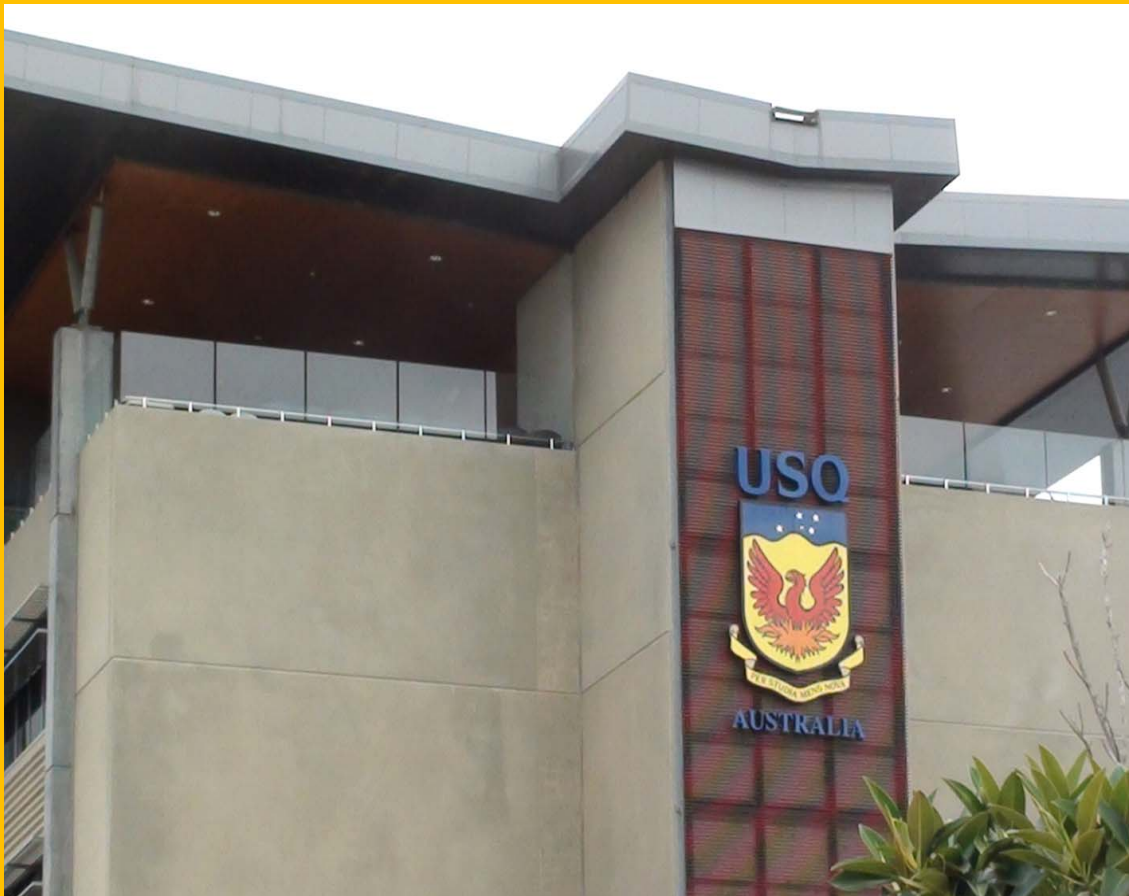


# **Geotechnique, Construction Materials & Environment**

**VOLUME 4(1)**



**Edited by  
Zakaria Hossain  
Jim Shiau**



GEOMATE 2014 BRISBANE, AUSTRALIA  
GEOTECHNIQUE, CONSTRUCTION MATERIALS AND ENVIRONMENT



PROCEEDINGS OF FOURTH INTERNATIONAL CONFERENCE – GEOMATE 2014  
GEOTECHNIQUE, CONSTRUCTION MATERIALS AND ENVIRONMENT BRISBANE,  
AUSTRALIA 19-21 NOVEMBER, 2014

# **Geotechnique, Construction Materials and Environment**

*Edited by*

**Zakaria Hossain**

*Graduate School of Bioresources  
Mie University*

**Jim Shiau**

*School of Civil Engineering and Surveying  
University of Southern Queensland*



THE GEOMATE INTERNATIONAL SOCIETY

Copyright @ 2014 by The GEOMATE International Society

All rights reserved. In principle, no part of this publication or the information contained herein may be reproduced in any form or by any means, translated in any language, stored in any data base or retrieval system, or transmitted in any form or by any means without prior permission in writing from the publisher.

Disclaimer: The editors and the publisher have tried their best effort to ensure the integrity and the quality of this publication and information herein. However, they give no warranty of any kind, expressed or implied with regard to the material contained in this book, and will not be liable in any event for the consequences of its use.

Published by:  
The GEOMATE International Society  
Tsu city, Mie, Japan  
E-mail: [geomate@gi-j.com](mailto:geomate@gi-j.com)  
[www.gi-j.com](http://www.gi-j.com)

ISBN Number: 978-4-9905958-3-8 C3051

## Table of Contents

Preface	xi
Organization	xii
<b><i>ID Keynote Papers</i></b>	<b><i>1</i></b>
1k PRACTICAL APPLICATION OF PROBABILISTIC METHODS IN GEOTECHNICAL ENGINEERING Stephen Buttlng	<b><i>2</i></b>
2k PERSPECTIVES FROM ACCURATE MEASUREMENTS OF THE STANDARD PENETRATION TEST Julian Seidel	<b><i>10</i></b>
<b><i>Technical Papers</i></b>	<b><i>11</i></b>
<b><i>ID Geotechnique</i></b>	<b><i>12</i></b>
4103 DESIGN AND DEVELOPMENT OF COMPOSITE FOUNDATION STRUCTURE FOR SOLAR SUPPORT SYSTEM Hossain, M.Z., Ojiro C., Ozumi, S., Harada, H. and Okuyama, S.	<b><i>13</i></b>
4113 DETERMINATION OF THE APPROXIMATE DYNAMIC COEFFICIENT OF FRICTION ON UNDERGROUND PIPES DUE TO VARIOUS BLAST SCENARIOS Akinola Johnson Olarewaju	<b><i>18</i></b>
4125 VERIFICATION OF RANDOM FINITE ELEMENT ANALYSIS FOR EVALUATING BEHAVIOR OF A CEMENT- TREATED SOIL COLUMN Tsutomu Namikawa	<b><i>24</i></b>
4132 INFLUENCE OF LIME ON STRENGTH AND COMPRESSIBILITY BEHAVIOR OF MARINE CLAY Nor Zurairahetty Mohd Yunus, Aminaton Marto, Faizal Pakir, Khairulanam Kasran and Mohd Akmal Azri Jamal	<b><i>30</i></b>
4141 SEISMIC BEHAVIOR OF SHORT GROUPED-PILES IN LIQUEFIABLE SANDY SOILS Chung-Jung Lee, Wen-Yi Hung, Chen-Hui Tsai, Yi-Chun Tu	<b><i>36</i></b>
4146 CHALLENGES IN ASSESSING THE INSTALLATION EFFECTS OF CONTROLLED MODULUS COLUMNS ON BEHAVIOR OF SURROUNDING SOILS Huu Hung Nguyen, Behzad Fatahi and Hadi Khabbaz	<b><i>44</i></b>
4147 EFFECT ON UNCONFINED COMPRESSIVE STRENGTH OF SAND TEST PIECES CEMENTED WITH CALCIUM PHOSPHATE COMPOUND BY ADDITION OF SCALLOP SHELL POWDER G. G. N. N. Amarakoon, Takefumi Koreeda, Satoru Kawasaki	<b><i>50</i></b>
4149 ENHANCING SLOPE STABILITY WITH VEGETATION Nicholas Hytiris, Michael Fraser and Slobodan B. Mickovski	<b><i>56</i></b>

4153	SMALL SCALE FIELD TESTS OF WATER INFILTRATION FOR COMPACTED SILTY LOESS SOIL Aiassa Martínez Gonzalo, Arrúa Pedro and Eberhardt Marcelo	62
4154	METHOD FOR HAZARD ASSESSMENT OF SLOPE FAILURES BASED ON INFORMATION PROCESSING TECHNIQUES Shinichi Ito, Kazuhiro Oda, Keigo Koizumi, Kyohei Umemura, and Yohei Usuki	66
4158	HYDRAULIC CONDUCTIVITY IN LOESSIC STABILIZED SOIL Alercia Biga Carolina, Arrúa Pedro, Eberhardt Marcelo, Aiassa Martinez Gonzalo	72
4159	MATHEMATICAL SIMULATION OF PILE INTEGRITY TEST (PIT) Ramli Bin Nazir and Osman El Hussien	77
4161	DEVELOPING DESIGN TOOLS FOR SHEET PILE WALLS Chane Brits and Jim Shiau	83
4165	SETTLEMENT BEHAVIOR OF DREDGED CLAY RECLAIMED LAND BY VACUUM CONSOLIDATION METHOD AND PROPOSAL OF ITS PREDICTION Ikeda H., Kawano M., Kiyoyama T., Yamamoto S., Takase E., Katagiri M., Ohishi K. and Yoshifuku T.	89
4166	SLOPE STABILITY AND ROCKFALL HAZARD ANALYSIS IN AN OPEN PIT ZINC MINE Maged Almandalawi, Greg You, Peter Dahlhaus, Kim Dowling and Mohannad Sabry	95
4171	A CONCEPTUAL MODEL OF ENVIRONMENTAL, GEOLOGICAL AND GEO-TECHNICAL RESPONSE OF DREDGED SEDIMENT FILLS TO GEO-DISTURBANCES IN LOWLANDS J. Rajaraman, K.Thiruvengkatasamy and S. Narasimha Rao	101
4174	3D NUMERICAL ANALYSIS OF A DEEP CIRCULAR EXCAVATION IN THE CITY OF RIO DE JANEIRO Jose Carlos Solis Tito, Celso Romanel	111
4178	STABILITY ANALYSIS OF THE SAIGON RIVERBANK SUBJECTED TO RIVER WATER LEVEL FLUCTUATION A. Oya, H.H. Bui, N. Hiraoka, M. Fujimoto, R. Fukagawa	118
4190	EFFECT OF LIGHT HYDROCARBONS CONTAMINATION ON SHEAR STRENGTH OF FINE SAND Rajab M. Abousnina, Jim Shiau, Allan Manalo, Weena Lokuge	124
4205	MONITORING THE STIFFNESS CHANGE IN CLAY WITH BENDER ELEMENT AND ELECTROMAGNETIC METHODS Chee-Ming Chan and Mohd Zarar Mohd Jenu	129
4208	NUMERICAL SIMULATION OF THE IMPULSE RESPONSE METHOD FOR RIGID PAVEMENT EVALUATION Hudson Jackson and Kassim Tarhini	134
4213	NUMERICAL ANALYSIS ON THE EFFECT OF JET GROUT PILES ON AN EXCAVATION LOCATED IN AN URBAN AREA Akula Pavan, Thiruvengadam Tamilmani	140
4217	USING DRILL BIT REFUSAL AS AN INDICATOR OF STRENGTH AT THE CORING INTERFACE B. Look, D. Lacey and D. J. Williams	145
4218	SPATIAL AND TEMPORAL VARIABILITY IN A RESIDUAL SOIL PROFILE Daniel Mellish, David Lacey, Burt Look and Chaminda Gallage	151
4230	INTERACTION ANALYSIS FOR OIL STORAGE TANK ON MARINE CLAY Pallavi Ravishankar B. and Neelima Satyam D.	157

4233	OPTIMIZATION OF TREATMENT AREA OF ENZYME MEDIATED CALCITE CEMENTATION: A NOVEL SOIL IMPROVEMENT TECHNIQUE Debendra Neupane, Hideaki Yasuhara and Naoki Kinoshita	162
4234	NUMERICAL ANALYSIS OF INFILTRATION INTO PERVIOUS CONCRETE-BASE SYSTEMS Bertrand Teodosio, Jaehun Ahn and Hyun-Suk Shin	167
4236	PROPAGATION OF HARMONICAL VIBRATIONS IN PEAT Darius Macijauskas and Stefan Van Baars	173
4237	SUBGRADE SUPPORT: A REVIEW OF SHORT-TERM AND LONG-TERM PERFORMANCE REQUIREMENTS Andreas Nataatmadja	179
4240	EVALUATION OF RE-LIQUEFACTION BEHAVIOR OF SEGREGATED AND UNIFORM SPECIMENS IN HOLLOW CYLINDRICAL TORSIONAL SHEAR TESTS Usama Juniansyah Fauzi and Junichi Koseki	185
4247	EFFECT OF FIBRE IN CONTROLLING DESICCATION CRACKS IN CLAY LINER SOILS Dr. Sobha Cyrus and Veena. V.	191
4250	CYCLIC BEHAVIOR OF RECYCLED CONCRETE AGGREGATE IMPROVED WITH LIME AND GYPSUM ADDITION Wojciech Sas, Andrzej Głuchowski Alojzy Szymański	196
4252	USE OF WIRE EXTENSOMETERS FOR MONITORING PAVEMENT PERFORMANCE IN AREAS OF SLOPE INSTABILITY J. N. Kirjan, D. F. Marks and J.S. Shiau	202
4253	GENERATION AND DISSIPATION OF PORE WATER PRESSURE NEAR TO PILE AND FAR-FIELD IN LIQUEFIABLE SOILS Suresh R Dash, Subhamoy Bhattacharya, Atul Prabhakaran and C. Sreenivasulu	208
4262	A COMPARATIVE STUDY ON THE RESISTANCES OF BUCKET FOUNDATION IN SAND WITH DIFFERENT INSTALLATION METHODS Ju-Hyung Lee, Jin-Ung Do and Sung-Ryul Kim	213
4280	OBSERVATION, MEASUREMENT AND ANALYSIS OF ORIENTED BOREHOLE CORE FOR LOCATING SLIP SURFACES IN FRACTURE ZONE LANDSLIDES IN SHIKOKU, JAPAN Tsunataka Furuya and Jing-Cai Jiang	217
4295	EFFECT OF LAYER THICKNESS AND BLOCK RATIO ON ROCK SLOPES MOVEMENT STYLE A. K. Alzo'ubi	225
4306	ESTIMATION OF THICKNESS OF LANDFILL BY GEOPHYSICAL EXPLORATION METHODS AT ILLEGAL INDUSTRIAL WASTES DISPOSAL SITE Minoru Yamanaka, Tomoaki Hachimura, Shuichi Hasegawa	232
4307	APPLICATIONS OF INNOVATIVE MATERIALS FOR PERFORMANCE IMPROVEMENT OF FLEXIBLE PAVEMENT OVER EXPANSIVE SUBGRADE Ravin M. Tailor, Dr. Navin C. Shah	238
4308	A PHYSICAL AND NUMERICAL INVESTIGATION INTO SINKHOLE FORMATION Brian Lamb and Jim Shiau	244
4309	EFFECT OF TEMPERATURE AND LIQUID CHEMISTRY ON GEOTECHNICAL AND HYDRAULIC PROPERTIES OF BENTONITE H. M. A. Rashid, K. Kawamoto, T. Komatsu, T. Saito. and P. Moldrup	250
4310	CASE STUDY OF GEOGRID REINFORCED SEGMENTAL RETAINING STRUCTURE Jia Xie, Barry Wai-Choo Kok, Jeroen Berends and Martin Silec	256

4315	CONSOLIDATION PARAMETERS FROM ATTERBERG LIMITS – NEW CORRELATIONS C H Solanki	262
4329	RESEARCH OF PERIMETER REINFORCEMENT OF THE FOUNDATION SOIL BY CEMENT-SAND MORTAR INJECTION M.L. Nuzhdin, L.V. Nuzhdin	267
4335	GEOTECHNICAL CHARACTERISTICS OF SYNTHETIC MUNICIPAL SOLID WASTE FOR EFFECTIVE LANDFILL DESIGN Oluwapelumi O. Ojuri. and Peter K. Adegoke	273
4344	INNOVATIVE GROUNDWATER TABLE MONITORING USING TDR TECHNOLOGY Vlastimil Chebeň, Marian Drusa and Michal Kuba	283
4363	DIFFERENTIAL CAPACITOR SENSOR OF WIRELESS SENSOR NETWORK FOR LANDSLIDE MONITORING S. M. A. Motakabber, M. I. Ibrahimy, and M. Z. Hossain	289
4364	BRIDGE SCOUR MONITORING BY USING RFID SYSTEM M. I. Ibrahimy, S. M. A. Motakabber and M. Z. Hossain	293
4368	MODELLING OF SHEAR STRENGTH PARAMATERS OF SATURATED CLAYEY SOILS M. Inanc Onur, Burak Evirgen, Ahmet Tuncan and Mustafa Tuncan	296
4369	DETERMINATION OF THE FREEZING EFFECT ON UNCONFINED COMPRESSION STRENGTH AND PERMEABILITY OF SATURATED GRANULAR SOILS Burak Evirgen, M. Inanc Onur, Mustafa Tuncan and Ahmet Tuncan	300
4381	QUANTITATIVE ASSESSMENT OF HUMAN RISKS POSED BY MINE DEBRIS FLOW Shuai Zhang, Limin Zhang	305
4386	A STUDY OF DYNAMIC SOIL STRUCTURE INTERACTION FOR PILED RAFT FOUNDATION WITH VARIABLE SUB SOILS Shukla S.J, Desai A.K. and Solanki C.H	310
<b>ID</b>	<b><i>Construction Materials</i></b>	<b>314</b>
4130	LIME LEACHABILITY STUDIES ON STABILIZED EXPANSIVE SEMI-ARID SOIL Arif Ali Baig Moghal, Muawia A Dafalla , Tamer Y Elkady and Mosleh Ali Al-Shamrani	315
4137	BEHAVIOR OF AN EPDM GEOMEMBRANE 18 YEARS AFTER ITS INSTALLATION IN A WATER RESERVOIR Manuel Blanco & Francisca Castillo, Nathalie Touze-Foltz, Bernat Amat, Escolástico Aguiar	320
4139	UNCERTAINTY OF BACK-CALCULATED VALUES IN PAVEMENT OVERLAY DESIGN WHEN USING THE FWD DEVICE Moshe Livneh	326
4145	UTILIZATION OF COCO COIR DUST AND PVC WASTE MATERIALS FOR WOOD-TILE QUALITY COMPOSITE BOARD Hermie M. del Pilar, Monesse Andrea Z. Antonio, Maricar A. Ilagan and Julius E. Seva	334
4155	UNCONFINED COMPRESSION TESTING OF CEMENT-TREATED DEMOLITION MATERIALS IN BASE AND SUB-BASE APPLICATIONS Alireza Mohammadinia, Arul Arulrajah, Jay Sanjayan, Mahdi Miri Disfani, Myint Win Bo, Stephen Darmawan	340
4157	RECENT FOAMED BITUMINOUS STABILISATION WORKS IN QUEENSLAND Lokanantham R. Logitharan, Kathirgamingam Somasundaraswaran and Jothi M. Ramanujam	346

4191	CHARACTERISTICS OF LIME STABILIZED EXPANSIVE SOIL FOR CONSTRUCTION OF FLEXIBLE PAVEMENTS S. Patel, L.M. Reddy and J. T. Shahu	353
4239	UPTAKE OF ADVANCED AND SUSTAINABLE ENGINEERING MATERIALS IN CIVIL INFRASTRUCTURE PROJECTS David S Thorpe	359
4243	A CASE STUDY – USE OF EXPANDED POLYSTYRENE BLOCKS IN LANDSLIDE REMEDIAL WORKS M. Boyer, K.Chew and Dr B. Look	365
4313	CRACKING AND BOND SPLITTING BEHAVIORS OF CORRODED LONGITUDINAL BARS IN REINFORCED CONCRETE BEAMS Yasuji Shinohara and Aris Aryanto	270
4314	SURFACE HEAT REDUCTION OF ASPHALT CONCRETE BY TOP FILLING WITH RECYCLED AGGREGATES AND MINERAL MORTAR Mohammad Raihanul Islam, Satoru Ishiguro, Masayoshi Yamanaka	376
4325	ASPHALT BINDER EXTRACTION FROM ASPHALT CONCRETE USING PULSED POWER TECHNOLOGY Rétyce Ivan Hervé Dodji Togbé Amoussou, Youhei Takanabe, Nobuyasu Oyama, Eva Arifi, Koichi Ishimatsu and Mitsuhiro Shigeishi	382
4345	ENGINEERING PROPERTIES OF CONCRETE INCORPORATING WASTE CARPET FIBERS Hossein Mohammad Hosseini, A.S.M. Abdul Awal, M. Zakaria Hossain	388
4365	EFFECTS OF MOISTURE CONTENT ON RESILIENT PROPERTIES OF RECYCLED CONCRETE AGGREGATES (RCAs) Chaminda Gallage, Shiran Jayakody and Jothi Ramanujam	394
<b>ID</b>	<b><i>Environment</i></b>	<b>400</b>
4117	CONSERVATION AND EXPLOITATION OF BANG GRASS EFFECTIVE IN PHU MY VILLAGE, VIETNAM Duong Minh Truyen, Le Hong Thia, Mashhor Mansor	401
4122	NUTRIENT TRANSFER AND TRANSFORMATION IN RIPARIAN GROUNDWATER WITH DIFFERENT LAND USE OF A LOWLAND WATERSHED, EASTERN CHINA Xuyin Yuan, Lei Han, Huan Wang, Shouquan Wang, Hailong Chen	406
4129	HEAVY METAL DESORPTION STUDIES ON THE ARTIFICIALLY CONTAMINATED AL-QATIF SOIL Arif Ali Baig Moghal, Mosleh Ali Al-Shamrani and Waleed M Zahid	411
4133	RECURRENCE INTERVALS OF METEOROLOGICAL DROUGHT EVENTS ACROSS EASTERN AUSTRALIA – IMPLICATIONS FOR DISTURBED LANDSCAPES Devanmini Halwatura, Alex M. Lechner and Sven Arnold	416
4135	EUTROPHICATED SEDIMENT REMEDIATION USING SHELL FRAGMENT AS REGIONAL UNUSED RESOURCES FOR NUTRIENTS ELUTION CONTROL Kazuhito Murakami, Saki Agatsuma, Michio Gomyo and Akiko Inoue-Kohama	421
4142	THE VELOCITY REDUCTION EFFECT OF OBSTRUCTING STRUCTURES ON FLOOD WATER FLOWS DURING ROAD CROSSING Abdul Naser Abdul Ghani, Ahmad Hilmy Abdul Hamid and NursriaFitah Kasnon	427
4168	ROLE OF A RETAINING WALL CONSTRUCTED OF NATURAL STONES IN PLANT BIODIVERSITY Taizo Uchida, Masaaki Furuno, Takashi Minami, Sampei Yamashita, Tadashi Uchiyama, Teruo Arase and Daisuke Hayasaka	432
4177	INFLUENCE OF EXOTIC PASTURE GRASSES AND FERTILIZATION ON THE VEGETATION RECOVERY OF LANDSLIDE SLOPES FORMED BY TYPHOON 9512 IN MIKURA-JIMA ISLAND, JAPAN Teruo Arase and Tetsuo Okano	438

4188	FUNDAMENTAL PROPERTIES AND ANALYSIS OF WATER QUALITY IN A RESERVOIR AFFECTED BY LITTLE WATER USE AND TEA PLANTATION Masaaki Kondo and Takamitsu Kajisa	444
4200	SMALL WATER DISTRIBUTION SYSTEM DISINFECTION BY-PRODUCT CONTROL: WATER QUALITY MANAGEMENT USING STORAGE SYSTEMS Sandhya Rao Polneni and Enos C. Inniss	450
4216	PESTICIDE SUSTAINABLE MANAGEMENT PRACTICE (SMP) INCLUDING POROUS BIOCHAR/GEOPOLYMER STRUCTURES FOR CONTAMINATED WATER REMEDIATION Ian P Craig, Jochen Bundschuh and David Thorpe	455
4220	AN EVALUATION MODEL OF MEDICAL TRANSPORT WITH TSUNAMI EARLY WARNING SYSTEM Norimitsu Koike, Susumu Kurahashi	458
4231	SEASONAL VARIATION OF THE ALIEN PLANTS INVASION INTO RIVER ECOSYSTEM Michiko Masuda and Fumitake Nishimura	464
4241	LANDFILL WASTE WATER TREATMENT BY PULSED DISCHARGE IN WATER DROPLET SPRAY Akio Takigawa, Keiichi Kato, Takashi Nakajima, Ryota Serizawa and Hiromu Tamba	472
4242	CHALLENGING FACTORS IN THE IMPLEMENTATION OF GREEN BUILDINGS IN MALAYSIA Che Musa Che Omar, Hooman Abadi, Kamarusin Moh Noor	477
4245	GEOTEXTILE ENCASED COLUMNS (GEC): WHY, WHERE, WHEN, WHAT, HOW? Dimitar Alexiew and Graham Thomson	484
4246	TSUNAMI-GENERATION WARNING SYSTEM USING THE EARTHQUAKE EARLY WARNING SYSTEM Susumu Kurahashi and Norimitsu Koike	490
4255	ANALYSIS OF THE RISK OF CONFLICT AROUND THE TRANSBOUNDARY WATER RESOURCES OF THE NORTHERN SAHARAN AQUIFER SYSTEM (NSAS) Mohamed Redha Menani	494
4260	EFFECT OF THE “120-DAY WIND” ON AGRICULTURAL AND ENVIRONMENTAL CONDITIONS IN HERAT, AFGHANISTAN Homayoon Ganji Abdul Saboor Rahmany Takamitsu Kajisa Masaaki Kondo and Hajime Narioka	500
4263	USE OF GENETIC PROGRAMMING BASED SURROGATE MODELS TO SIMULATE GROUNDWATER FLOW AND BIOCHEMICAL TRANSPORT PROCESSES IN CONTAMINATED MINE SITES Hamed Koochpayezadeh Esfahani and Bithin Datta	504
4266	DECONTAMINATION OF RADIOACTIVE CESIUM FROM OCEAN SLUDGE BY MICRO-BUBBLE AND MICROORGANISMS Kyoichi Okamoto and Takeshi Toyama	510
4268	SOLID WASTE MANAGEMENT THROUGH ECOLOGICAL FOOT PRINT ANALYSIS – A CASE STUDY IN KOCHI CITY, SOUTH INDIA Subha Vishnudas, Athira Ravi	515
4274	GROUND CONDITIONS AND THE LAND OPERATIONAL PARAMETERS DETERMINED IN THE PLANNING DECISIONS Grzegorz Kmiecik, Marta Szejnfeld, Hanna Szymczak, Anna Szymczak-Graczyk	520
4320	EFFECT OF FLOCCULATION AIDS ON THE ELECTRIC FIELD ASSISTED DEWATERING OF SOLID LIQUID SYSTEMS Mohammed Saedi Jami, Masashi Iwata, Md. Monjurul Alam and Md Zahangir Alam	524
4323	IMPORTANCE OF CORYDALIDAE AS AN INDEX OF METAL CONTAMINATION OF RIVER Akihiro Fujino and Hiroyuki Ii	528
4326	CHEMISTRY OF RIVER WATER, RIVER INSECT AND WATER PLANT IN THE KINOKAWA RIVER CATCHMENT Takuma Kubohara, Hiroyuki Ii	534



4328	COMPARATIVE ANALYSIS OF EMBANKMENT METHODS UTILIZING EXPANDED POLY-STYROL AND CONVENTIONAL METHOD IN MOUNTAIN ROAD IN JAPAN BY LIFE CYCLE ASSESSMENT Hideyuki Ito, Koichi Yamanaka, Shoma Nehashi, Atsushi Fukuda and Kunio Minegishi	540
4330	CU, ZN AND AS CONTAMINATION OF SEAWEED BESIDE SHIZUKI AND KANAYAMA METAL MINES IN JAPAN Hiroyuki Ii	545
4340	WATER BALANCE ANALYSIS CONSIDERING RUNOFF OF UNGAUGED CATCHMENTS IN IWAKI RIVER BASIN, NORTHERN JAPAN Soichiro Kageyama, Shingo Tomiyama, Makoto Ikeda and Hiroyuki Ii	551
4347	REMOVAL OF CESIUM FROM SEA SLUDGE THROUGH DECOMPOSITION OF ORGANIC MATTER WITH AQUEOUS HYDROGEN PEROXIDE Hirosuke Hirano, Takeshi Toyama, Nobuyuki Nishimiya and Kyoichi Okamoto	557
4383	THE EFFECT OF SUMATRA FAULT EARTHQUAKES ON WEST MALAYSIA Noushin Naraghi Araghi, Mohd. Nawawi, Syed Mustafizur Rahman and Rosli Saad	561
4202	DEVELOPMENT OF SOIL FORMATION CORRESPONDING TO CYCLIC STRESS – DERIVED SHEAR STRAIN BASED ON STRATUM INDEX FACTOR Abdull Halim Abdul	566
4324	UNEXPECTED HIGH CO <sub>2</sub> CONCENTRATION IN CLASSROOMS OF WAKAYAMA UNIVERSITY Masahiro Yamashita and Hiroyuki Ii	572
4337	ATTENUATION LANDFILL POTENTIAL EVALUATION FOR A MILLENNIUM CITY, IN NIGERIA Oluwapeluimi O. Ojuri	578
4338	SITE REMEDIATION IN NIGERIA: PROVEN AND INNOVATIVE TECHNOLOGIES (RECOVERY OF FREE HYDROCARBON FROM SOIL/GROUNDWATER) Oluwapelumi O. Ojuri, Samuel A. Ola, Olaolu G. Fadugba and Micheal A. Uduebor	585
4164	A CASE STUDY ON SLOPE REMEDIATION: A GREEN SOLUTION AND CONSTRUCTION REALITY Elisabeth Simbolon and Bindumadhava Aery	591
4305	AMMONIA REMOVAL CHARACTERISTICS OF POROUS CONCRETE WITH ZEOLITE FOR ENHANCING SELF-PURIFICATION ABILITY IN RIVER SYSTEM Fumitake Nishimura, Toshio Yamada, Motohiro Tanaka, Hirofumi Kassai and Michiko Masuda	597

## [Authors index](#)

[Contents of GEOMATE 2011 – Volume 1\(1\) & 1\(2\)](#)

[Contents of GEOMATE 2012 – Volume 2\(1\)](#)

[Contents of GEOMATE 2013 – Volume 3\(1\)](#)

## **Preface**

On behalf of the GEOMATE 2014 Organizing Committee, we would like to welcome you in attending the International Conference on Geotechnique, Construction Materials and Environment held at the University of Southern Queensland, Australia in conjunction with GHD, Australia, GEOMATE International Society, Japanese Geotechnical Society, AOI-Engineering, Useful Plant Spread Society, HOJUN and Glorious International.

On Friday 11 March 2011, at 14:46 Japan Standard Time, the north east of Japan was struck and severely damaged by a series of powerful earthquakes which also caused a major tsunami. This conference was dedicated to the tragic victims of the Tohoku-Kanto earthquake and tsunami disasters. The 2014 Geomate conference covers three major themes with 17 specific themes including:

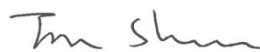
- Advances in Composite Materials
- Computational Mechanics
- Foundation and Retaining Walls
- Slope Stability
- Soil Dynamics
- Soil-Structure Interaction
- Pavement Technology
- Tunnels and Anchors
- Site Investigation and Rehabilitation
- Ecology and Land Development
- Water Resources Planning
- Environmental Management
- Public Health and Rehabilitation
- Earthquake and Tsunami Issues
- Safety and Reliability
- Geo-Hazard Mitigation
- Case History and Practical Experience

We have received very positive feedbacks; there have been paper submissions from 46 countries, including Algeria, Argentina, Australia, Bangladesh, Belgium, Brazil, Cameroon, Canada, China, Colombia, Egypt, Ethiopia, Germany, Ghana, India, Indonesia, Iran, Iraq, Israel, Japan, Libya, Luxembourg, Malaysia, Morocco, New Zealand, Nigeria, Pakistan, Palestine, Philippines, Poland, Russia, Saudi Arabia, Singapore, Slovakia, South Korea, Sudan, Taiwan, Thailand, Tunisia, Turkey, UAE, UK, Ukraine, USA, Vietnam. The technical papers were selected from the vast number of contributions submitted after a review of the abstracts. The final papers in the proceedings have been peer reviewed rigorously and revised as necessary by the authors. It relies on the solid cooperation of numerous people to organize a conference of this size. Hence, we appreciate everyone who support as well as participate in the joint conferences.

Last but not least, we would like to express our gratitude to all the authors, session chairs, reviewers, participants, institutions and companies for their contribution to GEOMATE 2014. We hope you enjoy the conference and find this experience inspiring and helpful in your professional field. We look forward to seeing you at our upcoming conference next year.

Best regards,

Dr. Jim Shiau, Conference Chairman



Dr. Md. Zakaria Hossain, Conference General Secretary



## **Organization**

### *Conference Chairmen:*

Dr. Jim Shiau, Senior Lecturer, USQ, Australia (Chair)  
Dr. Stephen Buttlng, S/Principals, GHD Geotech. (Co-Chair)

### *Conference Honorary Chairman:*

Dr. John Yeaman, Prof., Univ. of the S/Coast, Australia  
Dr. Sohji Inoue, E/Prof., Mie University, Japan

### *Conference Organizing Committee:*

Dr. Jim Shiau, Senior Lecturer Univ. of Southern Queensland, Australia  
Dr. Stephen Buttlng, Senior Principal GHD Geotechnics, Australia  
Dr. Ivan Gratchev, Lecturer, Griffith University, Australia  
Dr. Sohji Inoue, E/Prof. Mie University, Japan  
Dr. Toshinori Sakai, Prof. Mie University, Japan  
Dr. Zakaria Hossain, Prof. Mie University, Japan

### *National Advisory Committee:*

Dr. David Thorpe, Senior Lecturer, USQ  
Dr. Allan Manalo, Senior Lecturer, USQ  
Dr. Soma Somasundaraswaran, Lecturer, USQ  
Dr. Adrian McCallum, Lecturer, Uni. of Sunshine Coast, QLD, Australia  
Dr. Mark Jaksa, Prof. University of Adelaide, Australia  
Dr. Chaminda Gallage, Queensland Univ. of Tech. Australia  
Dr. Iyad Alkroosh, Curtin University, Australia  
Dr. Sammy Kwok, Geo. Eng. Cardno Bowler, Australia  
Dr. Jun Sugawara, S/Eng. Golder Associates Pty Ltd, Australia  
Dr. N. Sivakugan, A/Prof. James Cook Univ., Australia  
Dr. Robert Lo, A/Prof. UNSW Canberra, Australia  
Dr. Erwin Oh, Lecturer, Griffith University, Australia

### *International Advisory Committee:*

Dr. Fumio Tatsuoka, Prof. Tokyo University of Science, Japan  
Dr. Jing-Cai Jiang, Prof. University of Tokushima, Japan  
Dr. Toshihiro Morii, Prof. Niigata University, Japan  
Dr. Kimitoshi Hayano, Prof. Yokohama National Univ., Japan  
Dr. Sai Vanapalli, Prof. University of Ottawa, Canada  
Dr. M. Bouassida, Prof. National Sch. of Engg. of Tunis  
Dr. L.R. Austriaco, Prof. Angeles Univ. Found., Philippines  
Dr. A.S.M. Abdul Awal, Prof. Univ. Technology Malaysia  
Dr. M. Ibn Ibrahimy, Prof. Int. Islamic Univ., Malaysia  
Dr. Bujang B.K. Huat, Prof. Univ. Putra Malaysia  
Dr. Nemy Banthia, Prof. UBC, Canada  
Dr. Ian Jefferson, Prof. Univ. of Birmingham, UK  
Dr. John Bolander, Prof. Univ. of California, USA

Dr. Shamsul Chowdhury, Prof. Roosevelt Univ., USA  
Dr. Isabel Pinto, Prof. University of Coimbra, Portugal  
Dr. Kingshuk Roy, Prof. Nihon Univ. Japan  
Dr. Hj. Ramli Bin Hj. Nazir, A/Prof., UTM, Malaysia  
Dr. Aly Ahmed, A/Prof., Beni-Suef University, Egypt  
Dr. Chang-Yu Ou, Prof. National Taiwan University of Sci. & Tech.  
Dr. Raja Rizwan Hussain, A/Prof. King Saud Univ. Saudi Arabia

*Conference Secretariat:*

Mr. Ryan Kemp, Mr. Mathew Sams, Secretary,  
Faculty of Engineering and Surveying USQ Springfield Campus,  
Education City, Sinnathamby Boulevard, QLD, 4300, Australia,  
E-mail: Ryan.kemp@usq.edu.au, mathew.sams@usq.edu.au

Dr. Zakaria Hossain, General Secretary, Prof. MU, Japan  
Division of Environmental Science and Technology  
Graduate School of Bioresources  
Mie University, 1577 Kurima Machiya-cho  
Tsu-city, Mie 514-8507, Japan  
E-mail: geomate@gi-j.com  
Tel+Fax: +81-59-231-9578

*Editorial Committee:*

Dr. Jim Shiau  
Dr. Hossain Md. Shahin

*Executive Committee:*

Dr. Jim Shiau  
Dr. Stephen Buttling  
Dr. Zakaria Hossain  
Mr. Ryan Kemp  
Mr. Mathew Sams

Note- A: Associate, E-Emeritus

***Keynote Papers***

# PRACTICAL APPLICATION OF PROBABILISTIC METHODS IN GEOTECHNICAL ENGINEERING

Stephen Buttlings, BSc(Eng), ACGI, PhD, CEng, FICE, FIEAust, CPEng  
GHD Pty Ltd, Brisbane, Australia

## ABSTRACT

Despite the fact that probabilistic methods in engineering have been around for about 50 years, and their undoubted relevance to geotechnical engineering as a result of data uncertainty, they have not been widely adopted in everyday geotechnical design practice. There have been many publications, both books and technical papers, by eminent academic authors, but the knowledge of statistics required to make good use of the methods is held by few. In recent years, readily available commercial software has made it possible for probabilistic analyses to be carried out extremely easily, perhaps too easily, as the basic statistical knowledge is still required. Examples of misunderstandings of methods and misinterpretations of results will be shown, together with suggested ways in which these can be overcome and more appropriate use of the very powerful methods made.

*Keywords: Probabilistic analysis, slope stability, probability of failure, computer software*

## INTRODUCTION

Probabilistic methods have been around in civil engineering, and in geotechnical engineering, for quite some time, but yet they are not widely used and accepted in practice. If we look carefully at the work which has been done, it tends to be centred in academia, where the necessary understanding and knowledge can be expected to be available. On the other hand, the day to day practice may be left to engineers with a far lower level of skill, and this can, and indeed has, led to significant misunderstandings and misinterpretations of results.

## HISTORICAL PERSPECTIVE

Although they were specifically made with regard to the application of Bayesian Methods to updated parameter values based on some prior knowledge plus some site specific testing, the comments in Simpson & Driscoll [1] are believed to be relevant and have a wider implication:

The necessary skills in statistics are held by ***“very few designers who have committed their time to training and experience in geotechnical engineering. Attempts by statisticians to tackle geotechnical design have often ended in ridicule, and it is very difficult for one person to have a sufficient grasp of both disciplines that he can combine them sensibly.”***

Nevertheless we have excellent text books, such as two editions of Ang & Tang in 1975 [2] and 2007 [3], Duncan & Wright [4], and Phoon [5] amongst others, but their influence does not seem to have made its way into everyday engineering practice, and in particular into the assessment of

slope stability.

This is despite the fact that most of us acknowledge that engineering in general, and geotechnical engineering in particular, is concerned with parameters which have a high level of uncertainty. Ang & Tang [3] note that “the role of probability and statistics is quite pervasive in engineering.” This applies not only to soil properties, but also to rainfall and hence run-off quantities, wind forces on buildings, earthquake magnitudes, traffic volumes, and many more examples. In some of these the role of statistics is acknowledged and incorporated, especially in the case of rainfall, but in others we rely more on a factor of safety approach, believing that this will provide adequate protection, without needing to know how much. It is worth noting that the quotation from Ang & Tang [3] refers to the role of statistics and not to the use.

The chart in Figure 1 was first published by Christian et al [6], and has since been repeated by many others, including Nadim et al [7] and Pollock et al [8].

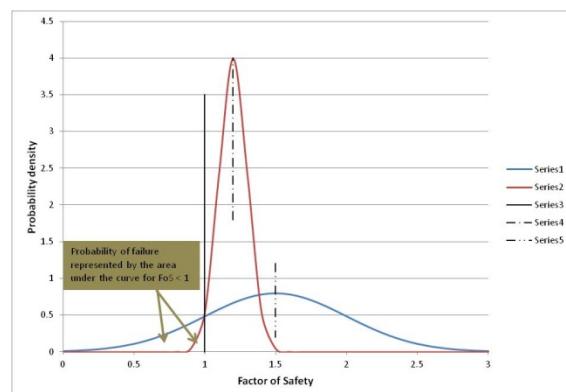


Fig. 1 Effect of data uncertainty on probability of failure for two mean Factors of Safety

It indicates the type of faith which practitioners have in the traditional use of factors of safety, derived from deterministic analyses, without considering data uncertainty. Because statistical analyses are frequently associated with large volumes of data, there is a very understandable concept that they can only be used in geotechnical engineering when we have large volumes of data, and that is rare. However there is no doubt that we are dealing with data uncertainty, and statistical methods also have wide application when we have very limited data. Duncan [9] has suggested the 6 sigma method amongst others, when there is little or no data, and this involves selecting the smallest possible value and the largest possible value, and assuming that they are separated by six times the standard deviation. Schneider [10] suggested selecting the lowest (a), highest (c) and most likely (b) values, and then defining the mean as:

$$\mu = \frac{a+4b+c}{6} \quad (1)$$

and the standard deviation as:

$$\sigma = \frac{c-a}{12} \quad (2)$$

Using either of these methods to consider the likely range of values of a parameter within a probabilistic analysis will probably produce a more meaningful output than picking a single value in a deterministic analysis.

This is not to say, however, that probabilistic analyses should replace deterministic analyses entirely. There is clearly a need for both, but probabilistic analyses are almost certainly not be given appropriate weight at the present time because of misunderstandings over their applications and benefits.

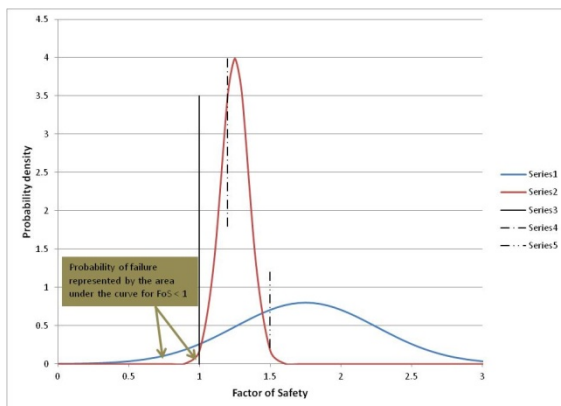


Fig. 2 Modified distribution with characteristic FoS = 1.5 and 1.2

In fact the curves in Figure 1 are considered to be slightly misleading, since it is considered that it is not normal practice in geotechnical engineering to

use mean strength for design. If we consider that a characteristic strength should be used, and that the characteristic strength may be defined as half a standard deviation below the mean, then this will give a more conservative answer. For simplicity of demonstrating the concept it is assumed that the distribution of factor of safety will be similar to the distribution of strength, and therefore use of a characteristic strength half a standard deviation below the mean strength will be equivalent to a Factor of Safety half a standard deviation below the mean Factor of Safety, then we can find the distribution of Factor of Safety which will give a characteristic Factor of Safety of 1.5 or 1.2 as in Figure 1. This is shown in Figure 2.

It is also noted that it has been recommended that slope stability analyses should be carried out using at least two computer programs, because of the complexities of the different algorithms within each program. In geotechnical engineering consultancy practice this is unlikely to occur as a result of commercial pressures both on time and licences.

## BASIS OF METHODS

In general the probabilistic methods involve determination of a distribution of values of a parameter, rather than a unique value as is used in deterministic analyses. Today we may also use statistical methods to determine our unique value as a characteristic value, to represent the data set, or the combination of a new data set with some previous knowledge. It has been found by various authors, e.g. Ang & Tang [3], and Bond & Harris [11], that soil strength parameters, being “physical properties based on a large number of individual, random effects”, will often be normally distributed about the mean value. However, great care is needed not to overuse this familiar and convenient model. Since the spread of the distribution needs to be defined as well as the mean value, the standard deviation is commonly used as a measure of spread. This is also often expressed as the Coefficient of Variation, or CoV, defined as:

$$CoV = \sigma/\mu \quad (3)$$

where  $\sigma$  is the standard deviation and  $\mu$  is the mean of the sample. Since it is known that 99.7% of all values in a normal distribution lie within the range of  $\mu \pm 3\sigma$ , it follows that if  $CoV > 33\%$  then some values will be negative. Data published by Duncan [9], Nadim et al [7] and Bond & Harris [11] has shown that  $CoV$  values for parameters such as apparent cohesion,  $c'$ , undrained shear strength,  $su$ , and coefficient of volume compressibility,  $mv$ , can range up to 40, 50 or even 70%, this would produce negative values if used with a normal distribution. Since for these and most engineering properties

negative values are not permissible, the normal distribution is unlikely to be appropriate if  $CoV > 30\%$ . This has also been discussed by Look [12].

On a project in Queensland, cement was being mixed with a bi-product of the alumina industry, known as red mud, in order to strengthen it to allow an upstream raise of the tailings dam. Trials were carried out, and in situ tests were used to measure the undrained shear strength of the treated material.

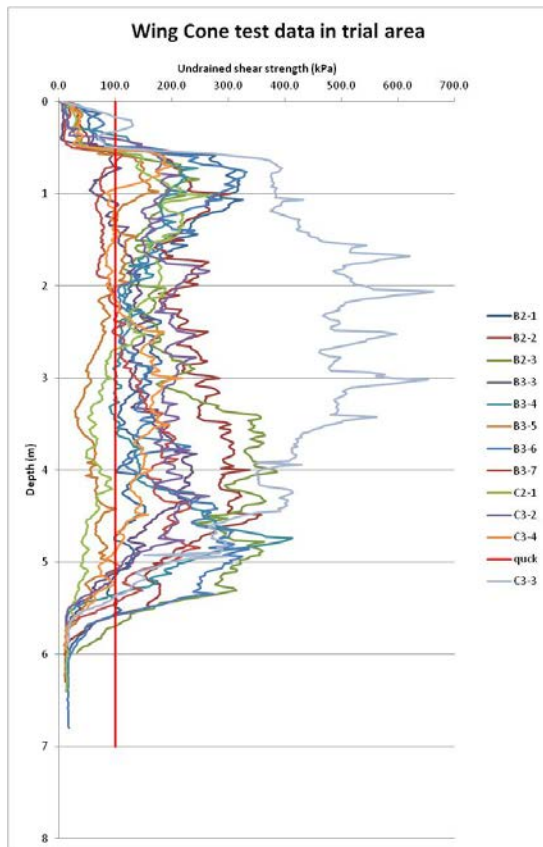


Fig. 3 Wing Cone Penetrometer profiles

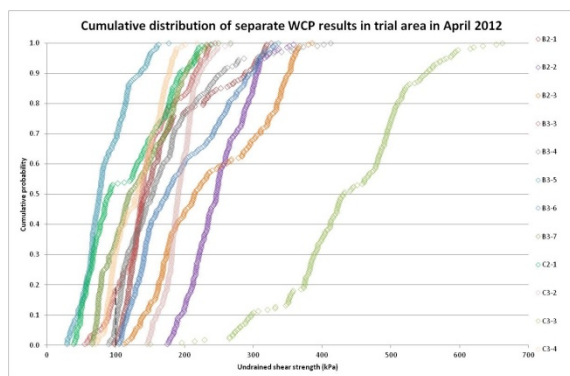


Fig. 4 Cumulative Distribution Function plots for 12 profiles of WCP data

The tests were carried out using a device called a Wing Cone Penetrometer, developed in Sweden as a variation on a Cone Penetrometer Test to smooth over minor spatial variations in strength. The results of twelve profiles are shown in Figure 3, which illustrates the scatter in the results. It is also apparent that many strength values are over 300 kPa, with some up to 700, while negative values are not possible. As a result the data does not fit a normal distribution.

Figure 4 shows the data for each profile plotted as a cumulative distribution function, and it can be seen that some follow a smooth trend, while others involve significant changes in gradient identify gaps in the strength distribution.

What is remarkable is that, when all the data are combined, making over 2,500 data points, the cumulative distribution function has a very close fit with a log-normal distribution curve, as shown in Figure 5.

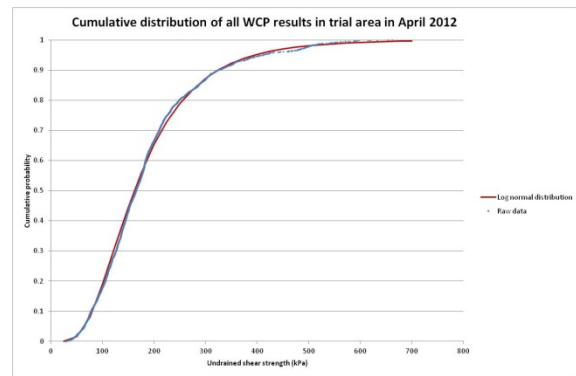


Fig. 5 Cumulative distribution function for 12 profiles combined

This would suggest strongly that a log-normal distribution is a good representation of the strength of this modified material. In other recent examples, a beta distribution was found to give a good representation of the probability distribution of some shear wave velocity results, seen in Figure 6, a log-normal distribution was found to work for some Lugeon test results seen in Figure 7, and an inverse Gaussian distribution gave the best fit for some Point Load Index test results seen in Figure 8.

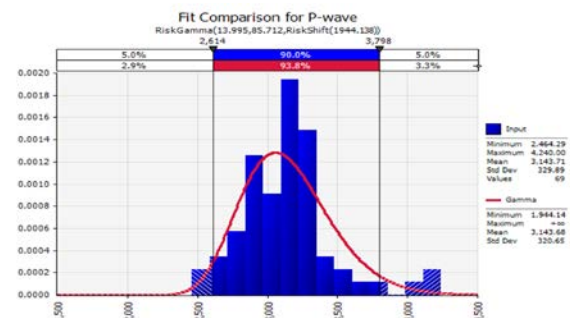




Fig. 6 A gamma distribution fitted through some P-wave velocity data

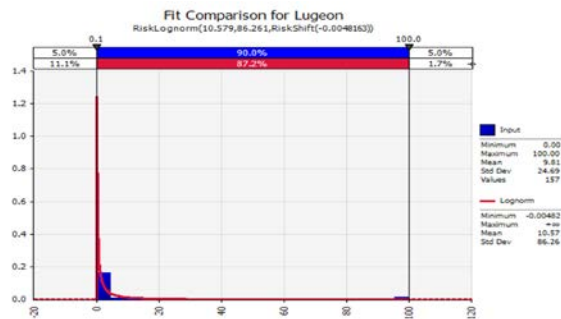


Fig. 7 A log-normal distribution fitted through some Lugeon test data

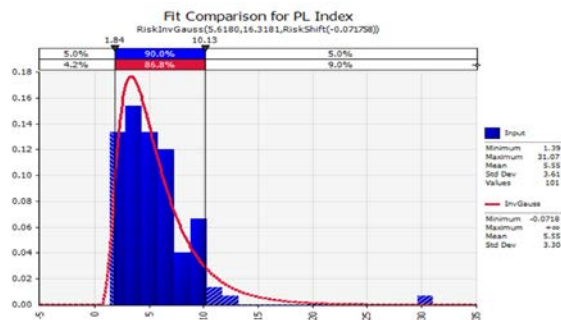


Fig. 8 An inverse Gaussian distribution fitted through some Point Load Index data

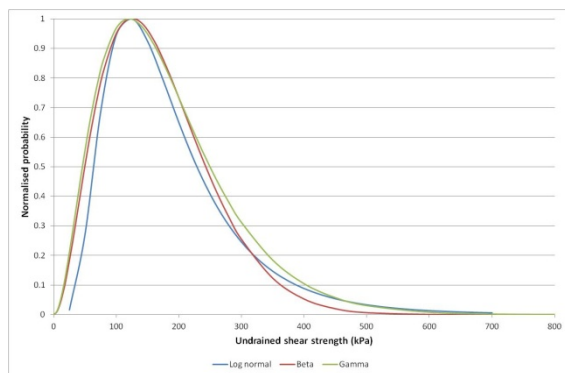


Fig. 9 Comparison of some skewed distributions

It is clearly essential to have a reasonable estimate of the probability distribution of the required parameters, in order to be able to select appropriate values to use in a probabilistic analysis. Nevertheless it is noted that several have a similar shape, such as the beta, gamma, and log-normal distributions, and it is unlikely that a significantly different outcome will result from their use. It is worth noting that the individual real data profiles in Figure 4 did not follow an idealized log-normal

profile closely, while the combination of all the data into one set produced the very close agreement with the log-normal curve shown in Figure 5. Figure 9 shows the log-normal probability distribution function for the data in Figure 5, as well as beta and gamma distributions which would be unlikely to be distinguishable when applied to actual data sets in real geotechnical engineering problems.

## SPECIFIC METHODS

### USE OF PROPRIETARY SOFTWARE

It is significant that, in the field of slope stability, two of the programs believed to be most widely in industry both offer probabilistic analysis as an option. This has made it easy for geotechnical engineers to carry out such analyses but, unfortunately, it has not ensured that they have the necessary skills. This is one of the common features of modern proprietary software. Many years ago such software was written and presented in complex code or programming language, and only people skilled in its use could understand and operate it. Now everything is windows-based, and user-friendly, and it has become increasingly difficult to ensure that software is only available to those with the requisite skills to operate it. This is especially true with the younger generation of computer literate engineers, who spurn hand calculations, and readily assimilate such things as finite element modeling without needing a grounding in the theory of stiffness matrices or constitutive modeling.

Returning to the subject of slope stability, it is very easy to click on the buttons in a program such as SLOPE/W to carry out a probabilistic analysis, without understanding how the analysis is carried out, or what the results mean. Examples have been published in which the authors have carried out probabilistic analyses, without understanding that they have not modeled spatial distribution of strength. By choosing a very simple geotechnical model, in order not to have distractions from the main point they were trying to make, the Monte Carlo method was only able to randomly select strength parameters, in this case  $c'$  and  $\phi'$ , and then apply them to the whole slope since there was a single soil layer. The resulting probability of failure, based on the proportion of critical failure surfaces which returned a factor of safety of  $< 1$ , was therefore the probability that the whole slope had uniform properties which did not provide enough resistance.

This helps to emphasise the difference between probabilistic and deterministic analyses. In the former, we choose suitably conservative strength parameters and apply them to the whole slope. But in the latter, in order for the probabilistic analysis and the Monte Carlo simulation to have any

meaning, there must be some realism to the random sampling, and applying one set of strength parameters uniformly to the whole layer is not it. Within the context of a probabilistic slope stability analysis, we need the random sampling to be modeling the spatial variability of strength, so we need there to be variations of strength within each layer.

In order to investigate this, the simple slope model shown in Figure 10 and analysed by Pollock et al [8] has been re-examined. First their results were regenerated, but it was found that the use of the optimization feature of SLOPE/W combined with

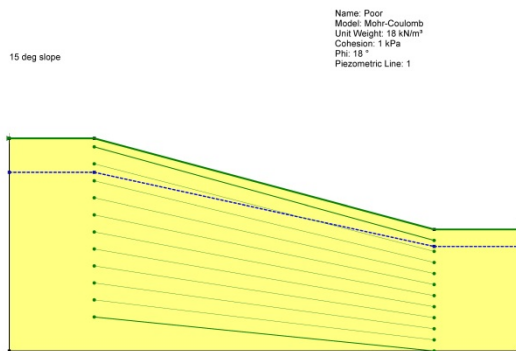


Fig. 10 Basic 15° slope analysed after Pollock et al [8]

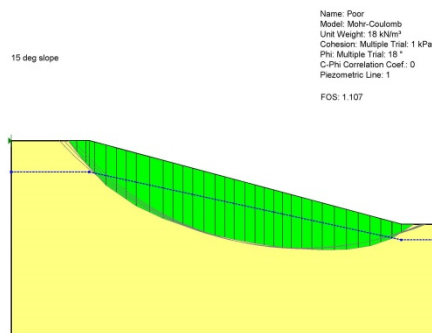


Fig. 11 Results of Morgenstern-Price analysis with optimization

the Bishop Method of Slices gave distorted results, even though they matched the output given in the paper. Instead the Morgenstern-Price method was selected, and this gave the results shown in Figure 11 and in Table 1.

A “standard” SLOPE/W analysis from Geostudio 2007 was used, except that the optimization function was turned on as it had been by Pollock et al [8]. The results were equivalent, except that they appeared to have used the Bishop Method of Slices, which gives a higher Factor of Safety when used with the optimization function than either the Morgenstern-Price method with optimization of the Bishop Method without.

The most striking thing about the results in Table 1 is the Probability of Failure at nearly 27%. Since no temporal variation has been allowed for in this analysis, it is only spatial variation that has been considered. This means that the Monte Carlo method, applied through 100,000 simulations, has randomly picked values for  $c'$  and  $\phi'$ , based on the mean and standard deviation supplied as determined Table 1 Probabilistic results from basic analysis

Mean F of S	1.1309
Reliability Index	0.707
P (Failure) (%)	26.925
Standard Dev.	0.185
Min F of S	0.69976
Max F of S	1.5791
# of Trials	100000

by Pollock et al [8], and then applied them to the whole slope. While it is understood that this is a special simple case chosen to illustrate a point with regard to the use of probabilistic analysis, it is also important to realize that such a distribution of strength will never occur in practice, since the random spatial distribution has not been modelled. Again this is an extreme case which has made the inappropriateness of this model clear because it is applied to the whole slope, but extreme care would also be needed when applying such a model to a multilayered slope, to ensure that the spatial variation of strength has been appropriately modelled.

The parameters which affect this are the auto-correlation distance, which relates to the distance over which properties, such as strength, are found to remain constant such that they can be modelled by a single strength selection in a Monte Carlo process. Using the same parameter over the whole area modelled is equivalent to using an auto-correlation distance =  $\infty$ . El-Ramly et al [13] reported that, for the lacustrine clays in the James Bay area of Quebec, Canada, auto-correlation distances of about 30 m were found to be appropriate. This has also been advised for quick clays in Norway. However, for older soils which may have been heavily over-consolidated and fissured, and for tropically weathered residual soils, very much shorter auto-correlation distances may be appropriate. Yu and Mostyn [14] suggested auto-correlation distances of 1 to 2 m.

In order to investigate the effect of this on the slope in Figure 10, the geometry was modified to have a mosaic of squares of soil of 2 m side, as shown in Figure 12.

The soil model was cloned such that all squares were notionally different soils, but with identical properties. This allowed the Monte Carlo simulation to allocate different strengths randomly to each “soil square” which, it may be argued, is a reasonable

approximation to the random spatial distribution of strength in nature. The effect on the results was dramatic.

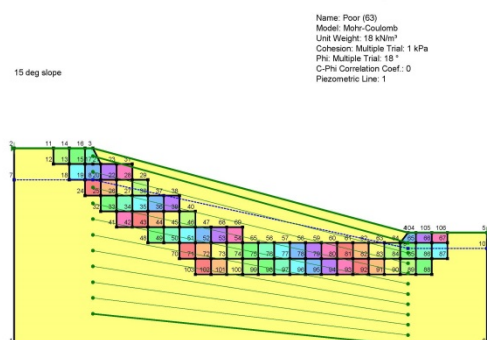


Fig. 12 Slope with mosaic of 2 m squares

The slip surface and the mean factor of safety were basically unaffected after 100,000 trials as seen in Figure 13, but the probability of failure had dropped by nearly three orders of magnitude, as shown in Table 2.

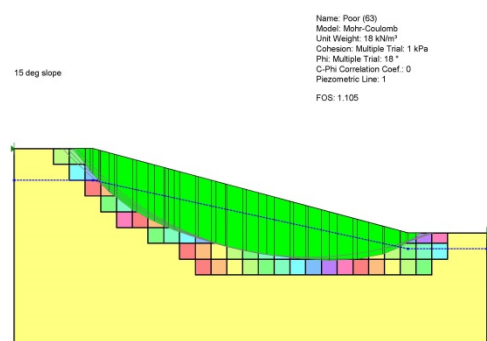


Fig. 13 Output from probabilistic analysis with mosaic of 2 m soil squares

Table 2 Probabilistic results from 2 m square analysis

Mean F of S	1.1294
Reliability Index	3.423
P (Failure) (%)	0.031
Standard Dev.	0.038
Min F of S	0.97796
Max F of S	1.2813
# of Trials	100000

The effect on the probability of failure of the number of Monte Carlo simulations was tested, and it was found that there was a small drop in the probability as the number of trials was increased from 10,000 to 200,000, as seen in Figure 14.

## ANNUAL PROBABILITY OF FAILURE

Another problem in application which has become evident relates to a misunderstanding of annual probability of failure. It is now commonly accepted that the term “risk”, when applied to

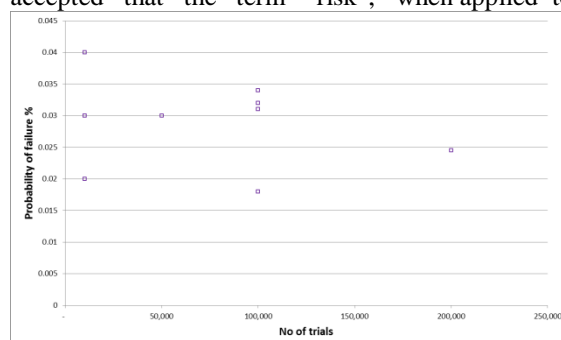


Fig. 14 Effect on probability of failure of number of trials for model with 2 m soil squares

landslides, is the product of likelihood and consequence. This in itself can lead to complications, because the general population may refer to risk in the context of probability, i.e. “the risk that something will happen”, or of susceptibility, i.e. “this is at a greater risk of slipping than that”. However, accepting that in landslide risk management, risk means the product of likelihood and consequence, in practice it seems to be easier to determine the consequences associated with a landslide of given dimensions, than it is to determine the likelihood that it will happen. There are a number of reasons for this, and obviously knowing the cause of a landslide is very high on the list, especially when we are referring to the cause of a landslide which has not yet happened. It is also generally accepted that there is a link between rainfall and landsliding, but details around the link are sketchy. What is the period of extreme rainfall which triggers landslides? Is it 10 minutes, an hour, 24 hours, 72 hours, or more? Is it different for different types of landslides, such as natural slopes, or fill slopes?

All of this makes the determination of an annual probability of extremely difficult, but nonetheless necessary if we are to establish likelihood in order to evaluate risk. It has already been noted that the readily available commercial software for slope stability will run a probabilistic analysis and produce an average factor of safety and also a probability of failure. What has happened is that users have not stopped to question what that probability of failure actually means.

It is easy to see that there is a connection between annual probability of failure, and probability of failure during a design life, with the latter probability increasing with increasing design life. This leads to the equation:

$$P_{DL} = 1 - (1 - P_a)^y \quad (4)$$

In which  $P_{DL}$  is the probability of failure during the design life of  $y$  years, and  $P_a$  is the annual probability of failure. This is illustrated in Figure 15.

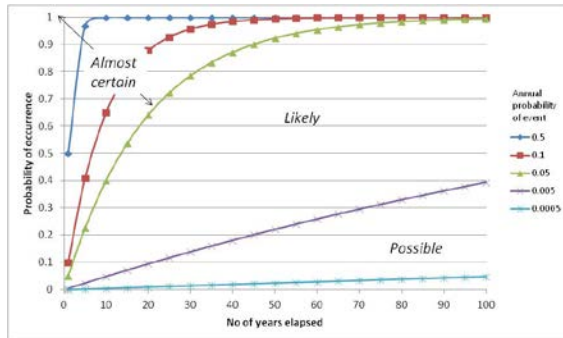


Fig. 15 Variation of probability of failure with design life.

In theory it would be possible, if the exact probability of failure during a given design life were known, to calculate the annual probability of failure. In practice this is exceedingly unlikely to happen, since circumstances dictate that it is more practical to determine an annual probability of failure than it is to determine a probability of failure during a design life. Unfortunately, what has happened on at least two occasions published recently, is that analysts have confused probability of failure, based on spatial variability, with probability of failure based on temporal variability, and have equated the spatial probability of failure with probability of failure during a design life. They have then tried to calculate an annual probability of failure by assuming a design life. This is clearly incorrect, since it leads to the conclusion that annual probability of failure decreases with increasing design life.

What needs to be done is that a reasonable geotechnical model is built, in accordance with the previous section, which makes due allowance for spatial variability. Superimposed on this we can then place different groundwater levels, with appropriate annual return periods. It will then be straightforward to determine a probability of failure which can be combined with the temporal probability to produce an overall annual probability of failure. These probabilities for each groundwater level can then be combined as in Table C6 in AGS [15].

#### USE OF CUSTOM MADE SOFTWARE

An examination of the literature tends to suggest that probabilistic analysis is still mainly carried out by academics within universities or research institutes, where the level of statistical understanding is suitably high, and time is available to write dedicated software, even if it makes use of readily

available materials such as Excel from Microsoft. Another example of this is the work of Cho [16].

In Example 1 in this study Cho [16] also looked at a uniform homogeneous slope, with a mean undrained shear strength = 23 kPa and a standard deviation = 6.9 kPa. With his 5 m high slope at 1(V) to 2(H) and 5 m below the toe to the rigid boundary, he found a deterministic factor of safety = 1.356. He then argued that the selection of the critical surface based on uniform parameters, followed by a Monte Carlo simulation of spatial variability, is unreliable since the spatial variability will inevitably affect the selection of the critical surface. This was demonstrated by analysis using his Random Field model, which is capable of modeling spatial variability. The effect was to identify a number of critical slip circles with factors of safety ranging between 0.834 and 0.983. However, an examination of the contours of undrained shear strength used in the different models suggests that an experienced geotechnical engineer would not carry out a deterministic analysis with an undrained shear strength of 23 kPa, because of the existence of large zones of lower strength material in what would be expected to be critical zones.

Cho [16] also examined the influence of cross-correlation between  $c'$  and  $\phi'$  for a homogeneous slope in his Example 2. He found the relationship shown in Figure 16 between Coefficient of Variation and cross-correlation, using both a fixed critical surface and his Random Field method.

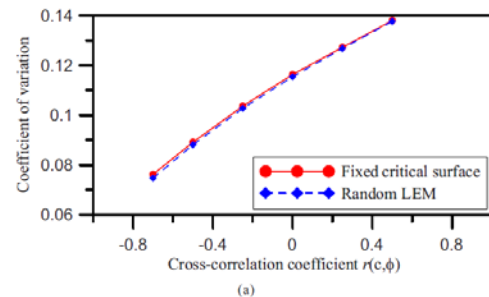


Fig. 16 Variation of Coefficient of Variation with cross-correlation coefficient after Cho [14]

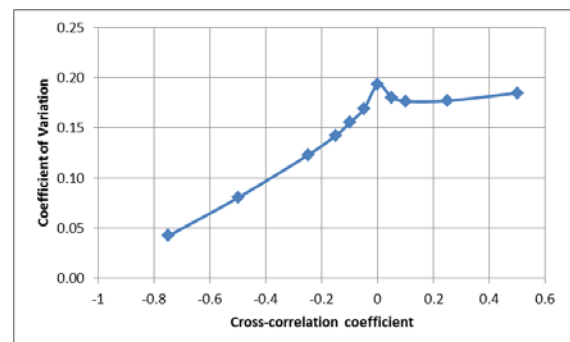


Fig. 17 Variation of Coefficient of Variation with cross-correlation coefficient using SLOPE/W

Attempts to reproduce this relationship in SLOPE/W using the same slope and soil parameters, and with a spatial correlation distance = 20 m, was not successful as there was an unexplained peak in the curve around a cross-correlation = 0, as seen in Figure 17.

This helps to illustrate the dilemma faced by practicing engineers. There is a lack of good understanding of the statistical processes involved in these analyses, and of the specialized jargon used by statisticians which is indecipherable to most of us, and there are now computer packages which appear to make the processes simpler, but involve the extreme danger of being able to produce answers without needing to understand the mathematical processes. In design offices all over the world, geotechnical engineers do not have the luxury of time to write custom software, or even adapt spreadsheets in ways which have been suggested by some authors (El-Ramly et al [13]; Low BK et al [17]; Wang et al [18])

## CONCLUSIONS

- 1 Probabilistic analyses are very powerful tools in the correct hands, and have particular application in geotechnical engineering as a result of data uncertainty.
- 2 The necessary statistical skills are held by very few people, and geotechnical engineers in general lack the necessary training in statistics.
- 3 Changes are needed in the education of geotechnical engineers, to make them more aware of engineering statistics, the tools available, and how to make proper use of them.
- 4 Proprietary software now offers some probabilistic analysis capability, but it is not well documented and explained, leading to serious errors in analysis and reporting.
- 5 Although it has been recommended that slope stability analysis is carried out using at least two computer programs, in actual geotechnical engineering practice this is unlikely to occur due to commercial pressures.

## REFERENCES

- [1] Simpson B & Driscoll R, "Eurocode 7 – a commentary", BRE Report BR 344, BRE, London, 1998.
- [2] Ang AH-S & Tang WH, Probability Concepts in Engineering Planning and Design, Vol I, Basic Principles. New York: Wiley, 1975.
- [3] Ang AH-S & Tang WH, Probability Concepts in Engineering – Emphasis on applications in civil & environmental engineering. 2<sup>nd</sup> Ed. New York, Wiley 2007.
- [4] Duncan JM & Wright SG, Soil strength and slope stability. New York, Wiley, 2005.
- [5] Phoon KK, Reliability-based design in geotechnical engineering – computations and applications London, CRC, 2008.
- [6] Christian JT, Ladd CC & Baecher GB, Reliability and probability in stability analysis, Journal of Geotechnical Engineering, ASCE, 120, 12, 2180-2207, 1994.
- [7] Nadim F, Einstein H & Roberds W, Probabilistic analysis for individual slopes in soil and rock, International Conference on Landslide Risk Management, Vancouver, 63-98, 2005.
- [8] Pollock D, Hurley G & Haberfield C, Linking equilibrium analysis and landslide risk assessment, Australian Geomechanics, 46, 2, 149-162, 2011.
- [9] Bond A & Harris A, Decoding Eurocode 7, London, Taylor & Francis, 2008.
- [10] Duncan JM, Factors of safety and reliability in geotechnical engineering, Journal of Geotechnical and Geoenvironmental Engineering, ASCE, 126, 4 307-316, 2000,
- [11] Look B, Appropriate distribution functions for characteristic values (to be published) 2013.
- [12] El-Ramly H, Morgenstern NR & Cruden DM, Probabilistic slope stability analysis for practice, Canadian Geotechnical Journal, 39, 665-683, 2002.
- [13] Yu YF & Mostyn GR, Random field modelling for the effect of cross-correlation, Proc. 13<sup>th</sup> International Conference on Soil Mechanics and Foundation Engineering, New Delhi, 4, 1389-1392, 1993.
- [14] AGS, Commentary on Practice Note Guidelines for Landslide Risk Management 2007, Australian Geomechanics, 42, 1, 115-158, 2007.
- [15] Cho SE, Probabilistic assessment of slope stability that considers the spatial variability of soil properties, Journal of Geotechnical and Geoenvironmental Engineering, ASCE, 136, 7, 975-984, 2010.
- [16] Low BK, Practical probabilistic slope stability analysis, Proc. 12<sup>th</sup> Panamerican Conference on Soil Mechanics and Geotechnical Engineering, MIT, Cambridge, Massachusetts, 2, 2777-2784, 2003.
- [17] Wang Y, Cao Z and Au SK, Practical reliability analysis of slope stability by advanced Monte Carlo simulations in a spreadsheet, Canadian Geotechnical Journal, 48, 162-172, 2011.

## **PERSPECTIVES FROM ACCURATE MEASUREMENTS OF THE STANDARD PENETRATION TEST**

Julian Seidel

Head, Specialist Foundation Engineering Consultancy, Australia

### **ABSTRACT**

The SPT or Standard Penetration Test is a much maligned in-situ test method which despite its failings, continues to be used extensively around the world, and is codified in standards such as ASTM-D 1586, BS 1377 and DIN 4094 to name a few. The test involves dropping a weight of 63.5kg from a height of 762mm onto a string of drill rods which drive a standard sampler 450mm into the material at the base of a borehole. The SPT N value is the blow count for the final 300mm of penetration, or equivalent. Despite the standardization of weight and drop height, there are considerable variations in the field implementation of the test which lead to variations in the SPT N. In addition, the way in which the blows are observed and recorded leads to inaccuracies. The authors have undertaken field studies into improved monitoring of SPT tests, and these have highlighted the deficiencies in current SPT evaluation processes. This paper will describe the field studies including the method of monitoring, provide results which highlight deficiencies, and provide some recommendations for future research and practice.

*Keywords: Standard Penetration Test, SPT, In-situ Testing, Monitoring, Measurement*

***Technical Papers***

***Geotechnique***



## **DESIGN AND DEVELOPMENT OF COMPOSITE FOUNDATION STRUCTURE FOR SOLAR SUPPORT SYSTEM**

Hossain, M.Z.<sup>1</sup>, Ojio C.<sup>2</sup>, Ozumi, S.<sup>3</sup>, Harada, H.<sup>2</sup> and Okuyama, S.<sup>3</sup>

<sup>1</sup>Graduate School of Bioresources, Mie University, Japan

<sup>2</sup>Cosmowinds Company Ltd., Nagoya, Aichi, Japan

<sup>3</sup>Beppu Construction Company Ltd., Yokkaichi, Japan

### **ABSTRACT**

Researches on solar plants are getting growing interest worldwide due to its renewable energy that combats climate change and assures a sustainable energy source. These researches are divided into mainly 3 categories such as 1) making current technology solar cells cheaper and/or more efficient to effectively compete with other energy sources; 2) developing new technologies based on new solar cell architectural designs; and 3) developing new materials to serve as light absorbers and charge carriers. This paper presents the design and development of a composite foundation structure for solar support system consisting of hollow circular steel pipe and thin cement-sand mortar layer. Field experiments of composite piles including pullout, compression (axial) and lateral tests were demonstrated and the results are summarized in this paper. Load-deflection relationships of pullout (uplift tension) tests, axial compression (pushing into ground) for pile-bearing tests and lateral tests of two sites are reported and compared for two different soils. It is concluded that the pullout, compression and lateral loads obtained from field tests are suitable to support solar panels against winds and weight of the solar systems.

*Keywords: Solar plants, Composite foundation, Pullout, Bearing capacity, Load-deflection relationships*

### **INTRODUCTION**

Energy production from renewable sources has become a crucial part for both industry and governments due to the growing demand for sustainable energy and climate change mitigation policy. The demand of solar plants is especially high in Japan after the tragic Tohoku-Kanto earthquake which occurred on Friday 11 March 2011, at 14:46 Japan Standard Time, in which the north east of Japan was severely damaged along with the destruction of Fukushima nuclear power plant. Literature review showed that there are many researches on the growing trend of creating renewable energy infrastructure, such as solar farms and wind turbines. To date, most of the researches available in the technical literature are on the technology of solar cells, architectural design of frame structures against winds loads and materials development for battery and light absorbers and charge carrier etc. Somekawa et al has conducted a research on the wind loads acting on the photovoltaic panels arrayed near ground and provided a design of frame structure against wind load [1]. There are some researches on the concrete foundations of solar plants that were found in the NEDO Organization, Japan [2]. These are mainly made of concrete and steel bars as of reinforced concrete foundation and cost-performance was not taken into account. In addition with these, researches on photovoltaic cells were performed by the Japanese Industrial Standards (JIS) [3,4]. Design wind pressure

coefficients on hip roofs of low-rise buildings with the variation of angle of solar panels were calculated by researchers of the Japanese Architectural Society and Aihara et al. [5,6]. In spite of the volume of information available on the upper part of solar system, very few researches are available on the solar foundation installed in the ground. Solar foundation that is directly related to the safety of the solar plants against severe climate such as typhoon, cyclones and heavy rains as well as bearing capacity of the structure; the cost-effective design of the solar foundation is indispensable for economic construction and long term performance of solar plants.

The object of this paper is to highlight some of these challenges and provides an alternative composite foundation for solar system that can facilitate the ease of installation, strength performance and minimize the construction cost. Composite pile presented in this paper are made of hollow steel pipe which supports the superstructure and sand-cement mortar between the pipe and the soil which provides the enough bearing capacity. The enhanced performance of composite pile comes from its synergetic action of steel with mortar and mortar with soil. Since, in composite pile, high tensile steel pipe provides adequate tensile and pullout resistance while the sand-cement mortar provides adequate frictional resistances and improved cohesion owing to its relatively greater surface area and roughness as compared to conventional foundation. If properly

designed, rough surface of mortar elements can grip the soil particles, and the frictional resistance needed for optimal design against pullout and compression failure can be significantly improved. Unfortunately, very little or no research attention has been given towards investigating pullout and compression response of composite foundation embedded in soil. In view of this objective, the pullout, compression and lateral response of composite pile embedded in two types of soil is studied initially and then these are optimized to obtain the necessary design strength. The paper reports the load-displacement relationships of composite solar foundation and development of the technique as well as failure modes from the pullout, compression and lateral tests results.

## SITE DESCRIPTION

The sites of the solar plants reported in this paper are located in Kasugai city, Aichi prefecture and in Matsuzaka city of Mie Prefecture, Japan (Fig.1). Both of the locations have strong winds especially during the typhoon. The types of soils are clayey and silty soils. The ground stratigraphy and the details of the soil properties can be found in elsewhere [8,9]. Both the grounds are usually saturated because of frequent raining throughout the year.



Fig.1 Sites of solar plants investigated in this research

## MATERIALS AND METHODS

The materials used are 76.3mm diameter steel pipe of lengths 1.5m and 2.0m and the sand-cement mortar mix with sand-cement ratio of 2.1 and water-cement ratio of 2:1. Outline of new solar foundation is shown in Fig.2. The anchoring length of the left pipe is 105cm and the right pipe is 125cm. In order to ease of pouring of the cement-sand mortar under the pipe, additional burrow of 10cm was done below the pipe (Fig.2).

### Work Procedure

The details of the work procedure are given the following flow chart (Fig.3).

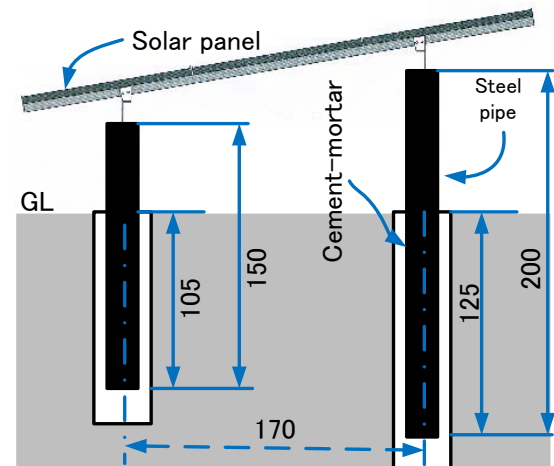


Fig.2 Outline of new solar foundation (cm)

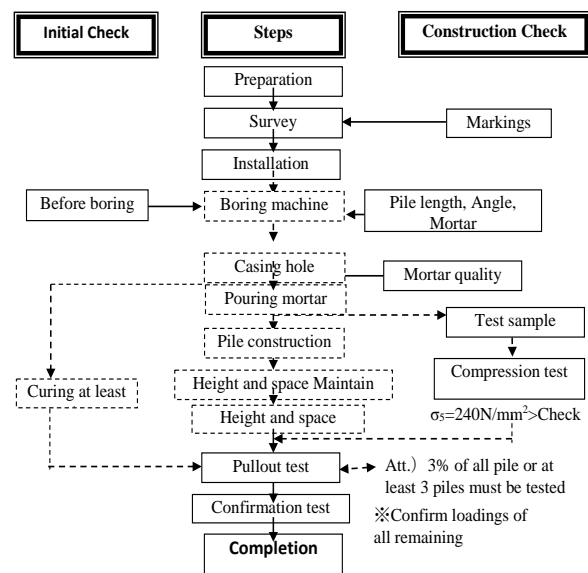


Fig.3 Work flow chart (Solid Line: Main Work, dotted Line: Specified Work, Construction Check: Formation and Quality Management)

### Drilling and Construction Method

The drilling was done using the rotary-percussion drilling machine (Fig.4). The equipment was set at the designated location where the pile needed to be installed and then it was adjusted vertically ( $\alpha = 90^\circ$ ). Careful attention was taken against the angle of drilling, direction of equipment and inclination of boring hole. Soil samples were collected from the boring hole and tested in the laboratory. After completion of drilling work, the mortar was pump into the drilled hole by using a pouring hose. The mortar was poured into at the bottom of the drilled hole in such a way that the water inside the hole was replaced by the sand-cement mortar. Finally, the steel pipe was placed into the sand-cement mortar

immediately upon pouring the mortar. All of these works were carried out according to the design and construction method of the Japanese Geotechnical Society (JGS).

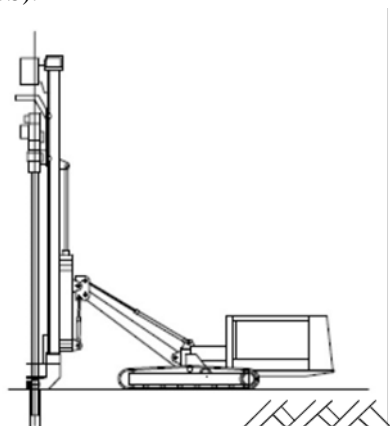


Fig.4 Rotary-percussion drilling machine used

### Method of Testing

The axial compression, tensile and lateral load tests were carried out in accordance with JGS 1811-31, 2002. A typical test setups for axial compression, tensile and lateral tests are shown in Fig.5-6. For axial compression, tension and lateral tests, pile head movements were monitored by the Linear Displacement Transducers (LDT). All LDT readings were recorded automatically with the increment of loads.

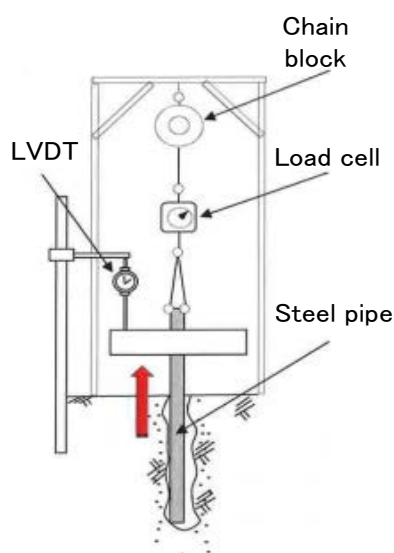


Fig.5 Outline of setup for axial compression and tensile load tests

### RESULTS AND DISCUSSION

The load displacement curves of Kasugai solar plants for pullout, compression and lateral loads are given in Fig.7-9, respectively. It is observed that the pullout load increases with the increase in displacement with a flat curvilinear nature (Fig.7).



Fig.6 Outline of lateral load tests

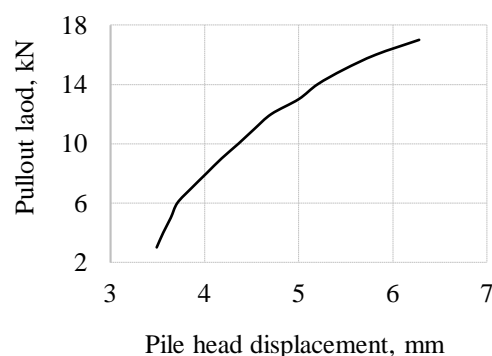


Fig.7 Pullout load-displacement relationships (Kasugai)

The maximum pullout load (17kN) was obtained at displacement of nearly 6.2mm. The compression load displacement curve can be characterized into three parts; which is like a reverse s-shape indicating a quick load increment at the initial stage and a straight line at mid-stage with a wider range of displacement from 8.7 to 10.7mm resuming its higher bearing capacity at the final stage. The maximum compressive load is recorded as 35kN at displacement of 10.9mm (Fig.8).

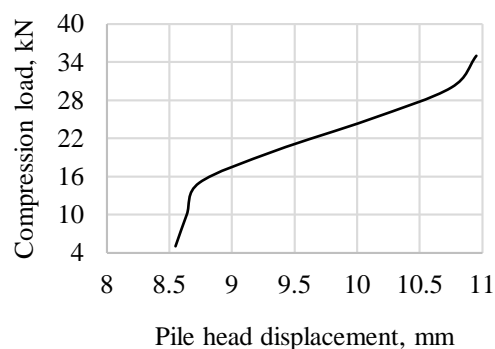


Fig.8 Compression load-displacement relationships (Kasugai)

The lateral load-displacement curve is seen as the combination of two linear parts. The first linear part is narrow range up to a displacement of about 2.7 mm at the initial stage while the second linear part is wider up to a displacement of about 13mm that corresponds to the failure of lateral load (8kN) (Fig.9).

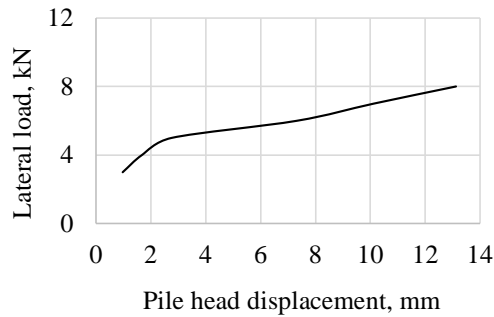


Fig.9 Lateral load-displacement relationships (Kasugai)

The results of pullout, compression and lateral load tests of two piles of Matsuzaka area are presented in Figs. 10-12. It can be seen from Fig.10 that the pullout load displacement curves for both the piles at Matsuzaka site showed the similar trend as of the Kasugai area pullout load-deflection curves. The uplift load for both the piles increased in curvilinear characteristics with a slight increase in the displacement. The maximum uplift loads for Matsuka are obtained as 15kN for both the piles.

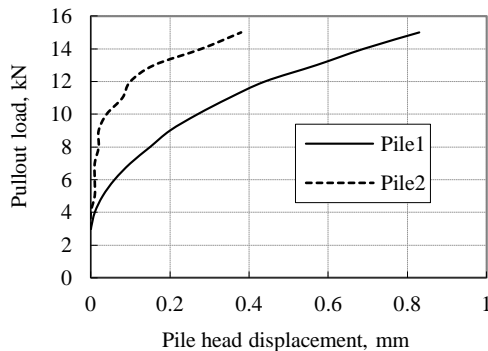


Fig.10 Pullout load-displacement relationships (Matsuzaka)

It can be seen from Fig.11 that the compression responses of both piles were non-linear. Both the piles showed very small displacement (nearly 0.7mm) in compression. For this case, the displacements in compression and tension are smaller. However, this behavior was conspicuously absent for Kasugai soil indicating the differences in load-deflection relationships for two soils in different locations. The maximum compression load for Matsuzaka area was noted as 20 for both the piles.

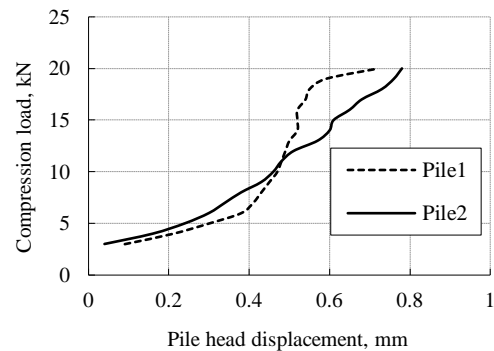


Fig.11 Compression load-displacement relationships (Matsuzaka)

The lateral load-displacement curve of Matsuzaka pile (Fig.12) can be characterized into three parts: the first linear part up to a displacement of 2mm, followed by the second linear component with a displacement ranging from 3mm to 14mm, and the third linear component with a near-horizontal slope up to a displacement of nearly 30mm. The maximum lateral load for Matsuzaka soil was obtained as 14kN at which the soil failure occurred along with lateral bending failure of the pile (Fig.13).

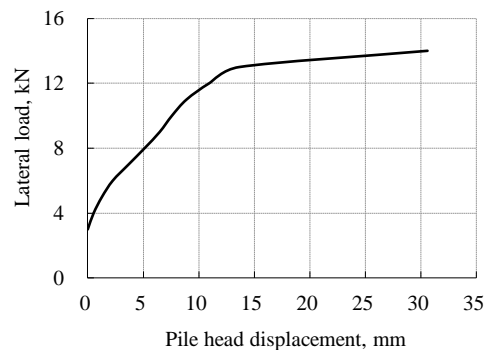


Fig.12 Lateral load-displacement relationships (Matsuzaka)



Fig.13 Bending failure of steel pipe after lateral test

## CONCLUSION

Composite foundation structures of solar support systems that have been designed and constructed in this research study are some of the examples in Japan. Results obtained have demonstrated that both the utility and the economy can be achieved using very simple techniques with locally available materials. Results obtained showed that the uplift pullout loads, compression loads and lateral loads of the piles are strong enough to support the solar plants against strong winds loads of about 40m/s and have the bearing capacity enough to support the weight of the solar plants. It is expected that the observations in this study will bring the new concept in gaining wide acceptance of composite foundation structures for the construction of strong, durable and cost-effective solar plants.

## ACKNOWLEDGEMENTS

The first author is grateful to Cosmo Winds Company Limited, Japan and Beppu Construction Company Limited, Japan for providing some of the field tests data and information noted in this paper.

## REFERENCES

- [1] Somekawa D., Koizumi T., Taniguchi T. and Taniike Y.: Wind loads acting on the photovoltaic panels arrayed near ground, The 22nd Wind Engineering Symposium, pp.157-160, 2012.
- [2] NEDO: New Energy and Industrial Technology Development Organization, <http://www.nedo.go.jp/>
- [3] JIS C8955: Japanese Industrial Standards, Design guide on structures for photovoltaic array, 2004.
- [4] JIS C8917: Japanese Industrial Standards, Environmental and endurance test methods for crystalline solar PV modules, 2005.
- [5] AIJ2004: Architectural Institute of Japan, Recommendations for Loads on Buildings, 2004.
- [6] Aihara T., Asami Y., Nishimura H., Takamori K., Asami R. and Somekawa D.: An area correct factor for the wind pressure coefficient for cladding of hip roof —The case of square plan hip roof with roof pitch of 20 degrees— The 22nd Wind Engineering Symposium, pp.339-344, 2008.
- [7] Cosmo Winds Company Limited, <http://cosmowinds.jp/solar/studio/>
- [8] Beppu Construction Company Limited, <http://www.o-beppu.co.jp/>



# DETERMINATION OF THE APPROXIMATE DYNAMIC COEFFICIENT OF FRICTION ON UNDERGROUND PIPES DUE TO VARIOUS BLAST SCENARIOS

Akinola Johnson OLAREWAJU

Civil Engineering Department, School of Engineering, Federal Polytechnic Ilaro, Ogun State, NIGERIA

## ABSTRACT

In this study, different types of blast scenarios and blast loads for various explosives were considered using [11]. Consequently, ground movement parameters were estimated and blast load durations for studying the dynamic effects of coefficient of friction on buried pipes due to blast loads were estimated. Simulated models for 'slip' and 'no-slip' conditions were analyzed using explicit code in ABAQUS. Dimensional analysis was used to process the results. It was observed that the ground shock parameters attenuate greatly in ground media as the distance increases. In addition, duration of blast play a significant role in the behavior of buried structures while the observed parameters reduced at coefficient of friction of around 0.8 compared to the conventional coefficient of friction for static analysis. Parameters thus determined would help in the study and designing of buried pipes to resist the effects of blast. Consequently, the environmental risk and hazards caused by blasts would be greatly reduced.

*Keywords: Blast, Underground, Coefficient of Friction, Simulation, Environment*

## 1. INTRODUCTION

Buried structures and facilities such as basements, foundations, mall facilities, storage facilities, etc could be fully buried or partially buried and these can be any structures of diver's shapes. Considering the severity of destruction due to blast; sufficient tremors could be created to damage substructures over a large area. At 138kpa of blast wave, reinforced concrete structures will be leveled resulting to loss of lives and property, disruption in production, land degradation, air pollution, etc. Blast occurs from terrorist's attacks, accidental explosion, wars, insurgent, nuclear reactors, accidental explosions from military formations, accumulation of explosive gases in pipes, etc. In view of these, there is need to estimate the blast load for the purpose of studying the dynamic behavior of simulated buried structures as well as the effects of coefficient of friction. The constituents of blast are basically the explosive, ground media, structural components as well as blast characteristics. In studying dynamic soil-structure interaction through modeling, experimental results are required in order to simulate the prevailing situations between all the constituent materials [8].

## 2. BACKGROUND STUDY

The analysis of soil-pipe interaction through modeling using numerical tools involves determination of variables such as pressure, displacement, strain stresses, etc around the pipe.

Analytically according to [6] and [10], axial friction force is determined using this expression,

$$F = \mu(W_p \gamma DH + W_p) \left( \frac{1}{12} \right) \quad (1)$$

where  $F$  = axial friction force (N/mm),  $\mu$  = coefficient of friction between pipe and soil,  $\gamma$  = density of backfill soil ( $\text{kg/m}^3$ ),  $D$  = outside diameter of pipe (m),  $H$  = depth of soil cover to top of pipe (m),  $W_p$  = weight of pipe and content ( $\text{kg/m}$ ). The soil density and friction coefficient (under static loads) are obtained from soil tests.

In impact related problems such as blast, it requires solution to equation of motion and analytical method may not provide accurate solutions to all the required variables. This is due to the dynamic nature of the problem as well as the blast duration which is short (i. e. transient). The non-linearity of the response of underground pipes due to blast loads lies in the definition of material (in this study, the material is considered as linear, elastic, homogeneous and isotropic), contact problem definition (boundary conditions), large displacements and rotations due to large loads (non-linear geometry) and time increment to ensure stability [2]. These responses could be suitably and easily studied by direct simulation, i. e. modeling using a suitable finite element numerical code, in this study, ABAQUS.

Considering the dynamic behavior of buried structures, a lot of works have been done on dynamic soil-structure interaction majorly for linear, homogeneous, and semi-infinite half space either linear or nonlinear using analytical or numerical methods [5], [7]. In this paper, blast

loads will be examined with a view to providing design parameters for the design of buried structures to resist the effects of blast loads in order to reduce environmental risk and hazards. From experience, the most common ways by which blast scenarios are expected to occur are: surface blast above the ground surface; open trench blast; underground blast below the ground surface with the explosives completely buried in the ground; and blast right inside the structures (whether the structure is buried in the ground or within the ground and the surface or on the ground surface). These are presented in Fig. 1.

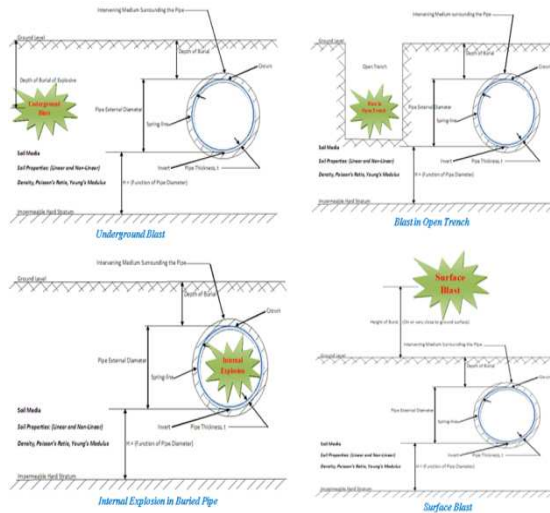


Fig. 1 Blast scenarios common to underground pipes

According to [11], the violent release of energy from a detonation converts the explosive material into a very high pressure gas at very high temperatures. It is followed by pressure front associated with the high pressure gas which propagates radially into the surrounding atmosphere as a strong shock wave, driven and supported by the hot gases. This pressure increase or shock front travels radially from the source of explosion with a reducing shock velocity which is always in excess of the sonic velocity of the medium [8]. The shock front arrives at a given location at time (ms). After the rise to the peak value of overpressure, the incident pressure decays to the ambient value in time which is the positive duration. The negative phase, shown in Fig. 2 with a duration which is usually longer than the positive phase and characterized by a negative pressure (usually below ambient pressure) have maximum values as well as reversal of the particle flow. The incident pulse density associated with the blast wave is the integrated area under the pressure-time curve shown in Fig. 2.

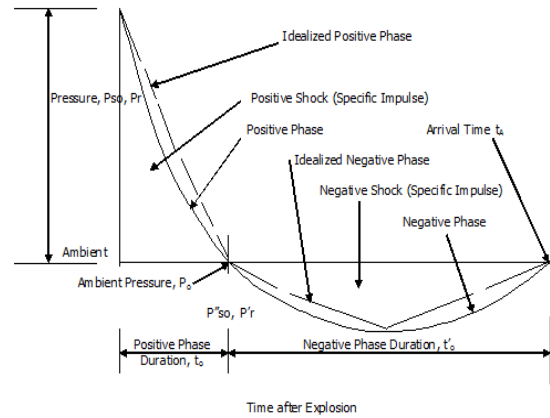


Fig. 2 Pressure-time curve

### 3. METHODOLOGY

In this study, in line with [11], blast load parameters were determined. For verification of blast load duration and dynamic effects of coefficient of friction on buried pipes, the soil of 100 m by 100 m by 100 m deep and pipes materials of 1.0 m internal diameter, 20 mm and 100 mm thick were modeled as elastic, homogeneous and isotropic as shown in Figs. 3 and 4 using the two elastic constants as obtained from different researchers and pipe manufacturers [1], [2], [3], [4]. Simulated models for 'slip' and 'no-slip' conditions were analyzed using explicit code in ABAQUS with 'no-slip' condition serving as control. In the 'no-slip' condition, it was assumed that perfect bond exist between the pipes and the soil while for 'slip' condition, coefficient of friction were varied.

The governing dynamic equation of motion is given as:

$$[m] \ddot{U} + [c] \dot{U} + [k] U = [P]; \quad \text{for } U(t=0) = U_0, \text{ and } \dot{U}(t=0) = \dot{U}_0 = v_0 \quad (2)$$

where  $m$ ,  $c$ , and  $k$  are element mass, damping and stiffness matrices,  $t$  is the time,  $U$  and  $P$  are displacement and load vectors and dots indicate their time derivatives [5]. The explicit dynamics analysis procedure in ABAQUS (finite element based numerical code) was used to solve eq. 2 [3]. The boundary conditions shown in the model (Fig. 4) were defined with respect to global Cartesian axes [2], [9].

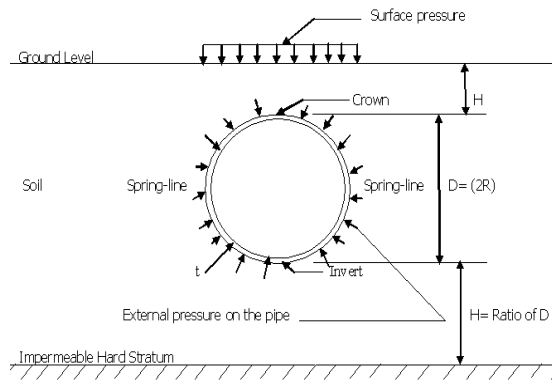


Fig. 3 Schematic diagram of underground pipe [8]

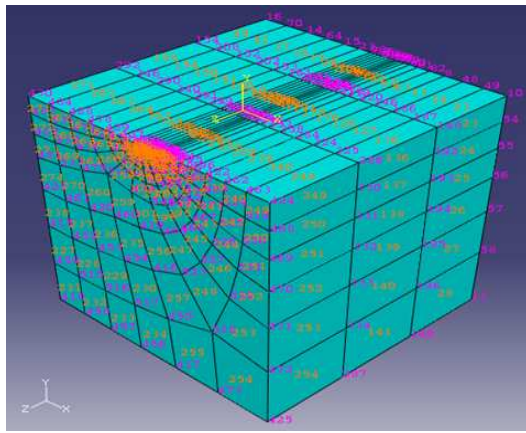


Fig. 4 Finite element model showing discretization [8]

Dimensional analysis was used to analyze the results of the dynamic effects of coefficient of friction on buried pipes due to blast loads [4]. All the dimensions are power law monomials of the form

$$[\alpha] = K L^a M^b T^c \quad (3)$$

where  $\alpha$  is the dimension of a physical quantity which would have a dimensionless quantity ( $[\alpha] = 1$ ),  $K$  and  $(a, b, c)$  are constants. This property is called dimensional homogeneity which forms the key to dimensional analysis [4].

#### 4. RESULTS AND DISCUSSION

In the case of underground blast, ground shock parameters which are equally known as the soil movement parameters translate into loading which the soil delivers to the buried structures. These parameters depend on both the seismic velocity and peak particle velocity. For a totally or partially buried charge located at a distance from the structure, ground movement parameters determined for stand-off distances are shown in

Fig. 5. In addition, the results of the peak side-on overpressure for surface blast for explosives ranging from 500kg TNT to 10000kg TNT are presented in Fig. 6. Furthermore, displacement and pressure of pipes buried in loose sand for various periods due to surface blast are presented in Fig. 7. The results of various observed response/behavior parameters at the crown, invert and spring-line of buried pipes against varied coefficient of friction are further processed using dimensional analysis and the dimensionless responses at the crown, invert and spring-line of buried pipes are presented in Figs. 8 to 11.

It must be noted that  $P$  is the intensity of surface pressure,  $P_{cr}$ ,  $P_{inv}$  and  $P_{spr}$  are the crown, invert and spring-line pressure respectively,  $H$  is the cover depth while  $D$  is the diameter of pipe,  $x$  is the displacement at the crown, invert and spring-line of pipes,  $P$  is the surface pressure intensity,  $\gamma$  is the unit weight of soil and  $r$  is the radius of pipe. These are shown in Figs. 8 to 11.

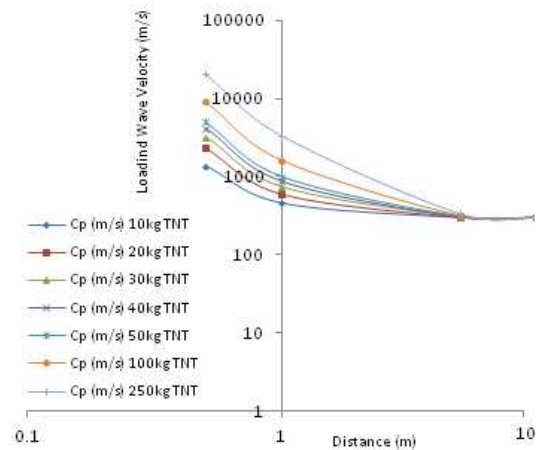


Fig. 5 Loading wave velocity due to underground blast

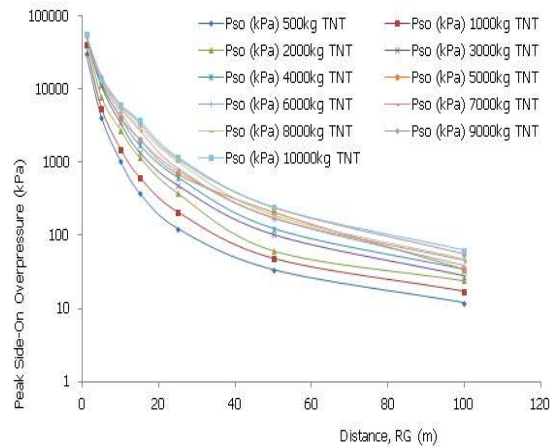


Fig. 6 Peak side-on overpressure due to surface blast



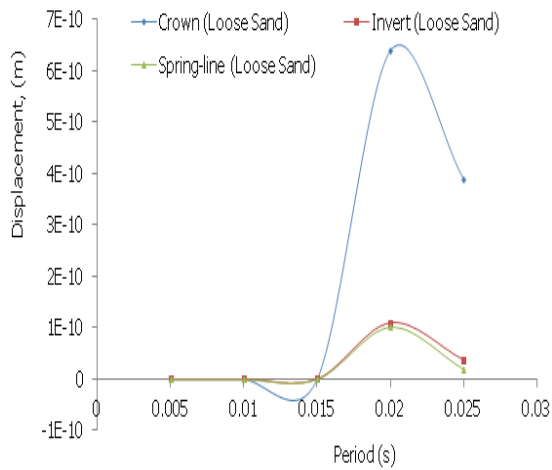


Fig. 7 Displacement in pipes buried in loose sand

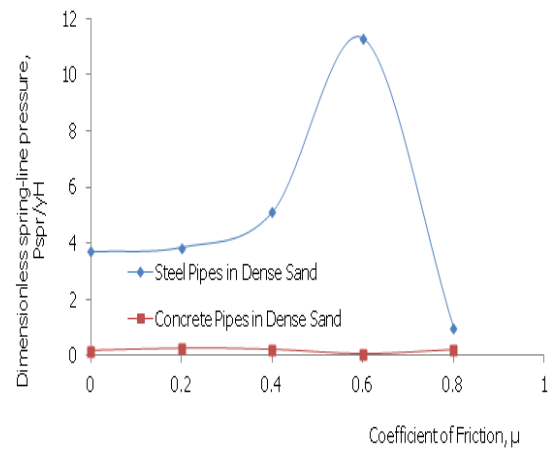


Fig. 10 Dimensionless spring-line pressure against coefficient of friction for underground blast

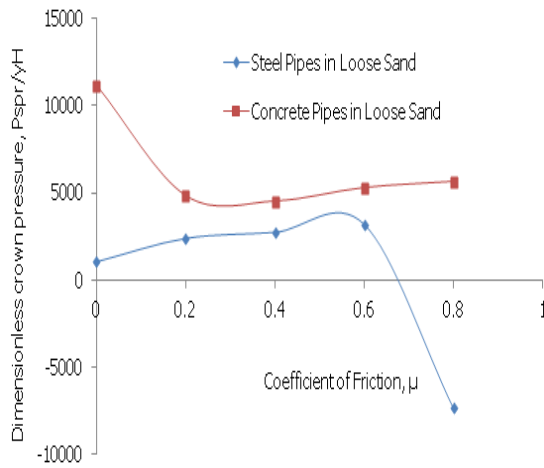


Fig. 8 Dimensionless spring-line pressure against coefficient of friction for surface blast

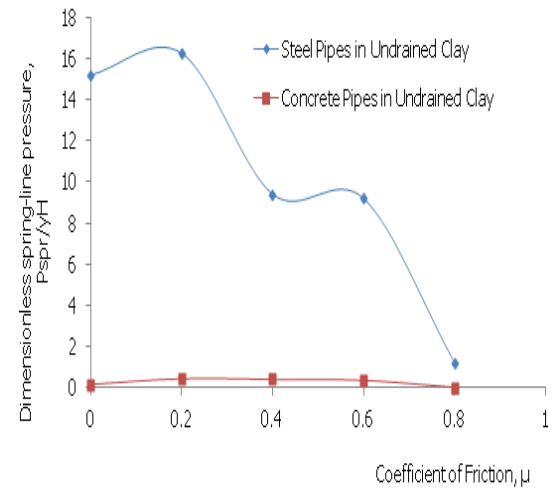


Fig. 11 Dimensionless spring-line pressure against coefficient of friction for underground blast

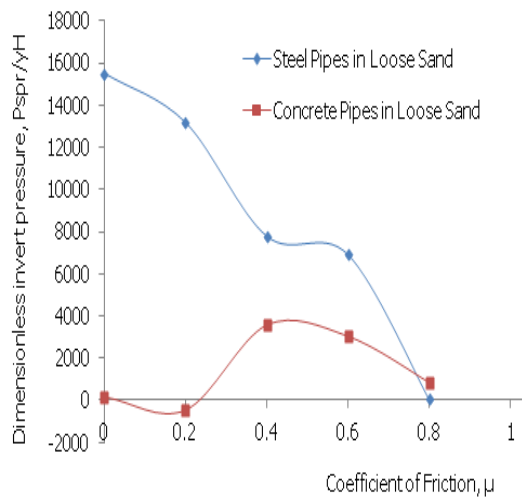


Fig. 9 Dimensionless spring-line pressure against coefficient of friction for surface blast

From Figs. 5 and 6, it was observed that energy attenuates greatly as the distances from the blast increases. In the case of underground blast, energy reduced to seismic velocity of the ground at less than 10m from the source of blast. Energy impulse from underground blast decreases as it travels for two main reasons, firstly, due to three dimensional dispersion of energy from blast, and secondly, due to work done in plastically deforming the soil matrix. Arrival time of blast wave depends on compression seismic velocity of the ground media. The arrival time is higher in saturated clay compared to other ground media. For the behavior of underground structures, especially pipes, arrival time of blast wave is the determining factor because it depends on the compression wave seismic velocity of soil. For structures above the ground surface, blast duration is the governing

factor. In line with [11], the blast wave parameters for the direct induced ground shock are the overriding factor for designing and studying the behavior of underground structures. At short duration which is common to blast, for low blast pressure due to surface blast, there is no behavior (i.e. response) of underground pipes even at small depth of burial.

One of the major challenges in the prediction of blast loads and duration is the complexity and difficulty in identifying the exact location, points or heights where the explosion will take place for surface blast. However, this problem is overcome by the fact that for parameters and guidelines to be suggested, there must be behaviors of underground structures (in this case pipes) due to blast loads. Efforts are tailored towards arriving at specific blast loads parameters and duration that produce behaviors or responses on underground pipes. Even if these loads are increased, response will also increase as well. In [11], the side-on overpressure and peak reflected pressure in the range of 2500psi to 8000psi and 30000psi to 100000 psi respectively do not have duration specified in the chart. For these pressures, durations have to be specified. This is scaled distance in the range of 0.1 to 0.45 and this does not mean that there is no duration for such blast pressures at such scaled distances. However, judgment has to be applied, to adjudge duration to such events. For scaled distances of 0.45 to 1.3 and 2.5 to 6, durations are almost the same irrespective of charge weight considered. It was observed from Fig. 7 that at less than 5ms of surface blast load duration, there is little or no behavior of underground pipes. This is noticeable in loose sand compared to other ground media. But as the duration of blast load increases, behaviors also increase. Since there must be behaviors in underground structures in order to provide design parameters and guidelines, duration of blast to be used should not be less than 20ms. Conservatively, to study the behaviors of underground structures due to blast, duration of 25ms is adequate for ground media [8].

For the purpose of the estimation of blast loads for various blast scenarios mentioned earlier on, in the dynamic behavior study of underground structures using finite element based numerical codes, in order to convert blast parameters from 0% increase of charge weight to 10% increase of charge weight, the following could be used as multiplication factor: 1.108 could be used for vertical and horizontal displacement while 1.0472 could be used for both vertical velocity and horizontal velocity. In addition, 1.02982 could be used for both vertical and horizontal acceleration. To convert the same blast parameters as above from 0% increase of charge weight to 20%

increase of charge weight specified by [11], 1.220 could be used for both vertical and horizontal displacement while 1.0936 could be used for both vertical velocity and horizontal velocity and 1.0595 could be used for both vertical and horizontal acceleration [8], [11].

In the result of the effect of coefficient of friction on the response of underground pipes due to blast loads as presented by [9], it was observed that there is variation in the results due to various parameters involved in the analysis. It became very much easier to interpret the results after evaluation using dimensional analysis. From the results of this study shown in Figs 8 to 11, at low coefficient of friction, the value of the dimensionless observed parameters is high in steel pipes due to ductility of steel pipes, while that of concrete pipes showed little or no increase due to brittleness of concrete pipes. Although the values of the dimensionless observed parameters for steel and concrete pipes reduced at coefficient of friction of 0.8.

From the results of the dimensionless responses of underground pipes shown in Figs. 8 to 11 obtained using dimensional analysis, it was observed that the observed parameters reduce at coefficient of friction of 0.8 for both surface and underground blasts. For all the ground media studied for the various categories of blasts considered in the dynamic analysis [9], in the design of underground pipes to resist effects of blast loads, coefficient of friction of average of 0.8 could be used. However, for practical applications for design purposes to resist effects of static loads, when test data are not available, the coefficient of friction of 0.3 (for Silt), 0.4 (for Sand) and 0.5 (for gravel) can be used. These coefficients of friction are the lower bound values equivalent to the sliding friction and static coefficient of friction can be as much as 70% higher than those stated above [6], [8], [9], [10].

#### 4. CONCLUSION

This paper has highlighted the basic steps in the estimation of loads arising from blast for the purpose of simulating the dynamic effects of coefficient of friction on underground pipes. Blast phenomenon and various blast scenarios applicable to underground structures were also examined and various durations for studying the behaviors of underground structures due to blast were equally examined. Dynamic effects of coefficient of friction on buried pipes were studied and coefficients of friction of friction were equally varied. Finite difference method in ABAQUS numerical code [1] was used to solve the equation of motion throughout time and dimensional analysis was used to evaluate the results. Practicable coefficient of friction for practical

applications in the design of buried pipes was suggested.

## 5. ACKNOWLEDGEMENTS

It is a project funded by Ministry of Science Technology and Innovation (MOSTI), Malaysia under e-Science Grant no. 03-01-10-SF0042 (Universiti Malaysia Sabah, Kota Kinabalu, Sabah, Malaysia).

## 6. REFERENCES

- [1] ABAQUS Inc., "ABAQUS Analysis User's Manuals – Documentation, Version 6.7- and 6.8-EF", Dassault Systemes Simulia, Providence, USA, 2009.
- [2] ABAQUS Inc.. Geotechnical Modeling and Analysis with ABAQUS, Dassault Systemes Simulia, Providence, Rhode Island, USA, 2009.
- [3] ABAQUS Inc.. ABAQUS/*Explicit: Advanced Topics*, Dassault Systemes Simulia, Providence, Rhode Island, USA, 2009.
- [4] Barenblatt, G.I.. "Dimensional Analysis", Gordon and Breach Science Publishers, New York, 1987
- [5] Kameswara RNSV, "Vibration Analysis and Foundation", 1<sup>st</sup> Ed., New Delhi, Wheeler Publishing Co. Ltd., India, 1998.
- [6] Lester, H.G. Chapter 4: The Pipe/Soil Structure – Actions and Interactions, 1-14, [http://plasticpipe.org/pdf/chapter4\\_pipe\\_soil\\_structure](http://plasticpipe.org/pdf/chapter4_pipe_soil_structure), 05/10/2010, 2008.
- [7] Olarewaju, AJ, Kameswara RNSV and Mannan, MA, "Response of Underground Pipes to Blast Loads", Earthquake-Resistant Structures - Design, Assessment and Rehabilitation, Abbas Moustafa (Ed.), InTech Publisher, Croatia, Europe, Feb., 2012, pp 507- 524.
- [8] Olarewaju, AJ, "A Study on the Response of Underground Pipes Due to Blast Loads", Ph.D Thesis, SKTM, Universiti Malaysia Sabah, Malaysia, 2013.
- [9] Olarewaju, A.J. "Estimation of blast loads for studying the dynamic effects of coefficient of friction on buried pipes by simulation", International Journal of GEOMATE, Geotechnique, Construction Materials and Environment, Tsu city, Mie, Japan, ISSN 2186-2982 (P), 2186-2990 (O), Sept., (received on Apr. 17, 2014), Vol. 7, No. 1 (SI No. 13), 2014, pp 1017-1024..
- [10] Peng L.C. "Soil-pipe interaction - Stress analysis methods for underground pipelines", AAA Technology and Specialties Co., Inc., Houston, Pipeline Industry, May, 67-76, 1978.
- [11] Unified Facilities Criteria, "Structures to Resist the Effects of Accidental Explosions", UFC 3-340-02, USA, 2008.

# VERIFICATION OF RANDOM FINITE ELEMENT ANALYSIS FOR EVALUATING BEHAVIOR OF A CEMENT-TREATED SOIL COLUMN

Tsutomu Namikawa<sup>1</sup>

<sup>1</sup>Civil Engineering Department, Shibaura Institute of Technology, Japan

## ABSTRACT

This paper presents a verification of the random finite element analysis approach for evaluating the compression behavior of a cement-treated soil column with spatial variability. In the verification, the unconfined compression tests of a full scale cement-treated soil column constructed by deep mixing method are simulated using the random finite element method. Samples of the full scale column are generated by means of Monte Carlo simulation and the finite element analysis with an elasto-plastic model which is developed for describing the mechanical behavior of the cement-treated soil is conducted for the generated samples. The statistical parameters of the cement-treated soil strength in the numerical analysis are determined from the strength of cored samples retrieved from the constructed columns. The numerical results indicate that the random finite element method evaluates the overall strength of the full scale column reasonably.

*Keywords: Cement-treated Soil, Spatial Variability, Finite Element Analysis, Monte Carlo Simulation*

## INTRODUCTION

It is well known that the strength of cement-treated soil ground by deep mixing is spatially variable, even at a single column. Therefore, such spatial variability has to be taken into account in design procedures to obtain the benefit of ground improvement. Finite element analysis combined with random field theory, called random finite element analysis, could be a powerful analysis tool for evaluating the behavior of the cement-treated soil ground [1]. Before adopting the random finite analysis in the design procedure, it is necessary to verify the random finite analysis for describing properly the behavior of the cement-treated soil ground with spatial variability.

This paper presents the verification of the random finite element analysis approach for evaluating the compression behavior of a cement-treated soil column with spatial variability. Futaki et al. (1996) [2] conducted the unconfined compression tests of full scale cement-treated soil columns constructed by deep mixing method. This full scale test is simulated using the random finite element method. On the basis of the statistical parameters of cored sample strength, full scale column samples are generated by means of Monte Carlo simulation and the finite element analysis with an elasto-plastic model which is developed for describing the mechanical behavior of the cement-treated soil is conducted for the generated samples. In this study, overall strength  $Q_u$  defined as the unconfined compressive strength of the full scale column is

mainly discussed. The comparison of the numerical and experimental results indicates that the random finite element method evaluates the overall strength of the full scale column reasonably.

## FULL SCALE COLUMN TEST

Futaki et al. (1996) [2] conducted the unconfined compression tests of deep mixed columns constructed at two sites. Group A test columns were constructed in cohesive ground having organic soil in the upper layer and Group B test columns were constructed in sandy ground. Four columns were tested in each group. The test columns are 1 m in diameter and 2.2 m in height.

## Cored sample strength

25 cored samples were retrieved from an upper cutoff portion of each test column; 100 cored samples were obtained for each group. The statistical values of the unconfined compressive strength  $q_u$  of cored samples are shown in Table 1. Using the sample mean  $m_{qu}$  and standard deviation  $s_{qu}$  of  $q_u$  in Table 1, the random field samples are generated by mean of Monte Carlo simulation.

The probability distribution of  $q_u$  is required to generate the random field samples. Several studies have been carried out to investigate the type of probability distribution of  $q_u$  [1], [3], [4]. These studies indicate that the normal or lognormal distribution provides a good fit for  $q_u$ . In this study, the Kolmogorov-Smirnov (K-S) test [5] was

Table 1 Statistical parameters of cored sample strength

Group	Mean $m_{qu}$	Standard deviation $s_{qu}$
A	3.48 MPa	1.46 MPa
B	3.78 MPa	1.20 MPa

Table 2 K-S test results for cored sample strength

Group	Probability distribution	D statistic	P-value
A	Normal	0.088	0.42
	Lognormal	0.067	0.76
B	Normal	0.117	0.13
	Lognormal	0.077	0.60

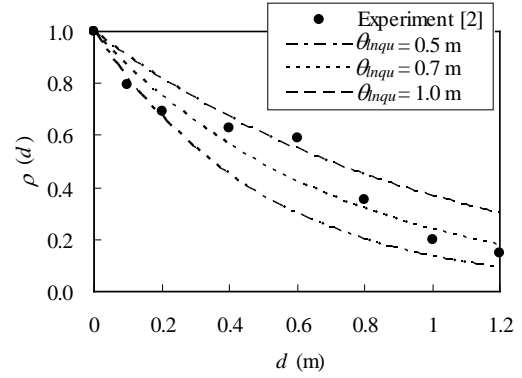
conducted to evaluate the goodness of fit for normal and lognormal distributions against the data for each group. The results of the K-S test are summarized in Table 2. Low values of the D statistic indicate a better fit of the data to the distribution than do high values. The K-S test result suggests that the lognormal distribution is better than the normal distribution for the probability distribution of the data. The P-value denotes the threshold value of the significant level in the sense that the null hypothesis will be accepted for all values larger than the P-value. The K-S test result shows that the P-value are much larger than 0.1 in all the cases of the normal and lognormal distributions, indicating that the null hypothesis that both the distributions are suitable for the probability distribution of  $q_u$  can be accepted at the 10% significant level. In this study, on the basis of the D statistic results, the lognormal distribution is assumed for characterizing the probability distribution of  $q_u$ .

The spatial correlation should be considered to describe the spatial variability appropriately. The exponential-type autocorrelation function is assumed for characterizing the spatial variability of  $q_u$ . The exponential-type autocorrelation function is defined as

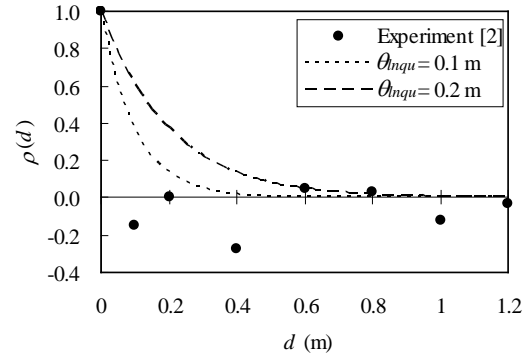
$$\rho(d) = \exp\left(-\frac{d}{\theta_{lnqu}}\right) \quad (1)$$

where  $\rho(d)$  = correlation coefficient;  $d$  = distance between the two points; and  $\theta_{lnqu}$  = autocorrelation distance in the random field of  $\ln q_u$ . Futaki et al. (1996) [2] calculated the correlation coefficient of the cored sample strength in each group. The correlation coefficient of the cored sample strength is shown in Figure 1. It can be seen that the strength correlates clearly in the Group A test column. Conversely, there is little spatial correlation of the

strength in the Group B test column. The correlation



(a) Group A



(b) Group B

 Fig. 1 Correlation coefficient of  $q_u$ 

coefficient calculated from Eq.(1) is also plotted in Figure 1. Here it is assumed that  $\theta_{lnqu}$  is not much different in magnitude from the autocorrelation distance in the random field of  $q_u$  [6]. The values of  $\theta_{lnqu}$  could be estimated to range from 0.5 m to 1.0 m for the Group A test columns and range from 0.0 m to 0.2 m for the Group B test columns.

### Unconfined compressive strength of a full scale column

Futaki et al. (1996) [2] obtained the overall strength  $Q_u$  of the full scale column from the unconfined compression tests. The obtained  $Q_u$  values range from 1.3 MPa to 2.2 MPa in the Group A test columns and from 2.5 MPa to 4.0 MPa in the Group B test columns.

### A DESCRIPTION OF RANDOM FINITE ELEMENT METHOD

Finite element analysis combined with random field theory, called random finite element analysis, was conducted to simulate the full scale unconfined compression test described in the previous section. In this analysis, Monte Carlo simulations were

performed involving the generation of realizations of the strength random field and the subsequent finite element analysis simulating the unconfined compression test.

### Generation of random field

As mentioned in the previous section, the lognormal distribution and exponential-type autocorrelation function defined in Eq.(1) are assumed for characterizing the probability distribution and spatial variability of  $q_u$ . The random field with the spatial correlation was generated by covariance matrix decomposition [7]. Using the Box-Muller method, the normal random numbers (white noise with the standard normal distribution) were calculated from uniform random numbers generated by the M-sequences method. Covariance matrix decomposition is a direct method of producing a random field with prescribed covariance structure. In this method, a random field vector  $\mathbf{X}(\mathbf{r})$  with the mean value  $\mu = 0$  is derived as

$$\mathbf{X}(\mathbf{r}) = \mathbf{L} \cdot \mathbf{u}(\mathbf{r}) \quad (2)$$

where  $\mathbf{L}$  is the lower triangular matrix of covariance matrix  $\Sigma$ , and  $\mathbf{u}(\mathbf{r})$  is a white noise vector with a standard normal distribution.  $\Sigma$  consists of  $\rho(d)$  calculated from  $d$  by Eq. (1).  $\mathbf{L}$  satisfies

$$\mathbf{L}\mathbf{L}^T = \Sigma \quad (3)$$

$\mathbf{L}$  is obtained using Cholesky decomposition.

The random number with the lognormal distribution was calculated from the normal random numbers. 100 realizations of the Monte Carlo process were performed for each case.

### Finite element analysis condition

Three-dimensional finite element analyses were performed using the finite element program developed by Shiomi et al. (1993) [8]. The finite element meshes for simulating the full scale column tests are shown in Figure 2. The sample is modeled as an isolated column of 1 m diameter and 2.2 m height. The mesh consisting of eight-node isoparametric elements is used. The majority of the elements are cubic with a length of 100 mm. The element length corresponds approximately to the standard height of cored samples. Therefore the local average process [7] has not been carried out in the analyses. The boundary condition for the sample is shown in Figure 2. The boundary conditions at the top and bottom surfaces are smooth. The loading process consists of applying uniform vertical displacement at the upper surface of the sample.

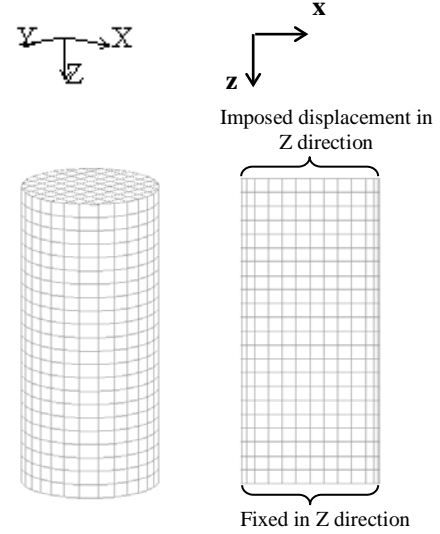


Fig. 2 FEM mesh

The variable unconfined compressive strength value of each element  $q_{ui}$  is given by

$$q_{ui} = \exp(\mu_{lnqu} + \sigma_{lnqu} x_i) \quad (i = 1, \dots, N_e)$$

$$\sigma_{lnqu} = \sqrt{\ln \left\{ 1 + \left( \frac{\sigma_{qu}}{\mu_{qu}} \right)^2 \right\}}, \quad \mu_{lnqu} = \ln \mu_{qu} - \frac{1}{2} \sigma_{lnqu}^2 \quad (4)$$

where  $\mu_{qu}$  is the mean of the strength,  $\sigma_{qu}$  is the standard deviation of  $q_u$ ,  $x_i$  is the standard normal random variable and  $N_e$  is the number of elements. The value of  $x_i$  generated by the method mentioned in the previous section is assigned to each element in the sample in the FE-analysis. The value of  $\mu_{qu}$  and  $\sigma_{qu}$  are determined from the mean and standard deviation of the cored sample strength as shown in Table 1. Here  $q_{ui}$  is classified into the discrete classes whose interval is set to be  $0.02\mu_{qu}$ .

Three different autocorrelation distances  $\theta_{lnqu}$  are considered in the simulation of each group. On the basis of the correlation coefficient of the cored sample strength shown in Figure 1, the values of  $\theta_{lnqu}$  were set to be 0.5 m, 0.7m and 1.0 m in the group A simulation, and 0.0 m, 0.1m, and 0.2 m in the group B simulation. Typical samples of the Group A columns are shown in Figure 3. The samples consist of 1936 elements. Dark and light regions depict “strong” and “weak” cement-treated soil, respectively. These spatial distributions of the strength are derived from the same probability distribution, that is to say, the lognormal distribution with the same probability parameters. The difference in spatial distribution is brought about by the difference of the autocorrelation distance  $\theta_{lnqu}$ .

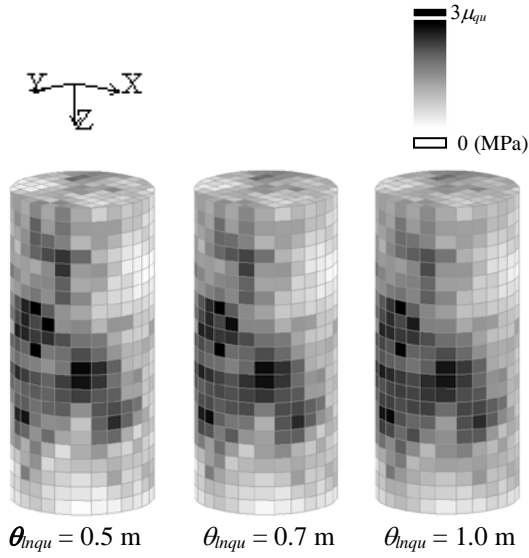


Fig. 3 Typical samples for FEM analysis (Group A)

An elasto-plastic model developed for cement-treated soils [9] was used in these analyses. This model can describe appropriately tensile and shear strain-softening behaviors in the strain localization zone after the peak stress state. In this model, the smeared crack band concept [10] is used to avoid mesh size dependency due to the strain localization. Thus the FE-analysis with the elasto-plastic model can simulate reasonably the post-peak behavior of cement-treated soils under various boundary conditions. The performance of the used model has been verified by the simulations for several laboratory tests of cement-treated soils [9], [11].

A list of elasto-plastic model parameters used in the numerical modeling and their values are shown in Table 3. These parameters for  $q_u = 1.7$  MPa were determined from the results of various laboratory tests in which cement-treated sand specimens with the unconfined compressive strength of 1.7 MPa were used [9], [12]. As indicated in Table 1, the elastic modulus  $E$ , the cohesion  $c$ , the tensile strength  $T_f$ , and the fracture energy  $G_f$  are regarded as the stochastic parameters. With the constant friction angle  $\phi$ , the value of cohesion  $c$  is determined from the value of  $q_{ui}$ . The values of  $E$ ,  $T_f$  and  $G_f$  are assumed to be proportional to the value of  $q_{ui}$ . Other parameters, Poisson's ratio  $\nu$ , the hardening parameters  $\alpha$  and  $e_y$ , the softening parameter  $e_r$ , the dilatancy coefficient  $D_c$ , the localization size  $t_{s0}$ , and the characteristics length  $l_c$ , are assumed not to vary with  $q_{ui}$ . The detailed descriptions of the material parameters and the numerical examples that can illustrate the applicability of this model are available elsewhere [9], [11].

Table 3 Material parameters for FE-analysis

Elastic modulus $E$	3000 MPa	Stochastic
Poisson's ratio $\nu$	0.167	Deterministic
Friction angle $\phi$	30 degree	Deterministic
Cohesion $c$	490 kPa	Stochastic
Tensile strength $T_f$	380 kPa	Stochastic
Hardening parameter $\alpha$	1.05	Deterministic
Hardening parameter $e_y$	0.0002	Deterministic
Fracture energy $G_f$	9.0 N/m	Stochastic
Softening parameter $e_r$	0.4	Deterministic
Dilatancy coefficient $D_c$	-0.4	Deterministic
Localization size $t_{s0}$	0.6 mm	Deterministic
Characteristics length $l_c$	100 mm	Deterministic

## NUMERICAL SIMULATIONS

Using the random finite element method, numerical analyses were carried out to simulate the behavior of the Group A and B test columns. Five realizations of the overall stress-strain relationship obtained from the numerical analyses are shown in Figure 4. In these stress-strain relationships, the stress is calculated from the total vertical load at the top surface and the strain is calculated from the vertical displacement of the top surface. For the Group A test with  $\theta_{inqu} = 0.7$  m, the stress-strain relationships vary widely before the peak stress state. Conversely, for the Group B test with  $\theta_{inqu} = 0.1$  m, there are no significant differences between the stress-strain relationships before the peak stress state. This is so because as the autocorrelation distance increases, the difference between the stress-strain relationships of the samples becomes large [1]. The experimental results are plotted in Figure 4 for comparison. The gradual stress increase during the initial loading process is observed in the experimental stress-strain relationships. This is attributable to the bedding error occurring at the top and bottom boundaries of the column. Consequently, there are significant differences between the numerical and experimental stress-strain relationships. It seems that such bedding error occurs significantly in the Group B test results. However, except the initial loading process, the calculated stress-strain relationships reasonably agree with the experimental stress-strain relationships.

The computed overall strength  $Q_u$  is summarized in Figure 5. The variability of  $Q_u$  increases as  $\theta_{inqu}$  increased. For the samples in the absence of spatial autocorrelation ( $\theta_{inqu} = 0.0$  m) for the Group B test, it can be seen that the variability of  $Q_u$  is quite low. Conversely, the variability of  $Q_u$  is high in the simulation for the Group A test in which  $\theta_{inqu}$  is



relatively large.

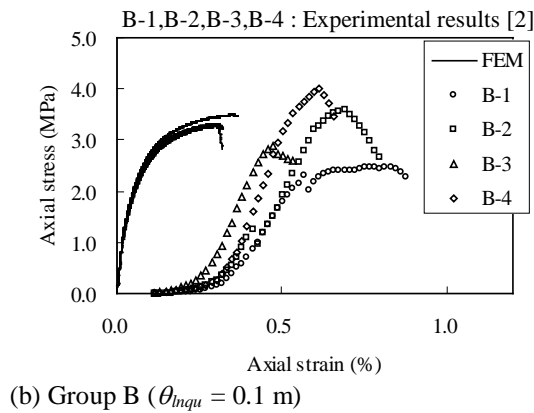
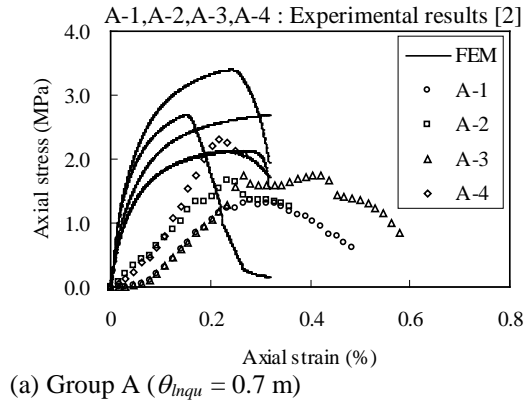
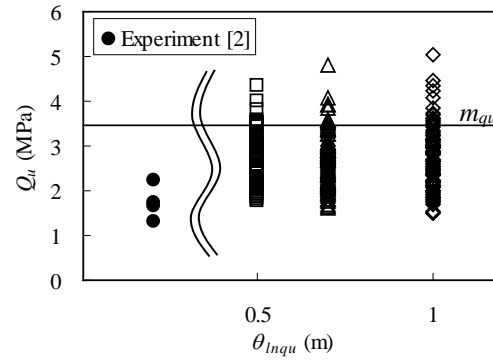


Fig. 4 Typical Stress-strain relationships

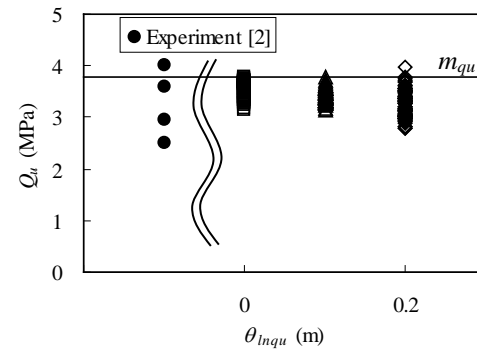
The experimental results are plotted in Figure 5 for comparison. In the simulation for the Group A test, most computed  $Q_u$  values become larger than the experimental  $Q_u$  values. The Group A test columns were constructed in cohesive ground with organic soil. In such cohesive ground, it is difficult to mix the ground thoroughly, with the result that the unmixed parts, that is, the defect parts, remain in cement-treated soil columns. The lognormal distribution used for the probability distribution of  $q_u$  cannot generate the low values of  $q_u$ , implying that the samples in the simulation do not contain defect parts. The probability distribution which can describe the defect parts in cement-treated ground should be examined in future studies.

In the simulation for the Group B test, the mean of the computed  $Q_u$  agrees reasonably with that of the experimental  $Q_u$ . However, the numerical result cannot describe the large variability of  $Q_u$  in the experimental result. As mentioned before, the variability of the computed  $Q_u$  depends on  $\theta_{Inqu}$ . The values of  $\theta_{Inqu}$  used in the numerical simulation were determined from the correlation coefficient reported by Futaki et al. (1996) [2] (Figure 1). The reported correlation coefficient may not represent sufficiently the spatial correlation of the strength in the Group B

test columns.



(a) Group A



(b) Group B

Fig. 5 Computed overall strength  $Q_u$

## CONCLUSIONS

Finite element analysis combined with random field theory, called random finite element analysis, was conducted for simulating the unconfined compression behavior of a cement-treated soil column. The objective of this study is to verify the applicability of the random finite element analysis to the evaluation of the overall strength of a cement-treated soil column. The comparison between the experimental and numerical results indicates that the random finite element analysis can describe the overall strength of a cement-treated soil column reasonably. However, there are some differences between both the results. In order to improve the numerical prediction, the probability distribution and the statistical parameters used in the analysis should be examined thoroughly in future studies.

## ACKNOWLEDGEMENTS

The author is grateful to Takenaka Corporation for their cooperation in the numerical analysis. The author also acknowledges the support of the Japan Society for the Promotion of Science (JSPS

KAKENHI Grant No. 25420509).

## REFERENCES

- [1] Namikawa T and Koseki J, "Effects of spatial correlation on the compression behavior of a cement-treated column", *Journal of Geotechnical and Geoenvironmental Engineering ASCE*, 139(8), 2013, pp. 1346-1359.
- [2] Futaki M, Nakano K and Hagino Y, "Design strength of soil-cement columns as foundation ground for structures", *Proceedings of IS-TOKYO'96 The second international conference of ground improvement geosystems*, 1996, pp. 481-484.
- [3] Honjo Y, "A probabilistic approach to evaluate shear strength of heterogeneous stabilized ground by deep mixing method" *Soils and Foundations*, 22(1), 1982, pp. 23-38.
- [4] Navin MP and Filz GM, "Statistical analysis of strength data from ground improved with DMM columns", *Deep Mixing 05*, 2005, pp. 145-154.
- [5] Kanji GK, "100 Statistical Tests 3rd Edition", *SAGE Publications*, 2006, pp. 76-77.
- [6] Griffiths DV and Fenton GA, "Bearing capacity of spatially random soil: the undrained clay Prandtl problem revisited" *Geotechnique*, 51(4), 2001, pp. 351-359.
- [7] Griffiths DV and Fenton GA, "Probabilistic methods in geotechnical engineering, Random field generation and the local average subdivision method", Springer, Wien, New York, 2007, pp. 201-223
- [8] Shiomi T, Shigeno Y and Zienkiewicz OC, "Numerical prediction for model No.1", Arulanandan & Scott (ed.) *Verifications of Numerical Procedures for the Analysis of Soil Liquefaction Problems*, Balkema, 1993, pp. 213-219.
- [9] Namikawa T and Mihira S, "Elasto-plastic model for cement-treated sand", *International Journal for Numerical and Analytical Methods in Geomechanics*, 31(1), 2007, pp. 71-107.
- [10] Pietruszczak ST and Mróz Z, "Finite element analysis of deformation of strain-softening materials", *International Journal for Numerical Methods in Engineering*, 17, 1981, pp. 327-334.
- [11] Namikawa T and Koseki J, "Evaluation of tensile strength of cement-treated sand based on several types of laboratory tests", *Soils and Foundations*, 47(4), 2007, pp. 657-674.
- [12] Namikawa T and Koseki J, "Experimental determination of softening relations for cement-treated sand", *Soils and Foundations*, 46(4), 2006, pp. 491-504.

## **INFLUENCE OF LIME ON STRENGTH AND COMPRESSIBILITY BEHAVIOR OF MARINE CLAY**

\*Nor Zurairahetty Mohd Yunus<sup>1</sup>, Aminaton Marto<sup>2</sup>, Faizal Pakir<sup>3</sup>, Khairulanam Kasran<sup>4</sup> and Mohd Akmal Azri Jamal<sup>4</sup>

<sup>1</sup> Senior Lecturer, Department of Geotechnics & Transportation, Faculty of Civil Engineering, Universiti Teknologi Malaysia, 86400, Skudai, Johor

<sup>2</sup> Professor, Department of Geotechnics & Transportation, Faculty of Civil Engineering, Universiti Teknologi Malaysia, 86400, Skudai, Johor

<sup>3</sup> Post-graduate Student, Faculty of Civil Engineering, Universiti Teknologi Malaysia, 86400, Skudai, Johor

<sup>4</sup> Bachelor Degree Student, Faculty of Civil Engineering, Universiti Teknologi Malaysia, 86400, Skudai, Johor

Corresponding author : [nzurairahetty@utm.my](mailto:nzurairahetty@utm.my)

### **ABSTRACT**

The presence of marine clay in Iskandar Malaysia Region, Nusajaya has caused expensive solutions in the construction of structures and roads. Alternatively, soil treatment is suggested to increase the strength of the unsuitable material to meet the constructions requirement for foundation and also to achieve the specifications for development work. In this study, a series of laboratory test will be conducted to determine the potential of lime to stabilize marine clay to form the basis of a strong, reliable land for construction of roads and building. Testing programme involves obtaining specimens of marine clays from various locations at Iskandar Malaysia Region, followed by laboratory tests to determine the physical and engineering properties with and without the addition of lime. The proportions of hydrated lime added are 3%, 6% and 9% to the untreated marine clay and tested at 7 and 28 days curing periods. Results show an increase in strength with increasing lime content. In addition, strength also increases significantly as early as 7 curing days and continues for 28 curing days. In agreement with the strength tests, compression characteristics improved with increasing lime content and as time prolonged. Hence, lime is successful and considered effective to improve the strength and compressibility behavior of Marine clay.

*Keywords: Marine Clay; hydrated lime, Compressibility*

### **INTRODUCTION**

Marine clay is a type of clay found both in the coastal and in several offshore areas spread over many parts of the world. The properties of saturated marine clay differ significantly from moist soil and dry soil. Marine clay is microcrystalline in nature and clay minerals like chlorite, kaolinite and illite and non-clay minerals like quartz and feldspar are present in the soil. The soils have higher proportion of organic matters that acts as a cementing agent. Marine clay soils in particular can present great problems in pavement design due to uncertainty associated with their performance [1], [2], [3], [4], [5]. They are often unstable beneath a pavement and they are the most susceptible to problems due to changes in moisture.

Nusajaya (about 4% of the area of Iskandar Malaysia) is one of the main focuses of several recent developments within the Iskandar region. However, the weak behavior of clay deposit in various site of development needs to be replaced or be specifically improved. Various ground

improvement methods have been introduced and tested, both in research and in practice. However their respective suitability are considered to be project-specific; being dependent on the existing soil's characteristics, cost and the stabilizers' potential impact or effectiveness for the proposed application. Chemical stabilization is one of the methods recommended to improve the properties of soil and lime stabilization is proven effective in most cases [6], [7], [8].

In order to develop a fundamental understanding of the engineering behavior of Malaysian marine clays, the influence of lime to improve the strength and compressibility behavior of Marine clay was investigated experimentally. Index testing such as Atterberg limit, specific gravity and compaction test were carried out initially on untreated specimen to determine the suitability of lime for lime-clay reactions. Meanwhile, strength and compressibility behavior were determined by unconfined compressive strength (UCS) test and oedometer test, respectively. In this study, the effectiveness of lime to stabilize Marine clay was

investigated on the basis of lime content and at different curing periods.

### 1.0 MATERIALS & SPECIMEN PREPARATION

In this research, Marine clay was the soil used and it was obtained from Nusajaya, an area in Gelang Patah, Johor. It was dredged from the seabed offshore the southern coast of the Nusajaya where there is an under-construction harbour project. The soil was dumped on the other part of the area. It was dark grey and highly disturbed by dredging. It was then collected in oil tanks and transported to the laboratory. The properties of the collected Marine clays in Nusajaya are shown in Figure 1. The hydrated lime used was supplied by Limetreat (M) Sdn Bhd, a company from Pasir Gudang, Johor. It was used as a chemical additive. The proportion of lime added to the soil was 3%, 6% and 9%. Table 1 summarizes the basic properties of Marine clay obtained in Malaysia, Thailand and India, and this data was compared to the properties of marine clay used in this study. Based on the comparison, Nusajaya marine clay shares the same properties as those from Kor Yo in Thailand, Eastern Cost of India and Kuala Muda Kedah in Malaysia as shown in Table 1.

Table 1 Summary of properties of Marine clays

Location	Kor Yo, thailand	Eastern coast of India	Kuala Muda, Kedah	Nusajaya Malaysia
Author	[3]	[4]	[5]	Mohd Yunus et. al (2014)
Gs	2.69	2.62	2.6	2.62
MDD (kg/m <sup>3</sup> )	1655	1430	1500	1600
OMC (%)	21	32	22	21

Results obtained from the compaction tests played an important role in the preparation of treated specimen. All the treated specimens were prepared referring to the respective maximum dry densities (MDD) and optimum moisture contents (OMC) of untreated soil. The required dry mass of soil samples was calculated with the reference of the mould volume and the MDD. Predetermined quantities of lime were then measured based on the dry mass of soil sample and mixed until homogenous. The soil specimen was then mixed with water content corresponding to the OMC.

Mixing process was carried within a reasonable time (approximately five minutes) to ensure that lime was not exposed to the air for too long. The specimens were mixed thoroughly and compacted in three layers into the 38mm x 76mm cylindrical

mould. The inner surface of the brass mould was layered with a thin, transparent sheet to minimize friction. After that, the specimens were extruded from the mould and wrapped with a cling film to preserve the water content and prevent from the carbon dioxide (CO<sub>2</sub>) exposure. The weight of the specimens was measured and cured in a controlled temperature room at 20°C and humidity greater than 90% for 7 and 28 days. Similarly, specimens of oedometer test were prepared based on OMD and MDD of untreated soil before being placed in the cylindrical metal ring with the dimensions of 75mm diameter and 20mm height.



Fig 1 Marine clay in Nusajaya

The results of index testing carried out on untreated Marine clay are summarized in Table 2. In general, soil is considered as suitable to be stabilized by lime because the plasticity index (PI) is more than 10.

Table 2 Physical properties of Marine clay

Properties	Marine Clay
Liquid limit (%)	58
Plastic limit (%)	36
Plasticity index (%)	22
Specific gravity	2.62
OMC (%)	21
MDD (kg/m <sup>3</sup> )	1600

### 3.0 TESTING PROGRAMME

Laboratory tests such as specific gravity test, Atterberg limit test and standard proctor test were carried out to determine physical properties of marine clay. The strength and compressibility of the lime stabilized soil was determined through UCS and oedometer test at 7 and 28 days of curing. Physical tests were carried out in the early stage as an initial step to indicate the suitability of soil for

lime stabilization. In the second phase of experimental work, hydrated lime was added to stabilize the marine clay. This study was carried out to investigate the effectiveness of lime to stabilize clay with different amounts of lime contents. The effectiveness of lime stabilization process was investigated by monitoring the improvement of strength and compressibility behavior of lime-clay reaction over time.

## 4.0 RESULTS AND DISCUSSION

### 4.1 Shear Strength Behaviour

Unconfined compression test is carried out to determine the maximum compressive strength of marine clay soil when lime is added. The summary of the data from unconfined compressive test (UCT) at different curing periods at different lime content is shown in the Table 2. The detailed calculation of each specimen is tabulated in Appendix. Table 3 shows the summary of the strength result obtained from all of the samples of marine clay at different curing period which is 7 days and 28 days. From table 3, for untreated sample of marine clay the strength of the sample remains the same for both periods which are 21kPa. Besides that, strength at 7 days increasing from 21kPa of untreated marine clay to 138, 294, and 379 for lime treated marine clay 3% 6% and 9% respectively. In addition, it shows that the increase of strength gained from untreated to 3% of lime at 7 days is 85.5%. Increasing of strength gained 3% to 6% of lime and 6% to 9% of lime are 53% and 22%. It shows that by increasing the lime, the strength of marine clay is also increased. Furthermore, by increasing the curing period, the strength of marine clay is also reinforced [9], [10], [11]. This can be shown by comparing 9% of lime at 7 days and 9% of lime used at 28 days, the strength is 379kPa and 517kPa. The difference is 138kPa which is rather high.

The results of the unconfined compressive strength is obtained and plotted at different curing periods as shown in Figure 3, and Figure 4. Figure 3 shows the effect of lime content at 7 curing days, while Figure 4 shows the effect of lime content at 28 curing days. The shear strength of each specimen is determined based on the peak strength of stress versus strain curve. Based on Figure 3 and 4, the result for the untreated is the same and it remains constant after achieving a peak strength which is 21kPa. In Figure 3, it can be seen that the strength slightly increases at 7 days before decreases at 28 days of curing.

The sample also increased gradually during first 7 and 28 days of curing. After 7 days, the increase became more rapid with sample treated 9% of lime showing the most increment. The small increases of strength during early days of curing

between 7 days and 14 days are because of the modification process within mixes. This is because of frictional component of shear strength. For nearly 28 days, there is an increase in strength but at a higher constant rate. This is due to the pozzolanic reactions between lime and soil [12], [13], [14].

Table 3 Summary of UCS data at different curing period

Sample	UCS (Kpa)	UCS (kPa)
	7 days	28 days
Untreated	21	21
Marine clay + 3% of lime	138	144
Marine clay + 6% of lime	294	423
Marine clay + 9% of lime	379	517

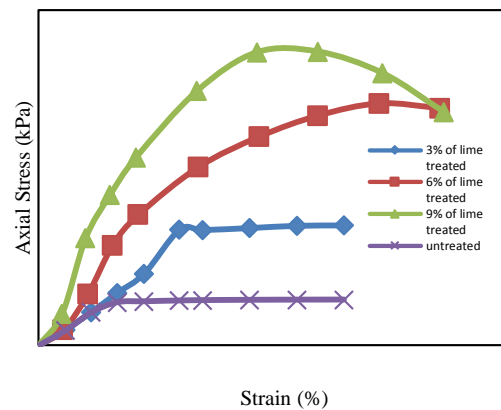


Figure 3 Axial stress versus Strain at 7 days

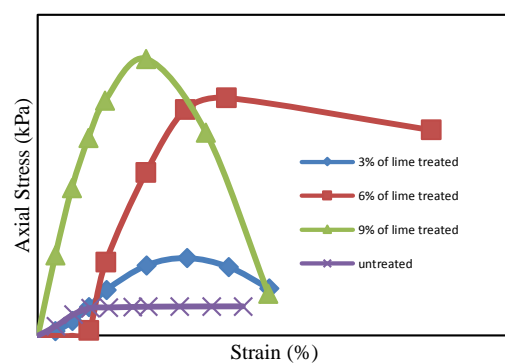


Figure 4 Axial stress versus Strain at 28 days

In general, the strength of marine clay with 9% lime at curing of 28 days is 517kPa which higher than the strength of marine clay with 3% and 6% lime. Comparing two result of 9% lime treated marine clay with different curing day, at 28 days the strength of marine clay is higher than 7 days. So, it is proven that curing process is a factor in

determining the strength of the treated marine clay. The lowest strength is 138kPa when the sample is added only 3% of lime and the curing period is 7 days. However, the strength of the soil slightly increase at 144kPa when the curing period is longer at 28 days and the concentration of lime is the same at 3%. The strength gradually increases by adding more concentration of lime which is 6%. It has been proven that 3% increase in strength is less significant, which shows that addition of 3% lime is not really effective to stabilize marine clay. However with further addition if 6% and 9% of lime content, the strength gains more significantly. The percentage of strength gained recorded for marine clay treated of 6% and 9% of lime content between 7 to 28 days are 30% and 27%. Prior to analysis, the strength of marine clay could be stabilized with high increasing concentration of lime. Therefore, based on the study, it is proven that the strength of lime-treated marine clay will be reinforced if the curing time is longer.

#### 4.2 COMPRESSIBILITY BEHAVIOUR

The odometer test was conducted on both untreated marine and treated marine clay. The untreated marine clay specimen was prepared and tested as a control specimen for comparison purpose with the treated specimens. Meanwhile, each duplicate sample was prepared for lime-treated marine clay at different curing period and lime contents, respectively. The proportions of lime added in this study were 3%, 6% and 9% and tested at curing period of 7 and 28 days. In this experiment, we use 12.5 kPa of sample as an initial load. The vertical compression under each load is observed at suitable intervals normally until up to 24 hours period. The load increment ratio (LIR=2) applied was 12.5kPa, 25.0kPa, 50.0kPa, 100kPa and lastly 200kPa while four decrement ratio were applied during reloading stage which were 50kPa and 12.5kPa. This section assesses the compressibility behaviour of lime-treated marine clay at different curing periods. The effect the lime-clay reactions is analysed in terms of changes in void ratio ( $e$ ), compression index ( $c_c$ ) and coefficient of consolidation ( $c_v$ ) which defines a soil's compressibility.

Table 4 summarises the initial properties of lime-treated marine clay after 7 curing days. In this study, each specimen was prepared to an initial water content equal to their respective compaction test OMC obtained from compaction test. Figure 6 illustrates the range of initial void ratio ( $e_i$ ) of the lime-treated marine clay. The  $e_i$  was calculated prior to applying the necessary loads. The compression index,  $c_c$  for untreated marine was 0.143,  $c_c$  was found to decrease to 0.040 with addition of 9% of lime.

Table 4 Summary of oedometer tests on lime-treated marine clay at 7 curing days.

Specimen	M0% L	M3% L	M6% L	M9% L
Diameter (mm)	50.0	50.0	50.0	50.0
Height (mm)	20.0	20.0	20.0	20.0
Initial void ratio, $e_i$	0.66	0.64	0.72	0.77
Compression index, $C_c$	0.143	0.066	0.050	0.040
Preconsolidation pressure, $P_c$ (kPa)	19.0	21.0	22.0	41.0

Table 5 summarises the initial properties of lime-treated marine clay after 28 curing days. In this study, each specimen was prepared to an initial water content equal to their respective compaction test. Figure 7 shows the range of initial void ratio ( $e_i$ ) of lime-treated marine clay. The  $e_i$  was calculated prior to applying the necessary loads. The effect of lime content on compressibility behaviour of lime-treated marine clay was further analysed at 28 days. Table 5 summarises the initial properties of lime-treated marine clay specimens at 28 curing days. The compression index,  $c_c$  for untreated marine is 0.143 and the value of compression is decrease to 0.028 for marine clay treated with 9% of lime.

Table 5 Summary of oedometer tests on lime-treated marine clay at 28 curing days.

Specimen	M0% L	M3% L	M6% L	M9% L
Diameter (mm)	50.0	50.0	50.0	50.0
Height (mm)	20.0	20.0	20.0	20.0
Initial void ratio, $e_i$	0.64	0.59	0.62	0.73
Compression index, $C_c$	0.143	0.047	0.040	0.028
Preconsolidation pressure, $P_c$ (kPa)	19.0	34.0	37.0	50.0

From figure 5 we can see that about 7 days curing period, the difference of void ratio of untreated marine clay is 0.114 while for marine clay treated with 3% of lime is about 0.03. For marine clay treated with 9% of lime the difference of void ratio is 0.022. It shows that the void ratio of lime-treated marine clay decreases with increasing lime content.



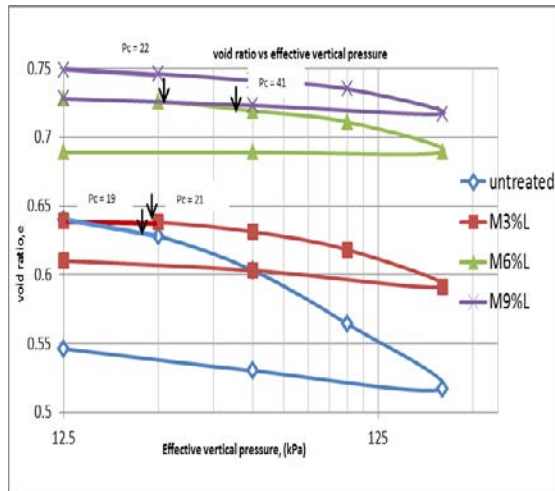


Figure 5 Effect of lime on compression curves of treated marine clay after 7 curing days

From figure 6 we can see that at 28 days curing period, the difference of void ratio of untreated marine clay is 0.114 while for marine clay treated with 6 % of lime is about 0.036. For marine clay treated with 9% of lime the difference of void ratio is 0.014. It shows that the void ratio of lime-treated marine clay decreases with increasing lime content.

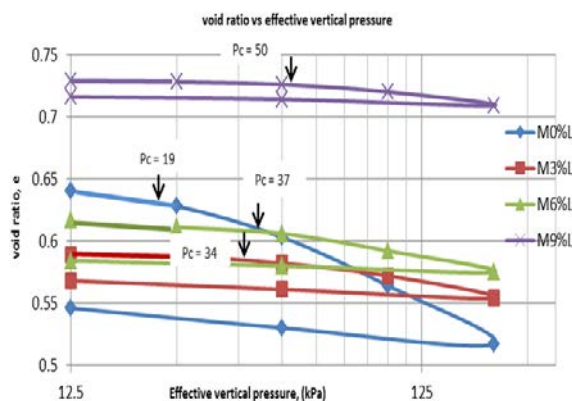


Figure 6 Effect of lime on compression curves of treated marine clay after 28 curing days

Figure 7 and figure 8 show the effect of lime-treated marine clay on coefficient of consolidation ( $c_v$ ) at 7 and 28 days respectively. The rate of consolidation could be determined by measuring the coefficient of consolidation ( $c_v$ ) obtained for each specimen at corresponding applied pressure.  $c_v$  was evaluated based on the Taylor method. Based on that figure, it can be seen  $c_v$  decrease with increasing lime content which indicates that specimens experienced less compressible behaviour. Consequently, a decrease in  $c_v$  values were observed on lime-treated marine clay with higher lime content [15], [16], [17]. From figure 8 we can see that, the coefficient of consolidation ( $c_v$ )

for 7 days curing period for untreated marine clay is  $8.3 \text{ m}^2/\text{years}$  at  $12.5 \text{ kPa}$  than it increases to  $8.61 \text{ m}^2/\text{years}$  at  $25 \text{ kPa}$  and for  $200 \text{ kPa}$  coefficient of consolidation is  $13.31 \text{ m}^2/\text{years}$ . At  $12.5 \text{ kPa}$ , marine clay treated with 9% of lime the coefficient of consolidation is decrease to  $5.6 \text{ m}^2/\text{years}$  compare to untreated marine clay which is  $8.3 \text{ m}^2/\text{years}$ .

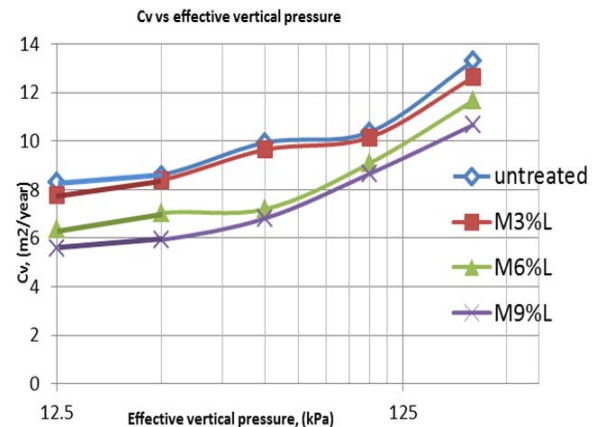


Figure 7 Effect of lime-treated marine clay on coefficient of consolidation ( $c_v$ ) at 7 curing days.

From figure 8 we can see that, the coefficient of consolidation ( $c_v$ ) for 28 days curing period for untreated marine clay is  $8.3 \text{ m}^2/\text{years}$  at  $12.5 \text{ kPa}$  than it increases to  $8.61 \text{ m}^2/\text{years}$  at  $25 \text{ kPa}$  and for  $200 \text{ kPa}$  coefficient of consolidation is  $13.31 \text{ m}^2/\text{years}$ . At  $12.5 \text{ kPa}$ , marine clay treated with 9% of lime the coefficient of consolidation decreases to  $5.5 \text{ m}^2/\text{years}$ , compared to untreated marine clay which is  $8.3 \text{ m}^2/\text{years}$

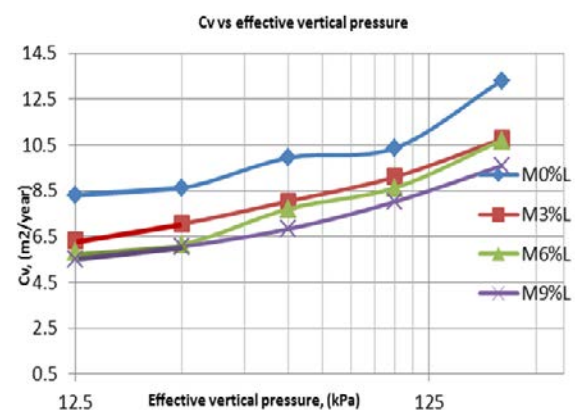


Figure 8 Effect of lime-treated marine clay on coefficient of consolidation ( $c_v$ ) at 28 curing days

## 5.0 CONCLUSIONS

The physical properties of untreated and treated lime stabilized the marine clays were investigated and discussed in this study. Plasticity chart the



marine clay can be classified as MH which is high silt. Since the value of Plastic Index (PI) is more than 10, the marine clay is suitable to be stabilized with lime. From the Standard Proctor Compaction Test, the maximum dry density (MDD) and optimum moisture content (OMC) is 1.55 Mg/m<sup>3</sup> and 21.20 % respectively while the specific gravity is 2.62. From the Unconfined Compression Test (UCT) test, it was illustrated that the strength development after 7 days is less significant. This is due to the process of modification. However, the strength treated soils increases rapidly at 28 days curing period. This phenomenon could be related to the process of stabilisation. Overall, this study proves that when lime is added into soils, the reactions between lime and clay particles change the properties of soils and these would increase the compression strength and shear strength of soil, which makes marine clay more stable. The consolidation test concludes that the void ratio of the sample decreases as the percentage of lime content increases from 3% to 9%. Then, the coefficient of consolidation ( $c_v$ ) of soil specimens with addition of lime decreases as the lime content increases compared to the untreated marine clay where specimen with 3% lime content increased about 18.4% from untreated marine clay at 7 curing period. Compression index ( $c_c$ ) value signifies the compressibility of a soil,  $c_c$  value decreases as lime content increases.

## 6.0 REFERENCES

- [1] S. Horpibulsuk, N. Yangsukkaseam, A. Chinkulkijniwat, and Y. J. Du, "Compressibility and permeability of Bangkok clay compared with kaolinite and bentonite," *Appl. Clay Sci.*, vol. 52, no. 1–2, pp. 150–159, Apr. 2011.
- [2] T. Petry and D. Little, "Review of stabilization of clays and expansive soils in pavements and lightly loaded structures-history, practice, and future," *J. Mater. Civ. Eng.*, no. December, pp. 447–460, 2002.
- [3] T. Chalermyanont, S. Arrykul, and N. Charoenthaisong, "Potential use of lateritic and marine clay soils as landfill liners to retain heavy metals.," *Waste Manag.*, vol. 29, no. 1, pp. 117–27, Jan. 2009.
- [4] S. Basack and R. Purkayastha, "Engineering properties of marine clays from the eastern coast of India," *J. Eng. ...*, vol. 1, no. 6, pp. 109–114, 2009.
- [5] Z. A. Rahman and W. Z. W. Yaacob, "Geotechnical Characterisation of Marine Clay As Potential Liner Material," *Sains*, vol. 42, no. 8, pp. 1081–1089, 2013.
- [6] N. L. Association, "Lime Treated Soils Save Time & Money," *Tech. Dig.*, 2005.
- [7] Sakr MA and Shahin MA, "Utilization of Lime for Stabilizing Soft Clay Soil of High Organic Content." *Geotechnical and Geological Engineering*, 2009, vol. 27, pp. 105-113.
- [8] Koslanant S, Onitsuka K and Negami T, "Influence of salt additive in lime stabilization on organic clay." *Geotechnical Engineering*, 2006, vol. 39, pp. 95-101.
- [9] Consoli, N.C., da Silva Lopes, Jr. L. and Heineck, K.S. (2009). "Key parameters for the strength control of lime stabilized soils." *Journal of Materials in Civil Engineering* 21(5): 210-216.
- [10] Consoli, N.C., da Silva Lopes, Jr.L., Prietto, P.D.M., Festugato, L. and Cruz, R.C. (2011). "Variables Controlling Stiffness and Strength of Lime Stabilized Soils." *Journal of Geotechnical and Geoenvironmental Engineering* 137(6): 628-632.
- [11] Davidson, L.K., Demeril, T. and Handy, R.L. (1965). "Soil pulverization and lime migration in soil lime stabilization." *HRB Record* 92, Highway Research Board, National Research Council, Washington, D.C., pp: 103-126.
- [12] Choquette, M., Andre Bérubé, M. and Locat, J. (1987). "Mineralogical and microtextural changes associated with lime stabilization of marine clays from Eastern Canada." *Applied Clay Science* 2(3): 215-232.
- [13] Rajasekaran, G. and Rao, N. (1997). "The microstructure of lime-stabilized marine clay." *Ocean Engineering* 24(9): 867-875.
- [14] Mohd Yunus, N.Z., Wanatowski, D. and Stace, L.R. (2012). "Effect of humic acid and chloride salts on the behaviour of lime-treated organic clay." PhD thesis, University of Nottingham, United Kingdom.
- [15] Burland JB, "On the compressibility and shear strength of natural clays." *Geotechnique*, 1990, vol. 40, no. 3, pp. 329-378.
- [16] Kassim KA and Huey CS, "Consolidation characteristics of lime stabilised soil." *Journal of Civil Engineering*, 2000, vol. 12, no. 1, pp. 31-42.
- [17] Tremblay H, Locat L, and Leroueil S, "Effect of organic matter on the compressibility of a soil treated with cement." *International symposium on coastal geotechnical engineering in Practice*, Sep 20-22, Yokohama, 2000, pp. 733-738.

## **SEISMIC BEHAVIOR OF SHORT GROUPED-PILES IN LIQUEFIABLE SANDY SOILS**

Chung-Jung Lee<sup>1</sup>, Wen-Yi Hung<sup>1</sup>, Chen-Hui Tsai<sup>1</sup>, Yi-Chun Tu<sup>1</sup>,  
Chin-Chen Huang<sup>2</sup>, Yuan-Chieh Wu<sup>2</sup>, Meng-Hsiu Hsieh<sup>2</sup>

<sup>1</sup> Department of Civil Engineering, National Central University, Taiwan.

<sup>2</sup> Institute of Nuclear Energy Research, Atomic Energy Council, Taiwan.

### **ABSTRACT**

A series of centrifuge shaking table tests was conducted to simulate the seismic responses of grouped-piles that was embedded in liquefiable sandy soils and subjected to earthquake loading. The grouped-piles connected with a pile cap were used to support 4 sets of model dry storage spent fuel casks. Different test conditions including the elevations of pile cap, and the grouped-piles embedded in the dry and saturated sand beds with the different levels of groundwater table are reported. Using pre-shaking the profile of shear wave velocity in the tested sand bed and the natural frequencies of both the sand bed and the grouped-piles were determined. The lower shear wave velocities and the lower natural frequencies were measured for the saturated sand bed, but no obvious difference in the natural frequency of the grouped-piles system with the pile cap embedded in the sand deposit were observed. The grouped-piles with the pile cap exposed to the ground surface and embedded in the saturated sand bed have the lowest natural frequency. The magnitudes of bending moment along pile depths would increase with the increases of base shaking. The lowest bending moment were measured for the grouped-piles with the pile cap embedded in the dry sand bed while the largest bending moments were observed for the grouped-piles with the pile cap embedded in the saturated sand bed and the groundwater table at the surface.

*Keywords: Seismic Response, Grouped-Piles, Liquefaction, Shaking Table Test, Centrifuge Modeling*

### **INTRODUCTION**

Dramatic failure of structures founded on pile foundations after a strong earthquake has led many researchers to investigating the behavior of grouped-piles supported foundations in liquefiable deposits [1; 2]. The liquefaction-induced pile foundation failures not only occurred in sloped grounds (lateral spreading) but were also observed in level grounds. The failure of pile foundation, resulting from that the bending moments or shear forces that are experienced by the piles exceed the bending or shear carrying capacity of the pile section, were often accompanied by settlements and tilting of superstructures. The damages rendered the supported-structures becoming useless or costing expensive to rehabilitate after big earthquakes. Therefore soil-structure interaction effects must be properly considered in the grouped-piles design especially embedded in the liquefiable sandy soils. Currently, piles in liquefiable soils are designed as beams to resist bending failure from lateral loads due to the inertia of the structure and/or slope movement (lateral spreading)[3].

Dry cask storage is an alternative method of temporary storing spent fuels that have already been cooled in a spent fuel pool. There are various designs of spent fuel dry storage cask system. With some designs, the casks are placed vertically on a concrete

slab that is founded with a grouped-piles foundation. The seismic responses of the grouped-piles system located at the liquefiable sites are critically concerned. In the study a series of model grouped-piles (2×2) centrifuge shaking table tests at an acceleration of 80 g was conducted to simulate seismic responses of a grouped-piles embedded in liquefiable sandy soil subjected to different magnitudes of earthquake loading.

### **GEOTECHNICAL CENTRIFUGE MODELING AND TESTING SETUP AND PROCEDURES**

#### **Testing Equipment**

The experimental work presented here was undertaken in the Centrifuge at the National Central University (NCU), Taiwan. The NCU Centrifuge has a nominal radius of 3 m and is equipped with a 1-D servo-hydraulically controlled shaker integrated into a swing basket. The shaker has a maximum nominal shaking force of 53.4 kN, a maximum table displacement of ±6.4 mm, and is operated at an centrifugal acceleration of up to 80 g. The nominal operating frequency range was 0–250 Hz. A laminar container with inside dimensions of 711 mm x 356 mm x 353 mm was constructed from 38 light-weight aluminum alloy rings arranged in a stack. Each ring

was 8.9 mm in height and was separated from the adjacent rings by roller bearings that were specially designed to permit translation in the longitudinal direction with minimal frictional resistance. The laminar container was designed for dry or saturated soil models and permits the development of stresses and strains associated with 1-D wave propagation [4]. A flexible 0.3 mm thick latex membrane bag was used to retain the soil and the pore fluid within the laminar container.

### Design and Fabrication of Grouped-Piles Model

Figure 1 is a typical layout of spent fuel dry storage system. The dry storage casks are placed on a concrete slab founded with a row of grouped-piles which are embedded in a medium dense to dense sand deposit and penetrated into the bed rock. Each concrete pile having a diameter of 1.8 m and  $EI=12772754 \text{ kN/m}^2$  are used to support a dry storage cask by means of the concrete slab. In the study 4 sets of spent fuel cask rest on a simplified 4 grouped-piles model ( $2 \times 2$ ) is used in the centrifuge modeling.

The grouped-piles model ( $2 \times 2$ ) as shown in Figure 2 was fabricated using 4 copper tubes with a 19 mm outer diameter and a 17 mm internal diameter. The length of pile was 160 mm and the embedment depth of the model pile in the sand bed was 125 mm both in model scale. Strain gauges were attached externally at nine positions on the pile shaft surface for two of four piles to measure the bending moment distributions along both the front pile and the back pile (MA and MB). These two model piles are named as the bending piles. The surface of model pile shaft was then resin coated for waterproofing. The coated model piles (22.5 mm in diameter) are designed to replicate a circular pile with a diameter of 1.8 m and having an embedment depth of 10 m when it was tested at an acceleration of 80 g. The ratio of pile length and diameter ( $L/D$ ) is around 5.5. The model pile exhibited flexural rigidity ( $EI$ ) of  $10350668 \text{ kN-m}^2$  in prototype scale. Here  $E$  and  $I$  are the Young's modulus and the inertia moment of the model instrumented pile, respectively. In addition the strain gauges are also attached on the pile shafts of the other two piles to measure the axial forces along the pile depths. These two piles are named as the axial piles. All the instrumented piles (two bending pile and two axial piles) were calibrated for establishing the relationships between the output voltages and bending moments (or axial forces) prior to the model tests. Therefore, the bending moment (or axial force) profiles on the front and back piles can be measured during the tests. The total weight of four model dry storage casks and the pile cap as shown in Figure 2 are 24.2 N in model scale. The height of gravity center of dry storage casks and the pile cap is scaled from the prototype.

### Sand Bed preparation and Testing Layout

A fine quartz sand (No. 306) was used to prepare the uniform dense sand deposit. The characteristics of the quartz sand are summarized in Table 1. The four grouped-piles were first screwed at the bottom of laminar container and then the quartz sand was pluviated with a regular path into the container from a hopper at a constant falling height and at a constant flow rate for preparing fairly uniform sand deposits having relative density of about 85%. Finally the saturation process was conducted for the saturated sand bed. In the case of saturation an acrylic plate was used to tightly cover the container for the saturation process of sand bed. Air was then simultaneously and continuously vacuumed out from both the inside and the outside of container. At the same time a de-ionized, de-air water-metulos solution having a viscosity of 80 times the viscosity of water was carefully dripped into the container to saturate the sand bed until the fluid level rose to the predetermined elevations. One day was required to saturate a sand bed.

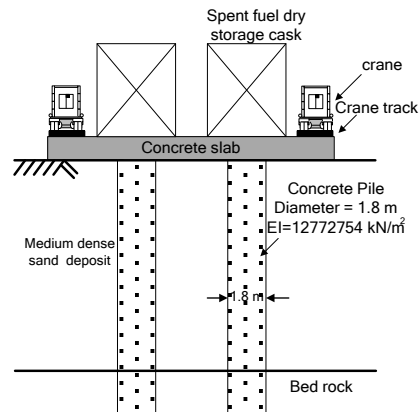


Fig. 1 Layout of spent fuel dry storage system.

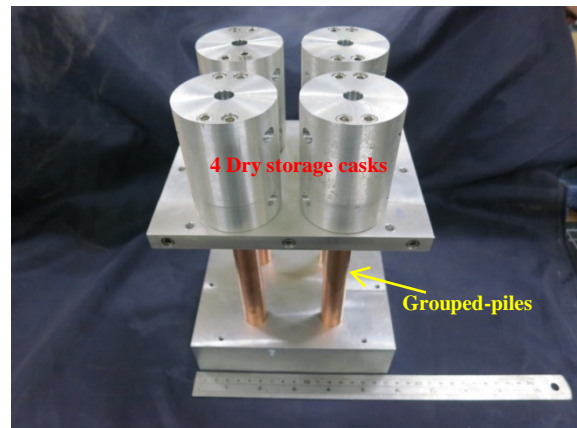


Fig. 2 Four model spent fuel storage casks rested on the concrete founded with grouped piles

Table 1 Characteristics of fine quartz sand.

$G_s$	$D_{50}$ (mm)	$D_{10}$ (mm)	$\rho_{\max}$ (g/cm <sup>3</sup> )	$\rho_{\min}$ (g/cm <sup>3</sup> )
-------	------------------	------------------	---------------------------------------	---------------------------------------

Quartz sand	2.65	0.193	0.147	1.66	1.44
-------------	------	-------	-------	------	------

<sup>1</sup> The maximum and minimum densities of the sand were measured in the dry state, according to the method (JSF T 161-1990) specified by the Japanese Geotechnical Society.

Five grouped-piles centrifuge model tests were conducted. Figures 3(a), 3(b), 3(c), 3(d) and 3(e) show the soil profiles and the instrumentation layouts used in the centrifuge modeling. Table 2 lists the testing conditions. The total depth of the sand bed for both the grouped-piles and the pile cap embedded in the sand bed is 14.6 m and that for the pile cap outcropping on the ground surface is 13.6 m both in prototypes. Two accelerometers were attached at two elevations on the spent fuel cask to measure the seismic responses. Each sand bed was equipped with 3 rows of vertically spaced accelerometers (A#) to record the propagation of shear waves from the base to the ground surface, as shown in Figure 3. At the elevations near those of the accelerometers, eight pore-water pressure transducers (P#) were installed for the saturated sand beds. A linear variable differential transformers (LVDTs) were installed on the ground surface to measure the time histories of surface settlement. The transducers were installed at similar locations in each test. Two laser displacement transducers (LDTs) were used to measure the horizontal displacements on the spent fuel casks. Three LVDTs were attached on the side wall of laminar container to measure the lateral wall displacements. All measurement points were located away from the boundaries of the laminar container to minimize boundary effects [4].

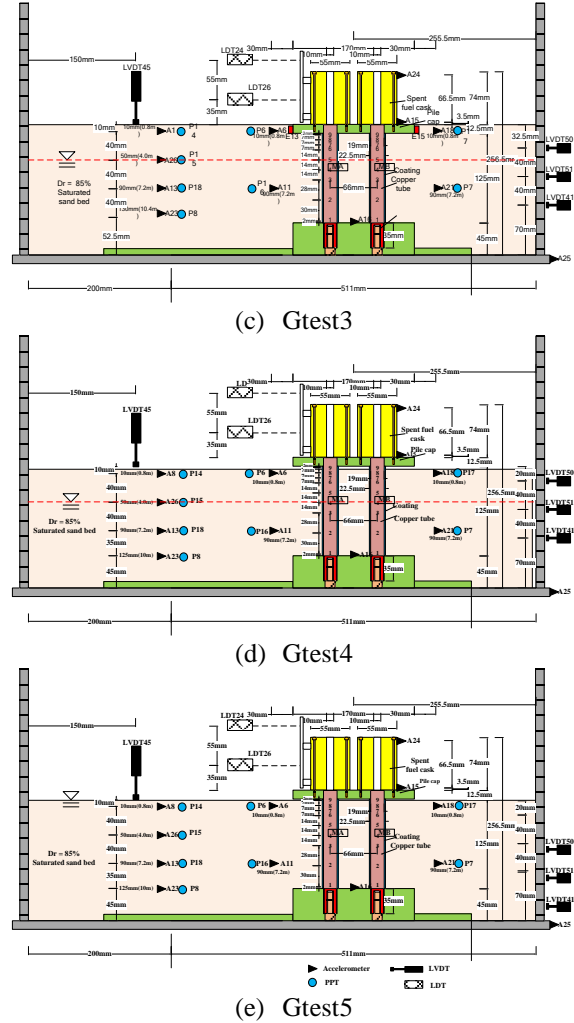
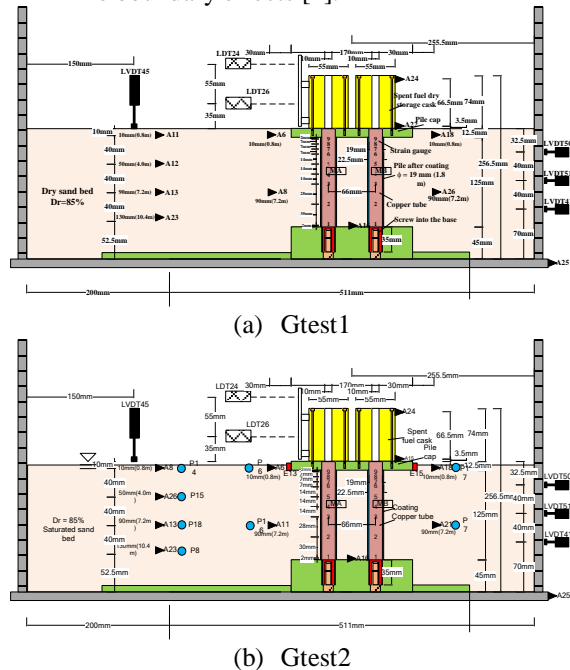


Fig. 3 Test setup and instrumentations: (a) Gtest1; (b) Gtest2; (c) Gtest3; (d) Gtest4; (e) Gtest5; the model dimensions are in centimeter and prototype dimensions (in parentheses) are in meters.

Table 2 Testing condition of grouped-piles

Test No.	Test conditions
Gtest1	Both the grouped-piles and the pile cap embedded in the dry sand bed
Gtest2	Both the grouped-piles and the pile cap embedded in the saturated sand bed having groundwater table on the ground surface
Gtest3	Both the grouped-piles and the pile cap embedded in the sand bed having the groundwater table 4 m below the ground surface
Gtest4	The grouped-piles embedded in the sand bed having the groundwater table 4 m below the ground surface but the pile cap outcropping on the top of ground surface
Gtest5	The grouped-piles embedded in the sand bed having the groundwater table on the ground surface but the pile cap outcropping on the top of ground surface

Figure 4 shows a test package resting on the NCU shaker is ready for testing. Comprehensive instrumentation and detailed measurements at various elevations and different positions are necessary to determine the seismic responses of the grouped-piles and the associated excess pore-water pressure generation and dissipation in the sand deposits during shaking. After completing the centrifuge flight safety checks, the centrifuge was accelerated at an acceleration of 10 *g* per step until it reached 80 *g*. The model was maintained at each *g*-level for 5 min. to ensure that the sand bed reached full consolidation at each overburden stress. Finally the model was subjected to different base shaking events with various amplitudes of base acceleration at an acceleration of 80 *g*. The time histories of acceleration, the pore-water pressure at various elevations, the bending moments and the axial forces on the piles, and surface settlement were recorded simultaneously. The measurements in the following sections are presented in prototype units unless specifically noted otherwise.

Table 3 lists the typical shaking events for the five tests (Gtest1 – Gtest5) in the study. The S1 event is a pre-shaking technique for measuring the  $V_s$  profile of sand deposits and identifying the natural frequencies of sand bed and soil structure system at the acceleration of 80 *g*. The pre-shaking technique is a non-destructive test. It uses a shaker as a wave generation source and a vertical array of accelerometers embedded in the sand bed and the accelerometers attached to the pile head as receivers [5]. After the pre-shaking events each model was subjected to multiple shaking events with amplitudes of base acceleration from small to large.

## TEST RESULTS AND INTERPRETATIONS

### Fundamental Frequencies of Sand Deposit and Grouped -Piles

The pre-shaking method (S1 Event as listed in Table 3) was conducted to measure the profile of shear wave velocity along the depths in terms of the vertical accelerometer array as shown in Figure 3. The shaker fired one cycle of a low, controlled amplitude sinusoidal wave (approximately 0.01 *g* in amplitude and 1 Hz, 2 Hz, and 3 Hz in frequency, both on the prototype scale) to provide a vibration source. A higher sampling rate of 30 000 samples/s was used to collect the acceleration time histories from the accelerometers those which were embedded in the sand bed and were attached on the spent fuel cask. Therefore the average shear wave velocity,  $V_s$ , of the sand deposit between the accelerometer pairs could be calculated using the following equation:

$$V_s = \Delta S / \Delta t \quad (1)$$

where  $\Delta S$  and  $\Delta t$  are the distance between adjacent accelerometers and the registered time difference between the first peaks of the accelerometer pairs, respectively. Figure 5 displays the typical test result of shear wave velocity profile for Gtest1. Figure 6 displays the amplification factors of the acceleration measured at various depths and at two different elevations on the spent fuel cask as shown in Figure 3(a). The peaks in the curves represent the nature frequencies of the sand bed and the entire soil-pile-casks system. Table 4 lists the measured average shear wave velocities and the measured nature frequencies of sand deposit and grouped-piles system. The dry sand bed has the highest nature frequency (Gtest1), the saturated sand bed has the lowest nature frequency. There are two nature frequencies measured from the grouped-piles, as listed in Table 4 and shown in Figure 6(b). The first one is the nature frequency of sand bed in which the grouped-piles are embedded and the second one is the nature frequency of grouped-piles system. The grouped-piles with pile cap embedded in the sand deposit have the highest natural frequency (4.1 Hz for Gtest1). By contrast the grouped-piles embedded in the sand bed having the ground water table on the ground surface and the pile cap outcropping on the top of ground surface have the lowest nature frequency (3.1 Hz for Gtest5).



Fig. 4 Test package resting on the NCU shaker

Table 3 Shaking events in the study

Test events	$a_{max(base)}$ /freq./No. of cycle g / Hz / cycles	Dr(%)
S1-1Hz	0.0083g / 1Hz / 1	88.6
S1-2Hz	0.0091g / 2Hz / 1	
S1-3Hz	0.0087g / 3Hz / 1	
S2	0.0118g / 1Hz / 15	86.6
S3	0.0373g / 1Hz / 15	86.7
S4	0.0858g / 1Hz / 15	87.3
S5	0.1491g / 1Hz / 15	87.9
S6	0.2112g / 1Hz / 15	88.0



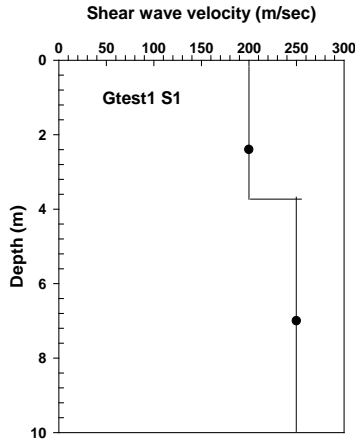


Fig. 5 Measured shear wave velocity profile of sand deposit for Gtest1

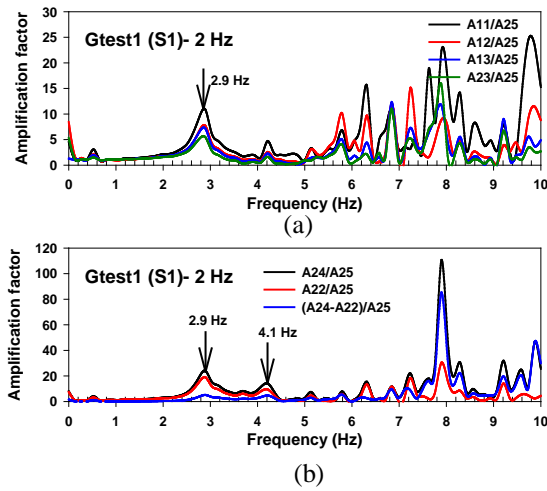


Fig. 6 Amplification factor vs. frequency for Gtest1: (a) measured at the sand bed; (b) measured at grouped-piles system

Table 4 Average shear wave velocities and natural frequencies of sand deposit and grouped-piles system

Test No.	$V_s^1$ (m/sec)	$f_n^2$ (Hz)	$1^{st} f_n^3$ (Hz)	$2^{nd} f_n^4$ (Hz)
Gtest1	225	2.9	2.9	4.1
Gtest2	170	2.4	2.4	4.1
Gtest3	170	2.9	2.9	3.97
Gtest4	170	2.4	2.4	3.6
Gtest5	160	2.1	2.1	3.1

<sup>1</sup>Measured average shear wave velocity of sand deposit;

<sup>2</sup>Measured natural frequency of sand deposit;

<sup>3</sup>Measured first natural frequency of grouped-piles system;

<sup>4</sup>Measured 2<sup>nd</sup> natural frequency of grouped-pile system

### Comparison of Time Histories of Acceleration and of Excess Pore Water Pressure at Different Depths

Figure 7(a), 7(b) and Figure 8(a), 8(b) show the time histories of acceleration of Gtest1 (S5) and Gtest5 (S5), those which were measured at the corresponding depths in the sand bed and at the spent fuel cask, respectively. The high frequency and high amplitude spikes in the histories of acceleration as shown in Figure 8(a) are observed. Figure 9 shows the measured time histories of excess pore water ratio of Gtest5 (S5) measured at different depths. Both the observed results show the top 7 m depth of the sand deposit becoming liquefying during big base shaking (the base acceleration  $\cong 0.3$  g).

After comparing the acceleration time histories the soil responses of these two models are quite different although nearly the same amplitude of input base acceleration. A single parameter that includes the effects of the amplitude and frequency content of the acceleration time history is the root mean square acceleration (RMS acceleration), defined as:

$$a_{rms} = \sqrt{\frac{1}{T_d} \int_0^{T_d} [a(t)]^2 dt} \quad (2)$$

where  $T_d$  is the duration of the acceleration and  $dt$  is the time interval of the acceleration time history. The larger the RMS acceleration value the higher the energy input to the sand deposit. An acceleration amplification ratio is defined as the ratio of the RMS acceleration value measured at different depths to the base input RMS acceleration value.

Figure 10 presents the RMS acceleration amplification ratios, those which were calculated from the accelerometer array embedded in the sand deposit and on the fuel spent cask; provide a comparison of amplification ratio profiles along the depths and on the spent fuel cask for Gtest1 to Gtest5 those which were subjected to different levels of base shaking. There was considerable amplifying effect on the acceleration measured on the top soil following shear waves propagating from the base to the surface on Gtest1 - Gtest4, but no amplification of ground response on the top 7 m of the sand deposit (Gtest5) were observed because occurrence of soil liquefying blocked the shear waves upward propagating. However the calculated amplification ratios on the spent fuel cask of Gtest5 had the largest magnitude. The spent fuel cask rested on the grouped-piles with a pile cap outcropping on the ground surface and that was embedded in the liquefied sand would experience the highest acceleration. The pile cap outcropping on the ground surface would greatly reduce the soil confinement; as a result, the spent fuel cask experienced the largest vibrations as shown in Figure 10(e).

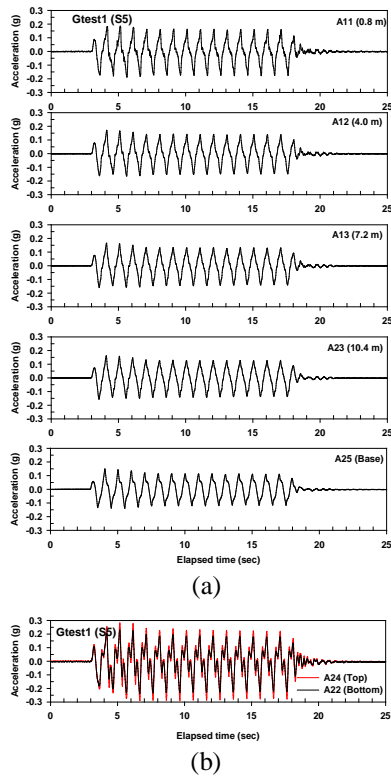


Fig. 7 Time histories of acceleration for Gtest1: (a) measured at different depths in the sand deposit; (b) measured at two elevations on the spent fuel cask

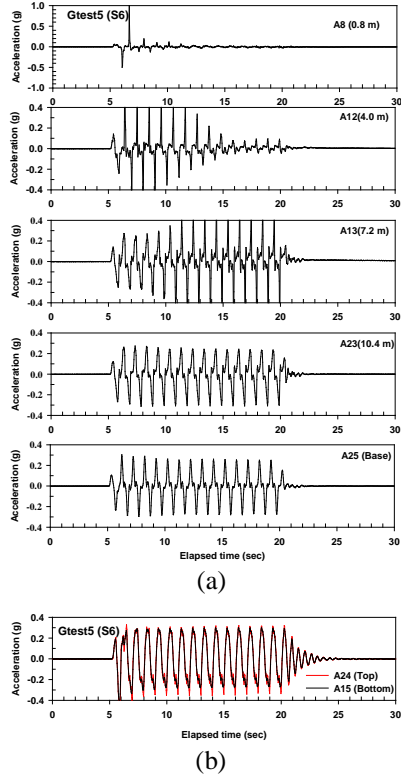


Fig. 8 Time histories of acceleration for Gtest5: (a) measured at different depths in the sand deposit; (b) measured at two elevations on the spent fuel cask

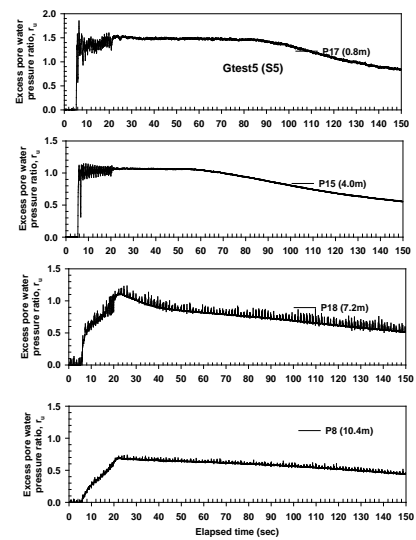


Fig. 9 Time histories of ratio of excess pore water pressure for Gtest5 (S5)

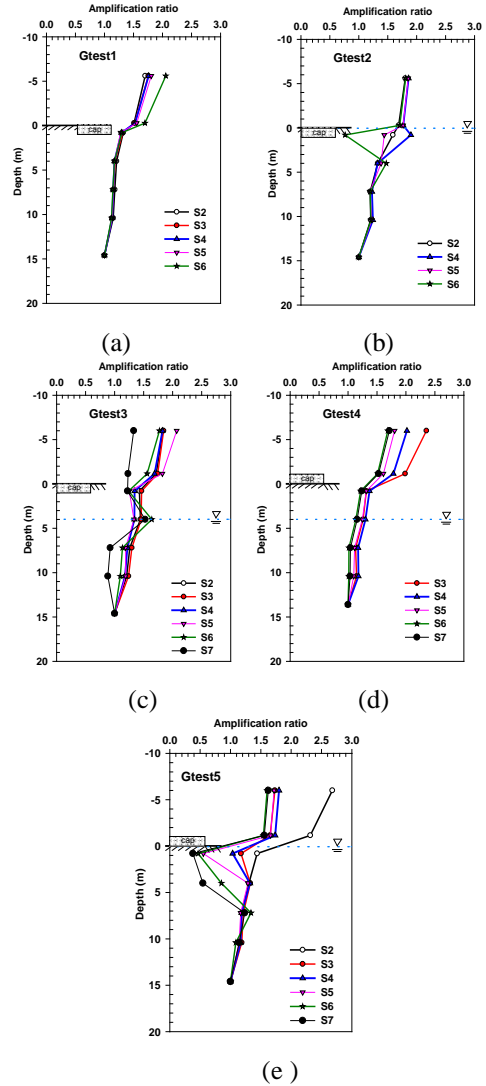


Fig. 10 Profiles of RMS acceleration amplification ratios along depths and on the spent fuel cask: (a) Gtest1; (b) Gtest2; (c) Gtest3; (d) Gtest4; (e) Gtest5



## Time Histories of Bending Moment along Depths on the Grouped-Piles

Figures 11(a) and (b) and Figures 12(a) and 12(b) show the time histories of bending moment measured from the pile head to the pile tip for Gtest1 (S5) and Gtest5 (S5), respectively. The grouped-piles and the pile cap both which were embedded in dry sand deposit (Gtest1) experienced the less magnitude of bending moments. Furthermore only top parts of piles (around 3.12 m in depth) experienced the bending moments. By contrast the grouped-piles embedded in the saturated sand bed and the pile cap outcropped to the ground surface experienced the largest bending moments. Nearly all the depths of pile shaft experienced the larger bending moment (Gtest5) compared to Figure 11. In addition the lower parts of pile also experienced the bending moments that different from the measured results of Gtest1. These resulted from the facts that the saturated sand became liquefying in the top of sand deposit and greatly losing the surrounding confinements to the piles if the cap of the grouped-piles exposed on the ground surface. Figures 13(a) – 13(d) display the relations of the measured maximum bending moment on the pile at MA9 (measured point is just below the pile cap) and the base acceleration or the acceleration measured on spent fuel cask for Gtest1 – Gtest5. The grouped-piles would experience the larger maximum bending moments on the pile in the case of exposing the pile cap on the ground surface than the case of the pile cap embedded in the sand deposit.

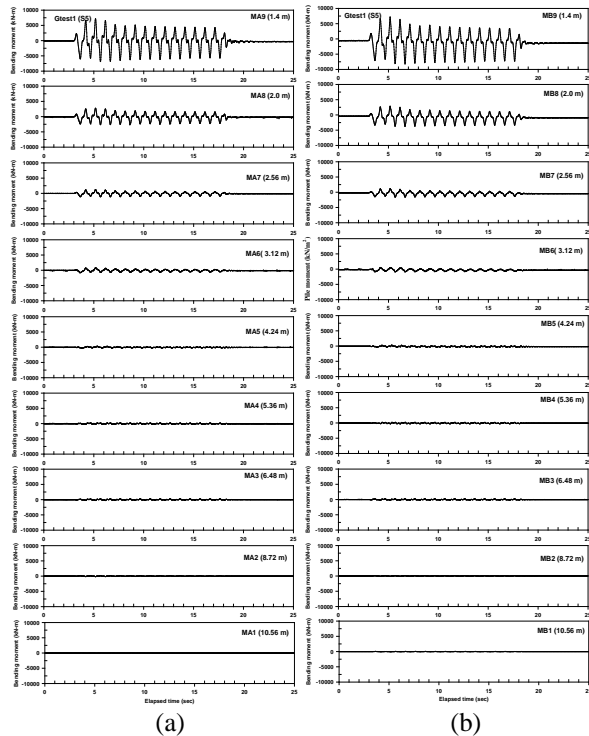


Fig. 11 Time histories of bending moment along the depths for Gtest1 (S5): (a) A pile; (b) B pile.

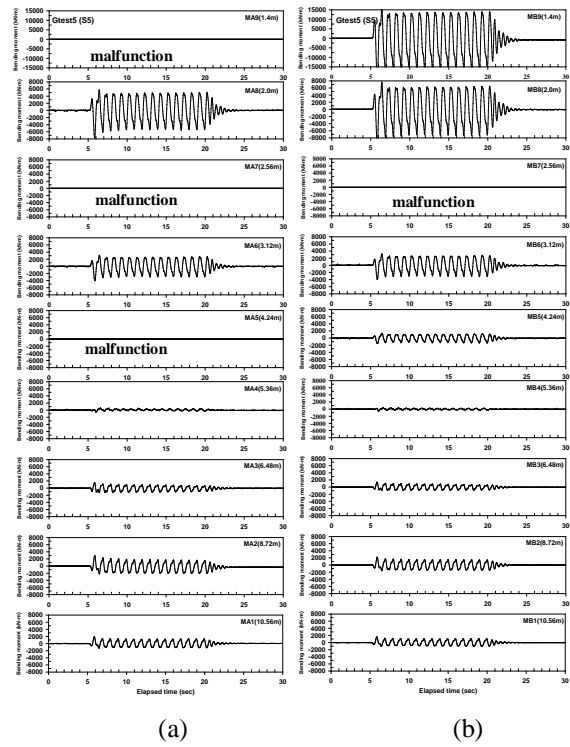
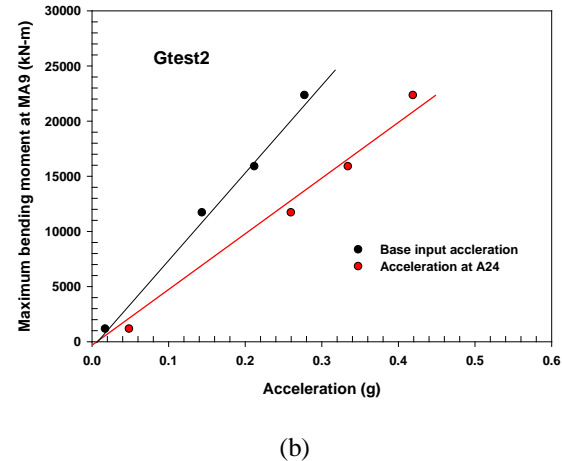
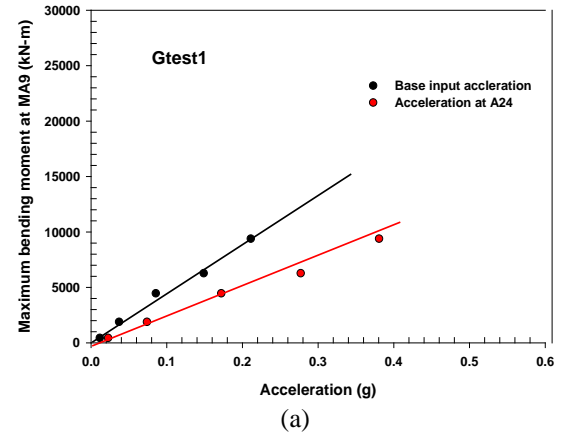


Fig. 12 Time histories of bending moment along the depths for Gtest5 (S5): (a) A pile; (b) B-pile



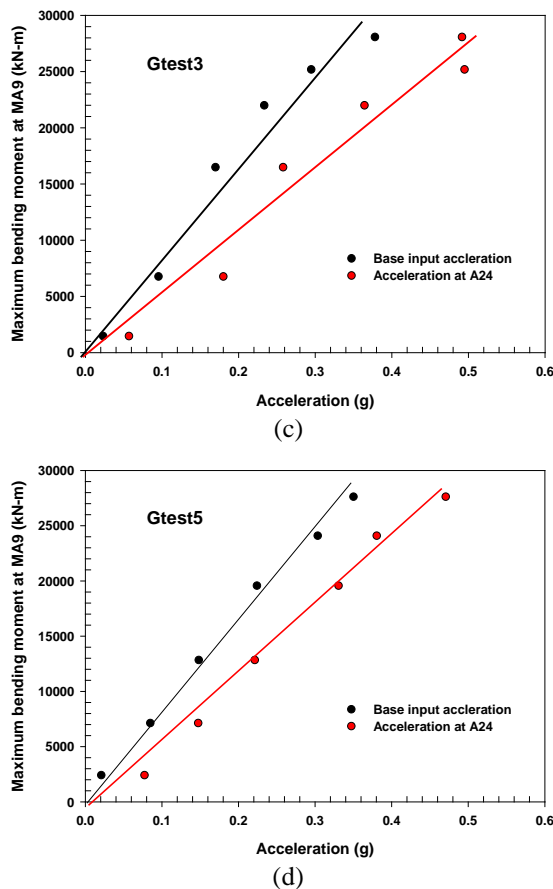


Fig. 13 Maximum bending moment measured at MA9 vs. base input acceleration and acceleration at spent fuel cask (A24): (a) Gtest1; (b) Gtest2; (c) Gtest3; (d) Gtest5

## CONCLUSION

A series of centrifuge shaking table tests was conducted to simulate the seismic responses of short grouped-piles that was embedded in liquefiable sandy soils and subjected to earthquake loading at an acceleration of 80 g. The grouped-piles connected with a pile cap were used to support 4 sets of model dry storage spent fuel casks. Different test conditions including the elevations of pile cap, and the grouped piles embedded in the dry and saturated sand beds with the different levels of groundwater table are reported in the study. Using pre-shaking technique the profile of shear wave velocity in the tested sand bed and the natural frequencies of both the sand bed and the grouped-piles were determined simultaneously. The lower shear wave velocities and the lower natural frequencies were measured for the saturated sand bed, but no obvious difference in the natural frequency of the grouped-piles system with the pile cap embedded in the sand deposit were observed. The grouped-piles with the pile cap those which were exposed to the ground surface and embedded in the saturated sand bed have the lowest natural frequency. The spent fuel cask rested on the

grouped-piles with a pile cap outcropping on the ground surface and that was embedded in the liquefied sand would experience the highest acceleration.

The pile cap outcropping on the ground surface would greatly reduce the soil confinement; as a result, the spent fuel cask experienced the largest vibrations. The magnitudes of bending moment along the pile depths would increase with the increases of the base shaking. The lowest bending moments were measured for the grouped-piles with the pile cap embedded in the dry sand bed while the largest bending moments were evidenced for the grouped-piles with the pile cap embedded in the saturated sand bed and the groundwater table located at the surface.

## ACKNOWLEDGEMENTS

The authors would like to express their gratitude for the financial supports (NL1020467) from the Institute of Nuclear Energy Research (INER), Atomic Energy Council, Taiwan, ROC and the National Science Council (NSC 100-2221-E-008-099-MY3), Taiwan, ROC. Without their financial supports, the study would not become possible.

## REFERENCES

- [1] Tokimatsu, K., Oh-oka, H., Satake, K., Shamoto, Y., and Asaka, Y. "Effects of lateral ground movements on failure patterns of piles in the 1995 Hyogoken-Nambu earthquake," *Geotechnical earthquake engineering and soil dynamics III*, Vol. 2, 1998, 1175-1186.
- [2] Rollins, K.M., Gerber, T.M., Dusty, L.J., & Ashford, S.A. "Lateral resistance of a full-scale pile group in liquefiable soils", *Journal of Geotechnical and Geoenvironmental Engineering*, ASCE, Vol.131, No.1, 2005, pp.404-414.
- [3] Yao, S., Kobayashi, K., Yoshida, N., and Matsuo, H., "Interactive Behavior of Soil-Pile-Superstructure System in Transient State to Liquefaction by means of Large Shake Table Tests," *Soil Dynamics and Earthquake Engineering*, 24,2004, pp.397-409.
- [4] Lee CJ, Wei YC, and Kou YC. "Boundary Effects of a Laminar Container in Centrifuge Shaking Table Tests", *Soil Dynamics and Earthquake Engineering*, Vol. 34, No.1, 2012, pp. 37-51.
- [5] Lee CJ, Hung WY, Tsai CH, Chen T, Tu YC, and Huang CH. "Shear Wave Velocity Measurements and soil-pile System Identifications in Dynamic centrifuge tests," *Bulletin of Earthquake Engineering*, Vol. 12, No.2, 2014, pp.717-734.

## CHALLENGES IN ASSESSING THE INSTALLATION EFFECTS OF CONTROLLED MODULUS COLUMNS ON BEHAVIOR OF SURROUNDING SOILS

Huu Hung Nguyen<sup>1</sup>, Behzad Fatahi<sup>2</sup> and Hadi Khabbaz<sup>3</sup>

<sup>1,2,3</sup> Centre for Built Infrastructure Research, University of Technology Sydney (UTS), NSW, Australia

### ABSTRACT

Ground improvement technique using controlled modulus columns (CMC) has become increasingly popular in recent years. A rotary displacement auger is screwed and pushed into the ground during installation, to create a vertical cylindrical cavity before concrete is injected to form a CMC. This process causes disturbance of the surrounding soils and results in lateral displacement. In certain circumstances, such displacement may cause damage to freshly grouted neighbouring columns or nearby structures.

This paper integrates the existing methods in assessing the lateral displacement of the surrounding soils due to CMC installation. Analytical, numerical and physical modelling techniques are discussed. The study aims to provide recommendations on novel techniques as well as important parameters for simulating CMC installation process and assessing the effect of this process on nearby freshly grouted CMCs and bridge piles.

*Keywords: Ground Improvement, Controlled Modulus Column, Horizontal Displacement, Cavity Expansion*

### INTRODUCTION

The use of controlled modulus columns (CMC) ground improvement technique has become a method of choice for projects with tight construction schedule or concerns related to contaminated ground. The technique uses a rotary displacement auger with a diameter of up to 500mm to create a hole, followed by concrete injection through the hollow stem while the auger is withdrawn (Fig. 1).

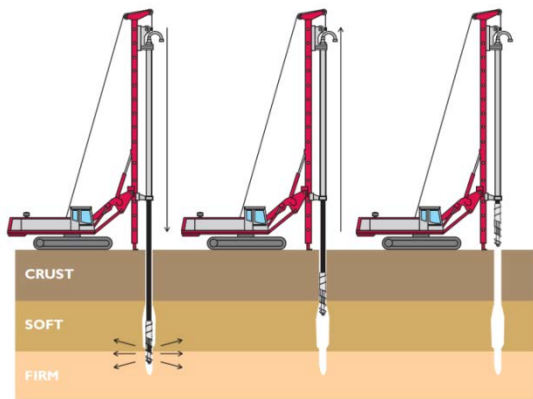


Fig. 1 CMC installation process by Menard [1]

The drill bit comprises the lower partial flight auger segment, the middle auger segment welded with helically wound blades and the upper portion (Fig. 2). The soils carried upward away from the tip by the auger flights are pushed away laterally by the blades. Therefore, the technique has the features of both screwed and jacked-in piling methods.

Based on the size of auger and the methods of piling, CMC can be considered as "large displacement piles", which may "cause a displacement such that significant stresses are induced in the surrounding soils, which may increase the load capacity of the pile and cause displacement of the surrounding soils" (AS2159-2009 – Piling – Design and Installation).

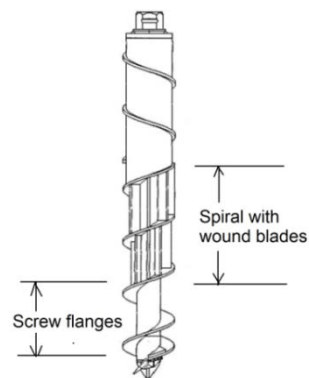


Fig. 2 CMC drill bit (courtesy of Menard-Bachy)

The displacement effects become more apparent in a number of circumstances, e.g. design of closely spaced columns in order to reduce differential settlement at the surface of the embankment. As a result, the installation-induced displacement at a new column could cause damage to freshly grouted surrounding columns. If installation is carried out near a bridge abutment, the displacement may cause lateral movement and impose additional load on the bridge piles. Such effects can be a major concern for

piling contractors and geotechnical engineers [2-4]. Plomteux *et al.* [2] reported a case study where the CMC column spacing of 1m was designed near the bridge abutment piles, which posed a risk that lateral displacement caused by installation could damage the surrounding freshly grouted columns. The construction method was modified with CMCs installed in two different interleave passes, each with 1.4m x 1.4m grids (Fig. 3).

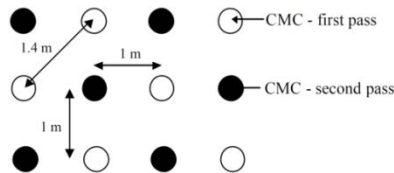


Fig. 3 Modification of CMC installation layout [2]

Similar strategy was adopted as in [3], where installation was commenced at the existing embankment and then working away from the existing embankment and piles. Although reported results from these modified installation patterns were positive, there is no solid justification for those selected patterns and how efficient they were in comparison to other possible installation patterns. To date the magnitude of such installation induced displacement remains unclear and, hence, requires further investigation. It is important to emphasise that properties of the CMC/soil interface play a significant role in performance of infrastructure built above the CMC improved ground [5, 6].

This paper highlights the challenges associated with the existing numerical, analytical and physical modelling methods in assessing the lateral displacement of the surrounding soils due to pile and column installation, and possibility of applying these methods to CMC. Recommendations for the needed improvement in predicting lateral displacement and simulation of the CMC installation are provided.

## INSTALLATION EFFECTS

The first phase of installation process involves formation of a cavity resulting from the auger penetration together with simultaneous rotation in a clockwise direction. Soil cuttings at the auger tip are carried upwards between auger flights, towards the auger segments with helically wounded blades, where the soils undergo further destructure and are displaced laterally. The surrounding soils especially sands are brought into passive state of stress during installation. Once desired depth is reached, concrete is injected through the hollow stem with a moderate pressure, while the auger is withdrawn.

The CMC installation is quasi-static, similar to slowly-jacked piles, but as opposed to “dynamic”

vibratory methods e.g. stone columns or driven piles. In contrast to jacked-in and driven piles, action of CMC auger rotation has large effects on the resulting radial stress changes [7]. Pucker and Grabe [8] found that the higher ratio of the auger rotation speed over the vertical penetration rate, the larger lateral displacement occurs.

In addition, installation induced displacement is quite distinct at different portions of the CMC column. Ground heave normally occurs near the ground surface, to depths ranging from approximately 2.5m to 4.0m [9]-[10]. In the middle region of the column, the installation results in a remarkable increase in soil density and stress level. Near CMC column base, the stress increase is insignificant [10]. In contrast, the base is the most influenced portion for jacked and driven piles [10].

## Installation-induced Changes in Soil State

Most current investigations were carried out for sand [7, 8]. During installation sand behaves under fully drained conditions since the excess pore pressure dissipates quickly. As the auger reaches the elevation of a soil element located in the vicinity of the soil/column interface, the total and effective stresses increases. However, as the auger passes that soil element, the soil within 1 diameter (1D) from the pile centre is loosened up [8] because of the slight change in cross section, from the displacement body towards the drill rod. Outside this thin zone, the soil densified significantly within a distance of 2D. Densified zone ranges from 6D for dense sand to 8D for loose sand. Long term effects in sand are considered as creep-induced ageing phenomenon [11], which has not been thoroughly investigated.

For saturated clayey soils, the behaviour during installation is often assumed to be undrained due to rapid auger penetration. The soils closer to the column fail in shear due to large deformation caused by the installation. Excess pore pressure is generated, which will initially reduce the radial effective stress. This failure zone is often referred as “plastic zone”, extending to a radius  $R = r_0[G/c_u]^{1/2}$ , where  $r_0$  is the pile radius,  $c_u$  is the undrained shear strength and  $G$  is the soil shear modulus [12]. Outside the plastic zone is “elastic zone” where excess pore water pressure is assumed zero. The clay behaviour also relates to over-consolidation ratio. For normally consolidated clay, there is an increase in both total stress and excess pore pressure  $\Delta u$ , but a decrease in effective stress [13]. For over-consolidated clay the total and effective stress increase everywhere but  $\Delta u$ , after increasing within a narrow zone near the pile wall, becomes negative in the next surrounding zone [13]. It should be noted that for a structured clayey soil due to increase in the mean effective stress as well as deviatoric stress, cementation degradation may occur influencing the deformation of the ground

immediately or long time after the installation [14].

Immediately after installation, the peak excess pore pressure falls off rather quickly [12]. Excess pore pressure decays during consolidation inducing elastic visco plastic deformation together with soil strength gain [15, 16]. At the end of consolidation, radial effective stresses around the column is greater than the in-situ horizontal effective stresses in the undisturbed ground with decreasing magnitudes with increasing distance from the pile centre within a zone of 10 times the column radius [17].

## ASSESSMENT OF INSTALLATION EFFECTS

The behaviour of soils affected by installation varies with time. For purposes of assessing installation effects on the surrounding environments, this paper focuses on short term effects. Since very limited assessment of CMC installation effects is reported except in [17], assessment methods will be discussed based on those used for different piling and ground improvement techniques.

### Analytical Methods

The advance of CMC auger to the ground comprises soil loosening by auger flights, followed by lateral compaction by the displacement body. If the loosening stage is ignored, the process can be considered as cylindrical cavity expansion. Unlike jacked and driven piles, CMC installation is not simply a cavity expansion process, but rather affected by the partial flight auger rotation, which reduces significantly normal stress on the pile shaft that would be estimated by cavity expansion theory [7]. The cylindrical cavity expansion is only applicable for the middle section of CMC. Near the column tip the installation resembles spherical cavity expansion while near the surface the confining stress is significantly lower and vertical displacement is normally dominant (i.e. heaving). Furthermore, since the column is drilled incrementally, the cavity expansion theory cannot simulate the installation process precisely. Despite of these limitations, cavity expansion method can be used for preliminary assessment due to its simplicity compared to more complicated methods.

Cavity expansion theory assumes radial displacement under plane strain conditions and no vertical strain, which is well described in Yu [18]. Pestana *et al.* [19] suggested that pile installation can be modeled as the undrained expansion of a cylinder within an infinite, homogeneous soil medium, and soil deformations can be estimated using Eq. (1).

$$\rho_r/r_0 = \sqrt{1 + (r/r_0)^2} - r/r_0 \quad (1)$$

where, a soil element at an initial radius  $r$  from the pile centre displaces towards a radius  $r + \rho_r$

under the expansion of the cylinder with a radius  $r_0$ . The predicted lateral displacement due to a closed-ended driven pile agreed quite well with the deflection measured using inclinometers.

Similarly, Kelly *et al.* [20] predicted stone column installation effects using estimation method for pile driving via Eq. (2) with inclusion of coefficient  $\beta$ , which is used to match predicted displacement with measured value. A  $\beta$  value of 0.6 was found to fit well with the measurement although  $\beta$  does not have any physical meaning, other than that the displacement caused by stone column installation is less than that caused by driving a solid pile with the same column diameter.

$$\rho_r = \sqrt{r^2 + \beta r_0^2} - r \quad (2)$$

where,  $\rho_r$  is the displacement at a distance  $r$  from the centre of column and  $r_0$  is the radius of the column.  $\beta$  value should be calibrated for each depth, which is a difficult task. Displacement can also be estimated using Eq. (3) presented by Yu [18]:

$$\rho_r = s_u/(2G)(1 + \ln(G/s_u))(r_0/r)^2 r \quad (3)$$

where  $s_u$  is the undrained shear strength. This equation allows estimation of soil displacement at various depths with  $G/s_u$  obtained from field tests, e.g. Seismic Dilatometer Marchetti Test (SDMT).

### Numerical Methods

More accurate assessment can be carried out using the finite element method (FEM) or the finite difference method (FDM). Advantages and challenges of various numerical techniques are discussed in this review. Numerical simulation of the penetration of a pile initially positioned above the ground surface is one of the challenges due to heavily distorted mesh and complex soil/auger contact. Instead, many studies omitted the physical shape of the auger, and simulated cavity expansion from a finite cavity with a prescribed horizontal displacement e.g. [17, 21]. More sophisticated analyses involved simplifying auger as a cone-shaped rigid body and often pre-installed into soils before simulation started [9]. Although installation of CMC, jacked-in and driven piles all results in a cavity to be filled with rigid piles or grout, the CMC installation is strongly affected by the auger rotation. Modelling auger effect is not possible in the 2D axisymmetric model but within a 3D system [8].

#### Updated Lagrangian analysis

Updated Lagrangian analysis such as “large strain mode” in the commercial software FLAC and “Update Mesh” feature in PLAXIS allows grid-point coordinates are updated at each step. This feature is

useful in simulation of cavity expansion with prescribed displacement along the boundary [22]. However, when dealing with extreme large deformation such as modelling the penetration of pile into the ground, especially with the use of finer meshes near the soil/pile contact, meshes are heavily distorted. Zones in these models however, have limiting distortions, which often cause “bad geometry” error message. For the program to continue to run, “Automatic Rezoning” feature (FLAC<sub>2D</sub> 6.0 or later) may be used to map existing stress onto a new generated, more regular mesh. So far this automatic rezoning technique has a number of limitations e.g. it does not allow use of interfaces and axisymmetric model and does allow only one soil model in the rezoned region. In addition, the techniques require user intervention, which could be quite computationally expensive.

#### *ALE and Eulerian-based analyses (CEL)*

Pure Lagrangian technique describes the motion of the mesh with each node moving together with materials. In contrast, pure Eulerian analysis describes the material deformation, relative to the spatially fixed mesh. The combined analyses forms the Arbitrary Lagrangian – Eulerian (ALE) adaptive meshing and Coupled Eulerian–Lagrangian (CEL) analysis, both available in commercial FEM software package ABAQUS.

ALE is available for both Abaqus/Standard and Abaqus/Explicit. However, ALE in Abaqus/Explicit is more robust and can handle a large variety of problems including severe distorted mesh, hence will be discussed further. ALE mesh is allowed to move independently of material deformation. In the first step the explicit Lagrangian analysis is performed. The resulted distorted mesh will require a new improved mesh. In the second step, the Eulerian analysis is performed, where variables in the previous analysis is transferred into the new mesh. ALE can deal with large deformation problem; however, since elements and connectivity (i.e. topology) do not change, high quality mesh may not be maintained during extreme deformation.

In contrast, CEL (only in Abaqus/Explicit) has spatially fixed mesh. Eulerian and Lagrangian bodies within the same model can interact via a contact definition e.g. a Lagrangian auger travelling into Eulerian yielding soil. Chosen portions of a CEL model can be modelled as Eulerian or Lagrangian. Since the Eulerian mesh is fixed in CEL, soil displacement has to be calculated by integrating node velocities of the Eulerian mesh recorded along a predefined path over time [8]. The installation of a screw displacement auger into dry sand was numerically simulated using CEL as in [8], however the results were not adequately verified against field measurements.

Overall, although both ALE and CEL seem to be the promising solutions to the very large strain problems, CEL is more computationally friendly since a fixed mesh means no mesh distortion and less solution convergence. These Abaqus/Explicit analyses, however, seem to offer only single-phase possibility with either fully drained or total stress undrained condition analyses [23]. Also, ABAQUS/Explicit currently only allows total stress or frictionless contact between bodies. The challenge would be to create a user’s subroutine into Abaqus to enable undrained effective stress analysis and frictional contact.

#### *Effects of initial radius on predictions*

There are two types of cavity expansion (1) from an existing cavity (2) from a cavity with an initial zero radius. While pile installation resembles cavity creation from an initial zero radius, numerical expansion must necessarily be modelled from a finite radius rather than from zero radius to avoid numerical difficulties (e.g. infinite circumferential strain). For simulation of the installation of a drilled displacement pile as in [7], a “finite initial radius”  $a_0$  of 0.015m was specified compared to a final pile radius  $r_0$  of 0.165m. The authors argued that this initial radius was sufficiently small to obtain limiting cavity pressure at the end of cavity expansion.

In fact, the restriction of numerical expansion from a finite radius in place for a zero initial radius would cause no inconsistency in the final results [24]. Various initial sizes of the existing cavity has been used but it is quite common to double the size of an existing cavity e.g. [10],[17]–[21]. Kosiński [10] simulated screw displacement pile installation using PLAXIS by modelling an initial cavity with a radius equal to half pile radius, and then doubled that cavity to the full size of pile radius in an axisymmetric model. While a smaller initial radius results in better prediction [7], a larger amount of expansion  $\Delta r = r - r_0$  will be required, which may eventually lead to heavily distorted mesh, especially with finer mesh. Again modelling for these cases is an extreme deformation problem.

#### *Constitutive models and parameters*

The choice of soil model is another challenge since soils are subject to complex loadings during installation. Selected models should capture highly non-linear inelastic behavior, decay of excess pore pressure, loading and unloading paths and density changes. Due to the complex shape of auger, cyclic effects in soils may need to be considered [8]. Well-established models such as Mohr Coulomb (MC) and modified Cam Clay (MCC) are incorporated in most of the commercial software packages. The MC failure criteria if used should account for stress-



dependent stiffness. For MCC model, since the soil surrounding the column is likely to be in critical state, this model can be quite representative. It can be noted that above water table, soils may be partially saturated and thus excess pore pressure should be predicted considering coupled flow-deformation behaviour of unsaturated soils [25].

Compared to MC and MCC, hypoplasticity is a relatively new type of soil model and has been increasingly utilized to solve large deformation problems [8, 9]. Various hypoplasticity models exist, noticeably by von Wolffersdorff [26] for sand and modified version by Mašín [27] for clay. Von Wolffersdorff [26] model for granular materials incorporates the intergranular strain and dependency of friction angle and stiffness on density changes and compaction. The model requires 13 parameters including critical state friction angle and void ratio. Despite of advanced features, determination of a large number of model parameters is a challenge.

Meanwhile, clay hypoplasticity model developed by Mašín [27] combines mathematical structure of hypoplasticity models with basic principles of the critical state soil mechanics. This model requires five parameters, similar to those of MCC model; however, it can provide a smooth transition between overconsolidated and normally consolidated states. Unlike MC, this hypoplasticity model correctly predicts the state dependent soil stiffness. Hypoplasticity models are not built-in in most commercial software packages, and implementation of these models is a difficult task.

### Physical Modelling

No laboratory experiment to assess CMC installation has been reported in the literature. Challenges during laboratory experiment would include auger fabrication (Fig. 1), setting up driving tools that can control torque and vertical crowd and complicated on-sample instrumentation. As an alternative approach to on-sample instrumentation, transparent artificial soils contained in a chamber with observable window allows the displacement field to be captured by photographs and analysed using “particle image velocimetry” technique. Such studies by Hird et al. [28] indicated that the displacement depends on rotation speed of the auger. However, rigorous scaling is hard to be achieved to translate the results into behaviour of a prototype CMC and artificial soils like glass offers little practical usefulness. Despite expected shortcomings, small scale models provide roughly similar trends of lateral displacements in full scale field tests.

Field tests are not often readily available for verification of numerical analysis, e.g. Rivera *et al.* [17] examined installation-induced stress around CMC column but has not verified using field results. In a separate case study, but rare, limited field tests

were carried out by Lehigh University [29], comprising installation of a 320mm-diameter CMC with four surrounding CMCs acting as reaction piles, instrumentation and one subsequent load test. The instrumentation included four push-in pressure sensors and four shape acceleration arrays (SAA) to capture stress change and displacement in soft silty soil throughout column installation and testing. At the end of installation, an increase in horizontal stress by 2kPa was recorded within 1D (i.e. one diameter) distance from the CMC, by 8kPa within 2D distance, and then with decreasing trend with increasing distance from the CMC. Some stress relaxation by approximately 2 to 3kPa was recorded at the end of the installation. However, after installation, the stress recorded around the central CMC increased and was greater than stresses recorded at the end of the installation. The recorded soil displacement showed a clear decreasing trend with increasing distance from the CMC. Although useful, this project included only a limited number of CMCs and tests for a particular soil type, without theoretical or numerical prediction.

### CONCLUSION

Concerns over the extent of installation effects on neighbouring structures should be addressed to assist the selection and evaluation of ground improvement techniques. This paper describes a number of challenges in assessment of CMC installation effects on the surrounding ground and structures. While the installation effects may be preliminarily estimated using well established analytical methods such as the cavity expansion theory, numerical methods provide a more comprehensive prediction tool, although there are still great geotechnical challenges remaining. Selection of a modelling technique and soil model that are able to account for very large displacement are of paramount importance. Although simple approaches may still have acceptable values in assessing the installation effects, the advanced methods CEL and ALE are the most promising. The other challenge is associated with the verification methods including small and full scale model testing. It is recommended that future CMC projects allow more field measurements as a basis to improve the assessment methods.

### REFERENCES

- [1] Pearlman, S., *Controlled Modulus Columns: Innovation in Ground Improvement*, in *Deep foundations*. 2012. pp. 73-75.
- [2] Plomteux, C., A. Porbaha, and C. Spaulding, "CMC Foundation System for Embankment Support—A Case History", in *GeoSupport*, 2004.



- [3] Hewitt, P., S.J. Summerell, and Y. Huang, "Bridge Approach Treatment Works On The Coopers Creek To Herons Creek Section Of The Pacific Highway Upgrade", in Sydney Chapter Symposium 2009.
- [4] Brown, D.A., "Practical considerations in the selection and use of continuous flight auger and drilled displacement piles", ASCE-Geotechnical Special Publication, (129), 2005, pp. 251-261.
- [5] Hokmabadi, A.S., B. Fatahi, and B. Samali, "Seismic response of mid-rise buildings on shallow and end-bearing pile foundations in soft soil", Soils and Foundations, 54(3), 2014, pp. 345-363.
- [6] Hokmabadi, A.S., B. Fatahi, and B. Samali, "Assessment of soil-pile-structure interaction influencing seismic response of mid-rise buildings sitting on floating pile foundations", Computers and Geotechnics, 55(0), 2014, pp. 172-186.
- [7] Basu, P. and M. Prezzi, Design and applications of drilled displacement (screw) piles, Publication FHWA/IN/JTRP-2009/28. Joint Transportation Research Program, Indiana Depart. of Transport'n & Purdue University, West Lafayette, Indiana, 2009.
- [8] Pucker, T. and J. Grabe, "Numerical simulation of the installation process of full displacement piles", Computers and Geotechnics, 45, 2012, pp. 93-106.
- [9] Larisch, M.D., et al., "Simulation of auger displacement pile installation", Int. J. of Geotechnical Eng., 2013.
- [10] Kosiński, A., "Numerical simulation of screw displacement pile interaction with non-cohesive soil", Archives of Civil & Mechanical Eng., 14(1), 2014, pp. 122-133.
- [11] Lim, J.K. and B. Lehane *Characterisation of the effects of time on the shaft friction of displacement piles in sand*. Géotechnique, 2014. 64, 476-485.
- [12] Randolph, M.F. and C.P. Wroth, "An analytical solution for the consolidation around a driven pile", Int. J. for Numerical and Analytical Methods in Geomechanics, 3(3), 1979, pp. 217-229.
- [13] Ladanyi, B., "Expansion of a cavity in a saturated clay medium", J. of Terramechanics, 1(2), 1964, pp. 96.
- [14] Nguyen, L.D., B. Fatahi, and H. Khabbaz, "A constitutive model for cemented clays capturing cementation degradation", International Journal of Plasticity, 56(0), 2014, pp. 1-18.
- [15] Le, T.M., B. Fatahi, and H. Khabbaz, "Viscous behaviour of soft clay and inducing factors", Geotechnical and Geological Engineering, 30(5), 2012, pp. 1069-1083.
- [16] Fatahi, B., T.M. Le, M.Q. Le, and H. Khabbaz, "Soil creep effects on ground lateral deformation and pore water pressure under embankments", Geomechanics and Geoengineering, 8(2), 2013, pp. 107-124.
- [17] Rivera, A.J., C.G. Olgun, T.L. Brandon, and F. Masse, *Numerical modeling of controlled modulus column installation in soft soils using a linear elastic perfectly plastic soil model*, in *Proceedings of NUMGE*. 2014, CRC Press. pp. 571-576.
- [18] Yu, H.-S., Cavity expansion methods in geomechanics. The Netherlands: Kluwer Academic Publishers, 2000.
- [19] Pestana, J., C. Hunt, and J. Bray, "Soil Deformation and Excess Pore Pressure Field around a Closed-Ended Pile", J. of Geotechnical and Geoenvironmental Eng., 128(1), 2002, pp. 1-12.
- [20] Kelly, R., T. Muttuvél, and K. Chan, *Lateral Displacements in Soft Soil Due to Installation of Vibro-Stone Columns Using the Dry Method*, in *Geo-Frontiers*. 2011, ASCE. pp. 549-556.
- [21] Castro, J. and M. Karstunen, "Numerical simulations of stone column installation", Canadian Geotechnical J., 47(10), 2010, pp. 1127-1138.
- [22] Ahmadi, M.M., P.M. Byrne, and R.G. Campanella, "Cone tip resistance in sand: modeling, verification, and applications", Canadian Geotechnical J., 42(4), 2005, pp. 977-993.
- [23] Elkadi, A.S.K., H. van Lottum, and H.J. Luger, *A 3D coupled Eulerian-Lagrangian analysis of the dynamic interaction of jack-up legs with the seabed*, in *Numerical Methods in Geotechnical Eng*. 2014, CRC Press. pp. 1255-1259.
- [24] Carter, J.P., M.F. Randolph, and C.P. Wroth, "Stress and pore pressure changes in clay during and after the expansion of a cylindrical cavity", Int. J. for Numerical and Analytical Methods in Geomechanics, 3(4), 1979, pp. 305-322.
- [25] Ho, L., B. Fatahi, and H. Khabbaz, "Analytical solution for one - dimensional consolidation of unsaturated soils using eigenfunction expansion method", International Journal for Numerical and Analytical Methods in Geomechanics, 2013.
- [26] von Wolffersdorff, P.A., "A hypoplastic relation for granular materials with a predefined limit state surface", Mechanics of Cohesive-frictional Materials, 1(3), 1996, pp. 251-271.
- [27] Mašín, D., "A hypoplastic constitutive model for clays", Int. J. for Numerical and Analytical Methods in Geomechanics, 29(4), 2005, pp. 311-336.
- [28] Hird, C., Q. Ni, and I. Guymer, "Physical modelling of deformations around piling augers in clay", Geotechnique, 61(11), 2011, pp. 993-999.
- [29] Suleiman, M.T., et al., Instrumented Static load test of CMC, Lehigh University, 2013.

## EFFECT ON UNCONFINED COMPRESSIVE STRENGTH OF SAND TEST PIECES CEMENTED WITH CALCIUM PHOSPHATE COMPOUND BY ADDITION OF SCALLOP SHELL POWDER

G. G. N. N. Amarakoon<sup>1</sup>, Takefumi Koreeda<sup>1</sup>, Satoru Kawasaki<sup>2</sup>

<sup>1</sup>Graduate School of Engineering, Hokkaido University, Kita 13, Nishi 8, Kita-ku, Sapporo, Hokkaido 060-8628, Japan

<sup>2</sup>Faculty of Engineering, Hokkaido University, Kita 13, Nishi 8, Kita-ku, Sapporo, Hokkaido 060-8628, Japan

### ABSTRACT

Chemical grout is composed of a calcium phosphate compound (CPC) which develops to form calcium carbonate (CC) precipitation throughout the soil and leading to an increase in soil strength. In this paper, initially the condition for CPC precipitation by using different mixtures of calcium and phosphate stock solutions were investigated and analyzed. For that, Toyoura sand test pieces were cemented by CPC solutions and cured up to 28 days and carried out unconfined compressive strength (UCS) test. Moreover, Toyoura sand test pieces were cemented by CPCs with scallop shell (SS) powder and cured and these specimens also analyzed with UCS tests. The UCS of the sand test pieces cemented by CPC with SS powder was larger than that of the test pieces with no added powders. The UCS of Toyoura sand test piece cemented with the CPC-SS powder method increased to a maximum of 156.9 kPa. Moreover, the best CPC-Chem mixture for cementation is CA: DPP with the concentration of Ca/P ratio is 0.5. In addition pH concentration, scanning electron microscope (SEM), and density before and after curing were observed. The results indicate that the density and the pH concentration of the sand test pieces cemented by CPCs with SS powder were larger than that of the sand test pieces with no added powders. SEM images of test pieces cemented with CA: DPP mixture by addition of SS powders not clearly identified a crystal formation among particles of Toyoura sand.

*Keywords: Calcium Carbonate; Calcium Phosphate Compound; Ground Improvement; Unconfined Compressive Strength*

### INTRODUCTION

Cement grouting is used as a ground improvement method for countermeasure against soil liquefaction during an earthquake [1]. However, cement grouting comprises several environmental problems such as high CO<sub>2</sub> emissions during cement production, high energy cost for re-excavation and hard to recycling the improved ground. Hence in present, grout materials produce by microorganism have been developed for ground permeability control and reinforcement [2]-[6]. Biogrouting is the process of ground improvement by biological action [7].

A novel ground stabilizer was developed to increase the number of options available among cementing mechanisms based on microorganisms [8],[9]. In addition, it is reported on a CPC chemical grout (CPC-Chem) that utilizes self-setting CPC mechanisms [10] and on a CPC biogrout (CPC-Bio) whose solubility is dependent on its pH [10] (Fig. 1), which can be increased by a microbial reaction.

CPC-Chem is easy to obtain, safe to handle, non-toxic, and recyclable, advantages that make it suitable for geotechnical application [8]. The maximum unconfined compressive strength (UCS) of sand test pieces cemented with CPC-Chem was found to be

63.5 kPa [8]. Our aim is to achieve a UCS value of 100 kPa, which is needed to avoid ground liquefaction during earthquakes [11]. This implies that the UCS of CPC-Chem is not sufficient for use as a ground stabilizer, necessity of a preferable mechanism for further increase in UCS.

An earlier research was said, the UCS of the test pieces with TCP and CC additives exceeded the targeted value of 100 kPa and increased to a maximum of 261.4 kPa and 209.7 kPa respectively [12]. This observations indicates that the existence of CC seed crystals can reinforce the strength of CPC grouts. The main component of scallop shells is CC, which are disposed of in large quantities as marine industrial waste (410,000 tons/year in Japan) [13]. Scallop shells are non-toxic to handle and inexpensive to obtain. Hence, scallop shells can be used for CC which is a favorable material in the geotechnical field from the view point of waste utilization and costeffectiveness.

In the present study, our aim was to improve strength by adding CPC with scallop shell powder. This study aims to exceed a maximum UCS of 100 kPa after 28 days of curing, which is the strength required to use the CPC and scallop shell powder combination as a countermeasure against soil

liquefaction during earthquake. UCS tests and scanning electron microscopy (SEM) observations were conducted on sand test pieces as a function of time. In addition, pH value and wet density were measured. Based on the results, we discuss the effect of the amount of added powders, variation in wet density ( $\rho_t$ ), pH and crystal form on the UCS.

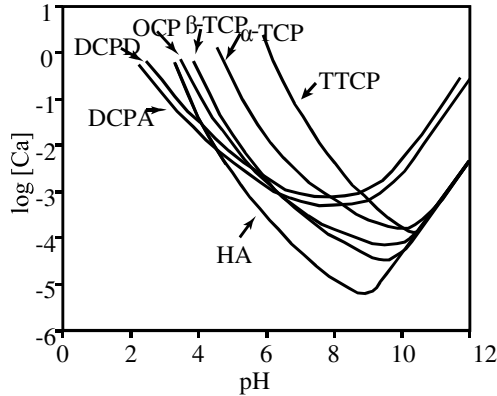


Fig. 1 Solubility phase diagrams for the ternary system,  $\text{Ca}(\text{OH})_2\text{-H}_3\text{PO}_4\text{-H}_2\text{O}$ , at 25 °C, showing the solubility isotherms of  $\text{CaHPO}_4$  (DCPA),  $\text{CaHPO}_4\cdot 2\text{H}_2\text{O}$  (DCPD),  $\text{Ca}_8\text{H}_2(\text{PO}_4)_6\cdot 5\text{H}_2\text{O}$  (OCP),  $\alpha\text{-Ca}_3(\text{PO}_4)_2$  ( $\alpha$ -TCP),  $\beta\text{-Ca}_3(\text{PO}_4)_2$  ( $\beta$ -TCP),  $\text{Ca}_4(\text{PO}_4)_2\text{O}$  (TTCP), and  $\text{Ca}_{10}(\text{PO}_4)_6\cdot (\text{OH})_2$ , (HA). The figure is adapted from Tung [10].

## METHODOLOGY

In this study, for the CPC-Chem, calcium acetate (CA) was used as a calcium solution and diammonium phosphate (DAP) and dipotassium phosphate (DPP) were used as phosphate solutions. The concentration of CA was varied from 1.5 M to 0.5 M and the concentration of DAP and DPP was constant as 3.0 M for prepare the CPC-Chem solution with two different Ca/P ratios (0.5 and 0.25). Then, Toyoura sand test pieces were cemented with CPC-Chem only and cured up to 28 days and analyzed with UCS tests. For this case, a standard sand test piece was made from 320.09 g of Toyoura sand (mean diameter  $D_{50} = 170 \mu\text{m}$ , 15% diameter  $D_{15} = 150 \mu\text{m}$ ) and 73.3 mL of CPC-Chem according to the previous report [8].

In addition, Toyoura sand test pieces were cemented with CPC-Chem (CA: DPP = 0.6 M: 1.2 M) by addition of scallop shell (SS) powder and cured up to 56 days and these specimens also analyzed with UCS tests. In this case, a standard sand test piece was made as same as previous case and it is called as 'CPC-Cont' sample. The examined test pieces were made with the combination ratios shown in Fig. 2. 1% (3.2 g) (Case SS-01), 5% (16.0 g) (Case SS-05), and 10% (32.0 g) (Case SS-10) of SS (mean diameter  $D_{50}$

= 25.12  $\mu\text{m}$ ) were mixed with 72.21 mL, 67.84 mL, and 62.38 mL of CPC-Chem respectively and added to weight of a standard sand test piece of 320.09 g for prepare CPC-SS samples.

It was uniformly mixed in a stainless-steel ball for 2 min and the mixture was divided into quarters, each of which was placed into a plastic mold container ( $\phi = 5 \text{ cm}$ ,  $h = 10 \text{ cm}$ ). The sand in the mold container was tamped down 30 times by a hand rammer after each of the four quarters was placed in the mold. The molded test pieces were subsequently cured in an airtight container at a high humidity for 28 days and 56 days at 20°C.

The UCS of the test pieces removed from the mold container after curing was measured at an axial strain rate of 1%/min with the UCS apparatus T266-31100 (Seikensha Co., Ltd., Japan). In all cases two test pieces were tested. The pH of the test pieces was calculated as an average of three measurements (top, bottom, and middle of each test pieces) using pH Spear (Eutech Instruments Pte., Ltd., Singapore). Segments of the UCS test pieces were observed by an SEM. The segments were naturally dried at 20°C for a few days and carbon-coated with a carbon coater. SEM observations were carried out at an accelerating voltage of 15 kV and at x 1000 magnification.

## RESULTS AND DISCUSSION

### UCS Test

In this study, Toyoura sand test pieces cemented by four reaction mixture sets of CPC-Chem were chosen. The measured UCS in this study ranged from 26.1 to 143.6 kPa. The maximum value was measured when the sand test pieces cemented with CA: DPP=1.5M: 3.0M mixture and Ca/P ratio was 0.5 (Fig. 3 (a)). The UCS is tended to increase with the curing time for 28 days for sample prepared with CA: DPP=1.5M: 3.0M mixture but the test piece at 14 days of curing time shows that the UCS is tended to decrease. It is assumed that some error could occur when preparing the sample. To clarify this result, further examination of the test pieces is needed in the future. There is no significant variation of UCS in the test pieces prepared with CA: DPP=0.75 M: 3.0 M mixture. Also, the UCS value of the test pieces cemented with CA: DPP=1.5M: 3.0M mixture (CA: DPP=0.5) is larger than the UCS value of the test pieces with CA: DPP=0.75M: 3.0M mixture (CA: DPP=0.25).

According to Fig. 3(b), the value of UCS is tended to constant for both CA: DAP=0.5 and CA: DAP=0.25. Also, the UCS value of the test pieces with CA: DAP=0.5 is larger than the UCS value of the test pieces with CA: DAP=0.25. Moreover, from the Figs. 3(a) and 3 (b), the UCS value of the test pieces with CA: DPP=0.5 is larger than the UCS value of the test pieces with CA: DAP=0.5.

Case Name	Control	CPC-SS Method		
	CPC-Cont	SS-01	SS-05	SS-10
Sand Weight (g)	Sand 320.09	Sand 320.09	Sand 320.09	Sand 320.09
Weight of adding powders (g)	Without powder	+	+	+
		SS 3.2	SS 16.0	SS 32.0
Volume of CPC- Chem (mL)	73.30	72.21	67.84	62.38

Fig.2 Conceptual image of the contents.

Figs. 4(a) and 4(b) show the relationship between UCS and Ca/P ratio for the sand test pieces cemented with CPC-Chem only. The results are given considering after 1 day and 28 days curing period. It comprises that the UCS value (Ca/P=0.5) is larger than the UCS value (Ca/P=0.25) for both testing cases such as CA: DPP and CA: DAP. The UCS value is larger after 28 days curing time than 1 day curing time. However, the rate of increase of UCS of sand test pieces cemented with CA: DPP mixture is larger in 28 days curing period than 1 day curing period (Fig. 4(a)).

In Fig. 4(b), when the test pieces cemented with CA: DAP mixture, the UCS values are nearly same after 1 days and 28 days curing period. Therefore, the rate of increase of UCS of sand test pieces cemented with CA: DAP solution is larger in 1 day curing period than 28 day curing period. However, it is assumed as an error and to get more precise result, further testing is required.

In addition, Toyoura sand test pieces cemented by four reaction mixture sets were chosen (adding CA: DPP = 0.6M: 1.2M mixture with no adding powders

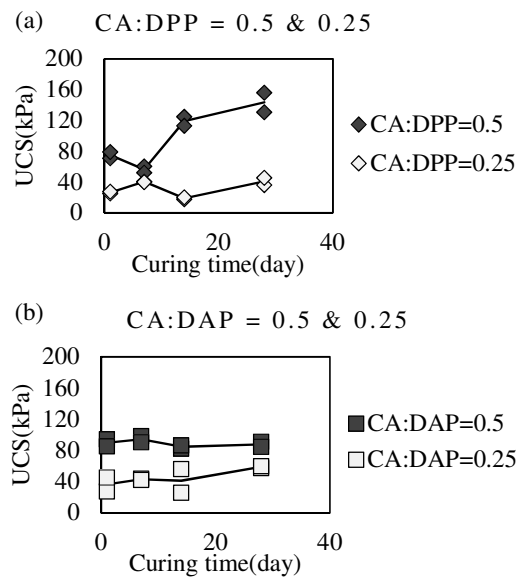


Fig. 3 (a) UCS of Toyoura sand test pieces cemented by CA: DPP=0.5 and 0.25. (b) UCS of Toyoura sand test pieces cemented by CA: DAP=0.5 and 0.25.

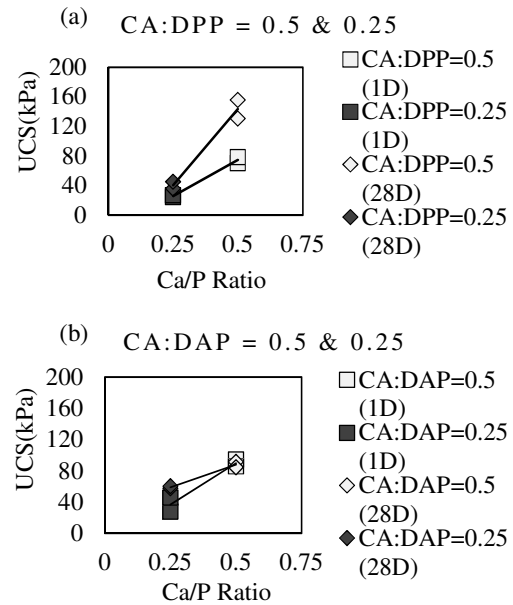


Fig. 4 Relationship between UCS and Ca/P ratio of Toyoura sand test pieces cemented by (a) CA: DPP=0.5 and 0.25. (b) CA: DAP=0.5 and 0.25.

and adding SS powder with different percentages: 1%, 5% and 10%). The measured UCS in this study ranged from 49.9 to 156.9 kPa.

The maximum value was measured when the sand test pieces cemented with CA: DPP=1.2M: 0.6M mixture by adding SS powder 10% (Fig. 5). The UCS of sand test pieces cemented by CPC with SS powder was larger than that of the test pieces with no added powders when considering cured time until 28 days. However, the UCS values of sand test pieces cemented by CPC with SS-1% and SS-5% after 56 days curing period is less than that of the CPC-Cont sample.

The test pieces with SS-10% show that the UCS is tended to decrease at 14 days curing period, it is assumed that some error could occur when preparing sample. To clarify this result, further examination of the test pieces is needed in the future.

### Effect of pH on UCS

Figs. 6(a) and 6(b) illustrate the effect of pH on UCS for the test pieces cemented by CPC-Chem (CA: DPP and CA: DAP). The pH of the test pieces range from acidic to weakly alkaline (6.4-7.5) for CA: DAP and the pH range from weakly alkaline to strong alkaline (7.0-8.7) for CA: DPP. Moreover the UCS is tended to increase with the increase of pH for CA: DPP (Fig 6 (a)) while the UCS was nearly constant when increase of pH for CA: DAP (Fig. 6(b)).

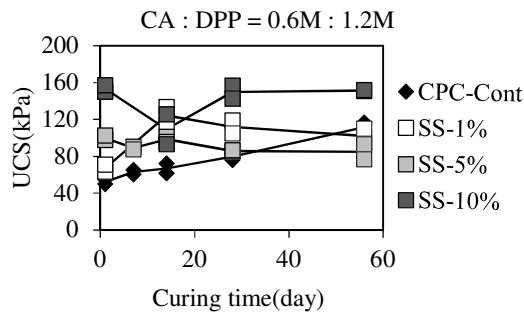


Fig. 5 Unconfined compressive strength (UCS) of sand test pieces cemented by CPC with SS.

According to Fig. 7, the pH is tended to increase with the time. Moreover, the pH value of CPC-SS sample is larger than pH values of CPC-Cont sample. When the concentration of SS powder is increased, pH value is tended to increase. Although, when pH is increased, UCS is tended to increase.

### SEM Observation

Fig. 8 shows SEM images of sand test pieces cemented with four reaction mixture set of CPC-Chem (CA: DPP=0.5 and 0.25 and CA: DAP=0.5 and 0.25) and the curing time was 14 days. Wisker-like

crystal structure was observed in the sample prepared with CA: DPP=0.5 mixture and other samples were not clearly observed any crystal formation.

SEM images of test pieces subjected to CA: DPP treatment with SS powders were not clearly identify a crystal formation among particles of Toyoura sand (Fig. 9). The increase in UCS seemed to be because of the binding of the sand particles by the precipitated CPC that enveloped the CC particles.

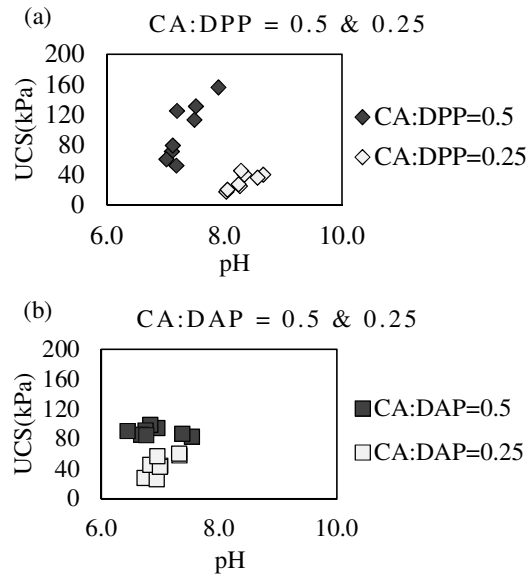


Fig. 6 (a) Relationship between pH and UCS for CA: DPP=0.5 and 0.25 (b) Relationship between pH and UCS for CA: DAP=0.5 and 0.25.

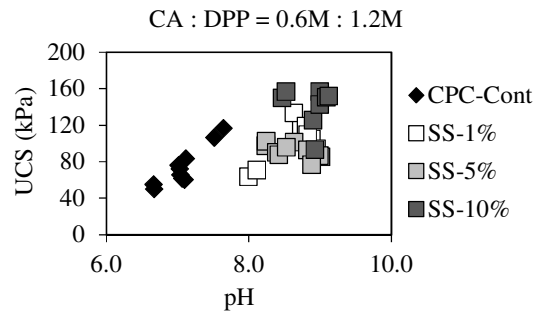


Fig. 7 Relationship between pH and UCS for CPC-Cont, and CPC-SS test pieces.

### Effect of Wet Density on UCS

The estimated wet density of the test pieces is shown in Figs. 10 and 11. Wet density (before) was calculated by measuring mold weight immediately after being produced and wet density (after) is defined as wet density immediately after cured. Fig. 10 shows wet density of the test pieces cemented with CPC-

Chem only. The results shows, UCS value is increased with increase of density only in CA: DPP=0.5. In addition, when curing time is increased the UCS is tended to increase. In other cases, the UCS value neither increase nor decrease with increase of wet density.

There is no significant difference between wet density, before and after the test. That is because there was no volume change such as expansion or shrinkage after curing.

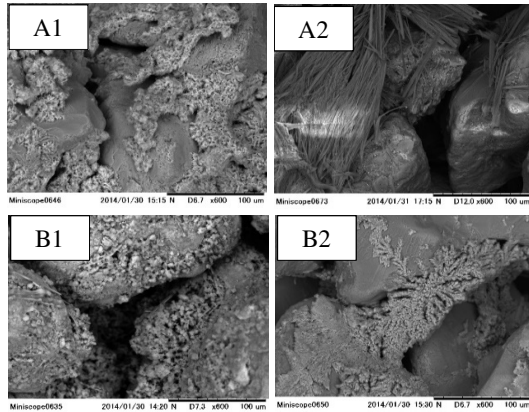


Fig.8 SEM images for test samples after 14 days curing period (600 X). (A1) CA: DPP=0.25, (A2) CA: DPP=0.5, (B1) CA: DAP=0.25 and (B2) CA: DAP=0.5.

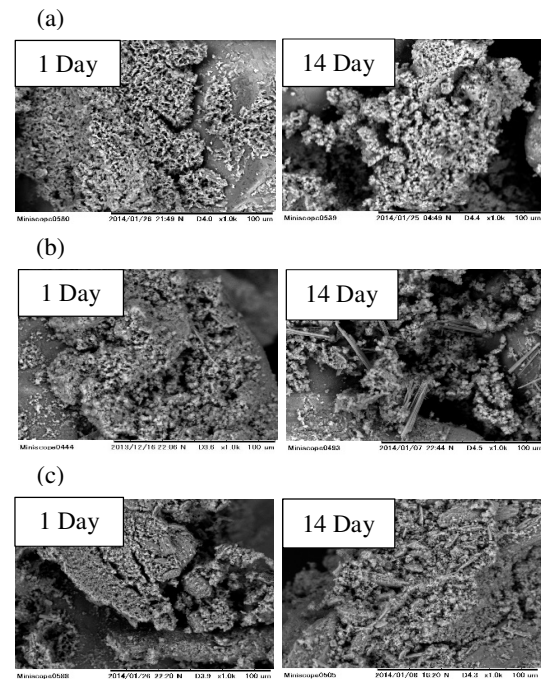


Fig.9 SEM images for test samples cemented with CPC by adding SS powder after 1 day and 14 days curing period (1000 X). (a) SS-1%, (b) SS-5% and (c) SS-10%.

In the case of the test pieces treated by the CPC-SS powder method, the wet density is larger than the test pieces cemented with CPC-Chem only. (Fig. 11). Also, it comprises that the UCS is tended to increase with increase of density. In addition, when the increase of SS and CC powders %, wet density is increased.

### Effect on Addition of SS Powder on the UCS

Figs. 3 and 5 show the UCS test results for Toyoura sand test pieces cemented with CPC-Chem only and CPC-SS powder respectively. It comprises that the UCS of test pieces cemented with CPC-SS is larger than that for CPC-Chem alone. Practically, the test pieces to which the SS powder with 10% was added show a UCS is larger than 100 kPa. This statement recommends that through control of the CC content, the CPC-SS and CPC-CC method would allow for adjustment of strength according to the required strength properties of the ground while maintaining a UCS of over 100 kPa. Considering results of UCS, pH, wet density and SEM images in CPC-SS powder method, the governing factors for increase the strength of the sample are pH and wet density.

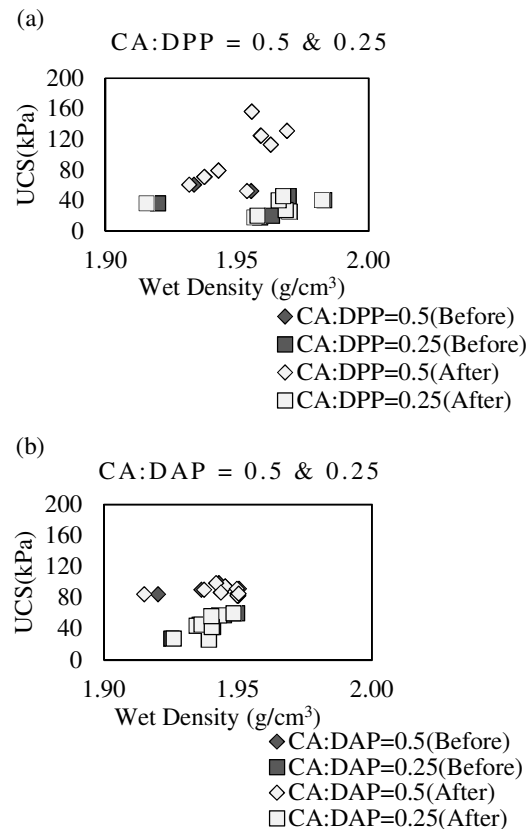


Fig. 10 Relationship between wet density and UCS (a) CA: DPP=0.5 and 0.25 (b) CA: DAP=0.5 and 0.25.

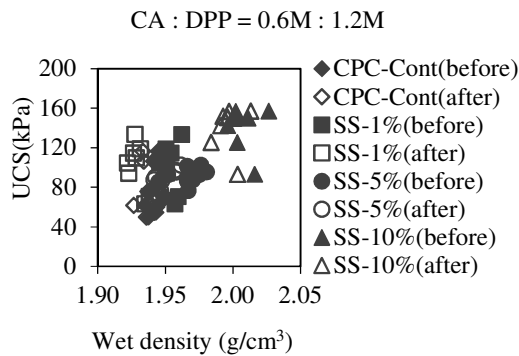


Fig. 11 Wet density of Toyoura sand test pieces cemented by CPC with SS.

## CONCLUSION

In this study, initially the condition for CPC precipitation using different mixtures of calcium and phosphate stock solutions was investigated and analyzed. It concluded that the best CPC-Chem mixture was CA: DPP with the concentration of Ca/P ratio is 0.5.

Further, the study was expanded to CPC powder method with using scallop shell powder. From this study, it was concluded that CPC-SS powder method had a significant potential for strength of the soil. The UCS of a Toyoura sand test piece cemented with the CPC-SS powder method increased to a maximum of 156.9 kPa. The aim of this study was to use CPC-Chem to achieve a maximum UCS of over 100 kPa, which was the strength required to prevent ground liquefaction. Using the CPC-SS powder method, we far exceeded this objective by achieving a UCS of over 150 kPa.

Finally, considering above viewpoints, CPC-SS powder method is more effective and reliable than CPC-Chem method for achieve a maximum UCS of over 100 kPa to prevent the ground liquefaction.

## ACKNOWLEDGEMENT

The work has been partly supported by a Grant-in-Aid for Scientific Research (No. 24300299) from the Japanese Ministry of Education, Sports, Science and Technology. This support is gratefully acknowledged.

## REFERENCES

- [1] Karol RH, "Chemical grouting and soil stabilization", 3rd ed., CRC Press, Boca Raton, FL, 2003.
- [2] Whiffin VS, Van Paassen LA and Harkes MP, "Geomicrobiology Journal", Vol. 24, 2007, pp. 417-423.

- [3] De Muynck W, De Belie N, and Verstraete W, "Ecological Engineering", Vol. 36, 2010, pp. 118-136.
- [4] DeJong JT, Mortensen BM, Martinez BC and Nelson DC, "Ecological Engineering", Vol. 36, 2010, pp. 197-210.
- [5] Harkes MP, Van Paassen LA, Booster JL, Whiffin VS and Van Loosdrecht MCM, "Ecological Engineering", Vol. 36, 2010, pp. 112-117.
- [6] Kawasaki S, Ogata S, Hiroyoshi N, Tsunekawa M, Kaneko K. and Terajima R, "Effect of temperature on precipitation of calcium carbonate using soil microorganisms", Journal of the Japan Society of Engineering Geology, Vol. 51, 2010, pp. 10-18 (in Japanese with English abstract).
- [7] Van Paassen LA, Harkes MP, Van Zwieten GA, Van der Zon WH, Van der Star WRL and Van Loosdrecht MCM, "Conference Proceedings", in Proc. 17th Int. Conf. on Soil Mechanics and Geotechnical Engineering, 2009, pp. 2328-2333.
- [8] Kawasaki S. and Akiyama M., "Unique grout material composed of calcium phosphate compounds", Int. Journal of GEOMATE, Vol. 4, No.1, 2013, pp. 429-435.
- [9] Akiyama M. and Kawasaki S, "Microbially mediated sand solidification using calcium phosphate compounds", Journal of the Japan Society of Engineering Geology, Vol. 137-138, 2012, pp. 29-39.
- [10] Tung MS, "Calcium phosphates: structure, composition, solubility, and stability, in: A. Zahid (Ed.), Calcium phosphates in biological and industrial systems", Kluwer Academic Publishers, Norwell, 1998, pp. 1-19.
- [11] Yamazaki H, Maeda K, Takahashi K, Zen K and Hayashi K, "Technical Note of Port and Harbour Research Institute", Vol. 905, 1998, pp. 1-29 (in Japanese).
- [12] Kawasaki S. and Akiyama M, "Enhancement of unconfined compressive strength of sand test pieces cemented with calcium phosphate compound by addition of various powders", Journal of Soils and Foundations, Vol. 53-(6), 2013, pp. 966-976
- [13] "Recycling Technology Guidelines for Harbor and Airport Construction and Maintenance", Edited in 2004, Ports and Harbours Bureau. <http://www.mlit.go.jp/kowan/recycle/>.



## **ENHANCING SLOPE STABILITY WITH VEGETATION**

Nicholas Hytiris<sup>1</sup>, Michael Fraser<sup>2</sup> and Slobodan B. Mickovski<sup>1</sup>

<sup>1</sup>Glasgow Caledonian University, Scotland, UK; <sup>2</sup> Mabey Hire Ltd, Scotland, UK

### **ABSTRACT**

Landslides can have serious impact on natural and human environment and their prevention and mitigation is of global concern. The ability of a slope to resist a landslide depends on the materials and the properties of which it is composed. This project focuses in the increased landslide resistance of a slope due to vegetation. The properties of the soil-root composite were measured in laboratory and, from these results, calculation and graphically based evaluation was used to determine their qualities for resisting landslide. The results show that vegetation roots had a stabilizing effect on the slope, limited to the rooting depth. Knowing the rooting depth (generally between 0.5 and 1.5 m) and dependent on the species, a correlation between the ratio of root weight to soil weight and the slope ability to resist landslide was implied from experimental results and a hypothetical design chart and equation were derived.

*Keywords: Geotechnical Engineering, Slope Stability, Root Weight Ratio, Root Reinforcement, Ecological Engineering*

### **INTRODUCTION**

Slope stability is an important aspect of the built and natural environment. Slope failures and landslides can have a significant human and monetary cost. Understanding and preventing these failures is an important facet of environmental civil engineering and the contribution of vegetation towards increasing slope stability.

The use of vegetation to stabilise slopes is a practice which has been used throughout the world. This form of slope stabilisation has been described as 'Ecological Engineering' and defined as 'the design of sustainable ecosystems that integrate human society with its natural environment for the benefit of both' (Mitsch, 1998). It is seen as a 'soft' engineering approach when compared to traditional, 'hard', methods of slope stabilisation, for example; soil nails, anchors, meshes, retaining walls, slope geometry modification etc. This, 'soft', approach offers many benefits such as increasing biodiversity, self-sustainability, cost effectiveness and visual aesthetics while being environmentally friendly (Mitsch, 1998).

. There are two types of slope, natural and artificial (Gray & Sotir, 1996).

Natural slopes are formed over time through geological and geomorphic processes, for example; mountain forming, river activity, glacial and tidal activity. These slopes are only stable if the soil of which they are constructed has sufficient strength to resist the gravitational forces exerted on the potential sliding mass.

Artificial slopes or earthworks are either cut into the ground (soil or rock) or built up as in spoil heaps, waste tips or embankments. Cut slopes and cuttings are made to provide access for infrastructure such as train tracks, roads, canals, etc .

Whitlow (2006) defines translational failure as 'linear movement along a bedding plane or a soil layer lying near to the (sloping) surface. Such movements are normally fairly shallow and parallel to the surface'.

It is important to understand the ways in which soil and vegetation interact in order to be able to assess the safety of a slope to prevent human casualties and economic losses.

### **VEGETATION BENEFITS FOR A SLOPE - OVERVIEW**

Freer (1990) comments that '...the most important and general problem is a shallow seated instability of a slope'. He goes on to say that this is at a depth of around 0.5-2m below the ground surface and that this is in fact the most widespread form of slope failure particularly in cuttings and embankments.

It can also be seen that vegetation roots anchor the vegetation and provide reinforcement of soil.

### **Factor of safety of unrooted and rooted soils**

Danjon et al (2007) studied the effect on slope stability of two White Oak (*Quercus Alba*) trees. The findings of their research say that depending on the potential slip surface, the factor of safety (FOS) varied from 2.8-3.7 and 1.8-2.0 for unrooted soil. When the mean value of the FOS increased significantly for surface depths of 0.3m, however as distance progresses to a depth of 1.2m these benefits diminish.

According to Whitlow (2006), the factor of safety for a slope may be calculated using the 'infinite slope model'. This formula is shown below.

$$F = \frac{C' + (\gamma z - \gamma_w h) \cos^2 \beta \tan \phi'}{\gamma z \sin \beta \cos \beta}$$

Where:  $C'$  - apparent cohesion of the soil ( $\text{kN/m}^2$ );  $Z$  - depth to shear plane (m);  $H$  - height of ground water level above shear plane (m);  $\gamma$  - density of soil ( $\text{kg/m}^3$ );  $\gamma_w$  - density of water ( $\text{kg/m}^3$ );  $\beta$  - slope angle ( $^\circ$ );  $\phi'$  - angle of friction ( $^\circ$ )

Morgan and Rickson (1995) give a modification of the formula from Whitlow for translational failure on an infinite slope when including the effects of vegetation, shown below.

$$F.O.S = \frac{(C' + C'R) + \{[(\gamma z - \gamma_w h_v) + W] \cos^2 \beta + T \sin \theta\} \tan \phi' + T \cos \theta}{[(\gamma z + W) \sin \beta + D] \cos \beta}$$

The above formula incorporates four additional variables to the F.O.S formula for soil alone. These are;  $C'R$  - the enhanced shear strength due to roots ( $\text{kN/m}^2$ ),  $T$  - tensile root force acting at the base of the shear plane ( $\text{kN/m}$ ),  $W$  - surcharge of the vegetation ( $\text{kN/m}^2$ ) and  $D$  - wind loading parallel to the slope ( $\text{kN/m}$ ). By adding these factors into the formula a F.O.S for soil including roots can be found. The authors comment that the most important variables in improving slope factor of safety are the enhanced shear strength and the tensile root force.

## EXPERIMENTAL WORK

It was decided that the direct shear test would be the most appropriate testing equipment to evaluate an improvement in resistance to translational failure due to root (vegetation) presence.

The direct shear test, measures normal and shear stresses directly on the failure plane. The shear box has dimensions: 60x60x25mm. The soil sample was cut/ extracted using a core cutter and placed inside the box. Samples of grass were extracted from the in-situ site using a core cutter of dimensions 60x60x25mm, this was pressed into the box. Testing was carried out according to BS 1377, 1990

In order to ascertain the cohesive strength ( $C'$ ) of soil alone and the pseudo-cohesion ( $C'R$ ) added by roots, incremental values of normal stress of 25.89, 39.51 and 53.14 kPa were applied to the samples. By comparison of these normal stress values against the values of shear stress obtained from the tests, graphs which showed the cohesive strength,  $C'$ , and the angle of friction,  $\phi$ , of the soil could be produced. Shear tests for each value of normal stress were carried out. The author was determined to evaluate whether the mass of vegetation within a sample would correlate to the increase in shear strength ( $\Delta S$ ) observed (if any) within the same sample. This root weight to soil ratio, 'root weight ratio' (RWR), is not strictly the same as the 'root area ratio' (RAR), the RAR is calculated by taking the diameter of all roots (generally larger roots, such as tree/ shrub roots) and

finding the ratio of root area to soil area. In the case of grass it was decided that this would be extremely time consuming/ difficult to record accurate measurements. Instead, the RWR (the weight of the vegetation mass within the sample against the weight of the sample as a whole) would be measured in an effort to see if this is an adequate substitute for RAR in the instance of grass.

The soil was determined by inspection to be 'topsoil'/ 'organic' and by sieve test to be a 'well graded sandy soil'. The moisture content was also assessed. After each sample of rooted soil had been tested in the shear box, the superficial vegetation was removed and it was washed in a 1.18mm sieve from the sieve test rig. This particular sieve size was selected in order to allow finer soil material to pass through its apertures retaining any organic material. The remaining vegetation was allowed to dry in the laboratory. By comparing the weight of the dried roots against the original weight of the sample, the RWR was found and this could be compared against the shear strength found for that sample.

## RESULTS AND ANALYSIS

### Direct shear testing of the soil without vegetation

By plotting the results of the shear test, shear stress over normal stress, the apparent cohesion of the soil was found to be,  $C' = 10 \text{ kN/m}^2$  and the peak angle of friction,  $\phi' = 16^\circ$ .

### Slope Factor of Safety for unrooted soil

The factor of safety for the soil was calculated from a formula described in Whitlow (2006)

$$F.O.S = \frac{C' + (\gamma z - \gamma_w h) \cos^2 \beta \tan \phi'}{\gamma z \sin \beta \cos \beta}$$

Apparent cohesion,  $C' = 10 \text{ kN/m}^2$  - Experimental result; Peak angle of friction,  $\phi' = 16^\circ$  - Experimental result; Density of soil,  $\gamma = 10.6 \text{ kN/m}^3$  - Experimental result; Depth to shear plane,  $z = 0.1 - 0.5 \text{ m}$ . This range of depths was chosen as according to Wu et al (1979), '...maximum depth of roots of grass and forbs in temperate zones is usually no greater than 0.5'. Therefore below this depth any slip plane will be subject to the shear apparent cohesion and peak angle of friction of the soil alone; Density of water,  $\gamma_w = 9.81 \text{ kN/m}^3$ ; Height of water table,  $h = 0.5 \text{ m}$  - This was chosen as a worst case scenario to give the lowest factor of safety possible for completely saturated conditions.

Angle of slope,  $\beta = 45^\circ$  - This was chosen as it is the upper limit of slope angle for the equation. Additionally, any slopes built of greater angles would likely use other technologies, for example geotextiles (Morgan et al, 1995).

F.O.S calculations are plotted below.

### Direct shear testing

Figure, shows the variation of the apparent cohesion,  $C' = 20 \text{ kN/m}^2$  and peak angle of friction,  $\phi' = 21.8^\circ$ . So, the apparent cohesion due to roots,  $C'R = C'$  (roots and soil) –  $C'$  (soil alone),

$$C' = 20 - 10 = 10 \text{ kN/m}^2.$$

In the case of vegetated soil, a modified version of the “drained infinite slope model” formula was used. This formula is from Morgan et al (1995) .

Experimental results: Apparent cohesion,  $C' = 10 \text{ kN/m}^2$  ; Apparent cohesion due to roots,  $C'R = 10 \text{ kN/m}^2$ ; Density of soil,  $\gamma = 10.6 \text{ kN/m}^3$ .

Depth to shear plane,  $z = 0.5 \text{ m}$  ; Density of water,  $\gamma_w = 9.81 \text{ kN/m}^3$ ; Depth of water table,  $h_v = 0.5 \text{ m}$ .

Assumptions: Surcharge of vegetation,  $W = 0 \text{ kN/m}^2$ ; Angle of slope,  $\beta = 45^\circ$  - Chosen to keep consistency with calculation; Tensile root force,  $T = 9.34 \times 10^{-3} \text{ kN}$  ; Angle between roots and slip plane,  $\theta = 45^\circ$ ; Wind loading force,  $D = 0 \text{ kN/m}$ .

Assumptions: The weight of the surface vegetation and its subsequent normal force on the soil are quantified as ‘W’, the surcharge. This surcharge is included in the calculation primarily due to the plausibly high force exerted on soils by trees, in this instance ‘W’ has been assumed to be zero as the surcharge exerted by grass is likely to be very small and of little consequence.

The tensile root force for the grass used experimentally was not tested. This testing would require specialized equipment that was unavailable. As a substitute for this, a value for tensile root force from a similar grass was used. This value was taken from Hengchaonovich (2003) for a similar grass, ‘common centipede grass’, as  $5 \text{ kN/m}$ .

The Wind loading force, ‘D’, is chiefly concerned with the effect of ‘wind throw’. In the case of grass, the surface area upon which wind can act is small in comparison to trees, additionally grasses tend to be flexible and unlikely to transfer a great deal of force to the roots.

Angle between roots and slip plane,  $\theta$ , has been taken to be equal to that of the slope angle,  $\beta$ , as it was assumed that roots had grown in a gravitropic manner.

#### Root area ratio (RAR) modification

Root area ratio is not uniform throughout its depth. Instead there is a tendency for RAR to decrease non-linearly to zero between the surface and its lowest depth. In order to account for this transition between soil with additional root cohesion,  $C'R$ , and soil with soil cohesion alone,  $C'$ , the  $C'R$  value has been factored down with depth according to a chart of root area ratio. Based on Figure 1, an average line was calculated and drawn in order to find suitable reduction factors to take depth into account. Figure 1 was created by averaging RAR

values over depth from a graph of similar grasses (Baets et al, 2008).

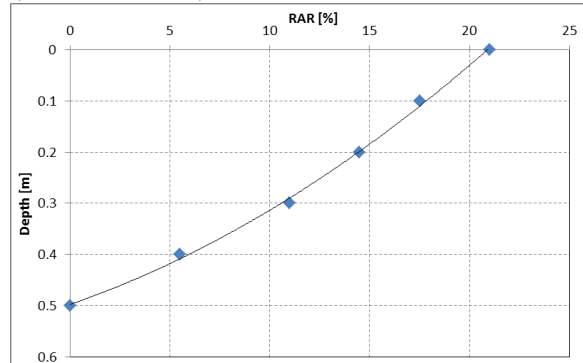


Fig. 1 – Comparison of RAR with Depth

#### Root Weight Ratio (RWR)

After testing, the rooted soil samples were washed clean of soil and the remaining roots dried and weighed. The ratio of the weight of the dry roots to the weight of the initial soil mass was calculated this was compared with the shear strength found by testing for each sample. The results of this test are shown in figure 2.

RWR				
Sample	Total Weight	Root Weight	Ratio	Shear Stress
1	65.1 g	13.7 g	21.045 %	30.83 kN/m <sup>2</sup>
2	64.1 g	13.2 g	20.593 %	27.5 kN/m <sup>2</sup>
3	68 g	14.4 g	21.176 %	31.94 kN/m <sup>2</sup>
4	104 g	9.6 g	9.2308 %	35.83 kN/m <sup>2</sup>
5	121 g	11.8 g	9.7521 %	35.28 kN/m <sup>2</sup>
6	61.6 g	12.4 g	20.13 %	29.44 kN/m <sup>2</sup>
7	83.5 g	11.2 g	13.413 %	42.78 kN/m <sup>2</sup>
8	60 g	12.1 g	20.167 %	39.17 kN/m <sup>2</sup>
9	60 g	11.7 g	19.5 %	41.11 kN/m <sup>2</sup>

Fig. 2 RWR Results Table

## DISCUSSION

### Soil properties

The in-situ soil was determined to have a density of  $1106.25 \text{ kg/m}^3$  and a moisture content of 33%. The soil was classified as ‘well graded sandy soil’ in accordance with the British Classification System for Engineering Purposes and visually identified as ‘topsoil’ / ‘organics’. All results and findings are only valid for these soil parameters pending further research.

### Shear strength and angle of friction

It can be seen from the shear test results of both unrooted and rooted soils that the individual samples yielded varying results. This variation in results could be attributed to the non-uniform nature of different samples in terms of soil composition and in the case of rooted soils, root mass. When the results for each value of normal stress were averaged they produced values which gave linear lines with upward trends when graphed. This would be expected from soil samples subjected to increasing values of normal stress as increased loading would create greater compaction of the sample and

therefore greater friction between particles/ roots and soil across the imposed shear plane.

The unrooted soil produced average values of shear strength of 18.33, 24.72 and 27.59kN/m<sup>2</sup> for normal stresses of 25.89, 39.51 and 53.14kN/m<sup>2</sup> respectively. The rooted soil produced shear strength values of 30.09, 34.81 and 41.02kN/m<sup>2</sup> for normal stress values of 25.89, 39.51 and 53.14kN/m<sup>2</sup> respectively. When graphed, this showed that the apparent cohesion,  $c'$ , of unrooted soil was 10kN/m<sup>2</sup> and of rooted soil, 20kN/m<sup>2</sup>, this apparent cohesion occurs under a normal stress value of 0kN/m<sup>2</sup> and is indicative of the strength of an unloaded soil. This indicates that the apparent cohesion due to roots,  $C'R$ , for this particular grass is equal to 10kN/m<sup>2</sup>, at least for the root mass found at 0.125m below the surface. From these results we see that the apparent cohesion of the soil has doubled due to the presence of roots.

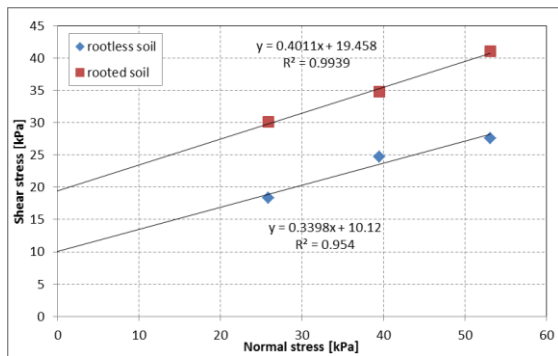


**Fig. 3 - Comparison of Shear stress over normal stress for unrooted and rooted soils.**

Figure 3 demonstrates the comparison of rooted and unrooted soils, it can be seen that shear stress over normal stress rises linearly with what would appear to be a constant difference in shear stress of 10kN/m<sup>2</sup>. This can be attributed to the presence of roots in the rooted soil samples.

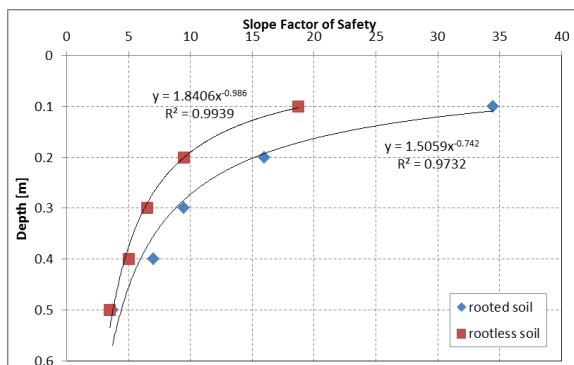


**Fig. 4 Slope Factor of Safety over Depth for rooted and rootless soil.**

Since a vegetated slope would require to be unobstructed on its surface so that sunlight may reach the vegetation, the only normal stress which

should be applied to the slope would be that of gravity and so the  $C'$  and  $C' + C'R$  values of unrooted and rooted soils are the most important values in this graph.

In figure 4, a comparison of factors of safety has been created for unrooted and rooted soil. We can see that the F.O.S for both soils decreases with depth, this would be expected as with additional depth, the horizontal force of a soil mass due to increasing area will increase, lowering its stability. We also see that with increasing depth the F.O.S of rooted soil reduces until at 0.5m it reaches the same value as rooted soil. This would be expected as due to the RAR modification applied to the rooted soil factor of safety formula,  $C'R$  decreases from 0.84 to 0 between 0.1m and 0.5m depth. This shows that any increased F.O.S due to roots can only exist where roots are present in the soil and is dependent on their density at that depth.

Since the soil type used in the experiment has yielded apparent cohesion values  $C'$  and  $C'R$ , of 10kN/m<sup>2</sup> and 10kN/m<sup>2</sup> respectively and given that calculated factors of safety have been high, a graph has been produced in which the apparent cohesion,  $C'$ , of the soil has been reduced from 10 to 0 kN/m<sup>2</sup> whilst keeping the apparent cohesion due to roots at 10kN/m<sup>2</sup>. An assumption has been made in maintaining the  $C'R$  value at 10kN/m<sup>2</sup>, this assumes that the vegetation will grow in a similar manner and to a similar density with depth as that of the soil used experimentally. The object of this comparison is to find the properties of a soil that may be improved to a useable standard by the vegetation used in this experiment. The slope angle used in this comparison will be 45° with a depth of 0.3m.

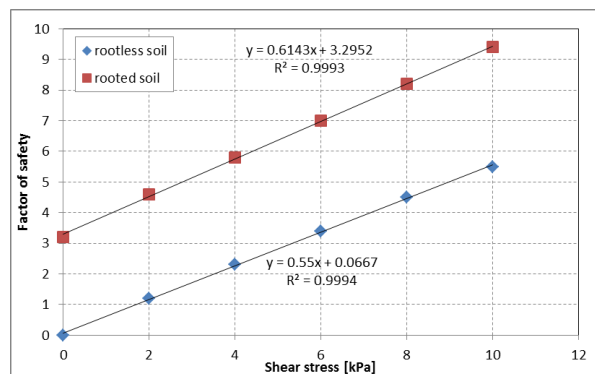


**Fig. 5 Factor of Safety over Shear Stress for Rooted and Rootless soil.**

In Figure 5, a comparison of the factor of safety for unrooted and rooted soil whilst lowering the apparent cohesion,  $C'$ , of the soil and keeping the apparent cohesion due to roots,  $C'R$ , constant is presented. In this diagram we see that in order to keep a factor of safety for slope stability above 1.5, a value of apparent cohesion,  $C'$ , of around 2.2kN/m<sup>2</sup> is required for unrooted soil. The factor of safety at this point for a soil rooted with the same vegetation

used in the previous experiments was around 5.

### Root weight ratio (RWR)

From laboratory experimentation, a positive correlation between RWR and shear strength was found and shown on figure 6. Sample 1 had a RWR of 21.045% and a shear strength value of 30.83kN/m<sup>2</sup>, Sample 2 had a RWR of 20.593% and a Cu of 27.5kN/m<sup>2</sup> and Sample 3 had a RWR of 21.176% and a Cu of 31.94kN/m<sup>2</sup>. Other samples exhibited this relationship however due to the problem of weight variance, the set of results for normal testing of 25.89kN/m<sup>2</sup> have been selected for further discussion as these results used samples with the smallest weight variance. To investigate this further, the relationship between RWR and Shear Stress was plotted along with the average shear stress of soil for the same normal stress, 18.33kN/m<sup>2</sup>.

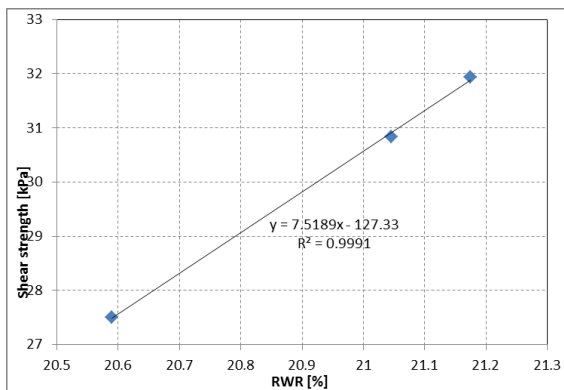


Fig. 6 – Shear Strength over RWR

Figure 7 shows the increase in shear stress from the first point, unrooted soil (e.g. 0% RWR) to the later three rooted soil points. The black line indicates the trend of the rooted soil points, this trend appears to be linear and as no greater values of RWR were found during the experiments, only assumptions can be made. An assumption would be that the RWR (%) in a soil must tend to an upper limit. The samples of rooted grass were from a mature lawn which has had over ten years of growing time, perhaps for this grass type and possibly the soil conditions present, values of RWR(%) will not exceed approximately 23-25% as this may be a limit.

Since there appears to be a correlation between RWR and shear stress, an assumption would be that between values of RWR of 0 and 21.176% (the highest value), shear strength must rise in a polynomial curve, the data points of which are plotted in figure 7.

The reasoning behind this assumption is based on two main facts evidenced by the experimental results:

A RWR of 0% must be equal to 18.33kN/m<sup>2</sup> as this is the shear stress of the soil itself under a normal load of 26.89kN/m<sup>2</sup>. The trend line in figure 7

cannot continue linearly as it would cross the RWR axis at roughly 16-17(%). This would indicate that when RWR is equal to 16-17%, shear stress is zero. This cannot be true as the shear stress of the soil alone is 18.33kN/m<sup>2</sup> under a normal load of 26.89kN/m<sup>2</sup>.

### Assumed polynomial curve

In figure 7 an assumed curve has been plotted based on the assumptions. This curve increases linearly before tending to a limit.

In an attempt to describe/ plot the hypothetical curve shown in figure 7, a polynomial equation was used. This equation was of a degree of three as there were four points and is shown below.

Solving for a, b, c and d respectively, an equation to describe the curve was attempted to be found. Unfortunately due to the lack of data for samples with RWR greater than 1 and less than 20.593% this produced an unsatisfactory curve with negative values.

In order to produce a satisfactory curve, three additional points were plotted on the hypothetical curve and these were used to create a formula which accurately described the hypothetical curve. The points were applied at RWR's of 5, 10, 15% and yielded approximate shear stress values of 19.5, 21 and 22.5kN/m<sup>2</sup> respectively. Once applied to the graph, a polynomial curve was drawn and an equation describing the curve derived.

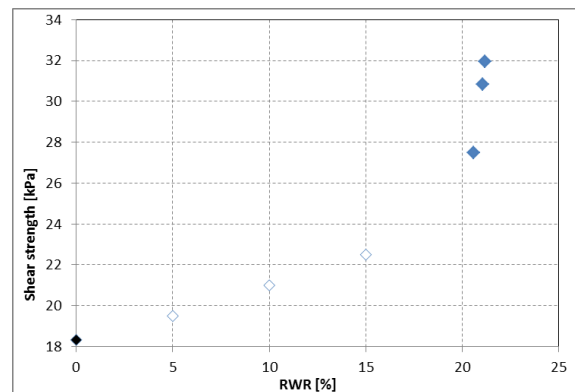


Fig. 7 – Shear Strength over RWR

The derived equation:

$$y = 0.0003x^4 - 0.0107x^3 + 0.1072x^2 - 0.0777x + 18.331$$

When modified to replace the axis denotations we arrive at a hypothetical formula to obtain shear strength from root weight ratio, shown below:

$$C'R + C' = 0.0003RWR^4 - 0.0107RWR^3 + 0.1072RWR^2 - 0.0777RWR + 18.331$$

“Total apparent cohesion (C'R + C') over root



weight ratio (RWR) equation.”

For values of  $C'R+C'$  in  $\text{kN/m}^2$ , RWR in percent (%) and where  $C' = 18.331 \text{ kN/m}^2$

## CONCLUSIONS

The aim of this project was to investigate the relationship between vegetation and slope stability in order to assess its benefits and to investigate whether a relationship between RWR and shear strength existed. The key findings of the project are discussed in the following sections.

Laboratory experiments have confirmed that vegetation roots increase the shear resistance, angle of friction and therefore the F.O.S of a soil however this increase is not uniform with depth. For the soil used in the experiments, vegetation was shown to improve the F.O.S by 75% at a depth of 0.1m however this diminished to 0% by 0.5m. It has been seen that, depending on the species of vegetation, roots may not grow to a depth below the shear plane, rendering them ineffective in slope stabilisation. Due to this, shear plane depth and root growth depth should be a major consideration when using vegetation to stabilise a slope. The grass tested in this project, could not be used to stabilise any slopes with shear planes deeper than 0.4m but could perhaps be useful if used in conjunction with other vegetation.

Work by Danjon (2007) discussed how areas of reduced  $\Delta S$ , increased shear strength due to roots, could occur between trees stabilising a slope. Perhaps the grass used in this dissertation or a similar variety could be used to improve  $\Delta S$  between trees to stop localised failures. Research by Norris (2008) and Huat and Kazemian (2010) discussed how artificially planting ‘live stakes’ on a slope at depths of up to two meters has been shown to be an effective form of stabilisation. This method is particularly attractive as it provides immediate stabilisation and can be planted at a depth of up to 2m which is greater than most vegetation roots can grow. This method is also easier to understand and model when compared to a root mass as the ‘live stakes’ act in a similar manner to soil nails.

## Root weight ratio (RWR)

The RAR of roots in a soil mass was found to be of great importance as this diminished with depth and correlated with  $C'R$ . The RAR with depth varied between vegetation species and this would have to be considered in order to create an effective ‘Ecological Engineering’ slope stability solution. The difficulty of measuring RAR for grasses was discussed as being difficult due to the small nature of grass root diameter (centipede grass roots averaged 0.66mm in diameter). For this reason, it was decided to see whether the RWR would be an adequate substitute.

When using samples of a similar weight, the

results strongly suggested a correlation between RWR and  $C'R$ .

Criticisms that could be made of the hypothetical formula include the fact that only one soil type/grass type was tested, low amount of data used to plot graphs and the assumptions made. Further research would be required to validate the results found in this research.

## REFERENCES

- Baets et al, 2008. Root tensile strength and root distribution of typical Mediterranean plant species and their contribution to soil shear strength. *Plant and Soil*. 305(1-2)
- Danjon, F., 2007. Using Three-dimensional Plant Root Architecture in Models of Shallow-slope Stability. *Annals of Botany*. 101 (8).
- Denzin, N. and Lincoln, Y., 2005. *The SAGE handbook of qualitative research*. 3<sup>rd</sup> ed. Sage Publications.
- Head, K.H., 2011. *Manual of soil laboratory testing, Volume 2, Permeability, shear strength and compressibility tests*. 3<sup>rd</sup> ed. John Wiley & Sons
- Freer, R., 1990. Bio-engineering: the use of vegetation in civil engineering. *Construction and Building Materials*. 5(1)
- Huat, B.K., and Kazemian, S., 2010. Study of Root Theories in Green Tropical Slope Stability. *The Electronic Journal of Geotechnical Engineering*. 15.
- Hyrtis N., Kapellakis I.E., De la Roij R and Tsagarakis K.P. “The Use of Olive Oil Residue in Solidification Process”. *Resources Conservation and Recycling Journal* 2 January 2004, p 129-139.
- Morgan, R. and Rickson, R., 1995. *Slope stabilisation and erosion control*. 1<sup>st</sup> ed. Taylor & Francis.
- Mickovski, S. B., Stokes, A., van Beek, L. P. H., Ghestem, M. and Fourcaud, T. 2011. Simulation of direct shear tests on rooted and non-rooted soil using Finite Element analysis. *Ecological Engineering*, 37 (10): 1523-1532.
- Mickovski, S.B., Bransby, M.F., Bengough, A.G., Davies, M.C.R., Hallett, P.D. 2010. The resistance of simple plant root systems to uplift loads. *Canadian Geotech. Journal* 47(1), 78-95.
- Mickovski S. B. and van Beek L. P. H. 2009. Root morphology and effects on soil reinforcement and slope stability of young vetiver (*Vetiveria zizanioides*) plants grown in semi-arid climate. *Plant and Soil* 324 (1-2 ): 43-56.
- Whitlow R. “Basic Soil Mechanics fifth edition Pearson education. (2006)
- Wu, T. H., 2007. Root reinforcement: analyses and experiments. *Developments in Plant and Soil Sciences*. 103 (21-30).

## SMALL SCALE FIELD TESTS OF WATER INFILTRATION FOR COMPACTED SILTY LOESS SOIL

Aiassa Martínez Gonzalo<sup>1</sup>, Arrúa Pedro<sup>2</sup> and Eberhardt Marcelo<sup>3</sup>  
<sup>1,2,3</sup>Facultad Regional Córdoba, Universidad Tecnológica Nacional, Argentina

### ABSTRACT

Silty loess soils are widely spread on Córdoba city, Argentina. The ability to use this soil improved by compaction on embankments it is of interest to different types of local constructions, with purpose of reducing settlements and infiltration. This work research the water infiltration through compacted silty soils from Córdoba by small scale field test. Four small test embankments were constructed on natural soil with different compaction conditions using local silty soils. The site was characterized by typical geotechnical laboratory and field tests. The infiltration tests were performed using double ring infiltrometers for a time period around of 2 months. Results were used to field permeability estimated ( $k_f$ ) and these were compared with laboratory results ( $k_l$ ). Conclusions regarding the behavior observed in the field are presented.

*Keywords: Embankment Test, Double Ring Infiltrimeters, Site Investigation, Córdoba Soil*

### INTRODUCTION

Compacted soils are frequently used for different engineering project. Soils excavated from nearest works may be utilized for embankment construction. This is an economic and sustainable alternative, but data are needed to characterize the mechanical and hydraulic performance of the material. Lagoons and other waterworks, require barrier systems generally include layers of compacted soil. In these cases it is of interest to determine the infiltration of water. Permeability tests are generally performed on samples in laboratory compaction molds, or undisturbed samples. However, these tests do not take into account possible effects of scale which can be noticed through large-scale laboratory [1] or field test [2], [3], [4]. The study presented in [5] explores, by laboratory and field test, the possibility uses of silty soil as landfill liner material. A test pad was constructed in field using different soil composition and different compaction effort. Sealed double ring infiltrometers were employed to hydraulic conductivity determination. Differences between the results of hydraulic conductivity obtained from laboratory and field were found. Laboratory values were lower [5].

This work research the field water infiltration through compacted silty soils from Córdoba [6], [7], [8]. Four small test embankments were constructed on natural soil with different compaction conditions using local silty soils. The site was characterized by typical geotechnical laboratory and field tests. The infiltration tests were performed using double ring infiltrometers. The results show the effect of scale compared with previous laboratory data on these soils, and the effect on field compaction conditions.

### MATERIAL AND METHOD

Soil used in laboratory and field experiments was a silty loess from Cordoba. The Table 1 reports principal properties.

Table 1 Properties of liner soil

Properties	Unit	Value
Liquid limit	%	26.7
Plasticity index	%	4.3
Fines (<0.074mm)	%	97
Fraction <0.002mm	%	5
Specific gravity		2.67
Class (ASTM D2487)		ML
Max dry unit weight	kN/m <sup>3</sup>	16.8
Optimal water content	%	19

Note: max dry unit weight and optimal water content are for Standard Proctor (ASTM D698).

For field infiltration test a small probe fills was constructed in the Universidad Tecnológica Nacional campus located on City Southern Cordoba City. The selected site was gated. The position of each cell was set and then excavations were undertaken (Fig. 1). For the excavation, a dimension plan of 1 m by 1 m was adopted and 0.55 m in thickness.

Soils excavations were scrapped because these contained many roots. Silty local materials were used, in depths of 3-5 m, in order to avoid impurities (Table 1), and prepared carefully to remove clods and mix well with added water. The construction of the cells was performed under controlled compacted soil layers. Each layer was compacted by dynamic



impacts. The compaction condition was controlled by the number of blows applied. Control tests as DCP (dynamic cone penetrometer) and in place unit weight were performed (Fig. 2).



Fig. 1 Construction stage.

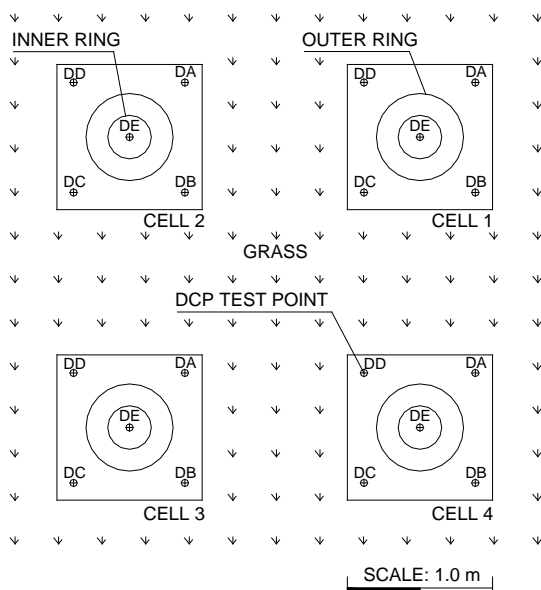


Fig. 2 Location sketch of cell.

Results of in place unit weight test were  $13.3 \text{ kN/m}^3$  (Cell 1),  $15.8 \text{ kN/m}^3$  (Cell 2),  $14.5 \text{ kN/m}^3$  (Cell 3),  $15.2 \text{ kN/m}^3$  (Cell 4). Relating to Standard Proctor the relative compaction were 79% (Cell 1), 94% (Cell 2), 86% (Cell 3), 90% (Cell 4). These values can be easily achieved in construction practice. Figure 3 shows DCP test results. Generally, a first surface layer of 5 cm with relatively low compaction is observed, then the embankment with a thickness of approximately 50 cm, followed by a layer of compacted natural soil to 65 or 70 cm deep. Finally, natural soil not affected by compaction, with a DCP index of 30 mm/blow is detected.

The infiltration tests were performed using

double ring infiltrometer. Inner ring of 30 cm diameter and outer ring of 60 cm were used. The water level was preserved approximately constant with a height of 5 cm. During the test progress, a waterproof cover was installed on each cell to prevent from rain event (Fig. 4). Additionally, a container for controlling evaporation occurred during the test was used. This determination not intended to provide weather information, it was made only for the purpose of correcting the volume of water infiltrated into the ring.

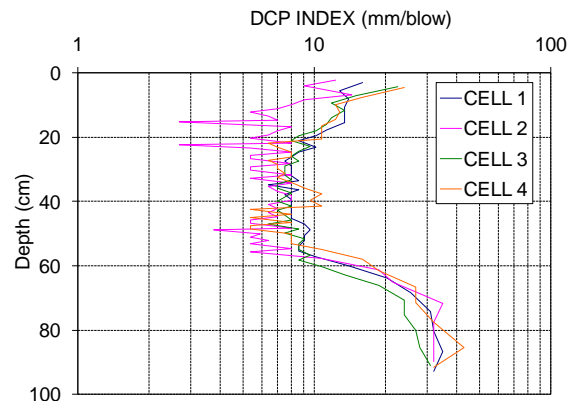


Fig. 3 DCP test results.

Infiltration tests were conducted at the site on the natural soil without compacting, in order to assess the influence of compaction. For this, the rings were installed on a prepared surface where it was removed coverage of grass and roots.



Fig. 4 Test in progress.

## RESULTS AND ANALYSIS

Measurements of water infiltration into the natural silty soil are shown in Fig. 5. To analyze the results the infiltration rate ( $I_r$ ) is adopted. Eq. (1) presents the formulation for field infiltration rate calculation.

$$I_r = \frac{\Delta V(t)}{\Delta t \cdot A} \quad (1)$$

Where  $\Delta V$ : volume infiltrate during time  $\Delta t$ ,  $A$ : inner ring area.

For natural silty soil the  $I_r$  results  $2 \times 10^{-6}$  m/s. This value characterizes the material located beneath the cells with compacted soil.

In the case of the compacted soil a correction was made for the infiltrate water, due the long test duration, and consequently the evaporation effect. Fig. 6 shows results of evaporation control test. In simplified form, a constant correction factor of 5.2 mm/day was adopted.

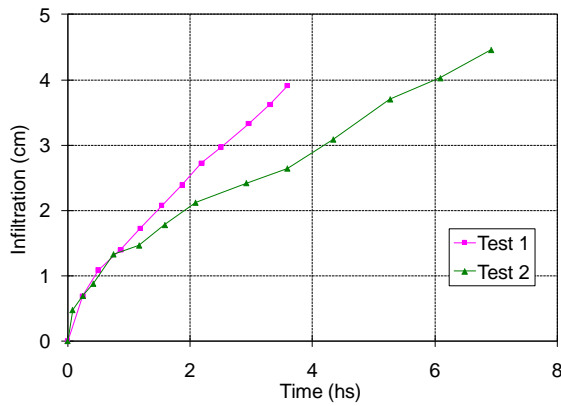


Fig. 5 Field infiltration test on natural silty soil.

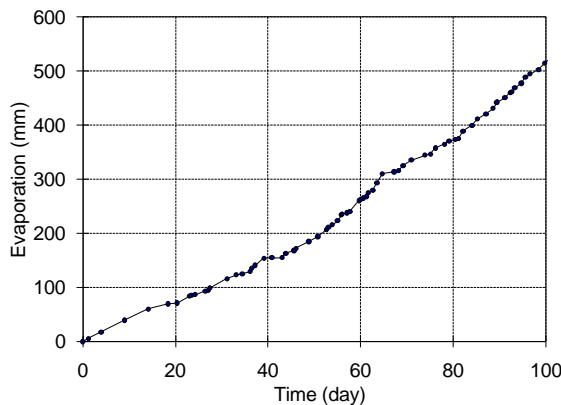


Fig. 6 Evaporation control test.

Fig. 7 shows corrected results of field infiltration test from cells. For compacted silty soil the  $I_r$  results  $2.0 \times 10^{-7}$  m/s (Cell 1),  $9.8 \times 10^{-8}$  m/s (Cell 2),  $2.4 \times 10^{-7}$  m/s (Cell 3),  $1.7 \times 10^{-7}$  m/s (Cell 4).

The comparison of results is performed by a factor relating infiltration rate of two cases (Eq. 2). Thus,  $\eta$  results 2.4 for cells 2 and 1. Comparing natural silty soil relative to the improvement by compaction, values for  $\eta$  between 8 to 20.

Concerning results of laboratory tests on samples compacted under similar conditions can be observed that in field values are similar without a clear scale effect.

$$\eta = \frac{I_{r1}}{I_{r2}} \quad (2)$$

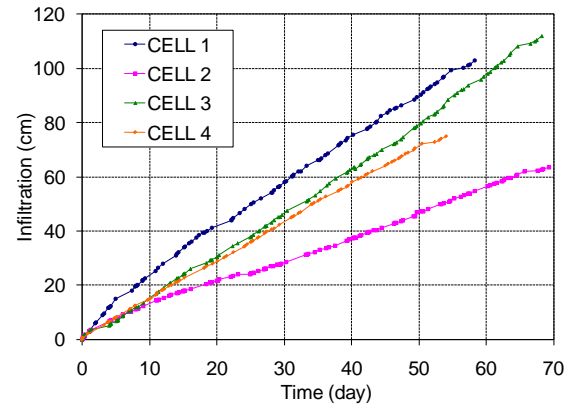


Fig. 7 Field infiltration test on compacted silty soil.

## CONCLUSION

In this paper, an experimental study of field infiltration tests on small silty soil compacted embankments is presented. The embankments were prepared under controlled compaction conditions. Cells were protected from the rain and the effect of water evaporation was contemplated due to the long test duration.

Compaction provides improved hydraulic performance, considerably reducing the rate of infiltration respect the natural soil. The condition of compaction affected the results. The greater relative compaction (Cell 2) determined the lowest cumulative infiltration, while the cell with lower relative compaction (Cell 1) presented the highest cumulative infiltration. Field results were similar to available laboratory compaction by similar conditions.

Despite soil compaction, the infiltration rate may be high for many project.

It could increase the relative compaction or incorporate some added material in order to attempt to reduce the infiltration rate. However, this work is one of the few local experiences with field infiltration tests on compacted silty soil. So, more embankments tests are needed in order to reach conclusions of general behavior.

## ACKNOWLEDGEMENTS

The authors thanks the support of Universidad

Tecnológica Nacional Facultad Regional Córdoba, Ministerio de Ciencia y Tecnología, Gobierno de la Provincia de Córdoba (PID-GRF), and FONCyT Agencia Nacional de Promoción Científica y Tecnológica (PICT).

## REFERENCES

- [1] Shackelford CD and Javed F, "Large-scale laboratory permeability testing of a compacted clay soil", *Geotechnical Testing J.*, Vol. 14, No. 2, June 1991, pp. 171–179.
- [2] Stewart JP and Nolan TW, "Infiltration testing for hydraulic conductivity of soil liners", *Geotechnical Testing J.*, Vol. 10, No. 2, June 1987, pp. 41–50.
- [3] Sai JO and Anderson DC, "Field hydraulic conductivity tests for compacted soil liners", *Geotechnical Testing J.*, Vol. 13, No. 3, September 1990, pp. 215–225.
- [4] Benson CH, Daniel DE and Boutwell GP, "Field performance of compacted clay liners", *J. of Geotechnical and Geoenvironmental Engineering*, Vol. 125, No. 5, May 1999, pp. 390–403.
- [5] Bozbey I and Guler E, "Laboratory and field testing for utilization of an excavated soil as landfill liner material", *Waste Management*, Vol. 26, 2006, pp. 1277–1286.
- [6] Arrúa P, Aiassa G., Eberhardt M and Alercia Biga C, "Behavior of collapsible loessic soil after interparticle cementation", *International J. of GEOMATE*, Vol. 1, November-December 2011, pp. 130–135.
- [7] Aiassa G. and Arrúa P, "Desempeño de barreras sanitarias simples de suelo loésico compactado", *Revista Tecnología y Ciencia*, Año 8, Noviembre 2009, pp. 26–40.
- [8] Aiassa G, Zeballos M, Arrúa P and Terzariol R, "Infiltración en suelos limosos compactados", *XIX Congreso Argentino de Mecánica de Suelos e Ingeniería Geotécnica*, Octubre 2008, La Plata, Argentina.

## METHOD FOR HAZARD ASSESSMENT OF SLOPE FAILURES BASED ON INFORMATION PROCESSING TECHNIQUES

Shinichi Ito<sup>1</sup>, Kazuhiro Oda<sup>2</sup>, Keigo Koizumi<sup>3</sup>, Kyohei Umemura<sup>4</sup>, and Yohei Usuki<sup>5</sup>  
<sup>1,2,3,4,5</sup> Osaka University, Japan

### ABSTRACT

Recently, the sediment disasters, such as slope failures, debris flows, landslides and so forth, caused by typhoon or cloudburst have occurred somewhere in Japan. The progression of global warming will increase the scale of typhoons and cloudbursts striking the Japanese Islands, so that it is a concern that the frequency of occurrence of sediment disasters may increase. Thus, it is necessary to identify the slopes with higher hazard to sediment disasters in order to establish disaster prevention planning. In this study, a method based on information processing techniques is proposed. In the proposed method, self-organizing map (SOM), cluster analysis, and Hayashi's second method of quantification are combined. The proposed method and only Hayashi's second method of quantification are applied to the periodical inspection data. As a result, the availability of the proposed method is confirmed by comparing the results of proposed method with only Hayashi's second method of quantification.

*Keywords: Sediment disasters, Self-organizing map (SOM), Hayashi's second method of quantification, Cluster analysis*

### INTRODUCTION

In Japan, where mountainous districts occupy 70 % of land, the sediment disasters, such as slope failures, debris flows, landslides and so forth, have occurred each year. Due to the progression of global warming, the intensity of rainfalls brought by the typhoons and cloudburst have become more severe, so the number of occurrences of the sediment disasters in Japan have also increased as shown in Fig. 1 [1]. Therefore, disaster prevention planning for the sediment disasters should be established. However, there are innumerable slopes in Japan, and there are limits to time and costs, so that it is difficult to examine all the slopes. Thus, first of all, it is important to identify the slopes with higher hazard to sediment disasters.

There are endogenous factors and exogenous factors of the sediment disasters. The endogenous factors mean the characteristics of the slopes, such as topographical features, geological features and so forth. The exogenous factors mean the trigger of the sediment disasters, such as rainfall, earthquake and so forth. It is difficult to forecast when, where, and how much rainfalls will be expected, so that it is useful to identify the slopes with higher hazard to sediment disasters based on the endogenous factors. In Japan, the detailed, periodical inspection [2] is performed in order to prevent future disasters. Therefore, a method for analyzing the characteristics of the slopes as easily and effectively as possible from the periodical inspection data in order to identify the slopes with higher hazard to sediment disasters is necessary. The method should be able to treat a large number of data,

so that artificial neural networks, mathematical statistics and so forth should be applied as analytical methods.

In this paper, a method that can identify the slopes with higher hazard to sediment disasters is proposed. In the proposed method, self-organizing map (SOM) [3], which is one of the artificial neural network techniques, and cluster analysis [4], which is one of the mathematical statistics, and Hayashi's second method of quantification [5], which is a quality determination method are combined.

In this study, the proposed method are applied to the periodical inspection data of slopes in order to identify the slopes with higher hazard to sediment disasters. Also, only Hayashi's second method of quantification is applied to the periodical inspection data of slopes. The purpose of this study is to confirm the availability of the proposed method by comparing two results that are from the proposed method with from only Hayashi's second method of quantification.

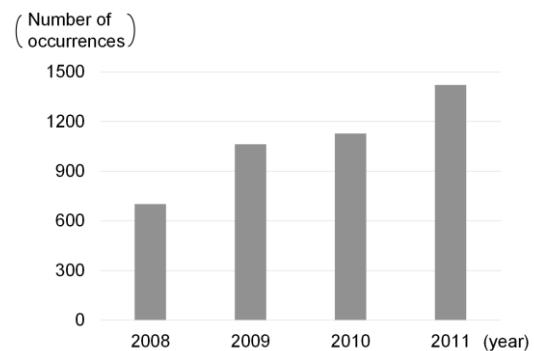


Fig. 1 Number of occurrences of sediment disasters in Japan

## ANALYTICAL METHOD

### Self-organizing map (SOM)

SOM is one of the artificial neural network techniques. The SOM is known to be an effective technique for analyzing high-dimensional data. In other words, high-dimensional vectors can be mapped to two dimensional space for visual understanding. The two-dimensional representation can then be used to observe patterns and correlations present in high-dimensional data. In addition, vectors with similar characteristics are placed closer on the two-dimensional map and dissimilar vectors are located farther apart. Therefore, in the case where SOM is applied to high-dimensional vectors, they can be classified into several clusters automatically. Fig. 2 shows an example of an analytical result of SOM. There are several parts with light gray color. Some vectors gather at each light gray part. That is, a set of some vectors gathering at a light gray part is a cluster.

However, SOM has a disadvantage. It is difficult to cluster high-dimensional vectors into several groups objectively. For example, from the result of Fig. 2, some users may cluster them into five groups surrounded with white circles as shown in Fig. 3. On the other hand, another users may cluster them into different five groups surrounded with black circles. The subjective judgment of the users controls the clustering based on visual mapping.

### Cluster analysis

A cluster analysis is one of the representative techniques in the mathematical statistics. It can divide objectively a set of high-dimensional vectors into several clusters which is fixed previously according to the similarity among the high-dimensional vectors. However, the cluster analysis also has a disadvantage. It is necessary to determine previously the number of clusters before conducting the cluster analysis. The number of clusters cannot be determined automatically unlike SOM. It is difficult to determine the number of clusters without preliminary analysis.

### Combination of self-organizing map and cluster analysis

In this paper, both SOM and cluster analysis are combined in order to overcome two disadvantage which are objective clustering in SOM and determination of the number of clusters. The analytical process is following. First of all, the number of clusters is visually determined by SOM. Then the number of clusters is applied to cluster analysis, and the objective clustering is performed. The results of cluster analysis are plotted on the map of SOM. If the number of clusters is wrong, the analytical results of SOM and cluster analysis are not

fitted as shown in Fig. 4. However, if the right number of clusters are applied to cluster analysis, the analytical results of SOM and cluster analysis are fitted as shown in Fig. 5.

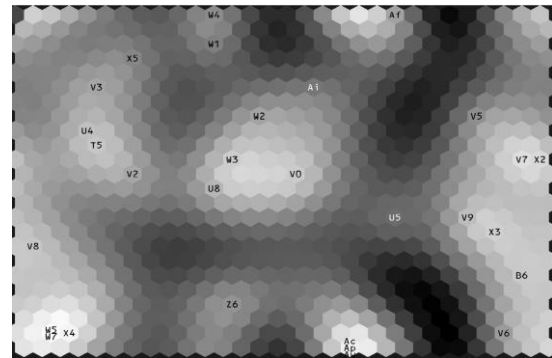


Fig. 2 An example of analytical result of SOM

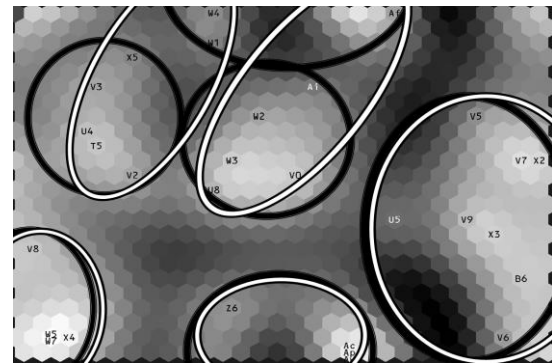


Fig.3 Different clusters of SOM by individual difference

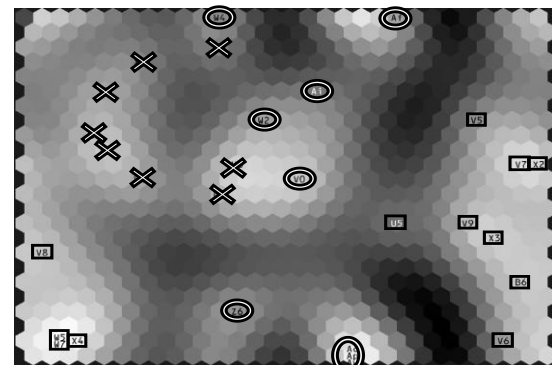


Fig.4 Analytical result of SOM and cluster analysis in case of applying wrong number of clusters

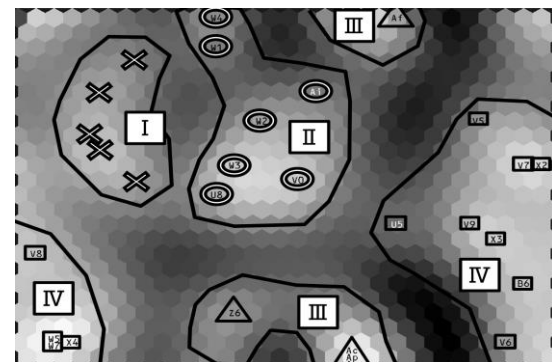


Fig.5 Analytical result of SOM and cluster analysis in case of applying right number of clusters

### Hayashi's second method of quantification

Hayashi's second method of quantification is a method of mathematical statistics. It is known as a representative technique of the quality determination method. This method treats categorical data and derives dependent variables from an explanatory variable. In other words, Hayashi's second method of quantification can divide one group into two groups.

Therefore, if Hayashi's second method of quantification is applied to slopes, the slopes are estimated to be failed or not failed.

### Method for identifying slopes with higher hazard

The authors proposed the method for identifying the slopes with higher hazard to deep-seated catastrophic landslides [6]. In this study, the proposed method are applied to the periodical inspection data of slopes in order to identify the slopes with higher hazard to slope failures. Namely, the proposed method are expected to identify the slopes with higher hazard to various type of sediment disasters by changing applicable data. Fig. 6 shows the flowchart of the proposed method. The proposed method has three stages.

At first stage, only failed slopes are grouped into several clusters through combination of a SOM and a cluster analysis. There are all sorts of failed slopes. All failed slopes do not necessarily have same characteristics. Therefore, the failed slopes are grouped into several clusters in which the failed slopes have almost similar characteristic in order to perform effectively following discriminant analysis.

At second stage, Hayashi's second method of quantification, one of the representative methods for discriminant analysis, can be applied to a set of slopes, which includes the failed slopes in a cluster and all of not failed slopes, in order to identify the slopes with higher hazard to slope failures. The slopes with higher hazard can be identified in this way.

At third stage, the slopes with higher hazard are given priority according to the sample score of Hayashi's second method of quantification. The sample score indicates the hazard of the slopes, such that the slopes with a higher sample score have a higher hazard to slope failures. Additionally, Hayashi's second method of quantification also give the score of the boundary between failed slopes and not failed slopes. In this study, the priority of the slopes was determined by the difference between the sample score and the score of the boundary. In other words, the slopes having a higher difference between the sample score and the score of the boundary are the slopes with the higher hazard.

In this way, the proposed method, which is based on SOM, cluster analysis, and Hayashi's second method of quantification, can identify the slopes with higher hazard and prioritize the slopes.

### APPLICABLE DATA

#### Periodical inspection data

In this study, the periodical inspection data of slopes are used. The periodical inspection data of slopes are integrated into the database, so the data will be stored and increased. Therefore, if the slopes with higher hazard to slope failures can be identified by using the data, it is useful for future disaster prevention planning.

The periodical inspection data that the slopes were inspected in 1996 is used. The data contain 128 slopes of expressway and 89 slopes of national road. There are 8 failed slopes of expressway and 29 failed slopes of national road in the periodical inspection data. Table 1 shows the parameters which estimate the hazard of each slopes, and the categorical data corresponding to each parameters.

#### Verification method

In this study, the training data and the identity data are used in order to confirm the availability of proposed method. Firstly, the periodical inspection data of slopes are divided into 7 to 3 ratio randomly. The training data are 70 % of data, and the identify data are 30 % of slopes. Secondly, the proposed method and only Hayashi's second method of quantification are applied to the training data. Herewith, the standards, such as the score of boundary and the categorical scores, that each parameters are quantified by Hayashi's second method of quantification, are established. Finally, the identify data are applied to each standards, and the number of failed slopes in the identify data which are estimated to failed is calculated. In the case where the proposed method has a high capture efficiency of the failed slopes which are estimated to failed, the availability of the proposed method is confirmed.

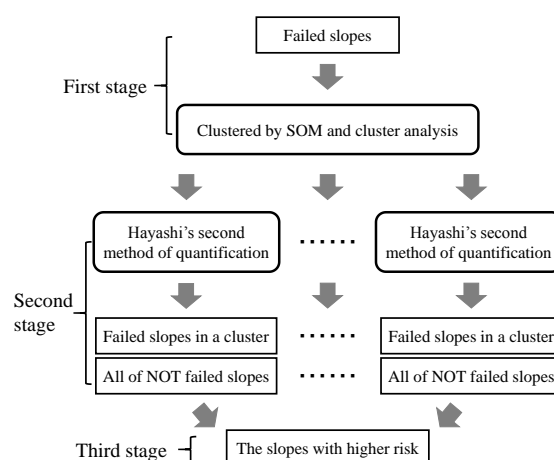


Fig.6 Method for identifying slopes with higher hazard

## ANALYTICAL RESULTS

### Only Hayashi's second method of quantification

Only Hayashi's second method of quantification were applied to the training data (26 failed slopes and 126 not failed slopes), and the standards, such as the score of boundary and the categorical score were established. Table 2 shows the analytical result that the identify data (11 failed slopes and 54 not failed slopes) are applied to the standards. From this result, 8 failed slopes in the identify data were estimated to failed, but 3 failed slopes in the identify data were estimated to not failed.

Table 1 Parameters and categorical data

parameters		categorical data
talus cone	0	0
	1	0.5
	2 or more	1
soil	stable	0
	medium	0.5
	fragile	1
lithology	stable	0
	medium	0.5
	fragile	1
formation	opposite slope	0
	dip slope	1
difference of permeability	small	0
	medium	0.5
	large	1
topsoil, loose part rock, boulder stone	stable	0
	medium	0.5
	unstable	1
spring water	without spring	0
	leakage	0.5
	spring	1
covering condition	construct	0
	compound	0.5
	vegetation, bare land	1
height of slopes	$H < 15$	0
	$15 \leq H < 30$	0.333
	$30 \leq H < 50$	0.666
	$50 \leq H$	1

Table 2 Analytical result of identify data by using only Hayashi's second method of quantification

		Real	
		Failed	Not failed
Estimate	Failed	8	6
	Not failed	3	48

### Proposed method

The proposed method were applied to the training data. At first, only failed slopes were classified into clusters by SOM and cluster analysis. Fig. 7 shows the analytical result of combining SOM with cluster analysis. The analytical result of SOM and cluster analysis are fitted as shown in Fig.7, so the failed slopes can be classified into four clusters. The characteristics of several clusters were checked and the distribution conditions of the failed slopes in each clusters in regard to each parameters were shown in Table 3.

There were 5 failed slopes in cluster 1. All of them were the slopes of expressway, and almost all of them were applicable to the parameters which had relatively lower hazard to slope failures. However, the failed slopes in cluster 1 had high height of slopes.

There were 8 failed slopes in cluster 2. All of them were applicable to fragile lithology. In addition, there were more slopes that were applicable to the dip slopes than cluster 1 and cluster 3.

There were 8 failed slopes in cluster 3. All of them were applicable to fragile soil, and almost all of them were applicable to fragile lithology. In addition, they had higher hazard about difference of permeability and topsoil, loose part rock, boulder stone.

There were 5 failed slopes in cluster 4. All of them were applicable to highest hazard categories about 4 parameters (talus cone, soil, lithology, formation). Therefore, the failed slopes in cluster 4 had the higher hazard to slope failures of the four clusters.

In this study, the characteristics of the failed slopes could be classified into the four clusters. Thus, the four clusters and not failed slopes made four groups. Namely, cluster 1 and not failed slopes formed group A, cluster 2 and not failed slopes formed group B, cluster 3 and not failed slopes formed group C, cluster 4 and not failed slopes formed group D. The each groups were then applied to Hayashi's second method of quantification, and the analytical result shown in Table 4.

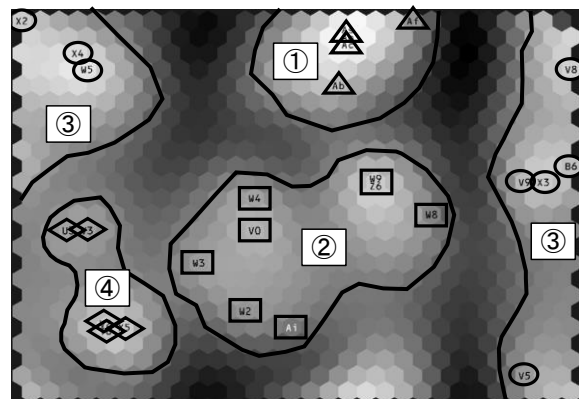


Fig.7 Analytical result of SOM and cluster analysis



Table 3 Distribution conditions of failed slopes in each clusters in regard to each parameters

(a) Cluster ①

parameters		number of slopes	parameters		number of slopes
talus cone	0	3	topsoil,	stable	5
	1	2	loose part rock,	medium	0
	2 or more	0	boulder stone,	unstable	0
soil	stable	4	spring water	without spring	1
	medium	1		leakage	4
	fragile	0		spring	0
lithology	stable	5	covering condition	construct	1
	medium	0		compound	4
	fragile	0		vegetation, bare	0
formation	opposite slope	5	height of slopes	$H < 15$	0
	dip slope	0		$15 \leq H < 30$	0
difference of permeability	small	5			$30 \leq H < 50$
	medium	0		$50 \leq H$	2
	large	0			

(b) Cluster ②

parameters		number of slopes	parameters		number of slopes
talus cone	0	3	topsoil,	stable	5
	1	2	loose part rock, boulder stone	medium	3
	2 or more	3		unstable	0
soil	stable	5	spring water	without spring	3
	medium	3		leakage	3
	fragile	0		spring	2
lithology	stable	0	covering condition	construct	5
	medium	0		compound	3
	fragile	8		vegetation, bare	0
formation	opposite slope	3	height of slopes	$H < 15$	1
	dip slope	5		$15 \leq H < 30$	2
difference of permeability	small	3		$30 \leq H < 50$	3
	medium	5		$50 \leq H$	2
	large	0			

(c) Cluster ③

parameters		number of slopes	parameters		number of slopes
talus cone	0	1	topsoil,	stable	0
	1	1	loose part rock,	medium	5
	2 or more	6	boulder stone,	unstable	3
soil	stable	0	spring water	without spring	3
	medium	0		leakage	3
	fragile	8		spring	2
lithology	stable	0	covering condition	construct	3
	medium	1		compound	2
	fragile	7		vegetation, bare	3
formation	opposite slope	8	height of slopes	$H < 15$	6
	dip slope	0		$15 \leq H < 30$	2
difference of permeability	small	1		$30 \leq H < 50$	0
	medium	6		$50 \leq H$	0
	large	1			

(d) Cluster ④

parameters		number of slopes	parameters		number of slopes
talus cone	0	0	topsoil,	stable	1
	1	0	loose part rock,	medium	3
	2 or more	5	boulder stone,	unstable	1
soil	stable	0	spring water	without spring	2
	medium	0		leakage	2
	fragile	5		spring	1
lithology	stable	0	covering condition	construct	3
	medium	0		compound	0
	fragile	5		vegetation, bare	2
formation	opposite slope	0	height of slopes	$H < 15$	4
	dip slope	5		$15 \leq H < 30$	1
difference of permeability	small	1		$30 \leq H < 50$	0
	medium	4		$50 \leq H$	0
	large	0			

Table 5 shows the final result which is total of Table 4. The result of Table 5 is difference from the result which simply add the number of failed slopes in Table 4 because there are some failed slopes estimated to failed in plural groups. Therefore, Table 5 is the final result which relieve the duplication of the analytical results. From the result of Table 5, all of the failed slopes in the identify data are estimated to failed.

Table 4 Analytical results of each groups by proposed method

(a) Group A

		Real	
		Failed	Not failed
Estimate	Failed	6	2
	Not failed	5	52

(b) Group B

		Real	
		Failed	Not failed
Estimate	Failed	2	8
	Not failed	9	46

(c) Group C

		Real	
		Failed	Not failed
Estimate	Failed	3	15
	Not failed	8	39

(d) Group D

		Real	
		Failed	Not failed
Estimate	Failed	3	0
	Not failed	8	54

Table 5 Final result of proposed method

		Real	
		Failed	Not failed
Estimate	Failed	11	25
	Not failed	0	29

## Discussion

From the results of Table 2 and Table 5, the precision of the analytical results can be improved by using the proposed method. In other words, there are 3 failed slopes in the identify data were estimated to not failed in the case of using only Hayashi's second method of quantification, but all of the failed slopes in the identify data are estimated to failed in the case of using the proposed method. Table 6 shows the result of the priority of identify data according to hazard by proposed method. The slopes with grey color shows the slopes which actually failed, and the slopes with white color shows the slopes which actually not failed. From the result of Table 6, the failed slopes with grey color have relatively higher priority according to hazard. Therefore, the proposed method can identify a lot of slopes with higher hazard and can prioritize the slopes with actually higher hazard. From the above results, the proposed method is sufficiently available to the first step for the disaster prevention planning.

Table 6 Result of priority according to hazard

priority	slope number	difference	priority	slope number	difference
1	U8	2.686	19	Bk	0.420
2	Bb	2.229	20	Ba	0.393
3	V7	1.945	21	Bd	0.368
4	W7	1.917	22	En	0.347
5	V6	1.789	23	X8	0.344
6	T5	1.710	24	Bg	0.230
7	U4	1.597	25	Aw	0.192
8	V1	1.584	26	De	0.192
9	U2	1.564	27	Ed	0.151
10	W1	1.385	28	Bo	0.128
11	T6	1.355	29	Y0	0.128
12	T9	1.331	30	W0	0.055
13	C9	1.312	31	Am	0.028
14	Z4	1.278	32	Ar	0.024
15	U6	1.121	33	Dj	0.024
16	Ej	0.797	34	Bw	0.024
17	Z5	0.700	35	Ch	0.024
18	U5	0.477	36	Bf	0.016

## CONCLUSION

In this study, a method based on information processing techniques was proposed in order to identify the slopes with higher hazard to slope failures. In the proposed method, self-organizing map (SOM), cluster analysis, and Hayashi's second method of quantification were combined. The proposed method

were applied to the periodical inspection data of slopes, and only Hayashi's second method of quantification were also applied to the data. Then, the availability of the proposed method was discussed. The main summarized as follows.

1. SOM, cluster analysis, and Hayashi's second method of quantification can be applied to the periodical inspection data.
2. The failed slopes can be classified into each clusters objectively by combining SOM and cluster analysis.
3. The slopes can be estimated to failed ones or not failed ones by using Hayashi's second method of quantification.
4. The proposed method can make the slopes into order according to hazard of sediment disasters.
5. The availability of the proposed method can be confirmed by comparing the results of proposed method with only Hayashi's second method of quantification.

## ACKNOWLEDGEMENTS

This study was funded by Grant-in-Aid for Scientific Research (24510254), for which I wish to express my gratitude here.

## REFERENCES

- [1] Ministry of Land, Infrastructure, Transport and Tourism, "Instance of Sediment Disasters", <http://www.mlit.go.jp/mizukokudo/sabo/jirei.html>, (2014/07/11) (in Japanese)
- [2] Road Management Technology Center, "Manual of periodical inspection of road (heavy rain, heavy snow)", 2009, pp. 20-37. (in Japanese)
- [3] Okita M, Tokutaka H, Hujimura K, Gonda E, "Self-organizing Maps and Tools", Springer Japan, 2008, pp. 1-13. (in Japanese)
- [4] Murase Y, Takada H, Hirose T, "Multivariate Analysis by SPSS", Ohmsha, 2012, pp. 273-298. (in Japanese)
- [5] Kan T, "Practice of multivariate analysis vol. 2", Company of Modern Mathematics, 2007, pp. 44-116. (in Japanese)
- [6] Ito S, Oda K, Koizumi K, "Method for hazard assessment to deep-seated catastrophic landslides due to heavy rain with both artificial neural network and mathematical statistics", The 14th International Conference of the International Association for Computer Methods and Advances in Geomechanics, 2014.

## HYDRAULIC CONDUCTIVITY IN LOESSIC STABILIZED SOIL

Alercia Biga Carolina<sup>1</sup>, Arrúa Pedro<sup>2</sup>, Eberhardt Marcelo<sup>3</sup>, Aiassa Martinez Gonzalo<sup>4</sup>  
<sup>1,2,3,4</sup> Grupo de Investigación y transferencia en Geotecnia, Estructuras y Fundaciones (GIGEF),  
Departamento de Ingeniería Civil, Facultad Regional Córdoba, Universidad Tecnológica Nacional,  
Argentina

### ABSTRACT

The loessic soils are the main geological storage available as a building material in Cordoba, Argentina. Infiltration tests were done using remoulded samples and a flexible wall permeameter. Water content, dry unit weight, and percentages of ionic stabilizer and bentonite have been studied. Experiment results were compared between mixtures with different percentages of additives. The results show the reduction of hydraulic properties of local soils to improve geotechnical structures.

*Keywords: Silty Clay, Infiltration Test, Flexible Wall Permeameter, Falling Head Method*

### INTRODUCTION

The loess soils have particles from 10 to 50 microns. In Argentina, covering a wide area and are naturally macroporous [1]. The increment in water content cause a dissolution of soluble salts and this reduce the shear strength [2]. In Córdoba city, usually geotechnical properties of loessic soils are modified by compaction or with chemical stabilizers [3]. Addition of sodium bentonite in soil has shown improvement of hydraulic properties [4]. During last year, artificial products have appeared in market, to reduce absorption capacity of loessic soils. In this paper, analyzes and compares the improvement in the hydraulic and mechanical properties of loess by incorporation of bentonite and base polymeric chemical stabilizer. Coefficient of permeability, absorption capacity and stress strain curves are show in this work.

### MATERIALS

#### Loessic soil - Bentonite

The soil used was obtained from boreholes at 1m depth, in Ciudad Universitaria, Córdoba. Sodium bentonite was used, provided by Minarmco SA deposits from Pellegrini Lake, Black River, located at north of Patagonia. Composed of 92% of motmorillonita, and lower percentages of quartz, gibbsite, feldspar, calcite and zeolites. It has a high sodium content product as a result of the presence of soluble salts and cations retained in the thickness of the diffuse double layer. The magnesium comes from octahedral positions of the clay structure, from soluble salts and exchangeable cations. Generally show high proportions of iron between 4% and 6%. It has a high cation exchange capacity, which varies between 76 and 97 meq/100g. The exchangeable

ions are  $\text{Na}^+$ ,  $\text{Ca}^{++}$ ,  $\text{Mg}^{++}$  and  $\text{K}^+$ , with a predominance of sodium cations, hence its classification [5]. It has high plasticity and high swelling capacity. Table 1 presents the principals geotechnical properties of the soils used in this work.

#### Base Polymeric Ionic Stabilizer (BPIS)

BPIS is a viscous liquid, colorless, without odor, miscible in water. It has a ph (13-14) and density is 1.05 gr/cm<sup>3</sup>. BPIS are composed of a biodegradable polymer, mineral salts and cationic surfactant (potassium polyacrylate, potassium hydroxide and Belzanconio chloride). The ionic stabilizer is an argentinian additive provided by Polydem Argentina SA, and it called Poly-Ses 028. The percentages of chemical composition are reserved by industrial protection. The chemical process of soil stabilization is produced by neutralization of the electrochemical activity of the clay particles (with negative electric charge) thus avoiding the adsorption of positive cations from water molecules, and so promote the attraction between particles ground, reducing the empty spaces and consequently increasing the density of the structure. The manufacturer ensures that the stabilizer BPIS modifies the surface tension of water on granular bodies and increases the contact angle of the water present in the interstices of the soil.

### METHODS

#### Soil/Bentonite and Soil/ BPIS mixtures

The materials were collected on trays at 20°C during 24hs. Soil passing sieve 100 was used. Soil

has been drying at 105 °C during 24 hs. The loessic soil comparison specimen was dry unit weight  $\gamma_d$  (kN/m<sup>3</sup>) = 12.4, initial water content  $\omega_{ini}$  (%) = 18.1.

Two groups of soil were selected, (a) loess and bentonite in dry weight in percentages SB1 = 3%, SB2 = 6% and SB3 = 9%, the  $\omega_{ini}$  (%) = 18.2, 18.2, 19.6, the  $\gamma_d$  = 12.8, 12.5, 12.7 respectively, and (b) loessic soil and BPIS with SE1 = 0.5 ‰, SE2 = 1.0 ‰ and SE3 = 1.5 ‰ incorporated in water. The  $\omega_{ini}$  (%) in static compaction was 18.5 16.3 17.7, and  $\gamma_d$  (kN/m<sup>3</sup>) 13.6, 13.7, 13.3 respectively. The specimens were 0.07m in diameter and 0.14m in high. Static compaction method was used to prepare samples, in cylindrical molds. The specimen test was built and compacted in three layers of equal thickness. Extraction of samples was performed using a hydraulic jack. In order to conserve water content, plastic bags were used.

Table 1 Materials properties

Properties	Loess	Bentonite
$\gamma_d$ (kN/m <sup>3</sup> )	12.2-14.5	--
$\gamma$ (kN/m <sup>3</sup> )	14.9-16.8	---
LL (%)	20.8-32.2	301
IP (%)	0-8	231
G <sub>s</sub>	2.68	2.71
P <sub>s</sub> 200 (%)	96	100
Clay content < 0,002 mm (%)	4	85
SUCS	CL-ML	CH
S <sub>s</sub> (m <sup>2</sup> /g)	1	731(*)
Ph	> 8	7-7.5
Sc (%)	0.38	< 0.1

Note:  $\gamma$  = natural unit weight, LL = Liquid limit, IP = Plasticity index, G<sub>s</sub> = Specific gravity, P<sub>s</sub> = passing sieve, S<sub>s</sub> = Specific surface, Sc = salt content. (\*) [12]

### Infiltration test

A flexible wall permeameter was used to evaluate hydraulic properties of samples. Variable-head permeability test was conducted [6].

Loess-bentonite samples were infiltrated in unsaturated and saturated condition. At the ends of each sample, filter paper and porous stones were used. Porous stones were saturated during 24 hours. During infiltration tests, the gradient was 10 [6]. Pressures for the camera, upper and lower head were taken as 117 kPa, 114 kPa and 100 kPa respectively. Deaerated water was used as permeant fluid.

In unsaturated condition, the infiltration rate ( $I_r$ ) is

adopted (Eq. (1)).

$$I_r = \frac{\Delta V(t)}{\Delta t A} \quad (1)$$

Where  $\Delta V$ : volume infiltrate during time  $\Delta t$ ,  $A$ : cross section specimen area. Under saturated condition the permeability parameter  $k$  is obtained with Eq. (2).

$$k = \frac{a L}{A \Delta t} \ln \left( \frac{PB_1 + \frac{V_{u(t_1)} - V_{l(t_1)}}{a}}{PB_2 + \frac{V_{u(t_2)} - V_{l(t_2)}}{a}} \right) \quad (2)$$

Where  $a$ : area of burette,  $L$ : length of sample,  $A$ : area of sample,  $\Delta t$ : lapsed time,  $PBi$ : bias pressure,  $V_{u(ti)}$ : volume reading of upper burette at time  $i$ ,  $V_{l(ti)}$ : volume reading of lower burette at time  $i$ . The saturation level was calculated as  $B = [(u_2 - u_1)/(\sigma_2 - \sigma_1)]$ . Where  $u_2 - u_1$ : increase in pore pressure,  $\sigma_2 - \sigma_1$ : increase in cell pressure. We consider that,  $B$  at 98% is saturation condition [7]. At the end of experiment, the water content was established in each sample.

### Unconfined compression (UC)

For UC test a mechanical press was used instrumented with a load cell with a capacity of 50kN and a digital comparator for recording displacements with a precision of 0.001 mm, to a constant deformation rate of 2.4 mm/min. UC tests is used to evaluate the stress-strain characteristics and the stiffness properties of the Soil-Additive-Mixture. Secant modulus at 1% of axial strain was defined.

### Capillary rise

To set the speed of capillary rise was used a metal container with the addition of distilled water. The specimens were placed on metal cylinders with 0.03 m height and slotted base. It was measured the rise of moisture in function of time.

## RESULTS DISCUSSION

### Infiltration test

The results of infiltration tests were  $\omega$  (3%) = 34.6 %,  $\omega$  (6%) = 26.4 %,  $\omega$  (9%) = 34.7 %,  $\omega$  (0.5 ‰) = 29.2 %,  $\omega$  (1 ‰) = 29.7 %,  $\omega$  (1.5 ‰) = 37.8 % and  $\omega$  (soil) = 29.5%.

Incorporating clay to the silty soil produces a decrease in the infiltration and also on the

permeability coefficient [8]-[10]. No records of permeability tests results were found on remoulded samples with densities near a value  $13 \text{ kN/m}^2$ . Figure 2 shows the response under infiltration conditions for stage was done. In unsaturated conditions, uncontrolled suction level, it has been pretending to simulate field conditions. In unsaturated conditions, non controlled suction level, we have tried to simulate field conditions.

Under saturation condition decreasing permeability coefficients with increasing percentage of bentonite is observed. The minimum value of permeability was obtained for samples with addition of 9% of bentonite.

The permeability parameter magnitudes were,  $k_{SB1} = 1.36 \times 10^{-6} \text{ m/s}$ ,  $k_{SB2} = 1.22 \times 10^{-6} \text{ m/s}$ ,  $k_{SB3} = 8.03 \times 10^{-7} \text{ m/s}$ .

One possible explanation for this behavior is a high exchange capacity cation of sodium bentonite, provided by the presence of sodium ions  $\text{Na}^+$ , providing attraction in the water particles, increasing the thickness of the diffuse double layer. Swelling of the ions  $\text{Na}^+$  also occurs, develop their full potential and affect the hydraulic conductivity. This behavior is accentuated with increasing bentonite

In Figure 2, is shown the hydraulic behavior of the specimens with the addition of stabilizer. It was observed a lower volume of fluid filtered with increases the contained of stabilizer in the blends.

Values being lower permeability, so the lowest permeability value is recorded for samples with 1.5 % stabilizer. The value obtained was  $k = 3.98 \times 10^{-6} \text{ m/s}$ .

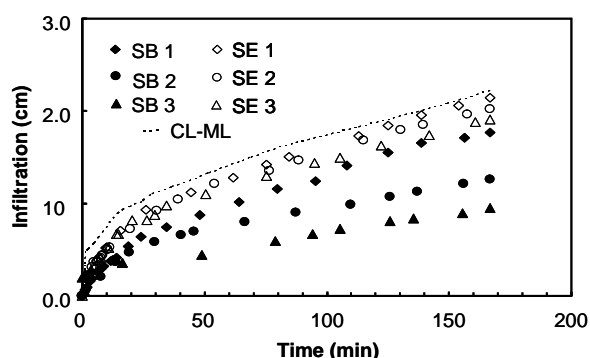


Fig. 2 Infiltration test on soil /bentonite and soil / BPIS samples

### Unconfined compression (UC)

The results of unconfined compression are shown on Fig. 4. The graphic shows that stiffness increase with bentonite content.

The increase of bentonite content causes an increase of the stiffness four times. The values obtained were  $E_{s_{SB1}} = 19.7 \text{ kN/m}^2$ ,  $E_{s_{SB2}} = 25.6 \text{ kN/m}^2$ ,  $E_{s_{SB3}} = 41.8 \text{ kN/m}^2$ .

There is no significant change in stiffness properties in soil-EIBP samples. The increment was

once more and a half. The values obtained were  $E_{s_{SE1}} = 11.6 \text{ kN/m}^2$ ,  $E_{s_{SE2}} = 16.6 \text{ kN/m}^2$ ,  $E_{s_{SE3}} = 16.8 \text{ kN/m}^2$  and  $E_{s_{SOIL}} = 10.1 \text{ kN/m}^2$ .

Higher compression resistance is achieved in samples with bentonite than BPIS samples. The value obtained was  $36.95 \text{ kN/m}^2$ .

### Capillary rise

Figure 4 shows the progress of hydration in the soil-bentonite specimens for capillary rise testing. The velocity of capillary rise increases with the amount of bentonite. Note that no significant difference was observed in samples with 3% and 6%.

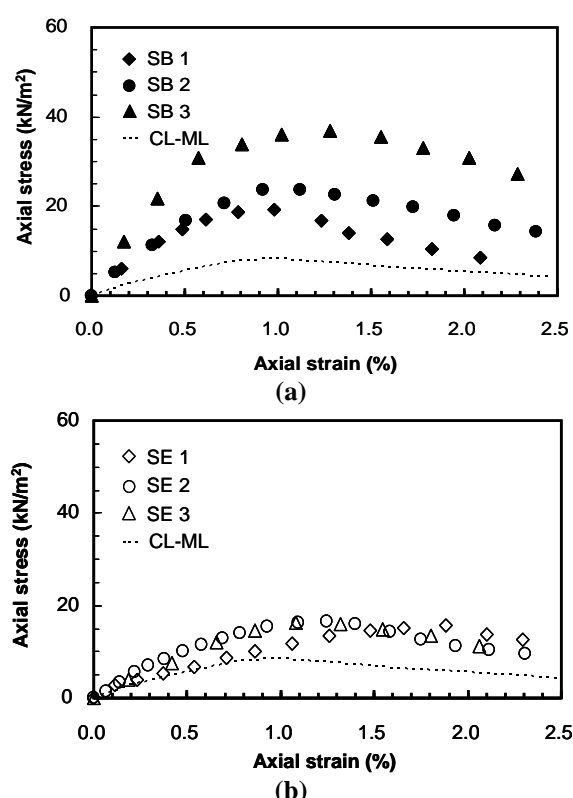


Fig. 3 Stress-strain curves unconfined compression test. (a) Soil/Bentonite. (b) Soil/BPIS

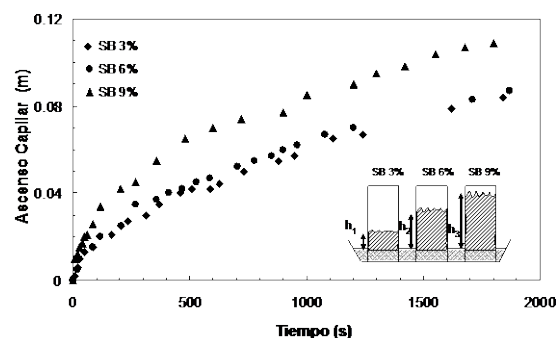


Fig. 4 Capillary rise. Soil/Bentonite

Figure 5 presents the results of the mixtures with ionic stabilizer. The results indicate that the speed of

capillary rise decreases with increasing stabilizer content.

An explanation of the phenomenon is the reduction of the electrostatic potential of the soil particles, precluding its adsorption capacity. Thus, negative charges present in the soil are neutralized, and prevent the absorption of positive charge present in the water molecules, producing an attraction between the solid particles, a rearrangement of the granular bodies and reduction of voids. Consequently, it produces a decrease of the film layer present in the soil particles [11].

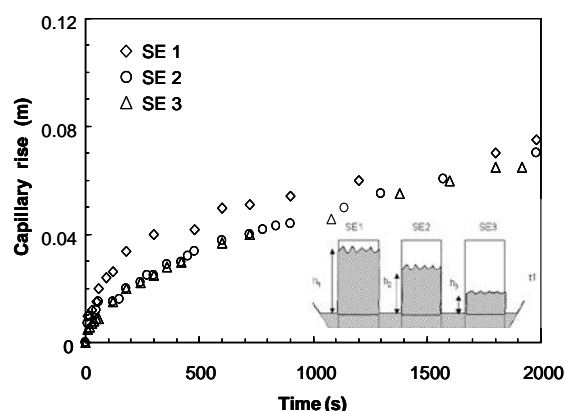


Fig. 5 Capillary rise. Soil/BPIS

An explanation of the phenomenon is the reduction of the electrostatic potential of the soil particles, precluding its adsorption capacity. Thus, negative charges present in the soil are neutralized, and prevent the absorption of positive charge present in the water molecules, producing an attraction between the solid particles, a rearrangement of the granular bodies and reduction of voids. Consequently, it produces a decrease of the film layer present in the soil particles [11].

## CONCLUSION

This paper has presented a study on mixtures of loess soil, bentonite and materials and revised the importance of interparticle interactions and their influence on the mechanical and hydraulically performance of the material. Water content, unit weight, and percentage of stabilizer have been studied. For low unit weights ( $\gamma_d = 13 \text{ kN/m}^3$ ) have been identified the main results as follows:

Hydraulic properties: (a) in unsaturated state, the infiltration volume decreases with increasing content of bentonite. (b) Soil / PBIS shows no reduction in volume infiltration compared to loess soil in the dosage used. In saturated condition, the behavior tendencies are similar to unsaturated conditions.

Unconfined compression: (a) It has been identified that the addition of bentonite increases the compressive strength by 400%. (b) Unconfined

compression test shows no increase of resistance with PBIS addition.

Capillary rise: (a) the capillary rise increase with the content of bentonite. (b) The capillary rise decreases with increase of EIBP content.

## ACKNOWLEDGEMENTS

The authors thanks the support of Universidad Tecnológica Nacional Facultad Regional Córdoba, Ministerio de Ciencia y Tecnología, Gobierno de la Provincia de Córdoba (PID-GRF), and FONCyT Agencia Nacional de Promoción Científica y Tecnológica (PICT).

## REFERENCES

- [1] Aiassa G, Zeballos M, Arrúa P and Terzariol R, "Infiltración en suelos limosos compactados", XIX Congreso Argentino de Mecánica de Suelos e Ingeniería Geotécnica, Octubre 2008, La Plata, Argentina
- [2] Arrúa P, Aiassa G., and Eberhardt M. "Behavior of collapsible loessic soil after interparticle cementation", International J. of GEOMATE, Vol. 1, November-December 2011, pp. 130–135
- [3] Arrúa, P.; Aiassa, G. and Eberhardt, M. Loess soil stabilized with cement for civil engineering applications. International Journal of Earth Sciences and Engineering. ISSN: 0974-5904. Vol. 5, No 1, 2012, pp.10-18
- [4] Aiassa G. and Arrúa P, "Desempeño de barreras sanitarias simples de suelo loessico compactado", Revista Tecnología y Ciencia, Año 8, Noviembre 2009, pp. 26–40.
- [5] Hyang-Sig Ahn, Ho Young Jo, "Influence of exchangeable cations on hydraulic conductivity of compacted bentonite." Journal of Applied Clay Science, Vol 44, 2009. pp.144-150.
- [6] ASTM. D 5084. Standard Test Methods for Measurement of Hydraulic Conductivity of Saturated porous Materials using a Flexible Wall Permeameter.
- [7] Fredlund, D.G; Rahardjo, H; Soils Mechanics for unsaturated soils. John wiley and Sons. 1993. NY. USA.
- [8] Cuisinier, O; Auriol, J.Cl; Le Borgne, T; Deneele, D; "Microstructure and hydraulic conductivity of a compacted lime-treated soil", Journal of Engineering Geology. Vol. 123, 2011 pp.187-193.
- [9] Qiong Wang, Yu-Jun Cui, Anh Minh Tang, Jean-Dominique Barnichon, Simona Saba, Wei-Min Ye "Hydraulic conductivity and microstructure changes of compacted bentonite/sand mixture during hydration". Journal of Engineering Geology. Vol 164, 2013 pp 67-76.

- [10] India Sudhakar M. Rao, Ravi K., “Hydro-mechanical characterization of Barmer 1 bentonite from Rajasthan, India”. Journal of Nuclear Engineering and Design. Vol 265. 2013. pp 330-340.
- [11] Mitchell K. James. Fundamentals of Soils Behavior. Editorial John Wiley and Sons. Inc. 1993.
- [12] Santamarina J., Klein K, Wang Y., and Prencke E. Specific surface: determination and relevance. 2002 Published on the NRC Research Press Web site at <http://cgj.nrc.ca>



## MATHEMATICAL SIMULATION OF PILE INTEGRITY TEST (PIT)

Ramli Bin Nazir<sup>1</sup> and Osman El Hussien<sup>2</sup>

<sup>1</sup>Associate Professor, Faculty of Engineering, Universiti Teknologi Malaysia, <sup>2</sup>PhD Student, Faculty of Engineering, Universiti Teknologi Malaysia

### ABSTRACT

Newly constructed piles are commonly tested using low strain integrity test in order to assess their integrity as part of pile foundation quality control program. Mathematical model based on numerical solution of wave equation, which incorporates soil effects, is formulated. This model accommodates soil resistance effects on the stress wave that propagates in pile body as a result of hammer impact. The numerical analysis is carried out using a computer program, which is developed based on the mathematical modeling of pile integrity test. The simulation program output is compared with real pile integrity test results, and the generated velocity values are found to have good similarity with in-situ test results. New procedure, which identifies pile integrity test limitations based on the established model, is illustrated.

*Keywords: Pile, Integrity, Numerical, Simulation*

### INTRODUCTION

Nondestructive testing techniques are routinely used in construction industry to evaluate material properties, structure components and to assess structure condition and performance without causing damage to the tested element during testing. Nondestructive testing methods are routinely used for quality control and damage assessment for hardened concrete. Static and dynamic load tests are the nondestructive testing techniques, which are widely used for pile foundations. Pile integrity tests are commonly carried out to evaluate the quality of recently constructed piles. Low strain integrity test (PIT) is the most common test used for evaluation of pile integrity.

Pile integrity tests are commonly carried out using acoustic testing techniques. Acoustic science includes the study of energy generation, transmission and reception in matter in terms of vibrational waves. Sonic sensation is the most common acoustic technique that used for assessment of materials. Low strain integrity test of piles involves examining the response of the pile to light impact that creates compressive wave within pile body. The low strain pile integrity test procedure requires measurement and analysis of force and velocity records generated as a result of the excitation at pile top caused by hand held hammer. The PIT equipment should have signal amplification capability to enhance analysis of signals that are reduced by soil and pile material damping. However, it may be difficult in some cases to differentiate between soil and pile responses [1].

A numerical simulation for dynamic testing of piles using Parallel Seismic Test was carried out to assess pile length as well as possible defects in pile

body [6]. An axisymmetric model using finite element techniques was used the pile and surrounding soil. A correction factor was suggested in the study in order to improve the accuracy of the model. The Parallel Seismic Test is considered to be time consuming test, while it requires drilling of receiver borehole adjacent to pile and fixing of receivers at different depths in the receiver borehole. Furthermore, the model was found to be less efficient in simulating real pile testing when the stiffness of soil near pile increases.

The test is carried out by striking pile top with small hammer. Stress wave will be generated as a result of the impact, which travels down pile body to pile bottom where it reflects back. The reflected wave generates measurable pile top displacement, and the pile is considered to be free from major damages when the stress wave is received at the correct time at pile top and no earlier reflections are received. A pile subjected to low strain integrity testing is shown in Fig. 1.



Fig. 1 Concrete pile subjected to low strain integrity test [7].

## MATHEMATICAL SIMULATION

Considering the pile shown in Fig. 2, which is divided to (n) segments, the pile has constant cross sectional area (A) and made of elastic material having a uniform density ( $\rho$ ) and modulus of elasticity (E). The pile is subjected to a dynamic force (F), which caused a linear displacement (w) in the (z) direction at time (t).

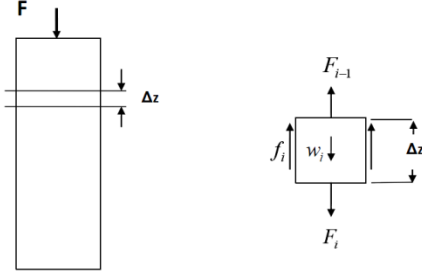


Fig. 2 Schematic diagram of pile subjected to dynamic force, and a selected pile segment.

The applied dynamic force will generate a stress wave, which propagates in pile body. The following equation, which is known as the wave equation, is considered as the basic equation in describing wave motion in pile body.

$$\frac{\partial^2 w}{\partial t^2} = c^2 \frac{\partial^2 w}{\partial z^2} \quad (1)$$

Where,

$$c = \sqrt{\frac{E}{\rho}} \quad (2)$$

The generated wave is subjected to damping effects produced from surrounding soil and pile material. Soil frictional forces are assumed to be proportional to pile segment displacement, while material damping force is proportional to pile segment velocity. Hence, wave equation incorporating soil and material damping effects can be written as follows [8]:

$$\rho A \frac{\partial^2 w}{\partial t^2} = E A \frac{\partial^2 w}{\partial z^2} - M w - C \frac{\partial w}{\partial t} \quad (3)$$

Where, (M) is the proportionality constant between soil frictional force and pile segment displacement, and (C) is pile material damping coefficient.

The (M) is the proportionality constant of the following correlation [5]:

$$f_i = \frac{G_s}{r_0 \cdot \ln\left(\frac{r_m}{r_0}\right)} w_i \quad (4)$$

Where ( $r_0$ ) is pile radius, ( $G_s$ ) is soil shear modulus and ( $r_m$ ) is the lateral distance from pile center where soil vibration caused by the dynamic force applied on the pile diminishes. Eq. (4) was derived considering the concentric cylinders shown in Fig. 3 and the equilibrium of soil element.

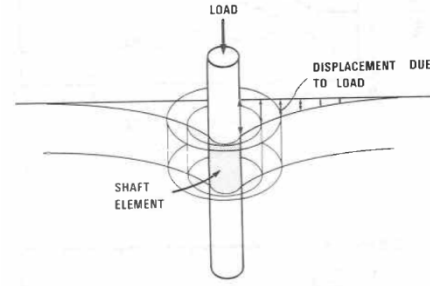


Fig. 3 Concentric shearing cylinders model [5]

In this model ( $r_m$ ) value is estimated using ground vibration attenuation equation [2]:

$$A_1 = A_0 (r_0 / r_1)^{(\gamma)} e^{\alpha(r_0 - r_1)} \quad (5)$$

Where, ( $A_0$ ), ( $A_1$ ) are vibration amplitudes at ( $r_0$ ), ( $r_1$ ) distances respectively, ( $\gamma$ ) is a coefficient depends on wave type and ( $\alpha$ ) is material damping coefficient.

The numerical solutions of Eq. (3) are as follows:

$$F_i - f_i A_{si} - C v_i = \rho A \Delta z \frac{v_i(t + \Delta t) - v_i(t)}{\Delta t} \quad (6)$$

$$v_i = \frac{w_i(t + \Delta t) - w_i(t)}{\Delta t} \quad (7)$$

$$F_i - f_i A_{si} - C v_i = E A \frac{w_{i+1} - w_i}{\Delta z} \quad (8)$$

Where ( $f_i$ ) is the skin friction generated at pile segment, ( $v_i$ ) is the pile segment velocity and ( $A_{si}$ ) is the surface area of that segment.

At pile toe, the force ( $F_r$ ) caused by reflected wave is correlated to the incident force ( $F_i$ ) is:

$$F_r = \left( \frac{Z_p - Z_s}{Z_p + Z_s} \right) F_i \quad (9)$$

Where, ( $Z_p$ ) is pile impedance and ( $Z_s$ ) is soil impedance.

Soil reaction ( $F_R$ ) at pile toe is calculated as per Kagawa correlation [4]:

$$F_R = E_{sb} r_{0b} \delta_{0b} z + 2(1 + \nu_{sb}) \sqrt{\rho_{sb} G_{sb}} r_{0b}^2 \delta_{0b} T_3 \nu_p \quad (10)$$

Where:

$F_R$  = Soil reaction at pile tip  
 $E_{sb}$  = Young's modulus of soil  
 $r_{0b}$  = Radius of pile tip  
 $\delta_{0b}$  = Soil reaction coefficient

$z$  = Pile tip displacement  
 $\nu_{sb}$  = Poisson's ratio of soil at pile tip  
 $\rho_{sb}$  = Soil density at pile tip  
 $G_{sb}$  = Shear modulus of soil at pile tip  
 $T_3$  = Polynomial function coefficient  
 $v_p$  = Pile tip velocity

Force transmission and reflection at pile toe is illustrated in Fig. 4.

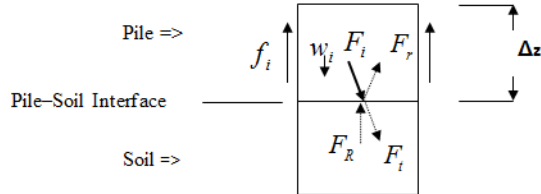


Fig. 4 Force distribution at pile toe

### MODEL PROGRAMMING

The assembled pile integrity test model including pile material and soil effects is programmed using MATLAB technical computing language. The input data is as follows:

Table 1 Program input parameters

No.	Input Parameter
1	Applied force amplitude
2	Number of segments
3	Pile length
4	Pile radius
5	Concrete density
6	Pile elastic modulus
7	Wave velocity in pile
8	Shear wave velocity in soil
9	Shear wave velocity in soil below pile tip
10	Soil density below pile tip
11	Poisson's ratio of soil below pile tip
12	Soil Reaction Coefficient
13	Polynomial function coefficient ( $T_3$ )
14	Concrete Damping Ratio
15	Wave type coefficient
16	Soil damping coefficient

The computer program is designed to carry out iterative calculations in order to analyze each pile segment producing velocity, displacement and force values for each segment. The program can generate automatic graphical output showing velocity,

displacement and force values in time domain. Sample of this graphical output is shown in Fig. 5.

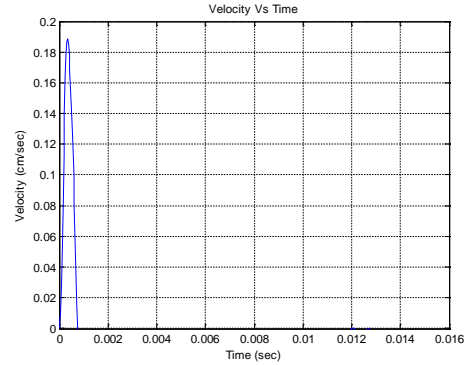


Fig. 5 Velocity at pile top in time domain generated from the computer program

### FIELD DATA COLLECTION

Raw and processed data was collected from a selected project. The project is located in Mesaieed Industrial Area in State of Qatar. Low strain integrity test results of 30 piles were used in the comparison. Pile toes were socketed in Limestone stratum, which is considered as high resistant layer.

There are complete sets of PIT and geotechnical data in this project. This includes borehole logs, pile drilling records, which include subsurface logging during piles construction and bored piles details.

The concrete piles are made of concrete and have nominal diameters of 0.9m. Subsurface condition at pile location consists of soft to medium dense silty sand overlies slightly to moderately weathered limestone stratum. Piles were casted at same tip elevation resulting in rock socket depths ranging from 5.6m to 7.0m approximately. The PIT tester used in the project is shown in Fig. 6.



Fig. 6 PIT tester and accessories

Piles tested using low strain integrity test, are categorized as one of the following categories:  
 Category A: Clear indication of sound pile and pile toe reflection.

1. Category (A1): Indication of sound pile above rock socket.
2. Category B: Clear indication of serious defect in pile.

3. Category C: Indication of possible defective pile.
4. Category D: Conclusion on pile integrity is not definite (Inconclusive).

The second category is associated with piles socketed deeply in bedrock. This category includes pile records do not show major impedance reduction; hence, piles in this category are considered having acceptable integrity with the limitation that this conclusion is for the pile section above rock socket. The fifth category is associated with pile test records that do not show toe reflection. This can be attributed to high soil resistance that dissipates the propagating wave energy [3]. The second and fifth categories show indefinite evaluation of pile integrity; hence, low strain integrity test is considered as inapplicable in the conditions associated with these categories.

### COMPARISON WITH INSITU TESTS

The output generated from the new model was compared with the collected field low strain integrity tests. Test results of 30 piles are used in the comparison. The following pile and soil data are used based on the actual pile details and subsurface soil condition:

Table 2 Pile and soil input data

Item	Value
Concrete Density, $\rho_c$ (t/m <sup>3</sup> )	2.5
Pile elastic modulus, $E$ (kN/m <sup>2</sup> )	$4 \times 10^7$
Pile Radius, $r_0$ (m)	0.45
Soil Density, $\rho_s$ (t/m <sup>3</sup> )	1.80
Rock Density, $\rho_r$ (t/m <sup>3</sup> )	2.30
Rock Poisson's Ratio, $\nu_r$	0.40
Wave velocity in concrete, m/s	4000
Shear wave velocity in soil, m/s	275
Shear wave velocity in rock, m/s	2000
Soil Reaction Coefficient	2.00
Attenuation coefficient( $\gamma$ ) for soil	2.00
Attenuation coefficient( $\alpha$ ) for soil	0.13
Attenuation coefficient( $\gamma$ ) for rock	2.00
Attenuation coefficient( $\alpha$ ) for rock	0.10
Concrete damping coefficient	0.015

Pile influence radial distance ( $r_m$ ) is calculated using Eq. (5) after substitution of the abovementioned pile-soil data. Wave amplitude attenuation trend corresponding to the radial distance is shown in Fig. 7. The velocity amplitudes at pile toe produced from insitu pile integrity test and the amplitudes predicted using the mathematical model are shown in Table 3.

The negative signs indicate upward movement, while the reflected wave, which is received at pile top, causes upward movement of pile.

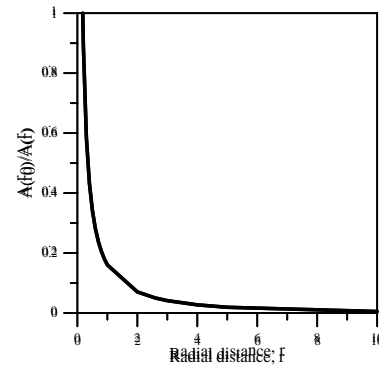


Fig. 7 PIT tester and accessories

Table 3 Velocity amplitudes at pile toe

Pile No.	PIT-W (m/s)	Model (m/s)
P-1	-0.00134	-0.00139
P-2	-0.00242	-0.00192
P-3	-0.00096	-0.00483
P-4	-0.00318	-0.00183
P-5	-0.00089	-0.00223
P-6	-0.00204	-0.0014
P-7	-0.00089	-0.00125
P-8	-0.00099	-0.00155
P-9	-0.00062	-0.00082
P-10	-0.0008	-0.00085
P-11	-0.0006	-0.00041
P-12	-0.0016	-0.00178
P-13	-0.0011	-0.0011
P-14	-0.00217	-0.00129
P-15	-0.00035	-0.00136
P-16	-0.00096	-0.00163
P-17	-0.00169	-0.00155
P-18	-0.00137	-0.00143
P-19	-0.00361	-0.00213
P-20	-0.00028	-0.00102
P-21	-0.00115	-0.00061
P-22	-0.00142	-0.00131
P-23	-0.0003	-0.00137
P-24	-0.00117	-0.00119
P-25	-0.00087	-0.00115
P-26	-0.0008	-0.00119
P-27	-0.00443	-0.00435
P-28	-0.00181	-0.00105
P-29	-0.00242	-0.00307
P-30	-0.00133	-0.00184

The velocity values in time domain for pile P-1 obtained from insitu testing and the mathematical modeling are shown in Fig. 8 and Fig. 9, respectively.

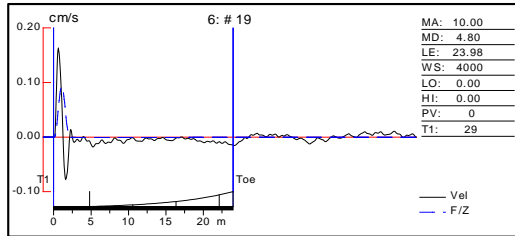


Fig. 8 Insitu velocity curve for pile P-1

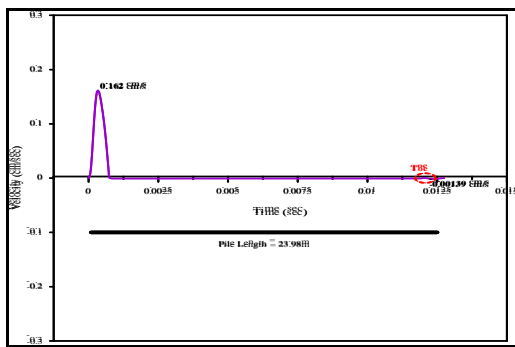


Fig. 9 Model velocity curve for pile P-1

The graphical comparison between the field results and the mathematical model shown in Fig. 10 demonstrates that both sets of results are having good similarity. Note that pile P-3 insitu result is considered as up normal while this pile was subjected to the highest impact force but resulted in a small velocity value received at pile top. Hence, model result for pile P-3 can be considered as more reasonable with respect to the amount of force applied.

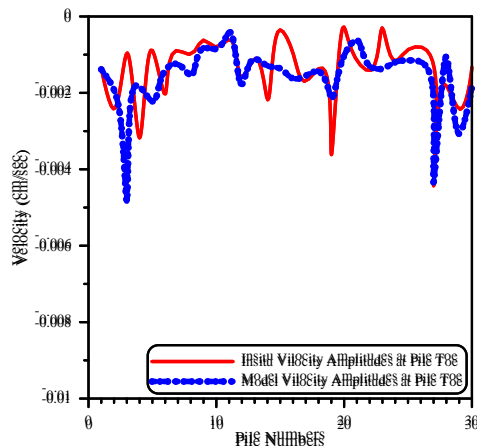


Fig. 10 Velocity amplitudes produced from insitu PIT and the mathematical model

The correlation between velocity amplitudes received at pile top produced from field and model results is shown in Fig. 11.

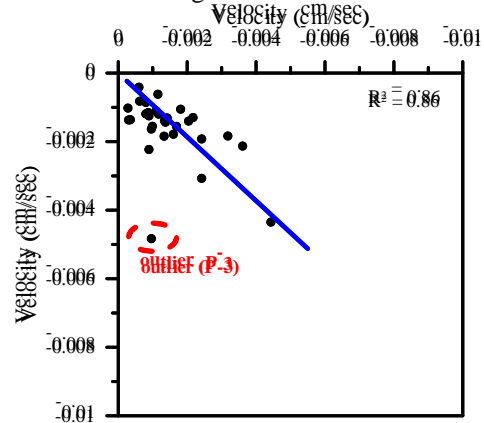


Fig. 11 Correlation between insitu and model velocity amplitudes

## EQUIVALENT IMPEDANCE CONCEPT

A new envelope is introduced, which is the “Equivalent Impedance Envelope”. This envelope can help in assessing the limitations of the PIT test for a certain pile cast in a certain soil strata. This envelope is based on expressing the losses in stress wave strength as change in impedance by calculating the equivalent impedance that causes the same amount of loss. The Equivalent Impedance Envelope for the stress wave amplitudes is shown in Fig. 12. This envelope is plotted for the points where significant change in equivalent impedance occurred, like change in soil layer or at pile toe.

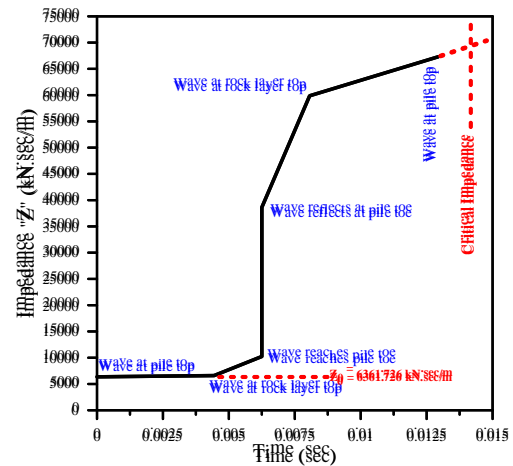


Fig. 12 The Equivalent Impedance Envelope

The “Critical Impedance” is the impedance when reached, the PIT hardware and software will not be able to properly identify the toe reflection; hence, inconclusive result will be reported. This impedance value can be used to identify the PIT test limitations

for certain pile and soil conditions.

## MODEL APPLICATION

The proposed modelling procedure provides a new methodology, which identifies the low strain integrity test limitations through quantifying soil resistance effects computed at pile circumference and pile toe. Furthermore, PIT test applicability can be identified through estimating the critical impedance, which is the impedance value when exceeded; the PIT test is no longer applicable. This helps in assessing the test suitability prior carrying out the test, which provides efficient tool for engineers to decide about including the PIT test in the quality control testing program based on site subsurface condition.

## CONCLUSIONS

The influences of soil friction at pile circumference and soil resistance at pile tip generated during testing of piles using low strain integrity test method are evaluated mathematically.

The mathematical model is based on introducing soil resistance at pile surface and pile toe in the basic wave equation.

The skin friction is assumed to be mobilized proportional to pile displacement, while soil resistance at pile toe is assumed to be caused by the change of impedance as well as the dynamic reaction at pile tip.

The introduced method of analysis had showed comparable results with insitu low strain integrity test results.

A new method, which evaluates low strain integrity test is introduced. This method can be used to evaluate the test limitations based on pile and subsurface soil conditions and the PIT tester sensitivity.

It is required to identify the sensitivity of the PIT equipment in order to assess whether model calculated values at pile toe can be recognized by the equipment or no.

## ACKNOWLEDGEMENTS

The authors would like to thank the Research Management Centre of Universiti Teknologi Malaysia (UTM) and Ministry of Education Malaysia (MOE) for providing financial support through research vote: R.J130000.7822.4L130 for this research.

Appreciation is also extended to Pile Dynamic Incorporation for providing the technical support related to PIT-S software.

## REFERENCES

- [1] American Society of Testing and Materials (ASTM), 2013, Section 4, Vol. 04.09, ASTM D5882, Standard "Test Method for Low Strain Impact Integrity Testing of Deep Foundations".
- [2] Amick, H., and Gendreau, M., "Construction Vibrations and Their Impact on Vibration-Sensitive Facilities". 2000. Proc., ASCE Construction Congress 6, Orlando Florida, pp. 1-10.
- [3] GRL Shaft Integrity Report No. 095017, March 2009, Qafco-5 Project, Mesaied, Qatar.
- [4] Kagawa T., "Dynamic Soil Reaction to Axially Loaded Piles", Journal of Geotechnical Engineering, Vol. 177, No. 7, July 1991.
- [5] Kraft, L. M., Ray, R. P., and Kagawa, T. (1981). Theoretical t-z curves, Journal Geotechnical Engineering Division, Proceedings Paper 16653, American Society of Civil Engineers, Vol 107(GT11).
- [6] Liao S., Tong J., Chen C., Wu T., "Numerical simulation and experimental study of Parallel Seismic test for piles", International Journal of Solids and Structures, 43, 2006.
- [7] Pile Dynamic Incorporation (PDI), Cleveland, Ohio, USA.
- [8] Rodriguez J. and Restrepo, V., September, 2008. Analytic Solution for one-dimensional propagation of waves and its adaptation to Results Interpretation of Pile Integrity Test (PIT). Proceedings of the Eighth International Conference on the Application of Stress Wave Theory to Piles 2008: Lisbon, Portugal.



## **DEVELOPING DESIGN TOOLS FOR SHEET PILE WALLS**

Chane Brits<sup>1</sup> and Jim Shiau<sup>1</sup>

<sup>1</sup>Faculty of Engineering and Surveying, University of Southern Queensland, Australia

### **ABSTRACT**

Nowadays, the engineering profession is discovering and using the computational powers of computer spread sheets in practice. They are used in bid preparation, budget, control, engineering design computation, and many other areas. However, the computational power of the computer-spread sheet is only the beginning of what can be accomplished. Success of geotechnical works relies on important factors such as proper planning, analysis and design of sheet pile walls. This paper aids in understanding the conventional methods used in the design of sheet pile walls better known as the limit equilibrium methods. It is aimed to develop an automated excel spread-sheet to be used in the engineering and geotechnical industry suitable for any sheet pile wall design by means of using the above mentioned methods.

*Keywords: FLAC, Sheet pile wall, Design, Analyses, Stability*

### **INTRODUCTION**

Sheet piles are widely used as retaining structures, especially in excavation support systems, slope stabilization, floodwalls, and waterfront structures. Sheet pile walls are known to be flexible structures, thus when the sheet pile moves away and into the soil respectively, active and passive pressure zones form on either side of the sheet pile wall. Thus when designing sheet pile walls it is necessary to determine the net pressure distribution exerted on the sheet pile for stability purposes as well as determining the bending moment distribution along the sheet pile wall for structural design purposes. This can be determined by means of analytical methods that have been around for many years [1] [2].

The analytical methods normally consist of many equations and may take a long time to solve by hand. Computers on the other hand has evolved over the past few decades and developing an automatic excel spread sheet in excel for design purposes decreases the time required to solve the equations as well as decreasing the possibility of any human errors that may occur. Although the analytical methods give a good indication of the soil-pile system, the hypotheses on which these methods are based upon are very conservative. Hence why developing numerical models in commonly known industrial available software programs such as Flac and Plaxis may be undergone in the future. This enables further information to be obtained, such as the wall

deformation, ground settlement and the location of failure surfaces.

### **CANTILEVERED AND ANCHORED SHEET PILE WALLS**

Sheet pile walls used to provide lateral earth support could be classified as either cantilever or anchored depending on the wall height requirements. Cantilever sheet pile walls are usually used with low wall height between 3-5 m and sometimes less due to limitations in availability of certain section modulus and their costs [3].



Fig. 1 Cantilever Sheet Pile (Hauraki Pilling LTD)

Cantilever sheet pile walls are suitable for places with tight space constraints due to the narrow base width of the cantilever wall.



This type of sheet pile wall depends on the passive resistance of the foundation material in front of the wall and the moment resisting capacity of the piles for stability. Therefore, it should not be used, where the foundation material may be removed during wall service life [4].

The anchored sheet pile walls are required when the wall height exceeds 5 m or when the lateral wall deflection is limited for design consideration [5]. Anchoring the sheet pile wall requires less penetration depth and also less moment to the sheet pile because it will drive additional support by the passive pressure on the front of the wall and the anchor tie rod. Anchored sheet pile walls are typically constructed in cut situations, and may be used for fill situations with special design consideration to protect the anchor from construction damage that may be happened by fill placement and fill settlement [3].



Fig. 2 Macalloy Anchored Sheet Pile (Iceland, 2002)

## POSSIBLE FAILURE MECHANISMS

Several failure modes for a sheet pile system must be considered in the design process. It is of upmost importance in design not for the sheet pile wall system to fail is it can lead to death and community disruption. These failures are known to be, deep-seated failure, rotational failure due to pile penetration inadequacy, overstressing of the sheet pile, and anchorage component failure. An investigation of load capacity of piles subjected to combined loading was performed; due to the fact that second-order bending effects reduce the lateral load capacity of the wall when piles are exposed to combined axial and lateral loads.

Deep-seated failure occurs when the complete soil

mass, containing the retaining wall system, rotates along a single failure surface. This type of failure is classed as a soil failure only, independent of the structural capacities of the wall and any anchorage system. Another form of rotational failure occurs when the retaining wall rotates due to the exerted soil pressures.

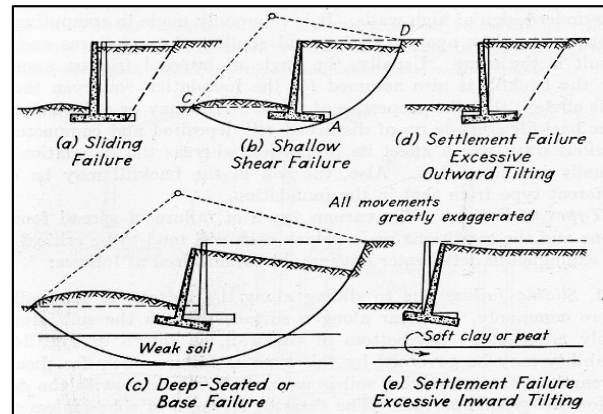


Fig. 3 Failure modes for cantilevered sheet pile walls [5]

The prevention of this type of failure can occur due to adequate wall penetration into the soil or by implementing an anchorage system.

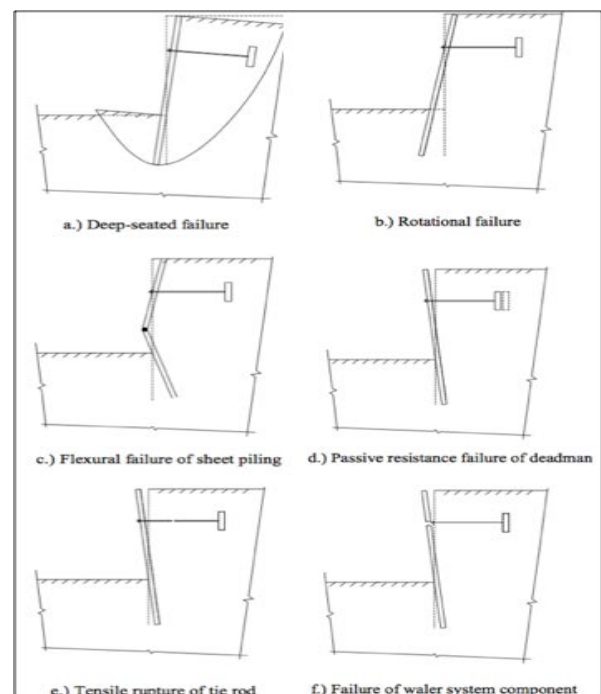


Fig. 4 Failure modes for anchored sheet pile walls [4]

The other failures that may occur in retaining wall systems are sheet pile overstressing, passive anchorage failure, tie rod failure and wale system failure. In the occurrence of pile overstressing due to both lateral and axial loads, a plastic hinge leading to failure will develop as a result. When the anchor moves laterally within the soil due to the force exerted on the anchor a passive anchorage failure will occur. The tie rod may fail if the required tensile capacity is not adequate, and the wale system may undergo a bearing failure if the loads are not evenly distributed.

### THE ANALYTICAL DESIGN PROCEDURE

The following analytical design methods for cantilever sheet pile walls have only briefly been discussed due to the conference paper limitations.

There are several sheet pile walls design methods, dating back from the first half of the 20<sup>th</sup> century; these original proposals have continuously and may currently being reviewed. Analytical methods are used for establishing equilibrium of the horizontal forces and moments developed along the wall, to define the embedment depth below the dredge line for either cantilever or anchored sheet pile walls by means of undergoing geotechnical design calculations. This paper based the necessary design calculation upon the earth pressures theories derived by Rankine. The Rankine theory assumes that the sheet pile wall has introduced no change in the shear stress at the soil-structure interface.

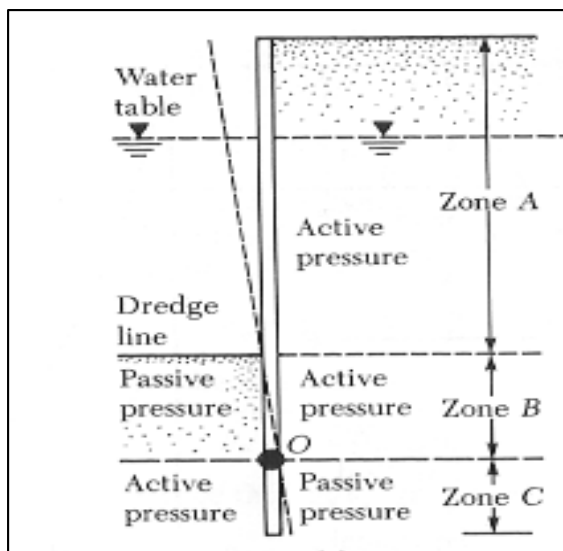


Fig. 5 Active and Passive Pressure Distribution [2]  
It has been assumed that straight planes represent the ground and failure surfaces and that the resultant

force acting on the backfill slope is acting in a parallel direction. Both active and passive pressure zones will develop on either side of the sheet pile wall as shown in the figure 5. When the sheet pile wall moves away from the soil an active pressure zone is formed however when the sheet pile wall pushes into the soil it forms a passive pressure zone.

To develop the relationship for the proper depth of embedment of sheet piles driven into a granular soil, for a visual representation reference is made to figure 6.

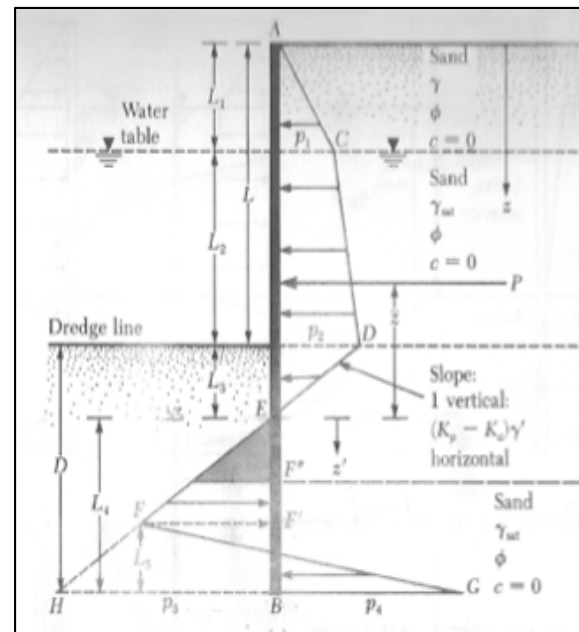


Fig. 6 Cantilever sheet piling penetrating sandy soils [2]

Due to the development of active and passive pressures on either side of the sheet pile wall, it is necessary to determine both Rankine's active and passive pressure coefficients:

$$K_a = \tan^2 \left( 45 - \frac{\phi}{2} \right) \quad (2-1)$$

$$K_p = \tan^2 \left( 45 + \frac{\phi}{2} \right) \quad (2-2)$$

It is important to note that after a geotechnical survey had been done, the designer will know certain input parameters. This is important information as it gives knowledge about the type of soil, the friction angle of the soil, the length above the dredge line as well as the soil cohesion.

Knowing this input data the active pressure on the right side of the sheet pile wall can now be determined:

$$p_1 = \gamma L_1 K_a \quad (2-3)$$

$$p_2 = (\gamma L_1 + \gamma' L_1) K_a \quad (2-4)$$

Indicated on figure 6 it is clear that the net pressure will be equal to zero at the point E, hence by using the ratio given as 1 vertical to  $\gamma'(K_p - K_a)$  in the horizontal the unknown length  $L_3$  can be determined:

$$L_3 = \frac{p_2}{\gamma'(K_p - K_a)} \quad (2-5)$$

The total pressure above the dredge line can now be determined by applying the area of known pressure exerting on the sheet pile wall and summing all the forces in the horizontal:

$$P = 0.5 p_1 L_1 + p_1 L_2 + 0.5(p_2 - p_1)L_2 + 0.5 p_2 L_3 \quad (2-6)$$

Summing the moments of all the pressure forces exerted on the wall about point E and dividing by the total pressure force P will provide the distance  $\bar{z}$  from E to the force P.

$$\bar{z} = \frac{\left[ 0.5 p_1 L_1 * \left( \frac{L_1}{3} + L_2 + L_3 \right) + p_1 L_2 * \left( L_3 + \frac{L_2}{2} \right) + 0.5(p_2 - p_1)L_2 * \left( L_3 + \frac{L_2}{3} \right) + 0.5 p_2 L_3 * \frac{L_3}{3} \right]}{P} \quad (2-7)$$

Thus the only unknown is the length of  $L_4$ , which is determined by deriving four equations containing the unknown length  $L_4$  by the formation of an equation for  $p_3$  by using the given ratio of 1 vertical to  $\gamma'(K_p - K_a)$  in the horizontal (2-8), determining the net pressure  $p_4$  at the bottom of the sheet pile by subtracting the total active pressure from the total passive pressure (2-9), summing the moments about the point B at the bottom of the sheet pile (2-10) and deriving an equation for the length  $L_5$ , which forms apart of the unknown length  $L_4$  (2-11):

$$p_3 = L_4(K_p - K_a)\gamma' \quad (2-8)$$

$$p_4 = (\gamma L_1 + \gamma' L_2)K_p + \gamma' L_3(K_p - K_a) + \gamma' L_4(K_p - K_a) \quad (2-9)$$

$$P(L_4 + \bar{z}) - (0.5 L_4 p_3) \left( \frac{L_4}{3} \right) + 0.5 L_5(p_3 + p_4) \left( \frac{L_5}{3} \right) \quad (2-10)$$

$$L_5 = \frac{p_3 L_4 - 2P}{p_3 + p_4} \quad (2-11)$$

The four equations above are then rearranged to determine  $L_4$ , solving an equation to the fourth power:

$$L_4^4 + A_1 L_4^3 - A_2 L_4^2 - A_3 L_4 - A_4 = 0 \quad (2-12)$$

Where  $A_1, A_2, A_3$  and  $A_4$  are given by [2]:

$$A_1 = \frac{p_5}{\gamma'(K_p - K_a)} \quad (2-13)$$

$$A_2 = \frac{8P}{\gamma'(K_p - K_a)} \quad (2-14)$$

$$A_3 = \frac{6P[2\bar{z}\gamma'(K_p - K_a) + p_5]}{\gamma'^2 (K_p - K_a)^2} \quad (2-15)$$

$$A_4 = \frac{P[6\bar{z}p_5 + 4P]}{\gamma'^2 (K_p - K_a)^2} \quad (2-16)$$

Where  $p_5$  is the passive pressure applied above point E, thus the decline in active pressure right above point E due to the large passive pressure being exerted on the left side of the sheet pile wall:

$$p_5 = (\gamma L_1 + \gamma' L_2)K_p + \gamma' L_3(K_p - K_a) \quad (2-17)$$

Knowing the length  $L_4$ , the sheet pile penetrating depth is simply:

$$D_{theoretical} = L_3 + L_4 \quad (2-18)$$

As a designer it is important to note that a certain factor of safety (FOS) has to be satisfied to avoid any possibility of the soil-system failure. This depends on the designer whether to apply a FOS to the calculated sheet pile penetrating depth, or to decrease the over estimated Rankine's passive pressure coefficient.

As mentioned earlier it is important to determine the maximum bending moment distributed on the sheet pile wall for design purposes. Thus we analyse the sheet pile as a normal beam to find the point of zero

shear force, hence at this point the maximum bending moment will occur:

$$Z' = \sqrt{\frac{2P}{(K_p - K_a)\gamma'}} \quad (2-19)$$

$$M_{max} = P(\bar{z} + Z') - [0.5\gamma'Z'^2(K_p - K_a)]\left(\frac{Z'}{3}\right) \quad (2-20)$$

### THE EXAMPLE

The following example is solved analytically using the analytical design approach discussed in the previous section. The example will also be solved in an excel spread sheet developed in the next section so that the relevance of developing design tools for sheet pile walls can be understood.

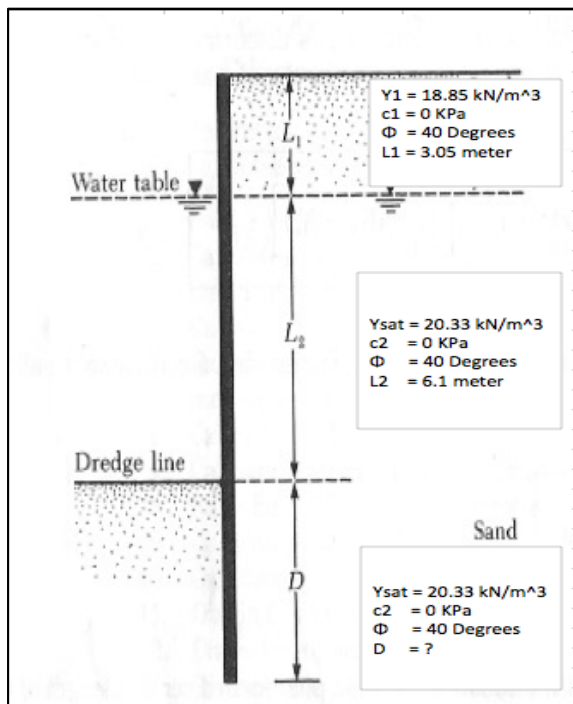


Fig. 7 Cantilever Sheet Pile penetrating sand [2]

After a geotechnical survey had been done, certain input parameters will be known. These input parameters give important information such as the length  $L_1$  and  $L_2$  above the dredge line. For the example in figure 7, the cohesion  $c_1$  and  $c_2$  of the soil has zero cohesion and the sheet pile wall is only penetrating sand. Also the friction angle  $\phi$  and the unit weight  $\gamma$  and saturated unit weight  $\gamma_{sat}$  of the sand are given in figure 7. Using equations (2-1) to

(2-20), the obtained solutions from this example are tabulated in table 1.

$L_4$	=	6.048 m
$D_{theor}$	=	6.62 m
FOS	=	1.3
$D_{actual}$	=	8.61 m
$L_{tot}$	=	17.76 m
$M_{max}$	=	779.18 kN.m

Tab. 1 Output for specific problem

The stability of sheet pile walls depends on the passive resisting capacity of the soil below the depth of excavation to prevent overturning. The depth of the sheet pile walls below the dredge line is determined by the difference between passive and active pressures acting on the wall. The theoretical depth ( $D_{theor} = 6.62 \text{ m}$ ) of penetration below the dredge line is obtained by equating horizontal forces by taking the sum of moments about an assumed bottom of piling. The designers would have to apply a FOS, normally between 1.2 and 1.4, to provide additional penetration depth such as  $D_{actual} = 8.61 \text{ m}$  in Table 1 to finalise their design.

The solutions obtained from the analytical methods should then be validated, by comparing with the solutions obtained from the excel spread sheet. This will be discussed in the following section.

### DEVELOPMENT OF EXCEL SPREAD SHEET

It was aimed at developing a spread sheet to automatically solve the complex derived analytical equations by means of only entering the known input data by the user clearly indicated by the labelled cells in Fig. 8.

INPUT DATA ONLY			
ABOVE WATER TABLE			
Depth of first soil layer	L1	=	3.05 m
unit weight of soil of the first layer	y1	=	18.85 kN / m <sup>3</sup>
cohesion of soil	c1	=	0 kN / m <sup>2</sup>
angle of friction of the soil for the first layer	phi	=	40 degrees
ABOVE THE DREDGE LINE			
Depth of second soil layer	L2	=	6.1 m
unit weight of soil of the second layer	ysat	=	20.33 kN / m <sup>3</sup>
cohesion of soil	c2	=	0 kN / m <sup>2</sup>
angle of friction of the soil for the first layer	phi	=	40 degrees
effective unit weight of soil $y' = ysat - y_{water}$	y'	=	10.52 kN / m <sup>3</sup>

Fig. 8 Required Input Data

The analytical equations are identified in the excel spread sheet under automatic analysis:

AUTOMATIC ANALYSIS	
$Ka = \tan^2(45 - \phi/2)$	$Ka = 0.217$
$Kp - Ka$	$Kp - Ka = 4.381$
$p1 = \gamma * L1 * Ka$	$p1 = 12.5 \text{ kN / m}^2$
$\gamma1 * L1$	$= 57.5 \text{ kN / m}^2$
$\gamma' * L2$	$= 64.16 \text{ kN / m}^2$
$\gamma' * L3$	$= 6.038 \text{ kN / m}^2$
$p2 = (\gamma L1 + \gamma' L2) Ka$	$p2 = 26.45 \text{ kN / m}^2$
$L3 = p2 / \gamma' (Kp - Ka)$	$L3 = 0.574 \text{ m}$
Area of Pressure diagram of layer 1	$P1 = 19.07 \text{ kN / m}$
Area of Pressure diagram of layer 2	$P2 = 118.8 \text{ kN / m}$
Area of Pressure diagram of layer 3	$P3 = 7.593 \text{ kN / m}$
Total area Pressure diagram	$Ptot = 145.5 \text{ kN / m}$
Centre of pressure of Area ACDE	$zbar = 3.68 \text{ m}$
$p5 = (\gamma L1 + \gamma' L2) Kp + \gamma' L3 (Kp - Ka)$	$p5 = 586.0 \text{ kN / m}^2$
$A1 = p5 / \gamma' (Kp - Ka)$	$A1 = 12.71$
$A2 = 8P / \gamma' (Kp - Ka)$	$A2 = 25.25$
$A3 = 6P * [2 * z * \gamma' (Kp - Ka) + p5] / \gamma'^2 * (Kp - Ka)^2$	$A3 = 380.2$
$A4 = P (6 * z * p5 + 4 * P) / \gamma'^2 (Kp - Ka)^2$	$A4 = 926.1$
depth of L4^4/4 using goal seek tool	$L4^4/4 = 24.19$
$\gamma = L4^4/4 + A1 * L4^3/3 - A2 * L4^2/2 - A3 * L4 - A4$	$\gamma = 7E-07$
$p3 = L4 * (Kp - Ka) \gamma'$	$p3 = 278.7 \text{ kN / m}^2$
$p4 = (\gamma L1 + \gamma' L2) Kp + \gamma' D (Kp - Ka)$	$p4 = 864.7 \text{ kN / m}^2$
depth of L5	$L5 = 1.22 \text{ m}$
$p6 = p2 - (D - L5) * (Kp - Ka) * \gamma'$	$p6 = -222 \text{ kN / m}^2$
Total length of sheet piles Ltot = L1 + L2 + D	$Ltot = 15.77 \text{ m}$
Total length of sheet pile by increasing the depth with a FOS	$* L * = 17.76 \text{ m}$
Total length of sheet pile by decreasing Kp with a FOS	$! L ! = 0 \text{ m}$
Point of zero shear force $Z' = \sqrt{(2 * P) / (Kp - Ka) * \gamma'}$	$Z' = 2.51 \text{ m}$

Fig. 9 Automatic analysis solved in excel

The important output figures such as length  $L_4$ , theoretical depth  $D_t$ , actual depth  $D_a$  and maximum bending moment  $M_{max}$  are indicated in figure 10.

Depth Of L4	$L4 = 6.047 \text{ m}$
Total Theoretical Depth Of Embedment $D = L4 + L3$	$Dt = 6.62 \text{ m}$
Total Actual Depth of Embedment $D = (L4 + L3) * FOS$	$Da = 8.61 \text{ m}$
Max Bending Moment $Mmax = P(z+Z) - [0.5\gamma' Z^2(Kp-Ka)]/[Z/3]$	$Mmax = 779 \text{ kN.m}$

Fig. 10 Output data

Due to the fact that the analytical methods and calculations does not provide the outputs graphically, a simple table has been developed to give graphical visual outputs for the deformation, shear force and bending moments distributed along the sheet pile wall in this development.

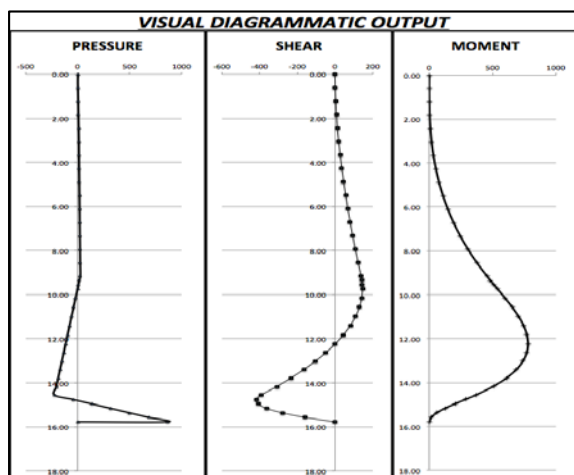


Fig. 11 Visual Diagrammatic Output Figures

The development of this excel spread sheet is useful in the design of sheet piles for undergoing parametric studies to make relevant comparisons and being able to get a result immediately with only changing the input data.

## CONCLUSION AND FUTURE WORK

Designing sheet pile walls using the analytical methods is a very tedious procedure and may take a long time. In the Engineering Industry time is money and being able to develop this design tool that can solve these equations automatically with the same accuracy, creating visual solutions and doing all of this in a much faster time with only the necessity of inputting known data, is a fantastic tool. The solutions obtained using the excel spread sheet is similar to the solutions derived from the analytical methods, thus the excel spread sheet has been proven both accurate and successful. Such a design tool is definitely needed and can be most valuable in the engineering industry.

However these analytical methods of design, has found to be very conservative due to several simplifications and assumptions made. Things like the ground settlement and possible surface failures are important information and cannot be obtained from the analytical methods. For future work, it is proposed to use numerical modeling such as FLAC 2D software to analyze soil-structure interaction and obtain critical information to provide higher accuracy of results.

## REFERENCES

- [1] J.E. Bowles, *Foundation Analysis and Design*, 5th ed. New York: McGraw-Hill, 1996.
- [2] Braja M. Das, *Principles of Foundation Engineering*, 3rd ed. Boston: PWS- KENT Publishing Company, 1990.
- [3] Geotechnical Engineering Bureau, *Geotechnical Design Procedure for flexible wall systems.*: New York State Department Of Transportation, 2007.
- [4] California Depratment Of Transportation, *Retaining Walls Design.*: Bridge Design Specifications, 2004.
- [5] Whitney Clark Huntington, *Earth pressures and Retaining Walls.*: Wiley, 1957.

## SETTLEMENT BEHAVIOR OF DREDGED CLAY RECLAIMED LAND BY VACUUM CONSOLIDATION METHOD AND PROPOSAL OF ITS PREDICTION

Ikeda<sup>1</sup> H., Kawano<sup>1</sup> M., Kiyoyama<sup>1</sup> T., Yamamoto<sup>2</sup> S., Takase<sup>2</sup> E., Katagiri<sup>3</sup> M., Ohishi<sup>3</sup> K. and Yoshifuku<sup>3</sup> T.

<sup>1</sup>Kyushu Regional Construction Bureau, MLIT; <sup>2</sup>Coastal Development Institute of Technology;

<sup>3</sup>Nikken Sekkei Civil Engineering, Japan

### ABSTRACT

One of the methods for increasing the capacity of disposal pond for dredged marine clay is the reduction of volume in already reclaimed dredged clay ground. In the vacuum consolidation method, the pore water in the reclaimed clay ground is squeezed by vacuum pumps, and ground surface settles. In this paper, the monitoring results of reclaimed land with dredged clay by the vacuum consolidation method are introduced. In addition, the results of reclamation analysis to obtain initial condition of reclaimed land before acting of vacuum pressure, the prediction and post analysis of ground behavior in the vacuum consolidation are described. The prediction procedure of vacuum consolidation method is proposed, and its evaluation is reported.

*Keywords: Dredged Clay, Vacuum Consolidation, Monitoring, Analysis*

### INTRODUCTION

The dredging of sea bottom sediment has been continuously conducted along the Japanese coastal area. One of the major purposes of dredging is the widening and deepening of existing navigation channels and anchorage areas to accommodate larger ship traffics. Dredging process normally comprises three phases that starts with the underwater excavation, then transportation and ends with disposal. The most common disposal method for dredged clay is to discharge dredged clay into a disposal pond in the sea surrounded by containment dikes.

As the construction of a disposal pond in the sea requires huge cost in general, it is becoming difficult to construct a new one. Therefore, the long use of existing disposal ponds has become important and urgent technical issue.

While the dredged clay is discharged into the pond, the clay layer increases its thickness and gradually approaches to the capacity of disposal pond. In parallel to the above process, the dredged clay layer is subjected to time-dependent self-weight consolidation and reduces its volume. Therefore the water content and consolidation characteristics of dredged clay at the time of discharging are influential factors for the life of disposal pond.

One of an extension of the life of disposal pond is the reduction of volume in already reclaimed dredged clay ground. The vacuum consolidation method with vertical drainage is one of ground improvement methods for very soft ground. In this method, the atmospheric pressure as the loading pressure is used, and the banking of fill materials is not necessary. The maximum pressure, however, may be 70 to 80 kPa at most due to the effectiveness of vacuuming pump.

At a part of the S3-area in Shin-Moji Oki disposal pond, a vacuum consolidation method was performed. In this paper, a construction example of the vacuum consolidation method for the reclaimed land with dredged clay is introduced. The results of monitoring and soil investigation after the vacuuming are described. In addition, the pre-analysis and post analysis for the vacuum consolidation method are reported. The key point of prediction of vacuum consolidation method for reclaimed land with dredged clay is emphasized.

### OUTLINE OF SHIN MOJIOKI DISPOSAL POND

Figure 1 shows the Strait of Kanmon between the Honshu and Kyushu Islands in Japan. Kanmon waterway located in this Strait is one of the busiest sea routes in Japan. To accommodate larger ship traffics, the dredging in this waterway has been conducted. For the protection of marine environment,



Fig. 1 Site of Shin-Moji Oki disposal pond



dredged materials, mostly clays have to be discharged into the Kanda Oki and Shin-Moji Oki disposal ponds shown in Fig.1.

Figure 2 shows the plan view of Kanda Oki and Shin-Moji Oki disposal ponds. The Shin-Moji Oki disposal pond is separated into three areas, S1-, S2- and S3-areas. The S1- and S2-areas were reclaimed at early stage, and are used as airfield. The S3-area is working as disposal pond at present. The rest capacity of S3-area decreases gradually, and the mud surface will arrive at the designed level in the next years.

In the S3-area, the additional embankment that constructed with mechanical dewatered clay lumps is mounted near the revetment for an increase in the capacity of disposal pond. The mechanical properties of dewatered clay lumps and its aggregates were reported by Moriki et al.<sup>1)</sup>.



Fig. 2 Plan view of disposal pond

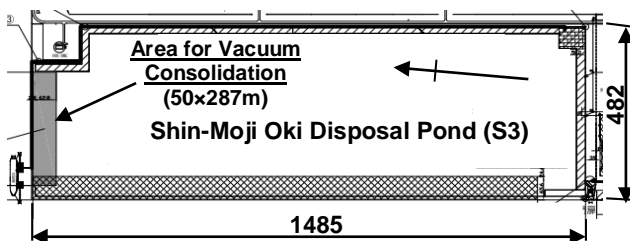


Fig. 3 Condition of S3-area

## MONITORING PLAN FOR VACUUM CONSOLIDATION

Figure 4 shows the schematic cross section of vacuum consolidation area near the North revetment. The left hand side is the North revetment constructed

with rubble mound and replaced sand. The original elevation of sea bottom was DL-6.7 m, and the alluvial clay having about 7 m of thickness overlaid the diluvial layer. The elevation of revetment was DL+8.0 m, and that of dredged clay layer was at DL+6.2 m.

In the design of vacuum consolidation, the upper and lower sealing layers were determined as 1 m of thickness according to the manual of vacuum consolidation drain method<sup>2)</sup>. The void water squeezed from dredged clay layer by vacuuming was gathered into horizontal tubes, and was flowed through them up to the vacuum pump. For the control of vacuum pressure, the origin, edge and tip pressures shown in Fig. 4 were measured. The origin pressure was the value of a vacuum pump. The edge and tip pressures were measured at the end of horizontal tube on the ground and at the tip of plastic board drain (PBD) as a vertical drain, respectively.

The pitches of vertical drains were set at 1.0 m and 1.7 m in the S-type area and R-type area, respectively. Here, the R-type area was designed as a buffer zone of vertical settlements between S-type and non-treatment areas.

The settlement plates were set at the grid with intervals of about 10 m. After about 30 days from the stop of vacuuming, the post soil investigations at the center of the S-type area and near the boundary of the R-type were performed at four lines and as shown in Fig. 4.

## VACUUMING AND MONITORING RESULTS

Figure 5 shows the settlement behavior of vacuum consolidation area measured by the settlement plates. The number of horizontal axis is the construction points from the edge of west revetment, and S-1 through S-4 are the positions of settlement plate in Fig. 4. In the initial condition before the installing of PBDs, the elevations were around 6.2 m. Figure 5 (a) is the state at the end of June before the vacuuming. The maximum consolidation settlement is about 1.2 m due to the disappearance of excess pore water pressure occurred after the installation of PBDs. Figure 5 (b) shows the ground elevations on

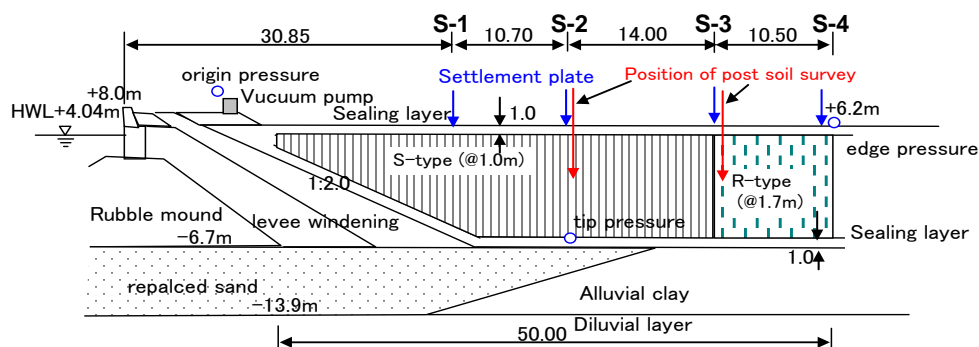


Fig. 4 Design of ground improvement and monitoring plan in vacuum consolidation



12/02/2013 and that was one month later after stopping the vacuuming. The total settlements after the installation of PBDs were 1 to 3 m. The maximum settlement of about 3 m generated around the cross point of No. 32 and S2 (No. 32-2).

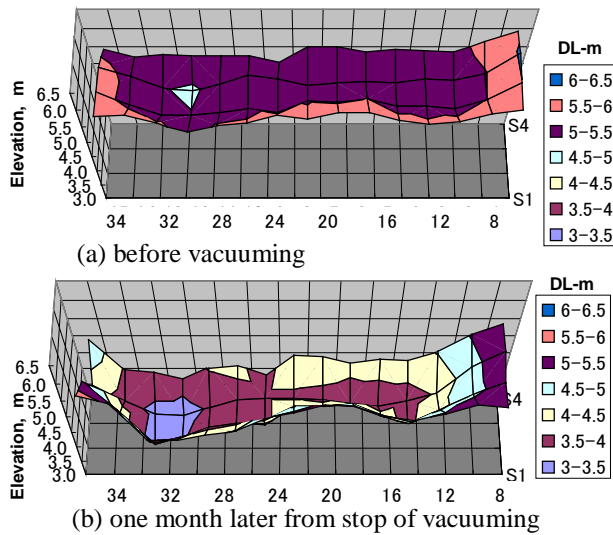


Fig. 5 Settlement behavior in ground improvement

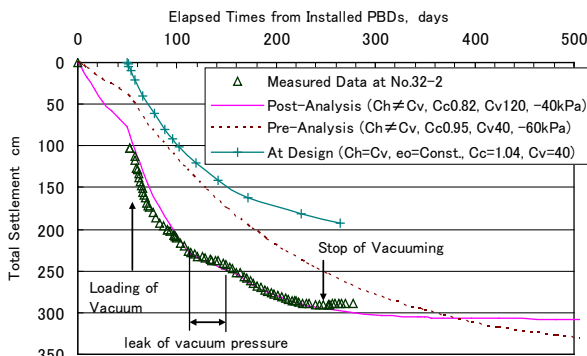


Fig. 6 Monitoring result and pre- and post- analysis

Figure 6 shows the time – settlement relation at the cross point of No.32 and S2 (No.32-2). The origin of horizontal axis is the installation of PBDs. In this figure, the prediction at design time are simulated.

The consolidation settlement at the point of No.32-2 before the vacuuming generated about 1 m after the installation of PBDs. The initial rate of consolidation settlement was high, and then decreased gradually. On the middle of this behavior during the vacuuming, a decrease in the rate of consolidation settlement occurred. This is the leak of vacuum pressure. After the change of vacuum pump after 150 days from the start, the consolidation settlement increased. After about 200 days from the installation of PBDs, the consolidation settlement converged to form 300 cm of total settlement. Using the approximation of hyperbolic curve, the time with consolidation degree 90 % was equivalent to 230 days from the install of PBDs.

## SOIL INVESTIGATION AFTER VACUUMING

The soil investigation was performed one month later after the stop of vacuuming. The sites of soil investigation were eight points set at the intersections between S2 and S3, and No.16, 24, 28 and 32. Figures 7(a) and 7(b) show the distribution of consolidation yield stress at the S2- and S3- lines, respectively. The anticipated vertical effective stress distributions at 60 kPa of working vacuum pressure and 80 % of working pressure are also drawn. The consolidation yield stresses of S2-line with the installing space of 1.0 m exceeded over 80 % of 60 kPa of vacuum pressure. The S3-line located at the boundary between S- and R-types did not reach 80 % of effective stress. The degree of consolidation was recognized to be dependent on the space of installed PBDs.

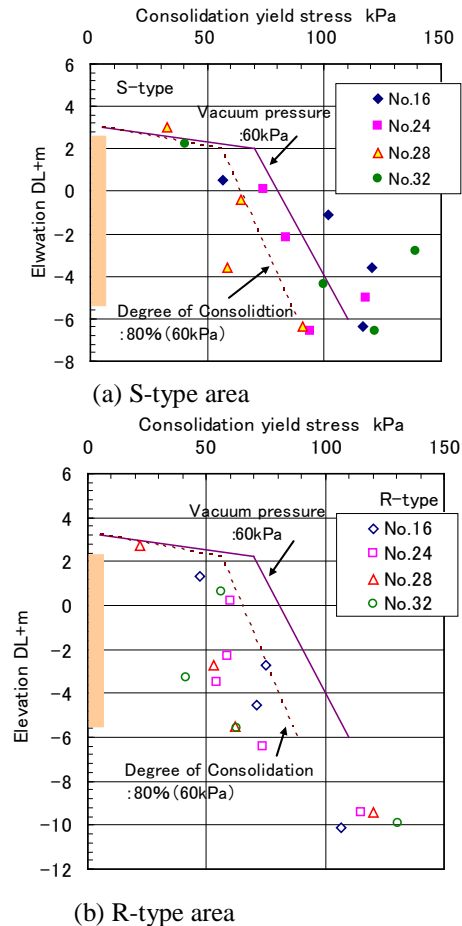
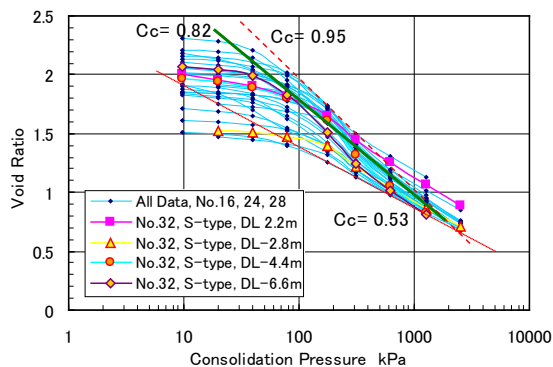


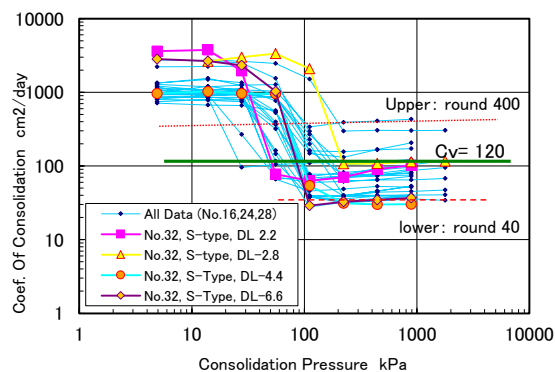
Fig. 7 Distribution of consolidation yield stress

Figure 8 shows the results of consolidation tests on the samples acted the vacuum pressure. The compression curves shown in Fig.8 (a) were represented from the over-consolidated to normal consolidated conditions, and the consolidation yield stresses were from 40 to 140 kPa mentioned earlier. The compression indexes,  $C_c$  ranged from 0.53 to 0.95. The coefficients of consolidation in the normal

consolidation condition were distributed from 40 to 400 cm<sup>2</sup>/day.



(a) compression curves



(b) coefficient of consolidation

Fig. 8 Consolidation characteristics

## BACK ANALYSIS FOR VACUUM CONSOLIDATION METHOD

Using the results of monitoring and soil investigation, several post-analyses were performed. The back analysis were used the  $C_c$ -method for consolidation settlement and Barron's Equation for progress of consolidation. To express the consolidation behavior of lower seal layer, the practical method for partial vertical drains proposed by Hitachi et al.<sup>3)</sup> was adapted.

### Evaluation for prediction at design

At the design of vertical drains, the elevation of reclaimed land was increasing as the dredged clays were poured into the disposal pond. Then, the ground model as uniform condition shown in Fig.9 (a) was assumed. The compression index was also set at 1.04 as shown in Fig.9 (b), and the coefficient of consolidation was 40 cm<sup>2</sup>/day as the lowest limit of test results.

The prediction at the design was shown as “+” in Fig. 6. To compare to measured data, the data was plotted from 50 days from installing of PBDs. This time was when the vacuuming started. The settlement was measured from the installation of PBDs, and was

approximately generated 100 cm just before the vacuuming and 200 cm during the vacuuming process. The prediction of design was not represented for the behavior after the installation of PBDs before vacuuming, and was expressed the behavior only after the vacuuming. The settlement after the installation of PBDs was the disappearance of excess pore water pressure accumulated during the reclamation of dredged clay. The model at the design did not consider this excess pore water pressure, and could not express the measured settlement.

### Determination of ground model at installation of PBDs

To predict the stress condition of reclaimed ground, the reclamation analysis named ‘CONAN’ was used. The CONAN was developed based on a generalized one-dimensional consolidation theory<sup>4)</sup>. The detailed procedure of this numerical method was described by Katagiri et al.<sup>5)</sup>.

The ground model including with consolidation parameters should be determined by numerical simulation of the reclamation stage. From the back analysis of preceding reclamation with dredged clay, the consolidation parameters are identified. Using these parameters the soil profile of the reclaimed ground at the installation of PBDs can be predicted by the CONAN.

Figure 10 shows the measured elevation of the north area of disposal pond monitored from 2003 to 2011. The result of reclamation analysis with the best-fit combination of consolidation parameters identified at the excavation area<sup>6)</sup> is simulated in the same figure. In this area, the Alluvial Clay layer presents within 5 m in thickness. The result of reclamation analysis was recognized to reproduce the measured data.

Figure 11 shows the distributions of void ratio and effective stress of the reclaimed ground in north area at the installation of PBDs obtained by the reclamation analysis. In Fig.11 (a), the measured data

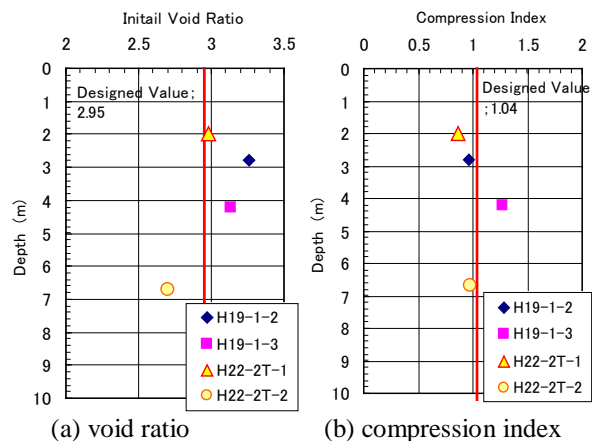


Fig. 9 Results of early soil investigations

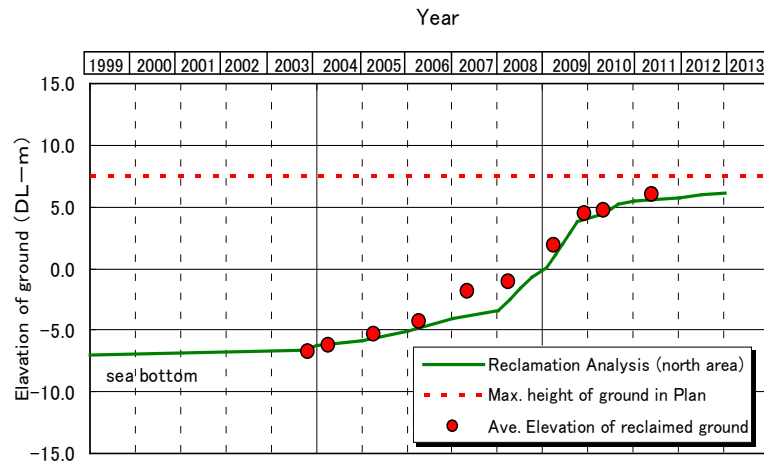


Fig. 10 Measured data and reclamation analysis result in the north area

shown in Fig. 9 (a) were also plotted at elevation converted with (DL+6.06 m) of ground surface. The result of reclamation analysis presents the measured data and to be believable as ground condition of reclaimed land with dredged clay. Figure 11 (b) shows the distribution of effective stress in reclaimed land. The pore water pressure is the difference between total stress and effective stress.

The pre-analysis in Fig. 6 is the prediction of the ground model obtained from Fig. 11. This analysis used the horizontal coefficient of consolidation depended on space of PBDs ( $Ch = (0.77 \cdot d - 0.24) \cdot Cv$ , d; space of PBD)<sup>6)</sup>. The consolidation parameters obtained from the soil investigation shown in Fig. 9 ( $Cc=0.95$ ,  $Cv=40 \text{ cm}^2/\text{day}$ ) were used. The vacuum pressure of 60 kPa was supplied. Whole settlement behavior after installing of PBDs to stop vacuuming was similar to measured data, but the magnitudes of settlement and consolidation rate were different.

#### Identified parameters of consolidation and their evaluation

In the post analysis, the parameters of consolidation and vacuum pressure were changed to fit the measured data. As a result, the  $Cc$  was identified as 0.82 and  $Cv$  was  $120 \text{ cm}^2/\text{day}$ . To identify the consolidation parameters, this fitting of time-settlement behavior was not enough and more evidence was needed. Figure 12 shows the analyzed water content distributions of reclaimed layer at  $U=90\%$ . In this figure, the initial condition before installing of PBDs and the water contents obtained from the soil investigation conducted after the stop of vacuuming were also plotted. The analyzed results except of the upper part, which is about 1 m as sealing layer were piled on the surveyed results at No.32. From these two evidences such as time-settlement behavior and water content distribution, the consolidation parameters used in the analysis could be identified.

These identified consolidation parameters were plotted in Fig. 8. Both the compression index and coefficient of consolidation were located in the middle of scattering data. It was concluded that the identified parameters were suitable for this ground condition.

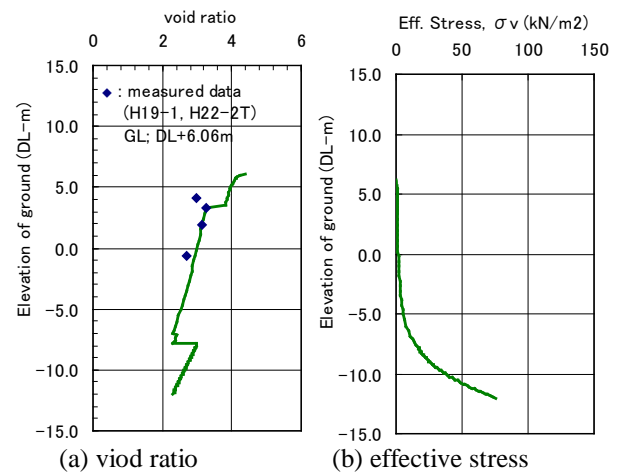


Fig. 11 Results of reclamation analysis

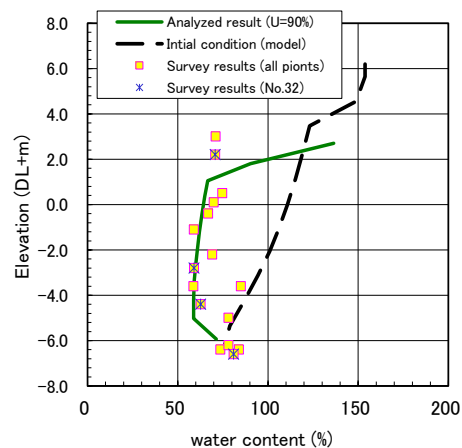


Fig. 12 Results of soil investigation and analysis

### Prediction procedure of vacuum consolidation method for a reclaiming land

From above consideration and knowledge, a prediction procedure of vacuum consolidation method for a reclaiming land is proposed.

A traditional procedure<sup>2)</sup> of prediction of vacuum consolidation method for a soft clay ground is i) determining the model ground using the results of soil investigation and ii) predicting the time-settlement behavior by Barron's equation and Cc-method. In a reclaiming clay ground, the elevation and ground condition are changed with time. The elevation and ground condition at the installation of vertical drains are different from those at the soil investigation. It is therefore necessary to predict the elevation and ground condition at the installation.

As mentioned earlier, the ground model can be determined by numerical simulation during the reclamation process. So, the consolidation parameters can be identified by back analysis, and the elevation and ground condition can be obtained by pre-analysis using CONAN<sup>5)</sup> program.

A prediction procedure of vacuum consolidation method for a reclaiming clay ground are proposed as follows; i) identifying the consolidation parameters by back analysis during reclamation process, ii) predicting the elevation and ground condition of reclaimed clay ground at the installation of vertical drains, iii) determining a ground model from the results of ii), and iv) predicting a settlement behavior of ground installed vertical drains under vacuuming. During the reclamation process, CONAN<sup>5)</sup> developed from a generalized one-dimensional consolidation theory<sup>4)</sup> can be used, Barron's equation while Cc-method may be used during the vacuum consolidation process.

The prediction by the proposed method is shown as a bold curve in Fig. 13. The gap between measured data (marked as "Δ") and prediction by the proposed method at 250 days from the installation of drains was 30 cm, and 10 % of predicted settlement. It is concluded that the proposed method is useful at the design of vertical drains for reclaiming lands.

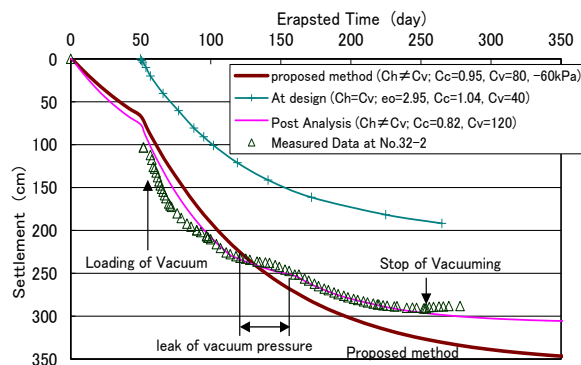


Fig. 13 Evaluation of proposed method

### CONCLUDING REMARKS

In this paper, the vacuum consolidation method for the reclaimed ground with dredged clay is introduced. The results of settlement behavior after the installation of vertical drains and soil investigation after the vacuuming are shown, and the pre- and back analysis are also described. From these considerations, a prediction procedure of vacuum consolidation method for reclaiming clay ground is proposed. The followings are obtained from this paper;

- 1) The ground model determined by limited ground information at initial design could not express the monitoring data. In particular, the settlement behavior after the installation of vertical drains was different.
- 2) The ground model determined from the result of reclamation analysis could be represented the results of monitoring and soil investigation.
- 3) From these considerations, a prediction procedure of vacuum consolidation method for reclaiming clay ground was proposed.

### ACKNOWLEDGEMENTS

The authors would like to thank the technical committee (Chairperson: Prof. K. Zen of Kyushu University) for their valuable advices.

### REFERENCES

- [1] Moriki, A., Katagiri, M. and Terashi, M.; Mechanical properties of dewatered dredged clay lumps, Proc. of 14th Asian Region Conference of Geo-mechanics and Foundation Engineering, Hong Kong, 2011, DVD-rom.
- [2] Association for VCD-Koho; Manual of Vacuum Consolidation Drain Method, 2010, pp.1-27. (in Japanese).
- [3] Hitachi, S., Yamamoto, H., Ikeda, D., Oikawa, K. and Nakanodo, H.; Consolidation of clay layer underlying vertical drain improved ground, Proc. of 29th JGS conference, 1994, pp.2107-2110. (in Japanese).
- [4] Imai, G.; Analytical examinations of the foundations to formulate consolidation phenomena with inherent time-dependence, Proc. of IS-Hiroshima '95, Vol. 2, 1995, pp.891-935.
- [5] Katagiri, M., Terashi, M. and Kaneko, A.; Back analysis of reclamation by pump-dredged marine clay – influence of ground water lowering –, Soils and Foundations, Vol. 41, No. 5, 2001, pp.73-86.
- [6] Ikeda, H., Kawano, M., Kiyoyama, T., Yamamoto, S., Takase, E., Katagiri, M., Ohishi, K. and Yoshifuku, T.; Application of vacuum consolidation method to sedimentation of dredged clay, Proc. of 58th Geotechnical Symposium, 2013, pp.85-92. (in Japanese)



## SLOPE STABILITY AND ROCKFALL HAZARD ANALYSIS IN AN OPEN PIT ZINC MINE

Maged Almandalawi<sup>1</sup>, Greg You<sup>1</sup>, Peter Dahlhaus<sup>1</sup>, Kim Dowling<sup>1</sup> and Mohannad Sabry<sup>2</sup>

<sup>1</sup>Faculty of Science, Federation University Australia; <sup>2</sup>School of Engineering, University of Western Sydney, Australia

### ABSTRACT

Rockfalls are a major safety hazard in open cut mines, particularly in large-scale deep pits. The geotechnical design relies on in-situ, site-specific, rock slope data to predict the trajectories and velocities of rockfalls that present a residual hazard in the mines. This paper presents slope stability analyses using both static general limit equilibrium methods and finite element stress analyses to estimate unstable areas and slope displacements in the mid-west slope at Handlebar Hill Open Cut Zinc mine at Mt Isa, Queensland, Australia. A conventional program - RocFall - was used for the slope rockfall risk assessment. Results indicate the possible slope benches involved in the initiation of rockfalls, and the maximum run-out distance, which could be defined as the pit's hazardous zone. A rockfall restraining system to absorb the impact energy of boulders and prevent them further falling was also modelled.

*Keywords: Factor of Safety, continuum modeling, shear strength reduction, RocFall, rockfall hazard barrier*

### INTRODUCTION

Rockfalls are a major risk in open cut mining as they often involve the unexpected detachment of rocks from a slope and their rapid movement by rolling or bouncing deeper into the pit. The rock fragments could come to rest on the lower benches or on the pit floor, generating high risk to workers, mine assets and the mine environment. The impacts depend on the size of the rockfalls, slope geometry, momentum of the rocks, the presence of obstacles and the site risk management.

Rockfall dynamics are largely a function of the mechanical properties of the rock and rock mass, location of detachment and downslope profile [1]. Falls have two successive mechanisms: the failure (i.e. rock detachment) and its propagation down the slope [2]. Once the potentially unstable areas have been identified, the potential run-out of the rockfalls can be evaluated using propagation models.

This paper presents analyses aimed at better understanding the rockfall hazard in the Handlebar Hill Open Cut (HHOC) zinc mine, approximately 20km north of Mount Isa in northern Australia (Fig 1). The study focuses on the slope stability of the mid-west pit, which is characterised by four geological domains with major discontinuities such as faults and shear surfaces dipping 60° - 70° to the west.

Standard models from the Rockscience suite of programs [3] were utilised to undertake the analyses. The main objective of the analyses was to identify the potential rockfall initiation areas and failure mechanisms, predict the sensitivity of the slope to

different triggering mechanisms and provide simulations that may inform the design of optimal slope geometry and restraint mechanisms.

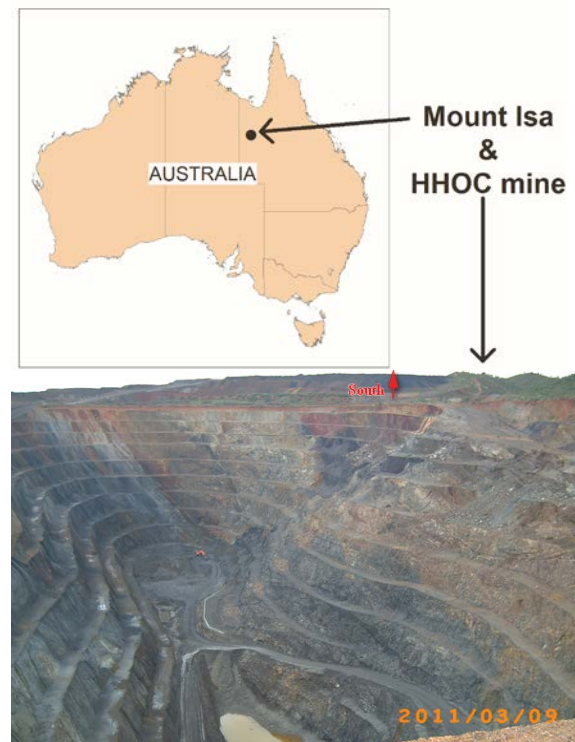


Fig. 1 The HHOC mine pit location and view looking south. This study focuses on the western wall, which is on the right hand side of the image.

## ROCK SLOPE STABILITY ANALYSES

Two software packages - Slide 6.0 and Phase<sup>2</sup> - were used to undertake a limit equilibrium analysis and construct finite element stress models of the pit slopes. The purpose of these analyses was to identify the most likely areas where rockfalls would be initiated. This information was then used as input into the rockfall simulation models.

### Limiting equilibrium analysis

Limit equilibrium analysis of the overall slope at the HHOC pit was analysed using Slide 6.0. Modern limit equilibrium software (such as Slide) is making it possible to handle ever-increasing complexity in the analysis. It is now possible to deal with complex stratigraphy, highly irregular pore-water pressure conditions, various linear and nonlinear shear strength models, almost any kind of slip surface shape, concentrated loads, and structural reinforcement [4]. All methods used in limit equilibrium analysis are based on a comparison of forces (moments or stresses) resisting instability of the mass with those that cause instability (disturbing forces).

In slope stability analysis, the Factor of Safety (FOS) may be considered as the ratio of resisting shear strength to the disturbing shear stresses at initial failure [5], with a typical FOS for open pit slope design ranging between 1.1 and 1.5. The potential failure surface is assumed to be directed by the linear Mohr-Coulomb relationship between rock shear strength and the normal stress applied on the slope failure surface.

The results of the general limit equilibrium analysis for the HHOC pit slope is shown in Fig 2. The critical surface specifies a minimum FOS of 1.21 for slope instability generated by the general limit equilibrium analysis.

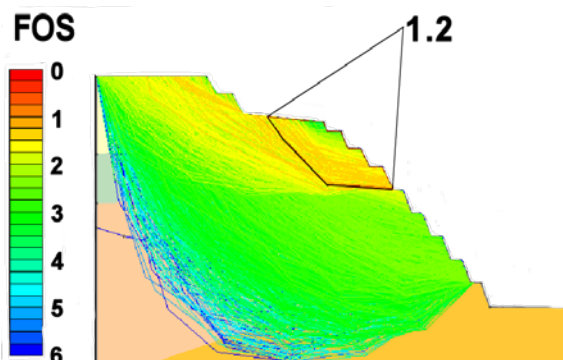


Fig. 2 FOS using limiting equilibrium analysis. (the critical surface shown has FOS = 1.21)

### Finite element analysis

For many decades, limiting equilibrium has dominated over any other method of analysis for soil/rock slope stability practitioners. Uncertainty is a key factor in slope design as an increase of one degree in excavated slope angle might make the slope unstable. Conventional slope practice is often based on a FOS which can not explicitly address the uncertainty, which ultimately led to the development of probabilistic finite element slope stability analysis [6]. In addition, the advantage of finite element methods for slope stability analysis over traditional limit equilibrium methods is that no assumptions needed to be made pre-analysis about the shape and location of the failure surface and geometry, such as the failure slice side forces and directions.

To reduce the limitations of conventional methods, the finite element shear strength reduction method was used in which the explicit material deformation and failure progression can be modelled. The strength reduction factor of the mid-west slope was modelled using the numerical method of the Phase<sup>2</sup> software. The results are shown in Fig 3.

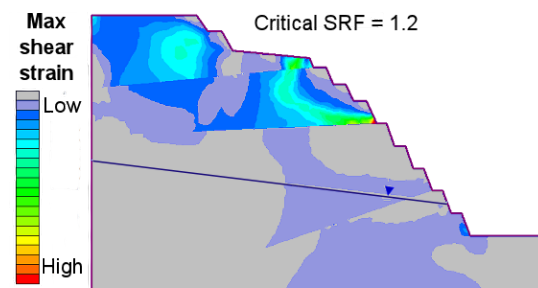


Fig. 3 Modelled strength reduction factor for the mid-west slope.

The resulting critical strength reduction factor (SRF) is 1.2 at maximum total displacement 0.026m.

### Rockfall mechanisms

The movement of a numerical-continuum body is a continuous time sequence of displacements. The rock material will occupy different configurations of size and shape at different times so that a particle occupies a series of points in space which describe a path line.

The displacement vectors and contours illustrated in Fig 4, shows that the most of rock displacements are close to the major discontinuities at the upper part of the slope surface. The slope is most likely influenced by the reduction in the strength (mechanical) properties of the rock masses in these zones.

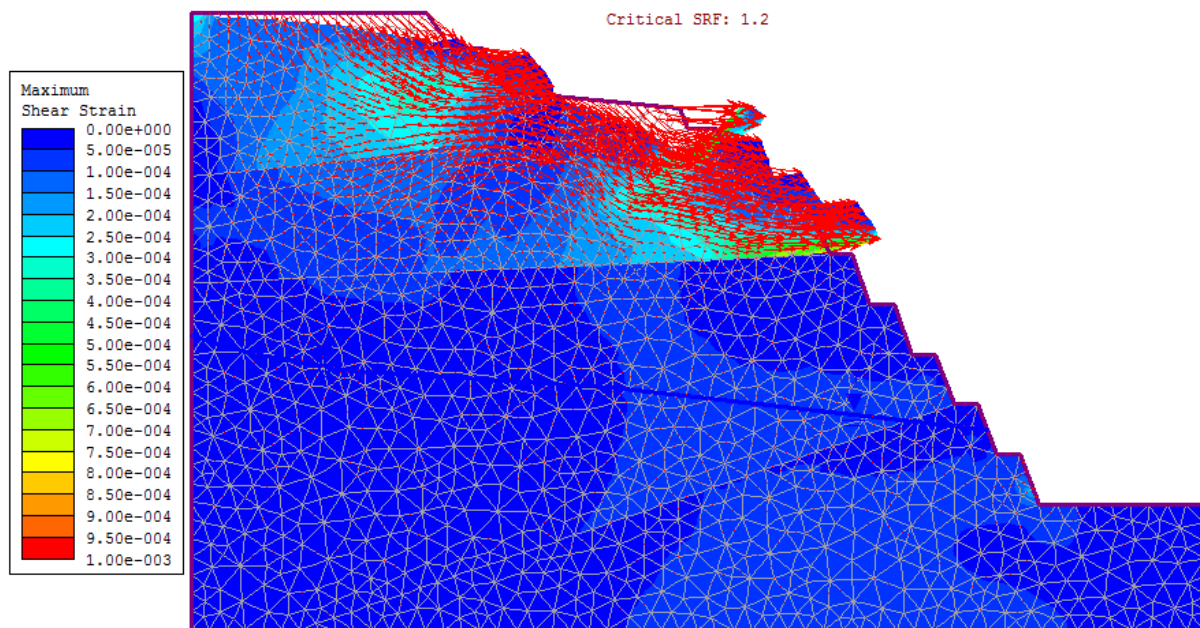


Fig. 4 Modelled displacement vectors of deformation showing the possible directions of block rotation and sliding modes.

Continuum modelling was used to determine the total displacements in the slopes and the locations of yielded elements in the rock mass shows critical state conditions as illustrated in Fig 5.

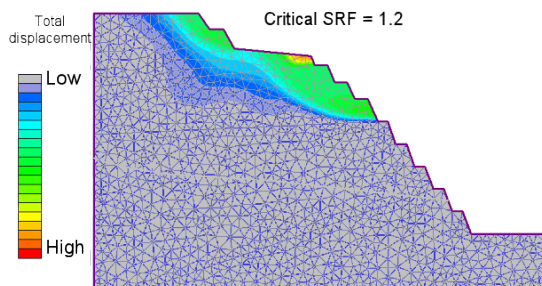


Fig. 5 The total displacement in the slope. The most critical displacement for the slope surface on which the proposed rocks could be detached, is located in the bottom of the ramp and nearby the upper benches around the haulage road.

Generally, rockfalls could be initiated by specific climatic conditions, which may create some changes to the forces acting on the slope. This is especially the case in tropical zones (e.g. the HHOC mine location), which experience a season of heavy rains. Rainfall events may rapidly increase pore pressures due to infiltration through the rock mass. At such times, the potential of rockfall initiation will probably be higher than during drier seasons.

For that reason, it is necessary to analyse the potential for rockfalls in high rainfall events. In addition investigating the causes of historical rockfalls (and mine accidents) can help planning to avoid future rockfalls.

## ROCKFALL SIMULATIONS

An assessment of rockfalls was undertaken to identify the potential fate of blocks that may detached from unstable pit slope faces and therefore, to improve the safety at the mine. The analysis was completed using RocFall, a program that simulates the trajectories of rocks falling from the slope. The trajectory is modelled as a two dimensional rockfall simulation largely based on the slope geometry. Using statistical analyses, the method calculates the probable trajectories, energy, velocity and bounce height envelopes for individual rock blocks. The entire slope can be modelled by the program, so that the ultimate resting locations of rockfalls can be determined, and the results are graphed with comprehensive statistics automatically calculated [3]. Besides the slope geometry, the program requires input data such as the slope roughness, restitutions of normal and tangential rock energy, coefficient of rolling friction and rock mechanical parameters.

To account for the uncertainty in the definition of the input parameters, stochastic variability is used. The determination of selected standard deviations for input parameters of detached boulders is required.



The potential rockfalls in the HHOC pit were initially modelled using a starting point located at the top slope vertex (0, 0), as shown in Fig 4. In this simulation, the source of the rockfalls is the Volcanics formation rock mass and their falling

paths are illustrated in Fig 6. A number of 50 detached rocks was used, each of 300 Kg weight and 28 Kn/m<sup>3</sup> density. The simulation calculated that all rockfalls would end on the haulage ramp.

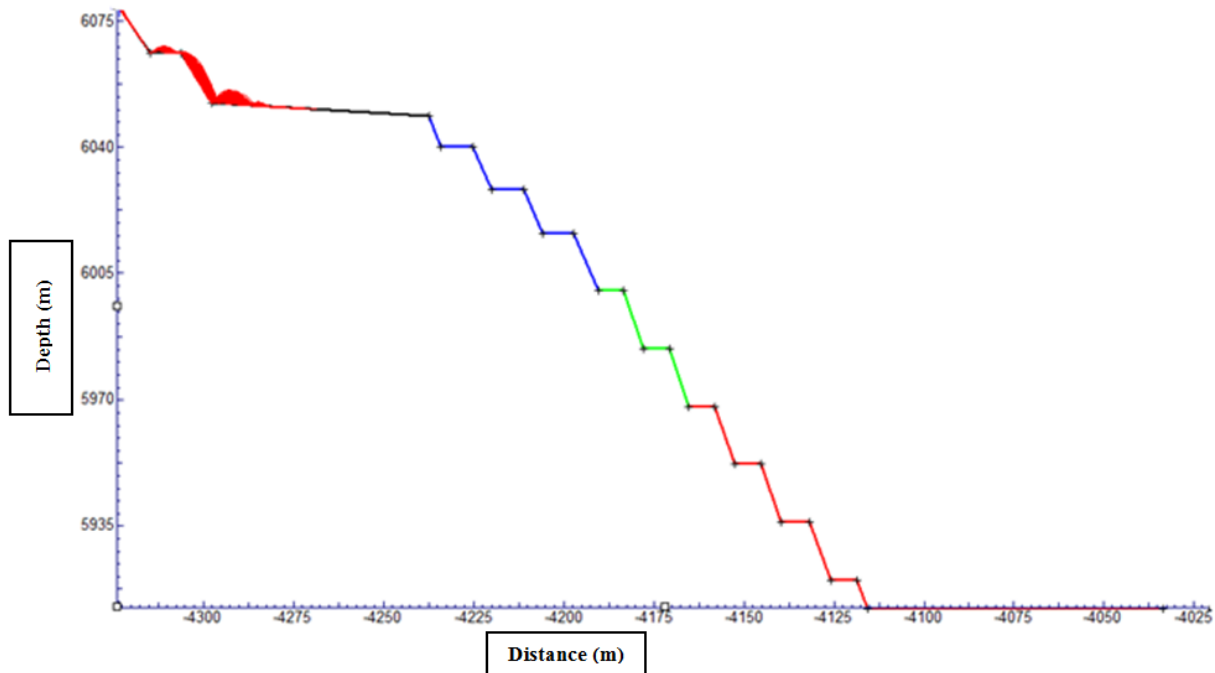


Fig. 6 Results of the simulation of a number of possible rockfalls from the top crest source area, using the model inputs listed in Table 1.

Table 1 The input parameters of rock mass materials used in the above simulation

Rock mass material	Rn (mean   std)	Rt (mean   std)	Phi (mean   std)	Roughness (std)	Colour
Volcanics	0.44   0.04	0.87   0.04	150   0	0	Black
Magazine Shale	0.46   0.04	0.89   0.04	160   0	0	Blue
Spears Siltstone	0.47   0.04	0.91   0.04	360   0	0	Green
Urquhart Shale	0.48   0.04	0.93   0.04	350   0	0	Red

A second simulation was run using a starting vertex in the Magazine Shale, which is from the lower bench following the the ramp on the slope surface. This area is regarded as a probable source for rock detachments based on the results of the modelled displacement vectors (Fig 4).

The rockfalls source point and their paths are illustrated in Fig 7 (A). The same number of 50 detached rocks were used, 300 Kg weight and 26.5 Kn/m<sup>3</sup> density for each falling block. The simulation predicts that many rockfalls would end on the pit floor and away from the toe of the slope.

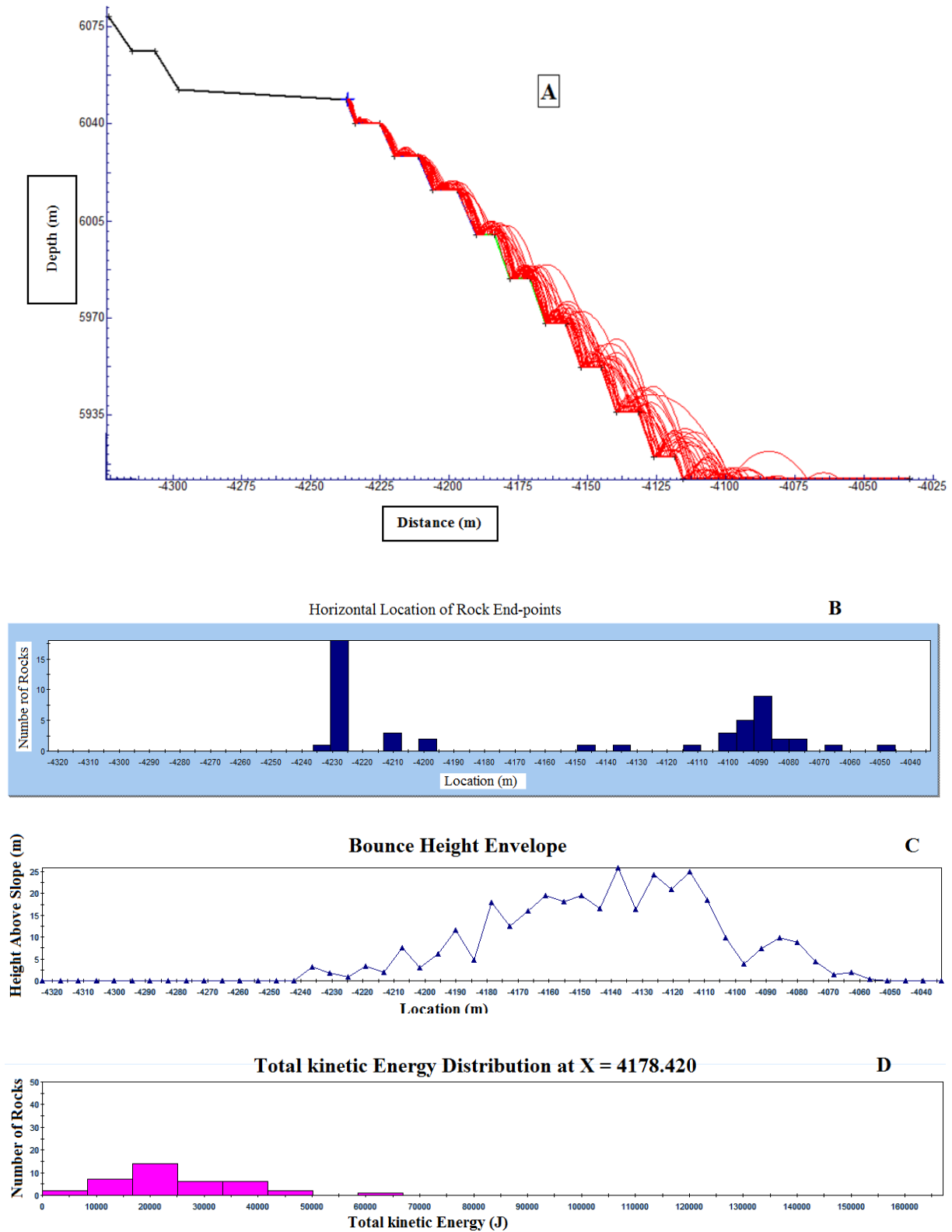


Fig. 7 The results of the RocFall simulations for the rockfalls sourced from the Magazine Shale on the top bench face. (A) Red lines show rockfall trajectories and the horizontal distances of rock end points. (B) The bar chart shows the distances and numbers of rockfalls from the source area. The majority of rockfalls travelled horizontally to a stop point, indicating that a probable hazard exists and that the installation of an effective protective system was required. (C) Shows the distributions of rockfall bounce heights above the ground level. (D) Shows the total kinetic energy distributed on the slope and the numbers of fallen rocks; the final impact energy on the ground is important for a safety design of the

protective barrier fence or windrow.

### Modeling a physical barrier for rockfalls

Assuming that rockfalls will be inevitable, then rockfall restraint must be considered.

A number of protective measures have been identified for the prevention of impacts on people and assets from rockfalls in open pit mines [7]. These include flexible rockfall barriers, identifying effective berm widths, bunds constructed on production berms and using draped mesh.

Windrows and catch barriers could be positioned to stop rockfalls from moving further down slope. Barriers and collectors can be modelled in RocFall as a line segment that can be positioned anywhere along a slope so as to intercept the paths of the rocks as they fall down the slope surface. The analysis includes the kinetic energy of the falling rocks and their impact energy could determine the location and capacity of the rockfall barrier. The proposed barrier protection structure at the HHOC mine was modelled as perfectly inelastic; therefore rockfalls that reach the barrier will finally stop. The rocks will not bounce back and just will fall straight down-wall to the foot of the barrier. The horizontal locations for maximum trajectories of falling blocks are shown in Fig 8.

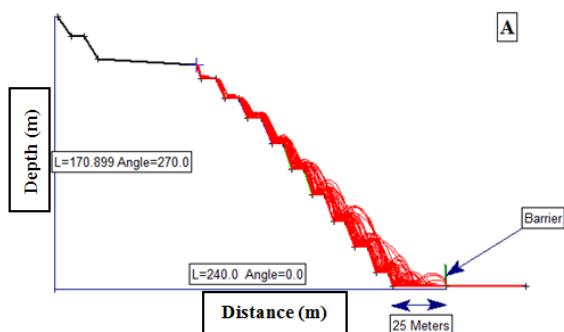


Fig. 8 Simulated horizontal location of rockfall end points utilizing a perfectly inelastic barrier 25 metres from the slope toe.

### CONCLUSION

Rockfalls are considered as a significant hazard in open cut mines. Blocks falling from high up on a slope can easily travel into the pit floor may destroy mining infrastructure and present a serious safety hazard for mine personnel. At the mid-west slope of the HHOC mine, the results of a general limiting equilibrium analysis indicate stable slopes with a FOS = 1.21. This deterministic analysis was verified through a finite element analysis using the shear strength reduction method. Modelled displacement

vectors illustrated the potential areas for slope instability and the potential areas of failures were contoured.

Rockfalls simulations confirmed the potential for individual rocks dislodged from the Volcanic rock formation at the slope crest to travel down slope and come to rest on the haulage ramp. By contrast, blocks falling from the top bench of the Magazine Shale rock mass, can possibly travel beyond the slope toe and onto the pit floor, presenting a hazardous zone. The models show that a barrier located at the foot of the slope on the pit floor, would be required to safely prevent the falling rocks reaching the mining operation zone.

The installation of a protective structure may partially control the rockfalls from the slope but the hazard cannot be fully eliminated.

### ACKNOWLEDGEMENTS

The authors sincerely extend their appreciation to Glencore Zinc Asset Australia for their support of this research project, and in particular, Dr Ahmed Soliman, Principal Geotechnical Advisor.

### REFERENCES

- [1] Cheng YK, 'Assessing Rockfall Hazards Using a Three-Dimensional Numerical Model Based on High Resolution DEM', Proceedings of the 22<sup>nd</sup> International Offshore and Polar Engineering Conference, June 17-22, 2012 Rhodes, Greece.
- [2] Jaboyedoff M, Dutt JP & Labiouse V, 'An attempt to refine rockfall hazard zoning based on the kinetic energy, frequency and fragmentation degree', Nat. Hazards Earth Syst. Sci., V: 5, 2005 pp: 621-632.
- [3] Rocscience Inc, 2010, 'Slide, Phase 2 & RocFall programs, Rocscience Inc. Toronto, Ontario, Canada. [www.rocscience.com](http://www.rocscience.com)
- [4] Krahn J., 2003, 'The limits of limit equilibrium analyses', The 2001 R.M. Hardy Lecture, NRC, Canada.
- [5] Cheng YM & Lau CK, 'Slope stability analysis and stabilization: New methods and insight', Routledge Press, USA. 2008.
- [6] Kainthola A, Verma D, Thareja R & Singh TN, 'A Review on Numerical Slope Stability Analysis', Int Jour of Sci, Eng & Tech Res (IJSETR), Vol 2, No 6, June 2013
- [7] Meyers A, 'Fundamental Techniques for Reducing Risk Associated with Instabilities in Mining Slopes', Int Jour Min & Geo Eng, Vol. 45, No. 1, December 2011, pp. 43-55.

## A CONCEPTUAL MODEL OF ENVIRONMENTAL, GEOLOGICAL AND GEO-TECHNICAL RESPONSE OF DREDGED SEDIMENT FILLS TO GEO-DISTURBANCES IN LOWLANDS

J. Rajaraman<sup>1</sup> K.Thiruvengatasamy<sup>2</sup> and S. Narasimha Rao<sup>3</sup>

1, Professor and Head, Department of Harbour and Ocean Engineering, AMET University, 135 East Coast road, Kanathur - 603 112, CHENNAI, INDIA. E-Mail [rajaraman.usha44@gmail.com](mailto:rajaraman.usha44@gmail.com)

2. Professor, Department of Harbour and Ocean Engineering, AMET University, 135 East Coast road, Kanathur 603 112, CHENNAI, INDIA. E-Mail [swamy2667@yahoo.co.in](mailto:swamy2667@yahoo.co.in)

3. Professor (Retd), IIT Madras, Director, Dredging Corporation of India (Govt. of India). E-Mail [snarasimharao@hotmail.com](mailto:snarasimharao@hotmail.com)

### ABSTRACT

In mineralogical evolution of clays, amongst the weathering phenomena, hydrolysis is very important. Clay minerals of 2/1 type, which first appear, are silica-rich with two tetrahedral silica sheets. The 1/1 clay minerals that follow have but one tetrahedral sheet and the last, gibbsite, has none at all. It is important to consider temperate and tropical environments. The kaolinite-gibbsite association is mostly characteristic of tropical environments. When all the silicates disappear to the gain of gibbsite, it is called total hydrolysis. Kaolinite and gibbsite are stable products in tropical environment. In temperate environment, weathering is often halted at the stage of 2/1 minerals (for example montmorillonite). This weathering can continue with kaolinite. In both cases it is partial hydrolysis only. This shows that the tropical environment is the only one to accumulate large quantities of gibbsite. In temperate climate only small amount of gibbsite is produced. In this paper a conceptual model of three layer system consisting of kaolinite, illite and montmorillonite is considered with symbols K, I, M respectively. The Geo- disturbance caused by dredging varies from pocket to pocket in the soil profile. The permutations and combinations of placed dredged materials are considered with different combination of the three clay types (KIM). All possible combinations will yield 24 different Geo-Technical sequences.

They are : KIM, MIK, IMK, KKK, III, MMM, KII, IKI, IIK, IKK, KIK, KKI, MII, IMI, IIM, KMM, MKM, MMK, KMI, IMM, MIM, MMI, MKI, and IKM. The link equation between drainage conditions and hydrolysis is identified as  $\tau = c + \sigma' \tan \phi$ . The cohesion  $c$  is controlled by hydrolysis (water) and  $\phi$  is controlled by residual friction of the mineral skeleton.  $\sigma'$  is effective normal stress. The above analysis is applied to important lowland Geo-technology problems in coastal areas such as sub-grade in pavement construction, land reclamation and fills to contribute to marine multi-inter-disciplinary research.

*Keywords: Hydrolysis Geo-disturbances Lowland-Geo-technology Residual friction Tropical, Temperate environment*

### INTRODUCTION

Many Geo-Technical engineering projects are not always under static loading alone, however, knowledge of dynamic properties and characteristics of soil is also important and needed for analysis and design. Dynamic loading can be grouped according to natural and anthropogenic origins: (a) natural sources of dynamic loads including earthquake, tsunamis, volcanic explosion, wind, rainstorm, waves, ice movement and current; and (b) anthropogenic sources of dynamic loads including machine vibrations, bomb blast, construction and quarry blasting, construction operation, traffic, ship impact and landing aircrafts. Each of these loadings

presents unique challenges to the geo-technical engineer. In this paper the effect of heavy rainfall on fills of dredged materials in coastal areas.

### Dredging Operation

Once the soil is disturbed, the chaotic conditions start. The only way to understand Geo-technical behavior / response of the dredged soil, is to extract order out of chaos. In this paper an attempt is made to take out order out of chaos. Dredged soil is influenced by many environmental factors.

Dredging itself creates chaotic condition in all Geo-technical aspects of the soil. Dredging causes loss of bonding stress, loss of fines with water.

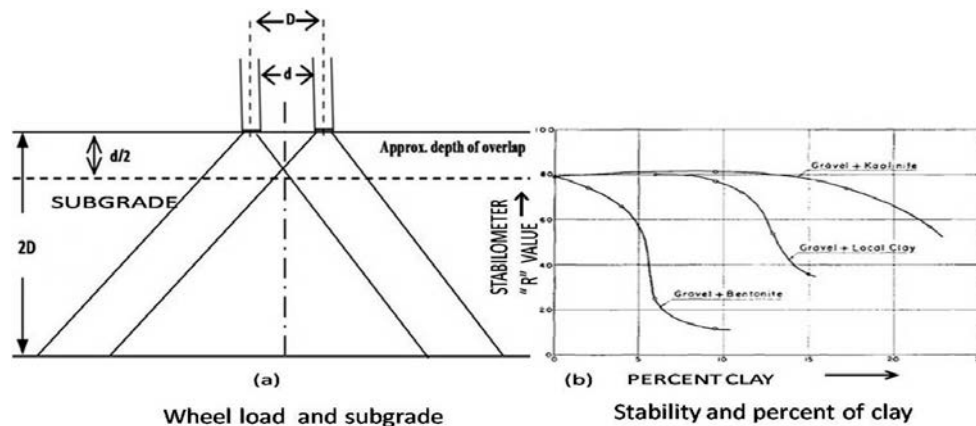


Fig.1 Stability Of Clay Minerals Under Wheel and Axle.

[1].

## STRENGTH OF SOIL INFLUENCED BY ENVIRONMENT FACTORS Clay Minerals and Stability

As the ability of soils to resist deformation depends very largely on the internal friction, wet clay has the effect of reducing or canceling out the frictional resistance. It may also be pointed out that the so-called cohesive resistance is induced almost entirely by the clay fractions, and therefore that clean sands are noncohesive. Again we must note the important part played by water, as finely ground dry clay particles exhibit no cohesive properties. If water is added to a dry soil, the cohesive resistance will normally increase with the addition of moisture and in most cases the frictional resistance will not be greatly impaired until a certain amount of moisture is added. Beyond this point, the friction will diminish but the cohesive resistance may continue to increase up to some point of higher moisture content, after which both values will diminish as the soil approaches a completely fluid state.

Metals are typical substances having little or no internal friction; in them, resistance values are almost entirely a result of the cohesive or tensile strength. Fig.1 (a) shows wheel load and subgrade in road construction in lowland coastal area. Fig.1 (b) is a chart showing characteristic curves illustrating loss in stability or internal resistance of a crushed sandy gravel due to the addition of increments of 1 plastic clay. The combined figures 1(a) and 1(b) clearly

indicates the instability created by Montmorillonite (Bentonite), Illite (local clay), and Kaolinite in the presence of water. Bentonite fails first followed by Illite. Kaolinite is more stable.

## Moisture Content and Clay Minerals

Moisture content in the soil mass is a major factor for controlling the state of stress of the soil. In general, an increase in the moisture content

or degree of saturation in soil will decrease the shear resistance as reflected by cohesion,  $c$ , or friction angle,  $\phi$ . This relationship is shown in terms of cohesion by figures 2 and 3.

Geo-Technical Behavior of Kaolinite, K, Illite, I, Montmorillonite, M in the presence of very heavy rainfall (moisture content very high %) of twenty four different combinations of KIM forming three layers of equal thickness.

Since moisture content is weight ratio Kaolinite is assigned 150 %, Illite 50%, followed by Montmorillonite 300%. The distribution of moisture content for saturated conditions for twenty four combinations of KIM will be :

1. KIM  $150 + 50 + 300 = 500$
2. MIK  $300 + 50 + 150 = 500$
3. IMK  $50 + 300 + 150 = 500$
4. KKK  $150 + 150 + 150 = 450$  (intermediate moisture)
5. III  $50 + 50 + 50 = 150$  (minimum moisture)
6. MMM  $300 + 300 + 300 = 900$  (maximum moisture)

Similarly calculating for KII,IKI,IJK, the % will be 250 each.

Similarly for others IKK,KIK,KKI, the % will be 350 each.

Then similarly MII,IMI,IIM will be 400.

KMM,MKM,MMK will be 750.

KMI, IMM, MIM will be 500,650 & 650 respectively.

And finally MMI,MKI,IKM will be 650, 500 & 500 respectively.

Considering all the combinations the % of moisture content varies from 150 to 900. Considering each combination of the twenty four figures the soil will be saturated if the % of rainfall over the dredged materials (Fill) reaches 900%. The cohesion becomes zero for the entire fill whatever may be the combination.

The important stages in the % of moisture content starts from III 150% (minimum) KKK 450% (intermediate) and MMM 900% (maximum %). The following figure explains how increase in degree of saturation decreases cohesion for weathered residual soil. The figure shows the effect of moisture content on cohesion for four basic clay minerals.

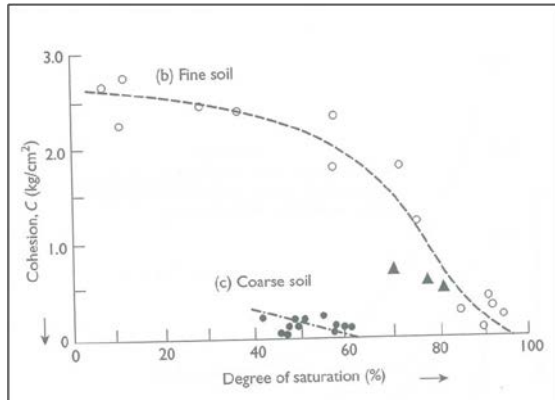


Fig. 2. Increase in degree of saturation decreases cohesion for weathered residual soils. [2].

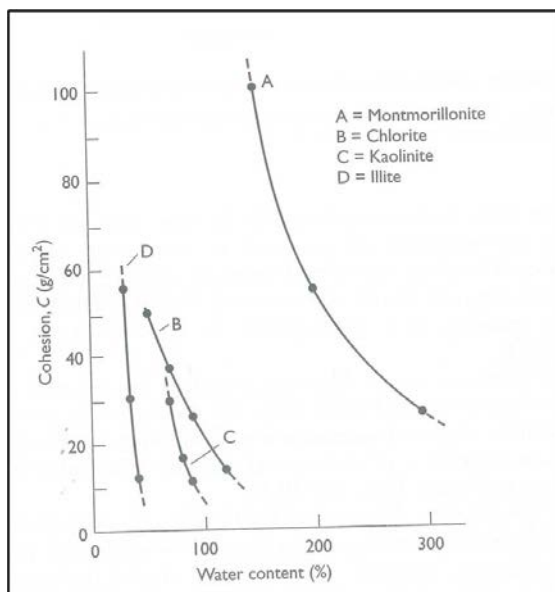


Fig. 3. Effect of moisture content on cohesion for four basic clay minerals. [3] [4].

The cohesion  $c$  becomes zero for Kaolinite at moisture content 150%, for Illite 50% followed by Montmorillonite 300%.

### Clay Minerals and Effect on Time

Shear strength of soils decreases with time, mainly caused by local environmental changes such as weathering, wet-dry cracking, creep and many

others. These environmental factors can cause the loss of bonding stress between soil particles, resulting in a gradual loss of shear resistance as shown in figure 4.

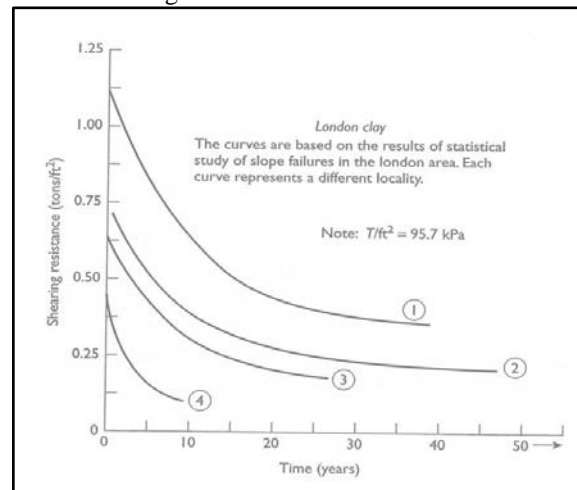


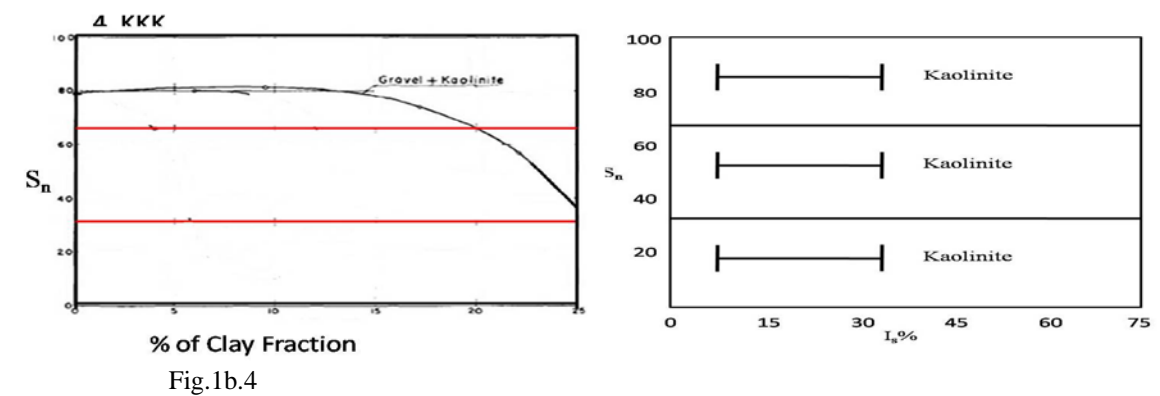
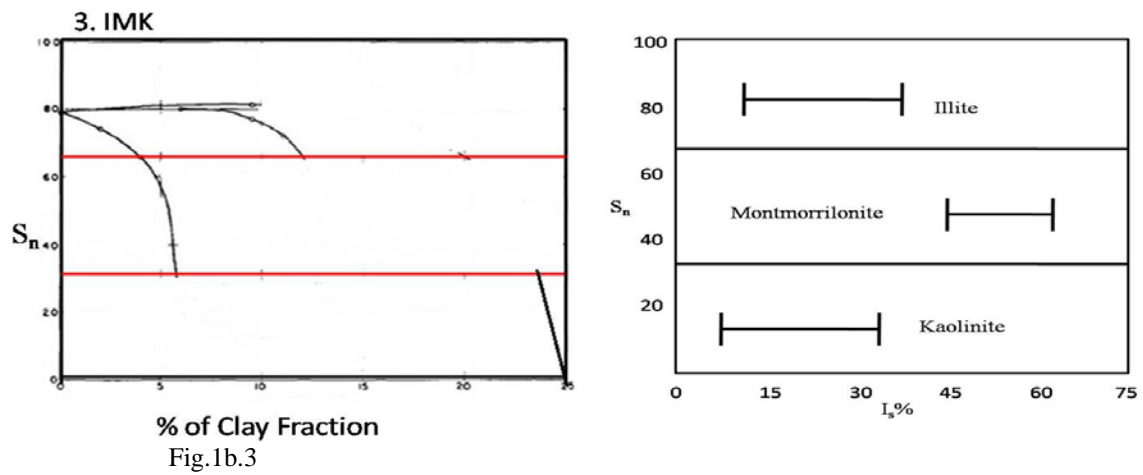
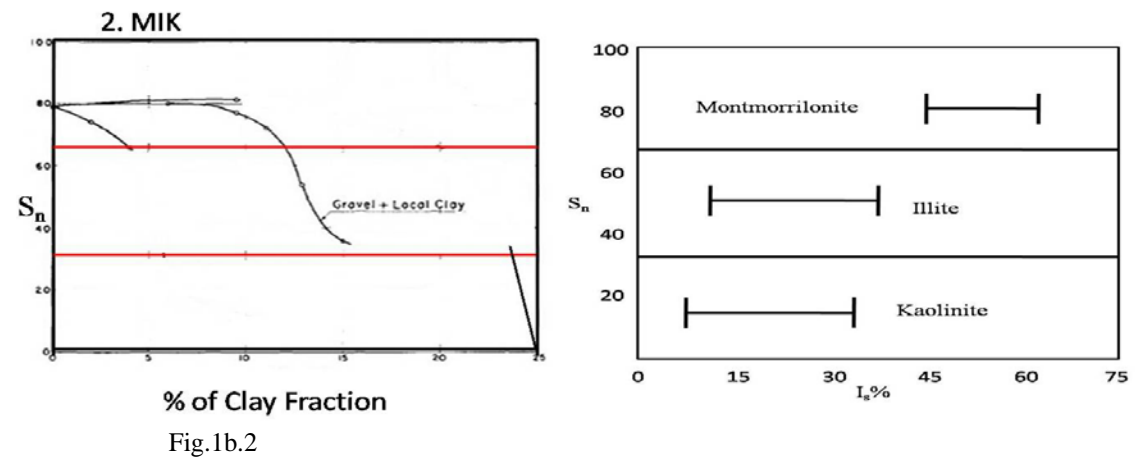
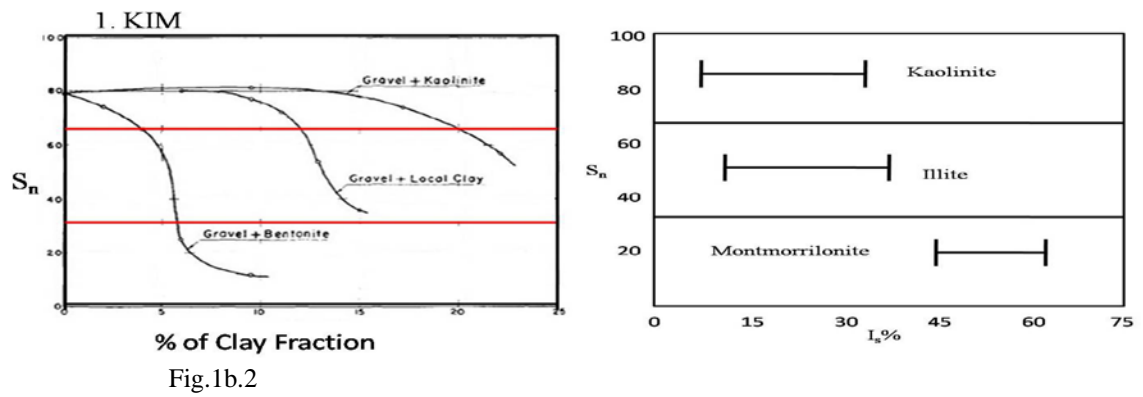
Fig.4. Gradual decrease of shear resistance of stiff clay with time. [5].

### GEO-TECHNICAL RESPONSE OF DREDGED MATERIALS

Lowlands Geo-technical problems are many. The dredged materials represent Geo disturbed soils with erratic variation in Geo-technical properties. In a rainy season in the beginning the rain first compensates soil moisture deficiency. Different clays absorb different amount of water. Upto shrinkage limit the stability is not affected by ever increasing amount of water. When there is very heavy continuous rain the different clays reach liquid limit with time lag. One layer of pocket will reach liquid limit and other may not. But when there is very heavy downpour (rain) all the layers reach their liquid limit state simultaneously and due to this shear failure occurs upto the depth influenced by shrinkage index. It is easier method to connect stability of dredged soils and shrinkage index to explain shear failure or liquefaction of the dredged fills. Ultimately the understanding of the mineralogy and consolidation properties of the dredged materials will help to explain stability related problems.

From Figure 1 a conceptual model of three layer system consisting of Kaolinite, Illite and Montmorillonite is considered with symbols K, I and M respectively. The layers in order before dredging has become chaotic after dredging. In order to take order out of chaos, 24 different combinations of K, I and M are considered.

**Figures 1b.1 to 1b.24 represent the assumed order out of chaos of clay minerals after dredging operations**





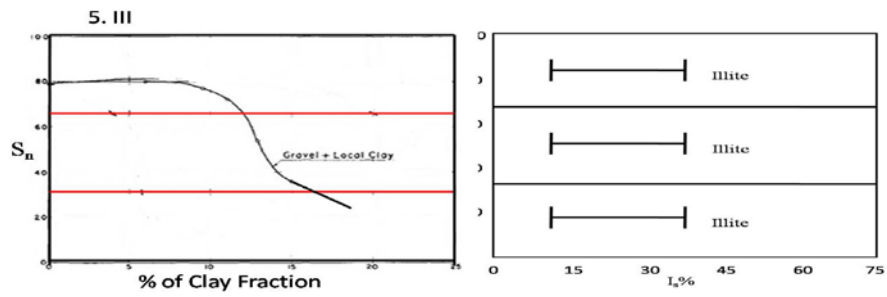


Fig.1b.5

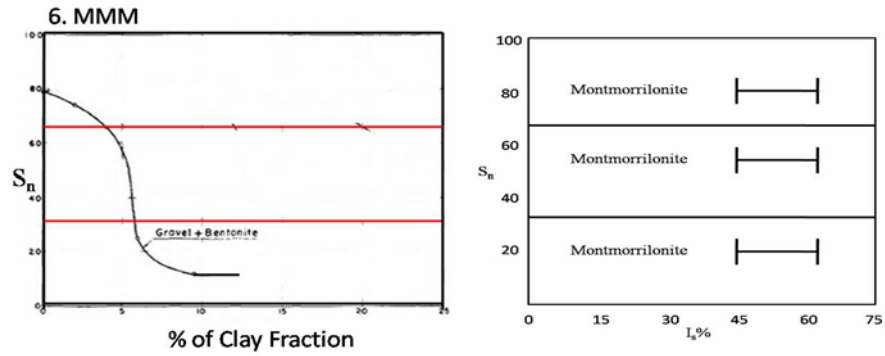


Fig.1b.6

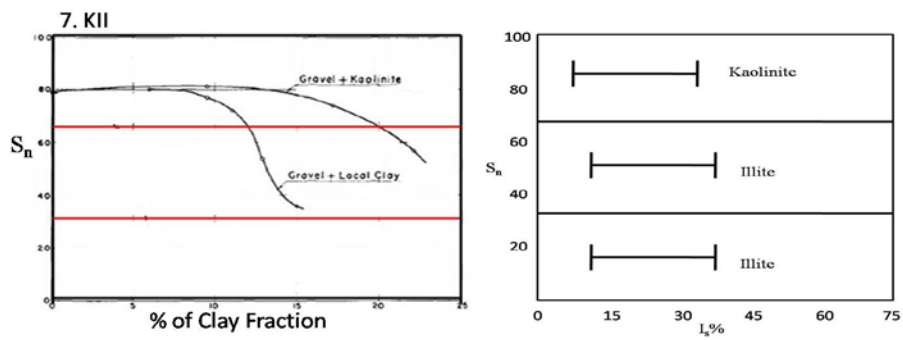


Fig.1b.7

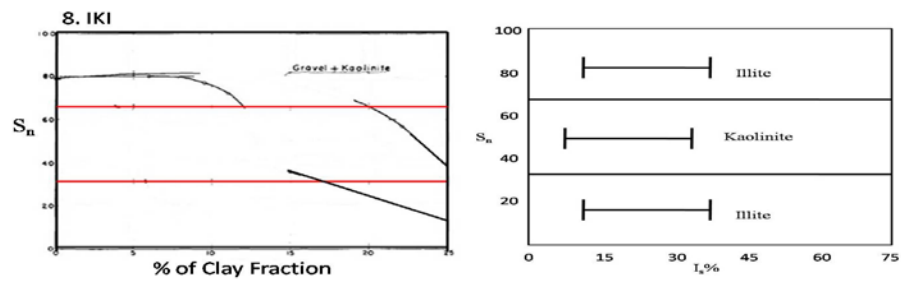


Fig.1b.8

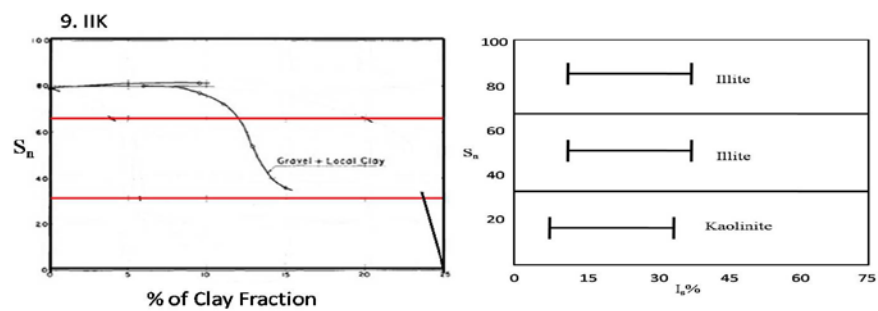


Fig.1b.9

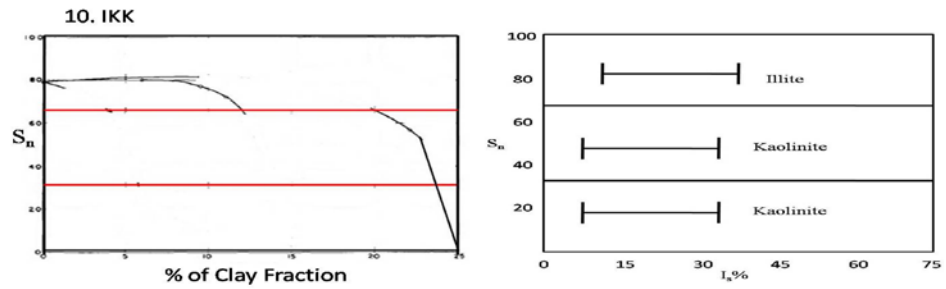


Fig.1b.10

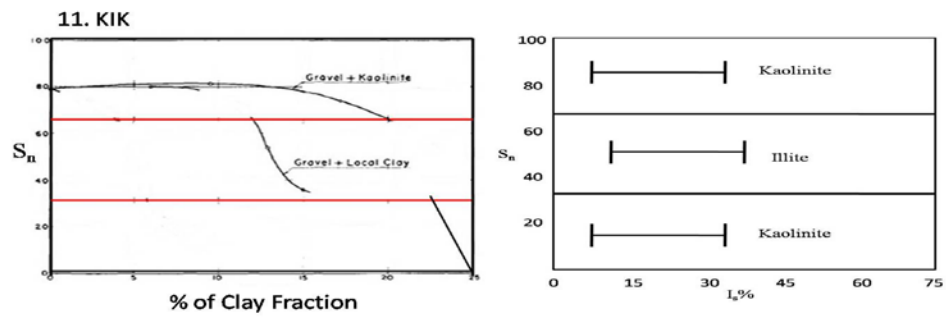


Fig.1b.11

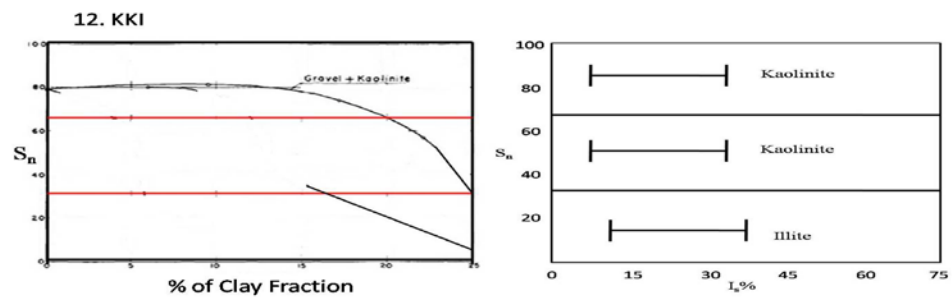


Fig.1b.12

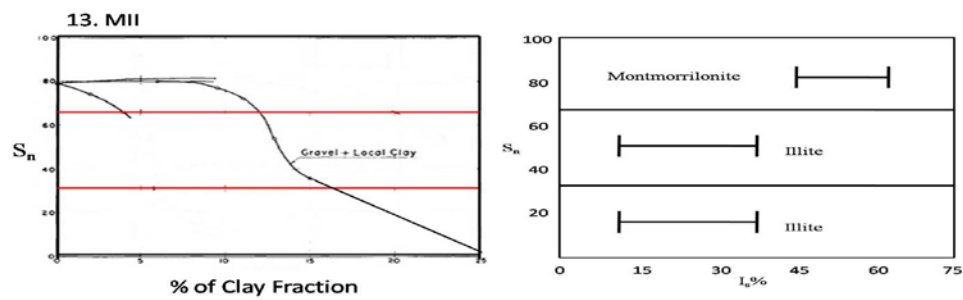


Fig.1b.13

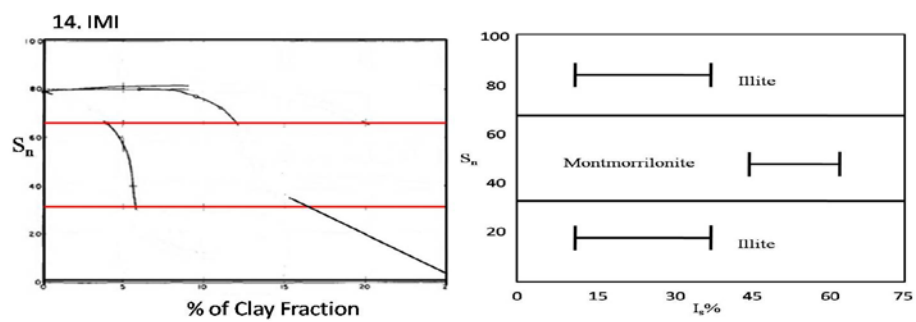
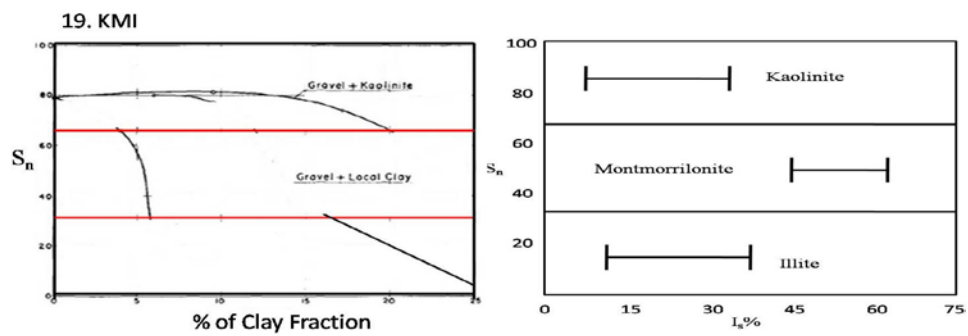
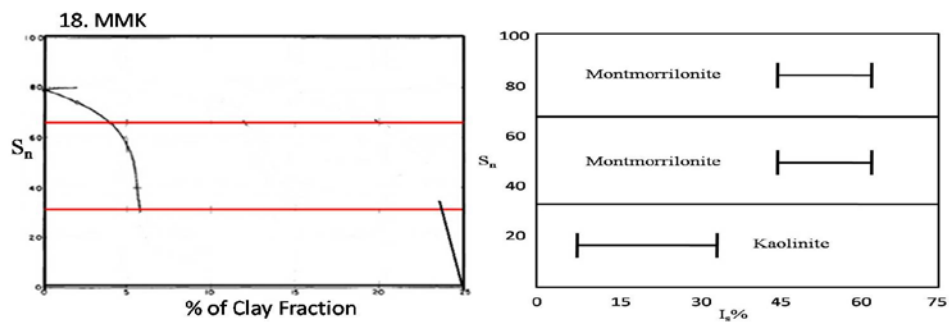
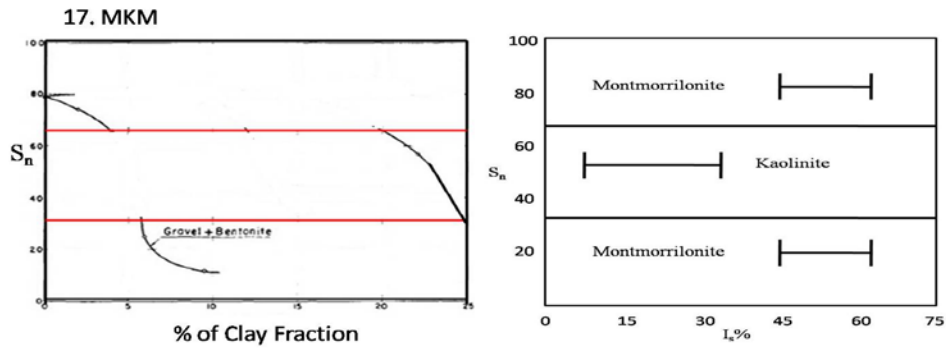
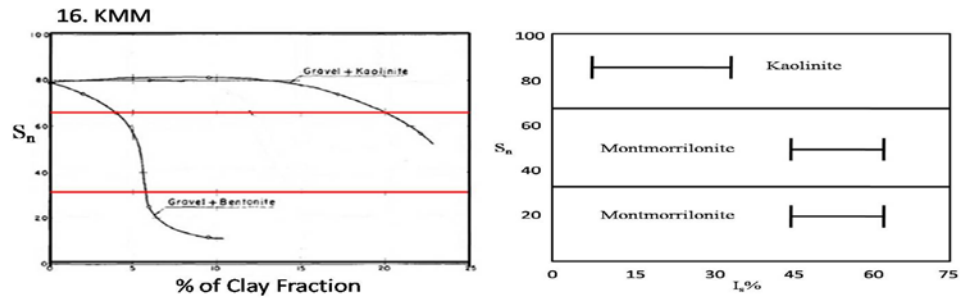
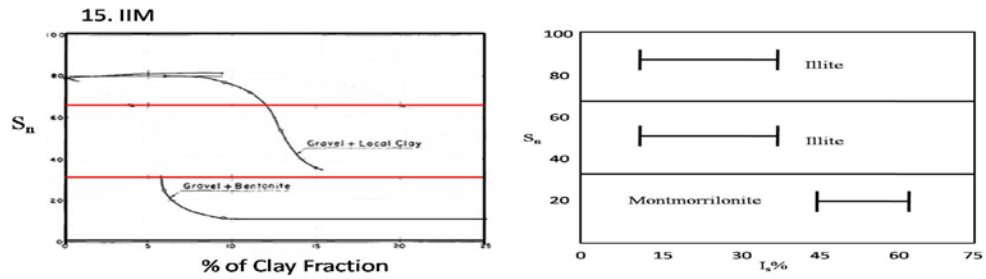


Fig.1b.14



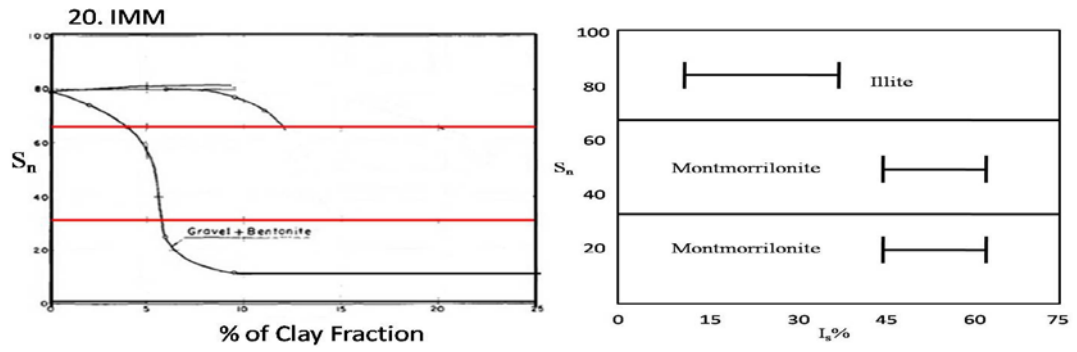


Fig.1b.20

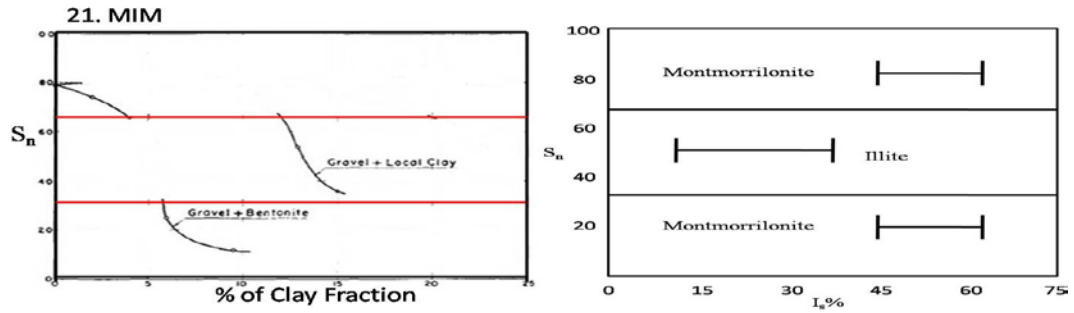


Fig.1b.21

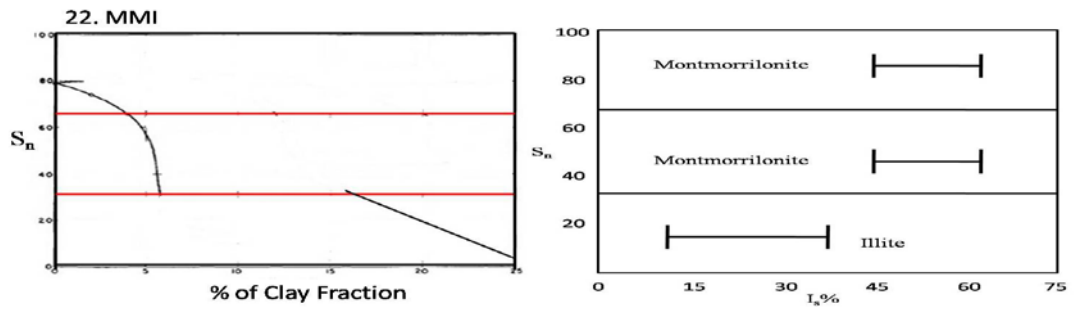


Fig.1b.22

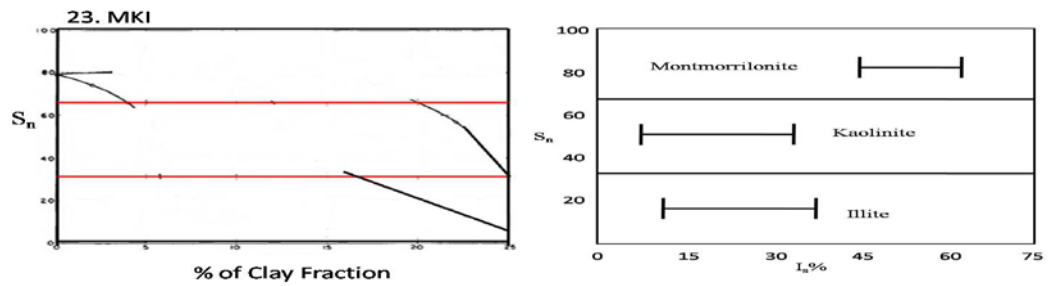


Fig.1b.23

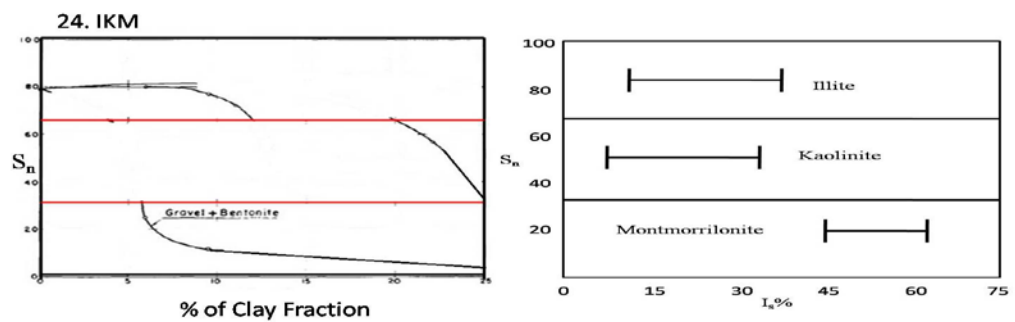


Fig.1b.24

### The Role of Co-efficient of Consolidation, $c_v$ , and Shrinkage Index, $I_s$ , in Dredged Materials

In Geo-technical Engineering it is always desirable to relate  $c_v$  to index properties of the sediments. Out of plasticity index and shrinkage index, in documented research papers it is found that  $c_v$  has a better correlation with shrinkage limit and hence it is used in the discussion. The important equations are : Coefficient of consolidation  $c_v$  (in m<sup>2</sup>/s) can be expressed as:

$$c_v = \frac{K}{\gamma_w m_v} \quad \text{Eq. (1)}$$

$$c_v = 3/100 (I_s)^{3.54} \quad \text{Eq. (2)} \quad [7]$$

For which correlation co-efficient is  $r = 0.94$  for equation 2

Where

$k$ =hydraulic conductivity (m/s)

$m_v$  =coefficient of volume change (m<sup>2</sup>/kN)

$\gamma_w$  =unit weight of pore fluid (kN/m<sup>3</sup>)

$I_s$  = Shrinkage index

It is well known that the coefficient of consolidation is a parameter that indicates the rate of compression of a saturated soil undergoing compression, which in turn directly depends on the hydraulic conductivity of the soil medium undergoing compression. The authors feel that for a soil that is more plastic as indicated by higher plasticity index or shrinkage index (Montmorillonite), hydraulic conductivity of the soil at any stress level will be less as compared to a soil that is less plastic. The reason being that the thickness of diffuse double layer (ddl) will be relatively larger for a highly plastic soil as compared to a less plastic soil. The thicker the ddl, the greater the reduction in the effective pore size for flow, and hence, reduction in the hydraulic conductivity of soil. This is the reason for  $c_v$  values being relatively higher for less plastic soils than for more plastic soils, though their liquid limit is nearly the same. As the effective consolidation pressure for a normally consolidated soil increases, the soil particles become more oriented and also come close to each other. As a consequence, for more plastic soils (Montmorillonite), the diffuse double layer repulsive forces mobilize, acting against the external loading, and hence, offer more resistance to compression (both rate and amount). This may be the reason for the decreasing trend of  $c_v$  versus  $\sigma'_v$  for more plastic soils. In the case of less plastic soils (Kaolinite, Illite) whose compressibility behavior is governed mainly by mechanical forces, as the consolidation pressure increases, the gravitational forces increase and will override the little repulsive pressure at the particle level in retarding the compression of soil, and hence, the increase in the rate of compression of the soil, i.e., an increase in  $c_v$  with pressure. This explains the varying trends of  $c_v$  versus  $\sigma'_v$  for soils with different plasticity properties.

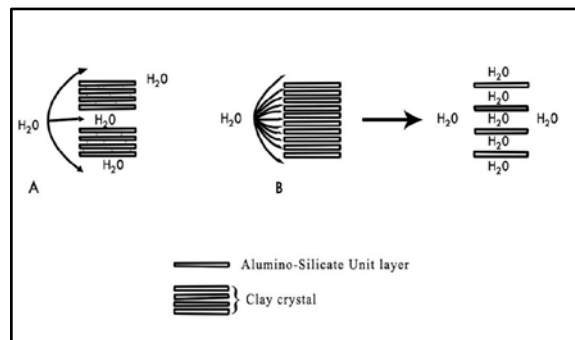
### CLAY MINERAL STRUCTURES

1. Kaolinite Group: Members of this group are considered 1:1 minerals because there is 1 tetrahedral sheet for every octahedral sheet. Within the octahedral layer there are generally aluminum atoms, and within the tetrahedral layer the cations are silicon.

2. Illite Group: Illite has a 2:1 structure and consists of a gibbsite sheet between two silica tetrahedral sheets, with the layers bounded together by potassium cations in the inter layer region. The octahedral cations are aluminum, magnesium or iron, and the tetrahedral cations can be aluminum or silicon.

3. Montmorillonite Group: Montmorillonite is a 2:1 mineral and consists of two sheets of silica tetrahedra on either side of a gibbsite sheet. Sodium (Na) Montmorillonite is a common form of the clay within bentonite, and expansive clay often specified in conjunction with drilling muds, borehole ceiling, and waste containment.

Fig.4. Moisture up take by clay minerals. A. with



non-expanding Lattice. B. with expanding Lattice. [6].

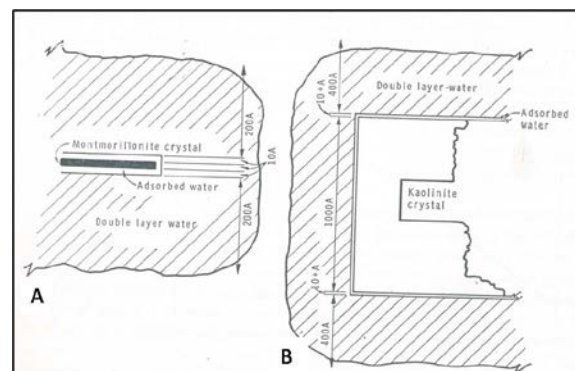


Fig.5. Relationships of clay crystals to surface and double layer water. (After Lambe, 1958 b, p.17).

A. typical Montmorillonite particle 1000Å/10Å.

B. typical Kaolinite particle 10,000Å/1000Å. [6].

## EXPLANATION FOR GEO-TECHNICAL RESPONSE OF DREDGED SEDIMENTS IN TERMS OF COAXIAL AND NON\_COAXIAL COMPONENTS OF SHEAR STRENGTH

The basic equation for shear strength is

$\tau = c + \sigma' \tan \phi$ . When moisture content is increased (Figs.2 and 3) the cohesion for all the clay minerals approximately reaches zero. The cohesion represents the coaxial component of shear strength or pure shear. Once the sediments lose their binding effect what remains is the only the residual angle of internal friction ( $\phi$ ) or non-coaxial component of shear strength or simple shear, which may not be sufficient to resist ever increasing water in lowland coastal areas. In this state shear failure or landslide will be the only choice.

## CONCLUSIONS

1. Dredging operations which is one of the anthropogenic activity, interferes and interrupts Geological formations and their processes. It creates imbalance to soils, flora and fauna, especially in the cases of 2/1 and 1/1 clay mineral types like Montmorillonite, Kaolinite and Illite.
2. The Geo-technical behavior of dredged sediments are drastically modified due to excessive rainfall.
3. The cohesion of the dredged sediments consisting of KIM ( Kaolinite, Illite and Montmorillonite) decreases with increase in moisture content and hence decreases shear strength of the sediment fill.
4. The water absorbing and retaining capacity even at higher moisture content percentage depends upon the type of clay minerals.
5. Retaining shear strength at very high moisture content depends upon the shrinkage index  $I_s$  where  $I_s = (W_L - W_{SL})$  Where  $W_L$  is liquid limit of the soil and  $W_{SL}$  is the shrinkage limit of the soil expressed in %.
6. When the shear strength approximately becomes zero the moisture content requirement for loss of shear strength varies from pocket to pocket variation in soil types. In other words the Montmorillonite combination (MMM) can tolerate moisture content upto 900% before failure in an ideal situation. And this combination, MMM is one of the 24 possibilities as shown in figure 1b.1 to 1b.24.
7. In the random variation of dredged materials and their Geo-technical properties depend mainly upon shrinkage index (which is different from shrinkage limit).
8. When clay minerals take water from dry state to liquid limit state the clay minerals with ddl (diffuse double layer) convert water into solid water which is included in ddl and offer resistance to effective

stress which in turn modifies co-efficient of consolidation and permeability of the sediments.

9. When dredged materials are used as a fill in coastal areas invariably saline water is included as pore water and hence the Geo-technical index properties are modified along with shear strength.

10. However, when there is heavy downpour of rain, all the above mentioned and discussed Geo-technical parameters which resist the incoming water or flood water fail in shear. No matter what the soil type is out of the 24 combinations which is only order out of chaos and not an exhaustive list of permutations and combinations and probabilities.

11. The dredged sediments should be treated as remolded samples.

12. The final conclusion is that water is more powerful than solids of the soils and sun is more powerful because it converts water into water vapor.

## REFERENCES

- [1] Francis N Hveem, "Importance Of Clay In Applied Soil Mechanics, Clays And Clay Material", 1952 Vol.1, No.1, pp.191-195.
- [2] Lumb P, "The Properties Of Decomposed Granite, Geo-Technique", 1962, Vol.12, No. 3, pp.226-243.
- [3] Shibuya T, "Geological Study Of Landslide Clay", KICT Report No.10 Kajima Institute of Construction Technology, Tokyo, July, 1973 pp.37
- [4] Fang HY, "Introduction To Environmental Geo-Technology", CRC Press, Boca Raton, FL, 1997 pp.652.
- [5] Skempton AW, "Long – Term Stability Of Clay Slopes", Geo-Technique Vol. 14 No.2 1964, pp.77-102.
- [6] Jacke Gillott, "Clay in Engineering Geology" Division of building research, National Research Council of Canada, Ottawa, Ont., Canada (Elsevier Publishing Company, 1968, pp.109-111.
- [7] Sridharan A, Nagaraj HB, "Coefficient of Consolidation and its Correlation with Index Properties of Remolded Soils" Geotechnical Testing Journal, Vol. 27, No.5 Paper ID GTJ10784

## 3D NUMERICAL ANALYSIS OF A DEEP CIRCULAR EXCAVATION IN THE CITY OF RIO DE JANEIRO

Jose Carlos Solis Tito<sup>1</sup>, Celso Romanel<sup>2</sup>

<sup>1</sup>Departamento de Engenharia Civil, Pontifícia Universidade Católica do Rio de Janeiro, Brasil; <sup>2</sup> Pontifícia Universidade Católica do Rio de Janeiro, Brasil

### ABSTRACT

At present, due to the need for engineering works of large scale, we have the challenge of solving problems related to deep excavations, where instability problems often occur. In this paper is presented the analysis and validation of the excavation of the service well PS – 39, of the executive project of collectors for treatment of sanitary sewage, located in the city of Rio de Janeiro. This well was constructed using a contention system of a wall of secant column, ring structure type of “shotcrete” covering the columns, and a slab of “jet grouting” anchored with passive tiebacks. The soil parameters of the different layers that compose the geotechnical profile, necessary for numerical modeling, were determined based on the geotechnical information available of the field instrumentation, laboratory data and specific literature review, considering the Mohr-Coulomb constitutive model. The results and interpretation, of the stresses and displacements during the excavation process, were determined using the PLAXIS 3D (2012) program. These results were validated with the measurements determined by instrumentation; then the numerical model will predict rationally the behavior of the set soil-structure during the excavation process. This allows to solve similar problems in advance, allowing proper planning.

*Keywords: Deep Circular Excavation, Validation of Analysis, Numerical Analysis of Excavation*

### INTRODUCTION

The different types of large-scale works that are built today require deeper excavations. In this type of excavation, failures often occur due to resistance problems or excessive deformations, presenting stability problems at different stages of the excavation, or in some cases, complete collapse. This has generated a growing interest in the evaluation of design methods, construction and control of excavations, and the different containment structures. This interest is also set in the numerical analysis of these problems, because from these models can be obtained important conclusions that will contribute to a better design of the work according to appropriate control systems.

The general objective of the research is to validate the 3D numerical analysis of the excavation of a circular well, based on the data from the field instrumentation available, through the application of the numerical method of finite elements using the PLAXIS 2D and 3D program.

### METHODOLOGY

The project of excavation of the service well PS-39, of the executive project of collectors for sanitary sewage treatment, is located in the Boas Vindas Avenue, in the District of Caju, in the city of Rio de Janeiro. Its location corresponds to the coordinates

N = 7469236000, E = 682000000, as shown in Fig. 1. The dimensions of the well are 16 m of deep and 8.60 m of inside diameter.

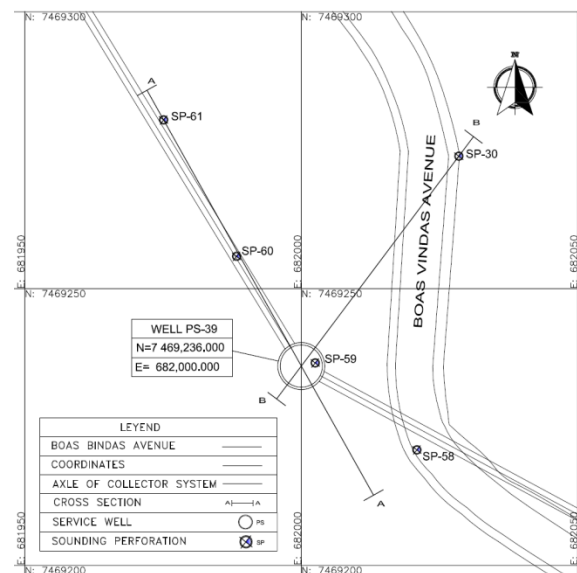


Fig. 1 Plan of location of the well PS-39 of the executive project of collectors for treatment of sanitary sewage.

The geotechnical information consisted of 5 perforations of recognition SPT, identified as SP-30, SP-58, SP-59, SP-60A and SP-61, conforming the



cross sections AA and BB, allowing to determine two geotechnical profiles for modeling the terrain, as shown in Fig. 2. From the SPT tests results, by determined correlations, were determined the index, physical and mechanical properties of the soil.

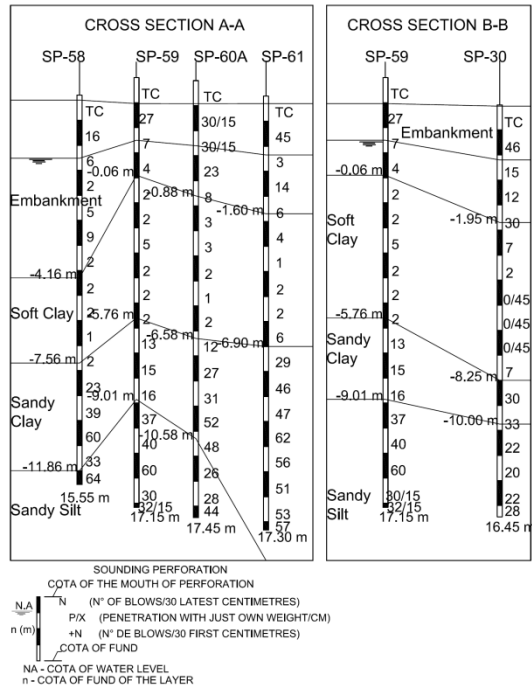


Fig. 2 Geotechnical profiles from geotechnical sections. The Section AA is formed by the soundings SP -58, SP -59, SP -60A, SP -61, and Section BB is formed by the soundings SP -59 and SP -30.

According to the geotechnical profile of the ground for the analysis of the excavation, determined according to the perforation SP-59 (presented in Fig. 3), the soil presents a layer of embankment with an average thickness of 2.9 m, followed by a layer of very soft clay, with an average thickness of 5.70 m. The next layer consists of a sandy clay, with an average thickness of 3.20 m. The last layer consists of a compact sandy silt (residual soil), with an average thickness of 21 m.

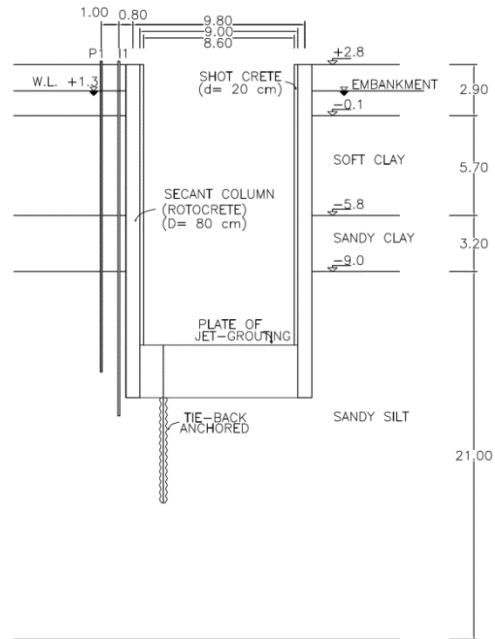


Fig. 3 Geotechnical profile for the excavation of the well PS -39.

The structure of primary containment consists of the secant columns, which have a diameter of 0.80 m, and are superimposed 0.20 m, in alternate columns were positioned 12 reinforcing bars ( $\phi = 25$  mm), these columns were performed with the technique of "wet-mixing" around the perimeter of the well to a depth of 19 m, which was modeled with a solid element with linear elastic behavior. The second containment structure is formed by a ring of shotcrete with 0.20 m of thickness, and built as the excavation progressed; this structure was modeled by plate elements with elastic behavior. The third structural element was a base plate with 3 m of thickness, made with 67 columns of "jet-grouting" with nominal diameter of 1.20 m and 32 columns with nominal diameter of 1.50 m, this plate was anchored with 25 passive tiebacks in the foundation ground. The jet-grouting plate was modeled with a solid element, and passives tie-backs with a combination of embedded piles and spring connections.

For analysis of the results is available the registers of measurements for the last stage of excavation, of the horizontal displacements registered with the inclinometer I-01. Also is available the registers of piezometric heads, determined during the period of excavation (consisting of 18 stages of excavation), registered with the piezometer P-03, at an average depth of 13.50 m, corresponding to the layer of silt.

The parameters used for modeling, according to the model of Mohr Coulmb were determined based on the results of field and laboratory test, data from field instrumentation, research results with similar

soils in different areas of the city of Rio de Janeiro, and specific literature review. These parameters allow validating the model with measurements from field instrumentation. The values used in the modeling are presented in Table 1a e Table 1b.

Table 1a Parameters of the soil layers that form the geotechnical profile.

Material		Embankment	Soft clay
Model		Mohr	Mohr
		Coulomb	Coulomb
Behavior		Drained	Undrained
Parameter	Unit		
$\gamma_{\text{unsat}}$	kN/m <sup>3</sup>	19	13.3
$\gamma_{\text{sat}}$	kN/m <sup>3</sup>	20	13.3
$e_0$	-	0.5	3.9
$k_x$	m/s	10 <sup>-5</sup>	10 <sup>-6</sup>
$k_y$	m/s	10 <sup>-5</sup>	10 <sup>-6</sup>
$k_z$	m/s	10 <sup>-5</sup>	10 <sup>-6</sup>
$c_k$	-	10 <sup>15</sup>	10 <sup>15</sup>
$K_{0x}$	-	0.43	0.59
$K_{0y}$	-	0.43	0.59
Model parameters			
$E'$	kN/m <sup>2</sup>	6000	1800
$\nu'$	-	0.3	0.3
$c'$	kN/m <sup>2</sup>	2	3.3
$c_u$			
$\phi'$	°	35	24
$\psi$	°	0	0
Interface			
$R_{\text{inter}}$	-	1	1

Table 1b Parameters of the soil layers that form the geotechnical profile.

Material		Embankment	Soft clay
Model		Mohr	Mohr
		Coulomb	Coulomb
Model		Mohr	Mohr
		Coulomb	Coulomb
Behavior		Drained	Undrained
Parameter	Unit		
$\gamma_{\text{unsat}}$	kN/m <sup>3</sup>	15	17
$\gamma_{\text{sat}}$	kN/m <sup>3</sup>	15	17
$e_0$	-	2.8	0.9
$k_x$	m/s	7×10 <sup>-6</sup>	10 <sup>-5</sup>
$k_y$	m/s	7×10 <sup>-6</sup>	10 <sup>-5</sup>
$k_z$	m/s	7×10 <sup>-6</sup>	10 <sup>-5</sup>
$c_k$	-	10 <sup>15</sup>	10 <sup>15</sup>
$K_{0x}$	-	0.58	0.38
$K_{0y}$	-	0.58	0.38
Model parameters			
$E'$	kN/m <sup>2</sup>	3000	5×10 <sup>4</sup>
$\nu'$	-	0.25	0.3
$c'$	kN/m <sup>2</sup>		10
$c_u$		25	
$\phi'$	°		38
$\psi$	°	0	0
Interface			

## DISCUSSION OF RESULTS

The finite element mesh of the three-dimensional model is shown in the Fig. 4. For the boundary conditions of this model, was adopted the standard boundary conditions, which are completely fixed in the base and only fixed perpendicular to the surface in the lateral planes. Concerning to the initial conditions, the stresses were generated by the  $K_0$  procedure, and the pore pressure calculation was established by the phreatic level.

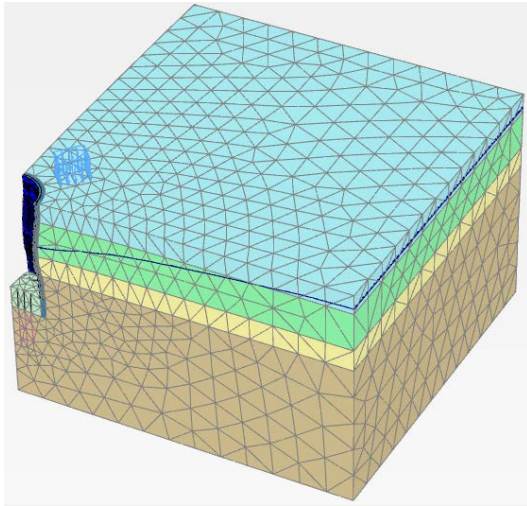


Fig. 4 Three-dimensional finite element model, for the last stage of the excavation (E18).

In the Fig. 5 is shown the horizontal distribution effective stress acting on both surfaces of the containment walls, for the four representative stages of the analysis, which are the initial conditions (E0), the first stage of excavation (E1) with a depth of 0.90 m, the intermediate stage of excavation (E9) with a depth of 8.60 m and the last stage of excavation (E18) with a depth of 16 m. In this diagram, the negative effective pressures correspond to those exerted on the inner surface (excavated side) and the positive on the outer surface (supported side). As the excavation proceeds, horizontal effective stress on the passive side is increased to its maximum value, acting directly on the plate of jet grouting.

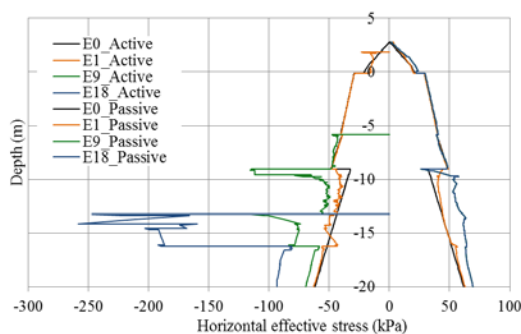


Fig. 5 Evolution of the horizontal effective stress on the active side and the passive side, during the excavation process.

To model the effect of the water flow is considered the flow at a steady state, because the mechanical analysis was established as a resistance analyze, excluding the effect of consolidation due to the short term of execution of the excavation, lasting almost a month.

In the Fig. 6 is presented the pore pressure

distribution in steady state, acting on both surfaces of the containment wall, determined for the four representative stages of the analysis, these are for the initial conditions (E0), the first stage of excavation (E1), the intermediate stage of excavation (E9) and last stage of excavation (E18). The negative pressure corresponds to exert on the surface at the active side, and the positive on the surface of passive pressures. In the first stage of excavation (E1), the levels and distribution of pore pressure are similar, because the excavation did not reach the water table. In the intermediate stage of excavation (E9) the pore pressure decreases to a height of 0.11 m, due to the abatement corresponding to this level of excavation. In the last stage of excavation (E18) can observe the effect of the stiffness of the structural element formed by the plate of "jet grouting", in the elevation of -13.2 to -16.2 m.

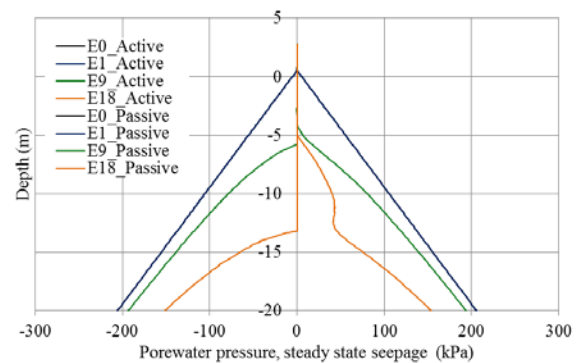


Fig. 6 Evolution of the pore pressure on the active side and the passive side.

In the Fig. 7a (1a), 5a (2a), 5a (3a), according to the charge distribution of total pressure, can be observed that the end of excavation, the drainage is established primarily through the layer of residual soil.

The excess pore pressure generated during the excavation process, considering established flow conditions are shown in Fig. 7b (1b), 5b (2b), 5b (3b). The most significant changes on the active side are due falling water level, corresponding to a decrease in pressure; and in the passive side are due to the excavation process, concentrated in the undrained layers. At the end, in the excavated side, the effect of excess pore pressure is zero, because the level of excavation reached the drained layer, but this had effect in the previous stages of the excavation.

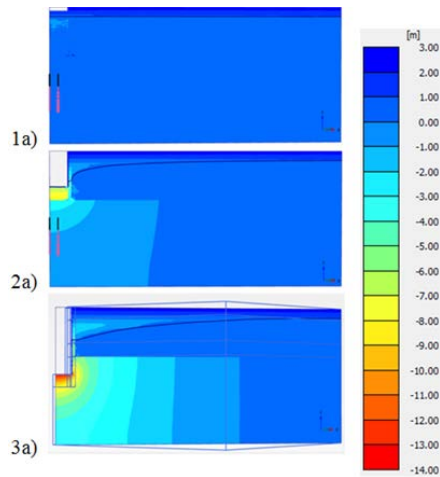


Fig. 7a Distribution of total pressure loads, in the condition of steady state flow, in stages with excavation depth (1a) 0.90 m, (2a) 8.60 m, (3a) 16.00 m.

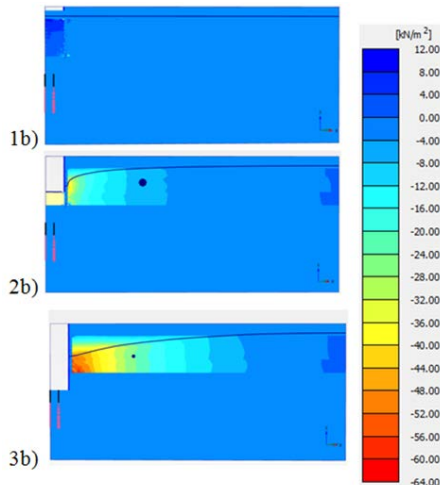


Fig. 7b Excess pore pressure, in the condition of steady state flow in stages with excavation depth (1b) 0.90 m, (2b) 8.60 m, (3b) 16.00 m.

In the Fig. 8, the profile of horizontal displacements of the control line (corresponding to the location of the inclinometer I-01) is presented. According to the diagram, the distribution of horizontal displacements with 3D modeling is similar to axi-symmetric 2D model. The modeling results show a pronounced curvature in the interface between the layers of soft clay and sandy clay with a convexity oriented toward the interior of the excavation. The displacements registered with 2D model show a marked discontinuity in the change of layer. At the end of the excavation, the maximum horizontal displacement in the control line was presented at elevation -5.5 m, with a value of 0.0143 m, which corresponds to the position of the interface soft clay and sandy clay. The minimum horizontal

displacement had a value of 0.000953 m corresponding to the elevation of 2.10 m, in the control line.

On the surface, the soil displacement is lower, accompanying the movement of the wall. The effect of flow in steady state has a minimum influence in the displacements. The effect of modeling the water flow in steady state in the 3D modeling, was concentrated in the layers of clay, producing a minimal influence in the displacements. It produced a contribution to the maximum horizontal displacement, of 0.00096 m.

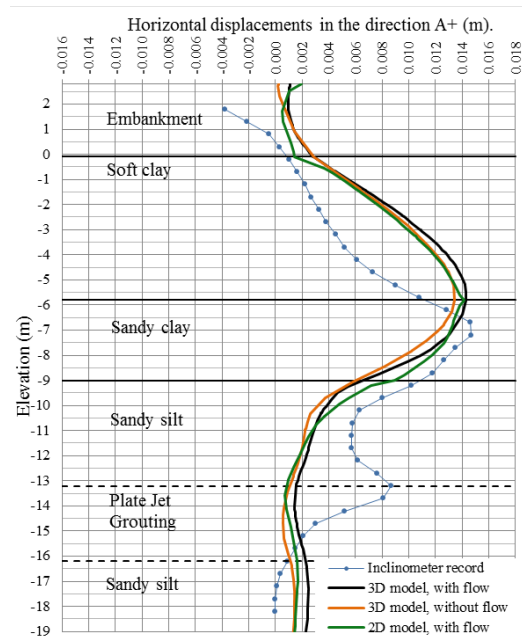


Fig. 8 Profile of horizontal displacements in the radial direction toward the center of the excavation.

In Fig. 9 is presented the piezometer heads registered during the 18 stages of the well excavation. The piezometer level present a fall of about 6 m, when the excavation reached the stratum of very soft clay (which is based on the elevation of -0.10 m). Also can be observed the validation of the 2D and 3D models with the piezometer heads recorded. The maximum difference between the determined head and the piezometric head was presented at the excavation stage 12 (corresponding to the date 14/10/1999). In the 2D model was 1.438 m and in the 3D model was 1.481 m, this depression was due to the flow that occurred in the drainage holes that were dropped off at the coating of shotcrete. This shows that the overlapping secant columns were not waterproof ring.

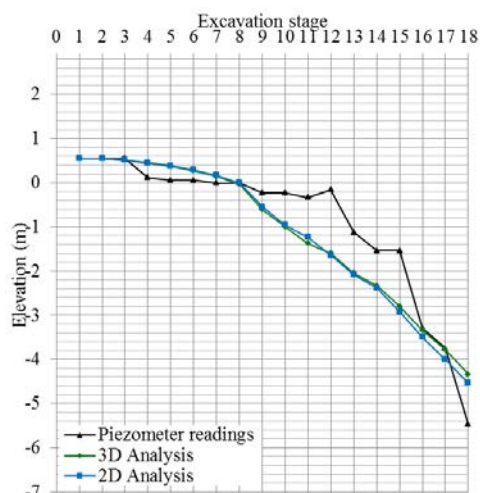


Fig. 9 Descent of the water level in the piezometer P 03.

## CONCLUSIONS

After collecting the index, physical and mechanical properties of the different soil types that form the stratigraphic profile of the well PS -39, according to the results of field and laboratory test, field instrumentation data, results of research conducted with similar soils in different areas of the city of Rio de Janeiro and specific literature review, the values used in the 3D numerical analysis were obtained.

Once established the values of the soil parameter, of the four layers corresponding to the stratigraphic profile of the well PS-39, required by the model Mohr Coulomb and using the PLAXIS 3D program, the maximum displacements were determined in the control line. In the last stage of excavation, the maximum horizontal displacement has a value of 0.0143 m at elevation -5.5 m, representing a ratio of the horizontal displacement/wall height of 0.000918. And according to the inclinometer readings, the maximum horizontal displacement at the elevation of -7.2 m, has a value of 0.0147 m. The difference between the displacements determined with the program and field measurements is 0.000403 m, representing a percentage of deviation of 2.74 % relating to the horizontal displacement registered in the inclinometer.

Concerning to the earth pressures acting on the secant columns, of the active horizontal pressure side. For the elevation of - 13.2m (corresponding to the bottom of the excavation) the horizontal effective stress is 246.87 kN/m<sup>2</sup>, for the elevation of -16.2 m (corresponding to the base of the secant column) the stress is 189.21 kN/m<sup>2</sup>. For the active horizontal pressure side, the horizontal effective stress for the elevation of 2.80 m (corresponding to the top of the secant column) is 1.439 kN/m<sup>2</sup>, and for the elevation of -16.2 m (corresponding to the

base of the secant column) is 64.296 kN/m<sup>2</sup>.

According to the 3D numerical analysis of the excavation, considering steady state flow, the effect of excess pore pressures in the wall of secant columns is greater in the soil content side, in the clay layer. This is due to undrained behavior of these soils, discharge process and decrease the water table, generating positive pore pressures (excess pore pressure suction) on the boundary of the excavation, increasing the effective stress. In the establishment of the boundary conditions for the analysis, the inside of the well acts as a drainage system, generating a progressive depression of the water level, as the excavation progresses. Thereby contributing to the horizontal movement, at the last stage of excavation, the interface of the layers of soft clay and sandy silt, in an amount of 0.00096 m.

The finite element method has many advantages due to its generality and ease of determination of clusters of complex calculation in analysis of two and three dimensions, constituting a tool to make a lot of analysis, preventing the occurrence of failures. This tool allows to determine an approximate representation of reality by modeling, using numerical analysis. Also allowing the drafting and designing of quality projects, obtaining results with adequate speed to the requirements and possibly offering better cost, therefore constitutes a competitive tool.

## ACKNOWLEDGEMENTS

The authors wish to thanks to the Pontificia Universidade Católica do Rio de Janeiro, for the support granted, which allowed the completion of this work.

## REFERENCES

- [1] Brinkgreve R. B. J., Engin E. and Swolfs W. M., PLAXIS 3D. Material Models Manual 2012. Holanda: Plaxis bv, 2012.
- [2] Massad, F., Escavações a céu aberto em solos tropicais Região Centro-Sul do Brasil. São Paulo: Oficina de textos, 2005.
- [3] Potts, D. M., "Numerical analysis: a virtual dream or practical reality?", *Géotechnique* 53, No. 6, 2003, pp. 535–573.
- [4] Rodríguez, A. R. and Mejía, H. C. Instrumentación de campo, Apuntes del libro: La Ingeniería de Suelos en las Vías Terrestres Carreteras, Ferrocarriles y Aeropistas Vol. 2. México: División de Educación Continua, Facultad de Ingeniería UNAM, 1984.
- [5] Sandroni S. S., "Os casos de escavações na região da cidade de Rio de Janeiro", *SEPE* 4, Vol. 2, 2000.

- [6] Schnaid, F. and Odebrecht E., Ensaios de campo, e aplicações à Engenharia de Fundações. 2a ed. São Paulo: Oficina de Textos, 2012.
- [7] Whitlow, R., Fundamentos de Mecánica de Suelos. México: Compañía Editorial Continental S.A. de C.V, 1994.
- [8] Zdravkovic, L., Potts, D. M. and John ST H. D., “Modeling of a 3D excavation in finite element analysis”, *Géotechnique*, Vol. 55, Issue 7, 2005, pp 497 –513.
- [9] Puller, M., *Deep Excavation: a Practical Manual*, 2nd. Ed. London, England: Thomas Telford, 2003.



# STABILITY ANALYSIS OF THE SAIGON RIVERBANK SUBJECTED TO RIVER WATER LEVEL FLUCTUATION

A. Oya<sup>1</sup>, H.H. Bui<sup>2</sup>, N. Hiraoka<sup>1</sup>, M. Fujimoto<sup>3</sup>, R. Fukagawa<sup>3</sup>

<sup>1</sup>Graduate school of Science and Engineering, Ritsumeikan University, Japan,

<sup>2</sup>Department of Civil Engineering, Monash University, Australia <sup>3</sup>Department of Civil Engineering, Ritsumeikan University, Japan

## ABSTRACT

The Saigon River, which flows through the center of Ho Chi Minh City, is of critical importance for the development of the city as forms as the main water supply and drainage channel for the city. In recent years, riverbank erosion and failures have become more frequent along the Saigon River, causing flooding and damage to infrastructures near the river. A field investigation and numerical study has been undertaken by our research group to identify factors affecting the riverbank failure. In this paper, field investigation results obtained from multiple investigation points on the Saigon River are presented, followed by a comprehensive coupled finite element analysis of riverbank stability when subjected to river water level fluctuations. The river water level fluctuation has been identified as one of the main factors affecting the riverbank failure, i.e. removal of the balancing hydraulic forces acting on the riverbank during water drawdown.

*Keywords: Stability analysis, Water level fluctuation, Seepage, FEM*

## INTRODUCTION

Many cities in south-east Asian countries have developed in downstream areas of the regions great rivers, and as a result they often suffer from flooding. Ho Chi Minh City (HCMC), located in southern Vietnam, is one of the leading economic and commercial hubs in South-East Asia. The Saigon River runs through the center of HCMC, provides its main source of water, and contributes to its industrial development. However, riverbank failure has recently become a serious issue especially at the flood events, with numerous reports of settlement and in some cases buildings collapsing. An example of a riverbank failure in the Thanh Da peninsula region (along the Saigon River) is shown in Figure 1. Furthermore, the increasing frequency of riverbank failures and subsequent flooding may hinder the future economic development of HCMC [1].

Some examples of riverbank failure countermeasures currently in use along the Saigon River are shown in Figure 2. These include: wooden piles to structurally reinforce river banks, and soil bags as temporary reinforcement measures. However, reinforcement of large sections of the river with piles is likely to be prohibitively expensive, sandbags are at best of a practical short term solution; an effective and economical countermeasure is required. However, in order to identify effective countermeasures it is necessary to first develop an understanding of the mechanisms leading to riverbank instability and failure and their causes. Investigating riverbank failure mechanisms has been a focus of our research group. The river water level fluctuation has been

identified as one of the main factors affecting the riverbank failure. [2] However, the seepage behavior due to water fluctuations and its effect on river bank stability have not been revealed. In this paper, field investigation results obtained at multiple points on the Saigon River are presented, followed by a comprehensive coupled finite element analysis of riverbank stability when subjected to river water level fluctuation.



Figure 1 Riverbank failure along Saigon River



Figure 2 Countermeasure by wood piles



Figure 3 Locations of the observation sites



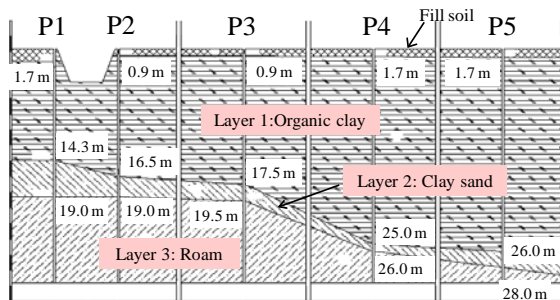


Figure 4 Soil layers at P1-P5

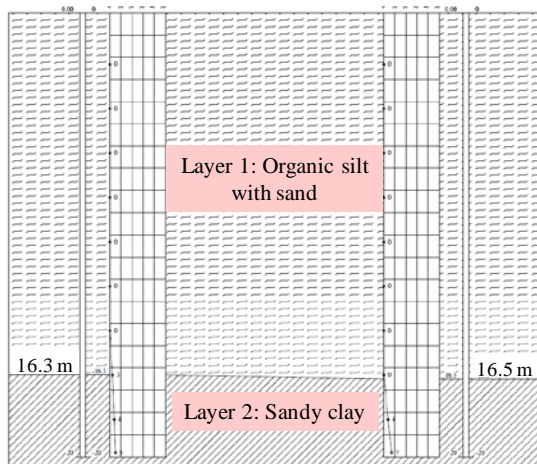


Figure 5 Soil layers at P6

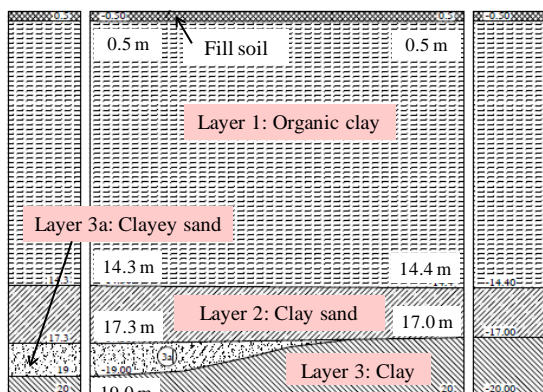


Figure 6 Soil layers at P7

## GEOTECHNICAL INVESTIGATION

Site investigations have been conducted at seven observation points along the banks of the Saigon River, most of which occur around the Thahn Da peninsula in HCMC (Figure. 3). Standard Penetration Tests (SPT) and comprehensive laboratory soil testing (Moisture content, Wet density, Specific gravity, Atterberg limits, Triaxial test or Direct shear strength test and consolidation test) based on ASTM criteria were performed on soil samples recovered from sites P1–P5 (blue dots), 2 points at site P6 (red dot), and site P7 (black dot). Bathymetry surveys of the Saigon River were undertaken using an Acoustic

Doppler Current Profiler (ADCP) at 3 locations (Figure 3). The results of ADCP testing are presented in Figures 7 to 9. Also, groundwater level and river water level were measured at site P7 (Figure 3).

### Sub-surface conditions

Three cross-sectional profiles have been determined at investigation site P1 to P5, P6 and P7, and cross sections are presented in Figures 4, 5 and 6 respectively.

Table 1 Soil parameters at P1-P5

Item	Layer1	Layer2	Layer3
$w_L$ %	70	36	
$w_P$ %	38	18	
$I_p$ %	32	18	
$w$ %	75	20	17
$\rho_t$ g/cm <sup>3</sup>	1.47	2.11	2.11
$\rho_d$ g/cm <sup>3</sup>	0.86	1.76	1.81
$G_s$	2.61	2.72	2.66
$S_r$ %	95.2	99.5	96.6
$c$ kN/m <sup>2</sup>	10.8	36.3	9.8
$\phi$ deg	4.38	15.7	28.1
$k$ m/sec	$6.2 \times 10^{-8}$	$4.8 \times 10^{-7}$	$6.1 \times 10^{-5}$
$N$	0-3	8-15	15-30

Table 2 Soil parameters at P6

Item	Layer1	Layer2
$w_L$ %	87.2	55.6
$w_P$ %	44.9	27.0
$I_p$ %	42.3	28.6
$w$ %	95.7	46.8
$\rho_t$ g/cm <sup>3</sup>	1.46	1.76
$\rho_d$ g/cm <sup>3</sup>	0.74	1.19
$G_s$	2.62	2.70
$S_r$ %	97.0	96.9
$c'$ kN/m <sup>2</sup>	11.8	16.6
$\phi'$ deg	18.9	23.2
$k$ m/sec	$4.02 \times 10^{-10}$	$1.62 \times 10^{-10}$
$N$	0	3-7

Table 3 Soil parameters at P7

Item	Layer1	Layer2	Layer3	Layer3a
$w_L$ %	73.4	39.2	51.1	
$w_P$ %	46.8	20.3	30.2	
$I_p$ %	26.6	18.9	20.9	
$w$ %	86.7	26.6	44.0	27.0
$\rho_t$ g/cm <sup>3</sup>	1.45	1.95	1.71	1.88
$\rho_d$ g/cm <sup>3</sup>	0.77	1.52	1.19	1.48
$G_s$	2.60	2.72	2.72	2.67
$S_r$ %	95.0	92.0	93.0	89.0
$c$ kN/m <sup>2</sup>	11.3	23.7	17.2	17.2
$\phi$ deg	9.43	12.3	23.4	7.55
$k$ m/sec	$5.95 \times 10^{-6}$	-	-	-
$N$	1-2	12-13	7-11	8

Soil parameters obtained from the soil testing are presented Tables 1, 2 and 3. Symbols used for the tables indicate as follows;  $w_L$ : Liquid limit,  $w_p$ : Plastic limit,  $I_p$ : plastic index,  $w$ : water content,  $\rho_i$ : Wet density,  $\rho_d$ : Dry density,  $G_s$ : Specific gravity of soil particle,  $S_r$ : Degree of saturation,  $c$ : cohesion,  $\phi$ : Friction angle,  $k$ : Hydraulic conductivity,  $N$ : SPT-N-value. At each of the investigation locations there were typically 2 or 3 distinct soil units. At P7, 4 soil layers were identified. At all locations, underlying the fill unit was a very soft organic clay/silt with a thickness varying from about 14 m to 26 m. The presence, and considerable thickness of this very soft soil, is of particular importance for slope stability assessment of the Saigon riverbank.

### Geometry of the bank

ADCP was used to investigate the three-dimensional distribution of flow-velocities in the Saigon River by obtaining three cross sections at locations shown in Figure 3. ADCP measures the river flow-velocities by transmitting ultrasonic waves into the floodway, and the results of this investigation are shown in Figures 7 to 9. Riverbank slopes of  $30^\circ$  occur at both sites, and heavy and thin lines in the river channels indicate the riverbed and the range of measurement, respectively.

### River water levels and ground water levels

Measurement of the groundwater level was carried out at three wells, numbered 1, 3, and 4; these are presented in Figure 10. Similarly, the river water level was measured using a water pressure gauge placed directly on the river bed.

Figure 11 shows variations in the groundwater level and river water level at observation site P7 over the duration of the experiment. A zero-value for the level of both river water and groundwater was set as equal to the ground level at 1. Groundwater level fluctuations reach a maximum of approximately 0.5 m, despite the low permeability of the soil. Larger fluctuations can be observed at observation points closer to the river, and the groundwater level is higher on at observation points furthest away. These data show that the Saigon River water level fluctuates by about 2 m in a single day, and the relationship between river water levels and groundwater levels.

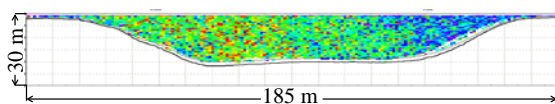


Figure 7 Cross-section at A-A' (ADCP No.1)

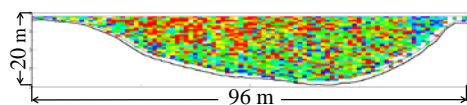


Figure 8 Cross-section at B-B' (ADCP No.2)

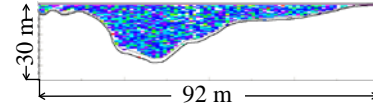


Figure 9 Cross-section at C-C' (ADCP No.3)

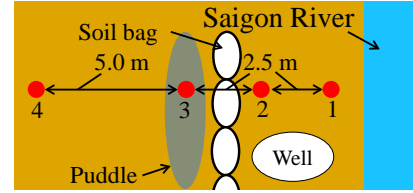


Figure 10 Set up condition of the wells

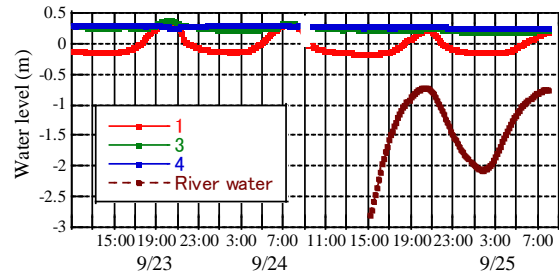


Figure 11 Groundwater level / River water level

### FLOW-STABILITY COUPLED ANALYSIS

Seepage flow-stability coupled analyses using commercial FEM software PLAXIS was conducted to examine how the water fluctuation and infiltration characteristic of the bank affect stability of the riverbank.

#### Analyses outlines

FEM analyses of the riverbank subjected to river water fluctuation were performed using PLAXIS [5]. Seepage flow-stability coupled analyses are undertaken. The analyses cover 3 points that site investigations are done. Soil properties at P7, P1-5 and P6 are applied to ADCP profiles No.1, No.2, and No.3 respectively. Soil properties at each site are combined with cross section at nearest points of each site for soil properties. Young modulus  $E$  is correlated from N-value of the ground, Poisson's ratio  $\nu$  is set at 0.33 which is typical value for geomaterials, and. Dilatancy angle  $\psi$  is set at 0.[6] Other parameters are determined by the results of laboratory soil tests mentioned above. Slope models are based on ADCP survey, and we develop the slope models by reading directly the line in the pictures. The slope model at No.1 is partly based on the field survey. Constitutive law is linear elastic perfectly plastic model (Mohr-Coulomb model). Shear strength reduction technique is applied to slope stability analyses. Unsaturated infiltration characteristic is determined by the Van-Genuchten model. Then, in order to assess seepage behavior in the bank, river water fluctuation is given as a boundary condition on

river side of the bank. The observed water fluctuation of 2 m is assessed as part of this analysis.

### Analyses conditions

*Conditions for No.1:* The geometry of the slope stability model is presented in Figure.12, analysis parameters are presented in Table 4. The model consists of 3 layers based on the subsurface conditions and soil parameters which were obtained from the site investigation. Soil permeability tests have not been conducted on Layer 2 and 3 materials at this stage thus hydraulic conductivity is assumed based on particle size distribution [7].

The initial water condition is based on an initial river water level and phreatic level set at 19.5 m from the bottom of the slope, this was determined by site survey. The water level is then linearly reduced to 17.5 m over a period of 4 hours, kept at 17.5 m for an hour, and then increased to 19.5 m over a period of 4 hours and kept at this level for an hour. Furthermore, initial phreatic line in the ground is assumed to be straight at 19.5m which is same as river water level.

*Conditions for No.2:* The geometry of the slope model is shown in Figure.13, and analysis parameters are shown in Table 5. The model consists of 3 layers based on the subsurface condition and soil parameters which were obtained from the site investigation. The initial river water level is set at 15.5m from the bottom of the slope, which is determined from the result of ADCP measurement. The initial phreatic line in the ground is assumed to be a straight line and the water level reduces 2 m over the period of 4 hours, kept at 13.5 m for an hour, increase to 15.5 m over the period of 4 hours and kept at this lever for an hour.

*Conditions for No.3:* Slope model is shown in Figure.14, and the analysis parameter is shown in Table 6. The slope model consists of 2 layers based on the results of the site investigation as well as other points. Initial river water level is set at 22.0 m, which is determined by result of ADCP measurement. initial phreatic line in the ground is assumed to be straight as well The water level take a descend of 2 m spending 4 hours as well as the point of profile A-A'. Then, it is kept at 13.5 m for an hour, takes an ascent of 2 m spending 4 hours and kept for an hour.

### Analyses results and discussion

For the analysis for No.1 (profile A-A'), results are shown in Figure.15 as potential failure surface obtained by stability analyses. The blue lines show

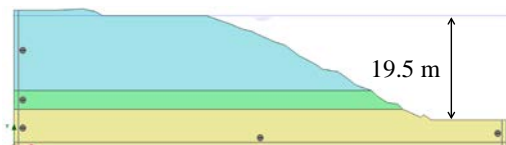


Figure 12 Slope model at A-A'

Table 4 Analysis parameter for A-A'

Item	Layer1	Layer2	Layer3
$\gamma_t$ (kN/m <sup>2</sup> )	13.2	19.1	16.8
$\gamma_{sat}$ (kN/m <sup>2</sup> )	14.1	19.2	17.6
$E$ (MPa)	4.20	27.3	22.4
$\nu$	0.33	0.33	0.33
$c$ (kN/m <sup>2</sup> )	11.3	23.7	17.2
$\phi$ (deg)	9.43	12.28	23.38
$\psi$ (deg)	0	0	0
$k$ m/s	$5.95 \times 10^{-6}$	$3.00 \times 10^{-8}$	$1.00 \times 10^{-8}$

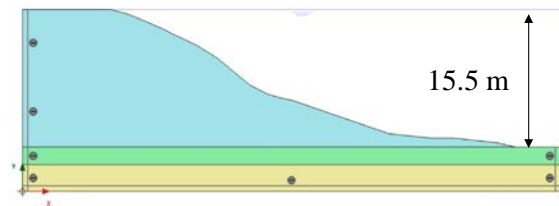


Figure 13 Slope model at B-B'

Table 5 Analysis parameter for B-B'

Item	Layer1	Layer2	Layer3
$\gamma_t$ (kN/m <sup>2</sup> )	14.72	-	-
$\gamma_{sat}$ (kN/m <sup>2</sup> )	15.2	20.7	21.1
$E$ (MPa)	5.60	33.6	64.4
$\nu$	0.33	0.33	0.33
$c$ (kN/m <sup>2</sup> )	10.79	36.3	9.81
$\phi$ (deg)	4.38	15.7	28.1
$\psi$ (deg)	0	0	0
$k$ m/s	$6.2 \times 10^{-8}$	$4.8 \times 10^{-7}$	$6.1 \times 10^{-5}$

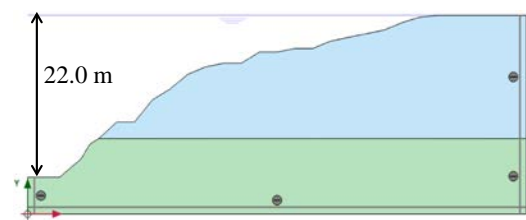


Figure 14 Slope model at C-C'

Table 6 Analysis parameter for C-C'

Item	Layer1	Layer2
$\gamma_t$ (kN/m <sup>2</sup> )	14.72	-
$\gamma_{sat}$ (kN/m <sup>2</sup> )	15.19	20.74
$E$ (MPa)	5.60	33.60
$\nu$	0.33	0.33
$c$ (kN/m <sup>2</sup> )	10.79	36.30
$\phi$ (deg)	4.38	15.66
$\psi$ (deg)	0	0
$k$ m/s	$6.2 \times 10^{-8}$	$4.8 \times 10^{-7}$



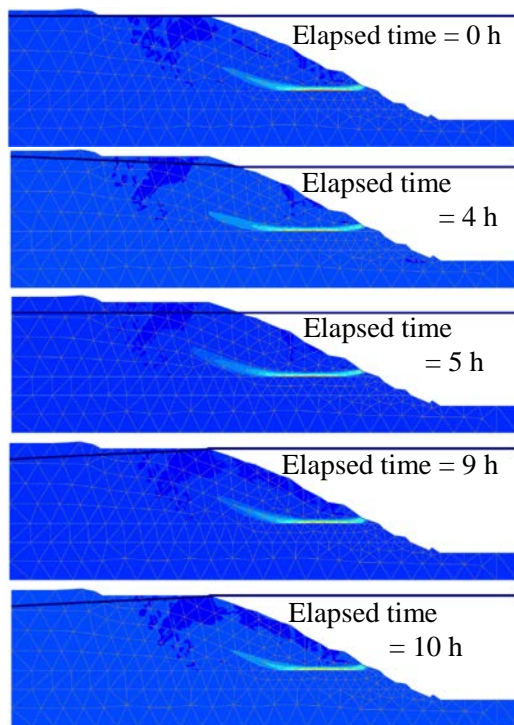


Figure 15 Potential failure surface on profile A-A'

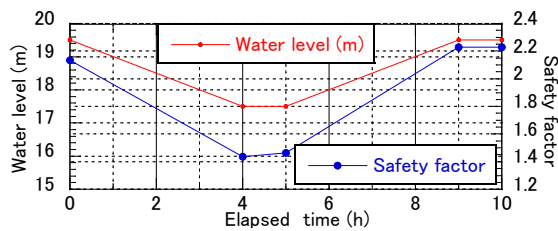


Figure 16 Safety factor on profile A-A'

the estimated the phreatic level in the ground. Safety factors are plotted in Figure 16 with river water level. When the water level goes down, the safety factor is lower. The riverbank slope is stable because of hydraulic pressure from the river when the water level remains high; however, when the river water level goes down, the hydraulic pressure dissipates and the slope becomes unstable. When the phreatic level in the river water level goes down, the phreatic level in the ground remains at a high level because of the ground's low permeability, and the weight of the soil remains high. It can be assumed that this leads to the instability of the slope. Furthermore, potential failure surface occurs in shallower point in lower water level stage, which indicates more massive slope failure can occur in this situation.

As for the analysis for No.2, results are shown in Figure 17 as potential failure surface obtained by stability analyses. The blue lines show the estimated the phreatic level in the ground. Safety factors are plotted in Figure 18 with river water level. At 5h, the water level ascent period, significant slip surface does not appear. In other stage of analyses, failure surfaces are observed on the boundary between layer 1 and 2.

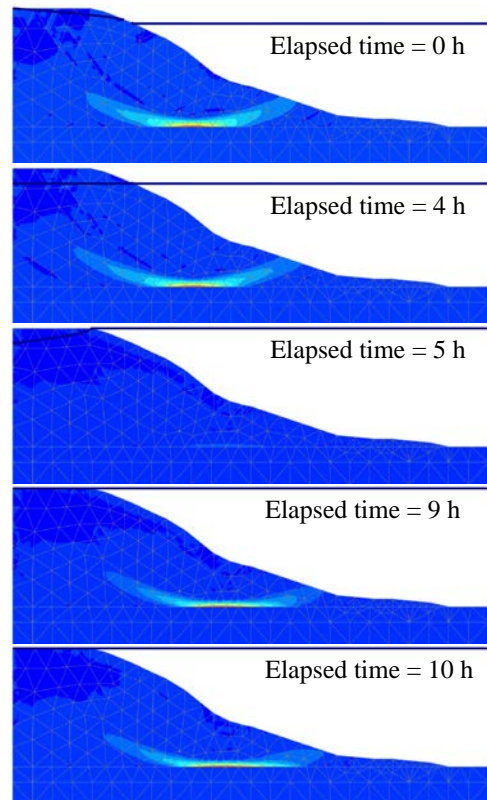


Figure 17 Potential failure surface on profile B-B'

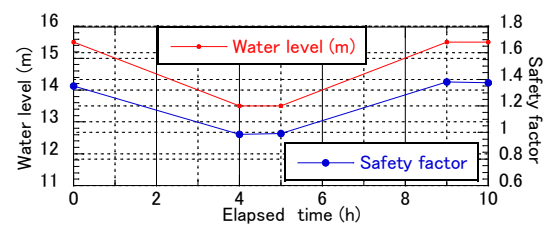


Figure 18 Safety factor on profile B-B'

A safety factor value under 1.00, which indicates the slope is unstable, is estimated in the period of water level descent. The maximum safety factor value of the slope at B-B' is lower than any safety factors of the slope at A-A' and C-C'. From the aforementioned factors, the slope is originally unstable, and gets more unstable due to water level descent.

The results of the analysis for No.3 (profile C-C') are shown in Figure 19 as potential failure surface obtained by stability analyses. The safety factors of the bank estimated stability analyses are plotted in Figure 20. The safety factor of the bank falls when the water level decreases and remains low, as is the case with profile A-A'. The phreatic level remains higher than the river water level, which is assumed to be the cause of the instability of the slope. The difference in safety factors for water level decent, the low water level period, water level ascent and the high water level period is smaller than that of other points analyzed. This is because the height of the slope is bigger than other points. As for slip surfaces,

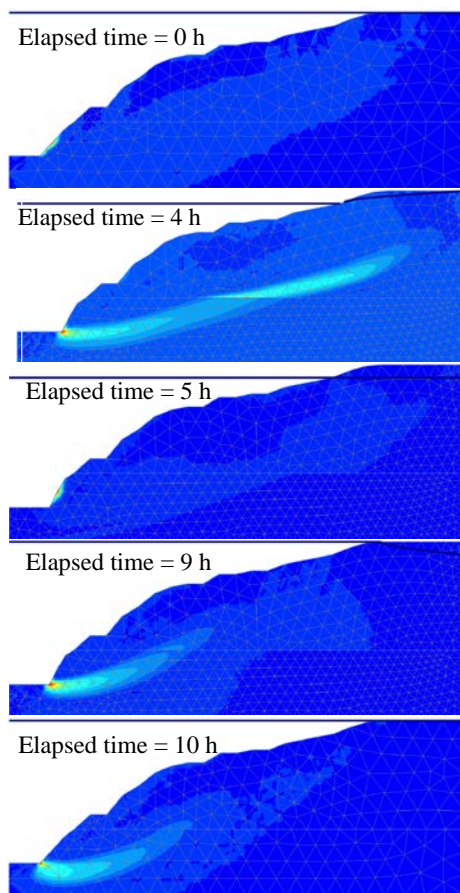


Figure 19 Potential failure surface on profile C-C'

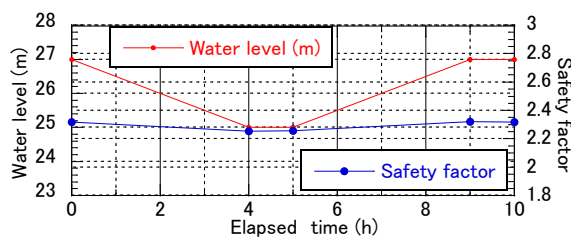


Figure 20 Safety factor on profile C-C'

significant ones do not appear when a water level is constant such as elapsed time 0 h and 5 h. On the other hand, 2 failure surfaces on the boundary of layer 1 and 2 and toe of the slope can be observed at elapsed time 4 h. There is a possibility that most massive slope failure occurs in this period.

## CONCLUSION

In this paper, geotechnical properties and hydraulic conditions along the Saigon River have been presented, and seepage flow-stability analysis was conducted. Soft clay soil is deposited as thick horizons, and the ground is mechanically weak at the all of points where we have carried out our investigation. As results of our analysis, we can observed that the safety factors of the slopes are degraded during water level descent and the low

water level period, which is a typical phenomenon that we can observe in the analyses of rapid drawdown of reservoir level in the dam.[8] These results suggest that river water fluctuation affects the stability of a riverbank, especially during water level descent because the phreatic level in the river water level goes down, the phreatic level in the ground remains at a high level because of the ground's low permeability, and the weight of the soil remains high, the slope is stable when water level is higher on the other hand. For future investigation, slope stability and seepage behavior due to cyclic water level fluctuations should be examined.

## ACKNOWLEDGEMENTS

This research was financially supported by Grants-in-Aid for scientific research (B) 23404012. Also, authors would thank Dr. LUU Xuan Loc (Ho Chi Minh City University of Technology) for his help in carrying the site investigations.

## REFERENCES

- [1] National report on disaster reduction in Vietnam, Socialist Republic of Vietnam, p.13, 2004.
- [2] Oya et al., Kansai Geo-symposium 2013, JGS Kansai Branch, pp.11-16, 2013. (In Japanese)
- [3] Report On Geotechnical Investigation (2011), Phan Tran Construction Foundation Geology CO.LTD, 2011.
- [4] Japan Road Association. 1987, Road Earthworks Manual, Maruzen Co., Ltd, Tokyo. (In Japanese)
- [5] Plaxis : Plaxis 2D Reference manual.
- [6] Technical note PWRI No. 4163, Public works research institute, Land slide research team, 2010. (In Japanese)
- [7] JGS. 2010, Laboratory soil test, Maruzen Co., Ltd, Tokyo. (In Japanese)
- [8] Plaxis : Plaxis 2D Tutorial manual.

## EFFECT OF LIGHT HYDROCARBONS CONTAMINATION ON SHEAR STRENGTH OF FINE SAND

Rajab M. Abousnina, Jim Shiau, Allan Manalo, Weena Lokuge

Faculty of Health, Engineering and Sciences, University of Southern Queensland, Toowoomba 4350, Australia

### ABSTRACT

Shear strength is one of the most important soil properties in geotechnical engineering and design. This property can be affected by several pollution sources such as crude oil. To investigate the effects of oil contamination, fine sand mixed with various amounts of light crude oil, ranging from 0 to 20% by mass were prepared. Direct shear test was conducted to determine the friction angle and cohesion of oil contaminated sand. Results showed that soil cohesion at its highest value of (10.7 kPa) at 1% oil contamination and decreases with as the oil contamination increases. Meanwhile, a slight reduction in the friction angle is observed when oil is added into the fine sand by as much as 20%. In general, the oil contamination is found to decrease the shear strength of fine sand. The results of this study will benefit engineers and decision makers in recycling or re-using of oil contaminated sand for building and construction.

**Keywords:** *Shear strength, Hydrocarbons, Contaminated sand, Cohesion, Friction angle*

### INTRODUCTION

Oil leaks can happen accidentally or intentionally during the exploration, production and operation, and transportation of crude oil. Despite the fact that most spillages of crude oil happened accidentally, there are some cases where crude oil was spilled intentionally, such as in the Gulf in 1991, where it was reported that about 1.1 billion litres of crude oil were purposely spilled into the Arabian Gulf, the Persian Gulf, and in the Kuwait [1, 2]. These are considered to be the largest oil spills in history. As a consequence of this intentional leakage, 700 km of coastline were severely polluted between Kuwait and Saudi Arabia, while approximately 49 square kilometers of the Kuwait desert was affected by this oil spillage. Furthermore, the explosions of the BP deep water horizon drilling rig in the Gulf of Mexico in 2010 caused a spill of around 91 million liters of oil, and as consequence it has affected about 110 km of Louisiana coastline. Whereas, 450,000 barrel of crude oil was intentionally discharged from oil-storage tank due to the human error cause tank fire at the Harouge Oil Operation petrochemical and refining complex at the Ras Lanuf Terminal in Libya in August 2008 [3, 4]. This intentionally spillage was done to avoid an explosion of that tank due to the fire caused by human errors during annual maintenance [3].

Most crude oil spills were caused unintentionally due to ageing facilities, lack of maintenance, and human error by the oil companies. Libya is one of the main countries exporting oil [5], and as such has been affected by the same source of sand contaminated with oil where large areas have been contaminated. Figure 1 (a) shows the major oil

pipelines, refiners, and major oil fields in Libya, while Figure 1 (b) shows the contaminated sand around the discharge disposal point of produced water, and Figure 2 shows the oil spillage in one of the Libyan oil fields.

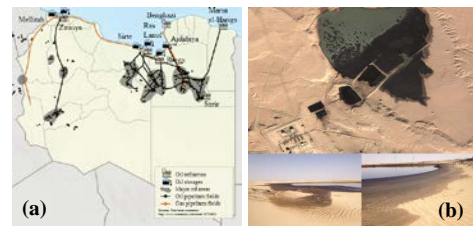


Figure 1: Libyan major oil pipelines, refiners and major oil fields [6].



Figure 2: Oil spillage

Selecting remediation method for the existing polluted sand requires knowledge of geotechnical properties and behavior of contaminated sand. Therefore, this paper presents the results of a laboratory study on the effect of light hydrocarbons on shear strength of fine sand. Light hydrocarbons and fine sand has been selected to represent the Libyan crude oil and sand in this study.

### SHEAR STRENGTH OF SAND

The shear strength of sand is a one of the most important parameters in the design of civil



engineering structures. The safety of any geotechnical engineering structure is based on the shear strength of the underlying sand [7]. All constructions, either in or on the land impose loads on the sand which supports the foundations of that particular construction or building. The load imposed on the sand may cause shear failure on the underlying sand that occurs when the imposed shear stress exceeds the maximum shear resistance (shear strength) which the sand can offer [8]. Therefore, shear strength of the sand is considered to be an important aspect in many foundations, such as the bearing capacity of shallow foundations and piles, the lateral earth pressure on retaining walls, and the stability of slopes of dams [9]. In addition to that shear strength of common engineering materials from a continuum mechanics viewpoint, such as steel, is governed by the molecular bonds which hold the material. The higher the shear strength of a material is the stronger the molecular structure [9]. Due to the particulate nature of sand, unlike that of a continuum, the shear strength depends on the interaction of anti-particles rather than the internal strength of the sand particles themselves [10]. Sand derives its shear strength from two sources: cohesion between particles and frictional resistance between particles. Cohesion is the cementation between sand grains or the electrostatic attraction between sand particles [8]. Hence, an understanding of the shear strength can play a great role in terms of the entity classification of the sand [10], which can assist engineers to derive the critical aspects of the overall sand mechanics in a specific environment. Hence, the main reason for shear strength test on the contaminated soil is to indicate whether the presence of light hydrocarbons affects the shear strength by investigating the difference between the shear strength of the sand without or with the presence of light hydrocarbons contaminant. This investigation on contaminated sand will help the geotechnical engineer to design the structure that will be built on crude oil contaminated sand.

## Experimental Approach

### Materials

Fine sand was chosen because it is similar to the sand in the Libyan Desert where the first author originated. Figure 3 shows the particle size distribution curve (PSD) of the fine sand based on AS 1141.11.1-2009 [11]. Fine sand was air dried to meet the condition of Libyan sand. Sieve analysis was initially carried out to obtain the particle grading curve of fine aggregate and it showed that the grain size of the sand particle is less than 2.36 mm.

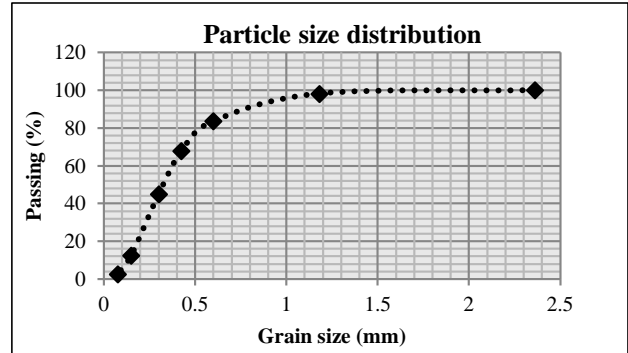


Figure 3: Particle size distribution curve of the sand

Mineral Fork w2.5 motor cycle oil was used as crude oil. This oil was selected because its density and viscosity are very similar to light crude oil (Table 1).

Table 1: comparison between light crude oil and Fork w2.5 Motorcycle oil

Specifications	Light crude oil	Fork w2.5 Motorcycle oils	Ref.
Density (Kg/L)	0.825	0.827	[12, 13]
Viscosity (mm <sup>2</sup> /s)	5.96	6.74	
Temperature (°C)	40	40	

### Direct Shear Test

A direct shear test was conducted using the ShearTrac-II system called “Geocomp” as shown in Figure 4 by applying shear to contaminated sand under constant vertical loading and according to AS 1289.6.2.2—1998 [14]. The test specimen was 24 mm thick and 63.5 mm in diameter, and it was loaded into the shear box with the aligning pins and bottom porous stone in place. Figure 5 show the process of direct shear (shear schematic).

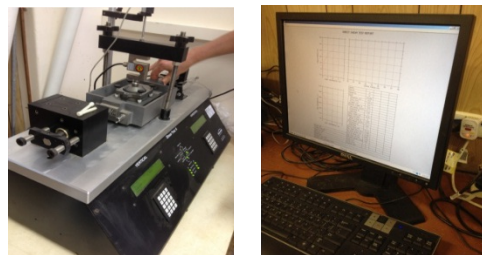


Figure 4: Direct shear (ShearTrac-II system hardware and software)

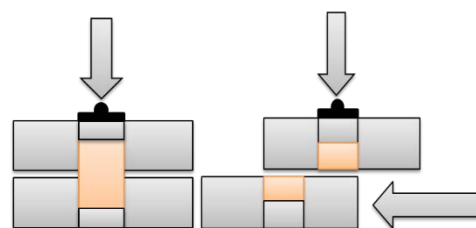


Figure 5: Shear Schematic



### Shear Strength Test Procedure

In this test, a thin soil sample is placed in the shear box consisting of two parallel blocks. The lower block is fixed while the upper block is moved parallel to the fixed one in the horizontal direction. The soil fails by shearing along a plane assumed to be horizontal. Ten samples were investigated with different contaminated soil (0, 0.5, 1, 2, 4, 6, 8, 10, 15 and 20%). Thus, a total of 30 tests were conducted under different normal stress (50, 100 and 200 kPa) respectively.

### Sample Preparation

The methods used in preparing the samples followed in the Australian Standard (AS 1289: 2001). Sample was filled up to the marked level then waited to keep the consistence of all samples See Figure 6.



Figure 6: Sample preparation

### Analysis

Effective stress and friction angle appear frequently in commonly used equations. Shear strength is related to these parameters by another parameter called cohesion, ( $c$ ). The below equation relates shear strength, effective stress, and cohesion. This is called Mohr-Coulomb failure criterion and is defined as follows [9]:

$$\tau = c + \sigma' \tan \phi \quad (1)$$

where:  $\tau$  = shear strength

$c$  = cohesion

$\sigma'$  = normal pressure

$\phi$  = angle of internal friction

### Results and Discussions

Figure 7 shows the shear stress as a function of normal stress with different oil content percentage for a series of direct shear tests

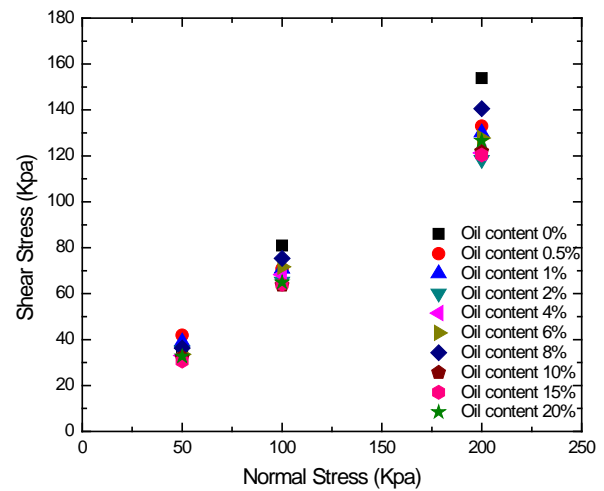


Figure 7: Shear stress (KPa) as a function of normal stress (KPa) with different crude oil content (%)

The results from the above charts are summarised in the Table 2, to clarify how the oil affected the strength parameters cohesion and friction angle. The calculated results (cohesion and friction angle) are to clarify the effects of oil contamination on the shear strength. These results are also presented graphically in Figures 8 and 9.

Table 2: Cohesion and frictional angle result

Oil content %	Cohesion (kPa)	Friction angle $\phi^\circ$
0	0.756	38
0.5	9.418	31
1	10.76	31
2	8.911	29
4	6.51	30
6	5.544	32
8	3.718	31
10	3.105	31
15	2.422	31
20	1.823	32

It can be seen from Figure 8 that a significant increase in cohesion was observed from 0% to 1% (uncontaminated sample and 1% oil contaminated sand). Interestingly, the cohesion decreases dramatically after reaching 1% oil contamination. The corresponding value of cohesion was observed as 1.823 kPa with an oil content of 20%. This particular trend may indicate the behavior of soil suction.

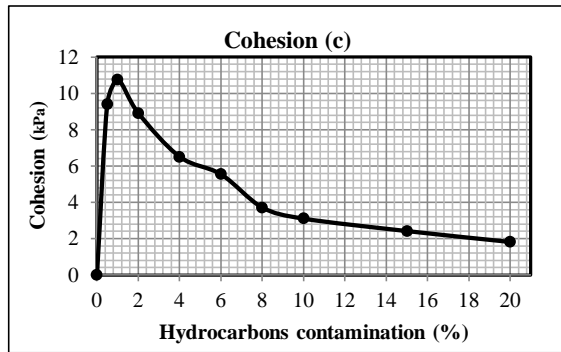


Figure 8: Cohesion as a function of crude oil contamination percentage (%)

The result of the shear strength test (Table 2 and Figure 8) illustrates a significant increase in cohesion value between the control sample and contaminated sand i.e. 0% to 1%. As can be seen from the figure, the cohesion is at its highest value of 10.76 kPa for sand with 1% oil contamination. This increase is reasonable because the moisture content of the dry sand used in these experiments was zero, so an addition of crude oil content has increased the moisture content of the dry sand and hence, it is noted that the peak value of the cohesion is obtained at 1% oil content. This observation agrees with a previous study [15], which concluded that the cohesion component of shear strength attains its peak value at around optimum moisture content and then decreases. This outcome of the previous study comparable with our observation since the cohesion value has decreased gradually with increasing oil contaminated percentage from 1% to 20% which also agrees with some previous studies that presented a similar trend on the shear strength parameter of contaminated soils [16, 17]. The reduction of the cohesion on the wet side is attributed to the soil particle coated by crude oil which leads to cohesion reduction between the soil particles. This observation is in agreement with the findings of Seed, et al. [18] they indicated that the cohesion reduction of the wet side is due to the thicker oil films around the soil particles and by increasing the crude oil content, the chance of inter particle slippage will be higher as well which resulting in a decrease in shear strength of the soil.

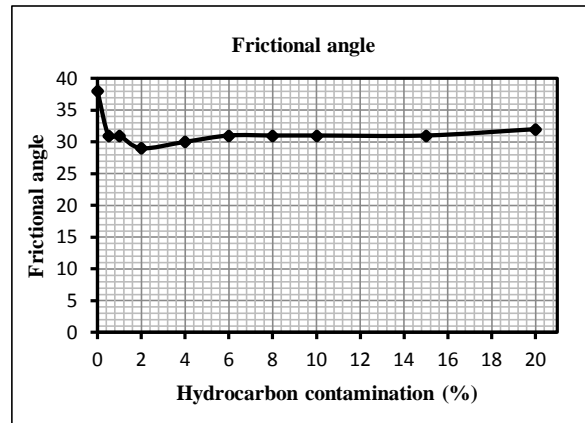


Figure 9: Frictional angle as a function of crude oil contamination percentage (%)

Figure 9 shows the frictional angle as function of the percentage of crude oil contamination. Based on the figure the uncontaminated fine sand has the frictional angle of 38°. A significant reduction of frictional angle was observed between the control sample (uncontaminated sand) and the contaminated samples (0.5%) where there was no significant variation of the frictional angle of the contaminated sand (0.5% to 20%). The frictional angle of oil contaminated sand is between 29-32°. The frictional angle of the contaminated sand has been decreased compared to the uncontaminated samples due to the lubrication effect provided by the crude oil, and this reduction of the internal friction is due to the inter-grain lubrication of the soil particles by crude oil. Thus, the characteristics of shear strength decline on oil contaminated sand can be specified due to mechanical interaction caused by high pore fluid viscosity.

Based on the analysis the shear strength values can be mathematically illustrated using the Mohr-Coulomb equation since both cohesion and frictional angle of oil contaminated sand were available.

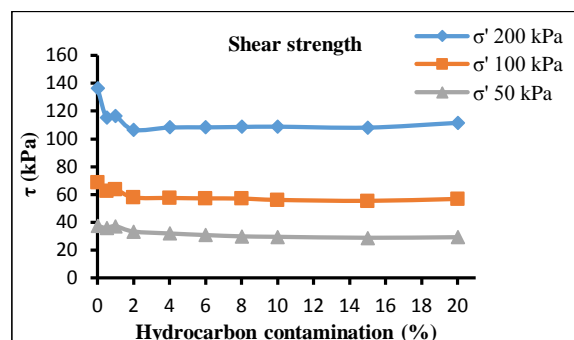


Figure 10: Shear strength as a function of crude oil content (%)

Figure 10 shows the soil shear strength as function of light crude oil content and it can be generally deduced that light crude oil pollution affects the shear strength of fine sand. The shear strength of

light crude oil contaminated sand was examined under different normal stresses i.e 200, 100 and 50 kN/m<sup>2</sup> respectively. Under shear stress of 200 kN/m<sup>2</sup> the reduction of shear strength varied from 11 up to 22% compared to uncontaminated sample (oil contaminated sand 0%), and under shear stress of 100 kN/m<sup>2</sup> the shear strength decreased from 7 to 19 % compared to uncontaminated sand, whereas when the applied shear stress was 50 kN/m<sup>2</sup> the reduction of shear strength varied from 1 to 23 %.

## CONCLUSION

This paper investigated the effects of light hydrocarbons contamination on the shear strength of fine sand. Based on the results of the study the following conclusions are drawn:

- The cohesion increased significantly with oil contamination of up to 1% and then decreased with increasing percentage of crude oil.
- A slight reduction in frictional angle was observed for fine sand contaminated with crude oil.
- Up to 20% reduction in soil shear strength was observed for oil contaminated sand.

These results provide a better understanding of the effect of light hydrocarbons on fine sand for the potential use of oil contaminated sand in building and construction. They are useful benchmarks for further investigation on oil contaminated sand as an alternative remediation method to reduce its adverse impact in the environment.

## ACKNOWLEDGEMENTS

The first author would like to acknowledge the scholarship provided by the Libyan Government during his PhD candidature.

## REFERENCES

- [1] H. Al-Sanad, W. Eid, and N. Ismael, "Geotechnical Properties of Oil-Contaminated Kuwaiti Sand," *Journal of Geotechnical Engineering*, vol. 121, pp. 407-412, 1995.
- [2] Mashalah Khamehchiyan, A. H. C. and, and M. Tajik, "The effects of crude oil contamination on geotechnical properties of Bushehr coastal soils in Iran," *IAEG*, pp. 6, 2006.
- [3] T. F. S. B. Products, "Storage Tank Fire Protection-Leave Nothing to Chance," 2008.
- [4] M. E. E. Survey, "Ras Lanuf Extinguished After Seven Days," *Middle east economic survey*, vol. 51, pp. 34, 2008.
- [5] G. Luciani, "The oil rent, the fiscal crisis of the state and democratization," *Democracy without democrats*, pp. 130-55, 1994.
- [6] U.S Energy Information Administration. (2011, 10/10). *Independent Statistics & Analysis* Available: <http://www.eia.doe.gov>
- [7] M. Budhu, *Soil Mechanics and Foundations*: John Wiley & Sons, 2008.
- [8] I. Smith, *Smith's elements of soil mechanics*: Wiley. com, 2013.
- [9] B. M. Das, *Advanced soil mechanics*: Psychology Press, 2008.
- [10] D. P. Coduto, *Foundation design*: Prentice Hall, 2001.
- [11] AS 1141.11.1, "Methods for sampling and testing aggregates - Particle size distribution - Sieving method," ed, 2009/Amdt 1-2011.
- [12] C. Ltd. (2009 ). *C. Putoline HPX Fork & Suspension Oil* Available: <http://www.championmotouk.com/product-info-t.php?Putoline-HPX-Fork-Suspension-Oil-pid10650.html>
- [13] SIMetric. ( 2011). *specific gravity of liquids*. Available: [http://www.simetric.co.uk/si\\_liquids.htm](http://www.simetric.co.uk/si_liquids.htm)
- [14] A. 1289.6.2.2, "Methods of testing soils for engineering purposes - Soil strength and consolidation tests - Determination of shear strength of a soil - Direct shear test using a shear box," ed, 1998.
- [15] E. Cokca, O. Erol, and F. Armangil, "Effects of compaction moisture content on the shear strength of an unsaturated clay," *Geotechnical & Geological Engineering*, vol. 22, pp. 285-297, 2004.
- [16] Z. Rahman, H. Umar, and N. Ahmad, "Geotechnical characteristics of oil-contaminated granitic and metasedimentary soils," *Asian J. Applied Sci*, vol. 3, pp. 237-249, 2010.
- [17] M. Khamehchiyan, A. Hossein Charkhabi, and M. Tajik, "Effects of crude oil contamination on geotechnical properties of clayey and sandy soils," *Engineering Geology*, vol. 89, pp. 220-229, 2007.
- [18] H. B. Seed, J. Mitchell, and C. Chan, "The strength of compacted cohesive soils, in Shear strength of cohesive soils," 1961.

## MONITORING THE STIFFNESS CHANGE IN CLAY WITH BENDER ELEMENT AND ELECTROMAGNETIC METHODS

Chee-Ming Chan<sup>1</sup> and Mohd Zazar Mohd Jenu<sup>2</sup>

<sup>1</sup>Faculty of Engineering Technology, Universiti Tun Hussein Onn Malaysia, Malaysia; <sup>2</sup>Research Centre for Applied Electromagnetic, Universiti Tun Hussein Onn Malaysia, Malaysia

### ABSTRACT

Soil's stiffness is usually measured in the laboratory in an indirect manner, such as by derivation from the gradient of a stress-strain plot. It requires numerous tests and may be compounded by error from the original measurement itself. As such, the bender element test has been rather popular among researchers for determining the small strain moduli of soils with minimal disturbance to the specimens. This paper examines the possibility of relating the bender element data with the dielectric constant obtained from the same soil specimen using an electromagnetic test setup. As both tests are non-destructive, they can be easily repeated on the same specimen over a period of time without the necessity of duplicate specimens. A clay sample was used in the present study, with varying water content corresponding to different 1-dimensional compression stresses. It was generally found that the resulting stiffness change was detectable from both the shear wave velocity ( $v_s$ ) obtained from the bender element tests, as well as the dielectric constant ( $\epsilon$ ) of the electromagnetic measurements, with fairly good correspondence between the two. These results shed light on the possibility of relating relevant geotechnical parameters with both the measurements for establishing a unique set of signatures for stiffness monitoring and determination in soils.

*Keywords: Stiffness, Bender element, Electromagnetic waves, Dielectric constant*

### INTRODUCTION

Extensive field as well as laboratory tests and measurements are necessary to ascertain the suitability of in situ soils for supporting a particular structure, often incurring significant costs and time consumption. This is especially so for the laboratory tests, where undisturbed soil samples must be retrieved, preserved and transported to the relevant facilities for the various tests. As such, it is always favourable to minimize test samples retrieval by implementing non-destructive measurements with ease of repetition and cross-check.

This paper attempts to describe one such endeavour by using the bender element and electromagnetic techniques to monitor stiffness change in clay soil. The soil sample was prepared from kaolin powder with the addition of various water contents. A series of oedometer tests were also carried out to simulate actual post-consolidation improved stiffness of the soil in correspondence with measurements using the bender element and electromagnetic methods. The data obtained were cross-correlated to determine the effectiveness of monitoring stiffness with both the methods.

### MATERIALS AND METHODS

The soil sample was prepared by admixing kaolin powder with water. These samples with different

water contents were used to establish the basic correlation between water content of the soil and the electromagnetic measurements. Oedometer test was also carried out with corresponding monitoring of the stiffness change with both the tests. As can be perceived, the soil's water content is the parameter linking measurements obtained from both the non-destructive tests, as elaborated in the ensuing section of the paper.

Bender elements are piezoelectric ceramic devices wired in such manner as to transmit and/or receive compression or shear waves. The direction of motion of the bender element inserted to normally no more than 5 mm of the ends of a soil specimen, whether perpendicular or parallel with the orientation of the specimen, produces the respective waves. It has become rather widely adopted in geotechnical testing in the past decade due to its simplicity, e.g. [1]-[4], though the definition of the wave arrival time remains very much an area of subjectivity. Nonetheless as long as caution is taken in conducting the test, and that the same arrival time identification method is used throughout the exercise, the errors or inconsistencies are expected to be systematic, e.g. reported by [5] & [6], and can be minimized with some normalization manipulations, for instance. The wave arrival time was determined by taking the time lapse between trigger of the wave (time zero) and first detection by the receiver, as depicted as the initial positive deflection in the received wave form

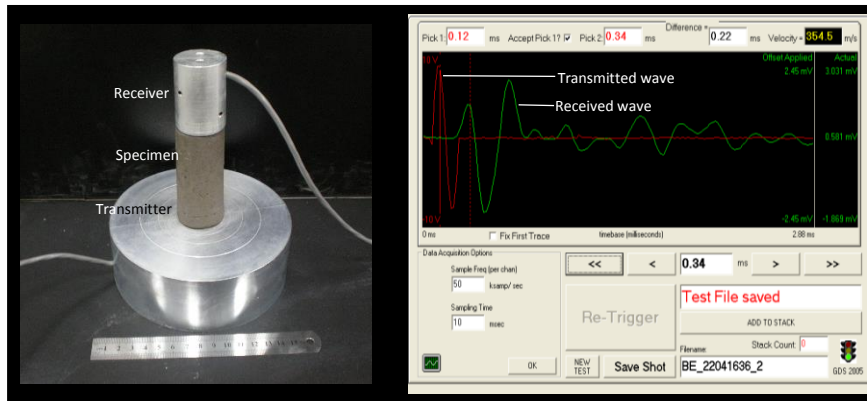


Fig.1  
Bender element test setup.

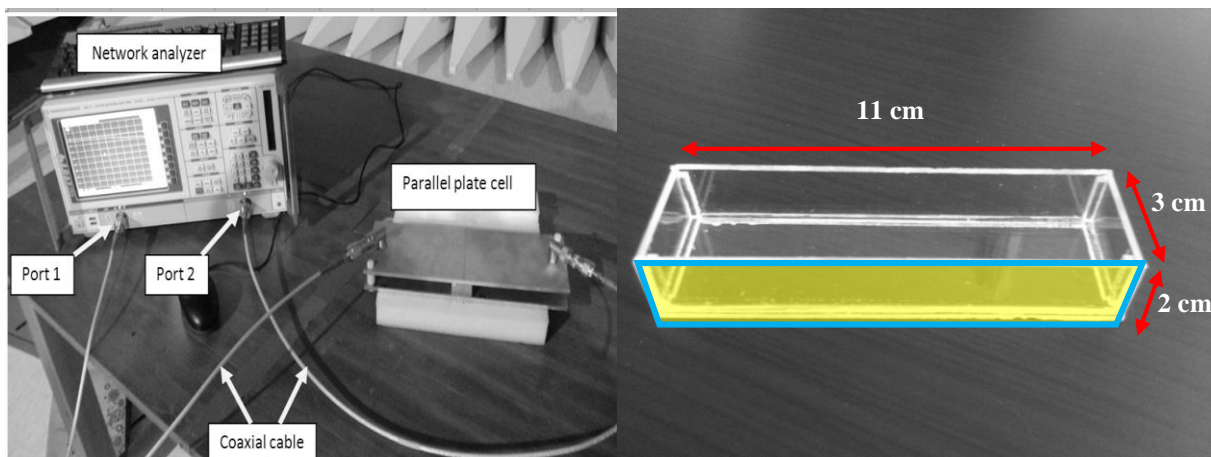


Fig.2 Electromagnetic test setup.

captured on screen. The shear wave velocity ( $v_s$ ) was then easily computed by dividing the tip-to-tip distance of the bender elements on both ends of the specimen with the arrival time determined. Note that only shear waves were adopted in the present work to avoid masking of the actual velocities by the compression wave propagating through the pore water instead of the soil skeleton, i.e. giving P-wave velocity of the water,  $\approx 1480$  m/s. The GDS BE system was used in the present study (Fig. 1). The specimens were cylindrical, 38 mm in diameter and 76 mm in height subjected to the bender element test (input frequency 650 Hz).

The electromagnetic method is a potential alternative method to determine key soil properties such as compressibility, strength and hydraulic conductivity. Referring to reports in [7], the high dielectric constant of water compared to soil solids makes the dielectric constant of moist soil highly dependent on the moisture content of soil, making it a viable tool for estimating the amount of moisture present in a soil mass. The dielectric permittivity is found to be the most suitable electromagnetic parameter for soil testing, attributed to the high-frequency permittivity parameters of waveforms produced by measurement systems with low attenuation. The properties of the waveforms are used to derive simple relations for estimation of low and

high frequency permittivity values from characteristic points of the waveforms [8]. The present study adopted a setup developed in-house (Fig. 2), which comprised of a network analyzer (Rohde & Schwarz), a pair of coaxial cable and a parallel plate cell. The soil sample was placed in a rectangular acrylic mould of 3 cm x 11 cm x 2 cm. The system was conditioned to measure S-parameters over the frequency range of 10 MHz to 14 GHz. The measured S-parameters were saved in a Matlab programme for subsequent computations of the relative permittivity or dielectric constant.

## RESULTS AND DISCUSSIONS

Fig. 3 shows  $v_s$  plotted against  $w$ , with a fairly good correlations indicated in the correlation coefficient, i.e.  $R^2 = 0.8808$ . With increased water content, the soil's structural skeleton essentially collapses into a liquefied mass. The solid particles are dispersed within the large amount of pore water present, resulting in excessive damping or impedance of the shear wave propagation. Note too that the perpendicularly traversing motion induced by the shear waves diminishes with reduced stiffness of the medium, such as a watery soil mass. As such, the shear waves take a longer time to travel between the transmitting and receiving ends of the specimens,



resulting in declining  $v_s$ .

On the other hand, the 1-dimensional compression curve was derived from a standard oedometer test on the soil specimen (Fig. 4), while Fig. 5 depicts the same data in terms of water content change. As consolidation causes gradual dissipation of excess pore water with an applied load, the settlement recorded (i.e. represented by the void ratio,  $e$ ) is directly proportionate to the water content of the soil specimen at the end of a particular loading stage. The  $w$  values shown in Fig. 5 were actual measurements taken of samples from the post-consolidation specimens. With expulsion of the excess pore water and zeroing of the excess pore water pressure, the exerted load was progressively transferred to the soil's skeleton. This consequently enhanced the soil's stiffness as a whole, with greater load-bearing capacity compared to its original form, i.e. stiffness improvement.

It follows that with  $v_s$  governed by  $w$ , and that  $w$  is of direct relation to the void ratio changes upon loading of the soil specimen,  $v_s$  can be correlated with  $e$  as shown in Fig. 6. With greater load applications in the oedometer test, more significant pore water dissipation took place, resulting in increased settlement or void ratio reduction. The outcome of the process was the stiffening of the soil matrix, as captured by the  $v_s$  increment in Fig. 6. Of course, with an oedometer cell incorporated with bender elements, actual real-time  $v_s$  changes could be monitored as the consolidation occurs, such as reported by [9]. The current indirect correlation method notwithstanding, it was considered suffice for the end-of-primary consolidation  $v_s$  values to be inferred from the corresponding water content.

Fig. 8 summarizes the electromagnetic measurement of dielectric constant ( $\epsilon$ ) on the soil specimen prepared at different water contents. The specimens subjected to the electromagnetic test were carefully prepared so as to have the same density and water content as the oedometer counterparts. Clearly a linear regression line can be plotted through the data points, indicating the rising trend of  $\epsilon$  with increased  $w$ . It ought to be mentioned that the measurement mechanism of the electromagnetic test setup is rather sensitive, leading to the scatter of data obtained. The scatter in Fig. 8 may be due to several factors, including the inaccuracy of water addition in the soil, the non-uniform distribution of water in the soil, the possibly variable calibration conditions, the misalignment (albeit small) of the mould placed in between the parallel plates, and possibly uneven contact surface of the soil with the top plate.

The electromagnetic field surrounding the soil was apparently significantly influenced by the water present in the soil specimen. The correlation in Fig. 8 enables estimation of the soil's improved stiffness via the water content, which is directly related to the compressibility of a saturated specimen. For practical

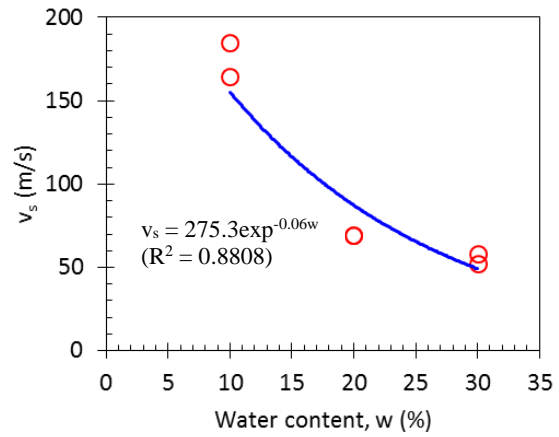


Fig.3  $v_s - w$ .

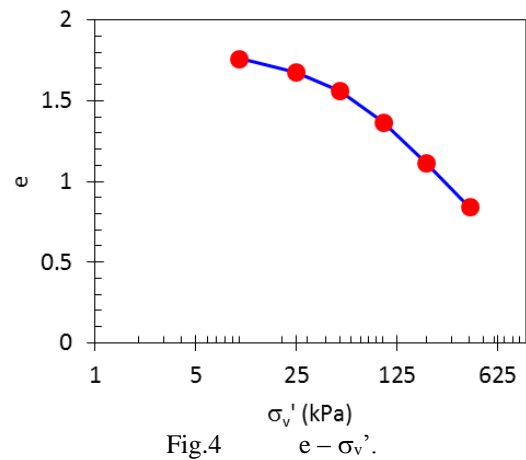


Fig.4  $e - \sigma_v'$ .

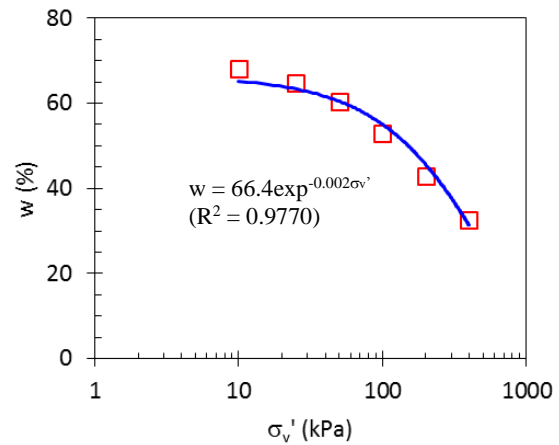


Fig.5  $w - \sigma_v'$ .

purposes, one would only need to identify the  $\epsilon$  or  $v_s$  value of a soil specimen to ascertain the stiffness, without having to subject the soil sample to the time-consuming oedometer test.

It is intuitive to expect that the rise in stiffness of a soil would be accompanied a proportional increase in strength as well. Fig. 9 relating the undrained shear strength ( $c_u$ ) and  $e$  was derived from the Author's past work with the same soil [10]. It is interesting to note that the change in  $\epsilon$  in the lower strength range (<200 kPa) is far less significant than in the higher strength range. As problematic in situ clay soils are usually



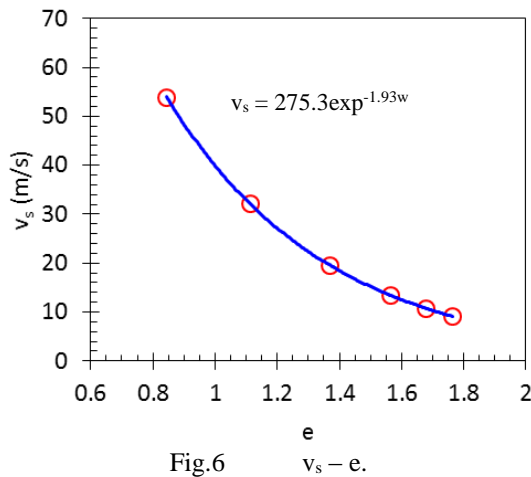


Fig.6

$v_s - e$ .

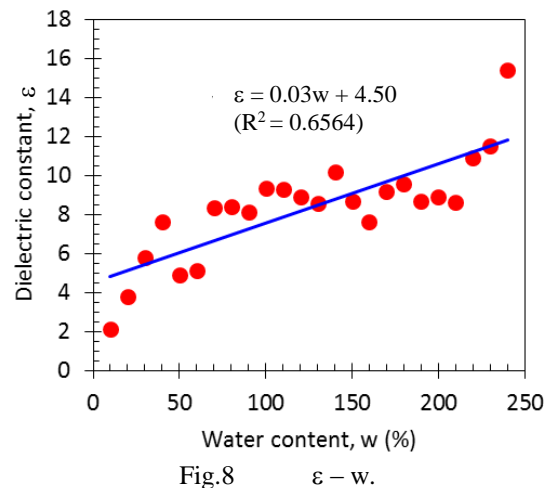


Fig.8

$\varepsilon - w$ .

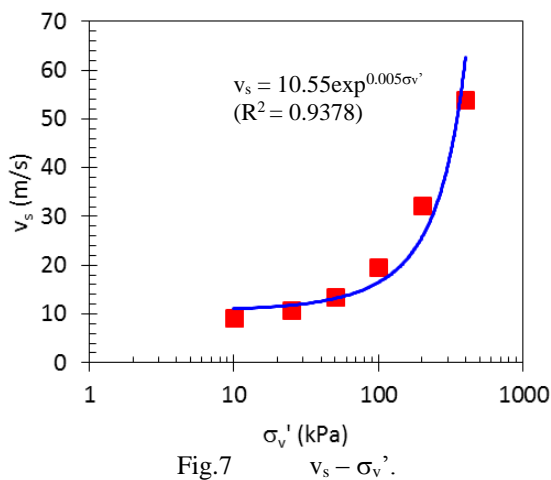


Fig.7

$v_s - \sigma_v'$ .

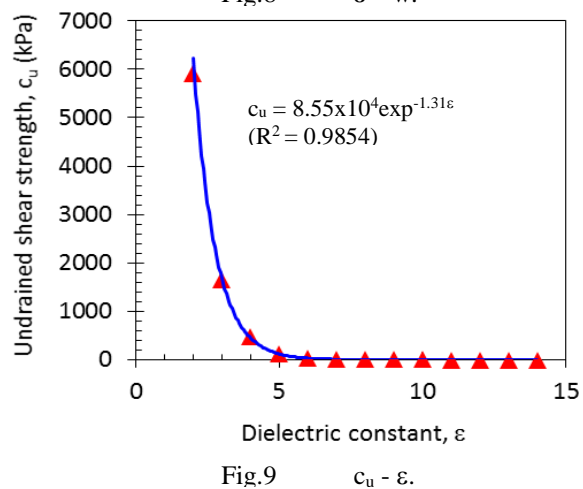


Fig.9

$c_u - \varepsilon$ .

found in the low strength range, the electromagnetic measurement technique appears to lack the sensitivity necessary to detect the changes. Furthermore soils do not normally have compressive strengths greater than 1 MPa (e.g. soft rocks), hence it is more relevant to examine the  $c_u - \varepsilon$  correlation within the common lower strength range for foundation clay soils. Nonetheless, it does show that the increment in strength corresponds with a reduction in water content, which in a clay soil indicates an improvement of the stiffness with expulsion of excess pore water via consolidation. The much higher  $c_u$  within the low  $\varepsilon$  range can be explained by the lower water content of the soil with advanced consolidation, and hence greater stiffness.

## CONCLUSIONS

The shear wave velocity ( $v_s$ ) and dielectric constant ( $\varepsilon$ ) were both non-destructive techniques for monitoring stiffness change in clay soils. The present work examined the measurements with an artificially prepared soil sample, i.e. kaolin at different water contents. It was found that the soil with higher water content gives lower  $v_s$  and higher  $\varepsilon$ , with corresponding decrease in void ratio ( $e$ ) and increase in stiffness respectively. Further work is currently in

progress to improve and refine the geo-characterisation techniques for application in a wider range of soil type and conditions, e.g. mixed and contaminated soils.

## ACKNOWLEDGEMENTS

Special thanks to W-K Loke who diligently carried out the laboratory work described in the paper. Funds were provided by the FRGS research grant, Ministry of Education, Malaysia.

## REFERENCES

- [1] Arroyo, M, Pineda, JA and Romero, E, "Shear wave measurements using bender elements in argillaceous rocks", ASTM Geotechnical Testing Journal, Vol. 33, No. 6, 2012, pp. 1-11.
- [2] Tanaka, H and Seng, S, "Properties of very soft clays: A study of thixotropic hardening and behavior under low consolidation pressure", Soils and Foundations, Vol. 52, No. 2, 2012, pp. 335-345.
- [3] Chan, C-M, "Bender element test in soil specimen: Identifying the shear wave arrival time", Electronic Journal of Geotechnical Engineering, Vol. 15, pp. 1263-1276.

- [4] Kawaguchi, T, Mitachi, T and Shibuya, S, "Evaluation of shear wave travel time in laboratory bender element test", in Proc. 15<sup>th</sup>. Int. Conf. on Soil Mechanics and Geotechnical Engineering, 2001, pp. 155-158.
- [5] Chan, C-M, "Variation of shear wave arrival time in unconfined soil specimens measured with bender elements", J. of Geotechnical and Geological Engineering, Vol. 30, No. 2, .2012, pp. 419-430.
- [6] Yamashita, S, Fujiwara, T, Kawaguchi, T, Mikami, T, Nakata, Y and Shibuya, S, "International parallel test on the measurement of  $G_{max}$  using bender elements", TC-29, ISSMGE, 2008.
- [7] Siddiqui, SI, Drnevich, VP and Deschamps, RA, "Time domain reflectometry development for use in geotechnical engineering", ASTM Geotechnical Testing Journal, Vol. 23, No. 1, 2000, pp. 9-20.
- [8] Savi, P and Maio, IA, "Soil permittivity estimation from time domain reflectometry (TDR) measurements: properties and guidelines", in Proc. Int. Conf. on Electromagnetics in Advanced Applications, 2007, pp. 288-291.
- [9] Chan, C-M, "One-dimensional compressibility of stabilised column systems with shear wave velocity measurements", Proc. 16<sup>th</sup>. South East Asian Geotechnical Conference, 2007, pp. 247-254.
- [10] Chan, C-M, Wong, W-K and Mohd Jenu, MZ, (2013). "On the geo-electromagnetic properties of clay: elementary characterization", in Proc. 1<sup>st</sup> Int. Conf. on the Science and Engineering of Materials, 2013.

## NUMERICAL SIMULATION OF THE IMPULSE RESPONSE METHOD FOR RIGID PAVEMENT EVALUATION

Hudson Jackson<sup>1</sup> and Kassim Tarhini<sup>1</sup>

<sup>1</sup>Faculty, United States Coast Guard Academy, United States of America.

**ABSTRACT:** The Impulse Response (IR) technique is a stress wave method that measures the structure's response to stress waves generated by an impact source. When applied to rigid pavements, the measured response contains complex information on the dynamic pavement properties that is primarily used in detection of voids or loss of support, and softening of the subgrade. The dynamic response of the pavement system is assumed to be similar to that of a single degree of freedom (SDOF) system. This assumption is useful for practical purposes but introduces inconsistencies and uncertainties in the data interpretation because it oversimplifies a complex dynamic problem. Results of a Finite Element parametric study analysis conducted to identify key factors that influence rigid pavement response during Impulse Response (IR) testing are presented. A dynamic modal analysis of a multilayer rigid pavement, assuming viscoelastic and elastic linear material properties, indicates that the mobility spectra from IR testing is predominantly influenced by the properties of the surface layer and the subgrade. The presence of voids beneath a rigid pavement results in increased mobility and less damped behavior of the pavement. The validity of the SDOF assumption in void detection in the reduction of field IR data is also examined.

**Keywords:** *Impulse response, Rigid pavement, Nondestructive testing, Voids, Flexibility spectrum, Finite element, Mobility*

### INTRODUCTION

The Impulse Response (IR) method is a surface reflection method that depends on the propagation of stress wave through the pavement system. The pavement is excited by an impact and the response measured. There are generally three major types of waves in an elastic half-space that are of interest for pavement testing, namely; compression (P), shear (S) and Rayleigh (R) waves. The nature of an impact and the medium of propagation determine which wave dominates. In a layered half-space, with two or more layers, the waves undergo reflections and refractions at each interface. Changes in the wave velocity, density or elastic modulus causes an impedance change. The fraction of the incident wave that is reflected from an interface is dependent on the impedances of both media.

Pavement systems can be considered as layered elastic systems. Waves generated by an impact travel through the structure producing disturbances within the pavement. The disturbances are generally small and in the elastic range; the effects can therefore be considered in terms of the propagation of elastic stress waves within the pavement. The generated waves are generally composed of widely distributed frequency components. The nature of the stress waves generated determines their ability to propagate through the various pavement materials and their ability to detect defects in the pavement system. In general, defects on the order of, or greater than, the wavelength of the propagating wave can be fully detected by the IR

method. The interaction of stress waves with internal discontinuities critically depends upon the relationship between wavelength and the dimensions and depth of the discontinuity [1].

The current IR data reduction procedure represents the dynamic response of the pavement-soil system as single degree of freedom (SDOF) system. Curve fitting between the actual response and that of a SDOF system is done to obtain the necessary modal parameters. The assumption of a SDOF response oversimplifies the problem and, although useful for practical purposes, introduces inconsistencies and uncertainties in the data interpretation [2]. The results obtained from the SDOF simulation are not always representative of the actual response of the pavement-soil system depending on the vibration mode, properties of the supporting soil and characteristics (geometry, rigidity) of the pavement due to a complex variation of stiffness and damping coefficient with frequency.

In order to investigate the validity of the assumption of the SDOF response and to improve data interpretation of the IR method used in the Seismic Pavement Analyzer, a finite element based parametric study of factors affecting the response of rigid pavements with and without voids was conducted. The first part of the paper discusses fundamentals of the IR technique used in pavement condition assessment. The second part deals with the finite element simulation of the IR test and effects of various parameters on the response and mobility spectra.

## OVERVIEW OF THE IMPULSE RESPONSE METHOD

The Impulse Response method also known as the Transient Dynamic method is a nondestructive testing method that is used in quality control and condition assessment of pavements and deep foundations. The IR method has been successfully used to determine the subgrade modulus and presence of voids or loss of support in rigid pavements [3, 4].

### Field Testing

The pavement is first divided into square grids and testing is done at the corner of each grid. The pavement is excited and the response measured at a nearby location. Spectra for both impact and response (particle velocity) are combined to obtain either the mobility, flexibility or impedance function of the pavement. IR testing has been incorporated into a device called the Seismic Pavement Analyzer (SPA). The SPA, shown in Fig. 1, is a device for nondestructive testing (NDT) of pavements, developed at the University of Texas at El Paso under the Strategic Highway Research Program [2]. Five different wave propagation techniques (spectral analysis of surface waves, impact echo, ultrasonic body waves, ultrasonic surface waves and impulse response) are incorporated into this device. The IR test done with the SPA uses the low frequency impact source and a nearest geophone G1, 25 cm away (Fig. 1). The rigid pavement is impacted to couple stress waves energy in the surface layer. A portion of the energy is reflected at the slab-base interface and a portion is transmitted to the subgrade. The load cell at the tip of the low frequency source records the impact energy, while the response, in terms of the particle velocity, is recorded by geophone G1.

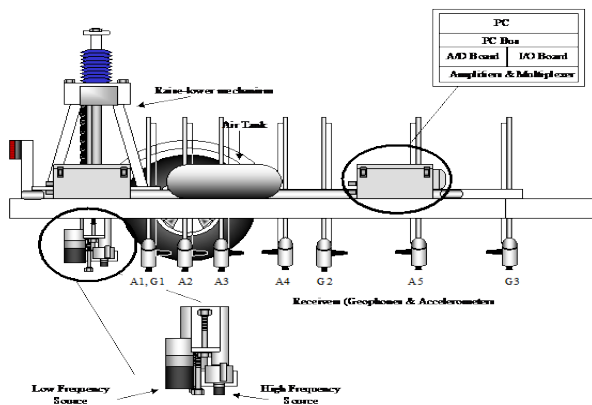


Fig. 1 Schematic of the Seismic Pavement Analyzer.

### 2.2 Data Reduction and Interpretation

The recorded load and velocity histories are then transformed to the frequency domain using a Fast-Fourier Transform algorithm. At each frequency, the

ratio of load to velocity, termed mobility, is determined. The mobility is integrated to obtain the stiffness. The mobility of pavement slabs with good support is fairly uniform up to a frequency of about 600 Hz, while a pavement with voids or loss of support has multiple resonant peaks. The underlying assumption of the IR method is that a rigid pavement system can be approximated by a response of a SDOF system, with the controlling stiffness being that of the subgrade.

Both the load and time histories and corresponding spectra are obtained from a load cell and a close low-frequency geophone (G1) respectively. The dynamic stiffness spectrum, representing the ratio of the two (load and displacement) spectra is matched by the response spectrum of a single degree of freedom system. The modal parameters of the SDOF system: the natural frequency, static stiffness and damping ratio are obtained to characterize the pavement. The natural frequency and static stiffness are used to evaluate the shear modulus, and the mobility and damping characteristics to detect voids or loss of support.

Detection of loss of support due to presence of voids underneath rigid pavements relies on a change in the pavement mobility. Voids cause a significant portion of the wave energy to be reflected back to the surface, resulting in an increase in mobility and a less damped response. Response of a slab with good support or sound contact can be described as a highly damped response, because a large portion of the impact energy can be radiated towards the interior of the medium.

### FINITE ELEMENT PARAMETRIC STUDY

A finite element parametric study was conducted to investigate the influence of factors such as pavement dimensions, Poisson's ratio, elastic modulus and flexural rigidity of the slab; layer thicknesses, elastic modulus of the base layer, the elastic modulus of the subgrade, and depth to bedrock on the dynamic response of a rigid pavement subjected to IR loading. ABAQUS finite element software was used in the simulation.

### Rigid Pavement Model Geometry

The cross section and pavement layer properties are shown in Fig. 2. The pavement is modeled as a multilayered viscoelastic system and is treated as a plane strain problem, symmetrical with respect to the point of load application. The finite element model is discretized using 8-node biquadratic plane strain elements with a width of 10cm in the horizontal direction. In the vicinity of the load, the mesh is refined using smaller elements. Both the concrete slab and base layers are discretized by 3 rows of elements each.

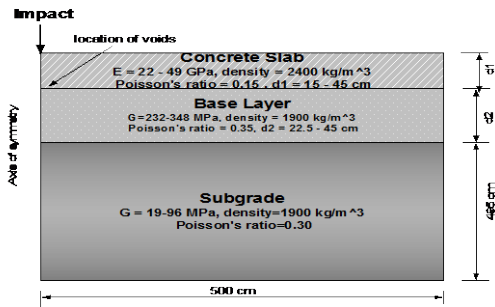


Fig. 2 Cross section and material properties of three-layer rigid pavement

Two finite element models, shown in Fig. 3, were used. In both models, the same mesh discretization and element type for the concrete slab and base layer are used. Four-node plane strain infinite elements are used in the description of the subgrade in both models. Using infinite elements eliminates the need to truncate the infinite domain and provide a means of effectively modeling extensive subgrade soil layers [5]. Model 1 represents a pavement supported on a uniform subgrade of finite thickness (stiff layer at a depth of 4.95 m). Model 2 better represents a half-space of infinite depth underneath a pavement.

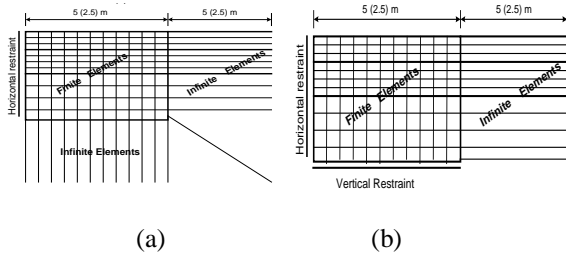


Fig. 3 Schematics of FE Model 1 (a) & Model 2 (b)

### Loading and Frequency Resolution

The loading was approximated by a Haversine function of 1.6 ms duration and maximum force of 5kN. This impact loading function was selected because it closely describes a typical hammer impact of the Seismic Pavement Analyzer (SPA). Time integration of 0.8 ms with 2048 increments was used, providing a maximum frequency of 625 Hz with a 0.61 Hz resolution.

### Layer Properties

Since the strain level induced in the pavement layers during IR testing is very low, materials of all the layers are described as linearly elastic. Each pavement layer is described by its shear modulus (shear wave velocity), mass density and Poisson's ratio. Damping is described as a Rayleigh type damping, with Rayleigh constants  $\beta$  and  $\alpha$  equal to 0  $s^{-1}$  and  $10^{-3}$  s, respectively. In this study, the maximum frequency of interest was about 600 Hz and the lowest frequency, 0 Hz. Substituting these values  $\beta = 0$   $s^{-1}$

and  $\alpha = 10^{-3}$  s into Rayleigh damping equation yields a damping ratio of 0 – 30 %. The damping ratio for the models was assumed to be in this range.

Voids were simulated by defining them as cracks, or by a removal of already generated elements. When described as cracks, voids were defined by two sets of elements above and below the crack connected to two sets of nodes of the same coordinates, but without a direct connection. The ranges of properties investigated are shown in Fig. 3 and summarized as follows:

- Concrete slab thickness-15, 22.5, 30, 45 cm
- Base layer thickness-0, 15, 22.5, 30, 40 cm
- Young's modulus of slab-22, 35, 50 GPa
- Shear modulus of base layer-232, 300, 385 MPa
- Shear modulus of subgrade-19, 76, 120 MPa
- Depth to bedrock-2.5, 5, 10, 25 m

### RESULTS AND DISCUSSION

The absolute mobility and stiffness spectra 25 cm (similar to the location of geophone G1 in the SPA) from the impact source are shown in Figs. 4 and 5. The mobility for model 1 and model 2 with H/R=10, increases with frequency and then decreases after reaching a peak value. The absolute stiffness generally increases with frequency. These trends are identical to that observed from IR field results from SPA testing. The mobility for both models are uniform for high values of depth to bedrock/width (H/B) ratios—i.e. deeper depths to bedrock.

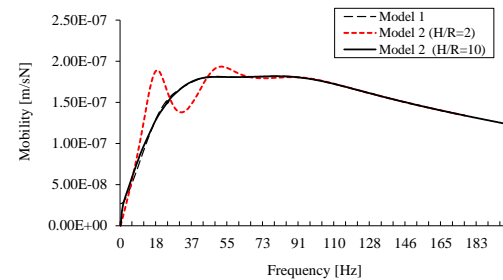


Fig. 4 Typical mobility spectra for models 1 & 2

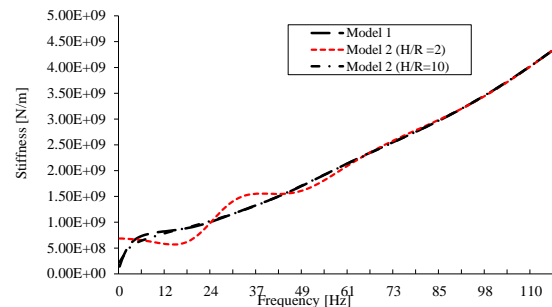


Fig. 5 Typical variation of absolute stiffness with frequency

The mobility and stiffness for model 1 and model 2 (with  $H/B = 10$ , implying extensive depth to bedrock) being similar is an indication that infinite elements suitable represent the subgrade as a half-space with no depth limitation. For model 2 with  $H/R = 2$  (implying shallow bedrock), multiple peaks are observed in the absolute mobility and stiffness spectra. Due to a slight rigid body motion caused by the use of infinite elements, a small static component is introduced resulting in a nonzero mobility at zero frequency (Fig. 5). Two prominent peaks at 17 Hz and 44 Hz, corresponding to the natural frequency of the subgrade to shear and compression waves, respectively, are evident in the mobility spectra of model 2 with  $H/R = 2$  (Fig. 4). It appears that the first peak (at 17 Hz) in the mobility spectrum is related, to a certain degree, to the amount of reflections within the model.

For a harmonic excitation, an analogy can be drawn between a SDOF oscillator and a massless 3D foundation on an elastic half-space [6]. The dynamic stiffness or impedance  $S(\omega)$  (for a particular frequency) is given by the following Eq. 1.

$$S(\omega) = K_s \left[ \left( 1 - \frac{\omega^2}{\omega_n^2} \right) + i 2\beta_d \frac{\omega}{\omega_n} \right] \quad (1)$$

Where,  $\beta_d$  is the critical damping ratio,  $\omega_n$  the natural frequency, and  $K_s$  the static stiffness of the slab–soil system.

The shear modulus of the subgrade can be calculated based on its relationship with static stiffness (Eq. 2) developed for a rigid circular foundation resting on a homogeneous half-space [7].

$$K_s = \frac{4GR_e}{1-\nu} \quad (2)$$

Where,  $G$  is the shear modulus of the subgrade,  $R_e$  the equivalent radius, and  $\nu$  Poisson's ratio of the soil.

Since pavement slabs are not circular,  $K_s$  must be corrected by applying a shape correction factor to account for the effect of length to breadth ratio on dynamic stiffness [7]. It can be seen from Eq. 1 that the dynamic stiffness of a SDOF system varies as a second degree parabola with the first part representing the spring function (real part of spectrum) and the second, the damping function (imaginary part of spectrum). By measuring the impedance, the parameters needed to characterize the system such as static stiffness, damping ratio and natural frequency, the appropriate pavement properties can be determined. In general spring function for both models increases and then decreases with increasing frequency. This trend is observed in field data of rigid pavements collected with the SPA

and is also typical for rectangular footings on a homogeneous half-space [8].

### Influence of Flexural Rigidity of Concrete Slab

Effects of slab thickness,  $d_1$ , and Young's Elastic Modulus,  $E_{sl}$ , can be combined into a flexural rigidity (FR) of the slab given by Eq. 3.

$$FR = E_{sl}d_1^3/12(1 - \nu^2) \quad (3)$$

The range of slab thickness and Young's modulus investigated are shown in Table 1 as well as the corresponding dimensionless stiffness ratios (SR), defined as:

$$SR = FR/G_sR_e^3 \quad (4)$$

Where,  $G_s$  is the shear modulus of the subgrade and  $R_e$  is the equivalent radius of the concrete slab. SR represents the relative flexural rigidity of the concrete slab to that of the soil subgrade.

Table 1 Range of flexural rigidity and stiffness ratio

Slab thickness $d_1$ [m]	Elastic Modulus of slab $E_{sl}$ [GN/m <sup>2</sup> ]	Flexural rigidity FR [MNm]	Shear Modulus of subgrade $G_s$ [MN/m <sup>2</sup> ]	Shear Modulus of base $G_b$ [MN/m <sup>2</sup> ]	Stiffness Ratio SR $\times 10^{-3}$
0.150	22	6.3	76	232	1.2
0.150	34.5	9.9	76	232	1.9
0.150	49.7	14.3	76	232	2.7
0.225	22	21.4	76	232	4.0
0.300	22	50.6	76	232	9.6
0.450	22	170.9	76	232	32.4

In general, mobility decreases with increasing flexural rigidity or stiffness ratio. Mobility is more sensitive to changes in flexural rigidity due to changes in slab thickness than to changes in Young's modulus. This is evident from Eq. 3; flexural rigidity varies with thickness to the third power. There is a general increase in stiffness with flexural rigidity with changes more pronounced at higher frequencies. The static stiffness,  $K_s$  was normalized to that of a "typical" rigid pavement. For the purpose of this study, the typical or standard rigid pavement was defined as one with a 450 mm slab, slab elastic modulus of 22 GPa, shear modulus of base layer and subgrade of 232 MPa and 76 MPa, respectively (i.e., flexural rigidity  $\geq 170$  MNm,  $SR \geq 0.032$ ). There is negligible change in static stiffness with increasing stiffness ratio. There was only a 1% change in static stiffness over the range of stiffness ratios investigated for model 1. The changes in static stiffness becomes more significant with decreasing  $H/B$  ratio for model 2. The normalized static stiffness increases logarithmically for model 1. Similar trends were observed for the individual variation of  $H/B$  ratios.



Peak (maximum) mobility decreases logarithmically with increasing slab flexural rigidity and slab-subgrade stiffness ratio for both models. However, model 2 is more sensitive to changes in the flexural rigidity of the slab due to the effect of the depth to bedrock on wave propagation within the pavement layers.

### Influence of Shear Moduli of Base and Subgrade

The results are presented in terms of shear modulus ratio GR, *defined as the ratio of the shear modulus of the pavement base layer to that of the subgrade*. Six different values of GR ranging from 2.0 to 12.0 were investigated. The shear modulus of the base was held constant at 232 MN/m<sup>2</sup>, while that of the subgrade was varied; this enabled the effects of subgrade shear modulus to be investigated. The shear modulus of the base layer (GR = 3, 4, and 5) was also varied while that of the subgrade was held constant at 76 MN/m<sup>2</sup>. The influence on the response due to changes in the shear modulus of the base layer are typically not significant. This is reflected in almost identical results for shear ratios of 3, 4 and 5 when G of the base was changed. Static stiffness decreases with increasing shear modulus ratio. A high shear modulus ratio implies a weaker subgrade compared to the pavement base layer. One of the key assumptions of the IR data reduction for rigid pavements is that the subgrade, being the weakest layer, dominates the response. The static stiffness is therefore expected to decrease with decrease in the shear modulus of the subgrade.

For GR = 12, which can be considered as a pavement with a weak subgrade support, more pronounced peaks in mobility were observed. These trends in mobility and stiffness are in agreement with the assumption that response to low frequency loading from IR testing is dominated by the quality of the subgrade support.

### Influence of Thickness of Base Layer

Effects of the thickness of the base layer were investigated by varying it from 0 (slab on grade with no base layer) to 45 cm, while maintaining the slab thickness at a minimum thickness of 15 cm. The shear modulus of the base ( $G_b$ ) and subgrade ( $G_s$ ) were also held constant at 232 MN/m<sup>2</sup> and 76 MN/m<sup>2</sup>, respectively (GR = 3.0). The results are expressed in terms of a dimensionless thickness ratio, TR, *defined as the ratio of thickness of the base layer ( $d_2$ ) to that of the concrete slab ( $d_1$ )*.

Mobility decreases with increase in thickness ratio. As the thickness of the base layer increases, the stresses and strain induced in the subgrade reduces because it acts as a stress cushion. This reduction in both the strain and slab oscillation results in a decrease in overall mobility. Similar trends were

observed for model 2. Both the static stiffness (SS) and peak mobility (PM) show a perfectly linear relationship with TR. SS increases while PM decreases linearly with TR. For the range of TR investigated, a 5% increase in static stiffness was observed for model 1 and 9% increase in model 2. These slight changes suggest that changes in base layer thickness do not have a profound effect on the static stiffness of the pavement-soil system. Peak mobility on the other hand, is more sensitive to changes in the thickness ratio. This implies that contribution of the base layer can be significant in some cases related to mobility and should not always be neglected in IR data reduction.

### Influence of Depth to Bedrock

The results are expressed in terms of H/B ratio, where H is the depth to bedrock and B is half the width of the pavement slab. Peak mobility increases with decreasing depth to bedrock. As expected, the static stiffness decreases with increasing depth to bedrock. For H/B = 10, the response approaches that of a pavement resting on a homogenous half-space. This is in agreement with work done by Gazetas, which suggests that, the response of a rigid circular disk on a stratum over a rigid base approaches that of the corresponding half-space for H/B = 8 [8]. The same trend is expected for rigid strip footings, but at higher H/B ratios.

### Influence of Voids

Three different void lengths, 60, 90 and 120 cm were introduced at the slab-base layer interface. The mobility of the pavement-soil system increases with increasing void length, with a slight shift of the peak to higher frequencies. As void size increases, the peak becomes more pronounced over a narrower frequency range. For model 2, as void length increases, the second peak mobility becomes significantly higher than the first. This is due to a stronger reflection of stress wave from the voids before reaching the horizontal boundary. Both damping and spring function decrease with increasing void size. This is in agreement with findings of Nazarian *et al* as well as field data collected on rigid pavements [3]. Changes are more pronounced for the damping function. Most of the energy from the impact is reflected back to the surface resulting in a reduction of damping of the pavement system when voids are present. This reduced damping implies higher displacements. If the loss of support is extensive, the slab tends to deform in a bending mode. Depending on the location of the void, and the magnitude of the impact, the slab deforms similar to a simply or fixed supported beam with multiple oscillations. In general, spring function decreases with increasing void size. As void size decreases, the

cross over frequency tends to increase, resulting in a reduction in natural frequency. It is evident from the results that the presence of voids or loss of support results in very significant changes in the mobility spectra.

### VALIDATION OF THE SDOF ASSUMPTION

For a SDOF system, the displacement response increases with frequency up to a resonance peak and then decreases as frequency further increases. The response spectrum has of a single peak. The trends observed from the numerical simulation do not support a SDOF approximation in all cases, especially for values of  $H/B < 10$ , and large void sizes relative to the slab thickness. Multiple mobility peaks are evident for lower  $H/B$  ratios as well as for large voids. These trends are also observed in IR field data collected using the SPA. The mobility spectra from two rigid pavement sections, with poor support and good support, respectively are shown in Fig. 7. Multiple peaks are evident in the pavement with poor subgrade support. In general, mobility (velocity/load) as well as the flexibility (displacement/load) of the pavement increases with voids, resulting in a slight reduction of the fundamental frequency as the support deteriorates. This indicates that above a given void size, the fundamental response of the system, in vicinity of the void, is completely altered due to the changes in support conditions. This phenomenon cannot be fully captured by a SDOF model. Hoffmann and Thompson also back-calculated rigid pavement parameters by matching the measured and theoretical SDOF frequency response and reported error of up to 33% [9].

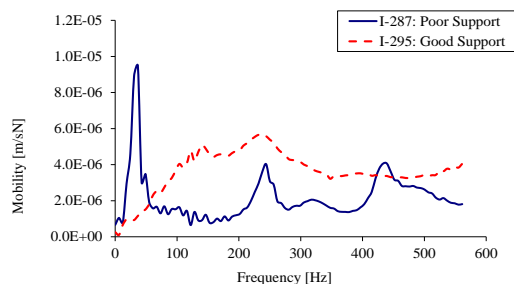


Fig. 7 Mobility spectra from SPA field data

### SUMMARY AND CONCLUSIONS

The results of a Finite Element parametric study conducted on a three layer rigid pavement models with unreinforced concrete slabs were presented. In general, the stiffness of the pavement system increases with increasing flexural rigidity of the concrete slab and thickness ratio, but decreases with increasing shear modulus ratio. Void or loss of support results in a significant increase in mobility and a reduction in the overall stiffness. Furthermore, significant differences in the response were observed

for void lengths larger than double the thickness of the slab. As support conditions deteriorate, the fundamental response of the pavement is altered, resulting in the response being dominated by higher modes of vibration. The effect of the thickness of the base layer on pavement stiffness is less pronounced, but in some cases may affect the overall pavement mobility response significantly.

### REFERENCES

- [1] Sansalone, M.J. and Streett, W.B., "Impact Echo: Nondestructive Evaluation of Concrete and Masonry." Bullbrier Press, Jersey Shore, PA, 1997.
- [2] Nazarian, S., Baker, M., & Crain, K. "Development and Testing of a Seismic Pavement Analyzer." Report SHRP-H-375, Strategic Highway Research Program, National Research Council, Washington, DC, 1993.
- [3] Nazarian, S., Baker, M., & Reddy, S. "Determination of Voids Under Rigid Pavements Using Impulse Response Method." Nondestructive Testing of Pavements and Back Calculation of Moduli: Second Volume, STP 1198, ASTM Publication, Philadelphia, PA, 473-487, 1994.
- [4] Gucunski, N., Vitillo, N. and A. Maher. "Pavement Condition Monitoring by Seismic Pavement Analyzer (SPA)." Structural Materials Technology IV—An NDT Conference, Atlantic City, New Jersey. 2000, pp337-342.
- [5] Hjelmstad, K. D., Zuo, Q. and Kim, J. "Elastic Pavement Analysis Using Infinite Elements." Transportation Research Record 1568, Washington, DC.
- [6] Roeset, M., "Stiffness and Damping Coefficients of Foundations." Dynamic Response of Pile Foundations: Analytical Aspects, ASCE, New York, NY, 1980.
- [7] Dobry, R., and Gazetas, G., "Dynamic Response of Arbitrary Shaped Foundations," ASCE Journal of Geotechnical Engineering, Vol. 112, No.2, New York, N.Y, 1986, pp109-135.
- [8] Gazetas, G., "Analysis of Machine Foundation Vibrations: State of the Art," Soil Dynamics and Earthquake Engineering, Vol. 2, No. 1, 1983, pp 1-42.
- [9] Hoffmann, M. S. and Thompson, M. R., "Mechanistic Interpretation of Nondestructive Pavement Testing Deflections" Transportation Engineering Series No. 32, University of Illinois, Urbana, 1981.

## NUMERICAL ANALYSIS ON THE EFFECT OF JET GROUT PILES ON AN EXCAVATION LOCATED IN AN URBAN AREA

Akula Pavan<sup>1</sup>, Thiruvengadam Tamilmani<sup>2</sup>

<sup>1</sup>AECOM Singapore Pte. Ltd., Singapore

<sup>2</sup>Bachy Soletanche, Singapore

### ABSTRACT

The development of infrastructure in limited land space is a challenging scenario. Infrastructure in limited land space regions (e.g. Singapore) does not provide freedom to develop at favourable locations instead forces the engineer to design at the possible locations. Clay with high organic content, commonly referred as Peaty clay is predominant in coastal areas. This clay being highly acidic ( $\text{PH} > 7$ ) and possessing very low shear strength is a critical factor to the design of infrastructure in the vicinity. Ground improvement adopted weak strata will have varying effect and may not be able to achieve the required strength. This paper discusses the effect of ground improvement (Jet Grout Piles) on the sloped excavation predominantly in Peaty clay. A 15m deep excavation which is 60 m wide is used for the *Finite element modeling*. Impact study on a tunnel located 40m from the excavation is presented (The study is carried out for various achieved Jet grout piles strengths of 100, 200, 300, 400 and 500 kPa). The stability of the slopes for the various strengths is also discussed (GeoSlope was used as the medium to perform the geotechnical analysis).

**Keywords:** Jet Grout Piles, Peaty clay, Sloped excavation, Impact study

### INTRODUCTION

Sloped excavation in an urban area poses threat by means of slope failure which will in turn damage nearby infrastructure. Hence, a conservative design approach has to be adopted to prevent slop failure during excavation. Slope failure is dependent on the undrained shear strength of the soil and it is favorable to execute excavation in sub soil conditions which have high strengths. In cases when the undrained shear strength is very low (1-2 kPa) ground improvement techniques has to be adopted.

Peaty clay also called as organic clay (due to the presence of organic materials which starts under aerobic and anaerobic conditions through incomplete decomposition of plant and animal matter) is highly acidic in nature and also has very low undrained shear strength. Unlike clays, in peaty deformation does not take place by pore pressure dissipation rather from a continuous rearrangement of soil particles under constant vertical effective stress after pore pressure dissipation Ground improvement technique usually adopted for peaty clay is Jet Grouted piles (JGP) or grouted stone column. Grouted stone column may not be used in the presence of critical structures nearby as it will cause unnecessary disturbances during the process. Jet grouted piles on the other hand do not cause these disturbances and hence are adopted in most of the cases. Triple tube Jet grout system is adopted for this paper. A challenging characteristic of peaty clay is that it hinders the formation of calcium silicate

hydrate when mixed with cement, thus it very difficult to achieve the target undrained shear strength.

Finite element modeling (PLAXIS) and limit equilibrium model was used to study the viability of the excavation nearby critical structure (tunnel) and green field respectively. The constitutive soil models are derived based on various conservative assumptions and hence will prevent under design of the ground improvement technique adopted. Modeling the ground improvement and predicting the ground settlement are accomplished using finite element modeling

### SUB SOIL CONDITIONS HEADINGS

Sub soil conditions are shown in Figure 1. It is evident that there is a predominant amount of peaty clay. Consists of 10m thick peaty clay layer (acidic in nature,  $\text{PH} > 7$ ) with a SPT value of 4-7. The organic clay layer is bedded upon a thick layer of peaty sand.

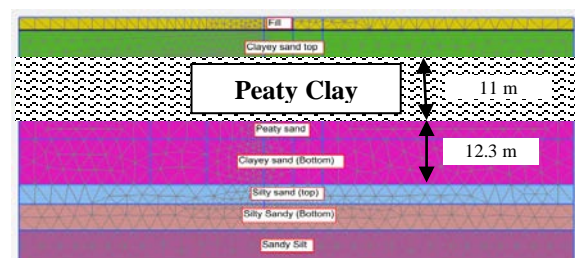


Fig. 1 Sub soil conditions

Peaty clay is a geological member of Kallang formation. Kallang formation is a recent formation and has alluvial, marine clay, Estuarine and littoral clays. The graph presented below shows variation of Estuarine clay with depth [2]. This graph was plotted based on the shear strength encountered in various part of Singapore.

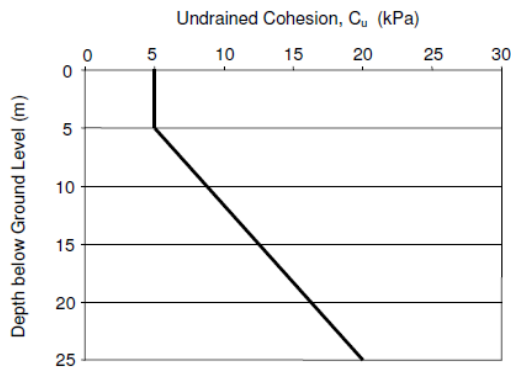


Fig. 1 Undrained Cohesion of Estuarine Clays (Source: LTA CDC, Singapore)

## EXCAVATION GEOMETRY

The excavation geometry is shown in Figure 3. The geometry of the excavation is adopted from the general sloped excavation scheme in Singapore. The excavation is 60 m wide and 30 m deep. Peaty clay is encountered from 8 to 18 m overlaying 5m deep 5m peaty sand. Two 10 m wide promenades are to be provided on either side of the excavation. Slope of 1:1.5 is considered on either side. The slopes are interrupted by two berms so as to increase the stability of the Slopes. Due to the sloped profile it is not possible to provide Earth retaining stabilizing scheme (struts and walers).

### Side A: Near Critical Structure

A Tunnel 20m away is considered as shown in Figure 3. The axis of the tunnel is 25m below ground level Peaty clay. It will be influenced by the excavation and hence advanced finite element modeling techniques is considered to study the impact of the excavation on the tunnel embedded in peaty clay. In order to reduce the influence of the excavation on the tunnel it is necessary to provide a Diaphragm wall 1m thick.

### Side B: Near Green Field

Impact of the excavation to green field areas is not a critical issue due to the absence of infrastructure and utilities in the vicinity. The Diaphragm wall provided for Side A will cut off the impact of excavation but due to the absence of Earth Retaining Stabilizing Structure (ERSS) for side B Slope stability is an important factor and it is

necessary to maintain a factor of safety of greater than 2 (Global and local slope stability).

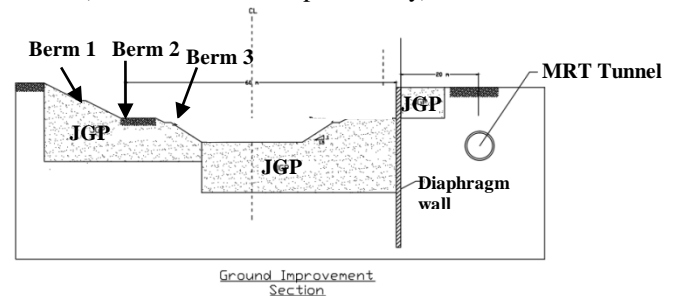


Fig. 3 Geometry of the excavation

## GROUND IMPROVEMENT SCHEME

The presence of weak sub soil strata (low undrained shear strength) such as peaty clay and peaty sand indicates the need for ground improvement before the start of the excavation [6]. Jet grout piles 1m c/c spacing with varying depths of treatment as shown in Figure 3. The varying depth of treatment was derived based on the minimum depth of Improvement required to satisfy the allowable deflection criteria on the tunnel (Horizontal displacement of 25 mm)

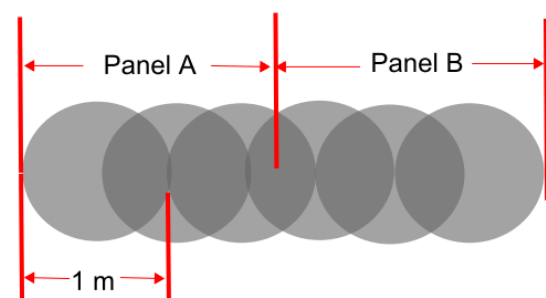
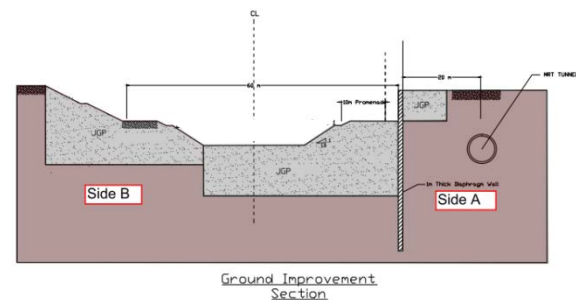


Fig. 4 Jet Grout pile – Plan and Elevation view

Triple tube coring can be used to carry out the ground improvement scheme as it reduces the time required and also attains a uniform mix of JGP. The uniformity can be checked by taking core samples at the overlap as shown in figure 4. The samples should be tested for 7 day and 28 day strengths.

## Ground Improvement Methodology

Methodology for the design used is an important factor in determining the efficiency of the model. The flowchart presented in figure 5. The governing criteria are the stability of slopes and impact of excavation on critical structures.

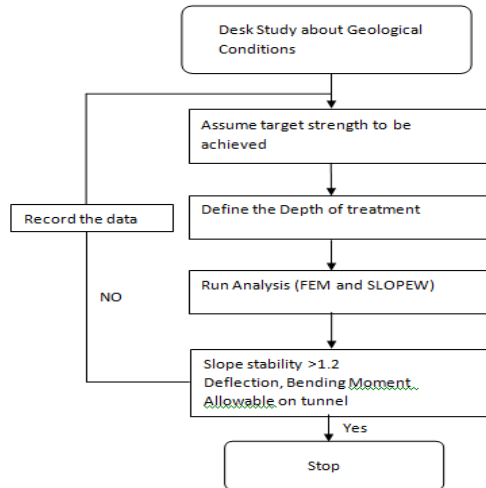


Fig. 5 Design Flowchart

## FINITE ELEMENT MODEL

The numerical tool used in this work is the commercial PLAXIS finite element program. PLAXIS 2D V12 is a 2 Dimensional Finite element analysis. PLAXIS allows using two elements with 6 or 15 node triangles. All analysis in this paper use 15 node analysis unless otherwise stated. Mohr Coulomb model (linear soil model) was adopted.

### Overview of Soil Model

Mohr Coulomb model (Method B - Stiffness and strength are defined in terms of effective property) was used for modeling the geological strata. MC model as shown in Figure 6 behaves elastically before failure. The important parameters used were  $E'$ ,  $C_u$  or  $C'$  for Undrained and Drained cases respectively. Peaty clay was assumed to be normally consolidated ( $OCR=1$ ). The drained stiffness of JGP was based on  $E'=0.5C_u$ . Moderatively, conservative parameters were taken from the LTA Civil design criteria thus preventing under design of the excavation.

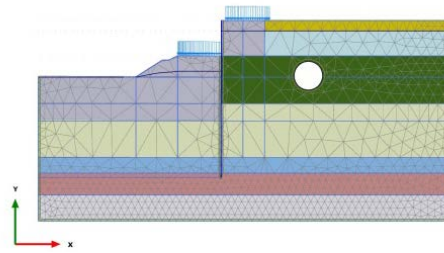


Fig. 6 – FEM Model (PLAXIS)

### Limit state Model

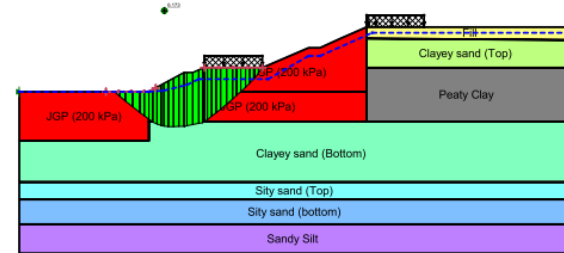


Fig. 7 Limit state model (GEOLSOPE)

Limit state model as shown in Figure 7 was used for finding the global and local factor of safety for the slopes near green field. Morgenstern and Price (1965) [13] method is used to iterate the global and local factor of safety. Morgenstern and Price [13] method is based on combined equations of force and moment equilibrium equations. A modified Newton-Raphson numerical technique was used to solve for factor of safety satisfying force and moment equilibrium equations.

$$X / E = \lambda f(x) \quad (1)$$

Where  $f(x)$  is a function that describes the manner in which  $X/E$  varies across the slope and  $\lambda$  a constant representing a portion of the function used when solving for factor of safety. Limitation of this method is that the direction of the resultant is arbitrary assumed.

## RESULTS AND CONCLUSIONS

### Slope Stability

Berm 1, Berm 2 and Berm 3 as indicated in Figure 4 were analysed for slope stability. A factor of safety greater than 1.2 was set as minimum criteria for the improvement strength to be considered. Figure 8 indicates the increase in global Factor of Safety (FOS) is insignificant and increase in undrained shear strength of the JGP did not affect the Global FOS. This is due to the formation of slip circle beyond the treatment zone.

The inverse phenomenon is observed in the stability of Berms. Berm 1 and Berm 3 are



intercepted by untreated Fill and Peat hence the increase in factor of safety is lower than berm 2 which is embedded in treated peaty clay. The trend indicates that the liner relationship between the undrained shear strength and the factor of safety is satisfied for the global and local slip surfaces and also is in accordance with Morgenstern and Price (1965) limit equilibrium formula

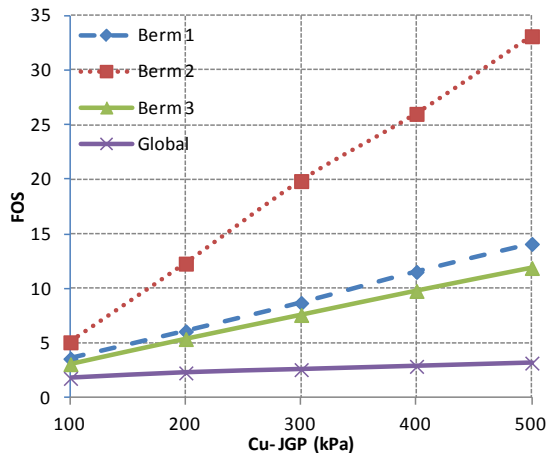


Fig. 8 – Slope stability (FOS) vs Cu – JGP

### Finite Element model

Finite element modeling was carried out to study the excavation impact on the diaphragm wall and tunnel located at 20m from the excavation.

#### Impact on Diaphragm Wall

The toe stability of the diaphragm wall is the governing factor and hence sufficient toe embedment to prevent rigid body movement is to be designed [7]. Figure 9 plots the deflection Vs depth (mRL) for different strengths of JGP. From the graph, we observe that the toe of Dwall has a lateral displacement of less than 10 mm and thus ensuring a factor of safety > 1 for toe stability.

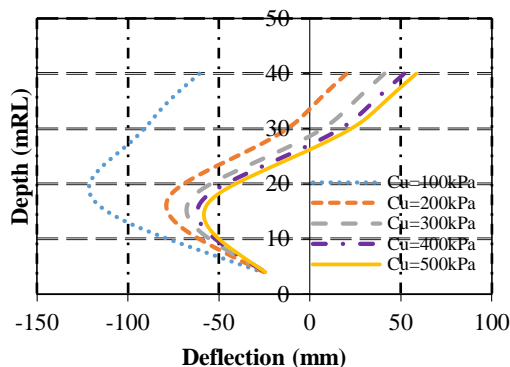


Fig. 9 Depth (mRL) vs. Deflection (mm)

Maximum deflection of 125 mm (towards the excavation) is observed at a depth of 20m due to

insufficient strength of JGP. Deflection can be controlled by means of providing struts. The deflection decreases as the strength of JGP increases which substantiate the validity of this model.

It is nominal to achieve strength of 200-300 kPa cause for strengths greater than 300 kPa the head of the wall moves towards the soil side which in turn will cause movement on the tunnel which is unfavourable.

It is evident from the figure 10 that the peak bending moment of 1100 kN/m is obtained at a depth of 30m (Cu = 500 kPa). At a depth of 15m the same strength of JGP causes the lowest bending moment of 430 kNm. The trend signifies that greater the Cu of the JGP greater the Bending moment at 30m and the inverse trend is observed at 15m.

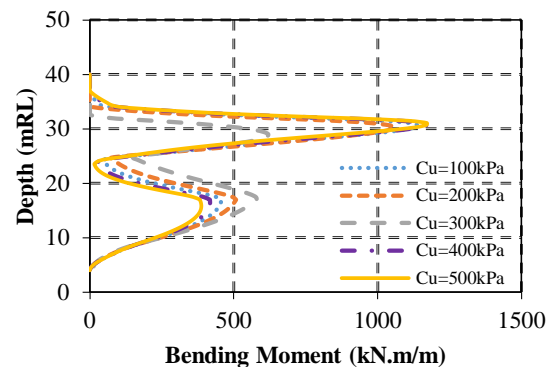


Fig. 10 Bending Moment vs. Reduced level

#### Impact on Tunnel

##### Bending Moment of Tunnel

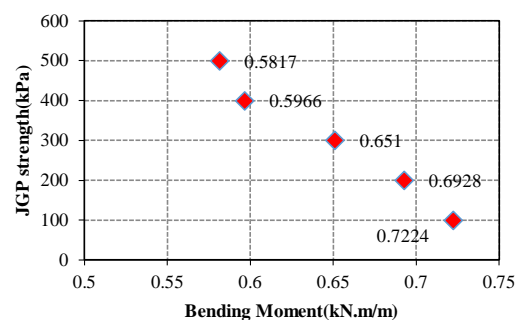


Fig 11. Bending moment vs Cu-JGP

A tunnel of 6.6m radius is introduced to see the effect of JGP. The impact of the ground improvement on the tunnel bending moment is compared. Figure 11 shows the comparison of bending moments for various strengths of JGP. The JGP had helped in reducing the Bending moments of the tunnels. It can be observed the bending moments are indirectly proportional to the JGP strength that is



higher the JGP strength lower is the bending moment. There is a 25% decrease in bending moment on an average between JGP strength of 100kPa & 500kPa.

#### Soil movement

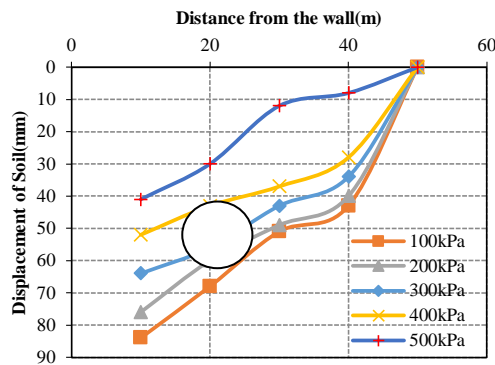


Fig. 12 comparison of various displacement behind the Diaphragm wall

Figure 12 shows the soil displacement behind the wall for a JGP strength of 500kPa. It is clearly inferred that soil movement reduces as we go farther from the diaphragm wall. There was an impact of tunnel on the displacement of soil but that was not very high. Maximum displacement of about 40mm was observed nearer to the wall. All the measurements were taken along a line at 32mRL.

#### ACKNOWLEDGEMENT

We would like to thank AECOM Singapore Pte. Ltd. and Bachy Soletanche, Singapore for their continuous support and encouragement.

#### REFERENCES

- [1] Biarez, J. and Hicher, P.Y. "Elementary Mechanics of Soil Behaviour", 1994.
- [2] "Civil Design Criteria for Road and Rail Transit Systems, Land Transport Authority, 2010 Singapore.
- [3] CP4: Code of Practice for Foundations (2003), Spring Singapore, Singapore
- [4] Dames and Moore (1983), Detailed geotechnical study – engineering report and detailed interpretative report, Mass Rapid Transit System, Singapore.
- [5] Indraratna.B., Basack.S., Rujikiatkamjorn.C (2013), Numerical Solution of Stone Column-Improved Soft Soil Considering Arching, Clogging, and Smear Effects. Journal of Geotechnical and Geoenvironmental engineering ASCE, Vol.139, No.3, pp.377-394

- [6] Sina, "A review of stabilisation of soft soils by injection of chemical grouting", Australian Journal of Basic and Applied Sciences, pp 5862-5868
- [7] South Carolina department of transportation geotechnical design manual (2010). pp 1-90
- [8] Hossain MZ, "For a chapter in a book", Soil Mechanics, 4th ed. Vol. 2, Sakai, Ed. Sankeisha: Publisher's Name, Year, pp. 11–60.
- [9] Author H, A Book. New York: Publisher, Yr, ch. 3.
- [10] Annnn B, "Unpublished work but accepted", accepted, Year.
- [11] Loganathan.N, Poulos.H.G, "Analytical Prediction for Tunneling-induced Ground movements in Clays", J. of Geotechnical and Geoenvironmental Engineering, Vol. 124, Sep. 1998, pp. 846-856.
- [12] Islam MR, "Conference proceedings", in Proc. 2nd Int. Conf. on GEOMATE, 2011, pp. 8-13
- [13] "Slope stability modeling with SLOPE/W2007", GEO-SLOPE International Ltd, 2007, ch. 2.

## USING DRILL BIT REFUSAL AS AN INDICATOR OF STRENGTH AT THE CORING INTERFACE

B. Look<sup>1</sup>, D. Lacey<sup>2,3</sup> and D. J. Williams<sup>2</sup>

<sup>1</sup>Foundation Specialists Group, Australia; <sup>2</sup>Jacobs, Australia; <sup>3</sup>The University of Queensland, Australia

### ABSTRACT

In residual soil profiles, there is often a gradational transition from soil through to the weathered rock profile. Across these indistinct interfaces, changes in drilling technique and testing also generally occur, with rock coring preferred in comparison to advancing boreholes by augering. However significant core loss may occur within low strength materials, and rock coring is more expensive than other investigative techniques. This quality - speed - cost - benefit analysis of investigation is continually completed by the drillers in the field, however the driller's knowledge is often omitted from borehole logs in favor of numerical engineering or geological logging.

By capturing "operational" changes in site investigation procedures, an indication of the material profile can also be made. Based on site investigations completed within South-East Queensland, drilling related data has been used to show associated soil and rock properties. Relationships (or lack of) between various drill bits and SPT 'N' values, rock strength, rock quality designation, rock defects or parent rock types are presented.

*Keywords: Residual Soils, Drilling, Coring Interface, Rock Strength, Standard Penetration Test, Drill Bits*

### INTRODUCTION

Intact rock strength and rock structure (e.g. defects, bedding, rock quality designation) are routinely used in the assessment of foundation bearing capacity. The state of rock weathering is also commonly used to first classify the material and is also an indicator of the likely field strength.

Where deep (piled) foundations are required the pile capacity can be judged during construction, either by piling refusal or rate of pile penetration. The type of drilling bit used, the rate of drill penetration, and the type and size of drilling rig can also be useful indicators of the strength of material. However these have not traditionally been used as there are so many variables (e.g. weight of rigs, which may vary considerably).

Drilling refusal can be identified as being dependent on both the intact strength and defect spacing in the rockmass, and thus should also be able to be used as a field assessment of rockmass strength. Similarly, drill bit "refusal" level, based on the driller's assessment of when wear and tear on the drill bits being used exceeds a productive rate of borehole advancement, is valuable experience that should be quantified for engineering purposes.

The cost to advance a borehole using rock coring is, on a per metre basis, over 4 times the cost using solid augers. This per metre rate excludes the cost of testing and sampling; e.g. completion of Standard Penetration Tests (SPTs) or obtaining an undisturbed sample. Typically, when an SPT exhibits "refusal" (> 50 blows) this is interpreted as indicating the material is of sufficient strength to be recovered via

the more expensive process of core drilling (i.e. low likelihood of core loss). Such a result also indicates that the continuation of drilling with solid augers would, in terms of penetration rate and wear and tear on drill bits, be less cost-effective for the driller and that profit (for the driller) could be optimized by the adoption of rock coring techniques. After the commencement of rock coring, SPTs are also generally not completed, additionally saving the driller time (for test set-up) and equipment wear.

These commercial assessments, made onsite, often determine the type and extent of *insitu* testing / samples that occur. However, the depth at which a change in drilling technique occurs is not necessarily a direct identifier for a significant change in geological interpretation of, for example, the weathering grade or rock strength at the depth.

It was suggested by [1] that the depth at which non-core and coring drilling techniques occurs should not be automatically considered an interface between extremely weathered (XW) to distinctly weathered (DW) rock. Cored material should not be considered to be a different weathering class to the non-cored material that exists immediately above. Specifically, as the soil to rock transition is a gradual change in residual soils, any identified interface is a subjective assessment, and is different from a clear interface which may be observed when alluvium soils overly bedrock (refer Fig. 1).

This paper compares the "refusal" depths identified using varying drilling techniques with other, quantifiable, rock properties such as rock defect spacing, rock quality designation (RQD), point load index strength indices ( $I_{s(50)}$ ), and the

results of SPTs. This information was then used to estimate likely founding depths for pile foundations.

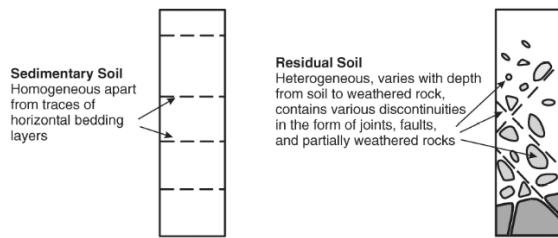


Fig. 1 Simplified residual and transported soil profiles (from [2])

### THE SOIL / ROCK INTERFACE

The question of the soil rock interface was raised by [3], whilst [4] discussed the effect of material type upon pile adhesion, and identified for a given material strength, the average adhesion of a pile in a mudstone, shale, sandstone or limestone rock was 4 times greater than that in clay (Fig. 2). This difference was attributed to smooth rock sockets being produced in soil (clay) materials and implied that rock sockets have increased roughness. This soil / rock interface and roughness factor for pile shaft resistance was explored further by [5], and [6] assessed weak rocks ( $UCS < 0.6$  MPa) and equated them to soil with an upper bound soil strength ( $S_u$ ) of 300 kPa. Yet despite the significant effect that the difference between materials defined as either “soil” or “rock” has on the applied pile shaft adhesion, this soil / rock interface continues to be poorly defined on bore logs, especially within residual soils.

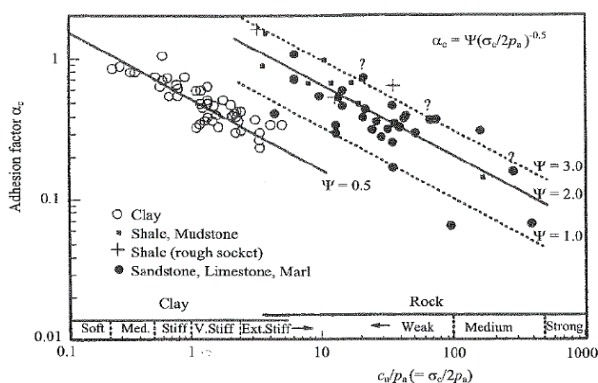


Fig. 2 Adhesion factors for normalized shear strength (from [4])

### Drilling techniques

Different drill bits are used during drilling to advance the borehole. These may include auger drilling with ‘V’ or Tungsten Carbide (TC) bits, or wash boring using a rotary blade, drag, rotary tricone or rock roller bits. The selection of drill bit is

based on the strength and types of soil or rock.

Once bit “refusal” occurs, rock coring will generally be required. Some investigations use rock coring as early as possible without taking the auger to refusal. This has the advantage of recovering continuous samples, but comes at a cost typically 4 to 5 times higher compared to non-core techniques. There will also generally be significant core loss and low RQDs associated with low strength rock.



The ‘V’ and TC bit would typically be expected to display “refusal” within extremely weathered and moderately weathered rocks with significant defects respectively, depending on rock type and assuming the employment of a heavy drilling rig. Table 1 compares the hardness of such drill bits with that of various soil and rock materials.

As a driller aims to avoid wear and tear on equipment, they select and change drilling bits based on what they perceive as drilling resistance, which is inferred by the thrust of the equipment. During rock coring, the selected core bit may vary between:

- o Saw-tooth – soil or very soft rock
- o Carbide – soft to medium strength rock
- o Diamond – soft to extremely hard rock

Thus, although it would be expected there would be a relationship between the depth of drill bit refusal and rock strength, observation of drill bit refusal would be not enough to provide a sound basis for rock strength or weathering assessment when used in isolation. However, when combined with other key rock indices, this data could provide an improved basis for the assessment of subtle strength change that may occur across the soil / rock interface.

Table 1 Comparison of hardness of drill bits with material types

Material	Moh's Hardness	Comments
‘V’ bit – Steel	7	
‘TC’ Bit – Tungsten Carbide	9	
Basalt	6	with 50% Feldspar
	5.5	with 50% Mafic
Sandstone	7	with 80% Quartz
Clays	2.5	Smectite, Kaolinite, Illite

## CASE STUDY - TC BIT 'REFUSAL' VS ROCK CORING

This case study illustrates how the use of information relating to TC drill bit refusal compared to information gained from completion of rock coring. It also illustrates the scope for incorrect classification of materials, if the capabilities of each of these drilling techniques are not understood by the supervising engineer.

Initially, three boreholes were drilled at a site in SE Queensland, in which NMLC rock coring was commenced from within 2m of the surface. The recovered rock core was logged and a suitable foundation design completed based on this information. Subsequently, additional probe holes (with no *insitu* testing) were carried out to assess potential variability of the subsurface profile across the site. Probe holes were extended to TC bit refusal, which was subsequently identified to have occurred within moderately weathered basalt.

Fig. 3 compares the "soil" samples obtained from the probe holes completed using the TC bit to rock core obtained from the same depth at an immediately adjacent borehole. The "soil" samples obtained were comprised of low to medium strength basalt rock fragments and, as the cored rockmass exhibited a natural fracture spacing of approximately 100mm, the rock material was able to be penetrated by the large (heavy) sized rig fitted with a TC bit.



Fig. 3 Moderately weathered basalt obtained via TC Bit and NMLC core drilling techniques

## DRILLING REFUSAL DATABASE

In order to compare material properties that can be inferred from the level of drill bit "refusal," data mining of several hundred site investigation reports has resulted in the construction of a database that includes the rock type, *insitu* test results, drilling rig type / size, and drill bit refusal within completed boreholes. For the three (3) categories of drill bits

typically used within Queensland, Australia – 'V', 'TC' and Rotary / Blade bits – this data was filtered by drill rig size and rock type. The discussion which follows is for large drilling rigs (i.e. rig  $\geq 10$  tonnes).

### 'V' Bit Refusal

Fig. 4 compares the dataset ( $n = 57$ ) of 'V' bit refusal observed in all rock types compared to the SPT 'N' value observed immediately adjacent to refusal. The log-logistic probability distribution function (PDF) was determined to best fit this data using 'goodness of fit' tests; however the more familiar log-normal function was also determined to provide a reasonable fit. Fig. 4 also indicates errors that may occur if the normal distribution is used to describe this data (e.g.  $N = -62$  at the 10% value).

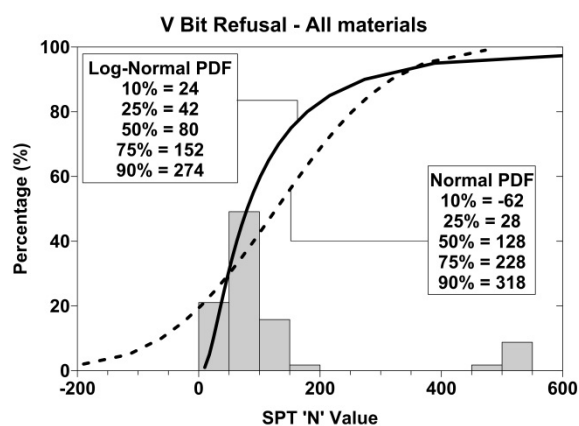


Fig. 4 SPT 'N' Value at depth of 'V' bit refusal, overlain with fitted PDFs ( $n = 57$ )

The mean and median SPT 'N' value corresponding to bit refusal of the 'V' bit dataset is  $N = 127$  and  $N = 80$ , respectively. Based on a statistical analysis adopting a log-normal distribution function, and range of  $N = 24$  to  $274$  is found to cover 80% of the dataset (i.e. 10% lowest and 10% highest values omitted). This equates to a multiplier of approximately 11, however much of this range is expected to be due to the extrapolation of the 'N' value from a discontinued SPT – defined either as (a)  $>30$  blows for  $<150$ mm penetration as per [7]; or (b) hammer bounce (in which a value of  $N = 500$  being then assumed). The Australian definition of SPT refusal (30 blows) has been discussed by [1], who demonstrated both the BS and ASTM standards allow a larger value before test termination. It was also noted that the BS and ASTM standards refer to using SPTs within rock materials, whilst the Australian Standards refers to soil materials only.

A concentration of data between the 10<sup>th</sup> percentile ( $N = 24$ ) and the mean ( $N = 127$ ) is also shown in Fig 4. This was interpreted to suggest that 'V' bit refusal can be expected to generally occur within this isolated range of SPT 'N' values, which would also limit the calculated multiplier to 6.

### Tungsten Carbide (TC) Bit Refusal

The dataset ( $n = 112$ ) of TC Bit refusal compared to inferred SPT 'N' values is shown in Fig. 5, whilst Table 2 presents a summary of the key statistics relating to this dataset when the data is categorized into various soil and rock materials. Table 2 suggests a distinct difference in 'N' value statistics based on material type, and suggests this data should not be considered as a single dataset.

Specifically, it has been considered the low 'N' values associated with the 'residual soils' category may be due to premature exchange of the TC bit (i.e. prior to bit refusal) with a rotary blade or drag bit (likely also associated with a possible change to wash boring drilling techniques). Thus the 'N' values correlated with TC bit 'refusal' is, in this case, thought to be associated with increasing drilling penetration rates rather than true bit 'refusal' due to increased strength of the material being penetrated. Of the 74 data records for which the TC bit 'refused' within rock material (shown in Fig. 6), 72% occurred within extremely weathered (XW) material, 14% within highly weathered (HW) material and 9% within a moderately weathered (MW) rockmass. The remaining 5% recorded refusal in slightly weathered (SW) to fresh (FR) rock.

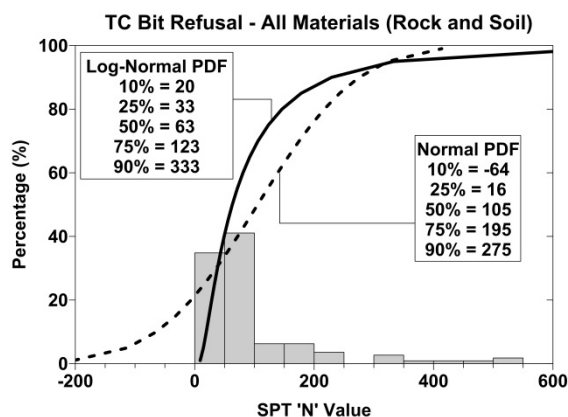


Fig. 5 SPT 'N' Value at depth of TC bit refusal – All material types ( $n = 112$ )

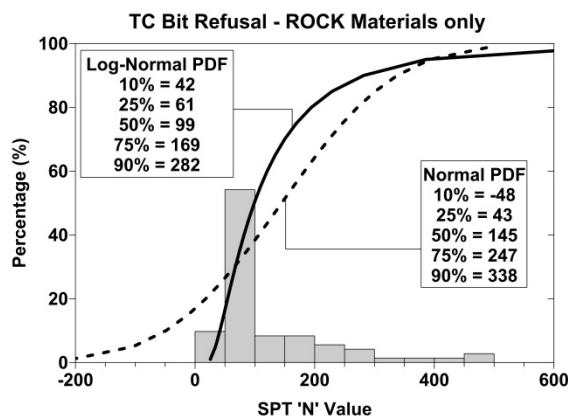


Fig. 6 SPT 'N' Value at depth of TC bit refusal – rock materials only ( $n = 74$ )

Table 2 SPT N\* statistics at 'TC' bit 'refusal' level – categorised by material

Material	COV (%)	SPT N* value (blows)			
		5%	10%	25%	Mean
Residual	80	10	12	18	35
Sedimentary/ Metamorphic	103	35	41	60	139
Igneous	99	34	42	63	139
All Rock	101	34	43	61	141
All Materials	135	15	19	33	106

For the cases ( $n = 54$ ) identified as indicating TC bit 'refusal' within XW rock, the high RQDs measured in rock core recovered immediately below the level of bit 'refusal' also suggests that use of an XW classification for the material was largely incorrect. This effect has also been described by [1].

The results of 'N' values corresponding to 'TC' bit refusal are very similar for all rock origin categories (igneous, metamorphic and sedimentary), as shown in Table 2. From this data it has been interpreted that the 'TC' bit can be typically expected to 'refuse' (or provide less efficient penetration) once rock materials exhibiting  $N \sim 100$  are encountered (using a large drilling rig).

In limited cases ( $n = 15$ ), a Point Load Index (PLI) test was completed immediately below the depth of TC bit refusal. The distribution of PLI results (i.e.  $I_{s(50)}$ ) for this dataset is plotted in Fig. 7. Using the best fit PDF (decaying exponential function), the mean and median for the dataset was calculated to be 1.5 MPa and 1.0 MPa, respectively.

For the data subset in which PLI testing was completed, the average N value at which 'TC' bit refusal was observed was  $N \sim 100$ . Adopting  $UCS \sim 10 \times I_{s(50)}$ , then for this dataset  $UCS \sim 100$  N. This is significantly above the relationship reported by [8], who suggested  $UCS \geq 10$  N. The conservatism in this proposed relationship was highlighted by [1], who instead proposed  $UCS > 30$  to 40 N (for medium to high strength rocks respectively) at the coring interface. The limitations of the existing Australian Standard relating to the completion of the SPT to acquire the N values within this range of rock strengths was also again highlighted.

The distribution of RQD values (%) for data in which RQD values were recorded immediately below the depth of TC bit 'refusal' is presented in Fig. 8 ( $n = 25$ ). From both visual inspection and PDF fitting, it was observed that the frequency of data is spread consistently across all RQD values, and thus no obvious relationship was interpreted to exist between RQD and TC bit 'refusal.'

Defect spacing of rock materials was similarly examined ( $n = 21$ ) at the depth of TC bit 'refusal,' from which it was assessed the mean and median defect spacing was 190mm and 100mm respectively.

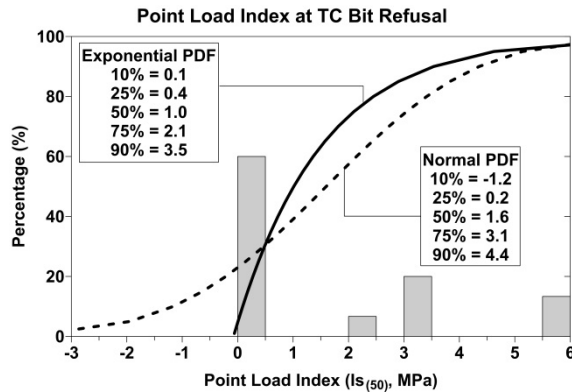


Fig. 7 Distribution of  $I_{s(50)}$  values for tests completed near 'TC' bit refusal ( $n = 15$ )

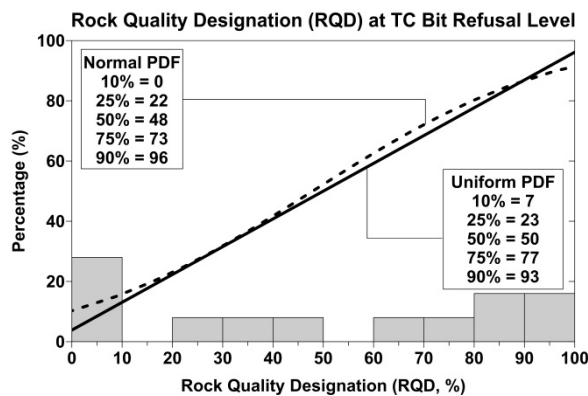


Fig. 8 RQD values near the TC bit refusal – all rock materials ( $n = 25$ )

#### Drag Bit (Rotary Blade) Refusal

The material properties present at the depth of drag bit refusal were assessed via a methodology similar to that described for the TC bit. The results of basic statistics calculated for  $N^*$  values (extrapolated  $N$  value),  $PLI$  values ( $I_{s(50)}$ ),  $RQD$  and the defect spacing are summarized in Table 3 (calculated adopting a fitted log-normal PDF).

Most material properties (i.e.  $N^*$  values, defect spacing and  $RQD$ ) exhibited at the TC bit refusal depth were reproduced almost identically within the drag bit dataset. In regards to rock strength ( $I_{s(50)}$ ), Table 3 indicates the strength at which bit refusal occurred is distinctly lower when compared to the TC bit refusal value, by a factor to 3 to 5. This is interpreted to suggest the TC bit would, with all other material properties being equal, penetrate through stronger rock than the drag (rotary) drill bit.

#### Rock Roller Bit Refusal

Similar statistics were calculated for the dataset relating to rock roller bit refusal, as presented in Table 4. These statistics show that  $RQD$  and defect spacing at the depth of bit 'refusal' is comparable to that observed for the TC and rotary blade bit databases. However, statistics relating to the SPT ' $N$ '

Table 3 Material properties at depth of drag (rotary) bit refusal in rock (values rounded)

Drag Bit Refusal Level	SPT $N^*$	$I_{s(50)}$ (MPa)	RQD (%)	Defect Spacing (mm)
25%	60	0.1	25	50
Median ( $\tilde{x}$ )	90	0.2	35	100
Mean ( $\bar{x}$ )	130	0.5	45	200
75%	160	0.5	75	370
90%	240	1.4	90	520

Table 4 Distribution of refusal in rock at rock roller bit refusal level (values rounded)

Rock Roller Bit Refusal Level	SPT $N^*$	$I_{s(50)}$ (MPa)	RQD (%)	Defect Spacing (mm)
25%	70	0.1	10	50
Median ( $\tilde{x}$ )	120	0.3	30	100
Mean ( $\bar{x}$ )	210	1.2	30	200
75%	205	0.8	55	210
90%	395	3.3	80	475

value at which rock roller bit 'refusal' was observed were 20% to 35% higher than those observed for any other drill bits analyzed. The average rock strength at bit refusal depth ( $I_{s(50)} = 1.2\text{MPa}$ ) corresponded to high strength rock, and was comparable to that calculated for the TC bit ( $I_{s(50)} = 1.5\text{MPa}$ ).

#### Summary of material properties at bit refusal depth

Table 5 provides a comparative reference of basic statistical values of the  $N^*$  and rock strength ( $I_{s(50)}$ ) observed at the depth of bit refusal for the various drill bit types analyzed.

Note that as the 'V' bit was not associated with drilling through rock materials, it only has SPT values attributed. This refusal value is, for a residual profile, interpreted to be generally associated with the soil / XW rock interface.

Examining the median and mean values presented in Table 5, key findings include:

- *SPT  $N^*$  value* – The rock roller refusal represents a higher SPT value as compared to the refusal levels of the other bits and can be expected to penetrate materials at least 1.5 times stronger than the 'V' Bit.
- *Rock Strength* – The TC Bit and rock roller bits appear to be able to penetrate rock materials up to medium to high strength. The blade bit stops in comparably weaker (low strength) rock.
- *RQD* – Limited relationship. Rock roller bit penetration may be limited to materials with lower RQDs than the blade or TC bit.



- *Rock Defect Spacing* – No difference between bit types. All limited to an average spacing of approximately 200mm.

Table 5 Summary of material properties at drill bit refusal depth

Bit Refusal		Percentile			
		25%	50%	Mean	75%
SPT N* Value	V	40	80	125	150
	TC	60	100	140	170
	Drag	70	100	125	150
	RR	70	120	210	205
I <sub>s(50)</sub> (MPa)	TC	0.4	1.0	1.5	2.1
	Drag	0.1	0.2	0.6	0.5
	RR	0.1	0.3	1.2	0.8
RQD (%)	TC	25	50	50	75
	Drag	25	35	45	75
	RR	10	30	30	55
Defect Space. (mm)	TC	45	100	230	235
	Drag	50	100	200	230
	RR	50	100	200	210

## PILE FOUNDING LEVELS

It has been shown by [9] that likely pile refusal of bridge PSC piles (450mm to 550mm diameter, for a set less than 5mm per blow) occurs at  $N^* \sim 100$  and 150 for sandstones and shales, respectively. These  $N^*$  values corresponds approximately to the typical values of TC bit refusal observed within sedimentary rocks ( $n = 51$ ,  $\bar{x} = 96$ ,  $\bar{x} = 139$ ), and thus driven pile refusal can be inferred to typically correspond to TC bit refusal. Typical rock properties for TC bit refusal depth, and thus attributable to driven pile refusal level, were included in Table 5.

In relation to bored piles, [10] demonstrated how the penetration rate for bored piles being constructed within a residual / XW rock profile, and drilling rig properties (e.g. torque, pressure, RPM of auger) could be used to determine site- and equipment-specific correlations with rock strength and type. The assessment completed in [10] was the construction phase equivalent of the material parameter study detailed within this paper.

## CONCLUSIONS

The interface between soil and weathered rock is not well defined, especially for residual soil profiles. In residual soils there is often a recorded disconnect in material properties across the soil-rock interface, often resulting in an instantaneous jump in strength or weathering properties. As identified herein, such jumps are likely attributable to drilling technique rather than an *insitu* condition.

This paper has constructed a dataset of the depth, material type and strength at which different drilling bit types have ‘refused.’ Typical material parameters corresponding to subsurface conditions at drill bit ‘refusal’ level has been identified, and correlation between refusal and strength ( $N^*$  and  $I_{s(50)}$ ) or defect spacing have been presented. It was also observed that some (PSC) pile driving refusal depths approximately correlate to TC bit refusal.

As the depth of drilling bit refusal provides useful information for interpreting *insitu* material properties and likely pile toe levels, it is thus recommended that: (a) the drilling supervisor should ensure different drill bits are used until bit ‘refusal’ is observed; and (b) bore logs should include this information, as well as details regarding the weight and size of drilling rig.

## REFERENCES

- [1] Look, B. (2004), “Rock strength at the coring interface”, *Australian Geomechanics Journal*, Vol. 39, No. 2, pp 105 – 110.
- [2] Wesley, L.D. (2010), *Geotechnical engineering in Residual Soils*, John Wiley and Associates
- [3] Kulhawy, F H, Trautmann C H and O’Rourke T D (1991), “The soil – rock boundary: What is it and where is it?”, *Detection of and construction at the soil rock interface* (GSP 28), Eds. W. F. Kane and B. Amadei, ASCE, New York
- [4] Kulhawy, F. H., and Phoon, K. (1993), “Drilled shaft side resistance in clay soil to rock”, *Proc. on Conf. on design and performance of deep foundations piles and piers in soil and soft rock*, GSP No 38, ASCE, pp 172 – 183.
- [5] Seidel, J. P. and Haberfield, C. M. (1995), “The axial capacity of pile sockets in rocks and hard soils” *Ground Engineering* pp 33 – 38.
- [6] Gannon, J.A., Masterton, G.G., Wallace, W.A. & Wood, D.M. 1999. *Piled Foundation in Weak Rock* (CIRIA Report No.181). UK, 80p
- [7] AS 1289 6.3.1 (1997), “Determination of the penetration resistance of a soil – Standard Penetration Test”, Australian Standards
- [8] Clayton, C. R. I. (1995), “The standard penetration Test (SPT) methods and use”, CIRIA Report 143.
- [9] Adams, B., Look B. and Gallage, C. (2010), Assessment of pile driving refusal using the standard penetration test, *Proc. of the 11th International Association of Engineering Geologists Congress*, Auckland, New Zealand, pp 2641 - 2648
- [10] Lacey, D., Kemp, A., and Sundaram, M. (2012) “Use of drilling rig instrumentation to assess subsurface profile and material characteristics during piling operations,” *Proc. of 11th ANZ Conference on Geomechanics*, Melbourne, Victoria, Australia, pp. 1316 – 1321

## SPATIAL AND TEMPORAL VARIABILITY IN A RESIDUAL SOIL PROFILE

Daniel Mellish<sup>1</sup>, David Lacey<sup>2,3</sup>, Burt Look<sup>4</sup>, and Chaminda Gallage<sup>1</sup>

<sup>1</sup>Queensland University of Technology, Australia; <sup>2</sup>Jacobs, Australia <sup>3</sup>The University of Queensland, Australia; <sup>4</sup>Foundation Specialists Group

### ABSTRACT

It is well understood that there is variation inherent in all testing techniques, and that all soil and rock materials also contain some degree of natural variability. Less consideration is normally given to variation associated with natural material heterogeneity within a site, or the relative condition of the material at the time of testing. This paper assesses the impact of spatial and temporal variability upon repeated *insitu* testing of a residual soil and rock profile present within a single residential site over a full calendar year, and thus range of seasonal conditions. From this repeated testing, the magnitude of spatial and temporal variation due to seasonal conditions has demonstrated that, depending on the selected location and moisture content of the subsurface at the time of testing, up to a 35% variation within the test results can be expected. The results have also demonstrated that the completed *insitu* test technique has a similarly large measurement and inherent variability error and, for the investigated site, with up to a 60% variation in normalised results being observed. From these results, it is recommended that the frequency and timing of *insitu* tests should be considered when deriving geotechnical design parameters from a limited data set.

**Keywords:** *Inherent soil variability, measurement error, temporal variability, coefficient of variation, Dynamic Cone Penetrometer, Moisture Content,*

### INTRODUCTION

Residual soil materials are known to be heterogeneous, and all *insitu* and laboratory tests are accepted to contain some aspect of uncertainty (equipment error; operator, spatial or temporal variation) associated with them [1]. In Limit State Design (LSD) allowances are made for this inherent variation and measurement error when determining design parameters or characteristic values from a dataset of soil test results (*insitu* and/or laboratory test results), by the selection of a (generally) conservative value for adoption in design. For example, the recommendation of [2] is in the absence of specific local test data, a characteristic value determined by statistical methods should produce a design parameter such that “a calculated probability of a worse value governing the occurrence of the limit state under consideration is not greater than 5%”.

It is also accepted that the results of material testing can be affected by moisture content [3]. Accordingly, the time of year that an *insitu* test is completed or a material sample obtained will influence test results, as the moisture content of the sub-surface varies based on recent climactic conditions. This is especially true of the near-surface and “active zone,” the region defined as the depth to which seasonal changes in moisture content occur.

As site investigations are often completed within

a single period of onsite work, and laboratory testing conducted upon representative samples taken during this limited duration of site visitation, all results are indicative of the material conditions at the single time of material sampling. Accordingly, when material parameters are determined for LSD, although spatial variability across the site and variation in results due to errors within the completed tests can generally be accounted for by suitable geological and analytical models respectively, no allowance for any temporal variability of results is routinely applied.

This paper summarises a field study completed to quantify the variation within the results of an *insitu* testing program repeated upon a single site over a period of 12 months, and the potential influence that the time of site testing may have on typical design parameters. Both the temporal and spatial variability of a simple *insitu* penetration test has been investigated by the repeated testing of a single site over a full cycle of seasons (and thus soil moisture content variation). This paper incorporates data presented by [4] as well as additional data collected to extend the duration of the study.

### TEST EQUIPMENT

The *insitu* test repeatedly utilised for this study was the Dynamic Cone Penetrometer (DCP), a simple, portable and low cost tool commonly used as

an indicator of strength and variation of the ground profile. An Australian Standard test method [5] was adopted for all tests completed at the test site.

The results, denoted Penetration Resistance (PR), produced by repeated hammer blows (weight drops) during the DCP test are reported as either: (a) the number of blows required to produce a rod penetration of a standard length; or (b) the length of rod penetration produced per single hammer blow.

DCP test results are, via generic correlations, used to infer relative density / consistency categories or to derive material parameters (e.g. shear strength, California Bearing Ratio (CBR) or modulus values).

Differences exist between the Australian [5] standard test equipment and that specified by other countries [6]. Specifically, the hammer weight, drop height and the dimensions of penetration cone may vary. However, as the energy imparted upon the rod is approximately equal, correlations derived by results of completed tests in any locality are often adopted by others without modification. Existing publications suggest that this assumption may [7], or may not [8], be appropriate.

## SITE DETAILS

The site of the repeated testing was a residential site located in Chapel Hill, a suburb of Brisbane, Australia. The subsurface was comprised of a residual soil profile transitioning into weathered phyllite rock by a depth of approximately 1.8m.

Particle Size Distribution (PSD) tests were completed upon the residual soil materials at depths of 0.25m, 0.75m and 1.25m, and a USC classification of Clayey Sand with Gravel was derived based on the resultant grading curves and Atterberg Limits. The completed PSD tests also indicated an 8 to 12% increase in gravel content across the depth profile analysed (i.e. higher gravel content with increased depth). This is typical of a residual profile, as indicatively shown in Fig. 1.

Fines were evaluated to be of medium plasticity, and the site location inferred an “active” zone of approximately 1.5m was expected to exist, as indicated by the applicable Australian Standard [9].

## STUDY METHODOLOGY

The completed study involved repeating a standard suite of insitu testing and sampling of the site five (5) times over a full calendar year. The selection of 12 months as the duration of the study was to enable a test variation over a full seasonal cycle to be observed.

Each period of testing involved the determination of site conditions and spatial variation across the site via repeated DCP testing. Three (3) locations (sub-sites A, B and C) within the Chapel Hill site were defined, offset from each other by 12 to 15 m. At

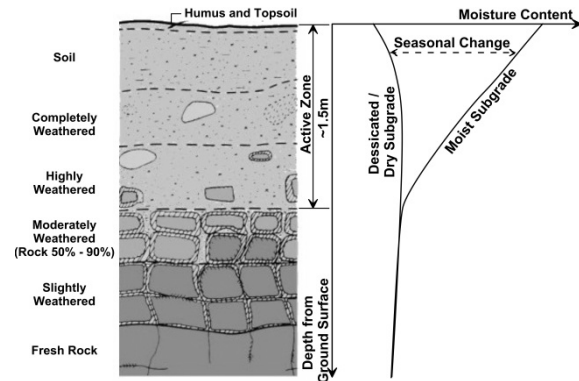


Fig. 1 Inferred weathered profile and expected “active” zone of site (after [9, 10])

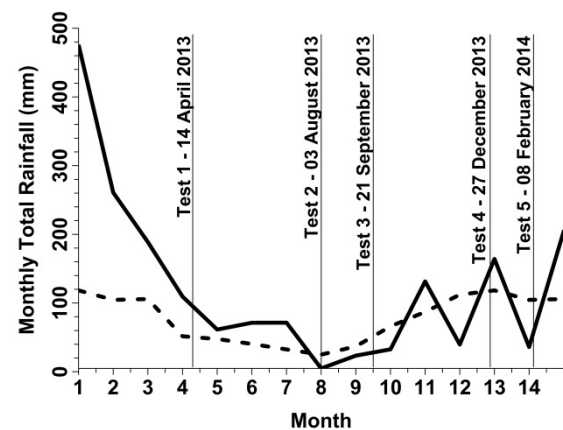


Fig. 2 Observed (solid) and median (dotted) monthly rainfall values and test intervals

each investigation phase, as identified in Fig. 2, multiple DCP tests were completed at each of the three (3) spatially discrete locations. By the assessment of the difference between the multiple DCPs completed at each sub-site and comparing the resultant averaged DCP profiles between each sub-site, the inherent variability of the soil, measurement error associated with the DCP test, and spatial variability across the test site was assessed. Similarly, by comparison of the DCP tests results obtained for each sub-site at each phase of investigation, and thus the change within the material state the period between tests, the temporal variability of the material was assessed.

*Insitu* moisture contents were determined for the initial 1.2 m profile within each sub-site, and thus the change in moisture content could also be compared to the variation in produced DCP profiles. This allowed the definition of the depth of the “active” zone within the site, and the variation of DCP penetration rate with field moisture content.

## RESULTS

For each period of testing, a typical DCP profile was produced at each sub-site by averaging, by depth, the PR values for all tests completed ( $n = 1$  to

Table 1 Coefficient of Variation (COV) of DCP profiles within identified material units, top 1.5m of subsurface

ID	Test Date	Co-efficient of Variation (COV) of each material unit (%), top 1.5m material profile					
		Site A		Site B		Site C	
		Range	Average	Range	Average	Range	Average
1	14 Apr. 2013	17 – 43	32	0 – 46	27	20 – 47	24
2	03 Aug. 2013	17 – 47	26	18 – 49	33	30 – 71	34
3	21 Sept. 2013	22 – 30	26	12 – 30	23	6 – 17	12
4	27 Dec. 2013	23 – 37	30	23 – 39	29	12 – 31	23
5	08 Feb. 2014	19 – 40	31	28 – 29	29	24 – 37	32

4). As shown in Fig. 3, a PR versus depth profile was produced, along with an estimate of the deviation from these values. This variation is shown as the maximum and minimum value envelope overlaid upon the averaged PR profile. Based on the average PR value, the encountered subsurface profile was also categorised into depth intervals of similar consistency or relative density.

#### *Inherent Variability and Measurement Error*

An assessment of normalised variation displayed within each sub-site's typical DCP profile was made, based on the calculation of a Coefficient of Variation (COV) value both for each individually identified material unit and averaged over all identified material units present within each sub-site. The COV values, as summarised in Table 1, is interpreted to present a combination of both the inherent heterogeneity of the soil material being tested and the measurement error associated with the DCP test methodology. By inspection of Table 1, it can be seen that the average COV encountered for comparative profiles is 27.4% across the full study length, and varies (with the exception of a single value) between 23% and 34%.

#### *Spatial Variation*

Spatial variability was assessed based on comparison of the results collected across the site at each of the five (5) testing periods. Average DCP

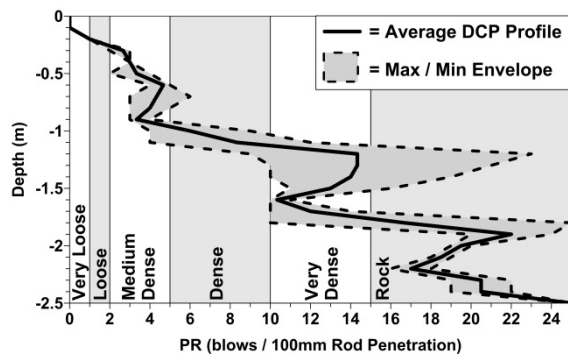


Fig. 3 Typical DCP plot showing averaged profile and range of observed values versus depth.

profiles produced at each sub-site were compared by observed PR value at regular (0.1m) depth increments, and combined to construct a single DCP profile representative of the full site for each date of test, as shown in Fig. 4.

After controlling for the variation in results due to testing / inherent error, as described previously, the spatial variability of the site observed at each test period was quantified by the calculation of residual COV values. Spatial variability (i.e. COV values above the variability associated with equipment and natural heterogeneity error) was observed in 59% of the results (44 of 75 records), with basic statistics of the quantified spatial variability for each test phase summarised in Table 2.

Within the normalised spatial variation calculated, values of up to 70% were observed, with a median and average of 4.5% and 9.5% respectively. Via inspection of the data and from formal assessment by linear regression no significant relationship between the spatial variability magnitude and depth was identified.

Accordingly, it is recommended that both inherent variability ( $\bar{x} = 27.4\%$ ) and spatial variation ( $\bar{x} = 9.5\%$ ) values should be assessed, and accounted for, equally across the full length of the DCP profile. The static COV calculated by this study (~37%) is similar to DCP repeatability reported by others [7].

#### *Temporal Variation*

Simple comparison between the data available for

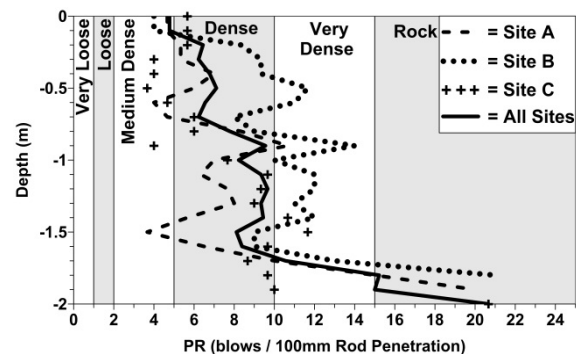


Fig. 4 Plot showing averaged DCP profiles (for tests completed in December 2013)

Table 2 Summary of spatial variation observed across site, by test period

Test ID	Normalised Spatial Variation (%)		
	Range	Average	Median
1	0.0 – 69.9	21.1	19.5
2	0.0 – 23.7	6.1	0.0
3	0.0 – 25.1	8.0	7.7
4	0.0 – 23.3	6.4	0.0
5	0.0 – 19.0	5.8	0.0
ALL	0.0 – 69.9	9.5	4.5

each sub-site produced a range and magnitude of variation observed across the full year of site testing, and produced a value of temporal variation for each 0.1m depth interval. The profile of temporal variation produced for each sub-site are shown in Fig. 5, and inspection of these profiles indicate the largest temporal variation is associated at the existing ground surface. The magnitude of temporal variation decays from above 45% at the ground surface to 0% at a depth of 1.0m. Below this depth the temporal variation appears to stabilise about an average value, with sub-site 'A' indicating a higher temporal variation at depths below 1.0m ( $\bar{x} = 26\%$ ) than the other two (2) sub-sites ( $\bar{x} = 3$  to 11%).

Linear regression analyses indicate the strongest relationship, assessed by correlation co-efficient ( $R^2$ ) values, consistently exists when the data is isolated from the ground surface to depths of 0.8m to 1.0m. This suggests that data below such depths does not display the same depth related relationship, and indicates the “active” zone of the investigated site is limited to a depth of approximately 1.0 m.

The observed general decrease in temporal variation over a specific depth interval extending from the ground surface is interpreted to be due to the variation in the moisture content present within this depth interval over the duration of the study. As moisture content influences DCP results, and the largest moisture content variation would be expected to occur at the surface level and decrease with depth

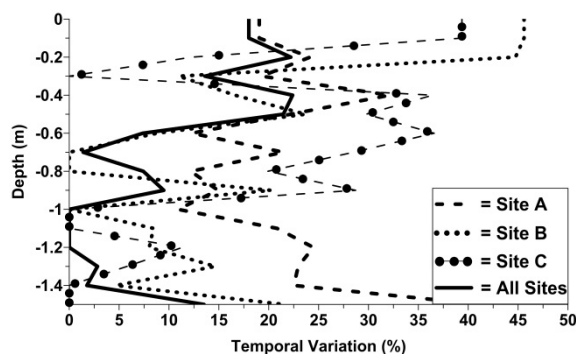


Fig. 5 Temporal variation within comparable DCP profiles over study duration

(refer Fig. 1), the temporal variation observed would also be expected to decrease with depth.

#### Total Observed Variation

Combining the three (3) isolated sources of variation, an estimate of total variation profiled against the initial 1.5m subsurface interval has been produced (Fig. 6). This indicates the magnitude of total variation varies from up to approximately 60% within the top 0.50m ( $\bar{x} = 54\%$ ), before decaying to oscillate about a lower bound value below depths of 1.0m ( $\bar{x} = 41\%$ ).

These derived values also fall within the range of variation associated with another commonly employed test, the Standard Penetration Test (SPT), as detailed by [1]. This previous study found the range of total variation of SPT testing in sand materials was 19 to 62% ( $\bar{x} = 54\%$ ).

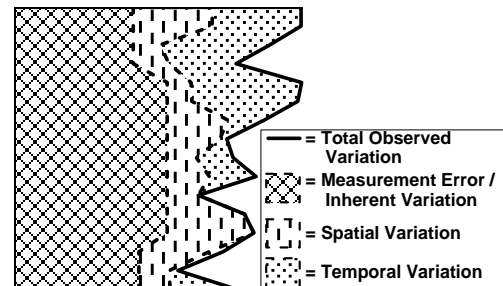


Fig. 6 Total observed variation with DCP results, categorised by source of variation and error

#### CORRELATION WITH SOIL MOISTURE CONTENT AND RAINFALL

Disturbed samples were obtained and the *in situ* moisture content determined ( $n = 49$ ) for a depth range of between 0.25m to 1.65m. The completed testing allowed the construction of a soil moisture content profile for each averaged DCP profile. The average and range profiles produced for the combined (full site) dataset is shown in Fig. 7, with the results calculated for the individual sub-sites summarised in Table 3.

Although the average field moisture content was observed to vary across the site, the largest range of variation over the 12 month study were consistently identified to exist at the surface, and then decrease with depth. It is also noted that within sub-site A, the moisture content increased with depth, which has been interpreted to be due to a temporal groundwater level located at 1.45m depth. However, at all sub-sites the minimum range in results was observed to exist at the 1.0m depth, again suggesting the “active” zone is located above this level. On average, the magnitude of moisture content variation at 1.0m

Table 3 Standardised range, average and COV of *insitu* moisture content, top 1.0m of subsurface

Depth (m)	Moisture Content (%)								
	Site A			Site B			Site C		
	Range	Mean	COV	Range	Mean	COV	Range	Mean	COV
0.25	8.7 – 23.3	14.7	41	8.8 – 20.6	15.3	33	16.5 – 21.0	18.1	9
0.50	11.3 – 19.4	14.5	23	11.0 – 17.6	14.7	17	9.5 – 16.9	12.6	22
0.75	11.3 – 19.9	15.4	20	8.4 – 14.6	12.8	20	5.7 – 12.9	9.6	33
1.00	17.3 – 23.4	20.1	12	10.8 – 12.3	11.5	5	6.5 – 10.9	8.8	23

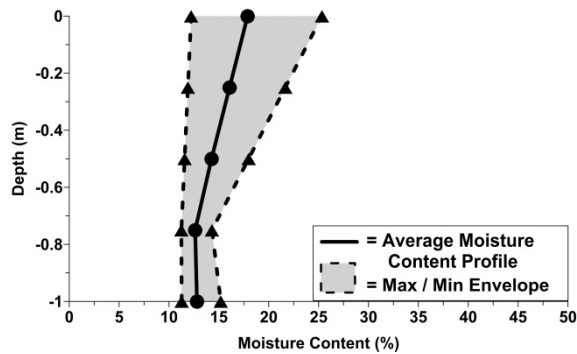


Fig. 7 Moisture content and range of variation observed over 12 month study duration

depth was 40% that observed at the sample taken closest to the surface (0.25m).

Correlation between the soil moisture content variation and the change in the PR results between consecutive test periods was completed to in order to demonstrate the relationship between the two (2) measured parameters. A statistically significant ( $n = 45$ ,  $p < .001$ ) linear relationship was determined for the difference in all results, as detailed in Eq. 1.

$$\text{PRV (blows/100mm)} = -0.39 \times \text{MCV (\%)} \quad (1)$$

Where, for the interval between repeated tests:

PRV = PR change (blows / 100mm penetration)

MCV = Moisture content change (%)

By isolation of the PR and moisture content values observed at each 0.25m depth increment, variations of the PVR:MCV linear multiplier and the

Table 4 Correlations between the observed moisture content variation and PR variation recorded during consecutive testing periods

Depth (m)	Sample size (n)	Relationship between PR and MC variation	$R^2$
0.25	12	PRV = -0.30 MCV	0.50
0.50	12	PRV = -0.56 MCV	0.24
0.75	12	PRV = -0.31 MCV	0.11
1.00	9	PRV = -0.49 MCV	0.43
ALL	45	PRV = -0.39 MCV	0.25

strength of the relationship ( $R^2$ ) were observed, as summarised in Table 4. The strongest relationship between moisture content and PR values occurred nearest to the surface (0.25m depth,  $R^2 = 0.5$ ) with the calculated  $R^2$  generally decreasing with depth.

Combining Eq. 1 and the annual range of moisture content variation experienced over the 2013 / 14 testing period (refer Fig. 7), the expected influence that moisture content has upon the DCP PR rate, and thus the variation of PR values based on the time of testing, has been estimated. This analyses indicated that the moisture content variation within the subsurface materials would be expected to produce an annual variation in DCP PR values of 4 hammer blows at the ground surface, and 1 to 2 hammer blows at the base of the “active” zone.

Comparing the calculated annual variation in PR values due to moisture content variation and calculating this range as a percentage of the “average” DCP PR profile calculated for the site, the equivalent percentage variation in PR result was also obtained. This indicated that the moisture content variation would result in  $\pm 25\%$  variation about the mean PR value for depths of up to 0.5m, and  $\pm 10\%$  variation in PR values over the remainder of the “active” zone. Such values approximately replicate the temporal variation magnitudes (refer Fig. 5).

As shown in Fig. 8, the total rainfall in the 3 month period preceding each suite of DCP testing [11] was compared to the proportion of averaged PR that indicated “dense” or above ( $\text{PR} \geq 5$ ) materials. A distinct increase in the proportion of the subsurface that reported such values occurs as the rainfall magnitude decreases and the subsurface is allowed to dry. Similarly, the profile showing the percentage of the top 1.5m subsurface profile interpreted to be “medium dense” or below ( $\text{PR} < 5$ ) largely reflects the shape of the profile of the total rainfall of the preceding three (3) months.

## IMPLICATIONS FOR DESIGN

CBR values are commonly derived from the results of DCP testing, and CBR values are then commonly incorporated into design as the basis for the estimate of a deformation parameter. Thus, the variation defined for the DCP PR values would also influence any correlated CBR values.



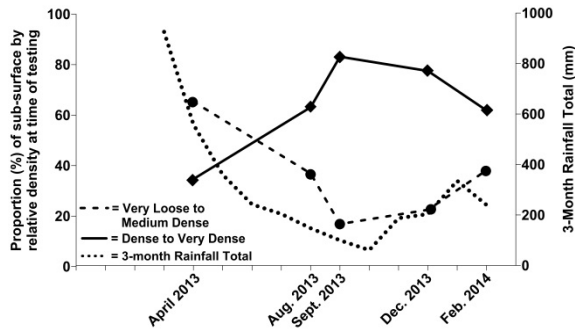


Fig. 8 Proportions of subsurface classified to intervals of relative densities compared to 3 month preceding rainfall total

By adoption of a generic DCP to CBR value correlation [12], the resultant range of CBR values produced by the derived variation associated with averaged PR values was calculated. The CBR range calculated for such values are summarised in Table 4, and indicate that for the one year that the site was monitored, *insitu* testing would have yielded resultant CBR values that would have displayed a variation of between  $\pm 46\%$  (at ground surface) and  $\pm 28\%$  (at 1.0m depth) about the average CBR value.

Table 4 *Insitu* CBR variation based on depth from surface and total observed PR variation

Depth (m)	PR Value		<i>Insitu</i> CBR (%)	
	Mean	Total Var. (%)	Min.	Max.
0.00	3.2	58	2.1	5.9
0.25	4.2	52	3.4	8.0
0.50	5.5	55	4.4	11.0
0.75	6.2	44	6.5	12.6
1.00	7.4	39	8.7	15.5

## SUMMARY AND CONCLUSION

A residential site in suburban Brisbane was monitored by repeated DCP testing over a twelve month period. The magnitude of various sources of test error and result variation associated with the DCP test has been derived from analysis of the recorded PR values (blows / 100mm rod penetration).

Inherent material variability and measurement error was calculated to average 27.4% and site-specific spatial variation was derived to average 9.5%. Thus, for any DCP completed at the site, a constant average variation magnitude of 36.9% was demonstrated to exist for any individual PR value.

The “active” zone was found to be approximately 1.0m deep at the site. An average temporal variation of 22% was observed to occur between the ground surface and a depth of 0.5m. Variation of PR values totaled 58% at the surface before decreasing to

approximately the static variation value (36.9%) at depths below of 1.0m.

Generic correlation between PR and *insitu* CBR values indicated the constant (36.9%) PR variation would result in a range of  $\pm 26\%$  about the CBR calculated from the mean PR value. Incorporating the maximum temporal variation (22%) would increase the resultant CBR range to  $\pm 46\%$ .

Accordingly, the results of DCP values should not be relied on for high accuracy, and the results of a DCP test should be viewed as representative of the site under the conditions at the time of testing only. Consideration for the season of testing and likely moisture content of the “active” zone of soil within annual variation should be considered when deriving characteristic parameters for geotechnical design.

## REFERENCES

- [1] Phoon, K.K. and Kulhawy, F.H. (1999). “Characterisation of geotechnical uncertainty”, *Canadian Geotechnical Journal*, Vol. 36 (4)
- [2] EN 1997-1: 2004. *Eurocode 7: Geotechnical design. Part 1: General rules*. CEN.
- [3] Das, B.M. (2011). *Geotechnical Engineering Handbook*, J. Ross Publishing, Ft. Lauderdale
- [4] Mellish, D. (2013). *Temporal and spatial variation of moisture content and its effect on the strength characteristics of soil*, B. Eng. Thesis, Queensland University of Technology
- [5] AS 1289 6.3.2 (1997). “Determination of the penetration resistance of a soil – 9kg Cone Penetrometer test”, Australian Standards
- [6] ASTM D6951 (2009). “Standard Test Method for Use of the Dynamic Cone Penetrometer in Shallow Pavement Applications”
- [7] Smith, R.B. and Pratt, D.N. (1983), “A field study of in-situ Californian Bearing Ratio Dynamic Cone Penetrometer testing for road subgrade investigations”, *Australian Road Research*, Vol. 13 (4)
- [8] Narendranathan, N., Archer, S. and Narendranathan, G. (2012). “Earthwork practices in civil & mining industries and advances in earthworks”, *Int. Conf. on Ground Improvement and Ground Control*, Wollongong, Australia, 30 Oct. – 2 Nov.
- [9] AS 2870 (2000). “Residential Slabs and Footings”, Australian Standards
- [10] Little, A.L. (1969). The engineering classification of residual soils, *7th Int. Conf. on Soil Mechanics and Foundation Engineering (ISSMFE)*, Mexico, Vol. 1, pp 1 – 10
- [11] Bureau of Meteorology (2014). Historical Rainfall Observations, [www.bom.gov.au/climate](http://www.bom.gov.au/climate)
- [12] Queensland Government (2010). Test Method Q114B – *Insitu* California Bearing Ratio (Dynamic Cone Penetrometer), *Materials Testing Manual*

# INTERACTION ANALYSIS FOR OIL STORAGE TANK ON MARINE CLAY

Pallavi Ravishankar B.<sup>1</sup> and Neelima Satyam D.<sup>2</sup>

<sup>1</sup>Research Scholar, <sup>2</sup>Assistant Professor, Geotechnical Engineering Laboratory, Earthquake Engineering Research Center, International Institute of Information Technology Hyderabad, INDIA

## ABSTRACT

The engineering behavior of marine clay is very different than that of the moist and dry clay because of its structural and mineral composition [1]. Marine structure is subjected to the waves which create a cyclic stresses inside the soil mass [2]. In this paper a cylindrical reinforced cement concrete tank with diameter 100m and 40 m height founded on soft marine clay of undrained shear strength of 10 kPa is considered for the analysis. The huge pile group is modeled by equivalent pier method and interaction factor method for the full and empty loading conditions. Settlement including the soil pile interaction has been estimated for both the cases mentioned above for different pile configuration including pile length, diameter and spacing of piles in a group. It has been observed that the spacing of the piles plays a vital role in estimating the settlements and stresses. With the comparison of the equivalent pier method (EPM) and interaction factor method (IFM) for settlement estimation, IFM is found to be more suitable for interaction analysis to achieve the safety of the tank.

*Keywords: Soil pile interaction, Oil storage tank, Settlement analysis, Pile foundation, Marine clay*

## INTRODUCTION

Due to an increase in the use of marine recourses like petroleum products, biological products etc. a coastal activities are increased tremendously. Due to this there is a huge necessity to build marine structures like offshore platforms, storage structures like fuel storage tanks, temporary halt structures, etc. Such offshore structures considered under heavy structures and give much impact on the soft clay settlement which affects the structural stability. Hence settlement analysis is needed to be performed for such type of structures. Originally very soft clay in sea bed or onshore clay called as marine clay, has very poor shear strength and shows shrinkage and swelling properties due to its structural arrangement and the minerals compositions like montmorillonite, chlorite, kaolinite and illite and non-mineral traces like quartz and feldspar. Along with these minerals and non-mineral compositions, marine clay consist of organic matter (

In the analysis, the settlement in the soil mass is estimated for the exact prediction of the response of the structure along with the soil behavior. In offshore structures the foundation is deeply embedded to hard strata, thus pile experiences the fluid foundation interaction as well as soil foundation interaction for the given loading conditions throughout the life span of the structure. It is now well recognized that the settlement of a pile group can differ significantly from that of a single pile at the same average load level.

There are a number of approaches commonly adopted for the estimation of the settlement of pile groups which employ the concept of interaction factors and the principle of superposition [20]. Few methods estimate the group settlement by modifying the single pile load-settlement curve, to take account of group interaction effects. Some of the methods are briefly explained in this section.

1. *The settlement ratio method:* In this method the settlement of a single pile at the average load level is multiplied by a group settlement ratio  $R_s$ , which reflects the effects of group interaction.
2. *The equivalent raft method:* In this method the pile group is represented by equivalent raft acting at some characteristic depth along the piles.
3. *The equivalent pier method:* In this method the pile group is represented by a pier containing the piles and the soil between them. The pier is treated as a single pile of equivalent stiffness in order to compute the average settlement of the group.
4. *The Interaction Factor Method:* In this method the settlement for one pile (reference pile) in the group is estimated and considering the interaction factor the settlement of the other piles in the group is calculated. The algebraic sum of the settlement value of all piles gives the settlement of the group.

5. *Numerical methods:* Different numerical techniques such as finite element method and the finite difference method have been used to find out the group settlement. While earlier work employed two-dimensional analyses, it is now less uncommon for full three-dimensional analyses to be employed [7].

In this research paper the equivalent pier method and the interaction factor method are used to perform a comparative analysis for estimating the settlement of the pile group including soil pile interaction.

#### Details of the storage tank considered for the study

Large ground storage is considered to be located in western part of India. A settlement analysis considering the soil pile interaction of marine deposits under static loading is carried out including the wind and gravity loading combination for the full and empty oil in the tank. The concrete oil storage tank of diameter 100m and height including free board is 40 m is supported by a initial set of pile foundation of diameter 0.4 m. Initially at a first iteration a pile is considered to be spaced on 3D to 6D and typical length of the pile is 10 m. General layout of the pile is explained in the Figure 1.

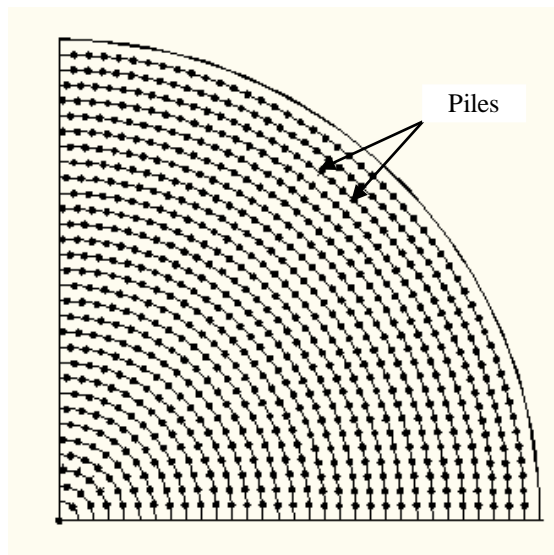


Fig. 1 General layout of the initial arrangement of the piles in a group.

Pile is provided with a uniformly thick pile cap of thickness 0.5 m. Fig. 2 explains the basic model geometry of the circular tank.

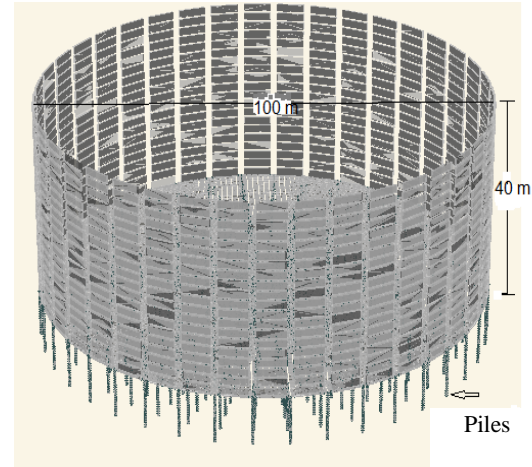


Fig. 2 Geometry of storage tank.

The tank is constructed to store oil of specific gravity 7.6 kN/m<sup>3</sup>. Large ground storage is supported by a local marine clay deposits. Table 1 explains the engineering properties local deposit.

Table 1 Soil properties considered for analysis [1]

Parameter	Unit	Value
Unit Wt.	kN/m <sup>3</sup>	16
Moisture Content	%	38
Shear Strength	kPa	10
Poisson's Ratio		0.35

The concrete grade is taken as M-30 for both tank and foundation system with the rebar reinforcement of Fe-415 steel grade.

#### ANALYSIS

##### Equivalent pier method (EPM)

Paulos and Davis (1980) proposed an Equivalent Pier method for heavy and large superstructures where a large pile group needs to analyze. Few researchers adopted a methodology of EPM to find out the settlement analysis for the huge pile group [25].

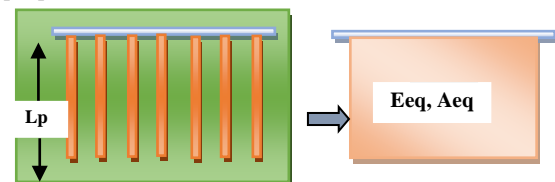


Fig. 3 Concept of equivalent pier method.

In this method the pile groups act as a whole pier to simplify the procedure for estimating the settlement of pile groups which equals that of single pile by means of load-transfer functions. The diameter of

the equivalent pier is given by the following equation

$$Deq = 2 \sqrt{\frac{Ag}{\pi}} \quad (1)$$

Where,  $A_g$  is the plan area of pile group.

### The Interaction Factor Method

For pile groups one of the common means of analyzing pile group behavior is via the interaction factor method [20]. In this method, referring to Fig. 3, the settlement  $w_i$  of a pile  $i$  within a group of  $n$  piles is given as follows:

$$W_i = \sum_{j=1}^n Pav * S1 * \alpha_{ij} \quad (2)$$

where,

$Pav$  = average load on a pile within the group;

$S1$  = settlement of a single pile under unit load (i.e., the pile flexibility);

$\alpha_{ij}$  = interaction factor for pile  $i$  due to any other pile  $j$  within the group, corresponding to the spacing  $s_{ij}$  between piles  $i$  and  $j$ , can be written for each pile in the group, thus giving a total of  $n$  equations, which together with the equilibrium equation solved for the a rigid (non-rotating) pile cap, in which case all piles settle equally. In this case, there will be a uniform settlement but a non-uniform distribution of load in the piles. Generally the interaction factors ( $\alpha_{ij}$ ) is computed from boundary element analysis and plotted in graphical form. In numerical analysis closed-form expressions are used for the estimation of interaction factors which provided the ease in prediction of group settlement behavior using numerical techniques [3]. The expression for the interaction factor is given as follows.

$$\alpha = A(s/d)^B \quad (3)$$

where,  $A = 0.57$  to  $0.98$

$B = -0.60$  to  $-1.20$ .

### Load Transfer function for individual pile in pile group

The analysis method [13], proposed originally by Coyle Reese and O'Neil [12], is an efficient method to predict the load settlement relationship for single piles subjected to vertical load for its simplicity and capability of incorporating the nonlinear behavior of soils. However, due to the emission of influence of pile-to-pile interaction on the deformation of the soil surrounding the pile, it is rather difficult to be extended to pile-group analysis. In this work, a load-transfer function is developed based on the analysis of the aforementioned interaction between individual piles in pile group. Pile  $i$ , supported by a

series of nonlinear springs along pile shaft or pile bottom to resist the vertical load  $P_i$  at the pile top, is taken out to be analyzed separately, as shown in Fig. 4. The stiffness of spring at the pile bottom can be conveniently expressed using the following equation suggested [12].

$$k = 4 * \frac{G}{\pi r(1-\mu^2)} \quad (4)$$

Where,  $G$  is the shear modulus and  $\mu$  is the poisson's ratio of soil.

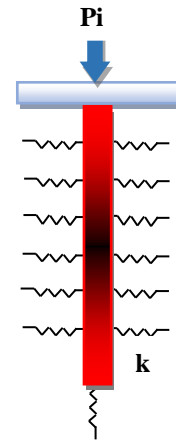


Fig. 4 Equivalent/Single pile with soil represented as a spring for soil pile interaction analysis [25].

### Pile interaction

In this study the main focus is given on the vertically-loaded pile groups consisting of  $n$  identical piles with the same length  $L$ , diameter  $d$ , pile space  $S$ , and elastic modulus  $E_p$  embedded in the homogenous soft soil. Generally, the resistance of the surrounding soils at the pile/soil interface, i.e. shaft frictional force named as  $\tau_z$ , is mobilized once the displacement of the piles occurs. The displacement of pile groups at a given depth is different from that of single pile under the same load due to the fact that the reinforcing effect caused by the interaction between some neighboring piles confines the displacement of soils along piles. Therefore, it is necessary to consider the interaction between individual piles in calculating the settlement of pile groups. The soils are assumed to be a series of nonlinear springs attached along the pile shaft to simulate the behaviors of soils subjected to shaft frictional force. Obviously, the stiffness of springs, denoted as the ratio of the shaft frictional force to the displacement of soils, is relative to the interaction between individual piles in pile group.

According to the formulation [25] to estimate the shear- deformation mechanism of surrounding soils

around piles subjected to the shaft frictional force  $\tau_{iz}$ , the displacement of a point of soils is expressed as

$$\frac{dy}{dz} = PZ(y)/(E_p A_p) \quad (5)$$

Considering the interaction between soil and pile and pile to pile in the group the interaction factor is proposed as

$$If = \frac{E_s}{E_p} \quad (6)$$

Hence the Modulus of the equivalent pier is modified as  $If * E_q$  considering the fact that the soil has been entrapped between the piles in the group.

## FINITE ELEMENT MODELLING

The tank is modeled using Finite element software SAP 2000 using circular wall as a shell element and slab as a plate element and piles as a 1-D element along with the soil modeled as a linear spring to capture the realistic soil pile interaction scenario (Fig. 5).

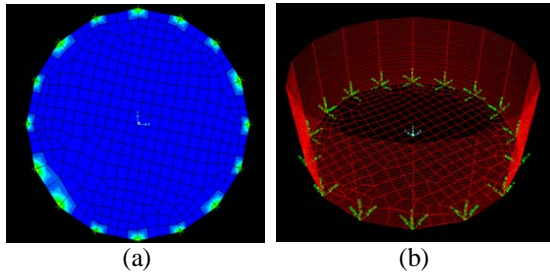


Fig. 5 Details of the finite element model for slab (a) and circular wall (b).

The analysis is carried out for considering single pile which takes load considering the group action and equivalent pier representing the pile group. The loading considered in analysis for is done for both empty and full condition of the tank.

In this method it is needed to consider a correction factor for the equivalent pier as soil trapped between the piles reduces the overall stiffness of the pile group. The correction in the equivalent stiffness of the soil group is calculated. The interaction analysis is carried out for linear static condition and the results are compared with the analysis case which excludes the interaction for all pile configuration. The parametric study is carried out for the different pile to pile spacing, pile diameters, pile length and the different D/L (diameter to side length ratio) ratio for the above mentioned conditions of the tank.

## RESULTS AND DISCUSSIONS

The settlement analysis is carried out for the huge water tank of diameter 100m and height 40m founded on the marine clay of very less shear strength using Equivalent Pier Method (EPM) and Interaction Factor Method (IFM) for different pile configuration of diameter, length and spacing considering the soil pile interaction including the linear spring with spring constant of equal to the soil coefficient. Fig 6a and Fig 6b shows the general settlement profile for the working load condition at the bottom node of the Equivalent pile for full and empty conditions respectively.

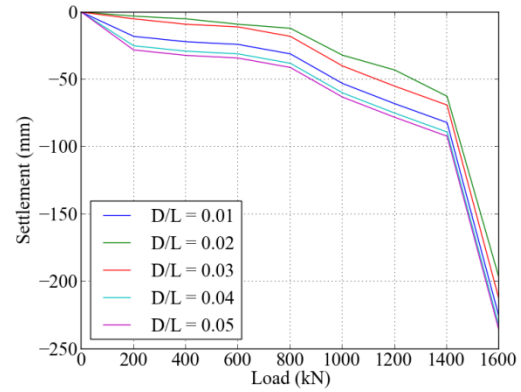


Fig. 6a. Settlement for tank by EPM (full condition).

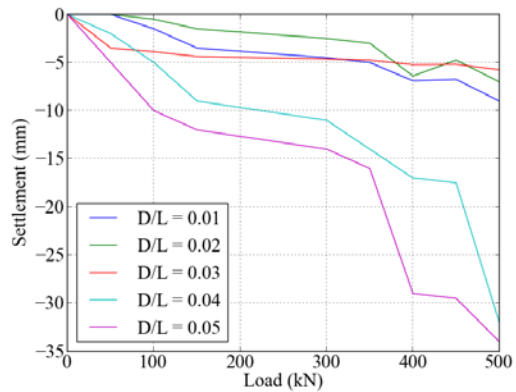


Fig.6b. Settlement for tank by EPM (empty condition).

The maximum settlement is calculated with interaction method considering the interaction between pile to pile using Eq. 2. The settlement for each pile is calculated manually considering the central pile as a reference pile and the maximum settlement for a pile group is estimated by performing a numerical summation of all settlement values obtained analytically. The settlement obtained by EPM and IFM is compared and the difference is shown in Fig. 7 for both empty and full loading conditions. The comparison for the



maximum settlement has been carried out for both empty and full loading conditions.

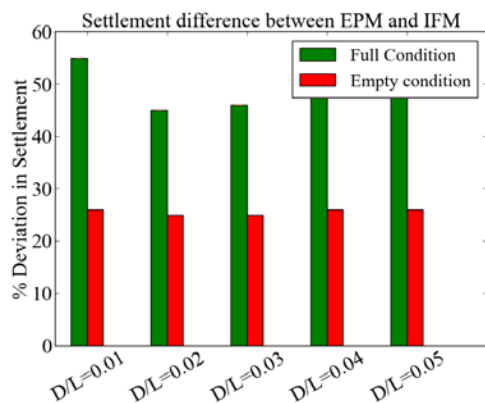


Fig.7 Percentage deviation in maximum settlement for critical load condition for EPM and IFM.

## CONCLUSIONS

The present study has drawn the following conclusions.

1. The Maximum settlement of the huge fuel tank for empty and full both conditions are found to be permissible range.
2. The settlement is found to be less for the pile configuration with D/L ratio 0.02 and for other ratios settlement is found to 20% more for the empty loading conditions where as D/L = 0.04 is proves to be an good choice as it gives minimum settlement for the full loading condition with EPM and IFM methods. Thus the pile configuration diameter 0.4 m, total length 10 m and spacing 1.6 m is found to be a good combination for the least settlement criteria.
3. Equivalent pier method proves to be simple to get the settlement of the huge fuel tank but interaction is need to explicitly provided with the springs which is a the lengthy method with respect to the calculation.
4. Interaction factor method accounts for interaction between soil and pile with springs and the pile to pile interaction with the formulation of the interaction factors thus this method is found to be more precise as in pile group pile to pile interaction is one of the important criteria.
5. The settlement values was found to be more by the interaction factor method (IFM) as compared to the equivalent pile (EPM) method which leads to fact that pile to pile interaction also plays a vital role in settlement

analysis.

6. The % deviation in settlement with EPM and IFM method is found to be more in the full load condition that the empty load condition of the tank which proves that the interaction between soil pile and pile to pile is more as the loading on the structure increases from the gravity load condition.

## REFERENCES

- [1] Basack and Purkayastha, "Engineering properties of Marine Clays from the eastern coast of India", *Journal of Engineering and Technology Research*, Vol.1(6), September 2009, pp.109-114.
- [2] S.S. Sharma and M. Fahey, "Cyclic deformation characteristics of cemented calcareous soil", *Deformation characteristics of Geomaterials*, 2<sup>nd</sup> ed., 2004, NRC Research Press, ISBN 905809604 1.
- [3] Mandolini, A. and Viggiani, C, "Settlement of piled foundations", *Géotechnique*, Vol.47 1997, pp.791-816.
- [4] Reese, L.C. and O'Neill, M.W., (1988). "Drilled shafts: construction procedures and design methods", Publication No. FHWA-H1-88-042.
- [5] Peaker, K.R.(1984). "Lakeview tower: a case history of foundation failure", *Proceeding in conference on Case histories in Geotechnical Engineering*, 1984 Missouri Rolla, pp.7-13.
- [6] Poulos, H.G., "Analysis of the settlement of pile groups", *Geotechnique*, Vol.18, 1968, pp. 449-471.
- [7] Poulos, H.G. (1988). "Modified calculation of pile group settlement interaction *International Journal of Geotechnical Engineering (ASCE)*, Vol. 114, 1988, pp. 697-706.
- [8] Poulos H.G., "Pile behavior Consequencees of Geolgical and construction imperfections", *International Journal of Geotechnical and Geoenvironmental Engineering (ASCE)*, Vol. 131, 2005, pp. 538-563.
- [9] Randolph, M.F. and Wroth, "Analysis of deformation of vertically loaded piles", *Journal of Geotechnical Engineering Division (ASCE)*, Vol.104, 1978, pp. 1465-1488.



## OPTIMIZATION OF TREATMENT AREA OF ENZYME MEDIATED CALCITE CEMENTATION: A NOVEL SOIL IMPROVEMENT TECHNIQUE

Debendra Neupane<sup>1</sup>, Hideaki Yasuhara<sup>2</sup> and Naoki Kinoshita<sup>3</sup>  
<sup>1,2,3</sup> Dept. of Civil and Environmental Engineering, Ehime University, Japan

### ABSTRACT

This paper evaluates a technique of enzyme mediated calcite cementation. In this technique, calcium ions and carbonate ions are allowed to combine within the soil specimen in-situ to produce  $\text{CaCO}_3$ . The precipitated  $\text{CaCO}_3$  solidifies and binds the soil particles resisting their movement, hence improving the mechanical properties of soil. The first part of this paper evaluates the improved mechanical properties of the sand specimens treated in a mold with a diameter of 5 cm and a height of 10 cm. An attempt is made to obtain a relation between the amount of precipitated calcite and the achieved mechanical properties. An increase in compressive strength up to 1.6 MPa is obtained while the calcite content is up to 4%. The second part of this paper evaluates the trend of distribution of the injected grout material in 1-m long vertical sand columns. Uniform distribution of injected urea and  $\text{CaCl}_2$  is achieved easily, but the solution volume is to be increased by 1.5 times to achieve the relatively uniform distribution of urease. Results show that the larger area treatment for the real site application may be possible.

*Keywords:  $\text{CaCO}_3$ , Urease, Precipitation, UCS, Concentration*

### INTRODUCTION

Soil improvement is necessary in places where the soil does not meet the engineering requirements. Due to the scarcity of land in the cities and planes, the relocation of the planned engineering structures may not be possible, even the soil is weak. The physical and mechanical properties of soil must be modified in order to meet the engineering requirements. The demand for new, sustainable methods to improve soil continues to increase, with more than 40,000 soil improvement projects being performed per year at a total cost exceeding US\$6 billion/year worldwide [1].

Recently, various soil improvement techniques are in practice. One of the emerging soil improvement techniques is the in-situ calcite grouting technique. This technique employs the enzyme of urease to dissociate urea into ammonium and carbonate ions. Urease enzyme purified from the jack bean, or the bacterial cells (e.g., *Sporosarcina pasteurii*) producing the urease enzyme, has been used as a catalyst to dissociate the urea [3]. The obtained carbonate ions precipitate in the presence of calcium ions. The precipitated  $\text{CaCO}_3$ , i.e., calcite, forms bridges between the soil grains, binding them and restricting their movement. A lot of works have been carried out recently in the field of in-situ calcite precipitation technique. But most of these works are confined on small scale samples. However, reference [5] has conducted large scale biogROUT

experiment. They achieved a uniaxial compressive strength (UCS) of up to 12 MPa and an increase in dry density of up to 37%. Nevertheless, the uniform distribution of the improvement is yet to be achieved. The control and predictability of the in-situ distribution of bacterial activity, reagents and the resulting mechanical properties due to precipitated calcite is yet not sufficient [5]. Homogenous distribution of bacteria and precipitated calcite is a great challenge on bacterial grouting because of higher flow velocity and pore sizes smaller than the size of bacteria [4]. Clogging may occur due to the bacterial absorbance in soil grains and it may limit the treatment distance [5].

Utilizing the enzyme itself may be alternative and more straightforward than using bacteria because the cultivation and fixation of bacteria (i.e., biological treatment) do not need to be considered [6]. The Enzyme Mediated Calcite Precipitation, EMCP, may be relatively simpler carbonate precipitation technique, in comparison with the bacterial methods, in order to achieve uniform calcite distribution.

In our current study, the EMCP technique that should improve the mechanical properties of soil has been evaluated. In the first part of this study, the EMCP technique is evaluated in small scale samples (i.e., with a diameter of 5 cm and a height of 10 cm). Sand samples are treated with grout material and the mechanical properties of improved specimens are examined. In the second part, the feasibility of this

technique is evaluated in larger scale in a way to achieve a larger treatment area with uniform distribution of the grout materials. In this part, the distribution of the injected grout material is examined throughout the sand packed inside a long tube with an internal diameter of 5 cm and a length of 98 cm.

## EXPERIMENTS

### Grout Materials

The grout used in this study is a combination of reagents, i.e., urea and  $\text{CaCl}_2$ , and an enzyme called urease. Urea and  $\text{CaCl}_2$ , having claimed purity levels greater than 95%, are obtained from the Kanto Chemicals Co. Inc., Tokyo, Japan. Urease, with the activity of 2970 Units/g obtained from Kishida Chemical Co. Ltd. Osaka Japan, has been used in the bio-catalytic dissociation of urea ( $\text{CO}(\text{NH}_2)_2$ ) (Eq. 1). The obtained carbonate ion precipitates in the presence of the calcium ion ( $\text{Ca}^{2+}$ ) supplied by the  $\text{CaCl}_2$  solution (Eq. 2).



Two different types of silica sands, keisa #6 and keisa #8, are used in large scale experiments to examine the flow and transport of the injected solution in sands with different hydraulic conductivity. The hydraulic conductivity of keisa #8 is 22 times smaller than that of keisa #6. The physical properties of these two types of sand are shown in Table 1.

### Evaluation Techniques

Different methods are followed to quantify the concentration of the grout materials and the amount of precipitated calcite. The concentration of calcium ion present in the solution is evaluated using ICP-AES. To evaluate the concentration of urea, the solution is mixed with the excess amount of urease. Afterwards, the concentration of the released ammonium ion is measured with the help of an ion meter [2]. The amount of precipitated calcite present in the treated sand is evaluated by acid leaching process. In this process, oven-dried treated sand is mixed with, Hydrochloric acid, HCl, until the gas bubble formations stops. The acid treated sand is dried in oven and the weight loss before and after acid leaching is calculated. The lost weight is assumed to be the weight of calcite.

### Small Scale Tests to Evaluate the Mechanical Properties

Small PVC cylinders with a diameter of 5 cm and height of 10 cm are homogenously packed with keisa #6 sand. A relative density of about 50% is maintained throughout the specimen.

Enzyme solution and reagent solution are mixed together. Concentrations of the reagent solution range from 1.0-1.6 mol/L and the urease concentration is fixed at 12 g/L. One pore volume of the solution, i.e., 85 mL, is poured into the sand samples from the top at the rate of 10 mL/min. It is allowed to drain from a small pin hole at the bottom of PVC cylinder. The treated sand specimens are carefully removed from the cylinder 24 hrs after the solution injection, and are dried inside the oven at 100 °C for 24 hrs. The oven-dried specimens are subjected to unconfined compression tests, to examine the mechanical properties. After the unconfined compression test, the amount of  $\text{CaCO}_3$  precipitated in the specimen is evaluated. Each of these experimental conditions is conducted two times to check the reproducibility.

Figure 1 shows the relation between  $\text{CaCO}_3$  precipitated and the mechanical properties achieved in the treated sand specimens. As is apparent in the figure, the noticeable improvement in strength can be observed after the precipitated  $\text{CaCO}_3$  approach a value of 2.5%. An almost linear increment in strength can be observed afterwards.

Table 1. Physical property of sands

Properties	Keisa #6	Keisa #8
$D_{10}$ [mm]	0.20	0.04
$D_{50}$ [mm]	0.34	0.10
Sp. Gr.	2.653	2.650
$e_{\max}$	0.899	1.333
$e_{\min}$	0.549	0.703
$k^*$ [cm/s]	0.044	0.002

\*k is hydraulic conductivity

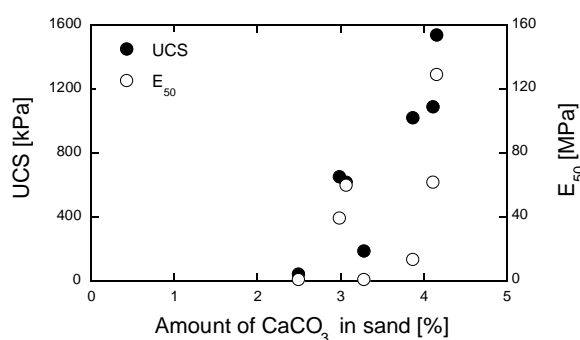


Fig.1 Relation between amount of calcite precipitated and the mechanical properties

However, there are some exceptions. A maximum strength of 1.5 MPa and stiffness of 129 MPa is achieved when the amount of precipitated  $\text{CaCO}_3$  in sand is about 4%.

### 1-D Flow Experiment

The feasibility of the grouting technique depends upon the volume of the treatment area that can be treated from one injection point. 1-D flow experiment is carried out to examine whether the treatment improved shape of about 2 m in diameter is possible or not. The acrylic pipe with an inner diameter of 50 mm and a length of 100 cm is used for the 1-D flow experiment.

#### Experimental set up

The schematic diagram of the acrylic cylinder test is shown in Fig. 2. The acrylic pipe contains removable caps with a porous stone at its two ends. The caps are connected with tubes with a diameter of 8 mm to inject and to drain out the grout material. The acrylic pipe contains 11 holes with a diameter of 2 mm at equal intervals as shown in Fig. 2. These holes are kept covered with silicone seals during sand packing and solution injection. The injection tube contains a ball valve, i.e., valve A, near the inlet

#### Sand packing

Sand is packed in the pipe in 5 layers, maintaining a relative density of about 50% in each layer. For the case of medium sand, the relative density of 50% is achieved easily with gentle compaction. But the fine sand is tamped with the help of a wooden tamper to achieve a relative density of 50%.

#### Solution injection

The sand sample is saturated with water before the solution injection. The tube connected to the bottom of acrylic pipe, i.e., injection tube, is filled with the injecting solution. Afterwards, one pore volume of injecting solution is poured into the tank and valve A is opened to commence the solution injection. The equal rate of injection, i.e., 60 mL/min, is maintained throughout the experiment. For the case of keisa #6, a 60 cm head is prescribed to maintain an injection rate of about 60 mL/min as shown in Fig. 2(a). For the case of keisa #8, a peristaltic pump is employed to maintain the equal rate of injection as shown in Fig. 2(b). Immediately after finishing the solution injection, 5 mL of sample solutions are pumped out of every hole with the help of syringes fitted with needle. The pumped solutions

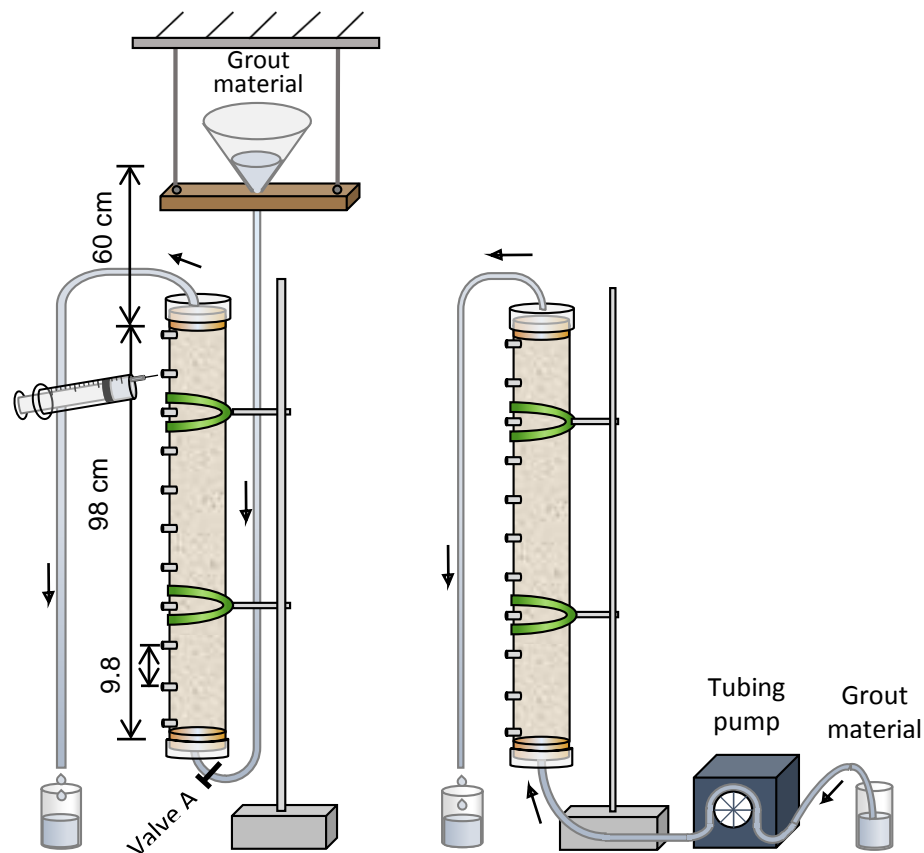


Fig.2 Experimental set up of 1-D flow test

of the acrylic pipe which is used to regulate the flow.

are collected in PP tubes separately.

conditions similar to Ea1), the concentration of

Table 2. Experimental conditions of 1-D flow experiment

Test name	Injecting solution	Injection volume (PV)	Head (cm)	Sand type	Dilution	Reacting solution	Evaluation method
Ca1	1 mol/L $\text{CaCl}_2$	1.0	60	Keisa #6	-	-	ICPAES
Ca2	1 mol/L $\text{CaCl}_2$	1.0	-	Keisa #8	-	-	ICPAES
Ua1	1 mol/L urea	1.0	60	Keisa #6	10 times	30 g/L urease	Ion meter
Ua2	1 mol/L urea	1.0	60	Keisa #8	10 times	30 g/L urease	Ion meter
En1	15 g/L urease	1.0	60	Keisa #6	10 times	1 mol/L urea	Ion meter
En2	15 g/L urease	1.0	80	Keisa #6	10 times	1 mol/L urea	Ion meter
En3	15 g/L urease	1.5	80	Keisa #6	10 times	1 mol/L urea	Ion meter
En4	15 g/L urease	1.5	-	Keisa #8	10 times	1 mol/L urea	Ion meter

The properties of the injected solution and mixing solution for various cases are shown in Table 2. The sample solutions of case Ca1 and Ca2 are subjected to ICP-AES to evaluate the amount of the calcium ion present in the solution. The sample solutions of the other cases are mixed separately with an equal volume of mixing solutions as shown in Table 2. The mixed solution is allowed 24 hours for the urea hydrolysis. After 24 hours, 1 mL of the mixed solution is taken and is diluted 10 times by mixing it with 9 mL of deionized water. The ammonium concentration of the solution is measured and the result is analyzed.

### Results

The vertical distributions of the individual grout materials are plotted. Vertical distribution of the calcium ion as evaluated by ICP-AES is shown in Fig. 3. As is apparent in the figure, distribution of the precipitated calcite is almost uniform throughout the height of the sample. It shows that the concentration of the  $\text{CaCl}_2$  solution can distribute uniformly throughout a distance of about 1 m from the injection. Vertical distribution of the ammonium ion for case Ua1 and Ua2 is as shown in Fig. 5. As is apparent in the figure, the concentration of the ammonium ion does not decrease remarkably in both of the sands, keisa #6 and keisa #8. Hence, the concentration of the urea solution injected into the sand distributes almost uniformly throughout a distance of about 1 m from the injection. However, the variation of distribution of urea seems to oscillate more than the variation of distribution of calcium ion. The variation of ammonium ion is relatively higher in keisa #8 sand. The vertical distribution of the ammonium ion for the case En1-En4 is shown in Fig. 6. As is apparent in the figure, the distribution of the ammonium ion for case Ea1 is uniform until a height of 60 cm from the inlet. Afterwards the concentration decreases. For Ea2 (i.e., head is increased to 80 cm keeping other

ammonium still decreases after 60 cm, however the

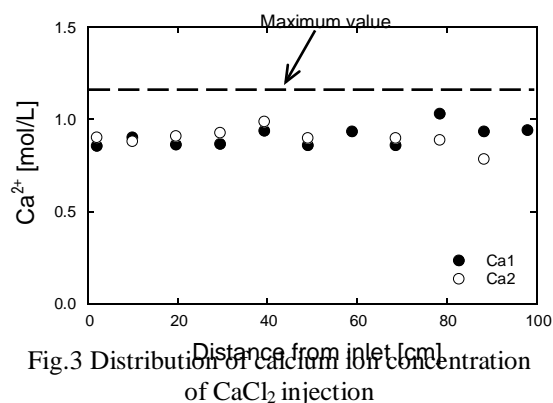


Fig.3 Distribution of calcium ion concentration of  $\text{CaCl}_2$  injection

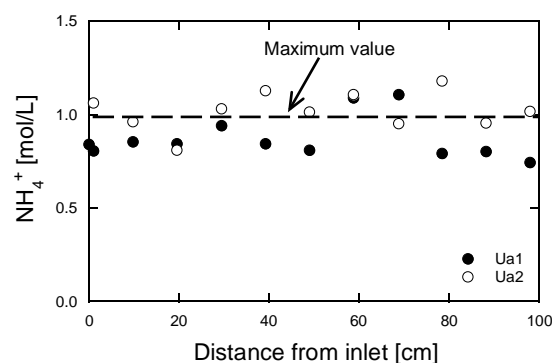


Fig.4 Distribution of ammonium ion concentration of urea injection

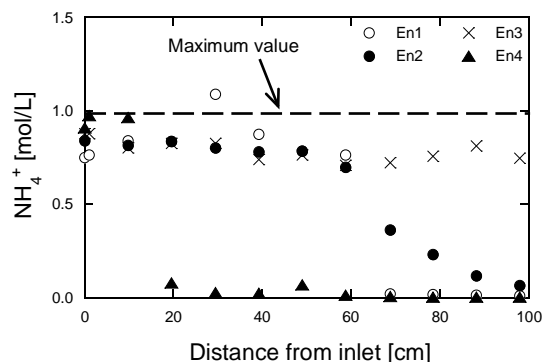


Fig.5 Distribution of ammonium ion concentration of urease injection

decrease is relatively gradual. In the next attempt to achieve the uniform distribution of the urease, volume of solution is increased. The distribution of ammonium ion is found relatively uniform in case Ea3, where the injection volume is increased to 1.5 pore volumes. With an increase in the volume of injection, the problem of non-uniform distribution of the urease content may be solved in keisa #6. To examine the distribution of urease in keisa #8, 1.5 pore volumes of solution is injected using a peristaltic pump. As is apparent in the figure, the urease content is observed only up to a few centimeters from the inlet. It may be due to the small pore size of keisa #8 sand. The relatively smaller pores may have resisted the flow of the colloidal particles of urease. These results conclude that the flow of urea and  $\text{CaCl}_2$  is relatively uniform over a vertical distance of almost 1m for both finer and coarser sand evaluated in this work. The uniform distribution of urease can be easily achieved in coarser sand by increasing the injection volume. Hence, the treatment distance of approximately 2 m may be feasible in EMCP technique.

## CONCLUSION

The efficacy of EMCP technique is evaluated in small scale laboratory samples. The results show an appreciable increment in mechanical properties. For the utilization of EMCP as an alternative soil improvement technique in engineering applications, the treatment area should be increased. The distribution of individual grout materials is evaluated in 1 m sand columns. The distribution of reagents is found to be uniform in both coarser and finer soil. In order to achieve the uniform distribution of urease in coarser soil, injection of higher volume of the solution is required. However, the injection technique employed in this work is found not appropriate to achieve a uniform distribution of urease in finer

sand. In the near future the mixed grout material is injected and the distribution of calcite throughout the sand column is evaluated. Afterwards, the similar test is replicated in 3- dimensional samples.

## ACKNOWLEDGEMENTS

This work has been partly supported by research grants from the Maeda Engineering Foundation, Tokyo, Japan and the Shikoku Create Association, Kagawa, Japan. Their support is gratefully acknowledged.

## REFERENCES

- [1] DeJong JT, Mortensen BM, Martinez BC, Nelson DC, "Bio-mediated soil improvement", *Ecol. Eng.*, Vol. 36, 2010, pp. 197-2010.
- [2] "Handy ion meter TiN-9001 instruction manual", Toko Chemical Laboratories Co., Ltd.
- [3] Harkes MP, Van Paassena LA, Booster JL, Whiffin VS, and van Loosdrehta MCM, "Fixation and distribution of bacterial activity in sand to induce carbonate precipitation for ground reinforcement", *Ecol. Eng.*, Volume 36(2), 2010, pp. 112–117.
- [4] Keykha HA, Huat BBK, and Asadi A, "Electro-biogrouting stabilization of soft soil", *Environmental Geotechnics*, 2013, pp. 1-9.
- [5] van Paassen LA, Ghose R, van der Linden TJM, van der Star, WRL, and van Loosdrecht M CM, "Quantifying biomediated ground improvement by ureolysis: Large-scale biogROUT experiment", *J. Geotech. Geoenviron. Eng.*, Volume 136 (12), 2010, pp 1721–1728.
- [6] Yasuhara H, Neupane D, Hayashi K, and Okamura M, "Experiments and predictions of physical properties of sand cemented by enzymatically-induced carbonate precipitation", *Soils Found.*, Volume 52(3), 2012, pp. 539–549.

## NUMERICAL ANALYSIS OF INFILTRATION INTO PERVIOUS CONCRETE-BASE SYSTEMS

Bertrand Teodosio<sup>1</sup>, \*Jaehun Ahn<sup>2</sup> and Hyun-Suk Shin<sup>3</sup>

<sup>1</sup>Graduate Student, Pusan National University, Korea

<sup>2</sup> Assistant Professor, Pusan National University, Korea

<sup>3</sup> Professor, Pusan National University, Korea

### ABSTRACT

Decrease in pervious area due to urbanization, and rapid change in climate prompted to reconsider our philosophy in stormwater management. One of innovative approaches for stormwater management is a concept called Low Impact Development (LID). Among other techniques of LID, construction of pervious pavement can utilize vast paved surfaces, traditionally impervious, allowing stormwater to infiltrate through its surface. In this study, the hydrologic performance of a particular pervious concrete system section was investigated using Finite Element Method (FEM) modelling. The influence of initial saturation and rainfall intensity to produce run-off were examined to imply possible design considerations. Further, rainfall data recorded from July 15, 2012 in Busan, South Korea was employed to probe the effect of evaporation and pipe installation in the hydrologic capacity and behavior of the pervious concrete system. The results and implications to hydrological design are discussed herein.

*Keywords: Low Impact Development, Pervious concrete, Finite Element Method, Infiltration, Run-off*

### INTRODUCTION

Flooding is recurring in most urban areas which affects economic growth. According to Crichton[2], total gross domestic product (GDP) losses due to stormwater run-off accumulation are approximately 14% and 2% for poorer and richer countries, respectively.

Inundation does not only lead to economic damage, it also causes bereavement in different affected regions. Conferring to the United Nations[5], above 90% of recorded death from natural disasters are related to water from the year 1975 to 2001 in Asia.

Possible methodologies to prevent severe flooding that could cause financial damage and life loss is through stormwater management. One of innovative approaches for stormwater management is a concept called Low Impact Development (LID). LID is an emerging practice to lessen inundation and hazards due to lack of pervious surfaces in an urban region. Among other techniques of LID, construction of pervious pavement can allow stormwater to infiltrate through its surface preventing or attenuating run-off occurrence.

To quantify the feasibility of a pervious pavement, the hydrologic performance should be investigated by obtaining the infiltration capacity and run-off threshold of a system. Generally, infiltration capacity can be obtained using calculation methods such as Darcy's Law, Horton's Equation, Curve Numbers, and Green-Ampt Model.

### INFILTRATION CAPACITY CALIBRATION

Infiltration is governed by the pull of gravity and capillary action. The soil characteristics including hydraulic conductivity, porosity, and ease of entry also affects the infiltration process.

In this study, Green-Ampt Model was compared to FEM model to verify the applicability of the used FEM software, SVOOffice's SVFlux[6].

#### Green-Ampt Model

The Green-Ampt Model[4][7] is a method to estimate infiltration which considers wetting front suction head ( $\psi$ ), volumetric water content ( $\theta$ ), saturated hydraulic conductivity ( $k_s$ ), and cumulative volume infiltrated ( $F$ ). Eq. (1) shows the formula to be used for rainfall intensity ( $I$ ) less than or equal to the saturated hydraulic conductivity to obtain the infiltration,  $f$ , at a specific time,  $t$ .

$$f = I \quad (I \leq k_s) \quad (1)$$

For rainfall intensity greater than the saturated hydraulic conductivity refer to Eq. (2).

$$f = k_s \left( 1 + \frac{\Delta\theta \cdot \psi}{F} \right) \quad (I > k_s) \quad (2)$$

Where  $\Delta\theta$  is the initial moisture deficit ( $\theta_s - \theta_i$ ) and  $\psi$  is the average suction at wetting front.

To obtain the cumulative volume of water infiltrated,  $F$ , Eq. (3) should be used.



$$k_s(t - t_s) = F - \Delta\theta \cdot \psi \cdot \ln(F + \Delta\theta \cdot \psi) - F_s + \Delta\theta \cdot \psi \cdot \ln(F_s + \Delta\theta \cdot \psi) \quad (3)$$

To calculate for the cumulative infiltration,  $F_s$ , refer to Eq. (4).

$$F_s = \frac{\Delta\theta \cdot \psi}{\frac{I}{k_s} - 1} \quad (4)$$

Where  $t_s$  is the time to achieve surface saturation calculated by getting the ratio of the cumulative volume of infiltration at moment of surface saturation,  $F_s$ , and rainfall intensity,  $I$ .

### Finite Element Method (FEM)

The infiltration of a single layer crushed limestone was modelled in SVFlux to compare with the Green-Ampt infiltration model. The material properties of the crushed limestone is presented in Table 1 and Table 2 for Soil Water Characteristic Curve (SWCC) and unsaturated permeability property, respectively.

Table 1 Crushed limestone SWCC [1]

Layer	$\theta_s$	a	n	m	h
Crushed Limestone	0.34	0.71	1.74	0.47	100

Note: a, n, m, h are constants from Fredlund-Xing Fit.

Table 2 Crushed limestone unsaturated k properties

Layer	$k_s$ (cm/s)	$k_{min}$ (cm/s)	p
Crushed Limestone	$1.1 \times 10^{-4}$ [3]	$1 \times 10^{-8}$	5

Note:  $k_{min}$  = minimum permeability;  
p=estimation constant for Modified Campbell

The comparison of infiltration models is shown in Fig. 1 and Fig. 2. The Green-Ampt model and FEM model for the infiltration of the single layer crushed limestone are almost coinciding with each other. The curves completely converges at around 35 minutes for all the applied infiltration intensities.

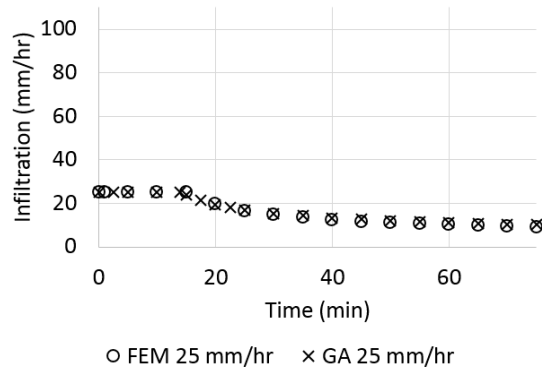


Fig. 1 FEM and GA models,  $I=25$  mm/hr.

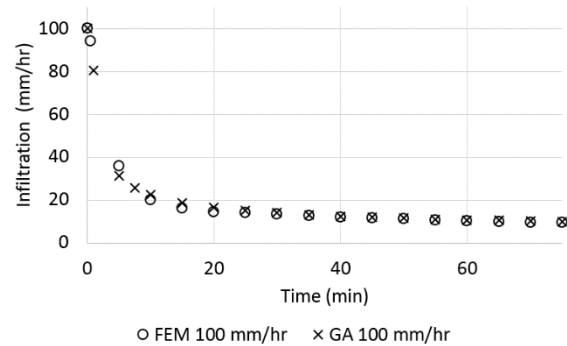


Fig. 2 FEM and GA models,  $I=100$  mm/hr.

### FEM INVESTIGATIONS

#### Initial Condition

For the following investigations, a pervious pavement system was modelled with two different layers. The top layer is a pervious concrete (PC) with properties listed in Table 3 and Table 4 based on experimental tests conducted. The height of the PC layer is 0.15 m.

Table 3 Pervious concrete SWCC

Layer	$\theta_s$	a	n	m	h
Pervious Concrete	0.32	2.23	1.63	8.60	0.21

Note: a, n, m, h are constants from Fredlund-Xing Fit.

Table 4 Pervious concrete unsaturated k properties

Layer	$k_s$ (cm/s)	$k_{min}$ (cm/s)	p
Pervious Concrete	0.129	$1 \times 10^{-8}$	5

Note:  $k_{min}$  = minimum permeability;  
p=estimation constant for Modified Campbell

The bottom layer is made-up of crushed limestone with properties listed in Table 1 and Table 2. The height of the bottom layer is 0.45 m. The width of the typical pervious pavement system is assigned to be 3 m.

The boundary conditions of the system was assigned to be zero flux at both sides and at bottom indicating that there might be a liner or a geomembrane installed to have no exfiltration. For the interface of PC and crushed limestone (CL), a no boundary condition was designated to allow flow. For the upper side of the PC layer, a direct rainfall was applied, hence, climate boundary condition was assigned. Refer to Fig. 3 for the boundary conditions designated to the pervious pavement system.

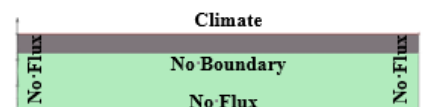


Fig. 3 Boundary conditions for PC and CL layers.

To investigate the effect of initial condition of the pervious system, the degree of saturation was assigned to be 0%, 25%, 50%, 75%, and 100%. The equivalent initial matric suction is listed in Table 5 for PC and limestone.

Table 5 Initial condition of the pavement system

Degree of Saturation	$\psi_i$ (kPa) PC	$\psi_i$ (kPa) Limestone
0%	-1.4	-250
25%	-90	-1x10 <sup>6</sup>
50%	-0.7	-3.7
75%	-0.28	-0.66
100%	-0.08	-0.05

The increment assigned for the iteration is 1 minute. For the initial condition saturation investigation, the end time is 900 minutes since this time is sufficient for the system to achieve full saturation. Fig. 4 presents the mesh for PC and limestone layers.

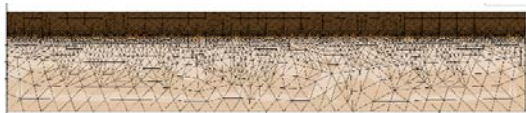


Fig. 4 FEM meshes for PC and limestone layers.

For the results of the five runs with constant pervious pavement section and material properties but different initial condition, refer to Fig. 5.

According to the graphs presented, the initial saturation affects the run-off threshold due to the differences in water storage availability. The curves is logical since the process of infiltration continues if there is a water storage available to fill additional water in the system. However, this graphs gives quantification to the time required to experience stormwater run-off for the specific section with SWCC and unsaturated hydraulic conductivity properties.

The run-off threshold for the pervious pavement system is 217, 183, 94, 10, and 3 minutes for initial condition equivalent to 0%, 25%, 50%, 75%, and 100% saturation, respectively.

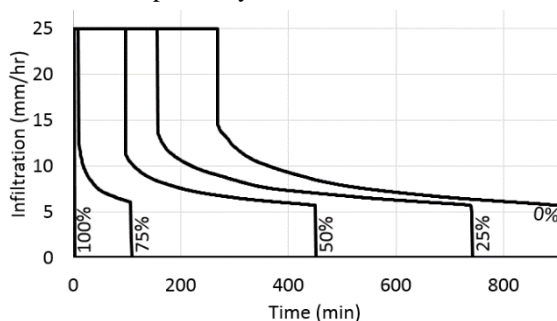


Fig. 5 Infiltration of pervious system having different initial saturations.

Concentrating in the water storage capacity, the total  $V_v$  of the system is 0.1994 m<sup>3</sup>/m<sup>2</sup>. Applying the constant rainfall intensity 25 mm/hr ( $4.17 \times 10^{-4}$  m/min), the time to fill the whole system is around 480 minutes for a dry initial condition. Due to the disparity of hydraulic conductivity of the two materials, run-off might occur after filling the PC layer. The total  $V_v$  for the said layer is 0.0483 m<sup>3</sup>/m<sup>2</sup>. It will take about 120 minutes for the PC layer to be filled. Referring to Fig. 5, the 0 % initial saturation system experienced a run-off at 217 minutes. The FEM value is between the computed time using  $V_v$  which has a range equivalent to 120 to 480 minutes. Same steps for calculating the range were made for the remaining system with increased initial saturation condition. The ranges are tabulated in Table 6.

Table 6 Range of possible run-off threshold

Initial Saturation	Min. (min)	Max. (min)	FEM (min)
0%	116	479	217
25%	87	359	183
50%	58	239	94
75%	29	120	10
100%	0	0	3

In system with higher initial saturation condition of 75% and 100%, it is reflected that the FEM run-off threshold was not in the range calculated. This effect is possibly due to the SWCC and unsaturated hydraulic conductivity of the materials.

The graphs for the cumulative run-off are displayed by Fig. 6. The cumulative run-off after 600 minutes for 0%, 25%, 50%, and 100% are 0.33 m<sup>3</sup>, 0.36 m<sup>3</sup>, 0.50m<sup>3</sup>, 0.70 m<sup>3</sup>, and 0.75 m<sup>3</sup>, accordingly.

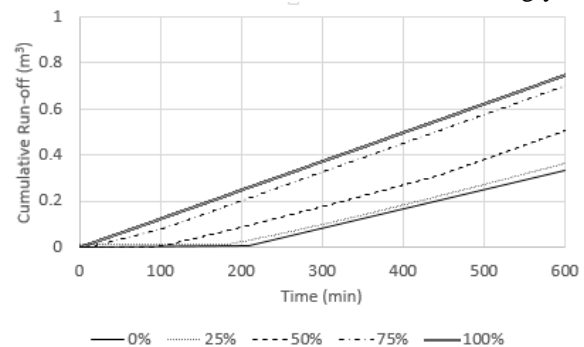


Fig. 6 Infiltration of pervious system having different rainfall intensities applied.

### Rainfall Intensity

To expand the range of analysis, rainfall intensity was assigned to be a variable with all the remaining parameters left constant. The constant initial condition chosen was 25% saturation since the optimum gravimetric moisture content can be obtained with this value according to experimental

tests. The rainfall intensities applied were 25, 50, 75, and 100 mm/hr and run-offs are experienced at time equal to 183, 62, 27, and 23 minutes, respectively. The infiltration curves are shown in Fig. 7.

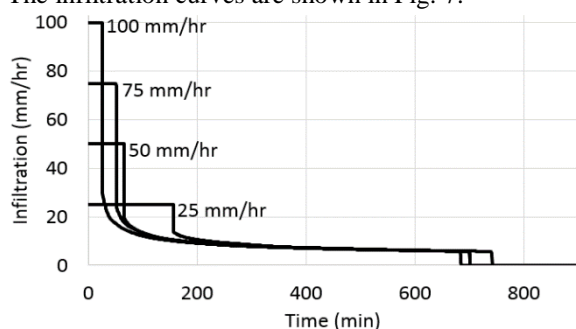


Fig. 7 Infiltration of pervious system having different rainfall intensities applied.

The cumulative run-off are 2.62 m<sup>3</sup>, 1.89 m<sup>3</sup>, 1.11 m<sup>3</sup>, and 0.36 m<sup>3</sup> for 100 mm/hr, 75 mm/hr, 50 mm/hr, and 25 mm/hr, respectively, for the rainfall intensity test simulation within 600 minutes. Refer to Fig. 8 for the cumulative run-off graphs of pervious pavement system with different rainfall intensities applied.

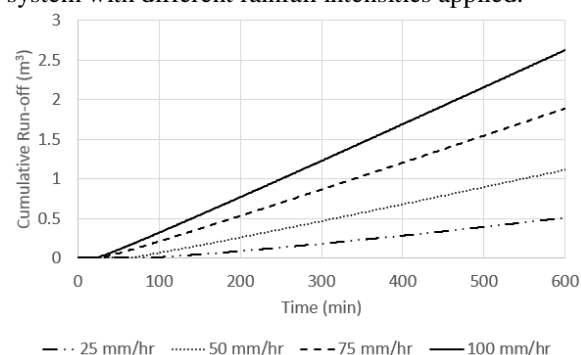


Fig. 8 Infiltration of pervious system having different rainfall intensities applied.

### Rainfall Data Application

A rainfall data was collected from July 15, 2012 in Busan, South Korea. The historical weather for the said day is listed in Table 7 which was used for the implementation of evaporation effect in the SVFlux software. The potential evaporation method used was constant while the actual evaporation method used was Wilson Limiting Equation.

Table 7 Historical weather in Busan, South Korea

07-15-12	T(°C)	H(%)	W(mph)
Max	29.4	94	21
Min	22.8	68	17
Ave	26.1	81	19

Note: T = air temperature; H = humidity; W = wind speed; C = potential evaporation constant.

To investigate the effect of the pipe, an opening

that has the ability to drain substantial water flow was drawn at the midpoint of the width on the bottom surface of the basalt layer. The boundary condition for the pipe was an excess pore pressure constant equal to zero ( $u=0$ ). The pipe is 100 mm in diameter. Fig. 9 illustrates the section with drain installed.



Fig. 9 Pervious pavement system section with pipe installed.

Table 8 FEM cases for run-off analysis concerning pipe and evaporation

Case	Pipe	Evaporation
1	None	None
2	None	Implemented
3	Implemented	None
4	Implemented	Implemented

There are four cases for the application of the collected rainfall data. At the preceding page, Table 8 presents the cases for examining the effect of pipe and evaporation in the hydrologic performance of the pervious concrete and limestone.

The rainfall data applied to the cases in Table 8 are plotted in Fig. 10.

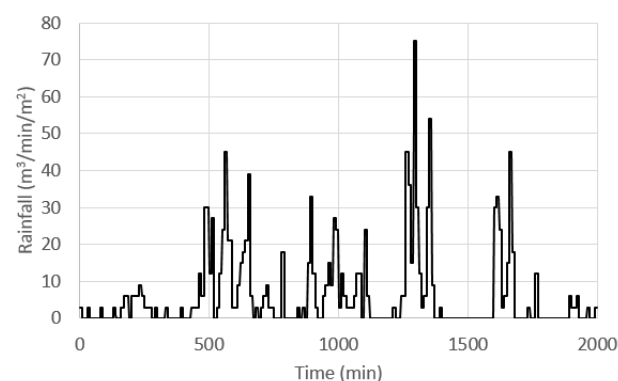


Fig. 10 Rainfall data (July 15, 2012) collected and applied in the FEM cases

Case 1 shows run-off without pipe installed and without evaporation implemented. It is evident from the graph that for a no exfiltration pervious pavement system and no evaporation implemented, notable volume of run-off should be experienced. Conferring to curve of Case 2, there is a small amount of reduction in the run-off due to the evaporation implementation which serves as an outlet at the top surface of the system. When pipe was installed, the run-off plummeted which is evident in both Case 3 and Case 4. The run-off graphs are shown in Fig. 11.

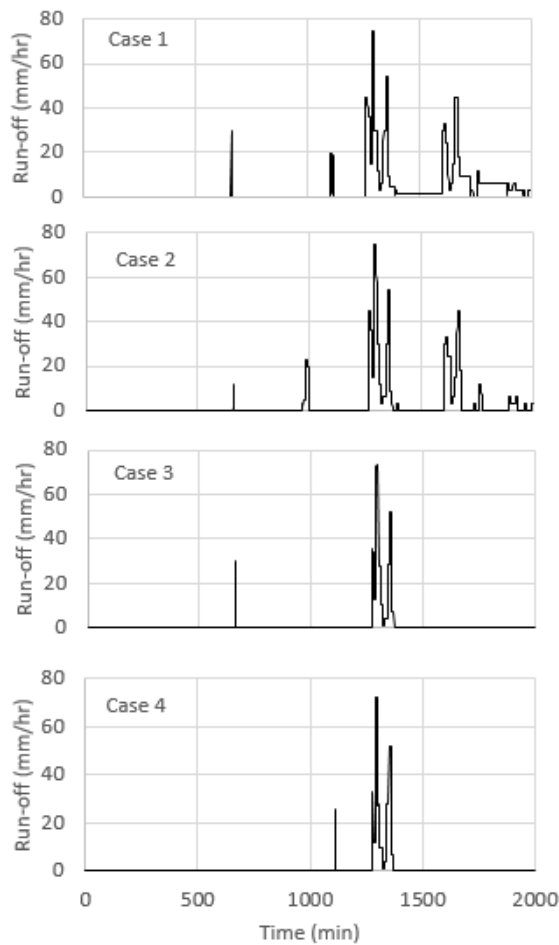


Fig. 11 Run-off graphs for rainfall data applied to pervious pavement system.

To quantify the run-off volume accrued, the cumulative run-off volume for each cases are plotted in Fig. 12. The maximum run-off volume collected for Case 1 is  $0.36 \text{ m}^3$ . By implementing evaporation in Case 2, the cumulative run-off volume decreased to  $0.28 \text{ m}^3$ . Case 3 and Case 4 collected  $0.13 \text{ m}^3$ .

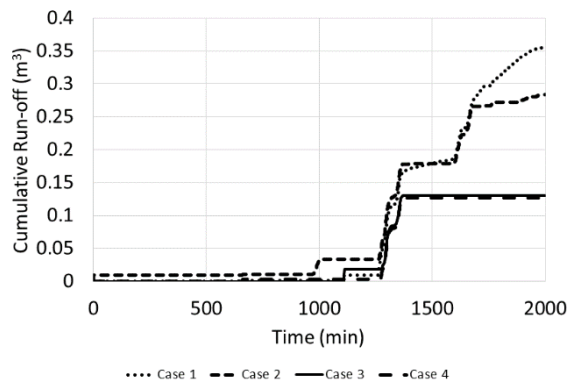


Fig. 12 Cumulative run-off graphs for rainfall data applied to pervious pavement system.

## CONCLUSIONS

In this study, three sets of experimental runs were conducted. The first set was conducted to investigate the influence of initial saturation condition (0%, 25%, 50%, 75% and 100%) of the pervious pavement system to the run-off buildup. A constant rainfall intensity of 25 mm/hr was applied. According to the data collected curves plotted, initial saturation, SWCC and unsaturated hydraulic permeability affects the behavior of water protrusion through the system. For a dry system until around 50% saturation, the run-off threshold time is in between the time to fill the PC layer (Minimum) and the time to fill the whole system (Maximum).

On the other hand, for initial saturation more than 50%, the run-off threshold time from the runs were not in between the computed range. For the 75% initial saturation, the run-off happened earlier. In the case of 100% initial saturation, the run-off happened late. The cause could be the initial matric suction assigned in the initial condition input based on the SWCC. The proximity of values of both PC and limestone for 75% initial saturation seems to have an effect to the analysis which resulted to earlier occurrence of run-off. While in the 100% initial saturation, the initial matric suction of PC has a higher value in comparison with the crushed limestone layer that could possibly ensued latter run-off occurrence. The pore pressure buildup might have an effect to the infiltration of water. Further examination should be conducted regarding this occurrences.

In relation with the cumulative run-off of the initial saturation investigation, there are no observable pattern that can be deduced from the curves plotted. However, 0% and 25% has almost similar run-off volume within 600 minutes. Similar case with the 75% and 100% initial saturation, the cumulative run-off volume's value are near.

The second set, focused on the effect of rainfall intensity applied to the system. The curves observed were reasonable. There is an inverse proportionality between the rainfall intensity applied and run-off threshold. As the rainfall intensity applied were increased, the time for run-off to occur decreased. Rainfall intensities of 75 mm/hr and 100 mm/hr have close run-off threshold time. A pattern can be observed in the cumulative run-off curves. Assuming that the baseline rainfall intensity is 25 mm/hr, increasing the rainfall intensity to 50 mm/hr (twice the baseline value) will increase the accumulated run-off volume by 208%. Similarly, applying rainfall intensity with a value thrice the baseline rainfall intensity would increase the cumulative run-off volume to 425%. Also, multiplying the baseline rainfall intensity (25 mm/hr) by four will increase the cumulative run-off volume by 628%. Hence, each time you increase the rainfall intensity by a factor, the

cumulative rainfall intensity will increase approximately 200% multiplied by the factor where 25 mm/hr rainfall intensity was assumed to be the reference.

The third set of simulation includes the application of the rainfall data collected from July 15, 2012. The rainfall data was used to investigate the run-off reduction by implementing pipe and evaporation. From the graphs obtained, the evaporation may have little significance when pipe was implemented to the system.

There is a 20% reduction in the cumulative run-off volume when evaporation is implemented. For a partial exfiltration system, 64% can be reduced in the cumulative run-off volume by installing a 100-mm pie at the center over the bottom surface of the limestone layer.

#### ACKNOWLEDGEMENTS

This research was supported by a grant from Advanced Water Research Program funded by Ministry of Land, Infrastructure and Transport of Korea government, and the Mid-Career Researcher Program (No. 2012-047702) funded by National Research Foundation of Korea government.

#### REFERENCES

- [1] Ba M, Nokkaew K, Fall M and Tinjum J, "Effect of matric suction on resilient modulus of compacted aggregate base courses", *J. of Geotechnical and Geological Engineering*, Vol 31, Issue 5, Oct. 2013, pp 1497-1510.
- [2] Crichton D, *International historical , political, economic, social, and engineering responses to flood risk*. Florida: CRC Press, 2011.
- [3] Cote J and Konrad JM, "Assesment of hydraulic characteristics of unsaturated base-course materials: a practical method for pavement engineers", *Canadian Geotechnical Journal*, Vol 40, 2003, pp 121-136.
- [4] Mein RG and Larson CL, "Modeling infiltration during a steady rain", *J. of Water Resources Research*, Vol 9, No. 2, Apr. 1973, pp 384-395.
- [5] United Nations, *Guidelines for reducing flood losses*. Geneva: United Nations International Strategy for Disaster Reduction (UNISDR), 2004.
- [6] Thode R and Fredlund M, *SVFlux Tutorial Manual*. Saskatchewan, Canada: SoilVision Systems Ltd., 2013, ch. 2.
- [7] Zhang J, *A laboratory scale study of infiltration from pervious pavements*. Australia: RMIT University, 2006, ch. 4.



## PROPAGATION OF HARMONICAL VIBRATIONS IN PEAT

Darius Macijauskas<sup>1</sup> and Stefan Van Baars<sup>2</sup>,

<sup>1,2</sup>Faculty of Science, Technology and Communication, University of Luxembourg, Luxembourg

### ABSTRACT

In order to check the reliability of man-made vibration prediction methods, vibration tests were performed on one of polders in the North-West of the Netherlands. The polder was chosen because it has a rather homogenous, thick and soft peat top layer. Here sufficient harmonical vibrations could be generated by a rather small shaker.

The shaker was designed and manufactured in order to produce harmonical vibrations at the soil surface. It consists of two counter rotating electric vibrators (with rotating eccentric masses) in order to produce a vertically oscillating force. For the recordings of the vibrations, six 2D or 3D geophones were placed on the soil surface and one 2D geophone was placed on top of the shaker.

The measured vibration amplitudes of the vertically oscillating shaker were compared with 1. Two different analytical methods used for the design of vibrating machine foundations, 2. The Confined Elasticity approach and 3. The Finite Element Method, for which Plaxis 2D software was used. Also the measured vibration amplitudes at the soil surface were compared with Barkan-Bornitz's solution and Finite Element Modeling.

*Keywords:* Soil Vibrations, Man-made Vibrations, Vibration Propagation, Soil Waves

### INTRODUCTION

For most developing countries the urban environment is getting larger and denser. Therefore civil engineers have to pay more attention to the effect of man-made vibrations. According to research by Hölscher and Waarts [2] the reliability of prediction methods for man-made vibrations is unfortunately disappointingly low. In order to check this conclusion, a field test was performed to measure the vibration propagation with an experiment on site.

In order to produce harmonic vibrations at the soil surface, a shaker was designed and manufactured. For the recordings of the vibrations, six 2D or 3D geophones were placed on the soil surface and one 2D geophone was placed on top of the shaker.

The measured vibrations of the shaker and the soil surface will be compared with analytical and numerical (FEM) solutions.

### SITE LOCATION AND STRATIGRAPHY

In order to produce sufficient harmonic vibrations on the soil surface with a rather small shaker, the potential site for the field test should fulfil two major conditions: it should be rather homogeneous and rather soft. Therefore a peaty site in the Netherlands was chosen. The test site is located about 10 km North-East from Amsterdam in the village of Uitdam. The test area is marked by letter "A" in Fig. 1.

Near the test area, other research has been made before, related to the strength of peat [3]. The area

used for the peat strength research is marked by letter "B" in Fig 1. In there, geological investigations have been carried out in May 2012. Three boreholes were drilled and they are marked by "c1", "c2" and "c3" in Fig. 1 and Fig. 2.



Fig. 1 Location of the test site (Google, Map data)

The top layer is a thin clayey layer with a thickness varying between 0.2 m and 0.5 m. Below this layer there is a peat layer of 4.5 m thick. It was reported that the bulk density of the peat layer  $\rho = 0.98 \pm 0.08 \text{ t/m}^3$  [3].

### EQUIPMENT AND SETUP

#### Shaker Design

In order to make the shaker transportable, two small counter rotating electric vibrators (with rotating eccentric masses) have been used to produce

a vertically oscillating force. This type of vibrator is frequently used in geotechnics (for example sheet pile driving or soil densification).

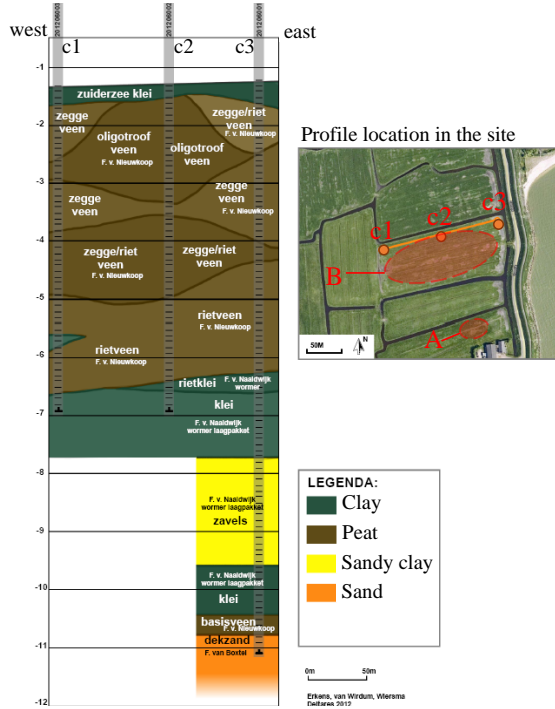


Fig. 2 Data from geological investigations [3]

The vibrators are connected to a plate of 40 cm in diameter and 2 cm in thickness. Additional square plates can be added on site to vary the total mass of the system. The whole is tightened together with bolts. This makes a total weight of the shaker variable up to a maximum of 300 kg (which makes the vertical gravity force 2.94 kN) and the vertical oscillating force (due to the rotating eccentric masses) can vary up to 2.06 kN.

### Vibration Tests Setup

The equipment used for the vibration tests, consists of a: 1) Shaker; 2) Frequency inverter; 3) Power generator; 4) Geophones; 5) Data acquisition box; 6) Laptop. All these components with their corresponding numbers are shown in Fig. 3.

### ELASTIC PROPERTIES OF THE SITE

In order to evaluate small strain stiffness parameters of the peat, pressure (P) and shear (S) wave velocity measurements were carried out. This was done by hitting the shaker with a hammer and measuring the arrival times at the geophones. The geophone on top of the shaker records the input wave.

The P-wave velocity was measured from the arrival time differences between of the first radial vibration peaks and the S-wave velocity similarly

but of the biggest vertical vibration peaks.

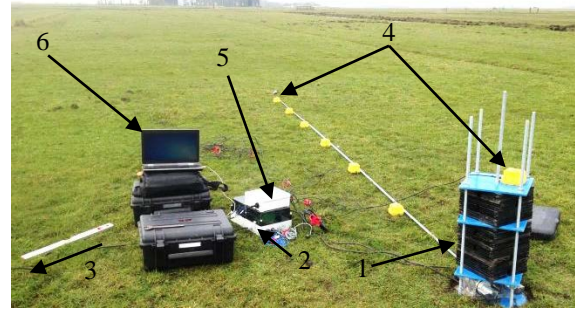


Fig. 3 Vibration test setup: 1) Shaker; 2) Frequency inverter; 3) Power generator; 4) Geophones; 5) Data acquisition box; 6) Laptop

The measured P-wave and S-wave velocities on site are respectively  $v_p = 66.9$  m/s and  $v_s = 17.4$  m/s. From the velocities of the body waves and the bulk density of the peat  $\rho \approx 1$  t/m<sup>3</sup>, according to Eq. 1, Eq. 2 and Eq. 3 the shear modulus  $G = 303$  kN/m<sup>2</sup>, the Poisson's ratio  $\nu = 0.464$  and the Elastic modulus  $E = 886$  kN/m<sup>2</sup> can be determined. The R-wave velocity can be calculated from the Poisson's ratio and S-wave velocity:  $v_r = 16.5$  m/s.

$$G = \rho v_s^2 \quad (1)$$

$$\nu = \frac{1 \left( \frac{v_p}{v_s} \right)^2 - 2}{2 \left( \frac{v_p}{v_s} \right)^2 - 1} \quad (2)$$

$$E = 2G(1 + \nu) \quad (3)$$

In order to compare the analytical solutions of the shaker vibration amplitude with the vibration amplitudes of the soil surface, the site will be modelled as an elastic isotropic homogenous half-space with the previously defined elastic properties.

### SHAKER VIBRATION AMPLITUDES

In 1904 Lamb [4] solved the problem of the wave propagation in three dimensions (also known as the dynamic Boussinesq problem). Based on Lamb's work, Reissner in 1936 [5] first developed the vertical response of a uniformly loaded flexible circular area resting on an elastic half-space. The vertical displacement amplitude at the center of the flexible loaded area is, according to Reissner, defined by:



$$A_R = \frac{F_0}{Gr_{pl}} \sqrt{\frac{f_1^2 + f_2^2}{(1 - ba_0^2 f_1)^2 + (ba_0^2 f_1)^2}}, \quad (4)$$

in which:  $F_0$  – amplitude of the vertically exciting force;  $r_{pl}$  – radius of the loaded circular area;  $f_1, f_2$  – displacement (compliance) functions;  $a_0$  – dimensionless frequency;  $b$  – dimensionless mass ratio. The dimensionless frequency and mass ratio are calculated as follows:

$$a_0 = \omega r_{pl} \sqrt{\frac{\rho}{G}}, \quad (5)$$

$$b = \frac{m_{vib}}{\rho r_{pl}^3}, \quad (6)$$

where:  $\omega$  – angular frequency;  $m_{vib}$  – total vibrating mass.

Bycroft [6] provided a solution for forced vibrations of a rigid circular plate attached to the surface of an elastic half-space for large values of the frequency ( $a_0 > 1.5$ , which is also the case in this article). Using Eq. (4), according to Kruijtzter [7] the compliance functions can be simplified to:

$$f_1 \approx \frac{3}{4a_0^2}, \quad (7)$$

$$f_2 \approx \frac{1.93}{a_0^3}. \quad (8)$$

Hsieh [8] modified in 1962 Reissner's solution and proved, that it is possible to have a mechanical analogue in a form of single-degree of freedom system. Later Lysmer and Richart [9] proposed a frequency independent mechanic analogue.

Lysmer modified the mass ratio:

$$B = \left( \frac{1-\nu}{4} \right) \frac{m_{vib}}{\rho r_{pl}^2} = \left( \frac{1-\nu}{4} \right) b. \quad (9)$$

And suggested an analogous spring stiffness  $K$  and damping ratio  $D$ .

$$K = \frac{4Gr_{pl}}{1-\nu}, \quad (10)$$

$$D = \frac{3.4r_{pl}^2}{1-\nu} \sqrt{G\rho}. \quad (11)$$

Using this, the vibration amplitude can be written as:

$$A_L = \frac{F_0 / K}{\sqrt{[1 - (\omega^2 / \omega_n^2)]^2 + 4D(\omega^2 / \omega_n^2)}}, \quad (12)$$

in which:  $\omega_n$  – natural angular frequency of the mechanical analogue system:

$$\omega_n = \sqrt{\frac{K}{m_{vib}}}. \quad (13)$$

Another analytical solution was suggested by Verruijt [10]. He suggests to neglect here the horizontal displacements (while they are very small compared to the vertical ones), which is called the confined elasticity approach. This approach was first proposed by Westergraad [11] and generalised for elastodynamics by Barends [12]. In this way the vibration amplitude of a rigid circular plate on a confined elastic half space becomes:

$$A_C = \left| \operatorname{Re} \left[ \frac{\left( \frac{\omega \exp(i\omega / \omega_c)}{\omega_c \sin(\omega / \omega_c)} - \frac{16B}{\pi m_c (1-\nu) \left( \frac{\omega}{\omega_c} \right)^2} \right)^{-1}}{A_s} \right] \right|, \quad (14)$$

in which:  $\omega_c$  – characteristic frequency;  $m_c$  – material constant,  $A_s$  – static displacement.

$$\omega_c = \sqrt{\frac{4G}{\rho r_{pl}^2}}, \quad (15)$$

$$m_c = \sqrt{\frac{2(1-\nu)}{1-2\nu}}, \quad (16)$$

The static displacement is defined as follows:

$$A_s = \frac{F_0}{\pi r_{pl} \lambda + 2G}, \quad (17)$$

in which  $\lambda$  – is the Lamé constant:

$$\lambda = \frac{E\nu}{(1+\nu)(1-2\nu)}. \quad (18)$$

These three methods described above will be compared to the measured vibration amplitude of the shaker on site.

## VIBRATION AMPLITUDES OF THE SOIL SURFACE

In this article only the vertical vibration amplitudes at the surface will be investigated. Barkan [1] suggested to distinguish between the near-field and the far-field.

For the near-field, vertical vibration amplitudes on the surface may be determined by:

$$A_{nf,s} = \frac{F_0 \omega}{v_s G} \cdot \sqrt{f_{1,s}^2 + f_{2,s}^2}, \quad (19)$$

where  $f_{1,s}$  and  $f_{2,s}$  – displacement (compliance) functions for the surface. Barkan [1] advised to use displacement functions solved by Shekhter [13].

For the far-field, an assumption was made that vibrations are caused only by R-waves, giving the following vertical vibration amplitudes:

$$A_{ff,s} = \frac{k_r F_0}{2G} \cdot \frac{k_s^2 \sqrt{k_r^2 - k_p^2}}{\partial g_k / \partial k_r} \sqrt{\frac{2}{\pi k_r r}}, \quad (20)$$

in which  $k_p$ ,  $k_s$  and  $k_r$  are P-, S- and R-wave numbers;  $g_k$  – function of wave numbers:

$$g_k = (2k_r^2 - k_s^2)^2 - 4k_r \sqrt{k_r^2 - k_p^2} \sqrt{k_r^2 - k_s^2}. \quad (21)$$

The distance, where  $A_{nf,s} = A_{ff,s}$  is the end of the near-field and beginning of the far field.

Another method to predict vibration amplitudes on the soil surface was suggested by Bornitz [14]:

$$\hat{u}_1 = \hat{u}_0 \left( \frac{r_0}{r_1} \right)^n e^{-\alpha(r_1 - r_0)}, \quad (22)$$

where  $\hat{u}_0$  is the amplitude of vibration at distance  $r_0$  from the source,  $\hat{u}_1$  is the amplitude of vibration at distance  $r_1$  from the source,  $n$  is the geometrical damping factor,  $\alpha$  is the material absorption coefficient. The benefit of the Bornitz's equation is limited, because the vibration amplitude  $\hat{u}_0$  at the distance  $r_0$  should be known a priori. However, the second part (i.e. exponential part) of the equation represents the material damping law which will be used together with Eq. 19 and Eq. 20. In this way the material damping will be considered. Based on Coelho [15] a material damping will be used for peat of  $D = 1\%$ .

Furthermore by assuming that, 1) most of the vibrations on the soil surface are caused by R-waves [16], [17], and 2) damping is frequency independent,

the material absorption coefficient can be determined by:

$$\alpha = \omega D / v_r. \quad (23)$$

The field test was performed with frequency  $f = 24$  Hz, therefore, the absorption coefficient here is  $\alpha = 0.09 \text{ m}^{-1}$ .

The Barkan-Bornitz equation will be used to predict the vibration amplitudes on the soil surface in the vicinity of the shaker.

## NUMERICAL SIMULATION

The field test was modeled with the Finite Elements Method (FEM). Plaxis 2D software was used. A 2-dimensional, axial symmetric model was built. The used geometry and mesh of the model can be seen in Fig. 4. The modelled area is 30 m in both length and depth. Measurement points for displacement recording were placed from radius  $r = 1.2$  m to  $r = 6.2$  m (reflecting positions of the geophones on the site). The soil is modelled with 15-node triangle elements.

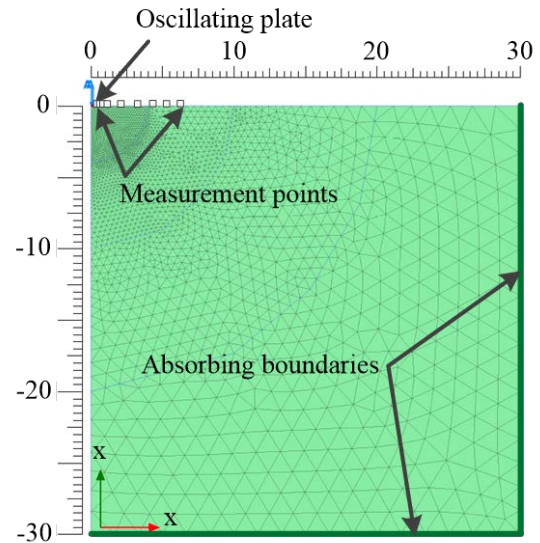


Fig. 4 FEM model: geometry and mesh

Elasticity properties defined from the P- and S-wave velocity measurements were used for the calculations. The shaker was defined as a plate element with axial stiffness  $EA = 21 \text{ GN/m}$ , bending stiffness  $EI = 17.5 \text{ MN/m}$  and weight  $w = 21.94 \text{ kN/m/m}$ . The selected weight corresponds to the total vibrating mass  $m_{tot}$ .

The general force-displacement matrix in Plaxis 2D is based on the following equation:

$$[M]\{\ddot{u}\} + [C]\{\dot{u}\} + [K]\{u\} = \{F\}, \quad (24)$$

where  $[M]$ ,  $[C]$  and  $[K]$  are mass, damping and stiffness matrices respectively,  $\{u\}$  is the displacement vector (with the first and second derivatives) and  $\{F\}$  is the force vector.

In Plaxis 2D, the Rayleigh damping is used, where  $[C]$  is a function of the mass and stiffness, defined by:

$$[C] = \alpha_R [M] + \beta_R [K], \quad (25)$$

in which  $\alpha_R$  and  $\beta_R$  determines the influence of mass and stiffness respectively.

The relationship between the Rayleigh damping coefficients and the damping ratio is:

$$\alpha_R + \beta_R \omega^2 = 2\omega D. \quad (26)$$

Solving Eq. 26 for two target frequencies and two target damping ratios yields:

$$\alpha_R = 2\omega_1\omega_2 \frac{\omega_1 D_2 - \omega_2 D_1}{\omega_1^2 - \omega_2^2}, \quad (27)$$

$$\beta_R = 2 \frac{\omega_1 D_1 - \omega_2 D_2}{\omega_1^2 - \omega_2^2}. \quad (28)$$

Nevertheless, in this simulation there is only one frequency  $\omega = \omega_1 = \omega_2$  and one damping ratio  $D = D_1 = D_2$ , therefore Eq. 27 and Eq. 28 can be simplified and the coefficients can be defined by:

$$\alpha_R = D\omega, \quad (29)$$

$$\beta_R = D/\omega. \quad (30)$$

In this case, for the vibration frequency  $f = 24$  Hz,  $\alpha_R = 1.508$  and  $\beta_R = 6.63 \cdot 10^{-5}$ .

## PREDICTIONS AND MEASUREMENTS

First of all the measured amplitude of the shaker vibration is compared to the predicted by the analytical methods. Predicted and Measured amplitude ratios (P/M) are calculated in order to evaluate how good the predictions are.

Table 1 shows that independently from the method used for a prediction, the amplitude of the shaker vibration has been predicted with at least 92 % accuracy. The highest P/M ratio is for the Confined Elasticity approach, which can be explained by the fact that horizontal deformations of the soil were neglected. It is also worth to mention that all methods over-predicted the vibration amplitude.

Not only the measured amplitudes of the shaker, but also of the soil surface in the vicinity of the shaker, have been compared with the predictions of

the analytical approach and also the FEM calculations.

Table 1 Comparison between the predicted and the measured shaker vibration amplitudes

Method	Amplitude [ $\mu\text{m}$ ]	P/M ratio [-]
Measured	292	1
Reissner	293	1.00
Lysmer	309	1.06
Confined Elasticity	316	1.08
FEM	302	1.04

The measured and the predicted vibration amplitudes can be found in Fig. 5.

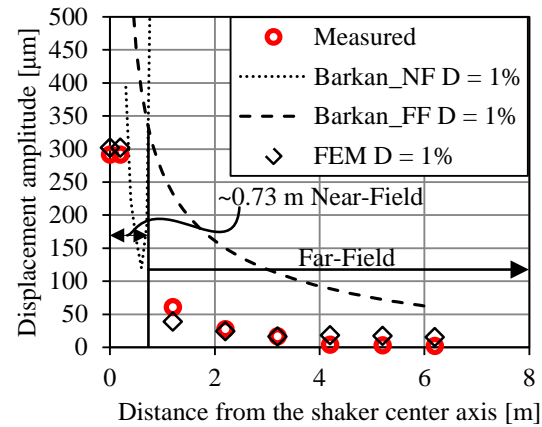


Fig. 5 Vibration amplitudes in the vicinity of the shaker

The P/M ratios between the predicted and the measured surface vibration amplitudes for the far-field can be seen in Table 2.

Table 2 Comparison between the predicted and the measured surface vibration amplitudes

Distance [m]	P/M ratio	
	Barkan-Bornitz Far-Field	FEM
1.2	4.2	0.6
2.2	6.6	0.9
3.2	8.7	1.0
4.2	31.4	4.5
5.2	36.5	5.5
6.2	48.9	7.2

The near-field of Barkan-Bornitz's method ends before the first measurement point (Fig. 5), therefore only P/M values for the far-field are calculated. The analytical approach strongly over-predicts the vertical vibrations, this can be due to the fact that the

method assumes only R-waves in the far-field, which could have led to misjudge of the destructive interference caused by body waves.

The FEM results are much better, but still under-predict the vibration amplitudes for the first 3 meters, and over-predicts further away. The weaker damping just next to the shaker and higher damping than expected further away from the shaker may be explained by the fact, that there is less vibration caused by the Rayleigh waves closer to the shaker and more vibrations caused by the Rayleigh waves further away from the shaker. This implies a different damping per different waves.

## CONCLUSIONS

The shaker vibration amplitudes can be predicted by three analytical approaches: Reissner, Lysmer and the Confined Elasticity approach and by numerical (FEM) calculations. The accuracy depends on the method used for the prediction, and ranges from 92% to 100%. This shows that the amplitude of the shaker can be predicted accurately enough for geotechnical purposes.

The soil surface vibration amplitudes can be predicted by Barkan-Bornitz's analytical approach and by numerical (FEM) calculations. The Barkan-Bornitz's approach over-predicted the amplitudes between 4.2 and 48.9 times. The FEM under-predicted the amplitudes for the first three meters and over-predicted up to 7.2 times for the last three meters. This shows that the amplitudes of the surface cannot be predicted accurately.

This confirms the conclusion made by Hölscher and Waarts [2], that the reliability of man-made vibration prediction methods is disappointingly low. This shows a demand of more research in the man-made vibration field.

## ACKNOWLEDGEMENTS

The authors express their acknowledgments to Mr. KJ Tromp from the village of Uitdam, who allowed using his land to perform the vibration experiments. Also to dr. C Zwanenburg for providing the geological investigations data of the site nearby.

## REFERENCES

[1] Barkan DD, Dynamics of bases and foundations. New York: McGraw-Hill Book Company Inc., 1962, Chapter VIII.  
 [2] Hölscher P and Waarts PH, "Reliability of vibration prediction and reducing measures", Final Report. Delft Cluster, Delft, 2003.

[3] Zwanenburg C, "De bepaling van sterkte-eigenschappen van veen", Geotechniek, Vol. Juli, 2013, pp. 26-32.  
 [4] Lamb H, "On the propagation of tremors over the surface of an elastic solid, Phil. Trans. Royal Soc.", series A., Vol. 203, 1904, pp. 1-42.  
 [5] Reissner E, "Stationäre axialsymmetrische durch eine schütternde Masse erregte Schwingungen eines homogenen elastischen Halbraumes", Ingenieur Archiv, Vol 22, Dec. 1936, pp. 381-396.  
 [6] Bycroft GN, "Soil-Structure Interaction at High Frequency Factors", Int. J. of Earthquake Engineering and Structural Dynamics, Vol. 5, 1977 pp. 235-248.  
 [7] Kruijtz G, The vertical motion of foundations and pontoons, Delft: VSSD, Reprinted 2006, Appendix 1.1.  
 [8] Hsieh TK, "Foundation Vibrations", in Proc. Of inst. Of Civil Engineers, Vol. 22, 1962, pp. 211-226.  
 [9] Lysmer J and Richard FE, "Dynamic response of footings to vertical loading", J. of Soil Mechanics and Foundations Division, ASCE, Vol. 92 No. SM1, January 1966, pp. 65-91.  
 [10] Verruijt A, Soil Dynamics. Delft, 2006.  
 [11] Westergaard HM, "A problem of elasticity suggested by a problem in soil mechanics: soft material reinforced by numerous strong horizontal sheets", Contributions to the Mechanics of Solids, Stephen Timoshenko 60<sup>th</sup> Anniversary Volume. New York: Macmillan, 1938.  
 [12] Barends FBJ, "Dynamics of elastic plates on a flexible subsoil", LGM-Mededelingen, Vol 21, 1980, pp. 127-134.  
 [13] Shekhter OY, "Consideration of Inertial Properties of Soil in the Computations of Vertical Forced Vibrations of Massive Foundations" NII, Symposium 12, Vibratsii Osnovaniy y Fundamentov, Moscow, 1948.  
 [14] Bornitz G, Über die Ausbreitung der von Großkolbenmaschinen erzeugten Bodenschwingungen in die Tiefe. Berlin: Springer, 1931.  
 [15] Coelho BEZ, Dynamics of railway transition zones in soft soils, PhD Thesis, TU Delft, 2010.  
 [16] Miller GF and Pursey H, "On the Partition of Energy between Elastic Waves in a Semi-Infinite Solid", Proc. Of the Royal Society of London, Series A, Mathematical and Physical Sciences, Vol 233, No. 1192, 1955, pp. 55-69.  
 [17] Macijauskas D and Van Baars S, "Decomposition of measured ground vibrations into basic soil waves", in Proc. of the 3rd Int. Symposium on Computational Geomechanics (ComGeo III), Krakow, Poland, 21-23 August, 2013.

## SUBGRADE SUPPORT: A REVIEW OF SHORT-TERM AND LONG-TERM PERFORMANCE REQUIREMENTS

Andreas Nataatmadja

Faculty of Health, Engineering and Sciences, University of Southern Queensland, Australia

### ABSTRACT

Subgrade performance is a function of a soil's strength and its behaviour under traffic loading. The subgrade should be stable to prevent excessive rutting and shoving during construction, provide good support for placement and compaction of pavement layers, keep pavement rebound deflections to acceptable limits, restrict the development of excessive rutting during the service life of the pavement and minimise effect of changes in moisture level.

In the case of weak subgrades, a capping layer of some thickness may be placed on top of the subgrade to facilitate field construction. This paper demonstrates that a semi-infinite effective subgrade stiffness can in fact be calculated for a combination of a capping layer and a semi-infinite subgrade. Furthermore, this paper discusses the importance of thickness and quality of capping layer, for both short- and long-term loading conditions. The recommended capping thicknesses have been benchmarked against the UK and US requirements.

*Keywords: Pavement, Subgrade, Capping Layer, Modulus, Elastic Analysis*

### INTRODUCTION

During construction, traffic is relatively low and is not as channelised as normal service life traffic. Nevertheless, because the traffic-generated subgrade stresses are relatively high during construction, a suitable capping material of an appropriate thickness may be placed on top of the natural subgrade to provide a stable foundation upon which pavement layers can be compacted. The capping layer (or working platform) itself may consist of several materials/layers. In this case, the effective (i.e. combined) strength of the subgrade and its capping layer can be used for the design of flexible pavements.

In the United Kingdom, for many years pavement foundations had been designed and constructed using established empirical relationships and a recipe specification [1]. The capping thicknesses vary from 0 mm to 600 mm (Fig. 1). However, irrespective of the thickness, the procedure assumes that all foundations achieve a similar minimum level of performance, and hence, are treated equally. A draft interim replacement specification offering 4 foundation types [2] is currently available but will not be discussed in this paper due to some technical differences [3].

Figure 1 was based on the assumption that a capping layer with as-compacted CBR value greater than 15 would provide an adequate platform for construction of the subbase when compacted to the appropriate thickness.

The capping thickness from Figure 1 was used in the UK to limit the permanent deformation caused by construction traffic to a maximum of 40 mm for

1,000 passes of a standard axle (single axle load of 80 kN). Note that this requirement is different from that of the Illinois Department of Transportation (IDOT) Subgrade Stability Manual [4], which specifies, through an analytical study, that the finished subgrade must have a minimum as-compacted CBR of 6% if untreated, or 10% if treated, and a maximum rut depth of 13.0 mm under construction traffic.

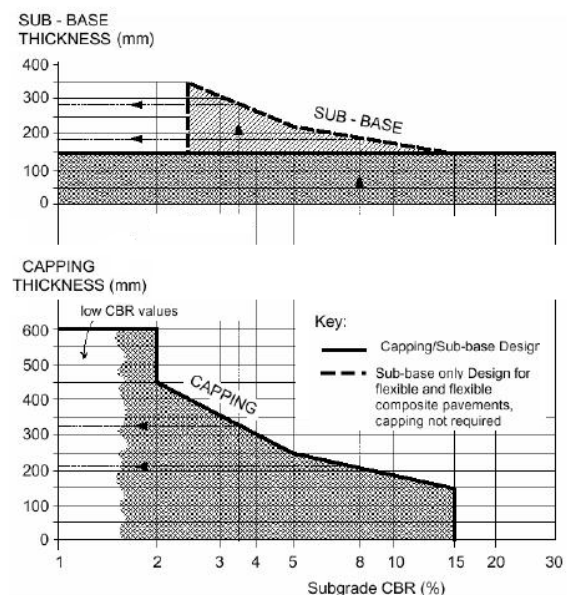


Fig. 1 Example of capping thickness requirement in the UK [1].

Figure 2 shows the IDOT's minimum capping thicknesses on top of subgrades of varying CBR

values. It is seen that despite the differences in their performance criteria, both the UK and IDOT methods yield similar thickness requirements. In the following sections, the choice of CBR and thickness for the design of a capping layer and the associated construction issues will be reviewed and discussed.

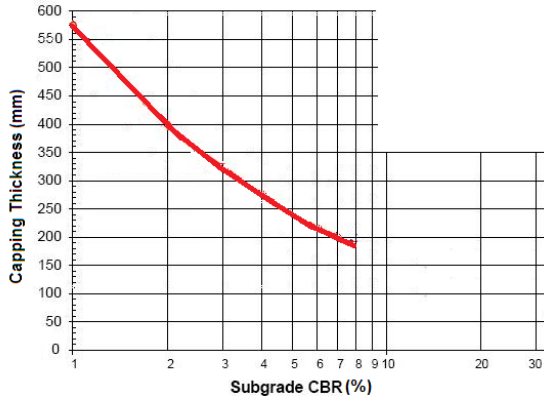


Fig. 2 IDOT's capping thickness requirements [5].

## STRUCTURAL CONTRIBUTION OF CAPPING LAYER

Clearly, given an appropriate thickness, the existence of a capping layer with a stiffness higher than that of the in situ subgrade would increase the effective stiffness of the subgrade. However, this effective stiffness cannot be assumed to be equal to the stiffness of the capping layer unless the capping layer is of a significant thickness.

A recent study [6] demonstrated that when two or more elastic layers are placed one on top of another, such as a capping layer on top of a subgrade, the layers will work together in such a way that they can be represented by an equivalent layer with an effective or combined modulus ( $E_e$ ) based on the work of Odemark [7]:

$$E_e = f \times \left[ \frac{\sum_{i=1}^n h_i E_i^{1/3}}{\sum_{i=1}^n h_i} \right]^3 \quad (1)$$

where  $E_i$  = modulus of layer  $i$  (MPa)

$h_i$  = thickness of layer  $i$  (m)

$f$  = correction factor

This equation is known as the Japan Equation in the Austroads Guide Part 2 [8], where  $CBR_i$  replaces  $E_i$ , with  $f=1$  and  $\sum h_i = 1$  metre. The Japan Equation [9] implicitly assumes the following condition:

- All layers are isotropic and have the same Poisson's ratio;

- Both the original structure and the transformed structure have the same stress & strain distribution ( $f=1$ ); and
- The existence of a semi-infinite subgrade thickness is ignored, i.e. only 1 metre total depth is considered (Fig. 3). In other words, the effect of applied stress is assumed to be negligible below this depth. This is an assumption that may be acceptable for designing concrete pavements but is erroneous in the case of flexible pavements.

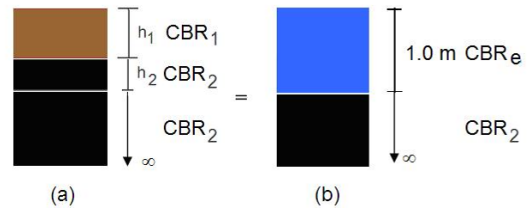


Fig. 3 Application of subgrade equivalency based on the Japan Equation [6].

Figure 4 shows the required capping thickness according to the Japan Equation to achieve an effective CBR of 6% for original subgrade CBR values of 1% to 6%. The capping materials shown in this figure have CBR between 8% and 15%. It is seen that for an original subgrade CBR of 2%, 750 mm thick capping layer of CBR 8% would be needed to produce an effective semi-infinite CBR of 6%. It will be shown later in this paper that such a thickness is insufficient if material anisotropy is considered.

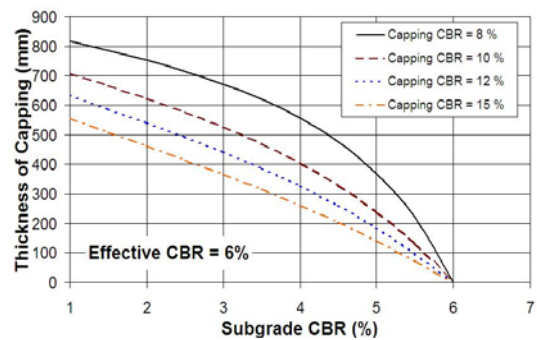


Fig. 4 Thickness of capping layer from the Japan Equation to obtain an effective semi-infinite CBR of 6% [6].

## ODEMARK'S METHOD WITH CORRECTION FACTOR

It has been shown above and also in [6] that the Japan equation (Eq. 1 above with  $f=1$  or Eq. 25 of



[8]) has a number of limitations. Therefore, the equation should not be used in the design of flexible pavements.

Attempts have been made to find a correction factor for the Odemark equation based on the method of equivalent surface deflection [6], [10].

The method of equivalent surface deflection is based on the premise that if a correct thickness of a capping layer of a certain CBR value is used over a subgrade with a certain CBR value, the two layer system can represent a semi-infinite subgrade with a single design (effective) CBR [10].

In accordance with the current Austroads mechanistic pavement design procedure, the previous study [6] assumed both capping layer and subgrade soil were cross-anisotropic with  $E_V/E_H = 2$ . The Poisson's ratio was assumed 0.45 for both the capping and subgrade layers. Sublayering of the capping was also done according to [8].

As reported earlier [6], the load chosen for the analytical work was a half-axle configuration with 550 kPa tyre pressure rather than 750 kPa since it is considered that the lower pressure would be more appropriate to represent the stress regime at the subgrade level. CIRCLY analyses were carried out to find the thickness of capping layer that can convert a subgrade with lower CBR values to an equivalent half-space CBR of various values for the same magnitude of surface deflection (i.e. method of equivalent deflection) under the centre of a dual wheel assembly.

The authors of [6] observed that the  $f$  values in Eq. (1) are variable, which support the results of [11]. When the ratios between effective CBR over original subgrade CBR are plotted against the  $f$  values, it becomes clear that  $f$  varies with the ratio between effective CBR to the original, semi-infinite, subgrade CBR. The following equation was suggested for finding the correction factor  $f$  for a capping thickness of up to 1.0 m (i.e. practical limit) and capping CBR values of up to 15%:

$$f = 1.5251 - 0.5251 \times \left[ \frac{CBR_e}{CBR_s} \right] \quad (2)$$

where  $CBR_e$  is the effective CBR and  $CBR_s$  is the original subgrade CBR.

Equation 1 can be rearranged to produce an equation that can be used to obtain the thickness ( $h_c$ ) and CBR value ( $CBR_c$ ) of a capping layer ( $h_c < 1.0$  m and  $CBR_c \leq 15\%$ ) for a nominated  $CBR_e$  value of the capping layer and subgrade ( $CBR_e < CBR_c$ ):

$$h_c = \frac{\left( \frac{CBR_e}{f} \right)^{1/3} - CBR_s^{1/3}}{CBR_c^{1/3} - CBR_s^{1/3}} \quad (3)$$

Using Eqs. (2) & (3), Figs. 5 and 6 were plotted to show the variation of capping thickness with the original subgrade CBR to achieve an effective CBR of 3% and 5%, respectively, for a maximum capping layer thickness of 1 m [6].

From Figs. 5 & 6 it can be seen that, theoretically, the effective (combined) CBR of the capping and subgrade materials will never be equal to the CBR of the capping layer unless a capping layer of infinite thickness is used.

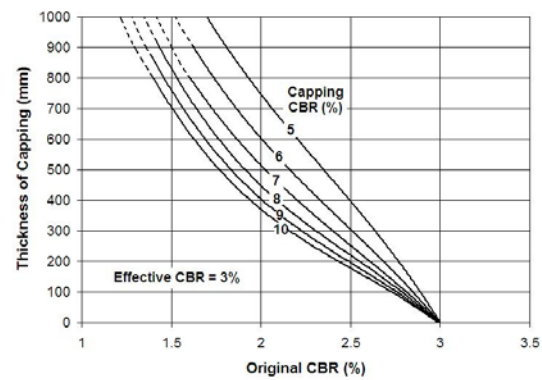


Fig. 5 Capping thicknesses to obtain an effective CBR of 3% [6].

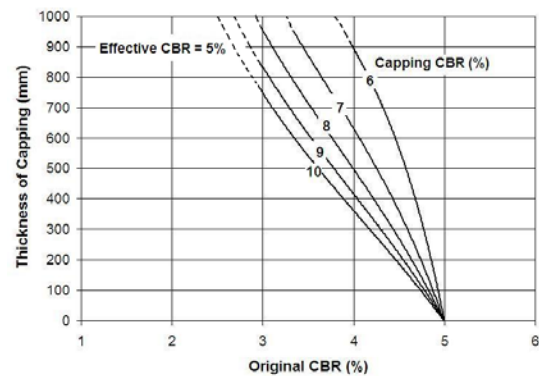


Fig. 6 Capping thicknesses to obtain an effective CBR of 5% [6].

## SHORT-TERM PERFORMANCE CRITERIA

During compaction, a maximum Benkelman beam deflection of 1.2 mm to 1.3 mm is often prescribed at the top of the subgrade layer to enable proper placement of the overlying layers. It can be shown analytically that this criterion corresponds with a minimum in situ CBR of 6% (see also Fig. 7).

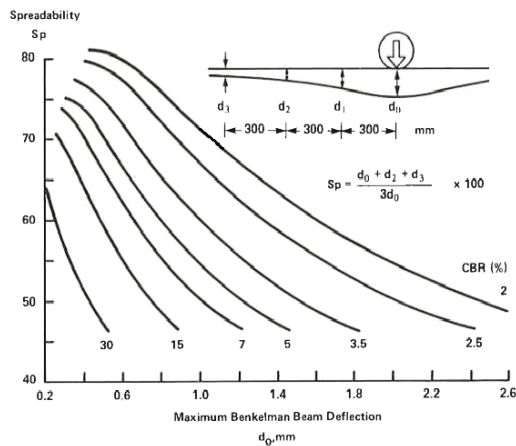


Fig. 7 CBR prediction based on Benkelman beam results [12].

To improve a subgrade in situ CBR say, from 4% to 6%, a capping layer may be used. If this capping material is compacted at the correct moisture content, an as-compacted capping CBR  $\geq 15\%$  would normally be achievable. With this in mind, a 500 mm of this material may be adequate to produce an effective CBR of 6% according to Eq. (3). However, if the capping material is compacted wet of optimum or subjected to an adverse moisture regime, the as-compacted CBR could drop to a lower value (Fig. 8) such that a thicker capping layer would be required. For example, if the as-compacted capping CBR drops to 10% due to unintentional wetting, a 750 mm capping layer would be required to improve the original subgrade.

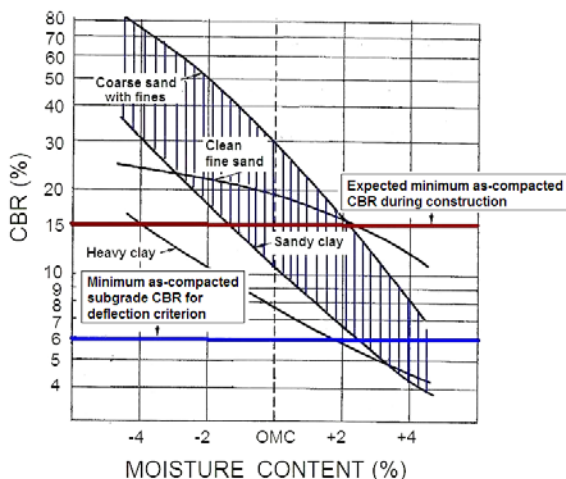


Fig. 8 Example of CBR variation due to moisture variation [13].

It should be noted that while the use of a capping thickness of suitable thickness will strengthen the

original subgrade, there is a possibility that the capping layer itself may not be strong enough to withstand construction traffic if the as-compacted CBR is less than 15%. Often it has to be either partially or fully replaced with a more suitable material or chemically modified during the construction.

Previous investigators [4] suggested that during compaction of a subgrade layer, the maximum deviator stress should be less than 75% of the subgrade's unconfined compressive strength. High subgrade deviator stresses ( $\sigma_{DEV}$ ) and Subgrade Stress Ratios ( $SSR = \sigma_{DEV}/Q_u$  where  $Q_u$  is the unconfined compressive strength) indicate high “subgrade rutting potentials” under the wheel load of construction vehicles or construction equipment (the same principle applies to the compaction of a capping layer if it the as-compacted CBR is less than 15%).

Construction vehicles typically have tyre pressure of about 500 kPa but compaction equipment may apply a much higher pressure in the order of 1,000 kPa [14]. To protect the subgrade from failure due to these applied tyre pressure, a sufficiently thick capping layer (as-compacted CBR  $\geq 15\%$ ) may be initially placed so that under the full loading of construction vehicles and construction equipment the subgrade is not overstressed.

This particular criterion, although most critical during compaction, is rarely considered by pavement designers as it is often assumed to be a part of the earthwork construction and layout. However, if this requirement is not satisfied, subgrade failure may occur during construction such that it would be difficult, if not impossible, to construct the next pavement layer.

As suggested by [15], it was assumed that the subgrade CBR =  $0.09 s_u$  (kPa), where  $s_u$  = undrained shear strength of the subgrade. Calculations were then performed with a tyre pressure of 750 kPa to find the minimum thickness of capping layer in order to protect the subgrade from failure using a multilayer isotropic elastic computer program CHEVRON (assuming capping layer CBR of 15%).

Figure 9 shows the calculated capping thicknesses compared with the UK requirement [1]. For subgrade CBR < 6%, the calculated capping thicknesses are lower than those of the UK requirement [1] since anisotropy was not considered. Overall, this figure suggests that a capping layer should always be placed on top a subgrade with an in situ CBR < 15%, and that a minimum capping thickness of 200 mm may be used on top of a

subgrade with an in situ CBR > 8%.

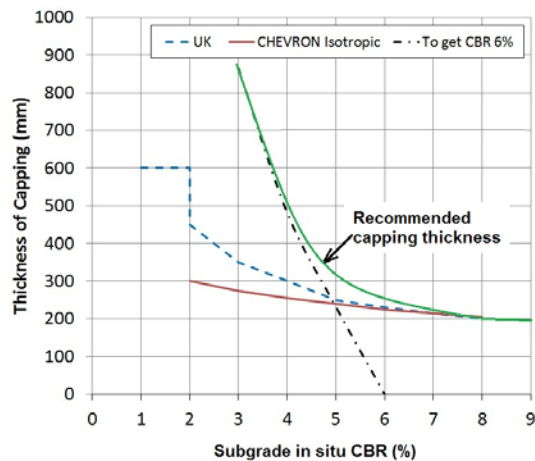


Fig. 9 Comparison of capping thicknesses.

Figure 9 also shows that there is a significant difference between the minimum capping thickness for subgrade protection (initial compaction criterion, failure stress criterion) and that for satisfying the deflection test (final compaction criterion, deflection criterion). The recommended capping thickness to satisfy both criteria is therefore shown. Considering the required thickness, in practice it may be difficult to satisfy the deflection criterion if the in situ subgrade CBR is less than 3%, unless a much stiffer capping layer or subgrade stabilisation is used (for which additional multilayer elastic analyses will be required).

### LONG-TERM PERFORMANCE CRITERIA

The choice of capping material is not only dictated by pavement construction and pavement design requirements. During construction, the as-compacted CBR is important; however, for pavement design a soaked CBR is often used. In the latter, if a capping material with a soaked CBR of 5% is chosen, there may be a risk that the long-term performance of the pavement could be compromised due to the possibility that the subbase layer may be weakened through undesirable interactions (Case 1, 2 and 3) between the two layers (Fig. 10). Note that Case 3 is not desirable but may have been accounted for if the subbase is assumed to be soaked during design.

Reference [16] presented Fig. 11, which shows the assumed aggregate thickness loss as a function of subgrade strength. From this figure, it may appear that the subbase layer is less likely to experience aggregate loss as long as the capping material has a minimum soaked CBR of 3%. However, it is possible that the capping material should have a minimum soaked CBR higher than 3% to completely eliminate the possibility of aggregate loss.

With regards to the possibility of mixing between a subgrade material and its overlying aggregate layer, Ref. [17] divides subgrade materials into four categories based on their CBR values (Table 1). Based on this, it appears that capping materials should have a minimum soaked CBR of 7%.

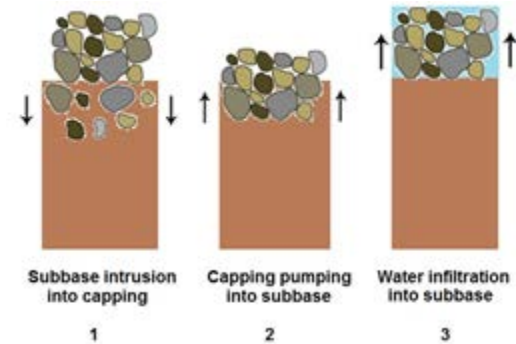


Fig. 10 Undesirable interaction between capping and subbase layers.

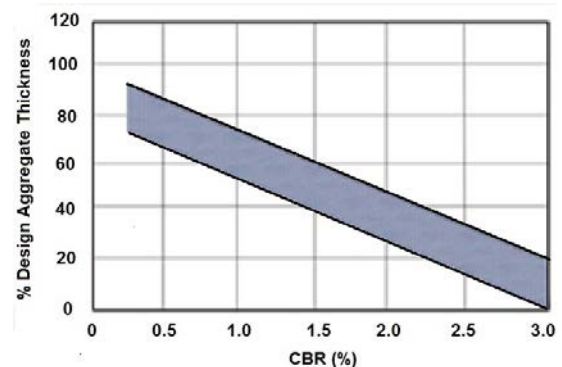


Fig. 11 Loss of aggregate vs. subgrade CBR [16].

Table 1 Subgrade quality in relation to the possibility of interlayer mixing [17].

Subgrade CBR (%)	Quality
< 3	This material is extremely poor quality. Substantial mixing will take place between the subgrade and the fill material.
3 - 7	Subgrade is generally acceptable for use in paved roads, but is of poor enough quality to allow mixing between the layers.
7 - 15	Subgrade consists of fairly good quality material which is unlikely to mix with the overlying material. Fines may however be carried with any excess pore water into the layer above thereby reducing the quality of the upper layer.
> 15	Subgrade is of good quality material.

It is interesting to note that Ref. [18] suggested

that geotextile separator be used for subgrade with  $\text{CBR} < 3$  and for subgrade CBR between 3% and 6.5%, the use of a geotextile separator is recommended. Therefore, without using a separator the soaked CBR of a capping layer should be  $\geq 7\%$ .

## CONCLUSION

This paper has reviewed and discussed the issue of calculating effective semi-infinite subgrade modulus for the combination of a capping layer and a semi-infinite subgrade. Some empirical methods for finding the effective semi-infinite subgrade CBR are presented and their validity examined.

It has been shown that the required thickness of capping layer is a function of its CBR and the subgrade in situ CBR. Recommendations have therefore been presented as to the choice of minimum capping layer stiffness and thickness, based on a minimum as-compacted CBR value of 15% at the time of compaction, in order to minimise the subgrade stress and deformation under construction traffic. The need to satisfy the Benkelman beam test criterion has also been outlined together with some related construction issues.

In addition, the need to keep soaked CBR value  $\geq 7\%$  for the capping layer has been discussed, to avoid the intrusion of the subbase material into the capping layer or the pumping of capping material into the subbase layer.

## REFERENCES

- [1] Highways Agency, "Design manual for roads and bridges", Pavement Design and Maintenance, Foundations, DMRB 7.2.2, HD25/94, HMSO, London, UK, 1994.
- [2] Highways Agency, "Design guidance for road pavement foundations (Draft HD25)", Interim Advice Note 73/06 (W) Revision 1, UK, 2009.
- [3] Brown, SF and Thom, NH, "Recent developments in pavement foundation design", Proceedings of the 18<sup>th</sup> International Conference on Soil Mechanics and Geotechnical Engineering, Paris, 2013.
- [4] IDOT, "Subgrade stability manual", Illinois Department of Transportation, Bureau of Bridges and Structures, Illinois, USA, 2005.
- [5] Tutumluer, E, Debakanta M and Abbas AB, "Characterization of Illinois aggregates for subgrade replacement and subbase", Report FHWA-ICT-09-060, Illinois Center for Transportation, Department of Civil and Environmental Engineering, University of Illinois at Urbana-Champaign, Urbana, IL 61801, USA, 2009.
- [6] Nataatmadja, A, Tao, SY and Chim, K, "Design subgrade CBR for flexible pavements: Comparison of predictive methods", Proceeding 25th ARRB Conference, Perth, WA, Australia, 2002.
- [7] Ullidtz, P, "Pavement analysis, development in civil engineering", Vol.19, Elsevier, Amsterdam, The Netherlands, 1987.
- [8] Austroads "Guide to pavement technology part 2: Pavement structural design", Sydney, NSW, Australia, 2012.
- [9] Japan Road Association, "Manual for asphalt pavement", Japan Road Association, Tokyo, Japan, 1989.
- [10] Reddy, MA, Reddy, KS and Pandey, BB, "Design CBR of subgrade for flexible pavements", IRC Highway Research Bulletin, India, 2001, p. 64.
- [11] El-Badawy, M and Kamel, MA, "Assessment of improvement of the accuracy of the Odemark transformation method", Int. Journal of Advanced Engineering Sciences and Technologies, 5 (2), 2011.
- [12] Lay, MG, "Handbook of road technology", Vol. 1, Gordon and Breach Science Publishers, New York, USA, 1990.
- [13] Road Research Laboratory, "Soil mechanics for road engineers", Department of Scientific and Industrial Research, Road Research Laboratory, HMSO, London, UK, 1952.
- [14] Garcia, G and Thompson, MR, "Working platform requirements for pavement construction", A White Paper Prepared for the Technical Review Panel, Project IHR-R30, Upgrade subgrade stability manual, Illinois Cooperative Highway and Transportation Research Program, USA, 2003.
- [15] Black, WPM, "The calculation of laboratory and in-situ values of California bearing capacity data", Geotech., 11, 1961, pp. 14- 21.
- [16] FHWA, "Task force 25 report", Department of Transportation, Federal Highway Administration, USA, 1990.
- [17] TRH, "Structural design of interurban and rural road pavements", Pretoria, South Africa, 1995.
- [18] California DOT, "Subgrade enhancement geosynthetic design and construction guide", California Dept. of Transport, USA, 2013.

## EVALUATION OF RE-LIQUEFACTION BEHAVIOR OF SEGREGATED AND UNIFORM SPECIMENS IN HOLLOW CYLINDRICAL TORSIONAL SHEAR TESTS

Usama Juniansyah Fauzi<sup>1</sup> and Junichi Koseki<sup>2</sup>

<sup>1</sup>Graduate Student, School of Engineering, The University of Tokyo, Japan

<sup>2</sup>Professor, Institute of Industrial Science, The University of Tokyo, Japan

### ABSTRACT

During the March 2011 Great East Japan Earthquake Disaster, there were a lot of evidences that sand deposits can liquefy repeatedly (or “re-liquefaction”) at the same sites after initial liquefaction during previous earthquake shaking. Unlike most prior studies, uniform and segregated specimens were used in this study. Uniform specimens were reconstituted by moist tamping and segregated specimens were reconstituted by depositing sand particles in three layers through water sedimentation. The latter specimen preparation was used to model a deposit of reclaimed land constructed by dredging and pumping method. In order to study re-liquefaction resistance and to examine the effect of segregated layer, undrained cyclic loadings were conducted on uniform specimens and segregated specimens of the same materials using hollow cylindrical torsional shear apparatus with the cyclic shear stress ratio, CSR, of 0.10, 0.12, 0.15, and 0.20 while maintaining the specimen height constant. In addition, the local deformations of specimens were observed by using a special image analysis technique.

*Keywords: Re-liquefaction, Segregation, Water Sedimentation, Katori sand, and Hollow Cylindrical Torsional Shear*

### INTRODUCTION

Liquefaction has been studied extensively since its first comprehensive observation of damage due to liquefaction during 1964 Niigata and 1964 Alaska Earthquakes, and fundamental advances have been made in understanding this phenomenon. The series of laboratory tests, model tests, field observation, and numerical modeling have led to a series of practical procedures for evaluating liquefaction resistance and estimating its effects [1]. During an earthquake shaking, excess pore water pressure is developed in saturated sandy soil leading to loss of strength and stiffness. The excess pore water pressure then starts to dissipate, generally through ground surface. The densification or reconsolidation accompanied by volume change occurred which is manifested by ground settlement [2-3].

Many studies have concluded that liquefaction resistance may increase with the increase of relative density such as reported in triaxial apparatus [4] and ground improvement projects [5]. However, there are a lot of evidences that liquefaction can take place repeatedly in natural deposits and reclaimed land. In 1983, Akita prefecture suffered serious damaged by overall liquefaction of alluvial sand due to 1983 Nihonkai-Chubu Earthquake ( $M_w$  7.7). One month later, an aftershock with lower magnitude ( $M_w$  7.1) hit the area and caused similar damage by liquefaction [6]. Reference [7] reported that during

the March 2011 Great East Japan Earthquake Disaster ( $M_w$  9.0), re-liquefaction was observed at a total of 62 sites in the Kanto region (35 sites are reclaimed land), where past liquefaction occurred during the 1987 Chibaken Toho-oki Earthquake ( $M_w$  6.7). Re-liquefaction was also reported during September 2010 ( $M_w$  7.1), February 2011 ( $M_w$  6.2) and June 2011 ( $M_w$  6.2) Canterbury Earthquakes [8]. It was found that sand deposits which had been liquefied, might be re-liquefied by a future earthquake even though with smaller amplitude than the previous one. In other words, the liquefaction resistance can decrease after first liquefaction.

Reference [9] is the first researcher who observed the re-liquefaction phenomenon in laboratory tests. It was found that liquefaction resistance decreases if it has been sheared beyond a threshold value. However, a different result was found using a large shaking table. Liquefaction resistance increased after first liquefaction even though no significant change in the relative density [10]. Later, it was found that mechanical behavior of sand relies sensitively on pre-strain or stress history. Reference [11] indicated that the residual strain is a main factor to control the liquefaction resistance in a subsequent re-liquefaction test. The small pre-shearing will result in hardening effect by which liquefaction resistance increase while large pre-shearing will cause opposite result. Further investigation revealed that re-liquefaction behaviors



are influenced by the effects of uniformity of void distribution, inherent anisotropy, induced anisotropy, and loading direction [12].

One limitation of previous re-liquefaction studies is the number of liquefaction stages. The number of re-liquefaction stages that can be performed was usually limited to two stages. In 2010, Reference [13] conducted liquefaction tests up to five stages using triaxial apparatus. It was found that the relationship of anisotropy induced in post-liquefaction and effects of different loading directions are not simple enough to be simulated by triaxial apparatus. One year later, liquefaction tests up to five stages were conducted by shaking table tests [14]. The results found that re-liquefaction resistance is not correlated with relative density or void ratio but the coefficient of consolidation,  $c_v$ , or proxy values such as  $D_{10}^2 D_r^{2.8}$  or  $D_{10}/C_u$ .

Recently, the University of Tokyo has develop a new laboratory apparatus to study re-liquefaction behavior called multi stacked-ring shear apparatus. The results show the pre-shearing history of soil is a major parameter that influences the re-liquefaction resistance [15]. However, this apparatus has a limitation. Its rigid metal rings boundary mobilizes friction in both vertical and circumferential directions which can affect the behavior during re-liquefaction tests. In this paper, undrained cyclic tests using hollow cylindrical torsional shear apparatus are conducted. Unlike the tests conducted in multi stacked-ring shear apparatus, the hollow cylindrical torsional shear apparatus uses latex membrane.

Furthermore, urban development has speared into unsuitable ground condition which, for instance, has loose sandy soil with high ground water table; hence liquefaction potential is high as well. Since reclamation became popular, areas of reclaimed land are prone to liquefaction. Most prior liquefaction studies have focused their efforts to establish a standard method of specimen preparation by which homogenous specimens can be formed in order to obtain reliable and repeatable results. However, reclaimed lands constructed by dredging and pumping method are not uniform due to different sedimentation velocities of soil particles in water. In this paper, segregated specimen and uniform specimen were used. Segregated specimen was used as a model of reclaimed land.

## HOLLOW CYLINDRICAL TORSIONAL SHEAR APPARATUS

A hollow cylindrical torsional shear apparatus as shown schematically in Fig. 1 was employed to conduct undrained cyclic loading. A two-component load cell having capacities of 15 kN and 0.3 kN.m respectively, was used to measure both the vertical load and the torque components. The confining

pressure was measured by a high-capacity differential pressure transducer (HCDPT) with a capacity of over 600 kPa. A LVDT (linear variable displacement transducer) was equipped to measure vertical displacement. Two potentiometers having diameter of 3.5 cm (main) and 5.0 cm, respectively were attached to the loading shaft and the top cap perimeter to measure the large shear strain. The measured vertical and shear stress were corrected for the effects of the membrane force [16].

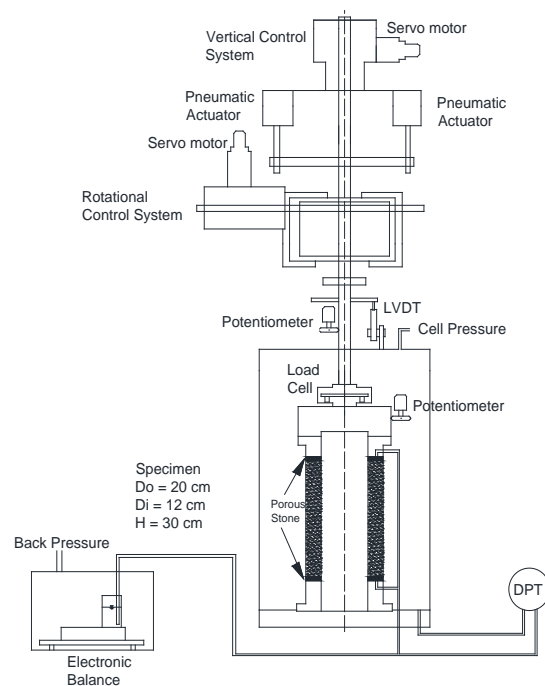


Fig. 1 Torsional shear test apparatus on hollow cylindrical specimen scheme.

## MATERIAL, SPECIMEN PREPARATION, AND TEST PROCEDURE

### Test Material

Katori sand passing through 4.75 mm sieve was used as test material. Its particles properties have mean grain size ( $D_{50}$ ) = 0.16 mm, coefficient of uniformity ( $C_u$ ) = 1.81, coefficient of gradation ( $C_c$ ) = 0.97,  $G_s$  = 2.65, maximum void ratio = 1.35, minimum void ratio = 0.92, and fines content of about 5% [17].

### Specimen Preparation

Details of this specimen preparation can be found in [17], but a brief description is made here. An acrylic pipe with length of 100 cm was used to elongate the height of mold for specimen preparation with water sedimentation (WS). A mixture of soil and water at a mass ratio of 1:2 was poured into the acrylic pipe using a funnel. The specimen consists of three sand layers and two silt layers. In addition, the



moist tamping (MT) method was used to reconstitute uniform specimen with fines content,  $fc$ , about 5% (Fig. 2)

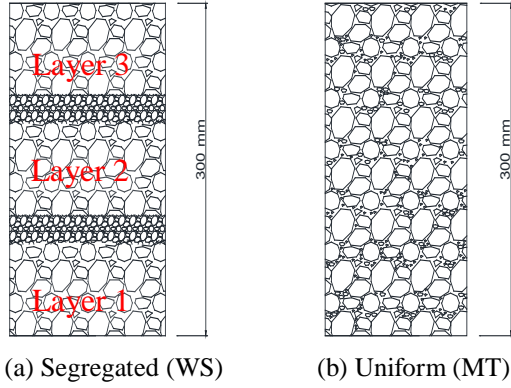


Fig. 2 Illustration of segregated and uniform sand specimens.

### Test Procedure

Re-liquefaction tests were conducted on hollow cylindrical specimens having initial height of 30 cm, inner and outer diameters of 12 cm and 20 cm, respectively. Prior to application of cyclic load, specimens were prepared at  $D_r = 18-22\%$ . Double vacuum method [18] was used during the saturation process due to large specimen size. *Skempton's B-values* could be achieved to be greater than 0.96 in all the specimens. After completion of saturation, the specimens were consolidated isotropically to effective stress,  $\sigma'_c = 100$  kPa ( $Dr_c = 26.7-27.9\%$ ). The first stage of liquefaction test was conducted after applying a drained creep loading for 15 min or even longer. The undrained cyclic loadings were applied with constant shear strain rate of 1%/min with single amplitude shear stress of 10 kPa, 12 kPa, 15 kPa, and 20 kPa (i.e., the cyclic shear stress ratio, CSR, of 0.10, 0.12, 0.15, and 0.20) while maintaining the specimen height constant. The first loading direction was on clockwise direction which will be hereafter defined to be positive. The specimens were considered to have been liquefied when the double amplitude of shear strain,  $\gamma_{DA}$ , reached 15%. At the end of liquefaction test, the global shear strain ( $\gamma_G$ ) was resumed to be zero while maintaining the undrained condition. The next stages of liquefaction were started by opening the drainage valve and re-consolidating the liquefied specimen into the same initial effective stress,  $\sigma'_c = 100$  kPa. An example of re-consolidation behavior of segregated specimen is shown in Fig. 3.

The next stages of liquefaction tests were conducted by following the same procedures as the one described in the first liquefaction test. The effective stress path and stress-strain behavior of segregated specimen during 1<sup>st</sup> and 2<sup>nd</sup> liquefaction

tests with CSR = 0.2 are shown in Fig. 4 and Fig. 5.

For the image analysis, dots with spacing of 5 mm x 5 mm grid were pasted on the outer membrane. A digital camera is employed to observe the dots movement. Details of this image analysis technique can be found in [17].

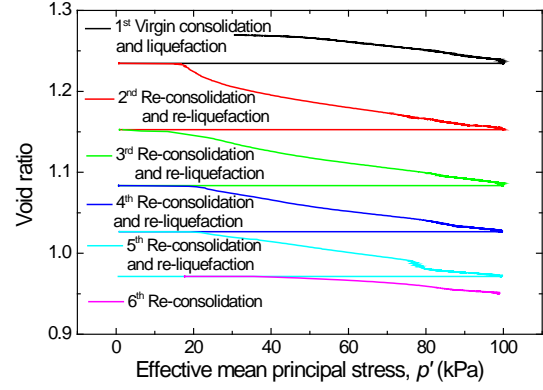


Fig. 3 Effective mean principal stress-void ratio relationship during re-liquefaction test of segregated specimen with CSR = 0.20.

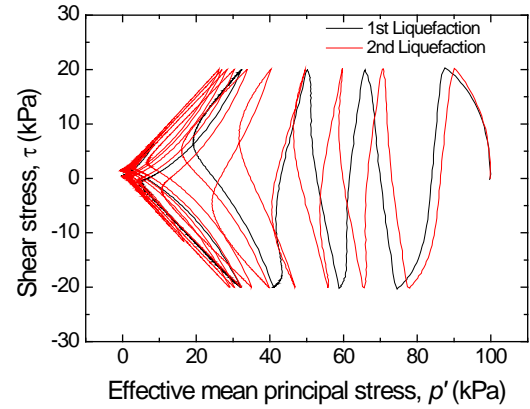


Fig. 4 Effective stress path for segregated specimen with CSR = 0.20.

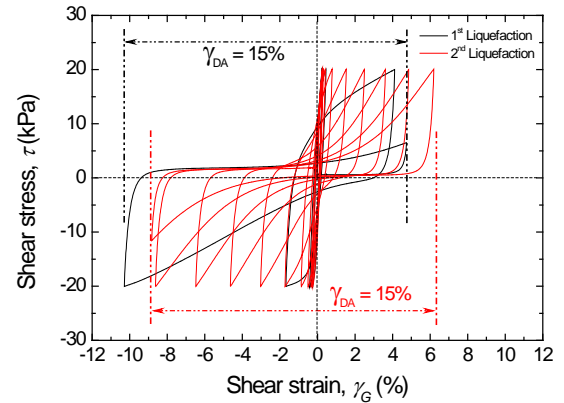


Fig. 5 Shear stress-strain relationship for segregated specimen with CSR = 0.20.

## TEST RESULTS AND DISCUSSIONS

In this section, the re-liquefaction behaviors of Katori sand are explained by experimental and image analysis results.

### Experimental Results

Figure 6 and Fig. 7 show the relationship between the stage of liquefaction and number of cycles to liquefy and relative density. Figure 8 shows the relationship between relative density and number of cycles to liquefy. Figure 9 shows an example of excess pore pressure generation at each stage of liquefaction. These figures indicate that the liquefaction resistance can decrease, keep constant, and/or increase in the second stage of liquefaction. Then, in the third and further stages of liquefaction, liquefaction resistance will increase. The liquefaction resistance of the segregated specimen increased gradually but that of the uniform specimen by moist tamping increased more significantly.

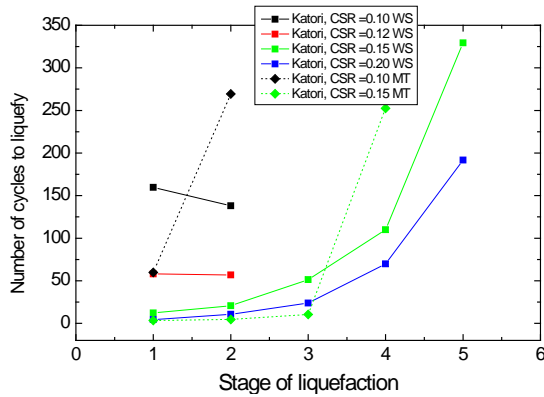


Fig. 6 Variation of liquefaction resistance with each stage of liquefaction.

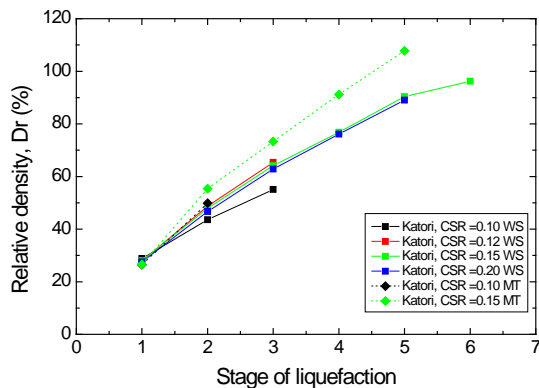


Fig. 7 Stage of liquefaction and relative density relationships.

All the specimens show densification during re-consolidation. However, the liquefaction resistance

does not always increase with the increase of relative density. This observation is consistent with the results from many previous studies that the increase of relative density is not the main factor of re-liquefaction behavior. These figures also show the increase in relative density of the specimen during re-consolidation follows a quadratic trend. Such trend is different from the observation made in [15] that the increase in relative density follows a linear trend.

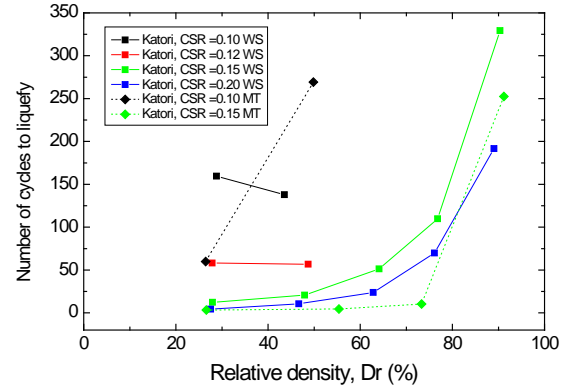


Fig. 8 Relative density and liquefaction resistance relationships.

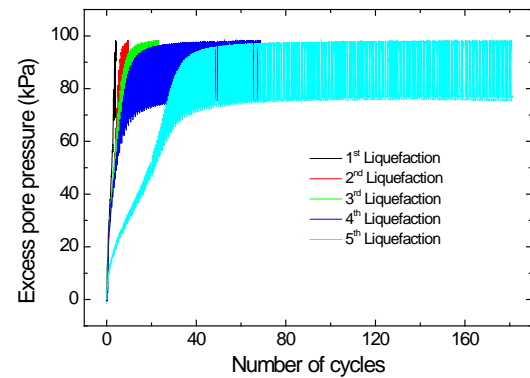


Fig. 9 Pore pressure generation during re-liquefaction tests. (Case: segregated specimen with CSR = 0.20)

### Image analysis results

Figure 10 and Fig. 11 show the distributions of local horizontal strain after consolidation (i.e., before each stage of liquefaction) for segregated and uniform specimens, respectively. These figures show that specimens undergo horizontal compression in the upper layer and expansion in the lower layer after each stage of liquefaction, suggesting that the diameter of specimen decreases at the top part and increases at the bottom part. It can be seen from the image analysis results that, after first stage of liquefaction, the specimen shapes are not uniform

anymore. This condition would affect the stress distribution during the next stage of liquefaction.

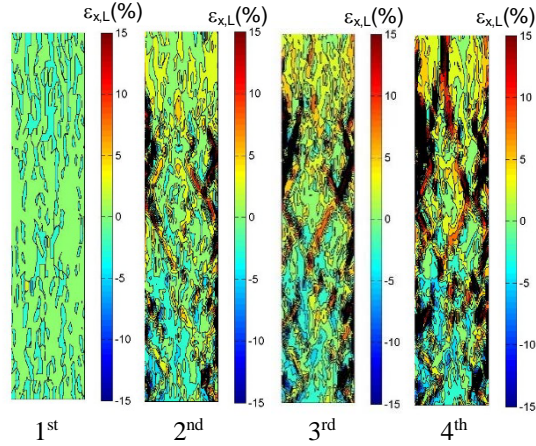


Fig. 10 Local horizontal strain of segregated specimen after consolidation (Case: CSR = 0.15)

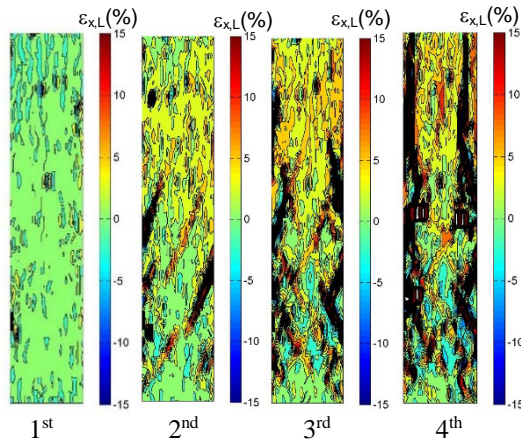


Fig. 11 Local horizontal strain of uniform specimen after consolidation (Case: CSR = 0.15)

The distributions of local shear strain during the first stage of liquefaction for segregated and uniform specimen (CSR = 0.15), respectively, are shown in Fig. 12 and Fig. 13. In addition, distribution of the local shear strains that are averaged at respective elevation is also plotted in these figures. In case of segregated specimens, at the interface between layer 1 and layer 2 (as defined in Fig. 2), and layer 2 and layer 3, higher concentration of local shear strain is observed. Such concentration appeared when the effective stress reduced close to zero. This behavior may be caused by a formation of water film when liquefaction happens. In case of uniform specimens, such concentration of local shear strain is not observed. However, the deformation of specimens are not completely uniform.

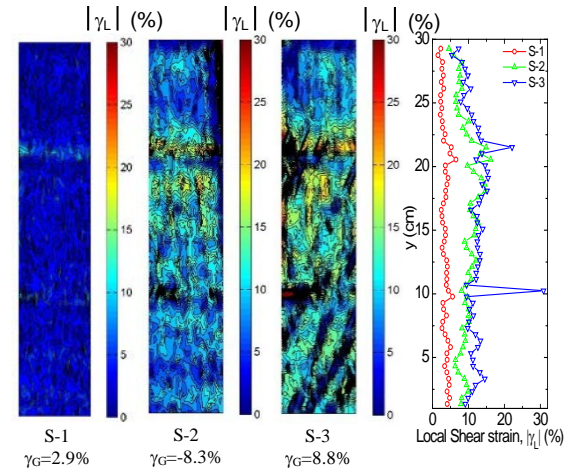


Fig. 12 Local shear strain of segregated specimen during first liquefaction (Case: CSR = 0.15)

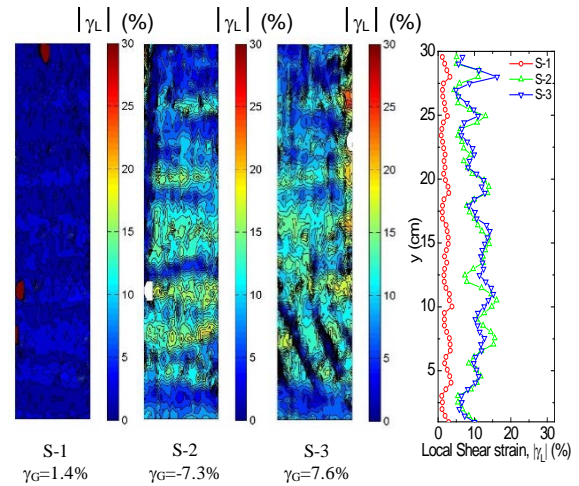


Fig. 13 Local shear strain of uniform specimen during first liquefaction (Case: CSR = 0.15)

## CONCLUSION

The re-liquefaction resistance of segregated and uniform specimens of Katori sand were investigated by undrained cyclic loading tests in hollow cylindrical torsional apparatus. From the test results, it was found that liquefaction resistance will not always increase with the increase of relative density after re-consolidation. The behavior of re-liquefaction of segregated Katori sand at second stage can be decrease, increase or constant. After that the resistance against liquefaction will increase. However, the behavior of uniform specimens show higher resistance after each stage of liquefaction. The specimen shapes in hollow cylinder apparatus are not uniform after the first liquefaction. This condition will affect the stress distribution in the specimen. There are still many behaviors that remain unclear, such as pre-shearing history, loading

direction, and specimen preparation. However, this study has started the study of re-liquefaction behavior using hollow cylinder torsional apparatus.

## ACKNOWLEDGEMENTS

The authors wish to express their sincerest gratitude to Mrs. Yukika Miyahita, Mr. Seto Wahyudi, and Mr. Takeshi Sato for their highly cooperative supports made during the development of image analysis technique and during the assembling works of both the mechanical and electronic components of the testing apparatus.

## REFERENCES

- [1] Seed RB, KO Cetin, RES Moss, AM Kammerer, J Wu, JM Pestana, MF Riemer, RB Sancio, JD Bray, RE Kayen, and A Faris, "Recent Advances in Soil Liquefaction Engineering: A Unified And Consistent Framework", Keynote Speaker in Proc. 26th Annual ASCE Los Angeles Geotechnical Spring Seminar, pp. 1-71.
- [2] Ishihara K, "Evaluation of Settlements in Sand Deposits Following Liquefaction during Earthquakes", *Soils and Foundations*, Vol. 32, No.1, Mar. 1992, pp. 173-188.
- [3] Tokimatsu K, HB Seed, "Evaluation of Settlements in Sands due to Earthquake Shaking", *Journal of Geotechnical Engineering*, Vol. 113, No. 8, Aug. 1987, pp. 861-878.
- [4] Toki S, F Tatsuoka, S Miura; Y Yoshimi, S Yasuda; Y Makiyara, "Cyclic undrained triaxial strength of sand by a cooperative test program", *Soils and Foundations*, Vol. 26, No. 3, Sept 1986, pp.117-128.
- [5] Mesri G, TW Feng, JM Benak," Post densification penetration resistance of clean sands", *Journal of Geotechnical Engineering* Vol. 116, Issue 7, Jul. 1990, pp. 1095-1115.
- [6] Yasuda S and I Tohno, "Sites of reliquefaction caused by the 1983 Nihonkai-Chubu earthquake." *Soils and Foundation*, Vol. 28, No. 2, Jun. 1988, pp. 61-72.
- [7] Wakamatsu K, "Recurrent Liquefaction Induced by the 2011 Great East Japan Earthquake Compared with the 1987 Earthquake", *Proceedings of the International Symposium on Engineering Lessons Learned from the 2011 Great East Japan Earthquake*, Mar. 2012, pp. 675-676.
- [8] Orense RP, T Kiyota, S Yamada, M Cubrinovski, Y Hosono, M. Okamura, and S Yasuda, "Comparison of Liquefaction Features Observed during the 2010 and 2011 Canterbury Earthquakes", *Seismological Research Letters*, Vol. 82, No. 6, Dec. 2011, pp. 905-918.
- [9] Finn WDL, PL Bransby, and DJ Pickering, "Effects of strain history on liquefaction of sand", *Journal of Soil Mechanic and Foundation*, Vol. 96, No. 6, Nov/Dec. 1970, pp. 1917-1934.
- [10] Seed HB, K Mori, and CK Chan, "Influence of seismic history on liquefaction sands", *Journal of Geotechnical Engineering Divisions*, Vol. 103, No. 4, Apr. 1977, pp. 257-270.
- [11] Ishihara K and S Okada, "Effects of large pre-shearing on cyclic behavior of sand", *Soils and Foundations*, Vol. 22, No. 3, Sep. 1982, pp. 109-125.
- [12] Oda M, K Kawamoto, K Suzuki, H Fujimori, and J Sato, "Microstructural interpretation on reliquefaction of saturated granular soils under cyclic loding", *Journal of Geotechnical and Geo-environmental Engineering*, Vol. 127, No. 5, May 2001, pp. 416-423.
- [13] Yamada S, T Takamori, and K Sato, "Effects on reliquefaction resistance produced by changes in anisotropy during liquefaction", *Soils and Foundations*, Vol. 50, No. 1, Feb. 2010, pp. 9-25.
- [14] Ha IS, SM Olson, MW Seo, MM Kim, "Evaluation of reliquefaction resistance using shaking table tests", *Soil Dynamics and Earthquake Engineering*, Vol. 31, No. 4, Apr. 2011, pp. 682-691.
- [15] Wahyudi S, J Koseki, and T Sato, "Characteristics of Re-Liquefied Behavior of Sand by Means of Image Analysis in Stacked-Rings Shear Apparatus", *Bulletin of Earthquake Resistant Structure*, Vol. 47, Mar 2014, pp. 15-26.
- [16] Tatsuoka F, S Sonoda, K Hara, S Fukushima, TBS Pradhan, "Failure and Deformation of Sand in Torsional Shear", *Soils and Foundation*, Vol. 26, No. 4, Dec. 1986, pp. 79-97.
- [17] Fauzi UJ and J Koseki, "Local Deformation Properties of Segregated Sand Specimen in Hollow Cylindrical Torsional Shear Tests", *Bulletin of Earthquake Resistant Structure*, Vol. 47, Mar. 2014, pp. 27-36.
- [18] Ampadu, SK and F Tatsuoka, "Effects of setting method on the behavior of clays in triaxial compression from saturation to undrained shear", *Soils and Foundations*, Vol. 33, No.2, Jun.1993, pp. 14-34.



## **EFFECT OF FIBRE IN CONTROLLING DESICCATION CRACKS IN CLAY LINER SOILS**

Dr. Sobha Cyrus<sup>1</sup> and Veena.V<sup>2</sup>

<sup>1</sup>Professor, Cochin University of Science & Technology, India; <sup>2</sup>Research Scholar, CUSAT, India

### **ABSTRACT**

The most general method adopted now a days for the disposal of Municipal Solid Waste (MSW) is by land filling. The desiccation of liner materials is a major factor affecting the performance of compacted clay liner landfills. This leads to the formation of cracks which provides pathways for moisture migration, increasing the generation of waste leachate and ultimately increases the potential for soil and ground water contamination. The problem of desiccation cracking is encountered when the clay liners are subjected to alternate wetting and drying, which are due to seasonal variations. The long term effect of these cracks is to reduce the sealing effect of the cover system significantly. Liner materials commonly used include bentonite enhanced sand mixture (BES) and locally available materials, which satisfy the norms as laid down in EPA. In the present study conducted on samples of BES subjected to alternate wetting and drying, the desiccation cracks has been quantified using crack intensity factor (CIF). Tests were also conducted on these soil samples amended with different percentages of polypropylene fiber.. For different fiber inclusions, (0.2%, 0.4 %, 0.6% and 0.8%), 3 cycles of alternate wetting and drying were performed. The behavior of BES for different percentage of polypropylene fiber was analysed .The study concluded that the problem of desiccation cracks in liner soils can effectively be addressed by fiber inclusion.

*Keywords: Desiccation, Amendment, Wetting and drying, Crack intensity factor, Digital image processing*

### **INTRODUCTION**

The major problem of the day is the solid waste disposal. Landfills are one of the solutions for this problem. The main component of an engineered landfill is a liner system at the base and sides, a leachate collection facility and a final cover system. The primary purpose of the liner system is to isolate the landfill contents from the environment and to protect the soil and ground water from pollution, originating in the landfill.

Desiccation of compacted clay liners is a major factor affecting the performance of landfills. During certain stages in the life of landfill, it could be subjected to seasonal changes, resulting in significant variation in water content leading to the desiccation of clay liner material. The development of tensile stresses facilitates the initiation of tensile cracks [2]. Cracks provide pathways for moisture migration into the landfill which increases the generation of waste leachate and ultimately increases the potential for soil and ground water contamination [1]. Use of fibres to reduce the desiccation cracking in liner soils has caught the attention of geotechnical engineers. The fibers increase the tensile strength of the clay and provide a ductile behavior that was not present in the samples

without fibers [5]. A model which describes the increase in tensile strength in terms of fiber properties, soil properties, and fiber/soil interface parameters has been developed [4]. Further, it was observed that there was definite improvement in the properties of the liner materials when it was reinforced with discrete random fibres. As such the desiccation cracks could be controlled with the help of fibre reinforcement [3]. Here an attempt is made to study the formation of desiccation cracks in Bentonite enhanced sand mixture soils when used as a liner material and containment of cracks with fibre amendments to BES soils.

### **MATERIALS**

#### **Soils**

##### *Bentonite*

Commercially available bentonite was used to prepare the BES mixture. The properties of bentonite used are given in Table 1

##### *Fine sand*

The commercially procured sand was dried and the portion passing through 425 $\mu$  sieve and retained

in 75 $\mu$  sieve was used for the study. Earlier investigators have added sand in different proportions to bentonite to reduce the volume change, and have suggested that a combination of 80% sand to 20% bentonite satisfies the liner requirements. The properties of sand used are given in Table 2.

Table 1 Properties of Bentonite

Particulars	Bentonite
Specific Gravity	2.8
Liquid limit(%)	293
Plastic limit(%)	52
Plasticity Index(%)	241
Shrinkage limit (%)	9
Grain Size Distribution	
Sand (4.75-0.075mm) (%)	0
Silt size (0.002-0.075mm)(%)	29.4
Clay size (<0.002mm) (%)	70.3

Table 2 Properties of fine sand

Particulars	Sand
Specific Gravity	2.64
Effective size $D_{10}$ (mm)	0.15
$D_{30}$ (mm)	0.18
$D_{60}$ (mm)	0.25
Uniformity Co-efficient	1.67

#### *Polypropylene fibre*

Polypropylene is the most common synthetic material used to reinforce soil. It easily mixes with soil and has a relatively high melting point which makes it possible to place the specimens of the fibrous soil in the oven and conduct the tests for moisture content. The amendment polypropylene fibre mesh was supplied by Taian Modern Plastic Co. Ltd, China. The properties of the fibre as given by the manufacture, is given in Table 3.

Table 3 Properties of Polypropylene Fibre Mesh

Particulars	Polypropylene fibre mesh
Average Diameter (mm)	0.1
Acid Resistance	Strong
Alkali Resistance	Strong
Tensile strength (MPa)	>450
Melting Point ( $^{\circ}$ C)	160-170
Water Absorption (%)	Nil

#### *Bentonite enhanced Sand (BES)*

The application of bentonite is currently the most accepted practice for lining purpose. In the study bentonite sand combination is taken as 20% bentonite and 80% sand. The properties of BES are given in Table 4

Table 4 Properties of BES

Particulars	BES
Specific Gravity	2.67
Liquid limit(%)	50
Plastic limit(%)	25
Plasticity Index(%)	25
Shrinkage limit (%)	25
Grain Size Distribution	
Sand (4.75-0.75mm) (%)	80
Clay size (<0.002mm) (%)	20

This has been adopted and this liner soil is termed as bentonite enhanced sand mixture (BES) in this study

#### **Preparation of samples**

In this study, the test specimens were compacted in Standard Proctor mould at their respective dry density, and 2% above optimum moisture content. In the preparation of the entire specimen, the air dried soil was mixed with an amount of water depending on the optimum moisture content of the soil. All mixing was done manually and proper care was taken to prepare homogenous mixture, at each stage of mixing.

When fibre was used as an amendment, the prescribed content of fibres was first mixed into the air dried soil in small increments by hand, making sure all fibres were mixed thoroughly to achieve a fairly uniform mixture and then the required amount of water was added. Afterwards the soil was sealed in plastic bags and allowed to hydrate for 24 hrs prior to compaction. The fibre content selected ranged over 0.2% to 0.8% depending upon the ease in mixing and the 'balling effect' experienced when higher fibre contents were tried.

## **METHODS**

### **Drying Procedure**

The prepared specimen was then placed in specially designed drier, Fig 1, which simulate the slow rate of drying that occur in the field, while maintaining reasonable test time cycle. The test



specimen were insulated on the sides using a thermal insulating material, so that only the top surface was exposed to heat and hence drying occurred from top. Thus the lab drying conditions simulated the field conditions precisely.



Fig 1 Photograph of Specially Designed Drier

Drying test was conducted till no significant decrease in weight of the specimen occurred. Considering the local climatic condition, a drying temperature of 40°C was selected.

#### Saturation Procedure

In order to saturate the sample specimen, a special arrangement was made. Rubber membrane of 10cm diameter was used. The dried sample along with the membrane was wrapped with a thick double layered plastic sheet of height slightly more than that of the sample. The top portion of the membrane was folded down over the edge of the outer cover. The bottom end of the sample was sealed to prevent entry of water from below. The so prepared sample was ponded with water by keeping them in a tub full of potable water.

This arrangement allowed water to enter into the specimen from top only which simulated the actual field condition. The membrane helped in preventing the lateral expansion of soil, allowing expansion only in the vertical direction

#### Determination of duration and number of Wet /Dry Cycle.

Tests were conducted in BES samples to determine the duration of drying and wetting periods. The compacted soil specimens were kept in drier until the weight of the specimen became stable. The weight of the sample was taken at every 24hrs interval. It was found that no significant change in weight occurred after 6 days of drying. Hence the

first drying period was kept as 6 days for BES sample.

In order to determine the duration of wetting period, dried samples were saturated by ponding with water. Every two days, soil specimens were taken from different samples for determination of water content from top, middle and base of sample. The experiments were conducted for 3 wet and dry cycles. The duration of wetting and drying cycles are as tabulated in Table 5

#### Measurement of Cracks

##### Digital Image Acquisition

The image acquisition was done using a digital camera HP Photo smart R507/R607 with HP instant share, 4.23 Mega Pixel. The colour image of the desiccated sample was taken. Digital image acquisition is the process by which a continuous visual scene is converted into a digital image file that can be saved, interpreted and redisplayed by computers.

Table 5 Duration of wet/dry cycles

Soil	Cycle No.	No. of days	
		Drying	Wetting
Bentonite	I	6	5
Enhanced	II	5	4
Sand (BES)	III	5	4

##### Development of Computer Algorithm

To obtain numerical information about the cracks in image, computer image processing algorithms were developed using MATLAB R2010a.

The RGB images taken by the digital camera are stored in the computer under the TIFF file format. The first stage in processing an image is to convert it to a gray scale image. The grayscale image provides a single value between 0 (black) and 255 (white) for each pixel in the image.

In second stage in crack determination, the grayscale image is binarized using a direct threshold method. The binarization is performed by setting a particular grayscale value as a threshold so that all the pixels that have grayscale values greater than or equal to the threshold value turn to white, while all the pixels that have grayscale values less than the threshold turn to black.

For the crack determined image the total cracked area can be determined by counting the number of black pixels in the image. The total number of black pixels then is converted into area units using a

defined scale. Counting the number of black pixels is easily done, either using one of the Matlab matrix commands or by writing a simple algorithm that scans through the image row by row and counts the number of the encountered black pixels.

The surficial cracked area was used for the determination of Crack intensity factor (CIF). Crack intensity factor is defined as the ratio of the cracked area to the total surface area of the sample.

## RESULTS AND DISCUSSIONS

### Compaction characteristics of fibre amended BES soils

Standard Proctor tests were conducted on Bentonite enhanced sand mixture (BES) using various percentage (0.2%, 0.4%, 0.6% and 0.8%) of fibre inclusion. The compaction characteristics of the soils are as given in Table 6. Since there was no significant change in the values of optimum moisture content and maximum dry density, the results without fibre inclusion were used for the study of desiccation cracks.

Table 6 Compaction characteristics BES with polypropylene fibre mesh

Fibre content (%)	BES	
	Max dry density ( $\text{kN/m}^3$ )	OMC (%)
0	17.8	17
0.2	18.0	17.3
0.4	17.6	16.8
0.6	18.1	17.4
0.8	18.4	17.5

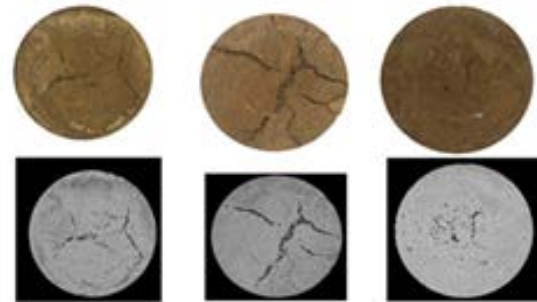
### Effect of fibre content on BES

The investigation of wet –dry cycle was done in the following sequence: drying of compacted soil, then wetting to saturation, followed by drying and so on. This sequence can be expected to simulate better field conditions.

The desiccation test for alternate wetting and drying cycles were conducted on unamended BES and BES with 0.2, 0.4, 0.6 and 0.8 percentage of fibre inclusion. The photographs taken at the end of each wet/dry cycle for unamended BES, BES with 0.2% and 0.8% fibre inclusion are presented in Fig.2, Fig. 3 and Fig.4 respectively.



(a) Cycle1 (b) Cycle 2 (c) Cycle 3  
Fig.2 Desiccated samples of unamended BES



(a) Cycle1 (b) Cycle 2 (c) Cycle 3  
Fig.3 Desiccated samples of BES fibre amended soils with 0.2% fibre content



(a) Cycle1 (b) Cycle 2 (c) Cycle 3  
Fig.4 Desiccated samples of BES fibre amended soils with 0.8% fibre content

A visual interpretation of the figure shows that at the end of cycle 2, the surficial cracks have increased and the amount of surficial cracks has decreased in cycle 3.

The effect of fibre amendment on BES is represented in the form of bar chart for ready reference, Fig.5. It is seen that the CIF increases up to second cycle and then it falls. The same phenomena were observed with increase in percentage of fibre inclusion. This shows that the maximum shrinkage takes place in the second cycle.

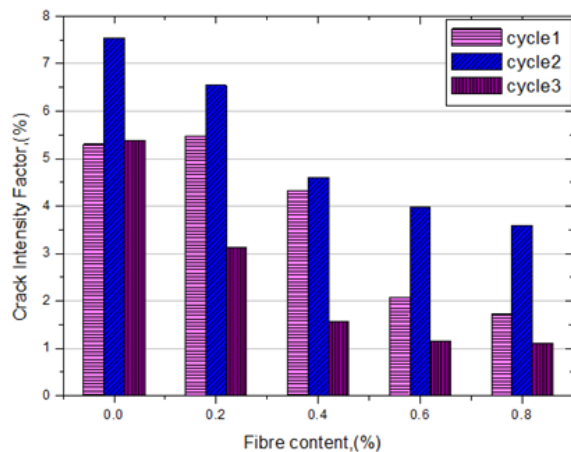


Fig.5 CIF with different % of fibre inclusion in BES for alternate wetting and drying cycles

The data obtained from the analysis of photographs of all cycles of desiccated samples of fibre amended BES is represented in Table 7. The observed value shows that, with increase in the percentage fibre inclusion, the percentage of CIF decreases. The very same pattern is noticed in all the 3 wet/dry cycles. The CIF decreases from 5.38% to 1.1% at 0.8% fibre inclusion in Cycle-3. The optimum value of CIF, 1.1% is when the percentage of fibre is 0.8%.

Table 7 Desiccation crack details of Fibre amended BES soil for various cycles

Cycle	Crack Intensity Factor (CIF)				
	Fibre content (%)				
	0.0	0.2	0.4	0.6	0.8
1	5.3	5.48	4.33	2.08	1.72
2	7.55	6.54	4.6	3.98	3.59
3	5.38	3.13	1.56	1.15	1.1

The depth of the crack was measured using thin wire gauges. The maximum depth of crack in centimeter with different % of fibre inclusion in BES for alternate wetting and drying cycle is given in Table 8. The maximum depth of crack steadily decreases with increase in percentage of fibre. From the point of view of depth of crack, the optimum value of fibre inclusion 0.8.

The study indicates that the CIF and the depth of crack decrease with the increase of fibre inclusion. It is further observed that the maximum value of CIF and depth of crack occurs during the second cycle and decreases during the third cycle. This may be due to the self-healing property of the soil.

Table 8 Maximum crack depth details of Fibre amended BES soil for various cycles

Cycle	Maximum depth of crack (cm)				
	Fibre content (%)				
	0.0	0.2	0.4	0.6	0.8
1	0.4	1.9	2.0	1.4	1.3
2	2.4	2.2	2.1	1.6	1.5
3	2.2	1.2	1.8	1.2	0.8

## CONCLUSION

The effects of fibre amendments in containing desiccation cracks in BES soils were studied. An attempt was also made to obtain the optimum value of fibre inclusion. The crack intensity factor and the depth of cracks were the parameters used for the study. The study reveals that the value of CIF decreases from 5.38% without fibre to 1.1% at 0.8% fibre inclusion in Cycle 3. The depth of crack was another parameter considered. It was observed that the maximum depth of crack steadily decreases with increase in percentage of fibre.

In short, the problem of desiccation cracks in BES soils can effectively be addressed by fibre inclusion.

## REFERENCES

- [1] Carol J Miller, Hong Mi, and Nazli Yesiller, "Experimental Analysis of Desiccation Crack Propagation in Clay Liners", *Journal of the American Water Resources Association*, 34(3), 1998, pp.677-686.
- [2] Costa S, Kodikara J, and Thusyanthan N I, "Modelling of Desiccation Crack Development in Clay Soils", in 12th International Conference of International Association for Computer Methods and Advances in Geomechanics (IACMAG), 2008, pp 1099-1107.
- [3] Cyrus S and Babu T Jose, "Studies on the Development and Control of Desiccation cracks in compacted clay liner soils", *Dyuthi digital repository*, Copyright © 2007-2011 Cochin University of Science and Technology.
- [4] Sami M Rifai, "Impact of polypropylene fibers on desiccation cracking and hydraulic conductivity of compacted clay soils", Ph.D. Dissertation, Graduate School of Wayne State University, Detroit, Michigan, 2000.
- [5] Shulley, Stacy, Leshchinsky, Dovand Ling, Hoe I (Corporate Author : Delaware Univ Newark) (1997), "Effects of Short Polymeric Fibers on Crack Development in Clays", DTIC online information for the defense community

## CYCLIC BEHAVIOR OF RECYCLED CONCRETE AGGREGATE IMPROVED WITH LIME AND GYPSUM ADDITION

Wojciech Sas<sup>1</sup>, Andrzej Gluchowski<sup>1</sup>, Alojzy Szymański<sup>1</sup>

<sup>1</sup>Faculty of Civil and Environmental Engineering, Warsaw University of Life Sciences, Poland

### ABSTRACT

In this paper, study on the use of reclaimed waste in Recycled Concrete Aggregate (RCA) was conducted. Reclaimed concrete problem has increased over the past decade, due to the replacement old concrete parts, such as rail substructures or pavement curb. The main idea of this article was the introduction of recycled materials to pavement engineering, which in Poland were usually deposited on waste landfills. Geotechnical study was undertaken to obtain physical and mechanical properties of RCA.

For better understanding of its exceptional behavior under repeated loading, cyclic triaxial test was conducted in various stages of loading. For the purpose of bearing capacity analysis, uniaxial tests were made. Moreover, RCA improvement of mechanical properties was proposed. Chemical stabilization with lime and gypsum was undertaken in order to ameliorate mechanical characteristics. While the mechanical stabilization is a cause of aggregates crushing, created fine fraction could be a stabilizing medium. Determination of resilient modulus  $M_r$  from repeated loading test for non-stabilized and stabilized material was also presented. The paper also includes an investigation of possible application of stabilized RCA as subbase in pavement construction.

*Keywords: Recycled Concrete Aggregate, cyclic CBR, Stabilization, Lime*

### INTRODUCTION

Recycled Concrete Aggregate (RCA) is a product of crushing process of concrete waste left from demolished constructions. Due to development of civil engineering and limited place for construction sites, old buildings are replaced by new structures. Such events are the cause of increasing of concrete debris on waste landfill.

In order to stop this unpleasant situation, many studies on possibility of recycling crushed concrete were made. In transportation geotechnics, for example, an application of RCA as subbase and improved subgrade was proposed. Interesting possibility of use RCA as noise barrier embankment is promising [1].

For RCA to be applied in pavement design as parts of road structures, its mechanical properties need to be described well. Many studies carried out over past decades, point out with a doubt that as artificial aggregate, RCA needs special tests in order for to obtain accurate strength properties.

Most obvious property which lights out problem of RCA is the greater angularity with comparing to natural aggregate. Moreover, surface of RCA is much rougher and aggregates display an unusual build. Voids in RCA are divided into two parts: accessible for water on surface, termed "surface pores", and those that are isolated, namely "internal pores" [2]. This occurrence of the voids results in higher degree of water absorption. This fact makes existing standards inaccurate for RCA testing.

These problems eliminate the possibility of using RCA as building material in the nearest future. Many tests conducted nowadays - for example direct shear test, triaxial tests and uniaxial compression tests - have shown that RCA is reliable and that this material shown good performance [3].

In case of pavement design it is important to obtain data about material cyclic loading. Among traditional cyclic triaxial tests, dynamic hollow cylinder tests are used for this purpose. Nevertheless, those methods are highly sophisticated and cannot be applied for such material like RCA. Applying this apparatus in pavement laboratories is expensive and simply too complicated.

In order to simplify the tests and shorten their time, another manner was proposed. Replacing empirical methods, such as the CBR test, is the greatest advantage in utilizing this procedure [4]. Repeated loading CBR or cyclic CBR (cCBR) methods use common CBR apparatus and similar procedures to obtain resilient modulus  $M_r$ , characteristic for cyclic phenomena.

Resilient modulus is calculated as follows:

$$M_r = \frac{\Delta\sigma_d}{\Delta\varepsilon_r} \quad (1)$$

where,  $\Delta\sigma_d$  is deviator stress pulse  $\Delta\sigma_d = \Delta\sigma_1 - \Delta\sigma_3$ ,  $\sigma_1$  is major principal stress,  $\sigma_3 = \sigma_2$  is minor principal stress, and  $\Delta\varepsilon_r$  is recoverable or resilient strain over deviator pulse  $\Delta\sigma_d$  [5].

Pozzolanic compounds which cause the grains combine with cement cannot be entirely exploited and part of them can be activated after crushing. Because of that, efforts to stabilize RCA, by adding

lime have been made. Calcium hydroxide induces reaction with pozzolanic compounds, as well as with siliceous or aluminous material.

The biggest advantage of using the repeated loading test is the possibility of gaining data relating to the permanent strain. This information can be used in the design of to pavement and shallow foundations [6]. Information about stress levels and performance of material during cyclic phenomena can also be obtained.

This knowledge can be better utilized simply because of ready to use results.

## MATERIAL AND METHODS

### Material

Tests were conducted on material obtained from demolished concrete from building demolition site. Concrete aggregates were an element of concrete walls and floor, whose strength class estimated from C16/20 to C30/35. Aggregates were in 100% composed from broken cement concrete. Grain gradation curve was adopted according to Polish technical standard [7] and placed between upper and lower grain gradation limits.

For estimation of physical properties, a series of tests was conducted. The sieve analysis led to classifying this material as sandy gravel (saGr), in reference to [7, 8]. Test results are shown in Figure 1. This distribution of particles from 31.5mm to 0mm is typical for soils used for subbase and support structures.

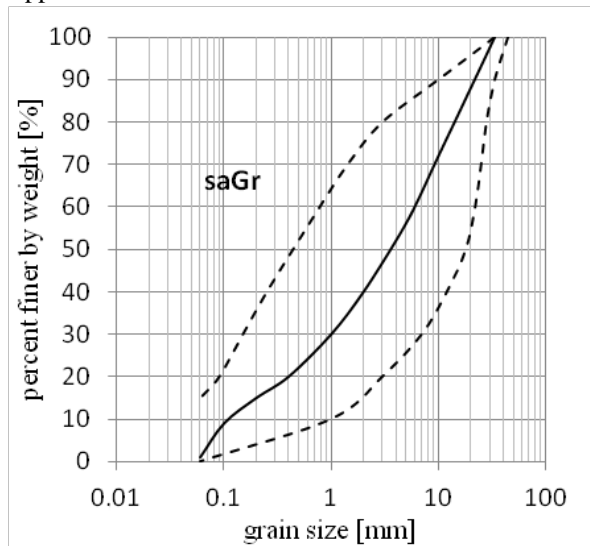


Fig. 1. Particle size distribution of tested soil.

Results of the Proctor test are presented in Figure 2. The test was conducted by compaction in the Proctor mold, whose volume equaled  $2.2\text{dm}^3$ , by using standard energy of compaction, equal to  $0.59\text{J/cm}^3$ . Optimum moisture content for sandy

gravel was  $w_{\text{opt}} = 8.67\%$  and maximum dry density of optimum moisture content was  $1.97\text{g/cm}^3$ .

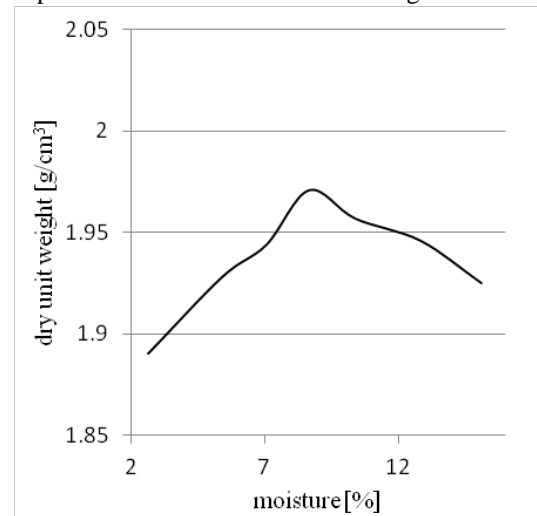


Fig. 2 The Proctor test results for sandy gravel.

### Methods

After the optimum moisture content has been estimated, the calculation of peak dry density  $\rho_{ds}$  for tested samples relative density was performed.

Observations during the Proctor tests show high water absorption of the material. Soil was compacted in three repetitions and registered data have been different each time. After 24 hours, tests were repeated on grains conditioned in constant moisture. After three repetitions, the recurrent results were obtained.

When marking of material physical properties and preparation of the samples were done, cCBR tests were performed. cCBR method was based on common CBR test. Main idea behind using this equipment came from its popularity. On the other hand, cyclic load triaxial apparatus is treated as an advanced machinery. Long existence of CBR method and its usefulness in pavement design, resulted in its worldwide spread. Although for mechanistic-empirical design CBR test becomes too empirical.

By using CBR mould and repeated loading apparatus, cCBR test method was established. The main principle of this test approach is to use standard CBR test procedure as a reference in order to study the later cyclic loading stage.

As was mentioned above, the first step is standard CBR test loading to 2.54mm. After reaching desired displacement with the use of plunger, unloading procedure was attempted, with the use of up to 10% of force obtained at 2.54mm. Loading and unloading is treated as the first cycle of cCBR test. Next cycles are determined by maximal and minimal force from the first loading. Test was

carried out with standard 1.27mm/min. velocity. Number of cycles is determined by the percentage of plastic strain in one cycle. cCBR method assumes that the test can be stopped, when 1% or less of plastic displacement in one cycle will occur. Amount of the cycles to obtain this condition usually oscillates around 50 [9, 10].

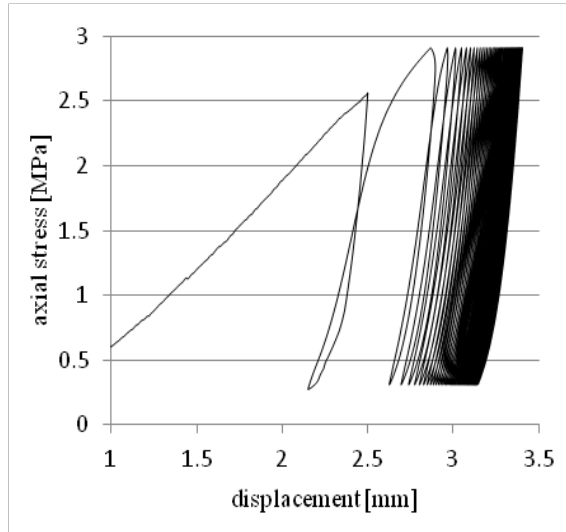


Fig. 3. Stress – displacement curve from cCBR test.

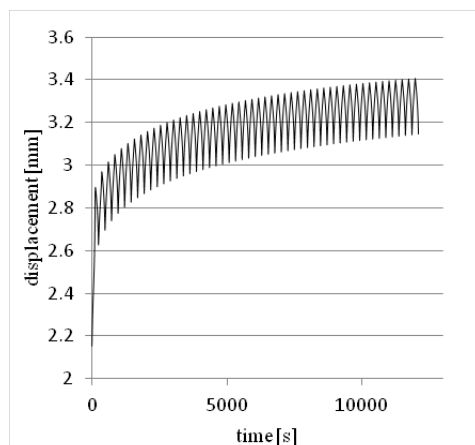


Fig. 4. Displacement – time curve from cCBR test.

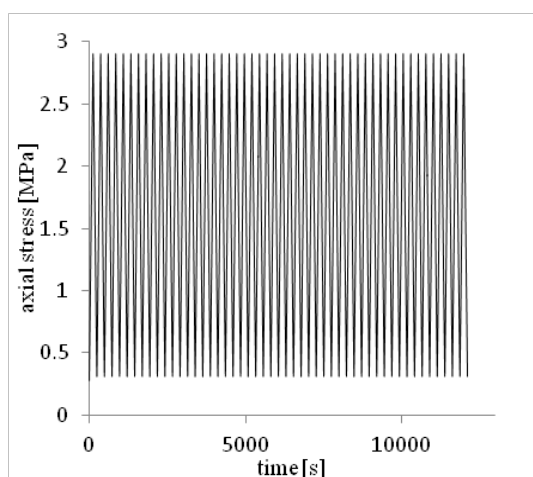


Fig. 5. Plot of cyclic wave from cCBR test.

Figures 3, 4 and 5 present exemplary cCBR test result. In this case, the tested material is RCA with 6% moisture content, compacted with normal Proctor energy. Figure 3 presents the relation of plot axial stress [kPa] to displacement [mm]. Figures 4 and 5 present plot of axial stress and displacement against time. Cyclic wave propagated in one axis stress state results in displacement, which is divided into two components: elastic - recoverable and plastic - irrecoverable displacement. These constitute the basis of numerous cyclic loading analyses. Figure 4 presents this phenomenon. At the end of every cycle, difference of displacement between analyzed test and cyclic test constitute the plastic displacement. Recovered displacements are represented by a difference between peak maximal strain and peak minimal strain in one cycle. In other words, the total plastic displacement increment is the value of minimal strain in each cycle.

### Stabilization

Stabilization of non-cohesive soils - especially coarse grained soils, with greater content than 50 percent by weight of 75 $\mu$ m grains diameter - is beneficial, if chemical stabilization could occur. Improvement can be much higher up to ten times when compared to untreated material [11].

RCA containing cement could still possess some unreacted pozzolanic compounds. Crushing process uncovers active pozzolanic compounds and leading to a reaction. In order to improve this reaction, lime and gypsum addition was undertaken. Lime as a hydraulic binder immobilized by pozzolan and produced calcium silicate hydrate. Moreover, addition of gypsum triggered the increase in hydration rate due to presence of RCA lime and gypsum, Ca and Al ions, in the mixture [12, 13].

In this study, RCA was stabilized with addition of lime and gypsum in amount of 5% and 0,5% respectively.

Material was stabilized in optimal moisture content, which was 8.7% for non-stabilized aggregate. This capacity was raised up to 10.7% due to water losses, caused by hydration.

After 50 cycles, the material reached resilient response to applied load and test was completed.

### RESULTS

Tests conducted on non-stabilized RCA have shown good performance of this material. During standard CBR test the CBR value reached from 36% for material compacted in 4% moisture content conditions, to 44% for RCA in optimal moisture content, although important feature of RCA performance under cyclic loading is characterized by displacement. It is easy to notice that the same penetration of plunger during the first load c is the



same as a tested value of overload to desired rut in pavement engineering in next cycles, but results in different plastic displacements. Lower moisture of RCA causes 3.5mm displacement with optimal moisture content conditions resulting in 3.0mm displacement. This phenomenon is clearly caused by degree of compaction of this material. Figure 2 presents Proctor's test results and differences of dry unit weight between 4.5% and 8.7% moisture content seem to be rather low, but due to their irregular shape, the grains could reduce rightly of RCA surface and create better conditions to assume better position of grains in skeleton.

The problem of the RCA rightly was observed in previous studies conducted in this research program. For example, direct shear tests friction angle results for 4% of moisture content and in optimal moisture content reached 44°, but in case of 4% moisture content, apparent cohesion was observed in quantity of 10kPa.

Stabilization process in details is presented in figures 6, 7 and 8. Plots present results of cCBR test in function of axial stress and displacement on fig. 6. Figures 7 and 8 present the changing in time of displacement and axial stress respectively.

After 24 hours from stabilization process, cCBR test conducted on this material presents improvement in CBR bearing capacity. CBR value has reached 72% and is 28% higher than results in optimal moisture content for non-stabilized sample.

During cCBR test, displacement reached during the 50<sup>th</sup> cycle equaled 2.47mm during the unloading phase, which is 0.53mm less than in case of non-stabilized sample. Detailed view is presented on figure 9.

RCA and especially stabilized RCA exhibit very resilient response to cyclic loading and this phenomenon can be observed in first cycles. Figure 10 presents results of cCBR test for stabilized RCA and an example of the second cycle of cCBR test for sandy clay. This plot picture presents RCA as the elastic displacement to cyclic load. In comparison to sandy clay tested by cCBR method, unloading path came back almost to beginning of load phase in single cycle. Sandy clay exhibits less resilient respond. Hysteresis loop did not close after the 50th cycle, which caused plastic displacement to increment.

In case of parallel stabilized and non-stabilized RCA, samples are more likely to exhibit resilient response as stabilized RCA, but this phenomenon occurs in a slighter manner.

These properties result in fast customization of this material to new load conditions. Material recovers its elastic properties in first few cycles, and rut depth in case of pavement engineering will not proceed or growth will be small. Plot of this phenomenon is presented in figure 10.

The analysis of plastic displacement for RCA is

presented in figure 11. Average functions of plastic displacement growth show that for stabilized RCA, acceleration of plunger penetration will be smaller than for the non-stabilized RCA.

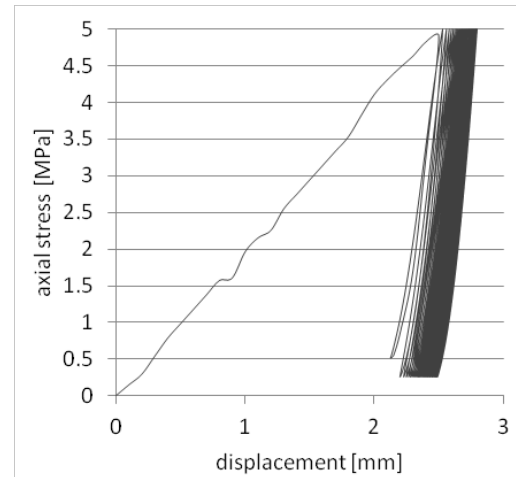


Fig. 6. Plot axial stress-displacement from cCBR test, for stabilized RCA.

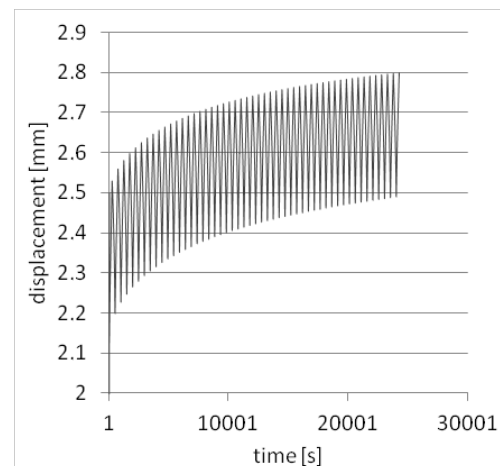


Fig. 7. Plot of cyclic wave from cCBR test for stabilized RCA.

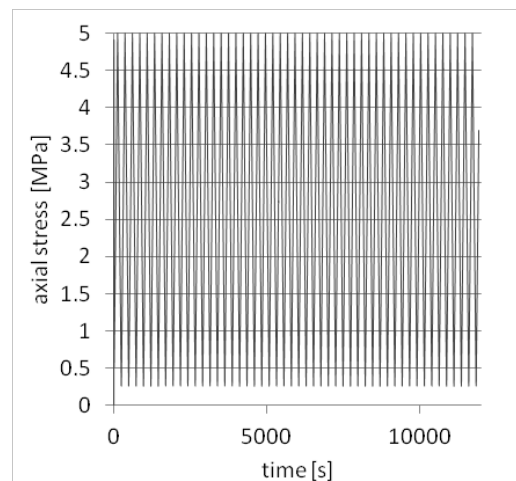


Fig. 8. Plot of cyclic wave from cCBR test for stabilized RCA.

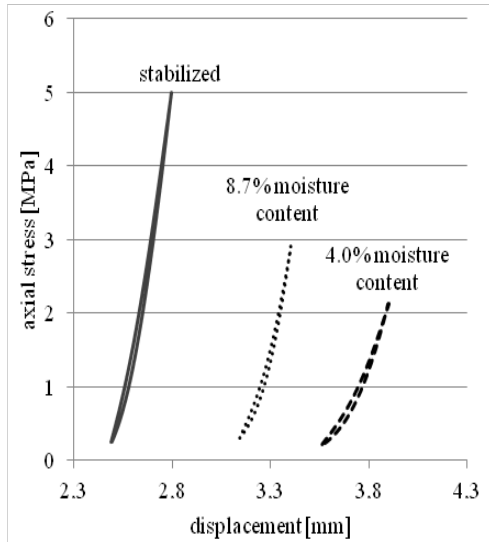


Fig. 9. Plot of last cycles from cCBR test for stabilized and non-stabilized RCA.

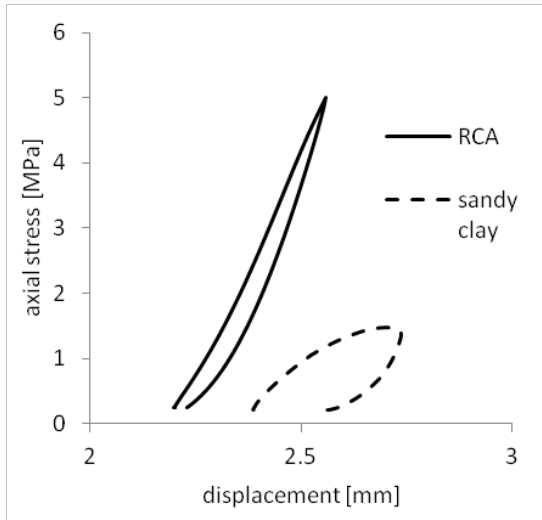


Fig. 10. Plot of results from cCBR test for stabilized RCA and sandy clay.

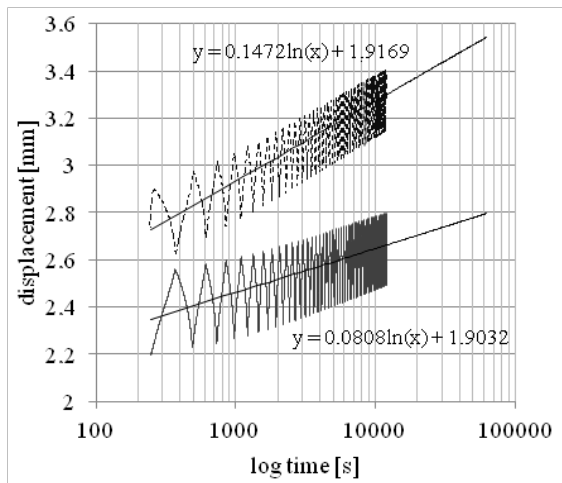


Fig. 11. Average functions of plastic displacement growth from cCBR test.

Stabilization process therefore became reason of stiffness increase in this material. This statement came from not only total displacement observation, but moreover from slope of the hysteresis loop, best seen in figure 9.

Resilient modulus which cannot be calculated directly from stress-displacement plot and is presented on equation (1), needs to be recalculated. In literature, such recalculation was presented in figure [14]. Equivalent modulus from repeated loading CBR, which in this case is named resilient modulus  $M_r$ , can be obtain as follows:

$$M_r = \frac{1.513(1-\nu^{1.104})\Delta\sigma_p \cdot r}{\Delta u^{1.012}} \quad (2)$$

where:  $\nu$  – Poisson's ratio [-] (in this study 0.35 for granular materials),  $\Delta\sigma_p$  – change between maximum and minimum axial stress in one cycle [MPa],  $r$  – radius of plunger [mm],  $\Delta u$  – recoverable displacement in one cycle.

Resilient stimulus for non-stabilized RCA calculated in this manner is equal  $M_r = 543.2 \text{ MPa}$  which is reasonable result [15], and  $M_r = 816.5 \text{ MPa}$  for stabilized RCA.

## CONCLUSION

Results of cCBR test on stabilized and non-stabilized RCA presented in this paper are as follows:

1. RCA as artificial aggregate behaves different than natural aggregates. This phenomenon came from its irregularity and rough surface.
2. Value of  $M_r$  for non-stabilized samples in optimal moisture content was 44% and 72% for stabilized specimen. In case of resilient modulus, values were as follow: 543.2MPa and 816.5MPa respectively.
3. Displacements due to cyclic loading were the smallest in stabilized specimens. Non-stabilized samples exhibit higher total displacement and its value rose with the decrease of moisture content.
4. Resilient modulus describes resilient response tested material in one cycle. Therefore no data about total displacement is available.
5. Material such as RCA generates resilient response much faster than, for example, cohesive soils such as sandy clay. Mobilization of elastic properties was highest in case of stabilized RCA.
6. Stabilization process demonstrates existence of free pozzolanic compound in crushed concrete. Addition of lime and gypsum as stabilization media could trigger hydration reaction.
7. Future studies should concern estimation of

optimal lime, water and gypsum content, evolution of displacements in more than 50 cycles and in other frequencies.

## REFERENCES

- [1] Krezel Z.A., McManus K., "Recycled aggregate concrete sound barriers for urban freeways." Waste Management Series Vol. 31, 2000, pp. 884 - 892.
- [2] Yogini S. Deshpande J. Hiller E., „Pore characterization of manufactured aggregates: recycled concrete aggregates and lightweight aggregates" Materials and Structures DOI 10.1617/s11527-011-9749-2A
- [3] Aurstad J., Berntsen G., Petkovic G. "Evaluation of unbound crushed concrete as road building material – Mechanical properties vs field performance." in Proc. 26<sup>th</sup> International Baltic Road Conference, Kuressaare, 2006.
- [4] Nazarian S., Pezo R., Picornell M., "Testing Methodology for Resilient Modulus of Base Materials". Research rep. 1336-1, Center for geotechnical and Highway Materials Research, 1996 ch. 2.
- [5] Taha T. R., Abbiss C.P., Rosyidi S.A.P. Chik Z., Ismail A. Nayan K. A.M. "Briefing: Study of the relationship between stiffness parameters for base materials." Proceedings of the ICE – Transport. Vol. 165(3), 2011, pp. 159-165.
- [6] Frost M.W., Edwards J.P., Fleming P.R., Arnold S.J. "Simplified laboratory assessment of subgrade performance parameters for mechanistic design of pavement foundations" Transportation Research Board, vol. 1913, 2005, pp.77-85.
- [7] PN – EN ISO 14688: 2a: Projektowanie geotechniczne – Część 1: Rozpoznawanie i badanie podłoża gruntowego.
- [8] WT – 4: Mieszanki niezwiązane do dróg krajowych. GDDKiA.
- [9] Sas W. Głuchowski A, Szymański A., "Determination of the resilient modulus  $M_R$  for lime stabilized Clay obtained from repeated loading CBR tests." Annals of Warsaw University of Life Sciences-Land Reclamation, vol. 44, 2012, pp. 143-153.
- [10] Sas W., Głuchowski A., „Metodyka wyznaczania modułów sprężystości ( $E$  i  $M_r$ ) na podstawie badania CBR pod obciążeniem cyklicznym." *Scientific Review – Engineering and Environmental Sciences*, vol. 57, 2012, pp. 171- 181.
- [11] Little D.N., Nair S., "Recommendation Practice for Stabilization of Subgrade Soils and Base Materials." NCHRP Document no. 144 web-only, 2009.
- [12] Degirmenci N., Okucu A., Turabi A., „Application of phosphogypsum in soil stabilization.", Building and Environment, Vol. 42 (9), 2007, pp. 3393-3398.
- [13] Poon C.S., Qiao X.C., Chan D., "The cause and influence of self-cementing properties of fine recycled concrete aggregates on the properties of unbound sub-base.", Waste Management, Vol. 26(10), 2006, pp. 1166-1172.
- [14] Araya A.A., "Characterization of Unbound Granular Materials for Pavements" PhD Delft, 2011.
- [15] Arm M., "Self-cementing properties of crushed demolished concrete in unbound layers: results from triaxial tests and field tests.", Waste Management Vol. 21(3), 2001, pp. 235-239.

## USE OF WIRE EXTENSOMETERS FOR MONITORING PAVEMENT PERFORMANCE IN AREAS OF SLOPE INSTABILITY

J. N. Kirjan<sup>1,2</sup>, D. F. Marks<sup>2</sup> and J.S. Shiau<sup>1</sup>

<sup>1</sup>Faculty of Health, Engineering & Sciences, University of Southern Queensland, Australia; <sup>2</sup>Department of Transport and Main Roads (TMR), Queensland, Australia.

### ABSTRACT

Geotechnical instrumentation has been widely used as the basis of early-warning monitoring systems that detect the impending failure of slopes, embankments dams and road pavements. In conjunction with remote wireless data acquisition systems, geotechnical instrumentation provides an invaluable risk management tool and enhances safety for road users. This paper outlines the investigation, design and installation of an instrumentation system for undertaking near real-time monitoring of a road pavement adjacent to an unstable slope located in Central Queensland, Australia. The arrangement of the monitoring schedule and alert protocols for the system are also discussed. The monitoring system provides data that is used to analyse ground movements and provides an alarm system to notify personnel of any road surface deformations that may impose a risk to road users. A system of 3 wire extensometers and a weather station, connected to satellite telemetry was installed on the remote site. The wire extensometer system provides a unique solution to the requirement for a reliable early-warning system on remote sites. The proven success and reliability of the system has provided a cost effective alternative to traditional instrumentation systems for monitoring pavements in the vicinity of unstable slopes.

*Keywords: Instrumentation, Early-warning system, Slope instability, Pavements.*

### INTRODUCTION

Slope instability can be one of the major causes of premature road pavement failure. These instabilities have the potential to cause costly damage to pavements and property as well as injury or loss of life. Much research has been undertaken into suitable systems and methodologies for mitigating the risks associated with unstable slopes and road pavements. One such methodology is the installation of instrumentation in the vicinity of the slope or the pavement itself. These systems can provide an early warning to any imminent failures, so remedial action can be taken.

Reference [1] states that slope stability monitoring involves selecting certain parameters and observing how they change with time. The two most important parameters are groundwater levels and displacements. Displacements may be characterised by depth of failure plane, direction magnitude and rate.

There are various types of instrumentation systems available for measuring the above parameters. These range from devices that measure surface movements such as simple survey monuments, to complex networks of strain gauges imbedded in the road pavement itself. Devices that measure groundwater levels also range from the very simple, such as observation bores, to complex, such

as remotely monitored networks of vibrating wire piezometers.

Over the years, the advancement in telecommunications systems, particularly the mobile network has paved the way for new and innovative remote monitoring systems. It is now possible for the collection of near real-time data anywhere on the planet. This advancement means that instrumentation has become a feasible risk management strategy in managing road pavement safety and performance in areas of slope instability.

This paper describes the implementation of a near real-time early warning system consisting of a network of wire extensometers coupled with a satellite telemetry system

### SITE HISTORY

During open cut mining operations on the western wall of the mine, small to large slips have occurred. The largest being in September 2000, and another in December 1999. Reference [2] states that the September 2000 failure appears to have occurred by slipping down a low strength faulted area in the western wall of the mine, with sub-horizontal shearing through approximately 40 m thickness of rock at the toe of the excavation. Reference [2] also states that the major factors in the development of the rock slide were considered to be the presence and low strength of material contained in the zone of the

western wall faulted zone, and the elevated groundwater pressures in this zone. Additional pressure relief drain holes were drilled in the lower west wall as a consequence of the September 2000 failure, and the mine was forced to cut back operations in this area [2]. It is also a point of interest that the September 2000 failure was preceded by cracking in the mine haul road.

According to Reference [2], on the evening of 18 July 2005, mine staff reported cracking in the road pavement, adjacent to the south-west wall. The total length of this cracking now extends over 100 m of the roadway, and at the closest point, the crack is only 50 m from the crest of the mine open cut pit (see Fig. 1 & Fig. 2). Geotechnical specialists were engaged, and recommendations were made to immediately seal the cracking and install survey monitoring prisms in this area in order to monitor possible ground movements.



Fig. 1 Location of cracking on the roadway in relation to the mine.



Fig. 2 Cracks on the roadway sealed with bitumen.

Although the survey data gathered from the prisms has provided some evidence that significant horizontal ground movement may be occurring, a site visit by TMR personnel highlighted some serious deficiencies in the installation of the prisms

themselves, which could possibly compromise the integrity of the data.

Reference [3] also highlight the shortfalls of the prism survey, and states that to date they have displayed a number of deficiencies, including occasional anomalous readings, significant gaps between readings (when instruments require repair) and finally, the display of erratic variations ( $\pm 5$  to 10 mm).

In summary, the survey prisms had shown some insight into the possible mechanism and magnitude of surface movements due to the unstable mine slope, and this was enough to warrant further and ongoing investigation as there is a significant risk to road users. However, the prism survey is a somewhat unreliable method of monitoring in its current condition, so this was a major motivation for TMR to investigate more reliable and accurate methods of monitoring the site.

## MONITORING SYSTEM DESIGN & INSTALLATION

Several types of instrumentation were considered as the basis of an early-warning monitoring system. These included FBG strain sensors, soil strainmeters and inclinometers. The type of instrument and the installation arrangement with respect to data acquisition and ongoing monitoring were critical factors in the selection of an appropriate system.

After careful consideration, wire extensometers were selected as the basis of the monitoring system as they had a number of advantages over the instruments mentioned above, most importantly they could be installed without any disturbance to the pavement surface.

### Wire Extensometers: Operating Principle

The wire extensometer, also known as a linear displacement transducer, is an instrument which enables the monitoring of a change in distance between two points. Typical applications of the wire extensometer include measurements of large displacements associated with landslides, monitoring rock-masses and surveying earth faults [3].

The device consists of an enclosure, in which a displacement transducer is housed. A long cable or wire is attached to the transducer at one end, and is placed under tension spanning the desired area. The end of the cable is attached to an anchor. Any movement between the anchor and the transducer unit will alter the output signal from the transducer, from which the displacement can be determined.

Reference [3] also state that their device has a sensitivity of 0.03 mm, an accuracy of  $\pm 1$  mm and a measurement repeatability of  $\pm 0.03$  mm.

## System Design

It was proposed that the instrumentation would be installed in three locations, two locations spanning the road pavement, and one location spanning the projected failure zone extended from the western wall of the mine. Each instrument would span around 35 metres, so this would easily enable the full width of the pavement to be monitored.

The instruments spanning the road pavement would be installed by means of horizontal boring under the road pavement, terminating at pits at either end for the anchor and wire extensometer transducer. The instrument spanning the cracking in the mine area could be installed by excavating a trench terminating at pits at either end.

Within the pits, concrete filled steel bollards would be installed extending below the base of the pits in order to provide a solid datum for the sensor and anchor ends of the installations. Adjustable brackets were designed and fabricated to allow the transducer to be mounted as high as possible within the pits. This is to help protect the devices from any

water ingress inside the pits. A cross-section of the instrumentation arrangement is shown in Figure 3 (below).

It was decided that temperature sensors would also be installed in the wire extensometer pits in order to monitor possible effects of thermally induced strains on the extensometer wires.

In addition, a weather station would also be included in the installation so accurate rainfall measurements could be undertaken. This could be easily connected to the chosen data acquisition system, therefore it would provide an important part of the early-warning monitoring system. The weather station selected was the Vaisala WXT520 weather station.

The telemetry and data acquisition system selected was a Campbell Scientific CR1000 data logger coupled with a Hughes BGAN 9502 satellite modem.

Finally, in order to provide a safe location for the telemetry and data acquisition system, a custom 8m tall mid hinged pole was designed and fabricated.

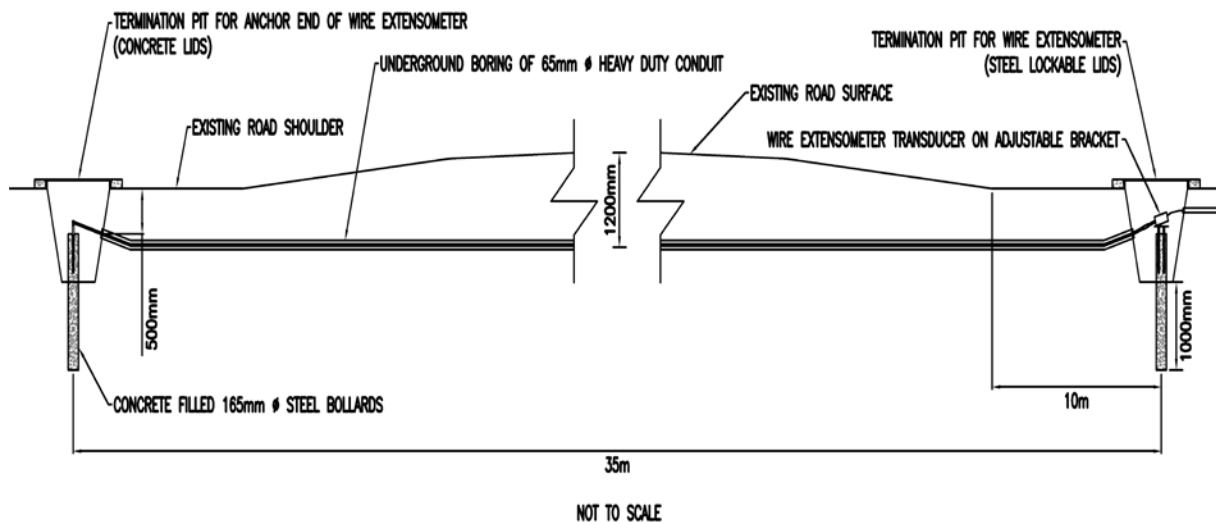


Fig. 3 Cross-section of instrumentation arrangement.

## Installation

The various components of the system were installed in two stages. The first stage involved the ground works, including excavation and directional boring, as well as the installation of bollards, brackets and communications pits. The final part of this stage was the installation of the footing cage for the hinged pole foundation.

The second stage of the installation involved the installation of the wire extensometers, weather station and associated hardware and wiring. The hinged pole was also installed along with the associated logging and data transmission hardware.

### Stage 1

Before the directional boring could commence, the locations were marked out carefully. Once the pits had been marked out, the pits were excavated and the drilling was undertaken, and the pits, bollards and brackets were then installed. Each pit was finished with concrete edging and lockable steel lids were also installed on the live end pits.

### Stage 2

The wire extensometers were then installed along with the communications pole and telemetry and data



logging system. During this stage, temperature sensors were also installed in the pits.

The wire extensometer and temperature sensor cables were then connected to the data logger. The devices were then calibrated and a function test was undertaken. Figures 4, 5 & 6 show selected completed components of the system.



Fig. 4 Live end completed installation.



Fig. 5 Completed installation showing logger box (bottom), satellite antenna (mid), weather station and solar panel (top).



Fig. 6 Telemetry system showing data logger, modem, power management and batteries.

## DATA ACQUISITION AND PRESENTATION

### Data Acquisition

The following section explains the 5 step processes involved in transferring the data from the instrument to the end user.

#### 1. Data logging

The Campbell Scientific CR1000 logger is programmed to collect data from the wire extensometers, weather station and temperature sensors every hour. The data is stored in the logger's memory until an upload is triggered.

#### 2. Data transmission

Every 3 hours, a relay is triggered to power the Hughes 9502 satellite modem. The satellite modem is connected to the CR1000 by a Campbell Scientific NL120 mounted on the CR1000 peripheral port. The satellite modem then makes a connection to the server and transfers data to the server through a File Transfer Protocol (FTP).

#### 3. Web server

In the web server, the software utility 'Cron' is running every minute to check for files that have been sent to the server. Cron is a software utility used to schedule activities at certain times. If a file is found, the Cron utility will execute a PHP script on the server. The PHP script will extract the file and compare the raw data values with the pre-defined trigger levels.

#### 4. Triggers and alerts

If any trigger values are found, an email will be sent via the SMS Gateway. The SMS Gateway will then convert the email to a SMS message. Finally, all data will then be saved to the server where it can be accessed remotely by registered users.

#### Data Presentation and Alarm Triggers

Upon successful log-in to the web server, the user is presented with a page which displays the most recent data from the wire extensometers, temperature sensors and weather station. This page is shown in Fig. 7.

Data plots for all devices can be accessed by selecting the appropriate date range through the device summary page. As an example, a plot for device WE2 is shown in Fig. 8 for the specified date range shown in the top left hand corner. Note that this plot displays a slight increase in displacement from late January 2013. This movement was attributed to

settlement of the pits and conduits after a period of heavy rainfall. The large data spikes are due to function tests undertaken on the devices during scheduled maintenance.

This plot also displays the trigger level thresholds for movement recorded by the extensometers, and is depicted by the red and amber lines on the plot. The trigger level threshold for the amber alert has been set at 25mm and the red alert threshold at 100mm. In addition to movement trigger levels, trigger levels for rainfall have also been defined. The amber alert rainfall trigger is set at >50mm and 125mm of rainfall in any 24 hour period will trigger a red alert.

As explained previously in the data acquisition process, when either trigger level is reached, SMS and email alerts will be sent by the system to key personnel. The actions to be undertaken upon receipt of alerts are detailed in the Site Emergency Management Plan. Receipt of an amber alert will prompt an immediate site inspection, and the receipt of a red alert will initiate an emergency site inspection a possible road closure.

**QUEENSLAND GOVERNMENT**

Monitoring Configuration FAQ

Jeremy Kirjan

[Help](#)
[Log Out](#)

Site:

Instrument Name	Last Reading
Battery	13/7/2014 18:10:00 Bat. Volt:12.63 Panel Temp. (Deg. Celcius):25.3
Rain Gauge	13/7/2014 18:10:00 Accumulated Rain Fall to present (24 h, mm): 0.00 Accumulated Rain Fall since midnight to present (mm): 0.00 Rain Fall intensity last 10 minutes (mm/h): 0.00 Rain Fall duration last 10 minutes (seconds): 0 Hail Intensity last 10 minutes (hits/cm2h): 0.00
Temperature	13/7/2014 18:10:00 Air Temperature (celcius): 20.6 Relative Humidity (%RH):22.5 Air Pressure (hPA):979.9
WE1 - Temperature	13/7/2014 18:10:00, Temperature (deg. Celcius):20.9
WE1 - Wire Extensometer	13/7/2014 18:10:00, Lateral Movement(mm):1.1
WE2 - Temperature	13/7/2014 18:10:00, Temperature (deg. Celcius):20.7
WE2 - Wire Extensometer	13/7/2014 18:10:00, Lateral Movement(mm):10.4
WE3 - Wire Extensometer	13/7/2014 18:10:00, Lateral Movement(mm):6.8
WE3 - Temperature	13/7/2014 18:10:00, Temperature (deg. Celcius):23.2
Wind	13/7/2014 18:10:00 Direction Avg (degrees): 269.00 Speed Min (m/s): 0.20 Speed Avg (m/s): 0.80 Speed Max (m/s): 1.60

iGEM ver. 2.0 - Copyright [Geotesta Pty. Ltd.](#), 2009

Fig. 7 Web server summary page showing most recent data for all devices.

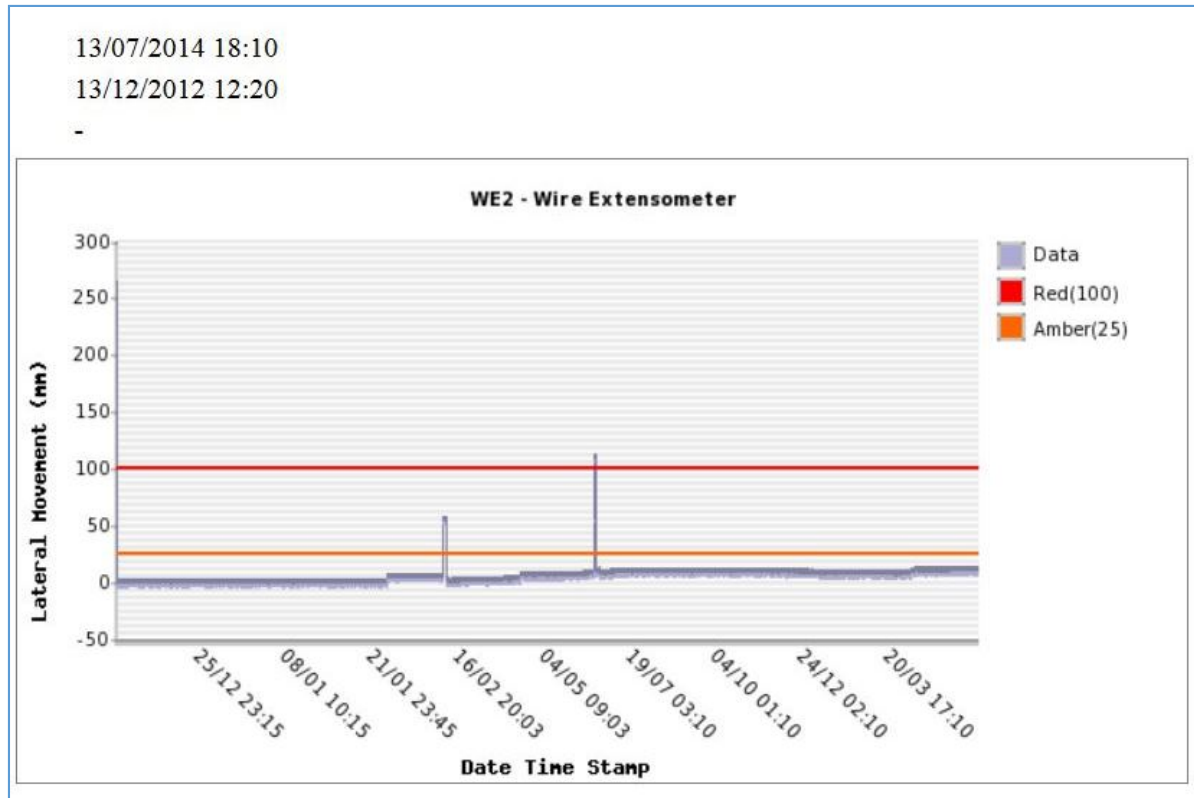


Fig. 8 Plot of data output from WE2.

## CONCLUSION

The wire extensometer early-warning instrumentation system has provided a unique solution to the risk management of the site. It should be considered as a viable alternative over conventional types of instrumentation for undertaking monitoring of road pavements or other structures which are prone to cracking and failure due to slope instability.

The fact that the system can be installed without any disruption to traffic should be considered as a key advantage of wire extensometers, as well as the ease of setup, access for maintenance and relatively low cost in comparison to the identified alternatives. The use of a mid-hinged pole as the base for the system communications is ideal for use in remote locations, as it provides protection from bushfire and vandalism while still allowing hassle-free access to the hardware for maintenance purposes.

## ACKNOWLEDGEMENTS

The authors would like to thank TMR Northern Region, in particular Cheryl Ridd, for the opportunity to undertake this project, also the staff from Geotesta for their ongoing assistance and technical support.

## REFERENCES

- [1] Kane, WF & Beck, TJ 2000, Instrumentation Practice for Slope Monitoring, Engineering geology practice in Northern California. association of engineering geologists Sacramento and San Francisco sections, viewed 31 May 2013, <<http://www.iti.northwestern.edu/tdr/publications/ipfsm.pdf>>.
- [2] Coffey Geotechnics 2011a, Report GEOTGARB00881AA-AG to Department of Transport and Main Roads, QLD, Coffey Geotechnics.
- [3] SISGEO 2011, Wire Crackmeter Datasheet, viewed 17 September 2013, <[http://www.sisgeo.com/wpcontent/uploads/2011/03/D241\\_EN\\_01Wire\\_Crackmeter.pdf](http://www.sisgeo.com/wpcontent/uploads/2011/03/D241_EN_01Wire_Crackmeter.pdf)>.
- [4] Bassett, R 2012, A Guide to Field Instrumentation in Geotechnics: Principles, Installation and Reading, Spon Press, New York.
- [5] Dunnicliff, J 1988, Geotechnical Instrumentation for Monitoring Field Performance, Wiley Interscience, Canada.

## **GENERATION AND DISSIPATION OF PORE WATER PRESSURE NEAR TO PILE AND FAR-FIELD IN LIQUEFIABLE SOILS**

Suresh R Dash<sup>1</sup>, Subhamoy Bhattacharya<sup>2</sup>, Atul Prabhakaran<sup>3</sup> and C. Sreenivasulu<sup>4</sup>

<sup>1</sup>Assistant Professor, IIT Bhubaneswar, India

<sup>2</sup>Professor in Geomechanics, University of Surrey, UK

<sup>3,4</sup>UG Student, IIT Bhubaneswar, India

### **ABSTRACT**

The degree of liquefaction as characterised by the excess pore water pressure plays an important role in defining soil strength and stiffness. The pile-soil interaction, if modelled using BNWF model, the strength and stiffness of the soil spring can suitably be reduced by using a reduction factor. This reduction mainly depends on the soil type, its SPT/CPT value and the degree of liquefaction. Ideally this reduction should be based on the excess pore water pressure near the pile. However, it is difficult to estimate the degree of liquefaction near the pile. Hence, the lateral resistance of liquefied soil at soil-pile interface is normally characterized by the degree of liquefaction expected in the soil at the site without considering the influence of pile.

Though, excess pore pressure near to the pile could be the governing parameter of soil resistance, it is hard to characterize the expected value of it in a field condition, as it depends on many parameters including soil type, shear loading, pile dimension, gap formation near to pile that facilitates easy dissipation of EPWP, soil densification during pile driving, etc. Hence, to understand the difference between the far-field and near-pile response of liquefied soil, one high quality centrifuge test results are studied in this paper. The pattern of excess pore water pressure generation and development has been compared for both near-pile and far-field. The results are critically reviewed and discussed in this paper.

*Keywords: Pile foundation, Liquefaction, Pore water pressure, Earthquake*

### **INTRODUCTION**

Pile foundations are long slender structural elements mostly used for foundations in weak soils, including seismically liquefiable areas. It is routinely used to support foundations bridges and high rise buildings where the loads are very high and the top soil is weak.

To define strength and stiffness of liquefied soil, the degree of liquefaction as characterised by the excess pore water pressure plays an important role. The pile-soil interaction, if modelled using BNWF model, the strength and stiffness of the soil spring can suitably be reduced by using a reduction factor. This reduction mainly depends on the soil type, its SPT/CPT value and the degree of liquefaction. Ideally this reduction should be based on the excess pore water pressure near the pile. However, as it is difficult to estimate the degree of liquefaction near the pile, the strength and stiffness of the liquefied soil at soil-pile interface is normally characterized by the degree of liquefaction expected in the soil at the site without considering the influence of pile [1].

It is often observed that the excess pore water pressure close to pile stays lesser than that occurs at free field for similar shear loading ([2], [3]) in 1g

model tests. Several centrifuge tests have also been carried out by [4] and [5] to study the effect of structure on liquefaction potential of the underlying soil, which showed that the pore water pressure built-up was quicker at free field than below the structure. Few field cases has also been reported by [6] and [7], which suggest apparent increase in liquefaction resistance due to the presence of structure. In contrast to the above observation, Liu and Quio [8] have suggested that the conditions for liquefaction are worse near to a structure than free field, based on a back-calculated damage investigation following Tangshan, China earthquake of 1976.

Although, it is expected that the liquefaction behavior of soil at far field (i.e., free field behaviour) and near field (close to structure behavior), the exact difference and their influence is very uncertain and depends on many site conditions. For pile foundation design, some researchers suggests to consider zero strength and stiffness of the liquefied soil [9], whereas, many other researchers [10], [11], believes that the liquefied soil bears certain strength and stiffness which shall be considered in pile foundation. The codes of practice of various countries does not say anything in this regard.

Sticking to any one of the two conditions as listed above, the design in some cases may become un-

conservative. For example, while calculating the buckling strength of pile in liquefiable soil, considering the strength of liquefied soil as 30% that of overburden (as per JRA 2000 [12], which specified the bending calculation due to lateral spreading of liquefied soil, see Fig. 1) may grossly overestimate the buckling load, making the design un-conservative.

Similarly, when modelling the lateral spreading of liquefied soil, considering zero strength of liquefied soil may underestimate the bending moment in pile, as the liquefied soil subjected to very large strain offers resistance due to particle interlocking.

Hence, it would be prudent to consider the strength and stiffness of the liquefied soil suitably to make the design conservative.

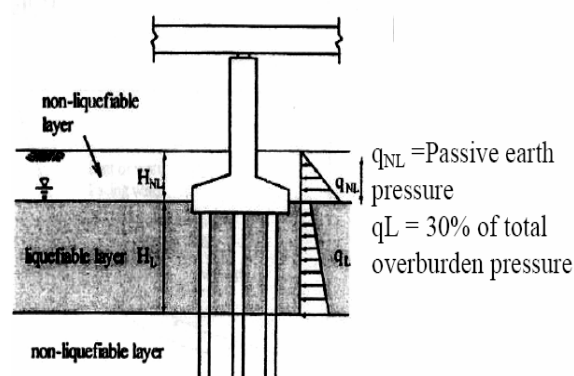


Fig. 1 Strength of liquefied soil as suggested by JRA (2000).

Therefore, to understand the difference between the far-field and near-pile pore water pressure behavior for pile-soil interaction in liquefiable soils and its implication in lateral strength of liquefied soil, a high quality centrifuge test results are studied in this paper. The pattern of excess pore water pressure generation and development has been compared for both near-pile and far-field. The pore water pressure measured very close to pile is termed as near-pile measurement, and the measurements those are done more than  $D$  distance from pile is termed as far-field measurement, where  $D$  is the diameter of the pile. The results are critically reviewed and discussed in this paper.

## EXPERIMENTAL SETUP OF PILE IN LIQUEFIABLE SOILS

A high quality centrifuge test data is used in this paper to study the near and far field pore water pressure response during seismic vibration.

The centrifuge test was carried out in the centrifuge facility Shimizu Corporation, Japan. The tests was carried out at centrifugal acceleration of 30-g. The stress and strain parameters were modelled by a factor of unity and the linear dimensions by the scale factor of 1:  $n$  (model: prototype), where  $n = 30$ .

The scaling parameters related to the centrifuge tests at centrifugal acceleration of  $n$ -g are presented in Table-1.

Table-1: Scalling laws for centrifuge modelling at  $n$ -g.

Parameters	Unit	Model / Prototype
Stress	$ML^{-1}T^{-2}$	1
Strain	--	1
Length	L	1/n
Time (Dynamic)	T	1/n
Acceleration	$LT^{-2}$	N
Seepage velocity	$LT^{-1}$	N
Pile bending stiffness	$ML^{-3}T^{-2}$	$(1/n)^4$
Natural frequency	$T^{-1}$	1/n

A laminar box was used in the test, which had 14 rectangular frames made up of square steel tubes. The frames were connected by thin linear bearings of 2mm thickness placed in between them. The inside of the container was lined with a 1mm thick rubber membrane for waterproofing of the box and to protect the bearings from soil. The inside dimensions of the box were 807mm long, 475mm wide and 324mm high.

## Test Layout

The model scale test setup used here is shown in Fig 2. For this centrifuge test, two pile groups were modelled on each side (side A and Side B) of the central partition wall. This kind of setup was beneficial in modelling both pile groups with the required soil/ structural parameter variation while keeping all other model parameters exactly same.

In this test setup, the free end quay wall was modelled near to one end of the container to simulate the soil flow condition (i.e. lateral spreading). In each of the tests, both the pile groups (A and B) were subjected to nearly identical conditions with respect to input motions and soil liquefaction.

Steel pipe of outer diameter 10mm and wall thickness of 0.2mm is used as pile in the test. Four layers of soil was placed in the test box, where top soil (soil-1) was unsaturated and all other three soils are saturated. The second layer of soil (soil-2) was prepared as medium loose saturated sand, which liquefied during the test. The pile was initially fixed to the bottom of the box. Four layers of soil were then filled in the box with required relative densities. The geotechnical properties of the sand layers are provided in Table-2.

The model was subjected to a varying magnitude base acceleration of a 60 Hz sine wave (2 Hz at prototype scale). The magnitude of base acceleration was gradually increased to make the liquefaction process more realistic, which went up to  $\sim 8g$  in 0.25s. This allowed the soil to liquefy in 5-6 cycles of



loading in the model. The base acceleration input in prototype scale is shown in Fig 3.

Table 2 Geotechnical properties of the sand used in the test

Item	Soil-1	Soil-2	Soil-3	Soil-4
Soil Type	Silica Sand-8	Silica Sand-8	Toyoura Sand	Silica Sand-3
$e_{max}$	1.385	1.385	0.951	0.974
$e_{min}$	0.797	0.797	0.593	0.654
$D_r$	50	50	90	90
$\gamma'$	12.85	7.652	9.908	9.496
	( $\gamma_t$ )			
$S_r$	10	100	100	100

**Note:**  $e_{max}$  and  $e_{min}$  = Maximum and minimum void ratio,  $D_r$  = Relative Density (%),  $\gamma'$  = Effective unit weight ( $\text{kN/m}^3$ ),  $\gamma_t$  = Dry unit weight ( $\text{kN/m}^3$ ),  $S_r$  = Saturation Ratio.

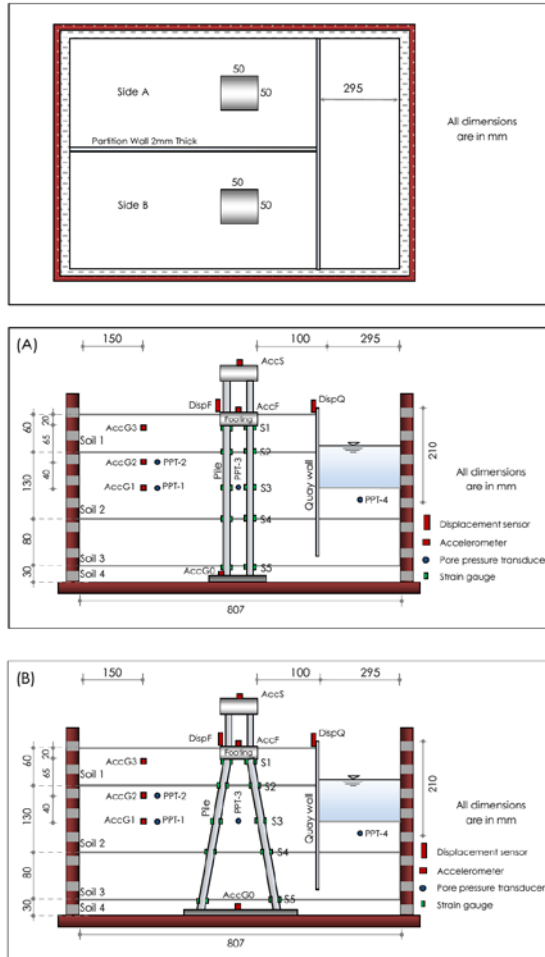


Fig. 2 Centrifuge test layout for pile foundation in liquefiable soils.

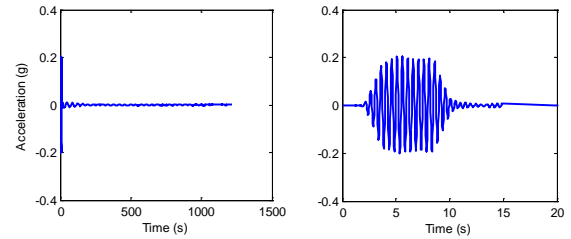


Fig.3 Base acceleration input in the centrifuge test

## OBSERVATION OF LIQUEFACTION FAR FIELD AND NEAR THE PILE

The near pile pore pressure observation was made behind the pile during the test. The value of EPWP, being a stress parameter, remains same for both prototype and model scale measurement in the centrifuge test. But, the time axis changes with a scale of 1 : n (model : prototype). The results here are presented in prototype scale.

Fig.4 shows the excess pore water pressure recorded near to the pile and far field for vertical piles (Side-A). It has been observed that the pore water pressure generation is slower near the pile foundation as compared to far field. The pore water pressure ratio for these two cases are also plotted in Fig.5. The soil near to pile took long time (10s) to reach full liquefaction, whereas the soil at same depth in free field fully liquefied at in (5s). This could be due to the availability of dissipation path at the pile-soil interface, which prevents the built up of pore water pressure. Hence it takes more time for the soil to fully liquefy near the pile in comparison with far field.

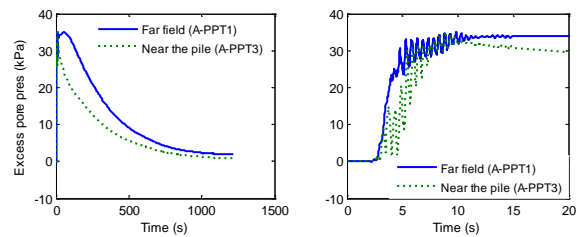


Fig. 4 Comparison of excess pore water pressure near to the pile and at the far field in Side-A model (Vertical pile group).

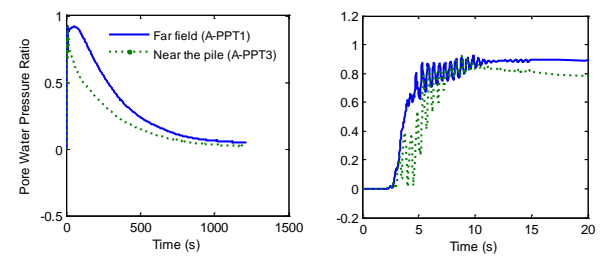


Fig. 5 Comparison of pore water pressure ratio near to the pile and at the far field in Side-A model (Vertical pile group).



Similar behavior has also been observed for inclined pile group (Side-B) as can be seen in Fig. 6.

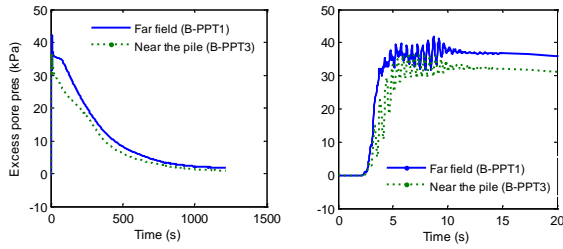


Fig. 6 Comparison of excess pore water pressure near to the pile and at the far field in Side-B model (Inclined pile group).

The pore water pressure ratio for inclined pile group is plotted in Fig. 7 for both near to pile and far field. It is clearly evident that even at the same depth, the soil close to the pile could not fully liquefy, but at free field full liquefaction has been observed. There is a slight overshooting of the pore water pressure ratio above 1. The maximum value of pore water pressure ratio should be 1, as this corresponds to fully liquefaction. However the observance of overshooting of this value can be attributed to (1) the actual effective stress at the measuring location might be more than the calculated value due to densification, and/or (2) settlement/dislocation of pore water pressure sensor during the test.

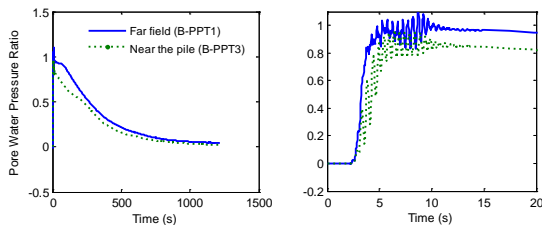


Fig. 7 Comparison of pore water pressure ratio near to the pile and at the far field in Side-B model (Inclined pile group).

Fig. 8 compares the excess pore water pressure near the pile for straight (Side-A) and inclined (Side-B) pile group. This figure shows that for inclined pile group the pore water pressure generation is slower than that of vertical pile group. This is because, the presence of pore pressure dissipation path is smaller in vertical pile group as compared to longer inclined path in inclined pile group.

The lateral resistance of soil at pile-soil interface has been estimated from the strain gauge reading at different depths of the pile. This lateral soil resistance with respect to soil-pile relative deformation is generally known as  $p$ - $y$  curves. The detailed procedure of estimating  $p$ - $y$  curves for this test can be referred in Dash (2010).

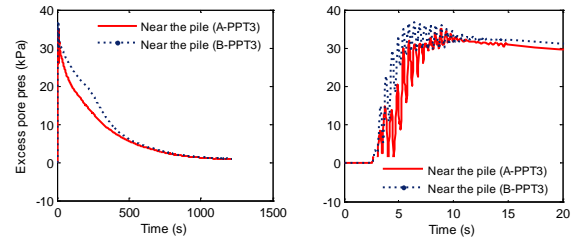


Fig-8 Comparison of excess pore water pressure near the pile for vertical (Side-A) and inclined (Side-B) pile group.

Fig. 9 shows the lateral soil resistance - displacement behavior ( $p$ - $y$  curves) at different times during the test. Viewing Fig. 9 in conjunction with Fig. 4 and 5 shows that the resistance of liquefied soil subjected to shear was partly attributed from the decrease in EPWP. This behaviour is similar to that observed in the laboratory element tests during monotonic shearing of liquefied soil, for example: Yasuda et al., 1999, 1998; Sitharam et al., 2009. In the initial phase of loading, free field pore water pressure reached a maximum value (that corresponds to effective stress = 0) in 3 to 4 cycles. But near to the pile, development of pore water pressure was dependent on pile vibration, and in each cycle the pore water pressure dissipation was also happening due to the availability dissipation path at soil-pile interface.

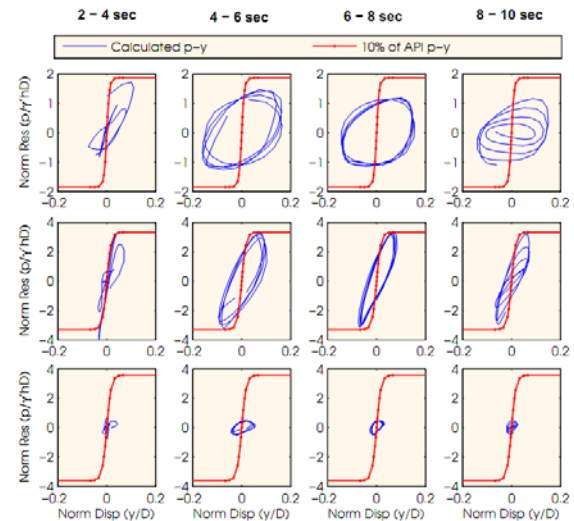


Fig. 9  $p$ - $y$  curves at different time range during test

Though, excess pore pressure near to the pile could be the governing parameter of soil resistance, it is hard to characterize the expected value of it in a field condition, as it depends on many parameters including the soil type, shear loading, pile dimension, gap formation near to pile that facilitates easy dissipation of EPWP, densification of the soil close to pile during pile driving, etc. Hence, the lateral resistance of liquefied soil at soil-pile interface is normally characterized by the degree of liquefaction expected in the soil at the site without considering the

influence of pile.

Hence, the lateral strength of liquefied soil (i.e., its  $p$ - $y$  behavior) has to be suitably chosen to make the design safe and conservative.

## CONCLUSION

The response of soil for possible near field and far field liquefaction of soils is different with variation in both depth and the spread. Design codes prove ineffective in analyzing possible modes of failure while over estimating other modes. The following recommendations may be followed for a conservative design of pile foundations in liquefiable soils.

While estimating the natural time period of the structure, the pile should be considered an integral part of the structure with the soil considered as zero strength at full liquefaction to full non-liquefied strength at no liquefaction to check the possible variation of the fundamental time period of the structure during an earthquake.

Where there is a possibility of the structure's natural time period transiting and falling within the predominant time period of the earthquake, possible effect of resonance shall be considered in the design. The liquefied strength shall be considered in such a way that the worst effect of resonance is observed.

For lateral spreading, loads on the pile foundations is larger. Thus a representative fraction of the non-liquefied strength can be considered, e.g., JRA 2002 code assumes 30% of overburden as the lateral pressure on pile for liquefiable soil flow.

While designing for possible buckling, lateral confinement is an important parameter and it may be conservatively assumed that liquefied soils offer no lateral resistance.

## ACKNOWLEDGEMENTS

The centrifuge data provide by Late Prof. Takashi Tazoh (Japan) of Shimizu Corporation is greatly acknowledged.

## REFERENCES

- [1] Rollins KM and Seed B, "Influence of Building on Potential Liquefaction Damage", J. of Geotechnical Engineering, Vol. 116, No. 2, Feb 1990, pp. 165-185.
- [2] Ishihara K and Matsumoto, "Bearing Capacity of Saturated Sand Deposits during Vibration", Proc. 4<sup>th</sup> Japan Earthquake Engineering Symposium, Tokyo, Japan, 1976, pp-431-438.
- [3] Yoshimi YK and Tokimatsu K, "Two Dimensional Pore Pressure Changes in Sand Deposits during Earthquakes", Proc. 2<sup>nd</sup> Int. Conf. on Micro-zonation, National Science Foundation," Vol. 2, 1978, pp. 853-863.
- [4] Whitman RV and Lambe PC, "Liquefaction: Consequences for a Structure", Soil Dynamics and Earthquake Engineering Conf., Southampton University, Vol.2, 1982, pp- 941-949.
- [5] Takemura J, Imamura S and Takashi Y, "Stability of Oil Tank Supported by Piled-Raft Foundation on Liquefiable Sand", Proc. of Sixth International Conference on Urban Earthquake Engineering, March 3-4, 2009, Tokyo, Japan
- [6] Watanabe T, "Damage to Oil Refinery Plants and a Building on Compacted Ground by the Niigata Earthquake and their Restoration", Soils and Foundation, Vol.15 No.3, 1966, pp. 27-40.
- [7] Ishihara K, Kawase Y, Nakajima M, "Liquefaction Characteristics of Sand Deposits at an Oil Tank Site during 1978 Miyagiken-Oki Earthquake", Soils and Foundation, Vol.20, No. 2, 1980, pp. 97-111.
- [8] Liu H and Quio T, "Liquefaction Potential of Saturated Sand Deposits Underlying Foundation of Structure", 8<sup>th</sup> World Conf. on Earthquake Engineering, Vol. 3, 1984, 199-206.
- [9] Bhattacharya S, "Pile instability during earthquake liquefaction", PhD thesis, University of Cambridge, UK, 2003.
- [10] Goh S, O'Rourke TD, "Limit state model for soil-pile interaction during lateral spread", Proc. of seventh US-Japan Workshop on Earthquake Resistant Design of Lifeline Facilities and Countermeasures against Soil Liquefaction, Seattle, 1999. p. 237-260.
- [11] Abdoun T and Dobry R, "Evaluation of Pile Foundation Response to Lateral Spreading", Soil Dynamics and Earthquake Engineering, Vol.22, No. 9-12, 2002, pp. 1051-1058.
- [12] JRA. Specifications for highway bridges, part V. Seismic design, 1996.
- [13] Dash SR, "Lateral Pile Soil Interaction in Liquefiable Soils", PhD Thesis, 2010, University of Oxford.
- [14] Yasuda S, Terauchi T, Morimoto M, Erken A and Yoshida N, "Post liquefaction behavior of several sands", Proc. of 11<sup>th</sup> European conference on Earthquake Engineering, Balkema, Rotterdam, 1998.
- [15] Yasuda S, Yoshida N, Kiku H, Adachi K and Gose S, "A simplified method to evaluate liquefaction-induced deformation", Proc. of Earthquake Geotechnical Engineering, Balkema, Rotterdam, 1999, pp. 555-566.

## A COMPARATIVE STUDY ON THE RESISTANCES OF BUCKET FOUNDATION IN SAND WITH DIFFERENT INSTALLATION METHODS

Ju-Hyung Lee<sup>1</sup>, Jin-Ung Do<sup>2</sup> and Sung-Ryul Kim<sup>3</sup>

<sup>1</sup>Senior Researcher, Geotechnical Engineering Research Div., Korea Institute of Construction Technology, Republic of Korea; <sup>2</sup>Research Specialist, Geotechnical Engineering Research Div., Korea Institute of Construction Technology, Republic of Korea; <sup>3</sup>Associate professor, Dept. of Civil Engineering, Dong-A Univ., Republic of Korea

### ABSTRACT

Model tests have been performed to investigate the vertical, horizontal and cone tip resistances of bucket foundations embedded in sand with different installation methods; suction force by pump and jacking force by actuator. Micro-cone penetrometer was used to evaluate the variation of the effective stress inside pile after model pile installation. As a result, in vertical pull-out test, the pile installed jacking force method shows 3 times larger resistance than installed suction force method. In horizontal pull-out test, the ultimate horizontal capacity and the slope of load-displacement curve for the model pile installed by suction force were decreased by 22% and 40% respectively compared to the pile installed by jacking force. In cone penetration test, inside cone tip resistance of the pile installed by suction force shows about 40% smaller than that installed by jacking force. It is because the effective stress was reduced due to upward seepage of inner pile in sand by suction force. Therefore, we can see that the effect of installation method on bucket foundation has to be considered to investigate the behavior of it experimentally.

**Keywords:** Bucket Foundation, Model Test, Vertical Resistance, Horizontal Resistance, CPT

### INTRODUCTION

The suction installation of bucket foundation into sandy soils induces seepage flow from outside to inside of bucket foundation; therefore, the downward seepage near the outside of bucket pie increases the effective stress while the upward seepage inside the bucket pile decreases the effective

stress [1] (Fig. 1).

The seepage effect helps bucket pile installation by reducing the penetration resistance during the installation, on the other hand, reduces the horizontal and vertical capacity of bucket foundation from the significant disturbance at the tip of the bucket foundation. Due to the complexity and difficulty in quantification of the suction installation effects (including seepage effect), many previous researchers generally neglect the effect of suction installation in their experiments. Therefore, in this study, the effects of suction installation on the resistance of bucket pile have been examined.

### TEST METHOD

To examine the effect of suction installation on the vertical and horizontal behavior of a bucket pile, the model pile was installed both by suction force and jacking force, respectively. When installed by jacking force, model pile had been penetrated into the model ground by actuator. When installed by suction force, model pile had been penetrated by imposing suction force using venturi pump. In this regard, the size of model pile, the penetrating depth, and velocity were controlled equally. The model pile were made of aluminum pipe with 1.2 mm thickness, 60.0 mm diameter and 180.0 mm length. The size of used soil chamber is 100 mm width, 100 mm length

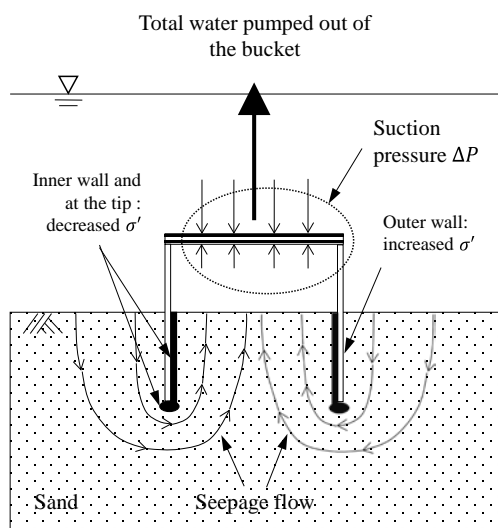


Fig. 1 Effect of seepage gradient on soil effective stress [1]

and 200 mm height. After the model pile installed, the pull-out test had been performed by using hydraulic cylinder. A displacement had been controlled as 100 mm/min [2], [3]. The vertical pull-out tests were performed after installation in 0 hour, 2 hours, 20 hours to check the set-up effect. The loading location of model piles are 67% of  $L$  ( $L = 180$  mm) from the pile top for the horizontal pull-out tests.

Joomoonjin sand from the East Sea in Korea were used in this study (Table 1). For vertical pull-out tests, the model ground was formed as 30% of relative density ( $D_r$ ) to estimate the resistance in loose state. The model ground of  $D_r$  70% was used for horizontal pull-out tests.

More details of the test program are summarized in Table 2.

Table 1 Engineering properties of Joomoonjin sand

$G_s$	$C_u$	$C_c$	$e_{min}$	$e_{max}$	USCS
2.62	1.43	0.9	0.929	0.620	SP

Table 2 Test programs for pull-out tests

Types	$D_r$	Loading point	Installation method
Vertical pull-out test	30%	Pile top	Suction / Jacking
Horizontal pull-out test	70%	67% of pile length	Suction / Jacking

For each test, a miniature cone penetration test was performed to examine the soil states of inside and outside the bucket pile. The cone penetrometer used in this study consists of 5 mm diameter of lower part and 12 mm diameter of upper part having micro strain gauge (Fig. 2).



Fig. 2 Micro cone (left) and input / output device (right)

## TEST RESULTS

### Vertical Pull-out Test

The results have been shown in Fig. 3. When comparing the maximum vertical pull-out

resistances, the initial uplift capacity shows that the piles installed by jacking force (about 30N) have about 3 times larger resistances than those installed by suction force (about 10N).

Also, the pile installed by suction force after installation in 20 hours indicates about 20% larger resistance than 0 hour. In general pattern, however, it can be concluded that the set-up effect seems insignificant in comparison with installation methods.

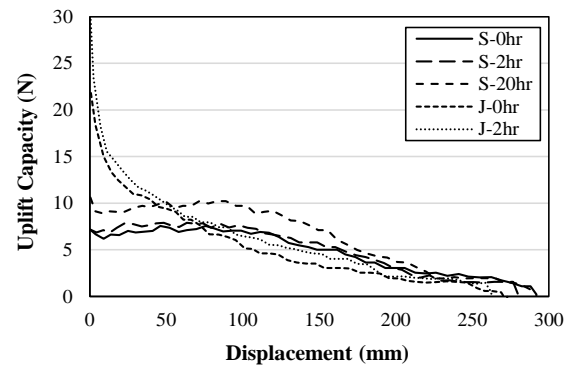


Fig. 3 Test results of vertical pull-out resistances on suction and jacked pile

### Horizontal Pull-out Test

Figure 4 shows the experimental results of the horizontally-loaded suction model piles installed by suction force and jacking force. The horizontal loading was placed at 67% from the piles' top without any loading inclination. In the Figure, the ultimate horizontal capacity and gradient (or stiffness) of "horizontal resistance-displacement curve" of pile installed by suction force were approximately 10% and 30% lower than those of pile installed by jacking force.

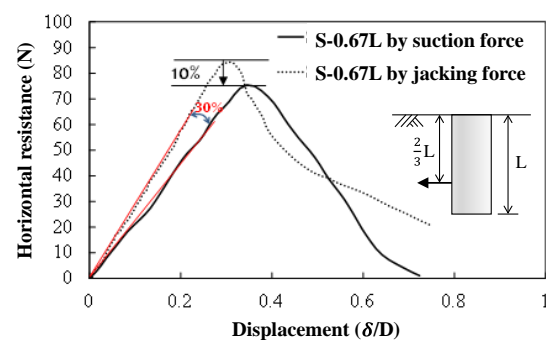


Fig. 4 Horizontal resistance-displacement curves of bucket piles installed by suction force and jacking force

### Cone Penetration Test

Like the above result, in cone penetration test (CPT), the cone tip resistance of the pile installed by

jacking force shows about 50% larger than those installed by suction force (Fig. 5).

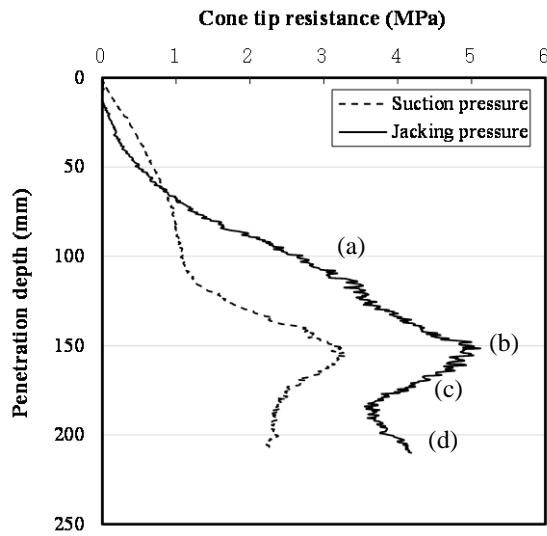


Fig. 5 Cone tip resistances on inside suction and jacked pile

In case of the pile installed by jacking force, before the micro cone escapes from the tip of the pile, the cone tip resistance just increased (Fig. 6a). But in close to the tip of the pile, the cone tip resistance suffered extremely high confining pressure by the pile wall (Fig. 6b). Sequentially, after escaping from the pile tip, the cone tip resistance rapidly decreased due to relaxation from high confining pressure (Fig. 6c). Lastly, after penetrating further, the cone tip resistance increased again due to original model ground (Fig. 6d).

In case of the pile installed by suction force, the pattern of the cone tip resistance were also almost same as Fig. 6a ~ Fig. 6c. In phase of Fig. 6d, however, the increase of resistance was not clear. The reason can be inferred due to the effect of suction installation.

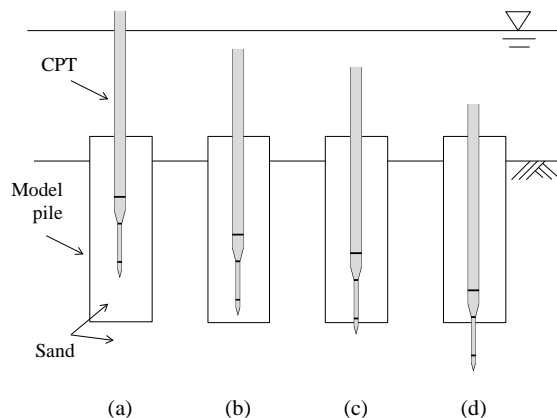


Fig. 6 Sequence of micro cone penetration

Fig. 7 represents the additional CPT results of inside and outside on bucket piles for the measurement of effective stress difference resulting from suction force. The solid and dashed lines in the figure are the CPT test results of the bucket piles installed by suction force and jacking force, respectively. The significant difference in CPT results of the inside and outside of the bucket pile results from the higher cone resistance due to the higher confinement inside of the pile wall.

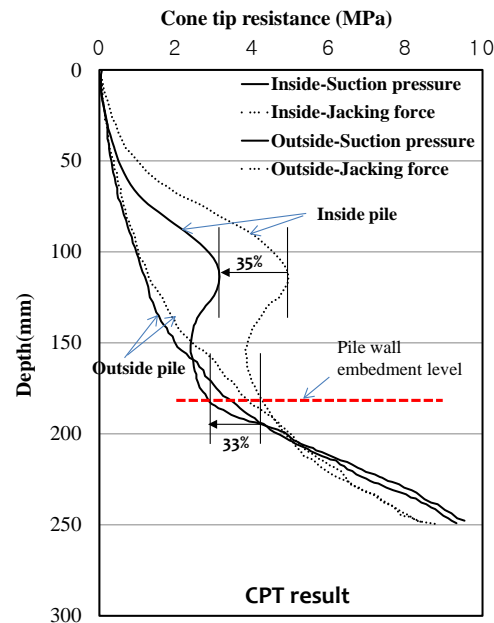


Fig. 7 CPT results of inside and outside on bucket pile by different installations

The suction installation effect on the cone resistances inside of the bucket pile is much greater than those outside of the pile. The CPT test results of outside on the bucket pile indicated that the cone resistances at depths of 100 mm and 200 mm of the jacked pile were 2% ~ 15% higher than those of the suction-installed pile. As also mentioned by [1], the downward seepage of outside on the bucket pile within dense sand (relative density approximately equal to 70%) may not increase the effective stress significantly. Contrarily, the cone resistance of inside on the suction-installed pile was 35% lower than that inside on the jacked pile. The much lower cone resistance inside of the suction-installed pile may be caused from the decreased effective stress induced by the upward seepage, as also insisted by [1]. The cone resistance at the suction-installed pile tip was about 33% less than that at the jacked pile tip.

It can be inferred that the lower cone resistances for suction-installed pile compared to those for jacked pile at any depth contribute to the lower horizontal capacity (about 10% difference as shown in Fig. 4) of the bucket pile. However, more precise

and extensive future research is required to identify the lower horizontal capacity for suction-installed pile.

## **CONCLUSION**

In this study, the effect of installation methods on bucket pile has been studied. As a result, the resistances of the pile installed by suction force and jacking force shown obviously different on vertical and horizontal pull-out resistances. This can be inferred because of decrease of effective stress caused by seepage flow from outside to inside of the pile. Thus, in the test on bucket pile, it can be concluded that the installation method affect on the bucket pile un-negligibly.

In summary, to examine the actual horizontal behavior of a bucket pile in sands, suction effect on the vertical and horizontal behavior of bucket pile plays an important role. Therefore, bucket piles were designed to be installed by suction force.

## **FUTHER STUDY**

To verify more effect on the installation methods, it seems necessary more to do test in terms of more detailed relative density, and not only inside resistances, but also outside resistances of the pile.

Finally, estimating changed friction angle of the model ground is the goal of this study.

## **ACKNOWLEDGEMENTS**

The research presented in this paper was conducted with funding from the project entitled "Development of Novel Technologies for Low-Cost and High Efficiency Bucket piles" at Korea Institute of Civil Engineering and Building Technology. The authors acknowledge the financial support from the institution.

## **REFERENCES**

- [1] Manh NT (2005), "Installation of Suction Caisson in Dense Sand and the Influence of Silt and Cemented Layers", Ph.D. Thesis, The University of Sydney.
- [2] Bang S, Jones KD, Kim KO (2011), "Inclined loading capacity of bucket piles in sand", *Ocean Engineering*, 38, pp.915-924.
- [3] Coffman RA, Fugro-McClelland Marine Geosciences, Inc.; El-Sherbiny RM, Rauch AF, Olson, RE (2004), "Measured Horizontal Capacity of Suction Caissons", *Offshore Technology Conference*, Houston, Texas U.S.A., OTC 16161.



## OBSERVATION, MEASUREMENT AND ANALYSIS OF ORIENTED BOREHOLE CORE FOR LOCATING SLIP SURFACES IN FRACTURE ZONE LANDSLIDES IN SHIKOKU, JAPAN

Tsunataka Furuya<sup>1</sup> and Jing-Cai Jiang<sup>2</sup>

<sup>1</sup>Graduate School of Advanced Technology and Science, The University of Tokushima, Japan

<sup>2</sup>Department of Civil and Environmental Engineering, The University of Tokushima, Japan

### ABSTRACT

This study employed oriented borehole cores for site characterization of two large fracture zone landslides in Shikoku, Japan. *In situ* and laboratory observations, geophysical measurement and digital imaging analysis of oriented borehole cores were performed to determine slip surfaces in the landslides that are in slow movement. The data obtained from each oriented borehole are (1) a depth distribution of rock quality designation, magnetic susceptibilities, the Equotip hardness values and wet unit weight of core samples, (2) geometric orientation of geologic discontinuities (cracks, joints, etc.), and (3) a depth distribution of numerical color values from digital imaging of borehole core. It is shown that a clearer change in rock quality designation, the Equotip hardness value and unit weight, and the orientation of cracks and joints was observed respectively near the slip surfaces, but the color values clearly varied only in one of the landslides and no change of magnetic susceptibility of core samples was found at both sites. The results demonstrate that it is capable of locating the slip surface in a fracture zone landslide by using the above-mentioned methods in combination.

*Keywords: Oriented core sample, Slip surface, Digital imaging, Equotip, Magnetic susceptibility, CIELAB model*

### INTRODUCTION

As a mountainous country, Japan has recognized a large number of active and potential landslide sites. These landslides can be divided into three categories, namely Tertiary type of landslides, fracture zone type and hot spring type [1]-[2]. Shikoku Island in the southeast part of Japan has been designated as a highly landslide-prone region with a large number of fracture zone landslides induced primarily due to tectonic activities. Many of these landslides are in relatively slow movement, some of which were restarted to move rather slowly due to heavy rainfall after a long term stop [3]-[4]. There also are natural slopes in Shikoku region that shows clearly landslide topography but so far there have been no movements to be observed or/and recorded [4]-[5].

An essential part of the investigation of a landslide is the determination of the depth and geometry of the slip surfaces that characterize it. For moving landslides the slip surfaces are easily inferred from data which can be obtained using surface movement observations, direct measurements of sub-surface displacements and geo-acoustic sensing. However, it is difficult to locate the slip surfaces in stationary and/or very slow-moving landslides, to which the above mentioned methods are usually not applicable. The available techniques for slow-moving landslides include direct observation of slip surfaces in exploratory and other excavations and in large diameter boreholes, observations on recovered samples,

inference from the contrast in properties between materials above and below a slip surface and sub-surface geophysical techniques [6]-[8]. However, using such methods to find slip surfaces usually requires careful logging of borehole data and certain experiences and skills [7]-[9].

Most of fracture zone landslides in Shikoku are distributed in the two geological strips sandwiched between the three tectonic lines (Fig. 1) [10]-[11]. The fractured state of bedrocks particularly near the tectonic faults and hydrothermal alteration of rock minerals into weaker clay minerals produced highly favorable conditions for landslides in the region. Such geological structures together with weathering of the bedrock minerals result in formation of multi-layers of clayey soil in different depth [10]-[11], and this causes the difficulties in locating slip surfaces for stationary and slow-moving landslides. Usually, it is required to use a number of different techniques in combination for site characterization of landslides in fractured geologic zones [8]-[9], [12].

This paper employed oriented borehole cores for determining slip surfaces in two large fracture zone landslides in Shikoku, Japan (i.e. the Azue landslide and the Kashio landslide). *In situ* and laboratory observations, geophysical measurement and digital imaging of oriented borehole core were performed. It was shown that the slip surfaces in fracture zone landslides could be located from the data obtained using the above techniques in combination.

## GEOLOGICAL CHARACTERISTICS

Shikoku Island is divided into four strips of geological formations by the three major faults in east-west direction, namely the Median Tectonic Line (also known as *Chuokozosen* which is the longest tectonic fault system in Japan and passes cross Shikoku Island), the Mikabu Tectonic Line and the Butsuzo Tectonic Line (Fig. 1) [13]. Most of the fractured zone landslides in Shikoku region are distributed in the Sanbagawa belt and the Chichibu belt between the three tectonic lines [10]-[11]. The Sanbagawa belt is a deposit of metamorphic rocks consisting mainly of green and black schist, and the Chichibu belt consisting of the three sub-belts forms a narrow strip of the Mikabu green stone as a metamorphic deposit along the tectonic line itself. The rock type in the Chichibu belt is sedimentary composed mostly of green schist, mudstone and conglomerate [10]-[11].

The Azue landslide is located in the Chichibu geological belt (Fig. 1). This slide took place just after slope failure and debris flow in the Azue area triggered by the heavy rainfall of typhoon Namtheun in 2004. Fig. 2 shows the slope failure and debris flow site in the Azue area [14], plan view and cross section of the Azue landslide. This huge slide block was found just above the main scarp of the Azue debris flow site. Numerous cracks were observed on the slope above the main scarp just after the event.

Surface and borehole investigations of the unstable block suggest that sliding surface reaches depths of up to 50m [14]-[16]. Stabilization works carried out to reduce the movement of the landslide mass are the construction of several water collection wells in the landslide mass for deep drainage. Fig.3 illustrates the slip surfaces observed from the water collection wells. The slip surface has developed at or close to the interface between the strong weathering green rock and the underlying bedrock. It is smooth and also exhibits striations or scratches in the down-slope direction. A thin layer of the slip-surface clay was formed along the failure plane where small size round gravel could be occasionally found.

The Kashio landslide is located in the south side of the Sanbagawa geological belt (Fig. 1). This huge slide occurred in fractured rocks consisting of pelitic (muddy) schist and basic schist. Due to large scale tectonic activity, the rocks around the landslide area are highly fractured and weathered. Fig. 4 illustrates plan view and cross section of the Kashio landslide. The average inclination of the slope surface is 24 degrees. The head of the landslide is located at 950 m above sea level, and the toe is located at 650 m near the Kashio river bed. The slide is divided into a main block and two small blocks in the lower part. The main block slide is structurally controlled, and occurred within the weathered pelitic (muddy) schist. The slide planes are located at depths of 10 to 30 m deep for the main block.

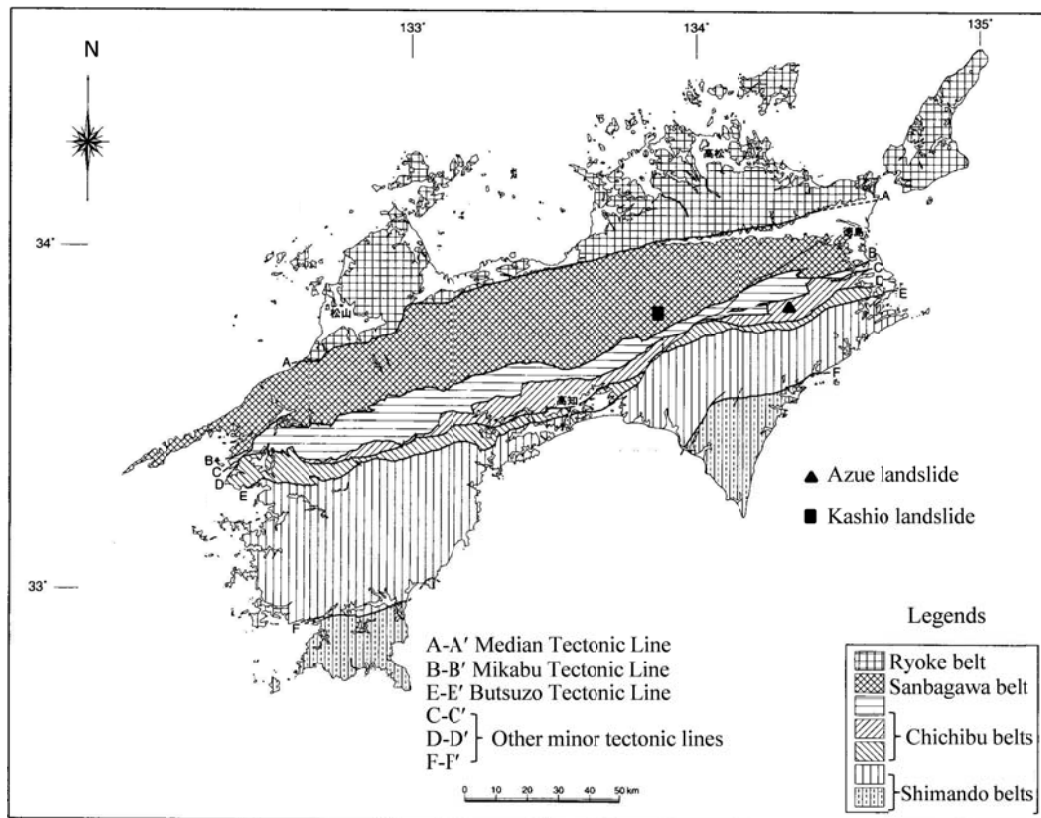
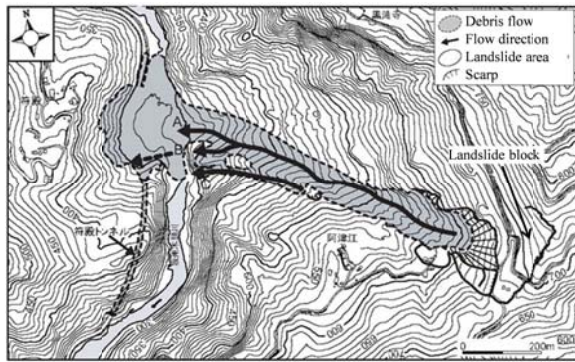


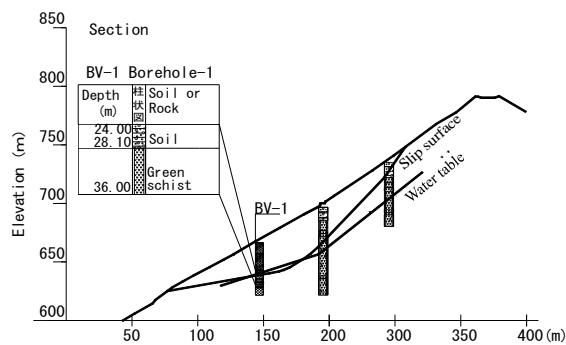
Fig. 1 Map of Shikoku showing major tectonic lines, geological belts and locations of two landslide sites in fracture zones (after [13])



(a) Plan view of the site of slope failure and debris flow in Azue area [14]



(b) Plan view of the landslide block



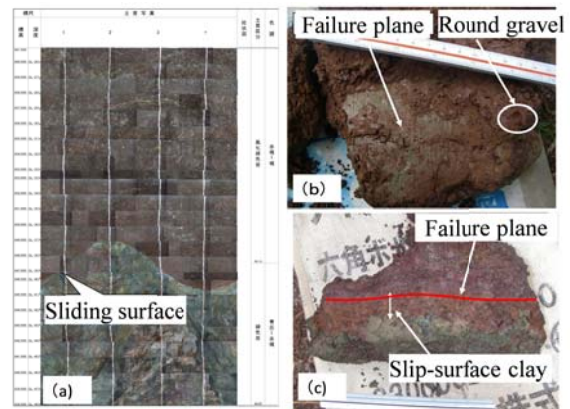
(c) Cross section of the landslide block

Fig. 2 Azue landslide

## METHODS

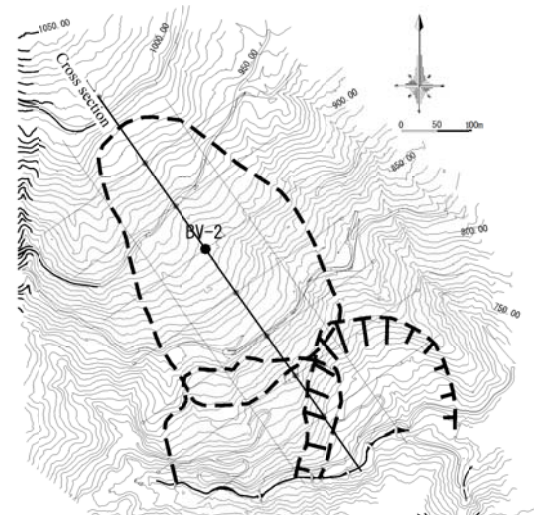
### Obtaining Oriented Core

Oriented borehole core provides data whereby the geometric orientation of geologic discontinuities (joints, faults, beddings etc.) may be determined. We employed an oriented drilling technique and double tube sampling system [17]-[18] for obtaining oriented core. As shown in Fig. 5, the system is composed of three parts: dual tube drilling rods, dual tube sampler and a direction fix rod. Dual tube

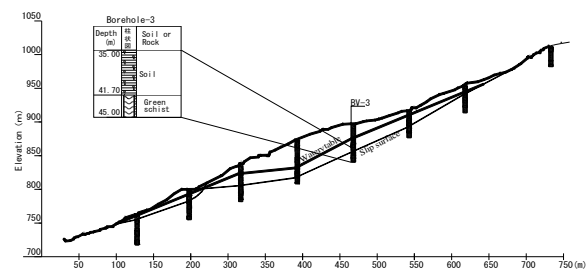


(a) Photograph of the wall of an excavated hole for water collection; (b) Slip surface with striations in downslope direction; and (c) Slip-surface clay along the failure plane

Fig. 3 Slip surfaces observed from the water collection wells in Azue landslide



(a) Plan view of the landslide area



(b) Cross section of the landslide block

Fig. 4 Kashio landslide

sampling uses two sets of probe rods to collect continuous soil rock cores. One set of rods is driven into the ground as an outer casing (tube). These rods receive the driving force from the drilling machine. The other set of rods are placed inside the outer tube. Outer tube rotates and allows for the removal of the cuttings while inner tube is fixed with the inside



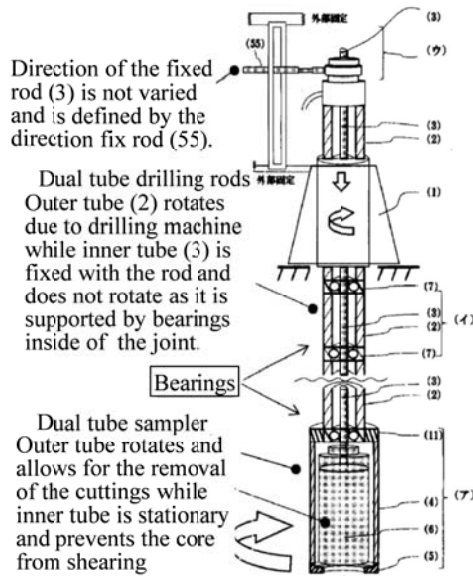


Fig. 5 Drilling/sampling systems for oriented core

rod and does not rotate as it is supported by the bearings inside of the joint. The direction fix rod is fixed on outer fixing arms and defines direction of the fixed rod together with the inner tube, allowing us to obtain oriented core samples.

### Oriented Core Treatment and Logging

The following steps are carried out for oriented core samples in laboratory:

- 1) Confirm and re-mark the base line on the core samples showing a known direction.
- 2) Clean the core of drilling fluids or mud in order to obtain clear photo image of the core outside.
- 3) Perform observation and sketching of the core through the full length for visual description logs.
- 4) Determine a new defined parameter called rock quality designation, which will be described in next section later.
- 5) Measure physical/geophysical properties of the core along the base line, including wet unit weight, magnetic susceptibility and Equotip values.
- 6) Photograph the core by rotating the core samples to obtain oriented, 360° photo image of the outer surface of the core. The digital images such obtained are analyzed later to calculate the orientation of discontinuities and to obtain color values of the core.

### Rock Quality and Fracture/Weathering Grade

#### Rock Quality Designation (RQD)

This parameter is defined by summing the length (between natural joints) of all core pieces more than 5cm long as a percentage of the total core length.

$$RQD(\%) = \frac{\text{Length (m) of core pieces} \geq 5\text{cm}}{\text{Total length (m) core run}} \times 100\%$$

Double tube sampling system used in this study

ensured high quality of the core [17]-[18] and a careful measurement of core pieces more than 5cm long was carried out along the base line marked on the core, as shown in Fig. 6.

#### Weathering grade and discontinuity description

The weathering/fracture grade is a measure of how the core properties (i.e. strength, mineralogy, etc.) have been changed from their original form. Table 1 shows suggested weathering/fracture grades and their associated description.

### Geophysical Measurement of Core Samples

#### Magnetic susceptibility

Magnetic susceptibility measures the 'magnetisability' of a material. In the natural environment around a landslide, the magnetisability tells us about the minerals that are found in rocks, particularly Fe-bearing minerals. It is used to classify different types of materials and to find the subsurface of a landslide [19]-[20]. In this study, magnetic susceptibility of the core was continuously measured along the base line using a KT-10 magnetic susceptibility meter by Terraplus [21]. Its sensitivity is  $1 \times 10^{-6}$  SI units with a measurement range of  $0.001 \times 10^{-3}$  to  $1999.9 \times 10^{-3}$  SI units and an operating frequency of 10 kHz.

#### Equotip values for rock hardness assessment

The Equotip is an electronic hardness testing device. It was originally designed for testing metals, but it has now been used extensively for testing rock hardness [22]-[24]. For the measurement of hardness of the core, we used an Equotip hardness tester produced by Proceq with a maximum hardness of 940 HV and an accuracy of +4L (+ 0.5%).



Fig. 6 Base line marked on the borehole core

Table 1 Weathering grades and descriptions

Grade	Field identification (Rocks)	Description (Discontinuities)	Description
W1	Original rock fabric is almost destroyed.	Structural discontinuities are perceived only between interface of W1 & W2.	Fracture structure
W2	Rock fabric is partially destroyed and rock is friable or changed almost to a soil.		
W3	The original fabric of the rock is visible. No clay soil is observed in rocks.	Discontinuities are open and gravel is disposed in cracks along joints etc.	Crack structure
W4	Rock may be slightly discoloured adjacent to discontinuities that partially exist in rock.	Discontinuities are slightly open along bedding joints, etc.	

## Digital Imaging Analysis

### *Geometric orientation of discontinuities*

The oriented, 360° photographs of the outside of the core are first treated and displayed as a 2-D image showing the core's entire outer surface. The images can then be used to locate and measure the dip and orientation of structural features (fractures, boundaries between different rock types) in the core, as shown in Fig. 7. This operation was carried out in this study by using the WELL CAD software [25].

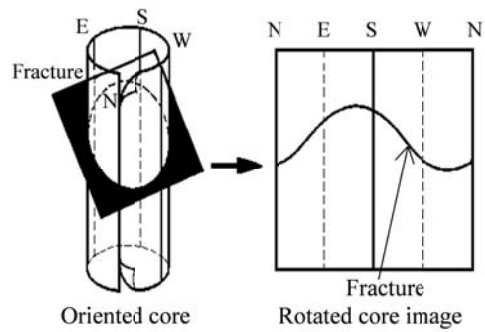
### *Color values based on CIELAB model*

CIELAB is an opponent color system based on the system of Richard Hunter called  $L^*$ ,  $a^*$ ,  $b^*$  [26]. This color system indicates distinctions between light and dark, red and green, and blue and yellow by using numerical values with three axes:  $L^*$ ,  $a^*$ , and  $b^*$ . The  $L^*$  axis represents lightness whose values run from 0 (black) to 100 (white). As a color can't be both red and green, or both blue and yellow (because these colors oppose each other), the values run from positive to negative on the  $a^*$  or  $b^*$  axis. On the  $a^*$  axis, positive values indicate amounts of red while negative values indicate amounts of green. On the  $b^*$  axis, yellow is positive and blue is negative. For both axes, zero is neutral gray. Therefore, values are only needed for two color axes and for the lightness or grayscale axis ( $L^*$ ). CIELAB color system is device independent and therefore become a very popular color model in practice. We used a SPAD-503 device for color measurement to obtain values of  $L^*$ ,  $a^*$ , and  $b^*$  of the borehole core.

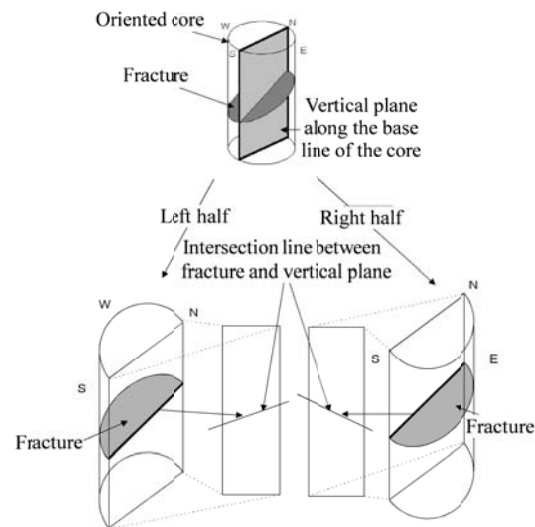
## RESULTS AND DISCUSSION

Results of observation and measurement of the cores of the Azue landslide are shown in Figs. 8 and 10(a). There are highly and slightly weathered green rocks above and below the slip surface at depth of 28.2m (Fig. 8), respectively.

Average unit weight measured between 24-28m/28-36m was  $2.36 \text{ kg/m}^3$  and  $2.76 \text{ kg/m}^3$ , respectively. The RQD defined for this study increased from 42% above the slip surface to 92% below the slip surface. A clear change in the Equotip value is also found near the slip surface. Fracture and crack structures are observed in the rocks above and below the slip surface, respectively. Discontinuities are oriented in a very narrow range in the vicinity of the slip surface but in a wide range in other depths. Their inclination is less than  $50^\circ$  above the slip surface and more than  $50^\circ$  for most discontinuities below the slip surface. Such a change in the structural fractures might be produced by large shear deformations along the slip surface and weathering. From Fig. 10 (a) it is seen that the magnetic susceptibility and the color values do not indicate a meaningful change near the slip surface in the Azue landslide.



(a) Oriented 360° core and rotated core image



(b) Calculation of strike and dip of planar fracture  
Fig. 7 Concept of calculating orientation of fracture

Results of observation and measurement of the core samples of the Kashio landslide are illustrated in Figs. 9 and 10(b). The rock type is politic schist. Weathering grade of the rocks at depth of 35~45m is from W1 to W4, gradually decreased, while there is highly (W1) weathered muddy schist above the shear band (slip surfaces) around a 41-42m depth.

The unit weight is increased with decrease in the weathering grade, ranging from  $1.6\sim 2.5 \text{ kg/m}^3$  for the W1-W3 grade rocks to  $2.6\sim 2.7 \text{ kg/m}^3$  for the W4 grade rocks. The decrease in the unit weight may be caused by increase of void ratio and water content due to grain refining of fractured rocks. The Equotip harness index and the RQD values measured are almost consistent with the distribution of unit weight, as shown in Fig. 10(b). A change of the color values of  $a^*$  and  $b^*$  and a positive peak value of  $L^*$  are also found near the shear band (slip surfaces). Note that such a peak of the color values of  $L^*$  also appeared at other depths. Rocks above and below the shear band can be categorized to fracture/crack structures, respectively. Discontinuities are oriented in a wide range in rocks of above and below the slip surfaces but in a very narrow range in the vicinity of the slip surfaces. No meaningful change in the magnetic susceptibility was found in the Kashio landslide.

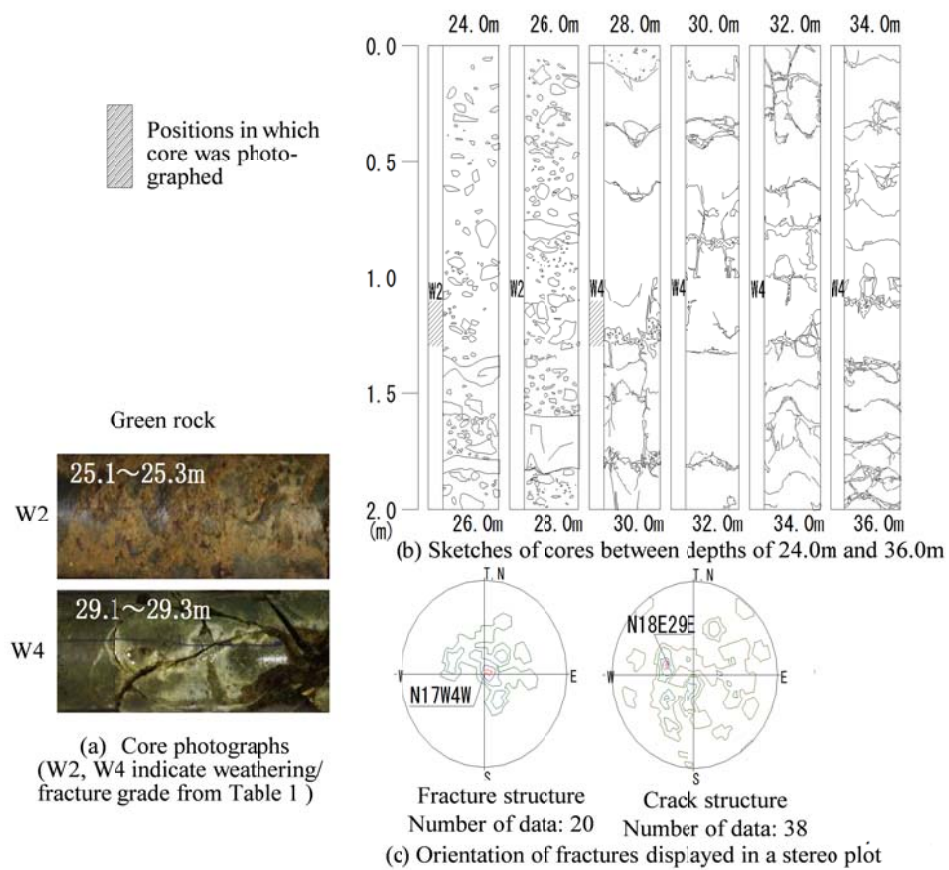


Fig. 8 Observation of core samples from Azue landslide

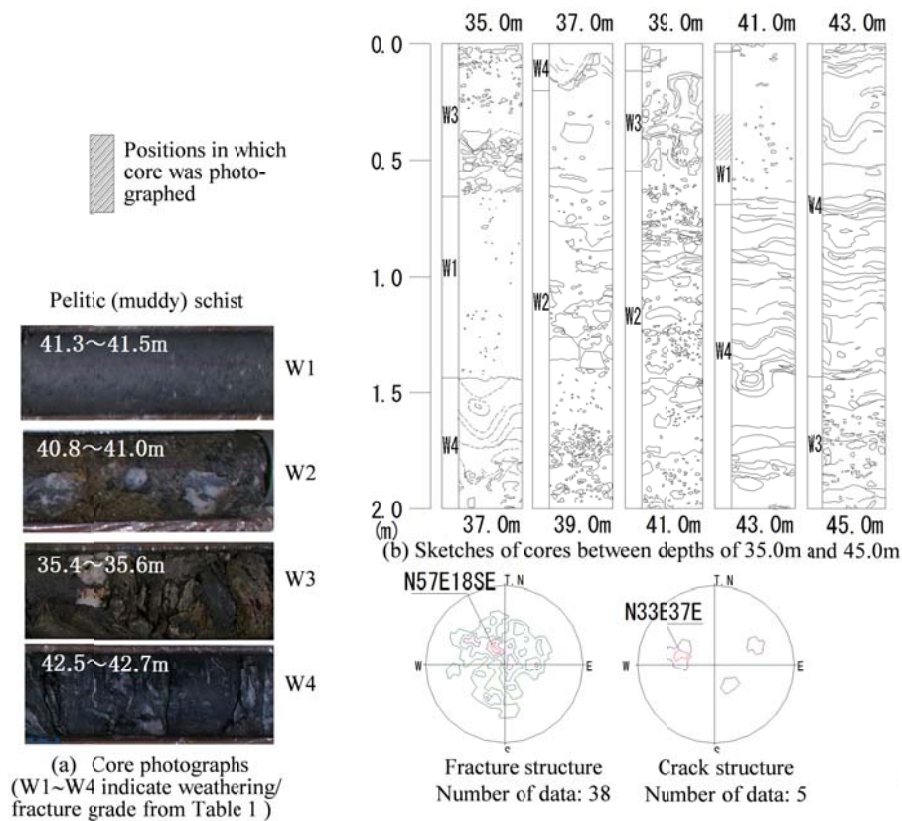


Fig. 9 Observation of core samples from Kashio landslide



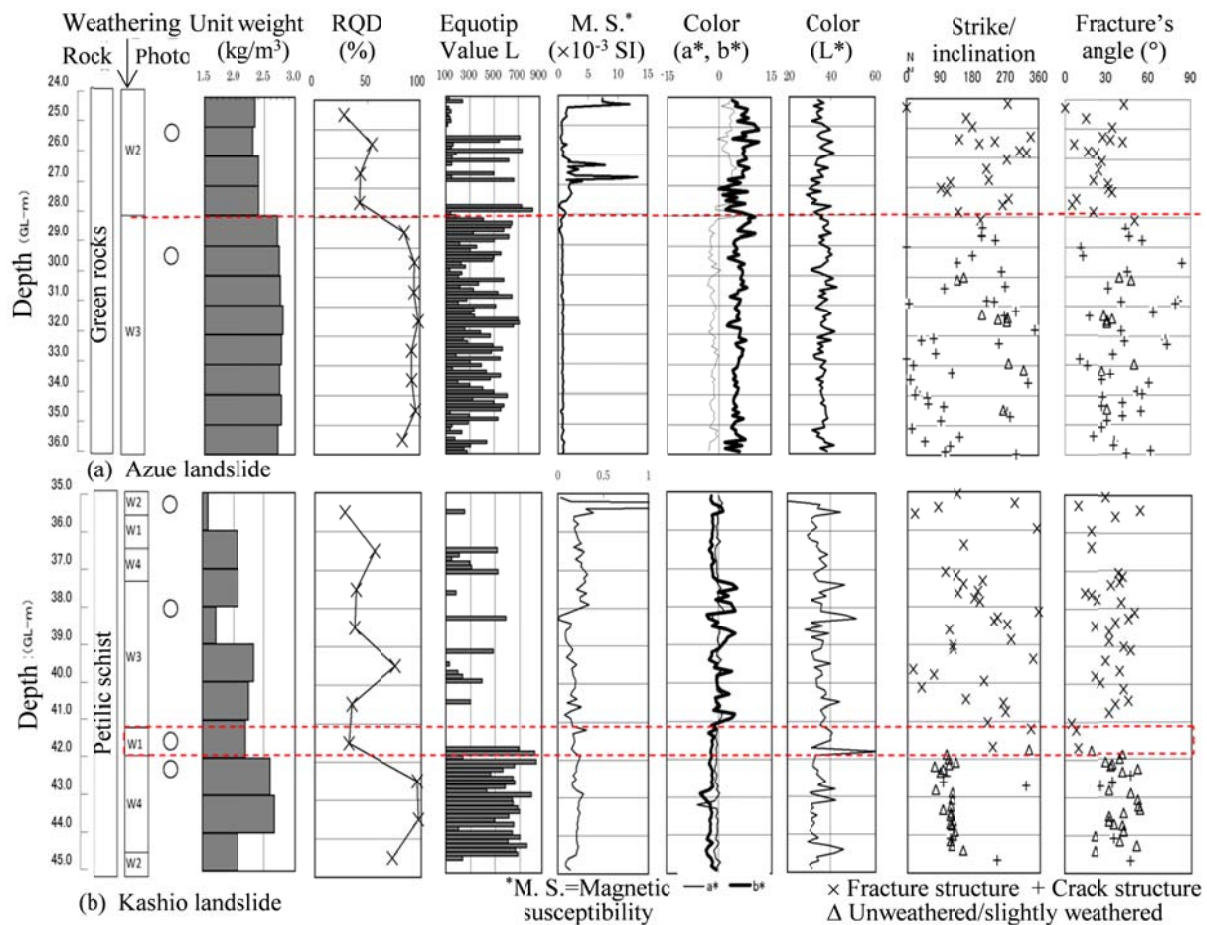


Fig. 10 Results of measurement and image analysis of the cores from Azue and Kashio landslides

Fractured bed rocks near the tectonic faults and hydrothermal alteration of rock minerals are the main reasons of fracture zone landslides in Shikoku, Japan. Such geological conditions together with weathering might result in different distributions of geologic discontinuities, rock quality designation, Equotip hardness, and numerical color values in rocks/soils above and below a slip surface. The information gained from observation, measurement and digital imaging analysis of oriented core samples, such as those shown in Figs. 8-10, allowed the successful determination of slip surface depths in fracture zone landslides.

## CONCLUSION

This study presented examples of laboratory observations, geophysical measurement and digital imaging analysis of oriented borehole core from two study sites in Shikoku, Japan where many fracture zone landslides are distributed. The data obtained from each site include (1) a depth distribution of rock quality designation defined in this study, magnetic susceptibilities, the Equotip hardness values and wet unit weight of core samples; (2) Orientation and inclination of geologic discontinuities (cracks, joints,

etc.) involved in the core samples, and (3) a depth distribution of numerical color values from digital imaging of borehole core. It has been indicated that a clearer change in rock quality designation, the Equotip hardness value and unit weight, and the orientation and inclination of discontinuities was observed respectively near the slip surfaces for both sites, while the color values clearly varied only near the slip surface in the Kashio landslide. In addition, no change of magnetic susceptibility of core samples was found at both sites. The results demonstrate that the data gained from observation, geophysical measurement and digital imaging analysis of oriented core samples can be successfully used to determine slip surfaces in fracture zone landslides.

## REFERENCES

- [1] The Japan Landslide Society, and National Conference of Landslide Control, "Landslides in Japan", <http://www.tuat.ac.jp/~sabo/lj/>.
- [2] Ministry of Land, Infrastructure, and Transport, "Landslides in Japan (in Japanese)", A booklet published by Sabo Publicity Center, Slope Conservation Division, 2000.

- [3] Kuroda K., Ando T., and Oka S. "The characteristics of landslides in groups in outer zone of southwest Japan" *Journal of the Geological Society of Japan*, Vol. 69, Jul. 1963, p.344.
- [4] Ueno S., "Prediction of a landslide by means of a topographic geologic investigation", *The Japanese Geotechnical Journal of Tsuchi to Kiso*, Vol. 45, No. 6, Jun. 1997, pp. 5-8. in Japanese.
- [5] Ueno S., "On the characteristics of landslides in the Izumi Group of Shikoku Island", *Journal of the Japan Society of Engineering Geology*, Vol. 41, No. 5, Dec. 2000, pp. 267-278. in Japanese.
- [6] Yamasaki T. "Plan of emergency landslide investigations and mitigation measures", *Key points in field work for landslide engineers No. 12*, *Journal of the Japan Landslide Society*, Vol. 44, No. 1, May 2007, pp. 58-64. in Japanese.
- [7] Kamoi Y. "An effect of standard penetration test in a slip surface detection based on Neogene landslides in Niigata, Japan", *Journal of the Japan Landslide Society*, Vol. 44, No. 1, May 2007, pp. 50-57. in Japanese.
- [8] Ono S., Yano K., Tanaka Y., and Yoshimine S. "Observation and judgment point of boring core for landslides in outer zone of southwest Japan", *Journal of the Japan Landslide Society*, Vol. 45 No.4, Nov. 2008, pp. 309-316. in Japanese.
- [9] Yoshimura T. and Mano M. "Estimation of slip surface by  $\gamma$ -ray and magnetic susceptibility measurements of boring core samples", *Journal of the Japan Landslide Society*, Vol.42 No.3, Sep. 2005, pp. 216-222. in Japanese.
- [10] Bhandary N. P. and Yatabe R., "Ring shear tests on clays of fracture zone landslides and clay mineralogical aspects", *Progress in Landslide Science*, Sassa et al. Eds. Springer, 2007, pp. 183-192.
- [11] Bhandary N. P., Yatabe R., and Takata S., "Clay minerals contributing to creeping displacement of fracture zone landslides in Japan", *Landslides: risk analysis and sustainable disaster managements*, Sassa et al. Eds., Springer, 2005, pp. 219-223.
- [12] Yamazaki T., Yamasaki T., and Hashimoto J. "Practical use of borehole televiewer in landslides", *Journal of the Japan Landslide Society*, Vol. 38, No. 1, May 2001, pp. 14-19. in Japanese.
- [13] Compilation Committee for Civil Engineering Geological Map of Shikoku, "Explanations for Civil Engineering Geological Map of Shikoku", *Japan Institute of Country-ology and Engineering*, 1998. in Japanese.
- [14] Yokoyama S., Murai M., Nakaya S., Nishiyama K., Ohoka K., and Nakano H., "Fractured zone landslides and debris flow at Azue, Naka Town, Tokushima Prefecture, induced by the heavy rainfall of Typhoon Namtheun in 2004", 113<sup>th</sup> National Conference of the Japan Geological Society, 2006. in Japanese.
- [15] Wang G. H., Suemine A., Furuya G., Kaibori M., Sassa K., "Rainstorm-induced landslides in Kisawa village, Tokushima Prefecture, Japan", *Journal of the International Consortium on Landslides No.3*, Vol.2, 2006, pp.232-242.
- [16] Hashimoto H., Kojima K., Sato, T., Hisazumi T., and Yamada M., "The landslide mechanism of Azue Landslide Area", *Journal of the Japan Landslide Society*, Vol. 42, No.6, Mar. 2006, pp. 493-498. in Japanese.
- [17] Takeda S., Komiya K., and Takeuchi I., "A hybrid sampling system for high quality cores from air bubble boring", *The Japanese Geotechnical Journal of Tsuchi to Kiso*, Vol. 54, No.4, Apr. 2006, pp. 16-18. in Japanese.
- [18] Suzuki Y., Tsukada M. and Higaki D., "A case study of improved core sampling using New Jet-Foam-Boring method in Chojia Landslide", *Journal of the Japan Landslide Society*, Vol. 45 No.4, Nov. 2008, pp. 304-308. in Japanese.
- [19] Wakizaka Y., Kozuma M., Watatani H., and Toyoguchi Y., "Characteristics of crushed rocks in a landslide body : An example of a landslide located in the Shimanto Belt", *Journal of the Japan Society of Engineering Geology*, Vol. 52, No. 6, Feb. 2012, pp. 231-247. in Japanese.
- [20] Kinoshita A., et al., "Physical and chemical properties around slip surface by assaying samples of well-cared cores from crystalline schist area in Shikoku Islands, southwest Japan", *Journal of the Japan Landslide Society*, Vol. 50 No.4, Jul. 2013, pp. 1-9. in Japanese.
- [21] Terraplus, "KT-10 v2 and KT-10R v2 Magnetic Susceptibility Meters", User manual.
- [22] Kawasaki S., Tanimoto C., Koizumi K. and Ishikawa M. "An attempt to estimate mechanical properties of rocks using the Equotip hardness tester". *Journal of Japan Society of Engineering Geology*, Vol. 43, 2002, pp.244-248. in Japanese.
- [23] Aoki H., Matsukura Y. "A new technique for non-destructive field measurement of rock-surface strength: an application of the Equotip hardness tester to weathering studies", *Earth Surface Processes and Landforms*, Vol. 32, 2007, pp. 1759-1769.
- [24] Harada T., Takehara T., Hamaguchi Y. and Morimoto K., "Slip surface formed on slate and serpentinite in the Chichibu Terrane", *Journal of the Japan Landslide Society*, Vol. 43 No.3, Sep. 2006, pp. 180-182. in Japanese.
- [25] ALT, "WELLCAD Software for borehole image analysis", user manual.
- [26] CIE: Commission Internationale de l'Éclairage, "CIELAB - Color Models - technical guides", 1976.

## EFFECT OF LAYER THICKNESS AND BLOCK RATIO ON ROCK SLOPES MOVEMENT STYLE

A. K. Alzo'ubi<sup>1</sup>

<sup>1</sup>College of Engineering, Abu Dhabi University, UAE

### ABSTRACT

In rock slopes, toppling movements are very common. In such slopes, the layers thicknesses and block ratio relative to slopes height might determine the type of slope movements and what will be the style of toppling. In this paper a numerical parametric study has been conducted to evaluate the effect of block ratio and block thickness, in both crystalline and sedimentary rock, on the style of rock slopes movement in slopes that are prone to toppling. The mechanical defects or joints of rocks can be either random or well defined sets depends on the rock mass origin, metamorphic, igneous, or sedimentary. Different styles of movements were observed numerically in this study ranging from block toppling to rock falls. The styles of movement were also compared to the ones observed in the field.

*Keywords: Slopes, Sedimentary, Toppling, Bed-Height ratio*

### INTRODUCTION

Rock slopes can be divided into two main categories: structurally controlled slopes, such as the planar and wedge failures, and the non-structurally controlled slopes in which rupture surface penetrate the intact rock to form circular or spiral failure surface. The structurally controlled slopes normally fail by shear, sliding along one or more continuous discontinuities, whereas, in the non-structurally controlled slopes, failure is a complicated process and involves failure in both the discontinuity and the intact material [1]. The assumption that single discontinuity controls the slope failure is a simplified approach for analyzing rock slopes and is applicable only for small scale slopes, while for large slopes, the continuity has limited validity unless a fault or any continuous large rock structure existed prior to failure.

Different modes of toppling movements have been observed in the field on both anacinal and cataclinal slopes. De Freitas and Watters [4] introduced the term "toppling" to describe the movements of rock slopes in rotation with steeply dipping beds. Goodman and Bray [7] extended the discussion of toppling mechanisms and showed that toppling in anacinal slopes is possible. Goodman and Bray [7] identified three modes of toppling: flexural toppling, block-flexural toppling, and block toppling. Later, [6] explored toppling in cataclinal slopes and extended Goodman and Bray criteria for toppling to accommodate the underdip toppling. Figure 1 shows an example of a toppling movement.

Cruden and Hu [2] described 16 topples in the Highwood Pass in Alberta. These researchers identified three modes of toppling based on the field

observation: block flexural toppling, which is characterized by gradual changes in the bedding orientation within the rock mass; multiple block toppling, which is characterized by more than one distinct zone of abrupt change; and block toppling, which is characterized by abrupt changes in the orientation between blocks between the toppling rock mass (the Chevron topple, [3]).



Fig.1 Rock falls/toppling in Hafeet Mountain, UAE.

Cruden and Hu [2] concluded that the different styles of toppling were associated with the joint spacing, bed thickness and slope angle, and used the block ratio to distinguish between different styles of toppling. Later, [5] further the investigation of the effect of the block ratio and concluded that using the block ratio to identify the toppling style is not the best way due to the overlap between the different modes of toppling. The following parametric study will investigate the effect of the joint spacing, the bed thicknesses, the slope angle, and joint-distribution on the style of toppling rock slopes by using the geological model proposed by [1].

## GEOLOGICAL MODEL

Terzaghi [1] proposed a geological model for rock slopes in hard-unweathered rock masses. The mechanical defects of rocks can be either random or well-defined sets. He described the mechanical model of stratified sedimentary rocks:

“Stratified sedimentary rocks consist of layers with a thickness averaging between a few inches and many feet. These are commonly separated from each other by thin films of material with a composition different from that of the rest of the rock. The bedding planes are almost invariably surfaces of minimum shearing resistance. They are likely to be continuous over large areas. The cross-joints, generally nearly perpendicular to the bedding joints, are commonly staggered at these joints. The cohesive bond along the walls of the cross-joints is equal to zero.

The intersections between the cross-joints and the bedding planes may be more or less parallel to one of two or more directions, or less parallel to one of two or more directions, or less commonly, the intersection may have a nearly random orientation. Because of the almost universal presence of bedding or cross-joints, stratified sedimentary rock with no effective cohesion ( $C_i=0.0$ ) has the mechanical properties of a body of dry masonry composed of layers of more or less prismatic blocks which fit each other. The boundaries between the individual layers of blocks constituting the masonry correspond to the bedding planes of the rock. The cohesion across the joints between all the blocks of each layer is zero, and most of the joints between the blocks of two adjacent layers are staggered at the boundaries between layers. The stability of a slope on a rock with the mechanical properties of such a body of masonry depends primarily on the orientation of the bedding planes with reference to the slope”. Cruden [8] also observed the same geological model. Terzaghi [1] also described a geological model for the crystalline rocks such as marble or granite as irregular-shaped crystalline particles, which fit each other like blocks between joints in a rock with a random joint pattern. The above-mentioned geological models are adapted in the present study.

## THE NUMERICAL MODEL

Terzaghi [1] and Cruden [8] described conceptual geological formations for rock masses in both sedimentary and crystalline rocks. Four numerical models, A, B, C, and D, were built based on the description of the geological model of rock masses, proposed by [1] and [8], to examine the effect of the block geometry and the slope face angle on the movement modes of rock slopes. The basic Numerical model used in this analysis is presented in Figure 2. It shows the details of the jointing and

the slope face angle variation between  $45^\circ$ - $60^\circ$ . The bedding was kept at a constant dip of  $80^\circ$ , while the bed's thicknesses were varied from 1.5 m to 3 m to 6 m for each slope.

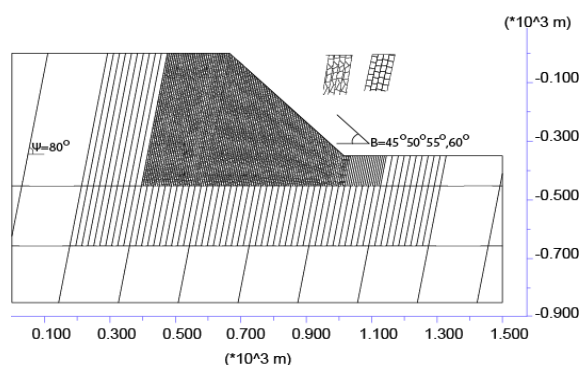


Fig. 2 Illustration of the numerical model geometry and joints details inside the beds

The effect of the bed's thickness and the slope face angle were tested by using two patterns of joints distributions. The first joint pattern was uniformly distributed and perpendicular to the bedding to simulate stratified sedimentary rock. The second pattern was irregular joint pattern intersecting the beds at different angles was used to simulate crystalline rocks. The insert in Figure 2 shows the joints patterns used in the numerical model. For the  $45^\circ$  models, the cross-joints were also changed from 8 m to 4 m to 2 m, to investigate the cross-joints spacing effect on the slope deformation style, producing block ratios between 5 and 0.1. A total of 30 models with different geometries were modeled and monitored to determine the toppling modes and behavior with numerical time. Table (1) shows the geometrical setup of the slopes used in this parametric study.

Table 1 Geometries of the toppling slopes used in this study

Slope	Face Angle ( $^\circ$ )	Bed thickness (m)	Cross-joints spacing (m)
A	45	6, 3, 1.5	8, 4, 2
B	50	6, 3, 1.5	8
C	55	6, 3, 1.5	8
D	60	6, 3, 1.5	8

## STRENGTH PROPERTIES

According to [1] and [8], the cross-joints and the beds have no cohesion, and the friction angle of the rock mass is the only strength parameter involved in stability analysis of the slopes. In this analysis, the cohesion and the tensile strength were assumed to be equal to zero, and a friction angle of  $30^\circ$  was used for both the cross-joints and the steeply dipping



joints. The cohesion along the beds can be easily destroyed and becomes equal to zero [1].

Although Patton [9] showed that the friction angle of rocks was composed of two components, the basic friction angle and the asperities, Cruden [10] showed that the friction angle in the Canadian Rockies could be reasonably estimated as the basic friction angle and zero angles of the asperities. Based on an experimental study using a tilt table, Hu and Cruden [11] concluded that the friction angle could have a range from 21.5° to 41.4°. Cruden [8] used a friction angle of 30° to build a process diagram to describe the type of slope movement based on the slope face and the beds' orientation. Table 2 shows the properties used in this parametric study for both the beds and the cross-joints.

Table 2 Elastic blocks and joints properties

Property	Elastic blocks	Joints
E (MPa)	20000	
Poisson's ratio	0.25	
$\phi$ (°)		30
C (MPa)		0
$\sigma_t$ (MPa)		0
Kn (GPa)		20
Ks (GPa)		5

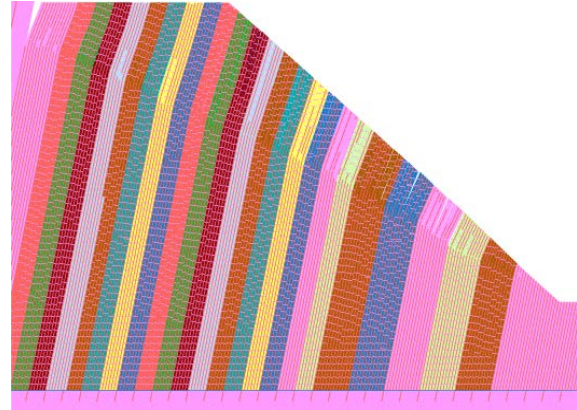
## MODES OF TOPPLING

Three modes of toppling were observed numerically: block-flexural toppling, multiple block-toppling, and block toppling (Chevron). Table 1 shows the different slopes' configurations used in this paper. All of these slopes are prone to toppling according to the Goodman and Bray's criteria. The effect of the block geometries and the slope face angle on development of the toppling mode investigated. The slopes were monitored with cycling to observe the mode of toppling formed. As topples deformed with cycling the style of toppling changed from flexural toppling to multiple toppling and eventually block toppling, the toppling style kept changing as cycling continued.

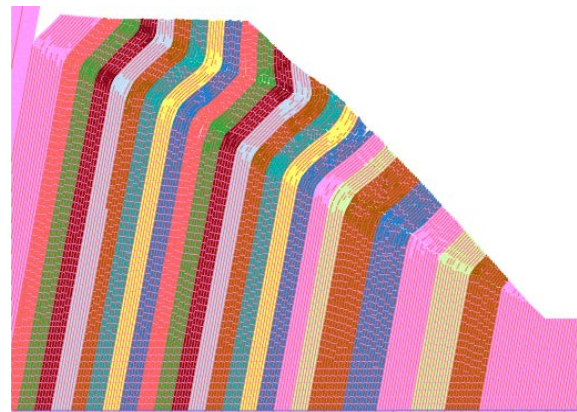
Figure 3(a) shows slope A (45°) with 3 m bed thickness and 8m cross-joints. This slope shows a gradual rotation of the rock columns with no rupture surface formation and experienced block flexural toppling mode. Cruden and Hu [2] and McAfee and Cruden [5] found block flexural toppling with no rupture surface formation in Highwood Pass topples.

The model in the figure is shown at 40,000 cycles. By allowing the model to cycle, two or more rupture surfaces were formed inside the slope: a pivot lower rupture surface and upper rupture surfaces, which formed a multiple block toppling that is characterized by more than one rupture

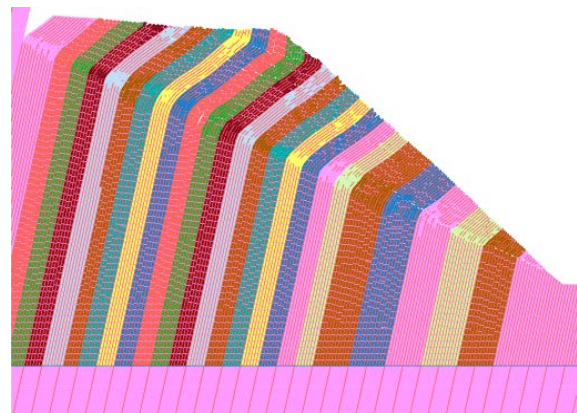
surface, Figure 3 shows the model at 120000 cycles. As the model allowed deforming with cycling, the toppling continued around the lower pivot rupture surface and the blocks above the upper rupture surface continued to topple. Eventually, the slope moved gradually from the multiple block-toppling to block-toppling mode which was described by [3] as Chevron, Figure 3 shows the model at 320000 cycles.



a) Block-flexural toppling, 40,000 cycles



b) Multiple block toppling, 120,000 cycles



c) Block toppling, 320,000 cycles

Fig. 3 Development of toppling style with time, (a) block-flexural toppling, (b) multiple block toppling, and (c) block toppling.

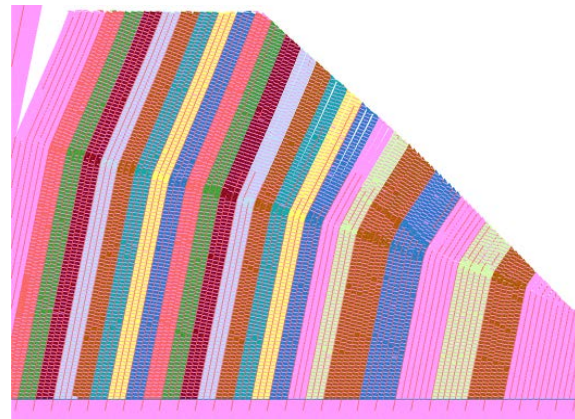
This deformation process and moving from stage to stage was observed in all the toppling models used in this study, for both regular and irregular cross-joints patterns, i.e. time is important factor in determining the toppling styles observed in the numerical simulation, the style is controlled by the time allowed for the slope to deform and move from stage to stage. McAfee and Cruden [5] concluded that weathering, which is time dependent process, caused the toppling to occur at the Highwood Pass. The next section will discuss the effect of the bed thickness normalized to the slope height as opposed to the block ratio on the toppling style.

### BED THICKNESS VERSUS BLOCK RATIO EFFECT

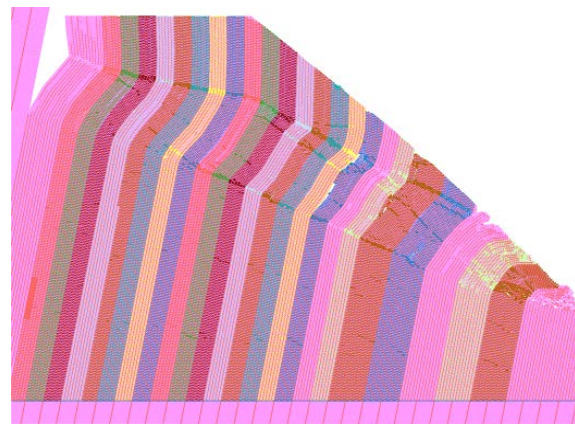
To normalize the bed thickness, the bed-height ratio is defined as the bed thickness to total slope height. Cruden and Hu [2] studied the effect of the block ratio on the toppling mode and suggested that the block ratio can determine the style of toppling. Two models with the same block ratio but different bed-height ratios were set up and tested numerically to determine if the toppling mode controlled by the block ratio or the bed-height ratio (1.5 block ratio and bed-height ratios of 0.017 and 0.0085 corresponds to 6 m and 3 m bed thicknesses, respectively). The two models had a 45° slope face. The slopes were monitored with time and compared at the same number of cycles (120000) and at the same numerical time (25 seconds).

Figure 4 shows the two models at 25 seconds. The slopes experienced two different modes of toppling despite that the same block ratio was used. The 0.017 bed-height ratio slope shows a block-flexural toppling while the 0.0085 bed-height slope shows a multiple block toppling at the same number of cycles. These results suggest that bed-height ratio, rather than the block ratios, plays an important role in determining the toppling style.

Martin and Kaiser [12] discussed the effect of the internal shears on rock slopes and showed the importance of these internal shears to accommodate failure along the basal shear plane. As mentioned earlier, the bed-height ratios were varied from 0.0043 to 0.017 to investigate their effect on the toppling mode as opposed to the effect of the block ratio in order to explain the mode of toppling. The smaller bed-height ratios introduced more shear planes in the rock mass than the high bed-height ratio, along which more sliding and shearing occurred at the instance at which the rock slope started moving. As the bed-height ratio became smaller the numerical simulations showed smoother rotational movements for the thin beds than for the thick beds. The comparisons between the different models were always made at the same number of cycles or the same numerical time.



a) Block-flexural toppling, 0.017 bed height (25 seconds)



b) Multiple block toppling, 0.0085 bed-height (25 seconds)

Fig. 4 Comparison of toppling style for two slopes at the same block ratio and different bed-height ratios, a) 0.017 bed-height ratio, b) 0.0085 bed-height ratio.

According to this numerical model parametric study, the rupture surface or pivot line also affected by the bed-height ratio, the thinner the beds, the steeper the rupture surface for the same slope face angle. Figure 5 shows the 55° slopes at three bed-height ratios, 0.017, 0.0085 and 0.00425, as shown in Figure 5, the rupture surface or the pivot line is shallower for the small bed-height ratio than the large bed-height ratio. In all the models, an uphill back scarp formed (see Figure 5), notice depth of the uphill back scarp in the models, it increased as the bed-height ratio increased.

This behavior occurred because the thin beds will introduce more shear planes, which allow more sliding and shearing between the rock columns than the thick beds (6 m) allowed. These shear planes between the beds accommodated more internal shearing and displacement and resulted in a smoother toppling movement than the toppling of the thick beds and shallower pivot or rupture surface.



Due to the increased amount of shear planes in the low bed-height ratio's slopes, the deformation due to the toppling movement was accommodated by shorter columns, and the pivot line or the rupture surface was formed closer to the surface and was steeper for the low bed-height ratio's slope than the high bed-height ratio's slopes, the rupture surface angle from the horizontal was measured and found to be as following:  $28^\circ$  for the 0.017 bed-height ratio,  $31^\circ$  for the 0.0085 bed-height ratio and  $33^\circ$  for the 0.0043 bed-height ratio.

### EFFECT OF THE SLOPE FACE ANGLE

At this parametric study, four slope face angles were modeled  $45^\circ$ ,  $50^\circ$ ,  $55^\circ$  and  $60^\circ$ . The results show that the mode or style of toppling was not affected by the slope face angle. By comparing the slopes at different face angles and the same bed thickness, the slopes were found to behave in the same pattern with the three modes of toppling: block-flexural, multiple blocks toppling and block toppling.

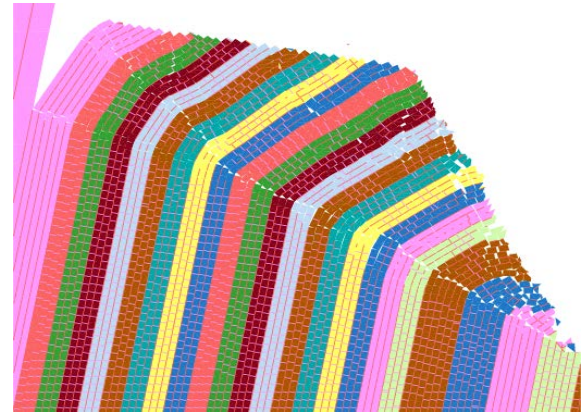
The low bed-height ratio slopes required more time to pass through this process of toppling, and in some cases it might need fracturing or removal of the failed material at the toe of the slope. The monitoring of the models showed that, the uphill scarp depth increased as the slope face increased, the uphill scarp for the  $60^\circ$  slope (0.017 bed-height ratio) was 123 m while the uphill scarp depth for the  $45^\circ$  was 83.4 m. This result was due to that, at steeper slopes the stresses was greater which resulted in higher stress-induced deformation. The high stress-induced deformations were accommodated by shearing along longer and deeper portions of the columns along the interface between the beds, and this resulted in deeper uphill scarp.

### ROCK SLIDES AND ROCK FALLS

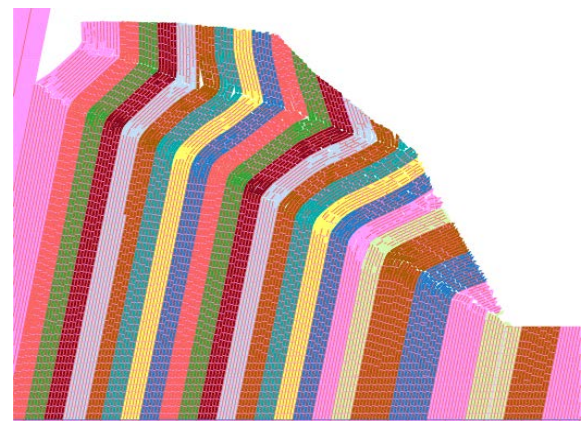
Toppling movement is characterized by shearing along the beds and rotation around the pivot line. This rotational movement may result in the formation of a rupture surface if enough rotational movement allowed.

This rupture surface evolves from the toe of the slopes, and propagates up the slope. Depending on the amount of rotation of the rock columns, the rupture surface may form partially or completely through the rock mass, i.e. through progressive development. Cruden and Hu [2] found topples that had been displaced by sliding along the rupture surface. The simulation revealed that the rupture surface was always initiated at the foot of the slope and propagated as the columns rotated and extended into the slope. In all models, the higher bed-height ratio slopes developed a rupture surface faster than the low bed-height ratio because the thin beds

allowed more gradual rotation and smoother curvature through the rock columns than the thick beds. Slopes with a  $45^\circ$  and  $55^\circ$  slope face angle tended to develop slopes susceptible to slide.



a) Block toppling, uphill scarp depth = 106.3 m, rupture surface at  $28^\circ$



b) Multiple block toppling, uphill scarp depth = 83.8 m, rupture surface at  $31^\circ$



c) Bed-height ratio = 0.00425

Fig. 5  $55^\circ$  slopes with three bed-height ratios and same number of cycles 320,000.

If further fracturing occurred and/or the cross-joints

were more closely spaced, the rock will slide and the debris will move down the slope. A slope with a  $45^\circ$  slope, 0.0085 bed-height ratio, and 2 m cross-joints were used to examine if sliding will occur at closer spaced cross-joints than 8 m.

Figure 6 shows the slope at failure and the sliding mass down the toe of the slope. In natural slopes, if natural damping did not stop the sliding mass, the material may travel away from the slope, as these failures may fail catastrophically at a high speed. McAfee and Cruden [5] noticed that five of the slopes at the Highway Pass developed a sliding mass away from the slope area. Note that rock falls were developed in the slopes with  $55^\circ$  and  $60^\circ$  degrees slope face angles especially at the 0.017 bed-height ratio. As the columns bent, the rock up the slope moved from flexural toppling, to multiple blocks toppling, to block toppling. At the stage of block toppling, the rocks at the top of the slope tended to detach from slope and fell catastrophically at very high speed, Figure 7 shows rock falls.

This behavior was observed more in the high bed-height ratio than the 0.085 and 0.0425 ratios because the slopes with high bed-height ratio moved easier and faster to block toppling stage, and left the upper part of the slope unsupported. The 0.0085 and 0.00425 bed-height ratio slopes tended to develop rock falls at the toe of the slopes. If erosion or any natural process removed the displaced material from the toe of the slope, or if the natural damping did not stop the rock falls at the toe the slope, the slopes would continue to move toward the block toppling stage and develop rock falls.

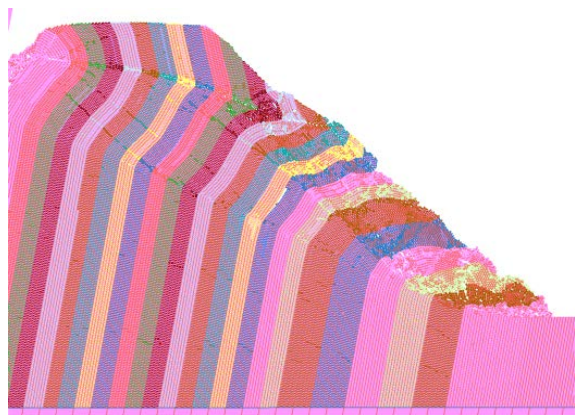


Fig. 6 Sliding proceeded by toppling

### TOPPLING IN CRYSTALLINE ROCKS

Unlike the sedimentary rock slopes discussed above, the foliated crystalline rocks may contain cross-joints with an irregular joints pattern. These joints can form at any angle with the steeply dipping joints. Nichol et al. [13] reported toppling in metamorphic and igneous rocks in natural rock slopes. This geological model is susceptible to

toppling due to the presence of the steeply dipping joints. As the cross-joints intersected the beds in different angles, the cross-joints were required to rotate and move more than the sedimentary rocks perpendicular cross-joints to form rupture surface. UDEC-DM [14] was used to create an irregular joints pattern at a random orientation inside the rock mass that contained steeply dipping joints (see the insert in Figure 2).



Fig. 7 Rock falls at  $60^\circ$  slope face angle and 0.017 bed-height ratio

The toppling mode, displacement, and formation of rupture surface were monitored and showed a similarity with the behavior of the sedimentary rocks. By comparing the two joints' patterns, the regular and irregular one, the later pattern was found to provides more planes that could accommodate sliding and shearing in the direction of the steeply dipping joints than the first pattern as the irregular joints' pattern contained joints in variable directions and some cross-joints might also have had the same orientation as that of the main joint set, which resulted in a steeper rupture or rotation surface than that of the sedimentary rocks. The three stages of toppling; flexural-block toppling, multiple blocks toppling, and block toppling occurred in these slopes, however, this behavior was more obvious in the sedimentary rocks.

Figure 8 shows the  $60^\circ$  foliated crystalline slope with a 0.017 bed-height ratio and irregular joints' pattern. By comparing Figure 8 and Figure 7, the two slopes at the same number of cycles, two different modes of toppling can be identified as the different joints orientations allowed shearing to be accommodated near the surface and delayed the transition from multiple block to block toppling. Further cycling permitted more deformation, which resulted in block toppling, Figure 9 shows the model at 720,000 cycles, this stage can be characterized as block toppling, notice the block falls, due to high slope face angle. Figure 10 shows an example of rock falls of steep slope. The slope shown in Figure is an example of a slope prone to topple; the rock



falls are shown at the heel of the slope.

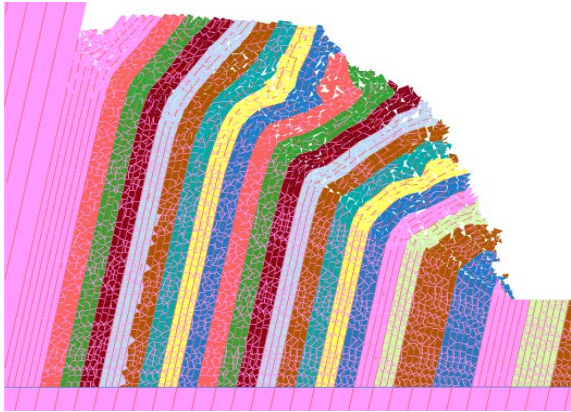


Fig. 8 Toppling at 60° slope face, and irregular joints pattern at 320,000 cycles

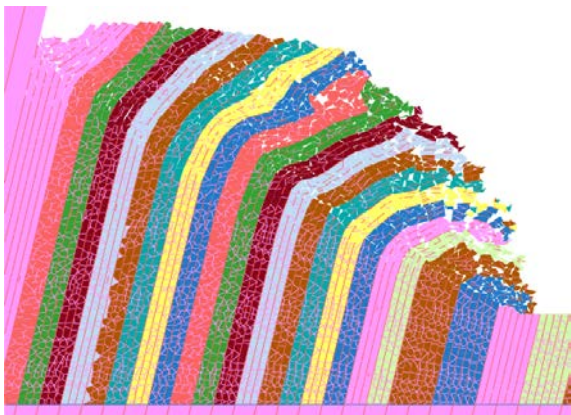


Fig. 9: Block toppling and rock falls, 60°slope, and 0.017 bed-height ratio at 720,000 cycles

## CONCLUSION

According to the numerical results presented in this study, the toppling style is more likely to be controlled by the time allowed for the slope to deform and move from stage to stage, the slope prone to topple moves with time from block-flexural toppling stage to block-toppling stage. The numerical modeling results suggest that bed-height ratio, rather than the block ratios, plays an important role in determining the toppling movement style. The smaller bed-height ratios introduced more shear planes in the rock mass than the high bed-height ratio, along which more sliding and shearing occurred at the instance of rock slope movement.

According to this parametric study, the rupture surface or pivot line also affected by the bed-height ratio, the thinner the beds, the steeper the rupture surface for the same slope face angle. In the field weathering with time, since the onset of toppling, might play an important role in controlling the movement style or stage. The steeper the slope the higher possibility of developing rock falls. The

rupture surface was initiated at the foot of the slope, as the columns down the slope were susceptible to more rotation than the columns up the slope.

## REFERENCES

- [1] Terzaghi, K. Stability of steep slopes on hard unweathered rock. *Geotechnique*, Vol. 12, 1962, pp. 251–270.
- [2] Cruden, D. and Hu, X.-Q. Topples on underdip slopes in the Highwood Pass, Alberta, Canada. *Quarterly Journal of Engineering Geology*, Vol. 27: 1994, pp. 57–68.
- [3] Cruden, D. and Varnes, D. Landslide types and processes. In *Landslides: Investigation and Mitigation*, Transportation Research Board. Special Report, Serial, edited by S. R. Turner, A.K., no. 247, 1996, pp.36–75. Washington D.C.
- [4] De Freitas, M. and Watters, R. Some field examples of toppling failure. *Geotechnique*, Vol. 23, 1973, pp. 485–514.
- [5] McAfee, R. and Cruden, D. Landslides at rock glacier site, Highwood Pass, Alberta. *Canadian Geotechnical Journal*, Vol. 33, 1996, 685–695.
- [6] Cruden, D. M. Limits to common toppling. *Canadian Geotechnical Journal*, Vol. 26, 1989, 737–742.
- [7] Goodman, R. and Bray, J. Toppling of rock slopes. In *Specialty Conference on Rock Engineering for Foundations and Slopes*, Vol. 2, 1976, pp. 739–760. ASCE, Boulder, CO.
- [8] Cruden, D. The shapes of cold, high mountains in sedimentary rocks. *Geomorphology*, Vol. 55, 2003, pp. 249–261.
- [9] Patton, F. D. Multiple modes of shear failure in rock. In *1st International congress, International Society for Rock Mechanics*, Lisbon, Portugal. Vol. 1, 1996, pp. 509–513.
- [10] Cruden, D. M. Rock slope movement in the Canadian cordillera. *Canadian Geotechnical Journal*, Vol. 22, 1985, pp. 528–540.
- [11] Hu, X.-Q. and Cruden, D. A portable tilting table for onsite tests of the friction angles of discontinuities in rock masses. *Bulletin International Association of Eng. Geology*, Vol. 46, 1992, pp. 59–62.
- [12] Martin, C. D. and Kaiser, P. K. Analysis of rock slopes with internal dilation. *Canadian Geotechnical Journal*, Vol.21(4), 1984, 605–624.
- [13] Nichol, S., Hunger, O., and Evans, S. Large-scale brittle and ductile toppling of rock slopes. *Canadian Geotechnical Journal*, Vol. 39, 2002, pp. 773–788.
- [14] Alzo'ubi, A., Martin, C., and Cruden, D. A discrete element damage model for rock slopes. In *Rock Mechanics, Meeting Society's Challenges and demands*, Vol. 1, 2007, pp. 503–510. Vancouver, B.C.

## ESTIMATION OF THICKNESS OF LANDFILL BY GEOPHYSICAL EXPLORATION METHODS AT ILLEGAL INDUSTRIAL WASTES DISPOSAL SITE

Minoru Yamanaka<sup>1</sup>, Tomoaki Hachimura<sup>2</sup>, Shuichi Hasegawa<sup>1</sup>

<sup>1</sup>Faculty of Engineering, Kagawa University

<sup>2</sup>Graduate School of Engineering, Kagawa University

### ABSTRACT

Serious environmental pollution has caused by illegal disposal of industrial wastes in Kagawa Teshima Island, Kagawa Prefecture, Japan. For restitution of Teshima, a distribution of the industrial waste by the drilling survey by past administration's research became clear roughly. But since the wastes was buried partially such as a pot into the sandy soil layer under the waste layer, it is necessary to investigate in detail the thickness of the wastes as removal of the waste layer progressed.

In this paper, the surface wave prospecting, the microtremor, the Electromagnetic method (EM) sounding and the Continuous wave radar sounding, which is new geophysical exploration methods, were carried out at the illegal industrial wastes disposal site for the purpose of estimating the thickness of the waste layer with sufficient accuracy.

*Keywords: Landfill, Investigation, Geophysical Exploration, Surface Wave Prospecting*

### INTRODUCTION

In order to estimate a volume of industrial wastes disposed illegally, it is necessary to measure a ground surface and to investigate a depth of the wastes by boring survey in general. The usual boring survey which uses water at the time of drilling has a possibility of making a contaminant expanding from a waste layer with concern of soil pollution. Because metal and rubber pieces may mix so much in wastes containing shredder dust (SD), it is very difficult to check the depth of wastes such a cone penetration test <sup>[1]</sup>. And more, the waste may be partially buried deeply such as pot at an illegal disposal <sup>[2]</sup>. Therefore application of geophysical exploration method which can detect continuous layer thickness distribution is desired strongly.

In this study, some geophysical exploration methods such as the surface wave prospecting and radar exploration were carried out at the illegal industrial waste disposal site, and the detection capability of continuous distribution of the waste layer was discussed.

### TESHIMA ILLIGAL DISPOSAL SITE

#### Topography and Geology

Figure 1 shows the plane of Teshima illegal disposal site. The site is at the seashore part of the northwest of Teshima Island, Kagawa Prefecture. As for the geology of the site, a granite rock, an alluvium soil, a reclamation soil, a banking soil and

the wastes are distributed from the lower part. The granite rock has many cracks, and the surface of granite has been weathered strongly <sup>[3]</sup>.

#### Amount of Treatment of Wastes

The industrial waste which reaches to about 675,000 tons will carry out from Teshima by March, 2016, and the carry out waste will be processed with incineration and melting style in the disposing facility in Naoshima island next to Teshima by the mediation provision of the pollution mediation with Kagawa Prefecture and Teshima residents <sup>[4] [5]</sup>.

Table 1 shows the amount of treatment of wastes and a polluted soil under wastes by estimating in as of March, 2011. The weight of wastes is increasing from 675 000 at the beginning to 938 000 tons because of an increasing of the waste density and a detection newly of wastes in banking layer soil under wastes layer. The polluted soil under the wastes layer will utilize as a cement material.

Table 1 Amount of treatment

Kind	Volume (Thousands m <sup>3</sup> )	Weight (Thousands tons)
Wastes	458.20	499.44
Polluted soil	70.20	122.85
Cover soil	19.40	33.92
Total	547.80	656.21



## GEOPHYSICAL EXPLORATION METHODS

### Survey Line of Investigation

Figure 1 shows the plane with survey lines of three types of geophysical explorations at the site.

The A-A' line was set on the sandy layer after the waste layer was removed, and the surface wave prospecting was carried out only at A-A' line. The B-B' line was set on shredder dust (SD) waste layer, and surface wave prospecting and microtremor were carried out at B-B' line. In addition, there is about 5 m difference in the ground level of A-A' line and B-B' line (see in Photo 1 (a),(b),(c)).

C-C' line and D-D' line of the direction from east to west the surface wave prospecting, the electromagnetic method (EM) sounding, and continuous wave radar sounding were carried out after excavating SD wastes accumulated on the south at B-B' line (see in Photo 2 (a),(b),(c))

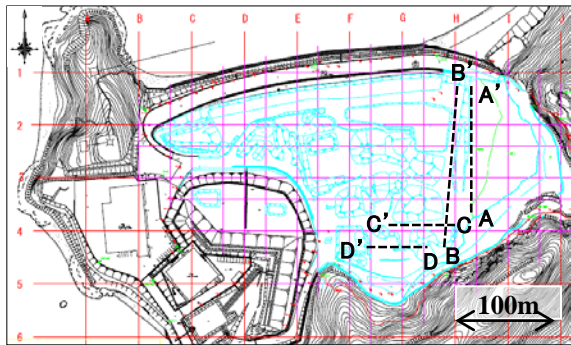


Fig.1 Plane with survey lines of three types of geophysical explorations



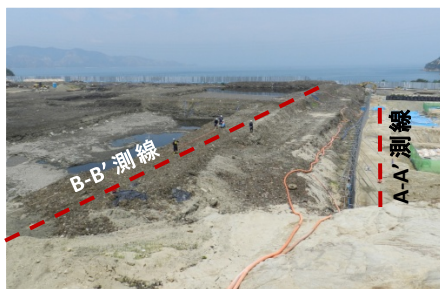
Photo. 3 Close view of SD wastes

Photo. 3 shows the close view of the SD wastes. It can be seen that a large piece of rubber or metal is contained in much quantity.

### Investigation methods

#### Surface wave prospecting

The Surface wave prospecting was carried out by using the high precision surface wave exploration equipment (McSEIS-SXW), and the land streamer type which draws on the surface of the waste layer was used because of roughness of the waste layer. The interval was 0.5 m for vibration points by hammer, and was 1.0 m for receiving points by 24 seismograph sensors. In order to make a seismograph catch certainly vibration transmitted in SD wastes deposited very loosely, it took care so that the base plate of the seismograph sensor might stick to waste.



(a) A-A' line and B-B' line



(b) Surface wave prospecting on A-A' line



(c) Surface wave prospecting on B-B' line

Photo. 1 State of exploration on A-A' line and B-B' line



(a) C-C' line and D-D' line



(b) EM sounding on C-C' line



(c) Continuous wave radar sounding on B-B' line

Photo. 2 State of exploration on C-C' line and D-D' line

### Microtremor

Measurement of microtremor was used the servo type accelerometer (McSEIS-MT NEO). Microtremor was measured every 10 m at a total of 15 places from the starting point of the B-B' line which carried out surface wave investigation. Because the surface level of the waste layer from 20 m to 70m at the B-B' line was downed by about 1 m from the level at the time of the surface wave investigation by progress of construction, the 1 m was considered when it analyze microtremor date.

### Electromagnetic method (EM) sounding

EM sounding is the method of analyzing the conductivity of the ground by observing the artificial induction electromagnetic field which occurs by the current sent through the coil or the loop. EM sounding was used together both measurements of type of EM31 and EM34. It becomes possible to obtain the image sectional view showing a ground conductivity structure by this combined use.

EM31 is a rigid boom type which fixed the transmitting coil and the receiver coil at a certain interval. EM31 is designed to measure by one person only, and is possible to investigate up to 6 m under surface at several hundred points per one day.

EM34 is the measuring device which separates the transmitting coil and the receiver coil. EM34 can be investigated up to about maximum 30m below by changing the distance of the coil separation.

### Continuous wave radar sounding

As for method of continuous wave radar sounding, it irradiates electromagnetic waves to ground surface, analyzes the reflected wave from some layers having different electric physical properties (conductivity etc.), and obtains the visible continued image. In order to obtain the analyzed reflective section image (time section image) under the line, the profile method was used in this study. In measurement by the profile method, using a transmitting antenna and a receiving antenna as a pair, it measured by keeping an antenna interval at 3 m and moving a transceiver antenna every 0.5 m. The analyzed reflective section

image (time section image) under the line is obtained by putting receiving records of measurement points in order.

## INVESTIGATION RESULTS

### Estimation of waste layer by surface wave prospecting and microtremor results

Figure 2 shows the analysis result of S-wave velocity  $V_s$  obtained by surface wave prospecting on the A-A' line on the sandy layer after the waste layer was removed. Since the  $V_s$  indicates 300 m/s over from 0 to 10 m in distance, it seems that the base rock (granite) layer is distributed near this. And it can be said that the high density sandy soil showing about 100 to 300 m/s of  $V_s$  is distributed from near 10 m of distance. In addition, at near 90 m of distance, because of influence of the noise by vibration of the exhaust hose crossing at this point was not able to be removed enough, it was considered as the white zone in this figure.

Figure 3 shows the relation between  $N_s$  by converting from  $V_s$  and  $N_d$  by converting from the penetration resistance value by the simple dynamic penetration test at 30 m in Fig. 5(a) and 80m in Fig. 5(b) on A-A' line.  $N_s$  is becoming large gradually to the depth estimated to be sandy soil which shows  $N_s = 30$  over at 30 m and at 80 m in both figures. And since  $N_d$  shows the properties of the sandy soil which is a matrix on the whole although  $N_d$  changes largely because a rod hits stones, it can be recognized that  $N_d$  is smaller a little than  $N_s$ . Here although the simple dynamic penetration test was carried out a total of 17 on A-A' line, it was almost the case that the test was not fully able to carry out because the rod hit frequency a gravel or a cobble stone in the surface layer.

Figure 4 shows the S-wave velocity  $V_s$  and the point of microtremor on B-B' line which is on the waste.  $V_s$  indicates about 300 m/s because of the base rock (granite) at near the starting point. And it can be clear that the waste layer that is  $V_s < 100$  m/s distributed from 15 m to the end of distance. The thickness of the waste layer can be estimated to be around 5 m judging from the value of  $V_s$ . Since the difference of the surface level between B-B' line

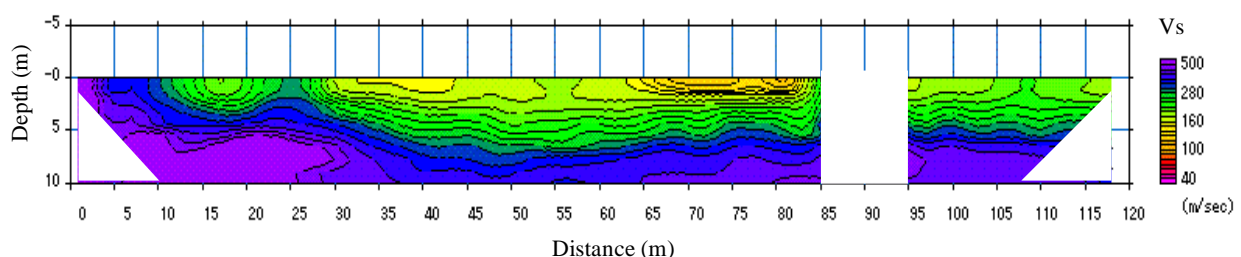
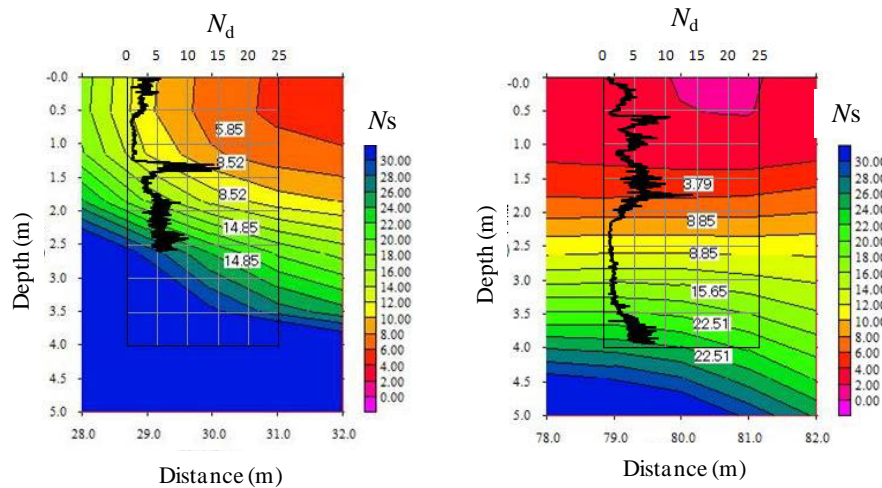


Fig.2 Analysis result of S-wave velocity  $V_s$  obtained by surface wave prospecting on the A-A' line





(a) Point at 30 m on A-A' line (b) Point at 80 m on A-A' line  
Fig.3 Relation between  $N_s$  from  $V_s$  and  $N_d$  from the penetration resistance value

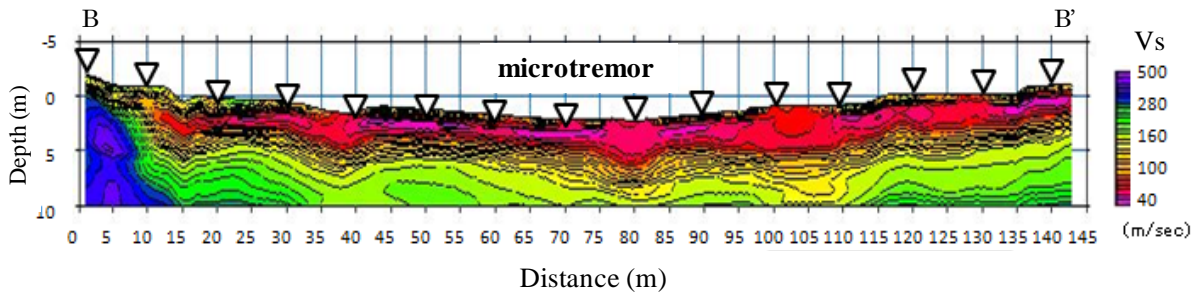
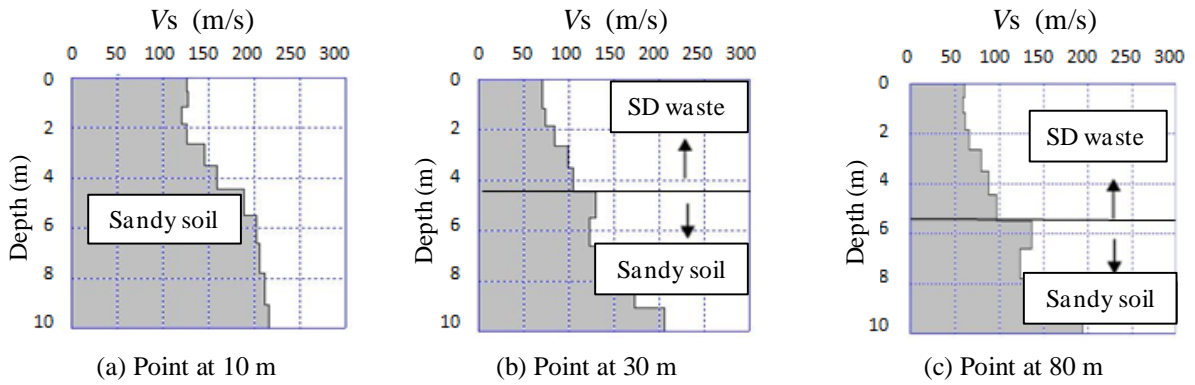
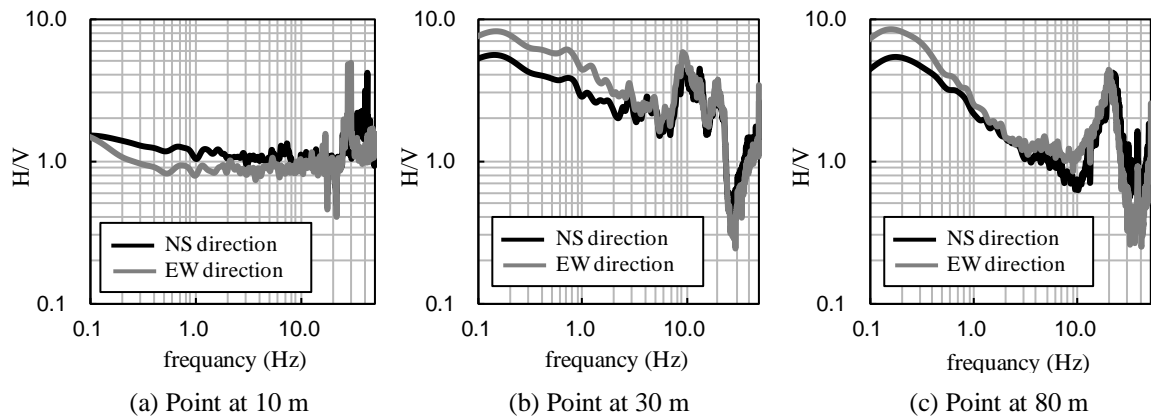


Fig.4 S-wave velocity  $V_s$  and the point of microtremor on B-B' line



(a) Point at 10 m (b) Point at 30 m (c) Point at 80 m  
Fig.5 Change of  $V_s$  toward depth at each point on B-B' line



(a) Point at 10 m (b) Point at 30 m (c) Point at 80 m  
Fig. 6 H/V spectral ratio on B-B' line

which is on the waste and A-A' line which is on the sandy soil is about 5 m from the point of direct survey, it can be confirmed that the thickness of the waste layer is about 5 m on B-B' line. Moreover, although the contour line of S-wave velocity shows a shape as a concave at 40 m, 80 m and near 105 m in distance, it suggests that a existence of undiscovered wastes into the sandy soil under the waste.

Figure 5 (a), (b) and (c) show the in-depth profile of  $V_s$  at 10m, 30 m and 80 m in distance individually. The waste does not accumulate at the point of 10 m in distance, and the  $V_s$  of sandy soil indicates more than about 120 m/s in Fig. 5(a). On the other hand, the waste accumulated at 30 m in Fig. 5(b) and at 80 m in Fig.5(c), it estimated that the value of S-wave velocity of the waste layer is  $V_s < 110$  m/s.

Figure 6 (a), (b) and (c) show the H/V spectral ratio obtained by analyzing a ground micro vibration by the microtremor at the same point as above Fig. 5. Frequency of 10 Hz or more was judged to be the frequency corresponding to the base rock. And since the site was near the seashore, the frequency of 1.0 Hz or less was judged to be the value having an influence of sea wave. Therefore the frequency which shows the value of a high H/V spectrum in the range with a frequency of 1.0 to 10 Hz was judged to be the frequency corresponding to the waste layer.

Now, the thickness of the waste layer can be calculated by the 1/4-wave rule shown in equation (1) using the frequency  $f$  corresponding to  $V_s$  of the waste layer and waste layer of an every place point.

$$H = V_s / 4f \quad \text{eq.(1)}$$

Here,  $H$  : estimated thickness of waste layer (m).

$f$  : frequency corresponding to waste layer obtained by the microtremor (Hz).

$V_s$  : S-wave velocity obtained by Surface wave prospecting (m/s).

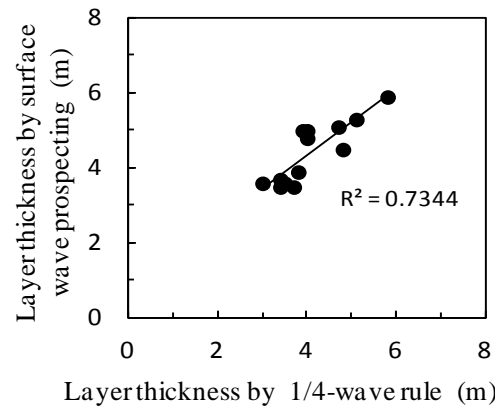


Fig.7 Correlation of layer thickness by surface wave prospecting and one by 1/4-wave rule

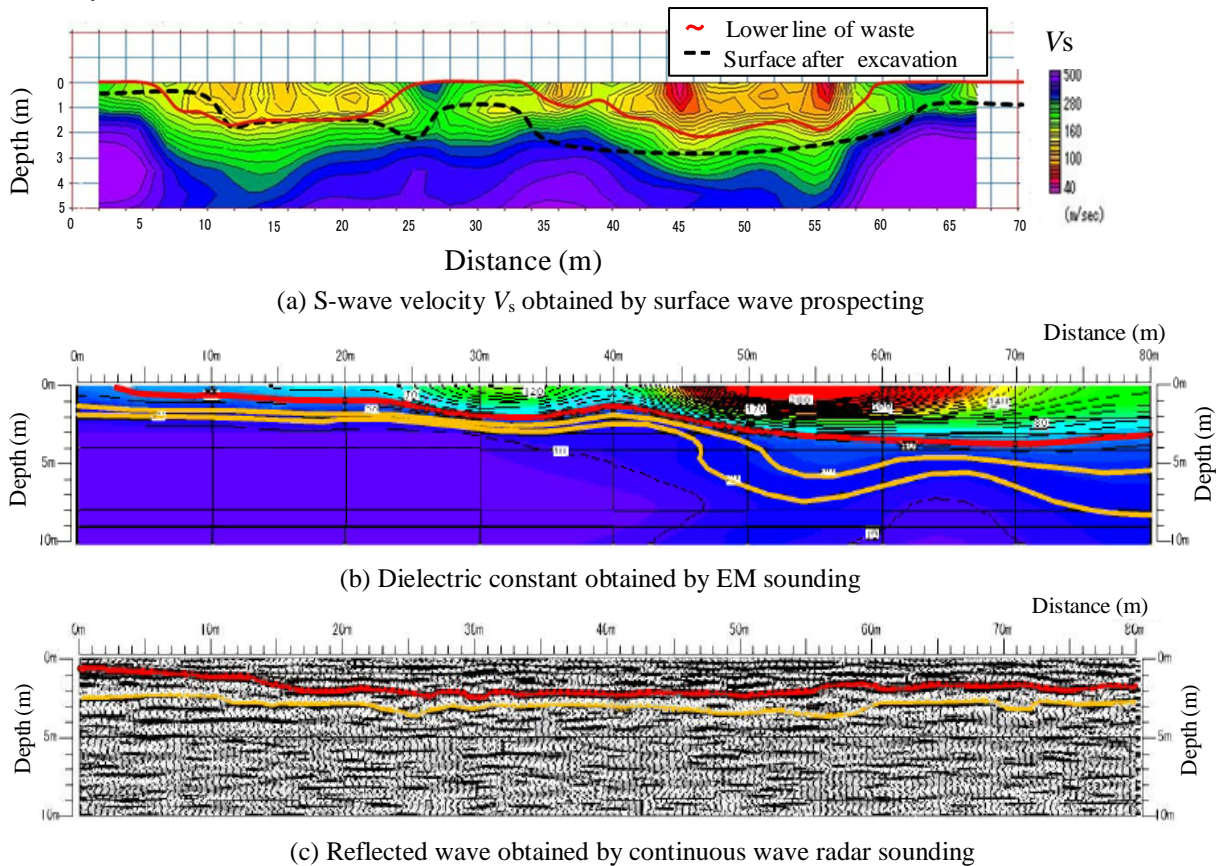


Fig.8 Results of geophysical exploration methods on C-C' line

Figure 7 shows the correlation of layer thickness by surface wave prospecting and one by 1/4-wave rule. It became clear that both layer thicknesses had positive correlation, and it can be said that the thickness of the waste layer by two geophysical investigation methods has enough accuracy.

### Estimation of layer thickness by EM sounding and continuous wave radar sounding

Figure 8 (a), (b), (c) show the decipherment result by three kinds of geophysical exploration carried out on the SD waste on C-C' line individually.

From Fig. 8 (a) which is result of the surface wave prospecting, the layer of the value of  $V_s=80\sim120$  m/s distributes in the surface on C-C' line, therefore this layer is estimated to be the SD waste layer. The red line in the figure means the boundary between the SD waste layer and the sandy soil layer. Since the red line falls largely at 8~25 m and 35~60 m in distance, it is considered that the waste is buried such as a pot. After the removal work of the SD waste was carried out after of proceeding the surface wave prospecting on C-C' line. The dashed black line shows the surface of sandy soil after the removal work. Although the lower boundary of the estimated waste layer correspond mostly to the surface of sandy soil at 10~20 m in distance, the surface of sandy soil seems to be deeper about 1~2 m in depth at other area. As this reason, it considered that the sandy soil mixed wastes a little under the SD waste and a discolored sandy soil which anxious about contamination was removed together. And more, although the value of  $V_s$  of the estimated SD waste on C-C' line is bigger a little than the one of the SD waste on A-A' line, it can be said that it is influence of increase of density of the SD waste in order to mix much sandy soils into the SD waste on C-C' line.

From Fig. 8(b) which is result of the EM sounding, the contrast of comparatively clear conductivity is detectable. The dielectric constant of the waste layer is 50 or more mS/m, and one of the base rock (granite) set as 20 or 30 mS/m each. Although there is a zone where a dielectric constant shows 150 mS/m or more at 45 ~ 70 m in distance, it can guess that the waste of different density is buried in this zone. And from Fig.8(c) which is result of the continuous wave radar sounding, the reflected wave of two lines was detected comparatively clearly. The above line was estimated as the reflected wave of undersurface boundary of the waste, and the low line was estimated as the reflected wave of upper surface boundary of the granite. On the other hands, as for the thickness of sandy soil layer, it can be read as 3 ~ 4 m by the surface wave prospecting, as 1 ~ 3 m by the EM sounding, and as 1 ~ 2 m by the continuous wave radar sounding.

## CONCLUSIONS

As a result of this study, important conclusions are summarized as follows.

- 1) The S-wave velocity of the SD waste of Teshima Industrial illegal disposal site is very low, it estimates about  $V_s=100$  m/s.
- 2) With the combination of the surface wave prospecting and the microtremor, it can estimate useful accuracy the thickness of the waste layer.
- 3) The surface wave prospecting is most suitable for estimation of the thickness of the SD waste layer among three kinds of geophysical exploration methods by this study.

## ACKNOWLEDGEMENTS

The authors would like to appreciate Mr. Masaya Komino of the waste management division, Kagawa prefectural office for his support in carrying out this study, Miss. Takako Takahashi of OYO Corporation for her technical advice for the surface wave prospecting, and Mr. Kiyoshi Yoshida of Kawasaki Geotechnical Engineering Co.,Ltd. for his technical advice for the EM sounding and the continuous wave radar sounding.

## REFERENCES

- [1] Hachimura T., Yamanaka M., Ohno H. and Hasegawa S. "New Investigation Methods to Estimate Waste Properties of Existent Landfills", Proc. of the 20th Int. Offshore and Polar Eng. Conf., ISOPE, Beijing, China, pp.739-742, 2010.
- [2] Yamanaka M., Ishida S., Hasegawa S. and Ikeda A., "Estimation of Layer Thickness of Landfill Waste by Geophysical Investigation Techniques", Proc. of Annual Conference of Shikoku branch of Japanese Geotechnical Society, pp.9-10, 2012. (in Japanese)
- [3] Hanashima M., Takatsuki H. and Nakasugi O., "A Case Study of Environmental Contamination Caused by Illegal Dumping of Hazardous Wastes", Waste Management Research, Vol.7, No.3, pp.208-219, 1996. (in Japanese with English abstract)
- [4] Kagawa Prefectural Management Committee for Disposal of Waste in Teshima, "Report on the Current Situation of Waste Disposal in Teshima", Waste Management Research, Vol.18, No.5, pp.304-314, 2007. (in Japanese with English abstract)
- [5] Kagawa Prefecture's Technological Examination Committee for treatment of Teshima' Industrial Wastes, "A Technological Examination for Treatment of Teshima's Industrial Wastes, Waste Management Research, Vol.12, No.2, pp.117-124, 2001. (in Japanese with English abstract)

## APPLICATIONS OF INNOVATIVE MATERIALS FOR PERFORMANCE IMPROVEMENT OF FLEXIBLE PAVEMENT OVER EXPANSIVE SUBGRADE

Ravin M. Tailor<sup>1</sup>, Dr. Navin C. Shah<sup>2</sup>

<sup>1</sup>Assistant Professor, S. V. National Institute of Technology, Surat, Gujarat, India;

<sup>2</sup>Director, Chhotubhai Gopalbhai Patel Institute of Technology, Bardoli, Gujarat, India

### ABSTRACT

Expansive soils are one of the most problematic materials that are widely encountered in significant land areas in several parts of the world; like Africa, Australia, India, United States and Canada. The South Gujarat region in India have majority of top soil as black cotton soil. The black cotton soil has characteristics of shrinking on drying and heaving on wetting. This soil being expansive creates several types of damages to pavement structures, and in some cases the pavement may even become unserviceable. The normal climate condition of study area shows short wet and long dry period which aggravate the problem of swelling and shrinkage. The IRC: 37 – 2001, Annexure – 4 suggest 0.6 to 1.0 m thick non-cohesive soil cushion on the expansive soil for road construction which led to higher cost for road construction. Also for new urban areas it is difficult to raise the embankment or to excavate the subgrade upto such a depth due to existing structures and under laying service lines. To provide economical solution along with feasible application two innovative materials were used namely, CONSOLID and Geotextile for flexible pavement. The CONSOLID application shows the great improvement of CBR values helping the overall stability of the pavement. The Geotextile provided below the pavement components to act against the heaving of the swelling soil at the same time it helps as drainage layer also. Field study is undertaken to observe the effect of Geotextile in flexible pavement performance and 2 specific boundary conditions are created for observations. The Observations shows about 50 % reduction in shrinkage effect for paved road reinforced with Geotextile subjected to drying and wetting cycles. Both the materials are having its unique advantage in the performance improvement of flexible pavement over expansive subgrade.

*Keywords: Expansive Soil, CONSOLID, Geotextile, Pavement Performance*

### INTRODUCTION

Roads are vital to link our communities and sustain the economy and quality of life in society. Roads constructed over the expansive soil observed with high maintenance expenditure inspite of high capital cost. These are because many roads in this region are failing prematurely due to the expansion of reactive soils underneath the roadway, causing safety issues and increases road maintenance costs.

Frost, Fleming and Rogers (2004) [1] outline the primary roles that a subgrade or pavement foundation must play in pavement design. The volume change at subgrade creates variety of failure in flexible pavement like cracking, rutting, potholes etc. Expansive soils are one of the most problematic materials that are widely encountered in significant Land areas in several parts of the world e.g. parts of Africa, Australia, India, United States and Canada. In these countries expansive soil is having great impact on the construction and maintenance costs of highways. The South West region of India is covered by top soil as black cotton soil. Fig. 1, map of soil deposits in Gujarat State shows that the

majority of South Gujarat area having black cottons soil as top layer.

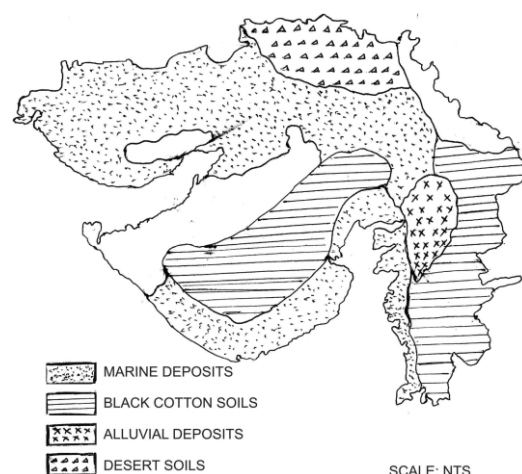


Fig. 1 Map of Soil Deposits in Gujarat State

To understand the phenomenon of expansion of swelling soil and to provide economical solution along with feasible application utilising various

strength of Geotextiles study started at the SVNIT campus, South Gujarat region of India. Geotextile is provided below the pavement components to act against the heaving of the swelling soil at the same time it helps as drainage layer also. Field study is undertaken to observe the effect of geotextile in flexible pavement performance and 2 specific boundary conditions are created for observations. Observations summarized shows about 50 % reductions in shrinkage effect for paved road reinforced with geotextile compared to road without geotextile.

Also the advanced material called CONSOLID system with two different types of soil were examined for better performance of south Gujarat soil. The samples are collected from SVNIT Campus in South Gujarat region and experimental work carried out for evaluation of CONSOLID system. Two samples are collected and named as, 1) SVNIT Road Side Shoulder Soil, and 2) SVNIT Campus Soil. The soil samples are found of MH and CH type of soil. The Soak CBR for MH type of soil for natural condition is 2.4% which improves about 45% With CONSOLID Treatment. Similarly, the Soak CBR for CH type of soil natural condition is 2% which improves about 27% with CONSOLID Treatment.

## EXPANSIVE SOIL

Expansive soils are clayey soils, mudstones or shales that are characterized by their potential for volume change on drying and/or wetting. Usually the clay content is relatively high and the clay mineral montmorillonite dominates. They are characterized by their high strength when dry; very low strength when wet; wide and deep shrinkage cracks in the dry season; high plasticity and very poor trafficability when wetted. Whenever insufficient attention is given to the deleterious properties of expansive soils, the results will be premature pavement failure evidenced by undulations, cracks, potholes and heave. Methods were developed for the identification and classification of expansive soils both locally and worldwide. In India IS: 1498-1970 [2] describe the methods to identify the expansive soil.

There are three basic particle size components of naturally occurring soil: sand, silt and clay. Plastic clays termed as expansive soils or active soils exhibit volume change when subjected to moisture variations (He-Ping Yang et al, 2007) [3]. Swelling or expansive clay soils are those that contain swelling clay minerals (such as montmorillonite and smectite) and can often be scientifically referred to as Vertosols. Vertosols are soils that contain clay minerals which, because of their natural physiochemical properties, possess a net negative electrical charge imbalance that attracts the positive

pole of dipolar water molecules and cations (Snethen, 1980) [4]. In addition, expansive soils have high degree of shrink-swell reversibility with change in moisture content. Petry and Little (2002) [5] discuss the history of clays and their engineering significance, dating back to papers written in the early 1930's.

The effects on buildings constructed on reactive soils with inadequate footings can be dramatic (Smith R, 2004) [6]. Road subgrades can be viewed as the footings/ foundations for road pavements, and if these footings are not adequate, structural damage can occur.

## STUDY AREA OBSERVATIONS

The research started based on the theme to provide effective solution against the moisture variation and differential swelling / shrinking of expansive soil in the area. There was planning of road construction at SVNIT campus near the observed site. The flexible road was proposed connecting transportation lab to workshop building on the back side of Civil Engineering Department. This site was selected for the further research work. Fig. 2 shows the aerial view of the site as observed in Google web page.

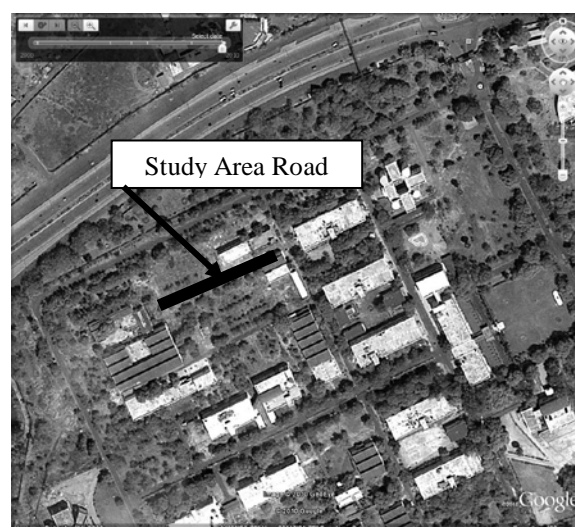


Fig. 2 Location of Road Joining Transportation Engineering Lab to Workshop, at SVNIT Campus, South Gujarat, India

The study by Jigisha (2008) [7] shows the average soaked CBR for typical South Gujarat undisturbed or compacted soil as 2.0 %.

Also study carried out by Yogendra (2008) [8] shows the similar type of observation for the South Gujarat region soil. Table 1 shows the Geotechnical Properties of Black cotton soil as observed by Yogendra (2008) [8].

Table 1 Geotechnical properties of black cotton



soil.

Property		Values
Grain Size	Gravel (%)	1
	Sand (%)	12
	Silt + Clay (%)	87
Atterberg's Limit	Liquid Limit (%)	55
	Plasticity Index (%)	27
Compaction Test	MDD (kN/cu.m)	15.50
	OMC (%)	21.75
Swelling Test	Free Swell Index (%)	70
CBR (%)		1.77
UCS (kN/sq.m)		59
Permeability (m/s)		8.75 x 10 <sup>-9</sup>

Also the samples are collected from the SVNIT campus to access the suitability with CONSOLID system. Various laboratory tests were carried out for the samples collected and mainly the CBR values are reported for the same. Table-2 shows the results for the same.

Table 2 CBR values of study area soils

Sample I.D.	1 - S.V.N.I.T. Road Side Shoulder Soil	2 - S.V.N.I.T. Campus Soil
Unsoak CBR %	5.7	4.7
Soak CBR %	2.4	2.0

### GEOTEXTILE FOR FOUNDING FLEXIBLE PAVEMENT ON SWELLING SUBGRADE

The proposed road is studied for its design and planning was done for the observation of the expansive subgrade behaviour. After taking necessary approval from authority it was decided to provide the Geotextile GARWARE made GWF-52-240 PP Grey Multi 240 Twill 5 M, just below the subbase layer for further observation.

The geotextile was laid in such a manner that 2 boundary conditions can be created for the site.

- 1) Road with both side covered ground (length between Transportation Engineering Lab and Water Resources Engineering Lab)
- 2) Road with one side covered and one side open ground (length along WRE lab & after WRE lab).

Figure 3 shows various stages of the road construction at site.



a) Geotextile above Murrum,



b) GSB spreading on Geotextile

Fig. 3 Road construction work in progress at site.

### Pavement Observations & Analysis

The following observations were started after finishing of the pavement construction upto grouting layer.

- 1) Visual observation for cracks and other changes
- 2) Ground profile reading to get amount of change in soil thickness with change in moisture content (i.e. change in season).

The visual observation shows that in some of the portion the Top Surface was deteriorated because of non-availability of appropriate Bituminous Layer. In general the area with Geotextile shows less undulation.

#### Ground profile survey

The leveling exercise carried out after pavement construction in Month of December 2010 to get the initial Ground Level RL. After one year during December 2011 further the ground level are surveyed and another ground level survey was carried out in June 2012.

The detailed observation are summarized and published by Tailor R.M. et. al. in year 2012 [9] and 2014 [10]. The summertime graphs shown in Fig. 4, 5 and 6 represents ground profile for various observations at Right, Centre and Left side.



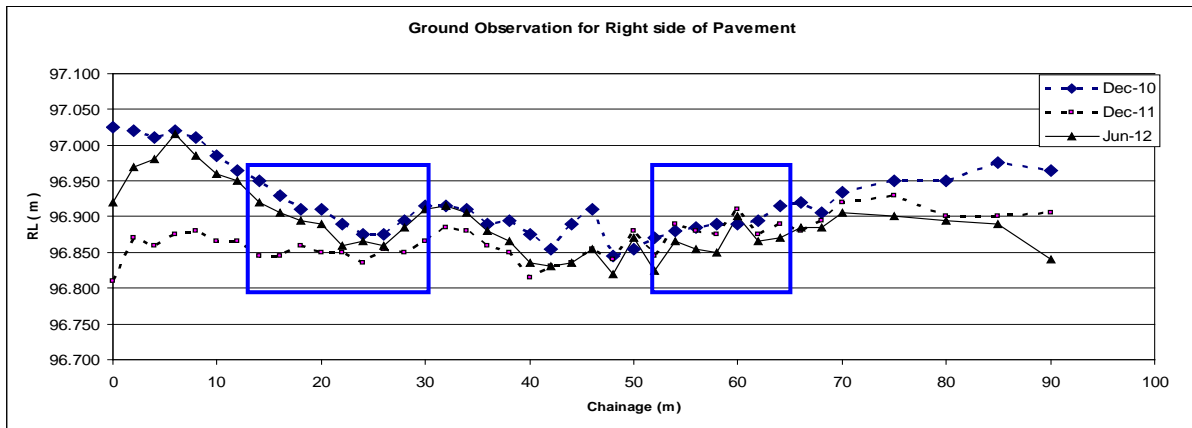


Fig. 4 Ground observation for Right side of Pavement.

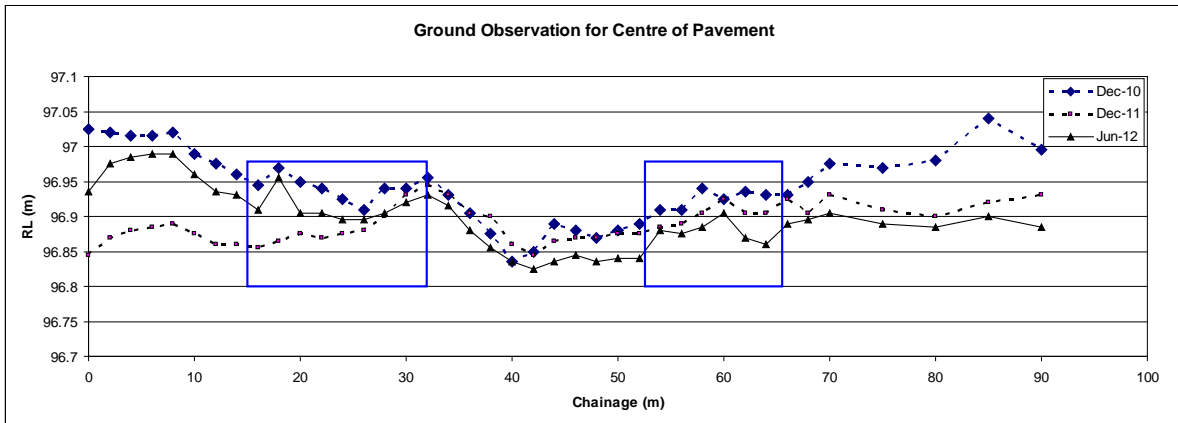


Fig. 5 Ground observation for Centre of Pavement.

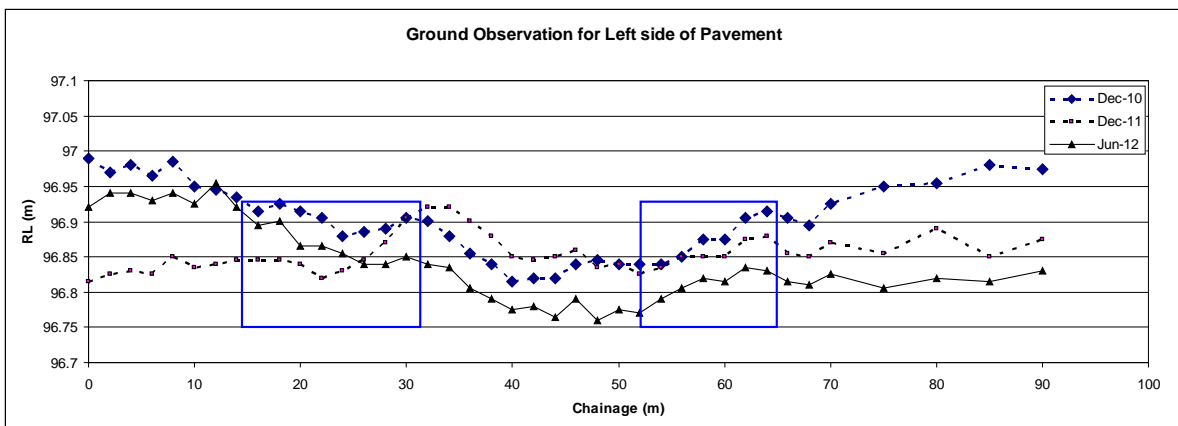


Fig. 6 Ground observation for Left side of Pavement

*Observations for WBM unasphalted pavement at Transportation Engineering Laboratory*

The subgrade was saturated clay. The typical road construction with structures on both sides and structure on one side were under observation. The other side is water logged and absence of topping

crust was also pervious to some extent. The textile was laid on subgrade in December 2010.

The December 2011 & June 2012 observations of elevation on road with nominal traffic shows:  
1) The introduction of geotextile fabric in sector of walls on both sides shows 40% reduction in shrinkage of fill & subgrade.

2) Wall on right & free surface on left, Chainage 54 – 90 m. The performance in December 2011 shows 43 mm average reduction of settlement of surface in fabric reinforced zone. (Reduction of about 60 % with reference to no reinforcement zone)

3) In middle sector with wall on right & free water access to left typical ingress of water can be seen to centre of road by December 2011. The left end shows ultimate heave where as right end shows settlement with little movement at centre in zone. In reinforced sector of this road overall performance shows settlement of 37 to 19 mm.

4) In general, trend shows shrinkage effect leading to settlement indicates drastic reduction of 50 % or more.

### CONSOLIDATE SYSTEM TO IMPROVE CBR

Sustainable production and consumption, leading to increased resource efficiency, is now high on the political agenda. Various alternatives are developed in form of advanced materials and waste utilization for resource intensive activities such as the construction of infrastructure including highways. The range of materials incorporated includes recycled asphalt, recycled concrete, ashes, slags, foundry sand, glass, plastic, rubber and other chemicals. Feasibility studies concerning the potential for the use of these materials are plentiful and some studies exist which have considered the engineering as well as environmental credentials of such practices. This particular study summarizes work conducted to date and investigates the engineering as well performance of CONSOLID system, which is combination of Consolidate444 & Solidry powder to replace conventional materials in non-bituminous layers of flexible pavement. Also same can be used to improve the soil CBR.

To study behavior of CONSOLID system with two different types of soil; samples are collected from Surat city and surrounding area in South Gujarat region and experimental works carried out for evaluation of CONSOLID system. The study for soil characteristics, Free Swell Index, Standard Proctor Test, Specific Gravity, CBR and UCS are conducted for natural and treated soil samples. Two samples are collected from the SVNIT campus and named as, 1) SVNIT Road Side Shoulder Soil, and 2) SVNIT Campus Soil.

The California Bearing Ratio test is penetration test meant for the evaluation of subgrade strength of roads and pavements. The results obtained by these tests are used with the empirical curves to determine the thickness of pavement and its component layers. This is the most widely used method for the design of flexible pavement. The CBR value of the specimen reflects on the strength of the specimen in soaked or un-soaked condition as tested in the laboratory. The soaked CBR values reflect the soil

behaviour in saturated condition and hence is very critical for the regions with heavy rainfall and retentive soil types. The soak CBR test is carried out after the submergence of sample in water for 4 days in accordance to IS: 2720 (Part 16) [11]. The test results are presented in Table 3 & 4 below for both samples.

Table 3 CBR values of SVNIT Road Side Shoulder soil with CONSOLID System.

Soil Condition	Natural Soil	Soil with CONSOLID System
Unsoak CBR %	5.7	54
Soak CBR %	2.4	45

Table 4 CBR values of SVNIT Campus soil with CONSOLID System.

Soil Condition	Natural Soil	Soil with CONSOLID System
Unsoak CBR %	4.7	32
Soak CBR %	2.0	27

The 1) SVNIT Road Side Shoulder soil sample found of MH type of soil while the 2) SVNIT Campus soil observed as CH type of soil. The Soak CBR for MH type of soil for natural condition is 2.4% which improves about 45% With CONSOLID Treatment. Similarly, the Soak CBR for CH type of soil in natural condition is 2% which improves about 27% with CONSOLID Treatment.

### CONCLUSION

The textile was laid on subgrade in December 2010. The December 2011 and June 2012 observations of elevation on road with nominal traffic shows:

1) The area without geotextile bothside building shows uneven change in ground profile while the area with Geotextile bothside building shows about 50 % reduction with uniform change in ground profile.

2) The area without Geotextile Rightside building shows the considerable change of ground in ground profile on lefthand side because of direct entry of rainwater on that side. The area with Geotextile Rightside building shows slight changes in leftside region.

3) Overall the observations show the positive impact of Geotextile laying in flexible pavement over swelling subgrade.

The overall visual observations also indicate considerable reduction in ground profile change for

flexible pavement embedded with Geotextile over swelling subgrade.

The CONSOLID system results shows great improvement in soaked CBR values from 2.4% to 45% for MH soil and 2% to 27% for CH soil, which encourage its utilization to improve subgrade condition.

## ACKNOWLEDGEMENTS

The authors are thankful to M/s Garce and Sachi Enterprise, Ahmedabad for funding the CONSOLID system project. Also thank to Dr. C.H. Solanki, Professor, Applied Mechanics Department, SVNIT, Surat for his continues support during the research work. Thanks are due to late Dr. M. D. Desai, Shri Jignesh Patel, Dr. Jigisha Vashi, Dr. Yogendra Tandel and Shri C. R. Patel for their unconditional support throughout the research work.

## REFERENCES

- [1] Frost W M, Fleming P R, and Rogers C D F, "Assessment of a Performance Specification Approach to Pavement Foundations", Transportation Research Record 1757, Soils Geology and Foundations, Transportation Research Board, Washington D.C, 2001, pp.100-108.
- [2] Classification and Identification of Soils for General Engineering Purposes, Indian Standard, IS: 1498-1970, Reaffirmed 2002, Bureau of Indian Standards, New Delhi, India.
- [3] Yang H P, Zheng J and Zhang R, "Addressing Expansive Soils", Institute of Special Soils, 2007, pp 64-69.
- [4] Snethen D R, "Expansive Soils in Highway Subgrades", U. S. Department of transportation, United States of America, 1980.
- [5] Petry T M, & Little D N, "Review of Stabilisation of Clays and Expansive Soils in Pavements and Lightly Loaded Structures - History, Practice, and Future", Journal of Materials in Civil Engineering, Nov/Dec 2002, pp. 447-460.
- [6] Smith R L, "Achieving the Goal of Management of Reactive Clays", Australian Institute of Building Surveyors Conference, Australia, (2004).
- [7] Vashi J, "Review of Geotechnical Parameter: CBR and Modulus of Subgrade Reaction (k) for Rigid Pavements", M. Tech (SMFE) dissertation, Applied Mechanics Dept., SVNIT, Surat, India, 2008.
- [8] Tandel Y, "Utilization of Copper Slag to Improve Geotechnical Properties of Soil", M.Tech (SMFE) dissertation, Applied Mechanics Dept., SVNIT, Surat, India, 2008.
- [9] Tailor R M, Desai M D and Shah N C, "Performance Observations for Geotextile Reinforced Flexible Pavement on Swelling Subgrade: A Case of Surat, India", International Journal of Civil Engineering and Technology, Volume 3, Issue 2, July- December 2012, pp. 347-352
- [10] Tailor R M and Shah N C, "Performance Improvement of Flexible Pavement on Swelling Subgrade Using Geotextile", Journal of Traffic and Logistics Engineering, Vol. 2, No. 2, June 2014, pp. 80-85
- [11] Methods of Test for soil - Part-16: Laboratory Determination of CBR, IS: 2720 (Part 16), 1987, Reaffirmed 2002, Bureau of Indian Standards, New Delhi, India.

# A PHYSICAL AND NUMERICAL INVESTIGATION INTO SINKHOLE FORMATION

Brian Lamb<sup>1</sup> and Jim Shiau<sup>1</sup>

<sup>1</sup>Faculty of Engineering and Surveying, University of Southern Queensland, Australia

## ABSTRACT

Sinkholes are a global phenomenon which can result in a major impact to a community. This paper aids in understanding the phenomena of sinkholes better through physical and numerical simulations. The research is conducted by closely examining a physical model to simulate the formation and collapse of a sinkhole and then by analysing sinkhole structures through utilizing finite difference software FLAC. The completion of 2D numerical models allows for numerous sinkhole simulations, with varying material properties and different overburden depth to cavity width ratios. The sinkholes are analysed through a strength reduction method, which can produce the factor of safety of the formation. By completing many simulations with different overburden depth to cavity roof width ratios the sinkhole phenomenon mechanics is explained. Future work is to conduct 3D simulation models for the investigation of sinkhole formation shape.

*Keywords: FLAC, FOS, Formation, Sinkhole, Stability*

## INTRODUCTION

Sinkholes are a global phenomenon which can have devastating consequences. There are many different causes, but all are based on the overburden's soil pressures. The pressures increase to a breaking point where then the overburden material, the material above an underground cavity, falls into the cavity, leaving in many cases a conical shape and circular ground opening.

This paper is focused on investigating sinkholes by generating idealised physical and 2D models, describing the sinkhole phenomena so it can be further explained. Fast Lagrangian Analysis of Continua (FLAC) software produced by the Itasca Consulting Group, Inc. is used for the 2D analysis.

## SINKHOLE DEFINITION AND CAUSES

Sinkholes are soil surface depressions caused by changes to soil and rock beneath the ground. These changes of the underground structure are caused by the production of a cavity and then the collapse of the overburden or overlaying material into the cavity [1]. This collapse creates a funnel-shaped depression with a hole at the center, this being a sinkhole.

Overburden is the overlaying material of a cavity. The Overburden's material properties and depth has a great effect on the dependence of a collapse.

Subsidence can occur gradually over time as a progressive event, known as dynamic subsidence. Subsidence can also occur very rapidly, for instance when a tunnel or pipeline collapses. Dynamic subsidence is the depressions formed on the overlaying overburden material before sinkhole formation [3].

Sinkhole collapse in most circumstances is an instantaneous event, producing extreme difficulty with in situ measurement during collapse failure [2]. This vastly increases the difficulty for investigating the formation, triggering mechanism and influential factors of specific ground failures and sinkhole events.

The relationship between the material properties of the overburden and overburden depth plays an important role in not only the mechanics of the failure, but also the cause. In limestone areas, a gradual solution of underground rock in groundwater passageways leads to subsidence instability of overburden and possible later collapse. Sinkholes of greater concern are those which are formed by a sudden collapse of an underground rock cavity. These occur often as initially small cavities, mainly on a soil and rock interface (Fig. 1) [1], [4]. Eventually, the cavity becomes large enough that the overburden can no longer support itself and collapses. Other causes include reduction in groundwater levels [5] from increased urbanisations' use of bore water. Mining also causes sinkholes due to the mined void causing instability in the overlaying material or overburden.

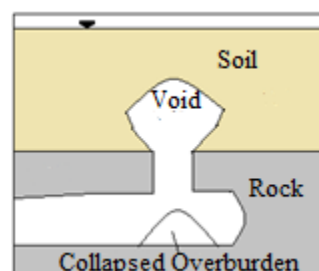


Fig. 1 An idealised model of a formed void.

In natural occurring sinkholes, the sinkhole size is a function of several variables such as the soil strength, position of water table, weathering of soil, cohesiveness of soil, depth of cavity and composition of the limestone rock [6]. Tunneling and pipelines can also create sinkholes or subsidence if they collapse, since they create underground voids [3], [4]. Earthquakes can directly trigger a sinkhole formation by disturbing the settled overburden to collapse.

## COLLAPSE MECHANICS

Reference [3] explains that subsidence ground movements have horizontal and vertical components. Vertical movement is at its largest in the central location of the subsidence, and gradually becomes less until the boundary of the subsidence is reached. The boundary is where there is no longer any ground surface deformation. Horizontal movement occurs in subsidence troughs as the surface tends to move towards the center of subsidence. This horizontal movement of adjacent points around the subsidence center moving closer to one another creates compressive strains of the surface. The compressive strains are at their maximum in the center of the depression and is reduced as it moves away from the center and adjacent points move further apart. Eventually, a point of zero compressive strain is approached, the inflection point where no horizontal displacement will occur. Beyond the inflection point the ground's neighboring points are moving further apart. This results in tensile strains on the ground's surface. The inflection point also, for the reason of being the location where tensile and compression are zero, is where the shape of the surface of subsidence changes between convex and concave [3].

The compressive and tensile strains as discussed above, either side on the inflection point, comprise the compression and tensile zones on subsidence. The forces can be represented as strains, because strain involves the dimensional change compared to the original position before being subject to tension or compression. Tensile strain pulls apart and compressive strain pushes inwards. The compressive zone makes up the central section of subsidence, above the center of failure above the cavity collapse. The tensile zone represents the remainder and often extends beyond the cavity failure. Soil has no or little tension, therefore this paper will focus on the failure of the overburden due to the compressive nature of the soil properties, as well as friction angle.

Once the overburden soil has reached a point where the strain is too great for stability, where the soil pressures distribution no longer keeps the overburden from collapsing, the overburden will fall into the cavity below, typically leaving a conical shape. In many cases the initial cavity produced is in rock, for example limestone which can become dissolved [5]. Figure 1, an idealised model of a formed void, shows

how the overburden soil material falls into the cavity below. It also shows the cavity opening chute in the rock.

## PHYSICAL MODEL

To physically model a sinkhole, first a test box was produced and then based on the initial design a complete acrylic box was created. The boxes are open at the top for access and have weep holes on the base for drainage. The cavity is built using sugar and then dissolved via an in situ water tube, to simulate limestone dissolution.

An initial design was made. Dimensions for the initial test, using a constructed wooden box with acrylic front, were 300 mm (length) by 200 mm (width) by 200 mm (depth). Figure 2 shows steps in the production of the model up to it being ready for testing. Picture 1 (Fig. 2) shows the acrylic viewing window. Picture 2 (Fig. 2) shows the drilled weep holes for drainage. Picture 3 (Fig. 2) shows a stone pebble base for added drainage. Picture 4 (Fig. 2) shows the first layer of sand and sugar, the material used to simulate a material subjective to dissolution, such as limestone. Picture 5 (Fig. 2) shows the halfway step of sand and sugar layering and the water pipe being laid into the model. Picture 6 (Fig. 2) shows the model about to be tested, and the use of the pipe to keep the sugar centrally placed at the face of the acrylic window.



Fig. 2 Preliminary design setup.

Figure 3 shows the cavity created and the circular shaped opening of the sinkhole. A conical shape is also evident as predicted and the circular extent of the opening onto the surface is highlighted in red. This preliminary investigation is encouraging and will be repeated with a new acrylic box to capture all earth movements, using slightly larger dimension to ensure the complete extend of the sinkhole formation is captured.



Fig. 3 Preliminary results of model tests.

The final full acrylic box design inside dimensions are 400 mm (length) by 250 mm (width) by 300 mm (depth).

## 2D FLAC MODEL

While physical soil conditions and overburden/cavity interactions have high complexity, the model uses simplification and assumptions to aid predict theoretical soil responses within cavity opening and overburden soil relationships. The sinkhole model assumes the use of Mohr-Coulomb failure criteria, with set soil characteristics of mass-density, elastic modulus, Poisson's ratio, cohesion and friction angle.

Table 1 shows the respective material properties in the analysis. The major characteristic of the undrained clay was the relatively high cohesion and zero friction angle. The drained sand was given zero cohesion and a non-zero friction angle. The c- $\phi$  soil was given the same cohesion and friction angle as the clay and the sand. The remaining material properties

were the same for each material for comparative analysis.

Table 1 Material Properties

Undrained Clay	
Material Property	Value
Mass-Density (kg/m <sup>3</sup> )	1900
Elastic Modulus (kPa)	1000
Poisson's Ratio	0.25
Cohesion (kPa)	30
Tension (kPa)	1.00E+7
Friction Angle	0
Dilation Angle	0
Drained Sand	
Material Property	Value
Mass-Density (kg/m <sup>3</sup> )	1900
Elastic Modulus (kPa)	1000
Poisson's Ratio	0.25
Cohesion (kPa)	0
Tension (kPa)	1.00E+7
Friction Angle	35
Dilation Angle	0
c- $\phi$ Soil	
Material Property	Value
Mass-Density (kg/m <sup>3</sup> )	1900
Elastic Modulus (kPa)	1000
Poisson's Ratio	0.25
Cohesion (kPa)	30
Tension (kPa)	1.00E+7
Friction Angle	35
Dilation Angle	0

Numerical results are investigated through the plots of plasticity state indicators, y displacement contours, elemental principal stresses and shear strain rate. Each material has six different cases, ranging from shallow to deep, each case had certain height to width ratio. The height (h) representing the height of the overburden material above the cavity and width (w) representing the length or diameter of the cavity roof, as shown in Figure 4.

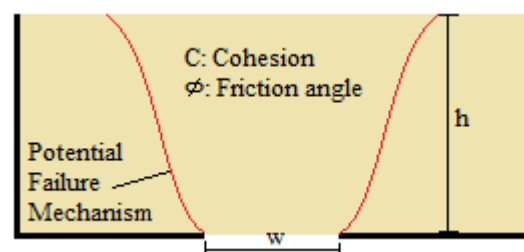


Fig. 4 Idealised sinkhole in 2D space.

In FLAC each case was constructed and the material properties set. The initial equilibrium was solved for and then a section width was released from the x and y fixed boundary condition, as shown in



Figure 5 a typical FLAC mesh. Then the model was solved through Factor of Safety (FOS) which is a measure of the shear strain rate and sinkhole failure. If the FOS is below one, then the properties of the soil are insufficient and the height by width (h/w) ratio is too small to prevent collapse.

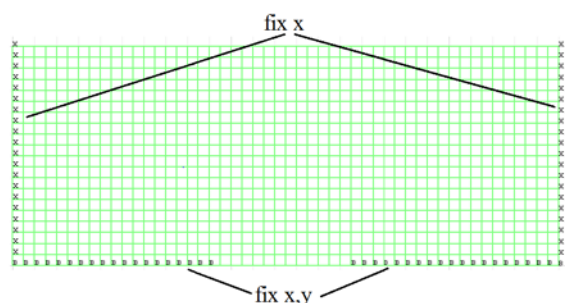


Fig. 5 A typical FLAC mesh (h/w=1.667).

## RESULTS AND DESCUSION

### Undrained Clay

Table 2 Undrained Clay Results

case	h/w	FOS	estress Max. Value	estress Min. Value
1	1.667	0.51	1.16E+05	-3.23E+05
2	2	0.592	9.99E+04	-2.82E+05
3	2.5	0.682	8.61E+04	-2.45E+05
4	3.33	0.795	7.30E+04	-2.23E+05
5	5	0.947	6.00E+04	-2.18E+05
6	10	1.189	4.18E+04	-2.13E+05

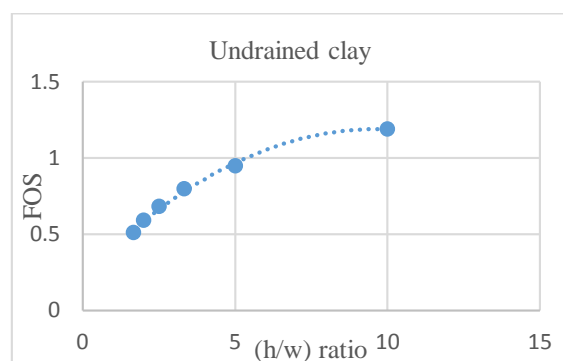


Fig. 6 FOS vs h/w ratio plot (undrained clay).

The clay results showed an increasing factor of safety with depth, or with increase of the h/w ratio (Fig. 6). This is as expected. Clay's cohesion has the ability to the support its self-weight above a cavity opening. The deepest case, or narrowest opening width had a factor of safety larger than 1, indicating a safe case with substantial self-support of its self-weight over the cavity opening

### Drained Sand

Table 3 Drained Sand Results

case	h/w	FOS	estress Max. Value	estress Min. Value
1	1.667	<0.03	8.81E+13	-2.84E+13
2	2	<0.03	1.96E+07	-5.18E+06
3	2.5	<0.03	2.96E+05	-2.50E+05
4	3.33	<0.03	9.82E+05	-4.25E+05
5	5	<0.03	3.29E+05	-2.56E+05
6	10	<0.03	-1.87E+03	-2.57E+05

Drained sand had an immediate failure in each case, due to the zero cohesion material property. The sand immediately fails under self-weight as the possibility of stability can only come from its non-zero (35°) friction angle. Factor of safety calculations in FLAC are not stable for immediate failure, due to its strength reduction process requiring a transition of strength until the limiting parameter is found to produce failure and the sand fails immediately, not allowing for this transition. Force relaxation methods through FLAC are evidently more relevant for weak soils [4]. Although factor of safety calculations have a more practical analysis by giving the stability of a scenario in the form of a single number.

### c-φ Soil

Table 4 c-φ Results

case	h/w	FOS	estress Max. Value	estress Min. Value
1	1.667	0.518	-1.96E-03	-5.65E+05
2	2	0.604	-2.43E-02	-5.09E+05
3	2.5	0.748	-3.30E-03	-4.21E+05
4	3.33	1.006	-6.74E-03	-3.46E+05
5	5	1.494	-2.17E-03	-2.53E+05
6	10	2.595	-1.53E+00	-2.16E+05

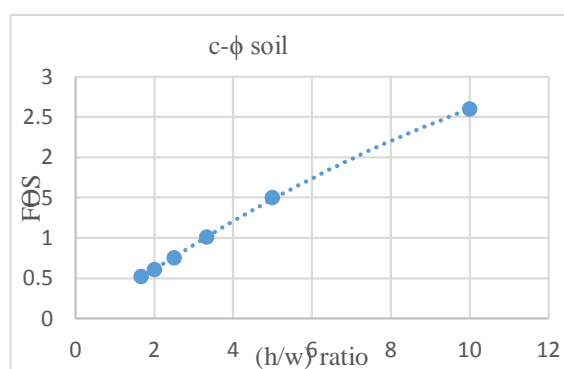


Fig. 7 FOS vs h/w ratio plot (c-φ soil).

$c-\phi$  soil had the most stable cases due to the inclusion of both the friction angle and cohesion. The trend increase from shallow to deep case, or wide cavity to narrow cavity with increasing  $h/w$  ratio was near linear (Fig. 7). Friction angle adds to the ability of a soil to withstand it's self-weight over a cavity along with its cohesion.

### Effective Principle Elemental Stresses

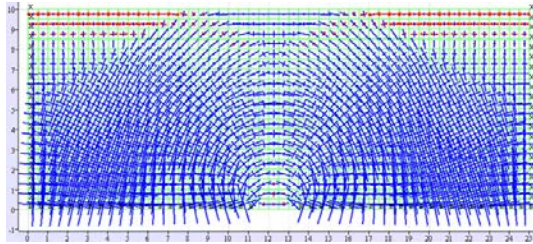


Fig. 8 Principle stress vectors (undrained clay;  $h/w = 5$ )

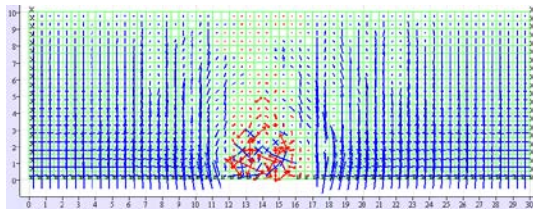


Fig. 9 Principle stress vectors (drained sand;  $h/w = 5$ )

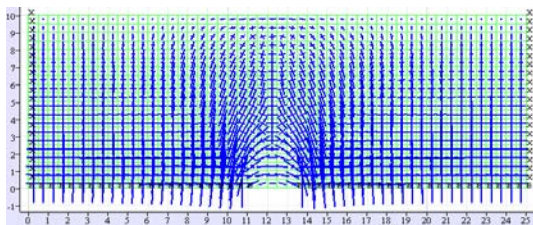


Fig. 10 Principle stress vectors ( $c-\phi$ ;  $h/w = 5$ )

The effective elemental principle stresses were plotted for each case. For the plots it is evident that an arching effect occurs in all cases, apart from cases 1 to 5 for sand, where the immediate collapse produced a chimney type failure. The arching process is a mechanism of stress relocation of the opening of a cavity to attempt to support the soils own self-weight before collapsing into the cavity. Increase the cavity width, or shallowness, stretches the arching effect, reducing the factor of safety and opportunity for stability.

### Plasticity and Shear Strain Rate

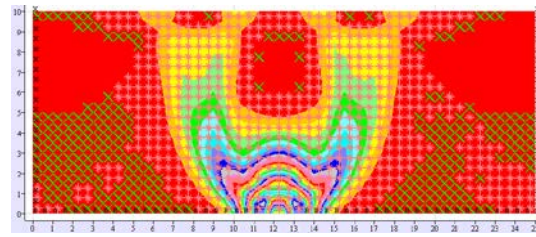


Fig. 11 Plasticity & max. shear strain rate vectors (undrained clay;  $h/w = 5$ )

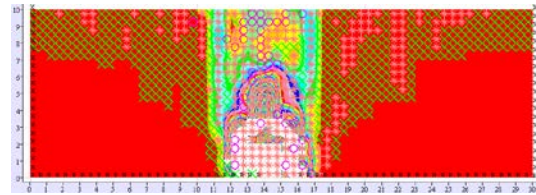


Fig. 12 Plasticity & max. shear strain rate vectors (drained sand;  $h/w = 5$ )

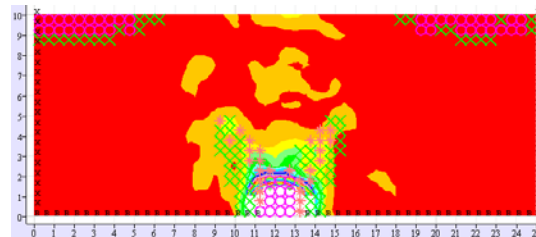


Fig. 13 Plasticity & max. shear strain rate vectors ( $c-\phi$ ;  $h/w = 5$ )

From the plasticity plots no indicator represents elastic, a green cross represents yield in the past and a red cross represents present yielding. The present yielding is an indication of the collapse failure plane, as with the shear strain rate and y-displacement contour plots. Shear strain rate being the rate of change of shear strain. Shear strain is a measure of deformation, the change in location of a particle from its original location perpendicular to a plane of the original location. Shear strain rate being an indication of the rate of deformation and thus is also a representation of the slip failure plane of the sinkholes. The shear strain rate for Drained Sand in cases 1 to 5 exhibited chimney failure.

### Y-Displacement Contours

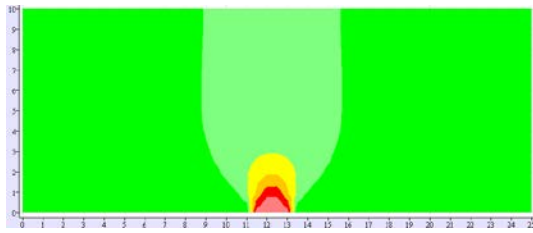


Fig. 14 Y-displacement contours (undrained clay;  $h/w = 5$ )

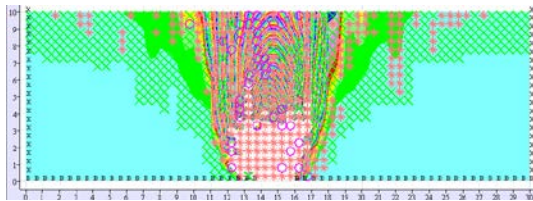


Fig. 15 Y-displacement contours (drained sand;  $h/w = 5$ )

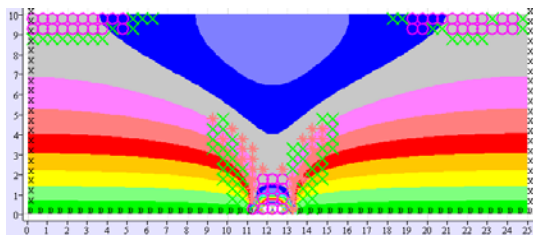


Fig. 16 Y-displacement contours ( $c-\phi$ ;  $h/w = 5$ )

The y-displacement contour plots represent the behaviour of the vertical movement or slump of the soil after the cavity is open. The more shallow the case, or wider the cavity, more of an extent the contours will cover. Undrained clay has narrower contours when compared to  $c-\phi$  soil and drained sand. Drained sand for cases 1 through 5 exhibited chimney type failure again.

### CONCLUSION

This paper has successfully demonstrated the collapse mechanism of a sinkhole via physical modeling. Through 2D analysis software FLAC,

factor of safety method of calculating the stability of sinkholes has been proven to be successful. The factor of safety calculation represents a practical method to determining the stability and safety of overburden above a cavity opening.

$c-\phi$  soil was more stable when compared to undrained clay and drained sand. Zero cohesion soils appear to fail immediately once the cavity is open. A non-zero friction angle though does aid in increasing safety and stability of overburden. An arching effect of soil stresses appears to play a key role in the stability of the overburden.

Future work is to attempt to model in three dimensions, for a more realistic sinkhole simulation. Also to conduct another, final physical model test based on the initial design.

### ACKNOWLEDGEMENTS

Appreciation is due to Mr. David Lamb for aiding with the construction of the initial physical model design.

### REFERENCES

- [1] Augarde, C Andrei, L Sloan, S 2003, Prediction of Undrained Sinkhole Collapse, Journal of Geotechnical and Geoenvironmental Engineering, March 2003 p.197-205.
- [2] Lei, M Gao, Y Jiang X, Hu, Y 2005, Experimental Study of Physical Models for Sinkhole Collapses in Wuhan, China, Sinkhole and the Engineering and Environmental Impacts of Karst.
- [3] Potential Impacts from Underground Mining 2006, Bureau of Mining, Pennsylvania Department of Environmental Protection.
- [4] Shiau, J, Kemp, R 2013, 'Developing a Numerical Model for the Stability Design of Tunnel Heading', Third International Conference on Geotechnique, Construction Materials and Environment, Nagoya, Japan.
- [5] Tharp, T 2003, Cover-Collapse Sinkhole Formation and Soil Plasticity, Sinkholes and the Engineering and Environmental Impacts of Karst, American Society of Civil Engineers.
- [6] Zisman, E.D 2003, Sinkhole Size, BTL Engineering Services, North Occident Street, Tampa, Florida.

## EFFECT OF TEMPERATURE AND LIQUID CHEMISTRY ON GEOTECHNICAL AND HYDRAULIC PROPERTIES OF BENTONITE

H. M. A. Rashid<sup>1</sup>, K. Kawamoto<sup>1,2</sup>, T. Komatsu<sup>1</sup>, T. Saito<sup>1</sup>, and P. Moldrup<sup>3</sup>

<sup>1</sup>Graduate School of Science and Engineering, Saitama University, Japan.

<sup>2</sup>Institute for Environmental Science and Technology, Saitama University, Japan

<sup>3</sup>Department of Civil Engineering, Aalborg University, Denmark

### ABSTRACT

This study investigated the effect of single-species salt solutions on geotechnical properties (swell index and liquid limit) and hydraulic conductivity of bentonite applying different cations, concentrations, and temperatures. Results showed that both the swell index and the liquid limit decreased with increase in salt concentration irrespective of the type of cation. Monovalent cations showed higher values of the swell index and the liquid limit compared to divalent cations. In general, the swell index of bentonite increased whereas the liquid limit decreased with increasing temperature for all cation types and concentrations. Significant and high correlations were found between swell index and liquid limit of bentonite at all three temperatures. Hydraulic conductivity of bentonite was found to increase with increasing temperature. No significant change in hydraulic conductivity with time was observed for all concentrations and cation types, and, overall, concentration and valance of cations had little effect on the hydraulic conductivity of bentonite.

*Keywords: Bentonite, Hydraulic conductivity, Liquid limit, Swell index, Temperature effects*

### INTRODUCTION

Geosynthetic clay liners (GCLs) are widely used as an essential component of bottom liner system of landfills for solid waste disposal. GCLs offer a final defense against the migration of landfill leachate into the underlying environment [1]. The main component of GCL responsible for its barrier performance is sodium bentonite, which is primarily composed of clay mineral sodium montmorillonite while the minor constituents include quartz, feldspars, carbonates and micas [2]. Sodium montmorillonite is characterized by its large specific area, high cation exchange capacity and high swelling potential which are responsible for the desirable physical and chemical properties of bentonite [3].

The biodegradation of organic waste inside landfill produces a chemical substance, leachate, which, when it comes in contact with the bentonite component of GCL, can alter its geotechnical and hydraulic properties as barrier material. In addition to the generation of leachate, the biodegradation of organic substances also generates heat, which can result in an increase of temperature inside the landfill up to 60 °C [4] - [7]. Chemicals in landfill leachate, coupled with a rise in temperature, can affect the geotechnical and hydraulic performance of bentonite. A number of researchers have investigated the effects of chemicals on the properties of bentonite [2], [8] - [15]. However, a very few researches have reported the combined effect of temperature and liquid chemistry on

geotechnical properties and hydraulic performance of bentonite. For example, Ishimori and Katsumi [1] has investigated the effects of temperatures (20 °C and 60 °C) on the swelling capacity and barrier performance of bentonite using deionized water (DI water) and three different concentrations (0.1 – 0.4 M) of NaCl solutions and found that swell and intrinsic permeability increase with increase in temperature. Other studies were focused on hydraulic conductivity [16] - [17] and hydro-mechanical behavior [18] using only water for specific applications in high level nuclear waste repositories. Therefore, the combined effect of temperature and liquid chemistry is still to be investigated to fully understand the behavior of GCL liners in long term performance of landfills.

This study investigated the effects of single-species salt solutions on geotechnical properties (swell index and liquid limit) and hydraulic conductivity of bentonite applying different cations, concentrations, and temperature. Thirteen solutions, (DI water and twelve salt solutions of four major exchangeable cations ( $\text{Na}^+$ ,  $\text{K}^+$ ,  $\text{Ca}^{2+}$ ,  $\text{Mg}^{2+}$ ), each at three different concentrations (0.01M, 0.1 M, 1M)) were used as hydrating liquids. The swell index and liquid limit tests were carried out using all the thirteen solutions at three different temperatures (20 °C, 40 °C and 60 °C). The hydraulic conductivity was evaluated using DI water, NaCl 0.01M and intermediate concentrations (0.1M) of all the four cation solutions at 20 °C and 40 °C. The hydraulic conductivity tests were followed by the pore size distribution analysis to understand the solute



transport phenomenon through the bentonite.

## MATERIAL AND METHODS

The bentonite used in this study was sodium bentonite extracted in powdered form from commercially available GCL (Bentofix®, NAUE GmbH & Co. KG, Germany). The bentonite passed through US sieve no. 200 (75  $\mu\text{m}$ ) was oven dried at 105 °C for subsequent testing. The particle density of bentonite for this typical GCL was 2.61  $\text{g}/\text{cm}^3$  [19]. The natural water content, liquid limit, plastic limit and swell index were measured using ASTM Standards. The results are given in Table 1.

Table 1 Physical Properties of Bentonite

Property	Unit	Value
Natural water content	%	11.78
Liquid Limit	%	559
Plastic Limit	%	51
Plasticity Index	%	508
Swell Index	$\text{mL}/2\text{g}$	30
Particle density	$\text{g}/\text{cm}^3$	2.61

The permeant solutions used in swell index and liquid limit tests were DI water and the salt solutions of NaCl, KCl,  $\text{CaCl}_2$  and  $\text{MgCl}_2$ . Concentrations of solutions were varied from 0.01 M to 1 and the tests were carried out at three different temperatures (20 °C, 40 °C and 60 °C). Hydraulic conductivity tests were carried out using DI water, NaCl 0.01M and intermediate concentrations (0.1M) of all the four cation solutions at two different temperatures (20 °C and 40 °C). The cations were selected because they are major exchangeable cations in bentonite  $\text{Na}^+$ ,  $\text{K}^+$ ,  $\text{Ca}^{2+}$  and  $\text{Mg}^{2+}$  [20]. Chemicals used for making solutions were purchased in powdered form and their formula weights were mixed with DI water to prepare the desired chemical solution.

### Swell Index Tests

The swell index tests were carried out in accordance with ASTM D5890. Initially, 2 g of oven dried bentonite was dusted into a 100 mL graduated cylinder filled with 90 mL of hydrating solution. Then, after the dusting of bentonite was completed, the cylinder was filled upto the 100 mL mark with the same solution washing the particles adhering to the walls of the cylinder. The cylinder was then covered with plastic wrap to prevent evaporation and carefully placed in a climate control room with a temperature maintained at 20 °C or placed in an oven for elevated temperatures (40 °C or 60 °C). The cylinders were kept undisturbed for 24 h prior to take the readings. The measurements were repeated

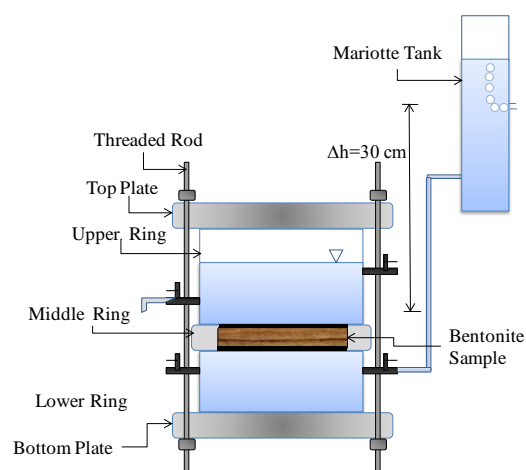
in triplicates and averages were used for subsequent analysis.

### Liquid Limit Tests

The liquid limit tests were carried out using the multipoint test method in accordance with ASTM 4318-10. The bentonite samples were prepared by thoroughly mixing the oven dried bentonite with each hydrating liquid at different moisture contents. The samples were then allowed to hydrate for at least 24 hours in double wrapped sealed plastic bags at specified temperatures (20 °C, 40 °C and 60 °C). To avoid evaporation during the hydration process, wet tissue papers were kept between the both wrappings. The samples were remixed before starting the experiment. A minimum of five trials were performed for each test and the liquid limit was determined using equation of the flow curve.

### Hydraulic Conductivity Tests

Constant head hydraulic conductivity tests were conducted using a rigid wall permeameter as shown in Fig. 1. The apparatus consisted of a lower ring, a middle ring and an upper ring placed between an upper and lower cap all made of acrylic. First, the bentonite samples were prepared with the permeating solution with a moisture content equal to its liquid limit for that particular solution, and allowed to hydrate for at least 24 h in sealed plastic bags. After 24 h, the prehydrated bentonite samples were placed in the circular middle ring with a porous filter at the bottom placed on the top of lower ring. Typically the inner diameter of the middle ring was 6 cm with a height of 1 cm, which represents the



dimensions of the sample.

Fig. 1 Schematic of hydraulic conductivity test apparatus

The lower ring was first filled with permeating solution, then sample was placed in the middle ring

by slight tamping, making due care to prevent entrapment of air bubbles inside the sample. A porous filter was then placed on top of the sample in such a way that the sample was sandwiched between the lower and upper porous filters to avoid washing off of the soil particles during the tests. After placing the sample and porous filters, the upper ring was placed on top of the middle ring and the cell was clamped after placing the top cap. To avoid leakage of water at the contact points, silicon grease was used.

The permeant solution was then supplied from a Mariotte tank to the sample through an inlet valve of the lower cell allowing the escape of air bubbles. Once the permeating solution started coming out of the sample ensuring that all air bubbles have escaped, the upper ring was then filled with the permeating solution up to a height equal to that of the lower ring and whole cell was made airtight. After that, the whole setup was placed in the climate controlled room with temperature maintained at 20 °C or in an incubator with a pre-set temperature of 40 °C. Permeant solution was then supplied to the sample from the Mariotte tank through an inlet valve of the lower ring while maintaining a constant head of 30 cm across the sample which correspond the hydraulic gradient. The effluent was collected from an outlet valve of the upper ring in a collecting jar at specified intervals of time. To measure the evaporation, a reference jar with an opening equal to the collecting jar was placed near the apparatus in the same environment and the evaporated volume was added to the measured volume to minimize the effect of evaporation during the test. The tests were continued for several days and hydraulic conductivity was calculated using Darcy's law [21].

The tests were conducted up to 100 days and electric conductivity (EC) and pH of the effluent was measured during the test period in addition to the hydraulic conductivity. After terminating the tests, weight of the each sample was measure and one part of it was taken to measure the moisture content ( $w$ ), porosity ( $\phi$ ), and void ratio ( $e$ ) while the rest was freeze-dried to measure the pore size distribution using Mercury Intrusion Porisometry (MIP).

## RESULTS

### Swell Index Tests

The swelling of bentonite can be explained as a two phase process [3]. First phase known as "crystalline swelling" occurs at small scale and a maximum of three to four layers of water molecules can be adsorbed in the interlayer around the interlayer cations which corresponds to less than 25% by mass. This phase is then followed by "osmotic swelling" where numerous layers of water

molecule enters the interlayer. The later phase can occur only when the exchange sites are occupied by monovalent cations [22] - [23] having  $\Delta$ radius (hydrated radius - ionic radius) to valance ratio of greater than 300 and more than three hydration shells (limited to  $\text{Na}^+$  and  $\text{Li}^+$ ) [3].

The swell index seems to be highly controlled by concentration of the solution in bulk pore water as shown in Fig. 2. It was observed that the swell index decreased with increase in concentration irrespective of the type of cation. This finding is consistent with the studies conducted by Jo et al. [10] who explained the phenomenon as a result of the moving out of the interlayer water due to gradient in free energy caused by the elevated concentrations in bulk pore water.

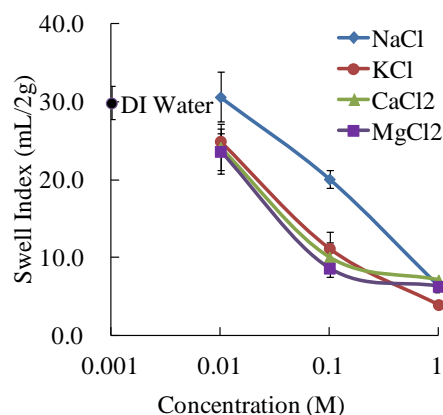


Fig. 2 Effect of liquid chemistry on swell index of bentonite

The highest value of the swell index was observed for the bentonite samples hydrated with NaCl solution at low concentration (0.01M) followed by the samples hydrated with DI water. As the bentonite is hydrated with NaCl solution, all exchange site are occupied by  $\text{Na}^+$  cation which take part in osmotic swelling phase resulting an increase in swell volume. All other cations were found to give similar values of swell index at all concentrations with the lowest value of the swell volume obtained for the bentonite samples hydrated with high concentration (1M) of KCl solution.

Temperature of the hydrating liquid was found to have significant effect at lower concentrations of monovalent cations as shown in Fig. 3 (a) and Fig 3 (b). At intermediate and high concentrations, however, the effect was insignificant. It was observed that for bentonite samples hydrated with DI water and low concentrations of monovalent cations, swell index increased with increase in temperature. Contrary to this, there exist a tendency of decrease in swell index with an increase in temperature at all concentrations for divalent cations as shown in Fig. 3 (c) and Fig. 3 (d).



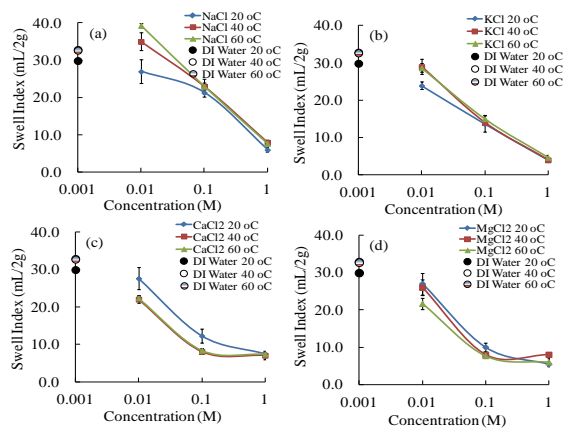


Fig.3 Effect of temperature on swell index of bentonite

### Liquid Limit Tests

#### Effect of liquid chemistry

Figure 4 is showing the effect of liquid chemistry on the liquid limit of bentonite.

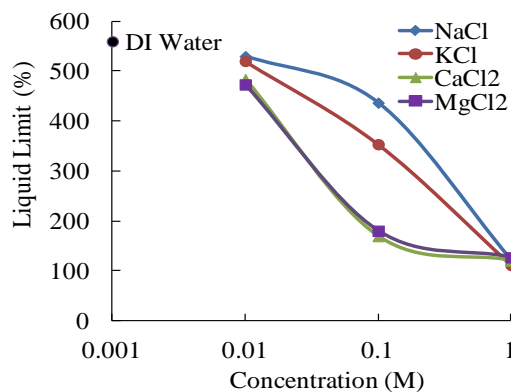


Fig. 4 Effect of liquid chemistry on liquid limit of bentonite

It was observed that liquid limit decreased with increase in salt concentration irrespectively of the type of cation. The liquid limit was highest (559 %) with DI water. The liquid limit was found to be similar at very low (0.01M) and very high (1M) concentrations irrespectively of the hydrating liquid. However, at intermediate concentration (0.1M), both monovalent cations show higher values of the liquid limit than divalent cations, with highest value of the liquid limit obtained for bentonite hydrated with NaCl solution. Both divalent cations showed similar values of the liquid limit at all concentrations.

#### Effect of temperature

The effect of temperature on the liquid limit of bentonite is shown in Fig. 5. In general, the liquid

limit was found to decrease slightly with increase in temperature. DI water showed the highest value of liquid limit (559%) when hydrated at 20 °C. The liquid limit was lowest at 60 °C (524%). A similar trend of decrease in liquid limit with increase in temperature was found with bentonite hydrated with NaCl solution at low concentrations. However, at high concentrations the effect of temperature was not significant. Temperature was found to have insignificant effect on the liquid limit of bentonite hydrated with KCl and divalent cation solutions (CaCl<sub>2</sub> and MgCl<sub>2</sub>).

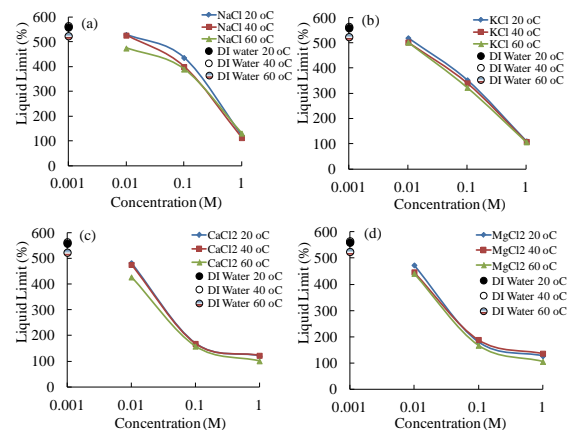


Fig. 5 Effect of temperature on liquid limit of bentonite

### Correlation between Swell Index and Liquid Limit

A comparison between the swell index and the liquid limit of bentonite is shown in Fig. 6. It was found that significant and high correlations exist between the both geotechnical properties at all temperature (Fig. 6 (a) – Fig. 6 (c)).

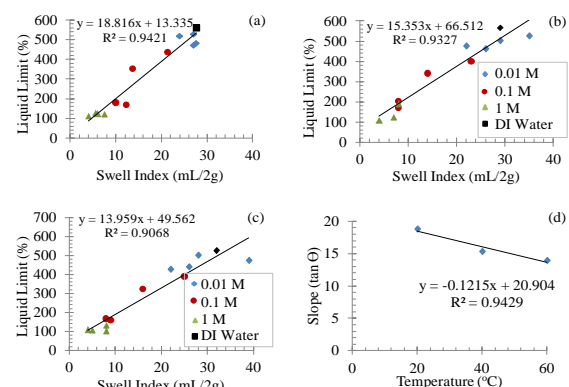


Fig. 6 Correlation between swell index and liquid limit

Figure 6 (d) is showing the relationship between slopes of the regression lines with temperature. It can be seen that the slope decreases with increase in

temperature which shows the temperature dependence of both the geotechnical properties.

### Hydraulic Conductivity

Hydraulic conductivity of bentonite was measured using all the thirteen permeant liquids. It was observed that for all cation types and concentrations, hydraulic conductivity do not change significantly with time. The duration of permeation (t), total pore volumes of flow (PVF), total porosity ( $\phi$ ) and void ratio (e) of each permeated sample is shown in table 2.

Table 2 Summary of hydraulic conductivity tests

Permeant Liquid	Conc. (M)	t (days)	PVF	$\phi$	e
NaCl	0.01	20	2.4	0.94	17.4
	0.1	109	8.9	0.91	10.17
	1	35	5	0.69	2.27
KCl	0.01	123	11	0.91	10.43
	0.1	78	41	0.90	9.93
	1	76	189	0.69	2.32
CaCl <sub>2</sub>	0.01	95	112	0.92	12.01
	0.1	111	71.8	0.81	4.42
	1	106	84.8	0.73	2.73
MgCl <sub>2</sub>	0.01	79	124	0.91	10.51
	0.1	89	29	0.82	4.79
DI water	1	97	51	0.71	2.45
	-	108	4.8	0.94	15.44

Figure 7 is showing the effect of concentration on average hydraulic conductivity of bentonite. Hydraulic conductivity was found to increase with increase in concentration for the samples hydrated with KCl solutions. For other cations, however, concentration was found to have little effect on bentonite samples even though the void ratio (e) inc-

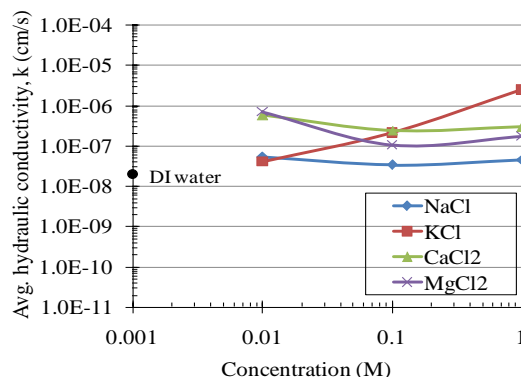


Fig. 7 Effect of cation concentration on hydraulic conductivity of bentonite.

reased and total porosity ( $\Phi$ ) decreased with the increasing salt concentration. This suggests that the water bound in the interlayer pores actually do not take part in the hydraulic conductivity of bentonite. Supporting this, the available pore space for the flow (the effective porosity of bentonite) did not change significantly with change in salt concentrations, see in Fig 8.

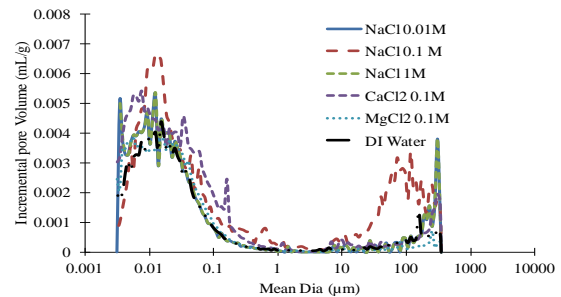


Fig. 8 Pore size distribution of bentonite samples permeated with DI water and salt solutions

Hydraulic conductivity test conducted at 20 °C and 40 °C showed that hydraulic conductivity as expected increases slightly with temperature; see Fig. 9.

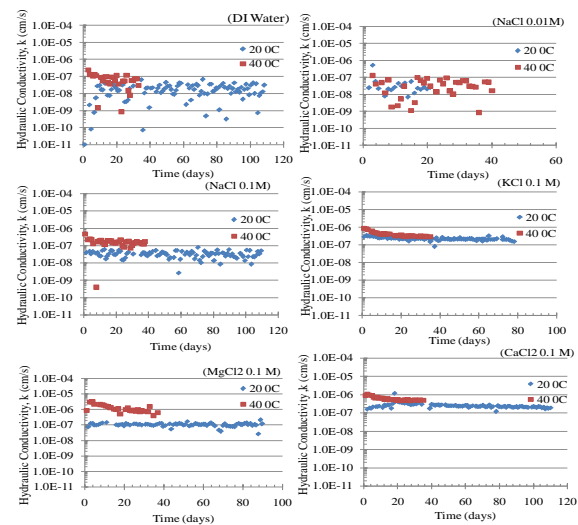


Fig. 9 Effect of temperature on hydraulic conductivity of bentonite.

### CONCLUSIONS

The study investigated the effect of temperature and liquid chemistry on swell index, liquid limit and hydraulic conductivity of bentonite. Concentration and type of cation were found to have significant effect on swell index and liquid limit of bentonite. However, the effect was small for hydraulic conductivity. It was found that the hydraulic

conductivity is mainly controlled by the effective porosity rather than the total porosity. Liquid limit was found to decrease whereas swell index and hydraulic conductivity were found to increase with increasing temperature.

## ACKNOWLEDGEMENTS

This work is partially supported by JST-JICA SATREPS project.

## REFERENCES

- [1] Ishimori H, and Katsumi T, "Temperature effects on the swelling capacity and barrier performance of geosynthetic clay liners permeated with sodium chloride solutions", *Geotextiles and Geomembranes*, Vol. 33, April 2012, pp. 25-33.
- [2] Bouazza A, Jefferis S, and Vanpaisal T, "Investigation of the effects and degree of calcium exchange on the Atterberg limits and swelling of geosynthetic clay liners when subjected to wet-dry cycles", *Geotextiles and Geomembranes*, Vol. 25, Dec.2006,pp.170-185.
- [3] Likos WJ, Bowders JJ, and Gates WP, "Minerology and engineering properties of bentonite", *Geosynthetic Clay Liners for Waste Containment Facilities*, CRC Press, 2010, ch.3.
- [4] Yoshida H, Hozumi H, and Tanaka N, "Theoretical study on temperature distribution in a sanitary landfill", in *proc. of the 2nd Int. Cong. on Env. Geotechnics*, 1996, pp. 323-328.
- [5] Rowe RK, Long term performance of contaminant barrier systems, 45th Rankine Lecture, *Geotechnique*, Vol. 55 (9), July 2005, pp. 631-678
- [6] Yesiller N, Hanson JL, and Liu WL, "Heat generation in municipal solid waste landfills", *J. of Geotech. and Geoenv. Engg.*, Vol 131 (11), Nov. 2005, pp. 1330-1344.
- [7] Koerner GR, and Koerner RM, "Long term temperature monitoring of geomembranes at dry and wet landfills", *Geotextiles and Geomembranes*, Vol. 24 (1), June 2005, pp. 72-77
- [8] di Maio, C, " Exposure of bentonite to salt solution: osmotic and mechanical effects, *Geotechnique*, Vol. 46 (4), 1996, pp. 495-707.
- [9] Ruhl, JL and Daniel, DE, "Geosynthetic clay liners permeated with chemical solutions and leachates", *J. of Geotech. and Geoenv. Engg.*, Vol. 123 (4), April 1997, pp. 369-381.
- [10] Shackelford CD, Benson CH, Katsumi T, Edil TB, and Lin L, "Evaluating the hydraulic conductivity of GCLs permeated with non-standard liquids", *Geotextiles and Geomembranes*, Vol. 18, April 2000, pp. 133 - 161.
- [11] Jo HY, Katsumi T, Benson CH, and Edil TB, "Hydraulic conductivity and swelling of non-prehydrated GCLs permeated with single species salt solutions", *J. of Geotech. and Geoenv. Engg.*, Vol. 127 (7), July 2001, pp. 557-567.
- [12] Shan HY, and Lai YJ, "Effect of hydrating liquid on the hydraulic properties of geosynthetic clay liners", *Geotextiles and Geomembranes*, Vol. 20, Feb. 2002, pp. 19-38
- [13] Kolstad DC, Benson CH, and Edil TB, "Hydraulic conductivity and swell of nonprehydrated geosynthetic clay liners permeated with multispecies inorganic solutions", *J. of Geotech. and Geoenv. Engg.*, Vol. 130 (12) Dec. 2004, pp. 1236-1249.
- [14] Katsumi H, Ishimori A, Ogawa K, Yoshikawa K, Hanamoto R, and Fukagawa, "Hydraulic conductivity of nonprehydrated geosynthetic clay liners permeated with inorganic solutions and waste leachates" *Soils and Foundations*, Vol. 47 (1), 2007, pp. 79-96
- [15] Kaufhold, S, and Dohrmann, R, "Stability of bentonite in salt solutions | sodium chloride" *Applied Clay Science*, Vol. 45, May 2009, pp. 171-177.
- [16] Cho WJ, Lee JO, and Chun KS, "Influence of temperature on hydraulic conductivity in compacted bentonite temperature effects of hydraulic conductivity of compacted bentonite", in *proceedings of waste material research society symposium on the scientific basis for nuclear waste management*, 1998, pp. 305-311.
- [17] Cho WJ, Lee JO, and Chun KS, "The temperature effects of hydraulic conductivity of compacted bentonite", *Applied Clay Science*, Vol. 14, Aug. 1999, pp. 47 - 58.
- [18] Villar, MV, and Lloret, A, "Influence of temperature on the hydromechanical behavior of compacted bentonite", *Applied Clay Science*, Vol. 26, Aug. 2003, pp. 337 - 350.
- [19] Rowe RK, and Lake CB, "Diffusion of Sodium and Chloride through Geosynthetic Clay Liners", *Geotextiles and Geomembranes*, Vol. 18, April 2000, pp. 103-131
- [20] Komine, H, and Ogata, N, "Predicting Swelling Characteristics of Bentonite", *J. of Geotech. and Geoenv. Engg.*, Vol. 130 (8), Aug. 2004, pp. 818-829.
- [21] Darcy H, "Les fontaines publiques de la ville de Dijon", 1856, Dalmont, Paris.
- [22] Norrish K, and Quirk J, "Crystalline swelling of montmorillonite, use of electrolysis to control swelling", *Nature*, Vol.173, Feb. 1954, 255 - 257.
- [23] Jellandar R, and Mareelja S, "Attractive double-layer interaction between calcium clay particles", *J. of Colloid and Interface Science*, Vol. 126 (1), Nov. 1988, pp. 194 - 211.

## CASE STUDY OF GEOGRID REINFORCED SEGMENTAL RETAINING STRUCTURE

Jia Xie<sup>1</sup>, Barry Wai-Choo Kok<sup>2</sup>, Jeroen Berends<sup>3</sup> and Martin Silec<sup>4</sup>

<sup>1</sup>Geotechnical Engineer, <sup>2,3</sup>Principal Geotechnical Engineer, Geoinventions Consulting Services, Australia. <sup>4</sup>Managing Director, Concrib Pty Ltd, Australia.

### ABSTRACT

A geogrid reinforced Keystone® segmental retaining wall structure was designed for a large industrial project in Redbank, southeast Queensland, Australia. The 230m long segmental retaining structure with a maximum height of 7.2m has recently been completed. Insufficient ground bearing capacity was identified due to the presence of soft to firm clay and ground improvement was required to address this issue. The worst ground condition appeared to be underneath the highest section of the structure, as it is located within the vicinity of the creek crossing. Considering the size of the Keystone® blocks, the significant height of the structure and the unsatisfactory ground condition, excessive wall deflection and differential settlement were the key issues for the design. In addition to the conventional stress-based limit equilibrium design approach, the strain-based approach was adopted to address these design challenges. This paper describes the design and analysis methodology adopted to mitigate the long term performance risk. The results of the finite element and limit equilibrium assessments will be presented and discussed.

*Keywords: Geogrid reinforced segmental wall, Ground improvement, Stress-based approach, Strain-based approach, Long term serviceability*

### INTRODUCTION

A new industrial development at Monash Road, Redbank, Queensland required an in total 230m long geosynthetics reinforced segmental retaining structure. The facing comprised the Keystone® modular masonry concrete units with the nominal unit dimensions of 203mm (H) x 457mm (W) x 315mm (D). The structure was reinforced by high-tenacity woven polyester geogrids at 600mm vertical spacing. The most critical section of the structure is in excess of 7.2m high and founded on soft to firm clay layer.

Geosynthetic reinforced soil structures were introduced in the 1970's. The use of dry-stacked columns of interlocking modular concrete units as the facing for geosynthetic reinforced retaining wall structures were first appeared in the mid-1980's, and has since increased rapidly [1], [2], [3]. McGown [4] pointed out that the geosynthetic reinforced soil structures were adopted in practice successfully first and researched and standardised later. Therefore, technically efficient and reliable design and analysis approaches have been of great concern for maintaining the confidence of the industry practitioners.

Stress-based limit equilibrium approach has been employed dominantly to date. The limitation of this approach is that it deals with all loads as pseudo-static loads and does not take the strains into account. To address this shortcoming, strain-based finite element design approach has been adopted lately. It studies the

stress-strain behaviour of the structure and provides more comprehensive solutions for structures sensitive to deflection or settlement.

This paper presents the design approach and analytical results of the most critical section of a geogrid reinforced segmental retaining wall. The design considers the stability and long term performance of the structure. Stability assessment was conducted by using limit equilibrium commercial software Slope/W. Displacement of the structure were simulated by finite element commercial software Phase2. The outcomes concluded from this case study could provide a helpful reference for design and analysis of geogrid reinforced Keystone® segmental retaining structure in south-east Queensland.

### DESIGN METHODOLOGY

#### Current Design Practices Review

The most common design and analysis methodologies of segmental retaining walls can be found in guidelines published by Federal Highway Administration (FHWA) [5]; the National Concrete Masonry Association (NCMA) [6]; and the American Association of State Highway and Transportation Officials (AASHTO) [7], [8]. All of these guidelines are based on stress-based limit equilibrium approach [9]. This approach generally treats all types of loads as pseudo-static loads and with no regard to the stress-

strain behavior of various structures under different loading combinations. This can lead to insufficient design considerations on the long term performance of the structure induced by displacement.

Apart from the conventional limit equilibrium approach, FHWA guideline [5] also suggests that both total and differential settlements should be considered, however, there is no standard method to evaluate the overall displacement of reinforced soil wall.

Berg et al. [10] and Greenway et al. [11] carried out systematic studies of the design methods and assessment techniques adopted in North America for Geosynthetic Reinforced Soil Structures since the 1970's. They revealed that slight modification has been made on design codes and guidelines to date. The design of the reinforced segmental retaining wall requires analytical models and performance data unique to this system [9]. More specific and comprehensive design approach should be adopted.

### Regional and Local Geology

The structure is located within close proximity to the Brisbane River, in the suburb of Redbank midway between Brisbane and Ipswich. The regional geology of the Ipswich Basin comprises sedimentary and igneous rocks of the Bundamba Group and Ipswich Coal Measures. According to previous geotechnical investigation of the area, the site was believed to be underlain by alluvial soils which in turn overlies sedimentary rocks of Ipswich Basin [12].

Additional site inspections were carried out prior to this project and Dynamic Cone Penetrometer (DCP) tests were conducted to verify the local geotechnical condition. The results indicated that the subsurface soils consist of soft to stiff alluvial clay up to 3.0m overlying stiffer alluvial soils. The worst ground condition appears underneath the highest section of the structure which is within the vicinity of a creek crossing.

### Design Requirements and Material Properties

The design life of the Keystone® segmental retaining structure is 120 years in accordance with Australian Standard (AS) 4678-2002 [13], categorized as major development zone by local council. The structure was designed to support the main access road into the industrial park with high vehicle volume. The critical section for design is 7.2m high and founded on the soft to firm clay layer up to 1.0m depth overlying 3.0m depth of firm to stiff clay.

The soil properties adopted in the retaining structure were determined based on the site investigation results and authors' previous project experiences in southeast Queensland, Australia. For limit equilibrium stability assessment, the adopted

soil parameters are listed in Table 1.

Table 1 Properties of the structure materials

Material Properties	Friction angle, $\phi'_d$ (Deg)	Unit weight, $\gamma$ (kN/m <sup>3</sup> )	Cohesion, $c'$ (kPa)
Reinforced Fill	36	20	0
Controlled Fill	28	18	5
Crushed Rock	45	20	0
Soft to Firm Clay	26	16	2
Firm to Stiff Clay	28	18	3
Stiff to Very Stiff Clay	30	19	5

Minimum embedment depth was computed as total wall height/20 in accordance with Roads and Maritime Services (RMS) Specification R57. To prevent potential bearing failure due to the excessive vertical stress and insufficient bearing capacity of the soft clay layer, a 750mm thick layer of crushed rock fill was adopted as the ground improvement option to replace the existing soft clay layer. In addition, a 300mm concrete footing was casted beneath the Keystone® blocks as raft foundation.

Uniaxial polyester geogrids Miragrid® 8XT were adopted as reinforcement in the design. The long term design strength of the reinforcement was determined by applying partial factors for durability, installation damage and creep for a 120 year design life. The long term design strength was adopted as 49.7kN/m.

A 20kPa uniformly distributed load was adopted to simulate the traffic loading on top of the structure. Groundwater was defined in accordance with the Q100 flood level recorded. The overview of the completed wall is shown in Fig. 1.



Fig. 1 Overview of the completed wall.



## Modelling and Analysis

The analysis conducted includes stress-based limit equilibrium modelling to assess the global stability of the structure, and strain-based finite element modelling to assess the displacement of the structure.

### *Stress-based approach – limit equilibrium analysis*

Commercial software Slope/W 2012 was employed to assess the global slope stability of the critical cross sections of the structure to achieve a minimum factor of safety (FOS)  $\geq 1.50$ . In this study, the proposed geometries with and without ground improvement layer were analyzed using the Morgenstern-Price method. The grid and radius method was adopted to define circular trial failure surfaces between specified coordinate limits and the critical failure surface with the minimum FOS was obtained [14].

Soil properties adopted in the stability assessments are listed in Table 1. Instead of adopting the conventional monolithic model for the Keystone® wall, a new constitutive model was developed based on the large scale direct pull-out test results undertaken by Bathurst, Clarabut Geotechnical Testing, Inc. in Canada. The normal stress versus shear stress relationship was modelled to simulate the shear capacity and the operational behavior of reinforcement at different wall heights. In this design, pore-water pressure was defined by piezometric line function in Slope/W based on the local Q100 flood level provided. It indicated a water table of approximately 3.0m above the ground surface at the critical wall section as shown in Fig. 2.

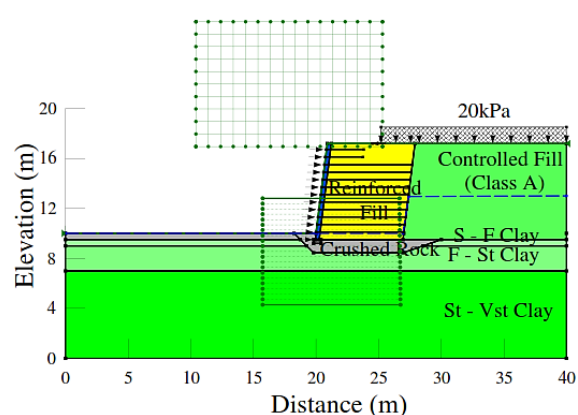


Fig. 2 Slope/W model of geometry with ground improvement.

### *Strain-based approach – finite element analysis*

Part of the design risks of this project were the potential wall deflection and excessive settlement due to the soft clay foundation layer and the significant

height of structure. Strain-based design approach was adopted to justify the design for long term performance. The commercial finite element software Phase2 was employed to assess the total, horizontal and vertical displacements.

The initial finite element analysis focused on the regulated maximum allowable settlement and wall face deflection of 50mm in accordance with AS4678-2002. However, this regulated allowance applies to all structures and does not consider the magnitude of structure height. This could lead to potential long term serviceability issue for structures with significant height. In this design, the potential cracking on the wall face induced by excessive tensile strain was a significant long term performance indicator. Bathurst and Simac [9] reported that modular concrete blocks have been observed to crack in reinforced segmental retaining wall structures. The appearance of cracking is not desirable from either aesthetic or structural point of view, especially for high structures consist of smaller concrete blocks. The differential settlement was summarized by Anderson [15] as one of the major sources causing cracking. In this design, the critical section of the structure was initially located on top of a 3.0m (W) x 1.5m (H) dimension concrete culvert which founded on soft clay area as shown in Fig. 3. This layer was then replaced by a layer of crushed rock fill as ground improvement option. The potential differential settlement between the combination of wall and culvert section versus the full height wall section was of primary concern.



Fig. 3 Overview of concrete culvert section.

Due to the lack of standard method to evaluate the serviceability problem caused by displacement, a methodology introduced by Mair et al. [16] for classifying the damage of masonry structures with prediction of ground movement and calculation of strains induced within the structure was adopted for this study. It established an important link between the estimated tensile strain and the potential damage category, which thus provided a principle for verifying the segmental block wall design from the serviceability assessment perspective.

Six categories of damage was defined by Burland et al. [17], numbered 0 to 5 in increasing severity.



Extensive case histories were analyzed by Boscardin and Cording [18], and the damage categories related to the magnitude of the tensile strain induced in the structure were summarized in Table 2. Based on this relationship, structures with induced tensile strain greater than 0.3% which classified category 4 to 5 represent severe to very severe degree of damage and require extensive or major repair. Therefore, the suggestion of 0.3% limiting tensile strain was adopted to compare with the computed differential strain from the finite element analysis to justify the serviceability of the structure.

Table 2 Relationship between category of damage and limiting tensile strain [18]

Category of damage	Normal degree of severity	Limiting tensile strain (%)
0	Negligible	0-0.05
1	Very slight	0.05-0.075
2	Slight	0.075-0.15
3	Moderate	0.15-0.3
4 to 5	Severe to very severe	>0.3

The finite element geometry was modelled with and without crushed rock fill ground improvement. The mesh was defined as a uniform pattern of approximately 1500 triangular elements with 6 nodes as shown in Fig. 4. The analysis will compute the variation of stress and strain throughout the mesh. The computed displacement outcomes were used to verify the long term serviceability of the structure.

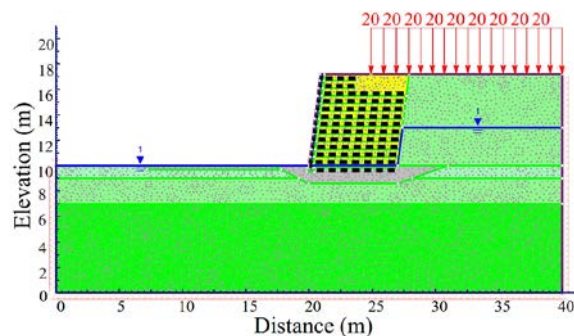


Fig. 4 Phase2 model with ground improvement.

## RESULTS AND DISCUSSIONS

### Effects of Soft Ground Improvement on the Slope Stability

To assess the stability of the structure in terms of FOS, the analysis introduced in previous chapter was conducted for different ground conditions. Prior to design, it was reported that the in-situ ground bearing capacity was sufficient and no ground treatment

would be required. However, the ground condition underneath the highest section of the structure was later found to be on a soft clay layer within a creek vicinity and ground improvement option was required. A 750mm thick layer of crushed rock fill was adopted to replace the soft clay layer. The crushed rock fill was designed to distribute the vertical stress uniformly into stiffer soil strata below and to prevent excessive wall displacement.

The Slope/W result shown in Fig. 5 shows that the FOS of structure founded on soft ground without treatment is 1.36 thus does not meet the minimum long term requirement of FOS 1.50 by local authority [19]. The Slope/W result illustrated in Fig. 6 indicates that the crushed rock fill effectively improved the ground condition and the FOS increased to 1.51 which satisfied the long term stability FOS requirement.

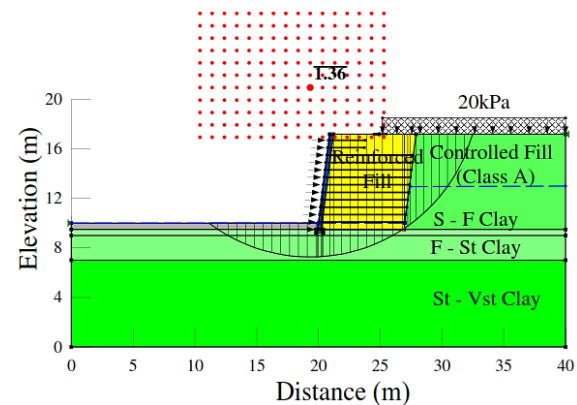


Fig. 5 FOS of geometry without ground improvement.

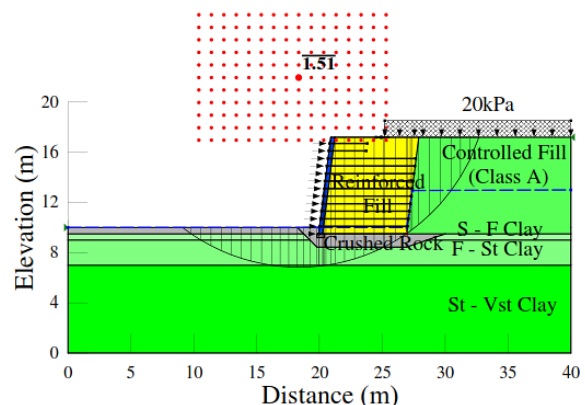


Fig. 6 FOS of geometry with ground improvement.

In order to further justify the effectiveness of the ground improvement method, the slope stability analysis of improved ground scenario were undertaken with different friction angle of the crushed rock ranging from 30 degree to 60 degree. The sensitivity check results illustrated in Fig. 7 presents the trend of the FOS increasing linearly with the

friction angle of the crushed rock fill. It was noted that in order to satisfy a FOS of 1.50, the crushed rock material must achieve a minimum friction angle of 45 degree. In this project, the crushed rock material was tested and verified in the laboratory before construction commenced.

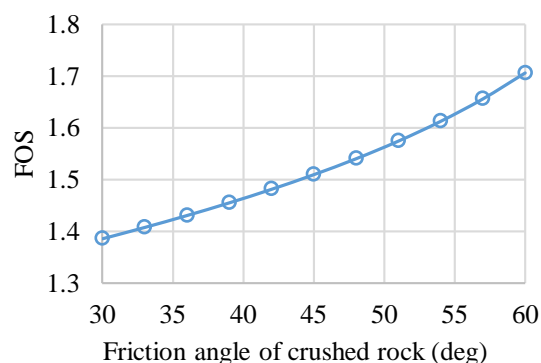


Fig. 7 FOS sensitivity check with different friction angle of crushed rock.

### Design Verification Using Strain-based Approach

As the long term excessive wall deflection and differential settlement were the key issues of this design, it was justified by using the strain-based approach described in previous chapter.

The finite element analytical results computed using Phase2 were adopted to justify the requirements stated in AS4678-2002 [20] which allows a maximum 50mm displacement. The comparison of the computed maximum horizontal and total displacement on the wall face of geometries with and without crushed rock fill are demonstrated in Fig. 8 and Fig. 9. The maximum horizontal displacement decreased from 52mm to 37mm, while the maximum total displacement decreased from 56mm to 38mm. Both results indicate that the crushed rock fill layer was effective on reducing the wall face displacements.

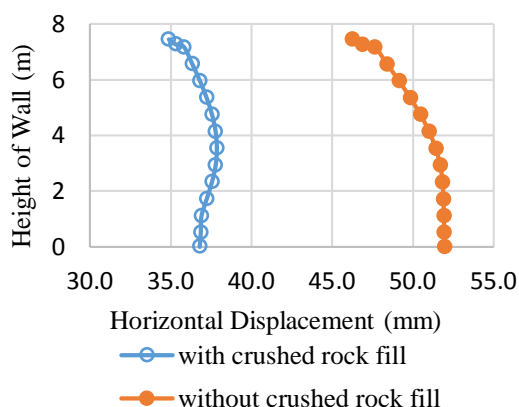


Fig. 8 Computed horizontal displacement along wall face with & without crushed rock fill.

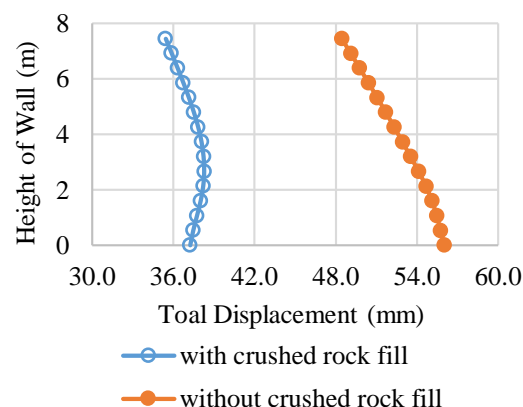


Fig. 9 Computed total displacement along wall face with & without crushed rock fill.

The strains percentage of wall displacement was then computed from the Phase2 results and checked for the serviceability requirement. The strains along wall face were calculated and the maximum value was adopted to compare with the 0.3% of limiting tensile strain described in previous chapter. The estimated maximum strain on the wall face was calculated as 0.26% based on total displacement outcome shown in Fig. 8.

The result indicates that the potential strains induced cracking on the face of the critical wall section could be classified as category 3. It corresponds to a moderate level of severity damage according to Table 2. Implication of typical damage and ease of repair and maintenance were suggested by Burland et al. [17]. This classification of damage could be conservative and the original paper suggested that there was no evidence of severe damage resulted from the tensile strains up to 0.3% by then. However, it provides a practical methodology for prediction of serviceability issue. Thus enables the design to be evaluated from the serviceability perspective which is unable to be addressed by stress-based analysis approach.

### CONCLUSION

The paper has focused on the design and analysis of the critical section of a geogrid reinforced segmental retaining wall that employs the Keystone® modular concrete units as the wall facing system. The stability of the structure was investigated by the conventional stress-based limit equilibrium approach. The long term performance of the wall face subject to displacements were analysed by strain-based finite element approach coupled with a serviceability evaluation methodology for masonry structures. The following conclusions were drawn from this case study:

- The long term performance of the wall under displacement is one of the key issues for the

design of Keystone® segmental wall with significant height. In order to fully address the design risks, the strain-based finite element approach for displacement analysis should be adopted in addition to the traditional stress-based limit equilibrium approach for stability assessment.

- The wall face cracking is a major performance indicator of reinforced masonry segmental retaining structure. The strain-based finite element approach could be extended by adopting a classification of damage methodology to examine the potential damage category based on the estimated tensile strains. Thus the long term serviceability could be evaluated in a more specific and comprehensive way with prediction of potential cracking damage in addition to the general displacement outcomes.

## ACKNOWLEDGEMENTS

The authors of this paper would like to acknowledge and thank Shadforths Civil Contractors, Keystone® Systems and Concrib Pty Ltd for their assistance and kind permission to publish this paper.

## REFERENCES

- [1] Anderson RB, Boyd FN and Shao L, "Modular block faced polymer geogrid reinforced soil walls U.S. postal service combined carrier facility", in Proc. On GEOSYNTHETICS'91, 1991, pp. 889-902.
- [2] Hill JJ and Berg RR, "Use of segmental wall system by Minnesota department of transportation", J. of Transportation Research Record, Vol. 1414, Dec. 1992, pp. 1-5.
- [3] Simac MR, Bathurst RJ and Goodrun RA, "Design and analysis of three reinforced soil retaining walls", in Proc. Conf. on GEOSYNTHETICS'91, 1991, pp. 781-789.
- [4] McGown, A, "The behaviour of geosynthetic reinforced soil systems in various geotechnical applications", in Proc. 2nd EU. Conf. on GEOSYNTHETICS, 2000, pp. 3-23.
- [5] Christopher BR, Gill SA, Giroud JP, Juran I, Mitchell JK, Schlosser F and Dunncliff J, Reinforced Soil Structure Volume I. Design and Construction Guidelines. Washington, D.C.: FHWA, 1990, ch. 3.
- [6] Simac MR, Bathurst RJ, Berg RR and Lothspeich SE, Design Manual for Segmental Retaining Walls, 3rd ed. Herndon: NCMA, 2010, pp. 250.
- [7] AASHTO/AGC/ARTBA, "Guidelines for the design of mechanically stabilized earth walls", In Situ Soil Improvement Techniques, 1st ed. AASHTO, 1990, pp. 4-18.
- [8] AASHTO/AGC/ARTBA, "Design guidelines for use of extensible reinforcements (geosynthetic) for mechanically stabilized earth walls in permanent applications", In Situ Soil Improvement Techniques, 1st ed. AASHTO, 1990, pp. 28-38.
- [9] Bathurst RJ and Simac MR, "Geosynthetic reinforced segmental retaining wall structures in North America", in Proc. 5th Int. Conf. on GEOTEXTILES, GEOMEMBRANES AND RELATED PRODUCTS, 1994.
- [10] Berg RR, Allen TM and Bell JR, "Design procedures for reinforced soil walls-a historical perspective, in Proc. 6th Int. Conf. on GEOSYNTHETIC, 1998, pp.491-496.
- [11] Greenway D, Bell R and Vandre B, "Snailback wall – first fabric wall revisited at 25-year milestone", in Proc. Conf. on GEOSYNTHETICS '99, 1999, pp.905-919.
- [12] Burkitt G, Redbank River Park Earthworks, Bulking Densities & Erosion Potential Assessment. Brisbane: Soil Surveys Engineering Pty Ltd, 2011, pp. 3-5.
- [13] Committee CE-032, "Design life", Australian Standard (AS) 4678-2002 Earth-retaining Structures, 1st ed. Standards Australia International Ltd., 2001, pp. 29.
- [14] GEO-SLOPE International Ltd., Stability Modelling with SLOPE/W 2012 Version: An Engineering Methodology. Alberta: GEO-SLOPE International Ltd., 2014.
- [15] Anderson RB, "Construction consideration for geogrid-segmental block mechanically stabilized earth retaining walls", J. of Transportation Research Record, Vol. 1414, Dec. 1992, pp. 12-15.
- [16] Mair RJ, Taylor RN and Burland BJ, "Perdition of ground movements and assessment of risk of building damage due to bored tunneling", in Proc. Conf. on GEOTECHNICAL ASPECTS OF UNDERGROUND CONSTRUCTION IN SOFT GROUND, 1996, pp. 713-718.
- [17] Burland JB, Broms B and De Mello VFB, "Behaviour of foundations and structures – SOA report, in Proc. 9th Int. Conf. on SMFE, 1977, pp. 495-546.
- [18] Boscardin MD and Cording EG, "Building Response to Excavation-Induced Settlement", J. of Geotechnical Engineering (ASCE), Vol. 115 (1), Jan. 1989, pp. 1-21.
- [19] Queensland Department of Transport and Main Roads Geotechnical Section, Geotechnical Design Standard-Minimum Requirements. Brisbane: Department of Transport and Main Roads, 2014.
- [20] Committee CE-032, "Construction tolerances", Australian Standard (AS) 4678-2002 Earth-retaining Structures, 1st ed. Standards Australia International Ltd, 2001, pp. 40.

## CONSOLIDATION PARAMETERS FROM ATTERBERG LIMITS – NEW CORRELATIONS

C H Solanki

Applied Mechanics Department, S V National Institute of Technology, Surat – 395 007 Gujarat, India,

### ABSTRACT

Various methods and empirical correlations are available to predict consolidation parameters. Use of empirical correlations for consolidation parameters cannot be generalized for all places and all soils. Empirical correlations should be used only after verifying its feasibility for particular region and type of soils. Consolidation test is expensive. Reliability is poor due to sampling disturbances. Time to investigate add more time to finalize the soil report. Normally soil report excludes the consolidation tests. In such cases empirical correlations are very useful to estimate consolidation settlement of shallow foundations. The test results and datasets containing index and consolidation parameters are used to conduct a statistical study to determine suitable correlations for estimating consolidation response of alluvial soil. This statistical analysis is carried out in order to obtain the most suitable and practically applicable relationships. New correlations are proposed for prediction of compression index and compression ratio using liquid limit, plasticity index, water content, voids ratio and porosity ( $n_o$ ) for alluvial deposits of Surat city & surroundings situated in the Gujarat state of India. Correlations obtained using atterberg limits having higher value of correlation coefficient. These correlations are use for prediction of compressibility parameters for all zones of Surat city and SUDA (Surat Urban Development Authority) region of South Gujarat in India.

**Key Words:** Alluvial Deposits, Atterberg limits, Empirical correlations, Soil Consolidation, Soil Properties.

### INTRODUCTION

[ 文  
意を引いたり、このスペースを使って注  
目ポイントを強調したりしましょう。こ  
のテキスト  
ボックスは、ドラッグしてページ上の好  
きな場所に配置できます。 ]

In the selection and design of foundation system, it is important to determine the types and properties of the soil. In a detailed investigation, the conventional approach is to perform subsurface investigation being to obtain for a sufficient number of soil samples which are then tested in the laboratory to obtain the necessary soil properties including consolidation parameters. The basic index properties are water content, dry density, void ratio, consistency limits. Consolidation tests are expensive and time consuming. In order to obtain realistic values, special sampling and testing techniques and testing systems are required. It is required to conduct these tests with the utmost accuracy and to adopt realistic and suitable procedures to evaluate and interpret the results obtained. However, the group of tests performed to obtain index properties of soil is relatively inexpensive and simple. They do not require much time or any sophisticated testing system. Hence, it is very useful to develop empirical correlations for

estimating the consolidation properties with soil index properties. The industrial growth and real estate activity in decade has been very fast. There are very few qualified equipped agencies to serve the sectors demand for soil investigations in time and at affordable price. The test for normal range of stress takes a more time. This constrain and normal practice to test typical one or two samples for a soil strata of approximately 3000 m<sup>3</sup> of the soil per unit could be statically unacceptable and occasionally misleading particularly for alluvial stratified layered deposits. Thus the expected accuracy of results and predicted final settlement or its time rate is highly variable. The aim of study is to establish fairly reliable forecast of consolidation parameters and finally total settlement at a specified time by passing statistically not acceptable tests with reference to time and cost both. New approach is evolved for quick analysis and to assess sensitivity of structure at a site for settlement. The derived parameters and approach can be new, quick and economical.

### Subsoil Characteristics

The study area is divided in to 10 zones of Surat City and SUDA (Surat urban development authority) situated in Gujarat state of India. Six zones are of Surat Municipal Corporation and 4 zones of SUDA. The subsoil characteristics of each zone are studied in detail from large number of datasets. A datasets containing index and consolidation parameters are

used to conduct a statistical study to determine suitable correlations for estimating consolidation response. This statistical analysis is carried out in order to obtain the most suitable and practically applicable relationships. This database can provide information regarding trends, relationships and statistical properties, a mechanism whereby test results can be checked and provides geotechnical information for preliminary design purposes. The soil characteristics of each zone are studied up to a depth of 8 m. This depth is stress zones for shallow foundations. Generally for multistoried buildings foundations are located at 3 to 4 m depth in the study region. The average soil properties up to depth of 8 m are shown in Table 1.

**Table 1** Average range of Subsoil characteristics for study area

Soil Properties	Most Range
Liquid Limit ( $w_L$ )	30 – 60
Plastic Limit ( $w_p$ )	20 – 30
Plasticity Index ( $I_p$ )	15 – 30
Void Ratio ( $e_0$ )	0.6 – 0.9
Dry unit weight $kN/m^3$ ( $\gamma_d$ )	14 – 16
Water Content ( $w$ )	15 – 30
Porosity ( $n_0$ ) %	40 – 46
% Fines	60 – 90
Clay %	20 – 30
Silt %	40 – 60
Compression Index ( $C_c$ )	0.24 - 0.37
Compression Ratio ( $C_c'$ )= $C_c/(1+e_0)$	0.14 – 0.18
Soil Classification	Low to High Compressible Fine Grained Soil
Differential Free swell	10 – 80
Mineralogy	Montmorillonite & Kaolinite

The consolidation characteristics such as compression index and compression ratio of west zone Surat are found less compared to other zones. The coarse-grained soil is predominant in west zone Surat. The properties covered in the table are liquid limit , plastic limit , plasticity index , void ratio, dry unit weight , water content , % finer , compression index and compression ratio.

### Statistical Summary of Subsoil characteristics and Empirical Correlations

Statistical summary of parameters such as mean, median, and standard deviation, coefficient of variance, skew ness, kurtosis and range are studied of all zones. This statistical analysis is done with the software statistixl. Statistical summary of subsoil characteristics of all zone of Surat and SUDA shows

that mean value range of liquid limit 38.5 – 51 %, plastic limit 20 – 25 %, plasticity index 20 – 27 %, void ratio 0.7 - 0.77 %, dry unit weight 15.2 - 16.0 gm/cc, water content 19 - 23 and % finer 55 - 84. Coefficient of variance for most soil properties in all zones found below 30% except very few cases. The lower values of skewness and kurtosis in all zones indicate symmetry of data. Various methods and empirical correlations are available to predict consolidation parameters are used for study area for determination of compressibility parameters. It is found that use of empirical correlations for consolidation parameters can not be generalized for all places and all soils. Empirical correlations should be used only after verifying its feasibility for particular region and type of soils. Consolidation test is expensive, and its reliability is also poor due to sampling disturbances. Time to investigate adds more time to finalize soil report. Normally soil report excludes the consolidation tests in the study area. In such cases empirical correlations are very useful to estimate consolidation settlement of shallow foundations. Laboratory test results of the study area used for deriving new correlations. New correlations are proposed for prediction of compression index and compression ratio using liquid limit, plasticity index, water content, void ratio and porosity for alluvial deposits of study area as shown in Table 2. Correlations are obtained using soil plasticity characteristics having higher value of correlation coefficient.

**Table 2** New Correlations

Correlation	Correlation Coefficient ( $R^2$ )
$C_c = 0.0061 w_L - 0.0024$	0.8435
$C_c = 0.4066 e_0 - 0.0415$	0.7223
$C_c = 0.0082 I_p + 0.0915$	0.7862
$C_c = 0.0107 n_0 - 0.1818$	0.7115
$C_c = 0.0091 w + 0.0522$	0.77
$C_c' = 0.0022 w_L + 0.0478$	0.9063
$C_c' = 0.0029 I_p + 0.0833$	0.8579
$C_c' = 0.0035 w + 0.0631$	0.6735

Correlations obtained using soil plasticity characteristics having higher value of correlation coefficient in compare to other soil properties. These correlations are use for prediction of compression index and compression ratio for different zones of Surat and SUDA region. Statistical summary of predicted values of compression index and compression ratio for Surat and SUDA are shown in table 4. New correlations derived for compressibility parameters of soil using index and plasticity properties are used for all zones of Surat and SUDA region. Experimental results are studied for soil index and consolidation properties. Available test datasets of Surat and SUDA gave reasonably good correlation

coefficient between soil plasticity and compression characteristics. Initially liquid limit and plasticity index are used separately for determining compression characteristics of alluvial soil. The average values of compressibility parameters are computed from values obtained using liquid limit and plasticity index correlations. From detail study of results, it is found that both parameters of soil may improve the correlation coefficient. The further study is carried out for determining consolidation parameters of soil using single or both parameters of soil. Large numbers of datasets of study area are used from S V National Institute of Technology and different agencies for deriving correlations of consolidation parameters. Empirical correlations are proposed for over consolidation ratio, coefficient of consolidation with soil plasticity characteristics. Correlations are also proposed for compression index and compression ratio using single or both parameters. Validations of new correlations are done with existing consolidation test datasets of other region. The proposed correlations derived by author for compressibility parameters of alluvial soil of above mention properties with correlation coefficient 0.75 and more are as follows for shallow foundations.

The ratio of pre-consolidation pressure and present overburden pressure is known as over consolidation ratio (OCR). Based on OCR soils are classified as normally consolidated, over consolidated or under consolidated. Selection of consolidation parameters such as compression index ( $C_c$ ), Recompression index ( $C_r$ ) or coefficient of volume change ( $m_v$ ) is on the basis of OCR for computing consolidation settlement. The correlations are also suggested by researchers to obtain Pre-consolidation pressure and Nagaraj and Murthy (1994), Chetia and Bora (1998) etc.

Based on the test data of study area following relation is derived for over consolidation ratio

Over consolidation ratio

$$(OCR) = 1.85 - 0.007 p_o - 0.225 (e/e_L) \quad R^2=0.793 \quad \dots\dots(1)$$

The rate of settlement of the soil layer takes place is essential from design consideration. This can be determined using coefficient of consolidation  $C_v$ . To obtain  $C_v$  it is essential to conduct a routine one-dimensional consolidation test. The various time fitting curves are available to evaluate  $C_v$ . This is time consuming process. Curve fitting procedures available in the literature are not completely satisfactory in evaluating  $C_v$  and hence large variation is obtained in the evaluated values by different procedures. Generally square root time fitting or Log time fitting curves are use for evaluation of  $C_v$ . The rate of settlement is directly related to the rate of excess pore pressure dissipation. Coefficient of consolidation  $C_v$  is useful in the determination of the time required for a

finite percentage of consolidation to occur. The coefficient of consolidation  $C_v$  generally decreases as the liquid limit of soil increases. The range of variation of  $C_v$  for given liquid limit is very high.  $C_v$  varies with both level of stress and degree of consolidation. For practical site settlement calculations, measure  $C_v$  relative to loading range applicable to site, and then assume this value to be constant. In the present study coefficient of consolidation is correlated with liquid limit and plasticity index of soil. It is observed that  $C_v$  for alluvial soil is giving higher value of correlation coefficient with plasticity index than to liquid limit. The correlation of  $C_v$  with liquid limit is also quite satisfactory.

Based on the test data of study area following correlations are derived for coefficient of consolidation

$$\text{Coefficient of consolidation using liquid limit} \\ (C_v) = 10^8 w_L^{-6.7591} \quad \text{cm}^2/\text{sec} \quad R^2=0.7867 \quad \dots\dots(2)$$

$$\text{Coefficient of consolidation using plasticity index} \\ (C_v) = 7.7525 I_p^{-3.1025} \quad \text{cm}^2/\text{sec} \quad R^2=0.9156 \quad \dots\dots(3)$$

$$\text{Compression ratio using liquid limit} \\ (Cc') = 0.0032 w_L + 0.0004 \quad R^2=0.7806 \quad \dots\dots(4)$$

$$\text{Compression ratio using liquid limit and plasticity index} \\ (Cc') = 0.002 w_L + 0.001 I_p + 0.037 \quad R^2=0.8674 \quad \dots\dots(5)$$

Fig 1(a) shows comparison of measured and predicted compression ratio from liquid limit and plasticity index.

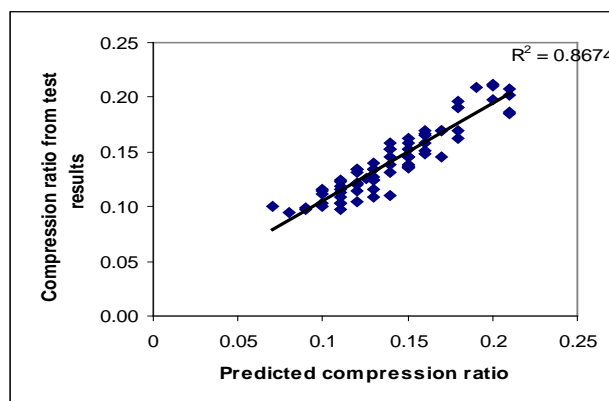
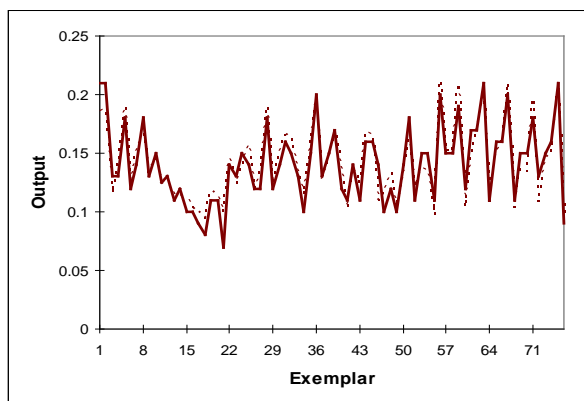


Fig 1 (a) Comparison of measured and predicted Compression ratio



Comparison of measured and predicted compression index using ANN (Artificial Neural Network) is shown in fig 1 (b).



**Fig 1 (b) Comparison of measured and predicted compression index Using ANN**

MSE	0.000141866
MAE	0.009728118
Min Abs Error	2.11004E-05
Max Abs Error	0.030127471
r	0.931366511

The software neurosolution5 was utilized for training, testing and cross validation. Various architectures of ANN along with numerous training algorithms were tried till satisfactory results were obtained.

The comparison of compression ratio from measured 135 numbers test data from literature and using above empirical correlation liquid limit and plasticity index both are determine. It is found that the values obtained using empirical correlations are close to consolidation test data. Compression ratio of soil is giving higher value of correlation coefficient with liquid limit and plasticity index both. Table 3 shows statistical comparison of compression ratio using test datasets of other region from literature and empirical correlation using liquid limit and plasticity index.

**Table 3 Statistical summary of compression ratio from test data and correlation**

Parameter	Cc' from test data	Cc' from correlation $W_L$ & $I_p$
Mean	0.175	0.178
Median	0.167	0.172
Std Error	0.004	0.003
Std Dev.	0.043	0.039
COV.	24.391	21.312
Sum	23.609	24.582
Minimum	0.103	0.126
Maximum	0.296	0.280
Range	0.193	0.154

Count	135.000	135.000
Skewness	0.678	0.823
Kurtosis	-0.151	-0.151

### Empirical Model for Computation of Settlement of Shallow Foundations

Empirical model is proposed using Visual Basic Program to predict the settlement of shallow foundations incorporating soil index and plasticity characteristics. The model incorporates the computation of over consolidation ratio, time rate settlement, magnitude of settlement and differential settlement of foundations. The model will be useful for foundation design incorporating the differential settlement of foundations. This model is proposed to obtain settlement of shallow foundation for fine grained alluvial deposits of same subsoil range. In this model input parameters are soil index & plasticity characteristics for obtaining settlement of foundations. The soil index and plasticity characteristics in addition to geometrical foundation parameters and load on the foundation are required to obtain settlement using this empirical model. The program is also prepared for predicting contact pressure between soil and footing (Safe or Allowable bearing Pressure) from input of required parameters. For Prediction of total and differential settlement soil properties and geometrical parameters used as input parameters are % finer, bulk unit weight of soil ( $\gamma$ ) water content ( $w$ ), liquid limit ( $w_L$ ), plasticity index ( $I_p$ ), specific gravity of soil grains ( $G$ ), standard penetration resistance ( $N$ ), width of footing ( $B$ ), length of the footing ( $L$ ), depth of the footing ( $D$ ), degree of consolidation ( $U$ ). Model computes area of footing, safe load on the footing with dry unit weight of soil ( $\gamma_d$ ), void ratio ( $e$ ), thickness of the compressible layer ( $H$ ), void ratio at liquid limit ( $e_L$ ), existing over burden pressure ( $p_o$ ), over consolidation ratio (OCR). Magnitude of settlement is determined using compression ratio of soil. The soil for which plasticity index is not known  $Cc'$  is determined using liquid limit. When liquid limit ( $w_L$ ) and plasticity index ( $I_p$ ) both are known compression ratio is determine using both parameters. Recompression index is taken as 10% of compression ratio.

For determining magnitude of settlement of normally consolidated soil geometrical factor is taken as 0.7 and for over consolidated soil taken as 0.5. Depth factor ( $D_f$ ) and Rigidity factor ( $R_f$ ) are taken as 0.8 in computation of magnitude of settlement. Modulus of elasticity is assumed or computes using standard penetration resistance ( $N$ ) in this model. The total settlement of the foundation is taken as sum of corrected immediate settlement and corrected consolidation settlement. The model also incorporates differential settlement between two

footings or two edges. Angular distortion is computed by giving center to center distance between two footings. If computed settlement is exceed the permissible settlement it highlights the values. These computations are used to check differential settlement for structural member of frame. The empirical model also includes computation of time rate settlement. Coefficient of consolidation is to be determined using liquid limit, if plasticity index is not known. When plasticity index of soil is known coefficient of consolidation ( $C_v$ ) is computed on using plasticity index. The model incorporates single drainage or double drainage. The output of time rate settlement is obtained in days.

## CONCLUSION

Empirical model is prepared to obtain settlement of shallow foundation for preliminary design. In this model input parameters are soil index and plasticity characteristics with some basic soil properties and geometrical dimensions. Model computes parameters such as over consolidation ratio. Coefficient of consolidation, compression ratio, immediate settlement, consolidation settlement and differential settlement. This model is enable the designer to decide safe bearing capacity or permissible bearing capacity which ever governs the design, Critical differential settlement zones in a structure to proportion foundations or stiffen structure and indicate critical sample site to minimize errors in transfer or remolding of samples collected by driller.

## REFERENCES

- [1] Celik, S. and Tan, O. (2005) Determination of Pre-consolidation pressure with Artificial neural network , Civil Engineering and Environmental system .22 (4) pp 217-230
- [2] Cherubini C & Giasi C I (2000), "Correlation equations for normal consolidated clays". Coastal geotechnical engineering in practice, Nakase & Tsuchida balkema Rotterdam pp 15 - 20.
- [3] Crumley, A. R. (2003) "Compressibility Relationships for soils in Puerto Rico" 12<sup>th</sup> Pan-American conference on soil Mechanics and Geotechnical Engineering Massachusetts Institute of Technology, Boston. pp. 1-5.
- [4] Koumoto, T. and Park, J. (2004), "New compression index equation". Journal of Geotechnical & Geoenvironmental Engineering ASCE 130 (2) pp 223 -226.
- [5] Lav, M. A. and Ansal, M. A. (2001) "Regression Analysis of Soil Compressibility" Turk Journal Environmental Science. Vol.25 pp 101-109
- [6] Nagaraj, T. S., Shrinivasa murthy B. R., and Vatsala, A. (1991), "Prediction of soil behaviors –part ii- saturated uncemented soil". Canadian Geotechnical Journal . Vol. 21 (1) pp 137 - 163.
- [7] Nath, A. and DeDalal S S (2004), "The Role of Plasticity index in predicting compression behavior of Clays" Electronic Journal of Geotechnical Engineering. pp 1-7
- [8] Robinson, R. G. and Allam, M. M. (2003) "Compression index of clays and silts" Journal of testing and evaluation ASTM 31 (1) pp 1-6
- [9] Senol A , Seglamer A (2000) "Determination of Pre-consolidation pressure with a new strain energy –log stress method " Electronic Journal of Geotechnical Engineering pp 1-11
- [10]Shahin, M. A. Maier, H. R. and Jaska, M. B. (2000) "Predicting settlement of shallow foundations using neural networks" Journal of Geotechnical and Geoenvironmental Engineering pp 785-793
- [11]Sridharan, A. and Nagaraj H.B. (2000), "Compressibility behavior of remolded fine grained soils and correlation with index properties". Canadian Geotechnical Journal 37 pp 712-722
- [12]Sridharan, A. and Nagaraj, H. B. (2004) "Coefficient of consolidation and its correlation with index properties of remolded soil " Geotechnical testing Journal ASTM 27 (5) pp 1-6
- [13]Yoon, G. L. Kim, B. T. and Jeon, S. S. (2004), "Empirical correlations of compression index for marine clay from regression analysis". Canadian Geotechnical Journal. .41 pp 1213 – 1221.

## **RESEARCH OF PERIMETER REINFORCEMENT OF THE FOUNDATION SOIL BY CEMENT-SAND MORTAR INJECTION**

M.L. Nuzhdin<sup>1</sup>, L.V. Nuzhdin<sup>2</sup>

<sup>1</sup>SPEC Company "O&F", Russia; <sup>2</sup>Novosibirsk State University of Architecture and Civil Engineering (Sibstrin), Russia

### **ABSTRACT**

The article analyzes the results of a series of laboratory experiments studying consolidation of foundations by perimeter reinforcement of the soil by rigid incompressible irregularly shaped inclusions. The experiments modelled consolidation of a shallow soil foundation base by directed high-pressure injection of mobile cement and sand mixtures. The essence of the method of high-pressure injection is pumping of a cement-sand mixture in the foundation under a pressure exceeding structural strength of the soil, as a result of which the massif continuity is broken and a cavity filled with cast-in-place concrete is formed in the soil. Laboratory tests in soil trays and a number of full-scale experiments on a test field were made in order to define rational design parameters of such consolidation. Several series of experiments were conducted: with different distance between inclusions in plan, with different depth of inclusions and etc.

*Keywords: Mortar injection, perimeter reinforcement*

### **INTRODUCTION**

The technology of reinforcement of foundation soil that is about using the targeted high-pressure injecting method is quite widespread in the city of Novosibirsk and in the West Siberian region of Russia. Technical essence of the method consists in feeding the workable cement-sand mortar in the ground base under pressure that is slightly higher than the structural strength of the ground. In this case the continuity of the ground mass is violated, and the formed cavities are filled with injectable mortar, after hardening of which in the foundation soil the incompressible inclusions are created.

The targeted high-pressure injecting technology consists in placing the injectors in certain geometrical order and simultaneous feeding of mortar through all the injectors. This allows creating in the ground the injection bodies of "given" forms. Thus, with the placement of the three injectors at the corners of the conditional equilateral triangle and with the usage of injectors with only one opening (at the lower end of the pipe) the flat disk-shaped body is formed. When positioning the injectors along a straight line and using injectors with slotted openings in their lower part in the base the vertical body oriented along a straight line is created. In both cases, the distance between the injectors, injection pressure, the consistency of the mortar and other parameters are assigned according to the calculations depending on the physical and mechanical properties of the ground.

Application of the targeted high-pressure injecting technology is quite productive and has

significant benefits. These are: the possibility to perform work in confined space (for example, from the basements of existing buildings); the absence of dynamic effect on the surrounding constructions; lack of coupling with the reinforced foundation (no interference with its condition); no need for special expensive equipment and materials; as well as the high efficiency of carried out reinforcing works with their low cost and quite a high speed of execution. In this case the reinforcement of the ground base and foundations can be done for existing buildings and facilities during their reconstruction and repair, as well as during the engineering preparation for new construction.

In Novosibirsk and other Russian cities the topic of reinforcing the ground base and foundations of historical buildings during their reconstruction, as well as reinforcing of existing buildings in order to avoid a negative impact on them during construction of new closely located buildings and structures is highly relevant.

With the variety of possible schemes for the reinforcement of the ground base and subsurface foundations, one of the most effective ones is outline reinforcement - insertion of a range of vertical elements (that consist of solid bodies) in the ground base along the edges of foundations. From a practical point of view, the reinforcing members that are made along the outline with a certain step function as a "compression wall" along the longitudinal edges of subsurface foundations, they also create some prestress of the ground base that is limited by the "compression veils" and the base of the foundation. These two factors can significantly

reduce the deformation of foundation soil.

For the effective commissioning of "compression walls" it is necessary to provide minimal vertical and horizontal displacements of reinforcing members, and to prevent horizontal ground heave from under the base of the foundation between the reinforcing members.



Fig. 1 Gravel chippings of different size, shaping solid incompressible inclusions in experiments on outline reinforcing in a small ground tray.

Vertical stability of the reinforcing members is achieved by immersing them to a certain depth. The upper part of the reinforcing member, due to frictional forces between the ground and its side surface, reduces stress in the ground, and the lower part of the reinforcing member due to friction transmits the load to the ground base. Clamping of the ground in the form of the created "arch roofs" during the loading prevents the ground punching.

The experiment of reinforcing inclusions formation while reinforcement of the ground foundation and the existing buildings foundation with the help of high-pressure injecting technology has proved to be efficient. Here (as with any other injecting) arises the question of allocation of effective inclusions geometrical parameters, such as the number and spacing between inclusions in "columns", inclusions diameter and the distance between them, etc.

#### Experimental set up in small and large ground trays

To define rational parameters of outline reinforcing of shallow foundation, created through pumping of cement-sand mixtures, a complex of laboratory research has been carried out on different scale models of foundations and reinforcing members. The experiments were carried out in a  $0.9 \times 0.38 \times 0.5$  m ground tray, filled with dry medium sand. As a model of foundation perimeter, a hard metallic rectangular  $0.37 \times 0.11$  m plate was used; and as a pier foundation – metallic square plate  $0.10 \times 0.10$  m.

Inclusions were shaped by gravel chippings with  $0.02 \dots 0.04$  m diameter. The sand was poured into the tray layer by layer without compaction, after

each layer gravel chippings were introduced into it with small effort, creating certain compaction, relatively shaping the compaction of the surrounding ground while injecting the cement-sand mortar.



Fig. 2 Gravel chippings arrangement while experimenting with effective parameters of perimeter plate outline reinforcement.

Vertical action, applied to the plate, was created with screw jack through spring dynamometer. Plate load was transferred as a point force through the support construction of the tray. High rigidity of metallic plates ensured even distribution of pressure on the ground over their bottom.



Fig. 3 Gravel chippings arrangement while experimenting with effective parameters of square plate outline reinforcement.

Measurement of plates vertical strain (settlement) was carried out through Maximov's deflectometer with division value 0.01 mm.

Laboratory research program consisted of 12 series (6 series for rectangular and 6 for square plate) 3-4 experiments in each, all experiments were repeated at least 3 times.

The following parameters varied while experimenting:

Dimensions of rigid inclusions:  $0.02 \dots 0.04$  mm ( $0.2b \dots 0.4b$ );

Outline reinforcement spacing:  $1d$ ,  $2d$  and  $3d$  ( $d$  – nominal inclusion diameter), approximately  $0.2b \dots 1.2b$ ;

Number of reinforcement layers: 3-10;

Gaps in depth between inclusions: 1d (tight laying), 2d and 3d;

In-plane distance from reinforcing members to the plate edges.

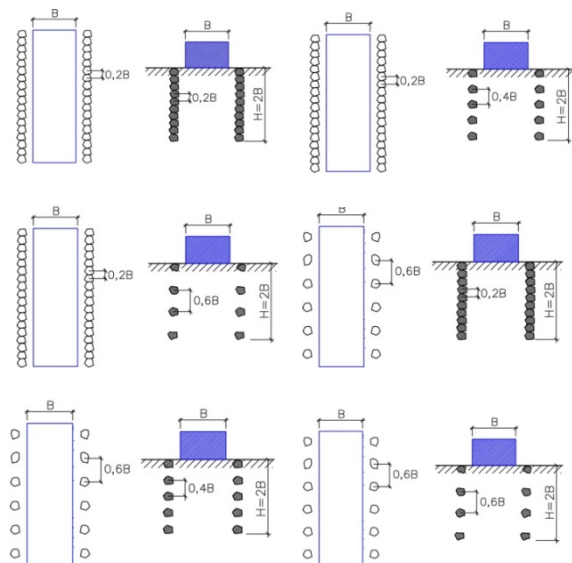


Fig. 4 Schemes of some experiments on studying the influence of geometrical parameters on the efficiency of outline perimeter plate reinforcement.

After each experiment, the sand and inclusions were taken out of the tray, the sand was sifted through, and a new experiment was being prepared.

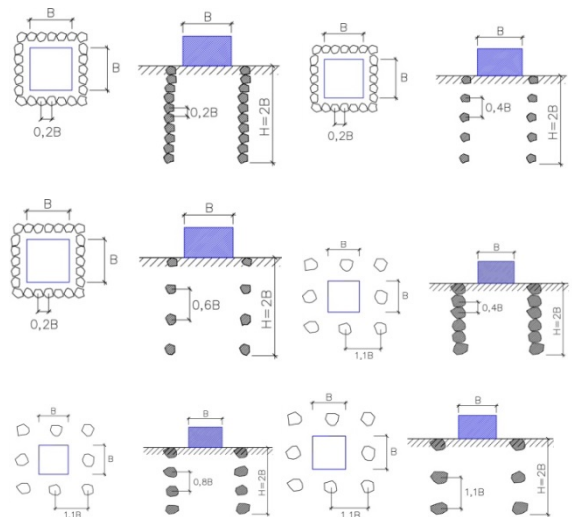


Fig. 5 Schemes of some experiments on studying the influence of geometrical parameters on the efficiency of outline perimeter square plate reinforcement.

Dependence diagrams «plate bottom pressure – plate subsidence» were constructed based on the obtained results.

In order to confirm qualitative dependence of experimental data, obtained in small ground tray, and quantitative evaluations of outline reinforcing influence on shallow foundations subsidence under load, a number of experiments in large ground tray and half-sized models was carried out.



Fig. 6 Experimental studies perimeter reinforced base of the square plate 5,000 cm<sup>2</sup> in area in the big soil tray on small packed sand (the loading device includes directional vibrator and allows transfer of vertical or horizontal dynamic loads to the plate in addition to static loads – this article does not examine the dynamic tests results).

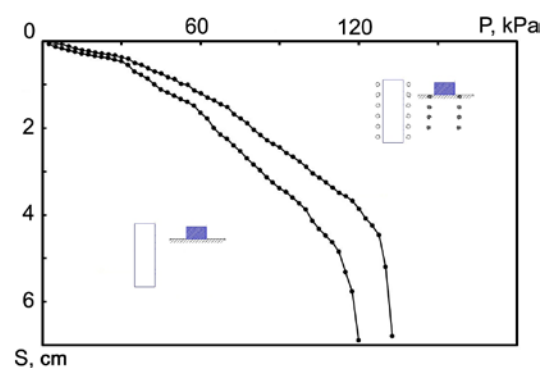


Fig. 7 Diagrams of perimeter plate subsidence on unreinforced base and on the base, reinforced with inclusions 0.2b with spacing 3d in plane and gaps 3d in depth.

Experiments in the big soil tray 300×300 cm and 200 cm deep were carried out on small packed air-dry sand with internal friction angle  $\phi = 37^\circ$ , pseudo cohesion  $c = 5$  kPa and deformation module  $E = 27$  MPa (see fig. 6). The tray had no rigid bottom below and under the sand there was slightly wet stiff silty clay with layer thickness more than 9 m. The load on the soil base was transferred by means of a hydraulic jack 1,000 kN set on a standard rigid plate 5,000 cm<sup>2</sup> in area. The plate settlements were registered by four



deflectometers with scale interval 0.1 mm. Measurements were made with time delays after deformations stabilization.

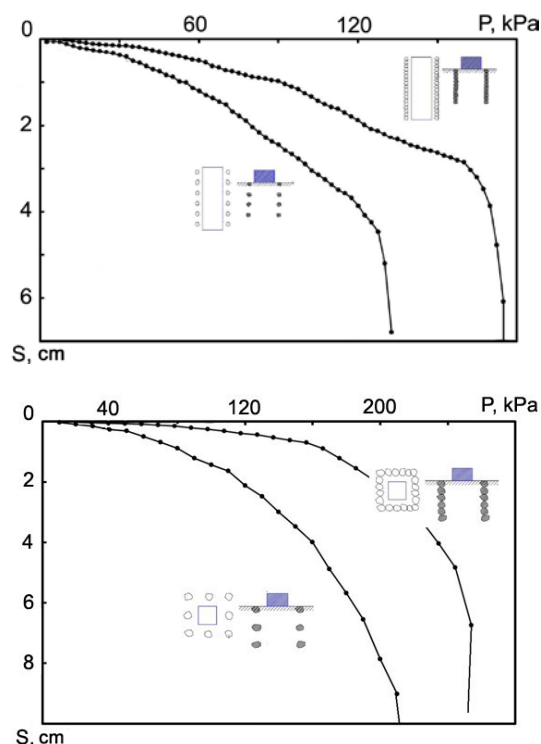


Fig. 8, 9 Diagrams of subsidence of perimeter and square plates on a base with contiguous outline reinforcement. The base is reinforced by the inclusions with a 3d lateral step and 3d gaps in depth with size 0.2b (Fig. 8) and 0.4b (Fig. 9).

Results obtained in laboratory conditions were experimentally checked during tests of a large-scale foundation model on a test field in natural soil conditions represented by slightly wet stiff silty clay with layers of lean clays and sand, having the following characteristics: internal friction angle  $\varphi = 27^\circ$ , pseudo cohesion  $c = 21$  kPa, deformation module  $E = 14$  MPa. As the foundation model we used a standard metal plate 5,000 cm<sup>2</sup> in area and stock reinforced concrete foundations with dimensions in plane 100×100 cm and 60×240 cm. Foundation models and plates were loaded by means of a system of beams, ballast weight (or anchoring system) and a hydraulic jack. Settlements and deformations of the surrounding soil surface were registered by a special reference measurement system, including deflectometers, watch-like indicators and reference points for geodetic. Experiments were made using a stress relaxation method, also called a method of controlled displacement (MCD). In our analysis of the efficiency of various ways of perimeter reinforcement of foundation soil of heavy-loaded

foundations we also used the results obtained in plate tests on several construction sites of Novosibirsk during reinforcement of sand, silty clays and lean clays.

### Laboratory research results

Efficiency of outline reinforcement with various parameters may be evaluated by comparing the diagrams of dependence of plate subsidence from the load (Fig. 7...Fig. 14). The diagrams are constructed on the basis of the experiments carried out on the small ground tray.

Analysed the results of the experiments we may come up with some general conclusions.

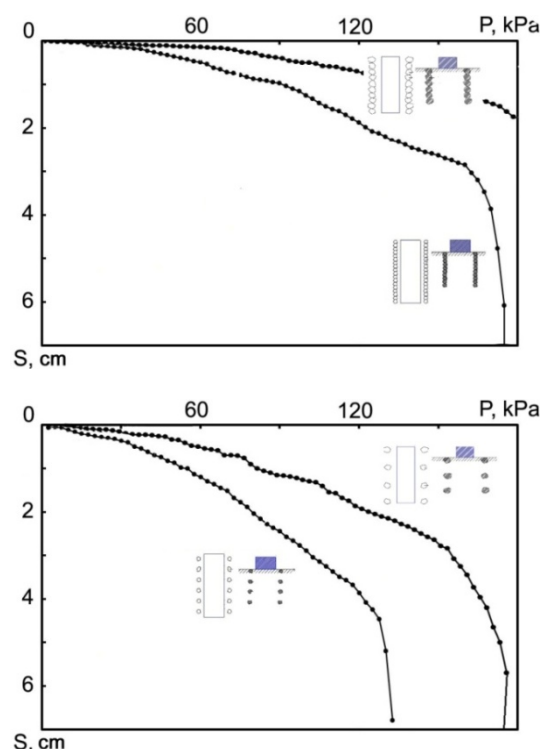


Fig. 10, 11 Diagrams of subsidence of a perimeter plate on a ground base reinforced with inclusions of different size (0.2b and 0.4b). Contiguous outline reinforcement (Fig. 10), distribution of reinforcing members with the step in plane of 0.3d and 3d gaps in depth (Fig. 11).

All the parameters of the reinforced ground foundation varied in experiments influence the end result – value of plate subsidence under load – in some degree. Even minimal reinforcement used in experiments (inclusions size 0.2b, step 3d on the plan, gaps of 3d depth) reduces subsidence for approx. 25% (Fig. 7) in comparison with an unreinforced base.

The most influence on the results for both perimeter and square plates is made by the



abundance of reinforcing members. Reinforcing members inserted tightly both in plane and in depth provide maximal compression effect and thus subsidence is minimal. In this case subsidence may be 100% (for perimeter plate) and 400% (for square plate) less than if the reinforcing members have gaps between each other. At the same time a significant increase of ultimate load on the base is observed.

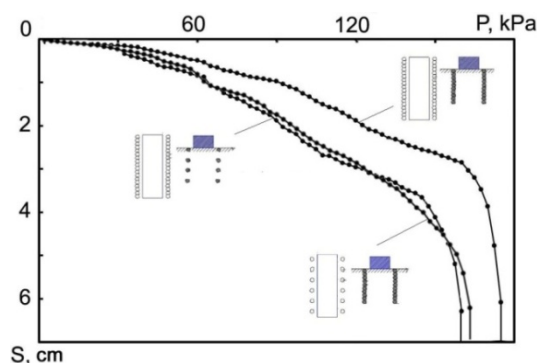


Fig. 12 Diagrams of subsidence of perimeter plate on a base with contiguous outline reinforcement with 0.2b inclusions and on a base with various distances: step and gaps in depth of 3d.

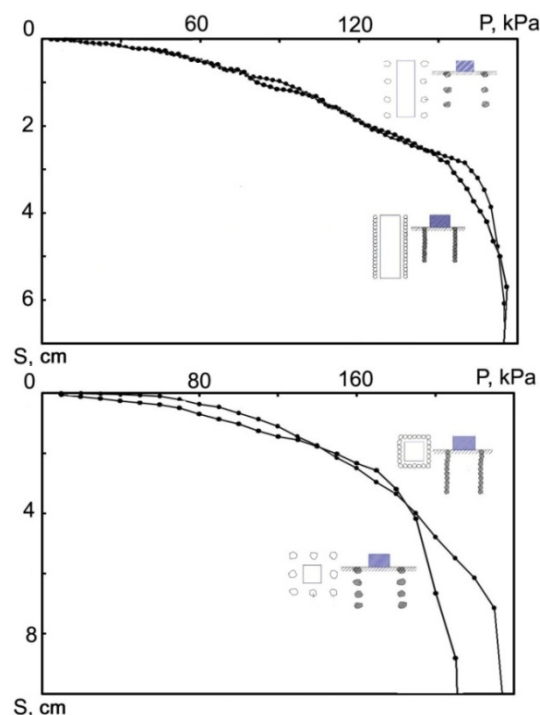


Fig. 13, 14 Diagrams of subsidence of perimeter and square plates on a base with contiguous outline reinforcement with elements of equal volume, inserted with different step and in depth gaps.

With the similar reinforcement scheme used, the size of inclusions is of large significance: if

inclusions with a size of 0.4b are used in contiguous outline reinforcement the subsidence at all stages of load is 2-3 times lower than in the same scheme of reinforcement with 0.2b inclusions. Significant increase of ultimate load on the base is observed by the reinforcement with larger inclusions.

If reinforcement was made with inclusion of the same size the plate subsidence directly depends on the distance between the reinforcing members. If the step between the members is increased laterally and height along, the subsidence increases as well. If the step between the members is increased in plane up to 3d (in contiguous vertical reinforcement) the subsidence increases for 75-100% in comparison with contiguous outline reinforcement. Results analysis revealed a curious fact that the similar vertical increase of gaps (in contiguous lateral step of the members) results in the equal increase of subsidence.

In both cases closer position of both laterally situated reinforcing members and inclusions in depth results in significant increase of ultimate load on a plate.

## CONCLUSION

Outline reinforcement around the subsurface foundations (plates) with high-pressure injections allows to reduce the subsidence of a ground base significantly in comparison with unreinforced base. Supporting of the existing foundations with such reinforcement results in the increase of base load-bearing capacity and makes extra loads possible.

## REFERENCES

- [1] Nuzhdin LV, "Account of interaction between a foundation frame and soil in pile foundation oscillations", in Theses of the Report at Nation. Scien.-Techn. Conf. "Soil mechanics and foundation engineering", SPb: SPbGASU, 1995, pp. 505-510.
- [2] Nuzhdin ML, "Prevention of non-uniform settlements of foundation plate by means of high-pressure injection" in Mat. of Int. Scien.-Techn. Conf. "Experience of construction and reconstruction of buildings and structures on weak soils", Arkhangelsk: Arkhangelsk State University, 2003, pp. 119-122.
- [3] Nuzhdin ML, "Use of cement-sand grouts to consolidate of soil foundations by means of directed high-pressure injection", in Int. Collection of Scien.-Techn. works, Issue 59, Kiev, 2003, pp. 430-433.
- [4] Nuzhdin ML, "Application of injection conductors to prevent occurrence of foundation plate tilts above the permitted standard by means of high-pressure injection" in Works of Int. Geotech. Conf. devoted to the Russian

- Federation Year in Kazakhstan “Geotechnical problems of large-scale and unique objects construction”, Almaty, 2004, pp. 351-354.
- [5] Nuzhdin ML, Nuzhdin LV, “Experience of high-pressure injection method application for erection buildings on plate foundation” in Proc. of XIVth Danube-European Conf. on Geotech. Eng. Key lectures, main lectures and abstracts of papers “From Research to Design in European Practice”, Bratislava, Slovak Univ. of Tech., 2010, p. 310.
- [6] Nuzhdin ML, Nuzhdin LV, “Erection many-storey buildings one plate foundation with application high-pressure injection method” in Proc. The 14th Asian Reg. Conf. on Soil Mech. and Geotech. Eng. (Hong Kong, China, 23-27 May 2011) “Soil Mechanics and Geotechnical Engineering: Challenges and Solutions”, Hong Kong, The Hong Kong Polytech. Univ., 2011, p. 219.
- [7] Nuzhdin ML, Nuzhdin LV, “Application high-pressure directional injection method for strengthen soil base” in Proc. of the IVth Central Asian Geotech. Symp. “Geo-Engineering for Construction and Conservation of Cultural Heritage and Historical Sites – Challenges and Solutions”, Samarkand, 2012, pp. 201-205.
- [8] Patent for invention No. 2352723 of the Russian Fed. «Method of adjustment of the vertical position of buildings and structures on plate foundations» by Nuzhdin LV, Nuzhdin ML, bulletin 11, 2009.

## **GEOTECHNICAL CHARACTERISTICS OF SYNTHETIC MUNICIPAL SOLID WASTE FOR EFFECTIVE LANDFILL DESIGN**

Oluwapelumi O. Ojuri<sup>1</sup>. and Peter K. Adegoke<sup>1</sup>

<sup>1</sup>Department of Civil and Environmental Engineering, Federal University of Technology, Akure, Nigeria

### **ABSTRACT**

Geotechnical characteristics of Solid Waste are crucial for effective landfill design and operation, including stability issues and integrity of lining components and sub-grade. This paper presents the results of laboratory investigation performed to determine the geotechnical characteristics of Synthetic Municipal Solid Waste (SMSW); simulating typical composition of municipal solid waste (MSW) generated in Akure metropolis, South-western Nigeria. Geotechnical tests performed include; basic index property tests, strength/compressibility test and the hydraulic conductivity test.

The two compactive efforts used are the modified AASHTO [American Association of State Highway and transportation Officials] and four times (4X) modified AASHTO to simulate higher compactive effort needed for field compaction of MSW. It was generally observed that the unit weight, specific gravity and shear strength of the SMSW increased with increase in compactive effort. Direct shear tests gave cohesion value of 7.6kN/m<sup>3</sup> for both modified AASHTO and 4X modified AASHTO compaction methods, while angle of shearing resistance for modified AASHTO compaction method was 42.4°, and 48.5° for 4X modified AASHTO compaction. In design of landfills the least shear strength failure envelope should be used for effective design. The hydraulic conductivity for both compactive efforts were within the same order of magnitude indicating that the modified AASHTO compaction was a good approximation of field compaction for the municipal solid wastes. Compressibility test on SMSW gave compression ratio of 0.20 with total compression of 33.0% under maximum load of 224kN/m<sup>2</sup>. This complies with the results reported in literature. Compression index ( $c_c$ ) was 0.4, initial compression ratio ( $r_0$ ) was 0.19, primary compression ratio ( $r_p$ ) was 0.71 and secondary compression ratio ( $r_s$ ) was 0.10. These provide the necessary information needed for the computation of expected settlement in the landfill.

*Keywords: Synthetic municipal solid waste, Geotechnical characteristics, Shear strength, Hydraulic conductivity, Compactive effort.*

### **INTRODUCTION**

Municipal solid wastes (MSW) as waste materials typically consist of food wastes, garden wastes, paper products, plastic, textiles, woods, metal, construction demolition wastes and soil. However, the composition of MSW varies from region to region and it depends upon lifestyle, demographic features and legislation [1]. The disposal of municipal solid waste (MSW) in the world is a problem that continues to grow with the growth of population and the development of nations. Since the beginning of the time people have needed to find a way of disposing their refuse, as far back as 18<sup>th</sup> century in England and France, Carters were paid by individuals to carry refuse and discard it in the outskirts of cities. Disposal of waste in open pit became a routine and Benjamin Franklin initiated the first municipal cleaning program in Philadelphia in 1757 [2].

The methods of waste disposal have continued to change with development and advancement of industrialized nations. In recent time wastes are not simply dumped into an open pit, due to health hazard posed by them and adverse environmental impact; hence, modern methods of disposing MSW were generally adopted. Sanitary landfill is the most common method of MSW disposal and probably accounts for 54% of United States MSW disposal, though it has been proven to be responsible for contamination of portable water in certain areas [3]. It is the most cost effective method of waste disposal adopted by most nations of the world compared to other waste management techniques, such as incineration and composting. Although, waste management authorities advocate recycling and reuse of waste material, many countries worldwide prefer land filling of MSW as an economic option [1]. However, in Nigeria the

most populous black nation in the world, sanitary landfill design and construction is not yet embraced as expected. This modern form of waste management technique should be considered in view of the deleterious environmental effects of open waste dumping on the geo-environment especially the surface water and underground water resources. It must be stressed that open dumping is still prevalent in most parts of Nigeria with the concomitant health consequences of this poor environmental management technique.

Integrity, sustainability and potential for future land reclamation of closed landfills depend upon the geotechnical characteristics of MSW stemming from the engineering properties of its constituents/elements. Though the failure of sanitary landfill may not be rampant, it does occur in different parts of the world. Modes of failure associated with; landfill sub-grade, waste and lining system was reported by [4]. Table I shows the engineering properties of MSW required for effective design of sanitary landfill.

Table I Engineering properties of MSW required for design [4]

Design case	Unit weight	Vertical compressibility	Shear strength	Horizontal in-situ stress	Hydraulic conductivity
Sub-grade stability	X		X	X	
Sub-grade integrity	X		X	X	
Waste slope stability	X	X	X		X
Shallow slope linear stability	X		X	X	X
Shallow slope linear integrity	X	X	X	X	
Steep slope linear stability	X		X	X	X
Steep slope linear integrity	X	X	X	X	
Cover system integrity	X	X	X		
Drainage system integrity	X			X	
Leachate/gas well integrity	X	X	X	X	X

## MATERIALS AND METHODS

### Study area

MSW generated within Akure was selected for this study. Akure is a growing urban area within latitudes 7° 10'N and 7° 20'N and between longitudes 5° 07'E and 5° 17'E in Ondo State, Nigeria. The mean annual temperature ranges between 24°C -27°C, while the annual rainfall, varies between 1500mm and 3500mm.

### Municipal Solid Wastes Composition

MSW sampled from various parts of Akure contain approximately the following components

by weight: 10% paper and cardboard, 54.0% food and other putrescible materials, 12.5% plastic, nylon and rubber, 4.3% metal and aluminium, 2.0% glass, 6.0% wood, 5.2% textiles and leather and 6.0% of soil like waste. Some previous studies have used synthetic municipal solid wastes (SMSW) to investigate the engineering properties of MSW [1], [5], [6] and [7]. Various components were further grouped into biodegradable and non biodegradable components according to [8]. These components were used for preparation of SMSW used in this study. The maximum aggregate size of the components was limited to 15mm to facilitate the use of conventional geotechnical testing equipments. Table II shows the SMSW composition used for this study.

Table II SMSW composition of Akure metropolis

Compositions	%	Material used
Non biodegradable	30	Gravelly lateritic soil
Biodegradable		
Garden waste	20	Grass clipping
Vegetable waste	15	Green leaves
Cellulose non paper	14	White bread
Paper waste	16	Shredded paper
Meat	5	Ground pork meat

## **Methodology**

Various tests carried out on SMSW samples are; moisture content, specific gravity, particle size distribution, compaction, compressibility and shear strength.

### *Moisture content*

The moisture content of SMSW was determined according to Part 2:3 of [9]. The SMSW was oven dried with the oven temperature being maintained at 60<sup>0</sup> c to avoid combustion of volatile material.

### *Specific gravity*

The specific gravity of prepared SMSW was determined according to Part 2:8 of [9]. The specific gravity test was carried out on both fresh and dis-aggregated compacted SMSW to investigate their variation as reported by [10].

### *Particle size distribution*

The grain size distribution of SMSW was determined using BS standard, according to Part 2:9 of [9]. The test was carried out on wet basis. The materials was washed using sieve no 200 (0.075mm), oven dried and sieved using BS set of sieves. After vigorous shaking for 10 minutes the material was allowed to settle down for 2 minutes and the weight of material retained on each sieve was recorded against it, and the percentage finer was determined. The sieve size was plotted against the percentage passing, on semi logarithm scale.

### *Compaction test*

Compaction tests were conducted on prepared SMSW samples. The tests were conducted according to Part 4:3 of [9]. The two compactive efforts used are the modified AASHTO and four times (4X) modified AASHTO to simulate higher compactive effort needed for field compaction of MSW while still maintaining the framework of a standard test method as reported by [10]. Factors affecting compaction were investigated during the tests. The method used in addition of water is non pre-wetted method (NPW), where only the first water added to the loose sample of SMSW was allowed to hydrate it for 18 hours. Subsequent water added, for higher target moisture content was compacted immediately, without further hydration time.

### *Compressibility Test*

Compressibility test was conducted on prepared SMSW samples with bulk unit weight of 8.2kN/m<sup>3</sup>

and moisture content of 50.3% in accordance with Part 5:3 of [9]. The oedometer used in this study was floating ring type with a circular brass ring of 60mm diameter and 20mm thickness, the specimen was compacted into the brass ring with porous stone at the top and bottom of the sample; compaction was done to get the initial bulk unit weight of the sample and the specimen was subjected to vertical load ranging from 0.01kN-0.64kN. Loading was done at 24 hours interval.

### *Direct shear test*

The shear strength parameter of prepared SMSW was determined by conducting direct shear tests on specimens from each SMSW unit weight variation. The test was conducted in accordance with Part 7:5 of [9]. Shear box used in this research was square type. SMSW was compacted into shear box having 60mm lengths and 20mm height. SMSW specimens were tested under different normal stress conditions. Initial wet unit weights are 8.2kN/m<sup>3</sup> and 11.1kN/m<sup>3</sup>; with moisture contents of 50.3% and 35% respectively from compaction result. Porous stones were place on the top and bottom of the sample content; vertical stress was applied to the sample and then sheared at a constant strain rate of 0.5mm/min.

### *Hydraulic conductivity*

Hydraulic conductivity test was conducted on two sets of prepared SMSW samples with three samples from each set, based on the two unit weight variation from compaction tests. The test was conducted in accordance with BS 1377 Part 5:5 of [9]. The initial bulk/wet unit weights of the samples were arrived at by compaction of the SMSW samples in permeameter cell with tamping rod.

## **RESULTS AND DISCUSSION**

### **SMSW Moisture Content**

The average value of moisture content taken from SMSW was found to be 31.5%, this fall within the range (25%-70%) reported in literature [1], [3], and [11]. However, the oven temperature was maintained at 60<sup>0</sup>c during oven drying to avoid combustion of volatile materials. Moisture content of waste depends on waste composition, climatic condition of the area, amount of organic content present in the waste and rate of decomposition. Therefore, higher moisture content is expected from older waste than for fresh waste; especially during decomposition process.

### SMSW Specific Gravity

The specific gravity of SMSW determined ranged between 1.39 and 1.53. These comply with the range of values reported in published paper for fresh waste [10]. However It is noteworthy to know that, the value of specific gravity is a function of compactive effort, the percentage of soil like material present in MSW and degree of decomposition of the waste; hence the higher boundary of the range would be expected for waste subjected to higher compactive effort, with higher percentage of soil like material or waste which decomposition process have commenced.

### SMSW Particle Size Distribution

The result of particles size distribution of SMSW shows that, approximately 30% of the sample was retained on 10mm sieve and remaining constituents are of sizes less than 10mm diameter. In addition to that, some of the materials used in generating synthetic waste are two dimensional; their sizes will not adversely affect the test results due to their relatively small thickness. Hence, SMSW used in this research would not over influence the results obtained using conventional equipment from soil mechanics laboratory. Figure 1 shows the graph of SMSW particles size distribution.

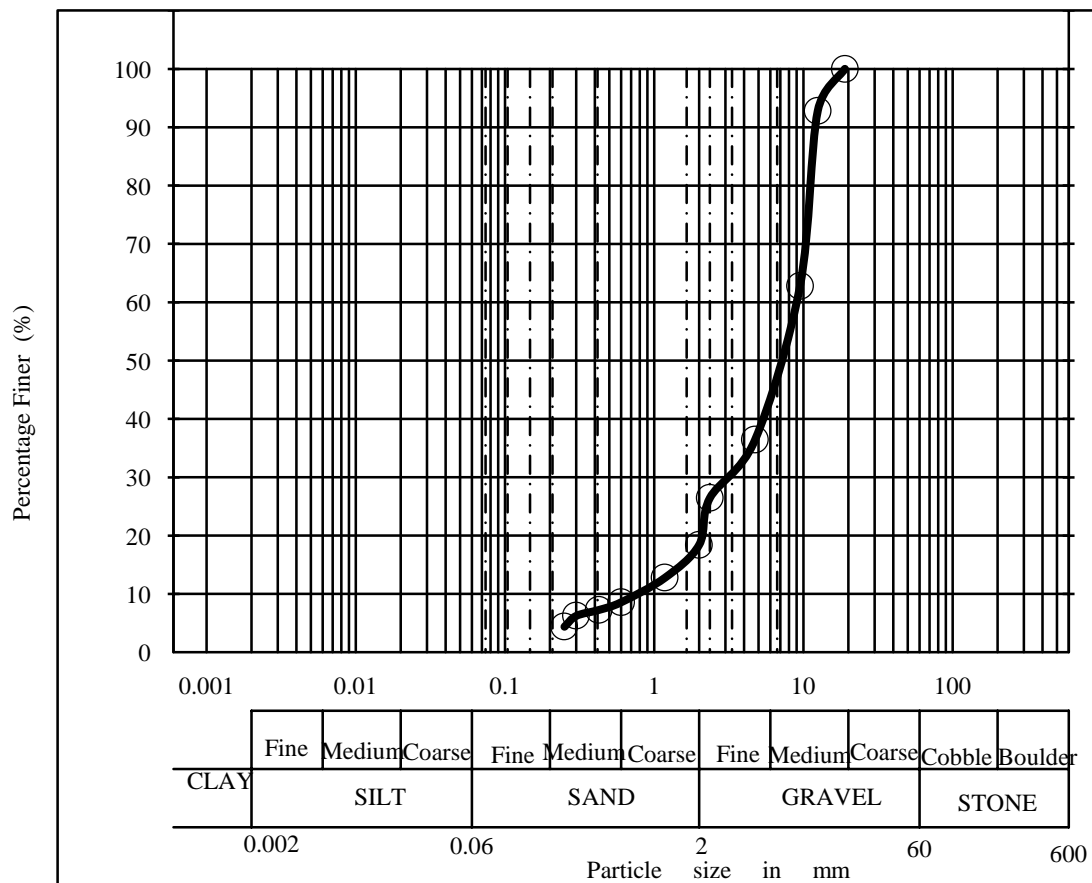


Fig. 1 SMSW particle size distribution curve

### SMSW Compaction

The maximum dry unit weight for modified AASHTO was 8.1kN/m<sup>3</sup>, while that of 4X modified

AASHTO was 10.9kN/m<sup>3</sup>; optimum moisture content for modified AASHTO and 4X modified



AASHTO were 50.3% and 35% respectively. These values fall within the range of values reported in

literature [10]. The curves for both methods are presented in Fig. 2.

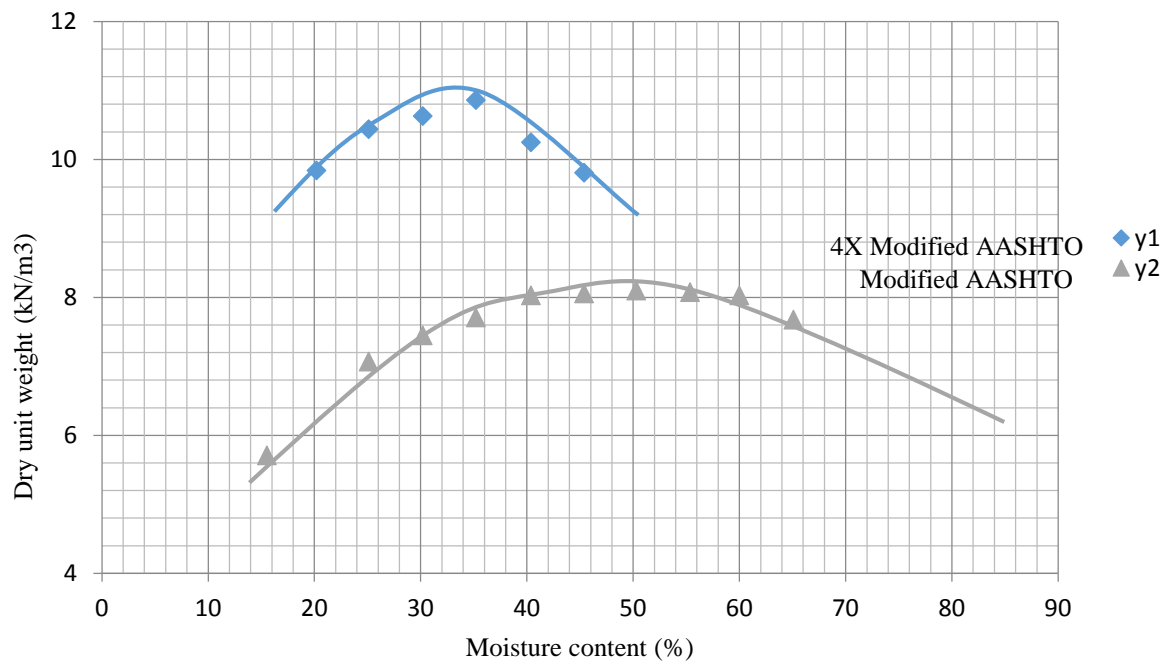


Fig. 2 SMSW compaction curve

The general shape of the compaction curves obtained for SMSW in the laboratory was consistent with the shape of compaction curves commonly obtained for soils. Dry unit weights increased with moisture content to a maximum value and then decreased with further increases in moisture content. Similar to soils, the additional solids content per unit volume was attributed to the lubrication of the particles from water addition, resulting in a denser packing arrangement. The water addition also produced a softening of the solid materials in wastes, increasing compressibility and decreasing rebound (significant for wastes) in response to compaction forces. The effectiveness of the moisture addition diminished at wet of optimum conditions as indicated by the decreasing dry unit weight ( $\gamma_d$ ) due to the replacement of solids with water. In general, the relative locations of the compaction curves for low and high effort were similar to those for soils. However, the decrease in dry unit weight at high moisture content for wastes

is not as prominent as that of soils because, the relative difference between unit weight of water and unit weight of solids is lower for wastes than for soils.

### SMSW Compressibility

Compressibility test on SMSW resulted in compression ratio of 0.20 with total compression of 33.0% under maximum load of 224kN/m<sup>2</sup>. This complies with the result reported in literature for fresh SMSW [1], [3], [5], and [7]. Compression index ( $C_c$ ) was 0.4, initial compression ratio ( $r_0$ ) was 0.19, primary compression ratio ( $r_p$ ) was 0.71 and secondary compression ratio ( $r_s$ ) was 0.10. These provide the necessary information needed for the computation of expected settlement in the landfill. However the effect of degradation due to decomposition of waste should be properly investigated as it may influence the amount of ultimate settlement.

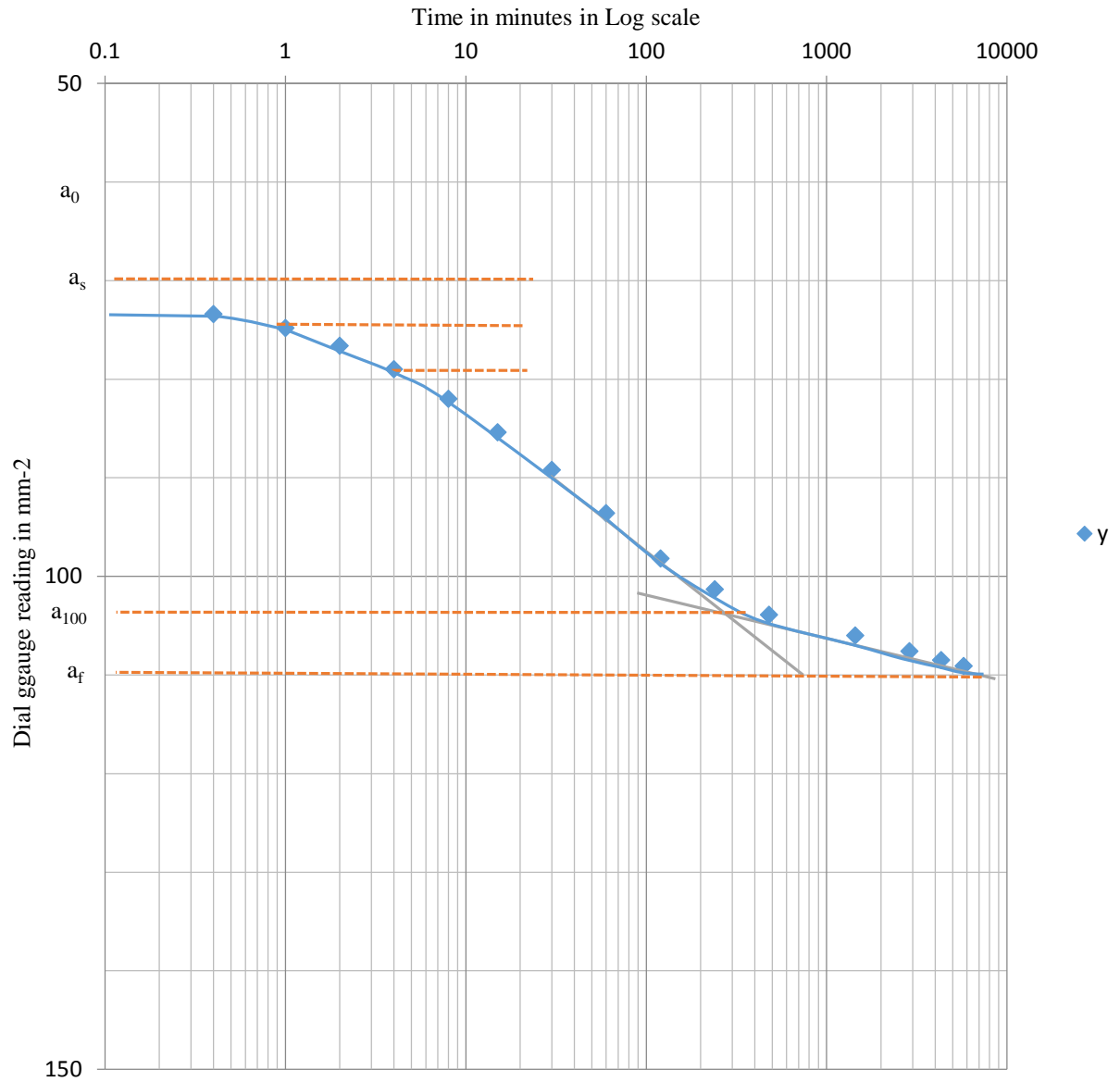


Fig. 3 SMSW Compression curve using Cassagrande's method

The initial compression ratio was calculated according to the following equations by [12].

$$r_o = \frac{a_o - a_s}{a_o - a_f} \quad (1)$$

Where  $r_o$  is the initial compression ratio;  $a_o$  is the start of compression process;  $a_s$  is the start of consolidation process and  $a_f$  is the limit of secondary consolidation process. The primary compression ratio can be expressed according to Eq. (2) shows below.

$$r_p = \frac{a_s - a_{100}}{a_o - a_f} \quad (2)$$

Also,  $r_p$  is the primary compression ratio;  $a_o$ ,  $a_s$  and  $a_f$  are as defined in Eq. (1) while  $a_{100}$  is the limit of primary consolidation process. Equation (3) represents the expression for secondary compression ( $r_s$ ), while  $r_o$  and  $r_p$  are as in Eq. (1) and Eq. (2).

$$r_s = 1 - (r_o + r_p) \quad (3)$$

#### Shear Strength

Direct shear tests resulted in cohesion of 7.6kN/m<sup>3</sup> for both modified AASHTO and 4X modified AASHTO compaction methods, while frictional angle for modified AASHTO compaction method

was  $42.4^\circ$ , and frictional angle for 4X modified AASHTO compaction method was  $48.5^\circ$  as indicated in Figure 4. The shear strength failure envelope for the two compaction variation is shown in Figure 4. Cohesion is within the range of results reported in literature for fresh wastes, however the angle of internal friction for sample compacted using 4X modified AASHTO (i.e. with  $11.1\text{kN/m}^3$  wet unit weight) was found to be slightly above the range reported in literature [13], [14], and [15]. This may be as a result of higher proportion of reinforcing component. Thus, in design of landfill the least shear strength failure envelope should be

considered for effective design. The shear stress versus shear displacement plots for the two variants of compactive efforts hence degree of densification (indicated by bulk unit weight  $[\gamma_b]$ ) for three normal stresses  $13.9\text{kN/m}^2$ ,  $27.8\text{kN/m}^2$  and  $41.7\text{kN/m}^2$  used for the direct shear test are presented in Figure 5. Shear stress versus horizontal displacement graph indicates a general bilinear plot for all normal stress values within the elastic zone. Plastic softening occurs close to the critical shear value, and the slope of shear stress versus horizontal displacement tends to flatten in the plastic zone.

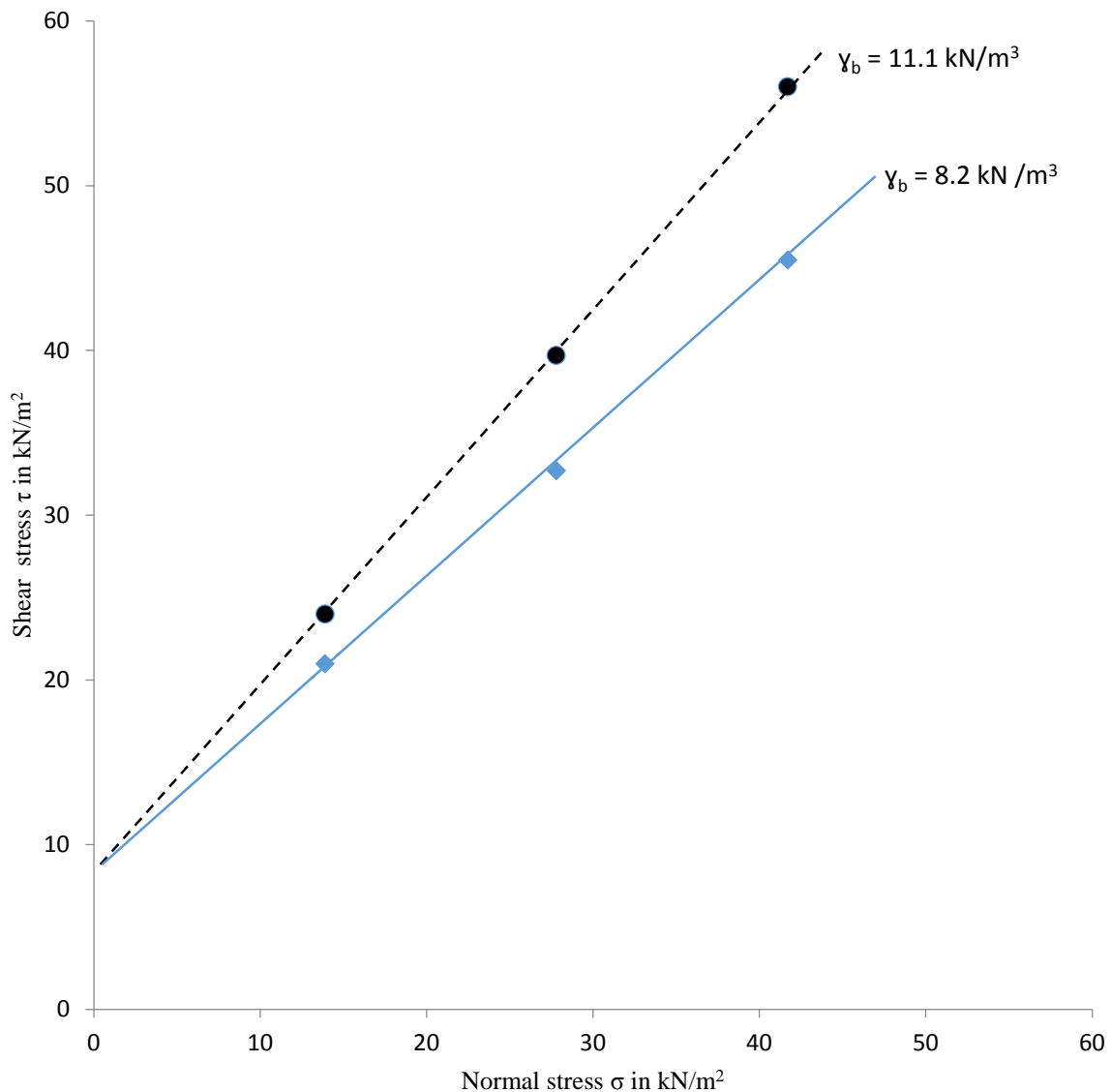


Fig. 4 SMSW shear strength failure envelope

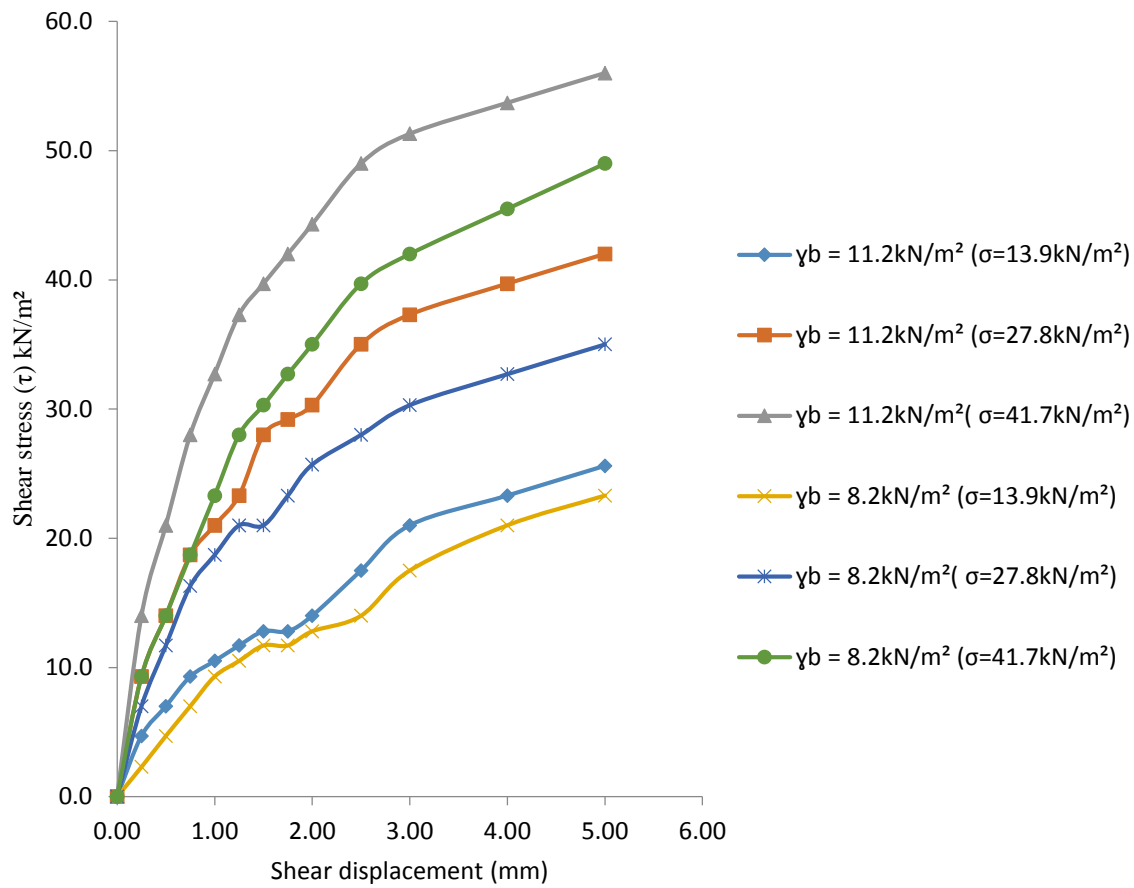


Fig. 5 SMSW shear stress curves

### Hydraulic Conductivity

Municipal Solid Waste hydraulic conductivity is important to landfill designers because of the influence it has on Leachate pressure distributions in the waste body and hence on the magnitude and distribution of effective stresses and, therefore, on shear strength [16]. Since shear strength is inversely proportional to compressibility/compression, the combined effect of hydraulic conductivity and compression is simulated by the SMSW.

Average hydraulic conductivity value in this research was  $2.16 \times 10^{-6} \text{ m/s}$  for samples with wet unit weight of  $11.1 \text{ kN/m}^3$  and,  $2.04 \times 10^{-6} \text{ m/s}$  for samples with wet unit weight of  $8.2 \text{ kN/m}^3$ . This shows that hydraulic conductivity values are relatively high, also only minimal variation in hydraulic conductivity was observed due to density change of the samples. Hydraulic conductivity of gravelly lateritic soil used to represent non biodegradable component of SMSW may be the reason for this behaviour. However, the results were within the range of hydraulic conductivity values as reported by [3], [17], [18] and [19]. A comprehensive report on waste hydraulic conductivity was given by [20].

### CONCLUSION

This article presents the geotechnical characteristics of SMSW of Akure metropolis South-western Nigeria. The wide spread of indiscriminate dumping of MSW all over Akure metropolis has lead to environmental degradation and poses a great threat to public health. In finding a permanent solution to this menace, proper waste management technique is needed, hence the need for construction of a sanitary landfill. In construction of a stable sanitary landfill three most important factors are considered, the stability of the lining system, the stability of sub-grade and the stability of the waste materials itself. The strength characteristics of SMSW simulating typical composition of MSW generated in Akure metropolis was determined in this work.

Knowledge of unit weight of MSW is required for all aspects of landfill design as reported in the literature. Initially the unit weight of waste is dependent on waste composition, the daily cover and the degree of compaction during placement. Mechanisms resulting in settlement of waste include physical compression and creep, raveling, and decomposition due to biodegradation of

organic components. For simplicity, the total settlement of a landfill can be taken as the combination of initial, primary and secondary compression. Initial compression includes reduction in voids due to removal of air. Primary compression includes the physical compression of components and consolidation. Secondary compression includes all creep effects and those relating to degradation. Knowledge of shear strength is required in order to assess the waste slope stability. Laboratory methods have been used widely but results from such studies should be interpreted carefully due to their association with disturbed samples. Out of the methods available, the direct shear box used in this work has been adjudged to produce the most reliable information. From the results of various test carried out on the SMSW the following conclusions could be drawn.

- 1) The unit weight of SMSW increased by 35% with 300% increase in compactive effort and specific gravity increased with 14%.
- 2) Shear strength of SMSW increases with increased unit weight (as a result of compaction), due to densification of the solids and increase in cohesion of wastes materials.
- 3) Compressibility of SMSW material is high; hence the expected settlement would be high.
- 4) Only minimal variation in hydraulic conductivity was observed due to density change of the samples.

## ACKNOWLEDGEMENT

The authors would like to acknowledge the contribution of Azeez, Gafar Adetunji in data collection for this work. The equipment used for this research was made available by the Department of Civil and Environmental Engineering, Federal University of Technology, Akure, Ondo State, Nigeria.

## REFERENCES

- [1] Reddy KR, Gangathulasi J, Parakalla NS, Hettiarachchi H, Bogner JE, and Lagier T, "Compressibility and shear strength of municipal solid waste under short-term leachate recirculation operations", *Waste Manage. Res.* Vol. 27, 2009, pp. 578–587.
- [2] Adebayo FA, "Basic elements of water supply and waste management", Supreme Printing Press, 2005, pp. 109–111.
- [3] Reddy KR, Hettiarachchi H, Parakalla NS, Gangathulasi J, and Bogner JE, "Geotechnical properties of fresh municipal solid waste at Orchard Hill Landfill", *Waste Management Journal*, In Print, 2008.
- [4] Dixon N, Ng'ambi S, and Jones DRV, "Structural performance of a steep slope landfill lining system", *Proceedings of the Institution of Civil Engineers Geotechnical Engineering* Vol. 157, 2004, pp. 115–125.
- [5] Dixon N, Langer U, and Gotteland P, "Classification and mechanical behaviour relationships for municipal solid waste; study using synthetic waste", *Journal Geotechnical Geo environmental Engineering*; ASCE, Vol. 134, 2008, pp. 79–90.
- [6] Hettiarachchi CH, "Mechanics of biocell landfill settlement", Dissertation, Doctor of Philosophy, Department of Civil and Environmental Engineering, New Jersey Institute of Technology, USA.
- [7] Langer U, "Shear and compression behaviour of undegraded municipal solid waste", Dissertation, Doctor of Philosophy, Loughbrough University, 2005.
- [8] US.EPA, "Municipal solid waste generation, recycling, and disposal in the United States: Facts and figures for 2006", <http://www.epa.gov/osw/nonhaz/municipal/pubs/msw06.pdf>, April 20, 2008.
- [9] BS (British Standard), "British Standard Institution, Methods of Test for Soils for Civil Engineering Purposes, Second Edition", Chiswick High Road, London W4 4AL, 1990.
- [10] James LH, Nazli Y, Shawna AVS, and Wilson WW, "Compaction characteristics of municipal solid waste", *Journal of Geotechnical and Geoenvironmental Engineering*; ASCE, Vol.136, 2010, pp. 1095–1102.
- [11] Landva A, Clark JI, "Geotechnics of waste fills: geotechnics of waste fills theory and practice", *ASTM STP* Vol. 1070, 1990, pp. 86–106.
- [12] Garg SK., "Soil Mechanics and Foundation Engineering", Khanna Publishers, 4575/15, Onkar House, Opp. Happy School Daryaganj, New Delhi, 2009, pp. 224–263.
- [13] Jones DRV, Taylor DP, Dixon N, "Shear strength of waste and its use in landfill stability analysis", *Proceedings Geoenvironmental Engineering Conference*. Thomas Telford, 1997, pp. 343–350.
- [14] Kavazanjian E, 2001, "Mechanical properties of municipal solid waste", *Proceedings Sardinia, Eighth International Waste Management and Landfill Symposium*, Cagliari, Italy, Vol. 3, pp.415–424.
- [15] Manassero M, Van Impe WF, Bouazza A, "Waste disposal and containment", *Proceedings Second International Congress on Environmental Geotechnics*, Osaka, Vol. 3, 1996, pp.193–242.
- [16] Jones DRV, Dixon N, "Landfill lining stability and integrity: the role of waste settlement",

Geotextiles & Geomembranes Vol. 23, 2005, pp. 27–53.

[17] Landva AO, Pelkey SG, and Valsangkar AJ, “Coefficient of permeability of municipal refuse”, Proc. of The Third International Congress on Environmental Geotechnics, Lisboa, Portugal, Vol. 1, 1998, pp. 63-67.

[18] Chen T, and Chynoweth DP, “Hydraulic conductivity of compacted municipal solid waste”, Bioresour. Technol. Vol. 51, 1995, pp. 205-212.

[19] Jain P, Powell J, Townsend TG, and Reinhart DR, “Estimating the hydraulic conductivity of landfilled municipal solid waste using borehole permeameter test”, Journal of environmental engineering, ASCE, Vol.132, 2006, pp. 645- 653.

[20] Powrie W, Beaven RP, “Hydraulic properties of household waste and implications for landfills”, Institution of Civil Engineers Geotechnical Engineering Journal, Vol. 137, 1999, 235–247.



## INNOVATIVE GROUNDWATER TABLE MONITORING USING TDR TECHNOLOGY

Vlastimil Chebeň<sup>1</sup>, Marian Drusa<sup>2</sup> and Michal Kuba<sup>3</sup>

<sup>1,2</sup>Faculty of Civil Engineering, University of Žilina, Slovakia; <sup>3</sup>Faculty of Electrical Engineering, University of Žilina, Slovakia

### ABSTRACT

This paper introduces an innovative and economically convenient measurement system that is based on a novelty method of installation, operation and remote control technology for ground watertable measurement. The technology is based on TDR (Time Domain Reflectometry) that employ a unique hollow coaxial cable. Installation is performed by CPT/DP penetration testing equipment, that in its nature, is relatively light, versatile, operative, and is not demanding of manpower or machinery. This method brings benefit to currently unreachable sites ex. steep slopes, places with little or no road access, option for setting up additional probes on existing structures etc., as the method doesn't require conventionally truck-mounted drilling rigs. Electronic origin of measurement offer the possibility of probe networking, remote sensing, automatic data acquisition and evaluation through developed software. Proposed measurement system has been laboratory tested, calibrated and installed on various sites over past 6 years in Slovak republic.

*Keywords: TDR, Groundwater Level Measurement, Coaxial Cable, Penetration Testing*

### INTRODUCTION

Slope instability has been an issue worthy of concern in applied soil mechanics engineering for decades. It causes serious losses to both private and public sectors all over the globe and has been studied throughout history by many researchers, scholars, academics, and practitioners from different perspectives. Unfortunately, landslides with severe consequences regularly occur in potentially unstable areas, which are not covered by a soil monitoring system due to lack of funding or priority. There are several factors which initiate soil movement, but the principal trigger mechanism is the presence of water, generally formed in ground water level - phreatic or pressure combined with geological, geomorphological and climate conditions in certain time and locality. Over past 10 years, demand for automatic and remote sensing monitoring systems for collecting required geotechnical data, mostly soil deformation and water level, initiated competition between electric based techniques. TDR technology (Time Domain Reflectometry) is a technology that has been employed for a variety of uses in electrical engineering. Since the 1930's, TDR has been used for examining electrical properties of cables and transmission lines, and measuring electrical properties of organic liquids. Universality and further enhancement of the technology during the 1990 is led to monitoring of landslide slope movements, soil electrical conductivity or water content measurement in soil [3]. TDR uses principle of radar, where an electric voltage pulse is reflected from point where inconsistency of electrical

properties occurs, e.g. a damaged cable, change in dielectric constant of environment and is sent back. Signal travel time, hence time domain, and known propagation velocity determine localization of signal reflection. The development of a new type of TDR probe for measuring groundwater level was started in order to meet requirements for reliable, low cost, remote sensing capable and possibility of installation in vehicle inaccessible areas. Proposed groundwater level sensing is based on air-filled coaxial cable resembled to an open pipe piezometer. Measurements of water level are determined by travel time analysis of the reflected signal from air-water interface, hence TDR piezometer. Laboratory testing and calibration as well as field installation experiments and actual field data are presented.

### LANDSLIDES IN SLOVAKIA

The role of monitoring of negative factors of slope deformation is a highly demanded in Slovakia. Altogether, more than 5.25 % coverage of land is endangered by slope deformations, furthermore about 98 km of motorways and 67 km of railway lines pass through landslides. The most known landslides occurred in Handlova in 1953, Riecnica in 1961 and in Velka Causa, Kapusany, Nizna Mysla in 2010. The most often trigger factor of slope deformations in Slovakia is effect of underground water combined with geological, geomorphological and climate conditions. According to statistics of national geological institute of Dionyz Stur, localization of slope deformation is mostly in zones

of Carpathian flysch belt, then Neovolcanic, West Carpathians and Central Carpathian Paleogene zone. The reason to implement TDR technology for deformation and groundwater monitoring in Slovakia was to find an attractive alternative to other water level measurement systems that would benefit in rapid and relatively easy installation, cost efficiency and suitability for remote sensing. Research and design of piezometer for phreatic water table based on TDR started in 2008 and later installed on three localities in Northern Slovakia – Dolná Tizina, Povazská Bystrica, and Brusno-Chrenovec. First two of them are presented in the article.

### TDR LABORATORY TESTING

In the period of 2008-2010 laboratory testing of new type piezometer for phreatic water table measurement based on TDR principle was carried out. Sensing probe was formed by a waveguide – hollow coaxial cable where dielectric is an air. This construction format allow water freely penetrate the cable according to principle of communicating vessels where water balances out to the same level as it settles. Determination of water level is principally trivial while air is replaced by water that has different dielectric constant Eq. (1) which results in signal reflection at exact point.

$$\varepsilon_w = K_w \cdot \varepsilon_0 \quad (1)$$

Testing scheme plotted on Figure 1 consisted of a tube representing a borehole, measuring waveguide - hollow coaxial cable and TDR unit. Two types of sensing waveguides with 50  $\Omega$  impedance were tested Heliflex HCA 58-50 with 5/8" and HCA 12-50 with 1/2" diameter. Water level was increased and decreased in many cycles while taking measurement by TDR and controlled and compared with measuring tape.

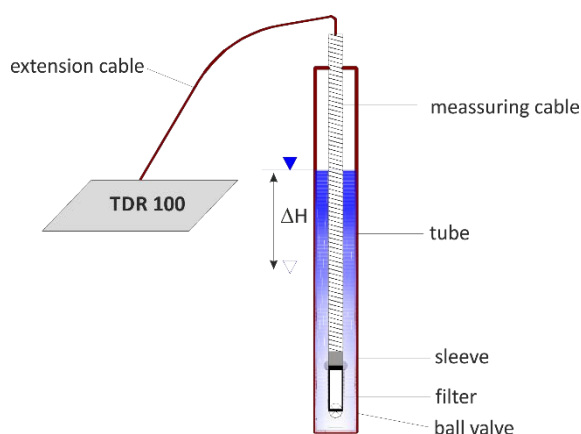


Fig. 1 Laboratory testing scheme

Acquired data were sorted, compared and analyzed. As in radar, TDR utilizes the roundtrip travel time in the air section to determine the water level, proper data reduction method of travel time determination and calibration of pulse propagation velocity was needed. The precise time of reflection that corresponded the position of the interface-required calibration, due to different velocity of propagation in lead and sensing cable. Waveguide with 5/8" diameter was feasible due to larger inner space where water can freely pass through.

### FIELD INSTALLATION AND TESTING

In 2010 and 2011 TDR piezometer probes were installed on three test sites in northern and western Slovakia, situated on slopes that are inaccessible to trucks. These sites were selected intentionally to confirm feasibility of installation using penetration test equipment.

#### Installation method

Installation of TDR piezometers were to small diameter holes of  $\varnothing$  35 - 40 mm carried out by static CPT or dynamic penetration equipment. Detail of special adaptor needed for installation to certain depth is shown on Fig. 2.

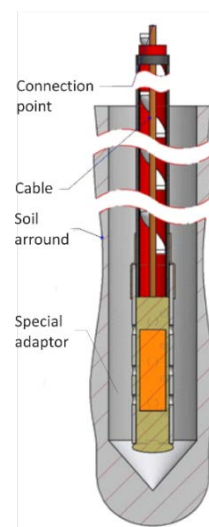


Fig. 2 Detail of installation using penetration equipment

Principally, determination of TDR ground water level is similar to standpipe piezometer which is based upon equilibration of standpipe water pressure with that at the measurement point and pore pressure is calculated in Eq.(2):

$$\Delta u = \Delta h \cdot \gamma_w \quad (2)$$

*Test site Povazska Bystrica*

Test site is located near town Povazska Bystrica in Northern Slovakia, where new bypass road was built in cut off of the hill in difficult geological conditions that was affected by landslides. Area belongs to the territory of hill called St. Helena, which ranks to orographic northwestern nesses of Strazovske Mountains. The relief in the studied area reflected the obvious connection between the resistance of rocks against weathering processes and morphology of the terrain. Orlovské layers make the top of the area of interest and are represented predominantly by sandstone containing thin marls or marlites inserts. Soft shape of lower part of the area is made up with sphaeroiderit layers with low resistance against weathering processes resulting in eluvial-deluvial deposits of clayey sediments that are susceptible to sliding.

Geotechnical monitoring of slope deformations was performed on the site mainly by inclinometers, and 3D inclinometers. Water pressure in layers important for stability calculations was measured by open pipe piezometers in certain depth level. There

were two or more significant water level horizons. In badly accessible places (I8, I8-P) TDR inclinometer and TDR piezometer were installed.

TDR piezometer I8-P was installed in the bore made by DP equipment. Sensing waveguide had length 7.9 m capturing the first water level horizon. Before embedding the waveguide, calibration measurement had to be performed with no water. Figure 3 shows two measurements of ground water level, the first one as of April 2010 and the most recent from June 2014. It is obvious that sensing waveguide is still in good condition and doesn't suffer any damage or deterioration of key parameters. As seen on the figure, apparent waveguide length is 8.6 m and has to be adjusted by signal velocity propagation  $v_p = 0.92$ . This is due to different propagation velocity in lead coaxial cable and sensing waveguide. Therefore, while taking measurements, the parameter  $v_p$  is set to 1.0. Last taken data say that groundwater was in 3.68 m depth. It must be noted that 0.6 m section of waveguide sticking out above the ground level should be subtracted.

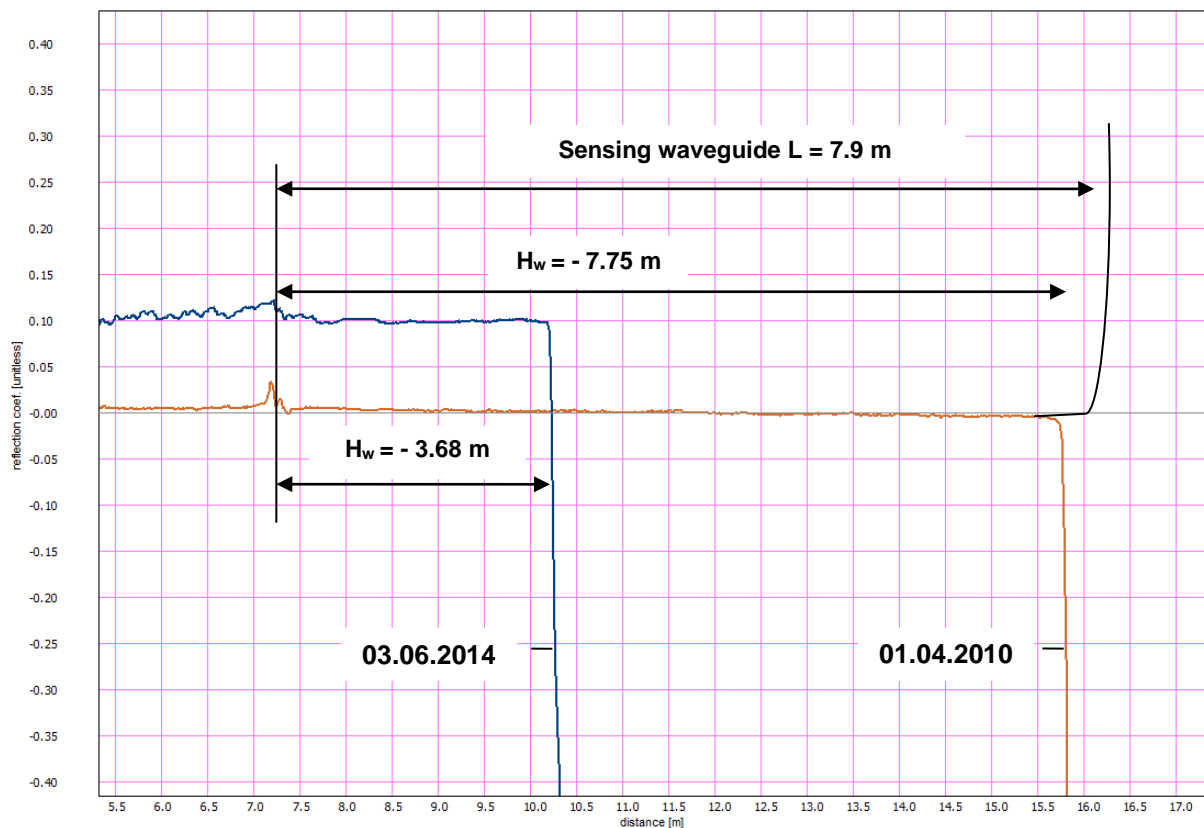


Fig. 3 Measurement of GW level in piezometer I8-P at Povazska Bystrica

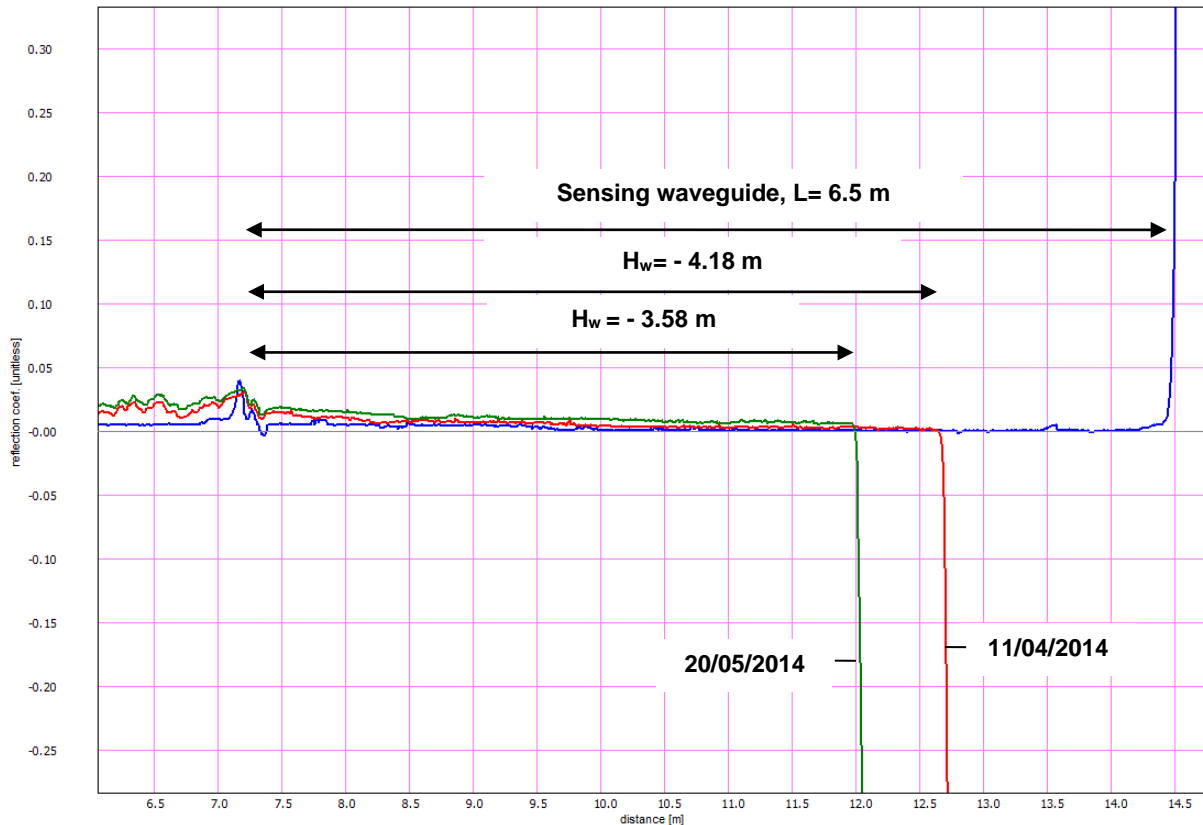


Fig. 4 Measurement of GW level at locality Dolna Tizina

#### Test site Dolna Tizina

Locality of Dolna Tizina is situated in Central Carpathian paleogene. According to the geomorphological division of the territory of the Slovak Republic, considered territory belongs to Fatra-Tatra region of Zilina basin subunit Varinske Podolie. Based on the documented visible external signs, whole area of slope deformation is a part of morphologically significant landslide activity, which has length of about 250 m and width of 130 meters. Within this relatively extensive active area two smaller partial landslides were identified in transportation and accumulation part. The primary cause in the development of landslide activity was erosion of local stream in the bottom part of area of interest.

Buoyancy effects of water and the presence of disturbed shear zones were the main trigger factors of the slope deformation. Ground water level at the time before remediation works reached the accumulation zone level 2 m below the ground surface, while two distinct horizons of GW level were found. Effectiveness of drainage wells, in particular, showed a significant decrease of buoyancy effects in the transportation and accumulation zone of the landslide.

The activity of slope failure started in 1997 due to excessive torrential rainfall when local road and

fencing were damaged. In 2001, the landslide was re-activated when creeping slide mass at accumulation zone endangered adjacent properties. In 2003, re-initiated movements were threat again. Later in 2006, slope failures extended to sides with decrease of terrain in the active zone from 2 to 2.5 m. Soil movement caused structural damages of house no. 358 that remained uninhabitable.

Owing the soil instability, a TDR piezometer was installed in 2010 employing dynamic penetration technique to create a bore. Waveguide calibration preceded its soil embedment. The same process with measured data described in previous section concerning calibration should apply. Figure 4 plots data of ground water level in last 1.5-month span. Relatively rainy end of April 2014 and beginning of May 2014 resulted in rise of groundwater level of 0.55 m.

#### AUTOMATIC DATA EVALUATION USING MEDIAN FILTER

In the next section, principles of automatic ground water level determination are proposed. Since the measurement system consists of cables that are not perfectly homogenous, noise can have notable influence on its performance. While TDR signature is a non-linear signal, the powerful method

has to be employed for waveform examination with respect to recognition of lead cable that can be several hundred meters long and sensing cable, which length is particularly up to 30 m. For automatic data evaluation, perhaps, the most fundamental form of signal manipulation is that of filtering, which describes a rule or procedure for processing a signal with the goal of separating or attenuating a desired component of an observed signal from either noise, interference, or simply from other components of the same signal. It is obvious from the TDR signal, that water level is in the point where sharp transition represented by waveform drop occurs. Localization of this point by numerical methods is a way to automatic water level detection. Therefore, use of running median filter - a nonlinear signal processing method in this application aiming at exploiting the system's nonlinearities or the statistical characteristics of the underlying signals. The running median was first suggested as a nonlinear smoother for time-series data [1].

Regarding definition of the running median filter, a discrete time sequence  $x(n)$  of  $N$  samples in time instants  $n = 0, 1, 2, \dots, N$  must be defined. The running median passes a sliding window of length  $M$  samples over the time sequence  $x(n)$  that selects, at each instant  $n$ , an odd number of  $M$  consecutive samples to comprise the observation vector  $\mathbf{x}(n)$  as Eq.(3):

$$\mathbf{x}(n) = [x(n-M+i)], \quad i=1, 2, \dots, M \quad (3)$$

The median smoother operating on the input sequence  $x(n)$  produces the output sequence  $y(n)$ , defined at time instant  $n$  as Eq.(4):

$$y(n) = \text{Median}\{\mathbf{x}(n)\} \quad (4)$$

Setting the symmetric observation window, operator  $\text{Median}\{\cdot\}$  is then defined as follows Eq.(5):

$$y(n) = \text{Median}\{\mathbf{x}(n)\} = \tilde{x}((M+1)/2) \quad (5)$$

where  $\tilde{x}((M+1)/2)$  is the  $((M+1)/2)$ -th element of the vector  $\tilde{\mathbf{x}}(n)$ . Vector  $\tilde{\mathbf{x}}(n)$  contains the same elements as the vector  $\mathbf{x}(n)$  but the elements in vector  $\tilde{\mathbf{x}}(n)$  are in ascend order of their values.

The reason of applying a running median filter consists in smoothing neighboring extreme values of the signal with no effect on subsequent evaluation.

After the waveform is smoothen using median filter as shown on Fig. 5, signal is processed in decision block and threshold procedure is performed finding discrete time index  $m$ , where signal exceeds pre-set level. It means, that index  $m$  is smallest

positive integer that satisfies condition  $y(m) > \text{threshold}$  or  $y(m) < \text{threshold}$ , meaning the former no water presence in cable, the latter water presence in cable.

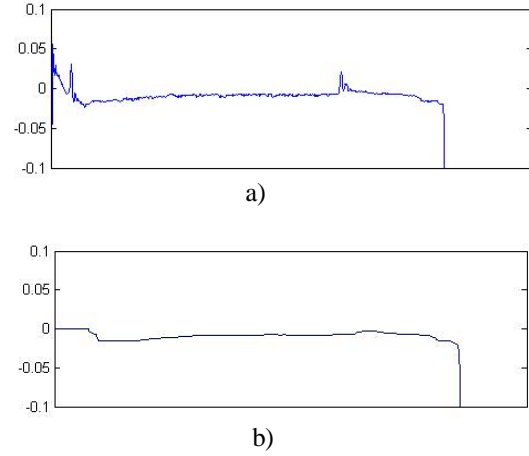


Fig. 5 TDR waveform a) as measured b) after median filtering

Adjusted index  $m$  value corresponds to signal travel time from transmitter to water level and back. Since propagation velocity is known, distance from reference point to water level can be obtained from Eq.6:

$$L_m = \frac{1}{2}(t_2 - t_1)v_L \quad (6)$$

where  $L_m$  is the length of sensing waveguide,  $t_1$  is reflected signal travel time in lead cable,  $t_2$  is reflected signal travel time in measuring waveguide. Hence, value of  $L_m$  is measured water level. Issue of system calibration is not discussed while quality and manufacturing precision of sensing waveguide guaranties its material characteristics.

## CONCLUSION

Despite the fact that air-dielectric TDR piezometer was first proposed by [3] in 1990's, its wide spread hadn't been yet very successful. A new type of TDR probe for groundwater level determination proposed in the paper, comprising of waveguide Heliflex HCA58-50 and Campbell Scientific hardware. We developed software for taking measurements and data processing. First field application was set 4 years back in 2010, when TDR piezometers were installed into a small diameter bore of 30-40 mm, created with equipment for dynamic or static penetration. This technique was proved feasible and viable on condition that skilled and experienced manpower. Recent data from two probes are presented showing that sensing waveguide as a key element, is in good condition

and still work. Assumption of clogging the inner space by fine particles of clay surrounding soil was not confirmed due to special sand filter at the bottom. Even if the clogging was the case, a probe replacement could be possible both physically and economically. The large pulse reflection at the air-water interface allows measurement at considerable distances, therefore when multiplexed one TDR point can cover area of hundreds meters benefitting in hardware cost reduction. New areas can be monitored with no or reduced access roads that suffer from potential of geohazard risk, e.g. steep slopes, dense forests, active landslides.

Electric nature of the technology is perfect not only for remote sensing but for automatic data processing and evaluation. Running median filter is used for smoothen TDR signature reducing noise, interference or reflection in the cable and for revealing water level at exact point where threshold value is exceeded.

Couplings and connectors are probably the weak link in the chain as they are exposed to humid and corrosive environment when installed unprotected.

Next research will head to building remote sensing measuring system with automatic groundwater level detection and improving reliability of the technology.

## ACKNOWLEDGEMENTS

The research is supported by European regional development fund and Slovak state budget by the project "Research centre of University of Zilina", ITMS 26220220183.

## REFERENCES

- [1] Arce R.A., Nonlinear Signal Processing. Hoboken, New Jersey: John Wiley & Sons, 2005
- [2] Chung C. et al., New TDR waveguides and data reduction method for monitoring of stream and drainage stage, *Journal of Hydrology*, Vol.505, 2013, pp. 346-351
- [3] Connor K.M., Dowding C.H., Geomeasurements by Pulsing TDR Cables and Probes, Boca Raton: CRC Press, 1999
- [4] Decký M., Drusa M., Pepucha Ľ., Zgútová K. Earth structures of transport constructions, Harlow, Essex: Pearson, 2013. - 180 s., ISBN 978-1-78399-925-5
- [5] Dowding, C. H., O'Connor, K. M., Geomeasurements by Pulsing TDR Cables and Probes, Boca Raton: CRC Press, 1999. ISBN 08-493-0586-1
- [6] Drusa M., Chebeň V. 2012. Implementation of TDR Technology for Monitoring of Negative Factors of Slope Deformations, *Proceedings of SGEM 2012 Vol. II. ISSN 1314-2704 p.143-150, DOI: 10.5593/sgem2012*
- [7] Drusa M., Chebeň V., Prohovníková P., 2013. Functionality of TDR Piezometers and Inclinometers for Monitoring of Slope Deformations In: *Sgem 2013: 13th international multidisciplinary scientific geoconference: conference proceedings. Vol. II. - Sofia: STEF92 Technology, 2013. - ISBN 978-954-91818-8-3. pp. 157-164.*
- [8] Drusa, M., Chebeň, V., Stolárik, L., Prohovníková, P.: Laboratory calibration of TDR measurements of underground slope deformations. In: *Theoretical foundation of civil engineering: XXII Slovak - Polish - Russian Seminar: Žilina, Slovak Republic, 09.09.2013 - 13.09.2013. Moskva : Izdatel'stvo ASV, 2013. ISBN 978-5-93093-986-6. - S. 437-442.*
- [9] Drusa, M., Chebeň, V. Bulko, R. 2014. New Technologies Implemented In Geotechnical Monitoring on Transport Constructions, In *SGEM 2014 Proceedings, Book 1 Vol.2 pp. 651-656, ISBN 978-619-7105-08-7, DOI: 10.5593/sgem2014B12*
- [10] Marschalko, M., Yilmaz, I., Křístková, V., Fuka, M., Kubečka, K., Bouchal, T.: An indicative method for determination of the most hazardous changes in slopes of the subsidence basins in underground coal mining area in Ostrava (Czech Republic). *Environmental Monitoring and Assessment* 02/2012; DOI:10.1007/s10661-012-2571-7
- [11] Mužík, J.: Analysis of Geotechnical Structures Using Meshless Local Petrov-Galerkin Radial Point Interpolation Method, In *SGEM 2014 Proceedings, Book 1 Vol.2 pp. 651-656, pp. 41-48, ISBN 978-619-7105-08-7, DOI: 10.5593/sgem2014B12*
- [12] Segalini, A, Carini, C.: Underground Landslide Displacement Monitoring: A New MMES Based Device, *Landslide Science and Practice*, vol. 2, 2013, Early Warning, Instrumentation and Monitoring - Margottini, Canuti & Sassa Eds. - Springer London pp. 87-93 - doi: 10.1007/978-3-642-31445-2
- [13] Yilmaz, I., Marschalko, M., Yildirim, M., Dereli, E., Bednarik, M., (2012) Preparation of the GIS based kinematic slope instability and slope mass rating (SMR) maps: an application to a railway route in Sivas (Turkey). *Bulletin of Engineering Geology and the Environment*. DOI: 10.1007/s10064-011-0384-5



## DIFFERENTIAL CAPACITOR SENSOR OF WIRELESS SENSOR NETWORK FOR LANDSLIDE MONITORING

S. M. A. Motakabber<sup>1</sup>, M. I. Ibrahimy<sup>1</sup>, and M. Z. Hossain<sup>2</sup>

<sup>1</sup>Faculty of Engineering, International Islamic University Malaysia, 53100 KL, Malaysia

<sup>2</sup>Graduate School of Bioresources, Mie University, Mie 514-8507, Japan

### ABSTRACT

Every year all over the world, many lives and properties are lost due to many geological catastrophes like, landslide or land-slip. Manual and electronic monitoring systems are used to predict the landslide happening period. The manual monitoring system is laborious and not practicable, then again, most of the electronic systems are complex and expensive. To monitor the natural disasters, a detecting system faces a lot of harder conditions. Natural tragedy occurs unexpectedly and damages the instrument system as well. The sensor system should be planned as a spread network with a simple positional identification device such as RFID. In addition, the network should have self-recovery, self-directed operation and actual data transmission facility in urgent situations. A distributed node network needs lot of sensors with complex structure and it is expensive too. This paper describes a simple and low cost system which comprises an underground pretension cable with a capacitor gage sensor attached at one end. A wireless sensor network has been proposed for a simple landslide monitoring system using RFID. The sensing node network can be operated by initializing mode, measuring mode and urgent mode depending on the situation. A switching mechanism is used to switch automatically to any one of these operating modes which makes a robust and dynamic control of data transmission system. A mathematical model has been developed for the system and verified by simulation. The result shows that an early prediction of the landslide is possible by using the proposed system.

**Keywords:** *Wireless Sensor Network, Landslide, Capacitor Sensor, RFID, Geological Catastrophe*

### INTRODUCTION

It is very hard to forecast an exact time, date and place of incidence of many natural disasters like a landslide. Worldwide, landslides cause about 1,000 deaths per year and property damage of approximately US\$ 4 billion [1]. Therefore, regular inspection and a record maintaining around the hazardous area is essential. If somehow we can catch some symptoms before the worst incidence, the information can help us to report to the residents and it can be useful to predict to operate the monitoring system efficiently. Existing manual solutions are insufficient and sometimes costly to landslide monitoring and prediction. Installing a single sensor for monitoring a wide hilly target area is not sufficient, since most of the cases the property on the hill is changed in about every 10-15 meters distance. Wiring with multiple sensors to a central data logger is also not practicable due to reliability and it requires frequent maintenance. Therefore, wireless sensor networks are used for real-time landslide monitoring system. A basic topology of a wireless sensor network is shown in Fig. 1. In this arrangement all nodes addressed by RFID tag are wirelessly connected to each other and finally these are linked with the local base station (LBS1). Each node has at least one sensor to measure the parameter of the land, such as temperature, land

movement, velocity and acceleration of the landslide of the target area. Practically a large number of nodes are used for landslide monitoring system. For simplicity of the structure, each node addressed by

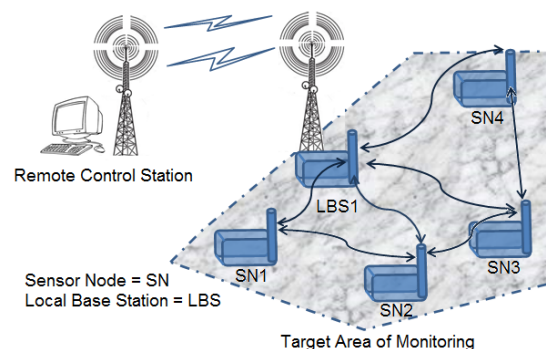


Fig. 1 Basic wireless sensor network for landslide monitoring

RFID tag, has a short distance communication facility (about 100m). It is sufficient to make a network for a large area. However, it is not enough to communicate with a secure distance during disaster time. Different algorithm and wireless protocol can be used among the nodes and LBS1 for communicating to each other. The LBS1 has a long distance communication facility with the remote control station, which is connected with server.

Therefore, the server can always receive real-time data of the sensor through LBS1.

A capacitor type sensor can be used for monitoring the land movement. A thin film strain gage pressure sensor with high accuracy pressure measurement is claimed [2]. A simple pretension underground cable attached with a strain gage at one end can be used to measure the pressure of the soil for the landslide monitoring system [3]. But it introduces noises and needs a complex thermal adjustment. A differential capacitor sensor of wireless sensor network for landslide monitoring has been proposed as shown in Fig. 2 which introduce less noise and low thermal adjustment. The differential capacitor sensor is simple, robust,

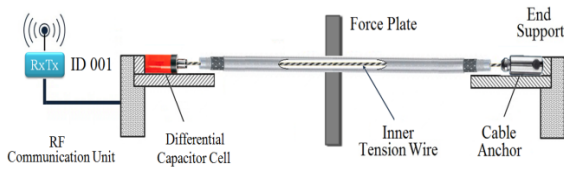


Fig. 2 Basic arrangement of a single sensor node for the proposed landslide monitoring system

reliable and chipper compares to other types of sensors. A slide movement of the soil is produced a force on force plate as well as the pretension wire. A variable differential capacitor is connected with one end of this wire. Therefore, due to the movement of the land there is a change of the capacitance in the differential capacitor cell. This capacitance change can be used to calculate the landslide prediction and detection. An electronic circuit (used to measure the capacitance change) and a small distance (about 100m) wireless communication system are used to make a sensor node. A number of the same kind of sensors setup or node can be used for monitoring a wide land area. Thus it is important to define each node carefully by a unique number by RFID tag within a wireless network to identify the exact location of the incidence. This ID number can be easily used to locate the landslide zone. A majority of the Wireless Sensor Network (WSN) arrangements are mainly data collection networks [4],[5]. The wireless sensor network will recurrently collect the respective data and collaboratively process measurements from the field under study before forwarding them to the central monitoring station. The central monitoring station will execute more computationally-intensive algorithms such as finite element modeling and parameter identification [6], [7] and will act as the expert interface to the system. A mobile communication system can be used to transmit the sensors sampled data and relevant information to a distant central database server computer for analysis purpose. The instant conveying of information will allow us to implement instant disaster rescue measures and to notify the

land user for protecting the people's lives and properties.

## SENSOR MODELING

A simplified force diagram of the proposed landslide sensor that is, pretension cable with differential capacitor cell is shown in Fig. 3. Assume that a pretension steel cable of length  $L$  is attached with two end supports under the ground. If the cable linear expansion coefficient is  $\alpha_L$  and the surrounding temperature of the cable is changed  $\Delta T$  degree Kelvin then the change of cable length  $\Delta L_T$  can be calculated as follows.

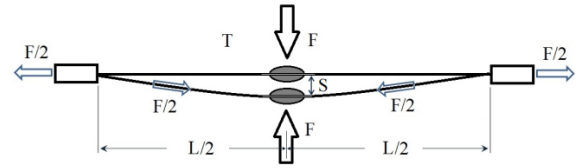


Fig. 3 Simplified force diagram of the proposed landslide pressure sensor

$$\alpha_L = \frac{1}{L} \frac{\Delta L_T}{\Delta T} \quad (1)$$

$$\text{Or, } \Delta L_T = \alpha_L L \Delta T \quad (2)$$

When the land is slightly moved to a distance  $S$  from its initial position then it will create a force  $F$  on force plate as well as on the cable. If the Yang's modulus of the cable is  $E$  then at force equilibrium condition be represented by Eq. (3).

$$E = \frac{F/A}{\Delta L/L} \quad (3)$$

Where,  $A$  is the cross sectional area of the cable and  $\Delta L$  is the change in length of the cable due to force.

Considering the temperature effect,

$$\Delta L = \frac{F(L + \Delta L_T)}{EA} \quad (4)$$

The work  $U_E$  done by the movement of the soil can be calculated by Eq. (5).

$$U_E = FS \quad (5)$$

The potential energy  $U_W$  stored in the cable can be calculated as follows.

$$U_W = \int_0^{\Delta L} F d\Delta L \quad (6)$$

From Eq. (4) and Eq. (6), it can be written as

follows.

$$U_W = \int_0^{\Delta L} \frac{EA\Delta L}{(L + \Delta L_T)} d\Delta L$$

$$\text{Or, } U_W = \frac{EA\Delta L^2}{2(L + \Delta L_T)} = \frac{\Delta LF}{2} \quad (7)$$

From Eq. (5) and (7), the potential energy  $U_C$  stored in the differential capacitor cell (supporting spring of the capacitor) can be calculated as follows.

$$U_C = U_E - U_W = FS - \frac{\Delta LF}{2}$$

$$\text{Or, } U_C = F\left(S - \frac{\Delta L}{2}\right) \quad (8)$$

Again, if the Yang's modulus of the spring of the differential capacitor cell is  $E_S$  then at force equilibrium condition can be calculated by Eq. (9).

$$F_S = \frac{E_S A_S \Delta L_S}{L_S} \quad (9)$$

Where,  $A_S$  and  $L_S$  are the cross section area and length of the supporting spring respectively,  $F_S$  is the force on the substrate and  $\Delta L_S$  is the change in length of the substrate due to force. So the potential energy  $U_S$  storage in the spring can be calculated as follows.

$$U_S = \int_0^{\Delta L_S} F_S d\Delta L_S$$

$$\text{Or, } U_S = \frac{E_S A_S \Delta L_S^2}{2L_S} \quad (10)$$

Combining Eq. (8) and Eq. (10), it can be written as follows.

$$F\left(S - \frac{\Delta L}{2}\right) = \frac{E_S A_S \Delta L_S^2}{2L_S}$$

$$\text{Or, } \frac{\Delta L_S}{L_S} = \sqrt{\frac{2F}{L_{GS} E_{GS} A_{GS}} \left(S - \frac{\Delta L}{2}\right)} \quad (11)$$

A basic construction of a differential capacitor cell is shown in Fig. 4. If the cell factor and the temperature coefficient of the differential capacitor

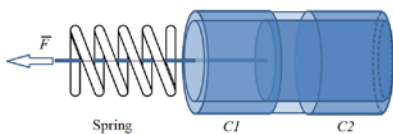


Fig. 4 Construction of a differential capacitor sensor cell

are  $k$  and  $\alpha$  respectively, then the change of

capacitance  $\Delta C$  of the differential capacitor cell with respect to the total capacitance  $C$  can be calculated by Eq. (12).

$$\frac{\Delta C}{C} = \left( \frac{k\Delta L_S}{L_S} + \alpha T \right) \quad (12)$$

Combining Eq. (11) and Eq. (12), the change of differential capacitance can be calculated by Eq. (13).

$$\Delta C = C \left( k \sqrt{\frac{2F}{L_S E_S A_S}} \left( S - \frac{\Delta L}{2} \right) + \alpha T \right) \quad (13)$$

From Eq. (4), if the Yang's modulus  $E$  of the cable is very large then  $\Delta T \approx 0$  and Eq. (13) can be rewritten as Eq. (14).

$$\Delta C = C \left( k \sqrt{\frac{2FS}{L_S E_S A_S}} + \alpha T \right) \quad (14)$$

Eq. (14) indicates that the change of capacitance of the differential capacitor cell is directly proportional to the square root of the force and displacement of the land.

## RESULT AND DISCUSSION

A PSPICE simulation has been studied for the proposed landslide sensor for monitoring system. The result is shown in Fig. 5. In this simulation it is considered that the Yang's modulus  $E$  of the cable is infinity and the temperature coefficient of the capacitor cell is very low. From Fig. 5 it is found that from the beginning there is a very slow landslide effect and about four months later the effect is more visible. The sensor ID number 001 (RFID tag number) shows that its capacitance is changing exponentially; it means a massive landslide will be happened within short time in the region under the sensor ID 001. The others sensor nodes also experienced some land slide effect.

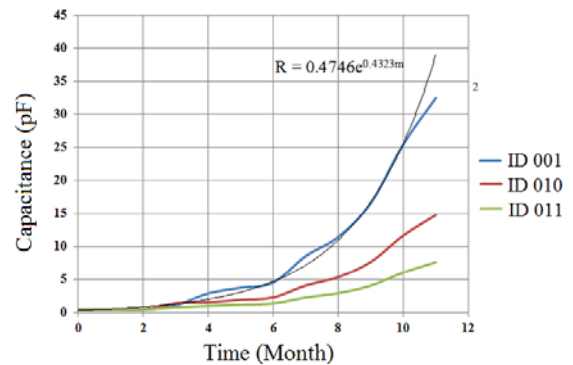


Fig. 5 Change of capacitance of the capacitor cell with time due to land movement

## CONCLUSION

A pretension cable and a differential capacitor sensor with RFID tagged ID can be used for landslide prediction and detection purpose. The change of cell capacitance is a direct indication of the landslide effect. This principle can help to develop a simple and low cost real time landslide or landslip monitoring system. According to the mathematical model Eq. (13) for an efficient system, the Yang's modulus of the cable must be very large. The steel and carbon fiber cable have a very large Yang's modulus and can be used in this development.

## ACKNOWLEDGEMENT

This research has been supported by the Ministry of Higher Education of Malaysia through the Fundamental Research Grant Scheme FRGS13-027-0268.

## REFERENCES

- [1] Lee S and Pradhan B, "Landslide hazard mapping at Selangor, Malaysia using frequency ratio and logistic regression models", *Landslides*, Vol. 4, No. 1, 2007, pp. 33-41.
- [2] Hongye W, Kun L, Zhichou A, Xu W and Xun H, "Ion-beam sputtered thin-film strain-gage pressure transducers", *Sensors and Actuators A: Physical*, Vol. 35, Issue 3, 1993, pp. 265-268.
- [3] Motakabber SMA, Ibrahimy MI and Anwar F, "Wireless Sensor Network for Landslide Monitoring", in proceedings of the 3rd International Conference on Geotechnique, Construction Materials and Environment, Nagoya, Japan, Nov. 13-15, 2013.
- [4] Szewczyk R, Polastre J, Mainwaring A and Culler D, "Lessons from a sensor network expedition", in proceedings of the 1st European Workshop on Sensor Networks, Jan. 2004.
- [5] Xu N, Rangwala S, Chintalapudi KK, Ganesan D, Broad A, Govindan R, and Estrin D, "A wireless sensor network for structural monitoring", in proceedings of the 2nd International Conference on Embedded Networked Sensor Systems, New York, USA, 2004, pp. 13-24.
- [6] Kuppusamy T, Sheng J, Parker JC and Lenhard RJ, "Finite-element analysis of multiphase immiscible flow through soils", *Water Resources Research*, Vol. 23, Issue 4, 1987, pp. 625-631.
- [7] Hoshiya M and Sutoh A, "Kalman Filter-Finite Element Method in Identification", *J. Eng. Mech.*, Vol. 119, Issue 2, 1993, pp. 197-210.

## BRIDGE SCOUR MONITORING BY USING RFID SYSTEM

M. I. Ibrahimy<sup>1</sup>, S. M. A. Motakabber<sup>1</sup> and M. Z. Hossain<sup>2</sup>

<sup>1</sup>Faculty of Engineering, International Islamic University Malaysia, 53100 KL, Malaysia

<sup>2</sup>Graduate School of Bioresources, Mie University, Mie 514-8507, Japan

### ABSTRACT

Bridge scour is an erosion which removes stream bed or bank material from bridge foundation due to flowing of water. Too much bridge scour is risky for the bridge foundation and causes sudden bridge to collapse without any warning. It implements significant impacts on the traveling public safety as well as the economy of the country. A number of parameters are associated with scour, thus different types of sensors are required to measure the individual affecting factor. A complex and expensive data logging from sensor and electronic communication systems are used to monitor the bridge scour in real-time to ensure the integrity of bridge structure. A high frequency band (13.56MHz) radio frequency identification (RFID) system has been proposed and that has been validated by simulation using PSpice software for direct scour monitoring scheme, which is simple and low-cost. A number of passive RFID tags have been piled surrounding the bridge foundation which are continually detected by the FRID reader. The erosion of the river bed carries out the RFID tag from nearby the bridge structure. As a result, the RFID reader can directly detect the absence of the tags as well as the amount of the scouring. Since, the design structure of the RFID system is simple, it is highly robust and easy to implement. The system can easily be implemented with an existing bridge structure and a wireless telemetry can be used to send the real-time data from the proposed system to a desktop computer in the monitoring lab.

*Keywords: Scour, Bridge Monitoring, Riverbed Erosion, RFID, Passive Tag*

### INTRODUCTION

An RFID system is simple in its structure which consists of two main components only: the reader and the tag (transponder) with their antennas as shown in Fig. 1. A passive RFID system, the tag does not contain an onboard power supply and harvests the energy from the reader transmitted RF wave for its operation. Since the passive tag has no battery, it is simple, low cost, long life and easy to maintain. The RFID technology permits the wirelessly two-way transfer of information from a reader to a tag via RF waves transmitted through antennas. Two major advantages of the high frequency band RFID system (13.56 MHz) to make it suitable for monitoring the bridge scouring. First, it does not need line of sight between the reader and the tag for communication. Second one, it can easily communicate through the metal, water, soil etc. Therefore, the tag can be detected even when it is buried in the bed substrate of the bridge. The high frequency band RFID system (13.56 MHz) can easily communicate up to 100m distances. Generally, the tags are buried at predetermined locations (depths) side by side with known lengths. The tags are subsequently driven into the bed substrate at the location where bridge scour holes are expected within the detection range of the reader antenna, which are installed directly above the tags. The tags are kept perpendicular to the RFID reader antenna plane, so that they can be continuously detected.

Once the scour takes place, the tags are washed out and thus they are not detected. Therefore, the result indicates that bridge scours have been occurred at the known depth, where the tags are initially buried. That will reduce the huge cost of physical monitoring for bridge maintenance. Mobile communication can be used to transmit relevant information to bridge maintenance and management units and road users when a bridge would be potentially damaged by manmade or natural disasters. The instant conveying of information will allow the bridge management units to implement

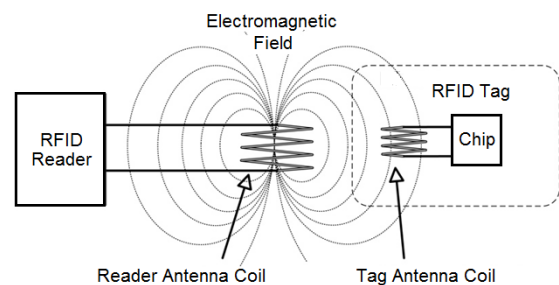


Fig.1 Basic RFID system

instant disaster rescue measures and to notify road users to avoid dangerous road sections, thus the people's lives and properties will be protected.

Bridge scour is the meaning of removal of soil, sand and rocks from around a bridge supports or piers as shown in Fig. 2. Rapidly moving water can



wash out the river bed materials and make scour holes, which can be threatening of the existence of a bridge structure [1]. Scour happens under the water and hard to see by naked eye. As a result, every year a number of bridges are collapsing all over the world and it damages lot of money and lives. The three main causes of bridge failure are collision, overloading and scour. It has been estimated that 60% of all bridge failure results occurred from scouring and other hydraulic-related causes [2].



Scour

Fig.2 Bridge scour [1]

Scour is a complex natural occurrence and a number of parameters are associated with it. Hence, to predict the bridge failures and real time scour monitoring, different types of sensors are required to measure the individual affecting factor [3, 4]. Among them sonar altimeter can be used to measure the distance between sensor and river bottom [5]. A change in distance-to-bottom is an indication of scour. Non-contact radar water level sensor can be used to measure the water level across a wide temperature range and varying water surface conditions [1]. Ultrasonic water velocity sensor and side-looking acoustic Doppler current meter can be used to measure bi-directional velocity of the water. The sensors read all the parameters including scouring, water levels and velocity of water flow. These sensor readings are transferred to a computer through wire or wireless communication systems. The reading is programmed to give an early warning to the computer. These sensors are generally selected and arranged based on local weather conditions, climate change effect, natural hazards and environmental conditions. Most of these type sensors are complex and very expensive.

## DEVELOPMENT OF RFID SYSTEM FOR SCOUR MONITORING

Design and development of a low cost RFID system which is related to the bridge scouring, is an exciting matter. An RFID system consists of a tag reader (also called the interrogator) and a passive tag. All communication between the tag and reader ensures completely through a wireless link which is sometimes called an air interface. Through a sequence of commands sent and received between

both devices called the inventory round. An RFID reader can identify an object, location, orientation etc. through the RFID tag. Fig. 3 shows an RFID reader antenna coil and tag arrangement surrounding of a bridge pier.

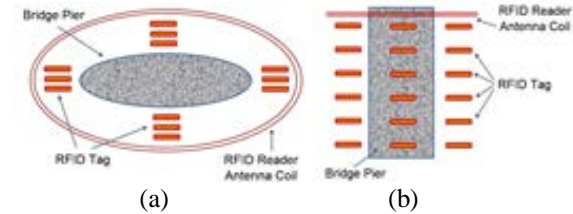


Fig. 3 (a) Cross sectional top view of the bridge pier and RFID tag arrangement (b) Cross sectional side view of the bridge pier and RFID tag arrangement

number or code and the reader can sequentially interrogate one by one of the tags with their code numbers. The tags are buried vertically in the river bed under the reader antenna coil as shown in Fig. 3(b) for the best performance. The scour will carry out the tag(s) from the vicinity of the reader antenna coil. As a result, no response will be found from the tag during the routine checkup of the reader by interrogation one by one of the tag with their corresponding code numbers. If a tag is not answered during the query of the RFID reader, the tag identification number gives a direct indication of the score position and its depth. For an improved service, the RFID reader can be interfaced with a wireless network communication system to communicate with the central control system, so that many bridge scour can be monitored simultaneously from a single place or a monitoring room.

The coupling factor between the RFID reader antenna and the tag antenna depends on geometrical parameters, distance and orientation of the antennas. In this case, the inductance values, number of turns of the coil of the tag are not involved. A simplified representation of the coupling factor  $k$  between a reader antenna coil and a tag antenna coil is represented by Eq. (1).

$$k = \frac{R_r^2 \times R_t^2 \times \cos(\theta)}{\sqrt{R_r \times R_t} \times \sqrt[3]{R_r^2 + d^2}} \quad (1)$$

Here,  $R_r$  and  $R_t$  are the radius of the reader and tag antenna coil respectively,  $d$  is the distance between the coils and  $\theta$  is the tilt along the axis of the coils.

## RESULT AND CONCLUSION

The PSpice simulation result of the coupling factor is shown in Fig. 4(a). There are two bumps, instead of having a good single peak in the



frequency response. These bumps, one for the tag antenna and the other for the reader antenna circuits respectively. It seems as two different resonant frequencies and which are well detached. This annoying effect is indeed what makes possible the design of an RF filter, made with cavities or helical resonators, slightly mistuned and carefully coupled to one another until the desired frequency response is obtained.

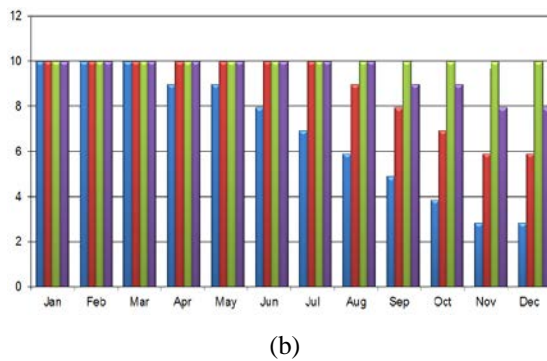
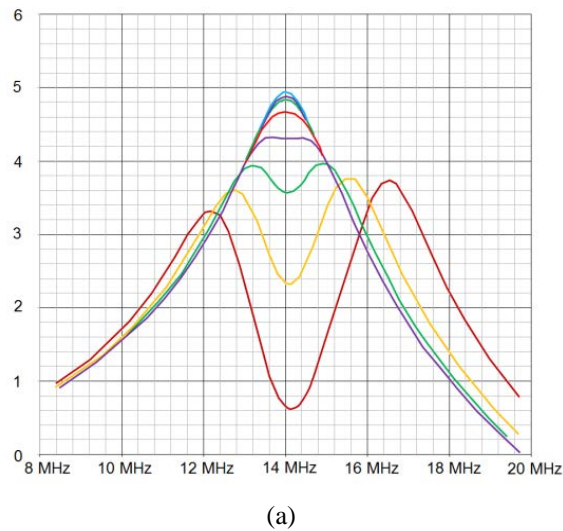


Fig. 4 (a) Coupling factor between RFID reader and tag antenna coils (b) Relation between scour and number of RFID tags

Fig. 4(b) shows the relation between bridge scour and an RFID tags. In this simulation 4 bridge piers with 10 RFID tags for each pier has been considered. From April to October is considered as the monsoon season, the result shows that a scouring starts at pier 1 from the month of April to November and finally

there is only 3 RFID tags are left surrounding of it. Similarly, scouring starts at pier 2 from the month of August to November and lastly, there is 6 RFID tags are left surrounding of it. Pier 4 also starts small scouring from the month of September. It is found that the bridge is in threatening condition of its existence due to huge scour with pier 1. Similarly, pier 2 also indicates moderate threatening to the bridge. However, the others have not significant indications to the bridge. It can be concluded that during the monsoon season the probability of bridge scouring is high.

## ACKNOWLEDGEMENTS

This research has been supported by the Ministry of Higher Education of Malaysia Government through the Fundamental Research Grant Scheme FRGS13-027-0268 entitled of the project “Analysis and Characterization of Chipless RFID Tag for Investigating the Scope of Uses in Malaysia”.

## REFERENCES

- [1] Anderson NL, Ismael AM and Thitimakorn T, “Ground penetrating radar: a tool for monitoring bridge scour”, *Environmental & Engineering Geosciences*, Vol. 13, No. 1, 2007, pp. 1-10.
- [2] Ballio F and Radice A, “A non-touch sensor for local scour”, *Journal of Hydraulic Research*, Vol. 41, No. 1, 2003, pp. 105-108.
- [3] Glaser SD, Li H, Wang ML, Ou J and Lynch T, “Sensor technology innovation for the advancement of structural health monitoring: a strategic program of US-China research for the next decade”, *Smart Structure and System*, Vol. 3, No.2, 2007, pp. 221-244.
- [4] Lin YB, Lai JS, Chang KC, Chang WY, Lee FZ and Ten YC, “Using MEMS sensors in the bridge monitoring system”, *Journal of the Chinese Institute of Engineering*, Vol. 33, No.1, 2010, pp. 25-35.
- [5] Lin YB, Chang KC, Chen CC, Wong SC, Lee LS, Wang YK and Gu MH, “Integrating real-time bridge scouring monitoring system with mobile location-based services”, *International Journal of Automation and Smart Technology*, Vol. 1, No. 2, 2011, pp. 51-62.

## MODELLING OF SHEAR STRENGTH PARAMETERS OF SATURATED CLAYEY SOILS

M. Inanc Onur<sup>1</sup>, Burak Evirgen<sup>2</sup>, Ahmet Tuncan<sup>3</sup> and Mustafa Tuncan<sup>4</sup>  
<sup>1,2,3,4</sup> Department of Civil Engineering, Faculty of Engineering, Anadolu University, Turkey

### ABSTRACT

Shear strength of a soil can be defined as the maximum shear stress that can resist by the internal forces of the soil. Shear strength must be determined to solve the soil stability problems. The shear strength parameters of the soil are cohesion and internal friction angle. These parameters can be determined in the laboratory by the direct shear test, triaxial test and unconfined compression test. However, laboratory tests take time and engineers want to define these parameters easily by using software. The development of the computer technology presents abilities to model the soil behavior in civil engineering applications. In this study, triaxial compression tests are performed on saturated clayey soils under different confining pressures. Unconsolidated-Undrained test is chosen to identify short term behavior. After the experimental procedure, the test is modeled by using the Plaxis program and the results are compared. Relationship between the results are presented.

*Keywords: Shear strength, Clayey soil, Triaxial compression test, Plaxis*

### INTRODUCTION

Defining the soil parameters is the first step of the all designs in geotechnical engineering. Especially, shear strength must be determined for soil stability problems. Shear strength of a soil is the maximum resisting capacity under shear stress. Soils gain this capacity from the internal forces. Shear strength is related to internal friction for coarse grained soils and cohesion for fine grained soils, respectively. The other factors affecting the clay soil strength can be such as effective stress, plasticity, cementation, moisture content, anisotropy and loading rate.

The soil strength parameters can be found by using triaxial shear tests (consolidated-drained CD, consolidated-undrained CU, and unconsolidated-undrained UU), direct shear test, vane shear test, unconfined compression test in the laboratory and standard penetration test, cone penetration test, pressuremeter test in the site. All of these test require maximum care and time because experimental errors can affect the results significantly. After determining the parameters, soil strength is calculated by using Coulomb theory, derived in 1776 [1]. Equation (1) is given below and shear strength ( $\tau$ ) is accepted just about shear stress on the failure plane [1].

$$\tau_f = c + \sigma'(\tan \phi) \quad (1)$$

where;  $c$  is cohesion  $\phi$  is angle of internal friction and  $\sigma'$  is effective stress.

Mohr-Coulomb failure criteria is used to define soil stress concept. Stress conditions at failure in a soil mass is given in Fig. 1.

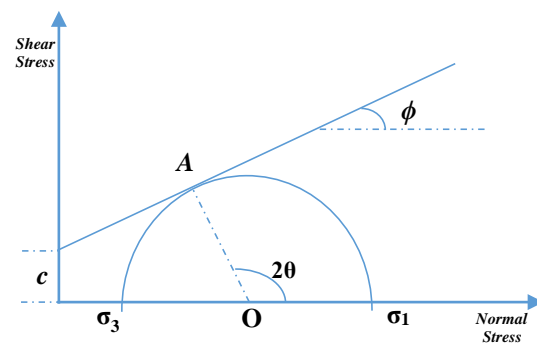


Fig. 1 Mohr's circle and failure envelope.

If the failure plane makes an angle  $\theta$  with the major principal plane, the normal stress and the shear stress on the plane are given in Eq. (2) and (3).

$$\sigma = \frac{\sigma_1 + \sigma_3}{2} + \frac{\sigma_1 - \sigma_3}{2} \cos 2\theta \quad (2)$$

$$\tau_f = \frac{\sigma_1 - \sigma_3}{2} \sin 2\theta \quad (3)$$

Many researchers studied shear strength of the soils in the literature. Some of them determined the parameters by using some laboratory tests and field tests or developed new test methods [2], [3], [4], [5]. Some researchers used numerical and statistical methods for modelling the soil strength [6], [7], [8], [9].

Nowadays, shear strength problems are solved by using software to save time. The soil behavior can be modeled by softwares using finite element or finite

differences methods. Thus, soil stability problems such as bearing capacity, slope failure etc. can be easily solved. In this study, triaxial compression tests are performed on saturated clayey soils under different confining pressures. Unconsolidated-Undrained (UU) test is chosen to identify short term behavior of clayey soil. After the experimental procedure, the test is modeled by using the Plaxis program and the results are compared. Relationship between the results are presented.

## MODELLING AND METHODS

In this study; Plaxis 2D performed to determine soil behavior. Plaxis is a commercially available program which is using finite element method and commonly used in civil engineering applications [10]. Example screen of the Plaxis menu is given in Fig. 2.

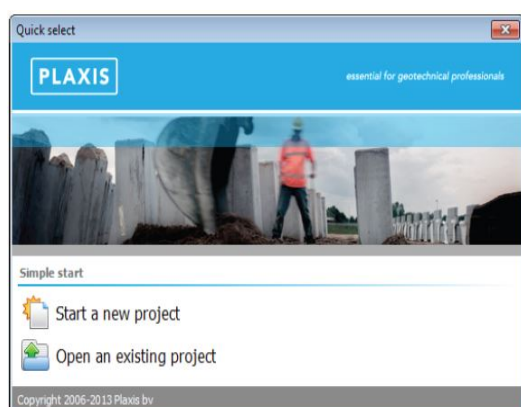


Fig. 2 Example screen of the Plaxis menu.

## Experimental Procedure

Test soil is taken from a construction site in the city of Eskisehir, Turkey. After boring, soil index properties determined such as moisture content, atterberg limits, specific gravity, sieve analysis, and hydrometer. Standard proctor tests are also performed on the samples. Basic characteristics of the soil are given in Table 1.

Table 1 Basic characteristics of test soil

USCS	MH-OH
$\omega_n$ (%)	30,20
$\omega_L$ (%)	85,00
$\omega_P$ (%)	20,00
$\omega_{opt}$ (%)	49,00
G <sub>s</sub>	2,52
Gravel (%)	0,32
Sand (%)	12,50
Silt (%)	64,18
Clay (%)	23,00

The reconstituted samples have 70 mm in diameter and 140 mm in length. In this study samples were prepared by compacting with optimum moisture content. Unconsolidated-Undrained triaxial test is performed on the compacted samples. The test procedures were designed according to the ASTM D2850. A test sample is given in Fig. 3.



Fig. 3 A test sample.

The confining pressures are chosen 10, 20 and 30 psi and the deviator stress are applied to the failure. Shear stress parameters are found by drawing the Mohr's circles. Detailed information is given in Table 2. Mohr's circles are also given in Fig. 4.

Table 2 Test Details

Sample	A	B	C
Confining Stress	10,0 psi	20,0 psi	30,0 psi
Deviator Stress	20,4 psi	28,7 psi	35,7 psi
Principal Stress	30,4 psi	48,7 psi	65,7 psi
Max. Strain	6,0 %	8,0 %	9,0 %
Cohesion	4,99 psi	4,99 psi	4,99 psi
Friction angle	16°	16°	16°

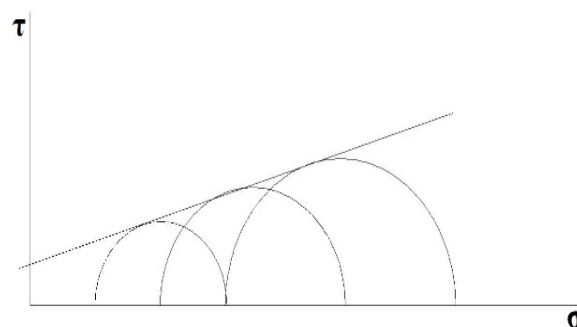


Fig. 4 Mohr's circles of the test samples.

## Modelling Procedure

Plaxis is using different soil models to define soil behavior such as Mohr-Coulomb Model, Hardening Soil Model, Soft Soil Model, Soft Soil Creep Model, Jointed Rock Model and Modified Cam-Clay Model. Mohr-Coulomb Model is chosen for this study. Because it is commonly used and not required extra soil parameters. The behavior is linearly elastic and perfectly plastic in this model that needs Young's Modulus, Poissons Ratio, and cohesion, internal friction angle and angle of dilatancy [10].

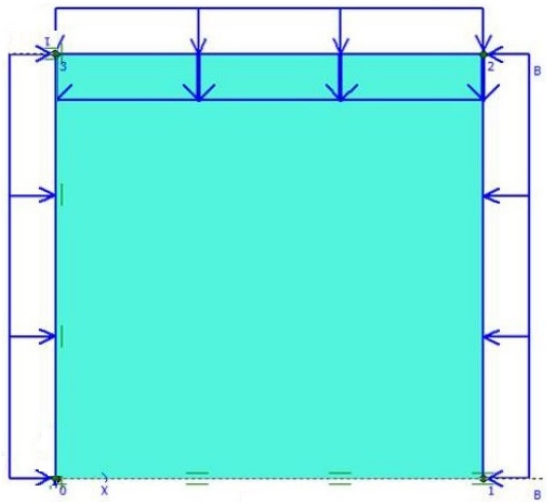


Fig. 5 Model screen.

Plaxis modelling is prepared with considering boundary conditions, loading and soil properties. Modulus of elasticity is calculated from the initial part of stress-strain graphs of the samples. Confining pressures are applied as the triaxial test at top and two sides. Three dimensional effect is ignored because of the 2D analysis. Deviator stress are applied at the top and the deformations are determined. Model details are given in Table 3.

Table 3 Model Details

Sample	A	B	C
Soil Model	Mohr-Coulomb	Mohr-Coulomb	Mohr-Coulomb
Cohesion	4,99 psi	4,99 psi	4,99 psi
Friction angle	16 <sup>0</sup>	16 <sup>0</sup>	16 <sup>0</sup>
Young Modulus	2875 kN/m <sup>2</sup>	2875 kN/m <sup>2</sup>	2875 kN/m <sup>2</sup>
Dilatancy angle	0	0	0
Poissons Ratio	0,3	0,3	0,3

## RESULTS

Plaxis models are performed and strains are calculated. Maximum strains are compared with the triaxial test results. The comparisons of the maximum strains are given in Table 4.

Table 4 Strain Values

Sample	A	B	C
Max. Strain (Triaxial Test)	6,0 %	8,0 %	9,0 %
Max. Strain (Plaxis Model)	5,9 %	8,1 %	9,1 %

The results shows approximately similar values despite the lack of three dimensional analyses. Mohr-Coulomb model is known as conservative model and gives safe results. In this study Mohr-Coulomb model simulate the results safely. Strain value in the Plaxis is a bit less in the first model but it is negligible.

## CONCLUSION

In this paper, the comparison between the laboratory tests and computer modelling are presented. Unconsolidated-Undrained triaxial test is performed in the experimental analyses and Plaxis 2D is performed to simulate these test results. The strain results under the loading and modelling are presented. Based on the results, the following conclusions can be drawn:

- The study shows similar results as the literature.
- Mohr-Coulomb model shows approximately similar values as laboratory tests, and gives safe results.
- If more sensitive results are desired 3D analysis should be done with considering the third dimensional confining effect.
- Presented values can be used in geotechnical applications.

## REFERENCES

- [1] Das BM., Principles of Geotechnical Engineering, Pws-Kent Publishing Co., 1990, ch 8.
- [2] Alikonis A., Amšiejus J., Stragys V., "Improvement of shear box apparatus and methodology of test", in Proc. Soil Mechanics and Geotechnical Engineering, The 12th European Conference, 1999, pp. 1053–1057.
- [3] Guo P., "Modified Direct Shear Test for Anisotropic Strength of Sand", Journal of

- Geotechnical & Geoenvironmental Engineering, vol. 134(9), 2008, pp. 1311–1318.
- [4] Matsuoka H., Liu SH., Sun DA., “A new in-situ direct shear testing method for rockfill materials sands and clays”, in Proc. Proc of the 15th International Conference on Soil Mechanics and Geotechnical Engineering, 2001, pp. 455–458.
  - [5] Vervečkaitė N., Amšiejus J., Stragys V., “Stress–strain analysis in the soil sample during laboratory testing”, Journal of Civil Engineering and Management, vol. 13(1), 2007, pp. 63–70.
  - [6] Amšiejus J., Dirgėlienė N., “Probabilistic assessment of soil shear strength parameters using triaxial test results”, The Baltic Journal of Road and Bridge Engineering, vol. 2(3), 2007, pp. 125–131. Author H, A Book. New York: Publisher, Yr, ch. 3.
  - [7] Dounias GT., Potts DM., “Numerical analysis of drained direct and simple shear tests”, Journal of Geotechnical Engineering, vol. 119(12), 1993, pp. 1870–1891.
  - [8] Jacobson DE., Valdes JR., Evans TM., “A numerical view into direct shear specimen size effects”, Geotechnical Testing Journal, vol. 30(6), 2007, pp. 512–516.
  - [9] Zhang L., Thornton C., “A numerical examination of the direct shear test”, Geotechnique, vol. 57(4), 2007, pp. 343–354.
  - [10] Brinkgreve, R.B, Vermeer, P.A. Plaxis Ver. 7.2 Manual Finite Element Code for Soil And Rock Analyses, Balkema, 1998.
  - [11] ASTM D2850 Standard Test Method for Unconsolidated-Undrained Triaxial Compression Test on Cohesive Soils

## DETERMINATION OF THE FREEZING EFFECT ON UNCONFINED COMPRESSION STRENGTH AND PERMEABILITY OF SATURATED GRANULAR SOILS

Burak Evirgen<sup>1</sup>, M. Inanc Onur<sup>1</sup>, Mustafa Tuncan<sup>1</sup> and Ahmet Tuncan<sup>1</sup>

<sup>1</sup>Department of Civil Engineering, Faculty of Engineering, Anadolu University, Turkey

### ABSTRACT

Artificial ground freezing usage gradually rises in civil engineering applications as a soil supporting system. However, many unknown fundamental parameters have been still waiting discovery, especially for granular soil. Granular soil can not carry its own weight during unconfined conditions. If water turns to ice that locates in the soil pores, it proceeds as a cementitious material. First step of design phenomena is to identify the material properties in geotechnical engineering. Within this scope, unconfined compression tests (UCC) and permeability tests are performed on frozen granular soils subjected to 1, 3 and 7 day-freezing periods to observe time effect. Experimental procedure are applied totally on 12 sand and gravel type of specimens with saturated cases after freezing application in the CDF/CIF freezing thawing machine. Stress - strain behaviors, ultimate load capacities and permeability of specimens are determined. This method will be used while taking undisturbed granular soil samples from the construction site.

*Keywords: Artificial Ground Freezing, Granular Soils, Unconfined Compression Test, Permeability*

### INTRODUCTION

Soil supporting system is an essential component for geotechnical engineering in many soil projects. Undergoing applications are such as laterally loaded piles, retaining walls and sheet piles, braced cuts for deep excavations and NATM or classic tunnel boring methods for tunnel constructions. All of them require dewatering if ground water table creates a risk in the site. Artificial ground freezing (AGF) presents easy, safety, eco-friendly and economical (without initial cost of machines) solution and dewatering as well.

Many researchers have studied artificial ground freezing and its effects on the soil properties. However, limited study have been found in the literature about fundamental mechanical properties such as unconfined compression strength and permeability of saturated frozen granular soils under normal conditions. Unconfined compression test application on the unfrozen granular samples are impossible having to avoid the dispersion of solid particles along the lateral direction according to without confining pressure around the soil media. However, triaxial test can be applied to the granular samples after difficult sample preparation with using vacuum and gradually pressure increment as a cell pressure. Another methods of UCC tests and triaxial tests have been performed inside the modified cold state cells that regulates the environmental temperature at constant value according to undergoing studies. But, proposed approach involves the basic UCC test while room temperature effects to frozen specimens. Evaluation the results of easy and

useful undisturbed sampling method without any modified cooling cell is purposed within this study.

Reference [1] presents that mechanical properties of frozen soil depends directly on water content. On the other hand, it is inversely proportional with the increase of consolidation pressure and sand content according to experimental results. Reconstituted soil samples that consist of silty - clay (inorganic clay of medium plastic) and sand (grain size ranged between 0.42 and 0.074 mm) mixtures were used during these tests. Sand content changes between 0, 10, 20, 30 and 50% of the total weight of solid material. Cylindrical specimens have 3.5 cm in diameter and 7 cm in height were used after subjected to 25, 50, 200 and 400 kPa consolidation pressures. Specimens were placed in the freezing chamber having a -14 °C temperature for 24 hours freezing period. Reference [2] gives that the specimens were prepared at higher dry density having more uniaxial compression strength than lower ones at the same strain rate and temperature for saturated frozen soils as a result of cohesion according to result of given equation in the paper. Remolded silty samples are used. Maximum (1.111) and minimum (0.503) void ratios were kept at constant temperature in freezing cabinet. They preferred the Eq. (1) as a function of strain - temperature according to investigations on the saturated frozen silty soil with different parameter ranges between -2 to -15 °C and  $1.10^{-6}$  to  $7.10^{-4} \text{ s}^{-1}$ , temperature and strain values, respectively.

$$\sigma_f = \sigma_o' (\theta/\theta_o)^i (\dot{\epsilon}/\dot{\epsilon}_o)^m \quad (1)$$



Where;  $\theta_0$  is reference temperature,  $\theta$  is negative temperature,  $\sigma_f$  is axial compression strength,  $\dot{\epsilon}$  is strain rate,  $\dot{\epsilon}_0$  is reference strain rate and  $m$  is the parameter changes due to dry density and temperature of samples. Reference [3] shows that ductile deformation type occurred at low water content in partially frozen soils. On the other hand, brittle type of failure was seen on frozen soils that have high water content. Residual compressive strength of frozen soils are independent of their dry unit weight at a particular temperature. However, it increases with decreasing temperature according to peak. Compressive strength observation was studied on saturated fine grained frozen samples with respect to the water content, dry unit weight and temperature parameters. Reference [4] indicates that some of the following practical advantages and disadvantages within the compressive strength observation under the effect of strain rate for both confined ( $-6^\circ\text{C}$  to  $-10^\circ\text{C}$ ) and unconfined cases ( $-2^\circ\text{C}$  to  $-15^\circ\text{C}$ ) of artificially frozen sand samples. Perfectly end platen preparation are not necessary for frozen soils. Soft platen material can eliminate the minor irregularities after freezing. Relatively short frozen cylindrical shaped samples can be used during strength determination after core drilling from construction site. Compatible platen usage reduces the stiffness of the test system and makes difficult to control test parameters.

In the AGF phenomena, free water that moves in the soil voids turns to ice as a cementitious material. So, concrete like material is obtained easily. But, many factors affect the artificial ground freezing applications in the site. For example, freezing duration, amount of given energy, used machine capacity, location of construction site as a function of weather temperature, construction period, cooling liquid and sizes of circulation pipes. In this study, effect of soil type and freezing duration on the uniaxial bearing capacity and permeability of saturated frozen granular soils were studied.

## MATERIAL PROPERTIES

Gravel and sand type of soil materials were used during experiments. First of all, fundamental geotechnical tests were performed. Figure 1 shows the grain size distribution curve as a result of sieve analysis. Physical properties of soil samples represent the common values of poorly graded granular materials as shown in Table 1.

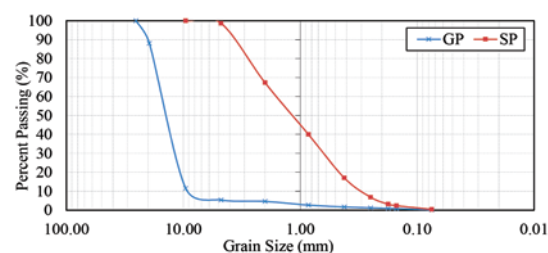


Fig. 1 Grain size distribution curve for samples

Table 1 Soil properties

Soil	I	II
Specific Gravity	2.54	2.58
Gravel (%)	94.60	1.30
Sand (%)	5.20	98.30
Silt & Clay (%)	0.80	0.40
$D_{10}$	9.10	0.30
$D_{30}$	11.00	0.62
$D_{60}$	15.00	1.60
$C_u$	1.65	5.33
$C_c$	0.89	0.80
Void ratio (e)	0.94	0.54
Type of Soil	GP	SP

Permeability is used to understand the water flow in soil media. This physical property affects the bearing capacity, settlement, shear strength and liquefaction potential of construction area. Proper dewatering process requires if ground water flow exists. Capacity of discharge increments also makes the removing of water difficult. In this case, AGF presents the useful dewatering technique even eliminating the seepage. Table 2 gives the common coefficient of permeability values [5].

Table 2 Coefficient of permeability values [5]

Soil Type	k (cm/sec)
Clean Gravel	1.0 - 100.0
Coarse Sand	1.0 - 0.01
Fine Sand	0.01 - 0.001
Silty	0.001 - 0.00001
Clay	Less than 0.000001

## EXPERIMENTAL PROCEDURE

Cylindrical specimens, 70 mm in diameter and 130 mm in height, were used. Six specimens were selected for unconfined compression tests and the others were used for permeability tests as shown in Fig. 2. Solid particles were placed without any compaction energy by using gravitational energy.

Then, freezing process was applied after saturation. First, unfrozen specimens were kept at  $-10^{\circ}\text{C}$  during 1 day before the tests as pre-freezing period. Then, specimens were removed from molds with hydraulic machine.



Fig. 2 Unfrozen gravel and sand specimens

Freezing of soil particles with lateral displacement under anisotropic and known principle stress is expected situation during both natural and artificial freezing process. However, freezing experiments are generally realized with eliminating displacement by using molds in the laboratory [6]. Accordingly, frozen specimens show volumetric expansion along the longitudinal direction from the top surface. Surface was levelled with spiral grinding machine as shown in Fig. 3.



Fig. 3 Surface levelling of expanded part

The prepared specimens were kept at constant temperature as  $-15^{\circ}\text{C}$  in a CDF / CIF freezing thawing machine during 1, 3 and 7 days as shown in Fig. 4. In spite of the apparent abundance of published experimental data on frozen soil behavior, some questions has not been answered, yet [6]. Some of them are such as unconfined compression strength and permeability change according to under thawing effect at room temperature after short term freezing periods.



Fig. 4 CDF/CIF freezing thawing machine

Six samples were subjected to axial compression force with  $1.0\text{ mm/min}$  loading rate to perform the unconfined compression test. Load rate was selected higher than normal value within the scope of eliminating the quick thawing process. Plexiglas were used at the top and at the bottom caps at  $-15^{\circ}\text{C}$ . Stress and strain values were collected with using Utest data acquisition system as shown in Fig. 5. Other six samples were used to perform permeability tests. Constant head permeability tests were performed at 300 mm constant head. Amount of water was collected simultaneously during 30 minutes for each specimen as shown in Fig. 6. Coefficient of permeability values are calculated according to these values.

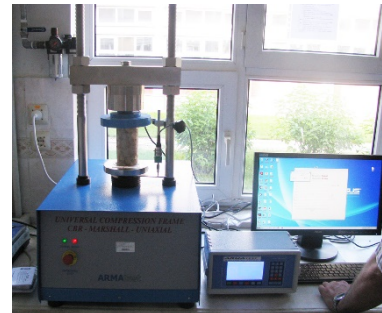


Fig. 5 Unconfined compression test device with data acquisition system



Fig. 6 Permeability test device

## RESULTS

Soil is known as heterogeneous material that consists of solid particles, air and water. So, unexpected stress and deformation behavior can occur inside the soil phases. Arrangement of particles is less important for frozen soil according to cementitious ice formations. Fine grained soil has more stress and strain capacity than coarse grained soil according to the results of unconfined compression tests as shown in Fig. 7. Unconfined compression strength values of poorly graded gravel specimens are determined as 1.64, 2.92 and 3.49 MPa for 1 day, 3 days and 7 days freezing periods, respectively. On the other hand, strength values are obtained as 2.94, 3.04 and 5.13 MPa during same periods for poorly graded sand specimens. Compressive strength of frozen samples increases with increasing time up to 7 days. Strain rates are approximately similar for sandy specimens. However, it is inversely proportional with increment of freezing period for gravel type of soils. Curves of both 3 days specimens and 1 day specimen of sandy soil are similar. Lower strength and higher strain values of 1 day gravel sample rises from partially freezing of solid particles and ice lenses.

All of the frozen specimens are started to thaw around 5 minutes as a result of constant head permeability tests on the frozen samples. If the freezing time increases, permeability of frozen sandy specimen decreases. However, coefficient of permeability value is inversely proportional with freezing time, unexpectedly. Coefficient of permeability of granular sample is about 5 times greater than the other one. Permeability test results of the samples are shown in Fig. 8.

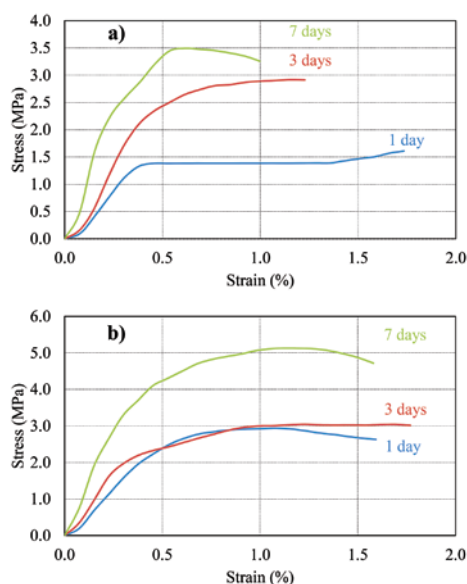


Fig. 7 Stress - strain behavior of frozen granular specimens, a. Poorly graded gravel, b. Poorly graded sand

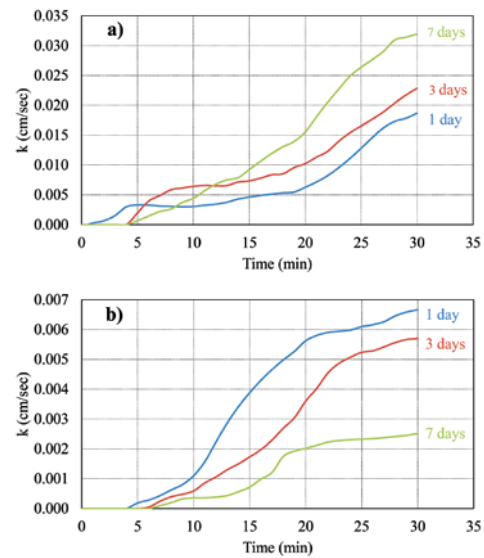


Fig. 8 Change in coefficient of permeability for frozen granular specimens, a. Poorly graded gravel, b. Poorly graded sand

Observed failure modes at the end of the compression tests are completely different for gravel and sand type of samples. Vertical cracks are occurred on the frozen gravel surfaces as shown in Fig. 9a. On the other hand, horizontal cracks are formed on the sand type of specimens as shown in Fig. 9b. All of the failure models are similar to concrete type of brittle material rather than soil like material. However, finer graded frozen soil material has more ductility than the coarser one.



Fig. 9 Failure mode and observed cracks on the samples a. gravel sample, b. sandy sample

Bursting behavior can occur on the frozen samples under very fast or slow loading rate [5]. If loading rate is too slow, ice turns to water - ice mixtures. If loading rate is too fast, frozen soil sample easily disperse due to the lack of cohesion or any finer material. Bursting phenomena was observed on the trial specimen under fast loading rate with using concrete compressive test machine as shown in Fig. 10.

## CONCLUSION

In this study, experimental analyses of twelve saturated frozen granular samples are examined with 1 day, 3 days and 7 days freezing time effect. The change in unconfined compression strength and coefficient of permeability values are presented. Based on the results, the following conclusions may be drawn:

Both brittle and ductile deformations and different strain values can be observed under same loading conditions according to the degree of water freezing in the pores or amount of fine material. Strength and deformation varies by the using area of the artificial ground freezing in the geotechnical projects.

Compressive strength of frozen samples increases with increasing time up to 7 days. Strain rates are approximately similar for sandy specimens. However, it is inversely proportional with increasing freezing time for gravel type of soils.



Fig. 10 Bursting formation under fast loading rate

All of the frozen specimens are started thawing around 5 minutes. If the freezing time increases, permeability of frozen sandy specimens decreases. However, coefficient of permeability value is inversely proportional with freezing time, unexpectedly. Coefficient of permeability for granular sample is about 5 times greater than the other one.

Presented values can be used for modelling of geotechnical projects both using finite element software and theoretical calculations as well.

## REFERENCES

- [1] Anagnostopoulos CA, Grammatikopoulos I, "The Effect of Freezing on the Strength of Silty-Clay-Sand Mixtures", *Electronic Journal of Geotechnical Engineering*, Vol. 10, 2005, bundle G.
- [2] Li HP, Zhu YL, Pan WD, "Uniaxial Compressive Strength of Saturated Frozen Silt", 8th International Conference on Permafrost, 2003, pp. 679-684.
- [3] Joshi RC, Wijeweera H, "Post Peak Axial Compressive Strength and Deformation Behavior of Fine-Grained Frozen Soils", in *Proc. Proceedings of the Fifth Canadian Permafrost Conference*, 1990, pp. 317-325.
- [4] Baker THW, Jones SJ, Parameswaran VR, "Confined and Unconfined Compression Tests on Frozen Sands", *Proceedings Fourth Canadian Permafrost Conference*, 1981, pp. 387-393.
- [5] Das BM, *Principles of Geotechnical Engineering*, Boston: Pws-Kent, 1990, ch. 4.
- [6] Ono T, "Lateral Deformation of Freezing Clay Under Triaxial Stress Condition Using Laser-Measuring Device", *Cold Regions Science and Technology*, Vol. 35, 2002, pp. 45-54.
- [7] Ladanyi B, "An Engineering Theory of Creep of Frozen Soils", *Canadian Geotechnical Journal*, Vol. 9, February 1972, pp. 63-80.



## **QUANTITATIVE ASSESSMENT OF HUMAN RISKS POSED BY MINE DEBRIS FLOW**

Shuai Zhang<sup>1</sup>, Limin Zhang<sup>2</sup>

<sup>1</sup> Department of Civil and Environmental Engineering, The Hong Kong University of Science and Technology, Clear Water Bay, Hong Kong

<sup>2</sup>Department of Civil and Environmental Engineering, The Hong Kong University of Science and Technology, Clear Water Bay, Hong Kong

### **ABSTRACT**

Prolonged rainstorms had triggered several large-scale debris flows along Provincial Road 303 near the epicenter of the 2008 Wenchuan earthquake. A lot of concrete-aggregate plants distributed along this road were buried by the runout debris, leading to a large number of fatalities. A Quantitative Risk Assessment (QRA) methodology is being developed for debris flows induced by various rainfall scenarios. QRA for these debris flow hazards is of significance to determine the probability distribution, consequence and human risk profile arising from these disasters. With the aid of Geographic Information System (GIS) platform, a potential channelized debris flow catchment in the study area is identified based on remote sensing images and field study. Rainfall intensity-duration thresholds for the local channelized debris flows are used to determine the occurrence probability under six rainfall scenarios for the purpose of hazard analysis. Subsequently, human losses of debris flow are assessed by considering the variations of rainfall events, and the final human risks can be obtained using a general risk model. Finally, the societal human risks are obtained, which provide a benchmark for studying the long-term human risks of these potential debris flows and engineering decision in the perspective of mining manufacture.

*Keywords: Debris Flow, Quantitative Assessment, Human Risk*

### **INTRODUCTION**

Debris flows are among the most frequent mass movement processes in mountainous areas (Kang et al. 2004; Jakob and Hungr 2005), and are attributed to an adequate supply of loose materials, surface runoff, and steep drainage channels (Takahashi 1981).

The 12 May 2008 Wenchuan earthquake in China triggered about 197,481 landslides (Xu et al. 2013). Numerous loose landslide deposits were retained on steep hill-slopes or in channels. Such deposits are in a quasi-stable state in the dry season but can provide source materials for debris flows in the wet season (Tang et al. 2011; Zhang et al. 2012; Zhang et al. 2013; Zhang et al. 2014). In the past four years, three large-scale debris flows occurred in the Pubugou Ravine near the epicentre of the Wenchuan earthquake on 24 June 2008, 14 August 2010 and 4 July 2011. Approximately 1.76 million m<sup>3</sup> of sediment was deposited during these three events. It is expected that debris flows will continue to occur in the coming years. Therefore, it is important to evaluate the risks of debris flows so that the potential loss of lives can be reduced in the future.

This research aims to develop a method to obtain the risk profile of mine debris flows along PR303 in Yingxiu area, and to conduct a case study on Pubugou debris flow to illustrate the methodology.

### **STUDY AREA**

The Pubugou Ravine is approximately 3.5 km from the epicentre of the Wenchuan earthquake, Yingxiu, in Sichuan Province, China (Fig. 1). The ravine is characterized by rugged mountains and deeply incised valleys. It has an area of 3.06 km<sup>2</sup> and elevations ranging between 1,100 m and 3,200 m. As shown in Fig. 1, the ravine consists of two sub-basins, namely the Xiezi Gully and the Wuming Gully. The Xiezi Gully extends 2288 m from the gully mouth to the topmost of the stream, having a local relief of 1580 m and a mean channel gradient of 28°. The Wuming Gully ranges from 1100 m to 1920 m, with a channel length of 977 m and a mean channel gradient of 27°.

The exposed lithology within the study area is mainly composed of four kinds of Proterozoic magmatic rocks; namely, diorite, biotitic granite, granodiorite and hornblende diorite. The maximum and mean annual precipitations within the study area are 1225 mm and 828 mm, respectively. Approximately 68% of the total precipitation falls between June and September. Zhang et al. (2012) and Chen et al. (2012) reported field investigations and numerical analysis of the landslide and debris-flow hazards in the study area.

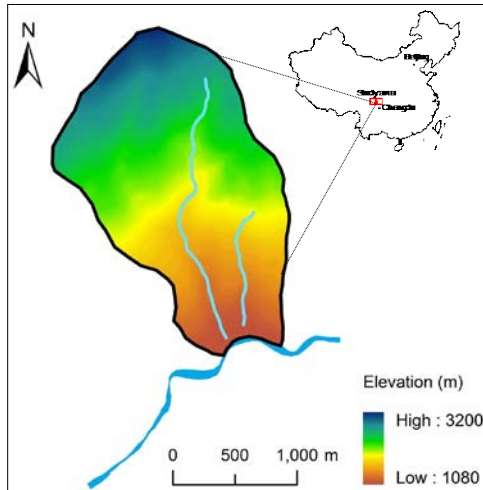


Fig. 1 Location of the study area

## HAZARDS IDENTIFICATION

During the Wenchuan earthquake, large-scale rock avalanches and landslides took place. A large amount of colluvium was retained on the hill slopes or deposited in the channels (Table 1 and Fig. 2). The landslide scars and the deposition zones together cover more than 50% of the terrain (Fig. 2). The volume of the deposited materials in the Pubugou Ravine was approximately 5.6 million m<sup>3</sup> (Table 2). After the Wenchuan earthquake, the hill-slope deposits are at a quasi-stable state under normal weather conditions. Upon a storm event during the rainy season, some of these deposits reactivate, slide down the slope and evolve into channel deposits. Some of the hill-slope materials may also evolve into hill-slope debris flows due to either post-sliding soil movements or bed erosion. The materials in the channels, no matter how far away from the highway, may gradually move to the gully mouth along the channel, which eventually run out as a channelized debris flow under rainstorm conditions. Several concrete-aggregate plants distributed near the gully mouth were buried by the runout debris, leading to a large number of fatalities (Fig. 3).

## ASSESSMENT OF HUMAN RISK POSED BY MINE DEBRIS FLOW IN PUBUGOU RAVINE

### Assessment model

In this section, the risk of debris flow in the Pubugou valley is assessed in terms of the potential loss of lives. The element at risk is taken as the passengers traveling on the road who may be buried by the runout debris should a debris flow event occur. The risk,  $R$ , is quantified by

$$R = p_f \times E \times V \quad (1)$$

where  $p_f$  = occurrence probability of debris flow;  $E$  = element at risk;  $V$  = vulnerability related to the run-out distance of the debris.

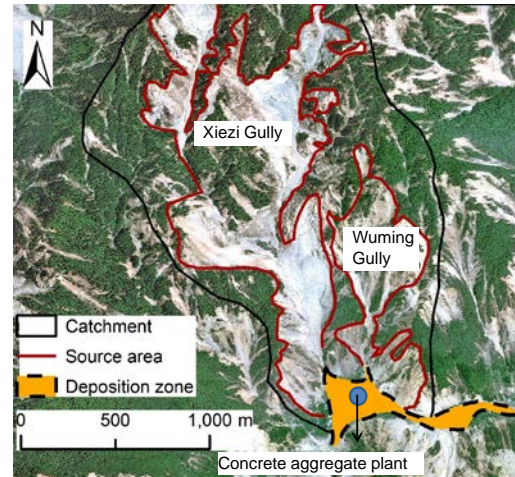


Fig. 2 - Distribution of the source materials within Pubugou Ravine

### Determination of occurrence probability

Rainfall is an essential predictor for the debris flow. It is well known that the correlation between the rainfall and the debris flow is the most widely used method to predict the occurrence of debris flow. Some precious rainfall-induced debris flow data had been collected, a statistical model (rainfall intensity – duration threshold model) is adopted to calculate the occurrence probability.

Logistic regression method is a useful tool for analyzing binary systems. The basic idea to predict the debris flow occurrence probability with logistic regression is to link the observed rainfall intensity and duration, i.e., the debris flow will either occurred or not occurred. The logistic regression model for debris flow prediction can be written based on Eq. (2) as follows

$$P_f = \frac{1}{1 + \exp\{-(b_0 + b_1 \ln I + b_2 \ln D)\}} \quad (2)$$

where  $b_0$ ,  $b_1$ , and  $b_2$  are unknown coefficients that can be calibrated using the maximum likelihood method. Based on the post-earthquake data including 27 occurred and 36 non-occurred debris flow cases, values for  $b_0$ ,  $b_1$ ,  $b_2$  are -7.776, 1.651, and 2.143, respectively.

According to the rainfall threshold model, the debris flow occurrence probability under the six rainfall conditions is obtained (Table 2). The empirical relations are statistically valid and provide threshold rainfalls for issuing warning signals.



### Landslide runout distance

The runout distance of a debris flow is the basis for estimating the element at risk and vulnerability of the landslide (as shown in Fig. 4). When a detailed study is not expected, the runout distance can be estimated using empirical relations. Here the relation proposed by Zhang et al. (2013) is adopted:

$$L_f = 2.04V^{0.18}H^{0.1}e^a \quad (3)$$

where  $L_f$  is the predicted runout distance (m);  $V$  is the volume of debris flow ( $m^3$ );  $H$  is the elevation difference of the mass movement (m);  $e^a$  is a discrete variable, which is expressed using a virtual discrete variable that represents either presence or absence of an attribute;  $e$  the natural logarithm base;  $a$  is 2.90 (Zhang et al. 2013).



Fig. 3 Runout debris destroyed the concrete aggregate plant near the gully mouth of Pubugou Ravine, and buried the road

Once the runout distance of debris flow is determined, the probability of runout debris reaching the element at risks ( $P_{Lf}$ ) can be quantified by applying Monte Carlo simulation, considering the uncertainties of the volume of debris flow (Table 2).

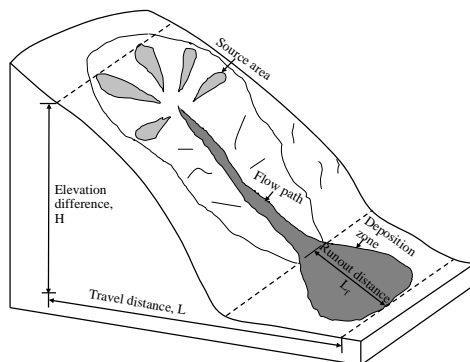


Fig. 4 Parameters related to runout distance of channelized debris flow

### Element at risk during normal operation of the road

The number of people,  $E$ , that can be buried depend on the traffic flow and the length of the roads that is buried by debris flows. Assuming a constant traffic flow over the road segment concerned,  $E$  may be expressed

$$E = \frac{WTn}{v} \quad (4)$$

where  $T$  = vehicles passing through the road per second;  $W$  = the length of road that is buried by the collapse of one or several deposits;  $v$  = average vehicle speed;  $n$  = average number of passengers in one vehicle.

According to the Grade-2 highways design requirements specified for PR303, The value of  $T$  is 1/6 vehicles per second and the design vehicle speed is 40 km/h at difficult parts of the road. The number of persons in a vehicle is 2.35, which is obtained during filed statistic analysis.

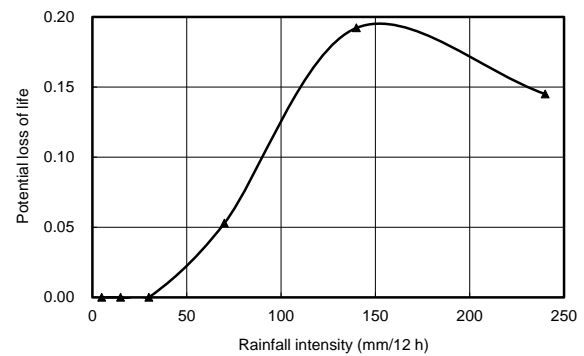


Fig. 5 Relationship between 12 hour rainfall and potential loss of life caused by channelized debris flows in Pubugou Ravine

### Vulnerability

In the study area, the width of the road is 8 m. As shown in Figs. 3 and 4, all the runout material that may run over the road, the calculated runout distance is 104 m. That means that all the debris will bury the road completely. Therefore, it is reasonable to assume that the vulnerability factor,  $V$ , is 1.0; i.e., the passengers will be buried once a landslide runs over the passengers (Finlay et al. 1999).

### Risk to human lives

Given the probability of occurrence, element at risk and vulnerability of debris flow, the human risk can be calculated using Eq. (1). The risk is measured

in terms of the potential casualty that could be caused by the debris flow.

Table 1 Volumes of loose materials deposited in channels and hill-slopes

		Xiezi Gully	Wuming Gully
Hill-slope deposits	Number of loose deposits	22	12
	Total area (km <sup>2</sup> )	0.64	0.23
	Volume (10 <sup>6</sup> m <sup>3</sup> )	3.63	1.31
Channel deposits	Total area (km <sup>2</sup> )	0.03	0.003
	Volume (10 <sup>6</sup> m <sup>3</sup> )	0.60	0.06
	Mean width (m)	36	13

The debris flow occurs within a short period so that all vehicles within the landslide area may be buried. In reality, once a debris flow occurred and the road is blocked by the first occurrence of landslide, the rest vehicles may attempt to escape from further landslides.

Table 2 Human risk of debris flow under different rainfall scenarios

Rainfall (mm/12 h)	240	140	70	30
Pf	0.99	0.77	0.12	0.0015
P <sub>Lf</sub>	0.96	0.74	0.23	0.0006
E	11.75	9.47	7.18	5.12
V	1	1	1	1
R	0.145	0.192	0.053	0

The risks at different rainfall scenarios are summarized in Table 2. The most serious human risk posed by the debris flow is 0.19 under the 140 mm/12 h rainfall condition followed by 0.15 under the 240 mm/12 h rainfall condition. The societal risk can also be graphically presented in the form of potential loss of life (PLL) (Fig. 5). The increment of risk is not significant when the rainfall intensity increases from 5 mm/12 h to 30 mm/12 h rain. However, the risk increases substantially when subject to a rain severer than 70 mm/12 h.

The societal risks of the debris flow under the six rainfall conditions can also be presented in an F-N curve in Fig. 6. One of the advantages of an F-N curve is that it provides additional information on the full range of credible fatal scenarios and the corresponding likelihood of occurrence (Wong et al. 1997). The societal risk acceptance criteria proposed by GEO (1998) are adopted in this paper as a benchmark, which is suitable for a study area with a reference toe length of 500 m or smaller. As shown in Fig. 6, the societal risks of the different rainfall scenarios are mainly located in the unacceptable region.

The impact of the debris flow on the traffic and concrete aggregate plant is significant, potentially involving over 10 casualties in a single slide event. To mitigate the risk, a warning system should be established to reduce the elements at risk when a storm occurs.

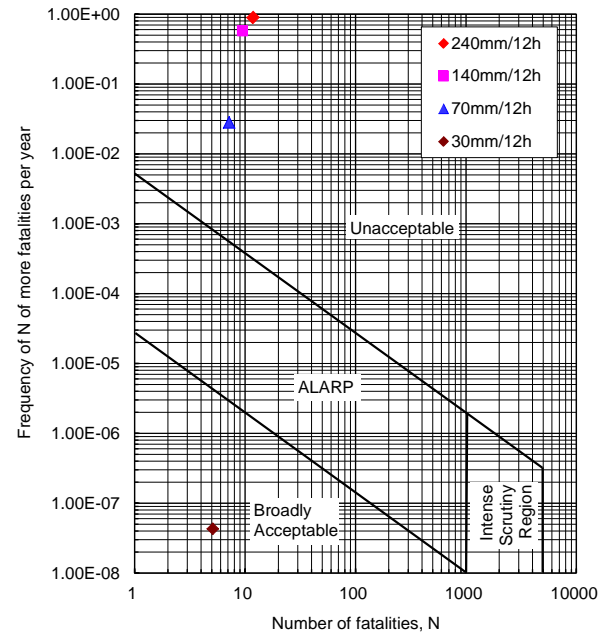


Fig. 6 F-N curves for debris flow in Pubugou Ravine after the Wenchuan earthquake in six rainfall scenarios

## CONCLUSIONS

The loose deposits formed during the 2008 Wenchuan earthquake on the steep terrains in the Pubugou valley near the epicenter are identified in a GIS platform. These deposits have very high probabilities of failure when subject to a storm and involve into a deadly debris flow. The risks to passengers on the road are also evaluated. Upon failure, the runout debris of debris flow in Pubugou Ravine could run out and beyond the road. Such debris flow could cause over 10 casualties in a single event under normal traffic flow conditions. The human risk under the conditions of 140 mm/12 h is higher than those under the other rain scenarios. Under the extreme rainfall condition of 240 mm/12 h, the failure probability is high and the consequence is very serious. However, the annual frequency is small; hence the final risk reflected in the F-N curve is not the worst. Such risk level is not tolerable; hence risk mitigation measures must be taken and an effective warning system established to reduce the risk level.

## ACKNOWLEDGMENTS

The work in this paper was supported by Sichuan Provincial Department of Transportation and Communications and the Research Grants Council of the Hong Kong SAR (Project No. 622210).

## REFERENCES

- [1] Chen, H.X., Zhang, L.M., Chang, D.S., and Zhang, S., 2012. Mechanisms and runout characteristics of the rainfall-triggered debris flow in Xiaojiagou in Sichuan Province, China. *Natural Hazards*, 62, 1037–1057.
- [2] Finaly, P. J., Mostyn, G. R., and Fell, R. 1999. Landslide risk assessment: prediction of travel distance, *Can. Geotech. J.*, 36, 556–562.
- [3] Geotechnical Engineering Office (GEO), 1998. Landslides and boulder falls from natural terrain: interim risk guidelines. GEO Report No. 75, Geotechnical Engineering Office, Hong Kong, 183 pp.
- [4] Jakob, M., and Hungr, O. 2005. Introduction of debris flow. In *Debris-flow Hazards and Related Phenomena*. Edited by M. Jakob and O. Hungr. Springer, Berlin, pp. 1-7.
- [5] Kang, Z.C., Lee, C.F., Ma, A.N, and Law, K.T. 2004. *China Debris Flow Studies*. Science Press, Beijing.
- [6] Takahashi, T. 1981. Estimation of potential debris flows and their hazardous zones. *Journal of Natural Disaster Science*, 3: 57-89.
- [7] Tang, C., Zhu, J., and Qi, X. 2011. Landslide hazard assessment of the 2008 Wenchuan earthquake: a case study in Beichuan area. *Canadian Geotechnical Journal*, 48: 128-145.
- [8] Wong, H. N., Ho, K. K. S, and Chan, Y. C. 1997. Assessment of consequence of landslides, in: *Landslide risk assessment-Proceedings of the Workshop on Landslide Risk Assessment*, Honolulu, Hawaii, USA, 19-21 February 1997, edited by: Cruden, D.M., and Fell, R., Balkema, Rotterdam, 111-149.
- [9] Xu, C., Xu, X.W., Yao, X., and Dai, F.C. 2013. Three (nearly) complete inventories of landslides triggered by the May 12, 2008 Wenchuan Mw 7.9 earthquake of China and their spatial distribution statistical analysis. *Landslides*, doi: 10.1007/s10346-013-0404-6.
- [10] Zhang, S., Zhang, L.M., Peng, M., Zhang, L.L., Zhao, H.F., and Chen, H.X. 2012. Assessment of risks of loose landslide deposits formed by the 2008 Wenchuan earthquake. *Natural Hazards and Earth System Sciences*, 12: 1381-1392.
- [11] Zhang, S., Zhang, L.M., Chen, H.X., Yuan, Q., and Pan, H. 2013. Changes in runout distances of debris flows over time in the Wenchuan earthquake zone. *Journal of Mountain Science* 10, 281–292.
- [12] Zhang, S., Zhang, L.M., and Thomas, G. 2014. Characteristics of Earthquake- and Rain-induced Landslides near the Epicenter of Wenchuan Earthquake. *Engineering Geology*, accepted.

## **A STUDY OF DYNAMIC SOIL STRUCTURE INTERACTION FOR PILED RAFT FOUNDATION WITH VARIABLE SUB SOILS**

Shukla S.J.<sup>1</sup>, Desai A.K.<sup>2</sup> and Solanki C.H.<sup>3</sup>

<sup>1</sup> Assistant Professor, Applied Mechanics Department, Sardar Vallabh Bhai National Institute of Technology, Surat, Gujarat, India E-mail: [sdv@amd.svnit.ac.in](mailto:sdv@amd.svnit.ac.in)

<sup>2</sup> Professor, Applied Mechanics Department, Sardar Vallabh Bhai National Institute of Technology, Surat, Gujarat, India, E-mail: [akd@amd.svnit.ac.in](mailto:akd@amd.svnit.ac.in)

<sup>3</sup> Professor, Applied Mechanics Department, Sardar Vallabh Bhai National Institute of Technology, Surat, Gujarat, India, E-mail: [akd@amd.svnit.ac.in](mailto:akd@amd.svnit.ac.in)

### **ABSTRACT**

The piled raft foundation system has recently been widely used for many structures, especially high rise buildings. In this foundation, the piles play an important role in settlement and differential settlement reduction, and thus can lead to economical design without compromising the safety of the structure. Foundation rafts are analyzed as a plate on elastic foundation with the representation of the foundation media using the Winkler idealisation. The elastic constant of the Winkler springs is derived using the sub-grade modulus. The post earthquake study of the structures reveals that the interaction of soil and foundation is playing a major role in the damage/response of structure. Perusal of literature reveals that very few investigations were done on the effect of variable sub soil on the behavior of structures supported on pile raft foundations. So in this research, an iterative dynamic analysis was performed using SAP2000 program to carry out three dimensional time history analysis of non-linear soil-foundation-building models under a great earthquake ground motions. The interaction between the soil and structure is represented by Winkler spring model. The obtained results confirmed that the dynamic characteristics of soil structure system should be recommended for conservative nonlinear seismic response of the high building since it mitigates of earthquake hazards.

**Keywords:** *Sub-grade modulus, Soil-Structure Interaction, Seismic Response, Time history analysis*

### **INTRODUCTION**

Piled raft foundations provide an economical foundation option for circumstances where the performance of the raft alone does not satisfy the design requirements. Under these situations, the addition of a limited number of piles may improve the ultimate load capacity, the settlement and differential settlement performance, and the required thickness of the raft. Buildings are susceptible to soil structure interaction effects due to the induced changes in the dynamic characteristics of soil during seismic excitation; particularly several buildings have been constructed on soft soil. Because of this detrimental effect, this paper aims at clarifying the soil structure interaction effect on the seismic response of buildings under strong ground motions to provide damage control and enhance the safety level of such buildings.

The load and deformation characteristics of the structural and geotechnical (soil) components of the foundations of structures can affect, and in some cases dominate, seismic response and performance. Recognizing this important fact, many structural engineers have included representations of foundation strength and stiffness in their seismic analysis models for many years. The modeling of the

soil and structural parts of foundations inherently accounts for the interaction of the soil and structure. There will also be energy losses due to internal friction of the soil. Because of these effects, the response of a structure on a soft foundation to a given earthquake excitation will, in general, be different from that of the same structure supported on a different sub soil. It is the influence of a soil structure interaction on the response of structures to earthquake motion that is the general subject of this paper.

### **BASIC CONCEPTS OF MODULUS OF SUBGRADE REACTION**

The concept of spring constant was first introduced by Winkler in 1867. He modelled flexible foundation, such as raft, to stand on an independent discrete spring elements or supports. In 1955, Karl Terzaghi, in his paper 'Evaluation of coefficients of subgrade reaction' proposed a method to estimate the magnitude of the spring constants. His approach, also known as subgrade reaction model, was then become popular and commonly used in the design of raft foundation.

In 1955, Karl Terzaghi (Liao, 1995) published a classic paper titled 'Evaluation of coefficients of

subgrade reaction', in which he presented recommendations for estimating the spring constants which have come to be commonly used to model the foundation sub grade in the analysis of mat foundations and other similar problems. Because of the complexity of soil behaviour, sub grade in soil-foundation interaction problems is replaced by a much simpler system called sub grade model. One of the most common and simple models in this context is Winkler hypothesis. Winkler idealization represents the soil medium as a system of identical but mutually independent, closely spaced, discrete and linearly elastic springs and ratio between contact pressure,  $P$ , at any given point and settlement,  $y$ , produced by it at that point, is given by the coefficient of sub grade reaction,  $k_s$  (Dutta and Roy 2002).

Starting with the pioneering work of McClelland and Focht (1958), beam-on nonlinear Winkler foundation (BNWF) models have been used for many years for analyzing the response of foundations, most notably piles, for static loads (Matlock, 1970; Cox et al., 1974) and dynamic loads (Penzien, 1970; Nogami et al., 1992; Boulanger et al., 1999). Key advantages of these models over continuum formulations lies in their ability to describe soil-structure interaction phenomena by one-dimensional nonlinear springs distributed along the soil-foundation interface. It is well-known that the modulus of the springs (also known as modulus of sub-grade reaction) is not uniquely a soil property, but also depends on foundation stiffness, geometry, frequency, response mode, and level of strain. A limitation of the approach relates to its one-dimensional nature. A spring responds only to loads acting parallel to its axis, so loads acting in a perpendicular direction have no effect on the response of the spring.

In this model the sub grade soil assumes to behave like infinite number of nonlinear elastic springs that the stiffness of the spring is named as the modulus of sub grade reaction. Nonlinear springs for shallow foundations have been used in conjunction with gapping and damper elements by Allotey and Nagggar (2003 and 2007) as well as Raychowdhury and Hutchinson (2009).

The direct method to estimate the modulus of sub grade reaction is plate load test that it is done with 30-100 cm diameter circular plate or equivalent rectangular plate (Reza & Janbaz, 2008). In general, the methods of determination of  $k_s$  can be classified as: [3]

- 1- Plate load test (Dutta and Roy 2002; Bowles 1998),
- 2- Consolidation test (Dutta and Roy 2002; Bowles 1998),
- 3- Triaxial test (Dutta and Roy 2002),
- 4- CBR test (Nascimento and Simoes 1957) and

- 5- Empirical and theoretical relations that are proposed by researchers (Bowles 1998; Elachachi *et al.* 2004).

Because of the limitation of available data and the uncertainty of soil condition, it was also roposed to use the empirical equations.

$$\text{Vesic} \quad k_s = \frac{0.65 E_s}{B(1-\nu_s^2)} \sqrt[1.2]{\frac{E_s B^4}{EI}}$$

The Vesic's equation clearly shows that the modulus of sub grade reaction depends not only on the width of the foundation,  $B$ , but also on the elastic parameters of soils,  $E_s$  and  $\nu_s$ , and on the shape factor of the foundation,  $I_p$ .

Table:- 1Range of modulus of subgrade reaction  
Use values as guide and for comparison when using approximate equations[1]

Soil		, kN/m <sup>3</sup>
Loose sand		48000 – 16000
Medium dense sand		9600 – 80000
Dense sand		64000 – 128000
Clayey medium dense sand		32000 – 80000
Silty medium dense sand		24000 – 48000
Clayey soil		
200<	$q_a \leq 200 \text{ kPa}$	12000 – 24000
	$q_a \leq 800 \text{ kPa}$	24000 – 48000
	$q_a > 800 \text{ kPa}$	> 48000

After broader idea of sub soil type's discussion, three major group of soil are selected for subsoil for the actual work problem. They are classified as under

The sub soils selected are c-soils-  $\phi$  soils and  $\phi$  soils. As c – soils the clayey soils with sub grade modulus 30000 kN/m<sup>3</sup>, as c-  $\phi$  48000 kN/m<sup>3</sup> and as  $\phi$  – soils medium dense sand with 70000 kN/m<sup>3</sup> modulus of sub grade reaction were selected and the further analysis was carried out and various outputs are compared for different sub soils as mentioned in above discussions.



Table :-2Values or value ranges for Poisson's ratio	
Type of soil	$\mu$
Clay, saturated	0.4 - 0.5
Clay, unsaturated	0.1 - 0.3
Sandy clay	0.2 - 0.3
Silt	0.3 - 0.35
Sand, gravelly sand	0.1 - 1.00
commonly used	0.3 - 0.4
Rock	0.1 - 0.4 (depends somewhat on type of rock)
Loess	0.1-0.3
Ice	0.36
Concrete	0.15
Steel	0.33

### PROBLEM STATEMENT

Foundation along with surrounding soil is considered for analysis. For analysis the building along with foundation was modelled as frame and shell element consisting of 9049 and 3305 elements. The Discretization of shell element was done at the rate of 1.2m x 1.2m with 0.3m of sub mesh

<b>Material properties:-</b> Grade of concrete :- M35 Poisson's ratio( $\mu$ ) :- as per the soil Type of pile :- friction pile Section of pile :- circular section
<b>Details of The Problem</b> Height - 90m Building Plane - 43.2 x 20.7m Column Dimension – 600mm x 600mm Beam Dimension – 250mm x 600mm Shear Wall Thickness – 300mm
<b>Foundation Data</b> Piled raft foundation Analyse Type – Flexible approach (Winkler's model) Thickness of raft –1 m , Area of raft – 1050.45 m <sup>2</sup> Pile Diameter, 1000 mm. Pile length (l)– 15m, 30m Spacing between piles :- 4.3 m atcentre,8.6 at edge Total no of piles:- 36 nos

A time history analysis was carried out using El Centro earthquake time history as shown in fig. 2

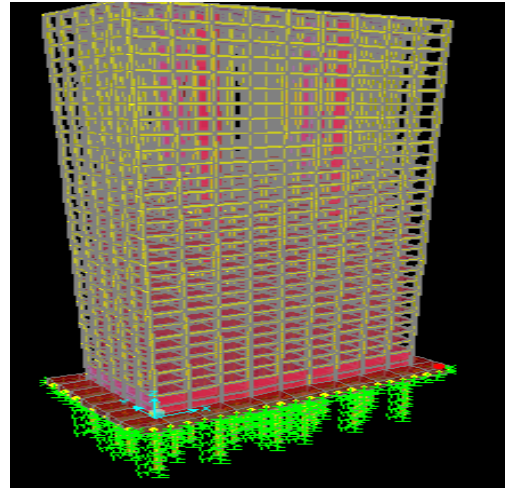


Fig:- 1 25 storey building supported on piled raft foundation

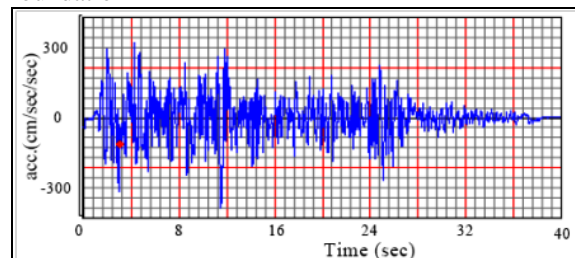


Fig:-2 A time history analysis was carried out using El Centro earthquake

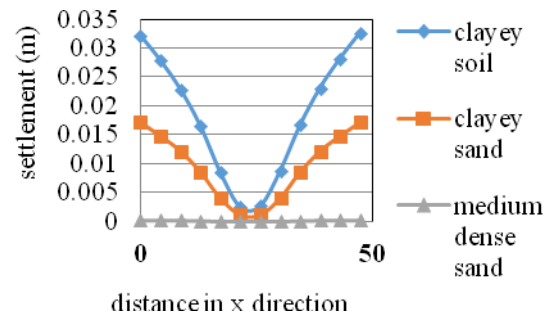


Fig: - 3 Settlement of raft in z direction for El Centro earthquake (l = 15 m)

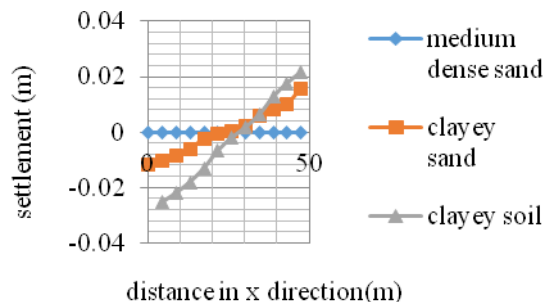


Fig: -4 For El Centro earthquake settlement in z direction l = 30 m



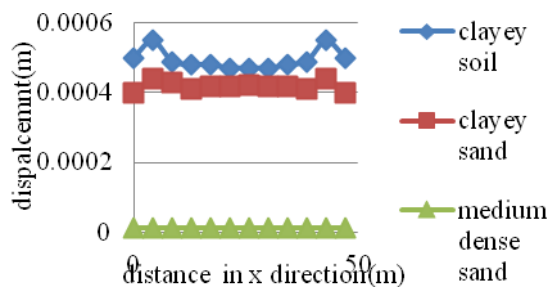


Fig. - 5 Displacement of raft in x direction for El Centro earthquake ( $l = 15$  m)

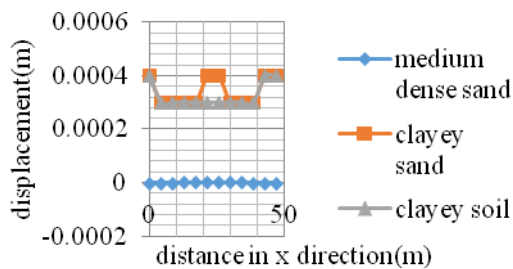


Fig. - 6 Displacement of raft in x direction for El Centro earthquake ( $l = 30$  m)

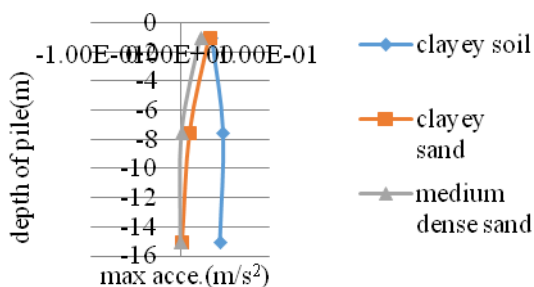


Fig. - 8 Maximum acceleration along the depth of pile for El Centro earthquake.  $l = 15$  m

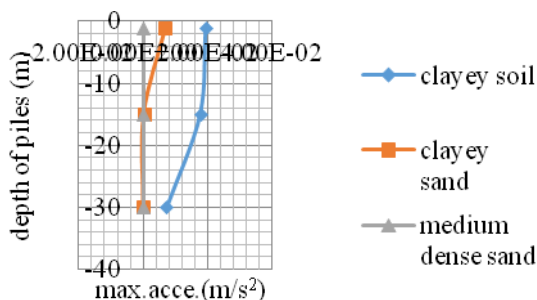


Fig. - 9 Maximum acceleration along the depth of pile for El Centro earthquake.  $l = 15$  m

## ANALYSIS AND RESULTS

### 1) settlement in raft for $l = 15$ m

c soil gives settlement in the range of 22 to 32 mm where as c- $\phi$  soil gives it in the range of 12 to 17 mm which shows reduction of 45 to 55 % and  $\phi$  soil

gave 1 mm to 2 mm which shows reduction of 99% structure remain steady in all sub soil conditions because settlement within permissible limits (65 to 100 mm for raft IS; 1904-1966) and for  $l = 30$  m , c- $\phi$  shows reduction of 65 to 70 % and  $\phi$  soil shows reduction of 99% structure remain steady in all sub soil conditions because settlement within permissible limits (65 to 100 mm for raft IS; 1904-1966)

### Displacement of raft for $l = 15$ m

c soil gives settlement in the range of 4 to 5 mm where as c- $\phi$  soil gives it in the range of 4 mm which shows reduction of 10 % and  $\phi$  soil gave 1 mm to 2 mm which shows reduction of 99% structure remain steady and for  $l = 30$  m c soil gives settlement in the range of 3 to 4 mm where as c- $\phi$  soil gives it in the range of 3 to 4 mm which shows reduction of 0 % and  $\phi$  soil gave .00 mm which shows reduction of 100% and structure remain steady.

## Conclusions

For medium duration earthquake the  $\phi$  soil behaves in desired manner. The settlement and displacement of raft gets reduced in considerable extent of and for short duration earthquake these results are even more effective considering all the three specified sub soil types. This exhibits excellent behaviour of medium dense sand ( $\phi$ ) soil as subsoil.

The frequency of occurrence of longer duration earthquake with high PGA is relatively very less but for medium to low duration earthquake it is very frequent. In that way performance of dense sand or medium dense sand as a sub soil results in reduced settlement and displacement to a considerable extent as compared to c and c- $\phi$  soil.

## References

- 1) Bowels J.E "Foundation Analysis and Design" 4th edition McGraw hill international edition.
- 2) Hamdy h. A, ahmedabd el "contribution of soil-structure interaction to Seismic response of buildings" journal of engineering sciences, assiut university, vol. 39, no. 4, pp. 715-750, july 2011
- 3) Indo-Norwegian Training Programme on Seismic Design of Multi-storey Buildings: IS 1893 vs. Euro code 8 May 26-28, 2014 at New Delhi
- 4) sadrekarimi J. Akbarzad M. "Comparative Study of Methods of Determination of Coefficient of Subgrade Reaction" ejge vol 14 bundle E, 2008
- 5) Kame .C.S., Sawant V.A. "A Parametric Study On Raft Foundation" The 12th International Conference of International Association For Computer Methods And Advances In Geomechanics (IACMAG) 1-6 October, 2008 Goa, India

***Construction Materials***

## LIME LEACHABILITY STUDIES ON STABILIZED EXPANSIVE SEMI-ARID SOIL

Arif Ali Baig Moghal<sup>1</sup>, Muawia A Dafalla<sup>2</sup>, Tamer Y Elkady<sup>3</sup> and Mosleh Ali Al-Shamrani<sup>4</sup>  
<sup>1, 2, 3</sup> Assistant Professor; <sup>4</sup> Professor; Department of Civil Engineering, College of Engineering,  
King Saud University, Riyadh

### ABSTRACT

The present study is aimed at examining the role of lime and the nature of leaching solution on the lime leaching characteristics of an expansive soil originating from the Kingdom of Saudi Arabia. Lime leachability studies were carried out in specially fabricated molds subjected to continuous leaching conditions. The specimens were compacted directly into specially fabricated perspex molds and cured for 7, 14 and 28 days under constant humidity conditions. In order to study the rate at which the calcium ions leach out from the lime treated clay matrix, water (leaching solution) was allowed to flow through the compacted specimen continuously for seven days and the resultant calcium concentration in the leachate was determined. The effects of various parameters like lime content, curing period and the pH of leaching solution on the lime leachability values has been studied. It is observed that, at a given lime content, the calcium concentration in the leachate reduces with curing period. Relatively higher amounts of lime leached under acidic conditions and the flow period does not affect the lime leaching patterns.

*Keywords: Expansive soil, Cementitious Compounds, Landfill, Lime, Lime leachability, Mineralogy.*

### INTRODUCTION

The expansive soils with their innate potential in exhibiting detrimental volume changes at different moisture conditions have been a cause of concern globally [1-2]. Major corrective measures to circumvent the problems posed by these soils include preloading [3], chemical treatment [4] and the use of cohesive non-swelling soil (CNS) cushion [5]. Lime is by far the most widely used chemical additive for the treatment of expansive soils. It has been proven suitable for clays or silty clays. In most of the applications such as structural fills, liners and landfill covers, road bases, and embankments etc., lime treated soils are often prone to the leaching of lime, which will reduce the lime content from the stabilized clay matrix affecting their performance [6]. Further, the lime leaching from the clay matrix severely hampers the rate at which pozzolanic reactions proceed, resulting in the increased material porosity as well as hydraulic conductivity and reduced mechanical properties. Hence, the durability of lime treated soils depends on the leachability of lime from the matrix. In this article, lime leachability studies on Al-Ghat soil, stabilized with lime have been conducted. The effects of various parameters like lime content, curing period and the pH of leaching solution on the lime leachability values have been studied. The mechanism with which the lime retention is achieved has also been brought out.

### MATERIALS

#### Soil

The tests were conducted on cohesive soil collected from Al-Ghat town, located 270 km to the Northwest of Riyadh (26° 32' 42" N, 43° 45' 42" E). Sampling was carried out at a depth of 3 m. The physical properties and chemical composition are reported in Tables 1 and 2 respectively. It has been classified as a high plasticity clay, as per unified soil classification system. The degree of expansivity was established based on measured modified free swell index (MFSI) values measured by means of sediment volume in carbon tetra chloride. For Al-Ghat the MFSI value was less than 1.5 cm<sup>3</sup>/g.

Table 1 Physical properties of the soil

Physical Property	Al - Ghat
Liquid Limit (%)	62
Plastic Limit (%)	30
Shrinkage Limit (%)	17
Plasticity Index (%)	32
Linear Shrinkage (%)	31
% Finer than 200 $\mu$ m	87.3
USCS Classification	CH

\*'USCS' refers to unified soil classification system;  
'CH' refers to clay with high plasticity.

Table 2 Chemical composition of the soil

Chemical Composition (%)	Al - Ghat
K <sup>+</sup>	1.1
K <sub>2</sub> O	1.3
Al	7
Al <sub>2</sub> O <sub>3</sub>	13.3
Si	9.8
SiO <sub>2</sub>	21
Ca <sup>+2</sup>	1.4
CaO	2

The predominant minerals present in the soil were determined by carrying out XRD using Bruker D8 Advance system. Sample was scanned from 2° to 60° (2θ) using 2.2kw cu anode long fine focus ceramic x-ray tube at a scanning rate of 1 degree per minute. Fig. 1 depicts comprehensive X-Ray Diffraction analysis. Apart from quartz, the predominant minerals include Kaolinite, Endelite, Dickite, Calcium sulfate hydrate and Calcium aluminium silicate.

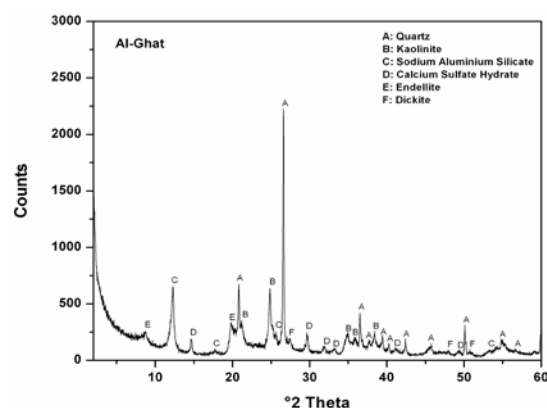


Fig.1. X Ray Diffraction analysis of Al-Ghat Soil

## Lime

Analytical grade Calcium Hydroxide, supplied by Winlab Chemicals, UK has been used in the present study.

## METHODOLOGY

### Lime leachability test procedure

The target lime content percentages of 2 and 4 were mixed to Al-Ghat soil on dry weight basis. The maximum proctor density values corresponding to each percentage of lime addition shown in Fig. 2 were determined by employing mini compaction test procedure developed by Sridharan and Sivapullaiah [7]. From Fig. 2, as the lime content increases the maximum dry density values were found to reduce with corresponding increase in optimum moisture

content for Al-Ghat. Remoulded samples with different lime dosages were tested for lime leachability in specially fabricated Perspex moulds, the details of which are shown in Fig. 3. The inside of the perspex mould was coated with a thin layer of silicon grease ensuring a good contact between the compacted material and the inner surface of the mould. All the tested samples were compacted to their maximum dry density and corresponding optimum moisture content values as per ASTM D5856-07 [8]. The top and bottom of the perspex mould were provided with perforated PTFE (Poly Tetra-Fluoro Ethylene) screens.

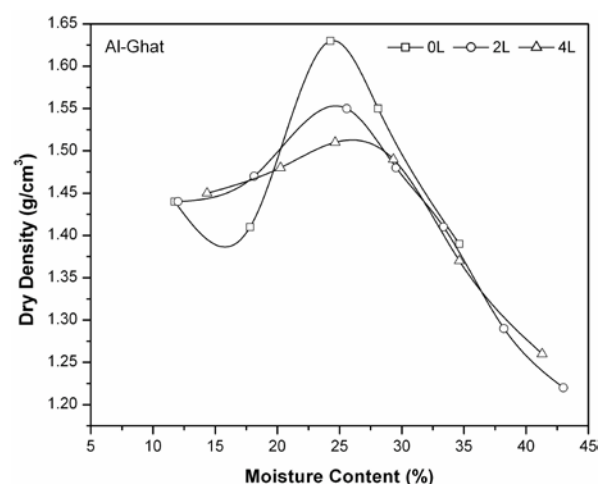


Fig. 2. Effect of lime content on the density characteristics of Al-Ghat soil

Chemically inert glass beads of 0.5 cm diameter were sandwiched between the two PTFE screens at both the ends ensuring uniform flow of water. The perspex mould with the compacted specimen was kept in a desiccator maintained at a relative humidity greater than 95%, and cured for 7, 14 and 28 days. After curing the specimen, the perspex mould was fitted into the position and connected to ultra-chemical resistant tubing (Tygon). Millipore grade water (for neutral water conditions) and acidified water (using 0.1N HNO<sub>3</sub> for pH 4 condition) was allowed to flow through the specimen and the entrapped air if any was removed using the air vent provided at the top of the perspex mould and leachate was collected in the graduated cylindrical jars. The concentration of the calcium in the leachate was determined immediately by PinAAcle 900T Atomic Absorption Spectrometer.

## RESULTS AND DISCUSSIONS

The leaching of calcium ions from pore solution forces the dissolution of calcium hydroxide which severely hampers the rate at which pozzolanic reactions proceed [2]. Hence in order to study the rate at which the calcium ions leach out from the lime treated clay matrix, water was allowed to flow

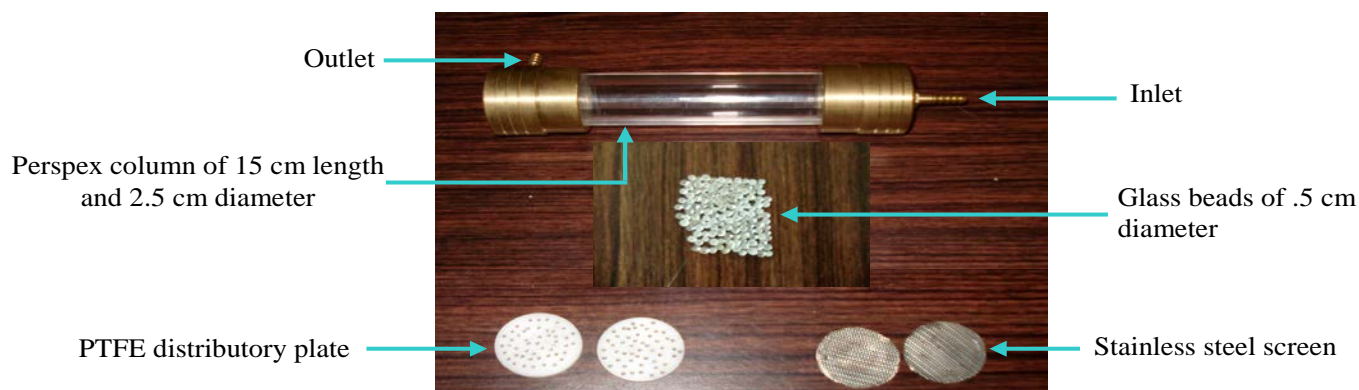


Fig. 3. Schematics of lime leachability test Apparatus

through the compacted specimen continuously for seven days.

The effects of various parameters like lime, curing period and the pH of leaching solution on the lime leachability behavior have been studied in detail. Fig. 4 shows effect of flow and curing periods on the lime leachability behavior of Al-Ghat soil under neutral conditions at 2% lime content. Prima facie, it appears that the flow duration does not affect the lime leachability and these values remain consistently same from the third day onwards. With increase in curing period, the leachability values are drastically reduced as lime is converted from more soluble form to less soluble form of calcium silicate hydrates. The cementation products formed at higher curing periods harden the clay matrix thereby reducing the lime leachability values considerably. Similar observations were noticed by Moghal and Sivapullaiah [6], and Moghal and Elkady [2] under identical conditions for different tested soils.

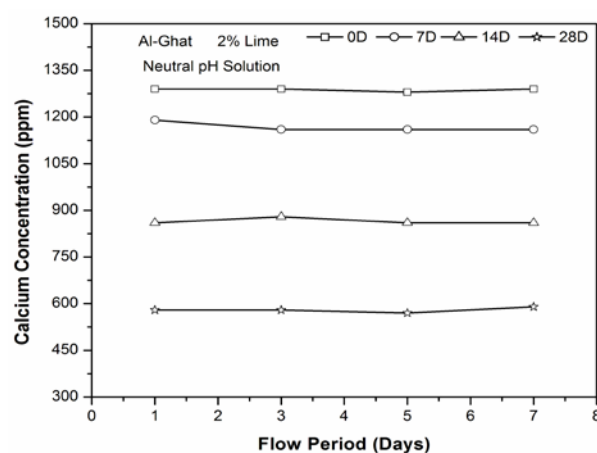


Fig. 4. Effect of flow period and curing period on the lime leachability behavior of Al-Ghat soil under neutral conditions at 2% lime content

With increase in lime content to 4%, the concentration of lime in the leaching fluid increases, particularly at lower curing periods as seen from Fig.

5. But with increase in curing periods, the solubility of silica from the clay is enhanced as the excess lime breaks the Si-O bonds in the silica rich phases of clay particles (Particularly Quartz as seen from Fig. 1). This dissolution of silica is better at 4% lime content compared to 2%, as it is nearer to the optimum lime content [9]. Apart from silica, alumina is also released from the mineral phase. This triggers a significant reduction in the lime leachability values at 4% compared to that at 2% lime addition at any given curing period.

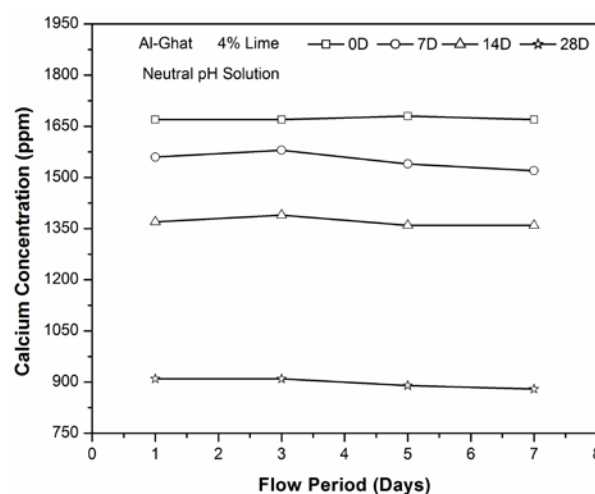


Fig. 5. Effect of flow period and curing period on the lime leachability behavior of Al-Ghat soil under neutral conditions at 4% lime content

#### Effect of Nature of Leaching Solution on the Lime Leachability Behavior

The surface of clay particles is rich with oxides of  $\text{SiO}_2$ ,  $\text{Fe}_2\text{O}_3$  and  $\text{Al}_2\text{O}_3$  as seen from Fig.1. When the pH of the leaching solution is reduced it severely hampers the dissolution of lime from clay matrix from these oxide surfaces. From Fig. 6, at 2% lime content, when the pH of the leaching solution was reduced to 4, lime leachability values increased to 61% compared to neutral solution at a given curing period. However with increase in curing period, there

is a significant reduction in the leaching of calcium ions from the stabilized matrix (Fig. 6).

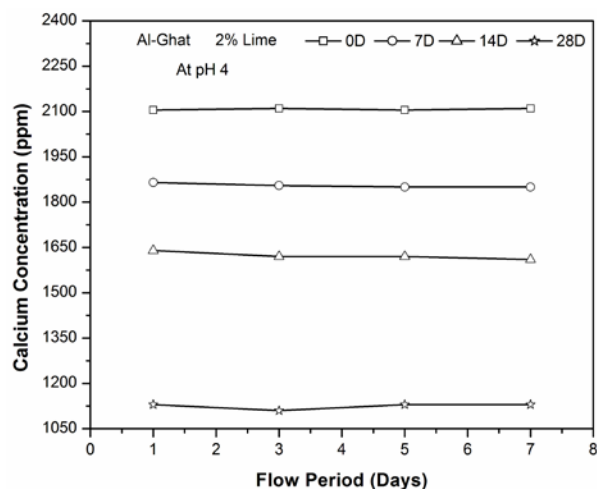


Fig. 6. Effect of flow period and curing period on the lime leachability behavior of Al-Ghat soil under acidic conditions (pH 4) at 2% lime content

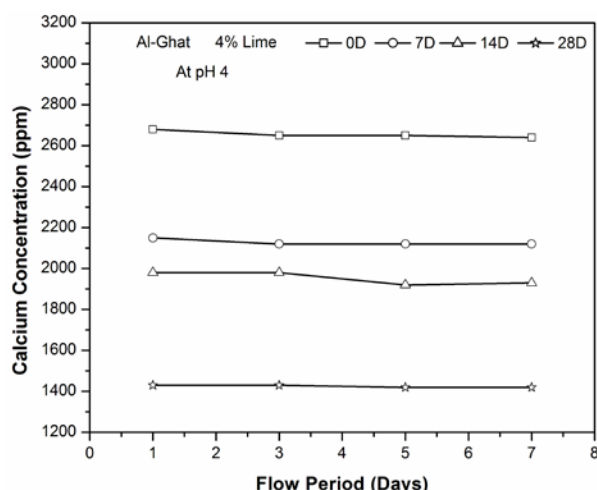


Fig. 7. Effect of flow period and curing period on the lime leachability behavior of Al-Ghat soil under acidic conditions (pH 4) at 4% lime content

Since soil lime reactions are time dependent, at lower curing periods, the cation exchange reactions (taking place between the ions such as sodium or potassium associated with the surfaces of the clay particles and calcium cations of the added lime) are predominant. This results in the modification of density of charged particles around diffused double layer. As a result when the pH of the leaching solution is reduced (around 4 in this case) the rate at which these cation exchange reactions occur are hampered, which result in increased release of calcium ions from the clay-lime matrix. This is particularly true at lower curing periods around 14 days as seen from Fig. 6. The

duration of flow period does not affect the lime leachability values (Fig. 6).

With increase in lime content to 4%, even at lower curing periods, apart from cation exchange reactions, flocculation reactions become predominant, which in turn hold the calcium ions intact, thereby reducing the lime leachability values at any given curing period (Fig. 7). Further at this lime content (4%) in addition to primary soil-lime reactions, secondary reactions (cementation and carbonation) are pronounced as well, where in the dissolved calcium ions react with silicate tetrahedral and aluminate octahedral sheets from the clay mineral lattices at their edges forming calcium silicate hydrate (CSH) and calcium aluminate hydrate (CAH) gels [10-12]. These cementitious gels are relatively in amorphous form at lower curing periods resulting at higher lime leachability values as seen from Fig. 7.

With increase in lime content from 2 to 4%, at a given curing period of 7 days, there is a 27% increase in lime leachability values, which is attributed to readily soluble gelatinous materials under aggressive environments (leaching solution pH 4). However with increase in curing period to 28 days, this difference in lime leachability values (at 2 and 4% respectively) reduces to 16.7%, as relatively more curing time is allowed which leads in the formation of cementitious compounds which are relatively crystalline in nature and are resistant to the acidity (pH 4) of leaching solution. Further, even at 4% lime content, the duration of flow period does not seem to affect the lime leachability values as seen from Fig. 7.

### Practical Importance of the Study

Chemically modified clays have great potential in the construction of base liners for waste containment facilities. One of the most overriding requirements for efficient functioning of a landfill liner material is to possess lower hydraulic conductivity values as it controls the migration of leachate and its toxic constituents into underlying aquifers or nearby rivers. In most of the cases, the pH of the leachate varies drastically in the acidic range which dictates the prevailing hydraulic conductivity and issues related to durability. The current study tries to simulate the acidic conditions a landfill liner might experience when it is constructed with chemically modified (lime treated) clay.

The amount of lime retained invariably reflects the long term performance and consequently addresses the issues related to the durability of the selected clay as a material for liner in the construction of a landfill. In this study, the ability of Al-Ghat soil to retain the stabilizer (lime) under aggressive leaching conditions is investigated and it is observed that even at pH 4, at varying lime contents, the amount of calcium leaching from the clay matrix is reduced, particularly when the samples cured (as



noticed from the curing period adopted in the study). Further, this study emphasizes and addresses the issues related to the use of locally available materials as a suitable choice for the construction of base liners for a landfills (both domestic and industrial).

## CONCLUSIONS

The durability of lime stabilized clays depends on the amount of lime retained in the clay matrix particularly when they are prone to leaching. The calcium leaching from the lime stabilized clay matrix severely affects the performance of the material and in most cases, the selected material may not meet the desired requirements. In this study, lime leachability studies on Al-Ghat soil, stabilized with lime were conducted. The effects of various parameters like lime content, curing period and the pH of leaching solution on the lime leachability values were studied. It was observed that lime leachability values increased with increase in lime content at any curing period. At a given lime content, the lime leachability values reduced with the increase in curing period as relatively more time is allowed for the formation of cementitious compounds.

When the pH of the leaching solution was reduced (pH 4), relatively higher lime leachability values were obtained. With increase in curing period, these gelatinous amorphous cementitious compound transform to crystalline form which resist the leaching of calcium due to their poor solubility. It was obvious that the flow duration does not affect the lime leachability pattern.

## ACKNOWLEDGEMENTS

This paper is a part of a research project that was supported by NSTIP strategic technologies programs, 11BU1489-02 in the Kingdom of Saudi Arabia. The authors would like to thank the Eng. Abdulla Bugshan Research Chair for Expansive Soils for providing the necessary facilities to carry out the experimental work.

## REFERENCES

- [1] Lu N, and Likos W, "Unsaturated Soil Mechanics", 2004, Wiley, New York.
- [2] Moghal AAB, and Elkady TY, "Durability Studies on Expansive Soils Treated with Lime," In the proc. of the International Conf. on Ground Improvement and Ground Control, 30th October to 2nd November 2012, held at Wollongong, Australia, 2012, pp.1187-1192.
- [3] Chen FH, "Foundations on expansive soils", 1988, 2nd Ed., Elsevier Scientific, Amsterdam, The Netherlands.
- [4] Puppala AJ, Wattanasanticharoen E, and Hoyos LR, "Ranking of four chemical and mechanical stabilization methods to treat low volume road subgrades in Texas", Transportation Research Record. 1819, Transportation Research Board, Washington, D.C., May. 2003, pp.63-71.
- [5] Sivapullaiah PV, Subba Rao KS, and Gurumurthy JV, "Stabilisation of rice husk ash for use as cushion below foundations on expansive soils", Ground Improvement, Vol. 8, No. 4, Jan. 2004, pp. 137-149.
- [6] Baig MAA, and Sivapullaiah PV, "Role of Lime Leachability on the Geotechnical Behaviour of Fly Ashes", International Journal of Geotechnical Engineering, Vol. 6, No. 1, Jan. 2012, pp. 43-51.
- [7] Sridharan A, and Sivapullaiah PV, "Mini Compaction Test Apparatus for Fine grained Soils", Geotechnical Testing Journal, Vol. 28, No. 3, May 2005, pp. 240-246.
- [8] ASTM D5856 – 07, Standard Test Method for Measurement of Hydraulic Conductivity of Porous Material Using a Rigid-Wall, Compaction-Mold Permeameter, 2007, West Conshohocken, Philadelphia.
- [9] Sivapullaiah PV, Sridharan A, and Bhaskar Raju KV, "Role of amount and type of clay in the lime stabilization of soils", Ground Improvement, Vol. 4, No. 1, Jan. 2000, pp. 37-45.
- [10] Eades JL, and Grim RE, "Reaction of Hydrated Lime with Pure Clay Minerals in Soil Stabilization," Highway Research Board, Washington, D.C. Bulletin No. 262, 1960, pp. 51-63.
- [11] Bell FG, "Lime Stabilization of Clay Minerals and Soils," Engineering Geology, Vol. 42, No. 4, July. 1996, pp. 223-237.
- [12] Moghal AAB, Al-Obaid AK, and Refeai TO, "Effect of Accelerated Loading on the Compressibility Characteristics of Lime-Treated Semiarid Soils", Journal of Materials in Civil Engineering, Vol. 26, No. 5, May 2014, pp. 1009-1016.

## BEHAVIOR OF AN EPDM GEOMEMBRANE 18 YEARS AFTER ITS INSTALLATION IN A WATER RESERVOIR

Manuel Blanco & Francisca Castillo<sup>1</sup>, Nathalie Touze-Foltz<sup>2</sup>, Bernat Amat<sup>3</sup>, Escolástico Aguiar<sup>4</sup>  
<sup>1</sup>CEDEX (Laboratorio Central de Estructuras y Materiales [Central Laboratory of Structures and Materials]),  
Ministries of Infrastructure and Agriculture and Food and Environment, Spain;  
<sup>2</sup>IRSTEA, France; <sup>3</sup>Firestone Building Products, Belgium; <sup>4</sup>BALTEN, Spain

### ABSTRACT

The purpose of this study is to evaluate the durability of an EPDM geomembrane installed 18 years ago in the water reservoir of El Boquerón (Canary Islands, Spain). To do so, samples were regularly taken from different places of the water reservoir. Samples were laboratory tested as follows: foldability at low temperature, static and dynamic puncture resistance, Shore-A hardness, tensile strength and elongation at break, seam strength and microscopic techniques. The obtained results confirm the EPDM geomembrane is still in good condition.

*Keywords: Geomembrane, Waterproofing, EPDM, Durability, Water Reservoir.*

### INTRODUCTION

In its report published in Paris in 1991, the International Commission of Large Dams indicated that the first geomembrane used in a hydraulic project was made from butyl synthetic rubber [1]. It was used in 1959 to waterproof the Kualapuu reservoir in Holokai (Hawaii).

In Spain, it was also this type of synthetic rubber which was originally used to waterproof water reservoirs. The use of this product began in the Ibi region, on the Mediterranean coast and extended across the entire country up to the Portuguese border, where Azud (small scale dam) in Matavacas (Huelva) was waterproofed in 1974 [2], [3].

Butyl rubber is a macromolecule which presents in its structure a large number of double bonds, of which the "TT" (trans-trans) chains are likely to be attacked by electrophilic reagents such as ozone and, consequently butyl geomembrane may experience significant degradation. The researchers looked for a synthetic rubber which was not susceptible to this phenomenon and they found this in the EPDM terpolymer. This macromolecule is comprised of three monomers: ethylene, propylene and diene, the latter being present in maximum concentrations of 5%. The first diene used was 1,3-butadiene which was then replaced by other types such as cyclopentadiene, considerably improving the initial performances [4].

### THE RESERVOIR

The El Boquerón reservoir is located in the area of Valle de Guerra, in the municipality of La Laguna in the north of the island of Tenerife (Figure 1 and Figure 2). The Canary Islands are located in a

geographical area where the maximum Global Solar UV Index in clear weather (Bournay E., 2007) is considered as high (index between 6.5 and 8.5). The technical characteristics of the reservoir are presented in Table 1.



Fig. 1 Geographical location of the reservoir.



Fig. 2 El Boquerón reservoir.

Table 1 Technical characteristics of the reservoir

Location	La Laguna
Capacity	51.747 m <sup>3</sup>
Height	11.0 m
Altitude	376.7 m
Perimeter	340.7 m
Thickness of EPDM geomembrane	1.50 mm
Area of the geomembrane laid	8,991 m <sup>2</sup>
Year of installation	1992

## FEEDBACK

### Initial Characteristics

Table 2 presents the initial characteristics of the EPDM geomembrane installed in the El Boquerón reservoir. The initial physical properties are compliant with the values declared on the manufacturer's technical data sheet. This data is consequently used as reference values for assessing the evolution over time of EPDM geomembranes.

Table 2 Initial Characteristics of the EPDM geomembrane

Characteristics (Standards)	Values
Average thickness (EN 1849-2)	1.51 mm
Shore A hardness (ISO 7619)	68
Foldability at -55 °C (EN 495-5)	Without fissures
Resistance to dynamic puncture* (EN 12691)	> 350 mm
Tensile Strength at break (ISO 527)	12.6 MPa
Stress at 300% elongation (ISO 527)	9.1 MPa
Elongation at break (ISO 527)	527%
Static puncture Resistance to puncture (EN ISO 12236)	
External surface	266 N/mm
Internal surface	266 N/mm
Depth of the plunger before perforation (UNE 104 317)	
External surface	40 mm
Internal surface	40 mm
Seam resistance by tensile-shear (EN 12316-2)	68 N/50 mm

### Evolution Over Time

After the EPDM geomembrane was installed, samples were taken regularly and tested in a

laboratory. Unless otherwise indicated, the values presented refer to samples taken from the north banks of the reservoir (bank most exposed to sunlight, and consequently most exposed to high UV and temperatures).

As far as the foldability test at low temperature is concerned (-55°C), no cracks or fissures were observed in the flexing area on the samples analyzed after 18 years of exposure. Similarly, during the dynamic puncture test, no fissures or any other type of degradation was noted in the impact area when the plunger was dropped from a height of 350 mm.

### Tensile Characteristics

Figure 3 shows the evolution in tensile strength at break, stress at 300% elongation and elongation at break over the 18 years since installation of the EPDM geomembrane. It can be seen that the tensile strength has not changed significantly, while elongation at break decreases noticeably. It can also be seen that the force necessary to obtain the same 300% elongation increases over time.

We note that after 18 years of exposure, the elastic elongation of the EPDM geomembrane is larger than 190% (remains elastic to breaking point), which is very high in comparison with the majority of thermoplastic geomembranes. This data is significant as the permissible elongation determines the ability of the geomembrane to adapt to differential settlements and irregularities in the soil and therefore defines its puncture resistance in real conditions.

The decrease in elongation at break and increase in stress at 300% elongation in the period is explained by the fact that, in the case of EPDM, during the oxidation phenomenon (induced by the temperature and UV exposure), the combination reactions of the carbon chains (cross-linking) has a prevails upon the cleavage reaction of the principal carbon chain [5]. Consequently, a decrease in molecular mobility and an increase in molecular mass can be seen [5]. These reactions are similar to the process of curing used during EPDM geomembrane production.

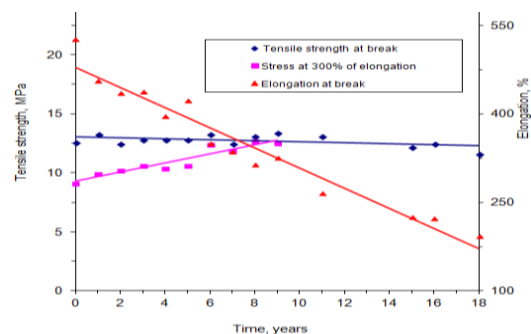


Fig. 3 Evolution over time in tensile strength and elongation at break, stress at 300% elongation.

### Shore A Hardness

The Shore-A hardness value has increased over time as shown in Figure 4. The increase in the Shore-A hardness can be explained by the decrease in molecular mobility as explained in the Section of the Initial Characteristics.

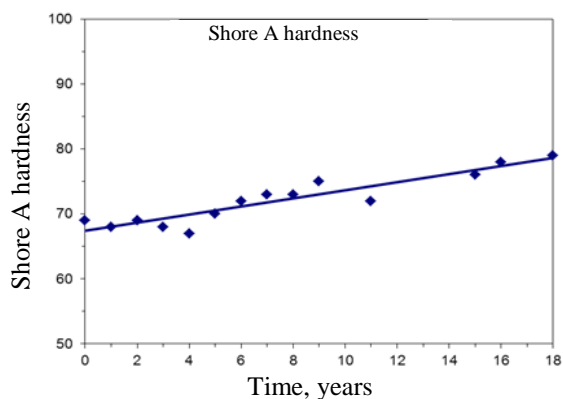


Fig. 4 Change in the Shore A hardness over time.

### Resistance to Puncture

Figures 5 and 6 respectively present the static puncture resistance and the distance travelled by the plunger before perforation. The distance travelled by the plunger before perforation is a measurement which allows for the evaluation of the resistance to puncture in actual conditions as it gives an idea of the adaptability of the geomembrane to the soil conditions. The resistance to puncture stays fairly constant in time (this is confirmed by samples taken after 21 years of exposition in this same water reservoir). On the other hand, the distance travelled by the plunger before perforation decreases accordingly given the decrease in molecular mobility (the same phenomenon that explains the decrease in elongation at break). It should be noted that this last value (27 mm after 18 years) remains very high and well above the measurements usually recorded on the vast majority of thermoplastic geomembranes [6].

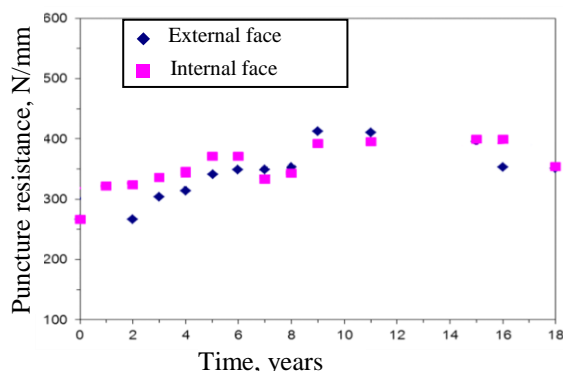


Fig. 5 Evolution in the resistance to static puncture over time.

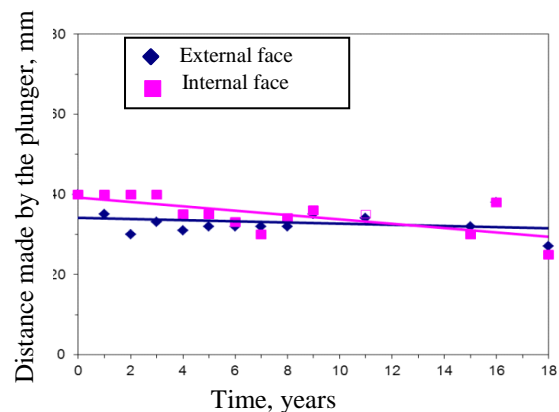


Fig. 6 Evolution of the depth of the plunger before perforation over time.

### Seam Resistance

After 18 years of exposure, the value for shear resistance of seams is 645 N/50 mm. Figure 7 illustrates that, during the first 8 years, the measurements for peel resistance of seams were relatively variable. The measurements taken in the following 10 years are more consistent and show that peel resistance is fairly constant.

The variability of peel measurements is explained in part by the seaming method used at the time that consisted of applying a butyl based glue for which uniform application was not guaranteed. This is one of the reasons why, for a number of years already, butyl glue has been replaced by other systems such as self-adhesive tape which ensures better quality consistency.

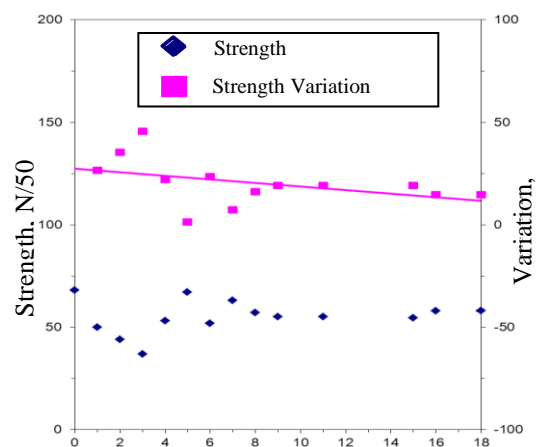


Fig. 7 Evolution of peel resistance of seams over time.

### Microscopic Analyses

Observations under reflection optical microscopy (magnified 40 times) and by scanning electron microscopy (magnified 90 times) have been

conducted according to the conditions documents in the literature [7] for the purpose of evaluating the condition of the geomembrane surface 18 years after installation (figure 8).

If we take into account the condition of the surface of an EPDM geomembrane that has not been exposed [8], we can see under reflection optical microscopy that after 18 years, the internal and external surfaces of the geomembrane seem to be in a good condition, with the internal surface presenting the best state of condition.

The scanning electron microscopy shows that eighteen years after installation of the geomembrane, the presence of a microporous structure can be detected confirming a slight degradation of the internal surface of the geomembrane. The external surface also presents some microcracks.

These microcracks seem relatively superficial and do not affect the mechanical resistance of the geomembrane, as proven in the evolution of the resistance at break and puncture examined above. This is explained by the highly cross-linked network of the EPDM geomembrane which distributes loads evenly across all carbon chains and limits the diffusion of potentially degrading elements [9].

These observations are to be compared with the results of the study on the surface condition conducted by Soriano et al. (2012) looking at different types of geomembranes. This study concluded that the impact of UV exposure is visible on these organic materials and that it is more significant on thermoplastic geomembranes than thermostable geomembranes such as synthetic rubbers [7].

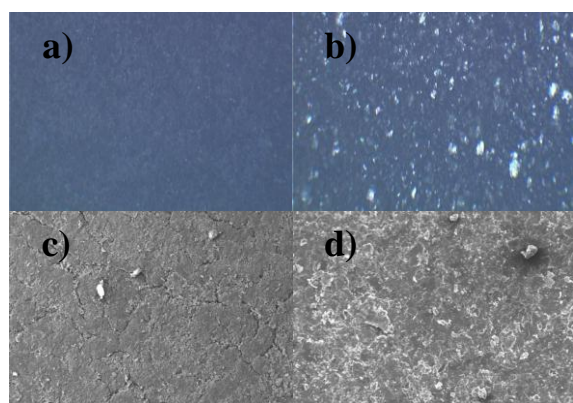


Fig. 8 18 years of exposition – microphotographs:  
- x40 of the (a) external surface and (b) internal surface taken using reflection optical microscopy.  
- x90 of the (c) external surface and (d) internal surface, taken using scanning electron microscopy.

### Influence of the Sampling Area on Samples

For the purpose of knowing the condition of the EPDM geomembrane in other areas apart from the

north bank, samples were also taken from the bottom (less exposed, due to protection from water) and the bank on the south side of the reservoir. Results obtained are presented in Table 3.

Regardless of their orientation and their degree of exposure, all samples analyzed after 18 years show a similar evolution in their mechanical properties. It is systematically observed that tensile strength is more or less constant, that elongation at break and the distance travelled by the plunger before perforation decreases significantly and that Shore-A hardness and resistance to static puncture increases over time. The results also show that the more apparent signs of ageing are observed on the samples taken from the north bank; the area that receives the most significant amount of solar radiation.

Table 3 Characteristics of the geomembrane according to exposure 18 years after installation

Characteristics	Ref.	Bank		Bottom
		N	S	
Tensile Strength, (MPa)	12.6	11.6	12.9	10.0
Elongation at break (%)	527	193	271	255
Resistance to puncture (N/mm)	266	351	367	371
Depth of the plunger before perforation (mm)	40	27	30	34
Shore A hardness	69	79	78	80
Seam resistance by tensile-shear (N/50 mm)	68	58	60	45

### CONCLUSION

The results obtained during the periodic inspection of the EPDM geomembrane installed in the El Boquerón reservoir allows us to draw the following conclusions:

- Both foldability at low temperature (-55°C) and resistance to dynamic puncture showed no cracks, breaks or any other indication of degradation after conducting the tests, proving the good state of conservation of the EPDM geomembrane 18 years since its installation;
- The tensile resistance that does not change significantly over the years; whereas elongation at break reduces significantly, a characteristic behavior of thermostable materials, as a result of the increase in the number of links between carbon chains (cross-linking); elastic elongation is larger than 190% after 18 years of exposure, which is very high for a geomembrane; this last property provides important information on the ability of the geomembrane to adapt to differential settling and irregularities in the soil;



- The Shore A hardness measurements increase over time; this is a consequence of the increase in the level of cross-linking in the geomembrane which reduces molecular mobility; the resistance to puncture is fairly constant and the distance travelled by the plunger before perforation, a measurement that allows us to evaluate the resistance to puncture in actual conditions, decreases over time; however, the value obtained after 18 years' exposure (27 mm) is greater than the measurement for the majority of thermoplastic geomembranes used in waterproofing;
- The shear resistance of the seams, testament to the quality of the seams, indicates that the seams between the panels are correct; the values for peel resistance of seams are relatively low and variable, given the use of an old seaming method which consisted of applying a butyl based glue to the seam area;
- The microphotographs taken by optical and scanning microscopy show a material in a good state of conservation; only micropores and some microcracks were detected but we note the complete absence of craters, fissures and microcracks;
- No significant differences in condition were observed between the samples taken from the bottom (covered by water) and the samples taken from the top of the banks (exposed to weather); the area most affected by ageing was the zone located on the north bank; given that the reservoir is located in the northern hemisphere, the north bank is the one facing the equator and consequently receives the largest amount of solar radiation (UV and temperature) which is responsible for the degradation of organic material.

After 18 years of exposure to demanding weather conditions (high temperature and UV rays), the EPDM geomembrane used in the El Boquerón water reservoir has retained the mechanical properties which are still well suited to this

## REFERENCES

- [1] International Commission on Large Dams. "Watertight Geomembranes for Dams". Paris: State of the Art Bulletin ICOLD N° 78, 1991.
- [2] Cea J.C. de, Asanza E., Blanco M. "Face Protection: Geomembranes Lining vs. Paint Coating". Montreal, Proc. 21 International Congress on Large Dams, 2003.
- [3] Blanco M., Castillo F., García F., Soriano J. "Las geomembranas sintéticas en la rehabilitación y mantenimiento de paramentos de presas. II". In Romeo et al. (eds.). London, Dam Maintenance and Rehabilitation Taylor & Francis Group, 2010, pp. 335-341.
- [4] Davis J. A., Hoff J. L., Kalwara J. J., Kane E. G. "A review of EPDM Systems Development Proc". Copenhagen, X International Congress: International Waterproofing Association, 1998, pp. 263-274.
- [5] Kumar A., Commereuc S., Verney V. "Ageing of elastomers: a molecular approach based on rheological characterization"; Polymer Degradation and Stability 2004; 2004, 751-757
- [6] Blanco M., Aguiar E., Castillo F., Soriano J., Noval A.M., Touze-Foltz N., Pargada L., Rico G., Aguiar E. "Comparative study of three different kinds of géomembranes (PVC-P, HDPE, EPDM)". BESANCON, 5th European Geosynthetics Congress, 2012, Volume 2. 25 030.
- [7] Soriano J., Blanco M., García M. A., Aguiar E., Leiro A., Rubín de Célix M., Mateo, B., Burgos J. Optical and scanning electron microscopy as advanced analysis methods to determine the condition of geosynthetic geomembranes. Valencia, Proc. Eurogeo5, 2012.
- [8] Blanco M., Aguiar E., García F., Vara T., Soriano J., Castillo F. "État de la géomembrane en EPDM de la retenue d' "El Golfo" dans l'île d'El Hierro (Îles Canaries)". Tours, Proc. 8eme Rencontres Géosynthétiques, 2011, 283-293.
- [9] Scott G. "Degradable polymers, Principles and applications, 2nd edition"; Kluwer Academic Publishers; 2002, pp.18-19.
- [10] EN 1849-2. Feuilles souples d'étanchéité - Détermination de l'épaisseur et de la masse surfacique - Partie 2 : feuilles d'étanchéité de toiture plastiques et élastomères. Bruxelles, Comité européen de normalisation.
- [11] EN 495-5. Feuilles souples d'étanchéité Détermination de la pliabilité à basse température. Bruxelles, Comité européen de normalisation.
- [12] EN 12691. Feuilles souples d'étanchéité - Feuilles d'étanchéité de toitures bitumineuses, plastiques et élastomères - Détermination de la résistance au choc. Bruxelles, Comité européen de normalisation.
- [13] EN ISO 527. Plastiques Détermination des propriétés en traction. Bruxelles, Comité européen de normalisation.
- [14] EN ISO 7619. Caoutchouc vulcanisé ou thermoplastique - Détermination de la dureté par pénétration - Partie 1 : méthode au duromètre (dureté Shore). Bruxelles, Comité européen de normalisation.
- [15] EN ISO 12236. Essai de poinçonnement statique (essai CBR). Bruxelles, Comité européen de normalisation.
- [16] EN 12316-2. Feuilles souples d'étanchéité - Détermination de la résistance au pelage des joints - Partie 2 : feuilles d'étanchéité de toiture



plastiques et élastomères. Bruxelles, Comité  
européen de normalisation.

[17]UNE 104 317. Matériaux synthétiques.  
Determinación del recorrido del punzón antes de

la perforación en geomembranas sintéticas  
impermeabilizantes instaladas en balsas.

## **UNCERTAINTY OF BACK-CALCULATED VALUES IN PAVEMENT OVERLAY DESIGN WHEN USING THE FWD DEVICE**

Moshe Livneh<sup>1</sup>

<sup>1</sup> Civil and Environmental Engineering Faculty, Technion-Israel Institute of Technology, Haifa, Israel

### **ABSTRACT**

Several pavement-design methods, among them the Israeli Flex-Design method for interurban roads and the new American FAARFIELD method for runways and taxiways, still rely on the subgrade CBR value together with its equivalent resilient modulus. The latter is determined from the CBR value by a predefined correlative equation. The use of these two methods for overlay or reconstruction design involves a determination of the existing subgrade CBR value by various in-situ testing methods, including the Falling Weight Deflectometer (FWD). For that test, the subgrade CBR value is calculated from the FWD back-calculated subgrade resilient value. Using just one of the predefined equations, however, makes the required design very uncertain. This uncertainty is demonstrated in the paper by two runways, one constructed with a conventional flexible pavement and the second with an all-asphaltic pavement. Both structures were designed for the same clayey subgrade with a design CBR value of 5%. Immediately after construction, both structures were tested by the FWD apparatus. For both structures, the 15-percentile MODULUS back-calculated subgrade resilient modulus yielded a high value for the case of an infinite depth to bedrock and a low value (about one half to one third of the infinite depth case) for the case of a back-calculated depth to bedrock. The consequences of these and additional outputs given by the old AASHTO and EVALIV forward-calculation procedures are discussed in light of the uncertainty they introduce into pavement overlay design.

*Keywords: Back-calculation, CBR, Forward-calculation, FWD, Overlay-design, Resilient-modulus*

### **INTRODUCTION**

Pavement-layer and subgrade moduli may be obtained from deflection-basin back-calculation analyses through any of a variety of calculation programs. These differing programs, however, render non-uniform solutions and, in certain cases, may even lead to erroneous conclusions. Moreover, for any given program, the initial input assumptions influence the moduli outputs, a situation that obviously puts into doubt every proposed program code. It also raises once more the following question: Which calculation program is the most applicable?

Even when a seemingly applicable calculation program is utilized, uncertainties associated with its outputs still exist. These uncertainties are well formalized in [1]: "It is, however, stressed that special care must be taken when trying to interpret deflection data to determine in situ pavement-layer properties. It is well known that real highway materials are neither truly linearly elastic nor are the in situ material properties and geometry uniform. Owing to generally poor problem conditioning, small anomalies between actual and assumed responses can lead to considerable differences between the predicted and actual moduli. These differences can be best minimized by incorporating judgment into a back-calculation algorithm." A similar quotation is given in [2]: "Experience obtained from the backcalculated programs shows that the

projects moduli may vary for each program. It is therefore necessary to use engineering judgment to ensure the calculated moduli are reasonable."

In contrast to those two quotations, the following quotation from [3] states: "The FWD is capable of providing accurate information on the stiffness of existing pavements using the EFROMD and ELMOD programs. The FWD test procedure is fast and accurate, and the stiffness values produced are considered to be more acute than field CBR test methods." Since its publication, many other technical papers have contradicted this quotation; see, for example, the findings of [4].

The present paper concentrates only on the consequences of obtaining subgrade moduli from deflection-basin back-calculation or forward-calculation analyses. (Note: pavement granular-layer moduli are discussed in an earlier paper; see [5]). The updated MODULUS 6.0 program [6] served the back-calculation analysis, as it is the leading program in Israeli practice. In addition, both the EVALIV [7] and the old AASHTO [8] programs served the forward-calculation analysis. The introduction of these two forward-calculation programs in this present paper stemmed from the attempt to follow the content of the following quotation: "Because of the unavoidable uncertainties involved in the fundamental assumptions of the theories and in the numerical values of the soil constants, simplicity is of much greater importance

than accuracy. If a theory is simple, one can readily judge the practical consequences of various conceivable deviations from the assumptions and can act accordingly.” [9]

Another issue dealt with in the present paper is a determination of the subgrade CBR value from the above back-calculated or forward-calculated subgrade resilient modulus. This calculation is necessary, as the Israeli Flex-Design method [10] for the flexible pavement design of inter-urban roads and the new American FAARFIELD method [11] for the flexible pavement design of runways and taxiways still use the subgrade CBR value as a major input in both new pavement and overlay/reconstruction calculations. This required CBR value is calculated from the back-calculated or forward-calculated subgrade resilient modulus by using a pre-defined transformation equation specific for each method.

Unfortunately, the above-mentioned procedure of obtaining the CBR value also leads to uncertain results as fully discussed in [12]. Thus, issues connected to both a correct determination of the sub-base resilient modulus and a correct transformation of the latter into the CBR value will be discussed in detail in the sections to follow.

## OBJECTIVES

The aforementioned issue of uncertainty will be demonstrated here by two runways, one constructed with a conventional flexible pavement having a total thickness of 1,560 mm, and the second with an all-asphaltic pavement having a total thickness of 900 mm. Both structures were designed for (a) a subgrade CBR value of 5% and (b) the same aircraft loading. Immediately after construction, both structures were tested by the FWD apparatus. Thus, in light of the foregoing background and the two recent FWD measurements, the objectives of this paper are as follows:

- Presentation of MODULUS back-calculated subgrade resilient modulus results, together with their consequences, from the two FWD measurements when the depth to bedrock is assumed to be (a) infinite and (b) equal to a back-calculated value.
- Comparison of the MODULUS back-calculated results with both the old AASHTO and the EVALIV forward-calculated subgrade resilient modulus results, including their consequences, from the above two FWD measurements.
- Elaboration of the uncertainty associated with a determination of the design subgrade modulus and the design subgrade CBR from the FWD measurements for the pavement-overlay design.

Finally, the paper offers a tentative procedure for determining the required stiffness and strength parameters for an existing subgrade, based on FWD pavement-surface deflection measurements.

## BACK AND FORWARD CALCULATIONS

As previously mentioned, the MODULUS 6.0 program [6] served to back-calculate resilient moduli of the subgrade and pavement layers for the two given structures. These back-calculations assumed that the depth to bedrock was (a) infinite and (b) equal to a back-calculated value.

Figure 1 shows the inequality of the subgrade resilient moduli outputs for the two given structures, the higher values being associated with the assumption of an infinite subgrade depth to bedrock. In addition, Fig. 2 shows the influence of the back-calculated depth to bedrock on the ratio of the back-calculated subgrade resilient moduli. This ratio is defined as the modulus obtained for the infinite-depth case divided by the same modulus obtained for the back-calculated depth. This figure clearly demonstrates the reduction of the ratio of the back-calculated subgrade resilient moduli with the increase of the back-calculated depth. Obviously, for a back-calculated depth approaching infinity, these two types of back-calculations should yield the same results.

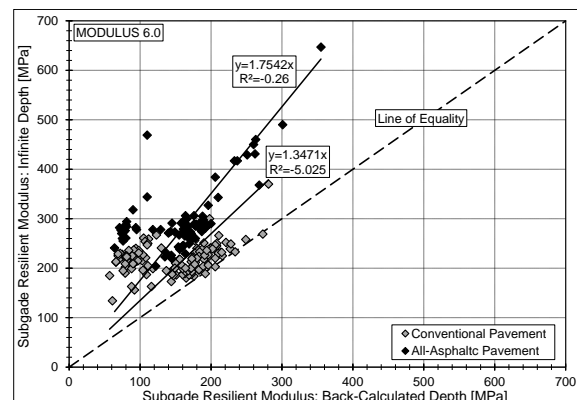


Fig. 1 Subgrade modulus for the case of infinite depth to bedrock versus subgrade modulus for the case of back-calculated depth to bedrock: MODULUS 6.0 outputs for the two given structures

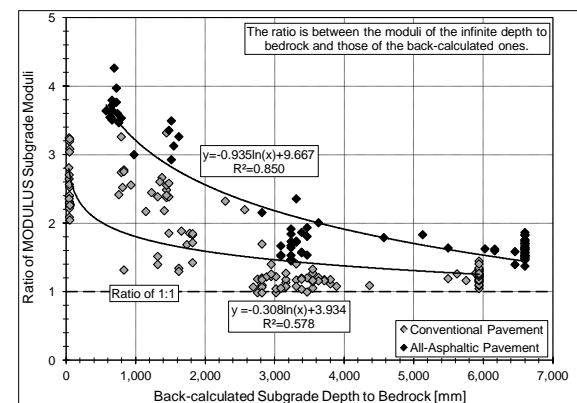


Fig. 2 Ratio of MODULUS back-calculated subgrade moduli with an infinite depth to bedrock to those with back-calculated depth versus the latter depth for the two structures

In addition, it can be stated that (a) the low values of the back-calculated subgrade depth to bedrock of Fig. 2 are very unrealistic; and that (b) the characteristics of the results associated with the conventional pavement are entirely different from those associated with the all-asphaltic pavement although the characteristics of the subgrade of both pavements are the same. All these facts point to the high rate of uncertainty of the moduli outputs involved in these back-calculation procedures.

Figure 3 depicts a comparison of the MODULUS back-calculated subgrade resilient moduli with the EVALIV forward-calculated moduli for the two given structures. The figure indicates that the EVALIV results are well correlated with the MODULUS results of the subgrade infinite depth to bedrock; i.e.,  $R^2=0.597$  for the conventional pavement and  $R^2=0.995$  for the all-asphaltic pavement. These findings are expected, as EVALIV also assumes an infinite depth to bedrock.

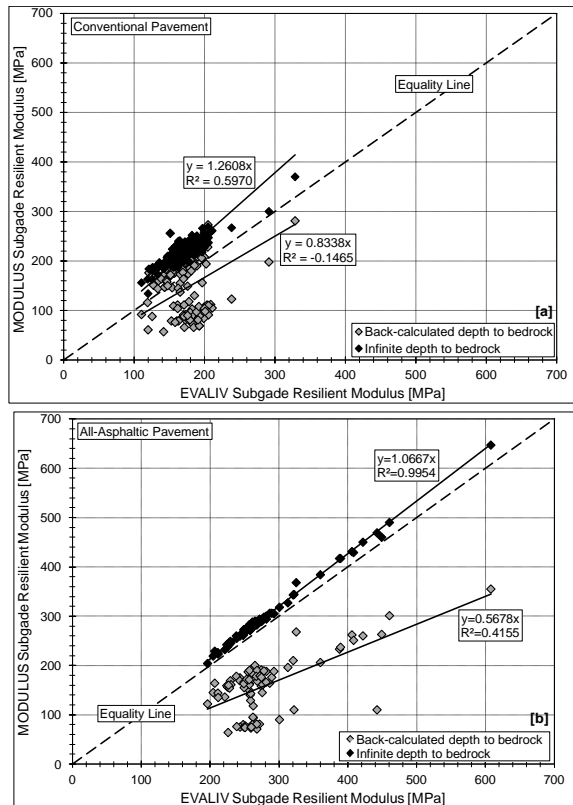


Fig. 3 MODULUS subgrade modulus for both cases of infinite and back-calculated depth to bedrock versus the old EVALIV subgrade modulus for (a) the conventional pavement and (b) the all-asphaltic pavement

Figure 3 also indicates that the ratio of the subgrade resilient modulus, obtained by dividing MODULUS by EVALIV, varies between 1.07 and 1.26 (i.e., around the expected value of 1.0) for the case of infinite subgrade depth to bedrock, and from 0.57 to 0.83 for the case of subgrade back-calculated depth to bedrock. The first value in each case relates

to the all-asphaltic structures, and the second values to the conventional structure.

Figure 4 depicts a comparison of the MODULUS back-calculated subgrade resilient moduli with the old AASHTO forward-calculated moduli when, in Eq. (1),  $C_a$  equals 0.33.

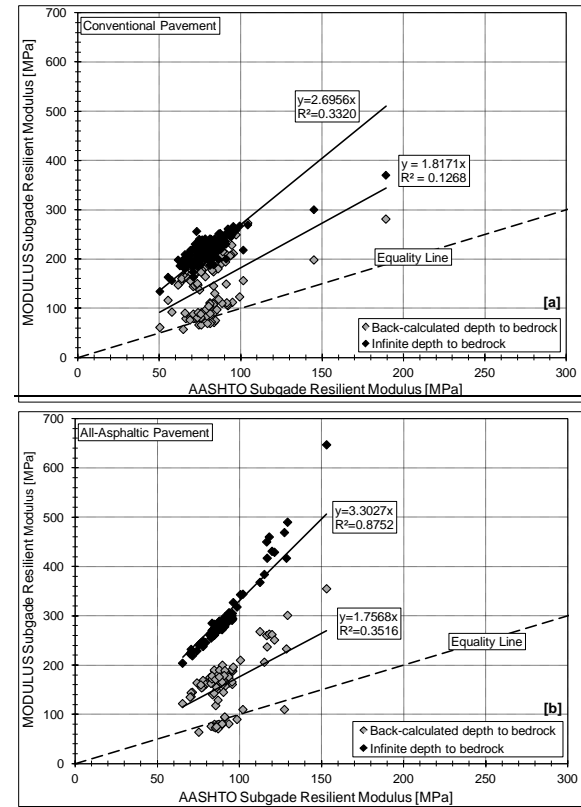


Fig. 4 MODULUS subgrade modulus for both cases of infinite and back-calculated depth to bedrock versus the old AASHTO subgrade modulus for (a) the conventional pavement and (b) the all-asphaltic pavement

To recall, the old AASHTO equation for calculating the subgrade resilient modulus is essentially Eq. (1).

$$E_s = \text{Min}\{C_a \times 0.24 \times P / (\delta_r \times r)\} \quad (1)$$

where  $E_s$  denotes the subgrade resilient moduli, in MPa;  $P$  denotes the FWD dynamic load, in N;  $r$  denotes the radial distance from the plate center, where the deflection measurement is recorded, in mm;  $\delta_r$  denotes the recorded deflection at a radial distance of  $r$ , in mm; and  $C_a$  denotes the correction factor, equal to 0.33. Note: Eq. (1) is derived from (a) Boussinesq stress-distribution theory for a homogenous medium with a Poisson ratio of 0.5 and an applied concentrated load, and from (b) the AASHTO correction factor of 0.33 in order to accommodate the relationship between the laboratory test results and the back-calculated results according to the original Boussinesq equation.

Figure 4 shows that only the old AASHTO results for the all-asphaltic pavement are well correlated with

the MODULUS results of the subgrade infinite depth to bedrock; i.e.,  $R^2=0.875$ . As for the conventional pavement, these results, in contrast to the EVALIV case, are badly correlated; i.e.,  $R^2=0.332$ .

Figure 4 also shows that the ratio of the subgrade resilient modulus, that obtained by MODULUS divided by that obtained by the old AASHTO, varies between 2.70 and 3.30 (i.e., around the expected value of  $1/Ca=1/0.33=3.0$ ) for the case of infinite subgrade depth to bedrock, and between only 1.82 and 1.76 for the case of subgrade back-calculated depth to bedrock. Again, the first value in each pair relates to the conventional structure, and the second to the all-asphaltic structure.

Finally, Fig. 5 describes the relationship between the EVALIV and the old AASHTO outputs, both for the subgrade resilient modulus. This figure points to the fact that the EVALIV results are well correlated with the old AASHTO results; i.e.,  $R^2=0.716$  for the conventional pavement and  $R^2=0.862$  for the all-asphaltic pavement. In addition, Fig. 5 indicates that the ratio of the subgrade resilient modulus, that obtained by EVALIV divided by that obtained by the old AASHTO, varies between 2.13 for the conventional pavement and 3.09 for the all-asphaltic pavement.

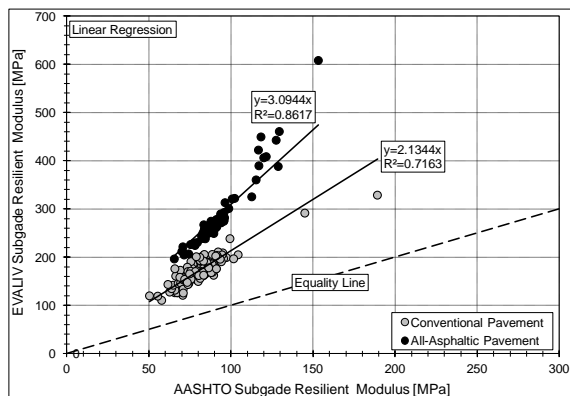


Fig. 5 EVALIV subgrade modulus versus old AASHTO subgrade modulus for the two given structures

### UNCERTAINTY OF CALCULATED MODULI

The preceding section clearly demonstrates the inequalities that exist among the subgrade resilient modulus outputs obtained according to all four calculative procedures. In order to sum up these inequalities, Fig. 6 depicts the cumulative percentage of these subgrade resilient modulus outputs obtained for the two given structures. Figures 6a and 6b both demonstrate the remarkable dispersion that exists in the MODULUS subgrade back-calculated outputs for the case of back-calculated subgrade depth to bedrock. This finding is not surprising, as Fig. 2 has already shown that a large proportion of the back-calculated subgrade depth to bedrock yields small, and even very small, unrealistic values.

Table 1 and Fig. 6 show that MODULUS/b (as defined in the notes to Table 1) and the old AASHTO subgrade modulus outputs for the two given structures are in essence the same. This finding was expected, as it follows the fact that the compacted and natural subgrade is actually the same, for these two given structures, each possessing a design CBR of 5.0%. In addition, the 15th percentile MODULUS back-calculated subgrade resilient modulus for the conventional structure yielded the value of (a) 193 MPa for the case of infinite depth to bedrock and (b) 86 MPa for the case of back-calculated depth to bedrock. For the all-asphaltic structure, these resilient-modulus values yielded values of 246 and 80 MPa, respectively. Considering these back-calculated results, it should be emphasized that many investigators agree with the following: "The success with which a calculated deflection basin is 'matched' with a measured basin is not a good indicator of the accuracy of the back-calculated moduli. It is possible to obtain small error terms with inaccurate moduli values" [13].

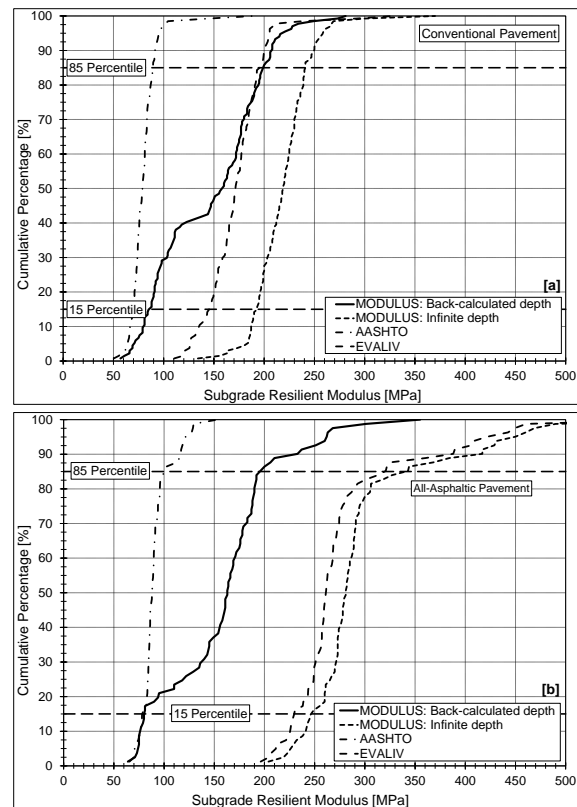


Fig. 6 Cumulative percentage of subgrade resilient-modulus outputs obtained according to all four calculative procedures for (a) conventional pavement and (b) all-asphaltic pavement

Table 2 contains the calculated values of the 15th and 85th percentiles of the calculated subgrade modulus: respectively, EVALIV outputs divided by MODULUS/b outputs and EVALIV outputs divided by old AASHTO outputs. These values were compared with the  $1/\text{slope}$  values given by the

constrained regression (linear regression through the origin) of Fig. 3 and with the slope values given by the constrained regression of Fig. 5. The comparable values as taken from these two figures with those of Table 2 are as follows:  $1/0.8338=1.1993$  for the fourth row of the table,  $1/0.5678=2.134$  for the third row, 2.344 for the second row, and 3.0944 for the first row. (Note: All rows are measured from the bottom of Table 2.) These values and those of Table 2 indicate that for the case of EVALIV divided by MODULUS/b, the two sets of values differ significantly, whereas for the case of EVALIV divided by old AASHTO, the two sets of values almost coincide.

Table 1: 15th and 85th percentiles of the back or forward calculated subgrade modulus as taken from Fig. 6

Pavement	Back or Forward-Calculative Procedure	Calculated Subgrade Modulus [MPa]	
		15th Percentile	85th Percentile
Conventional	MODULUS/b	86	197
	MODULUS/i	193	240
	AASHTO	69	89
	EVALIV	145	194
All-Asphaltic	MODULUS/b	80	196
	MODULUS/i	246	343
	AASHTO	79	100
	EVALIV	229	320

**Notes:** MODULUS/b denotes MODULUS 6.0 for the case of back-calculated subgrade depth to bedrock; MODULUS/i denotes MODULUS 6.0 for the case of infinite subgrade depth to bedrock.

Table 2: Ratio values of 15th and 85th percentiles of the calculated subgrade modulus: EVALIV divided by MODULUS/b and EVALIV divided by old AASHTO

Pavement	EVALIV divided by:	Ratio of Subgrade Modulus	
		Values of 15th Percentile	Values of 85th Percentile
Conventional	MODULUS/b	1.69	0.98
	old AASHTO	2.18	2.10
All-Asphaltic	MODULUS/b	2.86	1.63
	old AASHTO	3.20	2.90

**Note:** MODULUS/b denotes, as in Table 1, MODULUS 6.0 for the case of back-calculated subgrade depth to bedrock.

At this juncture, it is important to note that the ratio values of Table 2 differ substantially (i.e., they are much higher) from those calculated according to the correction equations given in [14] and [15]. Here it is worthwhile noting that the EVALIV forward-calculations of AASHTO pavement parameters were

developed in these two references. This finding adds additional weight to the uncertainty issue.

## UNCERTAINTY IN CBR DERIVATION

To sum up the previous findings, there is a serious lack of consistency in the interpretations made by various back- and forward-calculation programs for the same field data. This finding complies, as mentioned earlier, with that reported in [2] and, in addition, that in [16]. Furthermore, the limitations of back-calculation and forward-calculation of stiffness parameters in the field when utilizing non-destructive test methods include poor agreement between interpreted moduli and the corresponding laboratory-measured or in-situ directly measured moduli.

As mentioned previously, it is recommended in old AASHTO [8] that back-calculated  $E_s$  values according to Eq. (1) be multiplied by a correction factor of  $C_a=0.33$  in the determination of SN for design purposes. The analyses described in [8] pertain to the fine-grained AASHTO Road Test site plus fine-grained soil from seven other projects. No attempt was made in the old AASHTO study to investigate the relationship between back-calculated and laboratory  $E_s$  values for granular subgrades. It may be that back-calculated  $E_s$  values for granular subgrades would not require a correction factor as large as that required for a cohesive subgrade.

In this context, it should be added that a later research publication recommended a series of correction factors as a supplement to the old AASHTO design guide. Some of these correction factors are given in Table 3 [17]. In addition, other sources, as summarized in [12], indicate that this correction factor ranges from 0.2 up to 1.2.

Table 3: Some old AASHTO modulus correction factors for Eq. (1) obtained from the LTPP study [17]

Type of Structure above Subgrade	Correction Factor $C_a$	Coefficient of Variation [%]
Stabilized Subgrade	1.32	80
Full-Depth AC/PCC	0.52	37
Granular Base/Subbase	0.35	49

Other ratios have been documented in the technical literature, and a partial summary of them is given in [15]. All these values indicate again that even when the back- or forward-calculated subgrade resilient-modulus values are the "true" ones, their derived CBR values are uncertain, especially in light of the coefficient of variation values given in Table 3.

Equation (1), with  $C_a=0.33$  (the old AASHTO method), postulates that the relationship between  $E_s$  and its corresponding CBR value is as defined by



Eq. (2) for which  $k=10.3$  and  $m=1.00$ .

$$E_s = k \times \text{CBR}^{(1/m)} \quad (2)$$

where  $k$  and  $m$  are empirical parameters varying from source to source;  $E_s$  is the direct-cyclic triaxial test modulus or the corresponding FWD back-calculated modulus.

Equation (2) is displayed graphically in Fig. 7 for other frequently used values of  $k$  and  $m$  than those of the old AASHTO method. The  $m=1.00$  and  $14.0$  values were taken from [18]. The  $m=1.41$  and  $k=15.0$  or  $20.0$  values were taken from [19]. The TRL or the new AASHTO Mechanistic-Empirical Pavement Design Guide (MEPDG) expression was taken from [20], for which  $k=17.6$  and  $m=1.56$ . Further, the U.S. Army Corps of Engineers expression was taken from [21], for which  $k=37.3$  and  $m=1.41$ ; and that of the Georgia Department of Transportation for medium clay sand was taken from [22], for which  $k=21.5$  and  $m=2.09$ . Finally, the expression of the FAA's NAPTF for low to high-strength clays was taken from [23], for which  $k=23.2$  and  $m=1.46$ .

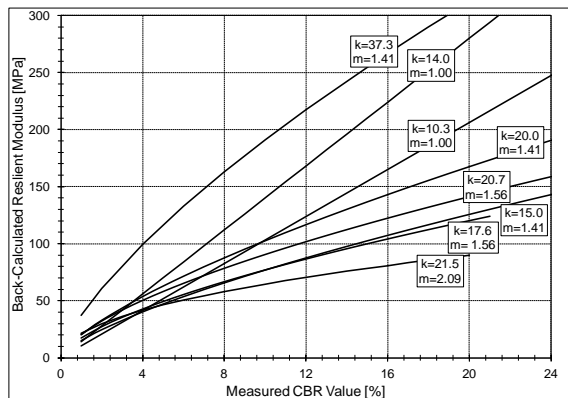


Fig. 7 Back-calculated subgrade resilient modulus versus CBR values according to various sources

Figure 7 indicates that the range of subgrade modulus estimations for a given CBR value is significant. For any given case, the lack of knowledge of its "true" expression may lead to considerable error, as much as 300% and more, in the modulus estimation for high CBR values. Part of the discrepancy in this CBR estimation comes from the range of  $E_s$  values that can be obtained from applying various back-calculation-program codes to the same deflection- bowl measurements.

In Israel, the default expression for the  $E_s$ -CBR relationship is defined by  $k=20.0$  and  $m=1.41$  or, alternatively, for the Flex-Design software, by  $k=14.0$  and  $m=1.00$ . For low CBR values, the difference in the subgrade modulus between these two expressions is insignificant.

In addition, it should be mentioned that the TRL or the new AASHTO Mechanistic-Empirical Pavement Design Guide (MEPDG) expression is

almost the same as that defined by  $k=15.0$  and  $m=1.41$ . On the other hand, the FAA's default expression for the FAARFIELD software does not utilize the above modified expression, but the old one, defined by  $k=10.3$  and  $m=1.00$ .

## TENTATIVE RECOMMENDED PROCEDURE

For a tentatively recommended procedure, it may be postulated that the EVALV procedure yields more reliable results, as it is based on all seven deflection measurements at a given location, and includes the important input of the total pavement thickness. In contrast, the old AASHTO procedure is based on only one deflection measurement at a specified lateral distance and excludes the thickness input. The questions now are the following: (a) What value is to be assigned to the correction factor for the EVALIV  $E_s$  output? (b) What values should be assigned to the  $k$  and  $m$  factors to calculate CBR from the corrected EVALIV  $E_s$  values?

It seems that the correction factor for the EVALIV  $E_s$  outputs ( $C_e$ ) is a function of the total thickness of the pavement. The data given in the present paper, together with that given elsewhere (see Fig. 8), indicate that the following tentative relationship may exist (see Fig. 9):

$$b = 4.3054 - 0.0017 \times H_p \quad (3a)$$

$$C_e = 1/b \quad (3b)$$

where  $b$  denotes the slope of the restrained linear regression (regression through the origin) of EVALIV  $E_s$  versus the old AASHTO  $E_s$ ;  $H_p$  denotes the total pavement thickness, in mm;  $C_e$  denotes the correction factor (multiplier factor) for the EVALIV  $E_s$  outputs.

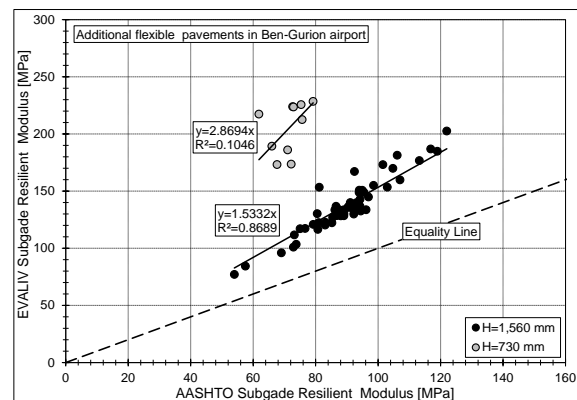


Fig. 8 EVALIV subgrade modulus versus old AASHTO subgrade modulus for additional flexible pavements at Ben-Gurion Airport

Thus, for a total pavement thickness of 900 mm, the correction factor ( $C_e$ ) is equal to 0.36; and for a total thickness of 1,560 mm, the correction factor ( $C_e$ ) is equal to 0.60. For the example of Table 1, in which the design value of EVALIV  $E_s$  is 229 MPa for the 900 mm pavement and 145 for the 1,560 mm

pavement, the corrected EVALIV Es values are  $229 \times 0.36 = 82.5$  MPa and  $145 \times 0.60 = 87.7$  MPa, respectively. These latter two values are almost identical, as they should be, since they refer to the same natural and compacted subgrade possessing, as mentioned earlier, a design CBR value of 5%. Here it is important to note that the Eq. (3a) expression should be verified by the directly measured and forward-calculated data of additional pavements.

As for the CBR derivation, it is tentatively suggested that Eq. (2) may be utilized for the case where  $k=15$  and  $m=1.41$  or for the case where  $k=17.5$  and  $m=1.56$ . This suggestion follows the new AASHTO Mechanistic-Empirical Pavement Design Guide (MEPDG) expression, which seems to be a modification of the old AASHTO expression. Note should be taken that the two expressions yield almost the same results for low CBR values as measured by the old AASHTO Road Test. Thus, the new expression modifies the old one in the region of medium to high CBR values.

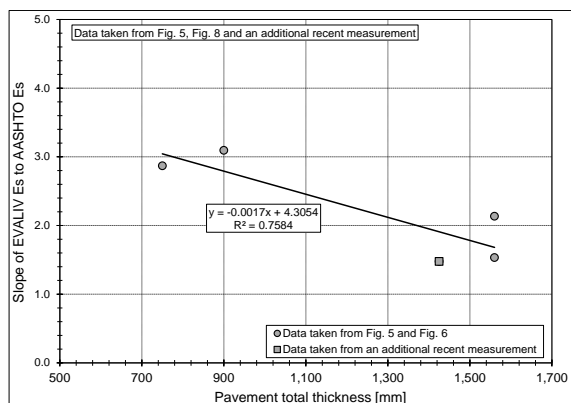


Fig. 9 Slope of EVALIV subgrade modulus versus old AASHTO subgrade modulus (the b parameter of Eq. [3]) in relation to total pavement thickness

To conclude, for the two corrected EVALIV Es values given above (i.e., 82.5 and 87.7 MPa), the corresponding CBR values are 11% and 12%, respectively. These values are higher than the design value (5%), as they refer to a dry-moisture state; i.e., to a state before possible wetting.

## CONCLUDING REMARKS

This paper presented back- and forward-calculations of FWD deflection bowls measured recently at Israel's Ben-Gurion International Airport. The calculations clearly demonstrate the inequalities that exist among the subgrade resilient-modulus outputs obtained according to four different calculative procedures. The consequence of this output is the introduction of uncertainty into the pavement overlay design.

In addition to the uncertainty involved in the subgrade resilient-modulus outputs, another

uncertainty is involved: this one in the calculation of the CBR value from these subgrade resilient modulus outputs. Various calculative expressions exist in the technical literature; however, the differences in their output may be very significant.

In spite of the above limitations, the paper concludes with a tentative suggestion of how to calculate (a) the proper subgrade resilient modulus from the FWD deflection measurements and (b) the CBR value from the above calculated subgrade resilient modulus.

## RECOMMENDATIONS

Together with the calculative procedure, it is very much recommended [see also 24] that the Es-CBR relationship in any rehabilitation design be assessed by conducting both FWD and in-situ CBR (DCP) tests on the existing pavements under consideration. It should be noted that this recommendation is similar to the following, given in [25]: "As a part of this process, some procedures include the testing of materials in the laboratory to define their stiffness (modulus) characteristics, in particular, undisturbed subgrade specimens. Cores from the asphalt concrete and other treated layers may also be obtained. These results are important to insure that the moduli determined by back-calculation are reasonable. Relative to the core data, it must be recognized that the back-analysis provide values for the bulk material while the cores provide spot values for the intact material."

Finally, it is worthwhile emphasizing the following statement, made in the old AASHTO guide [8]: "Users are cautioned that the resilient modulus value selected has a very significant effect on the resulting structural number determined. Therefore, users should be very cautious about using high resilient modulus values, or their overlay thickness values will be very thin."

## REFERENCES

- [1] Stolle, D. and Hein, D., "Parameter Estimate of Pavement Structure Layers and Uniqueness of the Solution," *Nondestructive Testing of Pavements and Back-calculation of Moduli*, ASTM, STP 1026, American Society for Testing Materials, 1989, pp. 313-340.
- [2] Zhou, H., Hicks, K.G., and Huddleston, I.J., "Evaluation of the 1986 AASHTO Overlay Design Method," *Transportation Research Record No. 1215*, Transportation Research Board, 1989, pp. 299-316.
- [3] Goode, J.I. and Mills, K.G., "Development of the Falling Weight Deflectometer for Economical Pavement Overlay Design," in *Proc. 16<sup>th</sup> Conf., Part 2*, Australian Research Board, 1992, pp. 19-35.

- [4] Livneh, M., "The Influence of Some Initial Assumptions on Back-Calculated Moduli," Road and Transport Research, Journal of the Australian Road Research Board, Vol. 8, No. 2, 1999, pp. 12-26.
- [5] Livneh, M., "Some Findings Concerning the Determination of Granular-Base Moduli for Flexible-Pavement Thickness Design," in Proc. of the 1st Inter. Conf. on Road and Rail Infrastructure, Opatija, Croatia, 2010, pp. 273-282..
- [6] Liu, W. and Scullion, T., "MODULUS 6.0 for WINDOWS: User's Manual," Report No. FHWA/TX-05/0-1869-2, Texas Transportation Institute, Texas A&M University System, College Station, Texas, 2001.
- [7] Livneh, M., "Combining FHWA and EVALIV Spreadsheets for Forward-calculating Subgrade and Pavement-Layers Moduli," in Proc. of the International Conference on Transport Infrastructures (ICTI 2010), São Paulo, Brazil, 2010.
- [8] American Association of State Highway and Transportation Officials (AASHTO), "AASHTO Guide for Design of Pavement Structures 1993," Washington, DC, 1993.
- [9] Terzaghi, K. and Peck, R.B., Soil Mechanics in Engineering Practice, John Wiley & Sons, Inc., New York, 1948.
- [10] Uzan, J., "A Pavement Design and Rehabilitation System," Transportation Research Record, No. 1539, Transportation Research Board, 1996, pp. 110-115.
- [11] Federal Aviation Administration (FAA), "Airport Pavement Design and Evaluation", Advisory Circular, AC 150/5320-6E, September 2009.
- [12] Livneh, M., "Uncertainty Associated with Pre-Defined Correlative Expressions of Various In-Situ Tests Outputs," in Proc. of the 2007 Federal Aviation Administration (FAA) Technology Transfer Conf., Atlantic City, NJ, 2007.
- [13] Briggs, C.R., Scullion, T., and. Mazer. K.R., "Asphalt Thickness Variation on Texas Strategic Highway Research Program Sections and Effect on Backcalculated Moduli," Transportation Research Record No. 1377, Transportation Research Board, 1992, pp. 115-127.
- [14] Livneh, M., "On Forward-Calculations of AASHTO Pavement Parameters from FWD Surface-Deflection Basins," in Proc. of the 2010 ATAP Symposium, South Korea, 2010, pp. 195-210.
- [15] Livneh, M., "An Alternative Forward-calculation Technique as a Screening Procedure for Review and Evaluation of Backcalculated Moduli," The International Journal of Road and Airports (IJRA), Vol. 1, No. 2, 2011, pp. 85-117.
- [16] Puppala, A.J., "Estimating Stiffness of Subgrade and Unbound Materials for Pavement Design," NCHRP Synthesis 382, Transportation Research Board, 2008.
- [17] Von Quintus, H.L. and Killingsworth, B.H., "Design Pamphlet for the Back-calculation for Pavement Layer Moduli in Support of the 1993 AASHTO Guide for the Design of Pavement Structures," Report No. FHWA-RD-97-077, FHWA, USDOT, Washington, DC, 1997.
- [18] Uzan, J., "A Pavement Design and Rehabilitation System," Transportation Research Record No. 1539, Transportation Research Board, Washington, DC, 1996, pp. 110-15.
- [19] Livneh, M., "Verification of CBR and Elastic Modulus Values Derived from Local DCP Tests," in Proc. of the 9th Asian Regional Conference on Soil Mechanics and Foundation Engineering, Bangkok, Vol. 1, 1991, pp. 45-50.
- [20] Powell, W.D., Potter J.F., Mayhew, H.C., and Nunn, M.M., "The Structural Design of Bituminous Roads," TRRL Laboratory Report 1132, Transportation and Road Research Laboratory, Wokingham, Berkshire, UK, 1984.
- [21] Green, J.L. and Hall, J.W., Jr., "Nondestructive Vibratory Testing of Airport Pavements: Experimental Tests Results and Development of Evaluation Methodology and Procedure," Report No. FAA-RD-73-205, Vol. I, Federal Aviation Administration, Washington, DC, 1975.
- [22] Webb, W.M. and Campbell, B.E., "Preliminary Investigation into Resilient Modulus Testing for the New AASHTO Pavement Design Guide," Office of Materials and Research, Georgia Department of Transportation, Atlanta, GA, 1986.
- [23] McQueen, R.D., Marsey, W., and Arze, J.M., "Analysis of Nondestructive Test Data on Flexible Pavements Acquired at the National Airport Pavement Test Facility," FAA, William J. Hughes Center, Airport Technology Research and Development Branch, AAR-410, Atlantic City International Airport, NJ, 2001.
- [24] Livneh, M., "Small-Scale Dynamic Devices for Subgrade and Granular Layers Characterization," in Proc. of the 3rd Transportation Engineering Specialty Conference, Canadian Society for Civil Engineering (CSCE), London, Ontario, 2000.
- [25] Monismith, C.L. and Brown, S.F., "Developments in the Structural Design and Rehabilitation of Asphalt Pavements over Three Quarters of a Century," Journal of the Association of Asphalt Paving Technologists, Vol. 68A, 1999, pp. 128-251.

## UTILIZATION OF COCO COIR DUST AND PVC WASTE MATERIALS FOR WOOD-TILE QUALITY COMPOSITE BOARD

Hermie M. del Pilar<sup>1</sup>, Monesse Andrea Z. Antonio<sup>2</sup>, Maricar A. Ilagan<sup>3</sup> and Julius E. Seva<sup>4</sup>

<sup>1</sup>Faculty, Malayan Colleges Laguna, Philippines;

<sup>2,3,4</sup> Malayan Colleges Laguna, Philippines

### ABSTRACT

Gearing on sustainable technology, two waste materials, coco coir dust and PVC were utilized to produce a wood-tile quality, high density composite board material. Adopting the technology in producing fiberboards, the use of PVC as binder to combine with dried coir dust (5% moisture content) was investigated. Three mix ratios of PVC:Coir Dust were used: 80:20, 70:30 and 60:40. The produced board from each combination was then subjected to mechanical and physical property tests. Their properties were compared using the analysis of variance. The mixing process involves the use of two-roll mill machine operating at 204°C while the pressing involves the heat press machine at 108°C and pressure of 450 psi for 3 minutes. The finished products highlight a glossy brown surface comparable to a wood tile, and can be readily manufactured without the additional veneer coating. Physical properties of the 3 ratios were tested against ordinary board. All 3 ratios exhibit 0% Water Absorption (WA) and Thickness Swelling (TS) while ordinary board showed 28.5% WA and 16.5% TS. Mechanical tests for the 80:20 ratio yielded a highest mean value of 55KPa·m on Impact Strength (IS) and 68.85MPa on Modulus of Rupture (MOR) while ordinary boards yielded 50KPa·m on IS and 7.51MPa on MOR. The least mean on different properties of the bio-composite material were compared with the means of commercial board product. This study found that the PVC-Coir Dust combination exhibited highly satisfactory performance based on the physical and mechanical properties as compared to the ordinary board

*Keywords: High density board, Coco peat, PVC pellet, Modulus of Rupture, Impact Strength*

### INTRODUCTION

Today's industry demands various sources of construction materials. Since the increasing problem in the supply of materials goes with the increasing problem in solid waste management, the use of technology in producing composite board materials out of plastic wastes like PVC and agricultural wastes like coco peat can be a practical alternative. Recycled materials converted to good use and reducing the energy required to make them are called "green building materials" (Kubba, 2010).

The intent to create green building materials from wastes and the opportunity to utilize the available technology, like technology in making Medium Density Fibreboard (MDF) and High Density Fibreboard (HDF), led to creating a composite board material using coco peat and PVC wastes.

The PVC waste was chosen as binder in making a composite High Density Board since among various waste materials, plastic wastes and municipal solid wastes are of great concern. Municipal solid wastes containing PVC when burnt gives rise to toxic gases like dioxins. In fact, disposal of plastics in an eco-friendly way is one of the thrusts of today's research (Vasudevan, 2012). Polyvinyl Chloride (PVC) at global level exceeds a demand of 35 million tons per year, second only to

the leader Polyethylene in the plastic industry. It is one of the most commonly used thermoplastic materials in worldwide polymer consumption (Sadat-Shojah M., 2011).

The Crown Asia Compounders Corporation (CACC) is one of the manufacturing companies in the Philippines. It manufactures plastic compounds and other plastic products for direct and indirect use in the construction and telecommunications industries. The company is currently located in Guiguinto Bulacan with an operating cost of 1,800 metric tons per year (Crown Pipes, 2011). Being a producer of PVC plastic pipes, the company yields residual PVC waste materials particularly on its plastic injector and converted into PVC pellets.

In this study, the base material for the bio-composite High Density Board product is the coco coir dust, also known as coco peat. A large amount of coir dust is produced in the process of extracting coco fiber. Coir dust is described as a brown spongy light weight particle which falls out when the fiber is shredded from the husk. It is estimated that the coir dust composed about 70% of the weight of the coconut husk (Tejano, 1985). The company Soriano Multi-Purpose Fibre Corporation (SMPFC) is one of the companies that produce coconut products in the Philippines. Being a subsidiary of the famous Foundation for a Sustainable Society, Inc. (FSSI), the company also operates in fibre-making

particularly in Laguna, Quezon and Albay (School, 2011). The coco peat waste products derived from the production of coconut products of a factory at San Mateo, San Pablo, Laguna were utilized in this study.

## METHODOLOGY

### *Materials and equipment*

The materials in producing the high quality HDB were sourced from the Soriano Multi-Purpose Fibre Corporation (SMPFC) in San Pablo, Laguna for the coco peat base material and Crown Asia Compounders Corporation (CACC) in San Miguel Bulacan for the binder PVC waste material. Figures 1a and 1b shows the appearance of the coco peat and PVC pellet upon purchase from SMPFC and CACC.



Fig. 1a: Coco Peat



Fig 1b: PVC pellets

The moisture content of the coco peat was determined using the oven-dry method. Oven-dry method is the most commonly used method in determining moisture content of a sample. The moisture content of the coco peat was determined by subtracting the weight of the coco peat before placing in to the oven to the weight of the coco peat after oven drying, this process will continue until the difference approximately reach zero. The equation below determines the percent of moisture content (MC), where it depends on the original weight ( $W_o$ ) and the final weight ( $W_f$ ) after oven drying.

$$MC = \frac{W_o - W_f}{W_o} \times 100\% \quad (1)$$

A moisture content of 5% or less qualifies for the HDB production. The use of sieves was employed to note the particle size of the coco peat, and the sieving procedure followed the AASHTO T 27, Sieve Analysis of Fine and Coarse Aggregate.

The commercial board, plywood, with similar thickness was used to compare with the mechanical and physical properties of the HDB composite boards. This plywood is commercially available at hardware stores in the Philippines.

### *Machines for the composite board production*

The machines used in the production of HDB are the two roll mill and the heat press. The two roll mill is equipped with rolls made of corrosion resistant steel and its surface is hardened and polished. The two rolls run at fixed speed at a fixed temperature. The temperature of the two roll mill was set at 204-210°C a bit higher to the melting point of the PVC. The mixing process for the coco peat and PVC was done as these components were continuously fed to the roll mill.

The heat press machine compress the HDB composition using two parallel plates. The heat press machine was set at 180°C and pressure of 3.11MPa sufficient to form the desired HDB.

The machines used, are found in the Industrial Technology Development Institute (ITDI) DOST Compound, Gen. Santos Ave., Bicutan, Taguig City, Philippines.



Fig. 2: The 2-Roll Mill Machine

Figures 2a shows the 2 roll mill machine used in this study.

### *Manner of Mixing and Percent Adhesion*

The 2-roll mill machine was used in mixing the PVC and coco peat. It rotates with temperature set at 204°C – 210°C, same as the melting point of PVC. The ratios of the PVC binder to the coco peat used were 60:40, 70:30, and 80:20. The PVC pellets were poured between the two roll mill to melt and the coco peat mixed as repeatedly kneaded by the rotating roll mill. After mixing, the mixture was placed in a 200 x 200 x 9.5 mm mold.

### *Heat Press on Mixtures*

The mold containing mixture was then placed between two parallel plates of the heat press machine with the temperature that was set at approximately 180°C and subject to a pressure of around 3.11MPa applied for 3 minutes. Trial mass mixtures were tested for hot compress to identify which density will provide a high quality board material which was judged according to appearance and texture.



Fig. 3: The finished HDB product with wood tile quality.

Figure 3 shows the physical appearance of the HDB composite product derived from the mixed coco peat and PVC binder.

#### HDB Specimen Handling

After heat press, the molder was removed from two parallel plates of heat press machine; the HDB was extracted from the molder with the use of hand protection to avoid breakage or damage to the HDB, and to avoid burn due to early contact between newly pressed HDB and the handler. The boards were cooled at room temperature and carefully sealed in plastic bag container upon cooling, before testing. The boards were then conditioned for 3 weeks in a room with temperature of 25°C and relative humidity of 65, before subjecting to physical and mechanical testing.

#### Physical Property test

The physical property tests employed for HDB and commercially available boards were *water absorption* and *thickness swelling*. The results of these tests were compared to determine if they are significantly different.

#### Water Absorption (WA) Test (ASTM D1037-99, 100-107)

The water absorption test measures the moisture content of HDB and the commercially available board (plywood). Portions of sample boards derived from the 200 x 200 mm boards were cut into 50 mm x 50 mm for each mix ratio. The specimens were weighed and placed in a container and immersed in water for 24 hours. When retrieved, the water at the surface of the sample boards were wiped out using filter paper or tissue and then weighed. The moisture content of each sample boards were computed using equation 2:

$$MC = \frac{W_w}{W_s} \times 100\% = \frac{W_A - W_s}{W_s} \times 100\% \quad (2)$$

where MC is the moisture content,  $W_w$  is the weight of the water being absorbed equivalent to the difference of  $W_A$  and  $W_s$ , the weight of the board before immersing in water and the weight after

immersing in water respectively (Hlaing and Kyi, 2011).

#### Thickness Swelling (TS) Test (ASTM D1037-99, 100-107)

The Thickness swelling test was conducted right after the water absorption test. After immersing the sample boards in water for 24 hours, the thickness of each board were measured using a Vernier Caliper. The measured thickness was compared to the thickness of the sample before immersion in water (Hlaing and Kyi, 2011). The test for TS and WA were based on the ASTM standard method D1037-99 (American Society for Testing and Materials, 200).

#### Mechanical Property test

The mechanical property tests for HDB and commercial board consists of tests for *modulus of ruptures (MOR)* and *impact strength (IS)*. The tests for strength were based on the ASTM code D1037. The results of these tests were compared to determine the significance of differences between HDBs and the least performing HDB with that of the CB performance.

#### Modulus of Rupture (MOR)

The *modulus of rupture* was determined using the *three point bend test*. The flexural test measures the force required to bend the HDB and the commercial board under three point loading conditions. Portions of the 200 x 200mm boards were cut into 50mm x 200mm to serve as specimen for testing in each mix ratio.

The MOR is used as an indicator of the sample boards' stiffness when flexed. Each sample board was subjected to a concentrated or breaking load at the centre of the sample board using the universal testing machine (UTM) with the bend fixture. After obtaining the value of the breaking load in each sample board, the MOR of each sample board was determined using the formula:

$$M = \frac{3PL}{2bd^2} \quad (3)$$

where M is the modulus of rupture, P is the breaking load, L is the span between the two supports,  $b$  and  $d$  are the width and the depth of the board samples respectively (Based on ASTM Code D1037).

#### Impact Strength (IS) Test (ASTM D256)

The impact strength (IS) test measured the amount of energy or load required to break the board specimens. The method of un-notched impact



strength was used for the IS test where the sample board was held horizontally supported at its ends with dimension 50mm x 10mm area and hit at its center by a pendulum. The IS was measured by the amount of energy per unit thickness of the specimen. The Humburg Pendulum Impact Tester was used in this study and the procedure was based on ASTM D256 standard.

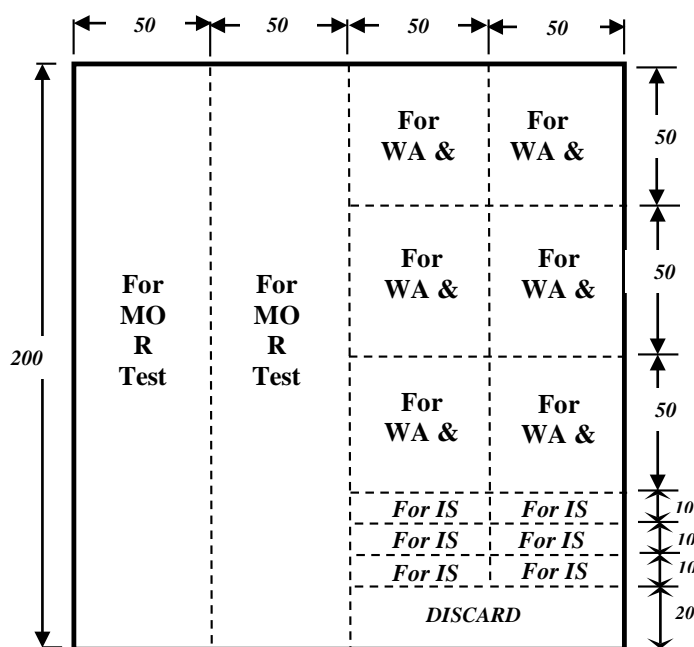


Fig. 4: Cutting pattern of test specimens for physical and mechanical testing (dimensions in mm.)

Figure 4 shows how the test specimens were cut in each mix ratio from board materials.

Table 1. Number of board materials, number of specimens, sizes for the physical and mechanical testing

Type of Board	Type of Test	No. of Specimen	No. of Board Required
HDB	Physical Test	WA 12	2 X 3 (mix ratios) = 6 boards
		TS 12	
	Mechanical Test	MOR 4	
		IS 12	
Plywood	Physical Test	WA 12	6 boards
		TS 12	
	Mechanical Test	MOR 4	
		IS 12	

The distribution of specimens produced for various tests of physical and mechanical properties of HDBs is shown in Table 1.

### Statistical tool

The Analysis of Variance was utilized to determine if there is a significant difference on the means of the HDBs produced using the 60:40, 70:30 and 80:20 ratio for the physical tests (WA and TS) and the Mechanical Tests (MOR and IS). The t-test was used to determine whether there is a significant difference on the means of HDB having the lowest value among the three mix ratios and the commercial board for each test.

## RESULTS AND DISCUSSION

### Physical Property Test

#### Water Absorption and Thickness Swelling Test

The 12 specimens - 50mm x 50mm for each 3 mix ratios of HDB and the commercial board (plywood) yields the mean Water Absorption shown in Table 2.

Table 2 Data on the Mean Water Absorption and Thickness Swelling (24 hours after immersion on water for all board' mix ratios).

Board Type	Ave. Density (g/cm <sup>3</sup> )	Mean WA (%)	Mean TS (%)
HDB (60:40 ratio)	1.3	0	0
HDB (70:30 ratio)	1.2	0	0
HDB (80:20 ratio)	1.3	0	0
Plywood	0.6	28.5	16.5

Based on results, the HDBs regardless of the mix ratio, exhibit the ability to prevent water absorption and thickness swelling, both registering zero percent! The commercial board records 28.5% and 16.5% on WA and TS, respectively. This is a promising quality of a developed product out of these materials.

### Mechanical Property Tests

#### Modulus of Rupture

The 4 pcs – 200mm x 50mm specimens cut in each mix ratio and commercial board yield the following means as shown in Table 3.

Results showed that the HDB, which yielded the highest and lowest MOR were the 80:20 and 70:30, respectively. The commercial board records a low 7.51MPa, which indicates that the composite HDB has a flexure quality far exceeding that of the commercial board.

Table 3 Means of the Modulus of Rupture Test for the different board specimens (HDB and Plywood)

Type of Board	Mix ratio	MOR Mean (MPa)
High density Board	60:40	53.91
	70:30	51.71
	80:20	68.85
Plywood	Not Applicable	

Using one way Analysis of Variance with 5% significance level for the 3 mix ratios of HDB, it shows that there was *no significant difference between the means of the MOR* derived from the 3-point bend (flexure test). Table 4 shows the ANOVA results of calculation.

Table 4 One Way ANOVA for the 3 composite boards

SOURCE	SS	df	MS	F	p
Between Groups	695.77	2	347.89	56.22	> 0.05 (Accept Ho)
Within Group	55.69	9	6.19		Null Hypothesis)
Total	751.46	11			

Table 5 showed that the 70:30 mix ratio yielded the lowest MOR (51.71MPa). This value was compared to the MOR performance of the commercially available plywood, which yielded 7.51MPa. Using the one-tailed test and 5% level of significance, the result shows that the lowest performing HDB has an MOR significantly, which is greater than that of the plywood. Table 5 shows the values in computing the test of significance.

Table 5 One-tailed t-test with 5% level of significance between 70:30 HDB and CB

BOARD TYPE	No. of Specimen	MEAN (MPa)	STD DEV	p value
70:30 HDB	4	51.71	1.91	$p_{comp} = 1.02 \times 10^{-5}$
Plywood	4	7.51	0.06	

The MOR of HDB 70:30 ratio is significantly greater than that of the plywood. Since  $p_{comp} < 0.05$ , which means that the flexural stress of the HDB far exceeds that of the plywood material.

The values in Table 5 show that the MOR of HDB 70:30 ratio significantly exceeds that of the plywood, therefore the HDB exhibits good quality in terms of flexure or bending stress resistance.

### Impact Strength (IS)

The 12 pcs – 50 mm x 10 mm test specimens for each type of board (60:40, 70:30, 80:20 mix ratios and plywood) were tested using the *Humburg Pendulum Impact Strength Test*. The results of the IS means are shown in Table 6.

Table 6 Mean of the Impact Strength Test for the different board specimens of HDB and CB

Type of Board	Mix Ratio	No. of Specimens	IS (KPa-m)	STD DEV
High Density Board	60:40	12	39.38	2.65
	70:30	12	51.88	3.54
	80:20	12	55.00	2.30
Plywood	Not Applicable	12	50.00	1.28

Table 6 shows that 70:30 yields the highest mean on IS, while 60:40 yields the lowest. Plywood has an IS mean comparable to the IS of any HDB mix ratio. This result suggests that plywood exhibit good quality in terms of impact resistance which is comparable to the IS of the HDBs.

Table 7 shows the values for the test of significance among the 3 mix ratios of the HDB.

Table 7 One Way ANOVA test for the 3 mix ratios of HDB

SOURCE	SS	df	MS	F	p
Between Groups	1639.875	2	819.938	99.010	
Within Groups	273.285	33	8.281		> 0.05 , therefore reject Ho
Total	1913.160	35			

A significant difference on the means of the HDBs produced were found among the 3 mix ratios, where the 60:40 ratio emerged as the highest, followed by the 80:20 ratio and least performing is the 70:30 ratio as shown in Table 7

The variation in values of the mechanical properties of the boards is summarized and shown in Figure 5, where the HDBs are noted to excel in the MOR performance while the plywood excel in the IS performance. HDBs with 80:20 mix ratio demonstrate highest performance in MOR while the

70:30 ratio is the least. The 60:40 ratio demonstrate the highest performance in IS while the 70: 30 is the least.

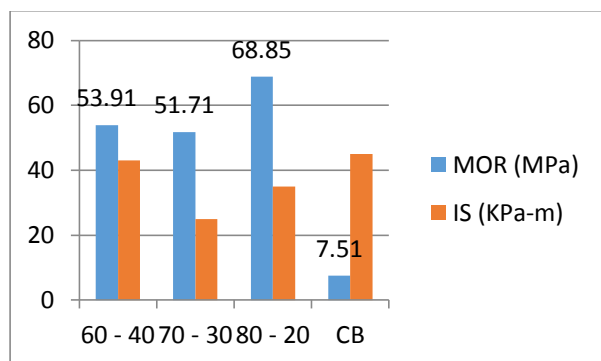


Fig. 5: Combined graph of the MOR and IS Means

## CONCLUSION

Based on the results on Physical and Mechanical Properties of the bio-composite HDB made of PVC waste and Coco Peat waste, the following conclusions were drawn:

1. The WA and TS of the composite HDB had shown excellent quality regardless of the mix ratio used. All specimens demonstrated 0% on both WA and IS tests. These results can be attributed to the plastic property of the binder PVC which comprises the greater percentage of the HDB component.
2. The mechanical test of the HDBs in resisting flexure or bending exhibit good performance compared to plywood. Among the mix ratios 60:40, 70:30 and 80:20, the best mixture was 80:20 recording an MOR of 68.85 MPa, while the 70:30 was the least performing with an MOR value of 51.71 MPa. Though statistics show that the MOR values of the 3 mix ratios do not differ significantly, the plywood had shown weak resistance in bending as reflected by its low MOR value of 7.51 MPa.
3. The plywood demonstrated impact resistance comparable to the HDBs. The 60:40 ratio exhibits best IS while the ratio 70:30 exhibited the least. The plywood has an IS mean of 50.00 KPa-m, which is quite high as compared to the 39.38 KPa-m value of the 60:40 HDB. The resistance of plywood against impact can be attributed to its physical structure since the board was produced through adhesion of wood ply, whereas the HDBs are of homogenous mixture bonded through heat and pressure.

4. The physical appearance of the HDB bio-composite product shows a quality comparable to a fine wood-tile. The surface exhibits a glossy surface which enhances the aesthetic feature of the composite material.

## ACKNOWLEDGMENT

The authors would like to acknowledge the support of Malayan Colleges Laguna in availing reference materials as well as the use of laboratory equipment in preparing and testing the composite board materials. Also, the Industrial Development Technology Institute (ITDI) of the Department of Science and Technology for allowing the authors use the 2 roll mill machine and hydraulic heat press for the production of the composite boards

## REFERENCES

- [1]Kubba, S. (2010). Chapter 6 - Green Materials and products. *LEED Practices, Certification and Accreditation Handbook*, pp.151 - 209.
- [2] Vasudevan, R. S. (2012). Construction and Building Materials. *onstruction and Building Materials*, pp.311 - 320.
- [3] Sadat-Shojah M., B. G. (2011). Recycling of PVC wastes. *Polymer Degredation and Stability*, Vol. 96, pp.404 - 415.
- [4] Crown Pipes. (2011). *Crown Pipes*. Retrieved January 28, 2014, from Crown pvc.com.ph: <http://www.crownpvc.com.ph/crownpipes/about/>
- [5]Tejano, A. (1985). State of the art of coconut coir dust and husk utilization: general overview- Paper presented during the National Workshop on waste utilization, coconut husk. *Philippine Journal of Coconut Studies*, Vol. 2, pp.4-11.
- [6] School, M. H. (2011). *Coconut Magic, Local specialties*. Retrieved January 30, 2014, from msc.edu.ph: [http://www.msc.edu.ph/cyberfair\\_2008/local\\_specialties/smpfc.html](http://www.msc.edu.ph/cyberfair_2008/local_specialties/smpfc.html)

## **UNCONFINED COMPRESSION TESTING OF CEMENT-TREATED DEMOLITION MATERIALS IN BASE AND SUB-BASE APPLICATIONS**

Alireza Mohammadinia<sup>1</sup>, Arul Arulrajah<sup>2</sup>, Jay Sanjayan<sup>3</sup>, Mahdi Miri Disfani<sup>4</sup>, Myint Win Bo<sup>5</sup>, Stephen Darmawan<sup>6</sup>

<sup>1,2,3,4</sup>Swinburne University of Technology, Melbourne, Australia; <sup>5</sup>DST Consulting Engineers Inc., Ontario, Canada; <sup>6</sup>Geotesta Pty Ltd, Melbourne, Australia

### **ABSTRACT**

One of the major challenges of current world and Australia is sustainable waste management. A major proportion of waste materials present in landfills are Construction and Demolition materials (C&D) which can be a suitable replacement for high quality quarry material. Conventionally, quarry materials were used as pavement foundations base and sub-base. With the increasing need of high quality quarry material in various industries and limitation of resources in many parts of Australia, replacement of traditional road building materials with alternative materials is a major concern from both environmental and economic perspectives.

The geotechnical properties of various cement-treated recycled demolition materials were assessed by Unconfined Compressive strength (UCS), results of which will be presented in this paper. The experimental program undertaken also included particle size distribution, modified Proctor compaction. The geotechnical properties obtained were compared with existing local road authority specifications for pavement base and sub-base applications. The method of sample preparation to achieve repeatability of the results has been discussed. The effect of curing duration on strength of the specimen has been analyzed. C&D materials were obtained from recycling facilities at Melbourne, Australia for the experimental program.

Unconfined compressive tests indicated that cement treated recycled material can be considered confidently as a pavement base or sub-base material in the field. The laboratory testing results indicate that temperature and humidity curing plays an important role in the strength development in cement-treated materials.

*Keywords: Cement Treatment; Pavement Base; Demolition Materials; Crushed Brick; Secant Modulus*

### **INTRODUCTION**

Construction and Demolition materials (C&D) account for a major proportion of the waste materials present in landfills in Australia. Developing a reliable technique for the evaluation of these reclaimed products as a base/sub-base material will increase level of confidence within industry regarding in-service performance of the recycled material and will result in a higher uptake of recycled materials in urban areas where cement treated sub-base pavements are commonly used. Reusing recycled materials will lead to lower carbon footprint from construction process, as using C&D materials have significant carbon savings compared to extracting virgin quarried materials [1, 2]. A considerable portion of waste materials presented in landfills worldwide contains C&D materials. Granular stabilization of unbound C&D materials such as RCA without any cementitious binder has been investigated in recent years in pavement and footpath applications [3-5]. The potential use of crushed brick blends in pavement sub-base systems

applications have been investigated and engineering properties of CB blends with other C&D materials were compared with typical state road authority specifications in Australia [6]. Stabilization of RAP materials with cement was attempted in various research projects to evaluate the effectiveness of cement treatments in enhancing the strength parameters and resilient characteristics of RAP aggregates [7, 8]. Recycled glass was proved to be applicable for light duty foot-path base application [9-11].

The objective of this research study is to evaluate the performance of cement-treated C&D materials in pavement base/subbase applications, particularly as a majority of metropolitan road pavements are traditionally constructed with cement-treated quarry aggregates. The assessment of the performance of cement-treated C&D materials, will lead to higher uptake of this alternative material and enable the diversion of significant quantities of C&D materials from landfills. The assessment of the performance of cement-treated C&D materials will also result in increased confidence in the usage of these

alternative low carbon materials by end-users, contractors and design consultants alike.

## MATERIALS AND METHODS

C&D materials comprising were collected from two different recycling facilities in Melbourne, Australia. The C&D materials which was investigated in this research are crushed brick (CB), recycled concrete aggregate (RCA) and Recycled asphalt pavement (RAP), with a maximum particle size of 20 mm. The laboratory program to determine the engineering properties of CB, RCA and RAP comprised particle-size distribution, hydrometer, Atterberg limits, water absorption, particle density, flakiness index, foreign materials content, organic content, Los Angeles abrasion, pH value, modified compaction, Unconfined Compressive Strength (UCS) tests. The characterization tests were initially performed to determine the properties of untreated C&D materials and also when treated with General Portland (GP) cement. The Strength and stiffness development of the materials due to cement-treatment was studied later by undertaking UCS.

Fig 1 shows the particle size distribution of C&D materials considered in this study before and after compaction. The particle size distribution curves of the untreated C&D materials were determined from sieve analysis and hydrometer tests. The particle size distribution plots were compared with upper and lower bound limits specified by the local state road authority [12].

The particle size distribution curves of the untreated C&D materials were determined from sieve analysis and hydrometer tests. CB has the finest gradation between the three tested C&D materials followed by RCA and RAP. The fines content of the materials are low and the fines were

found to be non-plastic. Since RAP has less than 5% fines fraction, hydrometer test was not conducted on this material. The gradation of RCA and CB moved to the left which shows the breakage in aggregates due to compaction effort. However, RCA gradation after compaction was not significantly altered compared to CB which shows RCA aggregates are stronger in nature than CB aggregates. On the other hand, gradation of RAP aggregates after compaction moved to right which is due to bitumen content of the RAP material causing the small aggregates to attach to each other during the compaction. Sieve analysis tests were conducted on materials obtained from three separate stockpiles of each C&D material obtained from the recycling site for consistency purposes. The minimum amount of 3 kilograms was sieved and the particle size distributions were plotted for each of the tested C&D materials [13]. A hydrometer was used to determine the particle size distribution for particles finer than the 75 $\mu$ m sieve [14].

Australian Department for Transport, Energy and Infrastructure suggested static compaction of material for preparing samples which is an appropriate technique to prevent the horizontal cracks along the layer interfaces for aggregates and increase possibility of repeatability of UCS samples [15]. MDD obtained from the modified compaction method was used to calculate the required mass to fill the known volume of mould in order to optimise the advantages of static compaction. Split compaction mould of 100 mm diameter and 202 mm length with a collar was used to facilitate the sample extrusion. Samples were compacted under constant pressure of 12.5 MPa in eight layers (with the thickness of 25 mm) with the OMC obtained from modified compaction curve to achieve the target density.

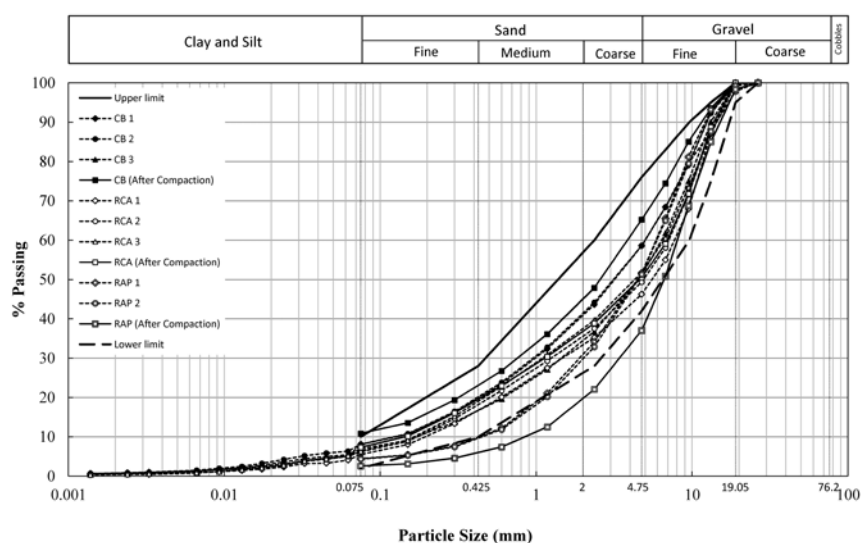


Fig. 1 Particle size distribution plots for C&D materials.

Typically, achieved densities of compacted materials were more than 95% of MDD. The surface of each layer was scarified before adding the materials for next layer to provide interlocking between the layers and to minimize the possibility of horizontal cracks in the specimen. The advantage of using the split mould, rather than open ended compaction mould was that the sample could be extracted from the mould intact with no scratches on the sides, leaving a smooth area to install local on-specimen measurement devices [3].

UCS tests were conducted on samples compacted with the aforementioned split mould under static loads to ensure the specimens were homogeneously compacted and were not damaged during removal and parallel end faces were maintained [16-18]. UCS test were performed on untreated C&D materials and materials treated by 2% and 4% of GP cement. The cement dosage in this study was limited to maximum of 4% by weight due to economic considerations of road construction.

In order to ensure that aggregates are fully soaked, materials are mixed with water and cured for 12 to 24 hours (based on material type) in room temperature before compaction. The cement is mixed with the respective C&D material prior to compaction. This will ensure that there is enough free water for hydration process and there would not be any loss of moisture due to water absorption. The moisture content of the material was determined immediately after compaction from the remaining mix and also after performing UCS tests. The cement-treated samples were cured in a fog chamber which maintained the humidity approximately 97% to 99% and at a chamber temperature of between 19°C to 22°C. Curing durations of 1 day, 7 days and 28 days were selected to evaluate the effect of curing on strength development.

## RESULTS AND DISCUSSION

Geotechnical properties of the untreated C&D materials are presented in Table 1. The pH values indicate that the C&D materials are alkaline by nature. The foreign material content of the C&D materials were visually assessed. RCA comprised of 1.2% CB material and 1.4% RAP material by weight and a very small fraction of other foreign material such as glass, wood and gypsum. CB contained up to 70% brick component, with the balance proportions comprising predominantly of RCA and less than 2% of other foreign materials. RAP contained less than 1% of foreign material.

UCS results for C&D material are presented in Fig 2, Fig 3 and Fig 4. Although only the 7 day curing period of UCS value is specified by the local road authority specification [19], the 28 day curing period tests were undertaken as an extra measure to determine the strength of the cement-stabilized C&D

material to evaluate the rate of increase in strength.

Table 1 Basic geotechnical properties of untreated C&D materials

Geotechnical Properties	CB	RCA	RAP
MDD* (Mg/m <sup>3</sup> )	1.99	1.96	2.06
OMC <sup>†</sup> (Mg/m <sup>3</sup> )	11.38	12.49	6.59
G <sub>s</sub> (Mg/m <sup>3</sup> )	2.65	2.67	2.61
USCS <sup>‡</sup>	GW	GW	GW
pH	10.92	11.85	9.79
Organic content (%)	1.72	3.07	5.15
Foreign material content (%)	1.8	2.9	0.5
Flakiness index	25.90	16.44	10.63
L.A. abrasion loss	35.47	30.80	20.81

\*Max dry density

<sup>†</sup>Optimum moisture content

<sup>‡</sup>Unified Soil Classification System

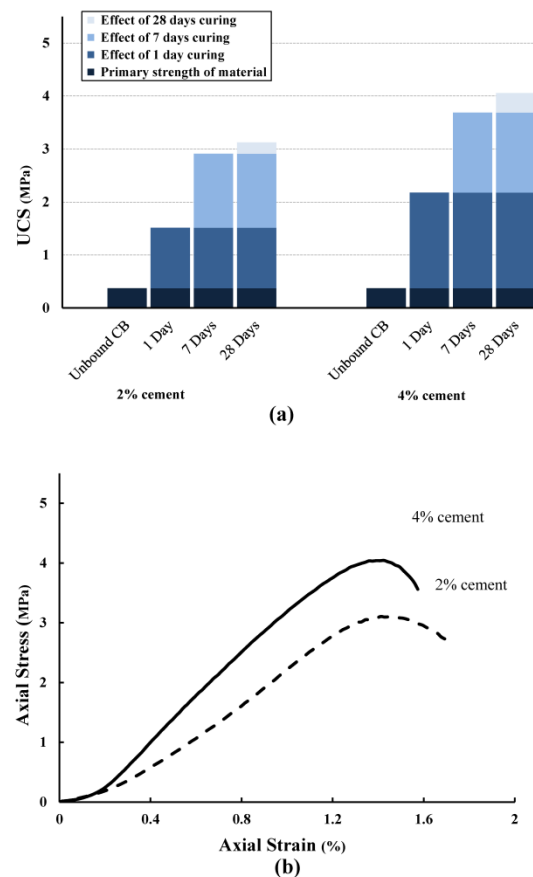


Fig. 2 a) Development of strength in CB with curing time and cement dosage, b) 28 days Stress-strain curves of CB stabilized with 2% and 4% cement.

Fig 2a shows the increase in strength properties of CB with curing time for 2% and 4% cement. Substantial increases in UCS values are evident between the cement-treated C&D materials



compared to the Control materials. It can be observed that the dominant increase is happening during the first 7 days and the strength development moderates significantly after the first 7 days of curing. Fig 2b shows the stress strain curve of 28 days treated CB with 25 and 4% of cement. The same strength development chart for RCA and RAP is presented in Fig 3 and Fig 4 respectively.

The hydration process was found to progress with time, creating a stronger bond between the aggregates, which leads to improvement in unconfined strength. Also it should be noted that higher cement content will increase the strength of bond between materials and will lead to higher UCS value. It is evident from the results that the hydration process slows down with time. In other words, the UCS starts to increase at a rapid rate at the beginning of the curing period and then starts to level off after 28 days. RAP was found to perform better than RCA and CB in all cases with the same cement content and under the same curing duration while RCA showed higher strength values compared to CB.

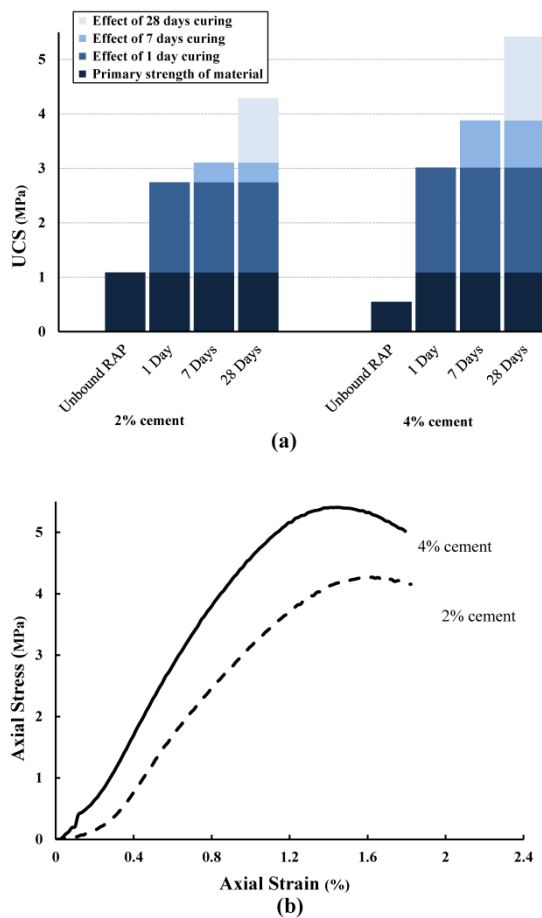


Fig. 3 a) Development of strength in RCA with curing time and cement dosage, b) 28 days Stress-strain curves of RCA stabilized with 2% and 4% cement.

The high strength results for RAP indicates that RAP used in this study was stronger and more durable than the RAP materials previously reported. This suggests that results of strength tests are reliant on the source of RAP.

Loading stiffness of material can be calculated from UCS test.  $E_{50}$  is the secant modulus at 50% of final strength and can be used for numerical analyzes. It can be observed from Fig 2b, Fig 3b and Fig 4b that there is an initial phase of stress strain curve that shows a moderate gradient due to sitting pressures. This is due to swelling of sample in curing period. In this delay phase, a considerable amount of strain will yield a very small increase in axial stress. The sharp increase in axial stress will start afterwards which is an indication of young modulus. The corrections for the initial lag phase have been done on the stress-strain graphs for calculation of secant modulus ( $E_{50}$ ). The procedure of this correction is as stated in CBR test [20]. It is worth mentioning that the samples failed at a maximum of 1.6% strain and show a rather rigid behavior with cement treatment.

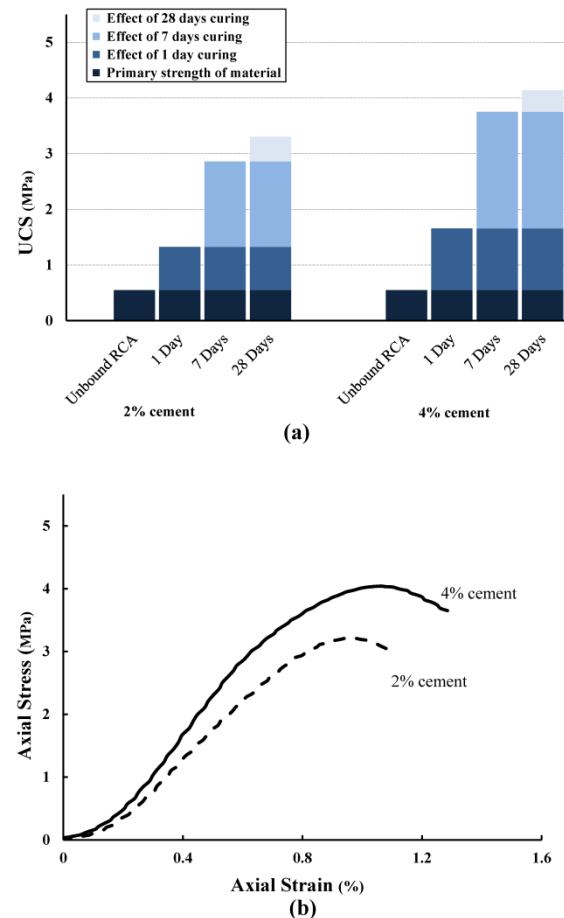


Fig. 4 a) Development of strength in RAP with curing time and cement dosage, b) 28 days Stress-strain curves of RAP stabilized with 2% and 4% cement.

Fig 5 shows the increase in  $E_{50}$  due to curing period for 2% cement treated C&D material. It can be observed that secant modulus increases significantly during the first 7 days. The 28 days stiffness of CB and RCA are very close to 7 days stiffness which implies that these materials reach to a significant amount of final stiffness after 7 days of curing. RAP is a moderately softer material in comparison to RCA due to bituminous presence among the aggregates. It can be observed that the increase in secant modulus continues after the first 7 days of curing significantly. This can be due to existence of free water in porous voids of RAP which will lead to growth of hydration process of cement in RAP, leading to a stronger bond between the aggregates. However, in case of CB and RCA the free water is absorbed by the aggregates, which slows down the hydration process. Comparing Fig 4a with Fig 5 shows that extra curing time wouldn't help in development of shear strength in RAP significantly, but it will lead to increase in stiffness of RAP. It can be concluded that extra curing period of RAP can develop fatigue properties of RAP.

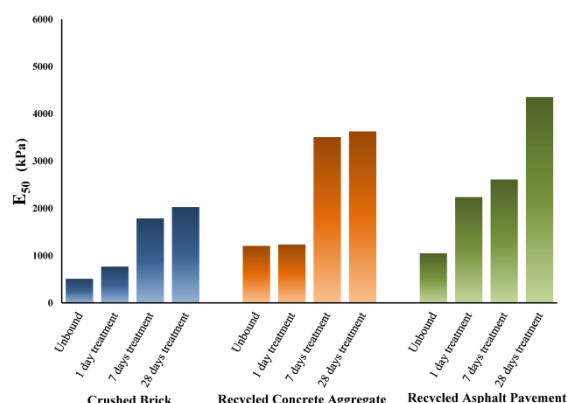


Fig. 5 Development of secant modulus ( $E_{50}$ ) in C&D material stabilized with 2% cement due to curing time.

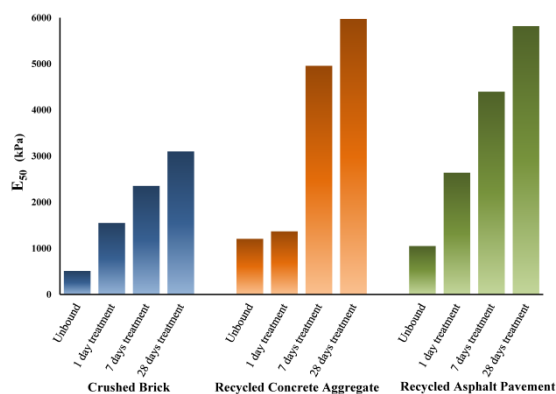


Fig. 6 Development of secant modulus ( $E_{50}$ ) in C&D material stabilized with 2% cement due to curing time.

## CONCLUSION

The geotechnical properties of cement-treated C&D materials were evaluated to assess their performance in pavement base and sub-base applications. The effect of curing duration on the strength of the C&D materials was analyzed for the UCS.

Based on the UCS results, RAP was found to require 2% cement and either 7 or 28 days of curing to meet the local road authority requirements while RCA and CB required 4% cement with 28 days of curing. RAP was found to have more strength than RCA and CB in all cases with the same cement content and under the same curing duration while RCA was stronger than CB. This can be attributed to the presence of bitumen which results in RAP aggregates having higher UCS strength than the other C&D materials for both the untreated and cement-treated scenarios. Initial dry density of RAP aggregates makes the initial strength of untreated RAP samples high.

This research study indicates that cement-treated C&D materials are viable construction materials for cement-treated pavement base/subbase applications. Their usage in pavement base/subbase applications would significantly lower the carbon footprint for future road constructions [21].

## ACKNOWLEDGEMENTS

This research was supported under Australian Research Council's Linkage Projects funding scheme (project number LP120100107).

## REFERENCES

- [1] Horpibulsuk S, Phetchuay C, Chinkulkijniwat A. Soil Stabilization by Calcium Carbide Residue and Fly Ash. *Journal of Materials in Civil Engineering*. 2012;24(2):184-93.
- [2] Kampala A, Horpibulsuk S, Chinkulkijniwat A, Shen SL. Engineering properties of recycled Calcium Carbide Residue stabilized clay as fill and pavement materials. *Construction and Building Materials*. 2013;46:203-10.
- [3] Gabr AR, Cameron DA. Properties of Recycled Concrete Aggregate for Unbound Pavement Construction. *Journal of Materials in Civil Engineering*. 2012;24(6):754-64.
- [4] Poon CS, Chan D. Feasible use of recycled concrete aggregates and crushed clay brick as unbound road sub-base. *Construction and Building Materials*. 2006;20:578-85.
- [5] Arulrajah A, Ali MMY, Piratheepan J, Bo MW. Geotechnical properties of waste excavation rock in pavement subbase applications. *Journal of Materials in Civil Engineering*. 2012;24(7):924-32.

- [6] Arulrajah A, Piratheepan J, Bo MW, Sivakugan N. Geotechnical characteristics of recycled crushed brick blends for pavement sub-base applications. *Canadian Geotechnical Journal*. 2012;49(7):796-811
- [7] Arulrajah A, Disfani MM, Horpibulsuk S, Suksiripattanapong C, Prongmanee N. Physical properties and shear strength responses of recycled construction and demolition materials in unbound pavement base/subbase applications. *Construction and Building Materials*. 2014;58(0):245-57.
- [8] Hoyos LR, Puppala AJ, Ordenez CA. Characterization of cement fiber-treated reclaimed asphalt pavement aggregates: Preliminary investigation. *Journal of Materials in Civil Engineering, ASCE*. 2011;23(7):977 - 89.
- [9] Disfani M, Arulrajah A, Suthagaran V, Bo MW. Shear Strength Behaviour of Recycled Glass-Biosolids Mixtures. 62nd Canadian Geotechnical Conference. 2009;Halifax, Canada.
- [10] Disfani MM, Arulrajah A, Suthagaran V, Bo MW. Geotechnical characteristics of recycled glass-biosolid mixtures. 2009. p. 201-4.
- [11] Wartman J, Grubb DG, Nasim ASM. Select engineering characteristics of crushed glass. *Journal of Materials in Civil Engineering*. 2004;16(6):526-39.
- [12] VicRoads. SECTION 812 - CRUSHED ROCK FOR PAVEMENT BASE AND SUBBASE. Contract Documents, VicRoads2011.
- [13] Standards Australia. Method for sampling and testing aggregates - Particle size distribution by sieving. Australian Standard 1141.11. Sydney, Australia: Australian Standard; 1996.
- [14] ASTM. Standard test method for particle-size analysis of soils. ASTM Standard D422 - 63. West Conshohocken, PA: ASTM International; 2007.
- [15] DTEI. Resilient modulus characterisation of granular unbound pavement materials. Adelaide, Australia.: Department for Transport, Energy and Infrastructure (DTEI),; 1991.
- [16] ASTM. Standard Test Method for Unconfined Compressive Strength of Compacted Soil-Lime Mixtures. ASTM Standard D5102 West Conshohocken, PA: ASTM International; 2009.
- [17] Standards Australia. Supplementary cementitious materials for use with portland and blended cement, Part 1: Fly ash. AS-358211998.
- [18] Standards Australia. Soil compaction and density tests - Determination of the dry density/moisture content relation of a soil using modified compactive effort. Australian Standard 1289521. Sydney, Australia: Australian Standard; 2003.
- [19] VicRoads. SECTION 815 - CEMENTITIOUS TREATED CRUSHED ROCK FOR PAVEMENT SUBBASE Contract Documents, VicRoads,2013.
- [20] ASTM. Standard Test Method for CBR (California Bearing Ratio) of Soils in Place. In: ASTM D4429 - 09a, editor. West Conshohocken, PA: ASTM International; 2009.
- [21] Arulrajah A, Ali MMY, Disfani MM, Piratheepan J, Bo MW. Geotechnical performance of recycled glass-waste rock blends in footpath bases. *Journal of Materials in Civil Engineering*. 2013;25(5):653-61.

## RECENT FOAMED BITUMINOUS STABILISATION WORKS IN QUEENSLAND

Lokanantham R. Logitharan<sup>1</sup>, Kathirgamalingam Somasundaraswaran<sup>2</sup> and Jothi M. Ramanujam<sup>3</sup>  
<sup>1,3</sup>Department of Transport and Main Roads, Queensland; <sup>2</sup> University of Southern Queensland, Queensland

### ABSTRACT

Adapting foamed bitumen stabilisation is considered as the most cost effective approach in Queensland to expedite the rehabilitation works, especially after the major flood devastation in 2011. This paper presents the key changes made as well as the recent practices adapted during a road rehabilitation work to increase the return from the investment. In this process, initially, the designed width for subgrade lime stabilisation has been modified to minimize the moisture entry into the pavement. The dry modulus, three days soaked resilient modulus and retain modulus were used to identify the suitable base material for construction. In addition, a trial site was used to examine the bulking effect on base layer when adding lime as secondary agent, which helped to estimate the exact depth for foamed stabilisation. A few innovative techniques such as a two-layer compaction to effectively condense stabilised subgrade, was used to improve the quality of the outcome were also highlighted.

**Keywords:** *Foamed bitumen, Flexible pavement, Pavement Rehabilitation, Stabilisation*

### INTRODUCTION

In Queensland, foam bitumen stabilisation (FBS) is becoming popular and widely accepted as a long term economic treatment for the base and sub-base layers in road rehabilitation works. Although the foam bitumen stabilisation method was introduced in Australia in 1960s, it never really gained acceptance until 1990s with the introduction of new reclaimers and the use of more experienced contractors [1]. In 1997, the first foam bitumen works was carried out in Queensland; however it is still new area for the road engineers especially when it comes to identification of suitable material as well as field testing that need to be carried out during construction to ensure quality outcomes. More specifically, a full depth reclamation works using foam bitumen still require a good knowledge-based approach and better specifications to achieve a quality outcome.

Traditionally, the most of the Queensland roads have been rehabilitated using the locally available material together with few (2~3%) adhesive agents. It was found that adding cement for unbound pavement change the properties of the pavement layer and become as bound/rigid pavement. When unbound gravels are strengthened by cementing, the particles that were stuck together raised a significant tensile strength, resulting in an unavoidable shrinkage effect, hence causing cracking of the pavement [2]. In contrast foamed bitumen provides a much more flexible pavement layer which reduces shrinkage cracks when using lime as secondary additive. Foamed bitumen stabilised pavement also act as a water proof layer and improve the plasticity and the stiffness of the unbound pavement material. In consideration of similar advantages into account,

currently foam bitumen stabilising is known as an environmental friendly, economical and innovative treatment for rehabilitation works compare to the other form of stabilisation works.

This paper discusses the steps taken from the design stage to completion of a rehabilitation work to a flexible pavement project in Oakey, Queensland. Specially, after the project was awarded to the contractor, the expertise from both client and contractor revisited the design, material specification and construction process to improve the quality of the outcomes. Thus, the aim of this paper is to highlight the technical changes made, analysis and testing adapted the follow-up actions undertaken on site to increase the return from investment.

### FOAM BITUMEN STABILISATION

Foamed bitumen is produced by injecting air and water droplets under high pressure into hot bitumen. In this process, as the water turns into steam, bitumen changes from the liquid state into foam [3]. When this foamed bitumen mixed with the suitable pavement materials it then helps to coat the fine particles within the material to make a bond between larger particles. This bonding is also sometimes referred as welding action between pavement partials.

### Advantages of using FBS

The advantages and disadvantages of using foam bitumen stabilising compared to other type of stabilising techniques are highlighted by several researchers [6][7]. The key advantages of using FBS are listed below:

- Significantly reduce or eliminate shrinkage cracks
- Increased resilient modulus for flooding/water entry areas
- Strong and flexible layer against fatigue failure
- Increased shear strength and reduced moisture susceptibility of granular material
- Reduced binder and transportation costs compared to other type of cold mixing.
- Foamed bitumen layers can be constructed in adverse weather such as light rain without affecting any conditions for workability.
- Energy conservation due to the only heating bitumen when stabilizing (no need to dry or heat the material)
- Reduced environmental and other side-effects resulting from the evaporation
- Reduced wastage as the existing material can be used with the imported material
- No risk of binder run off or leaking
- Saving in curing time as the traffic can be allowed as soon compacted

### Key requirements

The success of a foamed bitumen stabilisation is highly dependent on material characteristics, moisture content of the existing/imported material, bitumen class, characteristics of the foaming agent, tight quality process during the construction including use of correct equipment/machineries. Other factors which affect foaming properties of bitumen are foaming temperature, anti-foaming agents, foaming water content and bitumen chemical composition [4].

It is noted by several studies that when bitumen at a stage of foamed, it doesn't completely coat all aggregate surfaces but has an affinity for finer particles, those of 75 microns or less. This action with the fine particles forms a mortar or glue which effectively bonds with the other pavement materials together [5]. It has also been highlighted that the quality of fine is critical rather than the quantity. Therefore expected quality and chemical property of the fine particles should be well specified from the laboratory testing methods.

When foamed bitumen breaks and mixes with tiny particles the moisture contents within the tiny particles influences the strength of the created bond between the particles, so it is necessary to maintain a suitable moisture content for this purpose. If the imported/existing material for foamed bitumen works contain too much moisture or clayey then particles create lumps before the application of bitumen and foam will not be distributing evenly to create a strong bond. A moisture level that is too high lengthens the curing time, reduces the strength and density of the compacted mix, and reduces the coating of the aggregates [6]. On the other hand, insufficient

moisture reduces the workability of the mix which could result in inadequate dispersion of the binder. Therefore optimum moisture content should be maintained throughout the construction process.

Time required to mix the foam with the pavement material is critical in foamed bitumen works. Producing foam by adding water and air to a hot bitumen is an easy task than maintaining the foamed stage. Therefore appropriate expansion ratio and half-life should be used during the construction process. Expansion ratio is defined as being the ratio between the maximum achieved volume of the foamed bitumen and the original volume of the non-foamed bitumen [8]. Half-life of the bitumen is defined as time taken for the volume of foamed bitumen to settle to half of the maximum volume [7]. The type of foam most effective is one which has an expanded volume of 10 to 15 when injecting one to two percent of water to the hot bitumen[12].

Wirtgen Stabiliser (WR 2400, WR 2500) with the mixing chamber in the middle is the most suitable machine currently available for foamed bitumen stabilising work [13]. The selection of the roller and rolling pattern is critical for compaction works. Experienced final trim operator is critical to provide quality product within the tolerance specified in the MRTS.

### PROJECT DESCRIPTION

The project is located on Oakey-Pittsworth road which is 40 km from Toowoomba. This two-lane undivided highway segment with 2.6 km section has been identified for rehabilitation works. This section was severely affected during the 2011 and 2013 flood. Since its location subject to floods, a proper treatment is required to stand against future flood/rain events. The construction works had been awarded to RoadTek.

### Proposed Design

The Department of Transport and Main Roads (DTMR) has carried out the initial design where mechanistic design approach was carried using a pavement design software namely CIRCLY. The following traffic and materials parameters were used in the preliminary design: Maximum vertical design modulus for lime stabilised layer was 200MPa; Maximum design modulus for foam bitumen layer was 1200 MPa; Bitumen content for foam was 7% by volume; Strength of post cracked phase was 500MPa with Poisson's Ratio of 0.35, Project Reliability was 90%, Design Traffic was  $1.8 \times 10^6$  ESAs, and other design loading and subgrade rutting criteria as per Austroads 2004.

Initial design was carried out in 2012 during the preconstruction stage. The initial design considered the use of existing base and sub-base pavement

material or replacing it with suitable material. During the initial stage the moisture condition of existing pavement was considered critically when proposing mix design for foamed bitumen. As a result, it proposed to replace unsuitable material (250mm top) with imported Type 2.5 material as per specification given in Main Roads Technical Specification (MRTS) [11]. Further lime stabilising (300mm) was proposed to improve the strength of subgrade to eliminate the undesirable characteristics of the expansive soil. Lime demand test was conducted, and it was proposed to use 9% by mass that is 40kg/m<sup>2</sup> hydrated lime to stabilise the subgrade. The initial proposed FBS layer design was to use 3% bitumen and 2% General Blend cement (GB) by mass as primary and secondary stabilising agents respectively.

## MODIFICATIONS FOR IMPROVED QUALITY

After the contract was awarded, the following changes were undertaken jointly by the client and the contractor to improve the quality of the works. In this process, the team has revised initial design, identified proper sources for material and implemented additional control measures to ensure the quality outcomes from foam bituminous stabilisation process.

### Changes to subgrade design

Subgrade of this rehabilitation work has been identified as expansive soil. Expansive soil will expand during the wet season and shrink in dry season; therefore the base layer would fail on the expansive subgrade if not properly treated. In Queensland, lime is normally applied to modify expansive soils to improve strength characteristics, because lime improves the plastic properties, flocculating particles and it allows drying the material. In addition lime stabilising increases load bearing capacity and achieves long term strength retention [13]. Initial design for this work was to use lime (9% by volume) to stabilise the subgrade. The lane width of 4.8m (including median width) for a direction is proposed for subgrade stabilisation, however the design has been changed to stabilise 6m wide to include the additional 1.2 m section below the shoulder. This is to reduce the lateral moisture movements to the pavement. While expanding the width along the road it was noted that some of the sections contained small rocks and sandy soil which has to be treated with suitable process. The section encountered rocks have been treated by removing rocks. The area containing sandy soil had been treated by mixing with expansive soil. Although, initially it was decided to use triple blend, in order to maintain consistency across the road, later it has been decided to cross blend and stabilise the layers with lime. The

lime demand test has been carried out to identify the lime requirement (6% by mass).

### Material identification from mix design

With the foamed bitumen stabilisation it is essential that adequate fines must be available for the bitumen to bind with [7]. As per the material classification in Main Roads Technical Specification (MRTS), Type 2.5 and Type 2.3 material with 'C' grading can satisfy the requirement of a foam stabilisation works [11]. Therefore, undertaking initial investigation on available materials as well as carrying out mix design out of these materials was identified as critical steps.

A number of samples were prepared for varying amount of primary and secondary stabilising agent. The samples were prepared for a total of 16 different type of materials. These materials were taken from three different quarries. The following key tests were carried out in Herston Laboratory, Queensland (DTMR laboratory) to identify the suitable material for this rehabilitation work:

- Indirect tensile test to identify initial modulus after three hour curing at 25°C. A minimum expected strength of 700 MPa was set as target according the specification [13].
- Dry modulus was obtained after placing the specimen for three days at 40°C. Previously dry modulus were obtained after curing the sample at 60°C. However it has been modified considering softening point of the bituminous binder which allows its mobilisation and possible absorption into the aggregate [12]. Therefore currently, the DTMR, Queensland has been using 40°C as curing temperature.
- Three days soaked modulus was obtained after specimens soaked in water in vacuum chamber for 10 minutes at maximum pressure of 95 kPa.

When it comes to material selection, MRTS recommends the use Type 2.5 material as it can achieve high soaked modulus in mix design; however, there is no specific requirement for a minimum CBR value for type of materials that can be used. Therefore, the requirement for this project has been modified to achieve a minimum strength of CBR 45 for the base layer material.

Testing results revealed few issues when identifying the right material as the field soaked modulus was not achieving the minimum requirements. However this paper is only concentrating the construction issues. Therefore the detail technical issues will be discussed in elsewhere. In overall it was found that using material having finer particles increase the soaked and retain modulus more than material having more coarse particles.



## Changes to base layer design

Adding 2 % cement was proposed as secondary stabilising agent for the foamed bitumen work. Experience from as a similar site on the Warrego Highway showed that using cement as secondary agent would results in crack failures. The actual reasons for the failures are currently under investigation. Therefore, experts argued that using lime instead of cement would defiantly increase working time. Furthermore, using lime has the following advantages [7]: stiffens the bitumen binder, acts as anti-stripping agent, increases the initial strength of the material, and has a longer working time (up to 24 hours if need to rework). Therefore with the consultation of design engineers, lime has been proposed as a secondary agent.

## DETAIL OF CONSTRUCTION PROCESS

The construction works in this entire job has been equally divided into four sections, namely Lot 1, Lot 2, Lot 3 and Lot 4, as shown in Figure 1. This segmental approach allows a continuous passage of traffic in one lane with proper traffic control in place. Based on the test results, Type 2.5 material was used for Lot 1, Lot 3 and Lot 4, and Type 2.3 material was used to Lot 2.

- Primer sealing, allowing traffic and monitoring
- Spray sealing

### Subgrade stabilisation

Initially, an entire lot (eg., Lot 1) was milled out using profiler and existing material and was stockpiled away from site to use it for another project by the contractor. The lime stabilising method has been used to improve the subgrade. The lime demand test has been carried out and mix design showed the subgrade is to be treated with the lime at the rate of 40 kg/m<sup>2</sup>, which is equivalent to 9% hydrated lime by mass. Initially, the construction process has been planned to use 13~14 kg/m<sup>2</sup> spread rate in three runs. Matt/tray test has been carried out on-site to ensure the spread rate. However it was found that spreader operator encountered problem on maintaining consistence spread rate. As the hydrated lime is added with water it turned out to be bonded so the spread rate had been reduced to 10-11 kg/m<sup>2</sup>. Therefore number of run increased to runs which has been increased the cost and the project duration.

Design has also been modified on site by increasing stabilising width by 6m instead of original design of 4.8m for one direction. Each Lot has been further divided to five 260m sections to make the safer construction process (example, Sections A & B in Figure 1). Hydrated lime was spread for each section of 260m length, and subsequently mixed using stabiliser in three strips: two 2.4m sections (width) and one 1.2m section to achieve a total of 6m width. The lime stabilisation work has been carried out in two days in two adjacent sections (say Sections A & B). For example, subgrade lime stabilisation took two days in the following sequences: day 1 for 3 dry run in section A and 2 dry runs in Section B, and day 2 for 1 dry run in section A and 2 dry run in section B followed by wet run. The water truck was connected with stabiliser and proceeded with the wet run to both section A and section B.

The Section A and Section B were left over the night to cure and after second day sand replacement tests were carried out in these two sections to check the subgrade density with the required specification.

The MRTS-07A clause 8.4.16 [11] specifies the minimum requirement for the rollers to be used. Accordingly, 21Tonne Smooth drum and Padfoot rollers were used to compact 300mm lime stabilised layer. However the compaction at site has been carried out in two stages.

In this process, after completing lime applications, mixing and wet run the 150mm depth of material was removed using grader and bottom layer (150mm) was compacted using a 22 Tonne Padfoot roller. This initial layer was compacted by eight passes with full vibration. The next 150mm layer brought back and compacted using the same roller through 6 passes with full vibration. This segmental

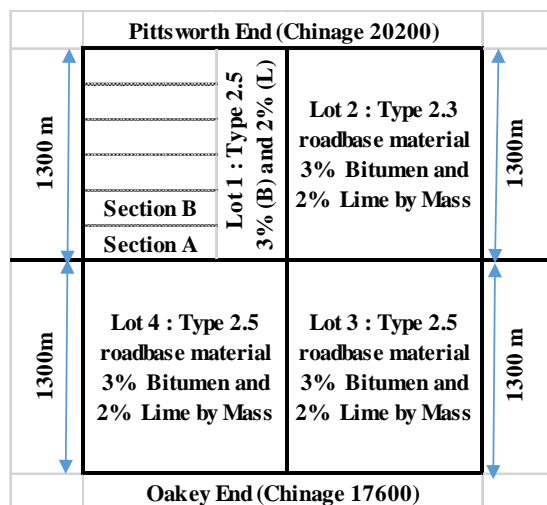


Fig.1 Site plan for segmental construction

After clearly dividing the lot's activities into the project plan, the following the construction works were carryout for each lot, separately:

- Removing 250mm unsuitable material using profiler
- Lime stabilising 300mm underneath foam bitumen layer
- Import 250mm layer of new base material
- 250mm depth of foam bitumen stabilising

compaction process reduces the risk of failure, especially when not achieving the required 'Relative Dry Density (RDD) of 97% (standard compaction) as specified in MRTS 11.07A clause 8.5.2 [11]. Once subgrade (300mm) was compacted, a grader was used to cut all Padfoot marks and trim the section within the tolerance specified in MRTS 11.07A [11]. Finally, smooth drum followed by multi tyred roller (12 Tonne) compacted the trimmed sections (3 passes with full vibration and three passes with half vibration). The sand replacement tests were carried out together with Dynamic Cone Penetration (DCP) tests on a few sections to ensure the required compaction. Both results show a satisfactory results, therefore at a later stage, DCP testing process has been adapted to speed up the construction process. According to the design, the stabilised subgrade should have a minimum California Bearing Ratio (CBR) value of 10. The test results show an average CBR values between 20 and 30.

### **Foamed bitumen stabilisation**

As soon as the completion of subgrade works and granular material (identified from the mix design) was delivered to the boxed out sections, the required tip rate for delivering material was calculated and provided to the supplier.

The material was delivered to the site with 65% to 70% of moisture content. As the success foam bitumen stabilising is heavily dependent on the moisture content of the material, the contractor has been informed about the high penalty for delivering material outside the tolerance level for the moisture content. As the materials were delivered, the moisture content has continuously been monitored closely on site. Then material were spread and compacted to 100% Relative Dry Density (RDD) as per the requirement of MRTS11.05 [11]. Then the section was compacted using a smooth drum (22 Tonne) with 12 passes and trimmed to the required level prior to commence the FBS. Once the section was trimmed to the required level the roller was used to tighten the material with back watering process using a water truck. The compaction process was carried out to ensure the section got the right amount of material (by mass) prior to commencing stabilising works.

A local contractor was appointed to supply the hot bitumen to the site, and the contract includes: load, cart, heat and supply at the required temperature. The bitumen has been supplied from Pinkinbar BP plant in Queensland, and it took 3 hours to transport the bitumen to the site from the plant.

The Class 170 bitumen has been loaded at 160 degrees. It is normal that when the bitumen is loaded into a road tanker, the temperature dropped by about 5°C-10°C and continues to fall by a further one or two degrees per hour while in transit [14]. In consideration of these facts, as soon as the bitumen

arrived on site the supplier starts to heat the bitumen, and it generally took an average of 3 hours to reach 180 degrees (heating rate 10 degrees per hour). When refining/transporting bitumen, anti-foaming agent (e.g. silicone oil) was added to reduce surface tension, as per guidance given in Shell Bitumen Handbook [4]. As the success of the foam bitumen stabilising relies on half life time and expansion ratio, the foaming agent (Terric 311) was added 30 minutes prior to the stabilising, i.e., a 100 liters (0.5% by mass : ie  $0.005 \times 20,000$  kg) of foaming agent was added for each 20 Tonne bitumen tanker.

Prior to commence foam bitumen stabilising (adding bitumen) the secondary agent (hydrated lime) was spread and mixed with the base materials. The use of hydrated lime helped to maintain the required right moisture before commencing the foam bitumen stabilisation. The quantity of the hydrated lime varies with the density of the road base material. As per the design, for the sections A & B, an application rate of 11.5 ~ 12 km/m<sup>2</sup> hydrated lime was used on site (~2% by mass). In this process, lime was dropped in two 2.4 m run to achieve 4.8m width. The Matt/tray test was carried out to ensure the drop rate is achieved as per the design requirement. As soon as spreader dropped the lime the water truck connected with the stabiliser and commenced the mixing the lime with granular base material. The moisture was controlled when mixing hydrated lime with granular material. In the construction process of FBS, the DTMR has introduced a term "Lower Reference Level (LRL)" which is the reduce level or bottom level of the foam bitumen stabilised layer. The material has been mixed to a depth 30mm above the lower reference level (in this case 220mm instead of 250mm) to ensure the stabliser is not mixing subgrade with the existing base material when mixing lime. A smooth drum (22Tonne) compactor followed the stabiliser and provide two passes with the full vibration and the grader was used to correct any irregularities on the mixed surface to ensure the surface is smooth just before staring the foam bitumen stabilisation. Then the trimble was used to check the surface level at different local points.

It should be noted as soon as add the lime, the material will bulk (about ~30mm) due to the change of volume, not the mass. Therefore a trail section was done to identify the bulking depth due to the lime stabilising. Then bulking depth was added to the design depth to identify the stabilising depth for foam bitumen stabilisation. Hence the final stabilising depth was calculated to include about 20mm of stabilised subgrade to ensure the compaction achieved was well below the lower reference level. In this case the full depth of foam bitumen stabilising was calculated to be 300mm as follows: 30mm bulking + 250mm actual stabilising + 20mm subgrade.

Foam bitumen stabilising continues straight after mixing the lime, and Wirtgen WR 2500 was used for foamed bitumen stabilizing (see Figure 2). The injection system in WR2500 consists of a microprocessor-controlled metering unit, an eccentric pump and an injection bar with 16 nozzles and feeding device. The pump delivers the liquid agent (e.g. water) from a tanker truck to the injection bar [8]. Test jet system of the Wirtgen 2500 was used to ensure correct bitumen expansion and half-life time during the foam bitumen stabilisation work.

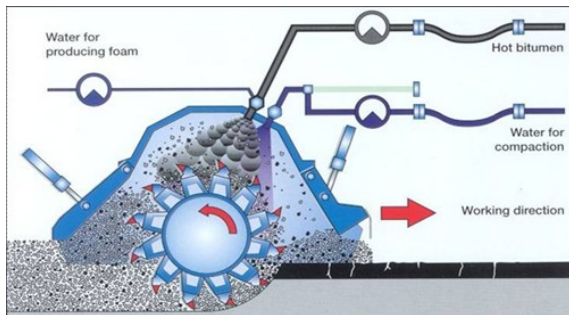


Fig.2 Foamed Bitumen mixing process [5]

Previous works show that the reducing the depth of the stabilisation shorten the life of the pavement. Therefore, depth of the stabilising layer is important to be achieved to the design depth. Once commence the foamed bitumen stabilising work the stabilising depth was measured using dummy level and Trimble to ensure the bitumen stabilising has been done to the designed depth. Further the temperature was constantly checked across the pavement behind the stabiliser to ensure all nozzles are working properly. The visual inspections were also carried out by squeezing stabilised material by hand to identify the bitumen has spreaded properly.

### Final compaction and trimming

Soon after completing the mixing process, initial compaction was carried out using padfoot roller (22Tonne) with 6 passes. The project team ensured that the stabilized pavement achieved required compaction and wasn't over-stiffening the pavement. Then a grader cut the padfoot mark, and trimmed the surface to the required level, followed by it a multi rubber tyred roller (24 Tonne) used to bring the final surface. At all times during the compaction process, it was monitored to eliminate any laminated layer due to the variation of vibration between layers.

### Sealing

The full width spread seal will not commence till complete entire job, but a primerseal was carried out to protect the pavement from adverse weather. The

traffic was not allowed on the stabilised pavement until the primerseal was complete and 24 hours to cure before allowing traffic. In this project Class 320 bitumen and 10mm aggregate was used for primerseal.

Initially, a Double/Double PMB seal with 14/7mm aggregate was designed for full width as final seal. However, the experts commented that transverse cracks might be appeared if a fabric was not used. In addition, Fyfe (2010) has highlighted a similar modification to the design, and the following were documented as justified advantages when using fabric seal: waterproof layer, bridging shrinkage crack, acts as a stress absorbing interlayer, and pro long surfacing life span [15]. Therefore, in this project, Type II-B geotextile was used. Finally, a fabric seal with tackcoat was carried out on top the primerseal before a double/double seal with 14/7 mm aggregate.

### CONCLUSION

After the severe floods in 2011 in Queensland, the application of foamed bitumen stabilisation technique in rehabilitation works has several success stories. This paper outlines the steps taken to improve outcomes while rehabilitating 2.6 km section of Oakey-Pittsworth road, Queensland. In this process of construction the stabilisation width of sub-grade layer increased, available materials were tested to maintain the required specification, a suitable secondary agent as a filler for FBS is introduced, and continued testing were undertaken to improve the quality of the outcome. A highly motivated collaborative relationship between DTMR (client) and RoadTek (contractor) provides a good platform to identify these key changes to improve the quality in this project. The documented scenarios highlight the recent approaches that could be applied for similar construction sites. This project could be considered as experiment for making changes to the specification by the road authorities.

### ACKNOWLEDGEMENTS

Authors would like to acknowledge the client, designers and field staff from Department of Transport and Main Roads Queensland (Philip Tweddell, Damian Volker & Belinda Krause), Regional Program Office 07 (David O'May) and RoadTek (Jason Dallinger & Kim Hankinson) for us to provide research opportunity and support through the job.

### REFERENCES

- [1] Vorobieff, G & Prestonnenene, N 2004, 'Bitumen Stabilisation – An Australian Perspective', NZIHT Stabilisation of pavements seminar, pp. 1-19

- [2] Wilmot, T & Rodway, B 1999, 'Stabilised pavements selecting the additive: cementitious, Polymer or Bitumen', *Proceedings of international congress on local government and public works*, pp.1-7, < <http://www.auststab.com.au>>.
- [3] Sunarjono, S 2009, 'Laboratory stiffness characterization of foamed cold-mix asphalt using indirect tensile stiffness modulus test', *dinamika Teknik Sipil*, Vol. 10, No. 1, pp.1-8.
- [4] Read, J & Whiteoak, D. (2003), *The Shell Bitumen Handbook*, Fifth Edition. Thomas Telford Publishing, Thomas Telford Ltd, 1 Heron Quay, London E14 4JD, pp 407 – 412.
- [5] Hiways Ltd (2014), *Technologies: Foamed Bitumen Recycling :Pioneering stabilisation technology in Australiasia and South Pacific*. Available from: <<http://www.hiways.com.au/stabilization/technologies/foam-bitumen-recycling>> [Accessed 6 Jun. 2014].
- [6] Muthen, KM 1998, 'Foamed Asphalt Mixes – Mix Design Procedure', *Report CR-98/077*, Sabita Ltd. and CSIR Transportek
- [7] Ramanujam, JM & Jones, JD 2000, 'Characterisation of foamed bitumen stabilisation', *Road System & Engineering Technology Forum*, Queensland, Australia. pp.1-23.
- [8] Wirtgen 2002, *Foamed Bitumen –The Innovative Binding Agent for Road Construction*, Windhagen,Germany, pp.1-32
- [9] Bowering, RH & Martin, CL 1976, 'Foamed Bitumen production and application of mixtures evaluation and performance of pavements', <<http://asphalt.csir.co.za/FArefs/Bowering%20&%20Martin.pdf>>
- [10] Lylemachinery.com, (2014). *Features for Wirtgen 2012 WR 2500 SK*, Available from <[http://www.lylemachinery.com/new\\_vehicle\\_features.asp?veh=292478&CatDesc](http://www.lylemachinery.com/new_vehicle_features.asp?veh=292478&CatDesc)> [Accessed 6 Jun. 2014]
- [11] MRTS 2009, *Transport and Main Roads Technical Specification and Standards*
- [12] Jameson, G 2013, 'Design and Performance of Foamed Bitumen Stabilised Pavements: Progress Report One', *Austrroads Technical Report*, AP-T247-13, pp.1-99
- [13] Wilson,P Ramanujam, J & Neary, A 2012, 'A new procedure for lime stabilising pavement subgrades for Queensland', *Shaping the future: Linking policy, research and outcomes*, Perth, Australia ,25th ARRB Conference
- [14] BP Australia Pty Ltd (2007), *Bitumen Basis : BP Bitumen Bringing Technology to the surface*, < [http://www.bp.com/content/dam/bp-country/en\\_au/products-services/bp-bitumen/all-pages/Bitumen-basics.pdf](http://www.bp.com/content/dam/bp-country/en_au/products-services/bp-bitumen/all-pages/Bitumen-basics.pdf)>
- [15] Fyfe, R 2010, 'Paving fabric seal design and performance on Australian roads', *2nd international and sealing conference-sustaining sprayed sealing practice*, pp.1-31

## CHARACTERISTICS OF LIME STABILIZED EXPANSIVE SOIL FOR CONSTRUCTION OF FLEXIBLE PAVEMENTS

S. Patel<sup>1</sup>, L.M. Reddy<sup>2</sup> and J. T. Shahu<sup>3</sup>

<sup>1</sup>Assistant Professor, Applied Mechanics Department, S. V. National Institute of Technology, Surat, India,

<sup>2</sup>Master Student, Applied Mechanics Department, S. V. National Institute of Technology, Surat, India,

<sup>3</sup>Professor, Department of Civil Engineering, Indian Institute of Technology, Delhi, India,

### ABSTRACT

A large portion of India roughly equal to 0.8 million sq. km, which is about 20% of the total land area, is covered with expansive soil popularly known as Black Cotton (BC) soil. This soil is considered problematic for road construction due to the presence of montmorillonite in its mineralogy which is capable of large volume changes from the dry to the saturated state. In this paper, an attempt has been made to stabilize the problematic expansive Black Cotton soil with lime for the effective utilization in the subbase course of flexible pavements. A number of cylindrical test specimens were prepared from BC soil with different lime (0-12%) contents and cured for 0, 7, 14 and 28 days. The geotechnical properties of different trial mixes, namely, unconfined compressive strength and resilient modulus were determined. The effects of lime content, curing period and curing temperature on unconfined compressive strength and resilient modulus were investigated. Different empirical models are proposed to estimate the resilient modulus of soil-lime mixes and model constants are determined. BC soil stabilized with a minimum lime content of 6% satisfies the criteria recommended by Indian Road Congress for utilization in subbase layer of flexible pavements.

*Keywords: Unconfined Compressive Strength, Repeated Load Triaxial Test, Resilient Modulus ( $M_r$ )*

### INTRODUCTION

India, being called as sub-continent has various geographical, geological and climatic conditions. In developing countries the socio-economic development depends upon the connectivity between the different parts of the country. India is enriched with different types of soils in which more part of the country is covered with black cotton soil which is good for agricultural purpose and in contrary, problematic for construction purpose.

Lime stabilization of black cotton soils waved back to several centuries in India and is a conventional method in so many countries. Since the pavement structure is subjected to traffic loading it is necessary to consider the cyclic loading effect in the design of the pavements. AASHTO [2] has recommended the use of resilient modulus in the design of pavements.

Resilient modulus ( $M_r$ ) is defined as the ratio of deviator stress to recoverable strain. Many organizations in the world do not have the necessary facilities to conduct the resilient modulus test. Therefore, state agencies and pavement designers use available empirical models to estimate resilient modulus of the pavement materials. Various engineering properties of lime stabilized soil have been reported in the literature [3], [4], [7], [9] and

[10]. However, a limited research has been reported in the literature on the behavior of stabilized subgrade under cyclic loading.

Singh et al. [12] reported an increase in resilient modulus value with the addition of lime and class C fly ash to CL soil cured for 28 days. Solanki et al. [13] and [14] observed an increase in resilient modulus of subgrade soils for each of three different additives, such as hydrated lime, class C fly ash and cement kiln dust. Reduction in resilient modulus beyond certain amount of lime content was observed in the literature [14]. Ranjan et al. [11] observed an increase in resilient modulus on addition of lime and cement to three different types of subgrade soils. With the increase in deviator stress, resilient modulus of untreated soil decreased and resilient modulus of treated soil increased [11].

The objective of the present study is to determine the effect of lime content, curing period and curing temperature on unconfined compressive strength and resilient modulus of different soil-lime mixes and to compare different empirical models for predicting the resilient modulus of soil-lime mixes.

The scope of the work includes conducting a series of unconfined compressive strength test and resilient modulus test on cylindrical specimens and carrying out regression analysis on different empirical models.

## EXPERIMENTAL PROGRAM

The experimental program consists of determination of unconfined compressive strength and resilient modulus of different soil-lime mixes.

### Materials

Black cotton soil was collected from SVNIT campus, Surat, India and lime was procured from the local market. The different geotechnical properties of soil as obtained according to Indian Standards were as follows: sand content = 17.5%, silt content = 46.5%, clay content = 36%, specific gravity = 2.7, liquid limit = 60.3%, plastic limit = 27.2%, plasticity index = 33.1%, free swell index = 66.7%, optimum moisture content (OMC) = 20% and maximum dry density (MDD) = 1.75 g/cc. The soil was classified as high plastic clay (CH) as per Indian Standard.

### Unconfined Compressive Strength Test

Unconfined compressive strength test was carried out on the soil mixed with different percentages of limes (3%, 6%, 9%, and 12%). First, soil and lime were mixed in dry state manually and then water corresponding to the OMC was added and mixed thoroughly. Next cylindrical specimens of 50 mm diameter and 100 mm high were compacted in three layers by static press to achieve the MDD of the mix obtained from modified Proctor compaction test. Samples were sealed in polythene bags and kept for curing. Specimens were cured in three different series for UCS test. In first series, specimens were cured at a temperature of 30°C for 0, 7, 14, 28 days. In second series specimens were cured at temperatures of 40°C and 50°C for 7 days. In last series specimens were cured for 3 days at 30°C and then soaked in water for 4 days before UCS test. UCS test was carried out by using a conventional compression testing machine at a strain rate of 0.6 mm/min.

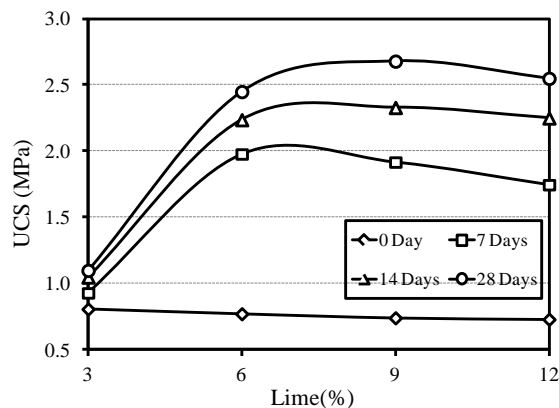


Fig. 1 Variation of UCS with lime content for 30°C curing temperature.

### Repeated Load Triaxial Test

Repeated load triaxial test (RLTT) was carried out on different soil-lime mixes. Cylindrical specimens of 50mm diameter and 100mm high were prepared in three different series same as that of UCS test. The test was carried out in accordance with AASTHO T 307 [1] method. First, the specimens were subjected to 3000 loading cycles during the conditioning phase and then tested for the determination of resilient modulus at fifteen different stress levels.

## RESULTS AND DISCUSSIONS

### Unconfined Compressive Strength

#### *Effect of lime content*

Figure 1 shows the variation of UCS with lime content. There is an increase in UCS values with increase in lime content up to certain extent and decrease thereafter. The lime content at which the compressive strength was maximum varies from 6% for 7 day curing to 9% for 28 day curing period. The strength gain in BC soil-lime mix is mainly due to the cementitious reaction which immediately begins by addition of lime in clay. The calcium ions of lime react with the silica and alumina present in the soil and form  $\text{CaO} \cdot \text{SiO}_2 \cdot \text{H}_2\text{O}$  and  $\text{CaO} \cdot \text{Al}_2\text{O}_3 \cdot \text{H}_2\text{O}$  known as C-S-H and C-A-H gel. These products act as a glue to bind the soil particles together resulting in a stabilized mass. With an increase in lime content, the quantity of gel formation increases, thus increasing the compressive strength. However, for lime content more than the optimum value, the lime particles remain unutilized and simply serve as weak filler in the mix resulting in the reduction of the strength. Similar variations of UCS for lime treated soil have been reported in literature [8].

#### *Effect of curing period*

Figure 2 shows the effect of curing period on UCS of different soil-lime mixes. UCS value increases continuously with curing period for all mixes; however the rate of gain of strength is high during the initial 7 days but slows down thereafter. As the pozzolanic reaction is a slow process the quantity of gel formation increases with an increase in curing period, thus resulting in high compressive strength.

#### *Effect of curing temperature and soaking*

Figure 3 shows the effect of curing temperature and soaking on UCS values for different soil-lime mixes. With the increase in curing temperature UCS



value increases for all lime contents. Higher curing temperature accelerates the cementitious reaction between soil and lime, thus increasing the strength. The soaked UCS values of the soil-lime mixes were found to be lower than the unsoaked UCS values. UCS values of different soil lime mixes at 7 day curing period before and after the cyclic tests were compared in Fig. 3. For third series of UCS tests, 7-day (3 days curing and 4 days soaking in water) UCS values of BC soil with 3%, 6%, 9% and 12% lime were 360, 1480, 1440 and 1310 kPa, respectively. IRC: 51 [6] recommends a minimum 7-day UCS value of 700 kPa for soil-lime mix to satisfy the strength and durability criteria for use in subbase course of flexible pavements. BC soil stabilized with a minimum lime content of 6% satisfies these criteria. UCS values obtained after cyclic test was higher than that obtained before cyclic test which may be due to the rearrangement and densification of soil particles during the application of cyclic loads. Similar trends were also observed for 14 and 28 days curing period. The variations of UCS values with curing temperature obtained in this study are consistent with the results reported in the literature [8].

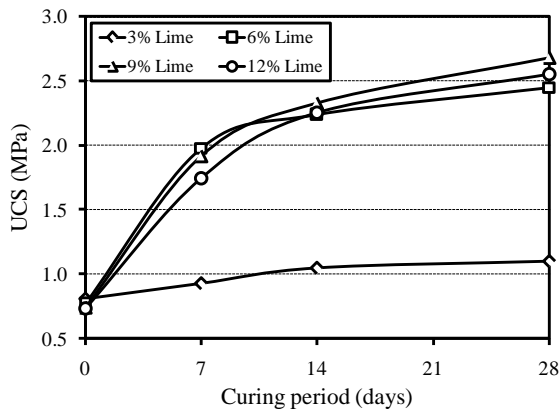


Fig. 2 Variation of UCS with curing period for 30°C curing temperature.

## Resilient Modulus

### Effect of lime content

Figure 4 shows the variation of resilient modulus with lime content for different curing periods at a deviator stress ( $\sigma_d$ ) of 93.1 kPa and cell pressure ( $\sigma_3$ ) of 34.5 kPa. There is an increase in resilient modulus value with increase in lime content up to certain extent (9% lime content) for all curing periods and decreases thereafter. For lime content more than the optimum values the lime particles remain unutilized and serve as weak filler resulting in the reduction of resilient modulus. Similar variations of the resilient modulus with lime content were reported in literature [5], [12], [13], and [14].

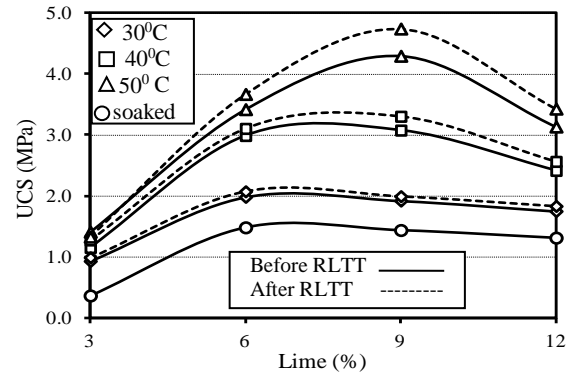


Fig. 3 Variation of UCS with lime content for different curing temperatures at 7 day curing period.

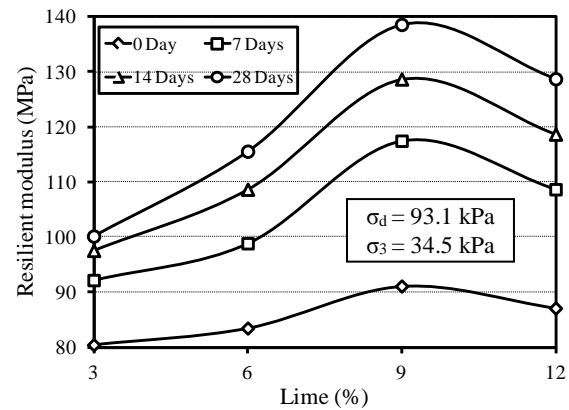


Fig. 4 Variation of resilient modulus with lime content for different curing period.

### Effect of curing period

Variation of the resilient modulus with curing period for different soil-lime mixes at a deviator stress ( $\sigma_d$ ) of 93.1 kPa and cell pressure ( $\sigma_3$ ) of 34.5 kPa is shown in Fig 5. The resilient modulus of all the soil-lime mixes increases continuously with curing period. However, the rate of strength gain is high during the initial 7 day curing and slows down thereafter. The amount of gel formation in the pozzolanic reaction increases with increase in curing period which binds the soil particles more efficiently resulting in higher stiffness.

### Effect of temperature

Figure 6 shows the variation of resilient modulus with lime content for different curing temperatures and soaking condition. There is an increase in resilient modulus with increase in temperature due to the accelerated pozzolanic reaction at higher temperature which shows that the lime stabilization is more effective in tropical countries where temperature is high. Resilient modulus of the soaked specimens were found to be higher than that of the

unsoaked specimens except for 3% lime content. This may be due to the development of pore water pressure during the cyclic test as the specimens were tested under undrained condition. The presence of pore water increases the resistance to the deformation resulting in higher stiffness.

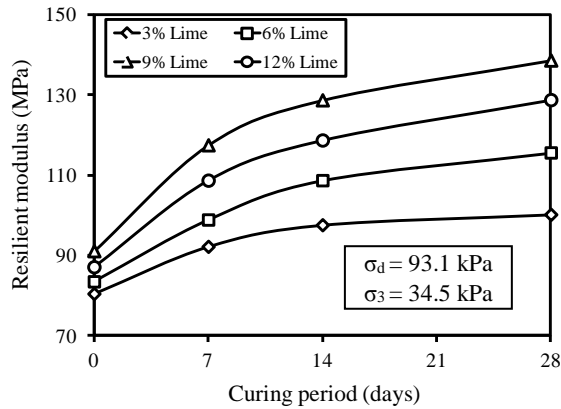


Fig. 5 Variation of resilient modulus with curing period for different lime content.

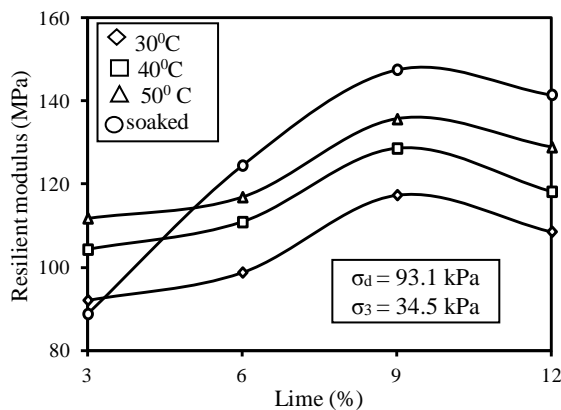


Fig. 6 Variation of resilient modulus with lime content for different curing temperature.

#### Effect of major principal stress

Variation of resilient modulus with major principal stress ( $\sigma_1$ ) for different soil-lime mixes are shown in Fig. 7 and Fig. 8. There is an increase in resilient modulus with increase in stress value for all lime content and curing period. Similar trend was also observed for other lime contents and curing periods.

Several constitutive stress based models for the estimation of  $M_r$  are available in the literature. In this study the fitness of four stress based models for the determination of  $M_r$  for soil-lime mixes are compared in Table 1. The residual sum of squares (rss) and the coefficient of determination ( $R^2$ ) obtained from the non-linear regression analysis were used to compare the “goodness of fit” for the

four models. The regression constants obtained were used for determining the predicted resilient modulus of the mixes. A graph was drawn between measured resilient modulus and predicted resilient modulus, and the corresponding  $R^2$  and rss values were determined. Comparison between the four models shows that the three parameter model provided a best fit regression equation for the determination of resilient modulus of lime stabilized soil.

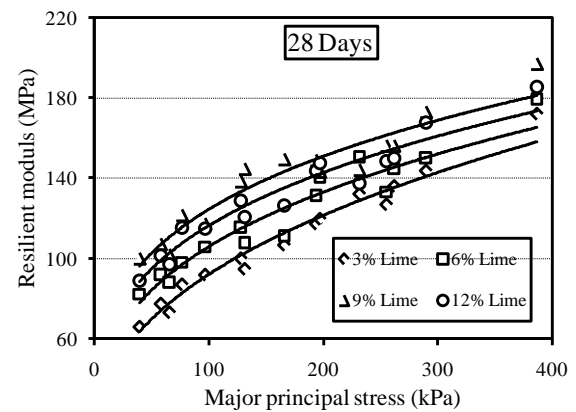


Fig. 7 Variation of resilient modulus with major principal stress for different lime content.

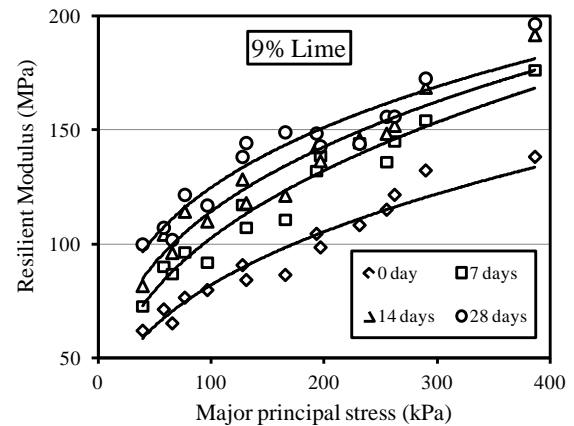


Fig. 8 Variation of resilient modulus with major principal stress for different curing period.

Table 1 Stress based models with  $R^2$  and rss values

Model	$R^2$	rss
$\frac{M_r}{P_a} = k_1 \left( \frac{\sigma_3}{P_a} \right)^{k_2} \left( \frac{\sigma_d}{P_a} \right)^{k_3}$	0.96	11651
$M_r = k_4 \sigma_d^{k_5}$	0.92	25920
$M_r = k_6 \sigma_1^{k_7}$	0.94	18766
$M_r = k_8 \theta^{k_9}$	0.86	41839

$P_a$  is atmospheric pressure equals to 101.3 kPa

$k_1, k_2, k_3, k_4, k_5, k_6, k_7, k_8$  are model constants

Model constants ( $k_1$ ,  $k_2$  and  $k_3$ ) of the three parameter model obtained for different soil-lime mixes were given in Table 2. The value of  $k_1$  increases with an increase in lime content upto 9% and decreases thereafter for all curing periods and curing temperatures. However, no consistent trends have been observed for values of  $k_2$  and  $k_3$ . Figure 9 shows the graph between predicted  $M_r$  using three parameter model and actual  $M_r$  of all the soil-lime mixes for fifteen different stress levels.

Table 2 Model constants of three parameter model for different lime content and curing period

$\frac{M_r}{P_a} = k_1 \left( \frac{\sigma_3}{P_a} \right)^{k_2} \left( \frac{\sigma_d}{P_a} \right)^{k_3}$						
Curing Period	Lime (%)	$k_1$	$k_2$	$k_3$	$M_r^p$	$M_r^a$
0 day	0	0.79	0.07	0.29	72.6	72.5
	3	0.94	0.16	0.30	78.2	80.4
	6	0.96	0.13	0.27	83.0	83.4
	9	1.03	0.09	0.27	92.6	91.0
	12	1.01	0.12	0.27	87.6	87.0
7 days	3	1.06	0.13	0.27	91.1	92.1
	6	1.16	0.16	0.24	97.0	98.8
	9	1.31	0.13	0.24	113.0	117.4
	12	1.24	0.16	0.24	103.7	108.6
14 days	3	1.08	0.08	0.30	98.0	97.5
	6	1.25	0.12	0.23	109.8	108.6
	9	1.39	0.06	0.26	129.0	128.6
	12	1.33	0.07	0.26	122.3	118.6
28 days	3	1.21	0.15	0.25	102.1	100.1
	6	1.33	0.13	0.20	114.7	115.5
	9	1.49	0.09	0.19	135.0	138.5
	12	1.40	0.07	0.23	129.4	128.6
7 days at 40°C	3	1.21	0.16	0.22	101.9	104.3
	6	1.25	0.12	0.25	108.8	110.9
	9	1.36	0.08	0.25	124.0	128.6
	12	1.33	0.11	0.24	116.6	118.2
7 days at 50°C	3	1.22	0.09	0.24	110.2	111.8
	6	1.30	0.10	0.21	116.6	116.9
	9	1.44	0.07	0.22	132.6	135.6
	12	1.36	0.08	0.23	124.5	128.9
7* days	3	0.98	0.12	0.35	84.6	88.8
	6	1.36	0.11	0.34	119.4	124.5
	9	1.50	0.03	0.28	144.0	147.5
	12	1.45	0.04	0.28	137.6	141.5

$M_r^p$  is predicted resilient modulus in MPa and  $M_r^a$  is actual resilient modulus in MPa at  $\sigma_3 = 34.5$  kPa and  $\sigma_d = 93.1$  kPa;

\*3 day curing at 30°C and 4 day soaking in water.

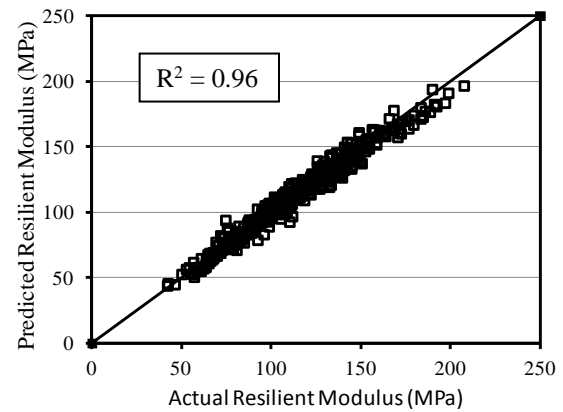


Fig. 8 Predicted  $M_r$  versus actual  $M_r$  for three parameter model.

## CONCLUSIONS

Engineering properties such as unconfined compressive strength and resilient modulus of soil-lime mixes were investigated and the following conclusions were drawn:

- UCS values increases with increase in lime content up to certain extent and decreases thereafter. UCS value was maximum at 6% and 9% lime content for 7 days and 28 days curing period, respectively. The rate of gain of strength is high during the initial seven days but slows down thereafter.
- Higher the curing temperature, higher is the UCS value obtained. It was observed that soaking of the specimens in water reduces its compressive strength for 7 day curing period.
- BC soil stabilized with a minimum lime content of 6% satisfied the strength criteria for use in subbase course as recommended by IRC 51.
- Resilient modulus of the soil-lime mixes increases with the increase in lime content upto 9% and decreases thereafter for all curing periods and curing temperatures.  $M_r$  value increases continuously with increase in curing period and curing temperatures. Resilient modulus of the soaked specimens were observed to be higher than that of the unsoaked specimens for 6, 9 and 12% lime contents.
- The performance of four stress based models were compared and observed that the three parameter model outperformed the other models with high coefficient of determination values providing good fit model constants for the determination of resilient modulus.

## LIST OF SYMBOLS

$M_r$  : resilient modulus  
 $\sigma_d$  : deviator stress  
 $\epsilon_r$  : recoverable strain  
 $\sigma_3$  : cell pressure  
 $\sigma_1$  : major principal stress  
 $\theta$  : bulk stress

## REFERENCES

- [1] AASHTO T 307, "Determining the resilient modulus of soils and aggregate materials", 2000.
- [2] AASTHO, "Guide for design of pavement structures", 1993.
- [3] Chakkrit S., Anand JP., Vivek C., Sireesk S., Laureano RH, "Combined lime and cement treatment of expansive soils with low to medium soluble sulfate levels", Geocongress 2008, ASCE, pp. 646-653.
- [4] George SZ., Ponnai DA., Little JA, "Effect of temperature on soil-lime stabilization", J. of Construction and Building Materials, Vol. 6 No. 4, 1992, pp. 247-252.
- [5] Hossain Z., Zaman M., Doiron C., and Solanki P, "Evaluation of mechanistic empirical design guide input parameters for resilient modulus of stabilized subgrade soils", ICSDEC 2012, pp. 510-518.
- [6] Indian Road Congress 51, "Guidelines for the use of soil-lime mixes in road construction", 1992.
- [7] Muhamed A and Wanatowski D, "Effect of lime stabilisation on the strength and micro structure of clay", IOSR J. of Mechanical and Civil Engg., Vol. 6, June 2013, pp. 87-94.
- [8] Nasrizar A., Ilamparuthi K., and Muttharam M, "Quantitative models for strength of lime treated expansive soils", Geocongress 2012, ASCE, pp. 978-987.
- [9] Pranay KC., Sai KV., Anand JP., Laureano H, "Evaluation of strength, resilient moduli, swell and shrinkage characteristics of four chemically treated sulfate soils from north Texas", GSP 136 Innovations in Grouting and soil improvement, ASCE 2005.
- [10] Radha KD., Vincent PD., Kim D, and Chen R, "Assessing the quality of soils modified with lime kiln dust measuring electrical conductivity with time domain reflectometry", J. of Transportation Research Board, 2006, pp. 101-109.
- [11] Ranjan KR., Pinit R, Shashank V., Anand J. P, "Resilient moduli behavior of lime cement treated subgrade soils", Geocongress 2012, ASCE, pp. 1428-1437.
- [12] Singh D., Rouzbeh G., Joakim GL., and Zaman M, "Laboratory performance evaluation of stabilized sulfate containing with lime and class C fly ash", Geoflorida 2010, ASCE, pp. 757-766.
- [13] Solanki P, Zaman MM, and Jeff D, "Resilient modulus of clay subgrade stabilized with lime, class C fly ash, cement kiln dust for pavement design", J. of Transportation Research Board, 2010, pp. 101-110.
- [14] Solanki P., Khoury N and Zaman MM, "Engineering properties and moisture susceptibility of silty clay stabilized with lime, class C fly ash, cement kiln dust", J. of Materials in civil Engg., ASCE, Vol.12, Dec. 2009, pp. 749-757.

## **UPTAKE OF ADVANCED AND SUSTAINABLE ENGINEERING MATERIALS IN CIVIL INFRASTRUCTURE PROJECTS**

David S Thorpe

Faculty of Health, Engineering and Sciences, University of Southern Queensland,

### **ABSTRACT**

Advanced and sustainable engineering materials, such as engineered fibre composites, geopolymer cement, and recycled concrete have the potential to reduce demand on scarce resources, improve safety, reduce greenhouse gas emissions and contribute to positive initiatives in civil engineering design and construction in areas like foundations and structural members. For example, engineered fibre composites can replace other materials (such as timber), because of their high strength to weight ratio, light weight and ease of installation. They can also have positive impacts on sustainability. While advanced materials have several advantages, their take-up by industry, and in particular small and medium enterprise companies (SMEs), has in a number of cases been relatively slow. This is likely to be the result of a number of factors, such as relatively high cost, financial risk in using an unproven technology, lack of suitable design standards, an unproven life cycle, uncertainty over long-term sustainability issues, and possible changed building and construction methods. Advantages and disadvantages of the use of selected advanced and sustainable materials in civil engineering projects are investigated. A weighted scoring methodology for improved evaluation of their advantages and disadvantages, with a view to aiding decisions, is proposed.

*Keywords: Advanced Materials; Sustainability; Innovation; Civil Engineering; Construction*

### **INTRODUCTION**

Advanced and sustainable engineering materials have the potential to make a positive contribution to civil engineering design, construction, operation and maintenance through reducing demand on scarce resources, improving safety and positively impacting on sustainability and resilience. While there have been a number of applications of these materials, their uptake at a more general level in civil engineering projects, and particular the small and medium enterprise (SME) building and construction sector, has tended to not been as rapid as it could.

A number of such materials have considerable promise in terms of innovation in engineering design, construction and asset management. Polymer composites, for example, are well-known for their use in manufacturing applications like aircraft. They have also had considerable use in non-critical structural applications such as bathrooms and vanities, cladding, decoration and finishing. It has been claimed that, in 1999, the construction sector was the world's second largest consumer of polymer composites, with 35% of the global market [1]. More recently, they have also been used in a number of applications like walers in corrosive environments, fibre composite bridge girders as alternatives to timber girders, railway sleepers, and repair and replacement of timber piles [2]. These structural applications of advanced materials promise to provide considerable efficiencies to the construction

process and contribute to sustainability through increased sustainability of scarce resources like old-growth timber. Other advanced and sustainable materials are similarly being successfully used in civil engineering applications.

The SME construction sector has been shown to be quite innovative in a number of areas, and in particular in the adoption of proven products and improved processes [3]. At the same time, there appears to be some reserve with respect to the development of less well-known or less well proven technologies. Price, for example, driven by the competitive tendering process, was found to be the main factor in a Welsh study on the adoption of pozzolans as substitutes for cement [4].

The decision-making process with respect to the adoption of new innovations (including new materials) is likely to be the result of a balance of barriers and enablers to adoption of innovations. Other factors, such as knowledge of the innovation, client requirements and legislative factors are also likely to impact on the decision to use advanced and sustainable materials.

This paper explores some of the issues, barriers and enablers with respect to this decision, discusses research with respect to innovation in small builders that illustrates the innovation process, and proposes a weighted scoring methodology for aiding the decision making process.

## EXAMPLES OF ADVANCED AND SUSTAINABLE MATERIALS

The materials selected for the discussion in this paper are engineered fibre composites, cement (pozzolanic substitutes for cement and geopolymers based cement) and concrete using recycled materials. These materials have been selected because of their potential impact on civil engineering developments.

One definition of composite materials is that they combine and maintain two or more distinct phases to produce a material superior to either of the base materials [5]. Polymer composites combine polymer resin (for example, polyester, vinyl and epoxy) with fillers and reinforcing fibres (such as glass, aramid and carbon) used as the primary means of carrying load, while the polymer resin protects the fibres and binds them into a cohesive structural unit, commonly called fibre composites [6]. As previously discussed, they have a wide range of applications in civil engineering and building, particularly in corrosive environments or as replacements for more traditional materials.

It has been claimed that in North America alone 10 billion tonnes of concrete are produced each year. This concrete has a definite impact on the environment. Strategies to meet the environmental challenge include the use of supplementary cementitious materials (such as fly ash and granulated blast furnace slag), use of recycled materials in place of natural resources, improved durability, improved mechanical and other properties (for example, doubling the strength of concrete in compression members to reduce the required amount of material) and reuse of wash water. There are both advantages and disadvantages with these processes. For example, while cement made with fly ash utilizes a waste material and is useful for mass structures because it has a delayed and different reaction from Portland cement, its relatively slow rate of strength development makes it unsuitable for applications requiring high early strength. The variation in the properties of fly ash between different electric power plants also raises an issue with respect to quality control. Recycled aggregate generally has lower densities than the original material used because of the cement mortar that remains attached to the original particles, and larger water absorption than virgin aggregate. The aggregate also varies in quality. Concrete made with recycled aggregate tends to have lower strength than concrete made with virgin aggregate. It is expected, however, that a shifting public attitude towards global warming is likely to increase the use of concrete containing recycled materials [7].

A geopolymer may be described as “the

inorganic aluminosilicate polymeric gel resulting from the reaction of amorphous aluminosilicates with alkali hydroxide and silicate solutions.” The material may have various names, including geopolymer cement (or concrete). It has been used on concrete of up to 70 MPa in strength, and can attain satisfactory high early strength if the temperature is above 20 degrees Celsius. Concrete made with this material as binder is claimed to have higher tensile and flexural strength, and lower drying shrinkage, relative to concrete made with Portland cement. It has been used in a range of applications like pavements, a retaining wall, water tanks, a boat ramp and precast bridge decks [8].

Carbon dioxide emissions from concrete made with this material have been compared that made from Portland cement. One such study, on a one cubic metre sample used in a Melbourne, Australia, bridge, reported that when obtaining raw materials, concrete manufacturing, and construction (transport and onsite placement) were taken into account that the carbon dioxide emission from the concrete made with geopolymer cement was 9% less than that from equivalent concrete made with Portland cement [9].

In summary, while there are a number of advantages with advanced and sustainable materials, there are also some disadvantages with them from the point of view of the product (material) itself. The following sections develop this discussion further.

## THE INNOVATION ADOPTION PROCESS

The uptake of advanced and sustainable materials and their associated processes can be described by the concept of innovation, which can be defined as the development of an idea, practice, or object that is perceived as new by an individual or other unit of adoption. According to Rogers [10], the generation of innovations has the steps of recognizing a problem or need, research (basic and applied), development, commercialization, diffusion and adoption and the consequences (changes that occur to an individual or a social system as a result of adoption or rejection of an innovation). In the adoption process, the potential user of the innovation makes a decision, the stages of which are gaining knowledge of the innovation, forming an attitude about it (persuasion), making a decision whether to accept or reject it, implementation of the new idea, and confirmation of this decision. All steps in the decision process involve communication.

The decision process is when an organization decides to adopt or not adopt a new product or process. There are rewards for early adopters of a process. There are also negative risks, such as potential financial loss. The materials discussed in



the previous section would tend to be mainly in the research or development phases of the innovation process. Thus, any adopter of one of these materials would be considered to be an early user of it.

The Queensland Department of Transport and Main Roads have further identified that in order to achieve the successful development of a product, it is necessary for all members of the interdisciplinary team to have a common and shared understanding of the material and service life conditions. In their consideration of engineered fibre composites, the major participants are the fibre composite designers, manufacturers, installers, infrastructure owners and academia [11]. There should be a shared understanding and clear lines of communication between these parties for successful adoption of the product.

#### **ENABLERS IN THE UPTAKE OF ADVANCED MATERIALS**

The process of forming an attitude about an innovation, which is the focus of the persuasion stage of the decision process, will require an assessment of items like relative advantages, compatibility, complexity, trialability and observability [12]. The assessment of these factors will require evaluation of the advantages and other enablers of the adoption of these materials, and of the disadvantages and other barriers to this adoption or uptake.

From the point of view of enablers of innovation in the Australian construction industry, a national survey of 383 construction industry firms [13] identified a number of drivers for innovation in the firms surveyed, which included efficiency, productivity improvements and customer needs. Better performing firms adopted a number of advanced practices, and invested in research and development.

Profit, market and legal related factors [14], and knowledge, along with its organization and dissemination [15], have also been identified as aids to innovation. A United Kingdom study found that in small construction firms, owners have the power to ensure rapid decision-making and thus facilitate rapid innovation, and that the process of innovation was behavioral and cyclical in nature [16].

A further potential driver of innovation for organizations undertaking civil engineering projects is the growing requirement for sustainable construction practices, including energy efficiency and resilience of buildings to extreme weather events [17]. Sustainability may come at an economic cost [18], which requires consideration.

Other enablers in the uptake of advanced and sustainable materials may include superior performance, improved client and community acceptance of modern energy efficient materials, and ease of construction and installation (such as with the relatively light fibre composite materials).

#### **POTENTIAL ISSUES IN THE UPTAKE OF ADVANCED AND SUSTAINABLE MATERIALS**

While there are a number of factors that facilitate the uptake of advanced and sustainable materials in civil engineering, a number of issues and barriers to this uptake have also been identified.

For example, the Queensland Department of Transport and Main Roads has identified a number of areas in which there are deficiencies between engineered fibre composites and other products such as concrete and steel. One of these areas is the lack of an Australian standard for this product. While there was a draft standard developed, it did not progress because of a lack of industry interest. Fragmentation and the use of Intellectual Property as a tool to closely guard information but also limit transparency surrounding manufacturing limits the openness of information published in papers. Ultimately, the lack of standards poses a professional indemnity risk for designers.

Other issues identified by the Department include uncertainty about the material properties with changes in temperature, and deficiencies in manufacturing and installation specifications, knowledge of design life and asset management procedures. The risk of brittle collapse is also an issue that remains unresolved. The Department is mitigating these risks by working with academics, undertaking trial installation of fibre composite replacement girders and undertaking structural health monitoring. It is also developing its own specifications [19].

While these processes might be useful for larger organizations, it is unlikely that the SME sector would have the financial strength to support the extensive development and testing required. There are also likely to be other barriers to the adoption of new materials by industry, and particularly its SME sector. For example, the Australian construction industry has been considered fragmented, adversarial and having low profit margins, low-bid tendering, inequitable risk sharing, small firm size, a lack of investment in technology, a cyclical nature, a large proportion of very small firms and a limited history of business deliverables from researchers

[20]. The small firm size tends to be an international trend [21]. It has also been found that cost-related factors are significant barriers to innovation, as are market-related factors and lack of skilled staff [22]. In summary, if the construction industry is to benefit from innovation, it has to change from an adversarial and blame culture to a sharing one [23].

Other negative factors that may have a bearing on the decision process to use advanced and sustainable materials in civil engineering projects, and in particular by SME firms, are likely to include the high cost of adopting and using these materials and the risks (particularly financial risks) of the new innovation not being successful.

### **RESEARCH INTO INNOVATION IN SMALL RESIDENTIAL BUILDERS**

In order to better understand the innovation process in the SME engineering and construction sector, the author undertook research in 2006 into innovation in the small firm residential building sector in South-East Queensland, Australia [24]. One hundred small residential builders constructing housing up to \$A750,000 in value were contacted, with 20 agreeing to a structured interview.

A qualitative methodology incorporating a semi-structured interview process was used. The objectives of the interview questions were to explore the extent of innovation in the firms selected, provide an understanding of how they developed or adopted innovations, assess the value of innovations to the firm and determine their readiness to adapt to changes in their operating environment.

Seven of the firms interviewed had four or fewer staff, 11 had five to 19 staff, and two had just over 19 staff. Of these firms 18 were primarily engaged in construction, and the other two in renovation and maintenance. Eleven of the firms undertook design as well as construction. All were involved in private sector residential work.

There were 50 examples of innovation in these firms. Of these innovations, 25 were associated with the development of a new or improved product. The majority of other innovations were associated with the development of a new or improved process. Eleven of the innovations were related to new or improved materials. Advanced materials like engineered fibre composites were however not listed by the builders.

Interviewees were also asked to select a particular innovation and discuss in depth why they developed or used it. The reasons given for their development ranged from an interest in a particular

aspect of improvement (for example, sustainability) to the specific business objective of improving productivity and/or efficiency.

A majority of the firms stated that the innovation was profitable, with none reporting a decrease in profits. Most firms did not feel that they had gained a competitive advantage by using the innovation, and there was uncertainty that using the selected innovation had reduced risk. However, all firms indicated that they would use the innovation again. This was a positive sign that the innovation had been of benefit to the firm.

Responses to questions about sustainability related innovations were varied, and included the positive responses that sustainable practices were good for business, made firms competitive and were a point of difference. Negative responses included the cost availability (of suitable materials), that some firms would only undertake sustainable practices if required and that tight margins were a barrier to adopting sustainable practices.

While not all of the firms reported problems in implementing the selected innovation, they expressed concerns with respect to the availability of suitable trades people. Cost (which also impacts on client expectations) and the need for legislation to keep up with industry advances were also cited as issues in this regard.

In summary, the SME builders, while generally supportive of innovations that utilized new or improved materials, had a number of reservations in areas like profitability and risk, and had concerns in areas like cost and availability of suitable materials.

### **A PROCESS FOR ASSESSING THE UPTAKE OF MATERIALS**

The above discussion has shown that while industry is interested in adopting innovative materials and processes, there are a number of factors that both encourage and discourage their use. A weighted scoring process has been proposed to aid the adoption decision process. This process focuses on the persuasion stage of that decision process, and in particular on the relative advantage of the innovation.

The stages in this process are to a) adopt a scoring system that enables factors expressed in different units of measurement to be included in the evaluation on an equivalent basis; b) weight the factors with respect to each other; and c) calculate a total weighted score combining the weights and the scores of individual factor values.

In order to provide an approach that permits a mix of quantitative and qualitative variables to be combined in the same analysis on an equivalent basis, each variable in the evaluation is assigned a score on the same rating scale. For quantitative variables, the score would be assigned on the basis of calculation, based on a formula that related the scores to actual variable values. Qualitative variables would be assigned a utility value derived from a risk profile based on the indifference point between various combinations of worst and best expected outcomes, given the probabilities of receiving each [25]. Stakeholder views would aid this process.

While there are a number of options for assigning the weights for each factor being assessed, one approach is the rational management process of Kepner and Tregoe [26]. This approach formulates a goal statement and considers the objectives supporting this goal by dividing them into musts (which are not negotiable) and wants. The wants are then grouped into related variables, and the groups are ranked using pair wise comparison or other techniques. Benefit and cost may be considered separately from the analysis, or else assigned a score and included in the analysis.

The final step is to calculate a total weighted score by summing the individual weighted scores, as follows:

$$T = \sum_{i=1}^n W_i S_i$$

Where:

T = Total Weighted Score

W<sub>i</sub> = Weight for factor i

S<sub>i</sub> = Score for factor i

This process is illustrated for engineered fibre composites, in which the alternatives of “adopt” and “not adopt” in the replacement of a timber bridge girder are compared. For simplicity, the analysis uses the selected factors of material, design life, ease of construction, availability of standards, ability to trial and sustainability. A scale of 0 to 10 is used to assign scores, which are multiplied by weights assigned to each factor and summed for each case, as shown in Table 1. In this table, “ease of construction” has been shown as “ease of building”, “availability of standards” has been shown as “available standards”, and “sustainability” as “sustain.” The abbreviation “Tot.” has also been used in the header rows for “Total.”

On the basis of the result in Table 1, the decision would be to probably adopt the material, subject to consideration of other factors like benefit and cost.

Table 1 Example Weighted Scoring Calculation for Adoption Decision - Fibre Composite

Factor Scores	Weight	Adopt		Not adopt	
		Item	Tot.	Item	Tot.
Material	0.25	8	2	2	0.5
Design life	0.15	6	0.9	4	0.6
Ease of Building	0.15	7	1.05	5	0.75
Available Standards	0.3	2	0.6	10	3
Sustain	0.15	6	0.9	2	0.3
<b>TOTAL</b>	<b>1.00</b>		<b>5.45</b>		<b>5.15</b>

## CONCLUSION

This paper has focused on the uptake of advanced and sustainable materials in civil infrastructure projects, with particular emphasis on their adoption by small and medium enterprise companies. It has overviewed the topic, discussed examples of advanced and sustainable materials, outlined the innovation process, discussed factors which aid (enablers) and prevent (barriers) with respect to uptake of these materials in civil engineering projects, discussed previous research into a similar area and outlined a possible approach to the adoption decision process.

It is concluded that as demonstrated in the research into innovation by small builders the industry is quite interested in adopting new materials and methods of design and construction, there are still reservations that prevent the complete uptake of advanced and sustainable materials in civil engineering projects. While advances in methods and the requirements of sustainable development may facilitate this process, there is a strong requirement for appropriate standards to be developed, increased trials of these materials in applications, and extensive communication to the industry about the benefit of using advanced and sustainable materials in their businesses.

## REFERENCES

- [1] Humphreys, MF, “The Use of Polymer Composites in Construction”, in Proc. 2003 International Conference on Smart and Sustainable Built Environment, November, 2003, Brisbane, Australia.
- [2] Aravinthan, T, “Fibre Composites in Civil Infrastructure – Research to Reality in Australia”, in Manalo, A and Kee-Jeung Hong

- (eds.) *Research to Reality: Promoting Fibre Composites in Civil Infrastructure*, February 2014, pp. 2-7.
- [3] Thorpe, D, Ryan, N., Charles, M., 'Innovation and small residential builders: an Australian study', *Construction Innovation*, Vol. 9, No. 2, 2009, pp. 184-200.
- [4] O'Farrell, M and Miller, CJM, "The barriers to new technology diffusion in the construction industry of South Wales", in *Current Issues in Small Construction Enterprise Development*, Welsh Enterprise Institute Monograph No. 4, ed. Miller, CJM. Packham, GA and Thomas, B, Pontypridd: University of Glamorgan Business School, 2002, pp.123-137.
- [5] Humphreys, MF, op. cit.
- [6] Humphreys, MF, op. cit.
- [7] Meyer, C, "Recycled Materials in Concrete", in Mindness, M (ed.), *Developments in the Formulation and Reinforcement of Concrete*, Cambridge, England: Woodhead Publishing Limited, 2008, pp. 208-230.
- [8] Aldred, J and Day, J, "Is Geopolymer Concrete a Suitable Alternative to Traditional Concrete?" in *37<sup>th</sup> Conference on our World in Concrete & Structures*, Singapore, August 2012.
- [9] Turner, LK and Collins, FG, "Carbon Dioxide Equivalent (CO<sub>2e</sub>) Emissions: A Comparison between geopolymer and OPC Cement Concrete", *Construction and Building Materials*, Vol. 43, 2013, pp. 125-130.
- [10] Rogers, EM, "Diffusion of Innovations", 5<sup>th</sup> ed., New York: Free Press, 2003, pp. 12, 136-168.
- [11] Pritchard, R, "an Infrastructure Owners Perspective of Fibre Composites", in Manalo, A and Kee-Jeung Hong (eds.) *Research to Reality: Promoting Fibre Composites in Civil Infrastructure*, February 2014, pp. 30-34.
- [12] Rogers, EM, 2003, op. cit., p. 170.
- [13] Manley, K, Allan, D, Blayse, A, Coillet, M, Hardie, M, Hough, R, MacKenzie-Smith, S, May-Taylor, W, McFallan, S, Miller, M, Swainston, M, Taylor, G, "BRITE Innovation Survey", Brisbane: Cooperative Research Centre for Construction Innovation, 2005.
- [14] Australian Bureau of Statistics, "Innovation in Australian Business 2003", ABS Catalogue No, 8158.0. Canberra: AGPS, 2005.
- [15] Egbu, CO, "Managing Knowledge and Intellectual Capital for Improved Organizational Innovations in the Construction Industry: an Examination of Critical Success Factors", *Engineering, Construction and Architectural Management*, Vol. 11, No. 5, 2004, pp. 301-315.
- [16] Sexton, M, and Barrett, P, "Appropriate Innovation in Small Construction Firms", *Construction Management and Economics*, Vol. 27, No. 6, 2003, pp. 623-633.
- [17] Australian Building Codes Board, "Discussion Paper - Resilience of Buildings to Extreme Weather Events", Canberra: AGPS, April 2014.
- [18] Meyer, C, "The Economics of Recycling in the US Construction Industry", in Chun, Claisse, Naik and Ganjian (eds), *Sustainable Construction Materials and Technologies*, London: Taylor and Francis Group, 2007.
- [19] Pritchard, R, op.cit.
- [20] Hampson, KD and Brandon, P, "Construction 2020: A Vision for Australia's Property and Construction Industry", Brisbane: Cooperative Research Centre for Construction Innovation, 2004.
- [21] European Commission, "Constrinnonet – Promoting Innovation in Construction Industry SMEs Project Final Report", Constrinnonet Project Consortium, 2004.
- [22] Australian Bureau of Statistics, op. cit.
- [23] Egbu, CO, op. cit.
- [24] Thorpe, D, Ryan, N., Charles, M., 2009, op. cit.
- [25] Hamburg, M, "Statistical Analysis for Decision Making", NY: Harcourt, Brace and World, pp. 631-644.
- [26] Kepner, CH and Tregoe, BB, "The New Rational Manager", Princeton, NJ: Kepner-Tregoe Inc.

## A CASE STUDY – USE OF EXPANDED POLYSTYRENE BLOCKS IN LANDSLIDE REMEDIAL WORKS

M. Boyer<sup>1</sup>, K.Chew<sup>2</sup> and Dr B. Look<sup>3</sup>

<sup>1,2</sup>Senior Geotechnical Engineer, Jacobs SKM, <sup>3</sup>Principal Geotechnical Engineer, Foundation Specialist Group, Australia

### ABSTRACT

This paper describes the use of expanded polystyrene blocks (EPS) as a lightweight fill as a means of stabilising a landslide. EPS is more commonly used for construction of embankments over soft ground. This case study describes the stabilisation of a fifty metre section of road in Queensland that was undergoing subsidence as a result of a large landslide. These works required re-grading of the slope and the installation of deep counterfort drains and horizontal drains, twenty-six metres in length. Part of the landslide was also stabilised using soil nails with high tensile steel mesh facing. The actual road was reconstructed using lightweight expanded polystyrene fill.

*Keywords: Landslide, Ground improvement, Lightweight fill, Expanded polystyrene, Soil nails*

### INTRODUCTION

Woombye-Montville road leads up the steep basaltic capped scarp on which the townships of Maleny, Montville and Mapleton are located in the Sunhsine Coast Hinterland, Queensland.

Multiple landslides occurred during and immediately following an unusual heavy rainfall event that also coincided with the January 2011 Queensland floods.



Fig. 1 Areas of subsidence and tension cracks

This landslide is believed to have occurred as a result of the combined effect of concentrated localised perched water flows (springs) and the damming effect of relatively low permeability colluvium that covers much of the lower slopes over which this road has been constructed [1]. This landslide is described as a deep seated rotational failure within the colluvial soils that extends back

beneath the road embankment into the adjacent cut slope. It was initially noted as a large area of subsidence with tension cracks in the road pavement as shown in Fig 1. Monitoring at this site indicated that further movement of the area was occurring in response to subsequent rainfall events.

### DESIGN DEVELOPMENT

#### Ground model

A ground model relating to this site was developed though detailed geomorphological mapping, geotechnical investigation and instrumentation which included piezometers fitted with dataloggers and inclinometers measuring ground movement with depth. The ground model and remedial measures are shown diagrammatically as Fig 2.

The location of critical slip surface was fairly well known where the back scarp and secondary scarp daylighted at the surface and where inclinometer movements have confirmed the location of deep slip surface within colluvial soils just above the underlying sandstone rock in this area. However, the location of the failure surface downslope could not be clearly inferred from investigations alone. Back analysis using limit equilibrium methods of circular slip analysis was used to predict the extent of the slip further down slope and establish soil parameters for further remedial design.

Groundwater conditions were inferred from either those recorded in piezometric wells or where visible seepage from the adjacent cut slope and toe of the slope could be observed during periods of

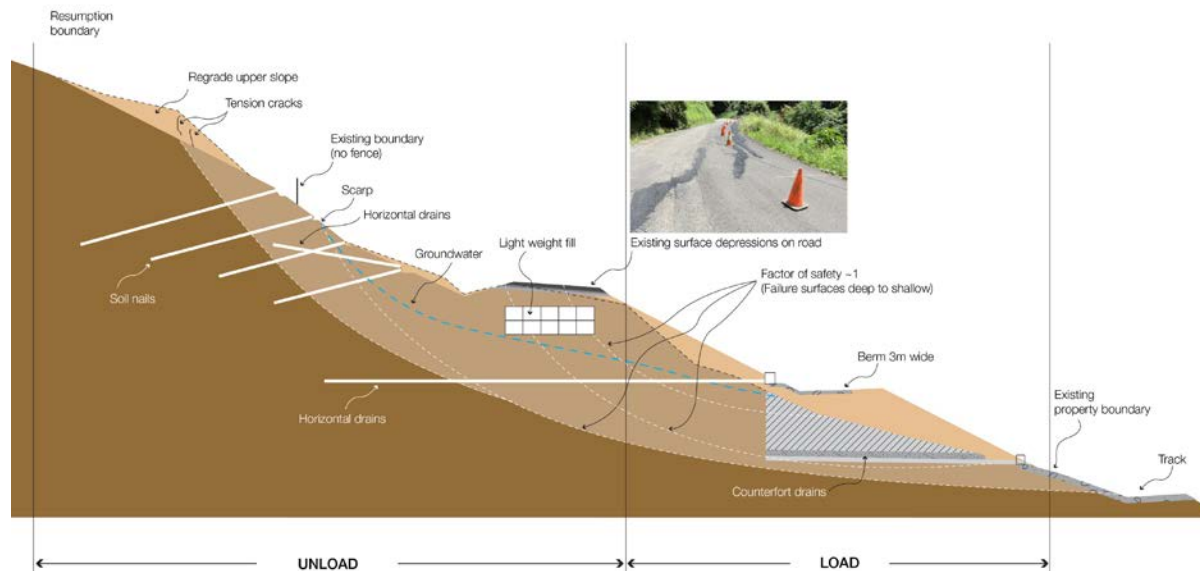


Fig. 2 Diagrammatic ground model showing failure mechanism and remedial design elements

heavy rain. Groundwater levels were found to rise and recede rapidly in response to rainfall and the lower part of the slope became fully saturated immediately after heavy sustained rainfall events.

### Design Concept

Hutchinson [2] describes the influence line approach to landslide analysis and stabilisation remediation. Influence lines indicate the optimum location of subsurface drainage measures and corrective cuts and fills. Detailed design of these works combined the three main principles of embankment stabilisation namely:

#### Unload

The driving forces imposed on this landslide were reduced by re-grading the upper part of the slope and reinforcing the cutting with soil nails. The road embankment was re-constructed using lightweight expanded polystyrene blocks.

#### Drainage

The site is drained using a combination of inclined drains into the soil nailed slope, deep counterfort drains and drilled horizontal wells up to twenty six metres in length.

#### Load

The site has been re-graded and fill has been placed over the toe of the landslide, increasing the stabilising forces imposed on the system.

This combination of loading and unloading the system and measures to control groundwater aims to address the balance of forces and provide the required global factors of safety as indicated by limit equilibrium computer analysis. Although this analysis indicated that a minimum global factor of safety could be achieved in the overall slope without the use of lightweight fill, this was adopted by the designers to account for uncertainty around the behaviour along pre-existing sheared surfaces and the upper level local stability of the road shoulder. It also made good practical sense to reconstruct the upper portion of the road embankment that had been damaged.

The analysis for global stability can be misleading as it indicates that the critical failure surface is the deep seated failure which matches the movement recorded by inclinometers. However, as is evident by secondary slip surfaces in the edge of the road embankment, less critical failure surfaces are present which present less than the acceptable factor of safety. EPS was employed to deal to stabilise the areas where these shallow slips surfaces were believed to be present.

### Design of Expanded Polystyrene (EPS)

#### Material Specification

A VH (very high density) class block moulded expanded polystyrene foam manufactured to AS1366 [3] was specified. This material has a unit weight of  $28 \text{ kg/m}^3$  ( $<1 \text{ kN/m}^3$ ) and a compressive



strength of 72 kN/m<sup>3</sup> and 164 kN/m<sup>3</sup> at 1% and 5% strain respectively. The blocks used contained a flame retardant.

#### *Set out and Construction Control*

The foundation to the EPS block was prepared by proof rolling, test (DCP) to confirm min CBR (3 %) which was to be trimmed to a tolerance of  $\pm 10$  mm over any 4000 mm distance. The design allowed for a “mud slab” comprising a thin layer of cement can be used prior to placing over lower blocks to create a level surface on which to construct the next layer. The maximum weight of compaction equipment was limited to 60 kN/m width or roller. Allowable stress at the surface of the EPS blocks was not to exceed elastic limit of blocks (165 kPa). The sand replacement method of compaction verification was specified where fill was placed directly in close contact to the EPS blocks as concerns were raised over the use of nuclear densometer which may present errors in calculating soil moisture as hydrogen gas exsolving from the EPS.

#### *Equivalent Subgrade Properties*

Long term compressive creep data was used to assess equivalent subgrade properties of pavements constructed over the EPS blocks. For comparison the grade of EPS used was similar to that of a CBR 2 % material at the stress range of concern.

#### *Design for Durability*

EPS blocks were encapsulated within a 1.5 mm HDPE membrane lapped no less than 300mm and sealed using asphaltic rubberised seam tape. Blocks were placed sufficiently low within the embankment to ensure no less than 600mm of soil cover to protect from fuel oil and fire degradation.

#### *Safety in Design*

Blocks were cast in factory moulds 0.6 m x 1.2 m x 5 m deemed the maximum size able to be carried by construction workers during placement. Although specified as flame retardant, freshly cast blocks were prone to pentane gas production and as such the design required blocks to be stored outside in the open air, covered only by traps to protect from weather and sunlight until installed. The risk of combustion around the EPS blocks required no

smoking during construction and the careful selection of cutting equipment and plant to limit the risk of ignition.

## **CONSTRUCTION**

### **Construction Challenges**

During construction the following issues were resolved during the placement of EPS blocks not envisaged necessary at the design stage.

#### *Set out and Construction Control*

EPS block set out requirements were limited to delineating an area within which EPS fill was to be placed. Subsequent layers were required to be laid transversely to the layer below to create an interlocking lattice structure which extended out beneath the edge of the pavement. In practice this proved difficult to accomplish without detailed set out drawings showing where individual blocks needed to be cut.



Fig. 3 Showing placement of EPS blocks

#### *Material Tolerances*

Tolerance between blocks – the design assumed that tolerances between adjacent blocks could be minimised to less than 10 mm. This proved initially difficult to achieve as the factory cast blocks did exhibit irregularities over their lengths. In order to minimise irregularities between blocks and ensure blocks were stable once in place a foundation was prepared using 150mm of good quality granular fill and a biaxial geogrid.

#### *Placement and Cutting*

Blocks were held in place using punched aluminium

grip plates. In order to ensure blocks were stable prior to placing a second layer kiln dried fine sand was specified to be brushed over the prepared surface and into gaps between the blocks. A small plate compactor was used over the blocks to assist in working the sand into place and ensuring the blocks were stable prior to placing a second layer. A hot wire saw was developed to reduce risk of combustion and create a clean cut edge which proved very effective and adaptable to accommodating irregular cuts at the ends of the blocks.

#### *Protection of HDPE during Construction*

The design was amended to cover only the top and sides of the blocks to avoid collecting water within a fully encapsulated HDPE cell. Damage was minimised by covering the HDPE with a lean mix screed as soon as practically possible.



Fig. 3 Showing placement of EPS blocks

#### *Protection of EPS during Construction*

Plant was carefully selected to prevent damage to the blocks. Only light rubber tracked plant was used to lay out material prior to compaction. A rubber tracked mini excavator (Cat 304D) was used to place material over the EPS blocks. A small front end loader (279C Pozzi Track) was used to push no less than 200mm of type 2.3 granular pavement material over the EPS blocks as a protective layer prior to compacting using a relatively small (250kg) vibrating plate compactor. Only when 400mm of cover was in place could a larger 2.8t twin drum roller be used in vibration mode. All plant was verified to ensure ground bearing pressures were limited to less than less than 72k N/m<sup>2</sup> (limit at which may cause 1 % strain of these VH grade EPS

Blocks).

#### *Construction of Overlying Pavement*

Placement of subsequent pavement layers proceeded in the normal manner although trafficking by trucks and heavy equipment is precluded until the pavement was completed. Crane mats were used to evenly distribute the load from delivery truck wheels. No traffic restrictions were necessary once the pavement was completed to design level. Final cover to the EPS blocks comprised some 870mm of compacted pavement material.

#### **Post Construction Performance**

##### *Monitoring Program*

Monitoring at this site has been undertaken, prior to, during and after these works. These monitoring records comprised deep inclinometers, surface monitoring points and groundwater monitoring wells with instrumented data loggers.

##### *Monitoring records*

Monitoring records noted significant (up to 20mm) deep and surface movement during construction (notably the drilling of deep horizontal relief wells and soil nails). Post construction surface monitoring of this site continued for five months up to June 2013.

No observable movement has been noted following construction over the monitoring period. This period of time includes two further large rainfall events which resulted in further landslides around the region between February and March 2013. Groundwater monitoring indicates that the horizontal drains have little effect on the groundwater in this area however the deep counterfort drains over the toe of the slope may limiting the extent at which groundwater can rise within the colluvium. Observations made during site visits indicate that the deep horizontal wells and deep counterfort drains below the embankment have intermittent flows (as is evidenced by iron staining around the outlets).

#### **CONCLUSIONS**

The strengthening and unloading (re-grading and lightweight fill) works were used to stabilise this section of embankment. Global slope stability analysis may lead to a design which considers the critical deep failure surface only (the lowest factor of safety). Design of stabilisation measures requires a consideration of all areas where the factors of

safety is unacceptable, and not only the deep critical condition. Thus EPS blocks were also used to stabilise the less critical failure surface areas at a shallow level.

No significant movement has been recorded since completion of these works or during subsequent heavy rainfall events. The use of expanded polystyrene block as a lightweight fill has been successfully used as part landslide remediation works. Additionally a great deal of practical knowledge regarding its installation has been accrued as part of this project.

#### **ACKNOWLEDGEMENTS**

The authors would like to acknowledge the Department of Transport and Main Roads Engineering and Technology department with whom this technical solution was developed.

In addition many of the innovative and practical solutions to the placement and construction were developed in conjunction with the departments contracting arm, RoadTek.

#### **REFERENCES**

- [1] Boyer, M, Chew, K. & Look, B (2013), A case study of a hillside slope instability in South East Queensland, Australian Geomechanics Vol 44 No 3, P77-84.
- [2] Hutchinson, J. N. (1984), "An Influence Line Approach to the Stabilisation of Slopes by Cut and Fill" Canadian Geotechnical Journal, Vol 21, P363-370.
- [3] AS 1366.3-1992 : Rigid cellular plastics sheets for thermal insulation - Rigid cellular polystyrene - Moulded (RC/PS - M)

# CRACKING AND BOND SPLITTING BEHAVIORS OF CORRODED LONGITUDINAL BARS IN REINFORCED CONCRETE BEAMS

Yasuji Shinohara<sup>1</sup> and Aris Aryanto<sup>2</sup>

<sup>1</sup> Tokyo Institute of Technology, Japan; <sup>2</sup> Institut Teknologi Bandung (ITB), Indonesia

## ABSTRACT

An experiment was performed to evaluate cracking induced by corrosion expansion and bond splitting behaviors of corroded longitudinal bars in reinforced concrete beam. An accelerated corrosion experiment by impressed current was conducted on reinforced concrete beam type specimens having different amount of transverse bars, diameter of reinforcement, and concrete strength with 6% of target corrosion weight loss of longitudinal reinforcement. The pull-out tests were also carried out to investigate the effect of corrosion on bond splitting behaviors. The test results showed that the corrosion cracking behavior greatly depends on concrete strength (porosity), and that stirrups contribute substantially to the residual bond splitting capacity after cracking.

*Keywords: Corrosion, Bond splitting, Bond-slip relations, Beam specimen, Concrete strengths*

## INTRODUCTION

A significant reduction of bond strength has been observed for corroded steel bar without stirrups [1] with increasing corrosion level, however, slight bond strength deterioration was observed when the stirrups have been introduced [2]. Actually, not only longitudinal bars but also stirrups may experience corrosion. The corrosion of stirrups may weaken the confinement of longitudinal bars by reducing in a cross section of stirrups, provoking extensive cover cracking [3] and diminishing of adhesion or friction between stirrups and surrounding concrete. The combined effect of corroded longitudinal reinforcement and stirrups has been investigated in a few studies [3].

The main aim of this study is to investigate the cracking induced by corrosion expansion and the bond splitting behavior of corroded reinforcements such as bond splitting capacity, mode of failure and bond stress-slip relationships. The relative influence of stirrups, longitudinal bar position and concrete strength were experimentally studied. From the test results, a formulation of bond-slip model and so on

for assessing the structural behavior of corroded structures were proposed and applied to a corroded RC column in order to estimate a degradation of structural performance due to corrosion.

## EXPERIMENTAL PROCEDURE Specimens And Materials

The effect of actual confinement by means of stirrups having different ratios and configurations was investigated in accelerated corrosion tests and pullout tests using beam type specimen. The effect of bar position on beams i.e. corner or middle bars and its position to casting direction i.e. top or bottom in casting were also evaluated.

Six rectangular beams were produced and tested. Each beam had two test regions, the corrosion and the non-corrosion regions (Fig.1). The specimen parameters are summarized in Table 1. In this study only longitudinal bars located at bottom side of beams were subjected to corrosion which has 400 mm of embedment length. On the right and the left side of embedment length the longitudinal bars were insulated using vinyl tape as non-corroded and un-

Table 1 Specimen's test parameters

No.	Designation	Concrete Strength (N/mm <sup>2</sup> )	Longitudinal bar			Target Corrosion Rate (%)	Transverse bars	
			No. bar	dia. (mm)	Ratio		Bar	Ratio
1 and 2	4L0T-∞S-NH&NC	24	4	19	1.29%	0 and 6	0	0%
3 and 4	4L2T-200S-NH&NC	24	4	19	1.29%	0 and 6	2-U6@200	0.15%
5 and 6	4L2T-100S-NH&NC	24	4	19	1.29%	0 and 6	2-U6@100	0.29%
7 and 8	4L4T-200S-NH&NC	24	4	19	1.29%	0 and 6	4-U6@200	0.29%
9 and 10	3L2T-100S-NH&NC	24	3	22	1.30%	0 and 6	2-U6@100	0.29%
11 and 12	4L2T-100S-HH&HC	48	4	19	1.29%	0 and 6	2-U6@100	0.29%

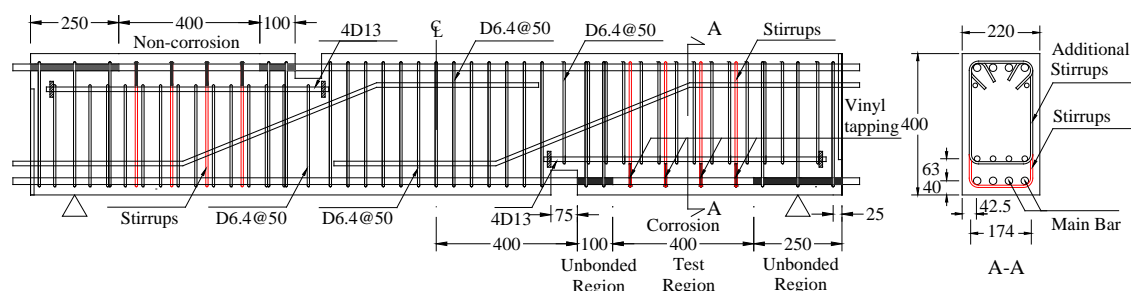


Fig. 1 Typical specimens and bar arrangements

bonded regions. The stirrups were also covered by vinyl tape in order to protect stirrup strain gages and to keep a constant confinement during corrosion test. Before the accelerated corrosion test, all specimens were cured for 28 days in the laboratory. Two concrete strengths of 24 and 48 N/mm<sup>2</sup> were used representing a normal and high strength concrete. The concrete was poured from the side of beams, so that the bond properties of left side is identical to that of right side. Thus, there are four bar positions in terms of casting direction, which is T, CT, CB, and B. The preheated high strength of steel bar was selected for longitudinal bars to avoid the yielding before bond splitting failure. Two bar diameters of 19 mm and 22 mm were used for longitudinal bars. The average yield strength and elastic modulus were 1053 and  $1.87 \times 10^5$  N/mm<sup>2</sup> for D19 and 980 and  $1.85 \times 10^5$  N/mm<sup>2</sup> for D22, respectively. For stirrups, high strength reinforcement was also used having average yield strength and elastic modulus were 1414 and  $2.0 \times 10^5$  N/mm<sup>2</sup>, respectively.

### Accelerated Corrosion Test

An accelerated corrosion test through the electrochemical process was performed. The typical accelerated corrosion set up for all specimens is described in Fig. 2. During accelerated corrosion process the specimens were placed on top of two supports and the tank containing 3% of NaCl solution was put below the specimen. The solution penetrated to the concrete through the water sponge. Thus, the corrosion attack took place from one

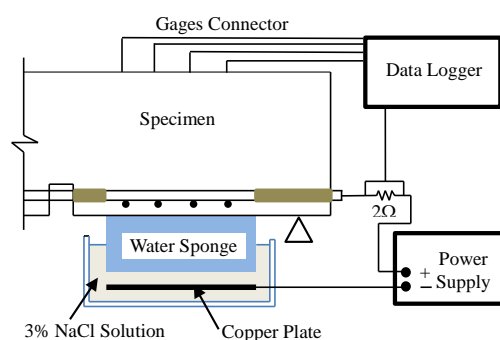


Fig. 2 Overview of accelerated corrosion setup

direction. The longitudinal bars were corroded up to approximately 6% of corrosion weight loss. The cracking of cover was visually observed and the crack width at certain locations was frequently measured using digital microscope [4]. Furthermore, a constant 10 Volt from the power supply was charged and the current flowed on each bar was monitored and recorded using data logger.

### Pullout Test

The specimens were tested in a simple three point loading. Because the beam has two test regions or specimens, corrosion and healthy regions, so after loading test was finished for one region, it was then continued with another test region in opposite loading directions by turning upside down. The outline of loading test set-up is described in Fig. 3. The loading was controlled by displacement and also it was controlled by measured strain at slit in the longitudinal bar. In addition, the slip of each bar was measured using LVDT which put at end of beams.

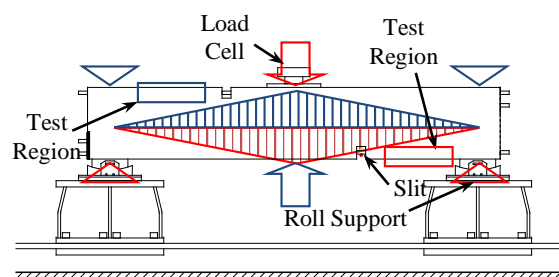


Fig. 3 Overview of test setup

## EXPERIMENTAL RESULTS

### Corrosion Weight Loss

At the completion of pullout testing, the corroded longitudinal bars were removed from their concrete beams and the corrosion product was chemically cleaned, and then it mechanically removed by steel wire brush and the weight loss was measured. The summary of corrosion rate for each bar and the average in each beam are shown in Table 2.

From Table 2 it shows that the corrosion rates of each bar at a beam are different, although the output



of current of each bar is relatively same. Larger corrosion rate was mostly obtained from the corner bar particularly bar located at top in casting (T). This trend was observed for all specimens. This can be due to the corrosion crack mostly occur at edge of beam, thus it allows water and oxygen to penetrate easily to the bars. In addition, the bar located at top of concrete casting tends to have higher porosity than the bottom bar due to settlement of fresh concrete. The different of corrosion rate of each bar are relatively large compared to the estimated corrosion rate by Faraday's law (6%). However, if the average corrosion rate in one beam is roughly consistent with the estimated corrosion rate.

Table 2 List of test variables for specimens

Designation	Bar Location				Ave.
	T	CT	CB	B	
4L0T-∞S-NC	10.6	4.7	3.8	5.6	6.2
4L2T-200S-NC	8.9	4.9	4.4	4.9	5.8
4L2T-100S-NC	8.2	4.4	5.4	6.3	6.1
4L4T-200S-NC	7.4	4.5	4.6	5.2	5.4
3L2T-100S-NC	7.4	3.9		6.3	5.8
4L2T-100S-HC	6.6	4.0	6.0	6.1	5.7

### Crack Patterns Caused By Corrosion Expansion

The first crack (crack initiation) on the concrete surface was visually observed within a few days after accelerated corrosion being started for all specimens. The crack patterns and crack width at final accelerated corrosion in Fig. 4. Generally, two major cracks were formed at the bottom cover of beams parallel to longitudinal cornered bar. The relations between observed maximum crack width and average corrosion penetration are also presented in Fig. 5. The average corrosion penetration was determined from the mean value of corrosion depth penetration for all longitudinal bars in one specimen. The corrosion penetration at first concrete cracking is around 30-60 micrometers for all specimens. For the 4L2T-100S-HC specimen, it clearly shows that the crack width is larger than specimens having normal concrete strength at similar corrosion levels.

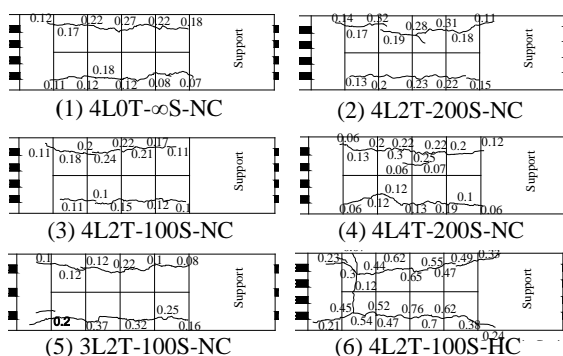


Fig. 4 Crack patterns at final accelerated corrosion

This can be attributed to lots of corrosion products localized in a crack because of lower porosity of high strength concrete, as reported by Kurumisawa et.al [5] and, the amount of pores greater than  $1\mu\text{m}^2$  is also increase for higher w/c ratio in Fig. 6. The stress of transverse bar in high strength concrete also increased in proportion to the crack width.

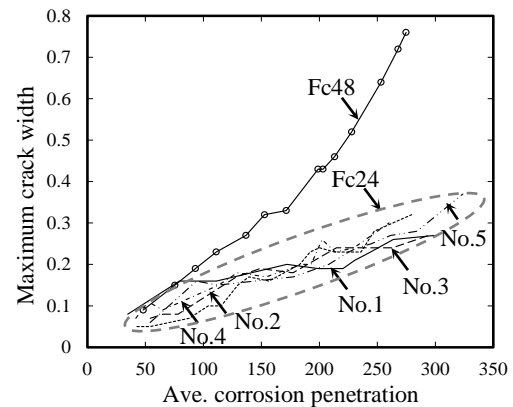
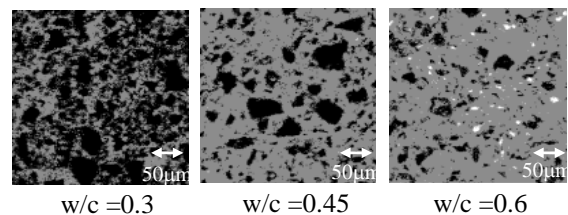


Fig. 5 Maximum crack width vs. average corrosion



■ : Only paste (no void)    ■ : Mix paste and void of  $1\mu\text{m}^2$   
□ : Fully void of  $1\mu\text{m}^2$

Fig. 6 Pore structure of hardened cement paste [5]

### Crack Patterns Caused By Pullout Test

Typical crack patterns at bond splitting failure viewed from side of beams are described in Fig. 7. Different types of crack patterns were observed from

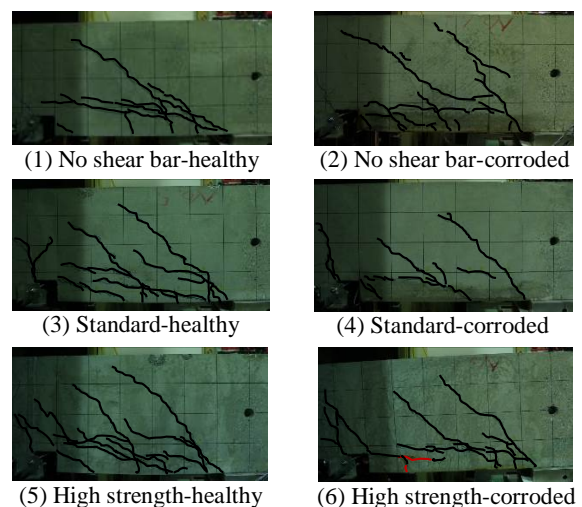


Fig. 7 Crack patterns at failure by pullout test



the test results depending of presence and absence of corrosion and stirrups. For uncorroded (healthy) specimens without stirrups a small number of inclined cracks were formed starting from the bottom support as observed from the side view of beam (Fig. 7(1)). The typical crack patterns for healthy specimens with stirrups were dominated by inclined cracks which have large number of cracks and more uniformly distributed along embedment length of longitudinal bars than specimen without stirrups. The typical crack patterns for corroded specimens were also dominated by inclined cracks, however, the cracks tend to propagate parallel to longitudinal bars or a smaller slope. This can be due to the damage of ribs on deformed bars by corrosion process, and may reduce a wedge action by ribs.

### Bond Stress-Slip Relationships

Fig.8 shows average bond stress-slip relationship for healthy and corroded specimens in the dash line and the solid line, respectively since the effect of bar location in casting direction on the bond stress-slip relationships was relatively small. The bond stress was estimated by dividing the tensile load acting on each longitudinal bar calculated from strain gages at slit on the longitudinal bar by the surface area of longitudinal bar along the embedment length. Thus, the results are the average bond stress along embedment length. The calculated bond strength for

healthy reinforcement based on the AIJ Guideline is also described by the dot line.

For the healthy and corroded specimen without transverse bars, as shown in Fig. 8(1), the maximum bond stress (bond strength) of both specimens is relatively small, around 2 N/mm<sup>2</sup> and it occurred at lower slip, less than 1 mm. The corroded specimen has a slightly higher maximum bond stress than the healthy specimen. This may be a possibility that the corrosion product filled the void at interface between reinforcement and concrete and enhanced the bond stress. However, after reaching maximum bond stress, the bond stress of the corroded specimen rapidly decreases due to the initial corrosion crack.

For specimens with transverse bars, the bond stress-slip relationship of specimen No. 3 to No. 12 (Fig. 8(2)-(6)) demonstrate that corrosion reduces the bond splitting capacity when comparing the bond strength between healthy and corroded specimens. It also shows that maximum bond stress for healthy specimens mostly occurred at larger slip more than 1 mm meanwhile for corroded specimens occurred at low slip smaller than 1 mm (brittle behavior).

As expected the presence of transverse bars increases the bond splitting capacity for healthy specimens. An increase in transverse bars ratio also increases the residual bond strength for corroded specimens. Moreover, it also shows that the presence of transverse bars enables to maintain the bond stress after reaching maximum bond stress at least

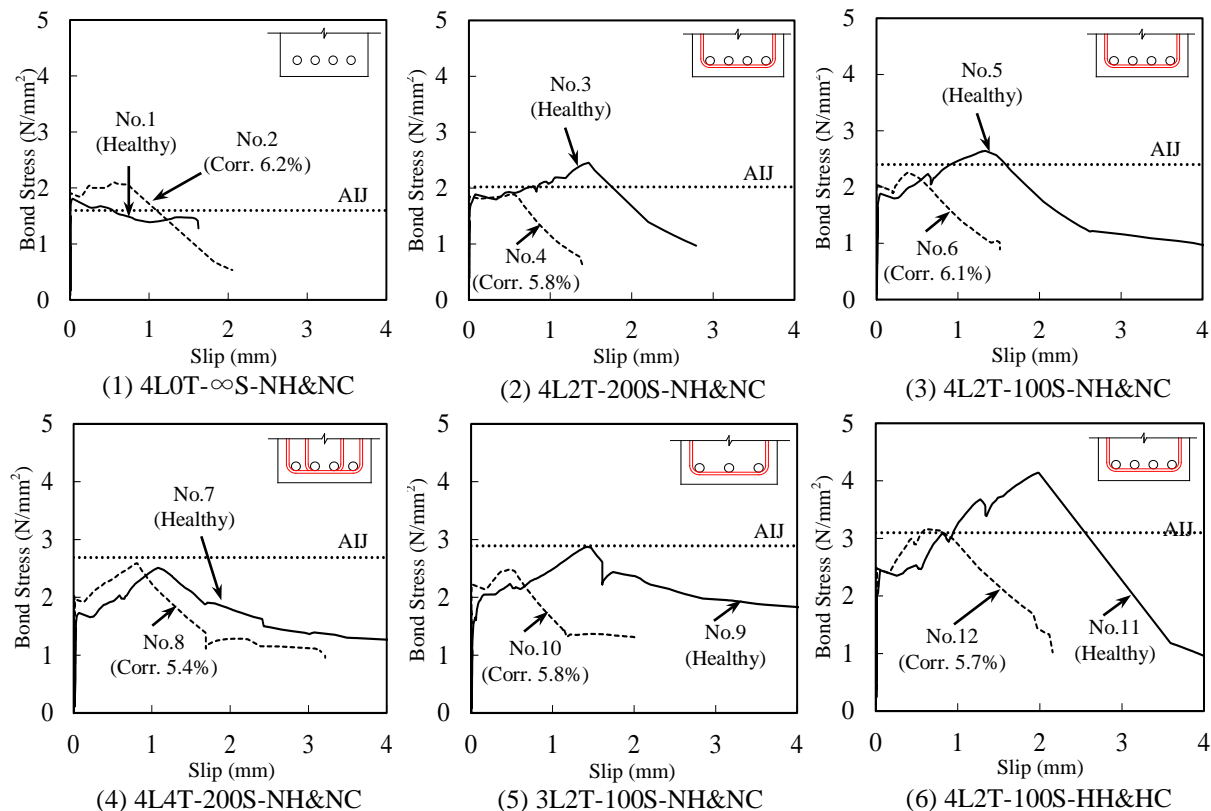


Fig. 8 Average bond stress-slip relationship

one third of maximum bond stress at larger slip because transverse bars can prevent bond splitting crack from widening. In addition, the initial bond stiffness is very high due to chemical adhesion between concrete and steel bars, as a result, a slip to the bond stress of 2 N/mm<sup>2</sup> at beginning is only about 0.02 mm, as reported by Aryanto et al. [4].

The bond-slip relationship for specimen with high concrete strength as shown in Fig. 8(6) has a larger maximum bond stress than for normal strength specimens, such as more than 4 N/mm<sup>2</sup> for healthy bars. This indicates significant contribution of concrete strength on bond capacity. However, the bond stress decreases rapidly after the maximum bond stress to lead a brittle behavior.

### Bond Splitting Capacity

The average bond strength of each specimen normalized with respect to that of the healthy specimen without stirrups (No.1) plotted against stirrups ratio is shown in Fig. 9. The test data conducted by Morita et al. [6] which have stirrups ratio of 0.58 was added into the graph. From Fig. 9, for healthy specimens an increase of bond splitting capacity was observed with increasing stirrups ratio as illustrated by linear regression curve, solid black line. As indicated by a linear regression of corroded specimens, dash line, the test results showed bond deterioration due to effect of corrosion. However, as shown in Fig. 9 an increase in transverse bars ratio generated higher residual bond splitting capacity. This shows substantial contribution of confinement provided by transverse bars in corroded specimens.

From Fig. 9, the decrease of bond strength of corroded longitudinal bar can be estimated for different confinement level, or considering the reduction area of transverse bar that might be occurred when transverse bar also experienced corrosion. Although the experimental data showed a scatter, the tendency of both effect of corrosion and transverse bars ratio was identified.

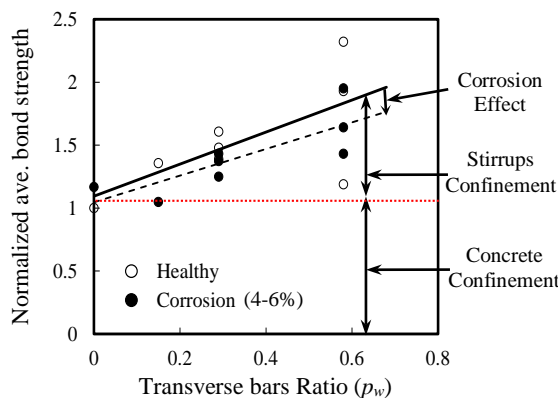


Fig. 9 Normalized ave. bond strength with respect to that of the healthy specimen without stirrups

### NUMERICAL SIMULATIONS FOR ASSESSMENT OF CORRODED RC COLUMNS

To simulate the effect of corrosion on structural performance of a corroded reinforced concrete column, FE analysis was carried out with special attention in transformation of material properties of reinforcements, concrete and bond properties due to corrosion. The configuration of column is based on the experimental test conducted by one of authors before. However, some modification was made by changing the longitudinal bar diameter and the steel strength of longitudinal and transverse bars to make the column failed in flexure for uncorroded columns. FE model are summarized in Fig 10. The mechanical properties of current concrete and reinforcement are summarized in Fig 11, corresponding to corrosion level. The steel bars used a bi-linear model without strain hardening. The stress generated on transverse bars due to expansion of corrosion product is considered to be taken into account in the analysis using the apparent yield strength. The bond stress slip relationship of longitudinal bar as estimated in this study were adopted, as shown in Fig. 12 .

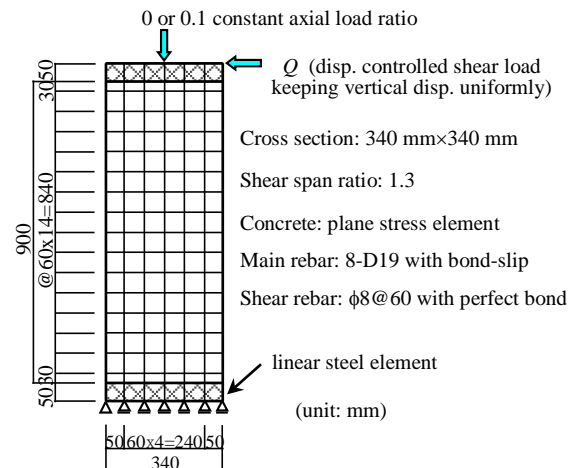
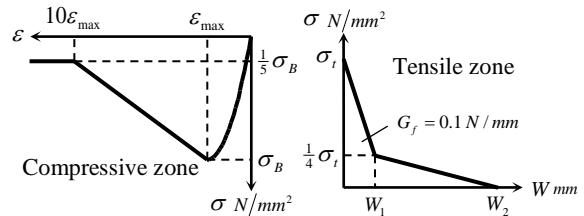


Fig. 10 Finite element model



	Concrete			Longitudinal		Transverse	
Corr. level	$\sigma_B$ N/mm <sup>2</sup>	$E_c$ N/mm <sup>2</sup>	$\sigma_t$ N/mm <sup>2</sup>	$\sigma_y$ N/mm <sup>2</sup>	$E_s$ N/mm <sup>2</sup>	$\sigma_{wy}$ N/mm <sup>2</sup>	$E_{ws}$ N/mm <sup>2</sup>
0 %	48	34300	2.8	345	2.00E+5	295	2.05E+5
3 %	32	26700	1.9	325	1.93E+5	208	1.98E+5
6 %	26	24100	1.5	304	1.86E+5	130	1.91E+5
10 %	26	24100	1.5	277	1.71E+5	39	1.82E+5

Fig. 11 Mechanical properties for concrete and rebar

Fig.13 shows the shear force and rotation angle of columns under no axial force and axial force ratio of 0.1. The shear force-rotation response of healthy column is firstly specified by formation of bending crack mostly located at top and bottom of column, followed by bending shear cracks and then yielding of longitudinal bar until reaching the maximum force as shown in Fig.13. Compared to the corroded columns, the cracking events and the yielding of longitudinal bar are almost the same with the healthy column except for specimens having an axial force and corrosion levels of 6% and 10%. From the analysis results it shows that larger corrosion level increases the possibility to have shear cracking at low load level. Moreover, the axial force promotes a shear failure before yielding of longitudinal bars as shown in Fig. 13 (2). This can be attributed to the lower apparent yield strength of transverse bar and bond deterioration induced by corrosion expansion. This analysis also leads to the recognition that the failure mode of RC columns can be changed with increasing corrosion levels from flexural failure preceded by yielding of longitudinal bars to shear failure before bar yielding which indicate a brittle behavior.

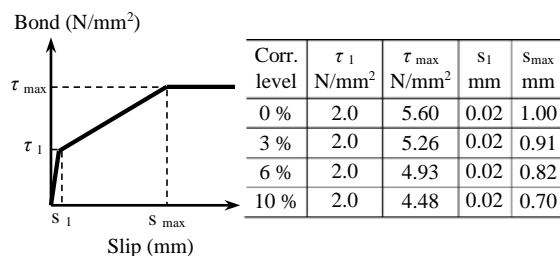
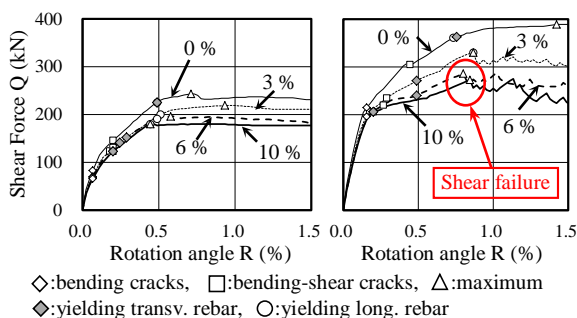


Fig. 12 Analytical model for bond-slip relationship



(1) No axial force (2) Axial force ratio=0.1

Fig. 13 Analytical model for bond-slip relationship

## CONCLUSION

- 1) Corrosion rate is not uniformly distributed among longitudinal bars in a beam and over perimeter of bar caused by the different of bar location in casting direction, the direction of chloride diffusion, and the supply availability of water and oxygen.

- 2) Concrete strength has a significant influence on the crack width growth rate and the stress increase of the transverse bars because of the difference of porosity in hardened cement paste.
- 3) The pullout tests show that the lower maximum bond stress and smaller slip at maximum bond stress are shown for corroded reinforcement and after reaching maximum bond stress, the bond rapidly deteriorates for corroded reinforcement.
- 4) An importance contribution of transverse bars to maintain residual bond splitting capacity for corroded specimens. The more transverse bar is provided, the higher residual bond splitting strength is generated.
- 5) FE analysis show that the failure mode of RC columns can be changed with increasing corrosion levels from flexural failure preceded by yielding of longitudinal bars to shear failure before bar yielding which indicate a brittle behavior.

## ACKNOWLEDGEMENTS

The authors acknowledge the supports of the Nuclear and Industrial Safety Agency as a part of the project on enhancement of Ageing Management and Maintenance of Nuclear Power Stations.

## REFERENCES

- [1] Aryanto, A. and Shinohara, Y., "Influence of Bond-Slip Relationship and Tensile Strength on Bond Behavior between Corroded Bar and Concrete," J. Structural and Construction Eng., AIJ, Vol.78, No.685, 2013, pp.559-567
- [2] Al-Sulaimani, G. J. et al., "Influence of Corrosion and Cracking on Bond Behavior and Strength of Reinforced Concrete Members," Structural Journal., ACI, Vol.87, No.2, 1990, pp.220-231
- [3] Hanjari, Z., Coronelli, D. and Lundgren, K., "Bond Capacity of Severely Corroded Bars with Corroded Stirrups," Magazine of Concrete Research, Vol.63, No.12, 2011, pp.953-968
- [4] Aryanto, A. and Shinohara, Y., "Cover Crack-width Propagation of Reinforced Concrete Members Induced by Corrosion," Proc. of the Japan Concrete Institute 2013, Vol.35, No.1, 2013, pp. 1123-1128.
- [5] Kurumisawa, K. and Tanaka, K. Difference in the void structure of each driving height of the cement paste. Proceeding Japan Concr. Inst. Res. 23, 781-786 (2001).
- [6] Morita et al., "Bond Behavior of RC Members with Corroded Longitudinal Reinforcement," Proc. Annual Meeting of AIJ, 2011, pp.411-414

# **SURFACE HEAT REDUCTION OF ASPHALT CONCRETE BY TOP FILLING WITH RECYCLED AGGREGATES AND MINERAL MORTAR**

Mohammad Raihanul Islam<sup>1</sup>, Satoru Ishiguro<sup>1</sup>, Masayoshi Yamanaka<sup>2</sup>

<sup>1</sup>Graduate School of Bioresources, Mie University, Japan

<sup>2</sup>Asahidoboku Co., Ltd., Yokkaichi, Japan

## **ABSTRACT**

The study was an attempt to elucidate the compressive strength of selected recycled aggregates and mineral material (slag) mortar in different curing condition, brightness and heat absorption characteristic of the pavements surface. Mortar was top filled on open graded asphalt concrete by vibrator. The compressive strength cylindrical samples sized with 5 cm Diameter And 10cm length were cured in 10°C, 20°C and 30°C. Light irradiation test conducted in environmentally controlled room with 30°C and 50% R.H., 3 hours light irradiation was applied on sample (30cmX30cmX5cm) pavements surface. At 30°C water curing samples showed the best result for all the RS mortar and 20°C water curing showed the highest compressive strength for all the oyster shell (OS) mortar except high early strength Portland cement (HSPC)-OS mortar due to the higher curing temperature. Highest compressive strength of HSPC-OS mortar was for 20°C air curing sample. In color and light irradiation test showed the same result and according to those test result; heat was absorbed and hold in pavement surfaces according to: OS-slag < HSPC-OS < OS < White Portland Cement-Sand < Slag-Sand < Sand < Asphalt.

*Keywords: Recycled Aggregates, Mineral Material, Mortar Strength, Color, Light Irradiation*

## **INTRODUCTION**

In Mie prefecture oyster farming is prospering and discharges a large quantity of oyster shell. Some of the shells are pulverized in factory after removing salt and utilized as an oyster shell [1].

WOS (waste oyster shell) sand can be resources of pure calcareous materials and effective in replacement of sand, indicating appropriate application of oyster shells, it is feasible to use in CLSM (controlled low-strength materials) [2].

In the financial year 2012 Japan produced 24639 thousand tons of blast furnace slag and 72.6% of that was used in cement industry [3].

Nowadays, there is an increasing interest in the utilization of waste materials. In the case of construction industry there was a growing trend towards the development and use of waste as supplementary cementitious materials [4].

Asphalt concrete is a temperature dependant material that may fall within a category of materials defined as brittle or quasi-brittle particularly at subzero temperatures [5].

Highways are rather high cost structures, and for that reason, it is obligatory that the materials to be used for their constructions should be appropriately designed [4].

Bitumen starts behaving like a Newtonian fluid at temperatures ranging from 30 °C to 70°C. Above these temperatures, bitumen may start flowing through any possible crack open in the pavement, in

a sort of capillary flow. This happens naturally when the temperature is high enough, for example during summer, although it can be also promoted artificially by induction heating or by microwave heating [6].

Objectives of this paper is to investigate the effect of curing temperature, air and water curing on mortar strength, to find out the most suitable curing condition of the recycled aggregate and mineral (slag) mortar and to the effective use of the experimental aggregates for surface heat reduction of asphalt concrete

## **MATERIALS AND METHODS**

### **Materials**

#### *Slag*

Blast-furnace slag was used in this study. It was collected as the steel industry by-product with specific chemical composition (**Table 1**). The slag was used with specific surface area of 4000 cm<sup>2</sup>/g and the density was 2.88 g/cm<sup>3</sup>.

#### *Cement*

Three types of cement were used in this study: Ordinary Portland Cement (OPC) with the density of 3.16 g/cm<sup>3</sup> and specific surface area of 3290 cm<sup>2</sup>/g; high early strength Portland cement (HSPC) with the density of 3.14 g/cm<sup>3</sup> and specific surface area of

4410 cm<sup>2</sup>/g and white Portland cement (WPC) with the density of 3.05 g/cm<sup>3</sup> and specific surface area of 3440 cm<sup>2</sup>/g.

### Sand

River bed sand was used in the study. Unit weight of the used sand was 2.60 g/cm<sup>3</sup> and the fineness modulus (FM) was 3.13.

### Oyster shell

The oyster shell is a waste product produced from oyster farming. Oyster shell aggregate collected from an oyster shell processing factory, Toba city in Mie Prefecture, Japan. Collected material pulverized in crushed form with the density of 2.29 g/cm<sup>3</sup> maximum size of 2 mm filled in commercial bag with specific specification

### Asphalt concrete

Asphalt concrete pavement block (30cmx30cmx5cm) was made and collected from Asahidoboku Co. Ltd., Yokkaichi, Japan

Table 1 Chemical composition of ground granulated blast furnace slag

Chemical compositions (%)	S-40	
	JIS A 6205	Test Value
Ignition loss	≤3.0	1.08
SiO <sub>2</sub>	-	33.24
Al <sub>2</sub> O <sub>3</sub>	-	13.87
FeO	-	0.32
CaO	-	42.51
MgO	≤10.0	5.32
TiO <sub>2</sub>	-	0.51
MnO	-	0.12
SO <sub>3</sub>	≤4.0	1.92
Na <sub>2</sub> O	-	0.20
K <sub>2</sub> O	-	0.31
Cl <sup>-</sup>	≤0.02	0.008

### Sample preparation

Mortar was prepared by different experimental materials with design mixing proportion. Cylindrical samples were prepared from mortar for the experiment with 50 mm diameter and 100 mm height. Binder aggregate ratio was 1:2 all cases. Slag was used 75% in OS mortar and 50% in sand mortar. Specific water binder ratio was used to prepare the mortar. For oyster shell mortar; water binder ratio was 1.1. For oyster shell-slag mortar; water binder ratio was 1.15. For River sand mortar in different conditions; water binder ratio was 0.5. The above mentioned mortar was filled on asphalt concrete pavement sample block (30cmx30cmx5cm)

by the help of vibrator with 1cm thickness.

### Test procedure

Three cylindrical samples were used for each age of curing. Samples produced from study aggregates were kept in 10°C, 20°C and 30°C constant room temperature for all the category just after to fill in the mould according to the experiment design and demoulded after three days, then, samples were cured in water at 10°C, 20°C and 30°C constant room temperature and in air at only 20°C constant room temperature, until the samples were used for compressive strength measurement at 3, 7, and 28 days. Compressive strength of each specimen was determined using universal testing machine with JIS A 1108[7].

Color test was performed with Digital Color Reader (CR -13, Konica Minolta Optics Inc.) by the direction of the instrument manufacturer which was followed by JIS Z 8721[8].

The asphalt-mortar samples were stored for the test in a controlled room at 30°C and with R.H. 50%. Every sample placed in cork sheet frame (30cm x 30cm x 5cm) and was kept in the light irradiation test room for 24 hours before the test for the purpose of temperature adjustment. The beam lamp Irradiation was continued on the sample block for three hours. The data logger was received and stored data for total about 15 hours.

The expressions of acronym used in this paper are shown in **Table 2**.

Table 2 Expressions of Acronym

Acronym	Original expression
OPC	Ordinary Portland cement.
HSPC	High early strength Portland cement.
WPC	White Portland cement
S-0%, 50%,.....	Mortar with specific % of slag content.
S-40/Slag-40	Slag with specific surface area of 4000 cm <sup>2</sup> /g.
RS	River bed sand.
OS	Oyster shell aggregate.
GGBFS	Ground Granulated Blast Furnace Slag.
Wc	Water curing
Ac	Air Curing (Temperature: 20°C; R.H.: 55-65% )

## RESULTS AND DISCUSSION

Compressive strength of RS mortar with OPC and no slag content (**Fig. 1**) in all ages was highest for 30°C water curing and at 28 days that was about 6.5% more than 20°C and 12% more than 10°C water curing and lowest for 10°C water curing. Strength for 20°C water and air curing was almost same up to 7 days and finally at 28 days the lower strength recorded for air curing samples even than 10°C water curing that was about 10.5% less than 20°C and 5% less than 10°C water curing.

About 30°C water curing is recommended for RS mortar with OPC and no slag content and air curing in this case should be avoided.

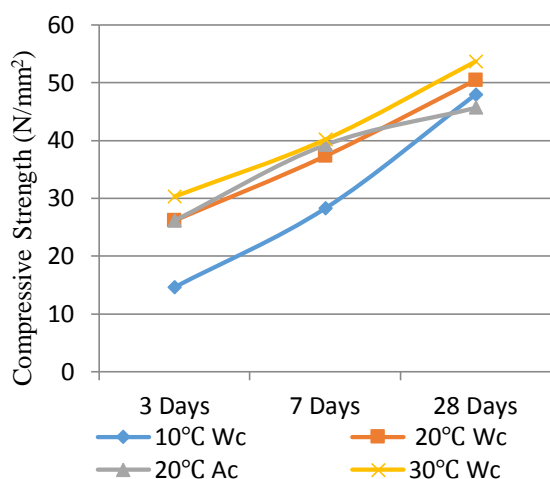


Fig. 1 Strength of RS mortar with OPC and no slag content.

Strength for RS mortar with WPC and no slag content (**Fig. 2**) up to 7 days was highest for 30°C water curing and at 7 days that was 4% higher than 20°C and 17% higher than 10°C water curing and lowest for 10°C water curing, finally at 28 days it was almost same for all cases except 20°C air curing. At 28 days 20°C air curing samples showed about 23% and 21% less strength than 20°C and 10°C water curing respectively.

For RS mortar with WPC and no slag content water curing at 10°C to 30°C will give the different strength at initial age but same on later age. Air curing could give initial higher strength and on later age it might be lower.

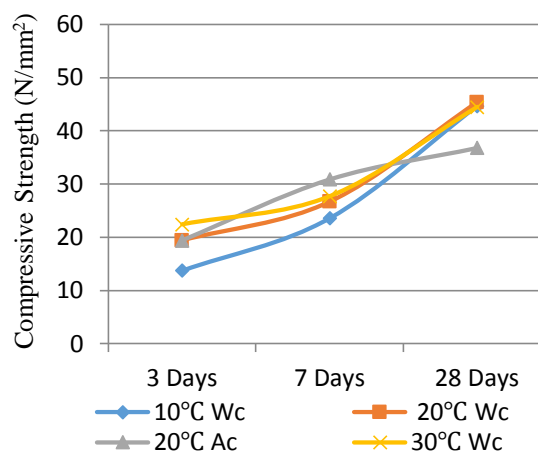


Fig. 2 Strength of RS mortar with WPC and no slag content.

Compressive strength of RS mortar with OPC and 50% slag content (**Fig. 3**) in all ages was highest for 30°C water curing and at 28 days that was about 19% more than 20°C and 66% more than 10°C water curing and lowest for 10°C water curing. Strength for 20°C air curing was almost same or more than 20°C water curing up to 7 days but at 28 days it was almost same as 10°C and 40% less than 20°C water curing.

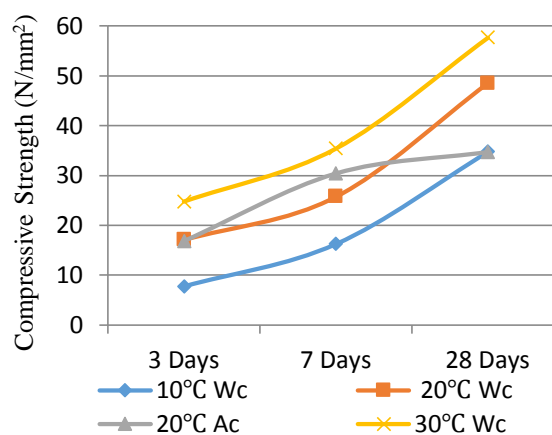


Fig. 3 Strength of RS mortar with OPC and 50% slag content.

Compressive strength of OS mortar with OPC and no slag content (**Fig. 4**) was highest for 20°C and 30°C water curing and lowest for 10°C water curing condition and at middle age all of that were almost same except 10°C water curing with lower trend. Finally 20°C and 10°C water curing samples showed the highest



and lowest compressive strength respectively whereas 20°C air curing and 30°C water curing samples showed the same result.

For 20°C water curing condition could be used for OS mortar with OPC and no slag content samples and 20°C air curing and 30°C water curing samples showed no difference in strength on later age.

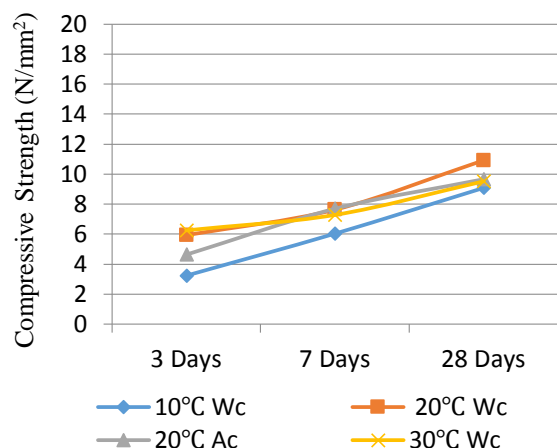


Fig. 4 Strength of OS mortar with OPC and no slag content.

In case of OS mortar with HSPC and no slag content (**Fig. 5**) at early age 30°C and 10°C water curing showed the highest and lowest compressive strength respectively, 20°C air and water curing samples showed the same result. At middle age 20°C air curing samples showed the highest strength within the all samples and finally it was highest; 14% more than 30°C and 31.5% more than 20°C water curing and strength in all other condition was almost same.

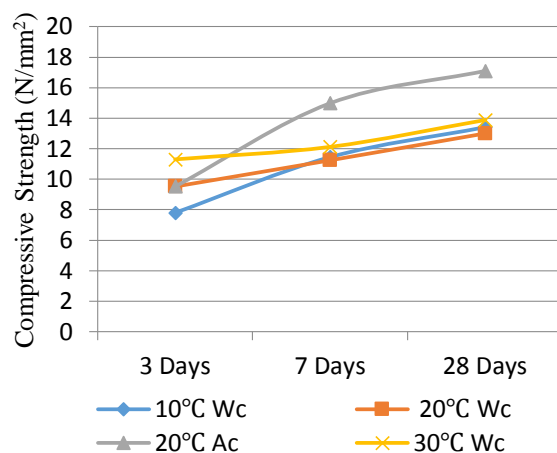


Fig. 5 Strength of OS mortar with HSPC and no slag content.

For OS mortar with OPC and 75% slag content (**Fig. 6**); 30°C and 10°C water curing sample showed the highest and lowest strength up to 7days. At final age 20°C water and air curing showed the highest and lowest strength whereas 10°C and 30°C water curing showed the same result.

20°C water curing condition could be suitable for long time strength gain whereas 20°C air curing showed the reverse trend.

For the above results of RS and OS mortar it was very much clear that higher curing temperature is preferable for the compressive strength due to the higher rate of hydration of cement and thus 30°C curing temperature gave the better result than 20°C and 20°C was better than 10°C condition. Feng Lin et al (2009) showed that the hydration reaction rate increases with the increase in temperature and the density of hydration products at higher temperature is higher [9].

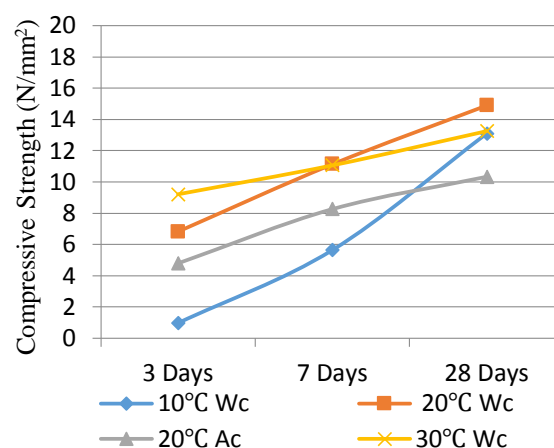


Fig. 6 Strength of OS mortar with OPC and 75% slag content.

Brightness of the study pavement was measured and expressed as numerical value. Brightness was directly related with absorption and holding the heat of the sample. Brightest sample showed the lowest surface heat in this study.

Within the study pavement OS-Slag mortar sample showed the highest brightness and the asphalt with no mortar filling showed the lowest (**Fig. 7**). Within the sand mortar pavements; WPC-Sand mortar showed the highest brightness and OPC-Sand showed the lowest and within the OS mortar pavements; OS-Slag mortar showed the highest and OS mortar showed the lowest brightness.

From the above discussion it could be said that heat will be absorbed and hold in experimental pavement according to: OS-slag<HSPC-OS<OS<WPC-Sand<Slag-Sand<Sand<Asphalt.

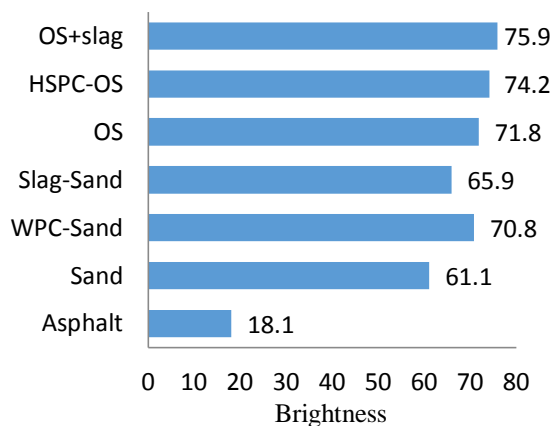


Fig. 7 Brightness of the sample pavements surface.

Asphalt pavement with top filling by OPC-Sand mortar reduced the bottom heat by 12% (6°C), WPC-Sand mortar reduced by 20% (9.2°C), OPC-Slag-Sand mortar reduced 17% (8°C), OS mortar reduced 22% (10.3°C), HSPC-OS mortar reduced 25% (11.2°C) and OS-Slag mortar reduced 29.5% (12.8°C) in compare with asphalt concrete pavement with no top filling (Fig. 8).

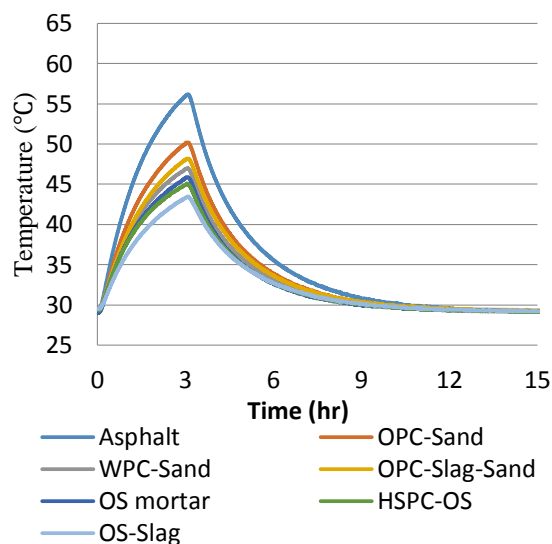


Fig. 8 Bottom temperature of the experimental pavements.

Asphalt pavement with top filling by OPC-Sand mortar reduced the surface heat by 18% (9.3°C), WPC-Sand mortar reduced by 28% (13.3°C), OPC-Slag-Sand mortar reduced 23% (11.5°C), OS mortar

reduced 30% (14.2°C), HSPC-OS mortar reduced 32% (14.8°C) and OS-Slag mortar reduced 36% (16.1°C) in compare with asphalt concrete pavement with no top filling (Fig. 9).

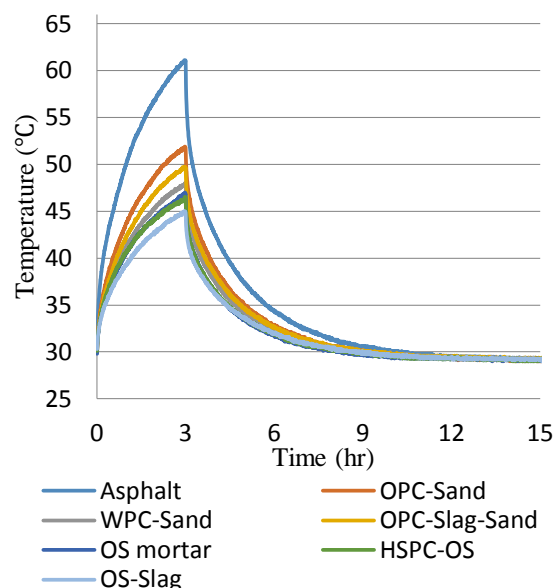


Fig. 9 Surface temperature of the experimental pavements.

From the above discussion heat was absorbed and hold in pavement samples bottom and surface according to: “OS-slag<HSPC-OS<OS<WPC-Sand<Slag-Sand<Sand<Asphalt” which supports completely the colour test results and proved the consistency of the both test results. This was due to the variation of brightness and absorption of heat by the experimental pavement surfaces.

Ishiguro et al. (2011) showed that heat reflecting pavements reduced their surface temperature due to the increasing in reflectance of solar radiation on the pavement surface [1]. K. Hayashi (2014) also mentioned that heat effects are caused by the heat absorption and reflectance with surfaces [10].

## CONCLUSION

About 30°C water curing is recommended for RS mortar with OPC and no slag content and air curing in this case should be avoided. For RS mortar with WPC and no slag content water curing at the temperature of 10°C to 30°C will give the different strength at initial age but same on later age. Air curing could give initial higher strength and on later age it might be lower. 30°C water curing is suitable for RS mortar with OPC and no slag content and air curing in this case should be avoided. For 20°C water curing condition could be used for OS mortar with OPC and no slag content samples and 20°C air curing and 30°C water curing samples showed no

difference in strength on later age. 20°C air curing was the most suitable condition for OS mortar with HSPC and no slag content and was one of the new learning of this study. 20°C water curing condition could be suitable for long time strength gain whereas 20°C air curing showed the reverse trend. According to the color test result it could be said that heat will be absorbed and hold in experimental pavement according to: OS-slag<HSPC-OS<OS<WPC-Sand<Slag-Sand<Sand<Asphalt. From light irradiation test result heat was absorbed and hold in pavement samples surface according to: “OS-slag<HSPC-OS<OS<WPC-Sand<Slag-Sand<Sand<Asphalt” which supports completely the colour test results.

## REFERENCES

- [1] Satoru Ishiguro and Masayoshi Yamanaka, “Heat Control of Pavement Surface Temperature Using Oyster Shell Lime”, First International Conference on Geotechnique, Construction materials and Environment, Mie, Japan, Nov.2011, pp. 353-356.
- [2] Wen-Ten Kuo, Her-Yung Wang, Chun-Ya Shu and De-Sin Su, “Engineering properties of controlled low-strength materials containing waste oyster shells”, Construction and Building Materials, Vol. 46, 2013, pp. 128–133.
- [3] NIPPON SLAG ASSOCIATION, Japan, (online),  
<<http://www.slg.jp/e/statistics/index.html>>
- [4] S\_ebnem Sargın , Mehmet Saltan , Nihat Morova , Sercan Serin, Serdal Terzi, “Evaluation of rice husk ash as filler in hot mix asphalt concrete”, Construction and Building Materials, Vol. 48, 2013, pp. 390–397.
- [5] S. Pirmohammad, M.R. Ayatollahi, “Fracture resistance of asphalt concrete under different loading modes and temperature conditions”, Construction and Building Materials, Vol. 53, 2014, pp. 235–242.
- [6] Alvaro García , Moises Bueno, Jose Norambuena-Contreras, Manfred N. Partl, “Induction healing of dense asphalt concrete”, Construction and Building Materials, Vol. 49, 2013, pp. 1–7.
- [7] Japanese Industrial Standards Committee. JIS A 1108: Method of test for compressive strength of concrete.
- [8] Japanese Industrial Standards Committee. JIS Z 8721: Color specification - Specification according to their three attributes.
- [9] Feng Lin , Christian Meyer Hydration kinetics, “Modeling of Portland cement considering the effects of curing temperature and applied pressure”, Cement and Concrete Research, Vol. 39, 2009, pp. 255–265.
- [10] K. Hayashi, “Study on concrete Material Technologies to Mitigate the Urban Heat Island Effect”, Concrete Journal, Vol. 52(3), Mar. 2014, pp. 273-279.

## **ASPHALT BINDER EXTRACTION FROM ASPHALT CONCRETE USING PULSED POWER TECHNOLOGY**

Rétyce Ivan Hervé Dodji Togbé Amoussou, Youhei Takanabe, Nobuyasu Oyama,  
Eva Arifi, Koichi Ishimatsu and Mitsuhiro Shigeishi  
Graduate School of Science and Technology, Kumamoto University, Japan

### **ABSTRACT**

Here, authors propose a pulsed power application to reclaiming aggregate from asphalt concrete lumps. This study aims at extracting asphalt binder from controlled specimens of asphalt concrete using pulsed power technology and evaluating the quality of the asphalt concrete recycled aggregate. Pulsed power was discharged into 5% asphalt content straight and modified asphalt concrete specimens. The results demonstrate that the extraction of modified asphalt binder from asphalt concrete is more difficult than that of straight asphalt and also requires more energy to produce approximately 1% asphalt content recycled coarse aggregate. Furthermore, the results suggest that recycled aggregate quality increases with increasing pulsed power energy.

*Keywords: Asphalt concrete, Modified asphalt, Recycled aggregate, Pulsed power technology*

### **INTRODUCTION**

In Japan, a considerable amount of construction waste consists of both ordinary and asphalt concrete while only half of the total amount of asphalt concrete waste is recycled as materials for surfaces, binder, or base courses [1].

Asphalt concrete is a composite material in which a bituminous material called asphalt cement binds coarse and fine aggregate, and filler. For road construction, either straight or polymer modified asphalt concrete can be utilized as binder. In the latter case, straight asphalt is modified to improve its binding properties with rubber or polymers incorporated into straight asphalt to improve resistance to rutting and cracking [2].

Asphalt concrete recycling has been promoted to satisfy the requirements to be cost-effective, environmentally responsible, and perform well. However, asphalt concrete recycling for modified asphalt pavement has some problems and does not lead to technical establishment.

While straight asphalt concrete is easily recycled relatively efficiently, recycled modified asphalt concrete presents problems of fatigue resistance [3]. Moreover, the incorporation of different types of asphalt concrete waste from various sources and the accidental mixing of debris cause inconsistencies and unpredictable behavior of recycled asphalt mixes.

Prevention of breakdown of recycling equipment during modified asphalt concrete recycling is essential [4]. Furthermore, the recycled asphalt mixture may be unpredictable and thus less durable due to the difficulty of mix design and the quality control by the reuse of modified asphalt waste.

Hence, implementation of asphalt concrete recycling methods that enhance quality of the recycled asphalt mixture by reducing the impact of deteriorated asphalt and modified asphalt binders is essential.

For ordinary concrete, the crushing processes to make recycling aggregate have been overcome by pulsed power discharge inside ordinary concrete waste to produce high-quality recycled coarse aggregate [5]. Reference [6] defined pulsed power discharge as a technique that spatially and temporally compresses and superimposes stored energy, thereby concentrating, controlling, and transmitting a large amount of power within a small space, for only a short time. This technique was less energy consuming and resulted in good quality aggregate that was as strong as the original aggregate to satisfy the JIS regulations for recycled coarse aggregate for concrete class H [7].

Unfortunately, to date, no study has investigated the applicability of pulsed power technology to recycle asphalt concrete. This study focuses on an application of pulsed power technology to solve problems associated with asphalt concrete recycling, notably modified asphalt concrete. Thus, the objectives of the present study are asphalt binder extraction from asphalt concrete specimens using pulsed power technology and quality evaluation of the recycled aggregate.

### **EXPERIMENT**

#### **Control Specimens**

Control specimens produced by Showa Rekisei Industries Co., Ltd. Kumamoto Mixture Factory,

Kumamoto, Japan were approximately 1.2 kg of both straight and modified type H [8] asphalt concrete specimens (Fig.1). Those characteristics are shown in Tables 1 and 2.



Fig. 1 Asphalt concrete control specimen

Table 1 Mix proportions of asphalt concrete controlled specimens

Coarse aggregate	Fine aggregate and Filler	Asphalt
57.60%	37.40%	5%

Table 2 Properties of straight and modified type H asphalt

Asphalt types	Softening point (°C)	Penetration (10 <sup>-1</sup> mm)	Ductility (cm)
Straight (S)	44.0 - 52.0	60 - 80	≥ 100
Modified H (MH)	95.0	45.0	93.0

### Pulsed Power Discharge into Asphalt Concrete

The authors have proposed a pulsed power application to extract asphalt binder from asphalt concrete. Pulsed power is a technology in which energy is accumulated over a relatively long period of time and then discharged in short pulses with controllable repetition rate thus increasing its instantaneous power [9].

Pulsed power energy (Eq. (1)) was discharged into both, straight and modified type H asphalt concrete specimens submerged in water (Fig.3) using a Marx generator (Table 3) under the conditions shown in Tables 4 and 5.

The pulsed power discharged energy is calculated using;

$$E = \frac{1}{2} C (V)^2 \quad (1)$$

where  $E$  is pulsed power discharged energy,  $C$  is the capacitance of the Marx generator, and  $V$  is voltage across the Marx generator.

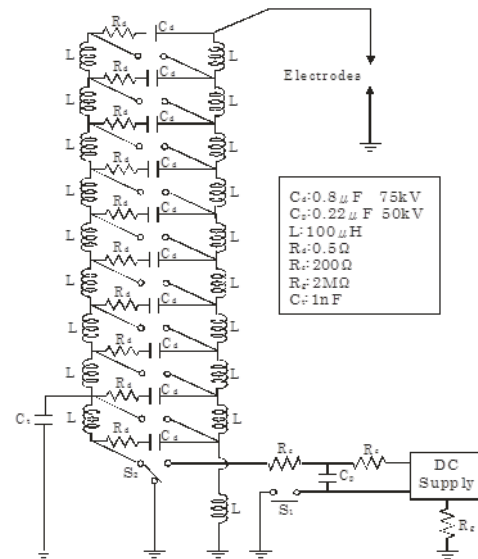


Fig. 2 Marx Generator

Table 3 Marx generator parameters

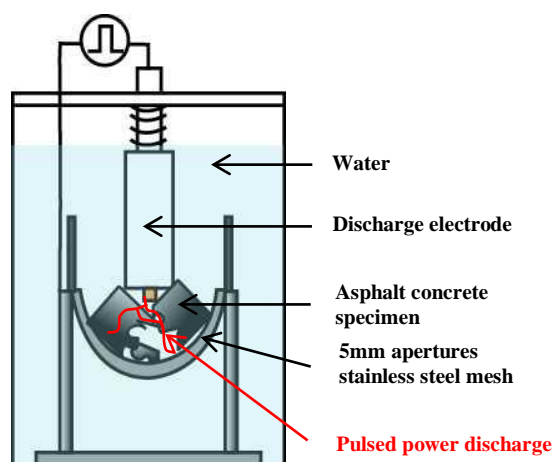
Voltages (kV)	30	40
Capacitance of the Marx generator (μF)	8	8

Table 4 Conditions of pulsed power discharge inside straight asphalt specimens

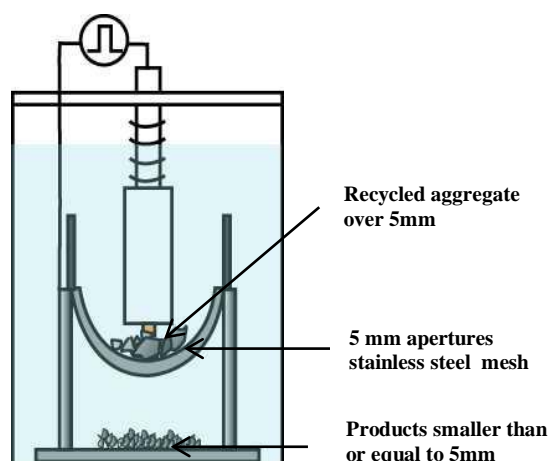
Voltage (kV)	Number of discharges on 5mm mesh	Number of discharges on 2.5 mm mesh	Total discharged energy (kJ)
30	25	25	180
30	50	50	360

Table 5 Conditions of pulsed power discharge inside modified type H asphalt specimens

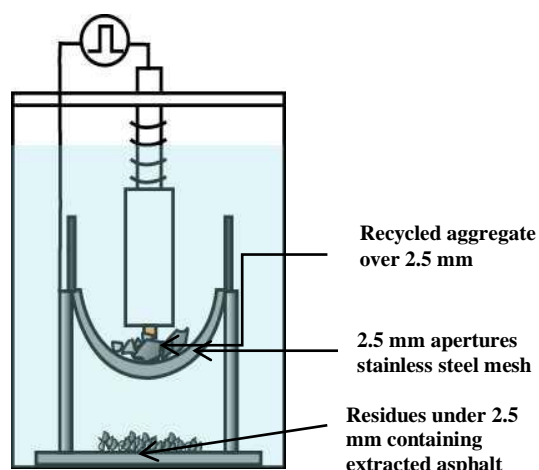
Voltage (kV)	Number of discharges on 5mm mesh	Number of discharges on 2.5 mm mesh	Total discharged energy (kJ)
30	50	50	360
30	75	50	450
30	100	50	540



a) Pulsed power discharge into specimens on 5 mm apertures stainless sieve



b) Production of recycled aggregate over 5 mm



c) Production of recycled aggregate over 2.5 mm and residues under 2.5 mm from products smaller than or equal to 5 mm

Fig. 3 Pulse power discharge apparatus [10]

Not only is asphalt concrete composed of asphalt binder and aggregate but also it is composed of air voids. The discharge of pulsed power inside asphalt concrete causes the dielectric breakdown of the gas inside air voids. As a result, the generated plasma induces shock waves followed by tensile stress that remove the asphalt binder from aggregate surface.

### Pulsed power discharge procedure

Pulsed power was discharged inside asphalt concrete controlled specimens on stainless steel meshes with apertures of 5 mm and 2.5 mm to separate them into both recycled aggregate over 5 mm; and over 2.5 mm and the residues under 2.5 mm containing the extracted asphalt binder. The process is as follows: at the start, after discharging the required pulsed power energy on the asphalt concrete specimens on the 5 mm mesh, the remaining recycled aggregate over 5 mm was collected. Then, on the 2.5 mm mesh, the same process was applied on the other part of the asphalt concrete specimens which size was smaller or equal to 5 mm to produce the over 2.5 mm recycled aggregate. At the end, the products which size was smaller or equal to 2.5 mm were categorized as the residues under 2.5 mm (Fig. 3 and Table 6).

Table 6 Size of pulsed power discharge products

Products	Recycled aggregate over 5mm	Recycled aggregate over 2.5mm	Residues under 2.5 mm
Size S (mm)	$S > 5$	$2.5 < S \leq 5$	$S \leq 2.5$

### Aggregate Recovery

To recover the original aggregate, asphalt was extracted automatically from over 5 mm and 2.5 mm recycled aggregate, and under 2.5 mm residues utilizing an asphalt extraction testing machine with propane as solvent at the Kumamoto Prefectural Center of Constructional Technology, Kumamoto, Japan. Next, asphalt was recovered utilizing the Abson method according to ASTM D1856-09 [11].

### Oven-Dry Density and Water Absorption Tests

Oven-dry density and water absorption tests were performed on all types of recycled aggregate according to Japanese Industrial Standards (JIS A 1109 and JIS A 1100).

Furthermore, oven-dry density tests were conducted on virgin aggregate used to make the control asphalt concrete specimens and recovered aggregate from asphalt concrete lumps recycled aggregate.



## RESULTS AND DISCUSSION

### Recycling Rates

As evident in Figs 4 and 5 with increasing pulsed power energy the recycling rate (Eq.(2)) of aggregate over 5 mm decreased markedly, contrary to that of over 2.5 mm recycled aggregate, which significantly increases from 128% to 141.3% for straight asphalt and from 123% to 163% for modified type H asphalt as a result of aggregate breaking.

$$R = \frac{PR}{PI} \times 100 \quad (2)$$

Here,  $R$  is aggregate recycling rate in percentage,  $PR$  is proportion of recycled aggregate in percentage, and  $PI$  is initial proportion of corresponding virgin aggregate in asphalt concrete specimens.

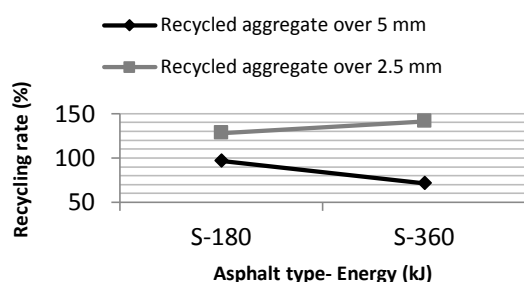


Fig. 4 Recycling rates of straight asphalt concrete aggregate

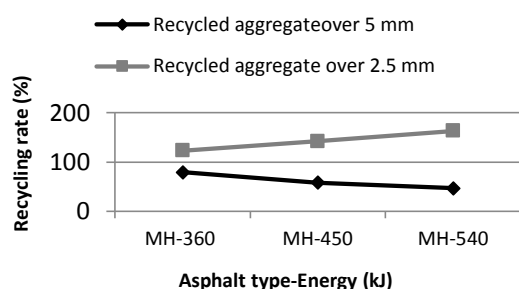


Fig.5 Recycling rates of modified type H asphalt concrete aggregate

### Asphalt Content of Recycled Aggregate

Straight and modified type H asphalt concrete specimens required 360 kJ and 540 kJ respectively (Figs. 6 and 7) to achieve approximately 1% asphalt content of recycled aggregate over 5 mm.

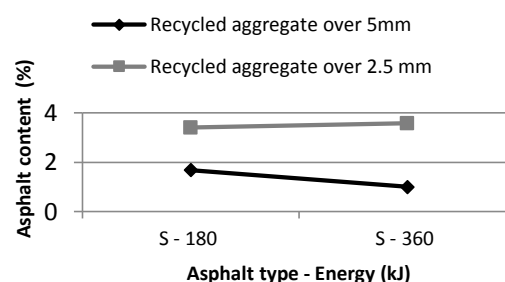


Fig. 6 Asphalt content of recycled aggregate from straight asphalt concrete specimens

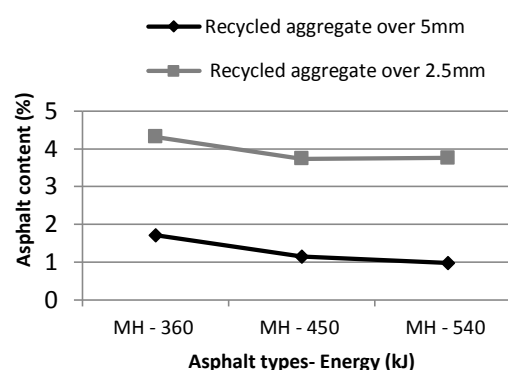


Fig. 7 Asphalt content of products from modified asphalt concrete specimens

As detailed in Fig. 6, for straight asphalt concrete specimens, asphalt content of recycled aggregate over 2.5 mm decreases to 3.41% and 3.58% from 5% (whole content in a specimen) at 180 kJ and 360 kJ as pulsed power discharged energy respectively. Asphalt content of recycled aggregate over 2.5 mm decreases as well reaching 1.69% and 1.01% at 180 kJ and 360 kJ respectively.

As indicated in Fig.7, for type-H modified asphalt concrete, asphalt content of recycled aggregate over 5mm decreases to 0.97% at 540 kJ as pulsed power discharged energy. Asphalt content of recycled aggregate over 2.5 mm decreases to 3.76% at 540 kJ.

These results show that the extraction of modified asphalt binder is not as easy as that of straight asphalt and requires more pulsed power discharge energy to produce the same asphalt content due to the presence of polymer modifier which increases its elasticity.

Furthermore, for both straight and type-H modified asphalt concrete, asphalt content tests revealed that finer recycled aggregate contained higher asphalt content. Although asphalt content of recycled aggregate over 2.5 mm is higher than that of recycled aggregate over 5 mm, asphalt content of

both recycled aggregate over 5 mm and 2.5 mm decreases when pulsed power discharged energy increases.

It could be inferred therefore that significant amount of asphalt binder was extracted from asphalt concrete specimens as part of the residues under 2.5 mm using pulsed power discharge.

### Oven-dry Density

Inspection of Fig. 8 indicates that oven-dry density of recycled aggregate over 5 mm from straight asphalt concrete specimens increases from 2.88 g/cm<sup>3</sup> to 2.94 g/cm<sup>3</sup> when pulsed power discharged energy increases from 180 kJ to 360 kJ. For type-H modified asphalt concrete, oven-dry density of recycled aggregate over 5 mm increases as well from 2.87 g/cm<sup>3</sup> to 2.94 g/cm<sup>3</sup> when pulsed power discharged energy increases up to 540 kJ. It is evident from the results of oven-dry-density tests that type-H modified asphalt concrete required more energy to achieve the same 2.94 g/cm<sup>3</sup> oven dry-density recycled aggregate over 5 mm compared to straight asphalt.

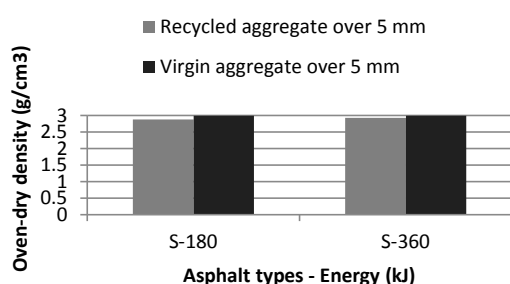


Fig. 8 Oven-dry density of recycled aggregate over 5 mm from straight asphalt specimens

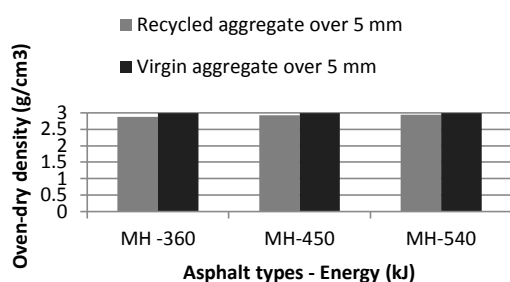


Fig. 9 Oven-dry density of over 5 mm recycled aggregate from modified asphalt specimens

For both straight and modified type-H asphalt concrete specimens recycled aggregate over 5 mm, the oven-dry density increases when pulsed power discharged energy increases and is almost equal to

that of the virgin aggregate utilized to make the corresponding specimens (Figs. 8 and 9).

Furthermore, an increase in pulsed power discharged energy appears to improve the oven-dry density of asphalt concrete recycled aggregate

### Water Absorption

The results of water absorption tests are shown in Figs. 10 and 11. For straight asphalt, the lowest water absorption ratio 0.73% was observed at 360 kJ for recycled aggregate over 5 mm. For type-H modified asphalt, the lowest 0.82% water absorption ratio was achieved by discharging 450 kJ as pulsed power energy. In other words, type-H modified asphalt concrete requires more pulsed power discharged energy to achieve approximately 0.80% water absorption recycled aggregate over 5 mm. According to these results it appears that the effect of pulsed power discharge on recycled aggregate over 5 mm water absorption is similar to that on its asphalt content and oven-dry density in terms of quality improvement.

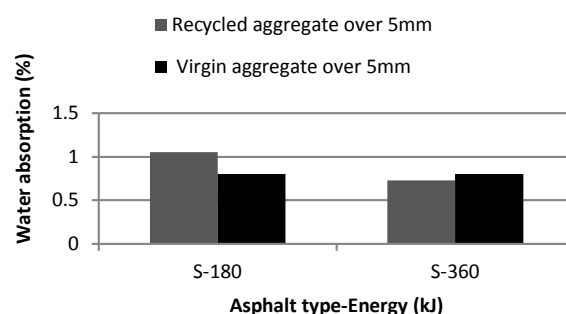


Fig. 10 Water absorption of over 5 mm recycled aggregate from straight asphalt specimens and virgin aggregate

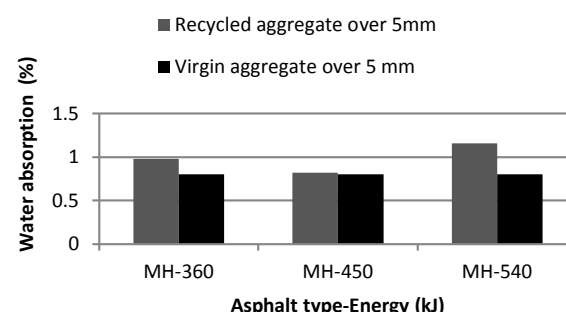


Fig. 11 Water absorption of over 5 mm recycled aggregate from modified type-H asphalt specimens and virgin aggregate

Furthermore, from Figs 10 and 11 it can be seen that the effect of pulsed power discharge on water

absorption of recycled aggregate over 5 mm from straight asphalt concrete specimens is in good agreement with that on recycled aggregate from modified type-H asphalt concrete specimens.

Despite the relatively higher water absorption ratio of over 5 mm recycled aggregate from modified asphalt concrete specimens at 540 kJ, water absorption decreases and becomes closer to water absorption of corresponding virgin aggregate when pulsed power discharged energy increases.

## CONCLUSION

Since pulsed power discharge inside ordinary concrete produced high quality recycled aggregate, the authors proposed its application to extract asphalt binder from asphalt concrete specimens.

In the course of this study, pulsed power was discharged into 5% asphalt content straight and modified type H asphalt concrete. The results show that pulsed power discharge affected aggregate gradation by increasing the recycling rate of aggregate over 2.5 mm up to 163% and decreasing that of over 5mm aggregate up to 47% due to aggregate breaking. Due to the high elasticity of modified type H asphalt binder, its extraction is more difficult than that of straight asphalt and requires more pulsed power discharged energy. Quality of recycled aggregate improved with an increase in discharged energy characterized by the decrease in water absorption and the increase in oven -dry density.

Further study should investigate the recovery of modified asphalt from the above-discussed residues under 2.5 mm and the separation of various types of polymer modified asphalt into decomposed polymer modifier and straight asphalt for separate recycling.

## ACKNOWLEDGEMENTS

The authors gratefully acknowledge the contributions of Associate Professor Takao Namihira, Dr. Yuichi Tomoda, Mr. Yasuo Miyazaki and the other members of Prof. Shigeishi's Group. The authors would like to express their sincere gratitude to Showa Rekisei Industries Co., Ltd. Kumamoto Mixture Factory, Kumamoto, Japan for providing the asphalt concrete specimens utilized in

this study.

## REFERENCES

- [1] Kubo, K.: Pavement Team, Public Works Research Institute, Japan: Recycling in Japan, 2009.
- [2] Japan Modified Asphalt Association, Polymer Modified Asphalt Pocket Guide. Japan Modified Asphalt Association (JMAA), 2010, pp. 3-5.
- [3] Tam V, "Comparing the implementation of concrete recycling in the Australian and Japanese constructions industries," *Journal of Cleaner Production*, Vol. 17, 2009, pp. 688-702.
- [4] Su K., Hachiya Y., Maekawa R., "Laboratory investigation of possibility of re-recycling asphalt concretes", *Proc. 6th ICPT*, 2008, pp. 435-442.
- [5] Inoue S., Iizasa S., Wang D., Namihira T., Shigeishi M., "Concrete recycling by pulsed power discharge inside concrete," *Int. J. Plasma Environmental Science and Technology*, 2012, pp. 183-188.
- [6] Akiyama H., *High-Voltage Pulsed Power Engineering*. Tokyo, Ohm-sha, 2003, pp. 1-2. (in Japanese)
- [7] Japanese Standards Association: JIS A 5021, "Recycled aggregate for concrete-class H," 2005.
- [8] Japan Modified Asphalt Association Standard, *Quality and Test Methods of Polymer Modified Asphalt for Road Pavement*. Japan Modified Asphalt Association (JMAA), 2007, p. 3.
- [9] Bluhm H., *Pulsed Power Systems: Principles and Applications*. Berlin: Springer, 2006.
- [10] Namihira T., Shigeishi M., Nakashima K., Murakami A., Kuroki K., Kiyon T., Tomoda Y., Sakugawa T., Katsuki S., Hidenori A., Ohtsu M., "Recycled coarse aggregate produced by pulsed discharge in water," *IEEEJ Trans. Fundamentals and Materials*, Vol. 6, Issue 3, 2006, pp. 197-198.
- [11] ASTM Standards: D1856-09, "Standard Test Method for Recovery of Asphalt From Solution by Abson Method," 2009, West Conshohocken, PA, DOI: 10.1520/D1856-09, [www.astm.org](http://www.astm.org).

## ENGINEERING PROPERTIES OF CONCRETE INCORPORATING WASTE CARPET FIBERS

Hossein Mohammad Hosseini<sup>1</sup>, A.S.M. Abdul Awal<sup>2</sup>, M. Zakaria Hossain<sup>3</sup>

<sup>1,2</sup> Faculty of Civil Engineering, Universiti Teknologi Malaysia, 81310 Skudai, Johor, Malaysia

<sup>3</sup> Graduate School of Bioresources, Mie University, Tsu-City, Japan

### ABSTRACT

This paper presents test results on physical and mechanical properties of concrete containing fiber from recycled carpet waste. Five concrete mixes namely plain concrete (PC) i.e. concrete without carpet fibers as control, and carpet fiber reinforced concrete (CFRC) mixes containing 0.5%, 1.0%, 1.5% and 2.0% polypropylene (PP) waste carpet fibers were made and tested for compressive, splitting tensile and flexural strengths, modulus of elasticity and shrinkage for periods of 1, 7 and 28 days. It has been found that carpet fibers reduced the workability and density of concrete. Concrete containing carpet fiber obtained lower compressive strength and modulus of elasticity than plain concrete. It is observed that carpet fibers effectively improved the splitting tensile and flexural strengths of concrete. The obtained values of shrinkage, however, confirmed that the shrinkage strain of carpet fiber reinforced concrete was higher than that of plain concrete. On the basis of short-term investigation, the one-year shrinkage values of both plain concrete and concrete containing carpet fiber were also predicted by extrapolating the data obtained during this period. The results indicate that waste carpet fibers can suitably be used as fibrous material for the production of fiber reinforced concrete with satisfactory engineering properties.

*Keywords: Fiber reinforced concrete, Waste carpet fibers, Workability, Strength, Modulus of elasticity, Shrinkage.*

### INTRODUCTION

The production and landfilling of waste are big problems throughout the world. Recycling of the waste materials and their use in construction industries are increasing in both the developed and developing countries. This has led to green and sustainable construction by reducing the cost of the production of construction materials and waste management. However, with the increasing utilization of the waste materials in engineering applications, it is necessary to understand their physical and mechanical properties. Concrete is the most widely used construction material. However, it has low tensile strength and low energy absorption [1]. Therefore, it is required to improve these properties and performance of concrete. An effective technique to obtain these properties of concrete is by adding small fraction of short fibers to the concrete [2,3,4]. Among others, the most common fibers used in construction are, steel fibers, synthetic fibers, such as nylon and polypropylene, glass fibers, natural fibers and fibers from pre and post-consumer wastes. Since the advent of fiber reinforcing of concrete, a great deal of testing has been led on different fibrous materials to determine the real characteristics and benefits for each product. Over the decades different types of synthetic fibers have been successfully used to reinforced concrete.

Synthetic fibers are developed mostly to supply the high demand for carpet and textile products.

Nylon and Polypropylene are the most synthetic fibers used in these industries [5,6,7]. Huge amount of carpet waste is produced and part of these wastes are in the form of fibrous materials. Generally, industrial carpet wastes are from face and back yarns. The face yarn is usually polypropylene or nylon fibers and the back yarn is mainly in the form of woven sheets (Fig.1). These fibers are mainly 50%-70% nylon and 15%-25% polypropylene. The advantages of using such recycled fibers include generally lower cost to process than virgin fibers, light in weight, good acid and alkali resistance and non-absorbent of water [2,5,8].



Fig. 1 Waste products from industrial carpet: a) face yarn b) back yarn.

The inclusion of carpet fibers is an innovative method to improve the physical and mechanical properties of concrete to use these waste material in construction industries instead of virgin materials. In

the last decades numerous researchers have investigated the effects of utilization of different types of fibers in plain concrete on its engineering properties. Wang [9,10], Vilkner et al. [11], and Zhou and Xiang [12] have studied the effects of addition of waste carpet fibers on physical and mechanical properties of concrete. They concluded that carpet fiber, decrease the workability and compressive strength of concrete with reference to concrete without using carpet fibers. However, carpet fibers have been shown to exhibit a positive response in terms of flexural strength, impact strength and toughness of concrete [1,12,13].

The addition of waste carpet fibers in the concrete mix is a new area of research which needs considerable attention. Although a number of research works were conducted on the utilization of this fiber in concrete to enhance general properties of concrete, it necessary to conduct in-depth study on the behavior of concrete with the wide range of mix proportions. Since a small amount of short fibers has been recommended for the improvement of the properties of concrete such as impact resistance and tensile strength [14,15,16,17], it paves the way to use PP carpet fibers to obtain desired properties in concrete mix. The main objective of this study is to investigate in detail the effect of the addition of waste PP carpet fibers on workability and density, compressive, tensile and flexural strengths, modulus of elasticity and shrinkage of concrete at different volume fractions of 0.5%, 1.0%, 1.5% and 2.0%. In addition, the engineering properties of carpet fibers such as tensile strength, density and melting point are also studied and presented.

## EXPERIMENTAL PROGRAM

### Materials and Mix Proportioning

Ordinary Portland cement (OPC) with a specific gravity of 3.13 was used in this study. A saturated

surface dry river sand passing through 4.75 mm sieve having water absorption of 0.70% was used as fine aggregate. The fineness modulus and specific gravity of river sands were found to be 2.4 and 2.6, respectively. Crushed granite of 10 mm size with specific gravity of 2.7 having 0.5% water absorption in a saturated surface dry (SSD) condition was used as coarse aggregate.

The waste carpet fibers used were obtained from ENTEX Carpet Industries Sdn. Bhd, Malaysia. In this study the multi-filament polypropylene carpet fibers having 0.45 mm diameters with 30 mm length were used and tested for their engineering properties. The properties of the carpet fibers are shown in Table 1. The mix proportions of carpet fiber reinforced concrete (CFRC) are given in Table 2. A control mix of plain concrete (PC) without any carpet fibers was also made for comparison and four fiber volume fractions,  $V_f$  of 0.5%, 1.0%, 1.5% and 2.0 were investigated. It should be noted that, no mineral or chemical admixtures were added in concrete.

### Testing of Specimens

The workability of all mixes was measured by the slump test in accordance with BS EN 12350-2:2009. Compressive strength test was conducted with 100 mm cube specimens (BS EN 12390-3:2009 and BS EN 12390-2:2009). Cylinders measuring 100 mm x 200 mm were prepared for splitting tensile strength test (ASTM C496 / C496M – 11) and 100 mm x 100 mm x 500 mm prism specimens were made for testing the flexural strength at 28 days (BS EN 12390-5:2009). The splitting tensile strength and compressive strength tests were measured at the age of 1, 7 and 28 days. A short investigation for a period of 28 days was carried out for the shrinkage test following (ASTM C 157 and ASTM C 490). All tests were performed at an average room temperature of 27 °C with the relative humidity, RH of 80 ± 5 %.

Table 1 Properties of polypropylene waste carpet.

Fiber	Fiber type	Length (mm)	Diameter (μm)	Density (kg/m <sup>3</sup> )	Tensile strength (psi)	Melting point (°C)	Reaction with water
PP waste carpet fiber	Multi-filament	30	450	940	4700	170	Hydrophobic

Table 2 Mix proportions of concrete mixes (kg/m<sup>3</sup>).

Mix	Water	Cement	Fine aggregate	Coarse aggregate	Carpet fiber
PC	215	430	840	910	0.0
0.5% CFRC	215	430	840	910	4.7
1.0% CFRC	215	430	840	910	9.4
1.5% CFRC	215	430	840	910	14.1
2.0% CFRC	215	430	840	910	18.8

## RESULTS AND DISCUSSION

### Workability and Density

Table 3 reveals the results for the workability and wet density of concrete mixes. The slump test was conducted to measure the workability of PC and CFRC. As expected, the workability of concrete containing PP waste carpet fibers with same water/cement ratio (0.50) in all mixes was reduced the slump values ranging from 10 to 40 mm. The sturdy fiber-matrix bond and the absence of superplasticizers would have caused this reduction in the slump value of concrete. It can be seen that the workability of CFRC depends on the fiber volume fraction. At  $V_f = 0.5\%$ , the slump value was reduced to 40 mm compared to the 55 mm slump value obtained for the PC. At higher volume fraction, for example, concrete with 2.0% fiber content, the slump values dropped to 10 mm. This indicates that the addition of PP waste carpet fibers dramatically reduced the workability of concrete mix. A similar observation has been made by Wang et al. [2], who reported the increase of waste carpet fiber content reduced the slump value even to near zero for high amount of fibers.

Table 3 Workability and density of fresh concrete.

Mix	Slump (mm)	Fresh concrete density (kg/m <sup>3</sup> )
PC	55	2385
0.5% CFRC	40	2328
1.0% CFRC	20	2290
1.5% CFRC	15	2210
2.0% CFRC	10	2150

In Table 3 it can be seen that the density of concrete decreased when carpet fiber was added to the mixture. Concrete containing PP carpet fibers showed a lower density than the PC. On average, 0.5% CFRC and 1.0% CFRC mixes exhibited 2.4% and 3.9% lower density respectively as compared to the PC. Further increase in fiber volume fraction reduced the density; at  $V_f = 2.0\%$ , the reduction in

density of about 10% was observed. This is because of the lower density of the PP carpet fibers (940 kg/m<sup>3</sup>) that ultimately affected the whole concrete. Therefore, this reduction in the density of concrete is an advantage of using these waste carpet fibers to reduce the overall weight of structure.

### Mechanical Properties

#### *Compressive strength and modulus of elasticity*

Table 4 summarizes the results obtained for the compressive strength, tensile strength, flexural strength, and modulus of elasticity of waste carpet fiber reinforced concrete.

The addition of multi-filament fibers at 0.5% dosage, a decrease of 8.6% in compressive strength was observed. Further increase in fiber content reduced the compressive strength further comparing with that of plain concrete. This has also been evidenced in the investigation by Wang et al. [2] and Vilkner et al. [11] where the addition of carpet fibers into the concrete was found to attain lower compressive strength. Although the compressive strength of fiber reinforced concrete was affected by the presence of carpet fiber, the failure mode, however, exhibited a considerable change from fragile to a ductile state. Due to bridging action of the fiber, the cube specimens did not crush into pieces rather holds their integrity up to the end of the test. At typical failure mode of the 100 mm cube specimen under compressive strength test is illustrated in Fig 2.

The values of modulus of elasticity shown in the Table 4 are obtained from the expression (Eq. 1), given by Neville and Brooks [18], where  $E_c$  is the modulus of elasticity and  $f_{cu}$  is the cube compressive strength of concrete. The expected 28-day modulus of elasticity following the expression as recommended by BS 8110-2:1983.

$$E_{c, 28} = 20 + 0.2 f_{cu, 28} \quad (1)$$

The results obtained in this study visibly shows that the modulus of elasticity of concrete containing carpet fibers in association with its lower compressive strength was lower than that of plain concrete.



Table 4 Mechanical properties of plain concrete and carpet fiber reinforced concrete.

Mix	Mechanical properties							
	Compressive strength (MPa)			Splitting tensile strength (MPa)			Flexural strength (MPa)	Modulus of elasticity (GPa)
	1-day	7-day	28-day	1-day	7-day	28-day	28-day	28-day
PC	23.4	38.2	46.5	1.6	2.2	2.7	5.3	29.3
0.5% CFRC	19.9	34.1	42.7	1.8	2.8	3.1	6.2	28.5
1.0% CFRC	15.2	28.7	29.1	1.9	2.7	3.3	5.4	25.8
1.5% CFRC	18.0	29.3	30.7	2.1	2.9	3.5	5.1	26.1
2.0% CFRC	11.4	21.7	25.5	1.9	2.6	3.0	4.4	25.1



Fig. 2 Failure mode of concrete cube under compressive load.

For example, the 28-day modulus of elasticity of plain concrete with the equivalent compressive strength value of 46.50 MPa was found to be 29.30 GPa. A slightly lesser value of 28.54 GPa was obtained for concrete with 0.5% of carpet fibers having a 28-day compressive strength of 42.70 MPa. This is to be expected, because the relationship between compressive strength and modulus of elasticity of concrete indicates that modulus of elasticity increases with an increase in the compressive strength of concrete, although there is no accurate form of the relationship.

#### *Splitting tensile and flexural strengths*

The splitting tensile strength of both normal and fiber reinforced concrete measured at different curing periods of 1, 7 and 28 days are also given in Table 4. Data presented in Table 4 suggest that along with curing time, the addition of carpet fiber in concrete mix had a positive response on tensile strength of

concrete. The 28-day splitting tensile strength of concrete without any fiber, for example, was 2.7 MPa. At the same age a higher value of 3.5 MPa was obtained for concrete with 1.5% carpet fiber.

The flexural strength of concrete containing carpet fiber at 28 days for each mix is also presented in Table 4. As can be seen in this Table the flexural strength of CFRC mixes were increased with respect to that of the PC mix. On average, flexural strength increased by 17% and 1.8% for 0.5% and 1.0% fiber content respectively when compared with that of plain concrete. It is interesting to note that flexural strength raised for fiber content of up to 1.0% and then further increase in fiber volume fraction reduced the flexural strength.

#### *Drying shrinkage*

The measured values of shrinkage over a period of 28 days are plotted in Fig. 3. It can be seen that the

shrinkage strain of concrete containing PP waste carpet fibers was higher than that of plain concrete. The magnitude of shrinkage of plain concrete at 28 days was  $490.44 \times 10^{-6}$ . At the same time about 9% higher value of shrinkage i.e.  $534.60 \times 10^{-6}$  was recorded for the concrete with 0.5% carpet fiber and this value continued to increase with the function of the fiber volume fraction. At each age, however, the difference in values are less. The adverse phenomenon may be attributed to the higher porosity in the concrete mixtures compared to that in plain concrete due to the addition of large amount of carpet fibers and voids produced by segregation of aggregates. A similar tendency has been observed by Wang et al. [2] who have used carpet fibers along with other recycled fibers in the concrete mix.

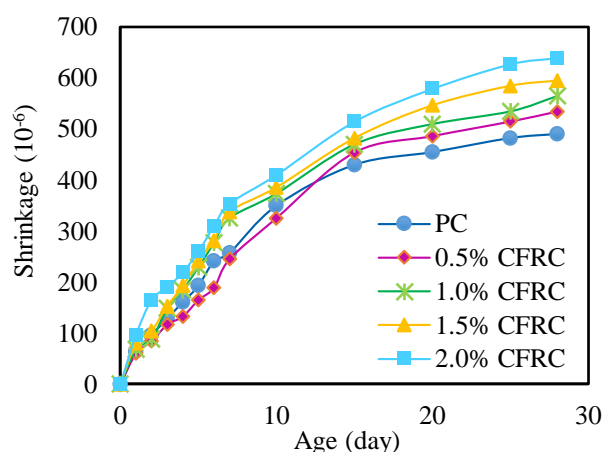


Fig.3 Shrinkage strain of PC and CFRC.

Various expressions are available for the prediction of the development of shrinkage with time. Among which, the equation developed by ACI 209R-92-1994, is perhaps the most elaborate. Although the equation can be used to estimate ultimate shrinkage of a wide range of moist-cured concretes, prediction of shrinkage by this equation is subject to considerable variation. An improvement in the accuracy of prediction of shrinkage is made by Neville and Brooks [18], in which long-term shrinkage values can be obtained by extrapolating the short-term tests of 28-day duration. The following expression was, thus, applied to predict the one-year shrinkage of plain concrete and concrete containing carpet fiber.

$$S_h(t, \tau_0) = S_{h,28} + 100 [3.61 \log_e(t - \tau_0) - 12.05]^{1/2} \quad (2)$$

Where  $S_h(t, \tau_0)$  = long-term shrinkage ( $10^{-6}$ ) at age  $t$  after drying from an earlier age  $\tau_0$ ,  $S_{h,28}$  = shrinkage ( $10^{-6}$ ) after 28 days, and  $(t - \tau_0)$  = time since start of drying (>28 days).

Following the above expression (Eq. 2), the one year prediction shrinkage strains for concrete with different amount of fiber are shown in Table 5. Data displayed in this Table indicate that along with the time, the addition of carpet fibers visibly increase the shrinkage strain values of concrete.

Table 5 One year predicted shrinkage values.

Mix	28-day Shrinkage ( $10^{-6}$ )	1-year Predicted Shrinkage ( $10^{-6}$ )
PC	490.4	789.8
0.5% CFRC	534.6	833.9
1.0% CFRC	565.0	864.3
1.5% CFRC	635.2	934.5
2.0% CFRC	667.3	966.7

## CONCLUSION

In this study the effects of the addition of industrial waste carpet fibers on properties of fresh and hardened concrete have been evaluated. Based on the experimental findings it is concluded that the addition of carpet fibers, in general, resulted in decrease in workability, density and compressive strength of concrete. Carpet fibers, however, effectively improved the splitting tensile strength by a maximum of about 30% at 1.5% of fibre content, and 17% of flexural strength at 0.5% fibre content as compared to that of concrete without any fibre. Meanwhile, concrete containing carpet fibers showed higher shrinkage strain values.

Although it is possible to predict long-term behavior from short-term data, long-term investigation including durability aspects have been put forward as recommendation for future study in order to understand fully the behavior of this material in concrete.

## ACKNOWLEDGEMENT

The authors wish to acknowledge the co-operation and technical support received from the staff of Structure and Materials laboratory of the Universiti Teknologi Malaysia (UTM) in conducting the experimental work. Special thanks to ENTEX Carpet Industries SND. BHD, Malaysia for making this research possible by providing waste carpet fibers.

## REFERENCES

- [1] Hsie M, Tu C and Song P, "Mechanical properties of polypropylene hybrid fiber-

- reinforced concrete," *Materials Science and Engineering A*, vol. 494, 2008, p. 153–157.
- [2] Wang Y, Wu H and Li C, "Concrete Reinforcement with Recycled Fibers," *Materials in Civil Engineering*, vol. 12, 2000, pp. 314-319.
- [3] Suna Z and Xu Q, "Microscopic, physical and mechanical analysis of polypropylene fiber reinforced concrete," *Materials Science and Engineering A*, vol. 527, 2009, p. 198–204.
- [4] Altun F, Tanrıöven F and Dirikgil T, "Experimental investigation of mechanical properties of hybrid fiber reinforced concrete samples and prediction of energy absorption capacity of beams by fuzzy-genetic model," *Construction and Building Materials*, vol. 44, 2013, p. 565–574.
- [5] Wang Y, "Fiber and Textile Waste Utilization," *Waste Biomass*, vol. 1, 2010, pp. 135-143.
- [6] Reis J. M, "Effect of Textile on the Mechanical Properties of Polymer Concrete," *Materials Research*, vol. 12, no. 1, 2009, pp. 63-67.
- [7] Wang Y, "Fiber Recycling in the United States," *School of Materials Science & Engineering*, Georgia Institute of Technology, Atlanta, Georgia, 2013.
- [8] Ucar M and Wang Y, "Utilization of recycled post consumer carpet waste fibers as reinforcement in lightweight cementitious composites," *International Journal of Clothing Science and Technology*, vol. 23, no. 4, 2011, pp. 242-248.
- [9] Wang Y, "Concrete reinforcement with recycled fibers from carpet industrial waste," *Materials in Civil Engineering*, 1997, pp. 103-104.
- [10] Wang Y, "Utilization of recycled carpet waste fibers for reinforcement of concrete and soil," *Polymer-Plastics Technology and Engineering*, vol. 38, no. 3, 1999, pp. 533-546.
- [11] Vilkner G, Meyer C and Shimanovich S, "Properties of glass concrete containing recycled carpet fibers," in *6th International RILEM Symposium on Fibre-Reinforced concretes*, Varenna, Italy, 2004.
- [12] Zhou J and Xiang H, "Research on Mechanical Properties of Recycled Fibers Concrete," *Applied Mechanics and Materials*, Vols. 94-96, 2011, pp. 1184-1187.
- [13] MirafTAB M, "Novel application of pre-and post consumer carpet wastes in concrete," 1999.
- [14] Schmidt H and Cieslak M, "Concrete with carpet recyclates: Suitability assessment by surface energy evaluation," *Waste Management*, vol. 28, 2008, pp. 1182-1187.
- [15] Song P, Hwang S and Sheu B, "Strength properties of nylon- and polypropylene-fiber-reinforced concretes," *Cement and Concrete Research*, vol. 35, 2005, pp. 1546– 1550.
- [16] Qian C and Stroeve P, "Development of hybrid polypropylene-steel fibre-reinforced concrete," *Cement and Concrete Research*, vol. 30, 2000, pp. 63–69.
- [17] Mazaheripour M, Ghanbarpour S, Mirmoradi S and Hosseinpour I, "The effect of polypropylene fibers on the properties of fresh and hardened lightweight self-compacting concrete," *Construction and Building Materials*, vol. 25, 2011, pp. 351–358.
- [18] Neville A and Brooks J, *Concrete Technology*, 2nd ed., Pearson, 2010.

## **EFFECTS OF MOISTURE CONTENT ON RESILIENT PROPERTIES OF RECYCLED CONCRETE AGGREGATES (RCAs)**

Chaminda Gallage<sup>1</sup>, Shiran Jayakody<sup>1</sup> and Jothi Ramanujam<sup>2</sup>

<sup>1</sup>Science and Engineering Faculty, Queensland University of Technology, Australia; <sup>2</sup>Queensland Department of Transport and Main Roads, Australia

### **ABSTRACT**

In pavement design, resilient modulus of a pavement material is one of the key design parameters. Resilient modulus of a granular pavement material can be measured using repeated load Triaxial (RLT) test or estimated using empirical models. For conventional granular pavement materials, a significant amount of resilient modulus data and empirical models to estimate this key design parameter are available. However, RCA is a relatively new granular pavement material and therefore no such data or empirical models are available. In this study, a number of RLT tests were conducted on RCA sample to investigate the effects of moisture content on its resilient modulus ( $M_r$ ). It was observed that the resilient modulus of RCA increased with a number of loading cycles but decreased as the moisture content was increased. Further, using RLT test results, empirical models to estimate the resilient modulus of RCA were enhanced and validated.

*Keywords: Repeater Load Triaxial, Recycled Concrete Aggregates, Resilient Modulus, Water Content*

### **INTRODUCTION**

Population growth and development /redevelopment activities in the globe have led to rapid increase in construction and demolition waste (C&D waste). Recycling of C&D waste has been identified as one of the best ways to manage C&D waste due to its environmental, social, and economic benefits. In 2008- 2009, Australia produced a total of 19 million tons of C&D waste [1] of which 55% was recycled. The C&D waste recycling sector in Queensland, Australia is reasonably well established and therefore Queensland government has targeted to increase the recycling of C&D by 50%, 60% and 75% successively in years 2014, 2017 and 2020 [1]. Therefore, it is needed to explore the applications of these recycled materials. About 40 % of C&D waste is demolished concrete and recycling concrete can generate aggregates called "Recycled Concrete Aggregates (RCA).

Roads are one of the biggest infrastructures in any country. In road construction, a large volume of aggregates is used as granular layers, stabilised granular layers, and aggregates for asphalt production. At present, crushed rocks are the preferred granular material used in road construction. Use of RCA as granular pavement material reduces the disposal of C&D waste to landfills and the depletion of natural resources (rocks).

Lack of data on properties and performances of RCA as a pavement granular material has limited its use in pavement structures. Further, the properties

and performances of RCA can be inconsistent due to the presence of impurities such as asphalt, brick, and glass in RCA. In addition, water content in RCA could have significant effect on the properties and performances of RCA as a granular pavement material.

Jr et al., [2] and Bennert et al.,[3] studied the performance of RCA and reclaimed asphalt pavement (RAP) using RLTs and concluded that RCA performed better than the RAP materials when considering the development of the permanent strain. Nataatmadja and Tan [4] reported that well-graded RCA produces a higher resilient modulus under low deviator stress and it may be caused by the un-hydrated cement within the RCA. Even though, some more studies on the performance characteristics of RCA are reported [5, 6], further studies are needed to investigate the effects of water content in RCA on its resilient modulus. Resilient modulus is one of key material elastic properties required in pavement design.

This paper presents the results of a series of RLT tests conducted on RCA samples with different moisture content. The results of the test series are then used to enhance the constitutive models, which are used to estimate the resilient modulus of granular materials, by taking the water content of RCA into account. Further, the applicability of the enhanced models to estimate the resilient modulus of the RCA is validated using additional RLT test data.

## TESTING MATERIAL

A commercially available RCA product termed as RM001 was employed in this experimental program. The material was obtained from a concrete recycling company in Queensland and it was sourced from clean concrete and can be considered free from other impurities such as glass, bricks, wood, soil, and asphalt. Figure 1 shows the texture of RM001.



Fig. 1 The appearance of RM001

Particle size distribution (PSD) of RM001 was obtained by performing sieve analysis in accordance with Australian standards, AS1289.3.6.1-2009 [7]. As shown in Fig. 2, the PSD of RM001 was plotted with upper and lower boundaries of PSDs of base layer granular materials specified by Queensland Department of Main Roads [8]. The RM001 has maximum and minimum particle size 25.4 mm and 0.18 mm respectively. It can be seen that the particles larger than 20 mm shifted the upper limit of specification and the particles smaller than 0.6 mm propped below the lower limit of the specification.

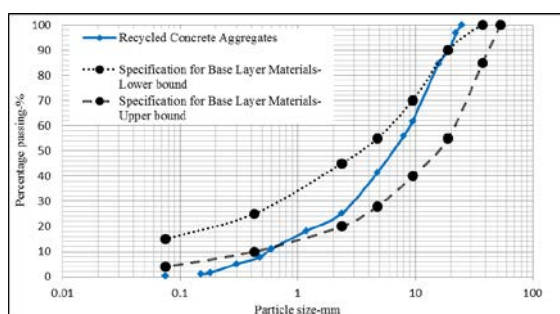


Fig. 2 PSD of test material (RM001)

RM001 was tested for atterberg limits in accordance with Australian and Queensland Department of Transport and Main Roads Queensland (QDTMR) standards [9-11], water absorption following the test method specified QDTMR [12, 13], and standard proctor compaction test in accordance with Australian Standards [14] and the results are shown in Table 1.

Atterberg limits of RM001 are within the range

specified by QDTMR for standard granular pavement material. However, the water absorption capacity of RM001 is much higher than that of standard pavement granular material. This could be caused by residual cement and cement mortar paste around the aggregates in RCA. When compaction properties of test material are compared with those of standard pavement granular material, RCA has smaller maximum dry density (MDD) and greater optimum moisture content (OMC) than that of standard granular pavement material. This could be due to lesser fines content and higher absorption capacity of RCA compared to standard granular pavement material.

Table 1. Physical properties of RCA

Property	Values	
	RCA (RM001)	Standard granular pavement material
Liquid Limit (PL) [%]	21.00	*Max: 25 [8]
Plasticity Index (PI)	5.40	*Max: 6 [8]
Linear Shrinkage (LS) [%]	1.00	*Max: 3.5 [8]
Water absorption (particles smaller than 4.25 mm) [%]	5.35	<10 [15]
Water absorption (particles greater than 4.25 mm) [%]	6.50	<10 [15]
Specific gravity (Gs)	2.64	2.85 [16]
Maximum dry density (MDD) [g/cm <sup>3</sup> ]	1.75	>1.79 [15]
Optimum moisture content (OMC) [%]	13.20	8-15 [15]

\*Max=Maximum

## TESTING APPARATUS

To obtain the resilient modulus of RCA samples, the Repeated Load Triaxial (RLT) apparatus of which the schematic diagram is shown in Fig. 3 was employed in this study. The apparatus can accommodate a cylindrical specimen with 100 mm diameter and 200 mm height. The confining pressure up to 1000 kPa is applied by pressurizing air in the cell and the applied confining pressure is continuously monitored by transducer connected to the cell. The pneumatic actuator connected to the vertical shaft can apply repeated load/stress with different waveforms on the sample under stress or strain controlled conditions. The actuator has the capacity to apply the maximum load of 12kN and has the maximum stroke of 30 mm. The vertical deformation of the specimen is calculated by averaging the vertical deformation measured by two



LVDTs attached to the vertical shaft as shown in Fig. 3. RLT test is commonly conducted under undrained condition and therefore no volume change unit is available. Saturated and unsaturated specimen can be tested in the apparatus with continuous monitoring of pore-water pressure by the transducer connect to the bottom of the specimen. LVDTs, Pore-pressure and cell pressure transducers, and load cell are connected to logging system to collect the responses of these transducers at specified time interval.

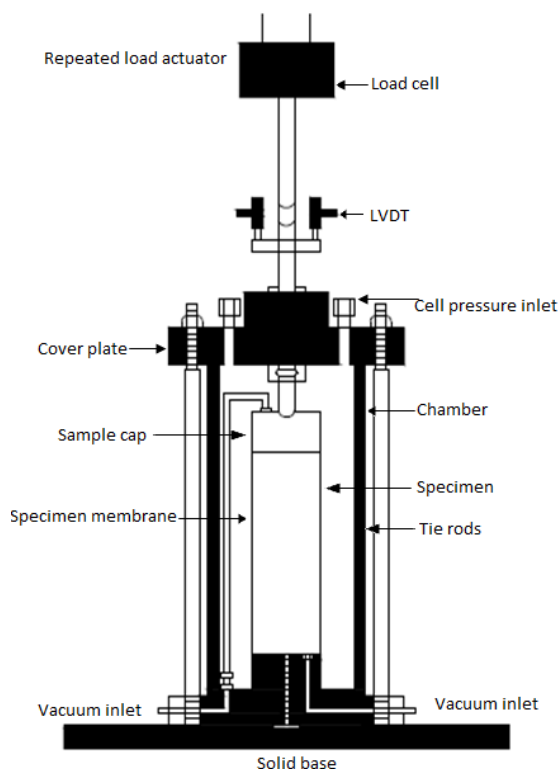


Fig. 3 The schematic diagram of RLT apparatus used

## METHODOLOGY

Table 2. Summary of test conditions

Moisture content (%)	Dry density ( $\text{g}/\text{cm}^3$ )	Confining pressure (kPa)	Degree of saturation (%)	Dynamic deviator stress (kPa)
11.6	1.75	125	60	175, 325, 475, 625
13.2	1.75	125	68	175, 325, 475, 625
14.5	1.75	125	75	175, 325, 475, 625
15.5	1.75	125	80	175, 325, 475, 625

Note: At each stress stage, 10,000 load repetitions were applied.

The resilient modulus ( $M_r$ ) of RCA and the effects of moisture content on  $M_r$  were investigated by performing a series of RLT tests on RCA specimens. As shown in Table 2, tests were performed using three dynamic deviator stresses ( $\sigma_d$ ) of 175, 325, 475, and 625 kPa, with confining pressure ( $\sigma_3$ ) of 125 kPa. Tests were conducted at four different water content values and the dry density equal to MDD was maintained for all tests.

## Specimen Preparation

Oven dried material was mixed with pre-determined water content (e.g: 11.6, 13.2, 14.5, 15.5 %) and left overnight in sealed containers for moisture homogenization. Then the material was compacted in to a split mould of 100 mm diameter and 200 mm height to achieve the pre-determined dry density of  $1.75 \text{ g}/\text{cm}^3$ . The compaction of the specimen was done in three layers. The bulk mass required to achieve the dry density of  $1.75 \text{ g}/\text{cm}^3$  in the mould was calculated and one-third of that mass was used for each layer and numbers of standard compaction blows were applied to reach one-third of the mould height. This method was repeated to other two layers to get a specimen prepared for a RLT test.

The compacted specimen was then enclosed in 0.8 mm thick rubber membrane and set in the RLT apparatus. The specimen was sealed at the top and the bottom of the specimen and 125 kPa confining pressure was applied and allowed to consolidate for about 2 hours.

## Loading and data interpretation

Once the sample was consolidated under 125 kPa confining pressure, the wave form shown in Fig. 4 was repeatedly applied under undrained conditions. For each sample, the wave form was repeated 10,000 times for each dynamic deviator stress ( $\sigma_d$ ) stage (e.g: 175, 325, 475, and 625 kPa).

Figure 5 shows a typical stress vs strain response for a RLT test and how to obtain resilient modulus ( $M_r$ ) and permanent/plastic strain (deformation) corresponding to a given loading cycle.

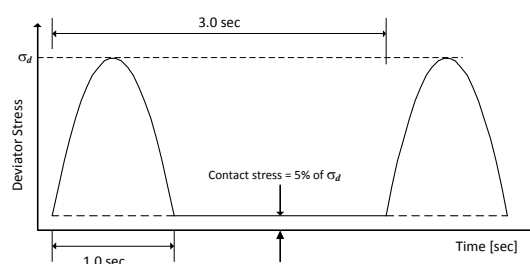


Fig. 4 Illustration of the vertical (deviator) stress waveform applied



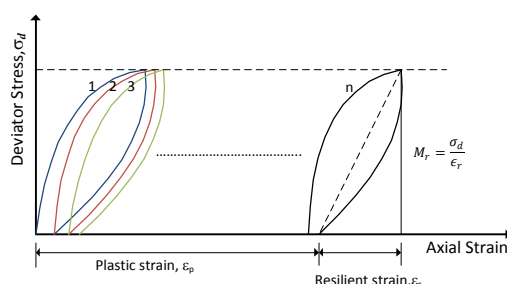


Fig. 5 Typical stress vs strain response in RLT test

## RESULTS AND DISCUSSIONS

A series of RLT tests were conducted under the conditions given in Table 2 to investigate the effects of water content on resilient properties (permanent deformation/strain and resilient modulus ( $M_r$ )) of RCA. Further, using the resilient modulus data obtained from the tests, a constitutive model was enhanced to predict/estimate the resilient modulus of RCA and its applicability was validated using additional test data.

### Accumulation of permanent (plastic) strain in RCA

Figure 6 depicts the accumulation of vertical plastic strain with numbers of loading cycles and how it is affected by the sample moisture content and dynamic deviator stress ( $\sigma_d$ ).

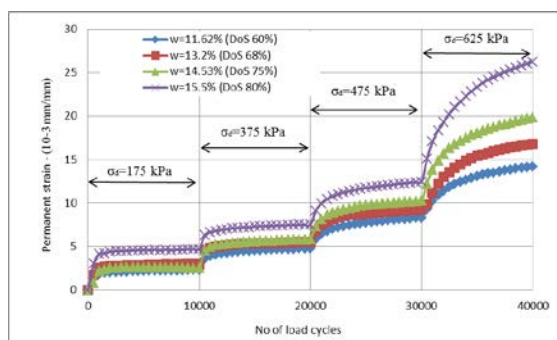


Fig. 6 Accumulation of vertical plastic strain with numbers of loading cycles

As shown in Fig. 6, for a given confining pressure and a dynamic deviator stress, the plastic strain increases with numbers of loading cycles. However, the rate of increase in plastic strain (plastic strain per loading cycle) decreases with numbers of loading cycles tending to achieve a long-term, steady-state response (no accumulation of plastic strain and each response is hysteric). This implies that a finite amount of energy is absorbed by the material on each stress-strain excursion. Once a purely resilient response has been obtained, the material is said to have “shake down” and the maximum stress level that this condition is achieved

is termed the “plastic shakedown limit”. Numbers of researchers [17, 18] observed the shake down state and the plastic shakedown limit for pavement granular materials such as crushed rocks. It can be seen that RCA tends to behave like natural granular material under repeated load and the applied stress conditions in this experimental program seem to be less than the plastic shakedown limit of RCA except  $\sigma_d$ .

The vertical plastic strain increases with increase in sample moisture content and the principal stress ratio ( $\sigma_d/\sigma_3$ ). As the moisture content is increased, the particles are more lubricated to facilitate their movement into air-voids. This may increase the accumulation of plastic strain. As the stress ratio is increased, the lateral confinement becomes smaller compared to the dynamic deviator stress. This may allow greater lateral displacement in the sample that cause to increase the plastic vertical deformation.

### Resilient modulus of RCA

Figure 7 shows how resilient modulus ( $M_r$ ) of RCA varies with numbers of loading cycles. It can be seen that, for a given stress condition which is smaller than the plastic shake down limit of RCA,  $M_r$  increases significantly with the first few numbers of loading cycles and then it increases with decreasing rate tending to approach the steady-state condition (zero increase in  $M_r$  with loading cycles) which can be termed as shake down response. Densification of the sample with the first numbers of loading cycles could cause the increase in resilient modulus. Once a steady-state response is achieved, neither plastic strain nor the densification is accumulated or occurred and therefore, no increase in  $M_r$  with numbers of loading cycles can be observed once the steady-state response is achieved. A numbers of researchers [19, 20] observed this phenomenon for natural crushed rocks and it can be seen that RCA behave like natural crushed rocks under repeated loads though its  $M_r$  is much less than that of high standard granular pavement materials ( $M_r=300-700\text{MPa}$ ) specified by Austroads Ltd, Australia [21].

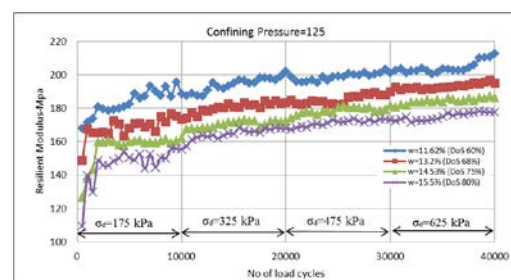


Fig. 7 The variation of resilient modulus ( $M_r$ ) of RCA with number of loading cycles

For each test with different water content,  $M_r$

was calculated at 10,000<sup>th</sup> loading cycle of each stress stage and the results are shown in Fig.8. It can be seen that  $M_r$  decreases with increase in material's moisture content and increases slightly with increase in stress ratio ( $\sigma_1/\sigma_3$ ) or bulk stress  $\theta$  ( $\sigma_1 + \sigma_2 + \sigma_3$ ).

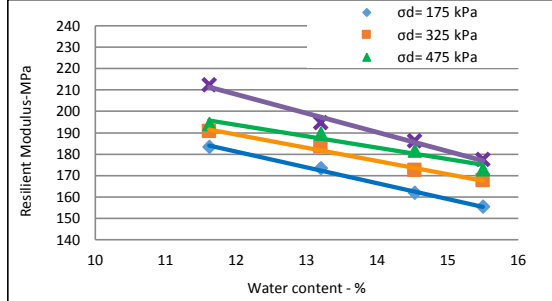


Fig. 8 The variation of resilient modulus of RCA with moisture content and stress level

More water in the sample lubricates the particles to reduce the frictional resistance between RCA particles and that eventually leads to reduce the stiffness ( $M_r$ ) of the sample.

#### Constitute model to estimate $M_r$ of RCA taking water content into account

It is not practicable to perform RLT tests to obtained  $M_r$  of pavement granular materials. Therefore, numbers of constitute models have been developed by researchers [22, 23] to estimate the  $M_r$  for granular road materials. There is no such model for RCA to predict/estimate its  $M_r$ , the following, more simple, constitute model is attempted to predict the  $M_r$  of RCA [22]:

$$M_r = k_1 p_a \left( \frac{\theta}{p_a} \right)^{k_2} \quad (1)$$

Where,

$M_r$  = Resilient Modulus

$p_a$  = Atmospheric pressure (103.4 kPa)

$\theta$  = Bulk stress ( $\sigma_1 + \sigma_2 + \sigma_3$ )

$\sigma_1$  = Principal vertical stresses

$\sigma_3 = \sigma_2$  = Principal radial stresses (confining pressure)

$k_1$  and  $k_2$  are model parameters

Non-linear regression analysis was used to fit the measured  $M_r$  in Fig. 8 to Eq. (1) and to obtain the model parameters  $k_1$  and  $k_2$  as a function of initial moisture content of RCA sample as shown below:

$$k_1 = -0.0435 w + 1.3397 \quad (2)$$

$$k_2 = 0.0088 w + 0.3009 \quad (3)$$

where,  $w$  = moisture content in percentage (%)

To validate the applicability of enhanced model to predict the  $M_r$  of RCA with different moisture content, a RLT test on RCA with 66 stress conditions was conducted according to the standard method of Austroad APRG 00/33-2000 [24]. The sample's initial moisture content was maintained at 13.8 %. Then, for all these 66 stress conditions,  $M_r$  was calculated and also predicted using Eq. (1), (2) and (3). Fig. 9 depicts the measured and predicted  $M_r$  values and they are well agreed. With further validation using the results of tests conducted at different moisture contents and stress conditions, it would be able to suggest the enhanced constitutive model to be used to predict/estimate the  $M_r$  of RCA.

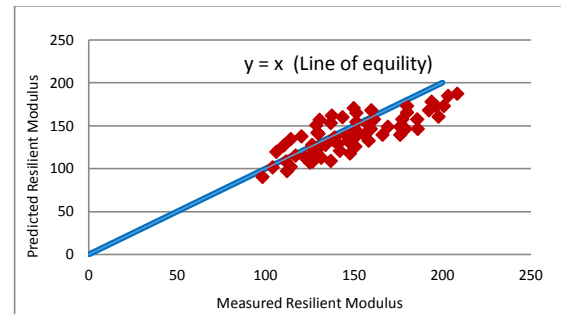


Fig. 9 Measured and predicted  $M_r$  for RCA sample with moisture content of 13.8%

#### CONCLUSION

In this study, the resilient properties of RCA and the effects of moisture content on these properties were investigated by a series of performing Repeated Load Triaxial tests. The following conclusions are drawn from this study:

- In terms of classification properties, RM001 (RCA) is comparable with standard granular pavement material specified by QDTMR.
- For a given stress condition, the resilient modulus of RCA decreases and the plastic strain of RCA increases with increase in moisture content.
- RCA tends to exhibit “shake down” response and “plastic shake down limit” that are observed in natural granular materials such as crushed rocks.
- The enhanced constitutive model will be able to use to predict the resilient modulus of RCA by taking moisture content and stress level of the material into account.

#### ACKNOWLEDGEMENTS

This paper is based on the second author's research completed as a partial fulfillment for the PhD requirements at Queensland University of Technology (QUT), Brisbane, Australia. Therefore, the first author acknowledges the scholarship received from QUT. The authors gratefully

acknowledge Alex Fraser Queensland for providing Recycled Concrete Aggregates (RCA) for this experimental program. Queensland Department of Transport and Main Roads (QDTMR) and Brisbane City Council (BCC) are greatly acknowledged for providing some of testing facilities. A special thank goes to Mr. Glen Barnes, senior laboratory technician at QUT, for his great support for conducting laboratory testing at QUT.

## REFERENCES

- [1] Hyder Consulting ECSRS."Construction and demolition waste status report". 2011.
- [2] Jr WJP, Maher MH, Bennert TA, Gucunski N."Behavior of construction and demolition debris in base and subbase applications". Recycled materials in geotechnical applications. 1998.
- [3] Bennert T, Papp WJ, Maher A, Gucunski N."Utilization of construction and demolition debris under traffic-type loading in base and subbase applications". Transportation research record 2000:33-9.
- [4] Nataatmadja A, Tan YL."Resilient Response of recycled concrete road aggregates". Transportation engineering. 2001.
- [5] Arulrajah A, J. Piratheepan MWB, Sivakugan N."Geotechnical characteristics of recycled crushed brick blends for pavement sub-base applications". Canadian Geotechnical Journal. 2012;49:796-811.
- [6] Conceicao Fd, Motta rdS, Vasconcelos KL, Bernucci L."Laboratory evaluation of recycled construction and demolition waste for pavements". Construction and building materials 2011;25.
- [7] Australia Cos."Methods of testing soils for engineering purposes". Method 361: Soil classification tests-determination of the particle size distribution of a soil-standard method of analysis by sieving. 2009.
- [8] MainRoads QDoTa."Main roads technical standards: MRTS05 - unbound pavements". Technical Specification 2010.
- [9] Australia CoS."Methods of testing soils for engineering purposes". Method 321: Soil classification tests-determination of the plastic limit of a soil-standards method. 2009.
- [10] Australia CoS."Methods of testing soils for engineering purposes". Method 391: Soil classification tests-determination of the cone liquid limit of a soil. 2002.
- [11] MainRoads QDoTa."Material testing manual". Test method NoQ106-1989 Linear shrinkage. 2011.
- [12] Roads QDoTaM."Test method No.Q214A-1996". Particle density and water absorption of aggregate (Fine Fraction). 2011.
- [13] MainRoads QDoTa."Material testing manual". Test method Q214B-1996, Particle density and water absorption of aggregates (Coarse fraction). 2011.
- [14] Australia CoS."Methods of testing soils for engineering purposes". Method 511: Soil compaction and density tests-determination of the dry density/moisture content relation of a soil using standard compactive effort. 2003.
- [15] Arulrajah A, Piratheepan J, Disfani MM, Bo MW."Geotechnical and Geoenvironmental Properties of Recycled Construction and Demolition Materials in Pavement Subbase Applications". Journal of Materials in Civil Engineering. 2013;25:1077-88.
- [16] Vegas I, Ibañez JA, San José JT, Urzelai A."Construction demolition wastes, Waelz slag and MSWI bottom ash: A comparative technical analysis as material for road construction". Waste Management. 2008;28:565-74.
- [17] Werkmeister S, Dawson AR, Wellner F."Permanent deformation behaviour of granular materials and the Shakedown concept". Transportation Research Record: Journal of the Transportation Research Board. 2001:75-81.
- [18] Cerni G, Cardone F, Virgili A, Camilli S."Characterisation of permanent deformation behaviour of unbound granular materials under repeated triaxial loading". Construction and Building Materials. 2012;28:79-87.
- [19] Vuong BT, Hazell D."Development of performance-based specifications for unbound granular materials". Road and Transport Research Journal. 2003;12:13-25.
- [20] Ekblad J, Isacsson U."Influence of water on resilient properties of coarse granular materials". Road materials and pavement design. 2006;7:369-404.
- [21] Jameson G, Group A."Pavement structural design". Guide to pavement technology part 2. 2008.
- [22] Seed HB, Mitry FG, Monismith CL, Chan CK."Prediction of flexible pavement deflections from laboratory repeated-load tests". National Cooperative Highway Research Program Report. 1967.
- [23] Witczak MW, Uzan J."The universal airport pavement design system". Report 1 of 4 Granular Material Characterization. 1988.
- [24] Vuong BT, Brimble R."Determination of permanent deformation and resilient modulus characteristics of unbound granular materials under drained conditions, In APRG DOCUMENT APRG 00/33(MA)". Austroads repeated load triaxial test method. 2000.

***Environment***

# CONSERVATION AND EXPLOITATION OF BANG GRASS EFFECTIVE IN PHU MY VILLAGE, VIETNAM

Duong Minh Truyen<sup>1</sup>, Le Hong Thia<sup>1</sup>, Mashhor Mansor<sup>2</sup>

<sup>1</sup>Cantho University, 3/2 Street, Cantho City, Vietnam;

<sup>2</sup>School of Biological Sciences, Universiti Sains Malaysia, 11800 Minden, Penang, Malaysia.

## ABSTRACT

Phu My located in Kien Giang province, South of Vietnam is a small village with the majority of the population made of a Khmer community. The weather conditions are not encouraging for locals due to serious flooding months. The soils and water are comparatively acidic. Therefore, only *Bang* grass (*Lepironia articulata*) – an indicator for the wetland habitats and *Nang* grass (*Eleocharis dulcis*) – the main food of an endangered Sarus Crane (*Grus antigone*) can thrive. *Bang* grassland area decreased due to the housing problem. To overcome the decrease of *Bang* grass and conserve this species, the project “Restoration and sustainable exploitation *Bang* grassland in Phu My, 2004” conducted to help locals make sophisticated handmade products from *Bang* grass. It is a good way to help the locals to benefit and conserve *Bang* grass.

**Keywords:** *Bang* grass (*Lepironia articulata*), *Phu My*, *exploitation*, *conservation*

## INTRODUCTION

Kien Giang Province is a diverse area of wetland ecosystems, including mangrove forests, brackish marshes, swamp and grasslands in Mekong Delta of Vietnam [1]. In Kien Giang, Phu My commune is a primitive wetland with heavy alum, organic soil and seasonally inundation. The main community in Phu My is Khmer people. Besides *Eleocharis dulcis*, *Eleocharis ochrostachys*, *Ischaemum rugosum*, *Melaleuca cajuputi*..., *Bang* grass (*Lepironia articulata*) is the main plant in Phu My [2]. Because of the alkaline soil, valuable food and agricultural crops are not taken. Therefore, *Bang* grass plays an important and essential role in social economic life of locals in the region. Cutting *Bang* grass to weave and make products and handicraft items is an important part for current revenues in Khmer community.

However, *Bang* grass is exploited significantly in a short time because locals transform land use into inappropriate agricultural models. It leads to the decrease of *Bang* grass area because of higher exploitive rate than natural restoration. The disappearance of *Bang* grass will affect enormously the socio-economy as well as ecological functions of environment and natural conservation. The model, which combines natural conservation with the participation of the community, is conducted in Phu My commune of Kien Giang province with the purposes: to preserve existing ecosystems, reduce financial burden for local governments in

conservation and improve people's lives and to assess the social and economic changes of the community involved in the project "Sustainable exploitation of grassland conservation *Bang* combining local trade village, Phu My commune, Kien Luong district" from 2004 to 2006.

## METHODOLOGY

According to Pham Hoang Ho [3], the location of vegetation classification *Bang* is described as follows: Order: Cyperales; Family: Cyperaceae; Genus: *Lepironia*; Species: *Lepironia ariculata* (Retz.) Domin



Fig. 1 *Bang* Grass (*Lepironia ariculata*) (according to Jackson and Jacobs [4]).

## Research Methodology

### 2.1.1 Collect basic information

Collecting information, documents, maps, research data related to pre-existing problems and

research areas, focusing on the study material of plants *Bang*, natural characteristics, socio-economic, management and development of the local villages. The information was collected at the following agencies: Technical Centre of Natural Resources and Environment (Department of Natural Resources and Environment Kien Giang), the People's Committee of Kien Luong district, People's Committee of Phu My commune, Department of Science and Technology.

#### Construct the questionnaires

Based on the different groups in the community living around the project area, constructing the questionnaires:

- Form I: households interviewed in 2004
- Form II: households participating spit and weave products from Bang grass
- Form III: intermediate households purchase products from Bang grass
- Form IV: employees working in the project or working at home

The investigators interviewed each household and reported information in different questionnaire. Data recorded will be encoded in a common code table. Enter data stored in an Excel spreadsheet, and processed with statistical software SPSS.

#### Methods of analysis of economic efficiency

- The economic efficiency of a model is calculated by the formula: profit = total revenue – total cost
- Determine the percentage of income of each model contributes to the total income per household in the year.

#### Maintain and develop the traditional craft villages for the local community

Use the rapid assessment of rural people's participation by conducting quick interviews of households who weaved *Bang* grass about techniques, methods and material preparation.

## RESULT

### Exploiting Bang grass from the local community

According to the survey in 2006, more than 64% of participating households exploited *Bang* grass. Activities were taken year-round and mostly in the rainy season. On an average day, an anchor puller pulled up 20 bunch (1 bunch of Bang is about 1.834kg). Approximately 1% of people pulled up

Bang grass every day and 42% pulled up after 10 days off.

Table 1 Exploitation of *Bang* grass in different months

Month	Exploitation level
1	**
2	*
3	*
4	*
5	*
6	**
7	**
8	**
9	***
10	***
11	***
12	***

Notes: (\*) : exploit rarely  
 (\*\*) : exploit averagely  
 (\*\*\*) : exploit significantly

bad quality  
 average quality  
 good quality

Table 1 shows the level of exploitation of the grass Bang Phu My community changes seasonally. In the rainy season from September to January, water flooded grasslands, Bang grass had good quality (height > 1.2m), and people exploited Bang grass the most. In the dry season from February to May, exploitation levels decrease due to poor quality of Bang grass (body broken, dry, reaching heights not suitable to exploit raw material), and people exploited the least. From June to August, flood started up and people started exploiting again.

Table 2 Total bunches of Bang grass exploited from locals

	Number of household
Households in the project area (*)	80
Total household living around the project area exploited Bang grass	229
Total bunches of Bang grass exploited from locals per year	1,671,700

Notes: (\*) On average, each household had one Bang grass puller, one person pulled 20 bunch /day (7,300 bunches/year).

Table 2 showed the total number of Bang bunches exploited from the local community (16717 million bunches/year). Compared with the findings of Tran Triet [2], the maximum number of total Bang



exploitation 1,2992 million bunches/year. This showed that exploited activities Bang of the local community after two years constructing the project increased to 372,500 bunches.

### Impact Communities to Bang Grass:

#### Exploit Bang grass

The community exploited *Bang* grass numerously in rainy season when Phu My commune was flooded fully. Pulling out and cutting were two ways, which used to exploit *Bang* grass:

+ Deracination: using hand to pull out the roots, just select the high stem to exploit. This method was used by 95% of the local community to exploit *Bang* grass in flooded season.

+ Cut: About 86% outside the local community used knife and cut the grass, including saplings in the dry season.

In summary, the exploitive activities of locals inside and outside the community increased and made the area of *Bang* grass decrease and degrade gradually. The main reasons were inappropriate technical exploitation and over exploitation of people to overcome self- regenerating capability in the rainy season.

#### The other impact

In 2006, grasslands were under significant impact of digging ditches, encroaching agriculture or melaleuca, hatching shrimp farm and burning grasslands. The ground water level was decreasing deeper by digging ditches in grassland, the surface soil had exposed to the air and led to the alkalization. The soil properties changed had brought about the vegetational cover on the surface changed. Those species under drought and aluminous conditions would be replaced by submerged species. The agricultural encroachment of households to take place in the contiguous area of meadows and agricultural land reduced grassland area, which had invested a lot of effort and money to renovate. As a result, 5% of local people often burned grasslands, alternating *Melaleuca leucadendra* in the dry season to log rough timber. Grasslands were habitats of many different species of animals and plants. Burning pastures would affect pasture conservation objectives and the living creatures and might changed the flora and fauna here.

### Impact of the project on the community

#### Raising awareness of community about Bang grass resources

In 2006, 64 of 122 households participated in *Bang* exploitation. Among them, 60 households knew information about the project and 44 households knew the boundaries of the project because the project set up landmarks and sentry - box. Collecting suggestions from community, 51% of people commented that *Bang* pasture would be forever and 49 % of respondents said that *Bang* pasture was declining by switching to farming, shrimp and over exploitation.

From the survey, there were 20 households recognizing the economic values of *Bang* grass. They built a dike and prevented strangers to exploit *Bang* grass. Technical exploitation of people changed more consistently, 64 households in the project used deracination method, selected the mature *Lepironia ariculata* with large diameter, height of 1m or more. Exploitable *Bang* grass time was different; only 3.1% of households exploited in rainy season when flooding occurred, around 6.3 % of households exploited all year around. Others exploited in freetime. Thus, after two years of project's implementation, communities living around understood the values of *Bang* grass (the economic and conservational values).

#### To create jobs for the local community

The project created jobs for the local community, especially for Khmer women. Total number of employees was 30 people; 26 people worked in 2005, 4 new people worked in 2006. Most products were made in the workshop of the project. They selected *Bang* grass and dried them to make handicraft items. Besides working at workshop, workers had worked at home.

Table 3 Income from production of the project

Activities	Capacity (product/day)	Income (USD/day)	Income (USD/month)
Weave cushions at home	2-3	0.71 – 0.85	21.20 – 25.44
Weave mats	8-10	0.94 – 1.41	28.27 – 42.40
Weave best color quality mats	2-3	0.94 – 1.41	28.27 – 42.40
Make baskets	7-10	1.41 – 2.12	42.40 – 63.60

From the result of socio-economic survey in 2006, who admitted into the project was local, encouraging Khmer people. If they knew to sew, they would be trained to become weavers. Otherwise, they were trained to be dyers or do other activities in production line of handbags, briefcases, hats. In case workers did not have time to work at the workshop, they could made cushions or mats at home. Table 1 shows that the income of workers made baskets was highest 42.40 – 63.60 USD/month. Workers weaved at home received from 21.20 – 25.44 USD/month. If compared with other jobs, working in the project had more stable income, fixed working time, improved skills, learned new methods to produce many kinds of products.

Income per year between farming and exploiting *Bang* grass were compared in table 4. Locals got about 3487.89 USD/year for farming while the income from exploitation *Bang* grass was 678.45 USD/year, about 5 times lower. This was the reason people changed to do farming and land use from pasture to rice fields. However, the lowest income might be -282.69 USD/year. Because farmers had a bad harvest, could not get the profits and got unpaid debts from buying chemical fertilizers and insecticides. Working in the project to make products from *Bang* grass, workers could get minimum 12.72 USD/year.

#### *The cost for exploitation Bang grass*

Community in Phu My commune exploited *Bang* grass without paying any cost. People often deracinated in wild *Bang* grasslands. Therefore, the costs were taken from travelling and eating. If people deracinated in project area, the cost would be 32.98 USD/basket. In case people made cushions at home, the material cost was 282.69 USD/mattress.

#### *The profits from exploitation of the project*

If people exploited natural *Bang* grass for sale raw materials and made cushions, the average profit per year would obtain 100.35 USD. Households with machine to press *Bang* had profits in the first year from 75.38 USD to 471.15 USD. The second year, profits rose from 84.81 USD to 1187.29 USD. The average profits were obtained from 33.92 USD to 376.92 USD. The project “Restoration and sustainable exploitation *Bang* grassland in Phu My, 2004” established in 12/ 2004, but until 12/2005 it has started a new business. The project purchased raw and dried materials to produce products such as mats, baskets books, briefcases and hats. The revenue

### **Economic Change**

Table 4 Comparison of income from farming and exploiting *Bang* grass

	Income (USD/year)	
	Farming 2 crops	Exploiting <i>Bang</i> grass
Low average	188.46	100.35
Average	338.19	126.46
Low	-282.69	12.72
High	3487.89	678.45

from the raw materials of business had been documented and reported every year.

### **Maintenance and development of traditional village for local community**

#### *Handicraft villages before 2004*

Weaving handicraft products was present in Khmer community anciently and inherited by the progeny and then it became the traditional industry of Phu My. In wartime, people weaved products such as cushions, baskets, hats, bags. Since 1990, only few items used and maintained until today.

#### *Manufacturing processes*

Every dry season, *Bang* grass withered. However, in rainy season, it began a new growth cycle. In harvesting time, people pulled up small handfuls, then bundled up bunches. After being dried, *Bang* grass had toughness, plasticity, sustainable strength and impermeability. Due to those characteristics, *Bang* grass was used as a raw material for weaving products. After drying, each stem was crushed on a small stone or a plank to flat it. Weaving instruments were a very sharp pointed piece of bamboo. First, using hands knitted a contour connecting the stems together. Continue knitting until the completion of the product. Hence, to complete a product people did not use any machinery. They only used hand to knit a product from raw materials.

#### *The consumer market*

Handicrafts products were mainly sold to locals, other cities in Vietnam and customers from Cambodia. Typically, most products sold in the rice season. Since the products were made from *Bang*

grass with many models, styles and colors, in 2005, products had expanded local markets and sold abroad. The baskets, mats, mattresses had been accepted in domestic markets, especially baskets had been exported to Japan.



Fig.2 Steps to knit a cushion: A. crushing instruments (pestle); B. crusing Bang grass; C. knitting a cushion.



Fig.3 Types of products: the types of bag; mats; pads; slippers; hats and dried materials.

From the mat and pad products providing by the local community, the project designed new products with multiple patterns, colors, different sizes.



Fig.4 The equipments used in the production Bang grass: Bang squeezer; looms; sewing machine.

The project maintained traditional ways of community that was weaving cushions by hand. However, there were improvements in machinery and equipment in production to save labor, save time and increased the capacity. Bang squeezers replaced hand tools. Looms used for weaving mats was shorter time than knitting by hand. Sewing machines used sewing baskets, contours in order to improve design and fit with current markets' demands.

## CONCLUSION

Handicraft village of the project had positive impacts on the local villages. Currently, productive technology and machinery used in production has been improved to help people reduce labor save time. From one model of product, locals expanded to develop about 20 types of baskets, mats, cushions and hats. Consumption of products was also expanding in domestic markets and international markets.

## ACKNOWLEDGEMENT

I would like to express my gratitude towards Universiti Sains Malaysia for funding the publication fee under the Individual Research Grant (1001/PBiologi/816217) and all the people who get involved in the project.

## REFERENCE

- [1] Nguyen, H.H., et al., *The relationship of spatial-temporal changes in fringe mangrove extent and adjacent land-use: Case study of Kien Giang coast, Vietnam*. Ocean & Coastal Management, 2013. **76**: p. 12-22.
- [2] Tran, T., *Combining biodiversity conservation with poverty alleviation - a case study in the Mekong Delta, Vietnam*. Aquatic Ecosystem Health & Management, 2010. **13**(1): p. 41-46.
- [3] Ho, P.H., *Cay co vietnam = An illustrated flora of Vietnam*1991, California: Pham Hoang Ho. v. <1 >.
- [4] Jackson, D.L. and S.W.L. Jacobs, *Australian agricultural botany*1985, Sydney, N.S.W. Beaverton, Or.: Sydney University Press ; International Specialized Book Services. viii, 377 p.

# NUTRIENT TRANSFER AND TRANSFORMATION IN RIPARIAN GROUNDWATER WITH DIFFERENT LAND USE OF A LOWLAND WATERSHED, EASTERN CHINA

Xuyin Yuan<sup>1,2</sup>, Lei Han<sup>1,2</sup>, Huan Wang<sup>2</sup>, Shouquan Wang<sup>2</sup>, Hailong Chen<sup>2</sup>

1. Key Laboratory of Integrated Regulation and Resource Development on Shallow Lakes of Ministry of Education, Hohai University, Nanjing, Jiangsu 210098, China;

2. College of Environment, Hohai University, Nanjing, Jiangsu 210098, China

## ABSTRACT

Riparian zone is a transition zone between terrestrial and aquatic systems, which can influence the water quality through nutrient dynamics. We investigate the changes of nutrients (N, P, C) in riparian zones with different land uses in a lowland watershed of eastern China, and illustrate the effect of land use on the nutrient transfer and transformation in riparian zones. Our results show the forest-dominated riparian land has high TN, moderate TOC and low TP concentrations with narrow variation ranges in space. The agriculture-dominated riparian land has moderate TN and TP, relatively low TOC, with large variations in space. Higher TOC and TP concentrations occur in the urban-influenced riparian land, and significant changes are observed in this area. Hydrologic regimes will significantly affect the nutrient distribution and transfer in riparian zones, which is associated with nutrient sources and soil properties. On the basis of lateral riparian profiles from inland to inshore, we conclude that nitrate and ammonia show low transfer ratios in forest-dominated and agriculture-dominated riparian lands respectively. But a high transfer ratio of TDP is observed in all riparian lands. TOC and DOC have a significant effect on the transformation of N and P species in dry season.

*Key words: Nutrient, Riparian groundwater, Land use, Watershed, China*

## INTRODUCTION

Riparian zone is a transition zone between terrestrial and aquatic systems, which can attenuate pollutants[1]. But riparian soils exhibit different effectiveness on removal of nutrients due to diversities of soil properties and geochemical behavior of nutrients [2]. Nutrients from different sources such as forest, agriculture and urban show varied concentrations and species in spatial and temporal distribution, which induce different extents of removal efficiency[3]. The nutrient characteristics are usually associated with land use and land cover, e.g. agricultural lands contain a high nitrogen concentration and urban sewage has a high phosphorus concentration[4,5]. In addition, the riparian environmental conditions will influence the biogeochemical cycle of nutrients.

Groundwater makes a pivotal role for the transfer and transformation of nutrients in riparian zones. Soil properties will affect the range and extent of nutrient transfer and transformation in groundwater [6]. To the best of our knowledge, an understanding of the linkage between nutrient partitioning and the land use is limited. Previous works of riparian zones take less attention to relationships between land use

and nutrient. The knowledge of interaction between nitrogen, phosphorus and carbon species in riparian groundwater needs expansion, which is important for understanding the contribution of terrestrial nutrients to aquatic systems.

The objectives of this paper are as followings. 1. To realize the spatial and temporal changes of nitrogen, phosphorus and carbon in riparian groundwater, and their relationships with land use in eastern Chinese watershed. 2. Analyzing the transfer and transformation characteristics of nutrients from lands to rivers. 3. To discuss the effect of organic carbon on nitrogen and phosphorus transformation.

## SAMPLING AND ANALYSIS METHODS

Tiaoxi watershed is located in the southwest of Taihu Lake, which covers hilly and plain topography. The mainstream of Tiaoxi River flow through the different lands, where reveals the forest-dominated land in upstream, the agriculture-dominated land in midstream and the urban-dominated land in downstream. Because of significant human activities, the ranges of riparian zones are less than 100m in the whole watershed.

Three profiles of each land type of riparian zone were chosen to study the nutrient characteristics in groundwater. These profiles were vertical with the river bank. Each profile has six sampling sites from 1m to 30m beside bank, and groundwater was collected at depth of 50cm to 100cm based on water table.

All groundwater in riparian zones were analyzed for TN, TP, NO<sub>3</sub>-N, NH<sub>4</sub>-N, dissolved reactive phosphorus (DRP) with colorimetric techniques approved by Ministry of Environmental Protection of China [7]. The groundwater samples were stored in chromic acid washed glass bottles at 4°C for TOC analysis with an Aurora 1030 TOC analyzer (USA). The filtered samples were measured for DOC.

## RESULTS AND DISCUSSIONS

### Nutrient distributions in groundwater of riparian zones with different land uses

Nitrogen, phosphorus and carbon concentrations of groundwater in riparian soils were shown in Table 1. It was evident that nutrients in urban groundwater were higher than those in woodland and cropland groundwater. But groundwater of cropland in summer had higher TOC and NO<sub>3</sub>-N. Compared to nutrients in surface water, nitrogen showed a slight decline, but phosphorus and carbon showed a significant decline. Because phosphorus and carbon mostly existed in the particulate form, and they were absorbed by riparian soils [8,9]. Among inorganic nitrogen, NO<sub>3</sub>-N showed a significant higher concentration in almost sites, indicating nitrate was dominated in groundwater of Tiaoxi River. The proportions of DRP to TP

in groundwater followed the order of urban riparian > cropland riparian > woodland riparian, which implied that changes of phosphorus species were related with land use. DOC concentration accounted for a high proportion of TOC, general more than 50%, decreasing with woodland groundwater > urban groundwater > cropland groundwater.

Nutrients in groundwater showed small seasonal changes in similar land use, although nitrogen, phosphorus and carbon showed a slight increase in winter usually. But the exceptional situation exhibited in a cropland riparian zone, denoting the significant effectiveness of cultivation condition on nutrients. The variations of carbon were larger than nitrogen and phosphorus, especially in an urban riparian area, perhaps originating from multi carbon resources in a same place [10]. Nitrogen and phosphorus species showed a significant seasonal changes which illustrated not only the source diversities, but also biogeochemical process in riparian zone[11,12].

Nutrients from different land use not only influenced the total concentration, but also their species in riparian groundwater. In woodland of lower intense cultivation, nutrients showed the lower concentrations. Changes of cultivation time and intense in cropland lead to large ranges of nutrient inputs in different seasons, particularly for nitrogen and phosphorus species. Urban riparian area usually received continuous sewage discharge form resident living, but nutrient concentration was significantly affected by rain runoff. This is why nutrients in summer are lower than in winter, due to less rain in winter.

Table 1 Nitrogen, phosphorus and carbon concentrations of groundwater in riparian soils around different lands

	Summer			Winter		
	Woodland	Corpland	Urbanland	Woodland	Corpland	Urbanland
TN	1.48 (0.83-2.49)	2.62(1.01-4.97)	3.21(1.38-6.44)	1.91(1.24-3.32)	2.72(1.67-4.90)	3.66(1.69-7.71)
NO <sub>3</sub> <sup>-</sup>	0.74(0.25-1.05)	1.73(0.77-2.70)	1.32(0.87-2.28)	0.61(0.29-0.93)	1.21(0.53-3.47)	2.45(1.15-3.71)
NH <sub>4</sub> <sup>+</sup>	0.04(0.02-0.06)	0.07(0.04-0.11)	0.13(0.06-0.36)	0.06(0.01-0.17)	0.10(0.03-0.24)	0.18(0.02-0.72)
TP	0.10(0.04-0.20)	0.09(0.04-0.13)	0.21(0.06-0.36)	0.07(0.04-0.09)	0.09(0.05-0.17)	0.11(0.06-0.19)
DRP	0.02(0.01-0.03)	0.04(0.01-0.08)	0.04(0.02-0.08)	0.04(0.02-0.06)	0.05(0.02-0.16)	0.07(0.03-0.10)
TOC	0.88(0.29-1.41)	1.87(1.19-2.81)	1.25(0.63-2.58)	1.13(0.68-1.78)	1.17(0.51-1.85)	2.57(1.64-3.54)
DOC	0.66(0.22-1.12)	0.89(0.45-1.63)	0.74(0.25-1.54)	0.78(0.36-1.17)	0.87(0.31-1.61)	1.12(0.44-2.08)

### Nitrogen and phosphorus transfer from land to river in the watershed

In order to compare the transfer characters of nutrients, the sampling sites of same distance from river bank were handled in each profile. The water samples were obtained at 1m, 5m, 10m, 15m, 20m and 30m from river bank. Varied plots of nitrogen, phosphorus and carbon

in riparian groundwater were displayed in Fig. 2. These nutrients showed an elevated trend from nearshore to offshore, where diversities existed for different elements. Nitrogen showed a significant increasing, and phosphorus and carbon showed a slight increasing along the riparian profile. As a whole, a wide range of nutrients appeared in cropland and urban

groundwater. But the concentrations of nutrient were stable in woodland groundwater.

TN in cropland riparian area, TP and TOC in urban riparian area decreased 52.0%-63.6%, 25.6%-31.9% and 13.7%-52.1% respectively at a 30m distance. But TN and TOC in woodland riparian area didn't show a significant variation at the sampling distance. In winter, significant decreasing of TN and TP exhibited in urban riparian area, with ranges of 57.3%-74.2% and 29.6%-37.0%. TOC in cropland riparian area decreased significantly with a range of 19.8%-37.9%. But TP in cropland and woodland had a small increase because fertilization added the phosphorus input in these areas [13].

#### Changes of nutrient species and transformation in riparian groundwater

Nitrogen and phosphorus species showed significant variations in groundwater under different land use. TN and  $\text{NO}_3\text{-N}$  revealed significant fluctuations in cropland area than

other areas in summer, but slight fluctuations in winter. Because soils tended to absorb particulate phosphorus and reduced the P concentrations in groundwater[14-15]. Than values of TN/TP were elevated. Cultivation enhanced the absorption progress of soil in riparian area due to extensive porosity. The proportions of DOC/TOC in cropland area were lower than in woodland and urban areas. This is the same origin that particulate organic carbon is easy to be absorbed by soils [16]. The seasonal variations of nutrients were complicated because of hydrological and environmental conditions. DRP/TP and DOC/TOC values in winter were higher than in summer. The concentrations of TN and  $\text{NO}_3\text{-N}$  increased in urban riparian area, which were associated with less dilution of sewage in winter. But variations of TN/TP and  $\text{NO}_3\text{-N}/\text{NH}_4\text{-N}$  didn't show significant rules in woodland and cropland areas.

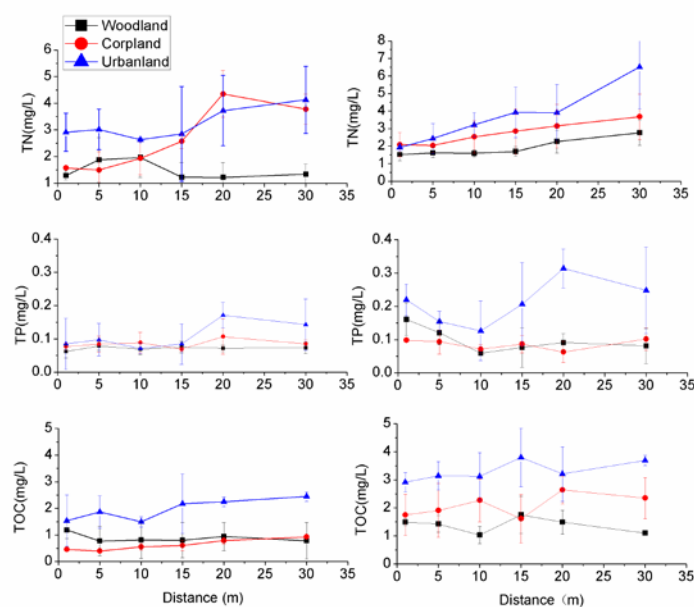


Fig.1 Nutrient changes of groundwater in riparian zones of different distances from river bank (Groundwater in summer shown in left, groundwater in winter shown in right)

Table 2 Nutrient ratios of riparian groundwater in different lands

	Summer			Winter		
	Woodland	Cropland	Urbanland	Woodland	Cropland	Urbanland
TN/TP	19.36(6.02-44.94)	35.11(8.44-92.68)	17.21(5.05-41.20)	28.11(14.25-58.19)	32.82(16.99-61.17)	33.42(11.84-86.25)
$\text{NO}_3\text{-N}/\text{NH}_4\text{-N}$	21.37(4.77-37.54)	26.14(12.23-35.08)	11.73(5.59-17.35)	19.93(3.75-94.74)	17.75(3.27-68.62)	22.18(3.28-69.34)
DRP/TP	0.26(0.14-0.53)	0.43(0.13-0.88)	0.23(0.07-0.64)	0.51(0.26-0.86)	0.62(0.42-1.32)	0.62(0.30-0.86)
DOC/TOC	0.76(0.66-0.84)	0.47(0.32-0.73)	0.60(0.39-0.91)	0.82(0.67-0.94)	0.58(0.32-0.85)	0.78(0.63-0.93)

Organic matter can influence nitrification and denitrification process of groundwater, and alter



the relative ratio of nitrate and ammonia [17]. By contrast, phosphorus is significantly affected by soil compositions like Fe and Al, and less affected by organic matter[18]. As shown in Fig.2, the correlations of TOC with  $\text{NO}_3\text{-N}/\text{NH}_4\text{-N}$  were better than with  $\text{DRP}/\text{TP}$ ,

and better correlations were shown in winter than in summer. These situations can be interpreted as the stable concentrations of nutrients in winter. Besides, the microorganism growth weakens in winter, reducing variation of nutrients, in particular for nitrogen.

### CONCLUSIONS

Nutrients of riparian groundwater of Tiaoxi watershed are significantly influenced by land use and land cover. Nitrogen and phosphorus show higher concentrations in groundwater of urban area than in woodland and cropland areas, but higher carbon concentrations are distributed in cropland area.  $\text{NO}_3\text{-N}$  and DOC are dominated species in riparian groundwater for nitrogen and carbon, but  $\text{DRP}$  in not for

phosphorus. Hydrological conditions also affect variations of nutrients in groundwater, which show the higher nutrient concentrations and better correlations in winter. The effects of organic carbon on nitrogen and phosphorus are also better in winter. Variations of nutrients in cropland area are significantly higher than in woodland and urban areas, manifesting effect of cultivation on riparian groundwater.

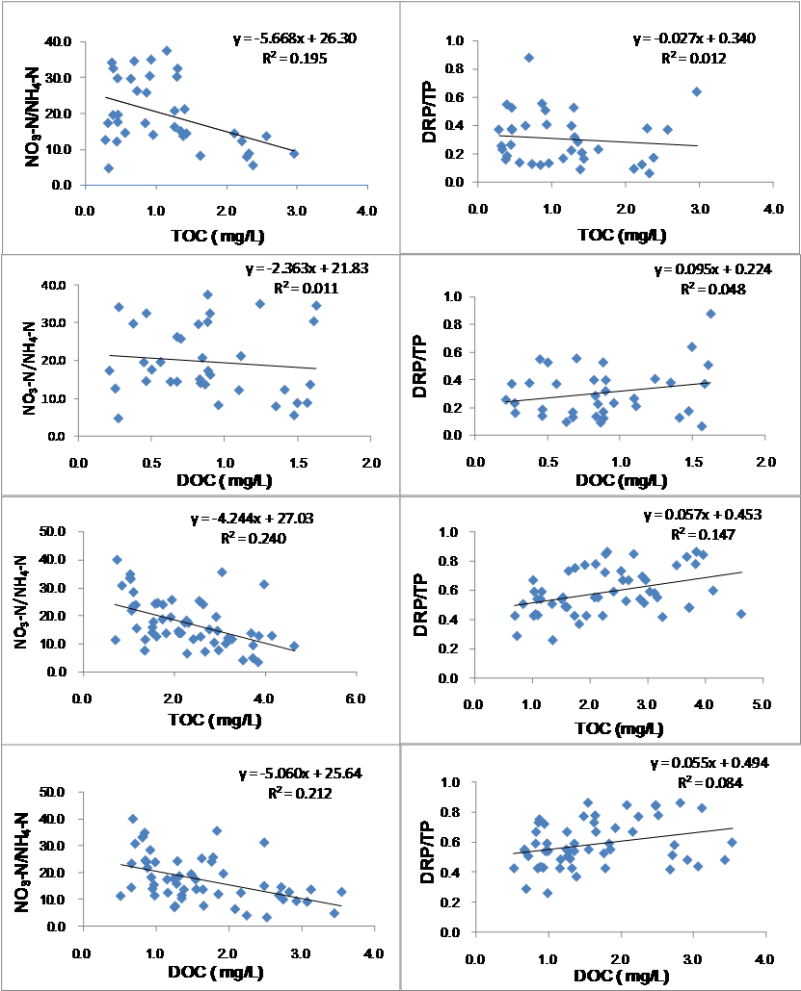


Fig.2 Correlations of TOC and DOC with  $\text{NO}_3\text{-N}/\text{NH}_4\text{-N}$  and  $\text{DRP}/\text{TP}$  in riparian groundwater. The upper four plots represent summer situations and the lower four plots represent winter situations.

### ACKNOWLEDGEMENTS

This study was financially supported by the International Technology Cooperation and

Exchange Fund from Ministry of Science and Technology of China (No.0102012DFA60830) and the Natural Science Foundation of China (No.41372354). Binwu Liu and Xiaoyong Luo are appreciated for their help in field work.

## REFERENCES

- [1] Mayer PM, Reynolds SK, McCutchen MD, Canfield TJ, "Meta-Analysis of Nitrogen Removal in Riparian Buffers", *Journal of Environmental Quality*, 2007, 36, pp.1172-1180.
- [2] Hill AR, Vidon PGF, Langat J, "Denitrification Potential in Relation to Lithology in Five Headwater Riparian Zones", *Journal of Environmental Quality*, 2004, 33, pp. 911-919.
- [3] Vidon PGF, Hill AR, "Landscape controls on nitrate removal in stream riparian zones", *Water Resour. Res.*, 2004, 40, W03201.
- [4] Carpenter SR, Caraco NF, Correll DL, Howarth RW, Sharpley AN, Smith VH, "Nonpoint pollution of surface waters with phosphorus and nitrogen." *Ecological applications*, 1998, 8, pp559-568.
- [5] Chen LD, Peng HJ, Fu B, "Seasonal variation of nitrogen-concentration in the surface water and its relationship with land use in a catchment of northern China." *Journal of Environmental Sciences*, 2005, 17, pp. 224-231.
- [6] Vidon PC, Allan C, Burns D, "Hot spots and hot moments in riparian zones: Potential for improved water quality management1." *JAWRA Journal of the American Water Resources Association*, 2010, 46, pp. 278-298.
- [7] China Ministry of Environmental Protection, *Monitoring and analysis methods of water and wastewater*. Beijing, Chinese Environmental Sciences Press, 2002, ch.3.
- [8] Schenk MK, Barber SA, "Phosphate uptake by corn as affected by soil characteristics and root morphology", *Soil Sci.Soc. Am. J.*, 1979, 43, pp 880-883.
- [9] Cronan CS, Piampiano JT, Patterson HH, "Influence of land use and hydrology on exports of carbon and nitrogen in a Maine river basin", *J. Environ. Qual.*, 1999, 28, pp. 953-961.
- [10] Meyer J, Paul M, Taulbee K, "Stream ecosystem function in urbanising landscapes", *Journal of the North American Benthological Society*, 2005, 24, pp. 602-612.
- [11] Neill C, Deegan LA, Thomas SM, Cerri C, "Deforestation for pasture alters nitrogen and phosphorus in small Amazonian streams", *Ecological Applications*, 2001, 11, pp. 1817-1828.
- [12] Saunders TJ, McClain ME, Llerena CA, "The biogeochemistry of dissolved nitrogen, phosphorus, and organic carbon along terrestrial-aquatic flowpaths of a montane headwater catchment in the Peruvian Amazon", *Hydrological Processes*, 2006, 20, pp. 2549-2562.
- [13] Kronvang B, Bechmann M, Lundekvam H, Behrendt H, Rubæk GH, Schoumans OF, Syversen N, Andersen HE, Hoffmann CC, "Phosphorus Losses from Agricultural Areas in River Basins: Effects and Uncertainties of Targeted Mitigation Measures", *Journal of Environmental Quality*, 2005, 34, pp. 2129-2144.
- [14] Aye TM, Nguyen ML, Bolan NS, Hedley MJ, "Phosphorus in soils of riparian and non-riparian wetland Zealand", *N. Z. J. Agric. Res.*, 2006, 49, pp. 349-358.
- [15] Hoffmann CC, Kjaergaard C, Uusi-Kämppe J, Hansen HCB, Kronvang B, "Phosphorus retention in riparian buffers: Review of their efficiency", *J. Environ. Qual.*, 2009, 38, pp. 1942-1955.
- [16] Billett MF, Deacon CM, Palmer SM, Dawson JJC, Hope D, "Connecting organic carbon in stream water and soils in a peatland catchment", *Journal of Geophysical Research*, 2006, 111, pp. 1-13.
- [17] Wigington PJ, Griffith SM, Field JA, Baham JE, Horwath WR, Owen J, Davis JH, Rain SC, Steiner JJ, "Nitrate removal effectiveness of a riparian buffer along a small agricultural stream in western Oregon", *J. Environ. Qual.*, 2003, 32, pp. 162-170.
- [18] Burger B, Reich P, Cavagnaro TR, "Trajectories of change: riparian vegetation and soil conditions following livestock removal and replanting", *Aust. Ecol.*, 2010, 35, pp. 980-987.

## HEAVY METAL DESORPTION STUDIES ON THE ARTIFICIALLY CONTAMINATED AL-QATIF SOIL

Arif Ali Baig Moghal<sup>1</sup>, Mosleh Ali Al-Shamrani<sup>2</sup> and Waleed M Zahid<sup>3</sup>

<sup>1</sup>Assistant Professor; <sup>2</sup> Professor; <sup>3</sup> Associate Professor, Department of Civil Engineering, College of Engineering, King Saud University, Riyadh

### ABSTRACT

In this study, the relevance of mineralogy on the desorption capacities of  $\text{Cu}^{+2}$  and  $\text{Pb}^{+2}$  from artificially contaminated Al-Qatif soil has been investigated. The desorption capacities of both  $\text{Cu}^{+2}$  and  $\text{Pb}^{+2}$  using ethylenediaminetetraacetate (EDTA) as decontaminating solution are determined. The effect of decontaminating solution dosage and liquid to solid ratio on desorption capacities are examined. Under identical conditions, the removal efficiency of  $\text{Pb}^{+2}$  ions are found to higher than  $\text{Cu}^{+2}$  ions. This has been attributed mainly due to the differences in surface charges of specific retention sites which hold these metal ions. Further, the heavy metal ion solubility and surface properties of respective clay minerals decide the desorption rate in soil systems as the pore fluid pH reaches the heavy metal solubility range or point of zero charge of the clay minerals. These studies provide valuable insight with regards to their applicability as potential barrier materials for containing industrial leachates.

*Keywords: Copper, Decontaminant, Desorption, EDTA, Lead, Mineralogy, Surface area.*

### INTRODUCTION

Soil is a basic building block for the most terrestrial ecosystems and a complex heterogeneous medium consisting of both solid and fluid phases. The ability of these soils in absorbing and desorbing metal ions from the aqueous phase assumes importance since it governs both the environmental and agricultural issues [1]. The clay fraction predominantly affects the metal ion concentrations in environmental systems owing to their ability in adsorbing these ions and further in releasing the same in part or whole when subjected to prevailing atmospheric conditions [2].

For ex situ systems, the contaminants are generally adsorbed on to the fine grained soil fraction and extraction of heavy metal ion complexes has been confirmed by the use of various chelating agents like citric acid, diethylenetriaminepentaacetic acid (DTPA), sodium ethylenediaminetetraacetate (EDTA), sodium nitrilotriacetate (NTA) and strong acid such as hydrochloric acid (HCl), nitric acid ( $\text{HNO}_3$ ) have been used to desorb metals from soils [3-6].

But, most of these research studies did not emphasize on the effect of clay mineralogy or the effect of  $\text{H}^+$  ions on the desorption response. Based on the solubility of heavy metals and the surface properties of clay minerals, desorption of heavy metal ions in soil systems occurs as the pH of the pore fluid in the soil reaches the solubility range of the heavy metal or is lowered to the point of zero charge of the clay minerals [6]. The amount of  $\text{H}^+$  ions available in the pore fluid and the nature of clay minerals are

considered important factors in desorption processes and need to be evaluated.

Two common types of heavy metal contaminants, copper and lead are considered in the study. Pollution of soil and water by copper may arise from copper mining and smelting and other industrial uses. Also, acute concentration of copper in solutions leads to Cirrhosis of the liver in children. On the other hand, lead is a non-essential element and it is not as bioavailable as other metals. It is a poisonous metal and its intake can damage nervous connections (especially in young children) causing blood and brain disorders. Long-term exposure to lead or its salts can cause nephropathy, and colic-like abdominal pains. Hence, in the present study, soil washing methodology has been employed to reduce the toxicity of  $\text{Cu}^{+2}$  and  $\text{Pb}^{+2}$ , by using a chelant in the form of EDTA, since chelating extraction of heavy metals has been proposed as an effective remediation technique for contaminated soils. The effect of liquid-solid ratio in enhancing the extractability has also been studied. The studies will enable to estimate the fraction of metal ion available for achieving selective recovery of  $\text{Cu}^{+2}$  and  $\text{Pb}^{+2}$  individually from the contaminated soil systems.

### MATERIALS

The tests were conducted on samples collected from Al-Qatif, a coastal oasis region located on the western shore of the Persian Gulf in the Eastern Province of Saudi Arabia (26° 56' 0" N, 50° 1' 0" E). The sampling was carried out at a depth of 3.0 m. The

physical properties and chemical composition are reported in Tables 1 and 2 respectively.

## METHODOLOGY

Particle size analysis based on laser diffraction as per ASTM B822 - 02 [7] was carried out on the selected soil sample. Laser diffraction relies on the fact that particles passing through a laser beam will scatter light at an angle that is directly related to their size. As particle size decreases, the observed scattering angle increases logarithmically. Larger particles therefore scatter light at narrow angles with high intensity whereas smaller particles scatter light at wider angles but with low intensity. From Figure 1, it can be seen that major portion of the selected soil has a gradation ranging from 0.1 to 10  $\mu\text{m}$ . This finer fraction is critical to the study as it affects desorption of  $\text{Cu}^{+2}$  and  $\text{Pb}^{+2}$  quite considerably.

The predominant minerals were determined by carrying out XRD using Bruker D8 Advance system. Samples were scanned from  $2^\circ$  to  $60^\circ$  ( $2\theta$ ) using 2.2kW Cu anode long fine focus ceramic X-ray tube at a scanning rate of 1 degree per minute. XRD patterns of samples were then compared with standard patterns [8]. Fig. 2 depicts comprehensive X Ray diffraction analysis. In addition to Quartz, Dolomite, Illite, Muscovite, and Palygorskite, the presence of Montmorillonite (a smectite group mineral known to induce significant swelling upon interaction with water) is noteworthy.

Table 1 Physical properties of the soil

Physical Property	Al - Qatif
Liquid Limit (%)	137
Plastic Limit (%)	60
Shrinkage Limit (%)	22
Plasticity Index (%)	77
Linear Shrinkage (%)	77
% Finer than 200 $\mu\text{m}$	99.1
USCS Classification	CH
Specific Gravity	2.71

Note: 'USCS' refers to unified soil classification System; 'CH' refers to clay with high plasticity

Table 2 Chemical composition of the soil

Chemical Composition	Al - Qatif (%)
$\text{K}^+$	1.8
$\text{K}_2\text{O}$	2.2
Al	3.3
$\text{Al}_2\text{O}_3$	6.3
Si	8.1
$\text{SiO}_2$	17.3
$\text{Ca}^{+2}$	0.7
CaO	0.9
CEC (cmol/kg)	137

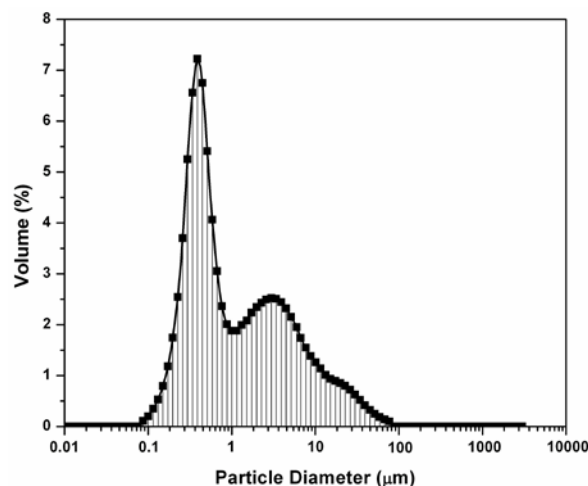


Fig.1 Particle Size Distribution Curve by Laser Diffraction Analysis

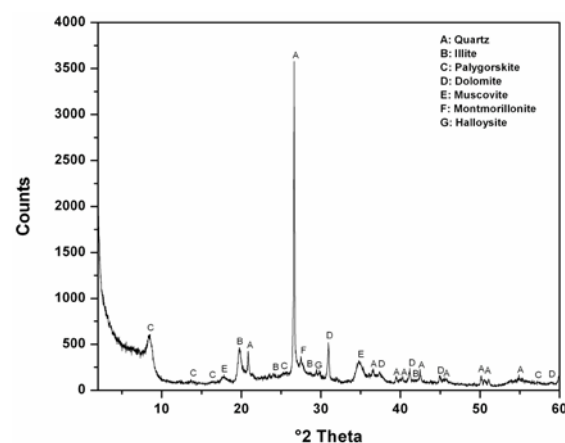


Fig. 2 X - Ray Diffraction Analysis

## Contamination Procedure

About 0.5 kg of oven dried soil was thoroughly mixed with deionized double distilled water in a 1:1 ratio, containing dissolved nitrate salts of copper nitrate,  $\text{Cu}(\text{NO}_3)_2$  and lead nitrate,  $\text{Pb}(\text{NO}_3)_2$  separately. The entire slurry was allowed to age at controlled temperature ( $23 \pm 0.5^\circ\text{C}$ ) for a period of 2 months. The slurry was mixed frequently during the course of aging period. At the end of aging period, the mixture was oven dried and acid digestion technique using US EPA Method 3050B [9] was employed on the respective samples below the boiling point to determine the  $\text{Cu}^{+2}$  and  $\text{Pb}^{+2}$  concentrations. Table 3 gives the metal concentrations of the selected metal ions before and after contamination.

## Desorption Batch Tests

Batch desorption experiments were carried out by mechanically shaking series of bottles containing the artificially contaminated soil samples at different

initial conditions. EDTA was used as a decontamination solution. The tests were carried out by placing 1g of soil in 100 ml teflon bottles followed by addition of varying volumes (10 mL, 20 mL, 40 mL and 50 mL) of the washing solution ( $\text{HNO}_3$ ). In order to determine the effect of concentration of decontaminating solution on the extractability of respective metal ion, the concentration of EDTA was varied as 0.1 M, 0.2M and 0.5M for each dilution ratio case. The samples were placed on a shaker table operated at 175 rpm at room temperature.

Table 3 Concentration of the metal ions

<i>Background concentration of the original uncontaminated soil</i>	
$\text{Cu}^{+2}$	13±0.5 mg/kg
$\text{Pb}^{+2}$	15±0.5 mg/kg
<i>Metal concentration of the contaminated soil</i>	
$\text{Cu}^{+2}$	833±2 mg/kg
$\text{Pb}^{+2}$	758±2 mg/kg

A 2-h reaction time was deemed sufficient based upon batch rate desorption tests conducted over a 48-h period. After mixing, the samples were allowed to settle for about 15 min and then filtered through a 0.45- $\mu\text{m}$  membrane filter. The accuracy was established by preparing replicate of three aliquots for each test. In the present study, it has been assumed that the metal concentration of the filtrate represents that released from the contaminated soil. Removal efficiencies were determined by dividing the heavy metal release quantities by the initial quantity in the soil. The residual concentration of the heavy metal ions ( $\text{Cu}^{+2}$  and  $\text{Pb}^{+2}$ ) in the filtered solution was determined using atomic absorption spectrophotometry (AAS). AAS calibrations were prepared from standard stock solutions.

## RESULTS AND DISCUSSIONS

Generally, when metal-containing compounds are dissolved in water, the metallic component exists as mobile ions in solution phase. But when these metallic ions are complexed by inorganic or organic ligands, they will be present in aqueous solution only at very low concentrations in the pH range of natural surface and subsurface waters. When the concentrations of these metals exceed the solubility of their corresponding hydroxide or carbonate phase at a given pH value, metal precipitates will intermingle and become an integral part of the soil matrix which is of prime concern [10]. The removal efficiencies of  $\text{Cu}^{+2}$  and  $\text{Pb}^{+2}$  using deionized double distilled water and EDTA solution from artificially contaminated soil are summarized in Table 4.

Table 4 Effect of chelant (EDTA) concentration and liquid to solid (L/S) ratio on the removal efficiencies of  $\text{Cu}^{+2}$  and  $\text{Pb}^{+2}$ 

Washing Solution	Removal efficiency (%)			
	DI Water	0.1M	0.2M	0.5M
<b>L/S Ratio 1:10</b>				
$\text{Cu}^{+2}$	19.1±0.5	55.3±0.5	68.7±0.5	81.2±0.5
$\text{Pb}^{+2}$	16.8±0.5	48.7±0.8	71.2±1.1	89±1.3
<b>L/S Ratio 1:20</b>				
$\text{Cu}^{+2}$	17.3±0.5	61.2±0.5	78.6±0.8	84.5±0.5
$\text{Pb}^{+2}$	15.7±0.5	58.6±0.7	81.3±0.5	90.6±1.2
<b>L/S Ratio 1:40</b>				
$\text{Cu}^{+2}$	15.6±1.7	76.5±1.6	85.3±1.3	91.1±0.9
$\text{Pb}^{+2}$	18.6±0.5	69.7±0.5	89.1±0.5	93.7±0.5
<b>L/S Ratio 1:50</b>				
$\text{Cu}^{+2}$	18.2±0.5	80.1±0.7	86.7±0.7	94.3±1.1
$\text{Pb}^{+2}$	14.8±0.5	77.6±0.7	91.1±0.5	96.2±0.7

The implication of using DI water is to arrive at the fraction of the metal that is weakly bound to the soil particles and is readily available for mobilization. It can be seen from Table 3 that, the fraction of  $\text{Cu}^{+2}$  and  $\text{Pb}^{+2}$  metal ions are strongly bound and is virtually independent of the soil to DI water ratio. Hence, the removal efficiencies are quite low and it is evident that, the remaining fractions of the metals are considered to be strongly bound and immobilized within the soil matrix under natural-water conditions. Also, with DI water, the resulting removal efficiency is due to rapid dissolution of weakly bound  $\text{Cu}^{+2}$  and  $\text{Pb}^{+2}$  ions retained at easily co-ordinated sites on the outer surfaces of clay matrix. Similar observations have been made by Abumaizar and Smith [11] when DI water was used to decontaminate Cd, Pb, Zn and Cr metal ions. Generally, in contaminated soils the total amount of metal ion concentration in the aqueous and solid phases is at levels much higher than those found in the solution phase. The solubility values of the metal ions are typically very small and it will not yield satisfactory removal efficiencies. Further, the respective metal ion solubility values are heavily dependent on predominant mineral phases that which are affected by pH and available ambient ligands.

The effect of 0.1M EDTA on the extractability of metal ions (Table 3) indicates that, there is a significant improvement in both  $\text{Cu}^{+2}$  and  $\text{Pb}^{+2}$  removal over flushing with DI water. The best removal efficiency for both the metal ions was obtained at a 1:50 soil to liquid ratio. Since, copper may be present in solution as either  $\text{Cu}^{2+}$  or  $\text{Cu}^{+}$ , although the more oxidized  $\text{Cu}^{2+}$  predominates due to the redox reaction in aerated water. Both copper and lead ions are prone to complexation, especially with hydroxide and carbonate ligands. The ideal mineral phases for metal complexation include those of oxide, hydroxide, carbonate and hydroxy carbonate, such as

$\text{MO}(\text{S})$ ,  $\text{M}(\text{OH})_2(\text{S})$ ,  $\text{MCO}_3(\text{S})$  and  $\text{M}_x(\text{OH})_y(\text{CO}_3)_z$  [12].

The presence of montmorillonite in Al-Qatif clay has been confirmed by Fig. 2 and the uptake of  $\text{Cu}^{+2}$  and  $\text{Pb}^{+2}$  metal ions is considered to occur primarily by ion exchange process on to this mineral site. The calcium sites in Al-Qatif clay (Table 2) have the ability to successfully displace a high proportion of the metal ions retained on the clay sites at higher molar concentrations of EDTA, thereby resulting in higher removal efficiencies for both the metal ions. But, at lower molar concentrations of EDTA, the calcium ions have limited ability to dissolve precipitated hydrous oxides of  $\text{Cu}^{+2}$  and  $\text{Pb}^{+2}$  and hence relatively smaller amounts are desorbed in the extracting solution. Also, with increase in EDTA concentration, competition from hydronium ions for the available oxide surfaces starts diminishing which also results in the increased removal capacities. Hence, relatively higher amounts of  $\text{Cu}^{+2}$  and  $\text{Pb}^{+2}$  are flushed out into the washing liquid.

The difference in removal efficiencies between the metal ions may be due to the differences in surface charges of specific retention sites like dolomite, illite, muscovite, and palygorskite (as seen from Fig. 2) which hold these metal ions and also due to the particle size distribution (the selected soil has a gradation ranging from 0.1 to 10  $\mu\text{m}$  as noted from Fig.1). The surface properties of carbonate and Fe-Mn oxide sites in Al-Qatif clay dictate the release of  $\text{Cu}^{+2}$  and  $\text{Pb}^{+2}$  as the pore fluid pH reaches the their solubility range or point of zero charge of the oxide sites, particularly at higher EDTA concentrations of 0.2M and 0.5M. From the batch chelant desorption tests, EDTA was extremely effective in decontaminating  $\text{Cu}^{+2}$  and  $\text{Pb}^{+2}$  from the artificially contaminated Al-Qatif soil. The removal efficiencies achieved were satisfactory and contaminated industrial repositories can be successfully treated with this technique.

## PRACTICAL IMPORTANCE OF THE STUDY

Heavy metal contaminated site is among the most common problem constraining cleanups and associated costs at industrial waste repositories in the Kingdom of Saudi Arabia. A typical soil washing technique involves, vigorous washing of the soil with water containing little amount of surfactants followed by solid/liquid separation for collecting the clay/silt fraction. This clay/silt fraction usually is treated by immobilization techniques and disposed off in a landfill while the bulk of the decontaminated soil is returned back to the site. But, in soils where heavy metals are present in higher concentrations soil washing alone would not suffice and chelants are required to reduce the toxicity to target levels. The current study addresses these issues and gives valuable insight in selecting appropriate extractant

(EDTA, in this case) for Al-Qatif soil in removing  $\text{Cu}^{+2}$  and  $\text{Pb}^{+2}$  metal ions. Depending on the target clean up level for respective metal ion, the feasibility of soil washing with EDTA may be readily determined using the data in Table 4 as a supporting guide. The employed technique is relatively cost competitive and extremely effective compared to existing methodologies.

## CONCLUSIONS

The decontamination of metal contaminated soils is primarily controlled by the dissolution of the metal-mineral bond followed by the dispersion of the target metal ion in the selected extractant or into an easily extractable or residual form. The results of batch washing tests indicate that  $\text{Cu}^{+2}$  and  $\text{Pb}^{+2}$  metal ions can be extracted from artificially contaminated soils independently using EDTA as a chelating agent. The use of DI water as a washing solution resulted in a lesser removal efficiency of  $\approx 17 - 20\%$ , for  $\text{Cu}^{+2}$  and  $\text{Pb}^{+2}$  metal ions, which confirms that these metal ions are strongly bound and are not readily mobilized in aqueous solutions. The effect of 0.1M EDTA on the extractability of metal ions indicates that, there is a significant improvement in both  $\text{Cu}^{+2}$  and  $\text{Pb}^{+2}$  removal over flushing with DI water. There was a threefold increase in removal efficiency with 0.1M EDTA compared to DI water alone. With increase in concentration of EDTA solution, relatively higher removal efficiencies of  $\approx 90 - 95\%$  were achieved. The mobility of  $\text{Pb}^{+2}$  ions was slightly higher than  $\text{Cu}^{+2}$  ions. The increase in liquid/solid ratio also aids in better removal efficiencies.

## ACKNOWLEDGEMENTS

This paper is a part of a research project that was supported by NSTIP strategic technologies programs, 12ENV2583-02 in the Kingdom of Saudi Arabia. The authors would like to thank the Eng. Abdulla Bugshan Research Chair for Expansive Soils and Prince Khalid Bin Sultan Chair for Water Research for providing the necessary facilities to carry out the experimental work.

## REFERENCES

- [1] Bradl HB, "Adsorption of heavy metal ions on soils and soils constituents", J. of Colloid and Interface Science, Vol. 277, Sep. 2004, pp. 1-18.
- [2] Farrah H and Pickering WF, "Extraction of heavy metal ions sorbed on clays", Water, Air, and Soil Pollution, Vol. 9, 1978, pp. 491-498.
- [3] O'Shaughnessy JC, D'Andrea RC, Canniff MR, St. Germain S, Venkataramanappa S, and Jacaulay MJ, "Evaluation of in situ soil flushing techniques for heavy metals removal from contaminated soils", *In the Proc. of the 48<sup>th</sup>*



- Purdue Industrial Waste Conference*. Lewis Publishers, Chelsea, Mich., 1993, pp.123–139.
- [4] Hong A, and Chen TC, “Chelating extraction and recovery cadmium from soil using pyridine-2,6-dicarboxylic acid”, *Water, Air, and Soil Pollution*, Vol. 86, 1996, pp. 335–346.
  - [5] Steele MC, and Pichtel J, “Ex-situ remediation of a metalcontaminated superfund soil using selective extractants”, *J. of Environmental Engineering, ASCE*, Vol. 12, No.7, July. 1998, pp. 639–645.
  - [6] Li LY, and Li RS, “The role of clay minerals and the effect of  $H^+$  ions on removal of heavy metal ( $Pb^{2+}$ ) from contaminated soils”, *Canadian Geotechnical J.*, Vol. 37, No. 2, Apr. 2000, pp. 296–307.
  - [7] ASTM B822 – 02, Standard Test Method for Particle Size Distribution of Metal Powders and Related Compounds by Light Scattering, 2002, West Conshohocken, PA.
  - [8] JCPDS, “Joint Committee for Powder Diffraction Studies: International Centre for Diffraction Data (ICDD)”, The Powder Diffraction File, 1999, Newtown Square, PA.
  - [9] USEPA, “Tests methods for evaluating solid waste, Physical Chemical Methods”, SW-846, Method 3050B, 1996, US Environmental Protection Agency, Washington, DC.
  - [10] Chen T, Macauley E, and Hong A, “Selection and test of effective chelators for removal of heavy metals from contaminated soils”, *Canadian J. of Civil Engineering*, Vol. 22, No. 6, Dec. 1995, pp. 1185–1197.
  - [11] Abumaizar RJ, and Smith EH, “Heavy metal contaminants removal by soil washing”, *J. of Hazardous Materials*, Vol. 70, Dec. 1999, pp. 71–86.
  - [12] Peters RW, “Chelant extraction of heavy metals from contaminated soils”, *J. of Hazardous Materials*, Vol. 66, Apr. 1999, pp. 151–210.

# **RECURRENCE INTERVALS OF METEOROLOGICAL DROUGHT EVENTS ACROSS EASTERN AUSTRALIA – IMPLICATIONS FOR DISTURBED LANDSCAPES**

Devanmini Halwatura<sup>1</sup>, Alex M. Lechner<sup>1,2</sup> and Sven Arnold<sup>1</sup>

<sup>1</sup>Centre for Mined Land Rehabilitation, Sustainable Mineral Institute, The University of Queensland, Australia. <sup>2</sup>Centre for Environment, The University of Tasmania, Hobart, Australia

## **ABSTRACT**

Droughts are one of the most devastating natural hazards, often causing severe economic and environmental damage. Across Eastern Australia climate is highly variable and frequent floods and droughts affect large areas over prolonged periods of time. Understanding the variations and trends in these weather extremes is critical for ecologists to assess the adequacy of management plans for anthropogenically affected landscapes such as agricultural or post-mining land, where water often plays a critical role for ecosystem persistence.

This study focuses on analysing drought events of four selected locations (Cairns, Melbourne, Wagga Wagga, Quilpie) across Eastern Australia using the Reconnaissance Drought Index (RDI). We used monthly total rainfall and evaporation data of the past 40 years (1972-2013) to identify drought events. We categorised the drought events according to their severity and duration and analysed separately the historic time series as two parts of 20 years (1972-1992 and 1993-2013). We calculated the recurrence intervals of droughts to assess trends in the occurrence of drought events. Results show that the recurrence intervals of Melbourne and Quilpie barely changed over time, while the drought recurrence intervals decreased in Wagga Wagga and Cairns. These findings have critical implications for any rehabilitation and management plans for post-mining and agricultural land.

*Keywords: Drought, Reconnaissance Drought Index, Recurrence intervals, Land rehabilitation*

## **INTRODUCTION**

Human alteration from mining, urbanisation and industrial development can degrade lands, significantly impacting the natural environment [1]. Re-establishment of these lands has become a priority in this century. In recent years ecologists have focused more on global climate change [2] in average conditions such as mean temperature and rainfall. However, weather events such as intense storms, changes in El Niño and La Niña cycles, coastal flooding, extreme temperatures and droughts [4, 5] have intensified in the last decades and are the barriers for successful rehabilitation practices [5].

Droughts are one of the most harmful climatic events and often have significant impacts on environment and socio-economic assets all over the world, including Australia [6]. In proportion to its area, Australia has a very low percentage of runoff to rainfall. This, together with moisture deficits that occur for decades, makes Australia a very dry place [7]. Eastern Australia, in particular, has highly variable and frequent droughts that affect large areas over prolonged periods of time.

Eastern Australia comprises a broad range of agro-climatic environments which support globally significant biodiversity and holds vast mineral and

energy resources [8]. These environments include a number of abandoned and ongoing mines. There are over 34,000 recorded abandoned mines in the eastern states of Australia (New South Wales, Queensland, and Victoria) that potentially need restoration owing to the legislative requirement for maintaining a sustainable mining industry in Australia [9]. The quantification of severity, duration, and frequency of drought events is crucial for planning for successful regeneration of these post-mined lands.

Drought analyses vary according to their purpose. Meteorological droughts are the most frequently studied type of drought, and standardized drought indices, such as the Reconnaissance Drought Index (RDI), provide the foundation for quantifying the duration, severity, and eventually the frequency or recurrence of meteorological drought events [10]. Drought severity, duration and frequency of occurrence are some of the key drivers of ecosystem rehabilitation because water availability is the primary abiotic factor for ecosystem rehabilitation in semi-arid climates [8].

The objective of this study was to quantify the severity and duration of drought events at four selected locations in Eastern Australia based on the RDI. Two historic time series of rainfall and

evaporation data for the past 40 years (1972-1992 and 1993-2013) were used to estimate the recurrence intervals of droughts for each of these sites in order to investigate climatic trends. We conclude by discussing the potential use of the method outlined in this paper as a management and risk assessment tool for rehabilitation of disturbed landscapes.

## METHODOLOGY

We selected four sites across Eastern Australia (Cairns, Melbourne, Wagga Wagga, Quilpie) (Figure 1) across different agro-climatic classes [11] and agricultural environments [12] (Table 1). For these sites rainfall and potential evaporation (PET) data was most comprehensive, i.e. longest (40 years) and most complete [13]. For a detailed description of the methodology described in this paper refer to [8].

Table 1. Climate indices and climatic classifications of selected locations across Eastern Australia.

Location and climate classification[14]	R/PET [15]	R <sub>w</sub> /R <sub>s</sub> <sup>a</sup>	
		1972-1992	1993-2013
Cairns (Tropical)	0.91	0.12	0.11
Melbourne (Temperate)	0.51	1.20	1.11
Wagga Wagga (Temperate)	0.30	1.75	1.23
Quilpie (Temperate)	0.14	0.73	0.51

<sup>a</sup> Based on average of three months of rainfall during the winter (June-August) and summer (December-February)

We estimated drought severity and duration using RDI at a 3-monthly time scale [16] based on monthly rainfall and PET. The standardized RDI<sub>st</sub> is given as:

$$RDI_{st}(k) = \frac{y_k - \bar{y}_k}{\hat{\sigma}_k} \quad (1a)$$

with

$$y_k = \ln \frac{\sum_{j=1}^{j=k} P_j}{\sum_{j=1}^{j=k} PET_j} \quad (1b)$$

where  $\hat{\sigma}$  is the standard deviation,  $y_k$  is the month  $k$  during the year,  $\bar{y}_k$  is arithmetic mean of  $y_k$ , and  $\hat{\sigma}_k$  is the standard deviation of  $k$ ,  $P_j$  and  $PET_j$  are precipitation and potential evapotranspiration for the  $j^{\text{th}}$  month of the hydrological year [10].

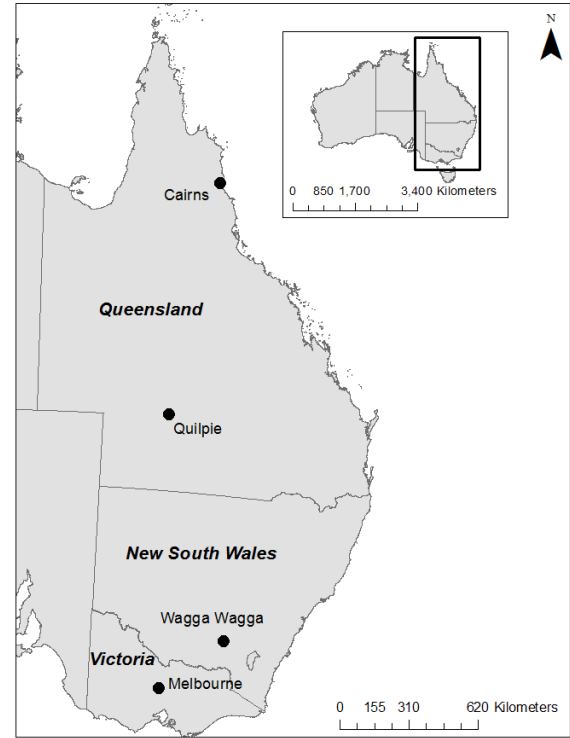


Figure 1. Selected locations of interest in Eastern Australia.

We categorized the drought events according to their severity and duration and split the historic time series into two parts of 20 years (1972-1992 and 1993-2013). Drought severity refers to the extent to which precipitation is below a threshold, whereas the drought duration is the period of rainfall deficit, preceded and followed by periods with no deficit [17]. Drought severity and duration were fitted to a gamma and logistic distribution, respectively [8]. We used the Frank copula to form a multivariate distribution of the fitted distributions of severity and duration. The copula parameter was then estimated according to the Inference Function for Margins (IFM) [8]. Recurrence intervals of drought events exceeding specific values of severity *or* duration (indicated by the logical operator “v”) were calculated as:

$$T_{RDI}^v = \frac{1}{P(S \geq s \vee D \geq d)} = \frac{1}{1 - C[F_S(s), F_D(d)]}. \quad (2)$$

## RESULTS

The recurrence intervals depicted in figure 2 describe site-specific rainfall patterns. In arid Quilpie the recurrence interval for droughts with a severity of 13 or duration of 17 months is one in 50 years, whereas in tropical Cairns the recurrence interval for the same drought is one in 100 years (1972-1992) or one in 1000 years (1993-2013). Temperate Wagga Wagga has a similar pattern of

prolonged and severe droughts as arid Quilpie (1972-1992) (Figure 2) with a recurrence interval of one in 50 years for a drought of severity 12 or duration of 18 months.

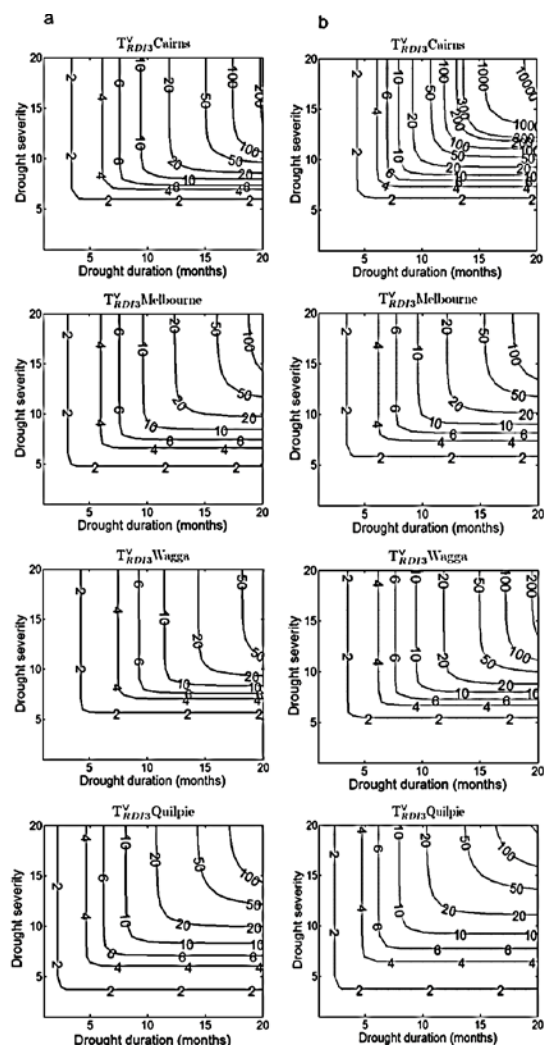


Figure 2. Recurrence intervals of drought events of any severity or duration of interest based on historic rainfall data for: (a) 1972-1992 and (b) 1993-2013.

For Quilpie and Melbourne there was very little difference in the frequency of drought events between the two 20-years time series (1972-1992 and 1993-2013), whereas for Cairns and Wagga Wagga the frequency of severe and prolonged droughts decreased over time (Figure 2). For all locations, except for Wagga Wagga, drought severity and duration increased between the first and the second period (Table 2). In the first period from 1972 to 1992, Wagga Wagga had the highest drought severity and duration, and Quilpie the lowest (Table 2). For the second period, from 1993 to 2013, drought severity and duration were highest in Cairns and lowest in Quilpie (Table 2).

Table 2. Mean severity ( $\mu_S$ ) and duration ( $\mu_D$ ) of selected locations across Eastern Australia and corresponding coefficients of variation  $CV_S$  and  $CV_D$  for short-term ( $RDI_3$ ) droughts from 1972 to 1992 and 1993 to 2013.

Location	$\mu_S$	$CV_S$	$\mu_D$	$CV_D$
<b>1972-1992</b>				
Cairns	4.5	0.5	6.1	0.4
Melbourne	4.3	0.7	5.3	0.5
Wagga Wagga	5.5	0.9	6.8	0.7
Quilpie	3.4	1.1	4.5	0.7
<b>1993-2013</b>				
Cairns	4.8	0.4	6.4	0.3
Melbourne	4.5	0.7	6.1	0.4
Wagga Wagga	4.6	0.6	5.7	0.4
Quilpie	3.5	1.1	4.7	0.7

## DISCUSSION

Land rehabilitation is a continuing issue in Eastern Australia due to below average rainfall resulting in decreased water availability along with high variable rainfall [8, 18]. However, across Eastern Australia, site specific rainfall and drought metrics have rarely been used [8, 19]. In this study we assessed trends in recurrence intervals of droughts for selected locations across Eastern Australia, extending a previous study on recurrence intervals as a planning tool for ecosystem establishment in post-mining landscapes [8]. The findings of this study and the methods developed may help to understand the variation of temporal drought patterns and encourage land managers to apply recurrence intervals of droughts as an early rehabilitation assessment tool.

Australia is often referred to as the driest inhabited continent on Earth as it includes a large in arid zone with significant temperature and precipitation variability [20]. Generally, the Australian climate can rapidly alternate between dry and wet periods, occasionally exhibiting sharp transitions or sudden shifts between the extreme events [21]. In Eastern Australia these climatic extremes are mainly controlled by large variations of the El Niño Southern Oscillation (ENSO) [8], which affects different regions at different times of the year [22]. These extreme climatic events impact on rainfall, influencing the average severity and duration of droughts, a primary abiotic factor driving rehabilitation (Table 2) [8].

The RDI<sub>3</sub> detected most severe and prolonged droughts in the tropical locations of Eastern Australia [8]. For the historic time series of 1972-1992 and 1993-2013 the most severe and prolonged droughts were detected in Wagga Wagga (temperate) and Cairns (tropical). The two locations have seasonal rainfall patterns, e.g. in Wagga Wagga winter rainfall is high, while in Cairns summer rainfall is high (Table 1). In arid Quilpie evaporation was high and seasonal rainfall patterns were absent. In contrast to tropical Cairns and temperate Wagga Wagga (Table 1), Quilpie has lower severity and duration of short term droughts and severe and prolonged long-term droughts [8].

The importance of rainfall variability including extreme rainfall patterns and below average rainfall has been highlighted in many research studies on ecosystem rehabilitation [8, 23, 24]. As plants are vulnerable to plant available water, identifying droughts and their characteristics play a critical role in ecosystem rehabilitation [25]. Recurrence intervals of short term droughts (Figure 2) can be used as metric for risk assessment, management and rehabilitation of degraded lands [19].

Estimated recurrence interval curves incorporate the severity and duration of drought events, also referred to as “design droughts” [8]. They provide the probability of occurrence of drought at a particular severity or duration so that land managers can assess the risk of failure of successful early ecosystem rehabilitation by selecting the suitable plant species for specific climatic conditions. Some plant species are highly sensitive to specific drought characteristics [26]. Similarly recurrence intervals along with known probabilities of plant establishment success for particular drought conditions provide a decision support tool for land managers to undergo a cost-benefit analysis prior to rehabilitation.

Finally, this study demonstrated how differences in recurrence intervals can be identified between two time-series and potentially be used to identify long-term trends. Our results support climatological studies that found increasing drought severity and duration to be more likely due to global climate change [5].

## CONCLUSION

Recurrence interval curves or design droughts can be used to identify the severity, duration and frequency of occurrence of droughts for a given location. These recurrence intervals can be used to analyze the risk of failure of initial ecosystem establishment due to

water deficit and should be implemented into rehabilitation plans of disturbed lands.

## REFERENCES

1. Dobson, A.P., A. Bradshaw, and A.á. Baker, *Hopes for the future: restoration ecology and conservation biology*. Science, 1997. **277**(5325): p. 515-522.
2. Harris, J.A., et al., *Ecological Restoration and Global Climate Change*. Restoration Ecology, 2006. **14**(2): p. 170-176.
3. Hobbs, R.J. and J.A. Harris, *Restoration Ecology: Repairing the Earth's Ecosystems in the New Millennium*. Restoration Ecology, 2001. **9**(2): p. 239-246.
4. Bridge, G., *Contested terrain: mining and the environment*. Annu. Rev. Environ. Resour., 2004. **29**: p. 205-259.
5. Mason, L., et al., *Adapting to climate risks and extreme weather: A guide for mining and minerals industry professionals*. 2013, National Climate Change Adaptation Research Facility, Gold Coast., p. 76 pp. .
6. Campbell, B., *Perspectives: Legislating change*. Nature, 2013. **501**(7468): p. S12-S14.
7. Gallant, A.J.E., et al., *The characteristics of seasonal-scale droughts in Australia, 1911-2009*. International Journal of Climatology, 2013. **33**(7): p. 1658-1672.
8. Halwatura, D., A.M. Lechner, and S. Arnold, *Design droughts as planning tool for ecosystem establishment in post-mining landscapes*. Hydrology and Earth System Sciences Discussions, 2014. **11**(5): p. 4809-4849.
9. Unger, C., et al., *Mapping and Prioritising rehabilitation of abandoned mines in Australia*. Proceedings Life-of-Mine, 2012: p. p259-266.
10. Tsakiris, G. and H. Vangelis, *Establishing a drought index incorporating evapotranspiration* European water 2005. **9/10**: p. 3-11.
11. Hutchinson, M.F., et al., *Integrating a global agro - climatic classification with bioregional boundaries in Australia*. Global Ecology and Biogeography, 2005. **14**(3): p. 197-212.
12. Woodhams, F., et al., *Carbon Farming Initiative: A proposed common practice framework for assessing additionality*. 2012: Canberra, August.
13. Bureau of Meteorology. *Bureau of Meteorology, Climate data*. 2013 [cited 2013 April]; Available from: <http://www.bom.gov.au/climate/data/>

14. Peel, M.C., B.L. Finlayson, and T.A. McMahon, *Updated world map of the Köppen-Geiger climate classification*. Hydrol. Earth Syst. Sci., 2007. **11**(5): p. 1633-1644.
15. UNEP, U.N.E.P., *World Atlas of Desertification*. 1992: London.
16. Zargar, A., et al., *A review of drought indices*. Environmental Reviews, 2011. **19**(NA): p. 333-349.
17. Ganguli, P. and M.J. Reddy, *Risk Assessment of Droughts in Gujarat Using Bivariate Copulas*. Water Resource Management, 2012. **26**: p. 3301–3327.
18. Tongway, D.J. and J.A. Ludwig, *Rehabilitation of Semiarid Landscapes in Australia. I. Restoring Productive Soil Patches*. Restoration Ecology, 1996. **4**(4): p. 388-397.
19. Audet, P., et al., *Site-specific climate analysis elucidates revegetation challenges for post-mining landscapes in Eastern Australia*. Biogeosciences, 2013. **10**(10): p. 6545-6557.
20. Barua, S., A.W.M. Ng, and B.J.C. Perera, *Comparative Evaluation of Drought Indexes: Case Study on the Yarra River Catchment in Australia*. Journal of Water Resources Planning and Management-Asce, 2011. **137**(2): p. 215-226.
21. Fenby, C. and J. Gergis, *Rainfall variations in south-eastern Australia part 1: consolidating evidence from pre-instrumental documentary sources, 1788–1860*. International Journal of Climatology, 2013. **33**(14): p. 2956-2972.
22. Bureau of Meteorology. *Australian Climate Influences*. 2014 [cited 2014; Available from: <http://www.bom.gov.au/watl/about-weather-and-climate/australian-climate-influences.shtml?bookmark=introduction>].
23. Hinz, C., G. McGrath, and A. Hearman. *Towards a Climate Based Risk Assessment of Land Rehabilitation*. in *1st International Seminar on Mine Closure*. 2006. Australian Centre for Geomechanics, Perth: Nedlands WA 6009 AUSTRALIA.
24. Hodgkinson, J.H., et al., *Climate adaptation in the Australian mining and exploration industries*. 2010, CSIRO Climate Adaptation National Research Flagship,.
25. Engelbrecht, B.M., et al., *Drought sensitivity shapes species distribution patterns in tropical forests*. Nature, 2007. **447**(7140): p. 80-82.
26. Arnold, S., Y. Kailichova, and T. Baumgartl, *Germination of Acacia harpophylla (Brigalow) seeds in relation to soil water potential: implications for rehabilitation of a threatened ecosystem*. PeerJ, 2014. **2**: p. e268.



# EUTROPHICATED SEDIMENT REMEDIATION USING SHELL FRAGMENT AS REGIONAL UNUSED RESOURCES FOR NUTRIENTS ELUTION CONTROL

Kazuhiro Murakami<sup>1</sup>, Saki Agatsuma<sup>1</sup>, Michio Gomyo<sup>1</sup> and Akiko Inoue-Kohama<sup>2</sup>

<sup>1</sup> Department of Life and Environmental Sciences, Chiba Institute of Technology, Japan; <sup>2</sup> Tohoku Institute of Technology, Japan

## ABSTRACT

Dominant species of Aoko, *Anabaena*, has a “function of nitrogen fixation from air”, so if there is even phosphorus in water, they can multiply explosively. This study aimed the removal of phosphorus by shells of regional unused resources as eutrophication countermeasure in Hasunuma Seaside Park Pond. As result, sprinkling crushed shells was essential to the removal of phosphorus and the increase control of phytoplankton such as *Anabaena spiroides*. Inhibition rate of phosphorus showed a high percentage with much quantity of dispersion. At the N/P ratio, all dispersion system showed the higher value in comparison with no-treated systems. Hardness showed a high percentage with much quantity of dispersion because of  $\text{Ca}^{2+}$  was eluted into water from shell body. The dominant species of phytoplankton was changed to *Chlorella* sp. and the growth of the phytoplankton was controlled until fifth or tenth day by  $\text{Ca}^{2+}$  eluted from shells fragment.

**Keywords:** Shell, Regional unused resources, Phosphorus removal, Water quality, Brackish pond

## INTRODUCTION

In the lakes of Japan, the achievement rate of chemical oxygen demand (COD) or biochemical oxygen demand (BOD) of environment standard is lower than those of rivers and sea, and eutrophication is under progressing condition. Fig.1 showed secular change of the environment standard of rivers, sea and lakes [1]. It showed high achievement rate of 92.5% in the river and 78.3% in the sea, but that of lakes showed low value of 53.2%. As reason for this, lakes are closed environment, and the resources of nutrient salt are flow from rivers and elution from sediment. Many countermeasures against eutrophication have been suggested and carried out. But it is not effective because there are problem of cost and maintenance management. Lake Tega and Lake Inba of Chiba prefecture in Japan are one of the most famous eutrophicated lakes. They are tackling water environment repair of dredge and raw water transmission business [2].

As eutrophication countermeasure of lakes, there are physical method such as sediment transaction, introduction of water purification and the change of flow path of influent water. But it has problem of cost and maintenance management. Another countermeasure is biological method such as removal of fishes. But it has problem of the breakdown of ecosystem. Therefore, a new method is demanded to solve these problems.

## MATERIALS AND MEYHODS

### Outline of Experimental Pond

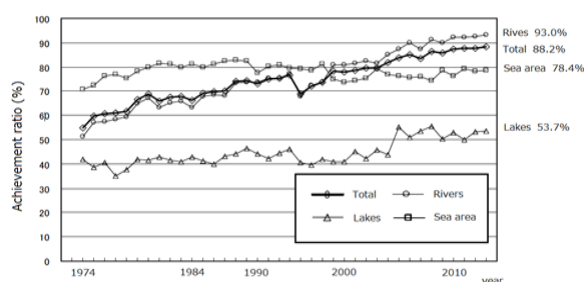
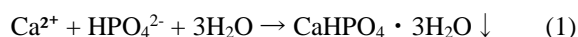


Fig.1 Achievement rate of environmental standards (COD, BOD) in lake, river and sea in Japan

Hasunuma Seaside Park Pond (Fig.2) in Sanmu city of Chiba prefecture locates at 350m inland from Kujukurihama coast. This pond is strong enclosed, and its surface area is about 10,000m<sup>2</sup>, water volume is about 7,400m<sup>3</sup>, the water depth is 0.74m in average. In past, a rental boat shop opened in this pond, but the problem of stink and deterioration of landscape occurred because Aoko occurred in every summer (Fig.3). Improvement works of drying in the sun and drainage work conducted, but Aoko occurred again in summer of next year [3].

Dominant species of Aoko at this pond is *Anabaena spiroides* (Fig.4). It has air nitrogen fixation ability. Therefore, they can multiplication explosively if there is enough phosphorus in water. The other side, many shells scattered in Kujukurihama coast on nearly of Hasunuma Seaside Park pond. Ca of the constituent parts of shell can adsorb phosphorus as formula (1) of below.



Shells are dumped as industrial wastes every year. Using these shells wisely, they can improve water quality and decrease industrial wastes. This study aimed the removal of phosphorus by physical adsorption and chemical combination with Ca eluted from shell fragments.

### Regional unused resources

In this study, *Anadara broughtonii* (Fig.5) was supplied as a regional unused resources. It is clam that belongs to species Aroodia family Arcidae. These shells inhabit in low tide area and bottom mud of inner bay. As character of shell, it has about 42 radial ribs. And its blood is red for it has Erythrocrutorin that similar to hemoglobin [4].

This shell was broken into 1-3mm size fragment (Fig.6). It sprinkled on the bottom mud of nutrients resources. Shells are scattered many in Kujukurihama coast of neighboring of Hasunuma Seaside Park Pond. And when its fragment sprayed on bottom mud, the surface of bottom mud looks bright by a reflection of the light.

### Experimental Methods

Water volume in the microcosm test is generally 300-1,000 ml[5]. From this reason, clear glass container (volume: 470ml, height: 14cm, diameter: 7cm,) was used in this study. Mud sediment of 100g collected from the pond was put in the bottom of the container to become flat, and pond water of 380ml was poured without disturbing the sediment. Crashed shells were sprinkled on sediment mud. The microcosm system was cultured in incubator. Culture period was 20 days, and culture system is no-treated system and sprinkled systems of 5, 10, 20, 30, 50, 80, 90, 100g/m<sup>2</sup>. Culture condition was 25 degrees(Celsius) in temperature and 2,400lux in illuminance (L/D=12/12hr). Measuring parameters were T-P (total phosphorous), PO<sub>4</sub>-P, T-N (total nitrogen), NH<sub>4</sub>-N, NO<sub>2</sub>-N, NO<sub>3</sub>-N, COD, chlorophyll a (Chl.a), pH, DO, hardness (Ca+Mg), and phytoplankton. Phytoplankton flora was observed in every 5 day.

## RESULTS AND DISCUSSION

### Phosphorus removal

Fig.7 and Fig.8 showed the inhibition rate of T-P and PO<sub>4</sub>-P. It showed high value because of there was much sprinkled in volume. It was the highest inhibition rate of T-P: 34.9% and PO<sub>4</sub>-P: 28%. In T-P, the inhibition rate became flat at sprinkled quantity of 5-30g/m<sup>2</sup> and 50-90g/m<sup>2</sup>. The inhibition rate of phosphorus did not change between each quantity of dispersion.



Fig.2 Hasunuma seaside park pond



Fig.3 Aoko in Hasunuma Seaside Park pond



Fig.4 *Anabeana spiroides* (Aoko)



Fig.5 *Anadara broughtonii* (shell)



Fig.6 Crushed shells fragment

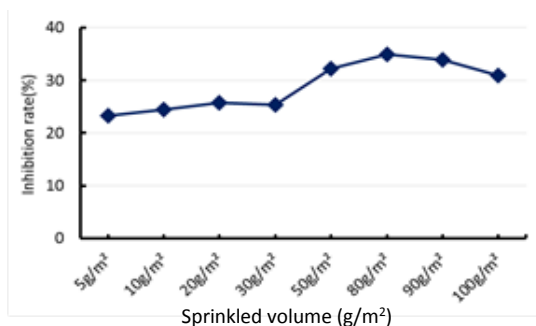


Fig.7 Inhibition rate of T-P in each microcosm

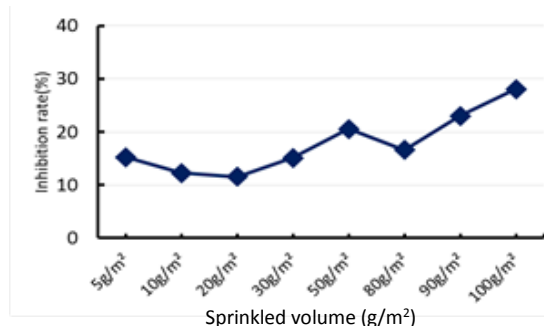


Fig.8 Inhibition rate of PO<sub>4</sub>-P in each microcosm

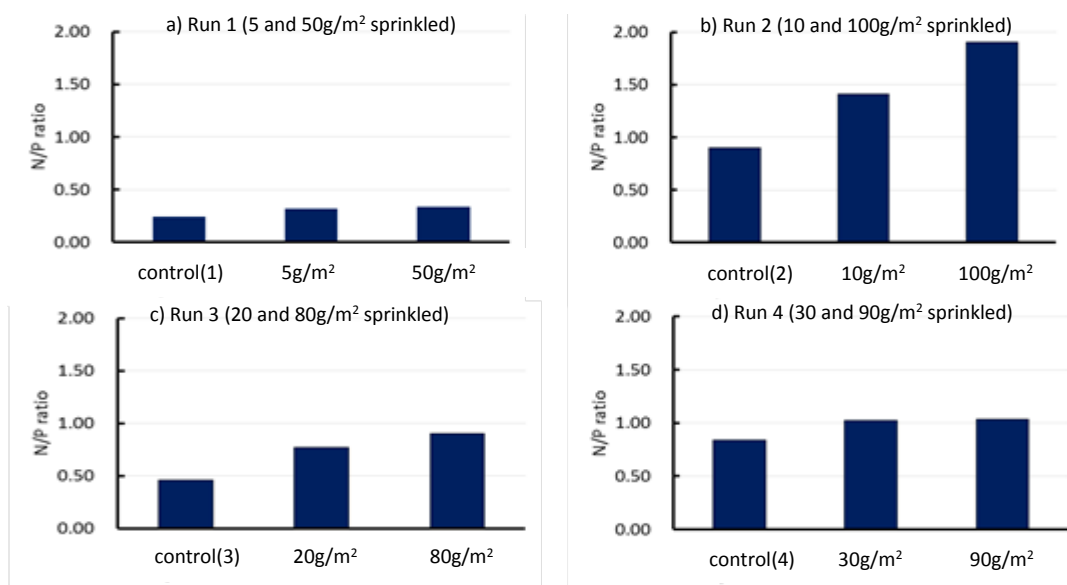


Fig.9 N/P ratio in each microcosm (20days after)

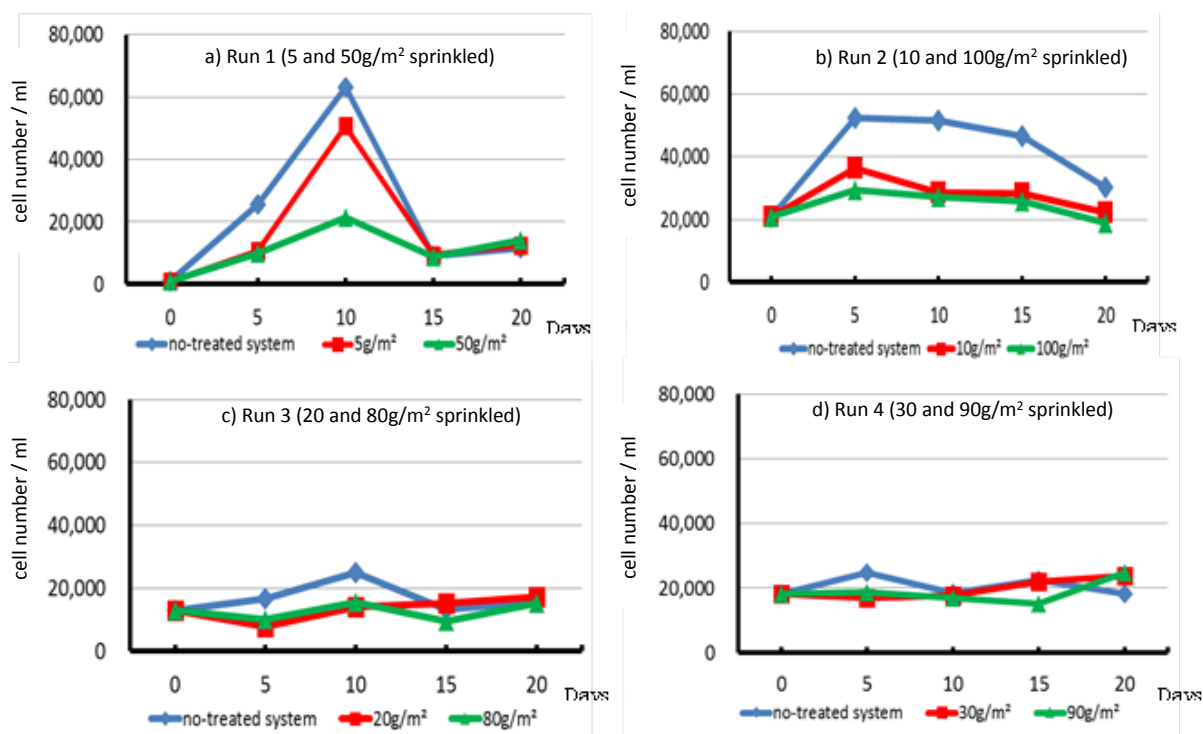


Fig.10 Total cell number of phytoplankton in each microcosm

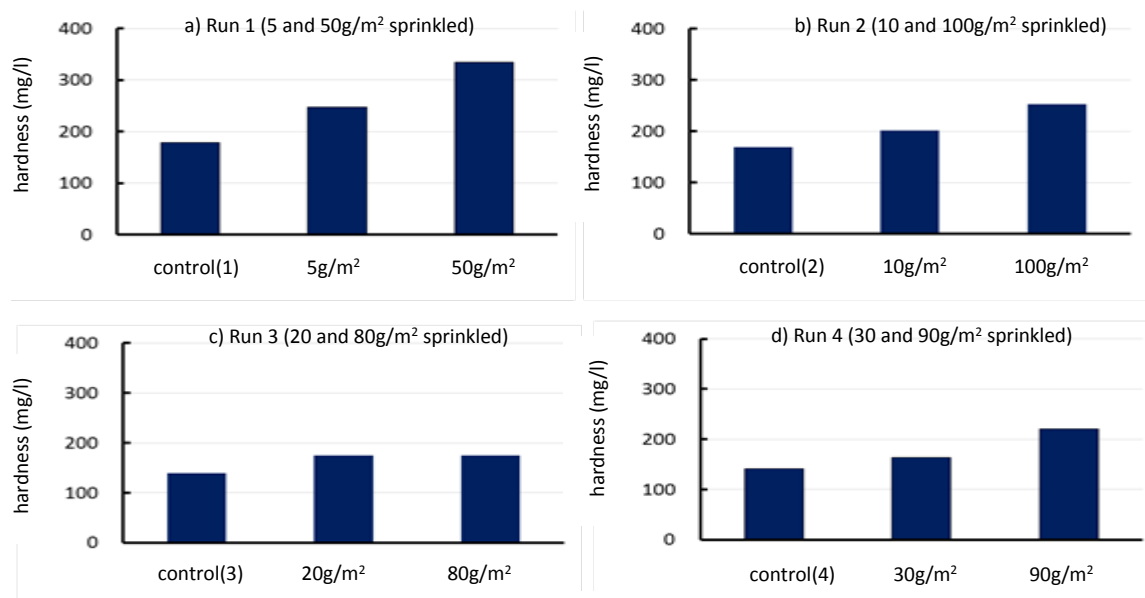


Fig.11 Hardness in each microcosm (20days after)

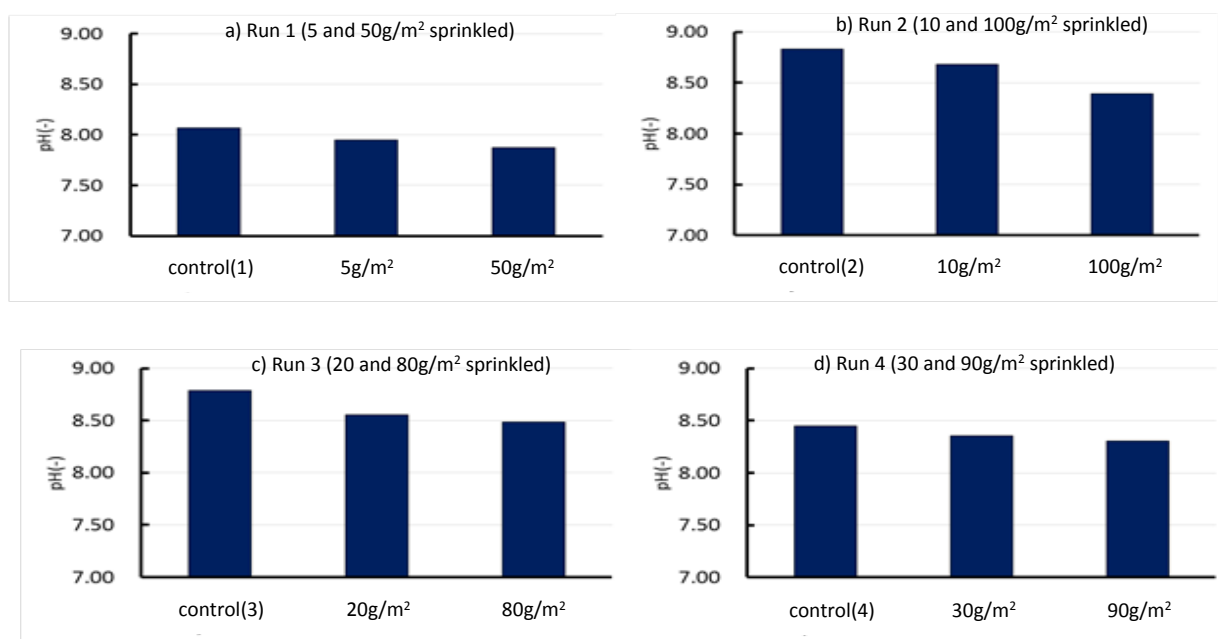


Fig.12 pH in each microcosm (20days after)

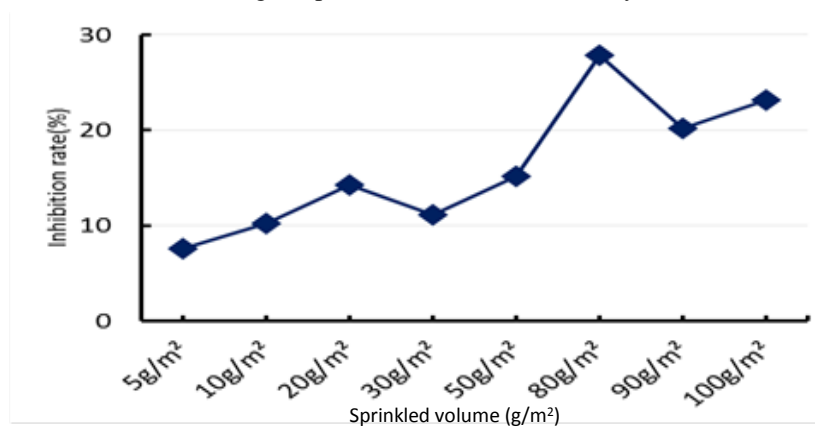


Fig.13 Inhibition rate of COD in each microcosm

The inhibition rate decreased at sprinkled quantity of 80g/m<sup>2</sup>-100g/m<sup>2</sup>. As reason for this, the sprinkled shell fragments overwrapped each other, and this cause is the decrease of surface area.

The solubility product of shells in water can be described as formula (2) of below [6],[7]. Therefore, combination adsorption quantity of phosphorus eluted from bottom mud and Ca<sup>2+</sup> eluted from shell fragments was particle. As this result, the mechanism of phosphorus adsorption in this study was considered as mainly physical adsorption.

$$[\text{Ca}^{2+}][\text{CO}_3^{2-}] = (3.6 \times 10^{-9})^2 \text{ (mol/L)} \quad (2)$$

#### N/P ratio in water

Fig.9 showed the N/P ratio in the microcosm. N/P ratio in all sprinkled systems showed high value than no-treated system. From this result, N/P ratio increased by Ca<sup>2+</sup> which adsorbed phosphorus and it changed to the direction of the proper N/P ratio from P excessive. However, N/P ratio is below 2.0 in all systems. Therefore, it was state of excessive phosphorus yet. The proper value of N/P ratio is about 10. In Lake Inba and Lake Tega in Chiba prefecture where well known as the most eutrophicated lakes in Japan, N/P ratio of these lakes are about 8.5 in summer [2]. However, N/P ratio in Hasunuma Seaside Park Pond of previous years was below 2.5[3], it was conditions of excessive phosphorus. In addition, *Anabeana spiroides* that dominant species of Aoko can breed if there is even phosphorus by air nitrogen fixation ability. Condition of phosphorus excess in Hasunuma Seaside Park Pond is serious problem.

#### Relationship between phytoplankton and regional unused resources

Fig.10 showed the daily variation of phytoplankton in microcosm system. The dominant species were *Chlorella* sp. in all systems. The population of sprinkled systems was less than no-treated system until fifth to tenth day. As reason for this, phosphorus concentration decreased by Ca<sup>2+</sup> that constituent of shell adsorbed phosphorus. By this, breeding of phytoplankton was controlled. Tsunami flowed in Hasunuma Seaside Park Pond by the Great East Japan Earthquake in March 2011, and breeding of *Anabeana spiroides* as dominant species of Aoko were controlled. But, water quality recovered to the state before the earthquake. Therefore, Aoko may occur again. In this study, sprinkled shells were effective to control phytoplankton that formed Aoko.

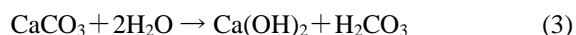
#### Hardness in water

Fig.11 showed hardness value in the each

microcosm. It showed a high value so that there was much sprinkled volume. As this result, it was thought that Ca<sup>2+</sup> that a component of the shells eluted in water. When there is much quantity of CO<sub>2</sub>, CaCO<sub>3</sub> which is constituent of the shell becomes easy to elute. In this study, quantity of photosynthesis by breeding controlled of phytoplankton accompany with sprinkle of shell reduced. By this, DO value becomes low of about 5mg/L. Therefore, the water becomes the anaerobic state, and it was thought that Ca eluted.

#### pH in water

Fig.12 shows the pH in each microcosm. pH is 8-9, and sudden change accompany with sprinkle of shells was not observed. As this reason, CaCO<sub>3</sub> eluted in water, it becomes formula (3) below.



Ca (OH)<sub>2</sub> is acidic. And H<sub>2</sub>CO<sub>3</sub> is alkaline. By this, water quality becomes neutral, and sudden change of pH was not seen.

#### Relationship between COD inhibition rate and sprinkle volume

Fig.13 shows the inhibition rate of COD in the microcosm. It showed a high value so that there was much sprinkled in volume. Ca<sup>2+</sup> eluted from sprinkled shells, and it was combination with phosphorus which is nutrients, and breeding of phytoplankton was controlled. Therefore, organic matter in the water was reduced, COD inhibition rate was higher.

#### CONCLUSIONS

This study focused Ca which constituent of shells as the regional unused resources which was many scattering in Kujukurihama coast. It removed phosphorus by physical absorption and Ca<sup>2+</sup> that eluted from shells, and it aimed to improvement from eutrophication state of water. The results were as follows.

- 1) With sprinkling the shell as regional unused resources, phosphorus that eutrophication material by chemical combination and physical adsorption of shells was controlled.
- 2) With sprinkling the shell, N/P ratio changed to the direction of the fair N/P ratio from P excessive. However, N/P ratio was below 2.0 in all systems. Therefore, it was state of excessive phosphorus yet.
- 3) COD inhibition rate was higher. Because Ca<sup>2+</sup> eluted by sprinkled shells, and it was combination with phosphorus which is nutrient salts, and breeding of phytoplankton was controlled. Therefore, organic matter in the water was reduced,

4) Dominant species of phytoplankton was *Chlorella* sp. in all system. The phytoplankton population of sprinkled systems was less than no-treated system until fifth to tenth day.

#### ACKNOWLEDGEMENTS

Special thanks for the cooperation of Sanmu Local Maintenance Center of Chiba Prefecture, and this study was supported by Grant-in-Aid for Scientific Research of JSPS (KAKENHI) (24651029) and New LRI of JCIA (2012PT4-02).

#### REFERENCES

- [1] Ministry of the Environment, "Annual Report on the Environment in Japan", 2013.
- [2] Amano Y, Taki K, Murakami K, Ishii T and Matsushima H, "Sediment remediation for ecosystem in eutrophicated lakes", The Scientific World, Vol.2, 2002, pp.885-891.
- [3] Murakami K, Ishii T and Taki K, "Re-eutrophication caused by bottom sediment sun-drying in shallow and strongly enclosed park pond", Papers on Environmental Information Sciences, Vol.23, 2009, pp435-440.
- [4] Okuya T, "Marine Mollusca in Japan", Tokai University Press, 2001, 1173pp.
- [5] Murakami K, Gomyo M, Agatsuma S, Amano Y and Inoue-Kohama A, "Environmental condition index for estimation on eutrophic state of enclosed aquifer ecosystem", International Journal of GEOMATE, Dec, 2013, Vol. 5, No. 2 (Sl. No. 10), 2013, pp. 706-711.
- [6] Driscoll CT, "Experimental watershed liming study, Kluwer Academic Publishers, 1996, 248pp.
- [7] Murakami K, Ishii T, Taki K and Matsushima H, "Waterplant purification in experimental mesocosm system with long-term observation", in Proc. 2nd IWA-ASPIRE Conference and Exhibition, 2007, CD-ROM.



# **THE VELOCITY REDUCTION EFFECT OF OBSTRUCTING STRUCTURES ON FLOOD WATER FLOWS DURING ROAD CROSSING**

Abdul Naser Abdul Ghani<sup>1</sup>, Ahmad Hilmy Abdul Hamid<sup>2</sup> and Nursriafitah Kasnon<sup>3</sup>

<sup>1,2</sup> Sch of Housing Building and Planning, USM, Malaysia; <sup>3</sup> Postgraduate Student, Sch of Housing Building and Planning, USM, Malaysia.

## **ABSTRACT**

Laboratory experimental investigations were conducted to identify suitable shape and dimension of objects as well as its capability to reduce flow velocity. The first stage of the study was to identify suitable shape and its arrangement. In this test a scale of 1:20 was used in a flow table experiment. The water flow pattern was recorded focusing on the distance and amplitude of the pattern as water flow pass the obstructing objects. The second stage of the investigation involved a hydraulic model investigation. In this investigation, the velocity reduction effect of the selected objects shapes were studied. The results are classified into three distinguishable patterns of diffusion. Two objects shapes and arrangements selected for use in the hydraulic model investigation indicated its capability to reduce flow velocity satisfactorily consistent with the flow pattern in the preliminary findings.

*Keywords: Flood, Road Crossing, Water Velocity, Velocity Attenuator*

## **INTRODUCTION**

In a general flooding scenario, water levels rise causing areas neighboring water bodies and some road stretch to be flooded. The primary effects of flooding include loss of life, damage to buildings and other structures such as roadways and canals. Flooded roads and transport infrastructure make it difficult to mobilize aid to those affected or to provide emergency health treatment [1].

The most regular and frequent type of disaster in Malaysia is flooding. When large amount of rainfall occurs, and the fact that it is more frequent these days, especially over a short period of time - drain, rivers and low lying areas will be filled with waters. With the ever increasing and higher frequency of events, the rainfall runoff will turn into floods or flash floods. In its way to lower area and finally the sea, the floodwater will cross urban, residential, industrial and agricultural area causing damages not only to properties but also creating hindrance for escape and blocking emergency access to the affected areas.

Road infrastructure is the main access for escape and emergency supplies. In flood events, some part of low lying roads will be inundated creating blockage for vehicle movement. Statistics clearly point out the high risk of driving in and around flooded roads and low lying areas [2].

Intensive literature search indicated very few previous works or information related to how floodwater exert pressure on crossing vehicles or human and how the pressure can be attenuated. Most of the previous and current works deals with flood risk assessment and mapping; scour of channel, river,

bridge piers and drains; policy and structural measures for flood control and abatement; and flood prediction. Figure 1 illustrates typical situation of floodwater during road crossing and how it affected the vehicles.



Fig.1 Dangerous crossing [3]

Yazici and Ozlay [4] proposed an evacuation route modeling to deal with transportation route planning during flooding - in other words, how to avoid flooded area. Meyer and Weigel [5] suggested an adaptive physical and management systems as an approach to mitigate potential problems. Physical approach of adaptive systems was studied by Pisani and Francesco [6] in the form of a moveable bridge that can be adjusted during floods. Meanwhile, Cai and Rahman [7] studied the used of road barriers as part of an emergency evacuation systems. A conceptual study of using Submerged Floating Tunnel (SFT) was carried out by Grantz [8].

Drobot et al. [9] described the risk factors of

driving into flooded road. They have also found out that more than half of flood fatalities involved vehicles driven into the floods. Cai et al. [1] and Kouyi et al. [10] used computer simulation to predict flood level on potentially flooded road and the distribution of discharges through cross road intersections. Fairweather and Yeaman [11] studied the influence of flooding on road pavement deterioration and recommended further research to better predict pavement failure. The question now in most flood event especially in Malaysia, at least, is how to make sure access for escape and emergency supplies can be safely provided.

Flowing floodwater exerts a pressure on an object such as a car or person. The pressure will be higher when the water depth increases. Friction between the tire and the slippery pavement will be reduced. Water, sand, or mud tends to replace the frictional forces that stabilize the vehicle.

In order to maintain the stability of a vehicle, forces from flowing floodwater crossing roads must be diffused to a minimum. This paper reports the result of investigations on the possibility of using road furniture as velocity attenuating objects.

## EXPERIMENTAL SETUP

Methodology used in this study were laboratory experiments. The experiments were conducted in the environmental and infrastructure laboratory and data were collected through observation and electronic data logging systems consist of sensors.

### Flow Pattern Experiment

The apparatus used in this experiment were water flow table, water color, adjustable stand, camera, and double cello tape to represent the shape and size of 2D obstructing objects. The apparatus were set up as shown in Fig. 2.

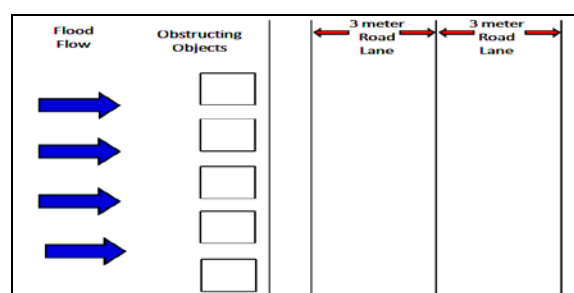


Fig. 2 Flow table set up.

Before doing the experiment for actual observation, pilot tests were conducted. The purpose of the pilot test was to help in finding some possibilities for the improvement possible hiccups before the actual experiment is conducted. It was also

to obtained typical water flow pattern as a result of the obstructing objects. This will help to ensure that the experiment can be conducted smoothly and will produce high quality meaningful results.

Three pilot tests using the scale of 1:50, 1:30 and 1:20 were carried out. The dimensional arrangement of the road surface for water flow simulation is as shown in Fig. 2 below. The 1:20 scale was finally chosen as the experimental scale because it gave the better presentation of diffusing effects. Tapes were carefully assembled on the water flow table for each test and the diffusing patterns were recorded by video camera.

The road shoulder and road are marked by the cello tape. The road shoulders are marked to represent 1 meter dimension on site and the road are marked to represent 3 meter on site. Figure 3 shows how the cello tape as diffuser model are fixed on the flow water table.

As the shape, size and arrangement of the various obstructing objects are expected to influence the diffusing capability of the systems, 18 such cases were established for testing. The experiment were conducted using the 18 pattern and size of diffusers as shown in Fig. 3 and the result were obtained by observing the outcome of the experiment by video. The diffusing pattern varies with the shape, orientation and size. The maximum size of diffusing object is 1 meter to scale of 1:20.

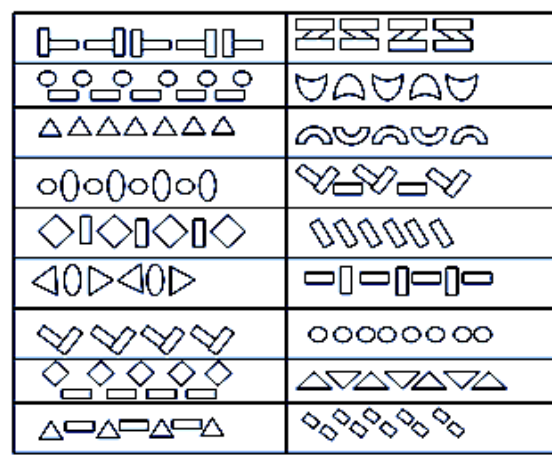


Fig. 3 Diffuser shapes and patterns.

### Hydraulic Model Investigation

The experiment were set up as in Fig. 4 in which two best object shape and pattern established from flow table experiments were used to study the velocity reduction effect in a 3D hydraulic environment.

Water were circulated into hydraulic flume as shown and sensors were placed before and after the diffusing objects. The sensors were also placed at the beginning, middle and end of the road cross section

to study the variation of flow after it passed through the diffusers. Velocity ( $V$ ) were recorded and readings were compared at every four locations of the road scale. This experiment maintained the scale of 1:20 and it correspond to 3 m width two lane road (i.e. road = 3m@15cm, road shoulder = 1m@5cm and diffuser model = 1m@5cm).

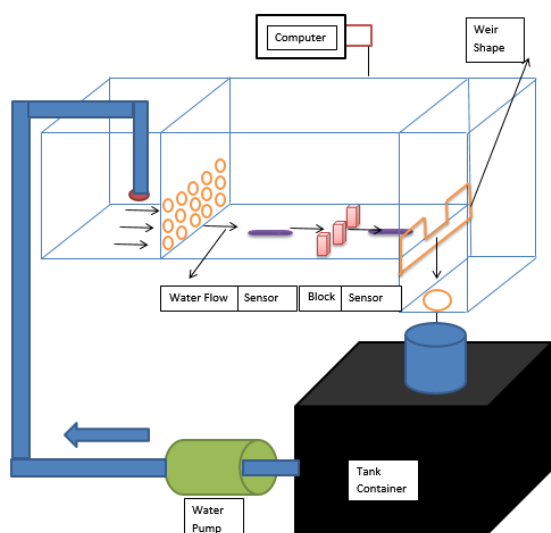


Fig. 4 Hydraulic model investigation.

## RESULTS AND DISCUSSIONS

### Flow Pattern

Based on the pilot tests carried out to identify diffusion patterns, two major characteristics of the diffusing water were identified and used as criteria for classification. The first characteristic is the “wave like” flow created by the obstructing object indicated that the water flow is being slowed down as it travels longer from one point to another. This include how long the wave like form remains while crossing the road. In some case, the wave diminishes before it reaches the other side of the road. In addition, there is also the amplitude of the wave in which higher amplitude indicating longer travel path.

The diffusing pattern can be divided into three categories. The first category is described as the diffusion pattern (wave) of the water flow after passing through the diffuser model is continuous until the road shoulder across the road. The amplitude of the wave are maintain the same until the end of the road shoulder.

The second category is described as the diffusion pattern (wave) of the water flow after passing through the diffuser model continue until the middle of the second lane and become straight to the end of road shoulder. The amplitude of wave remain similar until it diminished into straight line again. Straight line flow similar to the flow before the obstruction is

considered high velocity flow.

Category 3 is described as the diffusion pattern of the water is very little based on the smaller and shorter “wave like” flow created after the obstruction model. In this case the flow became straight again at the beginning of road crossing or no significant change in its flow pattern (straight flow). The amplitude of the wave are also small.

Out of the 18 obstruction patterns, two patterns can be considered as the pattern with the most capable of reducing water flow velocity. Figure 5 shows the recommended model that gave good effect on reducing the velocity of water flow across the road. They are two of the shape from category 1. This is because these object arrangement produced wave diffusion pattern until the end of opposite road shoulder and have high number of wave amplitude. The longer distance of the wave diffusion, the more velocity is being reduced. The higher number of wave amplitude, the more velocity reduces.

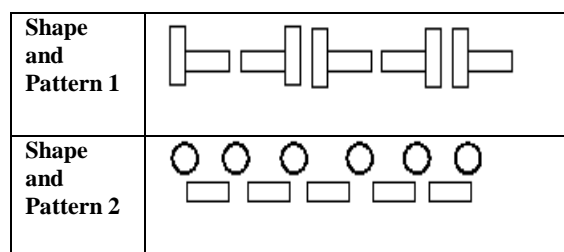


Fig. 5 Two best diffusing objects.

### Hydraulic Performance

The hydraulic investigations focused on the water velocity characteristics before and after passing through the two selected diffuser objects that have been identified in the flow table experiment previously.

Table 1 details the characteristics of water velocity as it travels before and passing the objects until it reach the end of the road section. It can be seen that both types of objects produce velocity diffusing characteristics consistent with the earlier flow pattern findings.

Table 1: Flow reduction Effect

Object Type	Average Velocity (cm/s)			
	Before	1	2	3
1	5.12 (100%)	3.98 (78%)	4.96 (97%)	6.31 (100%)
2	6.16 (100%)	3.89 (63%)	4.81 (77%)	6.10 (97%)

Note: 1, 2, 3 are locations along road cross sections as water travel across the model road.

The velocity reduction effect of object 1 can be further illustrated by the following Fig. 6. It can be

seen that the amplitude of water flowing waveform are diminishing towards the end of the road section. At point 1, i.e. just after the diffuser objects, velocity was reduced to 78% of the water velocity from before. It regains speed up to 97% of the original flow towards the end of the section and finally regain the full velocity as before.

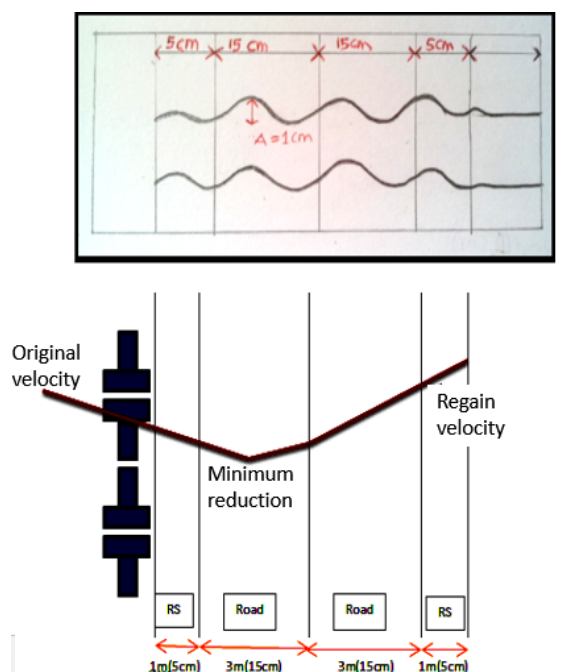


Fig. 6 Flow table pattern and velocity characteristics from Object 1.

As for object 2, flow table pattern is similar to object 1 but the diffusing effect goes beyond the end of road section as can be seen in Fig. 7 and Table 1. At the end of the road section the velocity is at 97% of the original water speed. Also the maximum diffusing effect of object 2 is 37% instead of 22% by object 1. This characteristics indicate better diffusing capability of object 2.

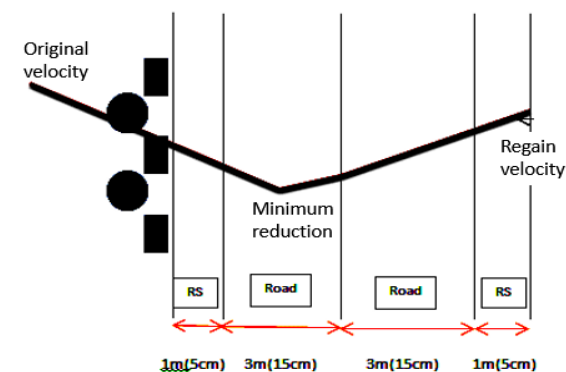


Fig. 7 Velocity reduction capability of object 2.

Possible arrangement of the objects can be illustrated by the following Fig. 8. It can be seen that

the objects can be placed as road furnitures in the form of planter boxes or corridor divider.

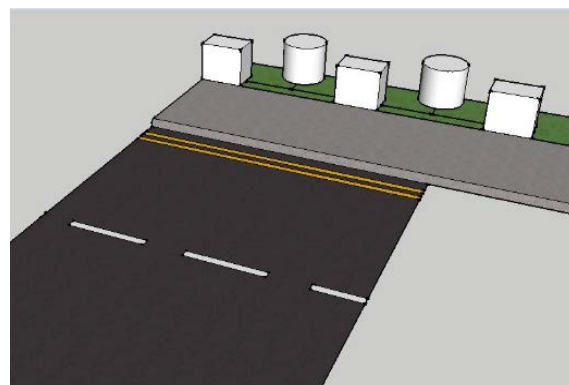


Fig. 8 Practical use of diffuser structures along flood stretch.

## CONCLUSION

Up to 37% reduction of flood velocity can be achieved by placing suitable objects along flooded stretch. This study has identified a suitable object shape and arrangement to reduce the floodwater velocity when it crosses road section.

## ACKNOWLEDGEMENTS

The authors would like to acknowledge financial support for this study by research grant no. 203/PPBGN/6711257 provided by Universiti Sains Malaysia/MOE Malaysia.

## REFERENCES

- [1] Hubo Cai, William Rasdorf, and Chris Tilley, "Approach to Determine Extent and Depth of Highway Flooding", *Journal of Infrastructure System*. Vol. 13, No. 2, June 2007, pp. 157-167
- [2] National Hurricane Center, "Never drive across a flooded road. Hurricane Preparedness". National Hurricane Center, USA.
- [3] The Star Newspaper. May 17, 2011
- [4] Yazici A. and Ozlay, K., "Evacuation Network Modeling via Dynamic Traffic Assignment with Probabilistic Demand and Capacity Constraint". *Transportation Research Record*. No. 2196. pp 11-20.
- [5] Meyer, M.D. and Weigel, B., "Climate Change and Transportation Engineering: Preparing for a Sustainable Future. *Journal of Transportation Engineering*". Vol. 137, No. 6, June 2011, pp. 393-403

- [6] Pisani, M. A. and Ballio, F., "Feasibility analysis of a movable bridge compensating for clearance deficit during floods". *Engineering Structures* 32 (2010). ASCE. Pages 3338\_3343..
- [7] Cai, H. and Asadur Rahman, "A Method to Develop and Optimize the Placement of Road Barriers in Emergency Evacuation for University Campuses". *Construction Research Congress 2010*. ASCE. Pages 409-419..
- [8] Grantz, W.C., "Conceptual Study for a deep Water, Long Span, Submerged Floating Tunnel (SFT) Crossing". *Procedia Engineering* 4(2010). Pages 61-70.
- [9] Drobot, S.D., Benight C. and Grunfest, E.C., "Risk factors for driving into flooded roads". *Environmental Hazards*, Volume 7, Issue 3, 2007, Pages 227-234.
- [10] Kouyi, G.L., N. Rivie`re, V. Vidalat, A. Becquet, B. Chocat and V. Guinot, "Urban flooding: one-dimensional modelling of the distribution of the discharges through cross-road intersections accounting for energy losses". *Water Science and Technology*. IWA Publishing, 2010, 61(8): pp. 2021-2026.
- [11] Fairweather, H. and Yeaman, J. (2014). "A study of the parameters affecting the performance of roads under extreme rainfall event". *Int. J. of GEOMATE*, Sept., 2014, Vol. 7, No. 1 (Sl. No. 13), pp.955-960



## ROLE OF A RETAINING WALL CONSTRUCTED OF NATURAL STONES IN PLANT BIODIVERSITY

Taizo Uchida<sup>1,2</sup>, Masaaki Furuno<sup>3</sup>, Takashi Minami<sup>1</sup>, Sampei Yamashita<sup>1,2</sup>, Tadashi Uchiyama<sup>2</sup>, Teruo Arase<sup>4</sup> and Daisuke Hayasaka<sup>5</sup>

<sup>1</sup>Faculty of Engineering, Kyushu Sangyo University, Japan; <sup>2</sup>Center for Landscape Research, Kyushu Sangyo University, Japan; <sup>3</sup>Graduate School of Engineering, Kyushu Sangyo University, Japan; <sup>4</sup>Faculty of Agriculture, Shinshu University, Japan; <sup>5</sup>Faculty of Agriculture, Kinki University, Japan

### ABSTRACT

The objective of this research is to evaluate the importance of vegetation of retaining walls made of natural stones (i.e., masonry revetment) in plant biodiversity. In this paper, plant compositions and the characteristics of masonry revetments were surveyed in terraced fields in Toho Village, southern Japan. In total, 43 families and 88 species were recorded in the spaces of the masonry revetments. Of these 88 species, 68 (77.3%) were herbaceous, excluding 13 (14.8%) ferns, and 7 (8.0%) species were woody plants. Native species accounted for 69 (78.4%) of the 88 species. Furthermore, numerous species not found in the horizontal environments around the terraced fields were also seen in the spaces of the masonry revetments. From these results, the authors consider that masonry revetments provide a habitat for plants and therefore contribute toward the conservation of plant biodiversity on a local scale.

*Keywords: Biodiversity, Revetment, Stone wall, Terraced field, Vegetation.*

### INTRODUCTION

Infrastructure elements such as roads, ports, bridges, power stations, and so forth, are fundamental structures and services that are necessary for supporting today's society. However, a large number of cut slopes and embankments, which accompany the introduction of infrastructure, have especially emerged in Japan, because forests account for the majority of the total land area of Japan (approx. 69%, excluding land submerged in water) [4]. Therefore, to prevent failure and erosion of cut slopes and embankments, revetment techniques have been rapidly developed and introduced. Some examples of these techniques are mortar sprayings, frame constructions, and precast segments including concrete blocks.

Since these structures often do not harmonize with their surroundings, a bio-engineering technique (planting and/or seeding for slope protection) has been actively applied over the last several decades, especially in Japan [22], to complement or enhance the peripheral scenery. The bio-engineering technique is also expected to ease global warming and reduce costs in other countries [8]. However, in a few cases, application of a bio-engineering technique is not suitable for protecting some slopes, e.g., those in extremely soft ground or on very steep land. At these places, retaining walls using lumber, natural stones and some other revetment material with less brightness and saturation, which can blend

into their surroundings, have recently been highly recommended in Japan [9].

In retaining walls using natural stones (hereafter referred to as "masonry revetments"), many narrow spaces appear between stones, and some plants, animals, and insects frequently colonize the spaces (Fig. 1). Among the colonizers, plants are generally considered as the major cause of collapse of masonry revetments and so become a target for removal.

As an alternative, the objective of this paper is to evaluate the importance of masonry revetment vegetation in plant biodiversity. In this study,



Fig. 1 Masonry revetment and some plants colonizing the spaces between stones.



therefore, plant compositions and the characteristics of masonry revetments were surveyed in a cluster of terraced fields. We examined a large number of masonry revetments under various different land uses in the same area.

## MATERIALS AND METHODS

### Study Site

The cluster of terraced fields used in this research is located at the Take section in Toho Village in southern Japan. The terraced fields, which are at an altitude of 280 to 420 m [21], are surrounded by artificial forests that are mostly *Cryptomeria japonica* and *Chamaecyparis obtuse*. The terraced fields are mainly used for rice although they have quickly changed into abandoned fields or fields for vegetables, grains, or housing in recent years. Nearly all of the slopes of the terraced fields are protected by masonry revetments with a southeastern aspect [21]. The dimensions of the revetments are approximately as follows: height 1 to 10 m, width 10 to 25 m, and inclination angle 70° to 80°. Also, the masonry revetments are the dry type [10], and on average they have 22 stones and a porosity of 7.5% per square meter.

According to data of the Automated Meteorological Data Acquisition System (AMEDAS) from 2004 to 2013, this surveyed area lies in the warm-temperature zone: the values of Kira's Warmth Index [12] range from 125.8 to 138.6 and the annual precipitation is 1,265 to 2,499 mm.

### Species Composition and Characteristics

Surveying of vegetation in the spaces between stones of masonry revetments was conducted from mid-September to early October, 2013. We examined 55 masonry revetments at random, using a survey quadrat located on vertical surface of the revetment at a height of 130 cm. The size of a quadrat was 100 cm long and 100 cm wide. The species composing the vegetation were recorded according to the methodology of the Braun-Blanquet cover-abundance scale [2]. In addition, the land-use type of each masonry revetment was classified as a paddy field, a dry field, an abandoned field, or "others", which included housing, parking lots, etc.

The plant nomenclature used in this paper followed that of Miyawaki et al. (1994), Baba (1999), and Shimizu (2003). All the recorded species were categorized by life form (dormancy form, disseminule form, radicle form, and growth form). The life forms were based on descriptions by Raunkiaer (1934) and Numata (1990). The invasive status (native or non-native) was also categorized based on published literature [1], [13], [18].

To compare the vegetation of the masonry

revetments with that of the surroundings, surveying of the vegetation was also conducted in 54 horizontal environments around the paddy fields, such as walkways between paddy fields, abandoned fields, and parking lots.

### Data Analysis

The Braun-Blanquet cover-abundance scale (r, +, I, II, III, IV, and V) was transformed as follows: r and +, 0.1%; I, 5.0%; II, 17.5%; III, 37.5%; IV, 62.5%, and V, 87.5%. Then, in Eq. (1), the summed dominance ratio (SDR) of each species [15] was calculated:

$$\text{SDR} = (F' + C')/2 \quad (1)$$

where  $F'$  and  $C'$  are the ratio of frequency and cover of each species to the numbers of the most abundant species, respectively.

To find out whether the characteristics of vegetation in the spaces of the masonry revetments were different by land-use type of the terraced fields, we conducted a Shapiro-Wilk test under the null hypothesis that the vegetation characteristics of the masonry revetments were equivalent across all land-use types [3], [23]. The vegetation characteristics employed were the following: total number of species, average number of species, Shannon-Wiener's diversity index ( $H'$ ), and percentages of native, herbaceous, and ferny species.

## RESULTS

In total, 43 families and 88 species were obtained in this survey. Native species accounted for 69 (78.4%) of the 88 species observed in the spaces of the masonry revetments surveyed. Moreover, of the 88 species, 68 (77.3%) species were herbaceous, excluding 13 (14.8%) ferns, and 7 (8.0%) species were woody plants. Of the 68 herbaceous species, 37 (54.4%) were ephemeral (annual and biennial) plants and 31 (45.6%) were perennials. Of the 43 families obtained in this survey, the most abundant families were Asteraceae (19/88 species) followed by Poaceae (9/88 species) and Leguminosae (4/88 species). Appendix 1 lists the plant compositions, land-use types, and life forms.

The species common to all land-use types (7/88 species) were *Acalypha australis*, *Boehmeria nipononivea*, *Equisetum arvense*, *Pteris × sefuricola*, *Stenactis annuus*, *Trachelospermum asiaticum*, and *Youngia japonica*. Conversely, species that emerged only in one specific land-use type were also observed. In only paddy fields, 15 species were observed, e.g., *Eclipta alba*, *Houttuynia cordata*,

Table 1 Vegetation characteristics of masonry revetment in each land-use type.

Land-use types	Vegetation characteristics						
	Number of survey plots	Total number of species	Average number of species	Shannon-Wiener's diversity index ( $H'$ )	Native species, %	Herbaceous <sup>†</sup> species, %	Ferny species, %
Paddy fields	29	55	6.2	5.260	83.6	72.7	21.8
Dry fields	8	35	6.6	4.917	82.9	65.7	25.7
Abandoned fields	14	53	8.4	5.395	81.1	75.5	15.1
Others	4	22	8.3	4.166	72.7	77.3	18.2
<i>P</i> -value	-	0.405 <sup>ns</sup>	0.164 <sup>ns</sup>	0.404 <sup>ns</sup>	0.103 <sup>ns</sup>	0.500 <sup>ns</sup>	0.954 <sup>ns</sup>

<sup>†</sup> Except for ferns. Woody species, %: 100 - [herbaceous species, %] - [fern species, %]. <sup>ns</sup>  $P > 0.05$ : not significant using Shapiro-Wilk test.

*Ixeris stolonifera*, *Lobelia chinensis*, *Osmunda japonica*, and *Vigna angularis*. In only dry fields, 6 species were observed: *Akebia trifoliata*, *Asplenium trichomanes*, *Chenopodium album*, *Gamochaeta coarctata*, *Lilium formosanum*, and *Sonchus oleraceus*. In only abandoned fields, 16 species were observed, e.g., *Cosmos sulphureus*, *Cryptomeria japonica*, *Miscanthus sinensis*, *Persicaria lapathifolia*, *Ranunculus silerifolius*, and *Rhynchosia volubilis*. In only the other fields for housing, parking lots, etc., 6 species were observed: *Arthraxon hispidus*, *Cosmos bipinnatus*, *Dioscorea polystachya*, *Echinacea purpurea*, *Lampranthus spectabilis*, and *Trisetum bifidum*.

Meanwhile, a total of 40 families containing 101 species were observed in the horizontal environments around the terraced fields. It should be especially noted that numerous species not recorded in the horizontal environments were obtained from vegetation of the masonry revetments (48/88 species; 54.5%).

From the species found in the masonry revetments only, many perennials (H and Ch; 39.6%) were obtained, as well as ephemeral plants (Th and Th(w); 35.4%). The dominant dispersal modes were anemochory (D1; 43.8%) or barochory (D4; 39.6%). In the radicle and growth forms, the majority of each form was "R5 (56.3%)" and "e (39.6%)", respectively. This implies that vegetation of the masonry revetments was spread primarily by seed.

On the other hand, no significant differences were found in the vegetation characteristics of the masonry revetments across the land-use types of the terraced fields ( $P > 0.05$ ) (Table 1).

## DISCUSSION

Numerous studies on vegetation colonizing hard surfaces such as pavement, rubble, roofs, ruins, building walls, and stone walls (masonry revetments) have been conducted, and it is widely understood that these surfaces are sufficiently able to support various taxa [5], [10], [11], [19], [20]. However, those studies are overwhelmingly concentrated in Europe [10], whereas information originating in other countries and regions regarding vegetation of hard surfaces, including masonry revetments, is lacking despite the importance of plant habitats.

In this study, 43 families and 88 species including 69 (78.4%) natives were observed between stones of the masonry revetments (Appendix 1). Our results are not surprising, because even hard surfaces such as cracks in pavement and mortared walls provide good opportunities for plants to colonize [10].

In environments with hard surfaces, ephemeral annuals or short-lived taxa (due to disturbance by human activities) tend to be dominant instead of perennials including woody plants [5], [7], [11]. However, many perennial herbs (45.6%; excluding ferns) and even woody plants (8.0%) were obtained in this survey, as well as ephemeral (annual and biennial) plants. Additionally, a large number of species not observed in the horizontal environments around the terraced fields were recorded.

On a local scale, therefore, we consider that the masonry revetments play an important ecological role in providing habitat for plants and in so doing, contribute toward the conservation of plant biodiversity. Incidentally, of the plants colonizing the masonry revetments, the main ecological types

were species, mainly Asteraceae and Poaceae, propagating by seed with gravity dispersal (barochory), or wind dispersal (anemochory) mechanisms. These observations are in total agreement with previous reports on hard surface vegetation [6], [7], [19].

On the other hand, vegetation characteristics such as the number of species, the diversity index ( $H'$ ), and the percentage of native species in the masonry revetments were not affected by the land-use types of terraced fields (Table 1). However, the plant composition of each land-use type was highly distinctive. Common species among land-use types could be defined as typical species in the masonry revetment vegetation, for example, *Acalypha australis*, *Equisetum arvense*, *Trachelospermum asiaticum*, and *Youngia japonica*. Conversely, the species observed only in a certain land-use type would be regarded as a peculiar plant, e.g., *Lampranthus spectabilis*, *Lilium formosanum*, *Oenanthe javanica*, and *Ranunculus silerifolius*, that is heavily dependent on its environment.

Moisture availability is the most important environmental factor for the development of hard surface vegetation [10], [16], [20]. That is, differences of moisture conditions in the masonry revetments, which accompany land-use change, would lead to varied plant composition. While infrastructure elements have long been mentioned as a force to reduce vegetation coverage, the masonry revetments installed in various locations with different moisture conditions could lead to plant biodiversity on a local scale.

In general, plants are considered to be the major cause of collapse of masonry revetments. Nevertheless, it is evident that masonry revetments play a significant role, not only in protecting slopes and embankments, but also in maintaining or ameliorating plant biodiversity on a local scale. Therefore, it would be a challenge to be tackled in the future to overcome or moderate a trade-off between plant biodiversity and maintaining masonry revetments.

Appendix 1 Species recorded in this survey, and they were listed according to plant composition of each land-use type.

Species	Family	Land-use types				Life form				Occurrence frequency (%)
		Paddy fields (n=29)	Dry fields (n=8)	Abandoned fields (n=14)	Others (n=4)	Dormancy	Disseminule	Radicoid	Growth	
<i>Acalypha australis</i> †, γ	Euphorbiaceae	II	II	+	III	Th	R5	D3	e	16.4
<i>Boehmeria nipononivea</i> †, §	Urticaceae	III	III	III	II	Ch	R3	D4	e	41.8
<i>Equisetum arvense</i> ‡	Equisetaceae	I	II	I	II	G	R1	D1	e	16.4
<i>Pteris × sefuricola</i> ‡	Pteridaceae	II	III	I	II	H	R3	D1	e	30.9
<i>Stenactis annuus</i> †, #, γ	Asteraceae	III	II	III	I	Th(w)	R5	D1	pr	49.1
<i>Trachelospermum asiaticum</i> ω	Apocynaceae	II	V	IV	V	Ch	R5	D1	l	25.5
<i>Youngia japonica</i> †, γ	Asteraceae	II	I	II	I	Th(w)	R5	D1	ps	25.5
<i>Echinochloa crusgalli</i> †, γ	Poaceae	II				Th	R5	D4	t	3.6
<i>Eclipta alba</i> †, #, γ	Asteraceae	+				Th	R5	D1	e	7.3
<i>Elatostema laetevirens</i> †, §	Urticaceae	II				H	R3	D4	e	1.8
<i>Eleusine indica</i> †, γ	Poaceae	+				Th	R5	D4	t	3.6
<i>Houttuynia cordata</i> †, §	Saururaceae	I				G	R1	D4	e	3.6
<i>Ixeris stolonifera</i> †, §	Asteraceae	r				H	R4	D1	p	1.8
<i>Lobelia chinensis</i> †, §	Campanulaceae	r				H	R3	D4	p	1.8
<i>Mallotus japonicus</i> ω	Euphorbiaceae	r				MM	R5	D2	e	1.8
<i>Oenanthe javanica</i> †, §	Umbelliferae	II				H	R4	D4	e	1.8
<i>Osmunda japonica</i> ‡	Osmundaceae	I				G	R3	D1	t	5.5
<i>Paederia scandens</i> †, §	Rubiaceae	+				Ch	R3	D4	l	3.6
<i>Phyllanthus urinaria</i> †, γ	Euphorbiaceae	r				Th	R5	D3	e	1.8
<i>Sonchus asper</i> †, #, γ	Asteraceae	+				Th(w)	R5	D1	pr	1.8
<i>Vigna angularis</i> †, γ	Leguminosae	III				Th	R5	D3	l	1.8
<i>Viola verecunda</i> †, §	Violaceae	+				H	R3	D3	b	5.5
<i>Akebia trifoliata</i> ω	Lardizabalaceae		I			M	R3	D2	l	1.8
<i>Asplenium trichomanes</i> ‡	Aspleniaceae		I			E	R3	D1	t	1.8
<i>Chenopodium album</i> †, γ	Chenopodiaceae		I			Th	R5	D4	e	1.8
<i>Gamochaeta coarctata</i> †, #, γ	Asteraceae		I			H	R5	D1	b	1.8
<i>Lilium formosanum</i> †, #, §	Liliaceae		I			H	R5	D3	e	1.8
<i>Sonchus oleraceus</i> †, γ	Asteraceae		II			Th(w)	R5	D1	pr	1.8
<i>Amphicarpaea edgeworthii</i> †, γ	Leguminosae			I		Th	R5	D3	l	3.6

## Appendix 1 Continued.

Species	Family	Land-use types				Life form				Occurrence frequency (%)
		Paddy fields (n=29)	Dry fields (n=8)	Abandoned fields (n=14)	Others (n=4)	Dormancy	Disseminule	Radicaid	Growth	
<i>Bothriospermum zeylanicum</i> †, γ	Boraginaceae			+		Th	R5	D4	b	1.8
<i>Capillipedium parviflorum</i> †, §	Poaceae			+		Ch	R3	D1	t	1.8
<i>Conyza canadensis</i> †, #, γ	Asteraceae			I		Th(w)	R5	D1	pr	3.6
<i>Cosmos sulphureus</i> †, #, γ	Asteraceae			+		Th	R5	D4	e	1.8
<i>Cryptomeria japonica</i> ω	Taxodiaceae			+		MM	R5	D1	e	1.8
<i>Euchiton japonicus</i> †, §	Asteraceae			+		H	R5	D1	b	1.8
<i>Ixeris japonica</i> †, §	Asteraceae			+		H	R3	D1	ps	1.8
<i>Miscanthus sinensis</i> †, §	Poaceae			I		Ch	R3	D1	t	1.8
<i>Persicaria lapathifolia</i> †, γ	Polygonaceae			+		Th	R5	D4	e	1.8
<i>Ranunculus silerifolius</i> †, §	Ranunculaceae			+		Th(w)	R5	D4	e	1.8
<i>Rhynchosia volubilis</i> †, §	Leguminosae			+		H	R5	D3	l	1.8
<i>Sagina japonica</i> †, γ	Caryophyllaceae			I		Th	R5	D4	b	1.8
<i>Setaria faberi</i> †, γ	Poaceae			+		Th	R5	D4	t	1.8
<i>Stellaria aquatica</i> †, γ	Caryophyllaceae			II		Th(w)	R5	D4	b	5.5
<i>Toxicodendron radicans</i> ω	Anacardiaceae			I		MM	R5	D4	l	1.8
<i>Arthraxon hispidus</i> †, γ	Poaceae				I	Th	R5	D4	t	1.8
<i>Cosmos bipinnatus</i> †, #, γ	Asteraceae				I	Th	R5	D4	e	1.8
<i>Dioscorea polystachya</i> †, #, §	Dioscoreaceae				I	G	R5	D1	l	1.8
<i>Echinacea purpurea</i> †, #, §	Asteraceae				I	Ch	R5	D4	e	1.8
<i>Lampranthus spectabilis</i> †, #, §	Aizoaceae				V	Ch	R5	D4	p	3.6
<i>Trisetum bifidum</i> †, §	Poaceae				II	H	R5	D4	e	3.6
<i>Lactuca indica</i> †, γ	Asteraceae	r	I	I		Th	R5	D1	pr	7.3
<i>Achyranthes fauriei</i> †, §	Amaranthaceae	II		I	I	H	R3	D2	e	14.5
<i>Artemisia princeps</i> †, §	Asteraceae	+	II	+		Ch	R2	D4	e	5.5
<i>Asplenium sarelii</i> ‡	Aspleniaceae	I	III	II		E	R3	D1	t	21.8
<i>Athyrium niponicum</i> ‡	Woodsiaceae	III	III		III	H	R2	D1	e	23.6
<i>Athyrium vidalii</i> ‡	Woodsiaceae	II	I	I		H	R3	D1	t	12.7
<i>Athyrium wardii</i> ‡	Woodsiaceae	+	II	I		H	R2	D1	e	12.7
<i>Boehmeria spicata</i> ω	Urticaceae		II	I		Ch	R3	D4	e	3.6
<i>Camellia sinensis</i> ω, #	Theaceae	II		IV		MM	R5	D4	e	5.5
<i>Chamaele decumbens</i> †, §	Umbelliferae	r	I	II		G	R5	D4	ps	10.9
<i>Chamaesyce maculata</i> †, #, γ	Euphorbiaceae	+			I	Th	R5	D3	b	5.5
<i>Clinopodium gracile</i> †, §	Labiatae	r		II		H	R5	D4	b	9.1
<i>Commelina communis</i> †, γ	Commelinaceae	II	I	II		Th	R5	D4	b	14.5
<i>Corydalis racemosa</i> †, γ	Papaveraceae	r	II	II		Th(w)	R5	D4	b	9.1
<i>Crassocephalum crepidioides</i> †, #, γ	Asteraceae	+		+		Th	R5	D1	pr	3.6
<i>Cyperus iria</i> †, γ	Cyperaceae	r	I			Th	R5	D4	t	3.6
<i>Deparia coniliti</i> ‡	Woodsiaceae	r	II	I		H	R2	D1	e	7.3
<i>Digitaria ciliaris</i> †, γ	Poaceae	III	II	II		Th	R4	D4	t	30.9
<i>Dunbaria villosa</i> †, §	Leguminosae		I	I		H	R3	D3	l	5.5
<i>Fatoua villosa</i> †, γ	Moraceae	r			I	Th	R5	D3	e	3.6
<i>Galinsoga quadriradiata</i> †, #, γ	Asteraceae	I	I	II		Th	R5	D4	e	20.0
<i>Gamochaeta pensylvanica</i> †, #, γ	Asteraceae		I	II		Th(w)	R5	D1	b	7.3
<i>Geranium nepalense</i> †, §	Geraniaceae	+	I	+		H	R5	D3	b	7.3
<i>Glechoma hederacea</i> †, §	Labiatae	+		I		H	R4	D4	p	5.5
<i>Hydrocotyle sibthorpioides</i> †, §	Umbelliferae	r			I	Ch	R4	D4	p	3.6
<i>Impatiens balsamina</i> †, #, γ	Balsaminaceae	II		I		Th	R4	D3	b	5.5
<i>Justicia procumbens</i> †, γ	Acanthaceae	I	I	III		Th	R5	D3	e	21.8
<i>Lemnaphyllum microphyllum</i> ‡	Polypodiaceae	II			II	E	R2	D1	e	5.5
<i>Lepisorus thunbergianus</i> ‡	Polypodiaceae	I	I			E	R3	D1	e	10.9
<i>Lygodium japonicum</i> ‡	Schizaeaceae	I		II		H	R2	D1	l	9.1
<i>Mollugo stricta</i> †, γ	Molluginaceae	r	I			Th	R5	D4	b	3.6
<i>Oxalis corniculata</i> †, §	Oxalidaceae	I		I	I	Ch	R4	D3	p	14.5
<i>Oxalis dillenii</i> †, #, §	Oxalidaceae		II	II		Ch	R4	D3	p	7.3
<i>Setaria viridis</i> †, γ	Poaceae		II	II	I	Th	R5	D4	t	10.9
<i>Stellaria neglecta</i> †, γ	Caryophyllaceae	r		II		Th(w)	R4	D4	b	5.5
<i>Taraxacum officinale</i> †, #, §	Asteraceae	I		+		H	R3	D1	r	7.3
<i>Thelypteris decursivopinnata</i> ‡	Thelypteridaceae	II		+		H	R3	D1	t	5.5
<i>Trichosanthes cucumeroides</i> †, §	Cucurbitaceae	+		II	I	G	R5	D4	l	12.7

In land-use types Roman numerals and other symbols for each species indicate SDR classes, defined as follows: r, under 5%; +, under 10%; I, under 20%; II, under 40%; III, under 60%; IV, under 80%, and V, above 80%. †, herbaceous species (excluding ferns); ‡, ferny species; ω, woody species; #, non-native species; γ, ephemeral herbs (annual and biennial plants), and §, perennial herbs. Highlight: species observed in masonry revetment only.

## ACKNOWLEDGEMENTS

We are deeply grateful to K. Kondo and S. Imado, Environ. Sci. Appl. Ecol. Lab., Kyushu Sangyo University, for their assistance with the field work. This research was supported by the Strategic Support for Research Project by Private University (No. S1203007) from the Ministry of Education, Culture, Sports, Science and Technology in Japan.

## REFERENCES

- [1] Baba T., 1999. Identifying woody species by their leaf appearances. Shinano Mainichi Shinbunsha, Nagano. 396 pp. *In Japanese*
- [2] Braun-Blanquet J., 1964. Pflanzensozologie. Grundzüge der Vegetationskunde, 3rd ed. Springer-Verlag, Vienna. 865 pp.
- [3] Davis J.C., 1986. Statistics and data analysis in geology, 2nd ed. John Wiley & Sons, New York. 656 pp.
- [4] Food and Agriculture Organization of the United Nations, 2010. Global forest resources assessment 2010. < <http://www.fao.org/forestry/fra/fra2010/en/>>.
- [5] Francis, R.A. and Hoggart S.P.G., 2008. Waste not, want not: The need to utilize existing artificial structures for habitat improvement along urban rivers. *Restoration Ecology* 16, 373-381.
- [6] Hayasaka D., Asasaka M., Miyauchi D. and Uchida T., 2011. Classification of roadside weeds along two highways in different climatic zones according to ecomorphological traits. *Weed Technol.* 25, 411-421.
- [7] Hayasaka D., Asasaka M., Miyauchi D., Elgene O.B. and Uchida T., 2012. Qualitative variation in roadside weed vegetation along an urban-rural road gradient. *Flora* 207, 126-132.
- [8] Islam M.S., Shahriar B.A.M., Islam M.S. and Shahin H.M., 2013. Study on growth of vetiver grass in tropical region for slope protection. In: Hossain M.Z. and Shahin H.M. (eds.), *Geotechnique, construction material & environment, The GEOMATE International Society*, Tsu. pp. 113-118.
- [9] Japan road association, 2009. Implementation guidelines for cut slope protection. Maruzen Co., Ltd., Tokyo. 521 pp. *In Japanese*
- [10] Jeremy L., 2011. Vegetation of urban hard surface. In: Niemelä J. (ed.), *Urban ecology*, Oxford, New York. pp. 93-102.
- [11] Jim C.Y., 2008. Urban biogeographical analysis of spontaneous tree growth on stone retaining walls. *Physical Geography* 29, 351-373.
- [12] Kira T., 1977. A climatological interpretation of Japanese vegetation zones. In: Miyawaki A. and Tüxen R. (eds.), *Vegetation science and environmental protection*. Maruzen Co., Ltd., Tokyo. pp. 21-30.
- [13] Miyawaki A., Okuda S. and Fujiwara R., 1994. Handbook of Japanese vegetation. Shibundo Co., Ltd., Tokyo. 646 pp. *In Japanese*
- [14] Numata M., 1990. The ecological encyclopedia of wild plants in Japan. Zenkoku Noson Kyoiku Kyokai, Tokyo. 664 pp. *In Japanese*
- [15] Numata M. and Yoda K., 1957. The community structure and succession of artificial grasslands (1). *J. Jap. Soc. Herb. Crops Grassl. Farm.* 3, 4-11. *In Japanese*
- [16] Payne R.M., 1989. The flora of walls in the Chew Valley, Somerset Archaeology and Natural History 133, 231-242.
- [17] Raunkiaer C., 1934. Life forms of plants and plant geography. Oxford University Press, London. 632 pp.
- [18] Shimizu T., 2003. Naturalized plants of Japan. Heibonsha Ltd., Publishers, Tokyo. 337 pp. *In Japanese*
- [19] Uchida T., Xue J.-H., Hayasaka D., Arase T., William T.H. and Lyn A.G., 2014. The relation between road crack vegetation and plant biodiversity in urban landscape. *Int. J. of GEOMATE* 6, 885-891.
- [20] Woodell S.R.J., 1979. The flora of walls and pavings. In: Laurie I.C. (ed.), *Nature in cities*. John Wiley & Sons, New York. pp. 135-156.
- [21] Yokoyama H., Yamashita S., Hitaka K., Uchida T. and Kurita T., 2013. Cultural landscape and tourism in Toho-Village, Fukuoka-Prefecture (2). *J. Indust. Manag. of Indust. Manag. Inst.* 45, 63-74. *In Japanese*
- [22] Yoshida H., 2007. Seeding on slopes in Japan for nature restoration. In: Hong S.-K. et al. (eds.), *Landscape ecological applications in man-influenced areas*. Springer, Dordrecht. pp. 311-328.
- [23] Zar, J.H., 1984. Biostatistical analysis, 2nd ed. Prentice Hall, Englewood Cliffs. 718 pp.

## INFLUENCE OF EXOTIC PASTURE GRASSES AND FERTILIZATION ON THE VEGETATION RECOVERY OF LANDSLIDE SLOPES FORMED BY TYPHOON 9512 IN MIKURA-JIMA ISLAND, JAPAN

Teruo Arase and Tetsuo Okano  
Faculty of Agriculture, Shinshu University, Japan

### ABSTRACT

Typhoon 9512 hit Mikura-jima Island, Izu Islands, Japan in 1995, producing many landslide slopes. Torino-o No. 3 landslide slope was planted with seedlings of native species (*Alnus sieboldiana* and *Miscanthus condensatus*) as part of vegetation recovery efforts and was subsequently seeded by helicopter in 2002 with exotic pasture grasses (*Agrostis stolonifera*, *Festuca* sp., and *Lespedeza cuneata*). To elucidate the impact of seeded exotic grasses in vegetation recovery, we designated seven plots in 2004, and surveyed vegetation every summer until 2013: four fertilized plots (fowl manure applied at 0.2 g/m<sup>2</sup>) and three non-fertilized plots. The planted native species seedlings grew steadily irrespective of fertilization, but with self-thinning in *A. sieboldiana* and a peak in maximum plant height in *M. condensatus* in 2008. Exotic pasture grasses decreased gradually and almost disappeared in 2013. Fertilizing temporarily enhanced the growth of *M. condensatus* and *Festuca* sp. but seemed to induce species competition. The growth forms of the invading species in herbaceous layer were different between the plots, which confirmed the enhanced competition by fertilizing.

**Keywords:** Exotic pasture grasses, Fertilization, Landslide slope, Mikura-jima Island, Vegetation recovery

### INTRODUCTION

In an insular ecosystem, such as an island, habitat for wildlife can easily be lost due to disaster or development. Island ecosystems are generally rich in endemic species but tend to be homogeneous in habitat, making them vulnerable to invasive species [10], [13]. Thus, insular ecosystems are considered to be prone to extinction events. However, it is more difficult to confirm the extinction of plant species than animal species because plants might survive unobserved in a very limited area of the original habitat [13].

Mikura-jima Island (area, 20.58 km<sup>2</sup>; location, ca. 180 km south of Tokyo) is an isolated island on the Izu Islands in the Pacific Ocean off the main island of Japan, where volcanic activity ceased ca. 7,000 years ago, leaving a long period for the development of the terrestrial ecosystem. It is covered with flora typical of that of the Izu Islands, has cliffs facing the sea with a large range in elevation (the highest peak is 850.8 m), and has many streams with abundant water [6], [12]. Mikura-jima Island was spared the deforestation for tourism or industry that took place on the other of the Izu Islands.

In September 1995, Typhoon 9512 hit Mikura-jima Island (Fig. 1). It produced many landslide slopes among the old-growth forests of evergreen broad-leaved trees (e.g., *Castanopsis sieboldii* (Makino) Hatusima ex Yamazaki et Mashiba, *Machilus thunbergii* Sieb. et Zucc., *Eurya japonica* Thunb. and *Buxus microphylla* Sieb. et Zucc.) [1].

The thin layer of volcanic ash soil was washed away, and the bedrock was exposed on the landslide slopes. After the typhoon, vegetation recovery efforts were begun with projects to build fascines (using fallen trees) to retain the soil and to transplant locality-certified seedlings of native species (*Alnus sieboldiana* Matsum. and *Miscanthus condensatus* Hack.) [9].



Fig. 1 Path of typhoon 9512. Open circles on the path indicate its location at 9:00 on each day. Figure based on original graph and data [7].



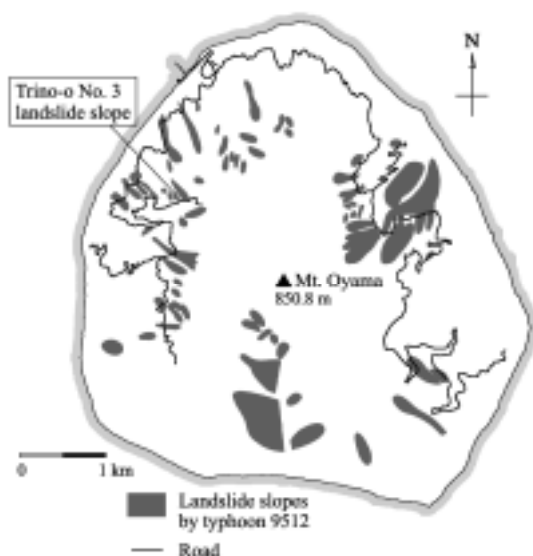


Fig. 2 Locations of landslide slopes formed by typhoon 9512 on Mikura-jima Island.

We focus on Trino-o No. 3 landslide slope, which is located on the northwest side of the island (Fig. 2). Vegetation recovery activities were carried out on this slope as described above. Exotic pasture grasses were seeded by helicopter after the locality-certified seedlings had become established; subsequently, the vegetation of the slope transitioned to a grassland community dominated by exotic pasture grasses in the next year [1], [9]. Then, in 2004, study plots were established, and one treatment group was fertilized once with fowl manure at 0.2 g/m<sup>2</sup>. In Japan, exotic pasture grasses have come to be used frequently for revegetation because of their rapid and homogeneous germination and growth. Recently, ecological conservation strategies call for the use of native species, except in urban areas. Therefore, the unintended introduction of non-native pasture grasses to Trino-o No. 3 landslide slope provides a valuable study site for examining the competition between native and non-native grass species.

Vegetation recovery in insolated ecosystems, such as on an island, should be carried out in ways that restore and do not disrupt the endemic ecosystem. The grassland vegetation established on Trino-o No. 3 landslide slope is undesirable, but it is noteworthy in the sense that it is difficult to design an exotic grassland in an insular ecosystem, even in the context of academic research. If we monitor the succession and the growth of each plant species, we will be able to obtain a rare data set for examining the effect of seeding exotic pasture grasses on landslide slopes on islands as a part of vegetation recovery efforts.

The strategy of using native plant species remains unproven: since their germination and growth are inferior to exotic pasture grasses, they

cannot rapidly achieve even ground surface cover. For future disaster prevention, it is desirable to transition from exotic pasture grasses to native species. However, exotic pasture grasses have been reported to prevent vegetation recovery: they prevent the establishment of trees [1], [4], change the direction of early succession [15], and may dominate the vegetation for long periods, e.g., 20 years [5], [8], [11], [15].

In the present study, we monitored the vegetation recovery on Trino-o No. 3 landslide slope of Mikura-jima Island for 10 years, from 2004 to 2013. In both non-fertilized and fertilized plots (fertilization was implemented in 2004 to support the growth of planted native seedlings which had inferior growth), we investigated the growth of locality-certified seedlings of native species, exotic pasture grasses and vegetation including newly invading trees and herbs.

## METHODS

### Site and Monitoring Plots

#### Site and Monitoring Plots

Mikura-jima Island is located ca. 180 km south of Tokyo in the Izu Islands. Over the past 5 years, the average annual precipitation was 2,910 mm and the average temperature was 17.9 °C. Trino-o No. 3 landslide slope is located at elevations ranging from

Table 1 History of vegetation restoration activities on Torino-o No. 3 landslide slope

Year	Work done
1995	Landslides and loss of vegetation caused by typhoon 9512 precipitation: 648.5 mm maximum wind speed: 67.8 m/s
1996	Start of transplanting trees (on the lower parts of the slope)
2000	Installation of founding fascines (1,100 m <sup>2</sup> , 19 steps) Transplantation of 800 <i>A. sieboldiana</i> seedlings (average of one seedling per square meter)
2002	Transplantation of 1,750 <i>Miscanthus condensatus</i> seedlings (average of 1.5 seedlings per square meter) Unexpected seeding of exotic pasture grasses by helicopter in fall
2003	Shift in vegetation to a grassland dominated by exotic pasture grasses
2004	Fertilization by hand to boost growth of planted native seedlings (fowl manure applied at 0.2 g/m <sup>2</sup> ) Establishment of monitoring plots

500 to 550 m above sea level with average slope of 27° and faces north. The bedrock around the site is andesite and basalt. Surrounding intact forest is dominated by evergreen broad-leaved trees, mainly *Castanopsis sieboldii*.

The vegetation recovery activities conducted at this site are listed in Table 1. The seeding of exotic pasture grasses occurred in 2002, and the amount of seeds and grass species is unknown; based on subsequent surveys, the species included bent grass (*Agrostis stolonifera* L.), a fescue (*Festuca* sp.) and a sericea lespedeza (*Lepedeza cuneata* (Dum. Cours.) G. Don).

In August 2004, seven plots of ca. 3 m × 2 m (5.5-7.4 m<sup>2</sup>) were established. To elucidate the effect of fertilization, we set three non-fertilized plots (C1 to C3) and four fertilized plots (F1 to F4). In subsequent years, growth and vegetation species were investigated in summer (early August).

#### Growth of transplanted species and exotic pasture grasses

Among the tree layer, transplanted trees of *A. sieboldiana* and other species were measured for plant height (H) and diameter at the base (D<sub>0</sub>), and the parameter D<sub>0</sub><sup>2</sup>H was calculated as an estimate of aboveground biomass. Since a phenomenon like self-thinning was observed in *A. sieboldiana*, we estimated the regression expression as follows:

$$1/x = a + by \quad (1)$$

where  $x$  is the mean plant density of *A. sieboldiana*,  $y$  is the mean individual D<sub>0</sub><sup>2</sup>H, and  $a$  and  $b$  are constants [16]. Data of other invading tree species were analyzed in the same way.

For the herbaceous layer, plant height was measured for *M. condensatus*, and the coverage percentage was determined for the exotic pasture grasses.

#### Vegetation survey

For the herbaceous layer, two layers were established based on height. The first herbaceous layer, taller than 1 m, was omitted from the survey because it comprised only *M. condensatus* growing along the fascines. For the second herbaceous layer, comprising exotic pasture grasses and invading native species, the coverage percentage of each species was determined.

Since several growth forms were observed in the second herbaceous layer, we classified the growth forms into four categories: b (branching form), e (erect form), l (climbing form) and t (tussocks). Each species was classified into one of these growth forms, and the coverage percentage for each growth form was summed.

Coverage percentage data were arcsine transformed prior to statistical analysis since they are considered to have a binomial distribution. Statistical operations were conducted by calculations in a spreadsheet (Microsoft Office Excel 2003).

## RESULTS

#### Growth of trees

Figure 3 shows the growth of *A. sieboldiana* and other invading trees over a period 10 years. In each of non-fertilized and fertilized plots, a phenomenon of self-thinning was confirmed in *A. sieboldiana*: the mean plant density decreased yearly, while individual D<sub>0</sub><sup>2</sup>H increased and tended to reach a

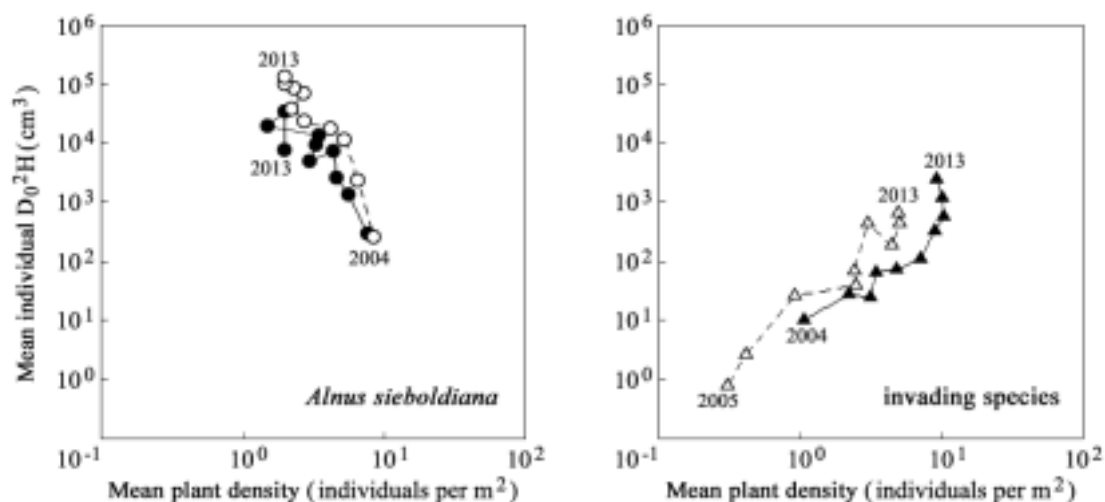


Fig. 3 Changes in the density and the average D<sub>0</sub><sup>2</sup>H per individual of *Alnus sieboldiana* in Torino-o No.3 landslide slope. The solid dots and solid line indicate non-fertilized plots, and the open dots and broken line indicate fertilized plots.

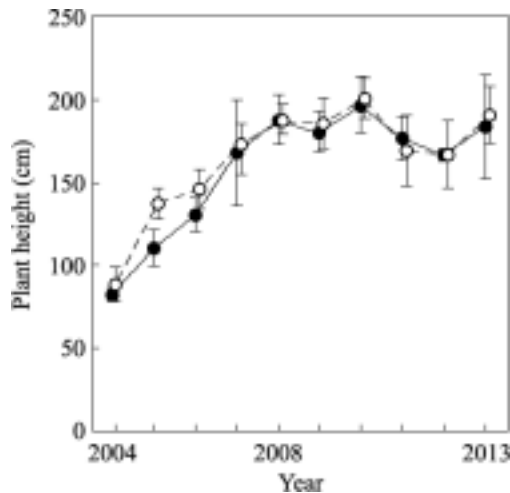


Fig. 4 Changes in the height of *Miscanthus condensatus* on the Torino-o No. 3 landslide slope. The solid circles and solid line indicate non-fertilized plots, and the open circles and broken line indicate fertilized plots. Error bars indicate  $\pm 1$  standard deviation (SD) ( $n=3$  for non-fertilized plots;  $n=4$  for fertilized plots).

plateau. Although individual  $D_0^2H$  tended to be greater in fertilized plots, analysis of co-variance detected no significant differences in the regression coefficients (F-test,  $p = 0.108$  and  $0.266$  for  $a$  and  $b$ , respectively) between the non-fertilized and fertilized plots.

In contrast, other invading trees increased in both density and individual  $D_0^2H$ , but the density appears to have reached a plateau in 2011 in each non-fertilized and fertilized plot. Invading trees were detected in 2004 in non-fertilized plots and in 2005 in fertilized plots. Both mean plant density and

individual  $D_0^2H$  tended to be smaller in fertilized plots, and significant differences were detected in 2011 and 2012 for mean plant density and in 2013 for individual  $D_0^2H$  (Wilcoxon's rank sum test,  $p < 0.05$ ).

#### Growth of *Miscanthus condensatus*, exotic pasture grasses and other invading herbs

Figure 4 shows the change in mean plant height of *M. condensatus*. Only in 2005, the mean plant height was significantly greater in fertilized plots than in non-fertilized plots (t-test,  $p < 0.05$ ). There were no significant differences in the following years, and plant height tended toward a plateau level in 2008 around which it fluctuated (from ca. 170 to 200 cm).

Coverage percentage of exotic pasture grasses is shown in Fig. 5. After 2005, the total coverage percentage of exotic pasture grasses decreased with the exception of in 2007, and no significant differences were detected between non-fertilized and fertilized plots (Wilcoxon's rank sum test). By species, *A. stolonifera* decreased yearly, while *Festuca* sp. and *L. cuneata* leveled off but showed decreases after 2008. *Festuca* sp. increased rapidly in fertilized plots in 2005 (the year after the fertilization), but no changes were observed in non-fertilized plots. In 2013, exotic pasture grasses were absent from non-fertilized plots. The remnants were still extant in one of the fertilized plots, but the coverage percentage was less than 1%.

#### Growth form of immigrated herbs

In the monitoring plots of Torino-o No. 3 landslide slope, volunteer seedlings of trees and composite species were representative of e (erect

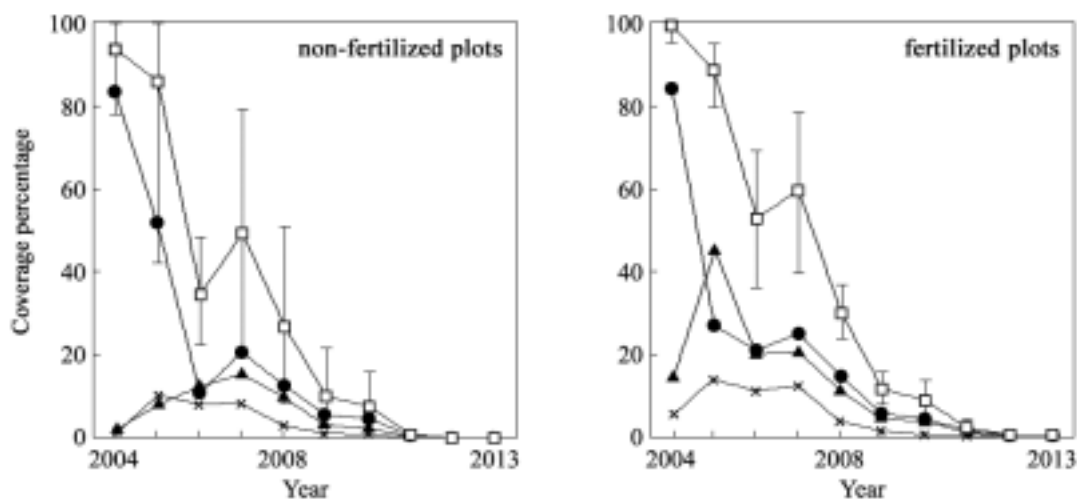


Fig. 5 Changes in the coverage of exotic pasture grasses on Torino-o No. 3 landslide slope.  $\square$ ,  $\bullet$ ,  $\blacktriangle$  and  $\times$  indicate the total, *A. stolonifera*, *Festuca* sp. and *L. cuneata*, respectively. Error bars indicate  $\pm 1$  SD ( $n=3$  for non-fertilized plots;  $n=4$  for fertilized plots).

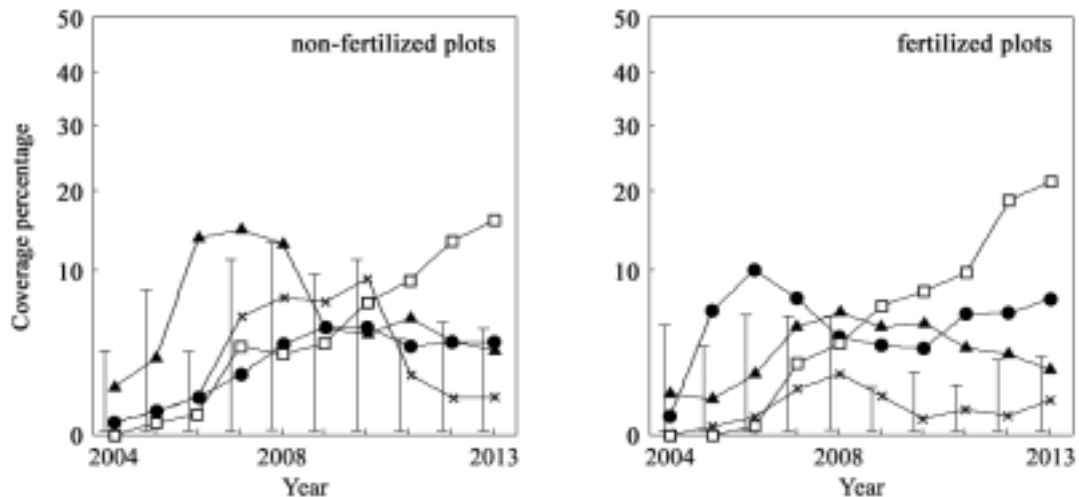


Fig. 6 Changes in the coverage of non-native plants in the herbaceous layer on the Torino-o No. 3 landslide slope with respect to growth form. ▲, ●, × and □ indicate erect form (e), climbing form (l), branched form (b) and tussock form (t), respectively. Each bar indicates the 95% confidence interval of difference between means based on Tukey's HSD.

form), *P. foetida* L. was representative of l (climbing form), *Viola grypoceras* A. Gray var. *hichitoana* (Nakai) F. Maek. was representative of b (branching form), and ferns such as *Stegnogramma pozoi* (Lag.) K. Iwats. were representative of t (tussocks form).

Figure 6 indicates the changes in coverage of invading herbs with respect to growth forms. In non-fertilized plots, e dominated from 2006 to 2008, but gave way to t. Significant differences were detected in 2006 ( $e > b, l, t$ ), in 2012 ( $t > b$ ), and in 2013 ( $t > e, b, l$ ) (Tukey's HSD,  $p < 0.05$ ). In contrast, in fertilized plots, l dominated from 2005 to 2007, but gave way to t. Significant differences were detected in 2005 and 2006 ( $l > b, t$ ), in 2009 and 2010 ( $e, l, t > b$ ), in 2011 ( $t > e, b; l > b$ ), and in 2012 and 2013 ( $t > l, e, b; l > b$ ) (Tukey's HSD,  $p < 0.05$ ).

## DISCUSSION

### Growth of *Alnus sieboldiana*, *Miscanthus condensatus* and exotic pasture grasses

In *A. sieboldiana*, the mean plant density decreased yearly, while the individual  $D_0^2H$  increased and tended to approach a plateau (Fig. 3). Analysis of co-variance did not detect significant differences in the regression coefficients between the non-fertilized and fertilized plots. Previously, we reported that individual  $D_0^2H$  was greater in fertilized plots than in non-fertilized plots based on data collected from 2004 to 2009 [1], but those differences diminished by 2013. This extended data set indicates that a single fertilization increased individual  $D_0^2H$  of *A. sieboldiana* with effects apparent for several years but diminishing in 10 years. However, the decrease in mean plant density cannot be explained, because the plots were not

covered completely by *A. sieboldiana*; that is, the self-thinning is not expected to be caused by competition between individuals. The Torino-o No. 3 landslide slope might be a severe environment for *A. sieboldiana*, as we observed lodging or slanting of trees in 2007 [1].

Average plant height of *M. condensatus* was significantly higher in fertilized plots than in non-fertilized plots only in 2005, the year immediately following fertilization. There were no significant differences in the subsequent years (Fig. 4). Therefore, the effect of fertilization was temporary for *M. condensatus*, lasting only a year in the present study.

Exotic pasture grasses tended to decrease yearly, and *Festuca* sp. increased rapidly in fertilized plots only in 2005 (the year following fertilization). Generally, excessive fertilization causes gramineous species to put out many offshoots and to form a large tussock, and then to decrease in density [14]. It is suggested that *Festuca* sp. is more susceptible to such effects of fertilization than *A. stolonifera* because the latter grows as a carpet-like community by putting down filiform stolons.

The length of time needed to transition from a community of exotic pasture grasses to one of native vegetation is said to range from over 5 to 10 years [5], [8], [11], [15], and over 20 years would be needed for harsh habitats, such as when the substrate is bare bedrock or wind-beaten bare ground [5], [11]. Simultaneous transplanting of exotic pasture grasses and trees is reported to accelerate the changes to the surrounding vegetation [11]. As a nitrogen-fixing pioneer tree, *Alnus sieboldiana* is hypothesized to improve the soil and protect herbaceous layer species by shading, thus facilitating the growth of *M. condensatus* and other invading native species.

### Change of Growth forms

Two phenomena are remarkable with regard to growth forms. First, different growth forms dominated the early period non-fertilized and fertilized plots; second, t (tussocks form) dominated after 10 years in all plots (Fig. 6).

In fertilized plots, l (climbing form) dominated in the early period. In contrast, e (erect form) dominated in the early period in non-fertilized plots. Climbing plants have an advantage in the competition: they can grow rapidly because they do not need to invest in supporting organs and can bring down other plants by winding or leaning [2]. Fertilization is reported to induce species competition within the community in the early period because it improves the growth of some nutrient-limited species [3]. Since fertilization temporarily increases the growth of *M. condensatus* and *Festuca* sp., severe competition could result within the herbaceous layer. The high abundance of climbing plants suggests that plants of other growth forms could hardly germinate or establish seedlings under such severely competitive conditions.

Plants of tussocks form in the study sites were mainly ferns: it is rare and unprecedented that the grasslands dominated by exotic pasture grasses give way to ferns in 10 years. The spores of ferns might have been carried by rainfall or wind from the surrounding intact forest, but their growth and propagation are not competitive enough to generate these shifts in numbers. In Fig. 6, only t (tussocks form) gradually and steadily increased during the 10 years of observation in both the non-fertilized and fertilized plots, and the decreasing exotic pasture grasses (*Festuca* sp. and *A. stolonifera*) are also of type t (tussocks form): this commonality suggests that ferns gradually replaced exotic pasture grasses by occupying the same niche in the herbaceous layer.

From the above, we can conclude that the community of exotic pasture grasses in this study was succeeded by native vegetation in 10 years irrespective of fertilization. Effect of fertilizing was temporary, and enhanced competition in herb layer.

### REFERENCES

- [1] Arase T, Okano T, Kimura T and Inoue S, "Influence of seeding exotic pasture grasses on the vegetation recovery of landslide slopes formed by typhoon 9512 in Mikura-jima Island, Izu Islands, Japan", J. of the Japanese Society of Revegetation Technology, Vol. 35, Feb. 2010, pp. 448-461
- [2] Bailey DR, "Weed control in tropical pastures", Tropical forege legumes, Skerman PJ, Cameron DG and Riveros F Eds. Rome: FAO, 1988, pp. 136-147.
- [3] Bazzaz FA, Plants in changing environment. Cambridge: Cambridge University Press, 1996, 320 pp.
- [4] Holl KD, Loik ME, Lin EH and Samuels IA, "Tropical montane forest restoration in Costa Rica: overcoming barriers to dispersal and establishment". Restoration Ecology, Vol. 8, 2000, pp. 339-349.
- [5] Imamoto H, Goto K, Shirai A and Washitani I, "Effect of the introduction of exotic grasses to solid rock slopes on the vegetation succession of the site". Ecology and Civil Engineering, Vol. 6, Aug. 2003, pp. 1-14.
- [6] Issiki N, Geology of the Mikurajima, Inambajima and Znisu districts. Yatabe: Geological Survey of Japan, 1980, 35 pp.
- [7] Japan Weather Association Ed., the yearbook of weather in 1996. Tokyo: the Printing Bureau, 1996, 265 pp.
- [8] Kodama S, Wada M, Shima K, Chiba K, "Effects of different introduced plant species on invasion and establishment of other plant species in the artificial slopes". J. of the Japanese Society of Revegetation Technology, Vol. 28, Aug. 2002, pp. 139-142.
- [9] Kyoju no Kai Ed., Saving earth (1) Practices to restore nature in Mikura-jima Island. Tokyo: Kyoju no Kai, 2004, 48 pp.
- [10] Loope LL, Hamann O and Stone CP, "Comparative conservation biology of oceanic archipelagoes -Hawaii and the Galapagos". BioScience, Vol. 38, 1988, pp. 272-282.
- [11] Nakano Y and Futami T, "Observation on plant succession at the past cut slope landscaping sites in Miyakejima Island". J. of the Japanese Society of Revegetation Technology, Vol. 30, Nov. 1987, pp. 383-388.
- [12] Ohba T, "Die Vegetation von Mikura-Insel leight 200km sudlich von Tokyo". Bull. of Kanagawa Prefectural Museum, Vol. 1, Feb. 1971, pp. 1-53.
- [13] Ono M, Wildlife in solitary island. Tokyo: Iwanami Shoten, 1994, 239 pp.
- [14] Sato K, Nishimura N and Takahashi M, Eco-physiological studies on the maintenance of density of forage crop swards, I". Grassland Science, Vol. 11, Jun. 1965, pp. 14-19.
- [15] Swada Y, Kubota K, Yashiro Y, Nishiwaki A and Tsuda S, "Vegetation established by the aerial seeding of pasture plants after a forest fire in a secondary forest in Shiga Prefecture, Japan". Japanese J. of Conservation Ecology, Vol. 13, May 2008, pp. 29-36.
- [16] Yoda K, Forest ecology. Tokyo: Tsukiji Shokan, 1971, 331 pp.

# **FUNDAMENTAL PROPERTIES AND ANALYSIS OF WATER QUALITY IN A RESERVOIR AFFECTED BY LITTLE WATER USE AND TEA PLANTATION**

Masaaki Kondo<sup>1</sup> and Takamitsu Kajisa<sup>2</sup>

<sup>1,2</sup>Graduate School of Bioresources, Mie University, Japan

## **ABSTRACT**

There are many reservoirs in trouble on eutrophication problem. This paper focused on a reservoir whose water has rarely been used for agriculture or drinking. The many tea plantations distributed in the dam basin are suspected to be the cause of the reservoir's eutrophication. It was investigated that eutrophication components such as nitrogen and phosphorus and how they relate to the tea plantations in the basin. With reference to phosphorus, trophic levels were determined with Vollenweider plots and Carlson indices. With reference to nitrogen, a field survey was carried out to investigate the properties of sulfate and then sulfate concentration was analyzed with a simple model. The various activities to improve the water quality of the reservoir are introduced. In conclusion, the dam reservoir water is typically eutrophic, and might be affected by the fertilizer in tea plantations. The motion of surface water in the dam reservoir is similar with the property of river, and then the sulfate concentration was analyzed with simple model.

*Keywords: Reservoir, Eutrophication, Tea plantation, Sulfate, Improvement activities*

## **INTRODUCTION**

The K dam reservoir in the north of Nara Prefecture, Japan, has an eutrophication problem causing a lot of blue-green algae to bloom every summer and needs to be protected from mold odors in the water because this water is used as drinking water. The many tea plantations distributed in the dam basin are suspected to be the cause of the reservoir's eutrophication.

It has been reported that the overfertilization to almost of the domestic tea plantations resulted that the surface water and groundwater surrounding the tea plantations had problems on water quality besides the K dam basin [1]-[3]. In order to improve the situation, many researchers tried to reduce the amount of applied fertilizer and improve the fertilization method. A rare successful water quality improvement of groundwater and river water was reported recently [4]. The K dam management office also has taken various steps to combat the water quality problem in the reservoir. For example, they have mown weeds on the slopes surrounding the reservoir, planted purification grasses around the tea plantations, planted buckwheat crops instead of tea tree crops, and created a floating island with aquatic plants for the purification of reservoir water, among other activities.

In this paper, the author gives a basic overview of the water quality of the K dam reservoir and discusses the concrete actions that have been taken to improve it. Of particular interest to us are eutrophication components such as nitrogen and

phosphorus and how they relate to the tea plantations in the basin. With reference to phosphorus, trophic levels were determined with Vollenweider plots and Carlson indices and performed comparisons with other domestic reservoirs, and with reference to nitrogen, a field survey was carried out to investigate the properties of sulfate and then sulfate concentration was analyzed with a simple model.

## **METHOD**

### **Parameters of Dam Reservoir and Basin**

Table 1 shows the parameters of the K dam reservoir and its basin. The K dam was built as a concrete gravity dam in 2001 and, according to the management officer, the sediment level at the bottom of the reservoir remains low even ten years after the completion. Water from the reservoir has rarely been used for agriculture or drinking in the past and a downturn in tea leaf consumption has significantly lowered what little water use there originally was. Ideas and activities for increasing the water usage of the reservoir are required besides as follows; water supply stations around the dam are available in the form of automatic vending machines, and farmers can buy reservoir water with coins and pour it into the tanks of pickup trucks to use the water more conveniently.

The basin area of the reservoir is 18.9 km<sup>2</sup>, the



Table 1 Parameters of the K dam and basin

Parameters	Value
Type of dam	Concrete gravity dam
Basin area	18.9 km <sup>2</sup>
Total reservoir capacity	$5.6 \times 10^6$ m <sup>3</sup>
Water surface area	0.329 km <sup>2</sup>
Mean depth	17.0 m
Residence time	0.31 year
Phosphorus load in 2008	683,553 gP•yr <sup>-1</sup>
Phosphorus load in 2009	997,690 gP•yr <sup>-1</sup>
Phosphorus load in rain*	15,500 gP•yr <sup>-1</sup>

\*value estimated by author

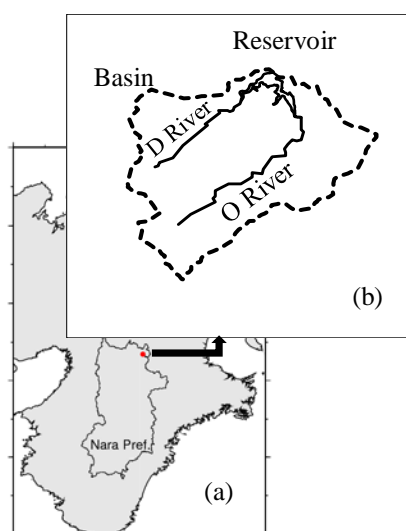


Fig.1 Location of the (a) K dam reservoir and (b) basin

total reservoir capacity is  $5.6 \times 10^6$  m<sup>3</sup>, and the water surface area is 0.329 km<sup>2</sup>, as shown in Table 1. Since the K dam was originally intended for irrigation and the provision of drinking water, the basin area and the reservoir capacity are small compared to dams with other purposes.

Two main rivers, D River and O River, flow into the dam reservoir, as shown in Fig. 1. A discharge channel M also flows into the reservoir between these main rivers. This channel is not included on the map due to its small discharge, but information pertaining to it is mentioned as necessary.

## Data

Data used in this paper were provided by the dam office and the part of data was measured and analyzed by the author. Dam control items were water temperature, inlet, and outlet flow, and weather data were precipitation and air temperature.

## Determination of Trophic Level in Reservoir

As nutrition issues have been linked to phosphorus, the trophic level in the reservoir was determined using a Vollenweider plot with phosphorus data. Trophic state index (TSI) was used as an additional index.

There are various methods of determine the trophic level, and in this work the Vollenweider method was selected due to its popularity [5]. There are two ways to make a Vollenweider plot: one, a flame method based on unit load data, and two, a method based on actual observed concentration and discharge data. The latter method was adopted and phosphorus concentration data was used from between 2008 and 2009.

TSI values were calculated using chlorophyll *a* and total phosphorus due to a lack of transparency data on the reservoir.

## Field Survey on Sulfate

Tea trees prefer sulfur and can grow in suitably acidic soil [6], [7]. Ammonium sulfate is often top-dressed into tea plantations during tea-picking season. Ammonium sulfate is the major quick-impact fertilizer described by (NH<sub>4</sub>)<sub>2</sub>SO<sub>4</sub> as a chemical formula [7]-[9]. Sulfur component circulates through the primary production process and accumulates in the sediment as hydrogen sulfide [10]. Fertilizer run-off from tea plantations causes severe water quality problems that have a national impact, which is why the author focuses on the sulfate in water here.

Sulfate is not measured by the dam office, so the author measured it specifically for this study. A monthly field survey was conducted between August and December 2011 during the formation of thermo-stratification.

Since the reservoir water is not used in great quantities, water turnover is small, so the motion of the reservoir water could be regarded as the same as river water during the formation of stratification.

The water in the field survey was sampled and measured at the surface layer in the reservoir and at the points where two rivers and the discharge channel flow into the reservoir. Water temperature, pH, dissolved oxygen, and electric conductivity were measured onsite as soon as sampling. Water samples were taken and sulfate was then measured in our laboratory. Other observed items included inorganic phosphoric acid, turbidity, chemical oxygen demand, and inorganic nitrogen such as nitrate-nitrogen, nitrite-nitrogen, and ammonia-nitrogen.

## RESULTS AND DISCUSSION

### Properties of Water Quality in the Reservoir

Figure 2 shows the changes of water temperature, pH, chlorophyll *a*, and dissolved oxygen (DO) with time for each layer in the reservoir. The water temperature results show that while the reservoir water was stratified in during summer, winter corresponded approximately to circulation.

The amount of phytoplankton in the summer increased at the sunlit surface layer of the reservoir, as shown in the results for chlorophyll *a*. Carbonic acid assimilation by phytoplankton caused the high value of pH and super saturation of DO. Upon rearranging the data in terms of the relationship between the water temperature and kinds of phytoplankton, while Bacillariophyceae tended to be dominant in water with a temperature below 15 degrees, Cyanophyceae was dominant over 15 degrees. This is in agreement with the general consensus that low water temperature is adequate for Bacillariophyceae while Cyanophyceae grows at high temperature [11], [12].

### Trophic Level in the Reservoir

Figure 3 plots data of other Japanese reservoirs [13] as well as a Vollenweider model of the K dam reservoir. The K dam reservoir was plotted using information from the 2008–2009 circulation seasons, and as shown, was obviously eutrophic.

Furthermore, the K dam reservoir was classified using the trophic state index (TSI) proposed by Carlson [14]. Data on chlorophyll *a* and total phosphorus at the surface layer between June and August was only used to determine TSI due to the lack of transparency data. The trophic level of the reservoir was classified as rank E in terms of the highest frequency, as shown in Table 2. Rank E was also given to the eutrophic level in the Vollenweider model, as in [14], [15].

The land use for each basin is shown in Fig. 4. Although the areas of the tea plantations are very small compared to the basin areas, a typical turbid water problem caused by blue-green algae occurred every summer. Since tea tree crops are grown commercially on the mountainsides, cultivation conditions could be responsible for fertilizer running off from the plantations. Figure 5 shows the change of phosphorus load calculated from the concentration in each river. Phosphorus load peaks appeared in April and October. According to the

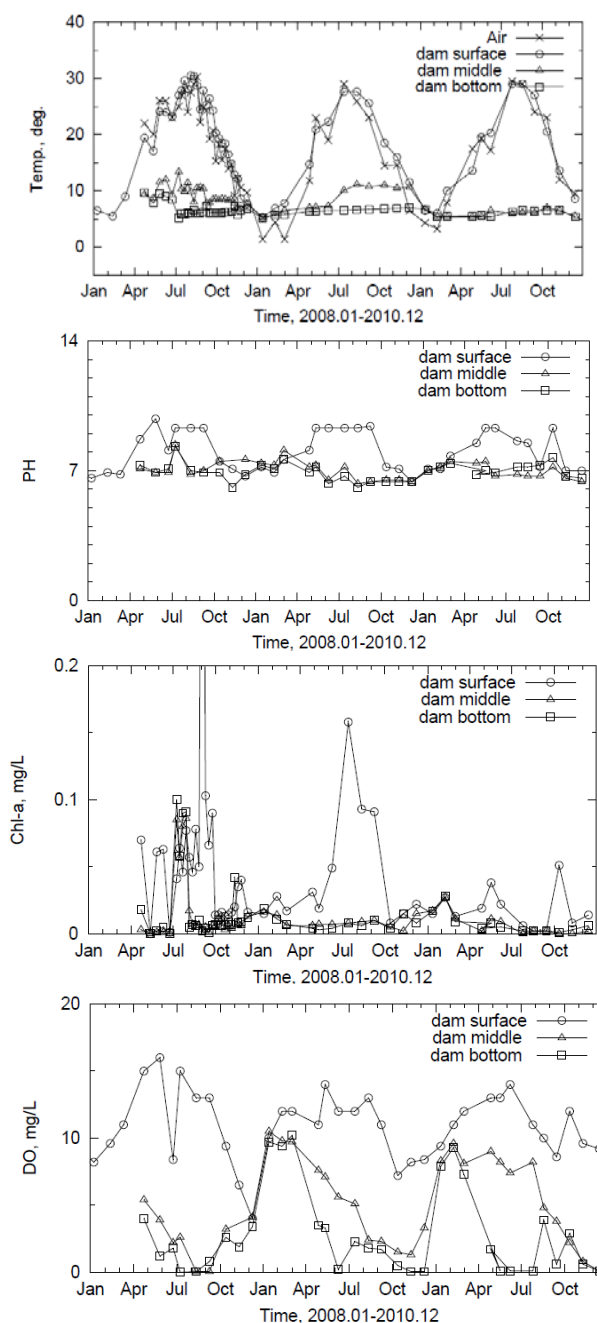


Fig.2 Changes of water temperature, pH, chlorophyll-*a*, and dissolved oxygen with time

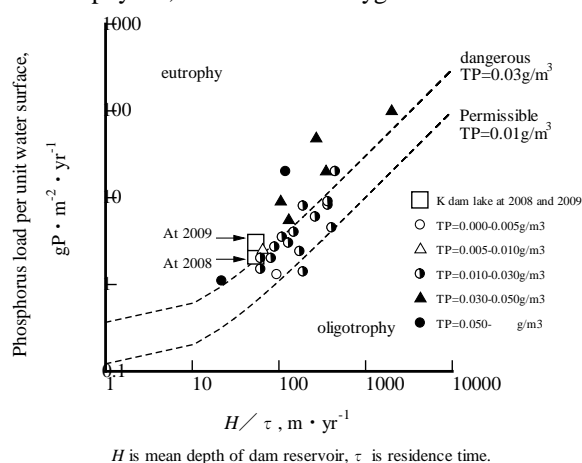


Fig.3 Plot of Vollenweider model on dam reservoirs

Table 2 Frequency of trophic state index of the K dam reservoir

Rank	Score of TSI	Frequency		Vollenweider model [15]
		TSI(chlorophyll <i>a</i> )	TSI(Total Phosphorus)	
A	Below 37	1	1	Oligotrophy
B	37 - 47	0	0	Oligotrophy - middle
C	47 - 53	0	1	Middle
D	53 - 61	0	2	Middle - eutrophy
E	Over 61	7	4	Eutrophy

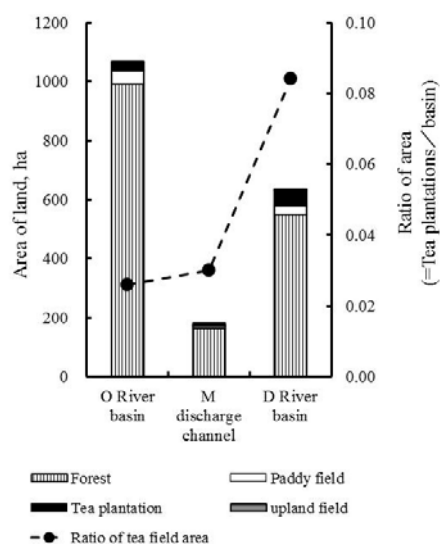


Fig.4 Land use for each basin and area ratio of tea plantations compared with basin (rearranging data provided by dam office)

standard of fertilizer for agricultural crops [16], base fertilizer is spread in the period running from late February through the middle of March and in early September. Rapeseed oil cake, an organic manure, is often used as a base fertilizer. It takes three weeks for rapeseed oil cake to decompose. The peaks of phosphorus load shown in April and October correspond to the decomposing stage of rapeseed oil cake. In general, phosphorus is absorbed in the soil and kept in the field. However, the sloped nature of tea tree fields causes soil particles with phosphorus to run off from the field and flow into the reservoir. While the soil in the field retains the nitrogen component in the form of ammonium, ammonium sulfate changes into nitrate nitrogen relatively quickly and the nitrogen component might run off

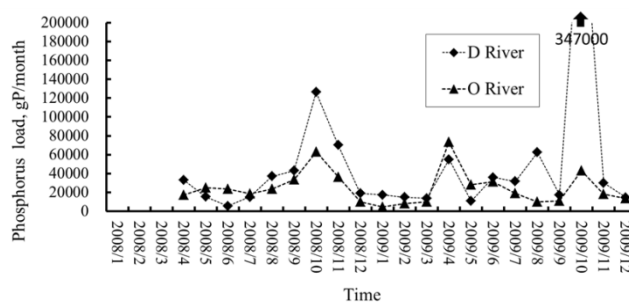


Fig.5 Changes of phosphorus load in river water with time

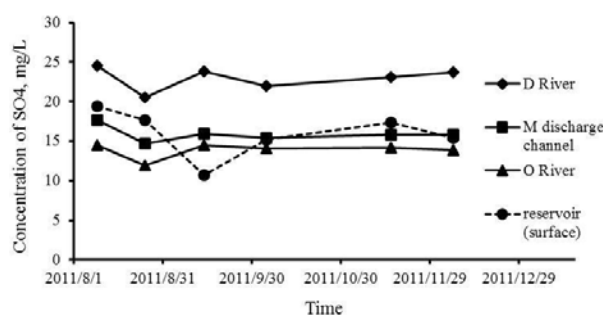


Fig.6 Changes of sulfate concentration observed in dam reservoir and rivers with time

from the tea plantation. As a result, ammonia fertilizers such as ammonium sulfate contribute to the water quality problem in the reservoir.

Attempts at improving the water quality in the reservoir include planting certain grasses around tea plantations that prevent soil from running off and placing floating plant islands in the reservoir itself to absorb nutrients.

### Sulfate Concentration and Its Analysis in Surface Layer

#### Results of field survey

Figure 6 shows the change of sulfate concentration observed at the reservoir's surface and at the rivers. The concentration of sulfate is larger in D River than the other rivers, as shown. According to Fig. 4, which illustrates the land use for each basin, the area ratio of a tea plantation compared with the basin area is 8.4 % on the D River basin, 3.0 % on the M discharge channel, and 2.6 % on the O River basin. Therefore, in light of the nutrient load mechanism discussed in previous section, the large ratio of the tea area on the D River basin seems to be connected to the high concentration of sulfate in the D River water.

Figure 7 shows the relationship between sulfate

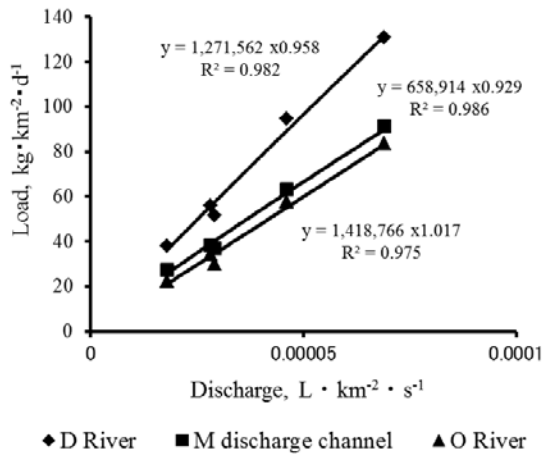


Fig.7 Relationship between sulfate load and river discharge

load  $L$  and discharge  $Q$ . The  $L$ - $Q$  values for each basin are calculated as

$$L_1 = 1,271,562 \cdot Q_r^{0.958} \quad (1)$$

$$L_2 = 658,914 \cdot Q_r^{0.929} \quad (2)$$

$$L_3 = 1,418,766 \cdot Q_r^{1.017} \quad (3)$$

where  $L_1$  is the load of sulfate in D River,  $L_2$  is the load of M River,  $L_3$  is the load of O River, and  $Q_r$  is the river discharge.

Since the concentration of sulfate increases along with the area of a tea plantation, it is reasonable to assume that load might run off from the plantations.

#### Analysis of sulfate concentration

Sulfate concentration was analyzed using a simple water quality model defined with river water inlet and reservoir outlet as shown in equation (4). This simple model was used because, although the author originally intended to use a circulation model of sulfur in water without an input-output system, the author wanted to investigate the rough validity. Little water use of the reservoir and reservoir stratification means that reservoir properties will remarkably agree with those of a river. Furthermore, biological processes and vertical mobility could be conversely estimated from the difference between the calculation result and the field survey measurements.

Water temperatures at each depth were measured at an intake tower of the reservoir and vertical profiles of water temperatures were used to estimate

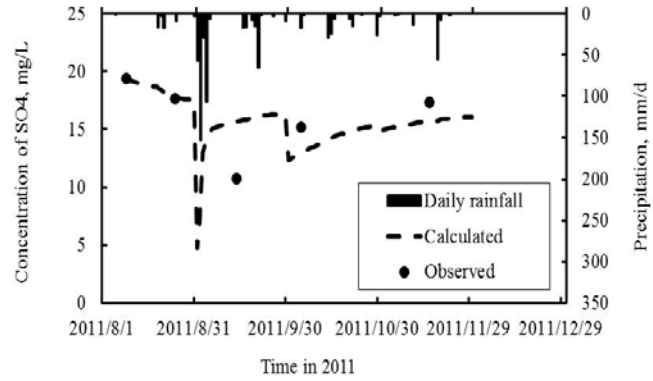


Fig.8 Comparison with calculated and observed data on concentration of sulfate

the depth of the surface layer as stratification depth. The reservoir was assumed to be stratified between August and December. Since the layer depth was varied with time, the model equation was naturally considered with the depth change.

$$\frac{d(VC)}{dt} = L_1 + L_2 + L_3 - QC \quad (4)$$

where  $C$  is the concentration of sulfate at the reservoir surface layer,  $V$  is the water volume of the surface layer given by multiplying water surface area by the depth of the surface layer,  $t$  is time, and  $Q$  is reservoir outlet.

Figure 8 shows the calculation result of sulfate concentration and daily rainfall. Sulfate concentration in the surface layer of the reservoir was calculated during stratification.

When the simple model was used to analyze the sulfate concentration, the calculated concentration value was in good agreement with the observed value. Our simulation was performed after the concentration of sulfate decreased in early September, and the concentrations of sulfate gradually increased until November. Concentration was quite low in early September. It seems that large typhoon No.1112 (TALAS) passed through the area at that time, and there was heavy rainfall.

#### CONCLUSIONS

A great deal of effort has been made by many Nara Prefecture officials and members of land improvement organizations to improve the water quality in the K dam reservoir. The author and laboratory members have also participated in these improvement activities as volunteers. In this paper, the fundamental properties of the K dam reservoir are reported using examples from the eutrophication mechanism and various water quality improvement methods.

The surface layer water of the K dam reservoir indicated approximately pH 10 during summer. Carbonic acid assimilation by much phytoplankton caused super saturation of dissolved oxygen in addition to high pH.

The value of mean depth divided by residence time was 55 m per year. Phosphorus load per unit water surface was  $2.1 \text{ g} \cdot \text{m}^{-2} \cdot \text{yr}^{-1}$  in 2008, and  $3.1 \text{ g} \cdot \text{m}^{-2} \cdot \text{yr}^{-1}$  in 2009. The TSI was the rank E level.

The reservoir water is typically eutrophic, and might be affected by the fertilizer in tea plantations.

The area ratios of tea plantations for each basin were less than 10 %. The concentrations of phosphorus and sulfate in rivers were described in order of the area ratios.

The motion of surface water in the dam reservoir is similar with the property of river, and then the concentration was analyzed with simple model.

It was observed that much rainfall brought about by typhoons decreased the concentration of sulfate and then the concentration gradually increased. The change of the concentration was simulated with the simple model.

## ACKNOWLEDGEMENTS

The author is indebted to the local public officials and dam management office for providing their cooperation and the valuable data for the study.

## REFERENCES

- [1] Yamamoto T, Nakasone H, Kuroda H and Kato T, "Diffuse nitrogen load pollution from collective tea field -case in Makinohara plateau, Shizuoka Prefecture-", J. of Japan Society on Water Environment, Vol.29, No.11, 2006, pp.745-748.
- [2] Ii H, Hirata T, Tanaka T, Nishikawa M, Nakajima T, and Umehara K, "Spring pond and river water chemistries derived from a tea plantation in central Shizuoka Prefecture", Proceedings of hydraulic engineering, JSCE, 44, 2000, pp.1155-1160.
- [3] Takeda I, Kunitatsu T, Kihara Y, and Mori Y, "Estimation of runoff pollutants of nitrogen, phosphorus and cod from a small catchment of tea field", J. of Japan Society on Water Environment, Vol.25, No.9, 2002, pp.565-570.
- [4] Hirono Y, Watanabe I, and Nonaka K, "Trends in water quality around an intensive tea-growing area in Shizuoka, Japan(Environent)" , Soil science and plant nutrition, Vol.55, No.6, 2009, pp.783-792.
- [5] Vollenweider R. A., "Advances in defining critical loading levels for phosphorus in lake eutrophication", Mem. Ist. Ital., Idrobiol., Vol. 33, 1976, pp.53-83.
- [6] Konishi S, "Technical system of agriculture : soil and plant nutrition" , Rural Culture Association, 1987, p.177.
- [7] Yoneyama T, Hasegawa I, Sekimoto H, Makino A, Matoh T, Kawai S, and Morita A, "Plant nutrition and fertilizers" , Asakura Publishing , 2010, pp.172-176.
- [8] Ishigaki K, " Studies on the nutritive characteristics of tea plant" , Bulletin of the Tea Research Station, Ministry of Agriculture and Forestry, 14, 1978, pp.1-152.
- [9] Ishigaki K, "Evaluation of ammonium nitrogen and nitrate on the tea plant as nitrogen source (part 1):on the concentration of nitrogen" , Tea Research Journal, 35, 1971, pp.57-64.
- [10] Wetzel R G, "Limnology, 2nd ed.", Saunders College Publishing, 1983, p.327.
- [11] Moss B, " Ecology of fresh waters " , Blackwell Scientific Publications, 1980, pp.74-75.
- [12] Water Resources Environment Technology Center, "Useful reading for water environment of dam reservoir" , Sankaido Publishing, 2002, p.64.
- [13] Morikita Y and Miura S, "Predictive techniques for eutrophication in dam reservoirs", Civil engineering journal, Vol.25, No.4, 1983, pp.181-186.
- [14] Japan Society of Civil Engineers, "The collection of hydraulic formulae", Maruzen Publishing, 1986, p.355.
- [15] Vollenweider R A, "Input-output models with special reference to the phosphorus loading concept in limnology" , Sch. Zeit. Hydrologic, Vol.37, 1975, pp.53-84.
- [16] Nara Pref., "Standard of fertilization management for agricultural crops", 2009, p.31.

## **SMALL WATER DISTRIBUTION SYSTEM DISINFECTION BY-PRODUCT CONTROL: WATER QUALITY MANAGEMENT USING STORAGE SYSTEMS**

Sandhya Rao Poleneni<sup>1</sup> and Enos C. Inniss<sup>2</sup>

<sup>1</sup>Ph.D. student, University of Missouri-Columbia, USA; <sup>2</sup>Faculty, University of Missouri-Columbia, USA

### **ABSTRACT**

Disinfection, a vital part of a drinking water treatment, using chlorine is the most widely practiced process in the world. The Stage-2 Disinfectant and Disinfection By-Product regulations force water utilities in the US to be more concerned with their distributed water quality. Compliance requires changes to their current operational strategy. Storage system management is an important part of the operational strategy of small scale utilities. This study quantifies changes in DBP formation and chlorine decay in storage systems under varying operational parameters such as mixing, contact time, and water movement using a physical model (Pipe Loop) of a distribution system. Effective operation of storage systems can yield greater than 30% decrease in DBP formation in distribution systems and maintain chlorine residual for a 50% longer period.

*Keywords: Clearwell, Storage Tank, Pipe Loop, Trihalomethanes, Chlorination*

### **INTRODUCTION**

Disinfection and distribution of treated water are vital parts of a drinking water utility's operation. Though they may seem like two completely different processes, their operation strategy needs to be complementary in order to maintain minimum disinfectant residual as part of the distribution system water quality management. Chlorination is one of the most widely used disinfection processes in water treatment plants because chlorine is a very effective disinfectant and is relatively easy to handle; the capital costs of installation are low; it is cost effective, simple to dose, measure and control; and, it has a reasonably prolonged residual [1]-[3]. Despite the benefits of chlorine, halogenated disinfection by-products (DBPs) are formed due to the interaction of aqueous free chlorine with natural organic matter (NOM), like humic substances, present in water [4], [5].

Small-scale water utilities are known to use different operational strategies to overcome their physical (infrastructure, source water quality, distribution system layout, storage system design etc.) and financial constraints to meet the water demand and provide consistent quality water to all its customers. In other words, though known to have infrastructural constraints small-scale utilities tend to benefit a lot by making necessary changes to the way they operate each of their units based on site-specific conditions and the formation kinetics of the contaminant in question. Water treatment process operation to maintain water quality with respect to numerous contaminants in distribution systems irrespective of seasonal changes and fluctuating

water demand is a complex process and hence requires a balanced approach. With the Stage-2 Disinfectants and Disinfection By-Product Rule regulation compliance date approaching (October 2014) many small-scale utilities in US are adopting techniques to balance protection against microbial risks with the risks posed by harmful by-products [6]-[8].

Storage tanks are an important part of infrastructure as well as the operational strategy of small scale utilities [9]-[15]. Many small scale water utilities are shut down for a part of the day and these tanks act as a reservoir of treated water at the treatment plant (clearwell) or in the distribution system (tower or stand-pipe) to meet the water demand of the town. They hold immense potential to either improve or degrade the water quality provided by the utility. External factors like atmospheric temperature, mixing conditions, size and shape of the tank, location of inlet and outlet valves, wall coating etc. play a vital role in quality of water coming out of the storage tanks [9]-[15]. The volume of water entering and leaving the tank and timeline of these events are the most important factors that dictate successful operation of storage tanks. Therefore understanding the changes in chemistry of water while in the storage systems can help utilities utilize these structures to maintain or improve the quality of water provided to their customers.

### **METHODS**

This research was conducted using a physical model of distribution system (Pipe Loop) built at the



City of Columbia, Missouri (USA) Water Treatment Plant using 10.16 cm (4 in) PVC pipe [16]. The scenarios discussed in this paper are: Normal Run, Storage Tank in Distribution System Run, Clearwell with proper mixing and fill-drain cycles Run and Clearwell without mixing and fill-drain cycles Run.

Normal run is used as the control or baseline for comparing other scenarios and is based on typical operation of a drinking water treatment process which involves treated water with disinfectant residual entering the distribution system. In order to simulate a Normal Run (NR), finished water from the City of Columbia water treatment plant (chlorinated water before ammonia addition) is allowed to enter the Pipe Loop via the Water Tank attached to it (Fig. 1). The water was recirculated in the looped system for 7 days with water samples collected at daily intervals.

In order to simulate storage tank in a distribution system scenario in the Loop, the finished water was allowed to fill the Loop via a storage tank attached to it. Once both tank and Loop were full, the valve between them was shut and the water was allowed to stay in the tank and recirculate in the Loop for 2 days. On day 2, the valve between tank and Loop was opened and one-third of volume of the tank was drained through the loop. The tank was filled to its full capacity at high pressure to ensure proper mixing. The process of draining one-third volume and refilling it with new water was continued for 4 more days before the Loop and the tank were drained completely to start the process all over again. Water samples were collected from the tank as well as the Loop at regular intervals. Samples were collected before draining and after refilling at both locations.

For clearwell with proper mixing and fill-drain cycles, the finished water was allowed to fill only the tank attached to the Loop on day 0 with high pressure and 1/3<sup>rd</sup> of the tank was drained after 24 hours using a valve at the bottom of the tank. The tank filled to its full capacity at high pressure to ensure proper mixing. The process of draining one-third volume and refilling it with new water was continued for 4 more days before the tank was drained completely to start the process all over again. Water samples were collected before draining and after refilling the tank at regular intervals.

For clearwell without mixing and fill-drain cycles, the finished water was allowed to fill only the tank attached to the Loop on day 0 and the water was allowed to sit in the tank for 7 days without any mixing or draining and filling with new water. Water samples were collected from the tank at regular intervals.

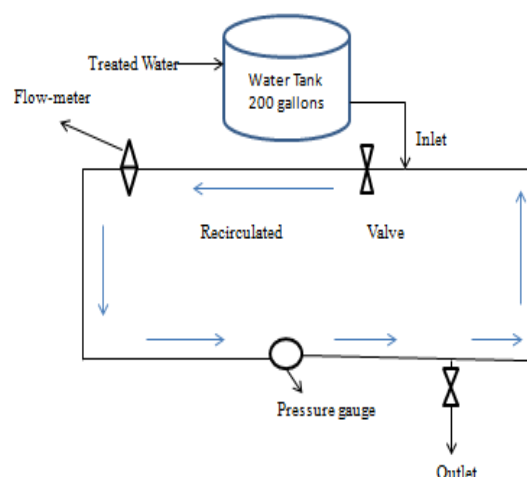


Fig. 1: Schematic of the Pipe Loop used in experiments to determine effects of distribution system management. Water tank shown was used to simulate clearwell and storage tank

All of the collected samples were tested for free and total chlorine residual, total organic carbon (TOC), pH, UV<sub>254</sub> and TTHM as a function of time over a period of 10 months. The TTHM concentration entering the Pipe Loop averaged 40 µg/L (half of MCL limit of 80) and pH averaged 8.5, which is considerably high for a chlorinated system. UV<sub>254</sub> was measured using Varian Cary 50 UV-Visible Spectrophotometer following Standard Method 5910 B [17]. Free and total chlorine residual was measured using appropriate DPD methods (Hach methods 8021 and 8167 [18] equivalent to Standard Method 4500-Cl G [17] and a Hach pocket Colorimeter II (Cat # 5870000) designed for collecting on-site measurements. TTHM concentrations were analyzed with a Varian 3800 Gas Chromatograph (GC) equipped with a Saturn 2000 Mass Spectrometer (MS) for detection following an analysis method similar to that described by EPA method 524.2 [19] and Standard Method 6232 C [17] was used. Total Organic Carbon (TOC) was measured using the combustion Infrared Method (Standard Method 5130B [17]). Statistical analysis of the data collected was done using MiniTab to ensure soundness of the conclusions. Analysis of Variance (ANOVA) and Paired t-tests were conducted on all the data with 90-99% level of significance.

## RESULTS AND DISCUSSION

### Normal Run Vs. Storage Tank In Distribution System Run

Water chemistry in storage systems is unique in many ways. Therefore, results are explained as

comparisons with a Normal Run (Fig. 2). This analysis is intended to statistically explain the effect of storage tank operation on water quality in terms of chlorine residual and trihalomethane concentrations.

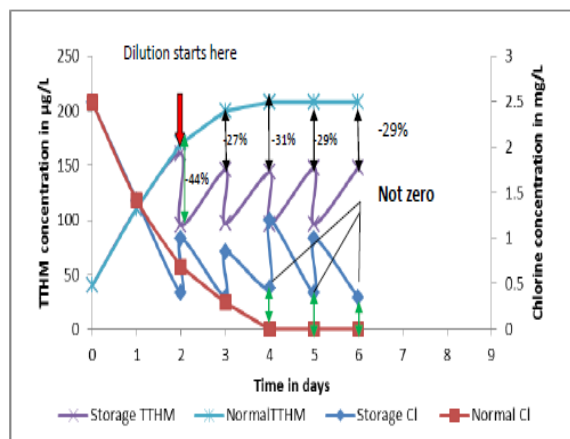


Fig. 2: Storage Tank run vs. Normal run chlorine residual and TTHM trends. The percent differences between the TTHM formation and chlorine decay values are also noted.

Data from the Loop and storage tank shows that the decay of chlorine residual and formation of TTHMs over time is dramatically different in Storage Tank run when compared to Normal Run. Relative to a Normal Run dilution by adding new water to the Storage Tank tends to decrease the concentration of TTHMs formed on average by 34% over a 6-day operation. In addition to that, this dilution helped maintain minimum residual in the system without additional chlorine unlike during the Normal Run when by the end of day 3, chlorine residual in the system decreased to zero. The TTHM concentration during the Storage Tank Run seems to be between 143 and 148 µg/L after 24 hours following the dilution for 4 days (compared to 200 µg/L for the Normal Run). This range depends on the concentration of TTHMs formed in the system before starting the dilution on day 2, which in turn depends on number of days the water is stored before the dilution process started. It is statistically proven with 99% level of confidence that these two strategies produce different trends in chlorine decay and TTHM formation over time under constant wall conditions.

The adverse effect of increased contact time and chlorine dosage on TTHM formation in the distribution system is explained in detail in our previous research [16], [20]. Therefore, storage time before the dilution process takes effect and contact time in the tank play an important role in water quality management in storage tanks. The stabilization effect of the dilution process is unique and can be a blessing to utilities if the tank is

operated properly. The adverse effects of biofilm formation, dead spots in the tank due to stratification and inappropriate positioning of inlet and outlet on water quality are extensively studied subjects. Hence it can be concluded that operation of the tank which involves constant mixing to avoid temperature stratification issues, proper maintenance in terms of coating to ensure absence of biofilm, optimal location for inlet and outlet, minimizing storage time by draining a considerable volume of water at short and regular intervals can be the difference between tanks improving versus degrading water quality in distribution systems.

### Clearwell With And Without Mixing And Fill-Drain Cycles

Clearwell is a storage tank located on the premises of a treatment facility and is used to store finished treatment water before it is allowed to enter the distribution system. Though the concept of storage time before dilution does not apply to clearwell as the finished water from the filtration unit directly enters the clearwell. Rather the effect of mixing, fill-drain cycles, and physical condition of the clearwell become predominant. For a large clearwell at any given time the mixed age of the water in the clearwell can be 2 to 4 days which demonstrates the adverse effect of increased contact time with the disinfectant. The difference between having and not having proper mixing and fill-drain cycles during storage time is shown using the data produced by two scenarios (Fig. 3). Storage tank data of Normal Run represents a system with no mixing and filling cycles whereas Tank Storage Run represents a system with complete mixing and regular filling cycles. Constant physical conditions are maintained in both systems.

Comparison of data from the two runs shows that the decay of chlorine residual and formation of TTHMs over time is dramatically different. Dilution with new water in the Storage systems Run tends to decrease the concentration of TTHMs formed on average by 30% over the 6-day operation relative to the Normal Run. The dilution process helped increase the chlorine residual in the Storage systems Run by 65% on day 4 and by 113% on day 5 relative to the Normal Run. On day 6 chlorine residual in the Normal Run decreased to zero when about 1.4mg/L is still left in the Storage system Run. It is statistically proven with a 99% level of confidence that these two strategies produce different trends in chlorine decay and TTHM formation over time under constant wall conditions.

These differences in TTHM concentration and Chlorine residual between these two strategies are solely due to mixing and filling conditions. Therefore, it can be concluded that, in the case of clearwells, the mixing and filling conditions play an

important role in management of water quality. Storage time before entering clearwell depends on the contact time of disinfectant requirements during filtration, therefore, it cannot be included in clearwell management. When operated under proper mixing and filling conditions, the clearwell can provide better water quality in terms of TTHM formation and chlorine residual without additional chlorine.

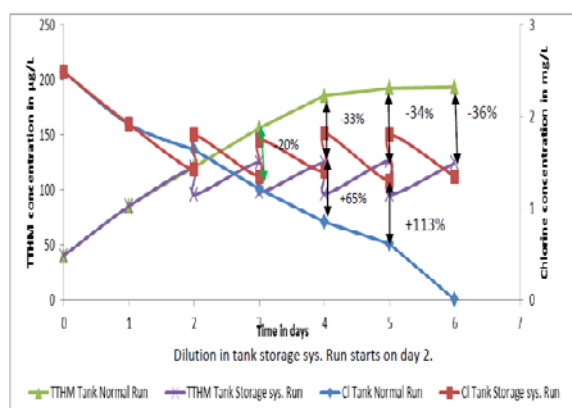


Fig. 3: Tank Normal run vs. Tank Storage run chlorine residual and TTHM trends. The percent differences between the TTHM formation and chlorine decay values are also noted.

The change in TTHM formation and chlorine decay kinetics between a high chlorine dosage scenario and usage of chlorine boosters scenario is explained in detail in our previous research [16], [20].

## CONCLUSIONS

Operational strategies affect water quality in terms of chlorine residual and TTHM formation in distribution systems. In the case of storage systems management, it is statistically proven that storage time before entering the tank, mixing conditions and fillings cycles play an important role in maintaining water quality in storage tanks located in distribution systems as well as clearwells located at the treatment facility. Storage time before entering the clearwell cannot be considered as a part of clearwell management as it is not controlled by the operation of the clearwell. Rather the primary disinfectant contact time requirements of the state directly influence this storage time. Proper mixing and fill-drain cycles can alone hold the potential to dictate whether a storage structure will improve or degrade the water quality in terms of chlorine residual and TTHM formation. Operators need to realize that any given operational strategy has potential to improve water quality with respect to one parameter and degrade it with respect to another. Finding a right

balance requires knowledge of system-specific conditions and factors of variability of water chemistry in distribution systems.

## ACKNOWLEDGEMENTS

Funding for this project was provided by National Institute of Hometown Security (NIHS). Analytical and technical support was provided by Missouri Water Resource Research Center (MWRRC), Columbia Water Treatment Plant (CWTP) and Vandalia Water Treatment Plant (VWTP).

## REFERENCES

- [1] Sadiq R, and Rodriguez MJ, "Disinfection by-products (DBPs) in drinking water and predictive models for their occurrence: a review", *J. of Science of the Total Environment*, Vol. 321, 2004, pp. 21–46.
- [2] U.S. Environmental Protection Agency, "National Primary Drinking Water Regulations: Disinfectants and Disinfection Byproducts", *Federal Register*, Vol. 63, 1998, pp. 69390-69476.
- [3] Warton B, Heitz A, Joll C, and Kagi R, "A new method for calculation of the chlorine demand in natural and treated waters", *J. of Water Research*, Vol. 40, 2006, pp. 2877–2884.
- [4] Adams C, Timmons T, Seitz T, Lane J, and Levotch S, "Trihalomethane and Haloacetic Acid Disinfection By-Products in Full-Scale Drinking Water Systems", *J of Environmental Engineering*, Vol. 131, 2005, pp. 526-534.
- [5] Rook J, "The chlorination reactions of fulvic acids in natural waters", *J of Environmental Science and Technology*, Vol. 11, 1977, pp. 478–482.
- [6] Carrico B, and Singer PC, "Impact of Booster Chlorination on Chlorine Decay and THM Production: Simulated Analysis", *J. of Environmental Engineering*, Vol. 135, 2009, pp. 928-935.
- [7] Clark RM, and Sivaganesan M, "Predicting Chlorine Residuals and Formation of TTHMs in Drinking Water", *Journal of Environmental Engineering*, Vol. 124, 1998, pp. 1203-1210.
- [8] Clark RM, Adams JQ, and Lykins BW, "DBP Control in Drinking Water; Cost and Performance", *J. of Environmental Engineering*, Vol. 120, 1994, pp. 759-782.
- [9] Besner MC, Gauthier V, Barbeau B, Millette R, Chapleau R, and Prevost M, "Understanding distribution system water quality.", *J. of American Water Works Association*, Vol. 93, 2001, pp. 101-114.
- [10] Clark R, Abdesaken F, Boulos P, and Mau R, "Mixing in Distribution System Storage Tanks: It's Effect on Water Quality", *J. of*

- Environmental Engineering, Vol. 122, 1996, pp. 814-821.
- [11] Germeles AE, "Forced plumes and mixing of liquids in tanks." J. of Fluid Mechanics, Vol. 71, 1975, pp. 601-623.
- [12] Grayman WM, and Clark RM, "Using computer models to determine the effect of storage on water quality", J. of American Water Works Association, Vol. 85, 1993, pp. 67-77.
- [13] Kennedy MS, Moegling S, Sarikelli S, and Suravallo K, (1993). "Assessing the effects of storage tank design on water quality" J. of American. Water Works Association, Vol. 85, 1993, pp. 78-88.
- [14] Mau R, Boulos P, Clark R, Grayman W, Tekippe R, and Trussel R, (1995). "Explicit mathematical models of distribution system storage water quality", J. of Hydraulic. Engineering, ASCE, Vol. 121, 1995, pp. 699-709.
- [15] Zachár AA, and Aszódi AA, "Numerical Analysis of Flow Distributors to Improve Temperature Stratification in Storage Tanks", J of Numerical Heat Transfer: Part A -- Applications, Vol. 51, 2007, pp. 919-940.
- [16] Poleneni SR, "Analysis and management of disinfection by-product formation in distribution systems", M.S. Thesis, University of Missouri. 2013, ch. 3.
- [17] APHA, AWWA, WEF, "Standard Methods for the Examination of Water and Wastewater," 20th ed. United Book Press: Baltimore, MD. 1998.
- [18] Hach, "Water Analysis Handbook." 3rd ed. Hach Company: Loveland, CO. 1997.
- [19] Munch JW, "EPA Method 524.2: Measurement of Purgeable Organic Compounds in Water by Capillary Column Gas Chromatography/Mass Spectrometry", Rev. 4.1, US EPA, Office of Research and Development: Washington, D. C. 1995.
- [20] Poleneni SR and Inniss EC, "Small Water Distribution System Operations and Disinfection By-Product Fate" J. of Water Resource and Protection, Vol. 5, pp. 35-41.

# PESTICIDE SUSTAINABLE MANAGEMENT PRACTICE (SMP) INCLUDING POROUS BIOCHAR/GEOPOLYMER STRUCTURES FOR CONTAMINATED WATER REMEDIATION

Ian P Craig, Jochen Bundschuh and David Thorpe  
Health, Engineering and Sciences, University of Southern Queensland, Australia

## ABSTRACT

As a result of agribusiness in Australia and across the world, water is contaminated with nutrients and pesticides which threaten riverine environments, wetlands, urban drinking water supplies and also marine assets such as the Great Barrier Reef (GBR). Much can be done and sustainable management practices (SMP) can be put into place to reduce water impacts from agriculture. Such an SMP strategy may take the form of improved spraying technology, improved integrated pest management, understanding pesticide environmental fate and behaviour, acquiring a better understanding surface and groundwater hydrology, and improved contaminated water remediation technologies. Required investment levels are insignificant compared to the economic advantages to be gained from adopting appropriate SMP across Australian and global agribusiness. Work in collaboration with biochemists needs to take place to develop enzymes which are naturally found in pesticide resistant insects or weeds. Biochar geostructural/geopolymer based technologies need to be developed, augmented with enzyme based products which need to be developed commercially. Such products or enhancers need to be targeted at specific pesticides (eg. ametryn, atrazine, simazine, diruron, ametryn, hexazinone, tebuthiuron, dieldrin, metalochlor, 2,4 D, triclopyr, picloram and bromacil). Surface runoff from is conventionally managed by retention lagoons facilitating water reuse on-farm, but these can be breached during heavy storms. Long term deep drainage from fields and seepage from lagoons can also lead to contaminated groundwater. Research, development and testing of appropriate non-leaking/reactive spillways and subsurface geostructures needs to take place across the various agricultural industries. It could be that a porous geopolymer concrete in combination with biochar may prove useful in the design of such structures. The potential for green or brown waste material derived biochar products, which could be readily manufactured from farm refuse and manure, needs to be thoroughly investigated in this regard. The challenge for engineers is to come up with geostructural designs which are efficient, cost effective and which will be taken up and embraced by Australian and world agribusiness.

*Keywords Sustainable, Pesticide, Herbicide, Contaminated Water, Biochar, Porous, Geopolymer, Enzyme*

## INTRODUCTION

Previously, agribusiness has attempted to reduce contamination of the environment by implementing Integrated Pest Management (IPM) [1] which refers to a strategy which seeks to reduce reliance on synthetic chemical pesticides. It involves i) managing pests below economically damaging levels rather than seeking to eradicate them ii) relying on non-chemical measures, and, iii) selecting and applying pesticides, when they have to be used, in a way that minimizes adverse effects on beneficial organisms, humans, and the environment. IPM involves integrating a range of tools and strategies for managing pests. These can be conveniently grouped in seven main objectives including i) using the correct spray equipment to produce the biologically optimum droplet size ii) optimising coverage iii) appropriate chemical selection, iv) preserving beneficial insects, v) preventing insecticide resistance vi) managing crop and weed hosts, vii) using trap crops effectively and viii) communication and training.

Field studies over the years have demonstrated that pesticide application using liquid based sprays is

probably at best only a few percent efficient [2]. Efficiency is defined simply in terms of the percentage of droplets reaching the intended target. These studies have indicated that droplet size seems to be the most important factor which determines this efficiency. Droplets produced by conventional hydraulic nozzles used in agriculture generally range in size from 30µm to 3000µm. Droplets with diameters less than 100µm have low sedimentation velocity and shallow trajectory, and are vulnerable to off target drift and loss to atmosphere. Droplets greater than 300µm which contain most of the volume of the spray, have high sedimentation velocity and steep trajectory, and are unlikely to strike a plant surface or pest. Even within a dense crop canopy, coarse droplets may bounce from a leaves, and therefore simply contribute to soil and/or groundwater pollution. Pesticide application efficiency could be increased dramatically if the percentage of droplets falling between 100µm and 300µm present in the spray was increased [3].

Investment is also needed in developing appropriate remediation technology to pesticide contaminated water which leaves cultivated field as

runoff. Green and brown waste derived biochar has recently shown significant potential in this regard. A particulate form of biochar is required to increase available surface area, with carbon particles held in a rigid and durable porous matrix, to prevent them being eroded away by a moving water stream. Recent developments in porous geopolymer concrete may perhaps provide an answer to this design challenge. Porous concrete/polymer materials developed for other purposes in civil engineering, may prove to be also very useful for Porous Reactive Barrier (PRB) designs [15], which trap contaminants from water flowing through them.

Such technologies when assembled together in a unified SMP strategy for sustainable agribusiness, will undoubtedly have the potential to significantly reduce pollution of atmosphere, soil, fresh water and oceans with pesticides.

## **PESTICIDE FATE AND BEHAVIOUR MONITORING AND MODELLING**

Pesticides residues can be found in the atmosphere, water, soil, vegetation and organisms. In water, pesticides can exist in a dissolved form, or can be attached suspended matter or bottom sediments. Pesticides are taken up by aquatic biota, possibly being excreted in metabolised form. Within a water system, transformation of pesticides can occur via chemical, physical and biological processes.

Pesticide runoff into natural water systems can occur during large rainfall or storm events. Weed control in urban areas is often adjacent to hard surfaces and roads with man-made drainage systems acting as a fast conduit to ocean. Correctly designed storm water harvesting infrastructure is often non-existent, or at best minimal. Farms are usually designed with retention storages whose combined purpose is to collect irrigation tail water and storm water runoff. However, during periods of high rainfall, on-farm storage of runoff can be breached, and pesticides are at risk of entering the river systems and making it out to the GBR [4].

The development of numerical models to describe pesticide fate and behaviour commenced in the 1970s, and were useful in understanding DDT found in birds of prey, in the wildlife at both poles, and also in dairy cattle directly affecting humans. Endosulfan was found in Australian export beef during the 1990s. HowLeaky software [5] launched by Qld Govt DNR, DAFF and EPA in 2003, represents the pinnacle of development for pesticide fate and behaviour modelling purposes. Evolution of the software arose from exhaustive testing and calibration earlier algorithms (USLE, CREAMS, GLEAMS, RZWQM, HSPF, PRZM, PERFECT). The HowLeaky model represents a one dimensional soil/water balance agricultural hydrology model for exploring the impact of different land uses and soil

management on water balance and water quality. It has a user interface which provides a highly visual representation of inputs and outputs. The software has been used to explore implications of different land uses (including crops, pasture and trees), climates, soil types and management (tillage, crop rotation, herbicide strategies) on hydrology, production index, erosion and off-site sediment loss, nitrogen, phosphorus and pesticide movement [6].

## **WATER REMEDIATION USING POROUS BIOCHAR GEOSTRUCTURES**

The use of ground iron based reactive barriers for TCE to ethane, Cr(VI) to Cr(III), some heavy metals and phosphorus has been investigated by the USEPA, but focus is now on non-living structures for pesticide/nutrient bioremediation, because of the problem of keeping the plants/microbes alive is alleviated. The advantage of using biochar geostructures is longevity and reduced maintenance costs. Added to soil in particulate form, studies have demonstrated that biochar can increase cation exchange capacity, enhance soil microbes and augment water retention [7,8]. These advantages are additional to its primary use as a soil carbon store for greenhouse gas reasons. It has also been suggested that biochar can reduce nutrient loadings in agricultural runoff. It is established that biochar on its own is showing promise also for the removal of some heavy metals [9] and uranium [10]. In trials in which particulate biochar was added to soil as a soil amendment, it was noticed that herbicide efficacy in controlling weeds was noticeably reduced [8]. The reason for this is presumably chemical binding of the herbicide active ingredient to the carbon particles. From this has very recently launched a series of investigations as to the potential effectiveness of biochar for removal of herbicides in water [11]. The potential for biochar derived from greenwaste has been assessed specifically for triazine based herbicides [12]. The potential for biochar derived from pig manure has been assessed for the herbicide paraquat by [13] and for carbaryl plus atrazine by [14]. Deep percolation of pesticides leads to long term pollution of groundwater resources and represents a new area which needs to be addressed. Preliminary investigations of biochar based geostructures commenced at USQ [15].

## **CONCLUSION**

Work in collaboration with biochemists needs to take place to develop enzymes which are naturally found in pesticide resistant insects or weeds. Biochar geostructural/geopolymer based technologies need to be developed, augmented with enzyme based products which need to be developed commercially [16]. Such products or enhancers need to be targeted at specific pesticides (eg. ametryn, atrazine, simazine,



diruron, ametryn, hexazinone, tebuthiuron, dieldrin, metalochlor, 2,4 D, triclopyr, picloram and bromacil). Deployment of and testing of appropriate geostructural designs needs to take place across the various agricultural industries. It could be that a porous geopolymer concrete in combination with biochar is used in the design of subsurface of surface structures. The potential for green or brown waste material derived biochar products, which could be readily manufactured from farm refuse and manure, needs to be thoroughly investigated in this regard. Surface runoff is managed by retention lagoons facilitating water reuse on-farm. Loss of contaminated water via field deep drainage presents a much tougher problem which up until now has not been satisfactorily addressed. The challenge for engineers is to come up with in-situ sub-surface geostructural designs which are efficient, cost effective and which will be taken up and embraced by Australian and world agribusiness.

## REFERENCES

- [1] Pimentel, D 2002. Encyclopedia of Pest Management. Vol 1. Marcel Dekker Inc. 02.
- [2] Graham-Bryce, I.J., 1980. Physical Principles of Pesticide Behaviour. Chapter Six – Behaviour of Pesticides in Air. Academic Press, London
- [3] Craig I, Hewitt A and Terry H, 2014. Rotary atomiser design requirements for optimum pesticide application efficiency. Crop Protection (submitted).
- [4] Henderson F and Croon F 2009. Overview of CSIRO Water Quality Research in the Great Barrier Reef 2003-2008. CSIRO:Water for a Healthy Country National Research Flagship.
- [5] Shaw M, Silburn DM, Thornton C, Robinson B and McClymont D, 2011. Modelling Pesticide Runoff from Paddocks in the Great Barrier Reef Using Howleaky?. 19th International Congress on Modelling and Simulation.
- [6] Carroll C, Waters D, Vardy S, Silburn DM, Attard S, Thorburn PJ, Davis AM, 2012. Paddock to Reef Monitoring and Modelling Framework for the Great Barrier Reef: Paddock and Catchment Component." Marine Pollution Bulletin 65 (4–9) 136-49.
- [7] Beesley L et al 2011. A review of biochar's potential role in the remediation, revegetation and restoration of contaminated soils. Environmental Pollution 159 (July, 2011) 3269-3282.
- [8] Jones DL, Edwards-Jones G and Murphy DV 2011. Biochar mediated alterations in herbicide breakdown and leaching in soil. Soil Biology and
- [9] Chen, J.; Zhu, D. and Sun, C. 2007. Effect of heavy metals on the sorption of hydrophobic organic compounds to wood charcoal. Environmental Science & Technology, 41(7), 2536–2541.
- [10] Kumar S, Loganathan VA, Gupta, RB and Barnett, MO 2011. An Assessment of U(VI) removal from groundwater using biochar produced from hydrothermal carbonization. Journal of Environmental Management 92 (2011) 2504e2512
- [11] Kearns, J., 2013. Sustainable Decentralized Water Treatment for Rural Developing Communities Using Locally Generated Biochar Adsorbents. ECHO Asia Notes May 2013 Issue 17.
- [12] Zheng W, Guob M, Chowa T, Bennetta DN, Rajagopalana N., 2010. Sorption properties of greenwaste biochar for two triazine pesticides. Journal of Hazardous Materials 181 (2010) 121–126
- [13] Tsai WT and Chen, HR 2013 Adsorption kinetics of herbicide paraquat in aqueous solution onto a low-cost adsorbent, swine-manure-derived biochar. Int. J. Environ. Sci. Technol. (2013) 10:1349–1356
- [14] Zhang, P, Sun H, Sun LYT, 2013. Adsorption and catalytic hydrolysis of carbaryl and atrazine on pig manure-derived biochars: Impact of structural properties of biochars. Journal of Hazardous Materials 244– 245 (2013) 217– 224.
- [15] Craig I, Shiao J, and Erdei L 2012. Contaminated soil/groundwater remediation using Permeable Reactive Barrier (PRB) techniques. Engineers Australia - Southern Region Engineering Conference, University of Southern Queensland, Toowoomba, 30 August 2012. Paper no. SREC2012-2A-4.
- [16] Scott et al 2010 A free-enzyme catalyst for the bioremediation of environmental atrazine contamination. Journal of Environmental Management May 2010.

## **AN EVALUATION MODEL OF MEDICAL TRANSPORT WITH TSUNAMI EARLY WARNING SYSTEM**

Norimitsu Koike<sup>1</sup>, Susumu Kurahashi<sup>2</sup>

<sup>1</sup>Department of Civil Engineering, Aichi Institute of Technology, Japan

<sup>2</sup>Disaster Prevention Research Center, Aichi Institute of Technology, Japan

### **ABSTRACT**

The Japanese Central Disaster Management Council announced a new damage estimate in the event of an earthquake with its epicenter in the Nankai Trough. The estimate shows the huge human damage. However, they mentioned the possibility of minimizing the casualty count by constant preparation for prompt evacuation to higher places in the event of a tsunami. This study aims to develop a reliability analysis model for medical transport activity considering a tsunami risk. The model includes a risk evaluation model developed to evaluate medical transport activity when a tsunami early warning system can be used. Our model is composed of the indices for those problems. By applying it to Chita Peninsula in Japan, it is demonstrated that the proposed model effectively implements the evacuation and medical transport planning. Some proposals are given for the road network in the area.

*Keywords: Risk management, Tsunami, Medical transport, Evacuation*

### **INTRODUCTION**

The Japanese Central Disaster Management Council recently announced a new damage estimate in the event of an earthquake with its epicenter in the Nankai Trough. The new estimate shows the huge human damage. However, they mentioned the possibility of minimizing the casualty count by constant preparation for prompt evacuation to higher places in the event of a tsunami. In response to this situation, many local tsunami evacuation plans have been reconsidered. Especially, the Tokai area is pointed out as a high tsunami risk area by the Nankai trough.

After a large-scale disaster, medical transport is very important for life-saving. D.Goldschmitt conducted some phases of a medical disaster response. First is the extrication. The purpose in this phase is to get victims out of the hot zone and to safety. Second is the field triage. The victims are evaluated to determine their needs for medical attention. The third is evacuation and transport. The phase is to transport them to the definitive care location or the emergency departments of local hospitals [1]. N.Koike et al. made an evaluation model for the transport of victims in an airplane accident in the third phase [2]. The model has been made for serious incidents like airplane accidents. The origin of the injured is one place just like an airport. In a large-scale disaster, however, many places may be defined as the origin, and the injured will be transported to some hospitals under the risk of a tsunami.

There are many previous studies about the evacuation. B.Wolshon published to a comprehensive review of evacuation plans of the area affected by hurricanes. In this review, he discussed the needs of emergency plan for special needs and low mobility groups [3]. The medical transport planning for victims and patients from view point of transport management may be needed.

This study aims to develop a reliability analysis model for medical transport considering the tsunami risk. The model includes a risk evaluation model developed to evaluate medical transport when a tsunami early warning system can be used. The tsunami early warning system determines the possibility of a tsunami by the seismic intensity and magnitude of the earthquake at almost the same time after an earthquake. The system serves to draw people's attention to the risk of a tsunami. There are two purposes of medical transport; one is a medical evacuation from one high-risk place to a safer place. Another is the emergency transport of injured to hospitals. Our model is composed of indices to evaluate such problems. Through applying them to the Chita Peninsula in Japan, it is demonstrated that the proposed model effectively implements the evacuation and medical transport planning.

### **METHODOLOGY**

#### **Outline of proposed method**

In the previous model, three risk factors were proposed for reducing the risk of death. One is the

left behind risk, which is an index to explain how long the injured must wait for pickup at the injury site. The second is the medical confusion risk, which is indicated by the arrival interval. Major injured persons are often brought to the hospital closest to the incident site, and smooth medical service is difficult. If they can be transported to a wider array of hospitals, the hospitals may accept a few injured within their ability. The third is the transport risk itself. It is the risk with a long transport time. As convalescence of the injured may be determined by many personal factors, it cannot be evaluated by only an index such as lifesaving time limit. The proposed indices are significant to compare some alternative plans.

For the evaluation of the medical transport with a tsunami risk, the left behind risk is out of the consideration. The problem is who and when will be rescued from high-risk places. For their rescue, a warning system to assure their fast evacuation is important. Our proposed model has included reducing the risk by improvement of the warning system.

### Medical risk indices

#### *Reducing risk by the warning system*

The best and unique countermeasure against a tsunami attack is to evacuate from the coast. However, it does not mean that all earthquakes cause a huge tsunami. When a tsunami is expected to cause coastal damage, the Japan Meteorological Agency (after this, JMA) issues a tsunami warning or advisory within 2-3 minutes after an earthquake. The tsunami information is transmitted immediately to disaster management organizations and media outlets. However, the best countermeasure is for people to flee coastal areas immediately after an earthquake. But the time to check the information from the government reduces the chance of evacuation. In Japan, the early earthquake warning system (after this, EEWS) is the earliest warning for the earthquake disaster. Kurahashi et al. have been developing early tsunami warning system used by the EEWS magnitude. K.Iida pointed out the earthquake magnitude is related tsunami occurrence [4]. The system includes the equation proposed by K.Iida. If the system can be put to practical use, the tsunami risk may well be reduced.

Fig. 1 shows an image between the time the risk of a tsunami is perceived and the time to reach a tsunami after an earthquake. “ $t_0$ ” is the time immediately after an earthquake. Time “ $t_1$ ” means the timing of the tsunami alert by the JMA. The perceived risk of tsunami will arise by the EEWS at this period. The time “ $t_2$ ” involves a person who has

received information of a tsunami reaching in or near the coast. This is certain information of the tsunami danger. And at the time “ $t_3$ ”, the tsunami is within sight, so people must escape to a safe place. The perceived risk can be exchanged for the probability of evacuation. Fig. 2 shows the relation between the time distribution and probabilities for evacuation. If the improvement by the EEWS can prompt evacuation immediately, the distribution of the probability of evacuating may shift to an early time. It will contribute to reduction of the number of tsunami victims.

Table 1 shows the evacuation ratio of people from the tsunami risk area after an earthquake. This is estimated by the empirical data in Japan from the Japanese Central Disaster Management Council. The estimation is considered to reflect people’s awareness about the risk of tsunami. In Case A, which is high awareness and effective warning, 70% of people can evacuate immediately, whereas only 20% of people can evacuate in Case C. It means the awareness and warning have a great influence on evacuation behavior.

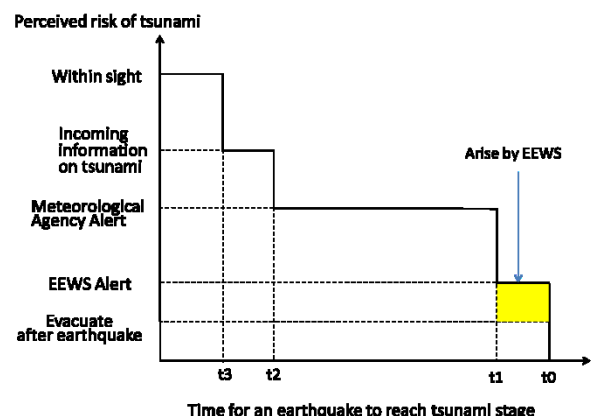


Fig. 1 Relation between time distribution and probabilities of tsunami

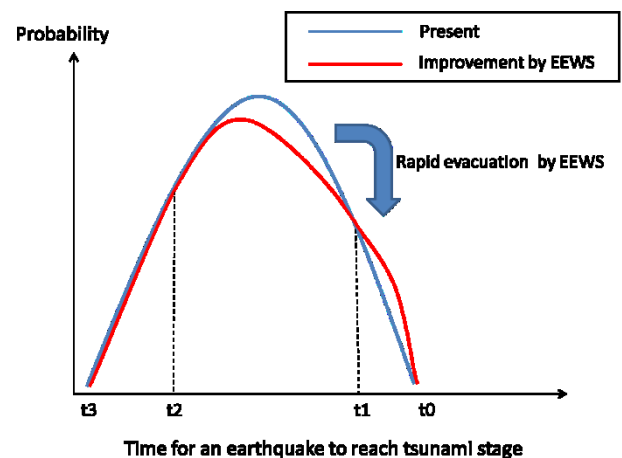


Fig. 2 Relation between time distribution and probabilities of evacuation

According to the above suppositions, the Japanese Central Disaster Management Council makes detailed estimates of the number of tsunami victims. The estimates show the numbers who cannot escape from a tsunami and who fail to escape in time.

As the EEWS provides information to escape immediately, it will reduce the number of victims who fail to escape in time. The EEWS as indicated by the present study will halve the number of victims who could not escape in time.

Table 1 Evacuation ratio at the report by Japanese Central Disaster Management Council

Items	Evacuate immediately after earthquake	Evacuate less quickening	Evacuation as imminent tsunami danger (%)
Case A	70	30	0
Case B	70	20	10
Case C	20	50	30

Case A: High rapid evacuation ratio and effective warning

Case B: High rapid evacuation ratio.

Case C: Low rapid evacuation ratio.

#### The risk factors

Fig. 3 illustrates the medical conditions transport after a tsunami. At first, people fail to escape and undergo injury. Second is the medical over-capacity risk. Because some nearby hospitals must accept many injured, those hospitals may be in disturbed due to over-capacity. To avoid over-capacity, they hope to transport to a nearby hospital, and are forced to transport long distances. In addition, some nearby routes cannot be used. This is the transport risk.

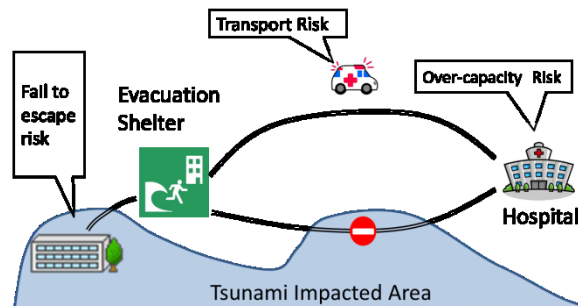


Fig. 3 Risk of injured persons

#### Modeling

The model area is divided into some zones which are set as the origin of medical transport.

Second, the distance  $D_{ij}$  is defined from origin zones  $i$  to hospital  $j$ .  $D_{max}$  is the farthest distance from all zones to the farthest hospital. As people try to go to the nearest hospital, possibility to select the hospital can be defined as Fig.4.

We define the hospital select coefficient from zone  $i$  to hospital  $j$  as follows;

$$Y_{ij} = (D_{max} - D_{ij}) / \sum_i \frac{(D_{max} - D_{ij})}{D_{max}} \quad (1)$$

The hospital select coefficient means the gravitation of the hospital  $j$  from zone  $i$ .

The Transport risk is written as follows;

$$TR_{ij} = Y_{ij} \times D_{ij} \quad (2)$$

When many hospitals are located near the damage area, the transport risk may be low, but when hospitals are far from the damage area, the risk may be high.

This model calculates how many injured people go to the hospital. However, the estimated number of injured persons is uncertain. In this paper, the relative damage estimation at the zone  $i$  is defined as follows;

$$E_i = V_i / \sum_i V_i \quad (3)$$

Where  $V_i$  indicates human damage in the area  $i$ . Although this index cannot show the absolute number of injured persons, we can discuss the priority of countermeasures for many injured.

Using the relative risk of human damage, the medical demand can be described with the hospital select coefficient and the relative risk of human damage.

$$RH_j = \sum_i Y_{ij} \times E_i \quad (4)$$

$RH_j$ : the medical over-capacity risk at hospital  $j$

$E_i$ : the relative risk of human damage at the zone  $i$

If the ability of all hospitals is almost equal, the ideal would be for the medical over-capacity risk  $RH_j$  to be dispersed around the hospitals.

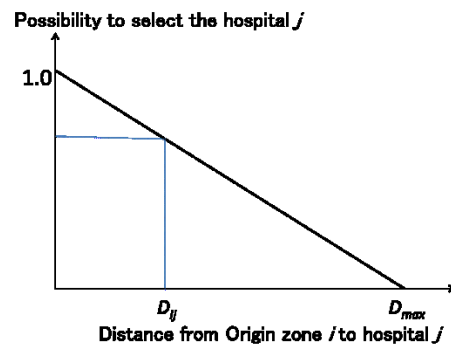


Fig. 4 Relation between distance and possibility to select the hospital  $j$

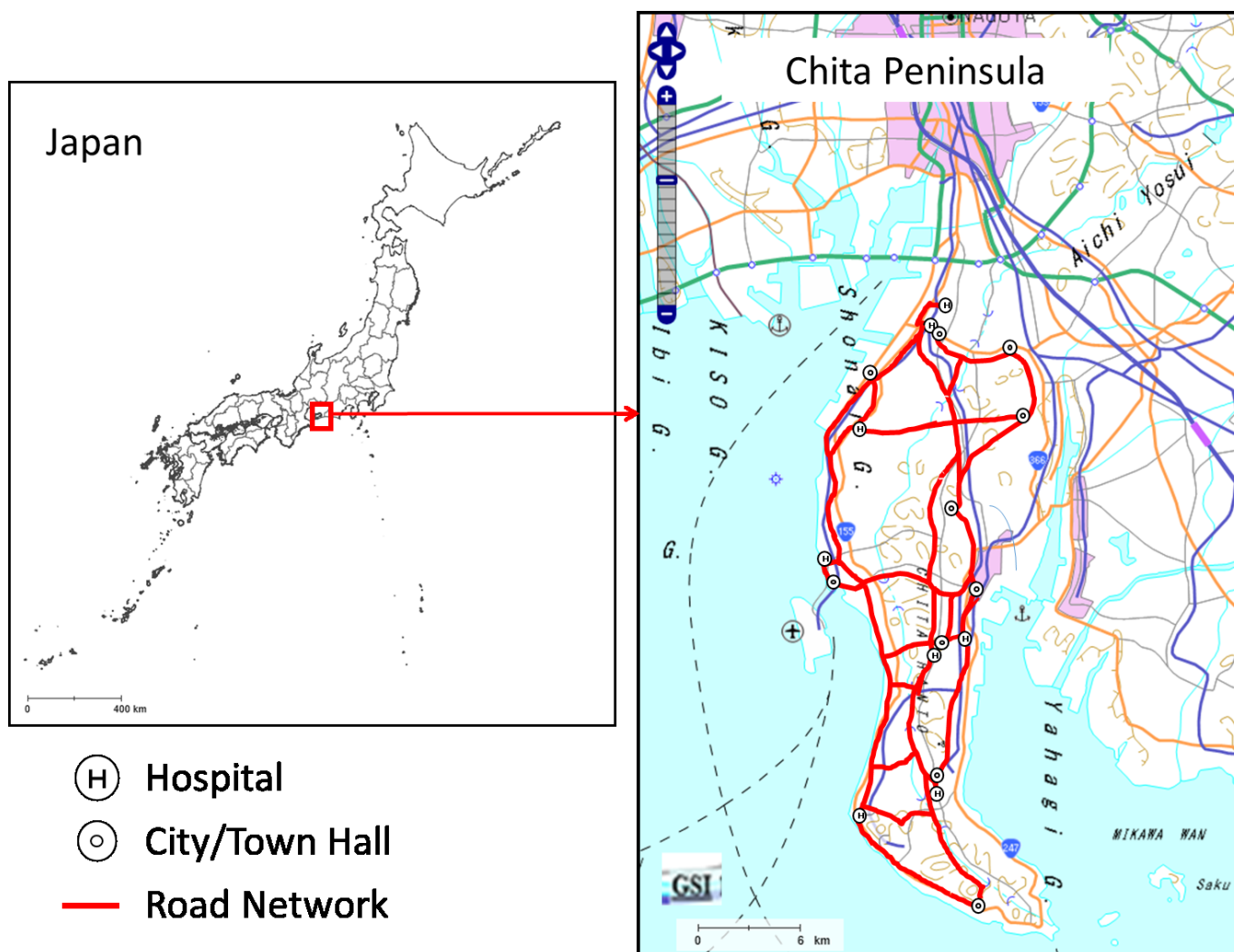


Fig. 5 Chita Peninsula road network and hospitals

Table 2 Hospital select coefficient

Area Hospital	Minami chita	Mihama	Taketoyo	Tokoname	Handa	Agui	Higashiura	Obu	Tokai	Chita
A	0.11	0.09	0.14	0.18	0.13	0.13	0.11	0.10	0.12	0.14
B	0.01	0.05	0.07	0.09	0.11	0.14	0.18	0.22	0.22	0.18
C	0.25	0.21	0.14	0.11	0.12	0.08	0.07	0.06	0.06	0.05
D	0.01	0.06	0.07	0.10	0.11	0.14	0.18	0.21	0.22	0.19
E	0.18	0.17	0.19	0.14	0.16	0.14	0.11	0.10	0.08	0.08
F	0.17	0.16	0.18	0.14	0.16	0.14	0.12	0.10	0.10	0.11
G	0.04	0.07	0.09	0.13	0.12	0.15	0.18	0.18	0.19	0.20
H	0.22	0.18	0.13	0.11	0.10	0.08	0.04	0.03	0.03	0.06

Table 3 Transport risk

Area Hospital	Minami chita	Mihama	Taketoyo	Tokoname	Handa	Agui	Higashiura	Obu	Tokai	Chita	Total
A	3.05	2.17	1.58	0.22	1.62	1.57	2.47	2.54	2.29	2.03	19.55
B	0.44	1.66	1.79	1.94	1.82	1.52	1.96	1.46	0.30	1.32	14.22
C	2.36	0.09	1.49	1.89	1.78	1.90	2.07	1.91	1.70	1.56	16.74
D	0.44	1.68	1.80	1.92	1.81	1.51	1.95	1.63	0.24	0.88	13.88
E	3.32	1.56	0.13	1.56	1.03	1.43	2.48	2.49	2.15	2.04	18.18
F	3.35	1.60	0.33	1.53	0.90	1.49	2.50	2.57	2.26	2.21	18.73
G	1.54	1.95	1.93	1.67	1.71	1.33	1.95	2.36	1.27	0.53	16.23
H	2.97	1.21	1.71	1.90	1.90	1.89	1.50	0.95	0.91	1.73	16.67
Total	17.47	11.92	10.76	12.63	12.56	12.63	16.89	15.91	11.12	12.29	

Table 4 Medical over-capacity risk

Area Hospital	Minami chita	Mihama	Taketoyo	Tokoname	Handa	Agui	Higashiura	Oubu	Tokai	Chita	Total
A	0.04	0.01	0.01	0.02	0.02	0.00	0.00	0.00	0.01	0.01	0.13
B	0.00	0.01	0.00	0.01	0.02	0.00	0.01	0.00	0.01	0.01	0.08
C	0.09	0.02	0.01	0.01	0.02	0.00	0.00	0.00	0.00	0.00	0.17
D	0.00	0.01	0.00	0.01	0.02	0.00	0.01	0.00	0.01	0.01	0.08
E	0.07	0.02	0.01	0.02	0.03	0.00	0.00	0.00	0.00	0.00	0.16
F	0.06	0.02	0.01	0.02	0.03	0.00	0.00	0.00	0.00	0.01	0.15
G	0.02	0.01	0.01	0.02	0.02	0.00	0.01	0.00	0.01	0.01	0.10
H	0.08	0.02	0.01	0.01	0.02	0.00	0.00	0.00	0.00	0.00	0.14
<i>Relative Risk of human damage</i>	0.37	0.10	0.06	0.13	0.16	0.03	0.03	0.02	0.05	0.05	

Table 5 Medical over-capacity risk of proposed system

Area Hospital	Minami chita	Mihama	Taketoyo	Tokoname	Handa	Agui	Higashiura	Oubu	Tokai	Chita	Total
A	0.03	0.01	0.01	0.03	0.02	0.00	0.00	0.00	0.01	0.01	0.13
B	0.00	0.01	0.01	0.01	0.02	0.01	0.01	0.00	0.01	0.01	0.08
C	0.08	0.02	0.01	0.02	0.02	0.00	0.00	0.00	0.00	0.00	0.16
D	0.00	0.01	0.01	0.01	0.02	0.01	0.01	0.00	0.01	0.01	0.09
E	0.05	0.02	0.01	0.02	0.03	0.01	0.00	0.00	0.00	0.00	0.15
F	0.05	0.02	0.01	0.02	0.03	0.01	0.00	0.00	0.01	0.01	0.15
G	0.01	0.01	0.01	0.02	0.02	0.01	0.01	0.00	0.01	0.01	0.10
H	0.07	0.02	0.01	0.01	0.02	0.00	0.00	0.00	0.00	0.00	0.14
<i>Relative Risk of human damage (improvement)</i>	0.30	0.11	0.07	0.14	0.18	0.04	0.04	0.02	0.05	0.05	

area.

## CASE STUDY

### Case study area

We have applied our model to the Chita Peninsula in Central Japan with its population of about 40 million. The administrative district is 10 blocks. There are 8 emergency hospitals. There is a high-risk area by tsunami attack in an earthquake with its epicenter in the Nankai Trough. Fig. 5 shows the road network from the city or town office to the emergency hospitals in Chita Peninsula.  $D_{max}$  is 40.9 km.

### Results

Table 2 shows the results of the hospital select coefficient  $Y_{ij}$ . For example, 25% of the people in the Minamichita area will go to hospital C. On the other hand, hospital B and D are far from the Minamichita area. Most people will not go to hospital B and D.

Table 3 shows the result of the transport risk. Minamichita has the highest transport risk. Because Minamichita is located in the southeast of the Chita Peninsula, many hospitals are far from the area. Hospital A has the highest transport risk. Because hospital A is located at the center of the Chita Peninsula, many people may come from all over the

Table 4 denotes the medical over-capacity risk. Because much human damage by tsunami attack is estimated, Minamichita is a high-risk area for human damage. Many people will go to hospital C from the Minamichita area.

Table 5 shows the medical over-capacity risk with the EEWS improvement. The relative risk of human damage is changed with the decreasing number of tsunami victims. For example, the relative risk of Minamichita goes down from 0.37 to 0.30. On the other hand, the relative risk of the Handa area increases from 0.16 to 0.18. It does not mean that the victims in the Handa area increase, but the victim ratio goes up. The total injured number of people will decrease. Comparing both cases, the medical over-capacity risk of some hospitals is changed. Because of decreasing the relative risk of human damage of the Minamichita area, the medical over-capacity risk of hospital C decreases.

Table 6 shows the result of the medical over-capacity risk and the ratio of bed number. We refer to the bed number as the scale index of hospitals. Comparing with the results and ratio of bed number, the medical over-capacity risk of hospital C, E, F and H are higher than the ratio of bed number, whereas the hospital A, B, D and G are lower. Although those hospitals have many beds, they are located far from the high-risk area.



Table 6 Medical over-capacity risk and ratio of bed number

Case Hospital	Normal	Improve	Ratio of bed number
A	0.13	0.13	0.16
B	0.08	0.08	0.15
C	0.17	0.16	0.15
D	0.08	0.09	0.18
E	0.16	0.15	0.08
F	0.15	0.15	0.04
G	0.10	0.10	0.18
H	0.14	0.14	0.07
	1.00	1.00	1.00

## DISCUSSION

We can observe the difference in the medical over-capacity risk for the normal and the EEWS warning situation. Especially, the medical over-capacity risk of some hospitals located near the water decreases. The improvement of initial behavior will avoid the over-capacity in the particular hospital.

The transport risk is shown for each zone and hospital. In addition, the medical over-capacity risk is not in proportion to the scale of the hospitals. It needs countermeasures for the high-risk zones and hospitals. For example, if the medical ability of the hospitals near the water is reinforced, the injured can avoid transport for a long time. The hospital select coefficient  $Y_{ij}$  is only decided by the distance  $D_{ij}$ . In future, one should consider how to select the hospital by a questionnaire survey.

In this paper, we presumed that all roads can be used. However, some road may be in fact damaged by the seismic and tsunami attack. If we set the scenarios of the road damage, this model can apply to evaluate the road network.

## CONCLUSION

This study proposed a reliability analysis model for the medical transport activity considering the tsunami risk. The model includes a risk evaluation model to evaluate medical transport activity when the tsunami early warning system can be used. Our model is composed of evaluation indices for those problems.

Through applying it to the Chita Peninsula in Japan, the proposal model serves to implement the evacuation and medical transport planning.

Because we set the relative risk of human damage in our model, we cannot compare the absolute number of injured persons between the normal and the improvement case. If detailed data of estimate number about of the human damage are available, we can evaluate the acceptable number of hospitals and the number of injured people.

## ACKNOWLEDGEMENTS

This research was partly funded by the Grants-in-Aid for Scientific Research <KAKENHI> (No.24590641).

## REFERENCES

- [1] David Goldschmitt; "Progression of disaster care", Medical Disaster response, CRC press, 2009, pp.145-162.
- [2] Norimitsu Koike, Eizo Hideshima, Koshi Yamamoto, Toshihide Fukai; "Study on reliability analysis model for transport of the injured at airplane accident," in Proc. Int. Conf. on ICTTS, Vol. 2, 2002, pp. 1047-1054.
- [3] Brian Wolshon; The role of transportation in evacuation and reentry: A survey of practice, Journal of transportation and safety & security, Vol.1, 2009, pp.224-240.
- [4] Kumizi IIDA; Magnitude and energy of earthquakes accompanied by tsunami, and tsunami energy, Journal of Earth Sciences, Nagoya Univ. 1958, pp.101-112.

## SEASONAL VARIATION OF THE ALIEN PLANTS INVASION INTO RIVER ECOSYSTEM

Michiko Masuda<sup>1</sup> and Fumitake Nishimura<sup>2</sup>

<sup>1</sup> Department of Civil Engineering, Nagoya Institute of Technology, Japan; <sup>2</sup> Department of Environment Engineering, Kyoto University, Japan

### ABSTRACT

Many alien species have invaded into fluvial environment. The invasion of alien species affect seriously damages to the biological diversity. Authors pointed out that invasion of alien plants is mainly occurred in spring, and recommended that the improvement of river environment should be done from summer to autumn in order for prevent invasion of alien species. However, there is little report about the phenomenon when the improvement of river was occurred from summer to autumn. So we investigated how the vegetation recovered at the improvement river area with no burial seeds in summer. During the investigation we removed all emerging seedlings in the half of the investigation area and always kept as the bare ground. As a result four of the following became clear, 1) seedlings of alien species could not easily invade bared area in summer, 2) only some seedlings of a few native species can be established in summer, 3) the vegetation by native species that recovered in summer prevented the invasion of alien species, 4) seedling removal hasten the invasion of alien species. The character that the seeds are able to emerge anytime and anywhere like the alien plants species are advantageous at the fluvial environment where rising of the river sometimes occurs. But the condition of river bed in summer is too severe to invade open area. Only a few native species can established their seedlings.

*Keywords: Four or Five Keywords (First Characters of Each Word are in Capital/Uppercase Letters), Italic*

### INTRODUCTION

The weed risk assessment (WRA) has been paid attention as a risk evaluation system of the species before alien species intentionally introduces into Japan. In Australia the operation results of the WRA system have exceeded twenty years [1]. Because the damage of the exoticism to biodiversity has become the largest problem worldwide, the WRA begins to be used also in Japan [2]. In the WRA, there is a check item concerning the item concerning a character of ruderal strategy. Actually, the invasion of alien species with ruderal strategy has become a big problem in Japan.

Now, the vegetation of the fluvial environments has been seriously affected by alien plants. In the river ecosystem the bare land is formed frequently by flood. The alien ruderal species easily invade the bare land faster than native species do [3]. The invasion of an alien plants have been diminishing the biodiversity at the river condition. Especially, the alien plant that invades the fluvial environment brought in to Japan by the seed medium. Therefore, genetic diversity is very high which adjusts easily to the each invading environment [4].

The authors reported that the strategy of alien plants has longtime seedlings emergence in spring in previous paper [5]. There we also suggested that the construction of river ecosystem should be finished during summer. But there is few seasonal research in

river ecosystem about alien plants seedlings invasion in bared land in summer.

The Ministry of Land, Infrastructure and Transport experimentally restored the old fluvial environment consist of round pebbles using 'Nature oriented river works' Toki river at central Japan. There were seeds of *Sicyos angulatus*, the species notorious alien species, in this area. So to recover the rich biodiversity of the river, all the surface soil and pebbles were washed in order to remove the burial seeds and installed there in 2010. The construction was finished in early summer fortunately. Then, we investigated how the invasion of alien plants in summer to autumn was done in the "Nature oriented river work". 1) Is there few alien plant species invasion compared native species in summer construction? 2) What kind of plant species invasion trespasses upon bared ground from summer to autumn? 3) Is the alien plants affect the native plant succession? It was paid attention to these three points, and analyzed.

### MATERIALS AND METHODS

#### The Study site

The study was carried out on a left bank of the Toki River at Miyamae, Tajimi City (35° 33' 56''N, 137° 12' 92''E, altitude 96.6 m). Toki river is a

upper river in the Shonai River water system of the extension 23km and 115 km<sup>2</sup> in the valley area. Because this river region had frequently received the flood damage, bank repair and a river dredge are continuing.

At the study area, the restoration of old fluvial environment was finished in 2010. The environment condition is a place of the old natural environmental condition without dam controls. This place is consists of round pebbles without burial seeds. And in order to everyone can easily access the river flow and enjoy nature condition, the loose inclination at lower riverbed is designed.

### Seedling emergence census

The restoration was done in the investigation place at June in 2010, where all the buried seeds were removed from the soil within 1m in depth. For seedling emergence census, 20 quadrats (1 x 1m) were set at 20m in higher bed part, medium part and waterside part on the hydrophilicity shore protection slope, each interval is 1m. The total area was 60m<sup>2</sup> (Fig 1, 2). Two treatments were done in each quadrat, one is seedling remained and the other is seedling removal. Two treatments were arranged like a checkerboard.

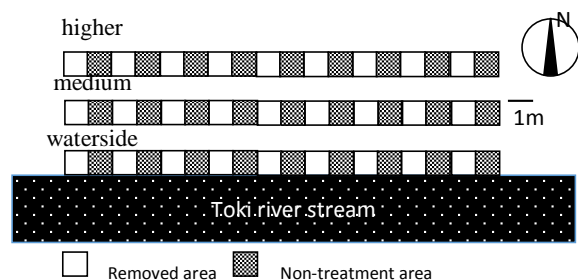


Fig. 1 The investigation areas map.



Fig. 2 The condition of investigation areas in June 23'2010.

The species of emerging seedlings was identified by comparison with the seedling specimen that had

been prepared by germinating the collected seeds under laboratory conditions. The recorded seedlings were checked by pigment ink. Census was carried out from June 30'2010 to Apr 24'2011 at every week intervals. Unidentifiable seedlings constituted only less than 0.1% of the total seedlings recorded during the study period except grass family. Using this data, it was compared the duration of seedling emergence between alien and native plants by Mann-Whitney test.

### RESULTS

In the census, we observed a total of 41 native plant species and 26 alien species. The number of species observed that emerging in each season at each treatment area showed in Table 1. In spring there are sometimes hard rain fall in the census area and we cannot count the seedling number exactly because hard rainfalls had flowed out seedlings. The number of native species is larger than that of alien species in each condition, treatment and seasons except for spring. The observed number of species is lower in summer in all area. But the number of native species is larger than that of alien species and the number of summer emergence species is smaller than that of autumn.

Table I. The number of species observed that emerging in each season at each treatment area. Native species normal exhibit and (alien species).

	Sum.	Autumn.	Win.	Spr.
Higher				
Removed	12 (8)	23 (16)	10 (7)	3 (2)
No treat	13 (7)	23 (17)	1 (2)	0 (0)
Medium				
Removed	10 (2)	21 (17)	4 (6)	0 (0)
No treat	6 (1)	16 (15)	1 (1)	1 (0)
Water side				
Removed	13 (7)	29 (16)	5 (5)	0 (0)
No treat	11 (8)	37 (22)	0 (1)	0 (1)

The duration of emergence in summer and autumn at each plot showed in Fig. 3 and 4 (more precisely data showed in Appendix 1-3). There were large differences observed the duration of emergence between native species and alien species in summer (Fig. 3). The duration of alien species seedling emergence was shorter than that of native species. Especially in medium plots alien species emergence were observed at one week, though native species emerged from one week to 5 weeks. In all area seedlings of *Digitaria ciliaris*, *Setaria viridis* and *Cyperus sp* were observed from 3 to 5 weeks, and a large number seedling emergence observed. In autumn, there was few differences

about seedling emergence duration between alien species and native species, but the longest seedling emergence were native species, *Eleusine indica*, *Cardamine scutata* and *Digitaria ciliaris*, in some area (Fig. 4). In removed area in autumn, durations of seedling emergence were longer than those of no treatment area. In alien species, *Cerastium glomeratum*, *Oenothera erythrosepala*, *Eragrostis curvula* and *Mollugo pentaplylla*, long durations of autumn seedling emergence were observed.

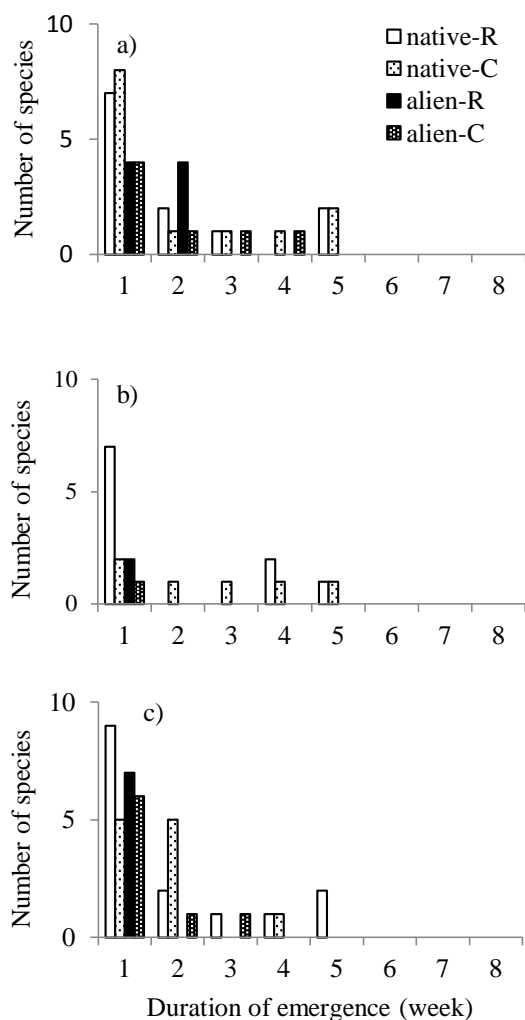


Fig. 3 The histogram of observed summer seedling emergence the durations. a) is the higher bed part, b) is the medium part, c) is the water side part. native-R is native species observed in removed area, native-C is native species observed in control area, alien-R is alien species in removed area, and alien-C is alien species in controlled area.

Mann-Whitney statistical tests were performed to examine the presence of differences in the duration of seedling emergence among native species and alien species at each season (Table II). In summer, the duration of seedling emergence of native species

in highest riverbed and waterside are longer those of alien species. In medium water condition plots there were only two alien species seedling emergence observed, so we cannot use this test, but alien seedling emergences were observed once time only. In autumn at control area of highest riverbed and medium water level there were differences between native species and alien species. But other condition there was no differences observed.

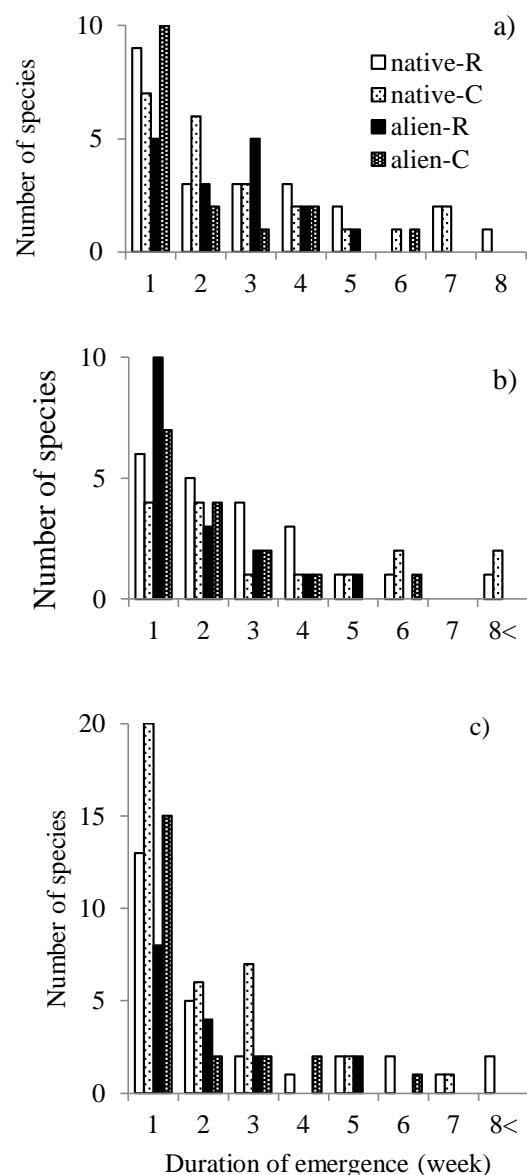


Fig. 4 The histogram of observed autumn seedling emergence the durations. a) is the higher bed part, b) is the medium part, c) is the water side part. native-R is native species observed in removed area, native-C is native species observed in control area, alien-R is alien species in removed area, and alien-C is alien species in controlled area.

Table II. The result of the Mann-Whitney U test for duration of seedling emergence of co-occurring native species vs alien species in different moist level plots.

season	Moist level	Removed	Control
Summer	highest	*	*
	medium	-	-
	water side	***	*
Autumn	highest	N. S.	*
	medium	N. S.	*
	water side	N. S.	N. S.

\*,  $p < 0.05$ , \*\*\*;  $p < 0.001$ ; N. S. means non-significant.

## DISCUSSION

Invasion of alien species into some areas has had a devastating impact on the native biodiversity [6]-[8]. Native species most vulnerable to the impact of alien species invasions are those which have evolved in isolation from high levels of competition. Especially the invasion of alien species in the river system, where continuous disturbance of each rainfall occurred, is the serious problem [9]. In order to manage the alien species Ministry of Land, Infrastructure and Transport has constructed many biotopes in river ecosystem. They removed burial seeds and vegetation of alien plants from the construction area, but the open areas are immediately occupied by alien species [10]. From the investigation of another biotope area [5], the alien plants invasion mainly occurred in spring, and there is rarely invasion in summer season. Then if the construction is finished in summer, alien invasion prevented by severe hot condition?

In our research the method to prevent alien species invasion is cleared. In summer more 10 native species can emerge in open area at severe condition, but there are few alien species occurred. And the number of alien seedling was very few, moreover the survival rate of seedling in very low. But some native species survived in severe conditions, the number of native species seedling is large, and establishment of vegetation cover can successful. Bared land in summer can easily prevent the alien species invasion. Only *Mollugo verticillata* is exception, they can emerge and survive in summer although there are few numbers (totally 10 seedlings in higher river bed area).

In autumn there is few differences in seedling emergence duration between native and alien species, both species emerged longer than that in summer. But some occupied vegetation effect observed. The prevention of alien invasion was observed in non-removed area. It seems there is no bared space where seedlings can emerge. The effect

of vegetation cover is more serious in alien species than native species.

It is continuing being said that removal of the alien species in fluvial environment is very difficult [11][12]. However, it was shown by our research findings in the summer that invasion of alien species was prevented. Moreover, if occupied by native species in a summer, alien species will become difficult to invade even if autumn condition. In order to press down invasion of alien species, construction plan in which an open space should be made to form in a summer is required. However although only *Mollugo verticillata* was a small number, it was able to invade into the fluvial environment of the summer. For this reason, in order to press down invasion of *M. verticillata*, it is thought that another technique is important.

## CONCLUSION

The following conclusions are drawn based on the study:

- 1) seedlings of alien species could not easily invade bared area in summer, 2) only some seedlings of a few native species can be established at the investigated area in summer, 3) the vegetation by native species that recovered in summer prevented the invasion of alien species, 4) seedling removal hasten the invasion of alien species.

## ACKNOWLEDGEMENTS

We wish to thank the member of Ministry of Land, Infrastructure and Transport Shonai River Office and Tokigawa Nature Observation Office for research support and permission to work in the river. We also thank the members of our laboratory for their assistance in the field works.

## REFERENCES

- [1] Pheloug PC, Williams PA, Halloy SR, "A weed risk assessment model for use as a biosecurity tool evaluating plant introduction," Journal of Environmental Management, vol. 57, 1999, pp. 239-251.
- [2] Nishida T, "Weed risk assessment-mainly in Australia and New Zealand," Ecology of Agriculture and Weed, Plant Species Biology Society, Ed. Bunichisogo, 2007, pp.121-136.
- [3] Imahashi M, Washitani I, "Examination of possibility of a river flood meadow restoration that uses seed bank," Conservation Ecology Research, vol. 1, 1996, pp.145-146.
- [4] Masuda M, "Invasion of alien plant: Status of *Coreopsis lanceolata* L. in Japan," Annual

- Journal of Engineering, Ehime University, vol. 21, Mar. 2000, pp.245-251.
- [5] Masuda M, Ito Y, Nishimura F, "Process of invading the alien plant species into the river ecosystem", in Proc. first Int. Conf. on GEOMAT, 2011, pp.437-442.
  - [6] Pullin AS, Conservation Biology. New York: Cambridge University Press, 2002, ch. 5.
  - [7] Groom MJ, Meffe GK, Carroll CR, Principles of Conservation Biology 3<sup>rd</sup> ed. Sunderland: Sinauer, 2005, ch. 8.
  - [8] Primak RB, Essentials of Conservation Biology 5<sup>th</sup> ed. Sunderland: Sinauer, 2010, ch. 10.
  - [9] Myers JH, Bazely DR, Ecology and control of introduced plants. Cambridge: United Kingdom at the University Press, 2003, ch. 5.
  - [10] Ministry of Environment, List of regulated living organisms under the Invasive alien species act, Tokyo: materials of Ministry of Environment, 2011.
  - [11] Muranaka T, Washitani I, "The population expansion predicted by a simulation model of an invasive alien species, *Eragrostis curvula*, in a middle-reach floodplain", Japanese Journal of Conservation Ecology, Vol. 8, 2003, pp. 51-62.
  - [12] Hatase Y, Oguri H, Matsue M, "Restoration effect of topsoil removal on the herbaceous community invaded by *Coreopsis lanceolata* in the vegetation of dry gravel", Japanese Landscape research, Vol. 75, 2012, pp. 445-450.



Appendix 1. the list of observed seedling emergence and duration of the emergence in each season at high river bed area.  
The number showed the times of emergence observation in each season.

removed native species	Summer Autumn Winter Spring				Non-removed	Summer Autumn Winter Spring			
<i>Acalypha australis</i>	1	2			<i>Acalypha australis</i>	2			
<i>Digitaria ciliaris</i>	3	7		2	<i>Digitaria ciliaris</i>	4	6		
<i>Setaria viridis</i>	5	7			<i>Setaria viridis</i>	5	5		
<i>Zizania japonica</i>	1	4	1		<i>Zizania japonica</i>	1	2		
<i>Cyperus sp.</i>	5	5	1		<i>Cyperus sp.</i>	5	3	1	
<i>Rumex acetosa</i>	1	1			<i>Phragmites japonica</i>	3			
<i>Cayratia japonica</i>	1				<i>Cardamine scutata</i>	1	4		
<i>Boehrspermium tenellum</i>	1				<i>Rumex acetosa</i>	1			
<i>Sonchus oleraceus</i>	1				<i>Artemisia indica</i> var. <i>maximowiczii</i>	1	1		
<i>Cardamine scutata</i>		3	1		<i>Sonchus oleraceus</i>	1			
<i>Phragmites japonica</i>	2	2			<i>Setaria viridis</i> form. <i>misera</i>	1	1		
<i>Portulaca oleracea</i>	1	1	1		<i>Portulaca oleracea</i>	1	2		
<i>Setaria viridis</i> form. <i>misera</i>	2	3			<i>Eleusine indica</i>	1	7		
<i>Eleusine indica</i>		5			<i>Chenopodium album</i>	1			
<i>Lespedeza juncea</i> var. <i>subsessilis</i>	1				<i>Poaceae</i>	7			
<i>Poaceae</i>	8	2			<i>Tarlis japonica</i>	3			
<i>Cyperus iria</i>	1				<i>Sonchus oleraceus</i>	2			
<i>Scirpus nichurae</i>	1				<i>Galium spurium</i> var. <i>echinospermon</i>	3			
<i>Galium spurium</i> var. <i>echinospermon</i>	4				<i>Setum bulbiferum</i>	1			
<i>Solanum nigrum</i>	2				<i>Stellaria media</i>	4			
<i>Oxalis corniculata</i> f. <i>erecta</i>	4				<i>Solanum nigrum</i>	2			
<i>Tarlis japonica</i>	1				<i>Paspalum scandens</i>	1			
<i>Stellaria media</i>		3	2		<i>Panicum bisulcatum</i>	1			
<i>Echinochloa crus-galli</i> var. <i>caudata</i>	1				<i>Trigonotis peduncularis</i>	2			
<i>Trigonotis peduncularis</i>	1	1			<i>Capsella bursa-pastoris</i>	1			
<i>Sagina japonica</i>	1	1	1		<i>Oxalis corniculata</i> f. <i>erecta</i>	2			
<i>Poa annua</i>		1			<i>Rorippa indica</i>	1			
<i>Persicaria hydrotyper</i>		1							
<i>Rorippa palustris</i>				1					
<b>Alien plants</b>									
<i>Trifolium repens</i>	2	4	1		<i>Trifolium repens</i>	4	3		
<i>Bidens frondosa</i>	1				<i>Bidens frondosa</i>	1			
<i>Ipomoea triloba</i>	1				<i>Ipomoea triloba</i>	2			
<i>Chamaecyparis nuda</i>	2	3			<i>Chamaecyparis nuda</i>	1			
<i>Mollugo pentagynia</i>	2	5			<i>Mollugo verticillata</i>	3	4		
<i>Chenopodium ambrosioides</i>	2				<i>Chenopodium ambrosioides</i>	1	1		
<i>Paspalum scandens</i>	1	2			<i>Amaranthus hybridus</i>	1			
<i>Phytolacca americana</i>	1				<i>Solanum carolinense</i>	1			
<i>Lamium purpureum</i>		3			<i>Cerastium glomeratum</i>	4			
<i>Cerastium glomeratum</i>		3	2		<i>Veronica persica</i>	1			
<i>Eragrostis sp.</i>	2		1		<i>Rumex sp.</i>	6			
<i>Eragrostis curvula</i>	4				<i>Lamium purpureum</i>	2			
<i>Gnaphalium peruvianum</i>	1				<i>Paspalum scandens</i>	1			
<i>Verbena brasiliensis</i>	3	1	1		<i>Eragrostis curvula</i>	2			
<i>Lamium amplexicaule</i>	1				<i>Veronica arvensis</i>	1			
<i>Rumex sp.</i>	1	1			<i>Veronica persica</i>	1			
<i>Vicia sativa</i> subsp. <i>nigra</i>	2	1			<i>Phytolacca americana</i>	1			
<i>Coreopsis lanceolata</i>	1				<i>Vicia sativa</i> subsp. <i>nigra</i>	1			
<i>Nuttallanthus canadensis</i>	1	1			<i>Verbena brasiliensis</i>	1			
<i>Veronica persica</i>	3	1			<i>Nuttallanthus canadensis</i>	1	1		
					<i>Veronica persica</i>	1	1		

Appendix2. the list of observed seedling emergence and duration of the emergence in each season at mid river bed area.  
The number showed the times of emergence observation in each season.

	SummerAutumWinteSpring				SummerAutumWinteSpring		
removed <i>Acalypha australis</i>	1	1		Non-removed <i>Acalypha australis</i>	1		
<i>Digitaria ciliaris</i>	4	3		<i>Digitaria ciliaris</i>	4	3	2
<i>Setaria viridis</i>	5	3		<i>Setaria viridis</i>	5	6	5
<i>Zoysia japonica</i>	1	4	1	<i>Zoysia japonica</i>			
<i>Cyperus sp</i>	4	2		<i>Cyperus sp</i>	3	6	
<i>Paederia scandens</i>	1			<i>Setaria viridis form. misera</i>	2	2	
<i>Rumex acetosa</i>	1			<i>Eleusine indica</i>	1	9	1
<i>Phragmites japonica</i>	1			<i>Poaceae</i>	10		
<i>Persicaria longisetia</i>	1			<i>Echinochloa crus-galli var. caudata</i>	2		
<i>Glycine soja</i>	1			<i>Torilis japonica</i>	4		
<i>Cyperus iria</i>		1		<i>Lactuca indica</i>	1		
<i>Poaceae</i>		8		<i>Stellaria media</i>	5		
<i>Echinochloa crus-galli var. caudata</i>	1			<i>Oxalis corniculata f. erecta</i>	2		
<i>Sonchus oleraceus</i>	2			<i>Wahlenbergia marginata</i>	1		
<i>Eleusine indica</i>	6			<i>Cardamine scutata</i>	2		
<i>Galium spurium var. echinospermum</i>	4	2		<i>Digitaria timorensis</i>	1		
<i>Cardamine scutata</i>	4			<i>Galium spurium var. echinospermum</i>	2		
<i>Setaria viridis form. misera</i>	2			<i>Portulaca oleracea</i>	1		
<i>Torilis japonica</i>	3			<i>Paspalum thunbergii</i>			
<i>Oxalis corniculata f. erecta</i>	5	1		<i>Persicaria lapathifolia</i>		1	
<i>Wahlenbergia marginata</i>	1			<i>Sonchus oleraceus</i>			
<i>Solanum nigrum</i>	1						
<i>Bothriospermum tenellum</i>	2						
<i>Stellaria media</i>	3	1					
<i>Trigonotis peduncularis</i>	2						
<i>Lapsana apogonioides</i>	1						
<i>Trifolium repens</i>	1			<i>Trifolium repens</i>	2		
<i>Bidens frondosa</i>	1			<i>Bidens frondosa</i>	2		1
<i>Chamaesyce nutans</i>		3		<i>Ipomoea triloba</i>			
<i>Mollugo pentaptylla</i>	2			<i>Chamaesyce nutans</i>	1	1	
<i>Chenopodium ambrosioides</i>	1			<i>Mollugo pentaptylla</i>	1		
<i>Amaranthus hybridus</i>	1			<i>Chenopodium ambrosioides</i>	1		
<i>Lamium purpureum</i>	3			<i>Amaranthus hybridus</i>	1		1
<i>Trifolium repens</i>	2			<i>Verbena brasiliensis</i>	3		
<i>Eragrostis curvula</i>	4			<i>Cerastium glomeratum</i>	6		
<i>Cerastium glomeratum</i>	5	1		<i>Eragrostis curvula</i>	4		
<i>Rumex sp</i>	2	1		<i>Rumex sp</i>	2		
<i>Chenopodium ficifolium</i>	1			<i>Bidens pilosa var. pilosa</i>	1		
<i>Lamium amplexicaule</i>	1			<i>Sorghum halepense</i>	1		
<i>Specularia perfoliata</i>	1			<i>Vicia sativa subsp. nigra</i>	2		
<i>Amaranthus hybridus</i>	1			<i>Lamium purpureum</i>	3		
<i>Verbena brasiliensis</i>	1	1		<i>Chenopodium ficifolium</i>	1		
<i>Nuttallanthus canadensis</i>	1	1		<i>Veronica persica</i>		1	
<i>Erigeron sp</i>	1	2					
<i>Trifolium campestre</i>		1					
<i>Veronica persica</i>	1						

Appendix 3. the list of observed seedling emergence and duration of the emergence in each season at low river bed area.  
The number showed the times of emergence observation in each season.

	Summe	Autum	Winte	Spring		Summe	Autum	Winte	Spring
remowec					Non-remow				
<i>Acalypha australis</i>	1				<i>Acalypha australis</i>	1			
<i>Digitaria ciliaris</i>	4	6			<i>Digitaria ciliaris</i>	1	2		
<i>Setaria viridis</i>	5	5			<i>Setaria viridis</i>	4	2		
<i>Zoysia japonica</i>	3	1	2		<i>Zoysia japonica</i>	2			
<i>Cyperus sp</i>	5	9			<i>Cyperus sp</i>	2	5		
<i>Paspalum scandens</i>	1				<i>Paspalum japonica</i>	3			
<i>Torilis japonica</i>	1	3			<i>Eleusine indica</i>	1			
<i>Eleusine indica</i>	1	6			<i>Portulaca oleracea</i>	2	3		
<i>Portulaca oleracea</i>	1	2			<i>Persicaria lapathifolia</i>	1	5		
<i>Persicaria lapathifolia</i>	2	1			<i>Portulaca oleracea</i>	2	2		
<i>Chenopodium album</i>	1	1			<i>Digitaria timorensis</i>	1	1		
<i>Phragmites japonica</i>	1				<i>Mimulus nepalensis</i>	1			
<i>Phyllanthus urinaria</i>	1	1			<i>Albizia julibrissin</i>	2			
<i>Solanum nigrum</i>	2	3			<i>Setaria faberi</i>	1			
<i>Setaria faberi</i>		1			<i>Persicaria longiseta</i>	2			
<i>Setaria viridis var. minor</i>	1	2			<i>Eragrostis ferruginea</i>	1			
<i>Poaceae</i>	8	1			<i>Rumex sp</i>	3			
<i>Cardamine scutata</i>	7				<i>Phragmites japonica</i>	1			
<i>Lindernia crustacea</i>	1				<i>Panicum bisulcatum</i>	1			
<i>Sedum bulbiferum</i>	1				<i>Solanum nigrum</i>	3			
<i>Oxalis corniculata f. erecta</i>	2	2			<i>Lophatherum gracile</i>	1			
<i>Sonchus oleraceus</i>	4				<i>Cyperus exaltatus var. iwawakii</i>	3			
<i>Stellaria media</i>	5				<i>Oxalis corniculata f. erecta</i>	5			
<i>Erigeron sp</i>	2				<i>Chenopodium album</i>	1			
<i>Sagina japonica</i>	2				<i>Cyperus iria</i>	1			
<i>Poa annua</i>	1				<i>Centipeda minima</i>	3			
<i>Bothriospermum tenellum</i>	1				<i>Poaceae</i>	7			
<i>Trigonotis peduncularis</i>	1	1			<i>Digitaria timorensis</i>	1			
<i>Galium spurium var. echinospermum</i>	1				<i>Cardamine scutata</i>	3			
<i>Rorippa indica</i>	1				<i>Bothriospermum tenellum</i>	1			
<i>Potentilla anemonifolia</i>	1				<i>Wahlenbergia marginata</i>	1			
<i>Artemisia indica var. maximowiczii</i>					<i>Trigonotis peduncularis</i>	1			
<i>Sagina japonica</i>		1			<i>Erigeron sp</i>	1			
					<i>Sagina japonica</i>	1			
					<i>Stellaria media</i>	2			
					<i>Potentilla anemonifolia</i>	1			
					<i>Artemisia indica var. maximowiczii</i>	1			
					<i>Lespedeza juncea var. subsessilis</i>	1			
					<i>Galium spurium var. echinospermum</i>	2			
					<i>Sonchus oleraceus</i>	1			
					<i>Sagina japonica</i>	1			
<i>Trifolium repens</i>	1	2	1		<i>Trifolium repens</i>		1		
<i>Bidens frondosa</i>		1			<i>Bidens frondosa</i>	1			
<i>Ipomoea triloba</i>	1				<i>Chamaesyce nutans</i>	4			
<i>Chamaesyce nutans</i>		2			<i>Mollugo pentapetala</i>	1			
<i>Mollugo pentapetala</i>	1	3			<i>Chenopodium ambrosioides</i>	1	1		
<i>Chenopodium ambrosioides</i>		1			<i>Oenothera erythrosepala</i>	1	7		
<i>Oenothera erythrosepala</i>	1				<i>Cerastium glomeratum</i>	3	1		
<i>Cerastium glomeratum</i>	1	3	1		<i>Lamium purpureum</i>	1			
<i>Lamium amplexicaule</i>	1				<i>Paspalum scandens</i>	2	1		
<i>Eragrostis curvula</i>		5	1		<i>Amaranthus hybridus</i>	1			
<i>Lamium purpureum</i>		1			<i>Galinsoga quadriradiata</i>	1	1		
<i>Rumex sp</i>	1	5			<i>Oenothera erythrosepala</i>	3			
<i>Specularia perfoliata</i>		1			<i>Verbena brasiliensis</i>	2			
<i>Plantago lanceolata</i>		1			<i>Sorghum halepense</i>	1			
<i>Verbena brasiliensis</i>		2			<i>Sisyrinchium rosulatum</i>	2			
<i>Mesicargo polymorpha</i>		1			<i>Cerastium glomeratum</i>	4			
<i>Paspalum scandens</i>		1			<i>Eragrostis curvula</i>	3			
<i>Gnaphalium pensylvanicum</i>		1			<i>Vicia sativa subsp. nigra</i>	1			
<i>Nuttallanthus canadensis</i>			2		<i>Trifolium repens</i>	1			
<i>Veronica persica</i>		2	1		<i>Chenopodium ficifolium</i>	1	1		
					<i>Lamium purpureum</i>	1			
					<i>Senecio vulgaris</i>	1			
					<i>Gnaphalium pensylvanicum</i>	1			
					<i>Nuttallanthus canadensis</i>	1			
					<i>Veronica persica</i>	1			
					<i>Nasturtium officinale</i>		1		

## **LANDFILL WASTE WATER TREATMENT BY PULSED DISCHARGE IN WATER DROPLET SPRAY**

Akio Takigawa<sup>1</sup>, Keiichi Kato<sup>1</sup>, Takashi Nakajima<sup>1</sup>, Ryota Serizawa<sup>1</sup> and Hiromu Tamba<sup>1</sup>  
<sup>1</sup>Department of Civil and Environmental Engineering, Maebashi Institute of Technology,  
460-01, Kamisatoro-cho, Maebashi, Gunma, 371-0816, Japan

### **ABSTRACT**

In this study, using the plasma generated from the pulsed discharge process, we examined the possibility of simultaneous degradations of dye substance and COD component in the landfill waste water. Furthermore, the possibility of sterilization by the plasma was investigated in the experiments. Experiments were performed to investigate the effects of voltage, repetition rate, charging time and O<sub>2</sub> coexistence on the sterilization and degradations of COD and dye substance. The experimental results show that the sterilization and simultaneous degradations of the dye substance and COD are possible by the plasma and the dye substance is easily decomposed by the plasma from COD. The degradations of the dye substance and COD were enhanced by the presence of O<sub>2</sub>, while the effect on the dye substance degradation is larger than COD degradation. The results reveal that sterilization is possible by plasma, and E. coli is completely dead as compared with the bacteria is difficult to kill completely by the plasma.

*Keywords: Landfill Waste Water, Plasma, COD, Dye Substance, Sterilization*

### **1. INTRODUCTION**

Many of the common final disposal site in Japan, non-combustible residue and ash comprised incineration of waste are mainly reclaimed. Many contaminants, such as SS, BOD, COD, dye substance, nitrogen content and salts etc. are contained in the effluent of these landfills [1]-[2]. In many disposal sites, the BOD value of the water meet the water quality standard value, but the COD does not reach the water quality standard value in many cases. The factor of COD component is dye substance, such as humic acid, fulvic acid etc.. These substances are difficult to decompose biologically, as so-called non-biodegradable organic matter.

Currently, landfill waste water treatment has been used physical treatment and biological treatment. However, biological treatments there are the following problems. That are, the processing time is long, the maintenance of micro-organisms is difficult, and can be not respond to change long-term leaching of water quality. Physical treatment methods commonly use aggregation, precipitation method etc., but there are the problems of sludge generation and high cost required to process.

In this study, using the plasma generated from the pulsed discharge process, we examined the possibility of simultaneous degradations of dye substance and COD component in the landfill waste water. Furthermore, the possibility of sterilization by the plasma was also investigated in the experiments. The pulsed discharges produce ozone, free radicals, ultraviolet radiation, and shockwaves in water, and can be utilized for a more effective water treatment [3]-[5].

Since the breakdown voltage in water is much higher than that in air, a large power supply and expensive pulse forming network are required. In this study, a pulsed discharge reactor is used to produce plasma in gas phase and wastewater is sprayed into the plasma for treatment. This system combines the advantage of using small, simple, and inexpensive power supply and pulse forming network for electrical discharges in air and directly utilizing ozone, as well as free radicals and ultraviolet radiations for treating the wastewater.

The experiments reported here were designed to investigate the effects of charging voltage, repetition rate, discharging time and O<sub>2</sub> coexistence on the sterilization and degradations of COD and dye substance.

### **2. EXPERIMENTS**

The experimental apparatus is shown in fig.1. The apparatus is combined of pulsed power generator, pump, O<sub>2</sub> cylinder, electrode and oscilloscope. The discharge chamber comprised of parallel electrodes enclosed in a vinyl chloride container (140mm×140mm×350mm). The size of frog electrode is 80mm in length, a width of 60mm, 12 mm needle length is fixed to equal 72 present on the surface. The plate electrode is made of stainless steel and sizes of width and length are 60mm, 80mm respectively. A showerhead for injecting droplets into the chamber is set at the lower part in the chamber. The experiments were carried out by using the real landfill waste water in this study. Waste water is sprayed into the reactor from a showerhead at a flow rate of 180ml/min. The sprayed water solution is collected in a container connected to the reactor and

is circulated to the reactor by a pump

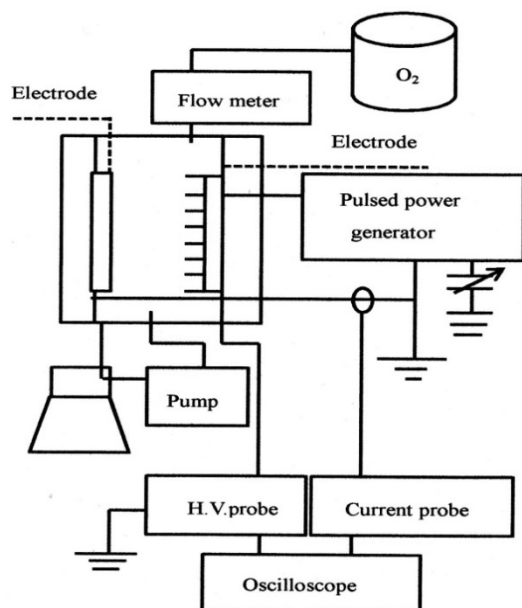


Fig.1 Schematic diagram of the experimental apparatus

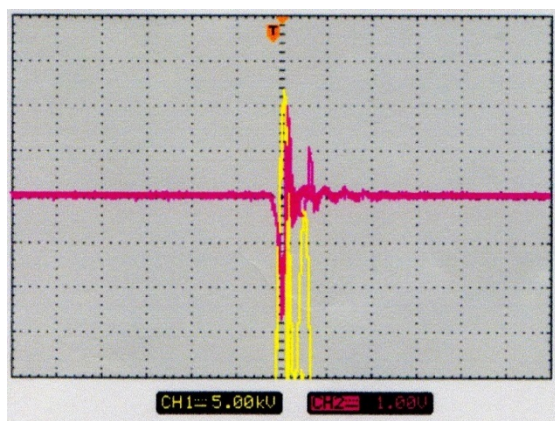


Fig.2 Typical waveforms of pulse voltage and discharge current

The voltage and current are observed by an oscilloscope (Iwatsu, DS-5110) via a 1/1000 high voltage probe (North Star, PVM-2), a 0.1V/A current probe (Person, 6600).

Table 1 Experimental conditions

No.	Voltage (kV)	Repetition rate (pps)	O <sub>2</sub> (ℓ/min)
1	32	100	0.5
2	37	100	0.5
3	42	100	0.5
4	42	65	0.5

5	42	80	0.5
6	42	100	0
7	42	100	0.1
8	42	100	0.25
9	42	100	0.5
COD:366mg/ℓ, capacity:500mℓ			
flow rate:180mℓ/min, cromaticity:1200°			

Table 2 Experimental conditions

No.	Voltage (kV)	Repetition rate (pps)	O <sub>2</sub> (ℓ/min)
A	35	65	0
B	35	80	0
C	35	100	0
E	40	50	0
F	40	50	0.5
G	40	50	1
E. coli :97CFU/ml, capacity:500mℓ			
flow rate:220mℓ/min, bacteria:115CFU/ml			

Discharging power varies with the changes of repetition rate and charging voltage. The sterilization and degradations of COD and dye substance were examined for the various discharging power and O<sub>2</sub> coexistence (table 1). The effects of O<sub>2</sub> presence and reptition ratio on the sterilization was also examined in this experiment (table 2). The ratio of decolorization of dye substance was measured with a UV and visible-light absorption spectrometer (Shimadzu, Uvmini-1240). The concentration of COD was measured with a COD<sub>Mn</sub> and E. coli and bacteria were measured with DD chiekkka-(Asone).

### 3. RESULTS AND DISCUSSION

#### 3.1 Effects of repetition rate and charging voltage on the ratios of COD decomposition and decolorization

The pulse energy changes with the changes of repetition rate and charging voltage and current. Fig.3 shows the effect of charging voltage on the ratios of COD decomposition and decolorization. When increasing the charging time from 0min to 30min, the COD decomposition ratios increases from 0% to 2%, 2%, 29% for the charging voltages of 32kV, 37kV and 42kV respectively. The COD decomposition ratios increase to 7%, 14% with the

change of the charging time from 30 to 120 minutes at the charging voltages of 32kV, 37kV, respectively. However, at the charging voltage of 42kV, the COD decomposition ratio increases from 29 to 36% in the same charging time. These results show that a constant voltage is required for the degradation of COD components by plasma. The results carried out at the charging voltage of 42kV also show that the component of COD can be roughly divided into indecomposable component and easily decomposable component. The easily decomposable component is decomposed in the initial treatment time and the indecomposable component remains in the process late. The ratio of decolorization increases with the increases of charging time and voltage. When increasing the charging time from 0min to 120min,

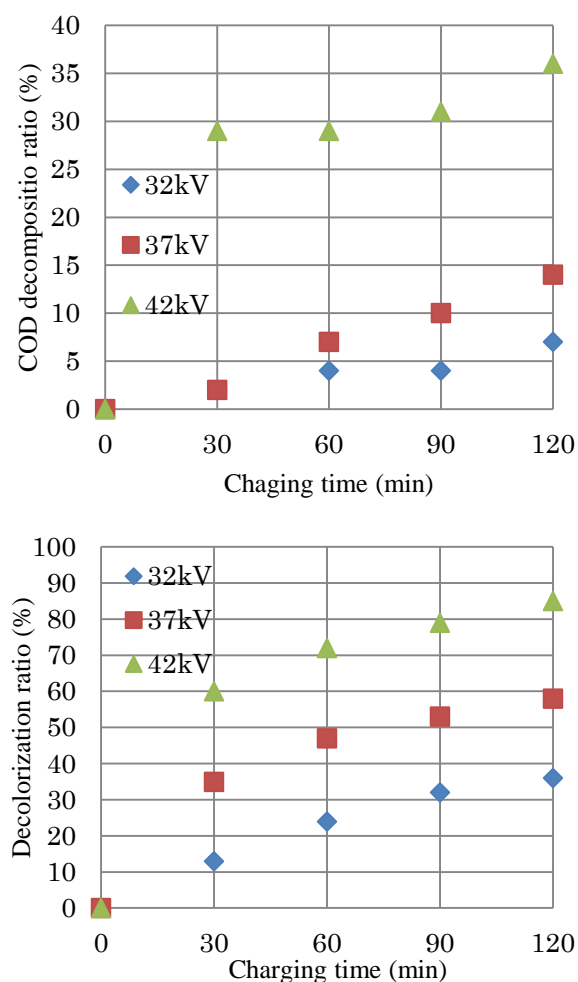


Fig.3 Effect of charging voltage on the ratios of COD decomposition and decolorization

the ratio of decolorization increases from 0% to 82 % at the charging voltage of 42kV. This maximum decolorization ratio of 82 % is much higher than that for the maximum decolorization ratio of 35% at the charging voltage of 32kV. Comparison of the effect of charging voltage on the ratios of COD

decomposition and decolorization shows that simultaneous degradation of the dye substance and COD are possible by the plasma and the dye substance is easily decomposed by the plasma from COD. Fig.4 shows the effect of repetition rate on the ratios of COD decomposition and

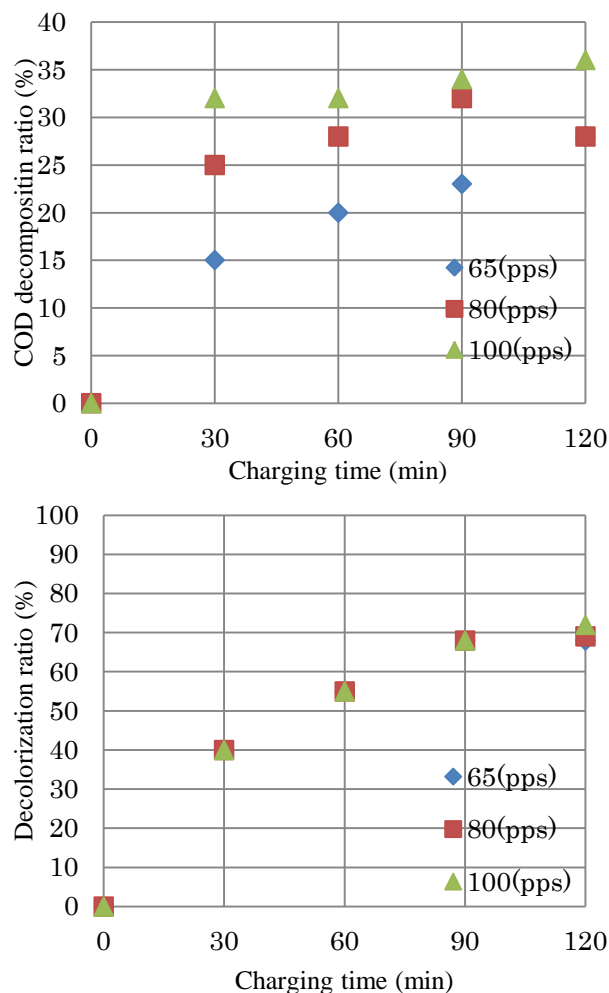


Fig.4 Effect of repetition rate on the ratios of COD decomposition and decolorization

decolorization. As the repetition rate of the applied voltage increases from 65 to 100 pps, the decomposition ratio of COD increase 8% in the range of the charging time, however, the variation in decolorization ratio show similar tendency for the change of the repetition rate from 65 to 100pps. These results show that the COD decomposition ratio is affected by the increase in the repetition rate and the decolorization is not affected by most to changes in the repetition rate.

### 3.2 Effect of O<sub>2</sub> coexistence on the ratios of COD decomposition and decolorization

Fig.5 shows the effect of O<sub>2</sub> coexistence on the ratios of COD decomposition and decolorization at the charging voltage of 42kV and repetition rate of



100 pps for the variation of O<sub>2</sub> gas flow from 0 to 0.5 l/min. When increasing the charging time from 0 to 120 minutes at the O<sub>2</sub> gas flow of 0 l/min, the

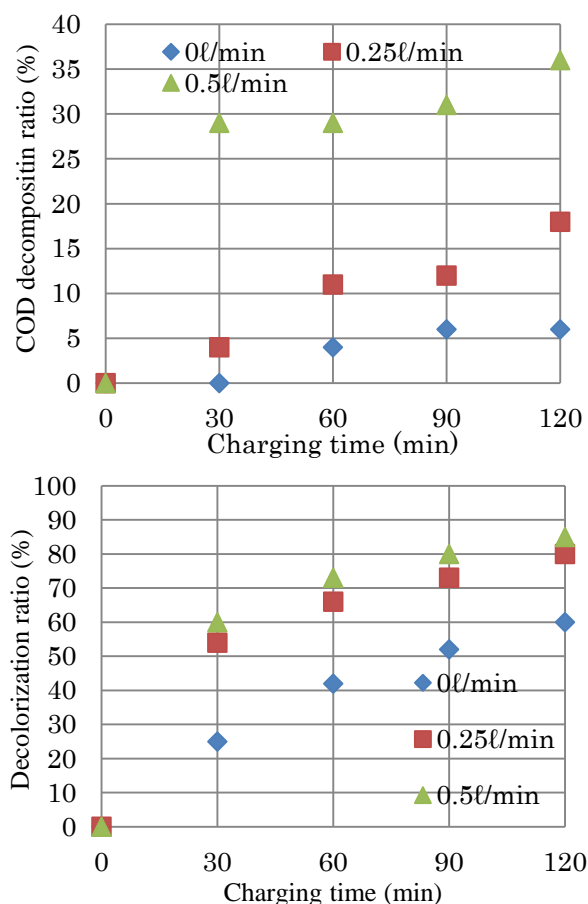
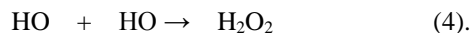
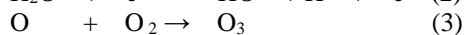
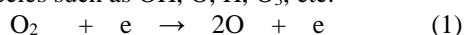


Fig.5 Effect of O<sub>2</sub> coexistence on the ratios of COD decomposition and decolorization

decomposition ratio of COD increases from 0 to 5%. However, The decomposition ratio of COD increases from 0 to 36% as the increasing of O<sub>2</sub> gas flow rate 0 to 0.5 l/min. This means that the variation of the O<sub>2</sub> gas flow rate from 0 to 0.5 l/min results in the increase of 31% of the COD decomposition ratio. On the other hand, when increasing the charging time from 0 to 120 minutes at the O<sub>2</sub> gas flow rate of 0 l/min, the decolorization ratio increases from 0 to 50%. When increasing the O<sub>2</sub> gas flow from 0 to 0.5 l/min, the maximum decolorization ratio increases from 50 to 82%. A basic mechanism of non-thermal plasma in electrical discharge processing for the treatment of wastewater is considered to be the formation of a strong electric field and strong non-thermal plasma where high-energy collisions of molecules with electrons generate various active species such as OH, O, H, O<sub>3</sub>, etc.



Comparison of the effect of O<sub>2</sub> flow rate on the ratios of COD decomposition and decolorization shows that the O<sub>2</sub> coexistence enhances decomposition rates of COD and dye substance by the generate O and O<sub>3</sub>, and effect of O<sub>2</sub> coexistence on the decolorization is higher than that decomposition of COD.

### 3.3 The possibility of sterilization in the landfill waste water treatment by the plasma

Fig.6 shows the experimental results carried out in the experimental condition 2, which investigated the possibility of sterilization in the landfill waste water treatment by the pulasma. It can be seen from the figure that the charging time over 20 minutes, the survival ratio of E. coli is 0%, and bacteria survived even 60 minutes. In addition, when increasing the charging time from 0 to 60 minutes, the survival ratio of bacteria is lower at the

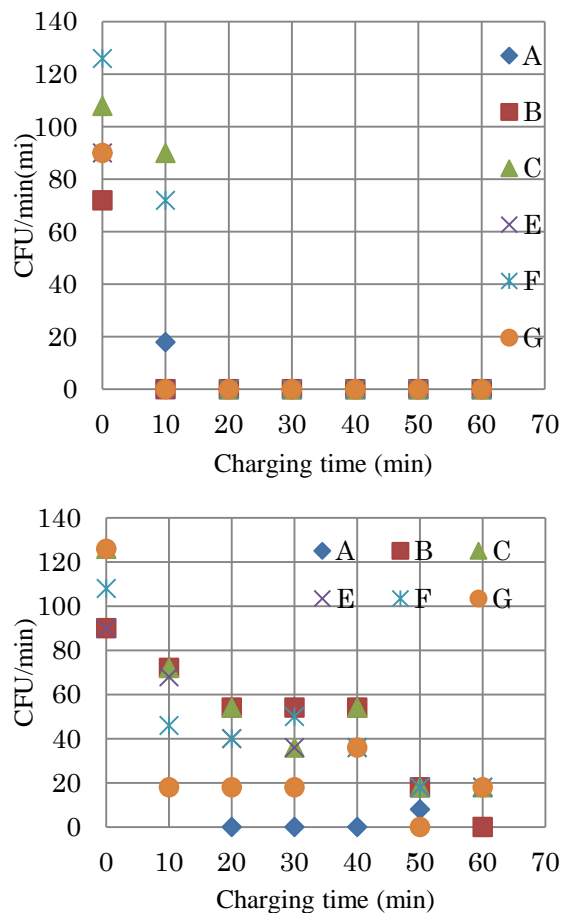


Fig.6 The effect of sterilization by using plasma

experimental conditions of A and F than that the other experimental conditions. These results indicate that the bacteria are difficult to kill by plasma completely and survival ratio was affected by the changes of repetition rate and O<sub>2</sub> gas flow rate.

#### 4. CONCLUSIONS

The effects of the repetition rate, charging voltage and O<sub>2</sub> coexistence on the ratios of COD decomposition and decolorization have been investigated by pulsed discharge in water droplet spray. The comparisons of the experimental results have clarified that the sterilization and simultaneous degradations of the dye substance and COD are possible by the plasma and the dye substance is easily decomposed by the plasma from COD. The degradations of the dye substance and COD were enhanced by the presence of O<sub>2</sub>, while the effect on the dye substance degradation is larger than COD degradation. The effects of repetition rate and O<sub>2</sub> coexistence on the sterilization has also investigated. It was found that sterilization is possible by the plasma, and E. coli is completely dead as compared with the bacteria is difficult to kill completely by the plasma.

#### 5. REFERENCES

- [1] Toji A, "Latest trend and introduction examples for leachate treatment", J.of Computer Science, Vol.31, 2008,pp.21-25.
- [2] Ishigaki T, Yamada M, "Property and treatment of landfill leachate in the world", J.of Computer Science, Vol.31, 2008,pp.26-30.
- [3] Nose T, Yokoyama Y, Nakamura A, Minamitani Y, "Effect of oxygen gas on the decomposition of dye by pulsed discharge in water droplet spray", The Institute of Electrical Engineers of Japan, Vol.131, 2011, pp.659-664.
- [4] Willberg D M, Lang PS, Hochemer RH, Kratel A, Hoffmann MR, "Degradation of 4-chlorophenol, 3,4-dichloroaniline, and an electrohydraulic discharge reactor", Environ. Sci. Technol. Vol.30, 1996, pp.2526-32534.
- [5] Clements J.S, Sato M, " Preliminary investigation of prebreakdown phenomena and chemical reactions using a pulsed high-voltage discharge in water", Vol. IA-23, 1987, pp. 224-235.

# CHALLENGING FACTORS IN THE IMPLEMENTATION OF GREEN BUILDINGS IN MALAYSIA

Che Musa Che Omar, Hooman Abadi, Kamarusin Moh Noor  
University Kuala Lumpur Business School (UniKL BiS), Kuala Lumpur, Malaysia

## ABSTRACT

Green building is the foundation of the sustainable construction development. Green building is redefining building practice and Malaysia is poised for early adoption in recondition of the potential economic and environmental benefits that accrue to it. The Malaysia government has played a strong role in ensuring environment sustainability by way of introducing necessary policies and implementing them. It has resulted in the promotion of green technology that presents the most viable way of meeting with the new green-related activities for environment conservation. In this research, the respondents were randomly selected from the professionals of Malaysian green building index (GBI) and the method applied for collecting data is questionnaire survey. All the questionnaires were sent out to the respondents manually or through e-mail. A total of 800 sets of questionnaire were sent out of 260 questionnaire were received based on Krejcie & Morgan table. The quantitative method was used for analyzing data through SPSS 19. Based on the results, the level of developing green building in Malaysia is not satisfied and government has a key role in the development of green buildings in Malaysia according to GBI. The main barriers can be listed as: deficiency of knowledge and skills, second lack of specific rules and regulations, third lack among of awareness and commitment, finally lack of sustainability elements based on green building rating like GBI.

*Keywords: green building, Green Building Index (GBI), construction development, sustainability*

## INTRODUCTION

In recent years, environmental issues such as climate change, energy crisis, and pollution receive a great attention from the construction industry in Malaysia. Transformation of building construction and operations are significant because the environmental impacts are expected to increase with population growth and changes in other factors such as demographic and economic factors. Various measures have been carried out to minimise the construction impacts towards environment and sustainable development was introduced to improve a quality of life for current people and future generation [1]. The Brundtland Commission defined sustainable development as the ability to make development sustainable to ensure that it meets the needs of the present without compromising the ability of future generations to meet their own needs [3]. In order to implement the sustainable development's goals in Malaysian construction industry, the government introduced green building. Green building has an important role in achieving the aim of sustainable development [4] which is to protect environment and to improve the quality of

human life. The construction industry generates the greatest environmental impacts among all the other industries. Green building designs and standards are developed to improve building operation energy and embodied energy efficiencies, and minimize energy and wastes [5].

Green building practices can play a key role in achieving sustainability in the construction industry [6]. Therefore, over the last two decades the construction industry has made efforts to develop green building practices [2]. Green buildings are about resource efficiency, lifecycle effects, and building performance. Smart buildings, whose core is integrated building technology systems, are about construction and operational efficiencies and enhanced management and occupant functions. There are several commonalities between integrating building's technology systems and constructing a sustainable or "green" building [7]. Many factors are promoting the rapid development of green buildings, including the increasingly serious environmental problems, the constant improvement of demands on architectural environment's quality, the introduction and development of a variety of green building

technologies, the successive implementation of accompanying “green building evaluation criteria” and other relevant policies and regulations.

All is well known, green building’s design is the premise and necessary conditions of green building development, which is itself a concept of sustainable development, and it emphasizes the adaptation to local conditions, times and issues [8]. Unfortunately, the implementation of green building concept in agricultural buildings (e.g. livestock barns, greenhouses, forage storages, etc.) are still limited. Some studies implemented similar approaches to that adopted by green buildings, but they neither fully addressed the concept of green buildings nor achieved its core. resource and material efficiency, and occupant's health and productivity. Kamana and Escultura (2011) defined “sustainable building” or “green building” as an outcome of a design which focuses on increasing the efficiency of resource use - energy, water, and materials - while reducing building impacts on human health and the environment during the building’s lifecycle, through better location, design, construction, operation, maintenance, and removal [9]. Pan et al. (2011) added that a green building is an outcome of a design philosophy which focuses on increasing the efficiency of resource use [10]. Deuble and de Dear (2012) stated that green buildings, often defined as those featuring natural ventilation capabilities, i.e. low-energy or free-running buildings, are now at the forefront of building research and climate change mitigation scenarios [11].

Table 1: Presents a comparison between “green buildings” and “non-green buildings” or “traditional buildings”.

Building Type	Green Buildings	Non-Green Buildings
Energy Consumption	Low	High
Indoor Environment Quality	Very Good	Good
Emissions	Low	High
Waste Management	Highly Efficient	Efficient
Building Materials	Environmentally Friendly	Not Environmentally Friendly
Project Practices	Sophisticated	Normal
Feasibility	>5% than Threshold	Threshold

There is deference between “green building” and “asean-construction”, where the concept of eco-

construction is a part of the whole concept of green building. The charter of the network for the development and use of natural resources in local construction of the Southeast Asian on Eco-construction and Sustainable Development defined the “eco-construction” as a holistic and integrated approach that aims to support access to a healthy habitat, primarily in rural areas, while ensuring conservation of natural resources and to build on the cultural and architectural heritage in construction. The eco-innovation in construction leads to the marketing of products, providing services and innovative solutions which include bioclimatic architecture, and enhancing use of local natural resource and highlight the skills of man and enterprise.

### Green Technology

Green technology refers to the development and application of products, equipment and systems to protect the environment and the natural environment and minimize or alleviate the negative effects of human activities [12]. Generally greenhouse refers to the normal greenhouse constructed for agricultural purposes and plants research. However, this study refers to green residential buildings where humans live. It also refers to residential buildings incorporating green technology with green space and energy efficiency that can provide the comfort, safety and healthy living environment. Green residential buildings are also constructed using sustainable development concepts that utilize green resources which can be found easily such as the wood (trees harvested and replanted), solar energy, hydroelectric power and wind power. Sustainable development is all about meeting the needs of the present (people) without compromising the ability of future generations in order to meet their own needs [13].

### What is a Green Building?

A Green building focuses on increasing the efficiency of resource use energy, water, and materials while reducing building impact on human health and the environment during the building’s lifecycle, through better siting, design, construction, operation, maintenance, and removal. Green Buildings should be designed and operated to reduce the overall impact of the built environment on its surroundings [17].

### Significant of Green Buildings

Green buildings are designed to save energy and resources, recycle materials and minimise the emission of toxic substances throughout its life

cycle. Green buildings harmonise with the local climate, traditions, culture and the surrounding environment. Green buildings are able to sustain and improve the quality of human life whilst maintaining the capacity of the ecosystem at local and global levels. Green buildings make efficient use of resources; have significant operational savings and increases workplace productivity. Building green sends the right message about a company or organisation – that it is well run, responsible, and committed to the future [17].

### Green Building Definition

According to GBI (2011), “A green building focuses on increasing the efficiency of resource use - energy, water, and materials - while reducing building impact on human health and the environment during the building’s lifecycle, through better siting, design, construction, operation, maintenance, and removal. Green Buildings should be designed and operated to reduce the overall impact of the built environment on its surroundings”. Buildings with green technology in Malaysia are considered new. But the efforts to develop a comprehensive green technology for buildings including residential are underway to ensure a better quality, comfortable and affordable to a wide range of social groups. The government of Malaysia is currently aware that green technology can be a practical, useful and an alternative approach for residential buildings [14].

1. Green buildings are designed to save energy and resources, recycle materials and minimise the emission of toxic substances throughout its life cycle.
2. Green buildings harmonise with the local climate, traditions, culture and the surrounding environment.
3. Green buildings are able to sustain and improve the quality of human life whilst maintaining the capacity of the ecosystem at local and global levels.
4. Green buildings make efficient use of resources; have significant operational savings and increases workplace productivity.
5. Building green sends the right message about a company or organisation – that it is well run, responsible, and committed to the future.

### Green Building Index?

The Green Building Index (GBI) is Malaysia’s industry recognised green rating tool for buildings to promote sustainability in the built environment and raise awareness among Developers, Architects, Engineers, Planners, Designers, Contractors and

the Public about environmental issues and our responsibility to the future generations.

The GBI rating tool provides an opportunity for developers and building owners to design and construct green, sustainable buildings that can provide energy savings, water savings, a healthier indoor environment, better connectivity to public transport and the adoption of recycling and greenery for their projects and reduce our impact on the environment [17].

GBI is developed specifically for the Malaysian-tropical climate, environmental and developmental context, cultural and social needs and is created to:

- Define green buildings by establishing a common language and standard of measurement;
- Promote integrated, whole-building designs that provide a better environment for all;
- Recognise and reward environmental leadership;
- Transform the built environment to reduce its negative environmental impact

Table 2: THE GBI RATING SYSTEM

BUILDINGS WILL BE AWARDED THE GBI RATING BASED ON 6 KEY CRITERIA:	
1	Energy Efficiency (EE)
2	Indoor Environmental Quality (EQ)
3	Sustainable Site Planning & Management (SM)
4	Material and Resources (MR)
5	Water Efficiency (WE)
6	Innovation (IN)

- 1) Energy Efficiency (EE): Improve energy consumption by optimising building orientation, minimizing solar heat gain through the building envelope, harvesting natural lighting, adopting the best practices in building services including use of renewable energy, and ensuring proper testing, commissioning and regular maintenance.
- 2) Indoor Environment Quality (EQ): Achieve good quality performance in indoor air quality, acoustics, visual and thermal comfort. These will involve the use of low volatile organic compound materials, application of quality air filtration, proper control of air temperature, movement and humidity.
- 3) Sustainable Site Planning & Management (SM): Selecting appropriate sites with planned access to public transportation, community services, open spaces and landscaping. Avoiding and conserving environmentally sensitive areas through the redevelopment of existing sites and

brownfields. Implementing proper construction management, storm water management and reducing the strain on existing infrastructure capacity.

4) Materials & Resources (MR): Promote the use of environment-friendly materials sourced from sustainable sources and recycling. Implement proper construction waste management with storage, collection and re-use of recyclables and construction formwork and waste.

5) Water Efficiency (WE): Rainwater harvesting, water recycling and water-saving fittings.

6) Innovation (IN): Innovative design and initiatives that meet the objectives of the GBI. Achieving points in these targeted areas will mean that the building will likely be more environment-friendly than those that do not address the issues. Under the GBI assessment framework, points will also be awarded for achieving and incorporating environment-friendly features which are above current industry practice.

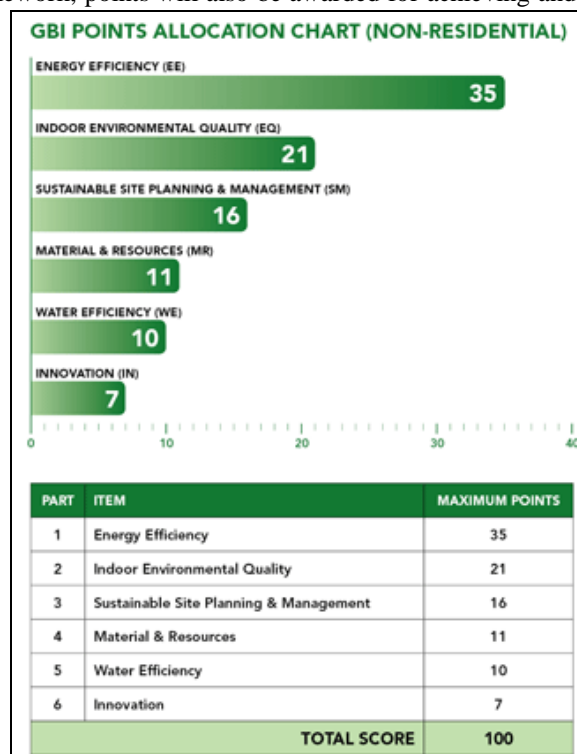
Table 3: THE GBI RATING TOOLS FOR RESIDENTIAL AND NON-RESIDENTIAL BUILDING

THE GBI RATING TOOLS	
NON-RESIDENTIAL	RESIDENTIAL
<p>The GBI Non-Residential Rating tool evaluates the sustainable aspects of buildings that are commercial, institutional and industrial in nature. This includes factories, offices, hospitals, universities, colleges, hotels and shopping complexes.</p> <p>Of the six criteria that make up the GBI rating, emphasis is placed on energy efficiency and indoor environmental quality as these have the greatest impact in the areas of energy use and well-being of the occupants and users of the building. By improving on the efficiency of active (mechanical and electrical) systems as well as incorporating good passive designs together with proper sustainable maintenance regimes, significant reductions in consumed energy can be</p>	<p>The GBI Residential Rating tool evaluates the sustainable aspects of residential buildings. This includes linked houses, apartments, condominiums, townhouses, semi-detached and bungalows. This tool places more emphasis on sustainable site planning &amp; management, followed by energy efficiency. This serves to encourage developers and home owners to consider the environmental quality of homes and their inhabitants through better site selection, provisions of public transport access, increased community services and connectivity, as well as improved infrastructure. Such achievement will help reduce the negative impact to the environment and create a</p>

realised. This can lead to a reduced carbon footprint and also offers long-term savings for the building owners.

better and safer place for residents and the community as a whole.

Figure 1: GBI POINTS FOR RESIDENTIAL AND NON-RESIDENTIAL BUILDING





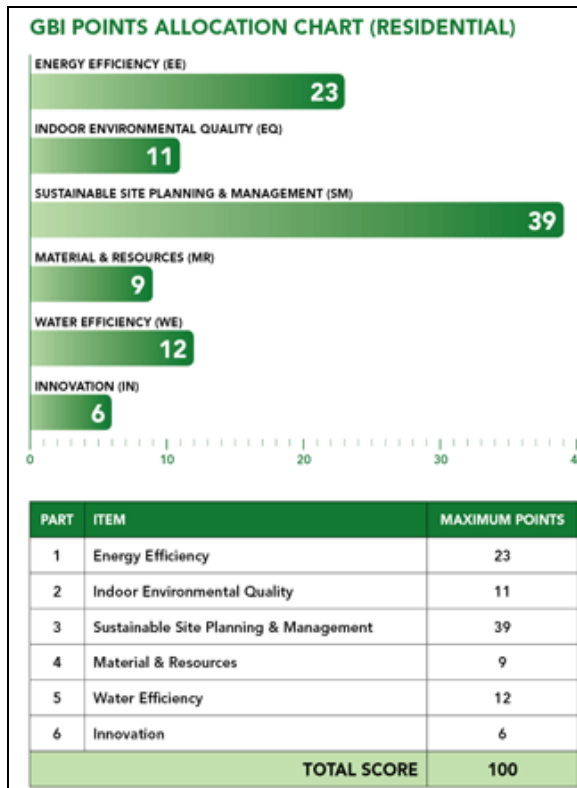


Table4: GBI CLASSIFICATION

GBI CLASSIFICATION		
Points	GBI Rating	Energy Efficient
86+	Platinum	>60%
76 to 85	Gold	50-60%
66 to 75	Silver	40-50%
50 to 65	Certified	30-40%

Table 5: COST OF GOING GREEN OVERALL

COST OF GOING GREEN OVERALL
-----------------------------

GBI	Ave M'sian Bldg	Meets MS1525	GBI Certified	GBI Silver	GBI Gold	GBI Platinum
kWh/m <sup>2</sup> /yr	250 Ringet	200 - 220	150 - 180	120 - 150	100 - 120	<100 Ringet
Energy Savings %	Base line	10 - 20	30 - 40	40 - 50	50 - 60	> 60
Incremental constructn cost %	Base line	0 - 3%	1% - 5%	5% - 8%	5% - 10%	7% - 13%

GREENBUILDINGINDEX SDN BHD | www.greenbuildingindex.org 2013

### Classification of Green Building Systems

Green building classification system is under the sustainable construction umbrella, and it is used to measure the sustainability of a building. Presently, the classification system has several standards and most countries have their own based on their particular climate, soil, environmental, and geographical location. Each country uses a different system to suit the social and cultural development of their respective countries (see Table 6). All the above classification systems for green building have the same objectives; to incorporate green technology in housing construction projects and new business premises. According to this study conducted in 2007 by Professional Builder [16], in Malaysia only, 92%

of respondents indicated that energy-efficient features either extremely important or very important with respect to new house of green building implementation especially for CO<sub>2</sub> reduction. It is also in line with the goals of the Malaysian government to reduce CO<sub>2</sub> emissions 40% from year 2008 onwards and overcome the problem of global warming according to the GBI. In addition, green building design can reduce the benefit of electricity consumption by up to 30%, the ability to reduce carbon emissions by 35%, reduce water consumption around 30% to 50% and help to reduce the cost to be produced Between 50% to 90% [14].

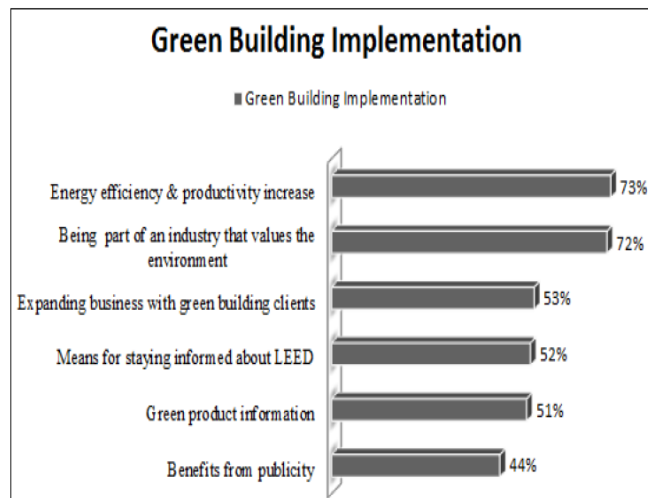
Table 6: CLASSIFICATION SYSTEM OF GREEN BUILDING

Green Building System	Country	Green Building System	Country
LEED (Leadership in Energy and Environmental)	USA	GBAS (China Green Building Assessment Method)	China
CEPHEUS (Cost Efficient Passive Houses as European Standards)	Germany	Protocollo Itaca/Green Building Council Italia	Italy
PromisE	Finland	Indian Green Building Council	India
Green Building Index	Malaysia	Green Mark	Singapore

### Green Buildings Implementation

According to McGraw Hill construction report in 2005 [15], the two (2) most cited perceptions why green buildings must be implemented are; (i) energy savings and productivity savings, and (ii) industry that values the environment. Other factors that the report cited are presented in Figure 2.

Figure2: reasons for green building implementation



### CONCLUSION

This paper has discussed the barriers of challenging factors in the implementation of green buildings in Malaysia. The problems related to green building construction were identified. The problems are common to all countries in term of energy efficient the major barriers are education and training, awareness, professional training, government support, financial support, legal implications and attitude. There are some barriers, which are more pronounced in Malaysia, for example, awareness,

government support and attitude of the population towards green building construction. The government should develop incentive schemes for the projects which adopt green ideas in buildings. The government should encourage in green building Construction for energy efficient. Another four aspects (i.e. managerial defects; social and cultural defects; political and legal defects; and environmental and biological defects) are less critical compared to technical aspect but it does not mean that they are not important and should not give an attention. By considering these critical factors, this study is expected to raising awareness for those who are involves in green building development in Malaysia.

The results of the study can be summarized three folds:

- The green building concept and exposure is still in its early stages in Malaysia and therefore need a strong and extensive awareness and acceptance by the community also a with close collaboration between all players in the construction industry.
- House buyers" perspectives towards green residential buildings are still vague and lack proper understanding. Perhaps, the present conditions (e.g., economy, financial, social and culture) prevented them from understanding the perceived benefits, challenges and something that we possessed today (e.g., natural environment, flora, fauna, and others) that need to be saved for future generations.
- The government's cooperation and intervention is needed intensely in providing more information, knowledge transfer and financial incentives sufficiently for green buildings, renewable energy, energy-efficient and hybrid technologies which can hopefully constitute an engine of growth for the 21st century.

### REFERENCES

- [1]. Samari, M., Godrati, N., Esmaeilifar, R., Olfat, P. and Shafiei, M.W.M (2013). The Investigation of the Barriers in Developing Green Building in Malaysia. Modern Applied Science, 7(2), 1-10.
- [2]. Gluch, P. 2006. Building green perspectives on environmental management in construction. PhD Dissertation, Chalmers University of Technology, Gothenburg, Sweden.
- [3]. Kates, R.W., Parris, T.M. and Leiserowitz, A.A. (2005). What is Sustainable Development: Goals, Indicators, Values and Practice. Environment: Science and

- Policy for Sustainable Development, 47(3), 8-21.
- [4]. Fisk, W.J. and Rosenfeld, A.H. (1998). Potential Nationwide Improvement in Productivity and Health from Better Indoor Environment. Paper presented at 1998 Summer Study on Energy Efficiency in Building, LBNL-41849, 23-28 August 1998, Washington, D.C.
  - [5]. Kwok, K.Y.G., C. Statz, and W.K.O. Chong. 2011. Carbon emission modeling for green building: A comprehensive study of methodologies. Proceedings of the International Conference on Sustainable Design and Construction (ICSDC): Integrating Sustainability Practices in the Construction Industry, pp. 9-17, 23-25 March, Kansas, USA.
  - [6]. Chatterjee, A.K. 2009. Sustainable construction and green buildings on the foundation of building ecology. *Indian Concrete Journal*, 83(5): 27-30.
  - [7]. Sinopoli, J. 2008. How do smart buildings make a building green? *Energy Engineering*, 105(6): 17-22.
  - [8]. Zhang, D., D. Liu, M. Xiao, and L. Chen. 2011. Research on the localization strategy of green building. Proceedings of the International Conference on Civil Engineering and Building Materials, 29-31 July, Kunming, Yunnan, China.
  - [9]. Kamana C.P., and E. Escultura. 2011. Building green to attain sustainability. *International Journal of Earth Sciences and Engineering*, 4(4): 725-729.
  - [10]. Pan, N.-F., R.J. Dzung, and M.D. Yang. 2011. Decision making behaviors in planning green buildings. Proceedings of the International Conference on Computer Distributed Control and Intelligent Environmental Monitoring, pp. 1710-1713, 19-20 February, Changsha Hunan, China.
  - [11]. Deuble, M.P., and R.J. de Dear. 2012. Green occupants for green buildings: The missing link? *Building and Environment*, 56(2012): 21-27.
  - [12]. KeTTHA (2011). Definisi Teknologi Hijau. Accessed on 29 January 2013. Available at: <http://www.kettha.gov.my/content/definisi>
  - [13]. Jennifer, P., and Jackson, T.O. (2008). *Green Buildings: Valuation Issues and Perspectives*.
  - [14]. Green Building Index, GBI Rating System, viewed 2011, <http://www.greenbuildingindex.org/how-GBI-works2.html>
  - [15]. Cryer, B., Felder, J., Matthews, R., Pettigrew, M., and Okrent, B. (2006). *Evaluating the Diffusion of Green Building Practices*.
  - [16]. YM Adnan, MN Daud, I Ahmad, A Aziz - Pacific Rim Property Research ... DETERMINING THE CRITERIA FOR THE CLASSIFICATION OF PURPOSE BUILT OFFICE BUILDINGS IN MALAYSIA, 2009 - [http://www.prres.net/Papers/PRPRJ\\_No\\_2\\_2009\\_Adnan.pdf](http://www.prres.net/Papers/PRPRJ_No_2_2009_Adnan.pdf)
  - [17]. Green Building Index. Accessed on 12 February 2013. Available at: <http://www.greenbuildingindex.org/index.html>

# GEOTEXTILE ENCASED COLUMNS (GEC): WHY, WHERE, WHEN, WHAT, HOW?

Dimitar Alexiew<sup>1</sup> and Graham Thomson<sup>2</sup>

<sup>1</sup>HUESKER Synthetic GmbH, Technical Director, Gescher, Germany

<sup>2</sup> HUESKER Synthetic GmbH, Area Director (Asia Pacific), Singapore

## ABSTRACT

The Geotextile Encased Columns (GEC) foundation system for embankments and dikes on soft soils was introduced some 20 years ago and is now considered State-of-the-art in Germany and step by step worldwide. The GECs consist of compacted non-cohesive fill similar to common sand or gravel columns with one decisive difference: they are confined in a high-strength woven geotextile “cylinder” (encasement) controlling their behavior.

Why: Why did the development start twenty years ago? What were the motivation and the main ideas at that time? What were the reasons for modifications in design procedures, materials etc over the years?

Where, when: What are the typical geotechnical and logistic circumstances for an optimal application? When and where does it make sense? What are the restrictions, if any?

What: What are the geomechanical mechanisms behind it? What are the proper materials (fill, encasement)? Which design procedures are sound and recommendable? What is the knowledge and experience today? What is the need of further research, if any?

How: How should GECs be installed properly and in an efficient way? How to control the construction process in terms of time and quality? How to eliminate problems, if any?

*Keywords: Geotextile Encased Columns, GEC, Embankments, Soft Soils*

## INTRODUCTION

While looking for embankments on soft soils, generally two groups of solutions exist:

Unsupported embankments (Fig. 1): there are four main options:

- build up embankment extremely slowly waiting for sufficient consolidation after every stage;
- replace the soft soil partially or totally;
- install a high-strength basal reinforcement providing overall and local stability and allowing building up the embankment much faster;
- combine the latter option with strip drains to accelerate consolidation and thus the construction process additionally.

Today only options "c" and "d" are of practical relevance. Despite all the pros and contras, the common attribute is that stability (Ultimate Limit State - ULS) can be controlled, but not the short- and long-term settlements (Serviceability Limit State - SLS).

Supported embankments (Fig. 2): the main common idea is to over-bridge the soft soil layers by supporting vertical elements of different types: rigid piles, trench walls etc. or "softer" solutions like different columns (compacted, cemented, mixed-in-place etc.). Herein the border between "pile-similar elements" and "soil improvement" seems to be fluent and depends on country, traditions etc.

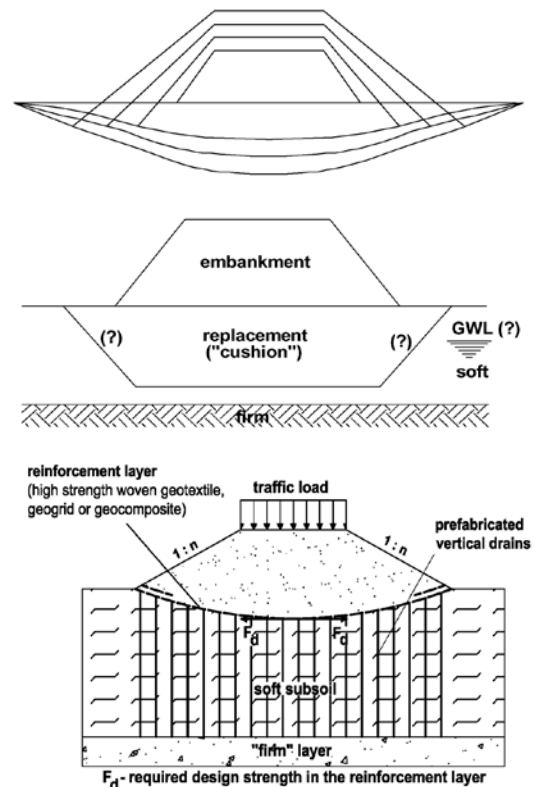


Fig. 1 Unsupported embankments on soft soil: options "a", "b" and "d" from top to bottom.

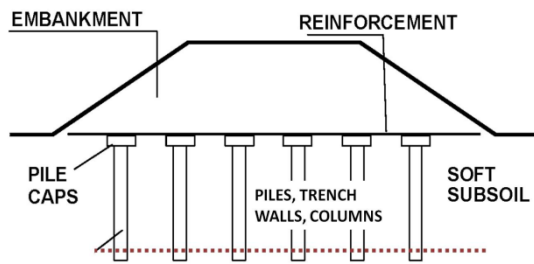


Fig. 2 Supported embankments on soft soil on rigid or semi-rigid elements like piles and columns.

Twenty years ago one specific solution more started: the Geotextile Encased Columns (GEC); they are discussed below in a more detailed way.

### WHY GEC?

The development of the GEC-System started in the early 90<sup>ies</sup>. It was initiated by the Contractor Möbius, Germany and developed in collaboration with Huesker Synthetic and Kempfert & Pa, Consultant.

The idea was to create a system providing:

Versus piles:

- lower costs
- ductility (especially lateral)
- permeability

Versus common granular columns (both in the short- and long-terms):

- mechanical stability even in extremely soft soils
- hydraulic stability
- protected from soft soil intrusion
- use of finer granular materials (e.g. sand) as fill

Versus both: lower installation energy consumption (today we call it “lower carbon footprint”).

Note: at that time execution of unbound granular columns was not allowed in Germany in soils with undrained unconsolidated shear strength  $S_U < 15 \text{ kN/m}^2$  due to the risk of bulging during execution or later under operation; today the limit is even higher:  $25 \text{ kN/m}^2$ .

Using sand was from interest because it is usually available and cheaper in typical soft soil areas.

It became soon obvious that a proper geotextile encasement could help to meet the goals.

The concept is depicted in Fig. 3.

### HOW?

A “triangle” of problems had to be handled:

A. A design procedure was needed for the analyses of the ULS (bearing capacity, overall

stability) and the SLS (settlements and possibly lateral embankment “spreading”).

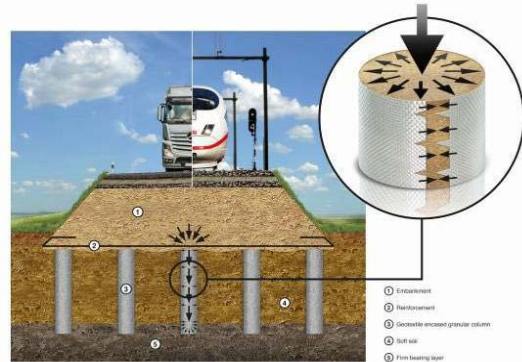


Fig. 3 The GEC-System: basic overview: embankment, horizontal reinforcement (if needed), encased granular columns, soft soil, firm substratum.

B. A proper geotextile encasement was needed to provide a sufficient lateral/radial confinement similar to a flexible oedometer (radial alias ring strength and tensile stiffness plus robustness) together with filter stability and separation capability.

C. A construction procedure was needed being so far as possible quick, easy and not expansive, using common equipment and causing only a limited damage to the geotextile encasement during installation.

### How to Design?

Intensive theoretical and practical research inclusive of 1:1 GEC tests and measurement programs was performed in the 90<sup>ies</sup> in Germany. A simplified design procedure had been suggested earlier in [1], but dealing only with the ULS aspect.

To make the long story shorter: in 2000 a proper verified design method [2] - [4] was finally established and is in the meantime after small modifications included in the German Code for geosynthetic reinforced systems [5]. It handles and solves in a “mixed” way both the ULS and SLS aspects (“mixed”, because it is based on a so called second order theory, say, the deformations of the GEC have influence on the stresses in the system and conversely). Main points are:

the two stages of design (“vertical”, dealing only with the vertical behavior of a column, and “horizontal”, dealing with the global stability of the embankment on GECs and adding a horizontal reinforcement on top of them if needed);

the consideration of some lateral counter pressure from the surrounding soft soil on the GEC, i.e. it is an interactive model;

the key role of the tensile stiffness of encasement



in the ring alias radial direction controlling by confinement the GECs behavior.

Assumptions, further explanations, detailed design recommendations and equations can be found in [2] - [7] both for the “vertical” and “horizontal” (global) design.

### How to Select the Encasement?

The confining encasement is a key component and the most substantial, decisive difference to “common” compacted granular columns (beside one other important difference: the possibility to use sand as a fill). The design asks for two parameters of it (reflecting correctly the physical reality and the common engineering sense):

Tensile stiffness (tensile modulus  $J$ , kN/m) in “ring” direction;

Design strength  $F_d$ , kN/m.

The leading factor is  $J$ , controlling the radial expansion of the column under load and thus its vertical compression, i.e. the settlement of its top, i.e. the settlement of embankment. Higher modulus results in less settlement. The modulus  $J$  is time-dependent due to creep and depends to 80-90% on the polymer used [8] and to 10-20% on the production technology of the encasement. Due to the additional need of separation and filter stability a woven geotextile proved to be the optimal solution. To eliminate the very negative influence of joints/seams mostly on  $F_d$ , but on  $J$  as well, modern encasements are seamless textile flexible cylinders delivered to the site “flat” as a roll (Fig. 4). The most established encasements today comprise two families from two different polymers, both of low creep, but with different moduli  $J$  and strengths  $F_d$ . Their Ultimate Tensile Strength (UTS) varies from 100 to 400 kN/m, the Ultimate Strain  $\varepsilon_{ult}$  from 10 % down to 5 % and the modulus  $J$  from 1000 to 6000 kN/m. Their typical diameters amount from 0.4 m to 0.8 m.



Fig. 4 Typical woven seamless encasement as delivered to the site before installation.

Summary: today the right choice of encasement is practically not a matter of availability, but of design optimization (see below).

### How to Select the Fill?

Generally a granular non-cohesive fill has to be used due to geomechanical (shear strength, low compressibility, insensitiveness to water, easier compactability) and hydraulic (water permeability) reasons. An important difference to the “common” compacted stone/gravel columns is the possibility to use sands. Typical recommended requirements are:

Less than 5 % of fines;

Angle of internal friction  $\phi > 30^\circ$ ;

Coefficient of uniformity  $C_U = 1.5$  to 6;

Coefficient of permeability  $k > 10^{-5}$  m/s and at least 100 times higher than  $k$  of the surrounding soil;

Oedometric (confined) compression modulus  $E_{oed} > 10 \times E_{oed}$  of surrounding soil.

In practice a wide range of materials can be used: from sands to rounded or crushed gravels and recycled materials as e.g. concrete debris (Fig. 5).



Fig. 5 Different fills for GEC in a field trial.

### How to Optimize the System?

The goal of the design is usually to limit the settlements to a prescribed value (SLS) ensuring in the same time bearing capacity and global stability (ULS).

Under given geotechnical conditions the design engineer can vary three factors [5], [6]:

The percentage of GECs  $a$ , % (area ratio of GEC area to total embankment foundation area); based on experience  $a = 10 - 20$  % is recommended; diameter and/or spacing of GECs can be varied;

Fill (e.g. sand or crushed gravel);

Ring tensile modulus  $J$  and strength of encasement.

Obviously the higher the “ $a$ ”, the better the fill and the higher “ $J$ ”, the lower the settlements. However, the fill is often a matter of availability in an acceptable distance from the construction site; normally in problematic low land soft soil areas sands are more accessible than gravels. The diameter of GEC can depend on the commonly available equipment in a country or region (see installation issues below). The parameters of real free choice are the area ratio and the modulus/strength of



encasement, the latter being also easy to transport to any place (Fig. 4).

Figures 6 and 7 show an example how increasing ring tensile modulus and/or area ratio reduce the settlement (same fill is assumed).

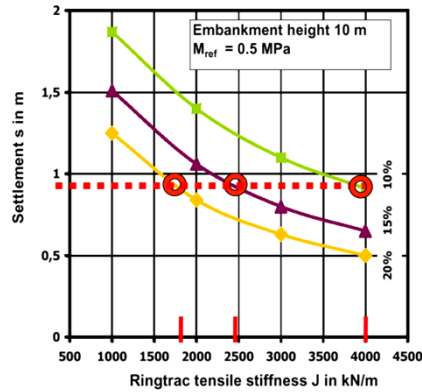


Fig. 6 Achieving the same settlement by different area ratios and ring tensile modulus.

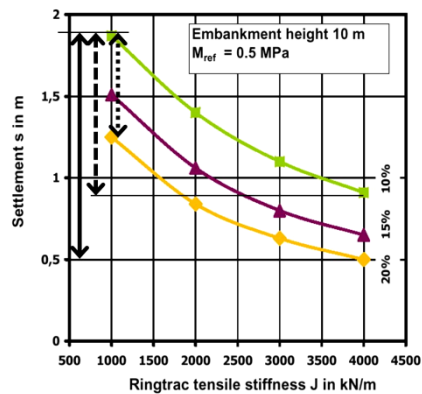


Fig. 7 Reduction of settlement by increase of area ratio, ring modulus and their combination.

Further simplified graphs of similar type for a first orientation can be found in [6].

It is usually more efficient to choose a lower percentage of GECs with higher tensile modulus  $J$ . The savings of fill material, equipment, energy, time, manpower and CO/CO<sub>2</sub> emission are significant. In the example above (Figs. 6 & 7) the increase of  $J$  from 1800 to 4000 kN/m reduces the area ratio from 20 to 10 %, it means only half the numbers of GECs need to be installed.

### How to Install the GECs?

The installation technique was refined over the years, but is generally quite simple [7]. Drive a steel pipe down by vibration; unroll and install the encasement into the pipe; fill it; pull the pipe up by vibration; the compacted GEC is completed (Fig. 8). In the case of the so called displacement method (Fig. 9) the pipe is closed by flaps during driving

down, and for the replacement method it is open and the local soil has to be excavated out (e.g. by a helicoidal spiral tool).



Fig. 8 Examples of completed GECs: in a sand platform, in streaming water, in sludge.

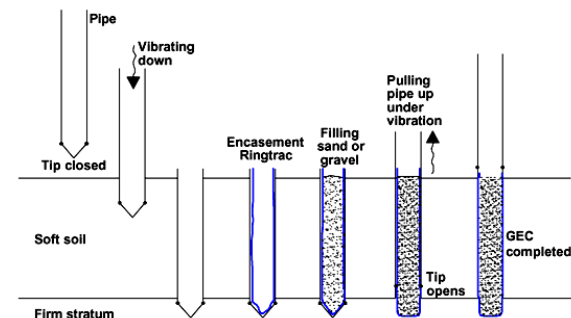


Fig. 9 Scheme of the so called displacement method of installation.

It is an advantage that steel pipes are available worldwide; the flaps can be easily produced and adapted; a wide range of vibro-hammers and bearing rigs is available as well, say, finally there is nothing too specific or sophisticated. The latter makes a difference more to the majority of "common" granular columns.

How to eliminate problems in advance:

- do not foresee a steel pipe with a too thin wall;
- look for pipe diameters being common in a country (it starts with metric/non-metric systems)

- it is often easier to adapt the design to the pipes commonly available than the reverse (see "how to optimize the system" above); note that the modern geotextile encasements (Fig. 4) can be easily customized - not so the pipes;

- use a high-class steel for the flaps;

- use high-frequency vibrators ( $> 30$  Hz) with

sufficient centrifugal force ( $> 2000 \text{ kN}$ ) and moment ( $> 500 \text{ Nm}$ ); resonance-free is not a must;

the working height of the mast of rig should be at least 2 to 3 m bigger than the length of the installation pipe;

it can be worth for larger jobs with e.g. more than 10.000 GECs to test two or three different vibrators before starting the job;

do not hesitate to contact a GEC-experienced professional regarding the equipment if you do not feel comfortable; it could save nerves and months of execution.

## WHERE/WHEN GEC?

Optimal applications:

in soft soils with a  $S_U < 30 \text{ kN/m}^2$ , even better  $< 20 \text{ kN/m}^2$  (possible down to  $S_U = 2\text{-}3 \text{ kN/m}^2$ ) and oedometric (confined) compression modulus  $E_{\text{oed}} = 0.5\text{-}3,0 \text{ MN/m}^2$ ;

for soft soil thickness of 8 to 30 m;

for embankments, dikes, stockpiles etc. of at least 1.5 m height;

from interest if system settlement in the range of 0.1 to say 0.5 m in the construction stage can be accepted and compensated (this is often the case); note, that because the GECs work also as "mega-drains", primary consolidation and settlements occur quickly; post-construction settlements are small;

from interest, if ductile (especially laterally) pile-similar elements being less sensitive to lateral soft soil pressure in depth are required (e.g. in the vicinity of stock piles or other directly founded loads);

from interest as ductile active foundation elements for the loads mentioned above, reducing the lateral trust in depth mentioned also above;

from interest in seismic areas keeping the integrity of granular columns under "shearing" seismic impact [9] - [11];

from interest if a disturbance of the groundwater regime is not acceptable (they are permeable and filter-stable);

from interest, if existing old embankments e.g. for railroads have to be upgraded for higher speeds increasing their static and even more dynamic stability [7], [10], [11].

## WHAT ARE GEC FINALLY?

This is a trial to add some missing points and aspects and to create a feeling what we are talking about.

GECs are bearing pile-similar elements; it is a matter of philosophy if they should be called "piles/columns" or a "subsoil improvement system".

They are end-bearing elements. Nevertheless, due to their "softer" behavior inclusive of the toe zone there is no need to enter the firm substratum by

more than one column diameter, say by 0.5 to 0.8 m in comparison to rigid piles with some meters.

Their behavior can be a priori controlled in a better way in comparison to non-encased granular columns due to the presence of an engineered produced in-plant element; the geotextile encasement.

They are not practically settlement-free like rigid piles, but most of the settlements occur before end of construction and can be easily compensated; however, the settlements are of other order of magnitude compared to non-supported embankments e.g. with basal reinforcement and strip drains (Fig. 1).

They work additionally as vertical drains with extreme drainage capacity.

The GEC-System is ductile and to a significant extent self-regulating and robust because of the interaction of fill, encasement, soft soil and horizontal reinforcement on top of GECs (if any).

Because of their permeability and filter stability their influence on the natural hydraulic environment is marginal.

Because of their permeability and filter stability and mainly due to the installation method by vibrators (say, the installation energy is applied with a high frequency of small rates) the generated dynamic pore water overpressure is smaller and dissipates quicker, say the "disturbance" of the soft soil is limited.

The geotextile encasement works primarily as reinforcement (although in a very specific way) providing (ring) tensile forces of key importance and secondarily as separator and filter.



Fig. 10 Position of the GEC System between two extrema: embankments on rigid elements and embankments without any support.

From a general engineering point of view the GEC-System can be positioned in terms of behavior, specifics and performance as shown in a very simplified way in Fig. 10.

## WHAT IS THE EXPERIENCE AVAILABLE?

In the meantime large with more than 30 significant projects and more than 2300 km of installed GECs. The most popular (German) design procedure [2], [5] seems to work properly being verified by measurement programs and practice; it is may be a bit conservative [7], [12]; further optimization is in progress. Since about ten years it

was always possible to create an optimized solution due to the huge range of geotextile encasements available today; no ULS or SLS problems known by reason of encasements. Problems arose sometimes during installation, e.g. slow installation progress; typical reasons are too light vibrators or low quality of pipe flaps, say the disrespect of basic rules.

## WHAT IS THE NEED OF FURTHER RESEARCH?

Until 2002 the activities in terms of research, measurement programs, design procedures and so on were concentrated mainly in Germany. Since about 2002-2003 international theoretical and practical research, measurement programs etc became more intensive because of the increasing worldwide application of GECs and the efforts to study additional aspects and applications of the system or to optimize design. Due to brevity all the publications in this context cannot be cited herein. Useful compact overviews can be found in e.g. [13], [14]. Generally some basics from the late 90ies were so far confirmed (e.g. [15]). An interesting research is under run dealing with the behavior, possible benefits and specialized design procedures in the case of seismic impact.

## ACKNOWLEDGEMENTS

Due to brevity the list of references herein include only a small part of the work done over almost twenty years in terms of executed projects, design, installation experience, research etc. by many engineers in Germany and worldwide from Brazil to Australia. They all have contributed significantly to the present State-of-the-art.

## REFERENCES

- [1] Van Impe WF, Soil improvement techniques and their evolution, AABalkema / Rotterdam / Brookfield, 1989.
- [2] Raithel M, „Zum Trag- und Verformungsverhalten von geokunststoffummantelten Sandsäulen“, Schriftenreihe Geotechnik, Heft 6, Universität Gesamthochschule Kassel, Kassel, Germany, 1999.
- [3] Raithel M, Kempfert HG, „Bemessung von geokunststoffummantelten Sandsäulen“, Die Bautechnik (76), Heft 12, Germany, 1999.
- [4] Raithel M, Kempfert HG, „Calculation models for dam foundations with geotextile coated sand columns“, Proceedings of the International Conference on Geotechnical & Geological Engineering GeoEng 2000, Melbourne, 2000.
- [5] EBGEO 2010. Recommendations for Design and Analysis of Earth Structures using Geosynthetic Reinforcements. German Geotechnical Society (DGGT), Ernst & Sohn, Essen-Berlin, 2011 (the English version).
- [6] Alexiew D, Brokemper D, Lothspeich S, "Geotextile encased columns (GEC): Load capacity, geotextile selection and pre-design graphs", Proc. Geofrontiers 2005, Austin, USA, 2005.
- [7] Alexiew D, Raithel M, Küster V, Detert O, "15 years of experience with geotextile encased granular columns as foundation system", Proc. Int. Symposium on Ground Improvement IS-GI, ISSMGE TC 211, Brussels, 2012.
- [8] Alexiew D, Sobolewski J, Pohlmann H, "Projects and optimized engineering with geogrids from "non-usual" polymers", Proc. 2<sup>nd</sup> European Geosynthetics Conference, Bologna, 2000, pp. 239-244.
- [9] Guler E, Alexiew D, Abbaspour A, Koc M, "Seismic performance of stone columns and geosynthetic encased columns", Proceedings ICEGE 2013 From case history to practice, Istanbul, 2013.
- [10] Di Prisco C, Galli A, Cantarelli E, Bongiorno D, "Geo-reinforced sand columns: small scale experimental tests and theoretical modelling", Proc. 8<sup>th</sup> Int. Conf. on Geosynthetics, Yokohama, Millpress, Rotterdam, 2006, pp.1685-1688.
- [11] Di Prisco C, Galli A, "Mechanical behaviour of geo-encased sand columns: small scale experimental tests and numerical modelling", Geomechanics and Geoengineering, available online 01 Sep 2011, 2011.
- [12] Raithel M, Alexiew D, Küster V, "Loading test on a group of geotextile encased columns and analysis of the bearing and deformation behaviour and global stability", Proc. International Conference on Ground Improvement and Ground Control (ICGI 2012), University of Wollongong, 2012, pp. 703-708.
- [13] Tandel YK, Solanki CH, Desai AK, "Reinforced granular column for deep soil stabilization: a review", International Journal of Civil and Structural Engineering, 2, No 3. 2012.
- [14] Tandel YK, Solanki CH, Desai AK. "Reinforced stone column: remedial of ordinary stone column", International Journal of Advances in Engineering & Technology, No 6, 2012.
- [15] Murugesan S, Rajagopal K, „Model tests on geosynthetic-encased stone columns“, Geosynthetics International, 14, No 6, 2007.

## **TSUNAMI-GENERATION WARNING SYSTEM USING THE EARTHQUAKE EARLY WARNING SYSTEM**

Susumu Kurahashi<sup>1</sup> and Norimitsu Koike<sup>2</sup>

<sup>1</sup>Disaster Prevention Research Center, Aichi Institute of Technology, Japan;

<sup>2</sup>Civil engineering, Aichi Institute of Technology, Japan

### **ABSTRACT**

We propose an early-warning system for providing tsunami refuge time using the magnitude and depth data provided by the Earthquake Early Warning (EEW) system of the Japan Meteorological Agency (JMA). The EEW provides an announcement of the estimated seismic intensity and expected arrival time at specific points and regions prior to the arrival of strong motion. The hypocenter and magnitude of the earthquake are estimated by using wave form data observed by seismographs near the epicenter. Inukai et al. (2009) proposed a method to determine whether a tsunami is generated by using the scaling relation between the magnitude and depth of the hypocenter. The probability that a tsunami is generated is calculated by using the EEW information (magnitude and depth) and Inukai's scaling relations. In this method, the information regarding the probability that a tsunami will be generated is issued within a few seconds by EEW. We incorporated this method into our system and verified the validity of our system.

*Keywords: Earthquake Early Warning, Tsunami Warning*

### **INTRODUCTION**

On 11 March 2011, a Mw 9.0 earthquake occurred off the Pacific coast of Tohoku, Japan (hereinafter referred to as the Tohoku earthquake). This was one of the largest earthquakes in terms of magnitude and consequence in the history of Japan. The huge tsunami generated by this earthquake struck the east coast along Tohoku, causing the deaths or disappearances of 19,000 people (Fire and Disaster Management Agency, 2012). The height of this tsunami was not properly transmitted during the disaster due to power failure, and people were not able to escape, since they did not believe a tsunami would strike their area. Currently, the Japan Meteorological Agency (JMA) issues tsunami warnings/advisories based on hypocentral parameters, such as the location, depth and magnitude, and the tsunami-simulation database system, which stores more than 100,000 cases of previously-conducted tsunami-propagation simulation results. This system allows tsunami warnings/advisories to be issued within about three minutes after the events occur. For the Tohoku earthquake, the tsunami warning of the initial warning was issued about three minutes after the occurrence of the earthquake. The prediction by the JMA was a magnitude of 7.9. However, the final moment magnitude was 9.0, and as a result, the tsunami warning was underestimated.

If adequate tsunami information is obtained (e.g., information on the possibility of tsunami generation), the actions needed to protect ourselves can be carried out. In particular, it is necessary to provide

such information as early as possible to those that require more time to take refuge, such as elderly people, physically handicapped persons, and people who live near the sea.

The JMA constructed the Earthquake Early Warning (EEW) system, which can provide the predicted S-wave arrival time and seismic intensity from an earthquake. In Japan, EEW was employed nationwide and became fully operational in October 2007. The seismic intensity and arrival times of S waves are calculated by EEW from the magnitude of the earthquake and hypocentral distance between the hypocenter and target site and the sites affected at the target site. The hypocenter and magnitude of an earthquake are determined as quickly as possible by using only the early parts of the P waves at a few stations close to the hypocenter. If this source information provided by EEW can be utilized, we may be able to calculate the probability of the generation of a tsunami.

The Disaster Prevention Research Center (DPREC), Aichi Institute of Technology (AIT), Japan, has organized a consortium that is composed of enterprises in this area in order to mitigate seismic disasters. One of the main research topics of DPREC is to re-distribute the EEW system.

We constructed a system that provides the information on the possibility of the generation of a tsunami by using the magnitude and depth of the occurrence of the earthquake as observed by EEW.

## EEW SYSTEM CONSTRUCTED BY AIT

The JMA has started to utilize EEW, which includes an origin time, a hypocenter, and a magnitude estimated by using the P-wave information observed at a nationwide seismometer network installed by JMA and the National Research Institute for Earth Science and Disaster Prevention. JMA provides an early warning to users including second suppliers within four seconds (average) after the detection of P-waves. DPREC receives the early warning and informs the offices and factories in the Mikawa area of Japan several to dozens of seconds before the arrival of strong motions. Figure 1 shows the conception diagram of the EEW system. Figure 2 shows the distribution system. JMA informs the early warning to the Japan Meteorological Business Support Center (JMBSC) via dedicated lines. DPREC receives the early warning from JMBSC via IP/VPN and distributes the warning to about 50 sites (offices and factories) via the internet within one second.

DPREC has also installed a seismometer network to obtain an observed seismic intensity in order to compare it with an estimated intensity. Furthermore, a PC monitor is installed at a central office and can display various information, such as the epicenter, magnitude, seismic intensity, and arrival time, which is estimated by EEW. It also can animate display P- and S-wave propagating fronts. DPREC obtains the observed seismic intensities from the observation sites via the web and sends back a map of the seismic intensities to simultaneously monitor the intensities at the other sites. The re-distributed EEW system developed by DPREC is currently installed at about 30 factories and successfully prevents seismic disasters.

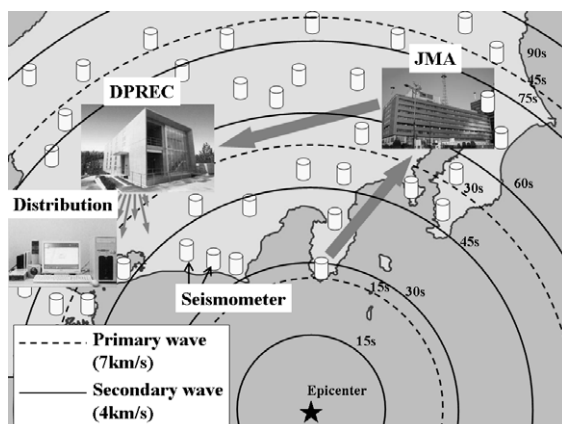


Figure 1 Conception diagram of the EEW system.

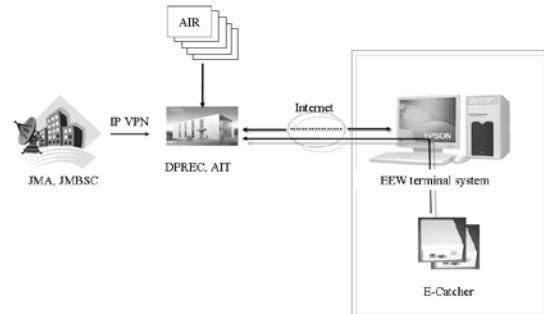


Figure 2 The EEW system of AIT

## RELATIONSHIP BETWEEN MAGNITUDE AND HYPOCENTER DEPTH

A tsunami is generated in the sea simultaneously with a large earthquake due to crustal deformation. The depth of the hypocenter is related to the generation of a tsunami. Inukai et al. (2009) proposed a method to determine the generation of a tsunami by using the scaling relationship between the magnitude and depth of the hypocenter. The data for this relationship were analyzed for 146 earthquakes in which a tsunami occurred. The equation for this relationship is

$$M = 0.005 D + 6.21,$$

where  $M$  is the magnitude and  $D$  is the depth of the hypocenter.

Figure 3 shows a graph depicting this relationship. The relationship shows that a tsunami is generated if an earthquake occurs beyond a magnitude of about 6.3 for shallow earthquakes.

Figure 3 also shows the line depicting the relationship between the magnitude and depth of the hypocenter by Iida. Inuduka's scaling law (2009) is more accurate than that of Iida.

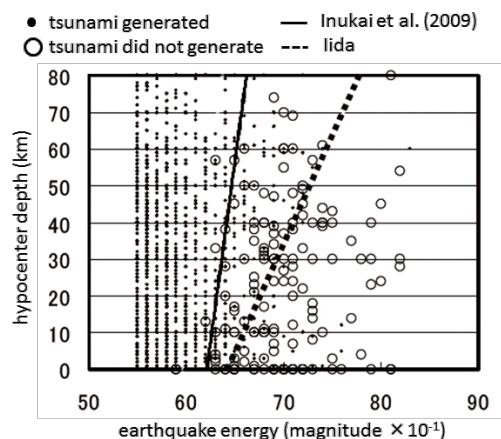


Figure 3 Relationship between the magnitude and depth of the hypocenter. The dots and circles indicate the events in which a tsunami was and was not generated, respectively. The thin line and dotted lines represent the Inukai law and Iida law,



respectively.

### CALCULATION METHOD ALGORITHM OF THE PROBABILITY OF THE GENERATION OF A TSUNAMI

The EEW system also provides source information (e.g., origin time, location of the hypocenter, and depth of the hypocenter). In addition, we can also obtain other information, such as the region of the sea, the inland area, and the accuracy of prevention. We constructed a method to provide the probability of the generation of a tsunami by using this information provided by EEW.

Figure 4 shows a flowchart of the algorithm of the calculation method of the probability of the generation of a tsunami.

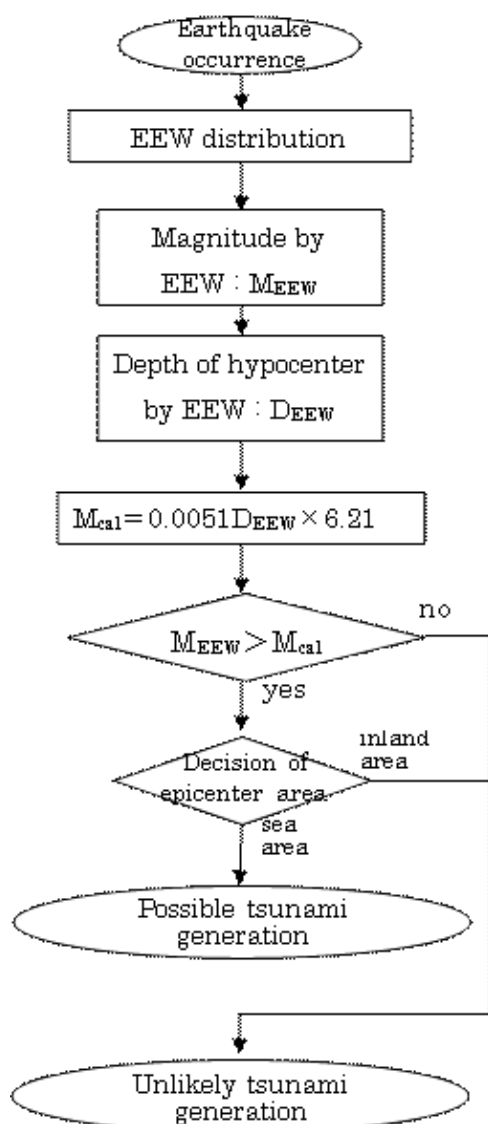


Figure 4 Procedures to calculate the probability of the generation of a tsunami.

### INSTALLATION OF THE EEW SYSTEM

We installed this algorithm into the EEW system. The information of the probability of a tsunami is shown on the PC monitor screen. Figure 5 shows the monitor screen, which can display the following information.

(1) The epicenter and dynamic state of the propagating P-wave (yellow) and S-wave (red) fronts from the epicenter to the predicting site (upper central). Estimated seismic intensity and a margin time prior to the arrival of strong motions at a target site (center).

(2) The seismic intensity and arrival time by EEW at the target site. The larger box is for the main site and the smaller boxes are for the other sites. The color of each box shows the seismic intensity. Red indicates a 5 lower or more of the JMA seismic intensity scale, yellow a scale 3 and 4, blue a scale 1 and 2, and gray indicates a scale 0.

(3) The information provided by EEW (e.g., origin time, received time of the warning, hypocenter, information number, magnitude, and depth of hypocenter) (bottom left).

(4) Real-time data of the seismic intensity observed by AIR-type seismometers installed at the five sites (bottom center).

(5) Communication status between the receiving and transmission servers at DPREC and the analyzed server at the target site (bottom left).

(6) The indication of the probability of a tsunami.



Figure 5 The monitor screen of the EEW system.

### VERIFICATION OF THIS SYSTEM USING THE 2011 TOHOKU EARTHQUAKE

We verified this system by using the 2011 Tohoku earthquake.



The EEW information is updated whenever the source information changes. During the 2011 Tohoku earthquake, the EEW information was updated 15 times. Table 1 shows a list of this information. We calculated the probability of a tsunami by using this system. As result, this information was provided during the third transmission of information, namely, after two seconds from the first transmission of information.

Table 1 EEW information for the 2011 Tohoku earthquake.

Information number	Delay time from no.1 information	Origin time	latitude of hypocenter	longitude of hypocenter	magnitude	depth of hypocenter	maximum seismic intensity
1	0:00:00	14:46:19	38.2	142.6	4.3	10	1
2	0:00:01	14:46:19	38.2	142.6	5.8	10	3
3	0:00:02	14:46:19	38.2	142.6	6.8	10	4
4	0:00:04	14:46:19	38.2	142.6	7.1	10	5.33
5	0:00:05	14:46:19	38.2	142.6	6.3	10	4
6	0:00:06	14:46:19	38.2	142.6	6.5	10	4
7	0:00:06	14:46:19	38.2	142.6	6.5	10	4
8	0:00:11	14:46:17	38	142.8	7.1	10	4
9	0:00:17	14:46:16	38	142.8	7.5	10	5.33
10	0:00:25	14:46:16	38	142.8	7.6	10	5.65
11	0:00:40	14:46:16	38	142.8	7.6	10	5.33
12	0:01:00	14:46:17	38	142.8	7.9	10	5.98
13	0:01:20	14:46:17	38	142.8	8	10	5.98
14	0:01:40	14:46:17	38	142.8	8.1	10	6.55
final	0:01:52	14:46:17	38	142.8	8.1	10	6.55

On the other hand, the tsunami warnings and advisories by JMA were provided within about three minutes after the earthquake. The initial warning issued at 14:49 JST on March 11 was based on the promptly-estimated JMA magnitude of 7.9, and “major tsunami” warnings were issued to Iwate Prefecture, Miyagi Prefecture, and Fukushima Prefecture. At the same time, “tsunami” warnings and tsunami advisories were issued for many other areas (Ozaki, 2011).

This system cannot provide the sea height; however, the probability of the generation of a tsunami can be quickly shown.

Figure 6 shows a timeline of the 2011 Tohoku earthquake.



Figure 6 Timeline of the 2011 Tohoku earthquake with the EEW information and tsunami warning.

## CONCLUSION

By using EEW information, we proposed a method that can produce the probability of the generation of a tsunami by using the relationship between the magnitude and depth of the hypocenter in accordance with Inukai (2010). This method was also incorporated into the EEW system. The probability of the generation of a tsunami can be shown on a monitor.

As a result of the verification of this system, in which the 2011 Tohoku earthquake was used, the information of the probability of the generation of a tsunami can be provided two seconds after the first transmission of information by the EEW system. This time is about three minutes for the JMA tsunami warning, which is more accurate than our system. However, data that can be transmitted faster can be very useful for early warnings, especially to warn those that have physical limitations.

## REFERENCES

- [1] Fire and Disaster Management Agency, “About the 2011 Off the Pacific coast of Tohoku earthquake”, website, [www.fdma.go.jp/bn/higaihou/pdf/jishin/144.pdf](http://www.fdma.go.jp/bn/higaihou/pdf/jishin/144.pdf), Year, 2011.
- [2] Inukai N, Noto H and Kato F, “Development of tsunami generating judgment model for tsunami warning”, 27nd Japan Society of Civil Engineers Kanto branch Niigata meeting research investigation exhibition, 2009.
- [3] Ozaki T, “Journal paper title”, J. of Computer Science, Vol. 1, Aug. 1987, pp. 23-49.
- [4] Islam MR, “Outline of the 2011 off the Pacific coast of Tohoku Earthquake (Mw 9.0) — Tsunami warnings/advisories and observations—”, Earth Planets Space, 63, 2011, pp. 827-830.

# ANALYSIS OF THE RISK OF CONFLICT AROUND THE TRANSBOUNDARY WATER RESOURCES OF THE NORTHERN SAHARAN AQUIFER SYSTEM (NSAS)

Mohamed Redha Menani<sup>1</sup>

<sup>1</sup> Earth Sciences Department, Faculty of Sciences, Batna University, Algeria

## ABSTRACT

The NSAS covers a surface about 1 000 000 km<sup>2</sup>, it's shared by Algeria, Libya and Tunisia. It's situated in a dry zone with a very weak current recharge but a big volume stored, estimated between 20 000 and 31 000 km<sup>3</sup>. Since 1970 to nowadays, the exploitation of the NSAS passed of 0.6 to more 2.5 km<sup>3</sup>/year. This situation provoked risks of water Stalinization, the reduction of the artesianism, the increase of drawdowns ... Which threaten the sustainable socioeconomic development engaged in the NSAS zone.

The rational and joint management of this aquifer became indispensable. The risk of conflict around transboundary waters is numerically estimated on the basis of the combination of weight and quotations of several indicators which have, directly or indirectly, an impact on the risk of conflict (degree of dependence to the transboundary waters, degree of satisfaction of the different needs, geopolitical context, geographic context and the water governance in each country).

*Keywords: Transboundary water resources, NSAS, risk of conflict, governance, joint management.*

## INTRODUCTION

The numerical indexation of the conflict risk around the transboundary water resources repose on the most representative indicators having weights proportional to their relative importance. However, each indicator varies in a rating field according to well defined criteria which take different values according to local conditions, thus providing a partial index of risk (weight x rate) and the sum of these partial indices provides the global risk index of conflict for a given region[1]. This approach allows a standardized assessment of the conflict around the transboundary water resources, based on indicators having fixed weights according to their relative importance (table 1).

Table 1 Risk Indicators and their respective weights

Indicators	Weights
Dependence degree to the transboundary water resources	5
Satisfaction degree of the water needs	4
Geopolitical context of the conflict zone	3
Geographic position in relation to the water resources	2
Water governance and achievements in water resources field	2

These indicators take different values in rating intervals which depend of the local conditions (example of the rating intervals for the first indicator in table 2).

Table 2 Rating intervals of the dependence degree to the transboundary water resources (Weight: 5)

Variation intervals	Rate
Total dependence	10
Partial dependence with difficulties of satisfaction of the needs by other resources (natural and technical difficulties)	8
Partial with possibilities of supplying by other resources but with a high capital cost	6
Partial with possibilities of supplying by other resources with an advantageous capital cost	4
Partial to weak with an effective supply by other resources	2

The combination between the fixed weight and the reached rate by each indicator in a given region leads to a partial index of the risk concerning this indicator and the sum of the partial indices provides the global conflict risk index around the transboundary water resources.

The rating intervals are based on criteria and standards which take into account results of research works carried out through actions at world scale which have not only integrated the quantitative and qualitative aspects of the resources, but also the economic, social, educative and political aspects.

According to the local conditions, risk indicators take values between 1 and 10; the greatest dimensions indicate a high risk of tension and conversely.

It's clear that these ratings must be established

for each country concerned by the transboundary water resources. The advantage of this method is its flexibility, i.e. the user can insert intermediate and specific steps which are not considered here and affect to them dimensions proportional to their relative importance by comparison with the proposed ratings.

The partial risk index is obtained by multiplying the fixed weight of an indicator by the rate reached by this indicator according to the local conditions.

$$(IPR = I_{iw} \cdot I_{ic})$$

IPR: partial index of risk

Iiw: indicator fixed weight

Iic: indicator rate (variable)

The total index of risk is the sum of the partial indexes:

$$GIR = \sum PIR = \sum I_{iw} \cdot I_{ic}$$

With GIR: global index of risk of conflict around the transboundary water resources

One note generally that two countries or more involved in a transboundary water conflict do not present the same global index of risk because conditions which prevail in each one of these countries are different. According to this procedure, the minimum conflict risk index is 25, whereas the maximum index is 158.

## THE NORTHERN SAHARAN AQUIFER SYSTEM (NSAS)

The northern Saharan aquifer system is shared between Algeria, Libya and Tunisia. It is situated in a high arid zone and covers a surface of approximately 1 000 000 km<sup>2</sup> with minor current recharge but with a large volume stored, estimated between 20 000 to 31 000 km<sup>3</sup> [2]. During the last 30 years, the NSAS exploitation passed from 0.6 to 2.5 billions m<sup>3</sup>/year, leading in major risks of salinisation of groundwater, the shortage of the natural releases and the depletion of water... which threaten the sustainable socioeconomic development committed in the whole zone. To counter at best these risks, a process of cooperation was introduced since 1998 under the aegis of the Northern Sahara Observatory (OSS) in partnership with institutions in charge of water resources in the 3 countries [3].

The NSAS water resources are very weakly renewable, nearly 1 billion m<sup>3</sup>/year, compared to the current exploitation esteemed at 2.5 billion m<sup>3</sup>/year. This data led to the conception of a hydrodynamics model that allows envisaging various exploitation scenarios of the water resources while taking into account perspectives of socioeconomic development in the 3 countries [4]-[5].

The NSAS extension is of 1 million km<sup>2</sup> of which 700 000 are in Algeria, 80 000 in Tunisia and 250 000 in Libya (Fig 1). This strategic aquifer

system will shelter on the horizon 2030 nearly 8 millions inhabitants.

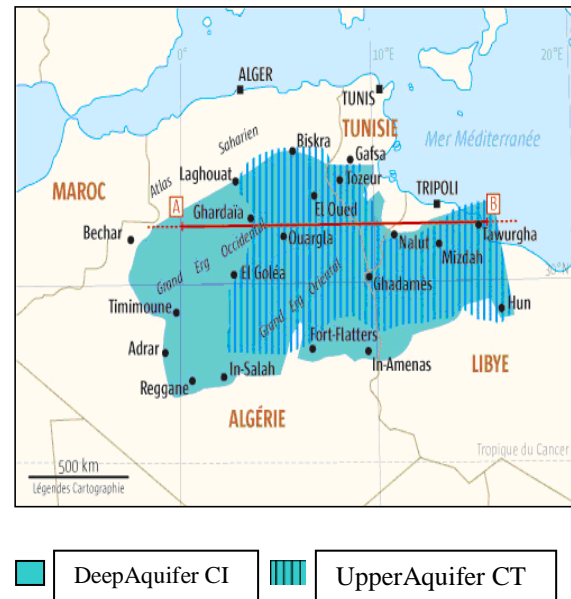


Fig. 1 Geographical position of the Northern Saharan aquifer system [3].

A summary cross geologic section of the system (see AB on Fig.1) is reported on Fig. 2.

The NSAS aquifer system has a complex structure [6]-[7] in which one can discern:

- The terminal complex (CT) constituted by calcareous series and sands which have a water reserve of nearly 11 000 km<sup>3</sup>;
- Gypseous marls series separating the two aquifers;
- The deep aquifer called CI (continental intercalaire), at variable depths (between 50 and 2300 m) confined in sand formation. The reserve stored in this aquifer is estimated at nearly 20 000 km<sup>3</sup>. Its water is warm (60 °C by places);
- Some intermediary aquifers with local importance.

The principal zones of recharge of the NSAS aquifer system are: the South Piedmont of the Atlas in the North-West (Algeria), The Tinrhert Mountains in the South (Algeria), the Dahar Mountains in the East (Tunisia), The Nafusa Mountains in the North-East (Libya).

Concerning the CI aquifer, the outlet zones are: the Touat-Gourara and the Tidikelt (Algeria), the El Hamma fault zone in Tunisia and the Tawargha source (Libya).

The outlet zones of the CT are principally: the salted Lakes (Marouan-Melrhir in Algeria and Gharsa-Djerid in Tunisia) and the golf of Syrte near Misrata in Libya).

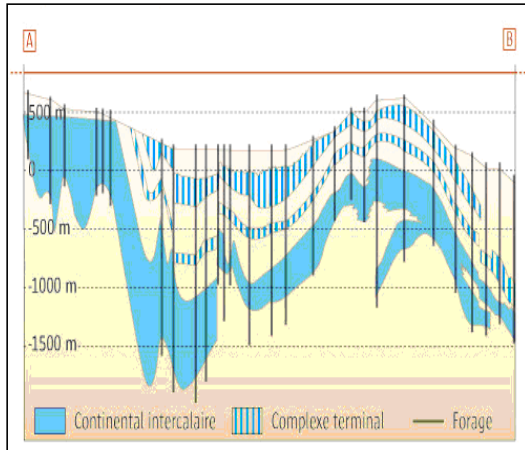


Fig. 2. Geological cross section of the NSAS [3]

Groundwater of the CT has 2 to 5 g/l of salts, those of the CI, 1 to 4.5 g/l. This high salinity is the origin of the deterioration of agricultural lands.

In 2008, The NSAS was exploited by 8800 catching points (3500 for the CI and 5300 for the CT) and the exploitation was 2.5 Billions m<sup>3</sup>/year (1.5 in Algeria, 0.55 in Tunisia and 0.45 in Libya).

It's clear that if this rhythm of exploitation continued, the NSAS zone will be exposed to serious risks of water depletion and a deterioration of its quality. Signs of this state are already perceptible.

Between 1950 and 2000, drawdowns increased from 25 to 50 m in many places.

According to the ERES model results, the potentialities of the NSAS are in an order of 156 m<sup>3</sup>/s.

## NUMERICAL INDEXATION OF THE RISK OF CONFLICT AROUND THE NSAS

### Dependance Degree To The NSAS

The three countries are situated in a dry region with very low atmospheric precipitations. The situation was analyzed by country under the following aspects:

- The renewable water resources potentialities, including surface water ;
- The non-renewable water resources captured, by distinguishing those of the NSAS;
- The actual capacities of the non-conventional water resources;
- The current water supply sources for the different uses;

The Ratio of withdrawals from the NSAS compared to the total production express the respective actual dependence degree of each country to the NSAS water resources. The dependence degree to the NSAS water resources

must also be analysed by comparison to the water exploitation index estimated as percentage of the annual renewable water resources. In the case of Libya, even if withdrawals from the NSAS represent a relative little ratio (nearly 9 %), this country is in total dependence of the non-renewable water resources of the NSAS (Northern Sahara Aquifer system) and of the Nubian Sandstone Aquifer System [8].

The dependence degree to the NSAS can be appreciated by the ratio of the withdrawals from NSAS to the total renewable water resources (Table 3).

Table 3 Withdrawals from NSAS (ratio)

	(WNRW) (Km <sup>3</sup> /y)	(TRWR) (Km <sup>3</sup> /y)	WNRW/TRWR (%)
Algeria	1.5	12.2	12.3
Libya	0.4	0.6	<b>66.7</b>
Tunisia	0.54	4.7	11.5

WNRW:Withdrawals of Non Renewable Water Resources from NSAS.

TRWR:Total Renewable Water Resources

Libya is in a position of high dependence to the NSAS water resources for satisfying its different needs [9].

Tunisia and Algeria are less dependent to the NSAS water resources. For these 2 countries, the improvement of the mobilisation of the renewable water resources can allows a substantial gain, in particular in Algeria where considerable efforts are made to increase the mobilization of surface waters through the construction of large dams to carry it from 7 to 9 Km<sup>3</sup>/year.

The degree of dependence to the transboundary water resources can be appreciated by the quotation indicated in table 4.

Algeria:The country as a whole can be considered actually as being in partial dependence to the NSAS water resources but the south of the country, in addition to the country's NSAS zone, is in total dependence of these resources. In addition the NSAS serves the extreme south (Tamanrasset) by hydraulic transfer from Ain Salah with 750 km of double conduct. The extreme south is situated at 2400 km far from the Mediterranean sea and an hydraulic transfer of desalinated water for example can't be envisaged, because very difficult technically and non-viable economically.

Libya: The Total Renewable Water Resources of Libya are insignificant compared to the water demand of this country. The dependence to the NSAS and the NSAS's water resources is complete even if these are non-renewable water resources.

Tunisia: The situation can be considered as being worse than in Algeria. Indeed, the water resources of the country are practically used with their threshold of renewal. The dependence to the

NSAS and to the non-conventional water resources will increase more and more. The South of the country is in total dependence of the NSAS' water resources

Table 4 Rating intervals of the dependence degree to the transboundary water resources (weight: 5).

Variation intervals	Rate	Country	PIR
Total dependence	10	Libya <sub>b</sub>	50
Partial dependence with difficulties of satisfaction of the needs by other resources (natural and technical difficulties)	8	Algeria <sub>a</sub> Tunisia <sub>c</sub>	40
Partial with possibilities of supplying by other resources but with a high capital cost	6		
Partial with possibilities of supplying by other resources with an advantageous capital cost	4		
Partial to weak with an effective supply by other resources	2		
Partial index of minimum risk ( $PIR_{min}$ ) = fixed weight. Minimum rate = 5. $2 = 10$			
Partial index of maximum risk ( $PIR_{max}$ ) = fixed weight. Maximum Rate = 5. $10 = 50$			

### Satisfaction Degree Of The Water Needs

The NSAS' water resources don't serve the NSAS' zone only but also other regions by transfer like in Libya notably and subsidiarily in Algeria. In the future, Algeria planners' project to proceed to hydraulic transfers from the NSAS towards regions situated in the north of the country. This index is obtained on the basis of the analysis of the different needs (domestic, agricultural and industrial uses) and the degree of their satisfaction in the 3 countries [10]-[11]-[12]. Due to the length of this analysis, only the final results are summarized in table 9.

### The Geopolitical Context

Considered under the conflict aspect, the geopolitical context of a region can be a critical factor. In the case of a political or armed conflict between countries, the management of the transboundary water resources endures the direct consequences. The cooperative committees of dialogue have then great difficulties in their

operation if they are not simply blocked. However, in regions marked by normal political relations, the risk of conflict decreases very appreciably.

By geopolitical context of the zone of conflict, it is the state of relations which bond countries of the area subject to a problem of transboundary water resources which is aimed here. It's obvious that if it's an armed conflict zone, the problem of water becomes an additional detonator. However, if the concerned states belong to a community space in which there are rules for the integrated water resources management and commissions especially for this type of conflict, the risk becomes weak then (Table 6).

Table 6 Rating intervals of the geopolitical context (weight: 3)

Variation intervals	Rate		PIR
Zone of armed conflict	10	Libya	30
Zone of diplomatic tension	8		
Zone of ethnic tension	6		
Normal relations between states	4		
Zone belonging to a communitarian space	2		
Existence of treaties, commissions of basins	1	Algeria Tunisia	3
Partial index of minimum risk ( $PIR_{min}$ ) = 3			
Partial Index of maximum risk ( $PIR_{max}$ ) = 30			

### The Geographic Position In Relation To The Transboundary Water Resources

The influence of the geographic position is related for example to the fact that a country situated in the upstream part of a river has more benefits by this situation that country located in the downstream part, either naturally or by a provoked way (non-consensual installations and river derivations, discharge of polluted water, not providing in time data relating to the rises of water which can cause grave floods in the downstream part. etc...). This factor concerns also transboundary aquifers, by taking into account recharge zones of these aquifers, pumping fields and natural outlet zones of these aquifers [13]-[14].

This concept integrates in an implicit way the environmental aspect. For example, pumping in captive aquifers provokes a drawdown in broad zones which exceed the pumping field itself.

A country is considered under "natural dominance" when for example the resources of which it depends are located out of its territorial limits, or when it is under bad hydro-climatic conditions compared to the riparian states (table 7).

The extreme case is when a country is under the two cases of domination (natural and provoked).

The results concerning this index are reported in table 7.

Table 7 Rating intervals of the geographical context (weight: 2)

Variation intervals	Rate		PIR
Under a natural influence	3	Algeria	6
		Tunisia	6
		Libya	6
Under a provoked influence	7		
Non concerned	0		0
Partial index of minimum risk ( $PIR_{min}$ ) = 6 Partial index of maximum risk ( $PIR_{max}$ ) = $14 + 6 = 20$			

These results are in relation with the natural outlets situated in Algeria and Tunisia (Salted lakes).

The 3 countries are under bad hydro-climatic conditions (dry zones) and have NSAS' groundwater natural outlets threatened.

#### Water Governance And Achievements In Water Resources Sector

Water governance is analyzed under criteria widely accepted in this field [15]. A great number of documents have been consulted for this analysis. These criteria are reported in Table 8.

Table 8 Rating intervals of the water governance and achievements (weight: 2).

	Rate	Algeria	Libya	Tunisia
Tarification (politic)	2	1.25	0.5	1.75
Institutions et Legislation	2	1.5	1.5	1.5
water metering and service quality		1.25	0.5	1.75
Access to water and to sanitation	2	1.5	0.5	1.5
Management of water supply and sanitation services, Global investments	2	1.5	0.75	1.25
		7	3.75	7.75
$PI = 2 * (10 - \sum x)$		6	12.5	4.5

Partial index of minimum risk ( $PIR_{min}$ ) = 2

Partial Index of maximum risk ( $PIR_{max}$ ) = 18

Each time a condition is filled, the rate affected at this condition is diminished of the total rate (10).

Better is the water governance, better is the water availability, decreasing in this sense the tension around this resource.

On the basis of the analysis of the indicators related to the water governance [15], it appears that the water governance in Tunisia is the best in the region by considering the priority accorded to the rational water resources management in the different uses [16]-[17]. The second position occupied by Algeria is due to the big investments in the water resources field (mobilisation of conventional and non-conventional, desalinisation of sea water, efforts in the management sector...) [18].

Libya occupies the last position because the centralized management of the water resources [19]-[20] and the uncertainty affecting in this period of troubles, the institutional and political framework.

#### The Global Index Of Risk (GIR)

The Synthesis of the partial index of risk gives the final result compiled in the table 9.

Table 9 Global index of Risk

Indicators	PIR		
	Algeria	Libya	Tunisia
Dependence degree	40	<b>50</b>	40
Degree of satisfaction of water needs	17.5	13.5	17.5
Geopolitical context	3	30	3
Geographic Position	6	6	6
Water Governance	6	12.5	4.5
Global Index of Risk	72.5	<b>112</b>	71

#### CONCLUSION

The indexation mode adopted allows placing Libya in a situation of a high risk of conflict around the NSAS' transboundary water resources compared to the riparian countries (Algeria and Tunisia)

This level of risk assessed at 112 points on a scale of 158, is due to the conjunction of many factors, of which the most important are a total dependence to the NSAS' water resources but also to the Nubian sand stones aquifer shared between Libya, Egypt, Tchad and Soudan, a situation of uncertainty and troubles inside the country with a high risk of secession between the different regions of Libya and finally a very low level of water governance compared to riparian countries.



The situation in Algeria and Tunisia is much better even the high level of exploitation of the national renewable water resources; the maximum is reached in Tunisia.

The relative good water governance in Tunisia risks furthermore to be stopped by the very significant drop of the investments in the water resources sector observed the last two years.

The current situation in Algeria is totally different. It is marked by a considerable level of investments in strategic projects in the water resources sector which will improve durably not only the water availability but also the creation of thousands hectares of irrigated agricultural areas, notably in the high lands regions.

The three countries are dependent of the NSAS' water resources and until recently, the mechanism of dialog initiated through the Sahel and Saharan Observatory (OSS) seems to have correctly functioned, even if a clear commitment of the 3 countries on the joined management of the NSAS water resources isn't yet notified.

## REFERENCES

- [1] Menani M. R. "A Numerical Method to Index the Risk of Conflict around the Transboundary Water Resources. Validation by a Studied Case." *Water Resources*, Vol. 36, No. 6, 2009, pp. 731-742.
- [2] Baba Ouled Sy. Recharge et paleorecharge du système aquifère du Sahara septentrional. Thèse de Doctorat en Géologie, Univ. De Tunis El Manar, 2005, 261 p.
- [3] OSS. "Le Système aquifère du Sahara septentrional (Algérie, Tunisie, Libye) Gestion concertée d'un bassin transfrontalier », Collection synthèse, n° 1 – Tunis, 2008, 56 p.
- [4] OSS. "Système aquifère du Sahara septentrional : une conscience de bassin. Modèle mathématique." Volume 4. 2002, 234p.
- [5] OSS "Système aquifère du Sahara septentrional – Essai de synthèse socio-économique." 2005, 73 p.
- [6] Bied-Charrenton M. "Le système aquifère du Sahara septentrional, une conscience de bassin." Synthèse de la première partie du projet (1999-2002) « OSS/NSAS », 2002, 17 p.
- [7] Margat J. "Les eaux fossiles". *Afrique contemporaine*, N°161 (Spécial) 1er trimestre, 1992.
- [8] Salem O. "National water policy review and Management of water scarcity In Libya. Partie I, la gouvernance et la politique dans le domaine de l'eau." Chapitre 6, 2002, pp. 87-103.
- [9] Salem O. M. "Water resources management in Libya". Workshop on Integrated Water Resources Management (IWRM) in Libya, Tripoli (11-12 April 2007).
- [10] Earth Trends "country profiles 1. Water Resources and Freshwater Ecosystems." ,Algeria, 2003.
- [11] Earth Trends "country profiles 2, Water Resources and Freshwater Ecosystems, Libyan Arab Jamahiriya." 2003.
- [12] Earth Trends "country profiles 3, Water Resources and Freshwater Ecosystems, Tunisia." 2005.
- [13] Mamou A., Latreche D. "Aquifères transfrontaliers de la rive sud de la méditerranée."Conference on The internationally shared aquifer resources management- Mediterranean (ISARM-MED) Key issues for sustainable management of Transboundary aquifers in the Mediterranean and South Eastern Europe. Thessaloniki, Greece, 21-23 oct. 2004.
- [14] Baba Ouled Sy, Besbes M. "Holocene recharge and present recharge of the Saharan aquifers. A study by numerical modeling". International symposium on Aquifers Systems Management, 30 may-1th June 2006, Dijon, France, pp 312-327,
- [15] Rogers, P. And Hall A.W. "Effective Water Governance, Global Water Partnership," 2003, TEC Background Papers no. 7.
- [16] Benabdallah S. "The Water Resources and Water Management Regimes in Tunisia." Proceedings of a Workshop in Tunisia (Series: Strengthening Science-Based Decision Making in Developing Countries), 2007, pp.81-87.
- [17] Horchani A. "Water in Tunisia. A National Perspective, Agricultural Water Management." Proceedings of a Workshop in Tunisia, Ed. National Academies Press, Washington, 2007, pp. 88-96..
- [18] Taibi R "Global Water Mediterranean Partnership", 24th February 2010, Madrid, Spain. Report and Recommendations, Final Document, May 2010. 34 p.
- [19] Al-Samarrai K., Al-Mejribi A. "Water Governance In Libya - Challenges and Responses. Global Water Partnership." Mediterranean, Workshop on integrated water resources management, Tripoli, Libya, 11-12 April 2007.
- [20] Salem O. "Management of Shared Groundwater Basins in Libya. In, Policies and strategic options for water management in the Islamic countries." Symposium, Tehran, Islamic Republic of Iran, 15-16 dec. 2003, UNESCO, pp. 89 97. IHP-IV Series on Groundwater n°73).

## EFFECT OF THE “120-DAY WIND” ON AGRICULTURAL AND ENVIRONMENTAL CONDITIONS IN HERAT, AFGHANISTAN

Homayoon Ganji<sup>1</sup> Abdul Saboor Rahmany<sup>1</sup> Takamitsu Kajisa<sup>1</sup> Masaaki Kondo<sup>1</sup> and Hajime Narioka<sup>1</sup>

<sup>1</sup>Graduate School of Bioresources, Mie University, 514-8507 Kurima-machiya-cho 1577, Tsu, Japan

### ABSTRACT

Due to impending climate change, the problem of extreme climate data for irrigation planning is critical, especially for areas in which data are limited. Herat province, which is located in West Afghanistan, experiences extremely strong winds, locally known as the “120-day winds”. The effect of these strong winds on reference crop evapotranspiration ( $ET_0$ ) is an important issue. The peak  $ET_0$  was given more than 10mm/day at Herat.  $ET_0$  exhibits a significant effect on hydrologic processes and agricultural crop performance. Therefore, this index is frequently used by the Food and Agricultural Organization. This study analyzes  $ET_0$  time-series data for both windy and non-windy seasons using the Penman–Monteith equation to determine seasonal differences in  $ET_0$ . To determine the most influential factors of  $ET_0$  rates, all factors are compared for an entire year, 2012. The wind component  $ET_{wind}$  is determined to be significantly influenced by the extreme wind velocities during the 120-day wind season. Based on the similar shapes of the time-series curves for monthly wind velocity and monthly vapor pressure,  $ET_0$  is determined to be significantly influenced by the synergistic effect of wind velocity and vapor pressure deficit.

*Keywords: 120-day winds; Herat, Afghanistan; Penman–Monteith method; Evapotranspiration*

### INTRODUCTION

Due to impending climate change, the consideration of extreme climate data for irrigation is essential for areas with limited data. However, studies of extreme strong wind conditions are rare. In Herat province in Afghanistan, strong winds (average speed 6 m/s)—locally known as the “120-day winds”—usually begin in early July and persist until late September.

During summer, the prevailing winds originate in the north at 10–15 knots (5.1–7.7 m/s). North winds occur 40%–45% of the time from June to August and 30% of the time in September. Peak gusts of 28, 31, 23, and 20 m/s were observed in June, July, August, and September, respectively [1].

Reference crop evapotranspiration ( $ET_0$ ), which is an important index of hydrologic budgets for different spatial scales, is a critical variable for understanding regional biological processes.  $ET_0$  is frequently employed as a variable in the estimation of evapotranspiration in rainfall-runoff and ecosystem modeling. Long-term changes in potential evapotranspiration can significantly affect hydrologic processes and agricultural crop performance. To obtain suitable daily estimates of evapotranspiration using the Penman–Monteith equation, a wind function that includes humidity, air temperature and solar radiation is necessary.

### AREA

Prior to the war, Afghanistan was well known for its agriculture and ample supply of food; wheat was the main food source. Herat province is located in West Afghanistan, with a geographical area of 54,778 km<sup>2</sup> and 1,241,410 ha of irrigated land; it belongs to the Harirud River basin (N 34° 20' 42" E 62° 11' 59").

Herat is characterized by a cold semi-arid climate, in which the average annual precipitation ranges from 152 to 214 mm; this precipitation is minimal and primarily occurs during winter and spring [2]. The summer climate is temperate, especially in June and July when the maximum degree of hotness ranges from 38 °C to 43 °C; however, the climate throughout the remainder of the year is also reasonable.

Using data from Climateps.com, Fig. 1 and Table 1 display the relative outline of Herat. In Fig 1, locations with low altitudes are shown in green, maximum average annual temperatures are shown in red, and the average annual precipitation is shown in blue.

Figure 1 lists the extreme data collected for North-Salang, which exhibits the highest ground levels, the coolest temperatures, and the highest amounts of precipitation in Afghanistan Table 1. Because data for the east side of the province is unavailable, the colors that represent the east side of this province are fixed.

In contrast with North-Salang, Zaranj exhibits the hottest temperatures and the lowest amounts of precipitation. Compared with other provinces, the data for Herat is similar to the data for Zaranj, i.e.,

high air temperatures, low ground levels, and low amounts of precipitation. Therefore, the majority of the province is shown in yellow in Fig.1.

## PURPOSE

This paper analyzes potential evaporation time-series data for both windy and non-windy seasons using the Penman–Monteith method in order to determine the differences in potential evapotranspiration, to promote modern methods of irrigation, and to propose changes in local methods of irrigation and rainfall irrigation. The effect that these strong winds exert on greater  $ET_0$  is an important issue.

A) Confirm the efficiency of raw data by establishing the numerical order by comparing each term shown in the reference.

B) Confirm the effect of wind velocity on  $ET_0$  during the period of the 120-day winds by evaluating each component of  $ET_0$ .

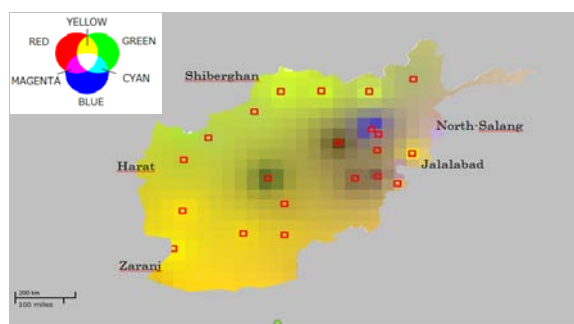


Fig. 1 Weather conditions for cultivating wheat in winter in Afghanistan. Red: intensity of hotness given by air temperature. Green: intensity of lowness of altitude. Blue: intensity of wetness given by precipitation. The data were downloaded from climatemps.com.

Table 1 Profile of the measured data

	Temperature (°C)	Altitude (m)	Rainfall (mm/y)
max	21.7 JALALABAD Red color	3366.0 NORTH-SALANG	82.7 (NORTH-SALANG) Blue color
average	13.5	1409.9	25.8
Min	-0.1	360.0	7.9 (FARAH)
HERAT	16.1	964.0	21.1

## BASIC EQUATION

$ET_0$  is an important index of hydrologic budget for different spatial scales and is a critical variable for understanding regional biological processes.  $ET_0$  is also an important variable in the estimation of actual

evapotranspiration in rainfall runoff and ecosystem modeling because it can significantly affect hydrologic processes and agricultural crop performance. To obtain suitable daily estimates of evapotranspiration using the Penman–Monteith method, which is a combination method, high accuracy is required. The Food and Agriculture Organization (FAO) has proposed a standardization of this method, which is known as the FAO-56 Penman–Monteith application. The daily average  $ET_0$  is given in mm/day according to Eq. (1), for example, in which solar radiation, air temperature, humidity, and a wind function are required [3].

$$ET_0 = ET_{\text{rad}} + ET_{\text{wind}} \quad (1)$$

$$ET_{\text{rad}} = 0.408 \Delta (R_n - G) \div \{\Delta + \gamma(1 + 0.34U_2)\} \quad (2)$$

$$ET_{\text{wind}} = \gamma \frac{900}{T + 273} U_2 dE \div \{\Delta + \gamma(1 + 0.34U_2)\} \quad (3)$$

$$dE = e_s - e_a \quad (4)$$

where  $ET_0$  is the reference crop evapotranspiration (mm/day),  $ET_{\text{wind}}$  is a wind term (mm/day),  $ET_{\text{rad}}$  is a radiation term (mm/day),  $\Delta$  is the slope of the saturated air vapor pressure curve (kPa/°C),  $R_n$  is the net solar radiation at the crop surface (MJ/m<sup>2</sup> day),  $G$  is the soil heat flux density (MJ/m<sup>2</sup> day),  $\gamma$  is the psychrometric constant (kPa/°C), 0.06 (kPa/°C) was used for Herat,  $T$  is the mean daily air temperature at a height of 2 m (°C),  $U_2$  is the wind speed at a height of 2 m (m/s),  $dE$  is the vapor pressure deficit (kPa),  $e_s$  is the saturated air vapor pressure (kPa), and  $e_a$  is the actual air vapor pressure (kPa).

## RESULTS AND DISCUSSION

Considering the accuracy of the collected data and the predicted basic equations, some features of the climate data for Herat are shown in Fig. 2 to Fig.5.

The collection of precipitation data for our analysis was challenging. This problem is not essential to  $ET_0$ ; however, details about this problem are shown in Table 2.

The collection of sunshine duration data was also challenging. These data was inaccessible because it could not be obtained from the National Climatic Data Center (NCDC). Although it is included in the FAO's database, a detailed annual analysis is not feasible because only average data is included.

However, we were able to observe cloud cover measured at Herat International Airport using weatherspark.com. Although this cloud cover fraction includes daytime information, we were able to confirm the experimental relation with the daytime ratio  $n/N$ , in which the daytime length  $n$  was obtained

from the Herat Metrological center the experimental results are shown in Fig. 2 and Eq. (5). In cases where the daytime length could not be obtained, Eq. (5) was helpful for the analysis.

$$n/N = 0.848 - 1.095 \times (\text{cloud cover fraction including nighttime}) \quad (5)$$

Where  $n/N$  represents the relative sunshine duration,  $n$  represents the actual duration of sunshine (h), and  $N$  represents the maximum possible duration of sunshine (h).

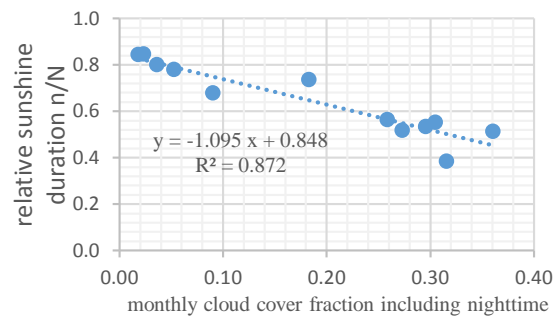


Fig. 2 Experimental relation between monthly cloud cover fraction, including nighttime, and relative sunshine duration in 2012.

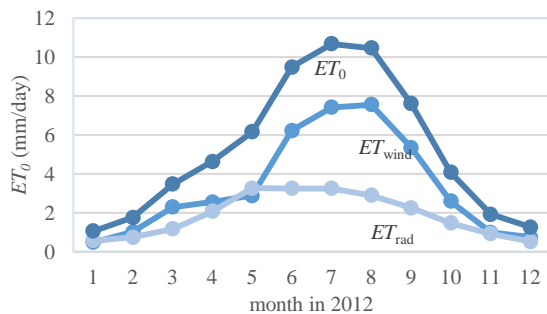


Fig.3  $ET_{rad}$ ,  $ET_{wind}$ , and  $ET_0$

2) In Fig. 3,  $ET_{rad}$  and  $ET_{wind}$  are shown with  $ET_0$  for the months in 2012 that correspond to basic eq. (1). The peak of  $ET_0$  was confirmed to exceed 10 mm/day. Although an extremely large order of  $ET_0$  was given, we have not way to express this largeness, because we can't compare that with another now.  $ET_{wind}$  was significantly larger than  $ET_{rad}$  from June to September during the period of 120-day winds.

3) In Fig.4, the monthly change of the  $U_2$ ,  $R_n$ , and  $dE$  are shown. These  $U_2$ ,  $R_n$  and  $dE$  are important valuables about  $ET_{rad}$  or  $ET_{wind}$  in eq. (2) and eq. (3).  $R_n$  and  $dE$  those have the peak at summer seem to be common. However, the occurrence of peak wind velocity  $U_2$  during the summer was also measured in Herat province. Therefore, it is not easy for us to separate and discuss about the impact of each of  $R_n$ ,  $dE$  and  $U_2$ . This kind of difficulty is expected to exist at where 120 days strong wind are blowing.

4) At last, for confirming the variable and stochastic  $U_2$  that increases during the summer, the relation between air temperature  $T$  and wind velocity  $U_2$  are shown in Fig. 5. In this Fig.5, the straight line demonstrates that  $U_2$  is linear to the air temperature  $T$ . We are presuming it so special straight line given for 120 days wind places.

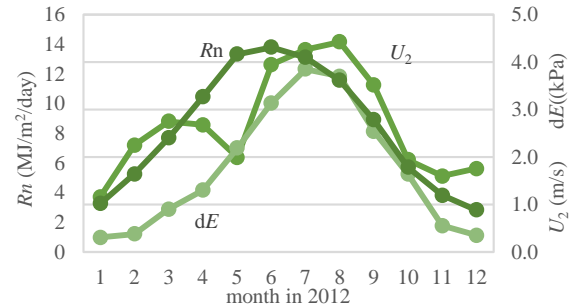


Fig. 4 Wind velocity  $U_2$ , vapor pressure deficit  $dE$ , air temperature  $T$ , and solar radiation  $R_n$

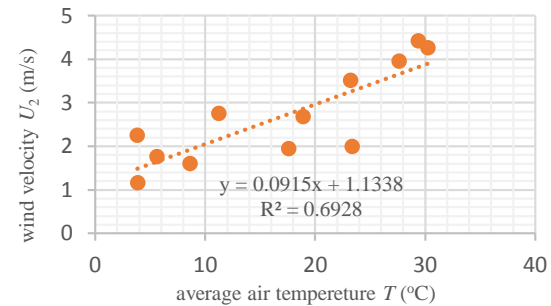


Fig. 5 Experimental relation between air temperature and wind velocity in which the data were monthly given in 2012.

## CONCLUSION

By analyzing  $ET_0$  time-series data for both windy and non-windy seasons using the Penman–Monteith equation, the next conclusions were given.

In the process of data treatment, the practical relation that has the large determination coefficient 0.872 between monthly cloud cover fraction and relative sunshine duration was confirmed.

The peak  $ET_0$  was more than 10mm/day. About 80% of this peak was consist of wind factor  $ET_{wind}$ . For this reason, 120-day winds can be expressed as the reasons of the large  $ET_0$  in Herat province.

In Herat province, by the occurrence of 120-day winds, the experimental solid relation having determination coefficient 0.6928 between monthly air temperature and wind velocity could be seen.

## ACKNOWLEDEMENT

To address the challenges of data collection, climate data is continually improving.

The feature of Accessible databases is shown in Table 2.

Table 2 Accessible online databases for irrigation planning (2014)

Name	Features
CROPWAT (FAO) CLIPWAT (FAO)	Mean rainfall data, Mean $ET_0$ and that's component data
NCDC (NOAA)	Air temperature, dew point, and wind velocity Basic daily data. The primary data from Figs. 2, 3, and 4.
Weatherspark.com	Cloud cover, wind velocity, air temperature, and humidity at the airport. Hourly data may be available. Payment is required. Used in eq. (5)
climatemps.com	Average air temperature and precipitation. Monthly average data. Used in Fig. 1.

## REFERENCE

- [1] AFCCC/DOPA: Herat Afghanistan, October, 2001.
- [2] Omid AB. R, Surface Irrigation of Afghanistan. Herat: Satarae Noghrae, 2009, ch. 8.
- [3] Richard G. Allen, Luis S. Pereira, Dirk Raes, Martin Smith: Crop evapotranspiration - Guidelines for computing crop water requirements - FAO Irrigation and drainage paper 56, FAO - Food and Agriculture Organization of the United Nations, Rome, 1998.

## USE OF GENETIC PROGRAMMING BASED SURROGATE MODELS TO SIMULATE GROUNDWATER FLOW AND BIOCHEMICAL TRANSPORT PROCESSES IN CONTAMINATED MINE SITES

Hamed Koohpayehzadeh Esfahani Esfahani<sup>1</sup> and Bithin Datta<sup>1,2</sup>

<sup>1</sup>School of Engineering and Physical Sciences, James Cook University, AUSTRALIA;

<sup>2</sup>CRC for Contamination Assessment and Remediation of the Environment (CRC-CARE), Mawson Lakes SA 5095, AUSTRALIA

### ABSTRACT

Transport of contaminant species undergoing chemical reactions in groundwater aquifers is a complex physical and biochemical process. Simulating this transport process involves solving complex nonlinear equations and requires huge computational time for a given aquifer study area. Development of optimal remediation strategies in aquifers may require repeated solution of such complex numerical simulation models. To overcome this computational limitation and improve the computational feasibility of large number of repeated simulations, Genetic Programming based trained surrogate models are developed to approximately simulate such complex transport processes. Transport process of acid mine drainage, a hazardous pollutant is first simulated using a numerical simulated model: HYDROGEOCHEM 5.0 for a study area resembling a mine site. Simulation model solution results for an illustrative contaminated aquifer site is then approximated by training and testing a Genetic Programming (GP) based surrogate model. To decrease the total number of GP formulations, the coordinates of observation locations are implemented as input data in the surrogate models. Comparison of the surrogate models and numerical simulation results show that the surrogate models can provide acceptable approximations of this complex transport process in contaminated groundwater aquifers.

*Keywords: Biochemical transport simulation, Genetic programming, Acid mine drainage, contaminated aquifers, surrogate models.*

### INTRODUCTION

Simulation of flow and transport processes for chemically reactive species in contaminated groundwater aquifers generally require extensive computational time. When repeated simulations are necessary to implement and solve optimization based decision model, e.g., to develop optimal aquifer management strategies, the computational burden may determine the feasibility of any methodology. To address this, trained surrogate models approximating the simulation model can be developed. These surrogate models are generally computer programs describing the relationship between output values (e. g., pollutant concentration at different locations and times) and input values (e.g., pollutant flux at potential pollutant source locations). Simulation of reactive species transport process (i.e. Acid mine drainage (AMD)) in contaminated groundwater aquifers is complex and computationally intensive. Therefore it is useful to develop trained and tested surrogate models to approximately simulate the transport processes. In this study, the flow and biochemical transport simulation model is replaced by trained genetic programming (GP) as surrogate models which can reduce consumption time.

An accurate description of the contaminant transport in aquifers is obtained if both chemical and physical behaviors of contaminant species are

incorporated. Solution of the transport process with chemical reactive species in groundwater was addressed by [1] and developed by [2-4]. One approach couples the non-reactive transport model MT3DMS [5] with various chemical reactive transport simulators [6-10]. HYDROGEOCHEM [11] was the first comprehensive three dimensional simulator of hydrogeologic transport and geochemical reaction in saturated-unsaturated media [11]. This code was developed to solve comprehensive heat, reactive geochemical and biochemical transport [12]. The proposed methodology uses HYDROGEOCHEM 5.0 (HGCH) as the simulation model for AMD transport process with chemically reactive pollutants for an illustrative study area with synthetic hydro-geochemical data. These simulation results are then utilized to train and test a GP based surrogate model.

AMD, which is the result of wastewater from metal mines or coal mines containing sulphur compounds [13], is hazardous contaminant sources for groundwater. Various sulphide minerals constitute AMD based on their chemical weathering reactions such as pyrite (FeS<sub>2</sub>), pyrrhotite (Fe<sub>1-x</sub>S), chalcopyrite (CuFeS<sub>2</sub>), arsenopyrite (FeAsS), etc. [14]. Beside mining activities, rocks' surface weathering in presence of water, oxygen and microorganisms produces AMD. These contaminants are considerable threats for water resources. In this study, the transport process of



copper and sulphate, hazardous AMD's compounds, along with their chemical reactions through the aquifer is considered.

A response matrix approach as an initial linear surrogate model was earlier used to simulate the aquifer responses [15], [16]. More recently proposed non-linear surrogate models include Artificial Neural Network (ANN) and Genetic Programming (GP) based surrogate models [17]. Reference [18] implemented ANN as a surrogate model to replace the flow and transport simulation in the non-dominated front search process as well as to save a huge amount of computational time. References [19] and [20] used GP as meta-model for simulation of pumping saltwater patterns in an optimization framework. Reference [20] demonstrated GP model have several advantages compared with conventional surrogate models and ANN surrogate models. These advantages are: simpler surrogate models, optimizing the model structure more efficiently, and parsimony of parameters. Use of GP surrogate model for groundwater contamination management, and development of a monitoring network design feedback methodology to identify unknown source characteristics was addressed by [21].

## METHODOLOGY

The current study proposes and evaluates a methodology, which includes two steps. In the 1st step, a numerical simulation model with specified boundary conditions, specified existing initial hydraulic and geochemical conditions, and with estimated hydrogeologic and geochemical parameter values is used to simulate flow and biochemical transport processes for hazardous compounds of AMD such as sulfate and copper, in a given contaminated aquifer. The specified illustrative aquifer resembles an abandoned (no longer in operation) mine site in Queensland, Australia, where similar contaminants are present and similar topologic and hydrogeologic conditions exist. In the second step, trained GP models are implemented to obtain pollution concentration at specified locations of the contaminated aquifer. These concentrations obtained using the surrogate model and those obtained by solving the implemented numerical three dimensional transient reactive contaminant transport simulation model (HGCH) are compared to evaluate the potential applicability of the GP based surrogate models.

### Simulation Model for Groundwater Flow and Biogeochemical Transport

The HGCH flow and transport simulation model consisting of the flow simulation model and physio-chemical transport model to obtain numerical

solutions. It is a computer program that numerically solves the three-dimensional groundwater flow and contaminant transport equations for a porous medium. The finite-element method is used in this simulation model. The general equations for flow through saturated-unsaturated media are obtained based on following equations [11]:

$$\frac{\rho}{\rho_0} \mathbf{F} \frac{\partial \mathbf{h}}{\partial t} = \nabla \cdot \left[ \mathbf{K} \cdot \left( \nabla \mathbf{h} + \frac{\rho}{\rho_0} \nabla \mathbf{z} \right) \right] + \frac{\rho^*}{\rho_0} \mathbf{q} \quad (1)$$

$\mathbf{K}$  is the Hydraulic conductivity tensor (L/T) and  $\mathbf{F}$  is the generalized storage coefficient (1/L) defined as:

$$\mathbf{F} = \alpha' \frac{\theta}{n_e} + \beta' \theta + n_e \frac{ds}{dh} \quad (2)$$

$$\mathbf{K} = \frac{\rho g}{\mu} \mathbf{k} = \frac{(\rho/\rho_0) \rho_0 g}{(\mu/\mu_0) \mu_0} \mathbf{k}_s \mathbf{k}_r = \frac{(\rho/\rho_0)}{(\mu/\mu_0)} \mathbf{K}_{so} \mathbf{k}_r \quad (3)$$

Where:

- $\theta$ : effective moisture content ( $L^3/L^3$ );
- $h$ : pressure head (L);
- $t$ : time (T);
- $z$ : potential head (L);
- $q$ : source or sink of fluid [ $(L^3/L^3)/T$ ];
- $\rho_0$  : fluid density without biochemical concentration ( $M/L^3$ );
- $\rho$  : fluid density with dissolved biochemical concentration ( $M/L^3$ );
- $\rho^*$ : fluid density of either injection (= \*) or withdraw (= ) ( $M/L^3$ );
- $\mu_0$  : fluid dynamic viscosity at zero biogeochemical concentration [ $(M/L)/T$ ];
- $\mu$ : the fluid dynamic viscosity with dissolved biogeochemical concentrations [ $(M/L)/T$ ];
- $\alpha'$ : modified compressibility of the soil matrix (1/L);
- $\beta$ : modified compressibility of the liquid (1/L);
- $n_e$ : effective porosity ( $L^3/L^3$ );
- $S$ : degree of effective saturation of water;
- $G$ : is the gravity ( $L/T^2$ );
- $k$ : permeability tensor ( $L^2$ );
- $k_s$ : saturated permeability tensor ( $L^2$ );
- $K_{so}$ : referenced saturated hydraulic conductivity tensor (L/T);
- $k_r$ : relative permeability or relative hydraulic conductivity (dimensionless);

The general transport equation using advection, dispersion/diffusion, source/sink, and biogeochemical reaction as the major transport processes can be written as follows:

$$\frac{D}{Dt} \int_V \theta C_i dV = - \int_r n \cdot (\theta C_i) V_i d\Gamma - \int_r n \cdot J_i d\Gamma + \int_V \theta r_i dV + \int_V M_i dV, i \in M \quad (4)$$

$C_i$ : the concentration of the  $i$ -th species in mole per unit fluid volume ( $M/L^3$ );

$v$ : the material volume containing constant amount of media ( $L^3$ );

$\Gamma$ : the surface enclosing the material volume ( $L^2$ );

$n$ : the outward unit vector normal to the surface;

$J_i$ : the surface flux of the  $i$ -th species due to dispersion and diffusion with respect to relative fluid velocity [ $(M/T)/L^2$ ];

$r_i$ : the production rate of the  $i$ -th species per unit medium volume due to all biogeochemical reactions [ $(M/L^3)/T$ ];

$M_i$ : the external source/sink rate of the  $i$ -th species per unit medium volume [ $(M/L^3)/T$ ];

$M$ : the number of biogeochemical species;

$V_i$ : the transporting velocity relative to the solid of the  $i$ -th biogeochemical species ( $L/T$ ).

### Surrogate Model

Genetic Programming (GP) models are used in this study to develop surrogate models to approximately simulate flow and transport processes. Trained GP models are developed using the simulated response of the aquifer to randomly generated source fluxes. The selected GP models can replace the numerical simulation model to obtain concentration of contaminants in observation wells. GP, a branch of genetic algorithms, is an evolutionary algorithm-based methodology inspired by biological evolution to find computer programs that perform a user-defined task. Essentially, GP is a set of instructions and a fitness function to measure how well a computer model has performed a task.

GP utilizes a set of input-output data which are generated randomly by simulation model. The numerical Simulation model creates  $M$  number of out-put sets from  $M$  number of input sets, which is generated by using random Latin hypercube sampling in a defined range. The performance of each GP program is evaluated in terms of training, testing, and validation using the set of input-output patterns. The testing data evaluates the model performance for new data without developing a new fitness function. To compare the GP and HGCH results at the same location, the normalized error is used as defined by the following equation:

$$f = \frac{1}{nt} \sum_{iob=1}^{nob} \frac{ABS(Chgch_{iob}^k - Cgp_{iob}^k)}{Chgch_{iob}^k} \quad (5)$$

ABS: the absolute value of

$Chgch_{iob}^k$ : the concentration simulated by the HGCH model at observation monitoring location  $iob$  and at the end of time period  $k$  ( $ML^{-3}$ ).

$Cgp_{iob}^k$ : the concentration estimated by the GP models at observation monitoring location  $iob$  and at the end of time period  $k$  ( $ML^{-3}$ ).

$nt$ : the total number of monitoring time steps.

$nob$ : the total number of observation wells.

### Performance Evaluation of Developed Methodology

To evaluate the performance of the proposed surrogate models and compare it with actual simulation model solution results, a hypothetical homogeneous and isotropic aquifer is utilized as an illustrative example as shown in Fig. 1. The grey area represent the contaminant sources  $S(i)$  which include distributed and point source. The monitoring networks are shown in Fig 2. Cells marked with green circle, wells set 1, are the grid locations containing a monitoring well which their data are used to train, test and validate GP models' formulations. Moreover, Cells marked with yellow and blue circle are the grid locations containing a monitoring well with their coordinates within, and beyond range of location coordinates implemented in GP formulations, respectively. Groundwater flow and solute transport process is simulated with hydro-geological parameters as given in Table 1. The synthetic concentration measurement data used for the specified polluted aquifer facilitates evaluation of the developed methodology.

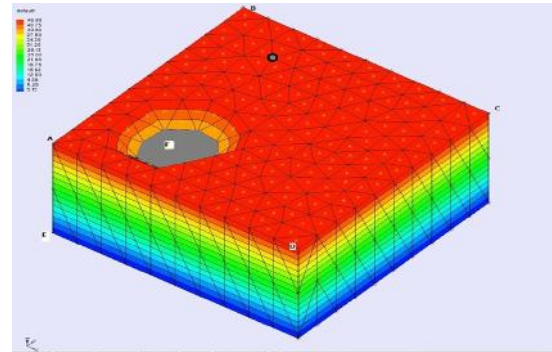


Fig.1 Example definition and flow boundary conditions (Total Head: A= 37 m, B= 40 m, C= 33m, D= 30 m; Level (F)= 37m)

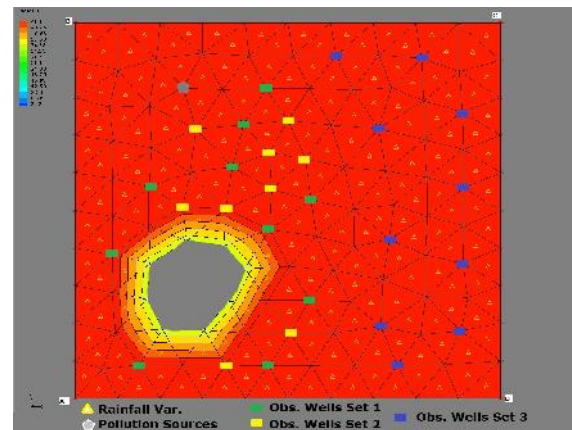


Fig. 2 Location of concentration measurements

In the incorporated scenario, copper ( $\text{Cu}^{++}$ ) and sulfate ( $\text{SO}_4^{--}$ ) are introduced as initial pollutants in sources, which are involved chemical reactions, which are showed in table 2.

Table 1 Aquifer's properties

Aquifer Parameter	Unit	Value
Length of study area	m	100
Width of study area	m	100
Thickness of study area	m	50
Node numbers		387
Element numbers		1432
Hydraulic conductivity, K	m/d	10
Effective porosity,		0.3
Longitudinal dispersivity, L	m/d	6
Transverse dispersivity, T	m/d	3
Horizontal anisotropy		1
Initial contaminant concentration	g/lit	0-100
Diffusion coefficient		0

Table 2 Chemical reactions during the contaminants' transport

Chemical Reaction Equations	Constant Rate (Log k)
$\text{Cu}^{++} + \text{H}_2\text{O} \rightarrow \text{Cu}(\text{OH})^+ + \text{H}^+$	-9.19
$\text{Cu}^{++} + 2\text{H}_2\text{O} \rightarrow \text{Cu}(\text{OH})_2 + 2\text{H}^+$	-16.19
$\text{Cu}^{++} + 3\text{H}_2\text{O} \rightarrow \text{Cu}(\text{OH})_3^- + 3\text{H}^+$	-26.9
$\text{Cu}^{++} + \text{SO}_4^{2-} \rightarrow \text{CuSO}_4$	2.36

The source activities are specified for eight similar time intervals of 100 days each. The actual pollutant concentration from each of the sources is presumed to be constant over a stress period. The pollutant concentration of copper as well as sulfate in the pit is represented as  $\text{Cpit}(i)$  and  $\text{Spit}(i)$  respectively, where  $i$  represents the stress period number, and also  $\text{C}(i)$  and  $\text{S}(i)$  represent copper and sulfate concentrations in the point sources, respectively at different time steps. An overall of sixteen concentration values for each contaminant are considered as explicit variables in the simulation model. The concentration measurements are simulated for 800 days since the start of the simulation. The pollutant concentration measurement at the observation wells starts at time  $t=100$  days and are measured after every 100 days at all the observation locations till  $t=800$  days. Figure 3 shows the pollutant concentration profile in the study area.

#### Genetic Programming formulation

Copper and sulfate concentration in sources are the two main input data sets which consist of sets of

concentration values for each of the 32 values,  $\text{Cpit}(i)$  and  $\text{C}(i)$  as well as  $\text{Spit}(i)$  and  $\text{S}(i)$  ( $i=1$  to 8), representing two sources, two kind of contaminants, and eight active stress periods. Although 128 GP formulations need to be generate in this scenario, the well coordinates are used as input data for GP models to decrease the number of GP models required. Therefore the numbers of models are reduced to 8 models for copper, as well as eight models for sulfate which are generated based on pollution concentration in sources and locations of data measurement. The corresponding output data consists of the resulting pollutant concentration measurements due to these source fluxes at all the 10 monitoring well at time  $t_1=100$ ,  $t_2=200$ ,  $t_3=300$ ,  $t_4=400$ ,  $t_5=500$ ,  $t_6=600$ ,  $t_7=700$  and  $t=800$  days. 1,000 data patterns comprising of inputs and the corresponding outputs are used in the GP models. Out of total data patterns, 40 % is used for training, 30 % for validation, and the remaining 20 % for testing. A Latin Hypercube distribution (MATLAB R2020b) was used for generating the random pollution values ranging between 0 g/lit and 100 g/lit, as the input. The corresponding output data was simulated using HGCH code. Discipulus<sup>TM</sup> (RMLTechnologies, Inc.) is used for training, validation and testing of the GP models.

## RESULTS AND DISCUSSION

The output data from HGCH are compared with GP model results at three arbitrary monitoring networks. The coordinates of first set of wells in the first network are implemented for GP models creation, and the coordinates of second and third monitoring networks are within and beyond the range of first well's location, respectively. These comparison results are shown in Figs 3, 4 and 5. Each time step is marked on the  $x$ -axis. Each of the bars corresponds to contaminant concentration in each well, obtained by HGCH and GP models. Fig 3 shows the HGCH and GP results in different time steps for wells set 1. Fig 4 and Fig 5 demonstrate these results for wells set 2 and set 3, respectively.

Figures 3, 4 and 5 show that the results obtained from GP models are very close to the simulated results obtained using a numerical simulation model. Although few wells' coordinates are used as input data for GP models, these models can estimate the concentration for all locations in the aquifer such as wells set 3, which shows acceptable results (Fig 5).

Figure 6 shows the summation of normalized error for each monitoring network in each period of time. As expected, generally GP models provide relatively accurate results for well set 1. However, errors for data set 2 and 3 are also small even though complex contaminant transport process with chemical reaction of species is involved in the evaluated scenario.

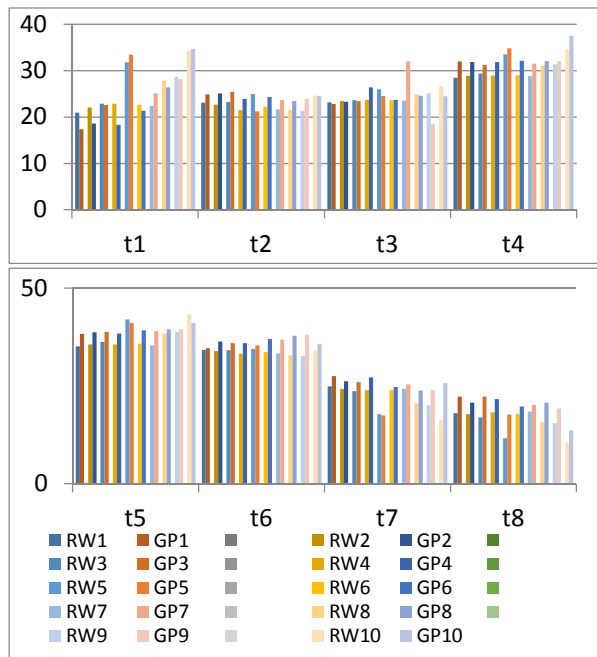


Fig. 3 Comparison data in wells set 1

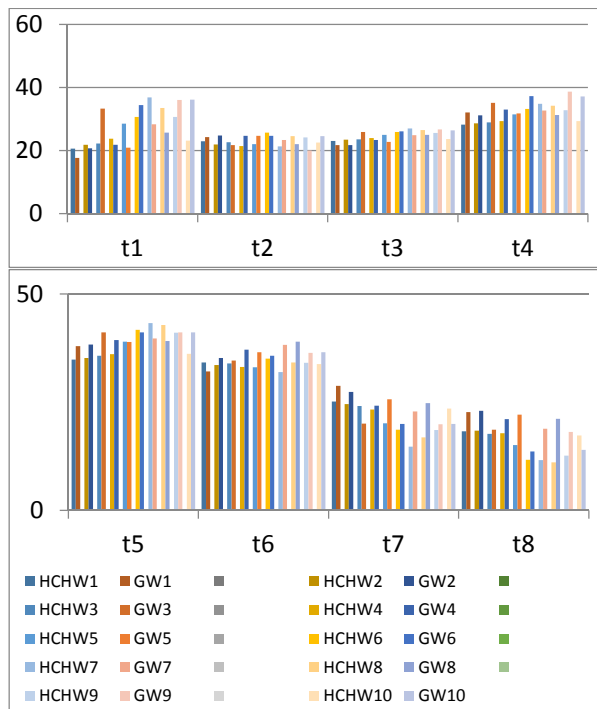


Fig. 4 Comparison data in wells set 2

## CONCLUSION

The developed methodology based on GP models for approximate simulation of the chemically reactive multiple species transport process appears to result in acceptable approximate representation of the transport process in a contaminated aquifer resembling an abandoned mine site. The developed GP models result in reducing the computational time

and complexity, and appear to provide acceptable results. However from the limited results in this study, it cannot be concluded if the surrogate models can replace the simulators in all situations. This method can be applied to real scenarios of contaminated aquifers where especially repeated running of numerical simulation models is required, e.g., in linked simulation-optimization model where computational time is a major constraint. GP based surrogate models can increase efficiency and feasibility of developing optimal management strategies for complex contaminated aquifers such as mine sites.

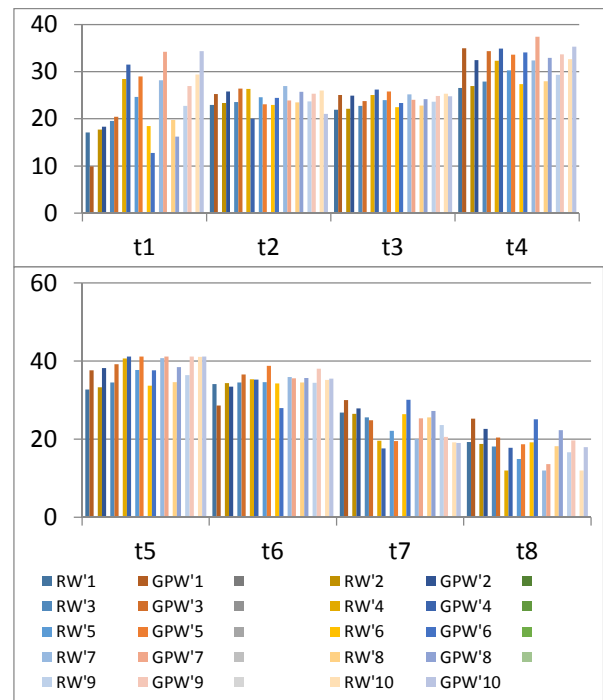


Fig. 5 Compare data in wells set 3

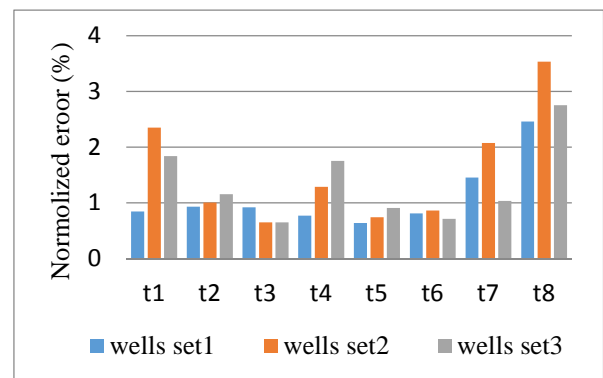


Fig. 6 Normalized errors for all wells sets

## REFERENCES

- [1] Parkhurst, D.L., Thorstenson, D.C. and Plummer, L.N., , "PHREEQE-A computer

- program for geochemical calculations", *J. of Water Resour. Invest.*, Vol. 210, 1982, pp. 80-96.
- [2] Herzer, J., Kinzelbach, W., "Coupling of Transport and Chemical Processes in Numerical Transport Models", *J. of Geoderma*, Vol. 44, 1989, pp. 115-128.
- [3] Tebes-Stevens, C., Valocchi, A. J., VanBriesen, J. M., Rittmann, B. E., "Multicomponent transport with coupled geochemical and microbiological reactions: model description and example simulations" *J. of Hydrology*, Vol. 209, 1998, pp. 8-24.
- [4] Prommer, H., Barry, D.A., Davis, G.B., "Modelling of physical and reactive processes during biodegradation of a hydrocarbon plume under transient groundwater flow conditions", *J. of Contaminant Hydrology*, Vol. 59, 2002, pp. 113-132.
- [5] Zheng, C., Wang, P.P., "MT3DMS: A modular three-dimensional multispecies model for simulation of advection, dispersion and chemical reactions of contaminants in groundwater systems"; Documentation and User's Guide. . Contract Report SERDP-99-1, US Army Engineer Research and Development Center, Vicksburg, MS., 1999.
- [6] Prommer, H., "PHT3D—A reactive multi-component transport model for saturated porous media. . Version 1.0 User's Manual, Technical report, Contaminated Land Assessment and Remediation Research Centre", The University of Edinburgh., 2002.
- [7] Parkhurst, D.L., Appelo, C.A.J., "User's guide to PHREEQC—A computer program for speciation, reaction-path, 1D-transport, and inverse geochemical calculations", Technical Report 99-4259, US Geol. Survey Water-Resources Investigations Report., 1999.
- [8] Waddill, D.W., Widdowson, M.A., "SEAM3D: A numerical model for three-dimensional solute transport and sequential electron acceptor-based bioremediation in groundwater", Technical report, Virginia Tech., Blacksburg, Virginia., 1998.
- [9] Parkhurst, D.L., Kipp, K.L., Engesgaard, P., Charlton, S.R., "PHAST e A Program for Simulating Ground-water Flow, Solute transport, and Multicomponent Geochemical Reactions", U.S. Geological Survey, Denver, Colorado., 2004.
- [10] Mao, X., Prommer, H., Barry, D.A., Langevin, C.D., Panteleit, B., Li, L., "Threedimensional model for multi-component reactive transport with variable density groundwater flow", *J. of Environmental Modelling & Software*, Vol. 21, Issue 5, 2006, pp. 615-630.
- [11] Yeh, G.T., Tripathi, V. S., "HYDROGEOCHEM: A coupled model of hydrologic transport and geochemical multicomponent equilibria in reactive systems", *J. of Environmental Science Division Publication*, No. 3170, 1991, Oak Ridge National Laboratory, Oak Ridge, TN.
- [12] Sun, J., A., "Three-Dimensional Model of Fluid Flow, Thermal Transport, and Hydrogeochemical Transport through Variably Saturated Conditions", M.S. Thesis. Department of Civil and Environmental Engineering, University of Central Florida, Orlando, FL 32816, 2004.
- [13] Kalin, M., Fyson, A., Wheeler, W. N., Review The chemistry of conventional and alternative treatment systems for the neutralization of acid mine drainage", *J. of Science of the Total Environment*, Vol. 366, 2006, pp. 395-410.
- [14] Nordstrom, D.K.a.A., C.N., "Geochemistry of acid mine waters, in Plumlee, G.S., and Logsdon, M.J., eds., The environmental geochemistry of mineral deposits, Part A: Processes, techniques, and health issues, Reviews", *J. of Economic Geology*, Vol. 6A, 1999, pp. 133-161.
- [15] Zhou, X., Chen, M., Liang, C., "Optimal schemes of groundwater exploitation for prevention of seawater intrusion in the Leizhou Peninsula in southern China", *J. of Environmental Geology*, Vol. 43, 2003, pp. 978-986.
- [16] Abarca, E., Vazquez-Sune, E., Carrera, J., Capino, B., Gamez, D., Battle, F., "Optimal design of measures to correct seawater intrusion", *J. of Water Resource Research*, Vol. 42, 2006, pp. 1142-1158.
- [17] Koza, J.R., "Genetic programming as a means for programming computers by natural-selection", *J. of Statistics and computing*, Vol. 4, 1994, pp. 87-114.
- [18] Dhar, A., Datta, B., "Saltwater Intrusion Management of Coastal Aquifers. I: Linked Simulation-Optimization", *J. of Hydrology Engineering*, Vol. 14, 2009, pp. 1263-1273.
- [19] Sreekanth, J., Datta, B., "Multi-objective management models for optimal and sustainable use of coastal aquifers", *J. of Hydrology*, Vol. 393, 2010, pp. 245-256.
- [20] Sreekanth, J., Datta, B., "Comparative Evaluation of Genetic Programming and Neural Network as Potential Surrogate Models for Coastal Aquifer Management", *J. of Water Resour Manage*, Vol. 25, 2011, pp. 3201-3220.
- [21] Datta, B., Prakash, O., Campbell, S., Escalada, G., "Efficient Identification of Unknown Groundwater Pollution Sources Using Linked Simulation-Optimization Incorporating Monitoring Location Impact Factor and Frequency Factor", *J. of Water Resour Manage*, Vol. 27, 2013, pp. 4959-4978.



## DECONTAMINATION OF RADIOACTIVE CESIUM FROM OCEAN SLUDGE BY MICRO-BUBBLE AND MICROORGANISMS

Kyoichi Okamoto<sup>1</sup> and Takeshi Toyama<sup>1</sup>

<sup>1</sup>CST, Nihon University, Japan

### ABSTRACT

The Fukushima nuclear accident of March 11, 2011, soil and water had been contaminated by radioactive cesium. Moreover, radioactive cesium was found in the ocean sludge in Tokyo Bay by flowing from rivers. Here, it cannot be easily removed the cesium which is adsorbed to the sludge. On the other hand, one of the authors had developed the decomposition system for ocean sludge with circulation type by micro-bubbles, which decompose and purification sludge by activating the aerobic bacteria, after creating an aerobic state by micro-bubbles. Here, based on the hypothesis that radioactive cesium is adsorbed on the surface of the sludge deposition. It is considered that radioactive cesium can be eluted, after decomposing the deposited sludge by using the decomposition system for ocean sludge with circulation type. If the cesium will be eluted in the water, we can fix the cesium to existing technology such as “Zeolite”. In this study, our objects is to consider the performance of removal of radioactive cesium after the decomposition of the deposited sludge, by using the decomposition system for ocean sludge with circulation type by micro-bubbles and activating microorganisms.

*Keywords: Decontamination, Radioactive Cesium, ocean Sludge, Micro-bubble, Microorganisms*

### INTRODUCTION

The Fukushima nuclear accident on March 11, 2011, soil and water had been contaminated by radioactive cesium. Moreover, radioactive cesium was found in the ocean sludge in Tokyo Bay by flowing from rivers. A report says it becomes 13 times of the cesium for 7 months from August, 2011 in [1]. Here, it cannot be easy to remove the cesium which is adsorbed to the sludge.

On the other hand, one of the authors had developed the decomposition system for ocean sludge with circulation type by micro-bubbles, which decompose and purification sludge by activating the aerobic bacteria, after creating an aerobic state by micro-bubbles.

Here, based on the hypothesis that radioactive cesium is adsorbed on the surface of the sludge deposition in [2], it is considered that radioactive cesium can be eluted, after decomposing the deposited sludge by using the decomposition system for ocean sludge with circulation type.

If the cesium will be eluted in the water, we can fix the cesium by the existing technology such as “Zeolite”.

In this study, our objects is to consider the performance of removal of radioactive cesium after the decomposition of the deposited sludge, and also show the mechanism of adsorption, elution and fix of cesium as our hypothesis, by using the decomposition system for ocean sludge with circulation type by micro-bubbles and activating microorganisms.

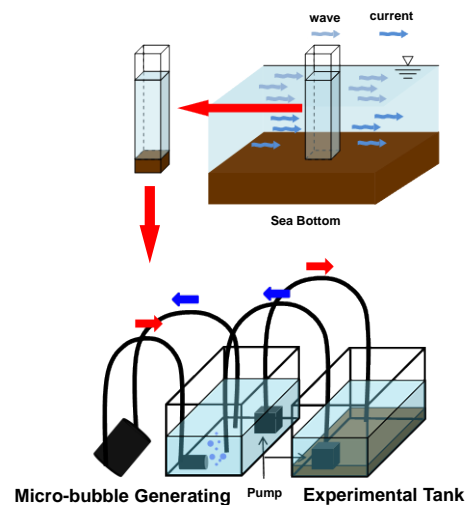


Fig. 1 Purification System of Circulation Type.

### DECOMPOSITION SYSTEM WITH CIRCULATION TYPE

It is very important to reduce sedimentary sludge in the ocean. Plans to reduce the sludge are usually dredging or sand covering. Dredging is a simple way and aims to cut off the sludge. But after cutting off, treating the dredged sludge takes much more time and, of course, cost. Sand covering, in general, gives a big load to living organisms and the ecological system.

So that, a more efficient way is needed to reduce



the sludge while not imparting environmental load in the local sea area. Here, attention was paid to micro-bubble technology for application to the purification of the sludge. The important point in this technique is to activate the bacteria existing in the area by micro-bubbles. Micro-bubbles (that is MB) can change conditions into an aerobic state. If the bubbling stops, the situation changes into anaerobic state, according to recent research. So, we selected a method for decomposing the sludge by microorganisms.

One of the authors had developed the decomposition system for ocean sludge with circulation type by micro-bubbles, shown in Fig.1, which decompose and purification sludge by activating the aerobic bacteria, after creating an aerobic state by micro-bubbles.

## MECHANISM ON FIXING OF CESIUM FROM ELUTION

In general, ocean sludge has a negative charge. When cesium with a positive charge flows from river, sludge was adsorbed cesium, shown in Fig 2. So that, sludge adsorbed cesium cannot eliminate by usual way.

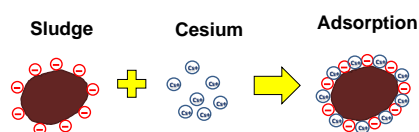


Fig.2 Mechanism on Adsorption of Cesium.

Here, we have a way by using of the decomposition system for ocean sludge with circulation type. After decomposition of the sludge adsorbed cesium by our system, cesium is eluted into water, shown in Fig 3. That is our hypothesis.

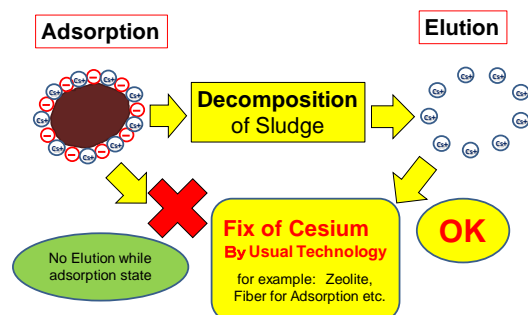


Fig.3 Mechanism on Fixing of Cesium from Elution.

## ELUTION EXPERIMENTS FOR CESIUM

### Procedure of Elution Experiment

The experimental devices consist of two parts, shown in Fig. 1. The water circulates through two tanks. In one tank (Width40xLength28x Hight28cm), micro-bubbles are generated. The micro-bubbles have micro-size diameter and high solubility. This means the water with high concentration of dissolved oxygen circulates through these tanks. The other part is the experimental tank (W60xL29xH35cm). We used sea-water 30(litter) and sludge 1(kg). Here, a micro-bubble generator is based on [3], [4] and the flow rate is 900 (litter/hour). The flow rate of water pumps connected each tanks are 300 (litter/hour).

We had caught the sludge and the sea water at Funabashi Port in Chiba Prefecture in JAPAN, as shown in Fig.4 and 5. Here, we had removed under 10cm of the sludge from seabed before sampling as experimental procedure, because we have to remove the initial value of cesium in the sludge, as shown in Fig. 6.

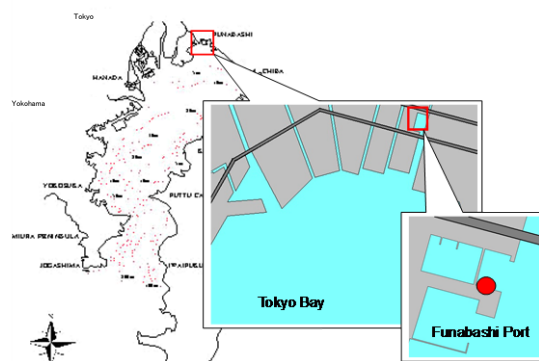


Fig.4 Catching Point of Sludge and Sea Water at Funabashi Port in Tokyo Bay.



Fig.5 Scene of Catching Sludge.

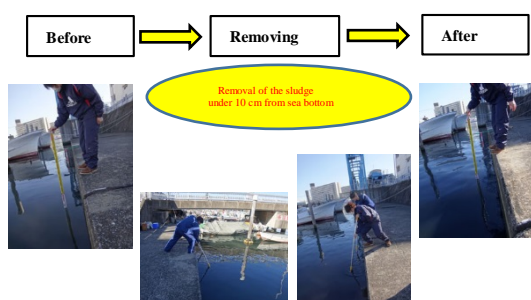


Fig.6 Removal of the Sludge under 10 cm from Sea Bottom.

We used the cesium chloride before 24 hours of starting time and the concentration of cesium ion is 100 (ppm). An air conditioner for water tank was set at the tank for generating microbubbles, for the purpose of setting water temperature 30 degree centigrade.

After setting the decomposition system for ocean sludge with circulation type by micro-bubbles, experiment starts at the same time of generating micro-bubble device.

After 6 hour, the microorganism activator was put in the experimental tank. Main staff of the activator is Kelp and including nutrients and some enzyme. Our used activator is reported to show effective results in purification for grease trap.

Dissolved oxygen (DO), water temperature and pH are measured by using of multi-parameter water quality meter. Ammonium nitrogen (NH<sub>4</sub>-N), total nitrogen (T-N) and total phosphorus (T-P) are measured by using of digital-water-analyzer by digital "Packtest", by water filtered after sampling in experimental tank.

### Experimental Conditions

As experimental conditions, Case 1 is a case of using the decomposition system for ocean sludge with circulation type by micro-bubbles, shown in Fig.7. Case 2 is no micro-bubbles and no circulation but is used the microorganism activator, shown in Fig.8.



Fig.7 Case 1 of Experiment for Elution of Cesium.

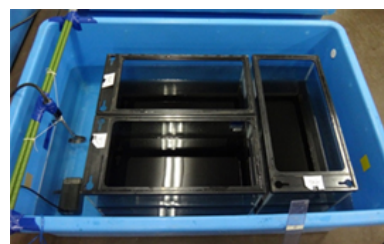


Fig.8 Case 2 of Experiment for Elution of Cesium.

### Results of water temperature, pH and DO as environmental condition

Fig.9-11 show the water temperature, pH and DO (Dissolved Oxygen) as the results of environmental condition of this experiment.

Water temperature is almost constant about 30 degree centigrade after 6 hours. pH is also constant about 7.2 to 7.8. DO in Case 1 is saturation state but DO in Case 2 rise because of mixing at putting microorganism activator after 6 hours, and then became constant. After 24 hours, DO value rise slowly, it seemed that water is mix by the work of sampling for measurement.

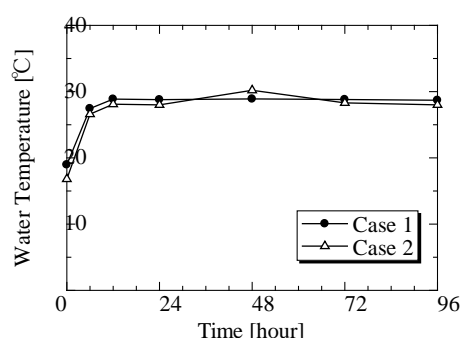


Fig.9 Changes in Water Temperature as environmental conditions.

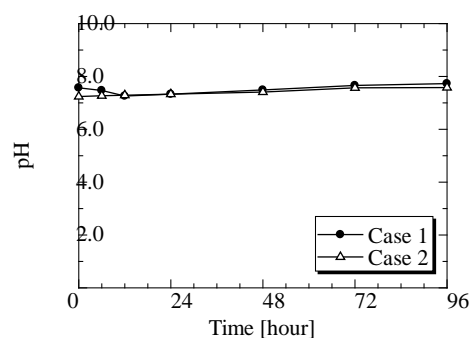


Fig.10 Changes in pH as environmental conditions.

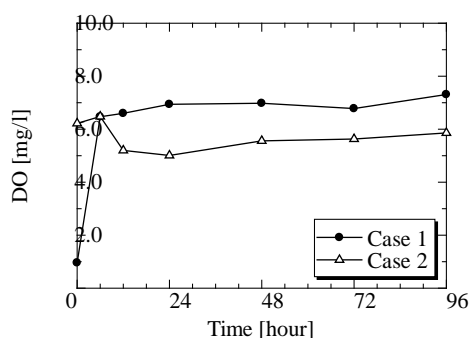


Fig.11 Changes in DO as environmental conditions

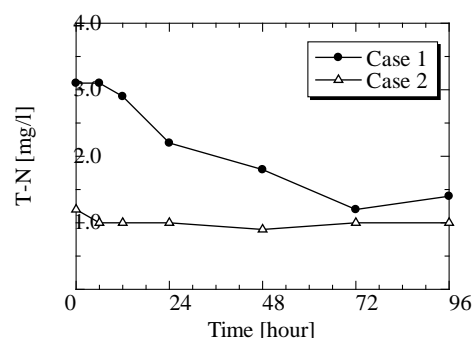


Fig.14 Changes in T-N.

### Results of H<sub>2</sub>S, NH<sub>4</sub>-N and T-N

Fig.12-14 are shown in results of H<sub>2</sub>S (Hydrogen sulfide), NH<sub>4</sub>-N and T-N.

H<sub>2</sub>S (Hydrogen sulfide) in Case 1 decrease rapidly, it seemed by the supply of Oxygen. Case 2 showed always lower limit of measurement, the reason is no H<sub>2</sub>S in sampling water by separation of water and sludge because of no movement of water.

NH<sub>4</sub>-N in case 1 has tendency of decrease but case 2 has no decrease. T-N in case of 1 also has tendency of decrease over 50% but case 2 has no decrease.

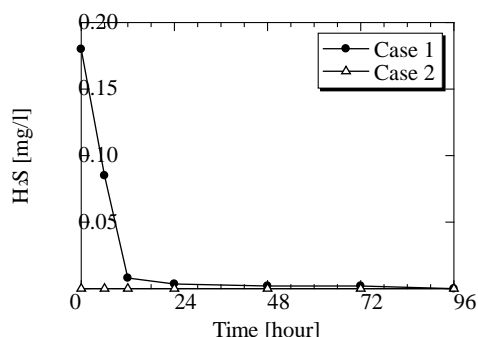


Fig.12 Changes in H<sub>2</sub>S.

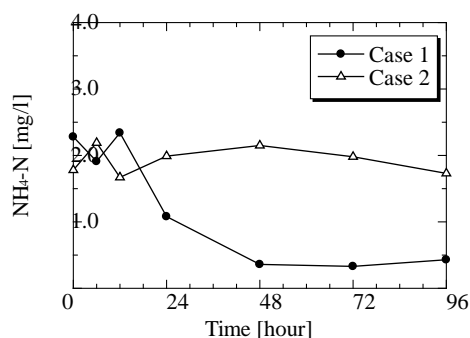


Fig.13 Changes in NH<sub>4</sub>-N.

### Results of Cesium (liquid)

The results cesium were obtained by the iron chromatography shown in Fig 15. The result of Case 1 is considered about 30.9% elution. Results of Case 2 is not bigger than initial value, this means no elution.

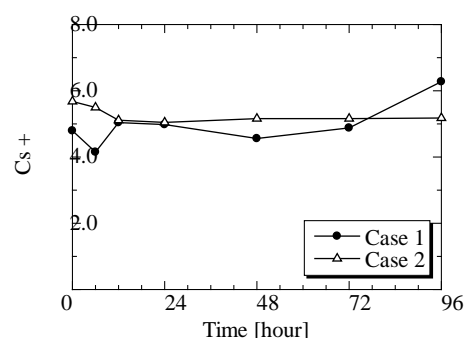


Fig.15 Changes in Cesium.

### Results of Cesium (solid)

We paid attention to cesium and silica (Si), as there are many chemical element in sludge. We used the energy dispersion type X-ray analysis device, because we can measure by the solid state. Weight ratio of cesium and silica (CS/Si) in solid of dry sludge are shown in Fig.16.

Ratio of case 2 increase 50% after 72 hours but final result is same of initial one. It seemed cesium in solid is no change of initial value.

Ratio of case 1 decrease at first after 24 hours, it increase at 48 and 72 hours and it decrease at 96 hours. This is considered that Cs elutes in water by decomposition of sludge at 24 hours and then cesium adhere again to unwrapped silica. It is considered "Re-adsorption" occur.

Mechanism of Re-adsorption is shown in Fig.17.

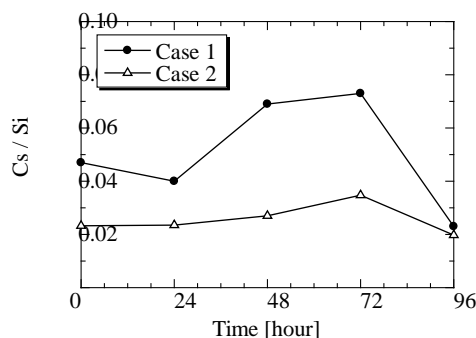


Fig.16 Changes in (Cesium)/(Silica).

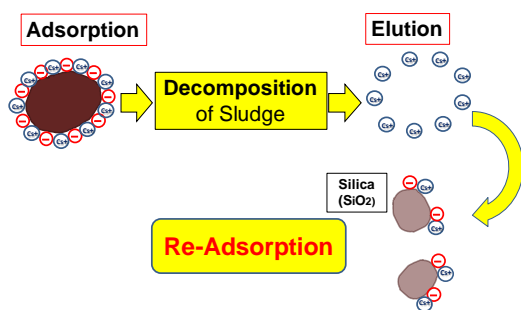


Fig.17 Mechanism on Re-Adsorption after Elution.

## CONCLUSION

We had carried out the elution experiments for cesium after decomposing the deposited sludge by using the decomposition system for ocean sludge with circulation type by micro-bubble and microorganisms.

From the results by iron chromatography,

(1) The elution of cesium is maximum 30.9% in sea water. It seemed it is very useful system.

From the results of the energy dispersion type X-ray analysis device, the weight ratio of cesium and silica (CS/Si) in solid of dry sludge denote,

(2) This is considered that Cs elutes in water by decomposition of sludge at 24 hours and then cesium adhere again to unwrapped silica. It is considered “re-adsorption” occurs.

(3) We showed the mechanism as our hypothesis, of adsorption to sludge of cesium, elution

of cesium after decomposition of sludge, and “re-adsorption”.

## ACKNOWLEDGEMENTS

The authors would like to express sincere thanks for chemical analysis to Hirosuke HIRANO, Graduate student of Nihon University, in Japan.

## REFERENCES

- [1] Yomiuri News Paper, 13 times by 7 months about cesium in ocean soil in Tokyo Bay, May, 13<sup>th</sup>, 2012.
- [2] OKAMOTO Kyoichi and TOYAMA Takaeshi: Ocean Decontamination: Removal of Radioactive Cesium from Ocean Sludge by Using Micro bubbles and Activating Microorganisms, The Japan Society of Naval Architects and Ocean Engineers, May, 2013.
- [3] Imai, T, Shioshige, K, Ukita, M, Sekine, M, Higuchi, T, Fukagawa, K and Fujisato, T. Development of Device for Dissolving High Concentration Gas for Purification at bottom layer around enclosed water area like Dam Lake, Proc. 39th Forum on Environmental Engineering of Civil Engineering Society, 10-12, 2002.
- [4] Matsuo, K, Maeda, K, Ohnari, H, Tsunami, Y, and Ohnari, H., “Water Purification of a Dam Lake Using Micro Bubble Technology”, Progress in Multiphase Flow Research I, pp.279-286, 2006.
- [5] OKAMOTO Kyoichi, HOTT Kenji, TOYAMA Takeshi and KOHONO Hideki, Purification System of Ocean Sludge by Activating Microorganisms, International Journal of GEOMATE (Geotec, Const. Mat. & Env.), Vol.6, No.1, pp.791-795, March, 2014.
- [6] OKAMOTO Kyoichi and HOTT Kenji, Purification System of Ocean Sludge by Using Coagulants and Activating Microorganisms, International Journal of GEOMATE (Geotec, Const. Mat. & Env.), Vol.4, No.2, pp.574-579, June, 2013.

## **SOLID WASTE MANAGEMENT THROUGH ECOLOGICAL FOOT PRINT ANALYSIS – A CASE STUDY IN KOCHI CITY, SOUTH INDIA**

Subha Vishnudas<sup>1</sup>, Athira Ravi<sup>2</sup>

<sup>1</sup>Faculty of civil Engineering Cochin University of Science and Technology, Kochi, India, v.subha@cusat.ac.in

<sup>2</sup>Research Scholar, Faculty of Civil Engineering Cochin University of Science and Technology, Kochi, India

### **ABSTRACT**

Urbanization directly contributes to waste generation, and unscientific waste handling causes health hazards and urban environment degradation. Solid Waste Management which is already a mammoth task in India is going to be more complicated with the increase in urbanization, changing lifestyles and increase in consumerism. Financial constraints, institutional weaknesses, improper choice of technology and public apathy towards Municipal Solid Waste (MSW) have made this situation worse. The current practices of the uncontrolled dumping of waste on the outskirts of towns/cities have created a serious environmental and public health problem. Ecological footprint analysis (EFA) is a quantitative tool that represents the ecological load imposed on the earth by humans in spatial terms. This paper narrates the solid waste management issues in Kochi city, the commercial capital of Kerala, South India, through the environment management tool Ecological Footprint Analysis.

*Key Words: Ecological Foot Print Analysis, Solid Waste Management, South India*

### **INTRODUCTION**

Our world is urbanizing at an unprecedented speed, as the global proportion of urban population has increased from 28.3% in 1950 to 50% in 2010 [1]. By 2015, there will be 23 cities with a population over 10 million. The percentage of urban population to total population in US, Europe and China is 83%, 73% and 47%, respectively, which is much higher compared to India, which is just 32%. As per World Bank studies, India, along with China, Indonesia, Nigeria and the United States, will lead the world's urban population surge by 2050. In India, according to the 2011 Census, the urban population grew to 377 million showing a growth rate of 2.76% per annum during 2001-2011. The level of urbanisation in the country as a whole increased from 27.7% in 2001 to 31.1% in 2011 – an increase of 3.3 percentage points during 2001-2011 compared to an increase of 2.1 percentage points during 1991-2001. . In 2050, urban India will be home to almost fourteen percent of the world's urban population [2]. A very high urban population growth has occurred in the states of Kerala and Andhra Pradesh; urban population growth rates have increased to 6.5% per annum in Kerala and 3% per annum in Andhra Pradesh during 2001-11 compared to just about 1% per annum during 1991-2001. Though the population growth rate is in a decreasing mode, Kerala have

82% as the decadal rate of urbanisation (2001-2011) as per Census 2011. 2011 census data positioned in the 19th rank in the level of urbanization [3]. As per Census 2011 Ernakulam is the most urbanized district of Kerala. The only two agglomerations with population more than 20 lakhs are Kochi and Kozhikode Urban agglomeration. The State Government is considering elevating the status of the city of Kochi, its commercial capital, as a metropolitan city. Kochi has been pushing its borders over the last decade relentlessly, throwing to wind all cautioning by planners that a city without a plan, without public spaces and without respect for its fragile ecological conditions can prosper only at a high cost. Rampant shortage of drinking water is just one. The condition of the roads, traffic congestions on arterial roads, little space for pedestrians and cyclists, rising levels of noise and air pollution, solid waste management nuisance are the others. The difficulty has been aggravated by lack of effective legislation, inadequate funds and services, and inability of municipal authorities to provide the services cost-efficiently. In the eye's of an ordinary man, the condition of the city is very bad in the present stage of unplanned manner especially in the case of solid waste management and transport system, and would wonder what will happen in the future if the city is raised to a metropolitan status. This paper narrates the solid waste management issues in Kochi city, the commercial capital of

Kerala, South India, through the environment management tool Ecological Footprint Analysis. As the ecological footprint analysis can give a quantified impact compared with the biocapacity of an area, many ecological footprint studies are initiated in many countries as a sustainability option. The ecological footprint of waste generation has been done in Khulna city corporation of Bangladesh and Digos city. In India, the ecological footprint study of the first of its kind has been done in India in Manali, Himachal Pradesh which was initiated by a Natural Resource Institute, University of Manitoba in June 1999.

## DEFINITION OF EFA

Ecological footprint analysis (EFA) is a quantitative tool that represents the ecological load imposed on the earth by humans in spatial terms. Ecological footprint analysis was invented in 1992 by William Rees and Mathis Wackernagel at the University of British Columbia. The ecological footprint of a defined population is the total area of land and water ecosystems required to produce the resources that the population consumes, and to assimilate the wastes that the population generates, wherever on earth the relevant land/ water are located [4] The footprint is the area, expressed in global hectares, needed to keep producing the food and fibre we use, absorb our wastes, generate the amount of energy we consume and provide the space for the roads, buildings and other infrastructure we rely on. Our ecological footprint is the sum of those areas (ecologically productive space) we need to sustain the lifestyle of each person. This would be the area of cropland necessary to produce the food we eat, the area of grazing land for producing animal products; the area of forest to produce wood and paper; the area of sea to produce the fish and seafood we consume; the area of land to accommodate housing and infrastructure; and the area of forest necessary to absorb the CO<sub>2</sub> from our energy consumption [5]

## STUDY AREA

The study area of research is the city of Kochi in South India, which lies between 9°48' and 10°50' Latitude and 76°5' and 76°58'E Longitude. The Kochi Municipal Corporation extends to an area of 94.88sq.km. As per census of India 2001, the population of Kochi Corporation is 5,95,575 and as per census 2011 the population is 6,01,574. Physical, social, political and economic factors have played their decisive role in the formation of land use

pattern in Kochi city. Constraints of landforms and lagoon system contributed to the concentration of economic activities to the water front areas. The existing land use pattern has resulted from the complex interactions of varied factors in the urban structures. The characteristic feature of the central city is the predominance of the area under water. The water sheet consists of backwaters, rivers, canals, tanks and ponds and altogether it forms 23.4% of the green land of the city. The net dry land available for urban use amounts to 71.86% of the gross land i.e. 68.18 sq.km. Truly there could be no ideal location than this, with its protected lagoons directly accessible from the sea, for a major terminal port and with its hinterland bountifully blessed by nature for a concentration of urban population and activities. But the present pattern of the city can be classified as that of haphazard growth with typical problems characteristics of unplanned urban development.

## EFA OF KOCHI CITY

The study shows that the consumption rate (EF=2.19gha) of the population in the city is very high and it is far exceeding the national average (0.8gha) and the nations biocapacity (0.4gha) and the available bio capacity per person in the world (1.8gha). It also shows that shelter footprint, which mainly depends on the house area usage and number of occupants, is very high in the city. The improper waste disposal at the source (residential units) is increasing the waste footprint of the population which results in the high goods and services footprint. The waste disposal is the second major component increasing the population's ecological footprint. For the detailed study of waste footprint of the city, a questionnaire survey was conducted for 500 representative samples in three different seasons i.e dry, wet and festival season, inside the Corporation boundary and random samples in the outskirts. The samples were selected based on density of population (high and low), location (away and near of CBD and major transportation nodes), mode of waste disposal (household level or community level), type of housing unit(individual plots, low rise building, row housing units, high rise building) and ownership of the building(individuals, government, builders). Samples were selected in such a way to include as many samples in these criteria. The wastes generated from samples were categorized into paper, glass, plastic, metal and organic waste (mainly food waste). The amount of paper waste was indirectly taken from the periodicals. The amount of glass and metal waste generated in a week was taken in account. The survey was done in three different



seasons (dry, wet and a festival season). In calculating the ecological footprint for household waste generation, methodology to assess the household ecological footprint, developed by M. Wackernagel and W. Rees were used. This study followed the simple methodology by Salequzzaman [6] applied to a particular area in Bangladesh. This methodology used global carrying capacity standards and utilizes the resource consumption and waste generation categories and the land use categories for those consumption and waste generation. Analysis of the data was done using waste footprint analyzer, which is a program developed based on the equations of ecological footprint of waste generation developed by William Rees and Mathis Wackernagel, the authors of the concept for inputting the survey data and estimating the footprint values in a visual basic platform. The analyser generated the footprint value in hectares per capita.

The average footprint of residents in the city area is above the national average. ( $2.19 > 0.8$ ). Also it consumption exceeds the available bio productive space per person in the world ( $2.19 > 1.8$ ). According to the Global footprint calculator if everyone like this we would need 1.3 PLANETS to sustain our life. The average footprint is highest in Ward No.58 (2.52gha) because of the high shelter footprint (1.21gha) because of high house area usage. The lowest ecological footprint is in Ward No. 53(1.79gha) . For all residents, the shelter footprint goes to the maximum followed by goods and services footprint, food footprint & mobility footprint. In most cases the shelter footprint constitutes about 46.37% of the footprint. Average house area usage is 400.45 sqft/person. This is contributing to high shelter footprint. The average male footprint is greater than the female footprint because the male mobility footprint is more than that of female. The average footprint of nuclear family footprint is more than that of joint family. Mobility footprint was directly proportional to the distance to the place of work or education. Low land area occupancy when compared to other units is reducing the average shelter footprint of high rise buildings. Therefore promoting well planned high density buildings will help us to conserve our bio productive space. The mobility footprint of the population in the wards near to the CBD and major transportation nodes is low because of their dependence on public transportation facilities when compared to the other wards.

From the solid waste management issues studied, it is understood that solid waste management problems is found to be the root cause for many other problem areas like water logging, mosquito threat, environmental pollution etc in the city and also it

affects the serene nature of the city. Nowadays the greed among the various manufacturing companies and inconsistent demands of the consumer have given way to turning a blind eye to the environment destruction due to waste disposal we bare down upon our finite planet. They are not bothered about the waste generation from their own houses and work places. But rather they blame the authorities for not disposing these wastes.

## WASTE FOOTPRINT OF KOCHI CITY

The analysis of waste footprint of the city found that the waste generation in Kochi City was 0.51kg/capita/day with an average household size 3.26. The solid waste components in the three seasons are shown in Figure 1. On an average the organic waste constitutes about 82%, 10% metal waste, 5% glass waste, 2.3 % paper waste and 1.4% plastic waste. In all the seasons the organic waste constitutes the maximum. In the festival season and the wet seasons the organic waste and the plastic waste seems increasing. Only paper waste is recycled. 53 people reported that newspapers and magazines are collected by agencies from households once in six months or more. The households are unaware of the type of recycling methods. Since the actual amount of recycled paper is difficult it was assumed that about 90% of the paper waste is recycled from each house. In order to assimilate these wastes an area of 0.011 hectare per capita is required in the dry seasons, 0.014 hectare per capita for the wet season and 0.013 hectare per capita for the festival seasons.

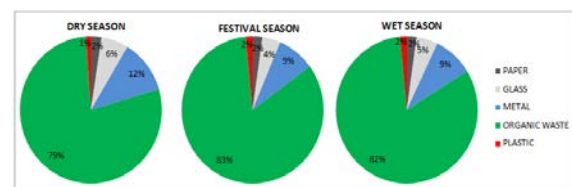


Fig. 1 Waste components in Kochi City

Even though the percentage of plastic in the solid waste is low compared to the other components, its percentage share of total footprint is relatively higher than other components except for metals. Metals also contribute to higher footprint. By land use category in the dry seasons about 102.16 sqm, 0.06sqm forest land and 12.74 sqm area of built up land is required per person.

The festival seasons demand 121.29sqm energy land, 0.07sqm forest land and 15.13sqm built up land for assimilating the waste generated by a single person in the Kochi city. For the wet season the figures are 114.20, 0.06 and 14.87 sqm respectively. This shows that during the festival seasons, the impact caused by the wastes in the city is comparatively high. Paper waste, organic waste and plastic waste seems increasing during the festival season and therefore the impact is caused by these components.

#### **Analysis Based On Density of Population**

The analysis showed that as the density of population is increasing the footprint is increasing as the amount of waste generated is more. The average footprint is more in the festival season. The per capita average footprint in sqm is about 145.83 in the festival season. The paper content in the dry seasons is high in the high density areas. But during the other seasons the composition of paper waste is more in the low density areas. The glass and metal content shows high composition during the dry and wet season in the high density areas. Organic waste and plastic content is more in the low density areas in all seasons.

#### **Analysis Based on Location and Household Income**

Residences which are near to CBD/MTN show high footprint values in the wet season and festival season. The footprint value is about 20% more when compared to that of the dry season. A similar trend is also noticed in the residences away from CBD/MTN. Analysis based on household income shows that the average footprint is comparatively high for the income group INR 10000 to INR15000 followed by the above INR20000 group. The footprint is high in the festival season for all income groups. The lowest contributor to waste footprint is the less than INR5000 income group.

#### **Analysis Based on Type of House and Ownership Details**

Almost all the housing types show high footprint values in the festival season. The average waste foot print value is comparatively low for individual plots except in festival season. Residences owned by builders showed low waste footprint values comparatively. The footprint values in the wet and festival season are high.

#### **Analysis Based on Mode of Disposal**

Community level disposals show high waste footprint values when compared to household level disposal methods. The waste footprint values are high in festival season. The low waste footprint values for household level disposals shows that the waste disposal at source itself is a sustainable option for proper solid waste management.

#### **CONCLUSION**

The Ecological footprint has a higher flexibility as it can be used for many different purposes. From the studies, it is revealed that the consumption rate (EF=2.19gha) of the population in the city is very high and it is far exceeding the national average (0.8gha) and the nations biocapacity (0.4gha) and the available bio capacity per person in the world (1.8gha). The study also revealed that shelter footprint, which mainly depends on the house area usage and number of occupants, is very high in the city. The improper waste disposal at the source (residential units) is increasing the waste footprint of the population which results in the high goods and services footprint. Consumption rate can be reduced by prioritizing strategies based on the component footprint values starting from the individual level. The analysis of ecological footprint of waste generation in the residential areas of Kochi city showed that with the present trend of waste generation and an assumed population growth rate of 4.5%, by 2051 the population will need about the full area of the city to assimilate the generated waste. The research anticipates a 39% reduction in footprint value through the programmes going to get launched in the city and suburbs. A maximum of 51% reduction in footprint value can be attained through the high optimistic value of recycling. The research highlights that as per the waste management hierarchy theories the source reduction proved the first order hierarchy in waste management in terms of waste footprint values. For effective footprint reduction through strategies, regions should develop their own ecological footprint calculators based on their consumption pattern and life style of the population. This calculator should be made available to the public through media. Provision should also be given in the calculator so that they can compare their current profile of consumption to a profile which reduces their ecological footprint thereby making the Ecological Footprint Analysis a public awareness tool in addition to a technical tool. This will make Kochi greener, cleaner, safer and self sustainable as in our good old days. To develop a calculator for

urban Kerala, corresponding footprint studies must be initiated at the national level. Therefore ecological footprint studies should be encouraged through R&D programmes and a footprint calculator should be developed especially for the urban areas of India.

## REFERENCES

1. World Bank , 2011. Doing Business 2011 India: Making a difference for entrepreneurs. Comparing business regulation of 183 economies, The International Bank for Reconstruction and Development (IBRD), Washington DC, USA
2. Swerts, E., Pumain, D., Denis, E., 2014. The future of India's urbanization. *J.Futures* 56, 43-52.
3. Government of Kerala, 2012. State Urbanization Report, Town and Country Planning Department, Kerala.
4. Wackernagel, Mathis and W. Rees. Our Ecological Footprint. Gabriola Island, BC: New Society Publishers, 1996
5. Athira Ravi , Subha V (2013). "Ecological Foot Print Analysis- An Overview", *American Journal of Engineering Research (AJER)* e-ISSN : 2320-0847 p-ISSN : 2320-0936 pp-12-19
6. M. Salequzzaman (2006). —Ecological Footprint of Waste Generation: A Sustainable Tool for Solid Waste Management of Khulna City Corporation of Bangladesh|| *Environmental Science Discipline*, Khulna University, Bangladesh

## **GROUND CONDITIONS AND THE LAND OPERATIONAL PARAMETERS DETERMINED IN THE PLANNING DECISIONS**

Grzegorz Kmiecik<sup>1</sup>, Marta Szejnfeld<sup>2</sup>, Hanna Szymczak<sup>3</sup>, Anna Szymczak-Graczyk<sup>4</sup>

Department of Urban Planning and Architecture<sup>1,2,3</sup>, Institute of Civil Engineering and Geoengineering, Faculty of Land Reclamation and Environmental Engineering, Department of Construction and Structural Engineering<sup>4</sup> University of Life Sciences<sup>1,2,3,4</sup>, Piatkowska Street 64E, 60-049 Poznan, Poland.

### **ABSTRACT**

Optimal land-use planning is a tedious and long lasting process, and in its genesis the actions which set itself the goal of creating spatial order and sustainable development are taken. Inherently, in almost each country planning policy, the basic instruments of planning action are the planning decisions.

They have been determined with the details of the location, purpose, method of use as well as the architectural form. As the result of these decisions, the possibility of designing and implementing a harmonious space that consider all factors and functional, socio-economic, environmental, cultural, aesthetic and compositional requirements are created. But whether planning decisions always protect interdisciplinary interests, even such an important aspect as the water ground conditions ?

The article based on specific example from Polish yard will appear the effects of skipping ground parameters issues related with the planning of building investment on particular area, which according to Polish legislation, are not treated as planning arrangements.

Consequently, the threats to the already existing water ground relations are very probable as far as the changing of these relations may have significant influence or even challenge the implementation of a specific building investment. This situation creates a huge risk including financial consequences and frequently has a significant impact on the future of the building investment process, including the danger of suspension of works.

*Keywords: Geotechnical conditions, Land zoning, Planning document, Investment costs.*

### **INTRODUCTION**

Undoubtedly the special planning is the art of organizing the environment, which despite to an aesthetic experience also performs important functions starting from the socio-economic through environmental or even teaching effects. However, foregoing art is easier to define, because the criteria for determining it are not only a matter of taste, but also refer both to the tough market or economic rules.

The combination of these different aspects in the creation of spatial plans requires the sustainable performance on many levels, and therefore it is reasonable to say that special planning is also an art unique, which should be guided by the law of democracy. Its essence is the ability to choose the alternative solutions, that in each case will create a harmonious and balanced extent. Notwithstanding, whether the certain solution reveal successful decide the future expense user, which is usually deeply embedded in the context and relationships with other people. Therefore, should the alternative choice was possible and equivalent, planning should be based on robust knowledge and understanding of the characteristics of the certain area as well as the empathy with respect to its current and future users.

The foremost means of expression of special planning are the planning decisions that as well as the local and regional level organize space striving to its most rational use.

### **THE CHARACTER OF PLANNING DECISIONS IN POLAND**

An underlying basis of each construction project is a detailed analysis of its cost-effectiveness namely cost estimation and efficiency of such plans.

The basis for obtaining the data for these analyzes are the planning decisions issued in the form of broader contextual local plans or zoning decisions usually for a single land area [1]. It contained therein information about acceptable method of zoning and land use as well as the architectural form. Moreover, the criteria determined in above way should be the result of not only the architectural and urban conditions but also environmental, cultural, historical, social, and what is very important, also groundwater factors. Only though properly constructed building conditions can give a full picture of the certain land property and allow to calculate its absorption i.e. the optimal management based on defined criteria. This attitude is directly associated with the market value of the

parcel and other economic aspects relating the building project or its execution.

As it is observed the spatial planning is also an 'art' that can be directly estimated and measured. Furthermore, it underlies all investment activity as obvious is the relationship that the greater amount of information about the area, the lower is the risk in decision-making regarding the purchase of property.

According to recent studies, more than half of all investment projects launched in Poland take place in areas avoided the zoning plans, based only on the legal provisions of the spatial planning bill concerning so-called "good neighborliness". Hereby the new objects and buildings are formed with the similar function as their neighborhood pre-existing buildings [2].

At the same time the other factors are often ignored such as groundwater conditions, which may significantly affect on the nature of the investment, regarding for instance the cost reasons.

Currently, the planning decisions very rarely define the conditions allowing the elimination of natural interactions on the planned investment and vice versa. Furthermore, if the investment does not constitute the significant impact on the decision of the environmental condition of the project or there is no indication for preparing the environmental report above decisions include very limited information about the characteristics or parameters of the substrate [3].

It may be surprising, especially in the context of the contemporary nature of the construction process, which consists plenty problematic factors concerning at least difficult land conditions and time or money limit. Whereas conditions associated with the parameters of the ground are one of the most cost and time consuming, that can greatly reduce the potential of the land and its attractiveness to future investor. Also, the environmental aspect should not be forgotten, because the effects of interference in the subsoil can be permanent and irreversible.

Thus, in planning documents, in addition to the typical architectural and urban planning parameters defining the acceptable dimensions of buildings, their height, form and building area should also be found the records of the land parameters that especially define the development of the plot and consequently its form of building.

Thereby we would obtain a full picture of the potential investment area, where in addition to the visible characteristics affecting to its market value such as location, access to communication, shape of the plot, its surface or equipment in the media, we would be able to determine the characteristics of the hidden handlers concerning the geotechnical parameters substrate, soil and water conditions or other environmental considerations [2].

Then, one could speak of the investment process in which the investor always has the right of

conscious choice and is not forced to choose the solution which is necessary and become apparent only upon the stage of design or workmanship. The planning decision should apply equivalent solutions correctly typed in the context of space so that the investor should be further guided only by his subjective investments purposes.

## PLANNING DECISIONS AND THE SELECTION CRITERIA OF THE TYPE OF INVESTMENT

Information about the geological and hydrogeological specific of grounds are very important and often fundamental when deciding about the commence of the investment or its character.



Fig. 1 View of historical park. Own photograph.

Above can be demonstrated on the building project of the multi-family housing in Poznan, the fifth largest city in Poland. The investment was planned on a very attractive market-plot, in the city center, adjacent to the downtown building from the beginning of the XX century and one of the most beautiful urban parks with its historic Palm House.



Fig. 2 View of historical park. Own photograph.



Despite the spectacular location the investment area was heavily degraded in the urban context as the result of many years of functioning the chemical plant in this place. Therefore, the planned investment gave the great opportunity to create a whole new quality of public space, adequate for this part of the city.



**Fig. 3 View showing the location of investment**  
**Performance of Geoprojekt.**

In relation to the lack of a Local Land Development Plan, the building parameters have been identified in the zoning decision issued for the parcel owned by the investor, without reference to the environmental values of the adjoining park. Consequently, multi-family housing was decided to design on the north-south axis, along the boundary of the botanical garden.

In order to the most efficient use of commercial values of the land it was assumed that the most architecturally and economically reasonable solution would be to design the underground car parking thus releasing space for main development. This resulted the fairly dimensional arrangement of the buildings and gave the usable amount of surface intended by the investor.

Implementation of the parking lot required pursuing an earthworks at a depth of 11.0 m below ground level. The analysis of geotechnical conditions of foundation the buildings showed that the ground soil had the complex ground water conditions as well as the level of ground water that imposed the necessity to perform the construction of an underground garage in the form of cavity/slot walls erected on the slab base [4].

Generally, the investment demanded complicated and expensive design solutions. However, preliminary analysis of soil and water conditions made on the basis of archival material before the purchase of the property suggested the possibility of such situation, allowing the investor calculate these extracurricular expenses in the overall cost of construction.

These water factors, together with the decision on building conditions were the main parameters of the investment. They have become the foundation of building project and cost estimates.

During the advanced design works it turned out that the planned investment would be a huge threat to the historic neighboring forest. There was also a feasible risk of changing the water conditions in this botanical park as a result of carried out excavations works or establishing some kind of baffle in the free movement of ground water, due to the method applied in construction project using cavity walls.

In the event of the above investment the planning decision refers only to the parameters of architectural and urban planning, instead analyzed additional conditions other than previously existing context of the building.

The above example shows that the standard approach applied in such a complex investment turned out to be insufficient, and the planned construction works could cause irreparable consequences for the environment and would make impossible to take any subsequent preventive action in this matter.

Merely performing the additional hydrogeological studies could gave a full picture of the situation. It was also presented that the results of the study may question the financial legitimacy of the implementation, as in the case of negative results the complete change of profile of the investment would be necessary. In fact without an underground garage residential development would probably be unprofitable especially in the view of high costs incurred for the purchase price in such a strategic location in the city. Thus, the investor has been deprived of choice and in return 'sentenced' to the selection of an unexpected solution. Ultimately, to maintain the whole investment it was necessary to change the function of buildings to the office one thus less favorable concerning the context of this part of the city. Paradoxically, skipping the groundwater issues, recognized as not planning assumption led to selection of less favorable urban solutions [5].

Therefore, evidently the zoning conditions for the areas with higher risk of natural hazards or extremely valuable for the city should apply the obligation of carrying out a specific range of geological and hydrogeological studies in order to recognize the subsoil. Obviously, this incurs certain costs but disproportionately smaller than the investment ones.

The relevant solution would be to create a database system with the ground conditions details which would greatly speed up an entire investment process, minimizes financial risk or improves design works. In addition, it could also be the perfect promoting and investor's drawing factor since the city possessing such comprehensive planning documentation could parallel simplify the entire building construction procedure, that will become much more attractive for the future investments.



## CONCLUSION

Typically, the basic criteria defined in planning decisions are: the architectural and urban parameters, determining acceptable size of buildings, their height, form or building area.

On the contrary with above remains the example discussed in this article which proves that the investment can be completely dominated by the land operational parameters not established in the legal decision. These parameters are strictly essential at the stage of developing the architectural and structural solutions, that usually reflect the existing building conditions. If planning decisions determine the underground building, it shall also contain the guidelines for geological or hydrological area. Additionally, in case of complex terrain conditions, the these architectural criteria should be described in a way that does not prohibit the investment integrally thus showing the possible directions to the investor that could freely decide the optimal course of investment.

In the example brought up in present paper there were several optional functions for the building from multi-family housing with a different combination of usable space and associated underground parking to office one. Any change of features would result the commencement of the administrative procedures of obtaining the required approvals or legal decisions. Consequently, issuing that decision required the new time-consuming results of research that in turn equals the suspension of the investment and had major financial implications for the investor. In contrast, the development of specific ground parameters at the design and planning stage would greatly accelerate the investment process and thus gave better control over the correctness of applied urban solutions.

## REFERENCES

- [1] The Act of 27 March 2003. of Spatial Planning and Regional Planning,
- [2] Gwozdz-Lason M. "Parameters of the Ground substrates in the context of its destination in Spacial Development Plans ", Mining and Geoengineering, Year 35, Issue 2, 2011,
- [3] Regulation of Infrastructure of November 9, 2004 - on the types of projects that may significantly affect the environment and the specific conditions for the eligibility of the project to prepare a report on the project on the environment effect (Dz.U.2010.213.1397).
- [4] Design materials of Geoprojekt-Poznan,
- [5] Kmiecik G, Szymczak H, "Planning decisions and the risk of change to the investment assumptions on the example of multi-family building construction project on Sniadeckich/Glogowska street in Poznan.", Architecture, Civil Engineering, Environment, Year, Book, 2014.

## EFFECT OF FLOCCULATION AIDS ON THE ELECTRIC FIELD ASSISTED DEWATERING OF SOLID LIQUID SYSTEMS

Mohammed Saedi Jami<sup>1</sup>, Masashi Iwata<sup>2</sup>, Md. Monjurul Alam<sup>3</sup> and Md Zahangir Alam<sup>4</sup>  
<sup>1,3,4</sup> Bioenvironmental Engineering Research Center (BERC), Department of Biotechnology Engineering, Faculty of Engineering, International Islamic University Malaysia, Kuala Lumpur, Malaysia; <sup>2</sup> Department of Chemical Engineering, Graduate School of Engineering, Osaka Prefecture University, Sakai, Japan

### ABSTRACT

Various construction techniques such as tunnel construction and earth drilling result in the production of huge amount muddy water with a high solid-to-liquid ratio. Consequently there is a need for disposing these large quantities of muddy wastewater. Dewatering by conventional belt press filters can achieve only small solids contents leading to high expenditure for the transport and disposal of these materials. Another option is the incineration. But since the water content is usually very high, energy consumption is the major concern. In this study, constant-current electroforced sedimentation (EFS) of zinc oxide is analyzed using the Terzaghi-Voigt combined model by neglecting the creep deformation of the material and the effect of adding dewatering aids on the enhancement of water removal is investigated. High current density yields higher dewatering. Increase in initial solid content slightly improves the effectiveness of dewatering. The addition of polyacrylamide as a dewatering aid enhanced the electroforced sedimentation.

*Keywords: Electroforced Sedimentation, Dewatering, Zinc Oxide, Polyacrylamide*

### INTRODUCTION

The process of disposal and re-use of wastewater is one of the most significant challenges in wastewater management. Besides, since such solid liquid system is usually highly compressible, mechanical dewatering is impeded due to a very high hydrodynamic resistance of the mixture.

It is possible to increase the settling velocity of highly concentrated material remarkably by applying direct current electric field with the increase of electric field intensity [1]. It happens mainly for electroosmotic flow which results from the movement of ions in the electric double layer along a solid-liquid interface toward one electrode or other because of the application of electric field. Electroosmosis has been applied in soil stabilization since before World War II [2]. L. Casagrande (1930-1962), had the main contribution in the development of the applications of electroosmosis in soil engineering, introduced that a permanent stabilization of soil could be attained by using aluminum electrodes [2].

The effects of flocculants aid in electroforced sedimentation of various aqueous suspensions were studied. Sedimentation rates of suspended kaolinite and clay are significantly improved by flocculants, whereas electroosmosis are not affected greatly [3]. On the other hand, anionic polymers increase the rate of electroosmotic dewatering of kaolinite [4]. In our previous study, constant current electroforced

sedimentation properties of kaolin and zinc oxide sediments were investigated and it was found that the addition of 1% polyacrylamide as dewatering aid enhanced the electroforced sedimentation of zinc oxide for a given current density [5].

It is well known that the moisture content remains unchanged at the sedimentation surface, whereas it decreases at the bottom of sedimentation column in the electroforced sedimentation and this has not been explained analytically yet [5]. The main objective of this paper is to investigate the electroforced sedimentation of zinc oxide in aqueous medium. The effects of total solid volume per unit cross sectional area, current density and the addition of flocculant aid were examined. The experimental data were also compared with model prediction.

### MATERIALS AND METHOD

#### Experimental

An acryl tube, height and internal diameter of 42 cm and 5.5 cm, respectively, was used as sedimentation column (Fig. 1) located in Bioenvironmental Engineering Research Centre, International Islamic University Malaysia. The electrodes, both made of stainless steel, are placed in parallel at the top and the bottom of the column. The electric field was applied by DC power in such a way that the bottom was cathode and top was anode as zinc oxide particles have positive charges. The slurry used in the experiments was prepared by

mixing a predetermined quantity of dry zinc oxide, polyacrylamide, and deionized water to form a suspension of known total solid volume per unit cross-sectional area. The slurry was then poured into the sedimentation column and left until gravitational sedimentation was completed and equilibrium height was achieved. Then direct current electric field was applied to achieve further sedimentation. The electric field was provided by a dc power supply with a capacity of 120 V and 0.5 A. The change in height of sediment was recorded. Experiments were performed under different current densities and different total solid volumes per unit cross-sectional area.

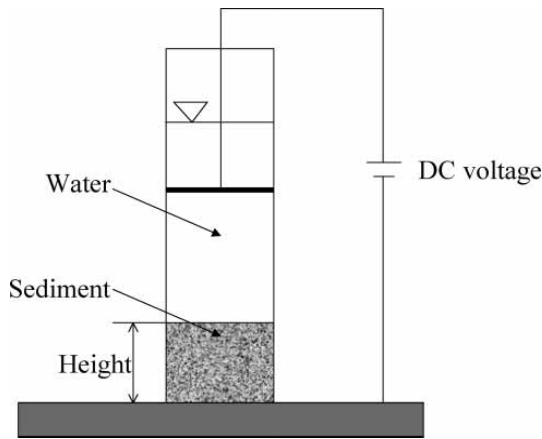


Fig. 1 Schematic diagram of experimental apparatus.

### Theory

For describing an electro-osmotic flow through a capillary tube, taking into account the applied electric field strength and the electric field strength in the electric double layer caused by the contact potential difference, the Navier-Stokes equation was solved about three decades ago [6]. The result was also extended to describe an electro-osmotic flow through porous media in much the same way as in the derivation of the Kozeny-Carman equation. The apparent liquid velocity  $q$  through the porous material is defined by the flow rate per unit cross-sectional area of the material and represented by [7].

$$q = \frac{\varepsilon^3}{kS_0^2(1-\varepsilon)^2\mu} \left( \rho_e E - \frac{dp_L}{dx} \right) \quad (1)$$

where  $k$  is the Kozeny constant,  $\varepsilon$  and  $S_0$  are the porosity and specific volume of the material respectively,  $\mu$  is the viscosity of the liquid,  $\rho_e$  is the

volumetric charge density of the liquid, and  $p_L$  is the liquid pressure.  $x$  and  $E$  are the spatial coordinate and the electric field strength in the direction of material thickness, respectively.

The first term of the right hand side of Eq. (1) represents an electro-osmotic flow in a porous material, while the second term shows a pressure flow in the material, both including the tortuosity and size of flow path. If  $E = 0$ , then Eq. (1) is reduced to the Kozeny-Carman equation which represents the apparent flow rate through a porous material under a liquid pressure gradient. Equation (1) was examined by use of incompressible sintered glass beads. Consolidation ratio ( $U_c$ ) is the measure of a progress of electroforced sedimentation. The equation for the calculation of  $U_c$  can be represented by the Eq. (2) [8].

$$U_c = \frac{H_1 - H}{H_1 - H_\infty} \\ = (1-B) \left[ 1 - \frac{32}{\pi^3} \sum_{n=1}^{\infty} \frac{(-1)^{n-1}}{(2n-1)^3} \exp \left\{ -\frac{(2n-1)^2 \pi^2 C_e}{4 \omega_0^2} \theta \right\} \right] + B[1 - \exp(-\eta\theta)] \quad (2)$$

where  $H_1$  and  $H$  are the initial and instantaneous height of the sediment and  $H_\infty$  is final height of the material, respectively.  $B$  is an empirical constant defined by  $B = a_c/(a_c + a_E)$  and represents the ratio of the creep deformation to the total deformation.  $U_c$  is zero at the beginning and becomes unity at infinity. There is a good agreement between experimentally measured  $U_c$  and theoretically calculated values by the use of Eq. (2) for the zinc oxide sedimentation [5].

### RESULTS AND DISCUSSION

Figure 2 illustrates the sedimentation rates of zinc oxide under three constant current densities. The rate of sedimentation increases with the enhancement of applied current density. In our previous study, similar trend was reported where the increase in the current density brought about increase in the solid compressive pressure which is responsible for enhance sedimentation [8]. Moreover, the rate of electroforced sedimentation of zinc oxide of two volumes per cross-sectional area ( $\omega_0$ ) was examined and the results are portrayed in Fig. (3). The consolidation ratio of zinc oxide with  $\omega_0 = 4.7$  mm is higher than that with  $\omega_0 = 5.8$  mm. There is an impact of initial volume of zinc oxide on the rate of consolidation ratio.

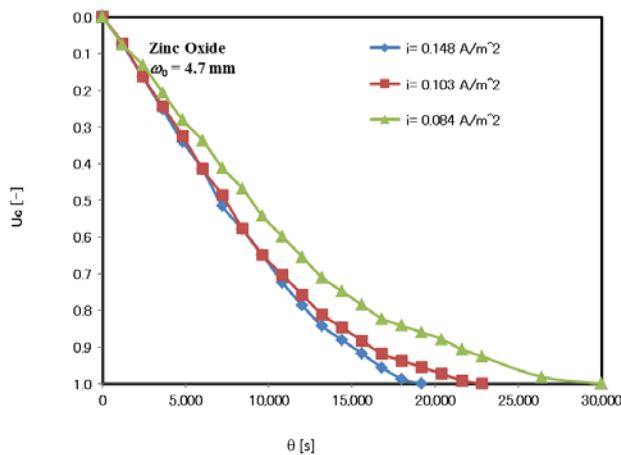


Fig. 2 Rate of sedimentation of Zinc Oxide under various current densities.

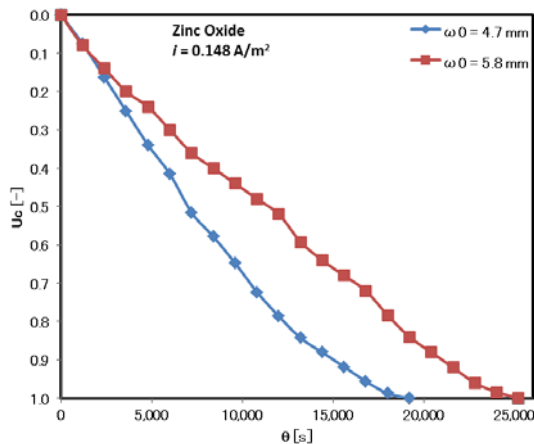


Fig. 3 Comparison of rate of consolidation ratio between two solid volumes per unit cross sectional area of Zinc Oxide.

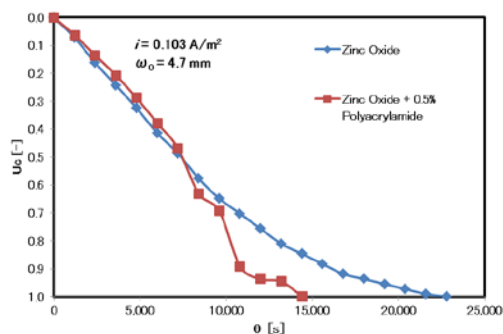


Fig. 4 Comparison between consolidation rate of Zinc Oxide and the mixture of Zinc Oxide and Polyacrylamide.

Figure 4 shows the effect of addition 0.5% polyacrylamide with zinc oxide as flocculants aid in

electroforced sedimentation. The consolidation rate is faster in the mixture of polyacrylamide and zinc oxide than without polyacrylamide. In consequences, it could be alleged that flocculant aid has an effect in dewatering. Figure 5 portrays the theoretical and experimental consolidation ratio of the electroforced sedimentation of zinc oxide. The theoretical values were found from calculation by using Eq. (2), where the creep ratio  $B$  was zero, thus the primary consolidation is main and there is no impact of the creep deformation. Experimentally measured data are well comparable with the theoretically calculated values.

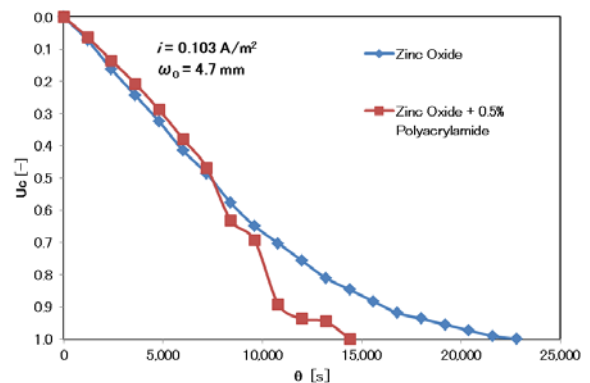


Fig. 5 Comparision of theoretical and experimental rate of sedimentation of Zinc Oxide under various current densities.

## CONCLUSION

This study assessed the effects of current density, total solid volume per cross sectional area, and addition of flocculation aid on the rate of electroforced sedimentation of zinc oxide. The main parameters influencing sedimentation were the applied current density and the addition of polyacrylamide in the zinc oxide slurry. After mixing the polyacrylamide with zinc oxide, the rate of consolidation ratio of zinc oxide increased remarkably. Beside this, the sedimentation rate of zinc oxide is enhanced with the increasing of current density. The initial weight of zinc oxide in slurry has less impact on electroforced sedimentation. Zinc oxide with  $\omega_0 = 4.7$  mm showed higher sedimentation than that with  $\omega_0 = 5.8$  mm. However, the electroforced sedimentation properties of other clay particles ought to be investigated.

## ACKNOWLEDGEMENT

This work was supported by Fundamental Research Grant Scheme, Ministry of Higher

Education, Malaysia (Grant no FRGS-13-029-0270) and we gratefully acknowledge the support.

## REFERENCES

- [1] Shirato M, Aragaki T, Manabe, A, & Takeuchi N, "Electroforced sedimentation of thick clay suspensions in consolidation region", *AIChE Journal*, Vol.25, Sep. 1979, pp. 855-863.
- [2] Adamson LG, Chilingar G V, Beeson CM, & Armstrong RA, "Electrokinetic dewatering, consolidation and stabilization of soils", *Engineering Geology*, Vol.1, 1966, pp. 291-304.
- [3] Lockhart NC, "Electroosmotic dewatering of clays. II. Influence of salt, acid and flocculants", *Colloids and Surfaces*, Vol.6, Apr.1983, pp. 239-251.
- [4] Dussour C, Favoriti P, & Vorobiev E, "Influence of chemical additives upon both filtration and electroosmotic dehydration of a kaolin suspension", *Separation Science and Technology*, Vol. 35, 2000, pp.1179-1193.
- [5] Jami MS, Iwata M, Muyibi S A, Karim M I A, Al-Khatib MAFR, & Mustapha M, (2013). "Enhanced electroforced sedimentation of various solid-liquid systems", *African Journal of Biotechnology*, Vol.10, Dec. 2011, pp.18906-18909.
- [6] Kobayashi K, Iwata M, Hosoda Y, and Yukawa H, (1979) "Fundamental study of electro-osmotic flow through perforated membrane", *Journal of Chemical Engineering Japan*, Vol.12, 2011, pp. 466-471.
- [7] Kobayashi K, Hakoda M, Hosoda Y, Iwata M, and Yukawa H, "Electro-osmotic flow through particle beds and electro-osmotic pressure distribution", *Journal of Chemical Engineering Japan*, Vol.12, 1979, pp. 492-494.
- [8] Jami MS, & Iwata M, "A New Method for the Theoretical Analysis of Electroforced Sedimentation Using Terzaghi-Voigt Combined Model", *Separation Science and Technology*, Vol. 43, 2008, pp.979-995.

## IMPORTANCE OF CORYDALIDAE AS AN INDEX OF METAL CONTAMINATION OF RIVER

Akihiro Fujino<sup>1</sup> and Hiroyuki Ii<sup>2</sup>

<sup>1</sup>Graduate School of Systems Engineering, Wakayama University, Japan;

<sup>2</sup>Faculty of Systems Engineering, Wakayama University, Japan

### ABSTRACT

Corydalidae is useful for evaluating a metal contamination of catchment. Metal concentration of river water is low and very changeable. River water contamination was caused by soil. However, soil analyzing is very difficult to reach average values because of variability of soil metal concentration. However, as Corydalidae eats many another insects in river and live in several years in river, metal derived from wide area of soil and water for long term is concentrated in Corydalidae body by food chain. Then it is easy to analyze metal concentration of Corydalidae because of high concentration. As a result, Cu, Mn and Zn were on the average, 410 ppm, 775 ppm, and 819 ppm in the polluted zone, the metal mine area. In the non-polluted zone, Cu, Mn and Zn were on the average, 26 ppm, 45 ppm, and 100 ppm. Metal concentration is quite different between polluted and non-polluted areas and then, it is very useful for index of metal contamination.

*Keywords: metal contamination, aquatic insect, Corydalidae, river, concentration factor*

### INTRODUCTION

Metal concentration of river water is low and very changeable. There is a method to quantify a metal concentration of algae adhering to a stone of a river bottom or an aquatic life, etc. instead of analyzing water directly. It is expected that metal contamination degree of a river can be evaluated by investigating an aquatic insect live in a river in several years especially. River water contamination was caused by soil, too. Then, to analyze soil also is necessary for determination of metal contamination. However, soil analyzing is very difficult because of variability of concentration. If an insect which condenses metal from water and soil is found out and its metal concentration is analyzed, the concentration will become an index for metal contamination for river and soil. Baetidae, a kind of may fly is reported to be useful as an environmental indicator for Cd and Zn and a caddis fly for Cd, Zn, Al, Fe, Cu, Ni, Mn, and Co [1]. Corydalidae eats many kinds of aquatic insects containing Baetidae and a caddis fly. Corydalidae was analyzed and a concentration factor was calculated. The concentration factor of *Stenopsyche marmorata* was compared with the concentration factor of Corydalidae, and it was investigated whether Corydalidae would be useful as a metal contamination environmental indicator living thing.

The maximum and the minimum of concentration factors of Mn for *Stenopsyche marmorata* were 490000 and 6410. The maximum and the minimum of concentration factors of Zn for *Stenopsyche marmorata* were 260000 and 25490.

The maximum and the minimum of concentration factors of Fe for *Stenopsyche marmorata* were 15 million and 51900. The maximum and the minimum of concentration factors of As for *Stenopsyche marmorata* were 18700 and 10000 [2]. Since there were not a concentration factor of Cu of *Stenopsyche marmorata* and a concentration factor of Pb, it cannot be compared.

Corydalidae is distributed in Japan, the eastern part and southern part of Asia, South and North America, South Africa, Madagascar, Australia, and New Zealand [3]. The larva of Corydalidae is living underwater for several years. The larva of Corydalidae lives under a stone of a river bottom and catch the other insects [3]. Therefore, it can be considered that the metal concentration in the larva of Corydalidae shows the pollution for river water and the river soil near an extraction point. The mining site which had produced gold, silver, copper, lead, zinc, and arsenic is upstream of Waidani, and mine water is flowing into the river.

### INVESTIGATION AREA

The river sampling places for Corydalidae were Waidani, Yoshinaga-cho, Bizen-shi, Okayama, and the Kotako River and the Sugitani River in Nara, and the Kogawa of Kozagawa River branch in Kozagawa-cho, Higashi-Muro-gun, Wakayama.

The closed mine produced gold, silver, copper, lead, zinc, and arsenic in the upstream of Waidani, and mine water is flowing into the river. In the Waidani area, there were three sampling areas of the lower reaches, the middle reaches and the upper



reaches. The Kotako River was in the limestone region. There is a hot spring in the fountainhead of the Kotato River and spring water flows into the river. The Sugitani River was close to the the Kotako River. the Kumano acidic rock was distributed in the Kogawa River catchment which is a non-polluted zone with no mine and [4]. The sampling points of the Kogawa River were in the upper reaches, the middle reaches, and the lower reaches.

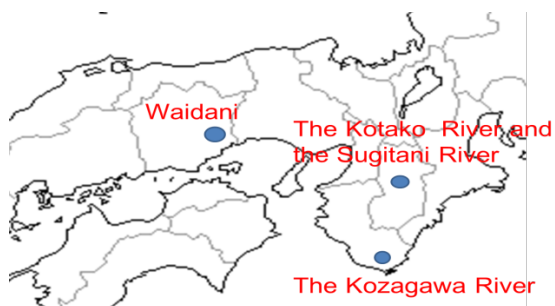


Fig. 1 Each investigation area in Honshu in Japan

## RESEARCH METHOD

River water and Corydalidae was extracted. The extracted Corydalidae was dried. The extracted river water puts in concentrated nitric acid. This is for abolishing the state in which the metal has adhered to the inner wall of bottle. The extracted dried Corydalidae is dissolved with concentrated nitric acid. After filtering the solution for river water with concentrated nitric acid and insect solution of concentrated nitric acid, solution was analyzed by ICP plasma-emission-spectrometry equipment.

In order to determine the original metal concentration of Corydalidae, it calculates from analysis result, the weight of a dried sample, and the quantity of the used concentrated nitric acid. Eq. (1) is a formula which calculates the metal concentration of Corydalidae. Eq. (2) is a formula which calculates a concentration factor.

$$\begin{aligned} \text{The metal concentration of Corydalidae} = & \\ \text{Analysis result} \times & \quad (1) \\ \frac{\text{Quantity of concentrated nitric acid}}{\text{Weight of a sample}} & \end{aligned}$$

$$\begin{aligned} \text{concentration factor} = & \\ \frac{\text{Metal concentration of Corydalidae}}{\text{River water metal concentration}} & \quad (2) \end{aligned}$$

## RESULTS

### Non-polluted zone

Table 1 is an analysis result of the river water metal concentration of the Kogawa River. There are no remains of a mine in Kogawa. The river metal concentrations of Cu, Fe and Pb in the upper reaches were 0.010, 0.021 and 0.061 ppm, respectively. The river metal concentrations of Cu, Fe and Pb in the middle reaches were 0.009, 0.053 and 0.055, respectively. The river metal concentrations of Cu, Fe and Pb in the lower reaches were 0.016, 0.019 and 0.016, respectively. Other metals were not detected.

Table 1 River water metal concentration of the Kogawa River(ppm)

	Cu	Fe	Mn	Pb	Zn	As
the upper reaches	0.010	0.021	0.002	0.061	0.003	0
the middle reaches	0.009	0.053	0.002	0.055	0.001	0
the lower reaches	0.016	0.019	0.001	0.065	0.001	0

Fig. 2 is Cu concentration of Corydalidae in the Kogawa River. Cu concentration of Corydalidae in the upper reaches was about 22 ppm to about 40 ppm. Cu concentration of Corydalidae in the middle reaches was about 22 ppm to about 35 ppm. Cu concentration of Corydalidae in the lower reaches was about 15 ppm to 40 ppm. The concentration factors of Cu of Corydalidae in the Kogawa River were the maximum of 13000, the minimum of 2200, and an average of 6700.

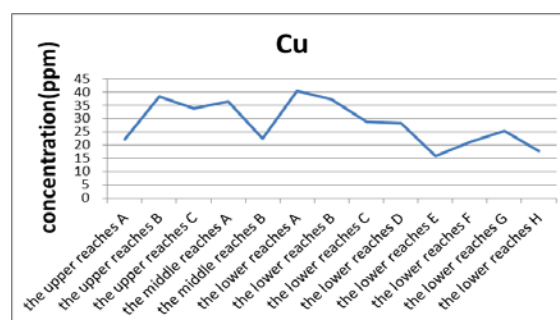


Fig. 2 Cu concentration of Corydalidae in the Kogawa River

Fig. 3 is Fe concentration of Corydalidae in the Kogawa River. Fe concentration of Corydalidae in the upper reaches was about 300 ppm to about 500 ppm. Fe concentration of Corydalidae in the middle reaches was about 350 ppm to about 500 ppm. Fe

concentration of Corydalidae in the lower reaches was about 300 ppm to 800 ppm. The maximum, the minimum and average of concentration factors of Fe for Corydalidae in the Kogawa River were 73000, 6400 and 34000, respectively.

Fe concentration of the river water in the middle reaches was 0.053 ppm, and was higher than those in the upper reaches and the lower reaches. However, one of the Fe concentrations of Corydalidae in the lower reaches was the highest concentration. Concentration of the Corydalidae did not relate with those in a river.

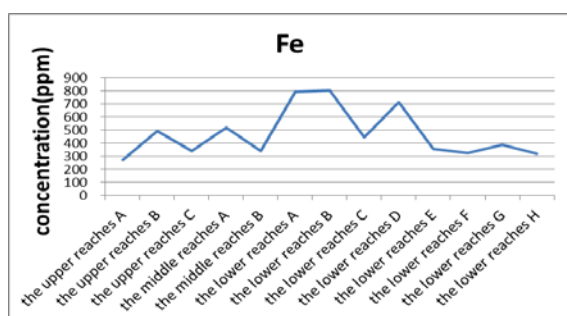


Fig. 3 Fe concentration of Corydalidae in the Kogawa River

Fig. 4 is Mn concentration of Corydalidae in the Kogawa River. Mn concentration of Corydalidae in the upper reaches was about 50 ppm to about 200 ppm. Mn concentration of Corydalidae in the middle reaches was about 50 ppm. Mn concentration of Corydalidae in the lower reaches was about 25 ppm to about 100 ppm. The maximum, the minimum and average of concentration factors of Mn for Corydalidae in the Kogawa River were 97000, 20000 and 44000, respectively.

Most Mn concentration of the river water in the Kogawa River was not detected. However, Mn concentration for Corydalidae in the Kogawa River was able to be detected to be 200 ppm and 100 ppm because of biological concentration.

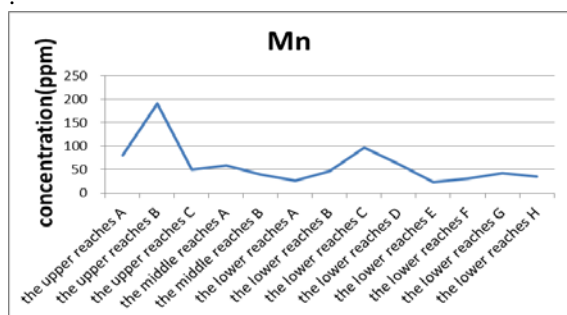


Fig. 4 Mn concentration of Corydalidae in the Kogawa River

Fig. 5 is Pb concentration of Corydalidae in the Kogawa River. Pb concentration of Corydalidae in

the upper reaches was about 4 ppm. Pb concentration of Corydalidae in the middle reaches was about 2 ppm to about 4 ppm. Pb concentration of Corydalidae in the lower reaches was about 1 ppm to about 4 ppm. The maximum, the minimum and average of concentration factors of Pb for Corydalidae in the Kogawa River were 1800, 20 and 720, respectively.

Pb concentration of the river water in the Kogawa River is about 0.060 ppm. However, Pb concentration of Corydalidae in the Kogawa River is about 3 ppm, and was hardly condensed by biological concentration.

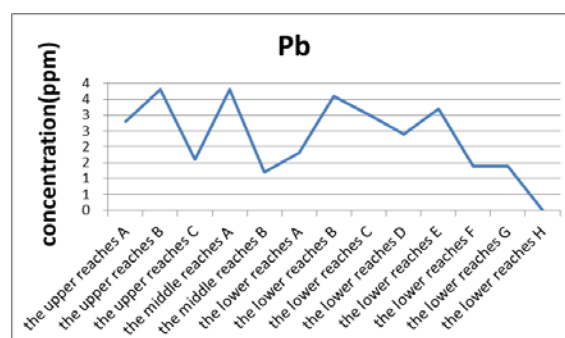


Fig. 5 Pb concentration of Corydalidae in the Kogawa River

Fig. 6 is Zn concentration of Corydalidae in the Kogawa River. Zn concentration of Corydalidae in the upper reaches was about 140 ppm to about 180 ppm. Zn concentration of Corydalidae in the middle reaches was about 100 ppm to about 160 ppm. Zn concentration of Corydalidae in the lower reaches was about 70 ppm to about 120 ppm. The maximum, the minimum and average of concentration factors of Zn for Corydalidae in the Kogawa River were 150000, 34000 and 62000, respectively.

Most Zn concentration of the river water in the Kogawa River was not detected. However, Zn concentration of Corydalidae in the Kogawa River was about 140 ppm because of biological concentration as well as Mn.

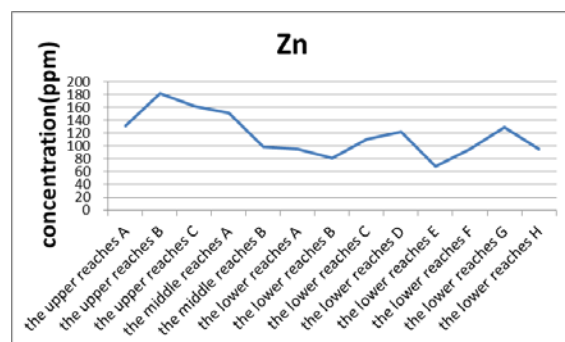


Fig. 6 Zn concentration of Corydalidae in the Kogawa River

Fig. 7 is As concentration of Corydalidae in the Kogawa River. As concentration of Corydalidae in the upper reaches was about 0.5 ppm to about 2 ppm. Most As concentration of Corydalidae in the middle reaches was not detected. As concentration of Corydalidae in the lower reaches was about 1 ppm to about 5 ppm. The maximum, the minimum and average of concentration factors of As for Corydalidae in the Kogawa River were 1800, 300 and 940, respectively.

As concentration of the river water in the Kogawa River was not detected. However, As concentration of Corydalidae in the Kogawa River is about 3 ppm, and As can also be concentrated in the body because of a biological concentration as well as Mn or Zn.

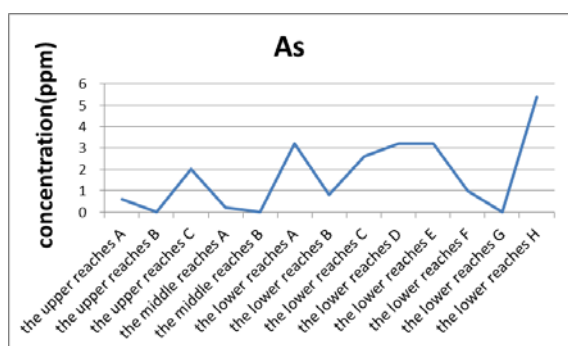


Fig. 7 As concentration of Corydalidae in the Kogawa River

#### Polluted zone and limestone region

Table 2 is the river water metal concentration near the Waidani, Kotako River, and the Sugitani River. The river metal concentrations of Cu, Fe, Mn, Pb, Zn, and As in the upper reaches of the Waidani were 0.080, 0.067, 0.007, 0.027, 0.700, and 0.013 ppm, respectively. The river metal concentrations of Cu, Fe, Mn, Pb, Zn, and As in the middle reaches of the Waidani were 0.021, 0.020, 0.022, 0.065, 0.300 and 0.024 ppm, respectively. The river metal concentrations of Cu, Fe, Pb, Zn, and As in the lower reaches of the Waidani were 0.006, 0.028, 0.056, 0.111 and 0.006 ppm, respectively. The river metal concentrations of Mn in the middle reaches of the Waidani were not detected. The river metal concentrations of Fe in the Kotako River were 0.008 ppm. The other metals were not detected. The river metal concentrations of Cu, Fe, Mn, Pb and As in the Sugitani River were 0.008, 0.082, 0.005, 0.006 and 0.028 ppm, respectively. Most Zn concentration in the Sugitani River was not detected.

Table 2 River water metal concentration of the Waikani, the Sugitani River, and the Kotako River(ppm)

	Cu	Fe	Mn	Pb	Zn	As
The upper reaches of Waidani	0.080	0.067	0.007	0.027	0.700	0.013
The middle reaches of Waidani	0.021	0.020	0.022	0.065	0.300	0.024
The lower reaches of Waidani	0.006	0.082	0	0.056	0.111	0.006
Kotako Riv.	0.001	0.008	0.001	0	0.001	0
Sugitani Riv.	0.008	0.082	0.005	0.006	0.002	0.028

Fig. 8 is Cu concentration of Corydalidae in the Waidani, Kotako River, and Sugitani River. Cu concentration of Corydalidae in the upper reaches of the Waidani was about 600 ppm. Cu concentration of Corydalidae in the middle reaches was about 300 ppm. Cu concentration of Corydalidae in the lower reaches was about 400 ppm. It turns out that Cu concentration for Corydalidae in the upper reaches is higher than those in the middle reaches and the lower reaches. Cu concentration of Corydalidae in the Kotako River and the Sugitani River was about 50 ppm. The maximum, the minimum and average of concentration factors of Cu for Corydalidae in the Waidani were 62000, 7600 and 28000, respectively. The concentration factor of Cu of Corydalidae in the Kotako River was 50000. The concentration factor of Cu of Corydalidae in the Sugitani River was 3000.

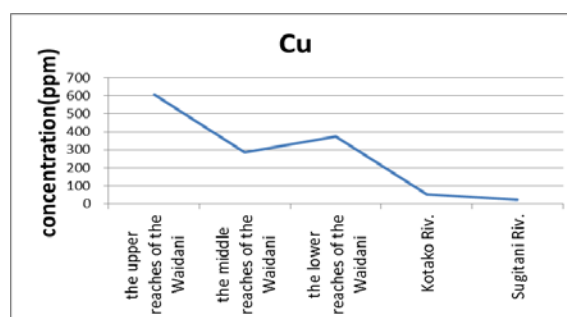


Fig. 8 Cu concentration of Corydalidae in the Waidani, the Kotako River, and the Sugitani River

Fig. 9 is Fe concentration of Corydalidae in the Waidani, Kotako River, and Sugitani River. Fe

concentration of Corydalidae in the upper reaches of Waidani and the middle reaches was about 1000 ppm. In the lower reaches, the high concentration was detected compared with the upper reaches and the middle reaches at 4000 ppm. Fe concentration of Corydalidae in the Kotako River was about 1000 ppm. Fe concentration of Corydalidae in the Sugitani River was about 3500 ppm. The maximum, the minimum and average of concentration factors of Fe for Corydalidae in the Waidani were 52000, 4500 and 23000, respectively. The concentration factor of Fe of Corydalidae in the Kotako River was 78000. The concentration factor of Fe of Corydalidae in the Sugitani River was 43000.

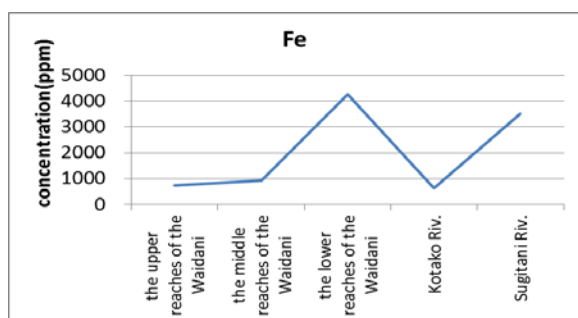


Fig. 9 Fe concentration of Corydalidae in the Waidani, the Kotako River, and the Sugitani River

Fig. 10 is Mn concentration of Corydalidae in the Waidani, Kotako River, and Sugitani River. Mn concentration of Corydalidae in the upper reaches of the Waidani and the middle reaches is about 250 ppm. Mn concentration of Corydalidae in the lower reaches is about 2000 ppm. Mn concentration of Corydalidae in Kotako River and the Sugitani River is about 250 ppm. The maximum, the minimum and average of concentration factors of Mn for Corydalidae in the Waidani were 29000, 9800 and 19000, respectively. The concentration factor of Mn of Corydalidae in Kotako River was 140000. The concentration factor of Mn of Corydalidae in Sugitani River was 29000.

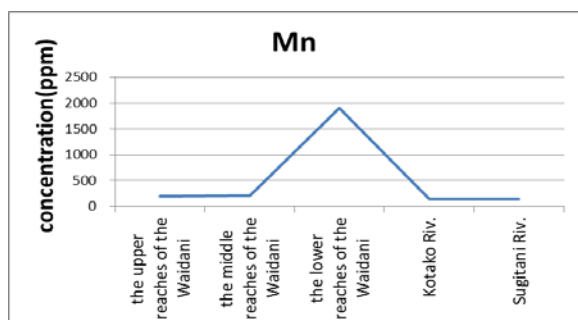


Fig. 10 Mn concentration of Corydalidae in the Waidani, the Kotako River, and the Sugitani River.

Fig. 11 is Pb concentration of Corydalidae in the Waidani, Kotako River, and Sugitani River. Pb concentration of Corydalidae in the upper reaches of the Waidani is about 90 ppm. Pb concentration of Corydalidae in the middle reaches is about 25 ppm. Pb concentration of Corydalidae in the lower reaches is about 10 ppm. The Kotako River and the Sugitani River are also the almost same concentration. The maximum, the minimum and average of concentration factors of Pb for Corydalidae in the Waidani were 3200, 100 and 1200, respectively. The concentration factor of Pb of Corydalidae in Kotako River and Sugitani River was not able to be calculated.

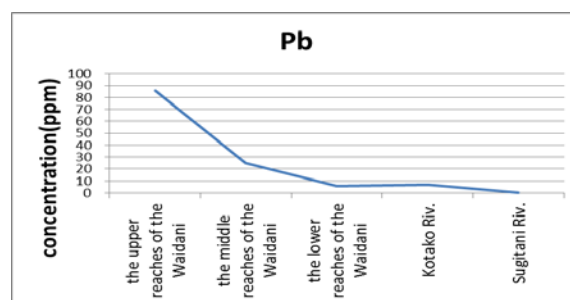


Fig. 11 Pb concentration of Corydalidae in the Waidani, the Kotako River, and the Sugitani River

Fig. 12 is Zn concentration of Corydalidae in the Waidani, Kotako River, and Sugitani River. Zn concentration of Corydalidae in the upper reaches of the Waidani is about 700 ppm. Zn concentration of Corydalidae in the middle reaches is about 600 ppm. Zn concentration of Corydalidae in the lower reaches is 1200 ppm. Zn concentration of Corydalidae in the Kotako River and the Sugitani River is about 100 ppm. The maximum, the minimum and average of concentration factors of Zn for Corydalidae in the Waidani were 11000, 1000 and 4600, respectively. The concentration factor of Zn of Corydalidae in the Kotako River was 120000. The concentration factor of Zn of Corydalidae in Sugitani River was 57000.

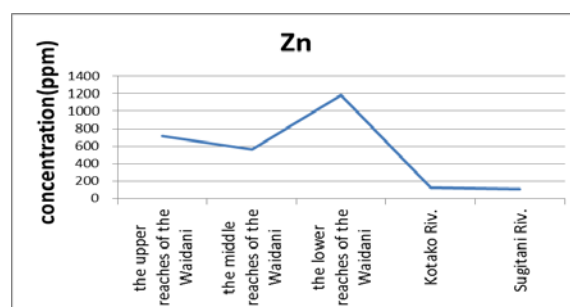


Fig. 12 Zn concentration of Corydalidae in the Waidani, the Kotako River, and the Sugitani River

Fig. 13 is As concentration of Corydalidae in the Waidani, Kotako River, Sugitani River. As concentration of Corydalidae in the upper reaches of the Waidani is about 250 ppm. As concentration of Corydalidae in the middle reaches and the lower reaches is about 220 ppm. As concentration of Corydalidae in the Kotako River and the Sugitani River is about 25 ppm. The maximum, the minimum and average of concentration factors of Mn for Corydalidae in the Waidani were 36000, 9000 and 22000, respectively. The concentration factor of As of Corydalidae in the Kotako River was not able to be calculated. The concentration factor of As of Corydalidae in the Sugitani River was 1000.

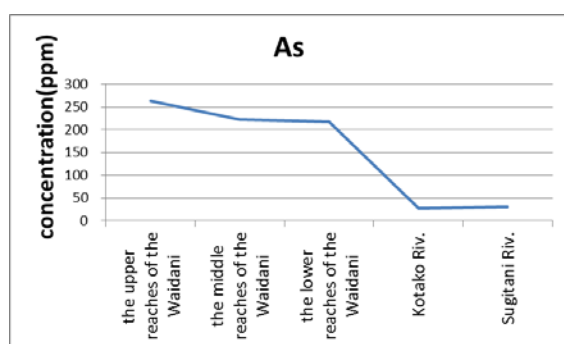


Fig. 13 As concentration of Corydalidae in the Waidani, the Kotako River, the Sugitani River

## DISCUSSION

The metal concentrations for river water and Corydalidae in the polluted zone and non-polluted zone were measured. It turns out that the metal concentration for Corydalidae in the polluted zone was higher than those in the non-polluted zone. However, Cu and Pb concentrations of river water in the polluted zone were not different from those in the non-polluted zone. In the polluted zone, Cu concentration and Pb concentration of Corydalidae are high concentration because of a biological concentration. The average concentrations of Cu, Fe, Mn, Pb, Zn and As of Corydalidae in the non-polluted zone were 28, 468, 60, 2, 117 and 2 ppm, respectively. The average concentrations of Cu, Fe, Mn, Pb, Zn and As of Corydalidae in the polluted zone were 421, 1970, 775, 38, 820 and 234 ppm, respectively. Metals, Cu, Fe, Mn, Pb, Zn and As are clarified to be concentrated in a body of Corydalidae larva.

The maximum concentration factor of Mn of Corydalidae was 140,000 and higher than those of *Stenopsyche marmorata*. The maximum

concentration factor of Zn of Corydalidae was 120,000 and higher than those of *Stenopsyche marmorata*. The maximum concentration factor of Fe of Corydalidae was 78000 and higher than those of *Stenopsyche marmorata*. The maximum concentration factor of Fe of Corydalidae was 36000 and higher than those of *Stenopsyche marmorata*.

The maximum concentration factor of Mn, Fe, and Zn for Corydalidae were very high as well as *Stenopsyche marmorata*, in this investigation, and then, Corydalidae is useful as an index living thing of Mn, Fe, and Zn.

Since the concentration factor of As for Corydalidae was a larger numerical value than those for *Stenopsyche marmorata*, it is useful as an index living thing for As.

## CONCLUSION

Corydalidae eats many kinds of aquatic insects as food. Then, metal derived from wide area of soil and water for long term is concentrated in Corydalidae body by food chain. The average of the metal concentration of Corydalidae under polluted zone was high. Metal concentration of Corydalidae is clarified to be influenced by river metal conditions.

The concentration factors of Fe, Mn, and Zn for *Stenopsyche marmorata* were higher than those for Corydalidae. The As concentrations and As concentration factors of Corydalidae were high in a river, then Corydalidae is effective for monitoring As, since its concentration factor is higher than those for *Stenopsyche marmorata*.

Therefore, it can be said that Corydalidae is useful as a metal contamination environmental indicator living thing of As.

## REFERENCES

- [1] Aizawa S, Kakuta K, and et.al "Evaluation of a caddis fly as a metal contamination environmental indicator living thing", *Bunseki Kagaku*, Vol. 43, 1994
- [2] Makoto S, and et.al "Shift of a radioactive material to a living thing from fresh water", *Radioactive Waste Management Center*, 1992
- [3] Yoshinori T, Takuzou Y, "The life history of *Parachauliodes continentails* in Sugihara river, Hyogo", *Hyogo Inland Water Living Thing*, Vol. 50, 1999, pp. 7-13
- [4] Sadahisa S, Ryoji K, "Mineral Resources Map of Chubu Kinki", *Geological Survey of Japan*, 2000



## CHEMISTRY OF RIVER WATER, RIVER INSECT AND WATER PLANT IN THE KINOKAWA RIVER CATCHMENT

Takuma Kubohara<sup>1</sup>, Hiroyuki Ii<sup>2</sup>

<sup>1</sup>Graduate School of Systems Engineering, Wakayama University, Japan;

<sup>2</sup>Faculty of Systems Engineering, Wakayama University, Japan

### ABSTRACT

Metal concentration of insect and plant was useful for determination of metal contamination and was proposed to be an effective index as metal contamination. Chemistry of water, river insect and water plant were studied in the serpentinite area, the closed mine area and another area of the Kinokawa River catchment in order to clarify influence of geological condition on water, insect and plant. Cu, Co and Ni concentrations of water were lower than those of insects and plants. Cu and Co in river insect and water plant were affected by Cu mines because those concentrations of river insect and water plant were high in the closed Cu mine area. Ni in river insect and water plant were affected by serpentinite because the concentrations of river insect and water plant were high in the serpentinite area. It was found that metals concentrations in moss, plant root and river insect were effective indicator for the influence of geological condition because Cu and Co concentrations of moss, plant root and river insects in the closed Cu mine area and Ni concentrations of moss and plant root in the serpentinite area were high.

*Keywords: Heavy Metals, Serpentinite, Closed Cu Mines, Insects, Plants*

### INTRODUCTION

Generally, the environment of water area is mainly evaluated by water quality. Moreover, most of water quality standards are established in order to keep the human life safely.

However, biodiversity is taken seriously in recent years. Therefore, in Japan, environmental quality standards for water pollution and preservation of aquatic life were established in November 2003.

However, chemistry of aquatic life is not investigated enough.

Therefore, in this study, chemistry of water, river insect and water plant was studied in order to clarify influence of geological condition on water, insect and plant.

### STUDY AREA

Fig.1 shows the location of study area. The Kinokawa River is located in Kinki. The Kinokawa River has its origin in Odaigahara, and flows to west along the median tectonic line. The flow is from South Nara through Kii plain into the Kii channel. Kinokawa is class A river, and the length is 136 km, total basin area is 1,750 km<sup>2</sup> [1]. The catchment in Wakayama prefecture is the research area.

Izumi Group composed of sedimentary rocks,

sandstone, mudstone, conglomerate and et al. is distributed in the northern part of research area, and Sanbagawa belt composed of metamorphic rocks, crystalline schist and et al. is distributed in the southern part, Hidakagawa Group composed of sedimentary rocks, sandstone and shale is distributed in the southeast part.

The Kinokawa River catchment has serpentinite and the closed Cu mines. The chemistry of Serpentinite is quite different from another rocks, in particular, serpentinite has high concentration of Mg, and Ni. The closed Cu mine produced a lot of Cu and Fe sulfide ore and waste water was low pH and high concentration of sulfate with metal.

### STUDY METHOD

We investigated chemistry of river water, river insect and water plant. Mg<sup>2+</sup>, Ca<sup>2+</sup>, Cu, Co and Ni concentrations in river water and Cu, Co and Ni in river insect and water plant were measured.

River water samples were kept cool and it was filtered with the membrane filter with 0.45 micrometer of pore size for analysis in laboratory. The sampled river insects and water plants were desiccated by dryer at first. After drying, they were dissolved with concentrated nitric acid and it was filtered with the membrane filter with 0.45 micrometer of pore size for analysis.



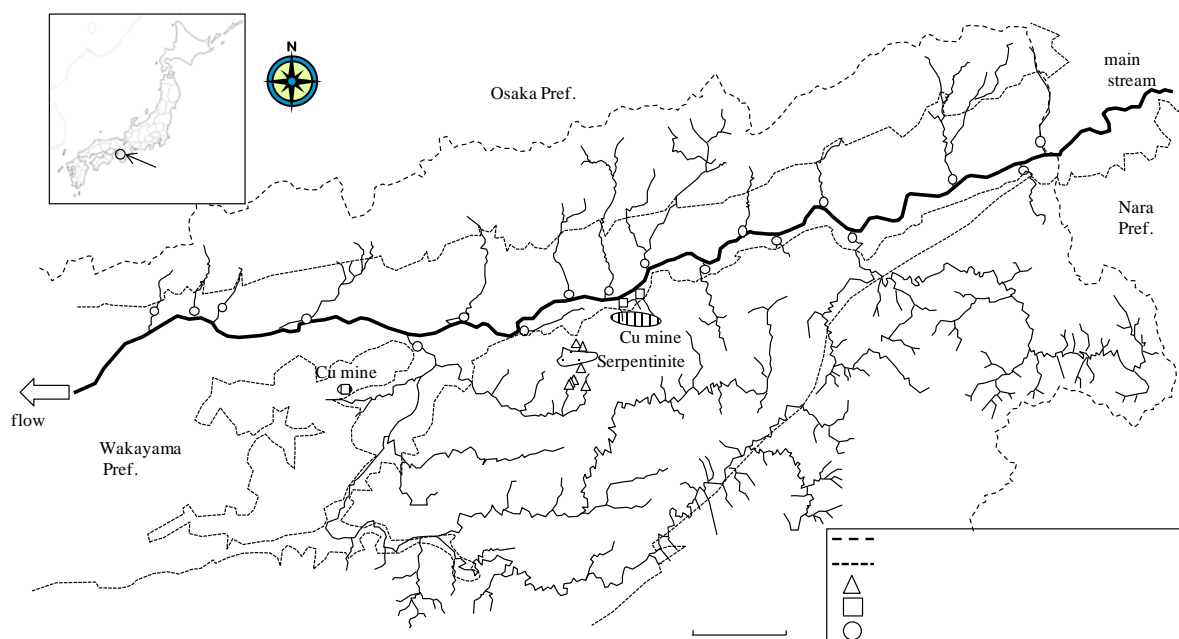


Fig.1 Study area.

$Mg^{2+}$  and  $Ca^{2+}$  were measured by ion exchange chromatography. Cu, Co and Ni were measured by ICP-AES. The actual detection limit of ICP-AES is 0.01ppm for Cu, Co and Ni.

Table.1 shows summary of field observation. About water plant except moss, the body divided into upper part, middle part, lower part and root. Therefore, one part is one sample.

## RESULTS AND DISCUSSION

### Mg/Ca Equivalent Ratio in River Water

Fig.2 shows Mg/Ca equivalent ratios in river water. Generally, it is known that Mg/Ca ratio in the river water is used for estimation of the geological condition in the catchment.

Mg/Ca equivalent ratios in the serpentinite area were from 0.25 to 24, those in another two areas were from 0.12 to 0.56. Then, Mg/Ca equivalent ratios in the serpentinite area were higher than another two areas. It is known that the serpentinite contains a lot of Mg. Therefore, river water in the serpentinite area was influenced by serpentinite.

### Heavy Metals in River Water

Figs.3, 4 and 5 show Cu, Co and Ni concentrations in river water. Cu concentrations in the closed Cu mine area were from under detection limit to 0.34ppm, those in another two areas were under detection limit. Then, Cu concentrations in the closed Cu mine area were higher than another two areas. But the highest Cu concentration was found at the mining sewage and the river water. Except the highest Cu concentration data, Cu concentrations

Table.1 Summary of field observation.

		the serpentinite area	the closed Cu mine area	the another area	total
water	observation time	July, Sep.2013, Feb., Apr.2014	Dec.2013, Apr.2014	Dec.2013, Jan.2014	
	sampling points	7	3	18	28
	number of samples	15	4	18	37
river insect	observation time	July, Sep.2013, Feb., Apr.2014	Dec.2013, Apr.2014	Dec.2013, Jan.2014	
	sampling points	7	3	15	25
	number of samples	19	6	19	44
	species	gammaridea, dobsonfly larva, caddice-worm, stonefly larva, dragonfly larva	crane fly larva, dobsonfly larva, dragonfly larva, corixidae, rat-tailed maggot	corixidae, crane fly larva, stonefly larva, dragonfly larva	
water plant	observation time	Feb., Apr.2014	Dec.2013, Feb., Apr.2014	Dec.2013, Jan., Feb.2014	
	sampling points	7	3	18	28
	number of samples	33	27	73	133
	species	fern, moss	coix, reed, japanese silver grass, fern, moss	coix, reed, paspalum	

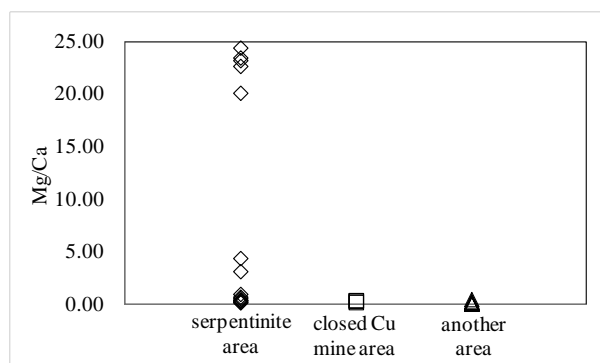


Fig.2 Mg/Ca equivalent ratios in river water.

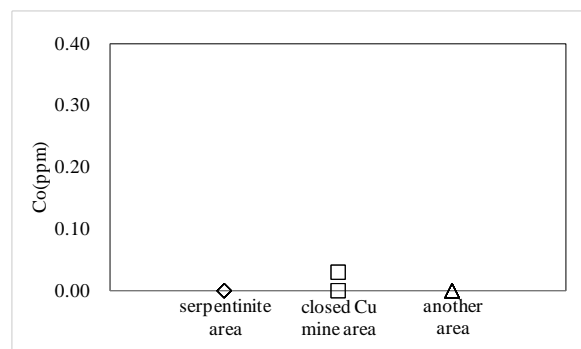


Fig.4 Co concentrations in river water.

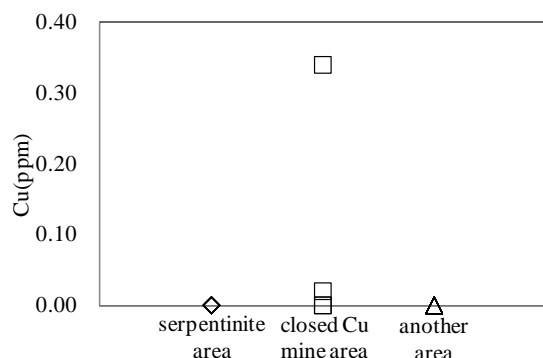


Fig.3 Cu concentrations in river water.

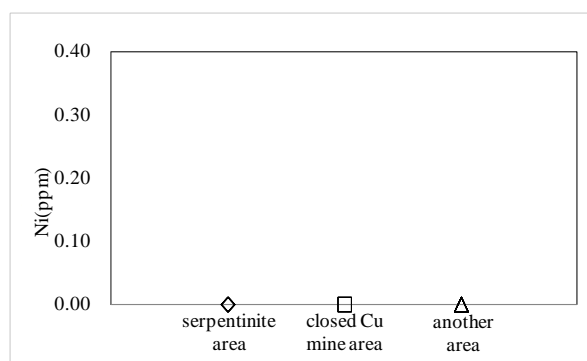


Fig.5 Ni concentrations in river water.

were almost under detection limit in all area.

Co and Ni concentrations were under detection limit in all area.

Therefore, although there are Cu mines and serpentinite in the catchment, Cu, Co and Ni concentrations in river water were very low, almost under detection limit except some sewage and river from the Cu mine.

### Heavy Metals in River Insect and Water Plant

Figs.6, 7, 8, 9, 10, 11 and 12 show Cu, Co and Ni concentrations in river insect and water plant. Fig.9 shows all Cu concentrations data, however, Fig.10 shows just less than 800mg/kg-dry for Cu concentrations.

In the closed Cu mine area, Cu concentrations of river insect were from 440 mg/kg-dry to 663 mg/kg-dry, Co concentrations of river insect were from under detection limit to 40 mg/kg-dry, Cu concentrations of water plant were from under detection limit to 10,000 mg/kg-dry, Co concentrations of water plant were from under detection limit to 61 mg/kg-dry. In another two areas, Cu concentrations of river insect were from under detection limit to 190 mg/kg-dry, Co concentrations of river insect were under detection limit to 10 mg/kg-dry, Cu concentrations of water plant were from under detection limit to 99 mg/kg-dry, Co concentrations of water plant were from under

detection limit to 10 mg/kg-dry. Then, Cu and Co concentrations of river insect and water plant in the closed Cu mine area were higher than another two areas. The Cu mines in the Kinokawa River catchment have cupriferous pyrite [2]. It is known that the cupriferous pyrite contains Cu, Co, etc [3]. Therefore, Cu and Co of river insects and water plants in the closed Cu mine area were affected by Cu mines.

In the serpentinite area, Ni concentrations of river insect were from under detection limit to 220 mg/kg-dry, Ni concentrations of water plant were from under detection limit to 270 mg/kg-dry. In another two areas, Ni concentrations of river insect were from under detection limit to 20 mg/kg-dry, Ni concentrations of water plant were from under detection limit to 30 mg/kg-dry. Then, Ni concentrations in river insects and water plants in the serpentinite area were higher than another two areas. It is known that the serpentinite contains Ni. Therefore, river insects and water plants in the serpentinite area were affected by the serpentinite.

### Comparison of River Water with River Insect and Water Plant on Heavy Metals

From Figs.3, 4 and 5, Cu, Co and Ni concentrations in river water were from under detection limit to 0.34ppm, under detection limit and under detection limit, respectively.

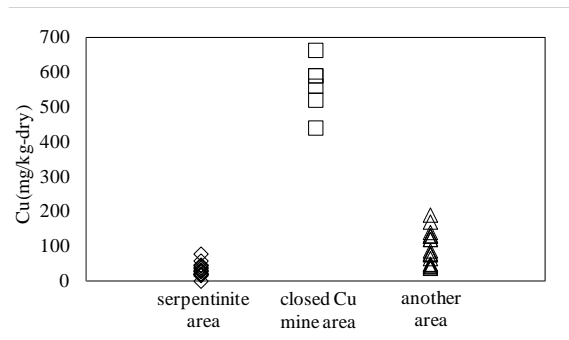


Fig.6 Cu concentrations in river insect.

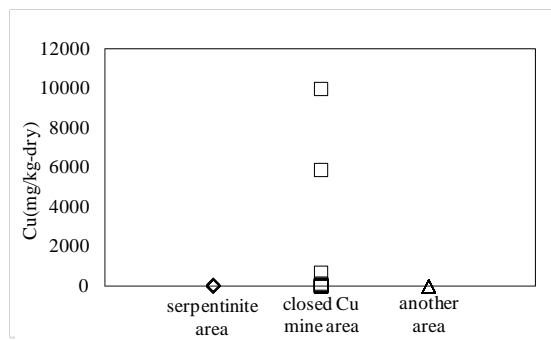


Fig.9 Cu concentrations in water plant.

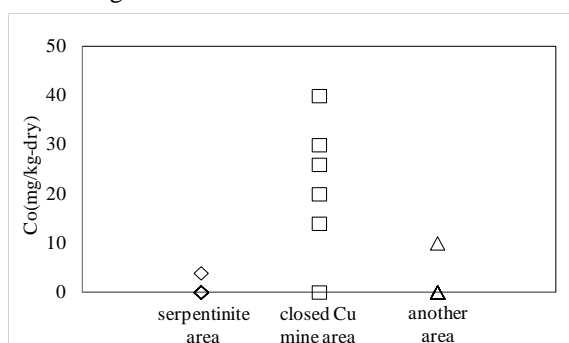


Fig.7 Co concentrations in river insect.

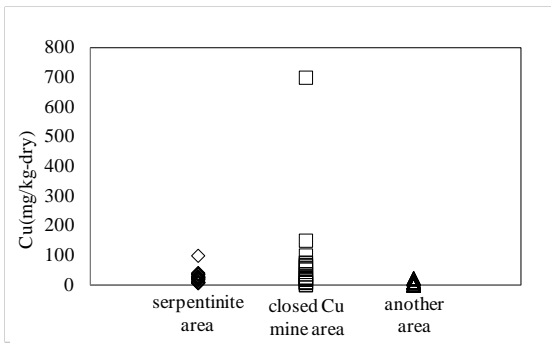


Fig.10 Cu concentrations in water plant (<800 mg/kg-dry).

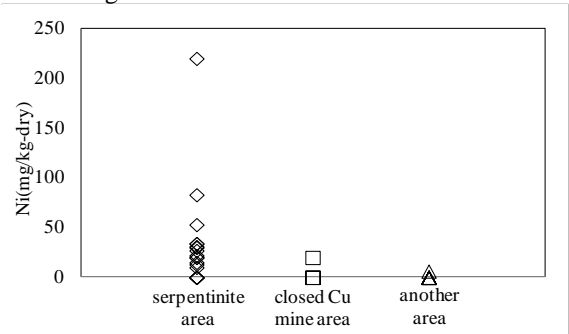


Fig.8 Ni concentrations in river insect.

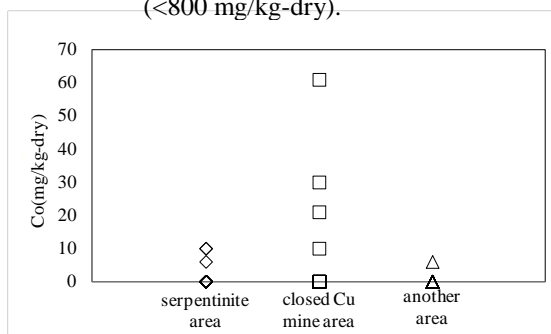


Fig.11 Co concentrations in water plant.

From Figs.6, 7 and 8, Cu, Co and Ni concentrations in river insects were from under detection limit to 663 mg/kg-dry, from under detection limit to 40 mg/kg-dry and from under detection limit to 220 mg/kg-dry, respectively.

From Figs.9, 10, 11 and 12, Cu, Co and Ni concentrations in water plants were from under detection limit to 10,000 mg/kg-dry, from under detection limit to 61 mg/kg-dry and from under detection limit to 270 mg/kg-dry, respectively.

As a result, heavy metals concentrations of insects and plants were higher than those of river water. Therefore, heavy metals in insect and plant were effective indicator for the influence of geological condition.

## Relationship between Heavy Metals and Geological Condition

From Figs.3, 4 and 5, although there are Cu mines and serpentinite in the catchment, Cu, Co and Ni concentrations in river water were very low,

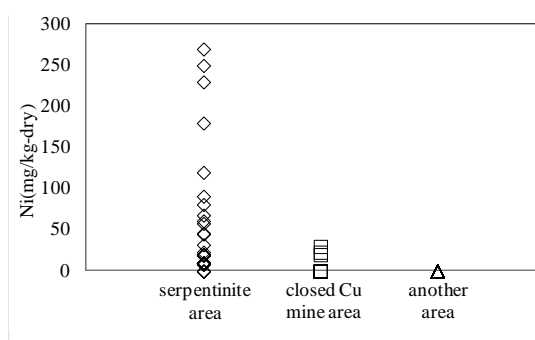


Fig.12 Ni concentrations in water plant.

almost under detection limit.

From Figs.6, 7, 9, 10 and 11, Cu and Co concentrations in river insects and water plants in the closed Cu mine area were higher than another two areas. Therefore, those of Cu and Co concentrations were useful for determination of influence of Cu mines.

From Figs.8 and 12, Ni concentrations in river insects and water plants in serpentinite area were higher than another two areas. Therefore, those of Ni

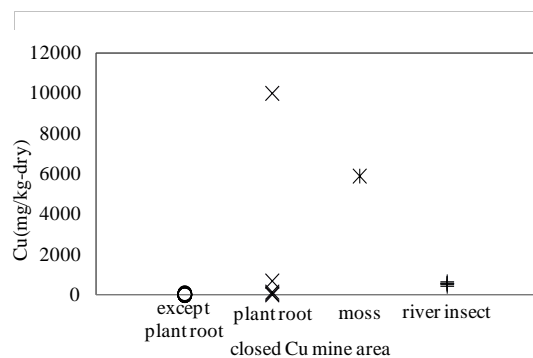


Fig.13 Cu concentrations of river insect and water plant in the closed Cu mine area.

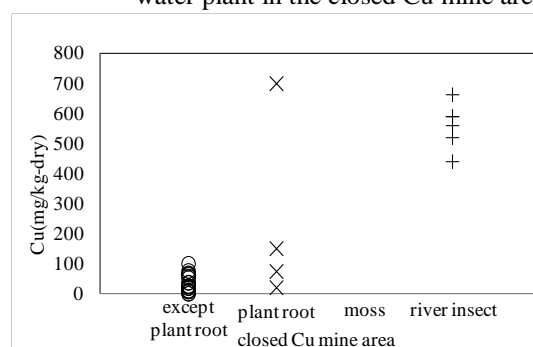


Fig.14 Cu concentrations of river insect and water plant in the closed Cu mine area (<800 mg/kg-dry).

concentrations were useful for determination of influence of serpentinite.

As the above, when the contamination was not able to be found by measurement of heavy metals in the river water, contamination was clarified by measurement of those in river insect and water plant. Therefore, it was thought that heavy metals in river insect and water plant become an important index as contamination.

### Compariosn of River Insects with Water Plants for Heavy Metals

Cu, Ni and Co concentrations of river insect and water plant were compared at the two fields, the Cu mine area and serpentinite area.

Figs.13, 14, 15 and 16 show the comparison results. Fig.13 shows all Cu concentrations data, however, Fig.14 shows just less than 800mg/kg-dry for Cu concentrations. Water plants were classified into moss (A) and other plant. Additionally, it classified other plants into root (B) and other part (stem and leaf) (C).

Cu concentrations of river insect were from 440 mg/kg-dry to 663 mg/kg-dry, Cu concentrations of water plant were from under detection limit to 10,000 mg/kg-dry. Then, Cu concentrations of water plant were higher than those of river insect.

Co concentrations of river insect were from under detection limit to 40 mg/kg-dry, Co

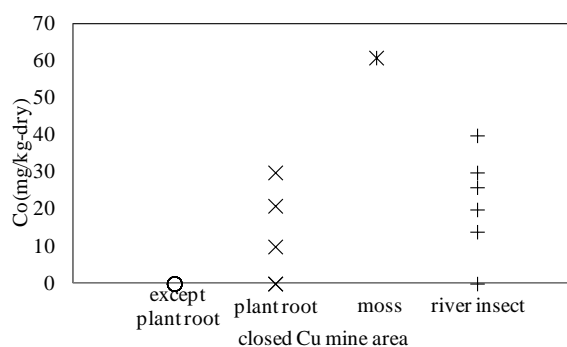


Fig.15 Co concentrations of river insect and water plant in the closed Cu mine area.

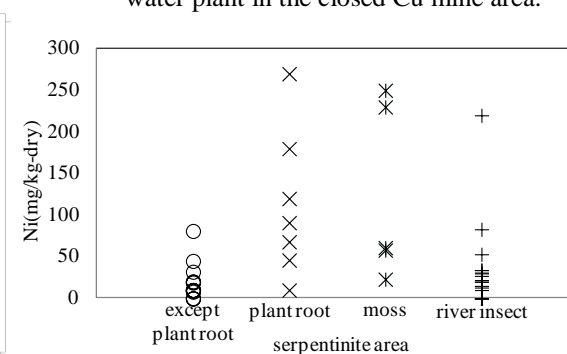


Fig.16 Ni concentrations of river insect and water plant in the serpentinite area.

concentrations of water plant were from under detection limit to 61 mg/kg-dry, Ni concentrations of river insect were from under detection limit to 220 mg/kg-dry, Ni concentrations of water plant were from under detection limit to 270 mg/kg-dry. Then, Co and Ni concentrations of water plants were almost the same range as those of river insects.

Cu and Co concentrations of river insects, (A) and (B) were from 20 mg/kg-dry to 10,000 mg/kg-dry and from under detection limit to 61 mg/kg-dry, respectively. Cu and Co concentrations of (C) were from under detection limit to 100 mg/kg-dry and under detection limit, respectively. Then, Cu and Co concentrations of river insects, (A) and (B) were higher than those of (C). Therefore, it was found that Cu and Co in river insect, moss and plant root were effective indicator for the influence of geological condition.

On the other hand, Ni concentrations of (A) and (B) were from 10 mg/kg-dry to 270 mg/kg-dry. Ni concentrations of river insects and (C) were from under detection limit to 220 mg/kg-dry, although most data below 100mg/kg-dry. Then, Ni concentrations of (A) and (B) were higher than those of river insects and (C). Therefore, it was found that Ni in moss and plant root was effective indicator for the influence of geological condition.

## CONCLUSION

In this study, chemistry of water, river insect and water plant was studied in the serpentinite area, the closed mine area and another area of the Kinokawa River catchment in order to clarify influence of geological condition on water, insect and plant.

It was thought that river water in the serpentinite area was affected by serpentinite because Mg/Ca equivalent ratios of river water in the serpentinite area were high.

Cu, Co and Ni concentrations of water were lower than those of insect and plant.

Cu and Co concentrations of river insect and water plant in the closed Cu mine area and Ni concentrations of them in the serpentinite area were high, although Cu, Co and Ni concentrations of river water in all area were almost under detection limit.

Therefore, it was thought that Cu and Co of insects and plants in the closed Cu mine area were affected by Cu mines. Moreover, it was thought that Ni of insects and plants in the serpentinite area were affected by serpentinite.

It was thought that heavy metals in moss, plant

root and river insect were effective indicator for the influence of geological condition because Cu and Co concentrations of moss, plant root and river insect in the closed Cu mine area and Ni concentrations of moss and plant root in the serpentinite area were high.

Therefore, metal concentrations of insect and plant were useful for determination of metal contamination and became an important index as contamination.

## REFERENCES

- [1] River Bureau Kinki Regional Development Bureau Ministry of Land, Infrastructure, Transport and Tourism, Kinokawa Basin, <http://www.kkr.mlit.go.jp/river/kasen/kinokawa.html>
- [2] Wakayama City Children's Science Museum, <http://www.city.wakayama.wakayama.jp/kodomo/sassi/ganseki/p9.htm>
- [3] Miyazaki Prefecture, <http://www.pref.miyazaki.lg.jp/shoukou/kougyou/m-geo/4th/index.htm>

# COMPARATIVE ANALYSIS OF EMBANKMENT METHODS UTILIZING EXPANDED POLY-STYROL AND CONVENTIONAL METHOD IN MOUNTAIN ROAD IN JAPAN BY LIFE CYCLE ASSESSMENT

Hideyuki Ito<sup>1</sup>, Koichi Yamanaka<sup>2</sup>, Shoma Nehashi<sup>3</sup>, Atsushi Fukuda<sup>4</sup> and Kunio Minegishi<sup>5</sup>  
<sup>1,2,4,5</sup> College of Science and Technology, Nihon University, Japan;  
<sup>3</sup> Nexco-Maintenance Kanto Company Limited, Japan

## ABSTRACT

In recent years, new composite geomaterials that were developed to reduce the weight are expected to be applied to soft ground and mountainous areas for preventing ground liquefaction and landslide in Japan. These new composite geomaterials have some problems such as taking much time for construction, increasing the construction cost and adverse impacts on environment. Thus, the conventional geomaterial is usually chosen than new composite geomaterials in Japan. However, there are few researches that analyzed the environmental impacts (for example, CO<sub>2</sub>, Nox, Sox and total life-cycle cost) of new developed composite geomaterials quantitatively from the perspective of LCA (life cycle assessment). Therefore, the purpose of this research is to estimate the total emissions of CO<sub>2</sub>, Nox, Sox and total life-cycle cost of 3 kinds of embankments constructed by conventional method (cut and fill), lightweight geomaterial mixed with expanded polystyrol beads and expanded polystyrol construction method in mountain road by applying the life cycle assessment.

*Keywords: Life Cycle Assessment, Lightweight Geomaterial Mixed with Expanded Polystyrol Beads, Expanded Polystyrol Construction Method, Life Cycle Cost*

## INTRODUCTION

In Japan, a lot of wetlands, rivers and coastal area have been reclaimed to increase agricultural land because the flat plains are narrow and limited. Thus, there are many potential areas that might cause the ground settlement and ground liquefaction. In addition, since it is difficult to acquire land for constructing roads in Japan, a lot of roads and buildings have been built in the mountains. On these backgrounds, recently new composite geomaterials have been developed in Japan to reduce the weight for applying to soft ground and mountainous areas for preventing landslide. Composite geomaterials are expected as landslide prevention works by weight saving.

In the existing researches, various composite geomaterials with additional values and new physical properties such as the cement stabilized soil, light weight treated soil with air foam method, liquefied soil stabilization method, and tire tip mixed soil are developed and estimated amount of CO<sub>2</sub> emissions at the manufacturing phase [1]-[2]. In addition, eco-efficiency assessment has been carried out by the simulation and sensitivity analysis as environmental assessment of composite geomaterials using construction sludge [3]. However, these existing researches are not compared with the conventional method and then estimated the emission of the air pollutants with considering all

life cycle including raw materials acquisition, construction, use and waste phase.

Therefore, the purpose of this research is to estimate the total emissions of CO<sub>2</sub>, Nox, Sox and total life-cycle cost of 3 kinds of embankments constructed by conventional method (cut and fill), lightweight geomaterial mixed with expanded polystyrol beads and expanded polystyrol construction method in mountain road by applying the life cycle assessment.

In this research, total amount of air pollutants and CO<sub>2</sub> emissions of conventional construction method by cut-and-fill and new methods using light weight geomaterial mixed with expanded polystyrol beads and expanded polystyrol construction method were estimated in consideration of all life cycles including the raw materials acquisition for construction, use, and waste phase. In addition, the total life cycle cost of these 3 construction methods were also calculated and performed the comparative evaluation of these construction methods.

## METHOD AND SYSTEM DETAILS

In this research, Mineoka area located in the southern part of Chiba prefecture was selected as a case study area because landside control works are conducted in mountainous roads (Fig.1). For comparative LCA analysis, we assumed conventional method, lightweight geomaterial mixed



with expanded polystyrol beads and expanded polystyrol construction method were adopted for constructing mountainous roads.

Also, we set a functional unit that provides a logical basis for comparing the environmental performance of alternatives for applying LCA to these 3 construction methods. We defined the target road condition (2 lanes, 7m wide and 1m long) as a functional unit as shown in the Fig.2. In addition, we hypothesized that the inclined angle of the mountain and road slope is 35 degree and 55 degree respectively, and then we set the ratio of cut and fill of conventional method is 3:1, the ratio of cut and fill of lightweight geomaterial mixed with expanded polystyrol beads and expanded polystyrol construction method is 1:3 (Fig.3).



Fig. 1 Location of case study area.

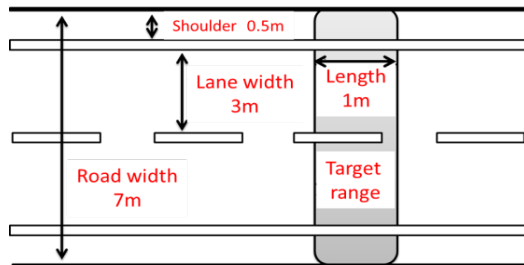


Fig. 2 Functional unit.

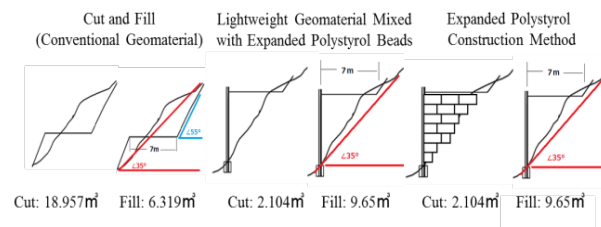


Fig. 3 Set condition of each construction method.

#### System Boundary of Each Construction Method

The system boundary of “cut and fill (conventional method)” is shown in Fig.3. The

limestone is transported to the plant for producing stabilizing material, and then the transported soil, sand, stabilizing material and water are mixed and leveled the ground at the road construction site. Cut and fill method is basically maintenance-free. At the waste phase, soil and sand are recycled after demolishing the road.

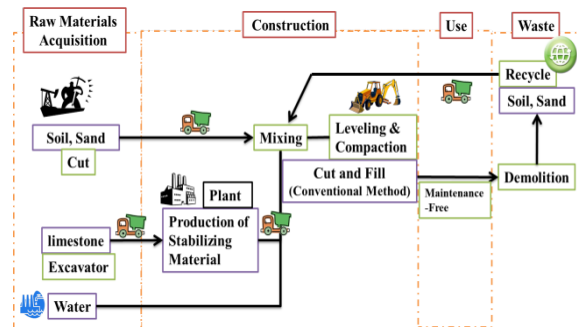


Fig. 3 System boundary of cut and fill method (conventional method).

Fig.4 shows the system boundary of lightweight geomaterial mixed with expanded polystyrol beads. Expanded polystyrol beads are produced in the plant at the phase of raw materials acquisition. At the construction phase, the limestone is transported to the plant for producing stabilizing material as well as “cut and fill (conventional method)”, and then the transported expanded polystyrol beads, soil, sand, stabilizing material and water are mixed and leveled the ground at the road construction site. Constructed lightweight geomaterial mixed with expanded polystyrol beads is also maintenance-free. Recycling method for lightweight geomaterial mixed with expanded polystyrol beads at the waste phase is not determined at present but we assumed the blowing separator is used for recycling soil.

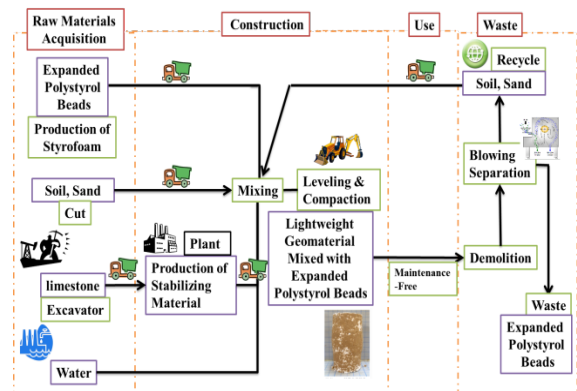


Fig. 4 System boundary of lightweight geomaterial mixed with expanded polystyrol beads.

Fig.5 shows the system boundary of expanded polystyrol construction method. Expanded polystyrol beads are produced in the plant at the raw

materials acquisition phase as well as lightweight geomaterial mixed with expanded polystyrol beads. The clamping materials that are used for expanded polystyrol construction method are manufactured from aluminum produced from imported bauxite and zinc smelt from sphalerites at the plant. The soil generated by excavation at the road construction site, styrofoam and clamping materials are used for expanded polystyrol construction. At the waste phase, all materials are disposed at the plant after demolishing the road.

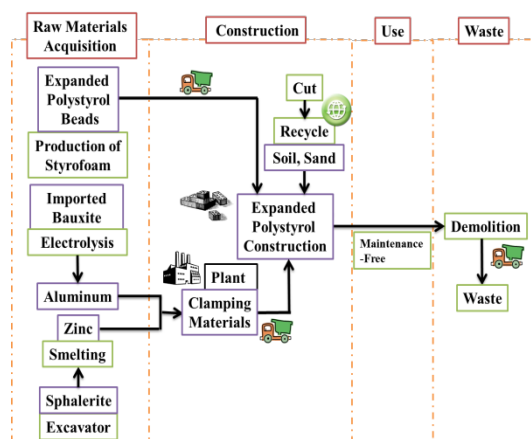


Fig. 5 System boundary of expanded polystyrol construction method.

### Method and System Details

For calculating the total amount of air pollutants and CO<sub>2</sub> emissions, we set the CO<sub>2</sub>, Sox and Nox unit (Table.1) and cost unit for each material (Table 2). These units were developed based on various databases and data such as LCA guideline for building [4], IDEA (Inventory Database for Environmental analysis) [5], LCA database developed by Life Cycle Assessment Society of Japan [6], database of Express Highway Research Foundation of Japan [7] and database of JEMAI-LCA PRO [8]". Cost unit for each material was estimated Input-Output Table of ministry of internal affairs and communications [9]. Regarding the power consumption of blowing separation that is used for recycling soil and sand for lightweight geomaterial mixed with expanded polystyrol beads, we estimated it based on the result of interview survey to a machinery manufacturer.

Estimated total amount of air pollutants and CO<sub>2</sub> emissions of each construction method by using these databases are shown in Table.3, 4 and 5.

Table 1 CO<sub>2</sub>, Sox and Nox unit.

Life-cycle	Materials	CO <sub>2</sub>	SOx	NOx
		(kg-CO2)	(g-SOx)	(g-NOx)
Raw Materials Acquisition	Soil, Sand (kg)	0.001963	0.003407	0.010598
	Limestone (kg)	0.004688	0.000865	0.001547
	EPS (kg)	1.31226	0.255529	1.165096
	Aluminum (kg)	9.218	76.8	30
	Zinc (kg)	1.443	5.92	1.327
Construction	Leveling (m <sup>2</sup> )	20.9	28.91883	48.17308
	Compaction (m <sup>3</sup> )	12.1	16.74248	27.88968
Transport	20t Truck (Diesel) (km)	1.18	1.45	3.64
	15t Truck (Diesel) (km)	0.962	1.18	2.97
	10t Truck (Diesel) (km)	0.742	0.91	2.229
	4t Truck (Diesel) (km)	0.472	0.56	1.45
	2t Truck (Diesel) (km)	0.323	0.4	1.0
Waste	EPS (kg)	2.64	0.544	1.22
	Metal (kg)	0.366	0.325	0.591
Energy	Electricity (Thermal power plant) (kwh)	0.425	0.17	0.13

Table 2 Cost unit for each material.

Materials	Unit	JPY
Polystyrene	JPY/kg	209.862
Crushed stone	JPY/kg	2
Limestone	JPY/kg	0.633
Aluminum	JPY/kg	76.539
Zinc	JPY/kg	186.132
Electricity (Thermal power plant)	JPY/kwh	16.19839
Diesel	JPY/L	78.979
Waste (Plastic)	JPY/kg	0.510976
Waste (Metal)	JPY/kg	0.998192
Leveling & Compaction	JPY/m <sup>3</sup>	934.2707

Table 3 Air pollutants and CO<sub>2</sub> emissions of cut and fill method.

Materials	Usage	CO <sub>2</sub> (kg-CO2)	SOx (g-SOx)	Nox (g-NOx)	Cost (JPY)
Soil, Sand (kg)	26539.8	52.1	90.4	281.3	53079.6
Limestone (kg)	405.5	1.9	0.4	0.6	256.7
Leveling & Compaction (m <sup>3</sup> )	6.3	208.5	288.5	480.6	5903.7
Soil, Sand (kg)	30.0	35.4	43.5	109.2	1077.0
Limestone (kg)	160.0	51.7	64.0	160.0	1579.6

Table 4 Air pollutants and CO<sub>2</sub> emissions of lightweight geomaterial mixed with expanded polystyrol beads.

Life Cycle Stage	Materials	Usage	CO <sub>2</sub> (kg-CO2)	SOx (g-SOx)	Nox (g-NOx)	Cost (JPY)
Raw Materials Acquisition	Soil, Sand (kg)	10615.0	20.8	36.2	112.5	21230.0
	Limestone (kg)	1105.7	5.2	1.0	1.7	699.9
	EPS (kg)	88.9	116.7	22.7	103.6	18656.9
	Soil, Sand (kg)	2944.9	5.8	10.0	31.2	5889.8
Construction	Leveling & Compaction (m <sup>3</sup> )	9.7	318.5	440.6	734.0	9015.7
Transport	Soil, Sand (kg)	30.0	28.9	35.4	89.1	877.5
	Limestone (kg)	160.0	51.7	64.0	160.0	1579.6
	EPS (kg)	160.0	51.7	64.0	160.0	1579.6
Waste	Demolition (kwh)	11.9	5.1	2.0	1.5	192.8
	EPS (kg)	88.9	234.7	48.4	108.5	45.4

Table 5 Air pollutants and CO<sub>2</sub> emissions of expanded polystyrol construction method.

Life Cycle Stage	Materials	Usage	CO <sub>2</sub> (kg-CO <sub>2</sub> )	SOx (g-SOx)	NOx (g-NOx)	Cost (JPY)
Raw Materials Acquisition	EPS (kg)	448.7	588.8	114.6	522.7	94156.5
	Aluminum (kg)	1.2	11.0	91.7	35.8	91.3
	Zinc (kg)	0.9	1.4	5.6	1.2	175.3
Construction	Soil, Sand (kg)	2944.9	5.8	10.0	31.2	5889.8
Transport	EPS (kg)	160.0	75.5	89.6	232.0	1944.1
	Soil, Sand (kg)	30.0	14.2	16.8	43.5	364.5
Waste	EPS (kg)	448.7	1184.5	244.1	547.4	229.3
	Metal (kg)	2.2	0.8	0.7	1.3	2.2

## RESULT

Fig.6 shows the results of estimated air pollutants and CO<sub>2</sub> emissions of each construction method at each life cycle phase. As the result, the expanded polystyrol construction method was the largest CO<sub>2</sub> emissions comparing with other methods because a large amount of CO<sub>2</sub> was discharged by production of styrofoam at raw materials acquisition phase and disposition of expanded polystyrol beads at waste phase. In regards to SOx emissions, the lightweight geomaterial mixed with expanded polystyrol beads was a bit larger than other methods due to higher SOx emissions at construction phase. In terms of NOx emissions, lightweight geomaterial mixed with expanded polystyrol beads was the biggest because of high NOx emissions at construction and transport phase.

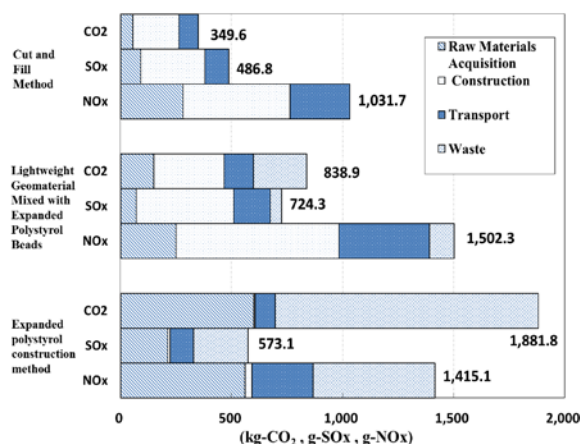
Fig. 6 Estimated amount of air pollutants and CO<sub>2</sub> emissions of each construction method.

Fig.7 indicates the results of estimated total life-cycle cost of each construction method. The cost of the lightweight geomaterial mixed with expanded polystyrol beads was the cheapest but the expanded polystyrol construction method was the biggest life

cycle cost than other methods. In general, the cost for polystyrol beads at raw materials acquisition phase was caused cost increase.

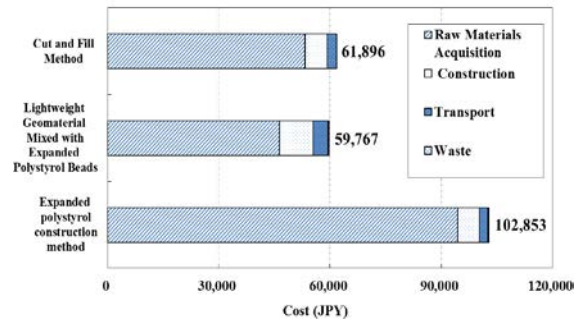


Fig. 7 Estimated total life-cycle cost of each construction method.

## CONCLUSION

As the result of comparative analysis of 3 construction methods including conventional method, we concluded that adding the polystyrol materials to the composite geomaterials increase the air pollutants and CO<sub>2</sub> emissions at raw materials acquisition and waste phase. If polystyrol materials will be recycled, these emissions might decrease than at present.

In this research, it was found that the cut and fill method (conventional geomaterial) was lower environmental impacts and life cycle cost than other construction methods. However, further study needs to perform comprehensive evaluation that included the perspective of safety degree for a fair comparison through life cycle impact assessment.

## REFERENCES

- [1] K Omine, H Ochiai "Evaluation of environmental impact and recycling efficiency for composite geomaterials using wastes", Proceedings of the sixth Japan National Symposium on Environmental Geotechnology, 2005, pp. 203–208.
- [2] H Ochiai, K Omine "Evaluation of environmental impact and development of mixed composite materials with new additional value." The Foundation engineering & equipment, Vol. 32, Aug. 2004, pp.9-11.
- [3] S Inazumi, H Otsu, T Isoda, Y Shigematsu "Evaluation of social environmental efficiency" on recycling of construction sludges as ground materials" Journal of geological engineering, Vol.68. 2012, pp.163-174.
- [4] Architectural Institute of Japan, "LCA guideline for building", 2006.

- [5] Advanced Industrial Science and Technology,  
“IDEA (Inventory Database for Environmental  
analysis)”, 2010.
- [6] Life Cycle Assessment Society of Japan,  
“LCA database”, 2003.
- [7] Express Highway Research Foundation of Japan,  
“Proposal of Estimation Method of CO<sub>2</sub>  
emissions on Road Projects”, 2004.
- [8] Japan Environmental Management Association  
for Industry,  
“JEMAI-LCA PRO”, 2000.
- [9] Ministry of Internal Affairs and  
Communications,  
“Input-Output Tables of Japan”, 2005.

## CU, ZN AND AS CONTAMINATION OF SEAWEED BESIDE SHIZUKI AND KANAYAMA METAL MINES IN JAPAN

Hiroyuki Ii

Faculty of Systems Engineering, Wakayama University, Japan

### ABSTRACT

Brown seaweed, *Sargassum thunbergii* is thought to be effective for As, Cu and Zn sensor. Green seaweed, *Ulva*, red seaweed, *Caulacanthus ustulatus* and *Ahnfeltiopsis flabelliformis* are thought to be effective for just Cu sensor. High Zn concentration and large volume of Zn drainage water from the closed Kanayama mine flowed into sea and drainage water and groundwater containing Cu Zn, As contacted with muck along the coast also flowed into sea in the closed Shizuki mine. Cu, Zn and As concentrations for many kinds of seaweed sampled at the two mines and no contamination places, the Kii and Izu Peninsula, were measured. Cu Zn and As concentrations for *Sargassum thunbergii* are 1000, several 100 and several 100 ppm at the Shizuki mine and 10, several 1000 and 100 ppm at the Kanayama mine, and 10, several 10 and 100 ppm at the no contamination places.

*Keywords: Seaweed, Metal sensor, Metal mine, sea metal contamination*

### INTRODUCTION

Many papers about metal concentration of seaweed are published and high bioconcentration factor of heavy metal was found for many kind of seaweed [1]–[2]. The relation between time or sea metal concentration and bioconcentration factor was clarified [3]–[5]. Metal concentration of seaweed at heavy metal contamination area was published and metal concentration for water and contaminated soil were also described [6]–[8]. However a monitoring of water and soil is important for evaluating contamination, it spends long term sampling and large number of sampling for reaching average value of metal concentration for water and soil because water and soil metal concentrations are variable for time and place. To measure metal concentration of seaweed is easier than to measure those of water or soil because metal concentration of seaweed is higher than those of water or soil because of bioconcentration factor and seaweed has long term information. Then, the purpose of this study is to find effective seaweed as a metal sensor. There are many kinds of seaweeds and then each bioconcentration factor is variable. Therefore, effective seaweed as a metal sensor needs wide distribution and changeable concentration depending on metal concentration of water and soil. Then, comparing seaweed at contaminated area and non contaminated area, we select effective seaweed as a metal sensor. In this study, Cu, Zn and As were selected because Cu, Zn and As were popular heavy metals in Japanese metal mine contamination area.

### METHOD

Fig.1 shows the study areas including 2 closed metal mines, Shizuki and Kanayama mines and 5 non contamination areas, North Senjyo, South Senjyo, Kada (Wakayama city), Saikasaki (Wakayama city) and Nawachi coasts. Both two small metal mines are facing sea. Drainage water and muck was accumulated on the coast. Seaweed was sampled along the coast. Sampling date for Kanayama is May 2013. Senjyo April 2013, Nawachi February 2014, Kada March 2014, Shizhuki July and Aug 2013 and March 2014, and Saikasaki May 2014. Sampled seaweed was dried and then dissolved with concentrated nitric acid solution. The solution after filtration was analyzed to be metal concentration by ICP-AS. Spring water and river water including adit drainage were also analyzed by ICP-AS.

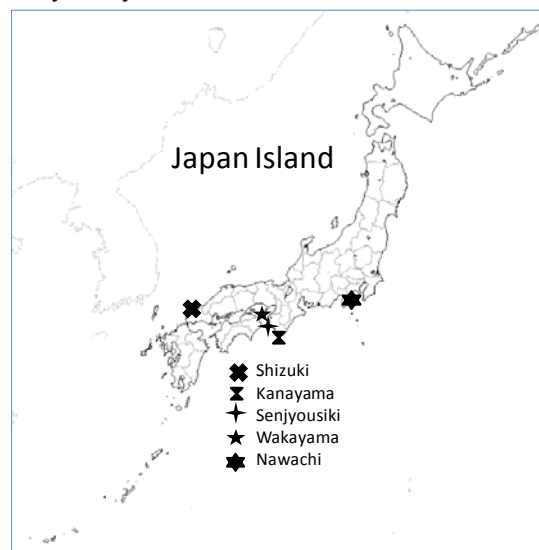


Fig. 1 Sampling points for seaweed



## RESULTS

### Condition for mine metal contamination area

Shizuki mine is copper mine at the Japan sea side and primary metal minerals are pyrite  $\text{FeS}_2$ , sphalerite  $\text{ZnS}$ , chalcopyrite  $\text{CuFeS}_2$  and arsenopyrite  $\text{FeAsS}$ . In this mine, there is a lot of muck along the coast. As the secondary metal mineral, atacamite  $\text{Cu}_2(\text{OH})_3\text{Cl}$  was also found at the spring point and at the surface of muck stone along the coast, sea water was thought to react with spring water containing copper from mine. Table 1 shows flow rate and Cu, Zn and As concentrations for drainage and spring water. Cu concentration was high, a few mg/l and Cu load reached 5kg. Cu contamination was thought to bring out. Zn and As contamination was also thought to bring out because of drainage water and metal mineral including Zn and As.

Table 1 This is the example for table formatting

	spring at coast	drainage from adit	
date	2013/7/12	2013/7/12	2014/3/28
flow(l/min)	0	3	0.6
Cu(mg/l)	9.377	3.019	1.472
Cu(kg/year)		4.76	0.46
Zn(mg/l)	0.328	1.071	0.748
Zn(kg/year)		1.69	0.24
As(mg/l)	0.013	0.084	0.038
As(kg/year)		0.13	0.01

Kanayama mine is located at the Kanayama Bay in the Kii Peninsula facing the Pacific Ocean. Although main production was Pb (Galena  $\text{PbS}$  5% of total metal mineral), main metal mineral is pyrite (50%) and sphalerite (40%). Chalcopyrite (5%) was also found in the vein. Drainage water from two vein flows into the Kanayama Bay. One drainage water flows into the bay through the river. The other drainage is spring on the coast facing the bay.

Fig.2 and 3 show Zn concentration and Zn load for spring and river waters. Zn concentration of spring and river were less than 50 to 90 mg/l and 1 to 5 mg/l. Flow rate for spring increased since 2009 till 2011 and then Zn concentration decreased. However, Zn load increased with flow rate and since 2011 Zn load for spring was 2000 to 4000 kg per year. Zn load for river was 1000 kg per year since 2011. Then total Zn load for the Kanayama Bay 3000 to 5000 kg per year and it is quite large Zn load for the small bay with 100 m length and 50 m width. Total Zn concentrations for the sea water in the bay were 0.2 to 1.9 mg/l and soluble Zn concentration with 0.45 filtered sea water were also 0.2 to 1.6 mg/l. Most Zn was soluble style and sea

water Zn concentration was also high.

Fig.4 and 5 show Cu concentration and Cu load for spring and river waters. Although Cu load reached several kg per year, Cu concentration was very low and 0.01 to 0.05 mg/l for spring and 0.005 to 0.01 mg/l for river since 2011. As concentrations for spring and river water were under detection limit 0.001 mg/l. Then, in the Kanayama mine area Zn contamination was quite large and Cu contamination was also thought to bring out. As contamination was not thought bring out or to be very small.

### Condition for no contamination area

Senjyo coast is 3 km northwest from the Kanayama Bay. Wakayama coast, Kada and Saikasaki are 70 km northwest from the Kanayama Bay. Nawachi is located at the Izu peninsula in the center of Japan facing the Pacific Ocean. The all coast was located far from the big city and mine area and then heavy metal contamination was not thought to bring out. However the Senjyo coast is close to the Kanayama Bay and metal contamination may occur.

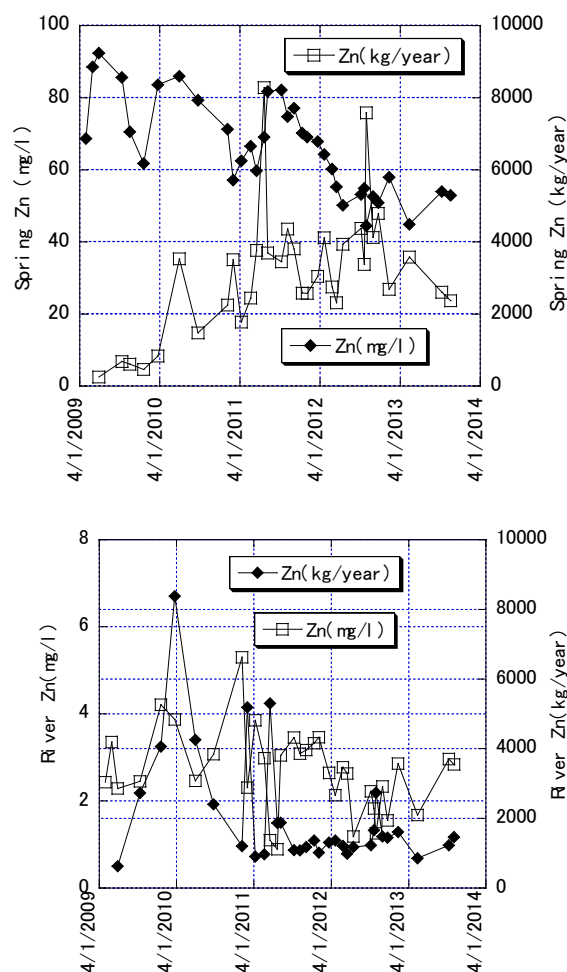


Fig.2 and 3 Zn concentration and Zn load from Spring and river in the Kanayama mine



# The relation between place and metal concentration of seaweed

Fig.6 shows Zn concentration of all sampled species of seaweed under the dry weight condition and place. In the Kanayama Bay, metal concentrations depend on distance from spring and the mouth of river and then sample points are described by distance from spring and river mouth. "UP" is close to spring or river mouth. Right direction from the "UP" shows far from spring. "O" is just located at the outside of the Kanayama Bay. "SS" and "SN" are south and north of Senjyo coast. "WS" and "WK" are Saikasaki and Kada coasts in the Wakayama city. "NW" is Nawachi coast. "SH" is Shizuku mine coast. Zn concentration in seaweed is extremely high in Kanayama Bay and reached several % down the spring. The maximum value is thought to be world record in natural. River stream area in the Kanayama Bay was also high. In the bay Zn minimum values for seaweed are 1000 ppm. Zn concentration just outside of the bay also keeps several 100 to several 1000 ppm. South of Senjyo coast is near the Kanayama Bay than North of

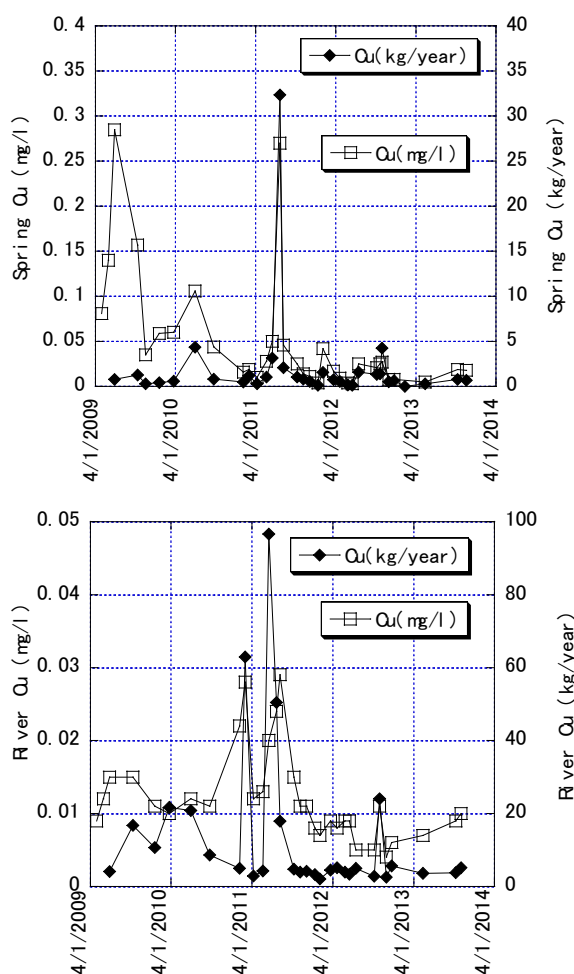


Fig.4 and 5 Cu concentration and Cu load from Spring and river in the Kanayama mine

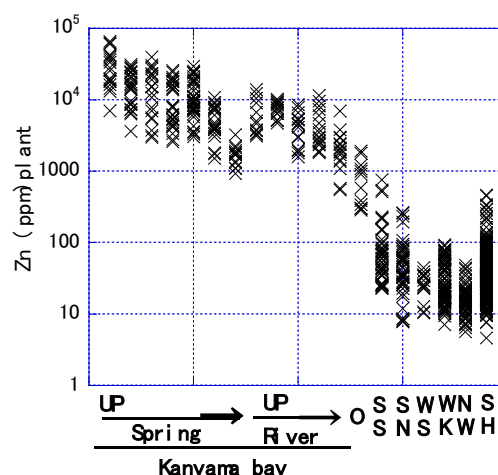


Fig.6 shows Zn concentration of all sampled species of seaweed and place.

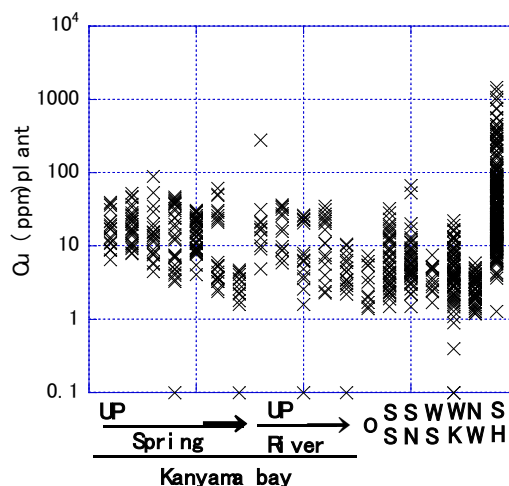


Fig.7 shows Cu concentration of all sampled species of seaweed and place

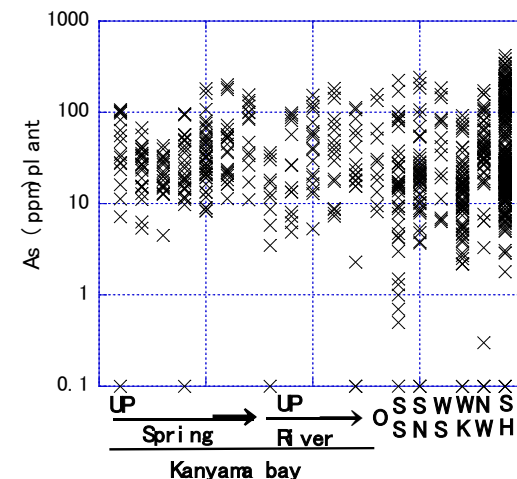


Fig.8 shows As concentration of all sampled species of seaweed and place

Senjyo coast. Zn concentration at south of Senjyo coast is relatively high to north of Senjyo, Saikasaki, Kada, and Nawachi. Zn concentration in the Shizuku mine coast is wide variable and reached several 100

ppm. Zn concentration at the north of Senjyo is also high relative to no contamination coast and then Senjyo area is thought to be contaminated by Kanayama mine drainage.

Fig.7 shows Cu concentration of all sampled species of seaweed under the dry weight condition and place. Cu concentration for seaweed at the Shimizu mine shows wide range and varied from several to 1000 ppm. Cu concentration of seaweed

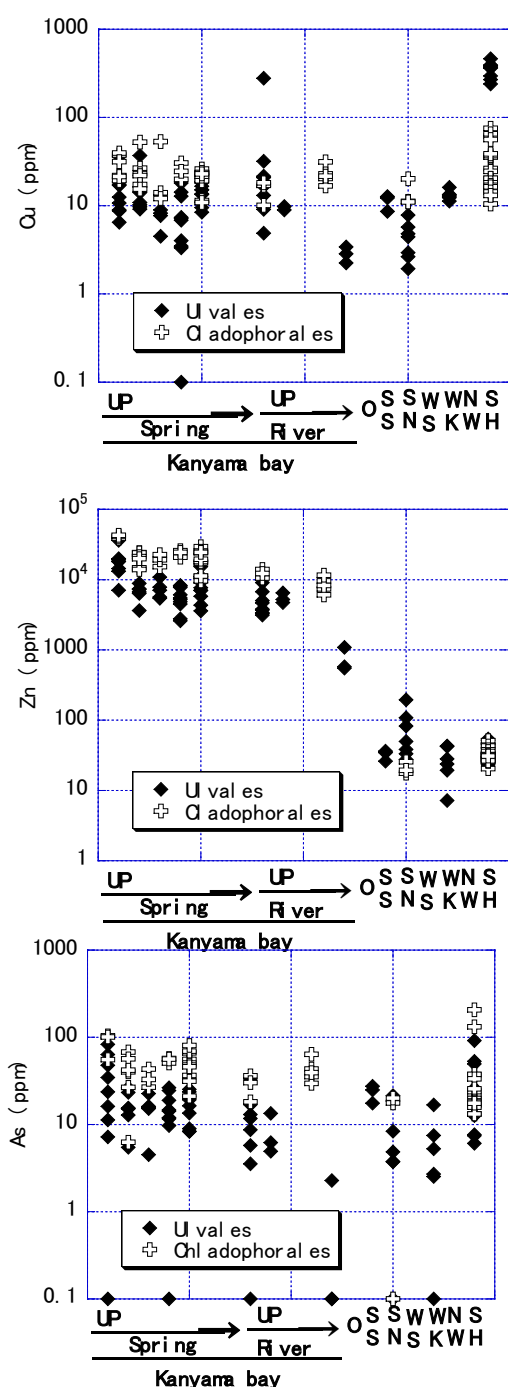


Fig.9 Cu, Zn and As concentration for green seaweed (Ulvaophyceae), Ulvaes and Chladophorales.

sampled at August and July 2013 in the Shizuki mine showed high values and it shows season changes. Cu contamination for seaweed was remarkable for the Shizuki mine. Cu concentration of seaweed in the Kanayama Bay is several to several 10 ppm and the same value as Senjyo and Kada coasts. However, Cu concentration decreased with distance from spring or river mouse to outside

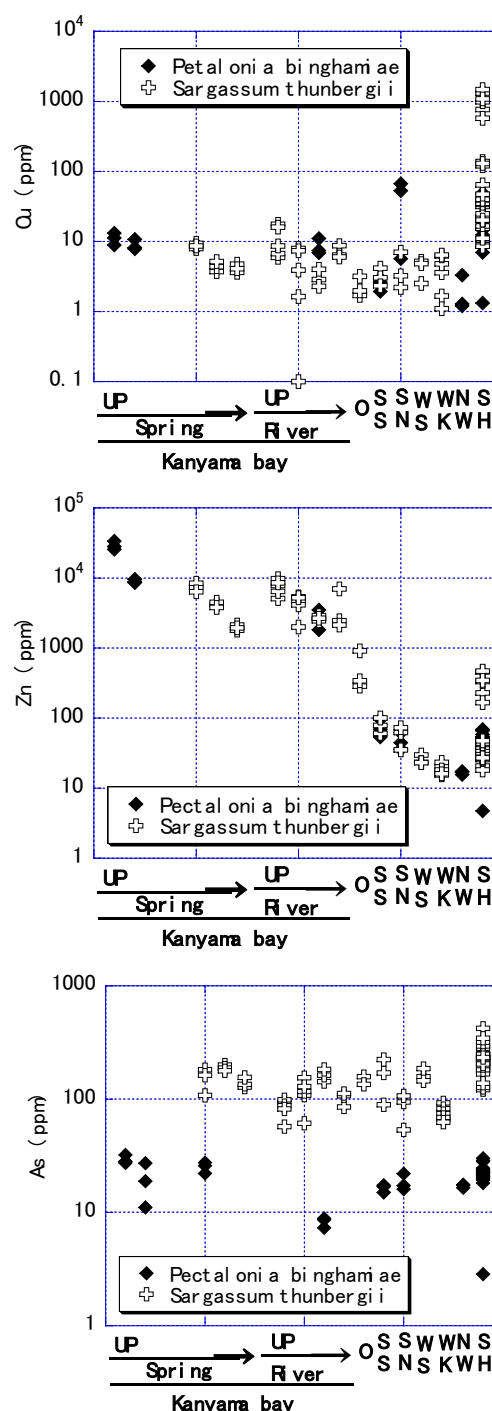


Fig.10 Cu, Zn and As concentration for brown seaweed (Phaeophyta), Pectalonina binghamiae and Sargassum thunbergii.

of the bay. Cu contamination was found from Cu concentration for seaweed in the Kanayama Bay. Cu concentration of seaweed at the Kada and Senjo in the no contamination area were relative to high to those at the Nawachi and Saikasaki coasts.

Fig.8 shows As concentration of all sampled species of seaweed under the dry weight condition and place. As concentration for seaweed in the Kanayama mine with no As mineral is not high relative to those sampled at another coast. As concentration for seaweed at the Shimizu coast shows wide range and varied from several to 100 ppm. As concentration of seaweed sampled at July and August 2013 in the Shizuki mine showed high values and it shows season changes for As as well as Cu. Muck from the Shizuki mine contains As mineral and drainage water contain 0.0n mg/l for As. Some samples shows high As values, however As concentration for seaweed was variable and some sample shows low values. Therefore, As concentration was thought to depend on species. Then, next, relationship between species and metal concentration is shown.

#### The relation between place and metal concentration of green, red and brown seaweed

Fig.9 Cu, Zn and As concentration for green seaweed (Ulvophyceae), Ulvales and Chladophorales. Ulvales and Chladophorales were popular green seaweeds at the sampling place and then effective candidate for a metal sensor covering a wide habitat. Cu concentrations of Chladophorales were uniform, 10 to 100 ppm under the different places. Cu concentrations of Ulvales were several 100 ppm at the Shizuku mine, several 10 ppm at the Kanayama mines and several ppm at the no contamination places. Ulvales is effective metal sensor for Cu because the concentration range was 100 times depending on the condition. Zn concentrations of Ulvales and Chladophorales were several 10000 ppm at the Kanayama mine and several 10 ppm at the no contamination places and the Shizuki mine. Both green seaweeds were not effective metal sensors for Zn because Shizuki mine was thought to bring out Zn contamination but Zn concentration of seaweeds at the Shizuki mine was low. As concentrations of Chladophorales were higher than those of Ulvales. As concentrations of Chladophorales were uniform, several 10 ppm to several 100 ppm and As concentration for Chladophorales of the Shizuki mine were not necessary high values. As concentrations of Ulvales were several 10 ppm at the downstream of spring in

Kanayama mine and the Shizuki mine and several ppm at the no contamination places and at the downstream of the river in the Kanayama mine. Both Chladophorales and Ulvales were not effective metal sensor for As because of narrow range concentration.

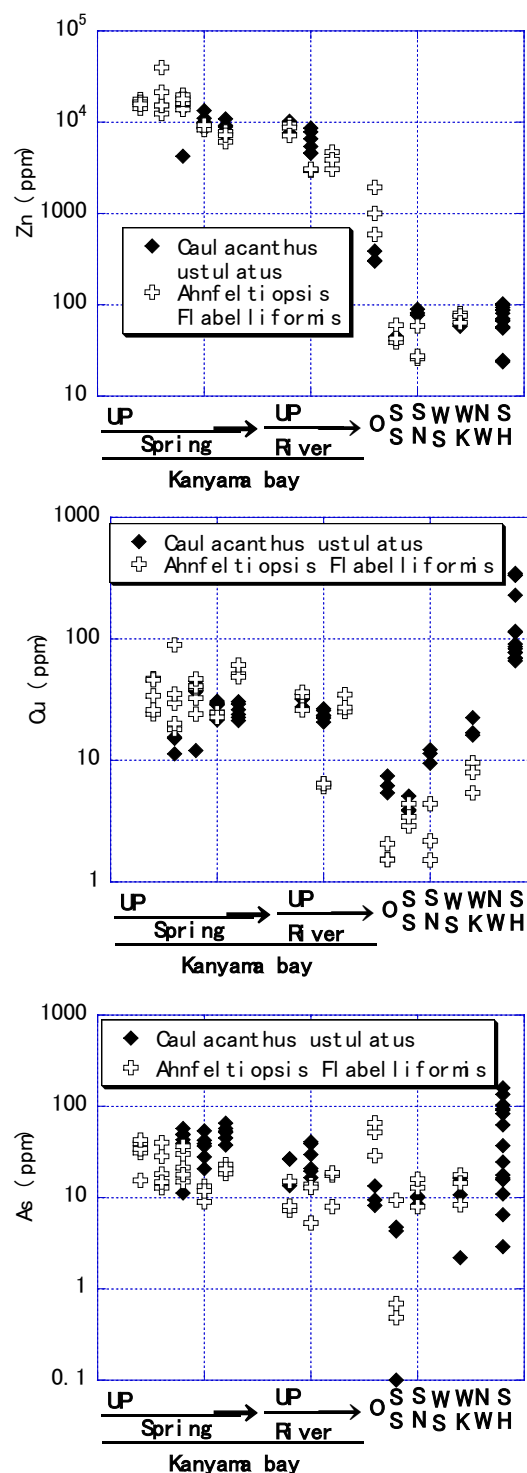


Fig.11 Cu, Zn and As concentration for red seaweed (Rhodophyta), *Caulacanthus ustulatus* and *Ahnfeltiopsis flabelliformis*.

Fig.10 Cu, Zn and As concentration for brown seaweed (Phaeophyta), *Pectalonia binghamiae* and *Sargassum thunbergii*. They were popular brown seaweeds at the sampling place and then effective candidate for a metal sensor. Cu concentrations of *Pectalonia binghamiae* were uniform, several to several 10 ppm and not high at the Shizuki mine. Cu concentration of *Sargassum thunbergii* at the Shizuku mine were high relative to another area having wide concentration range from 10 ppm to several 1000 ppm. Cu concentrations of *Sargassum thunbergii* were 10 ppm at the Kanayama mine and less than 10 ppm in the no contamination places. Therefore, *Sargassum thunbergii* was thought to be an effective metal sensor for Cu. Zn concentration of *Pectalonia binghamiae* were several 1000 ppm to several 10000 ppm at the Kanayama mine and several 10 ppm at the Shizuki mine and at the no contamination places. Zn concentration of *Sargassum thunbergii* were several 1000 ppm at the Kanayama mine, several 10 to several 100 ppm at the Shizuki mine and several 10 ppm at the no contamination places. Then, both brown seaweeds were effective metal sensor for Zn. As concentration of *Pectalonia binghamiae* were uniform values, however As concentration of *Sargassum thunbergii* were over several 100 ppm at the Shizuki mine and several 10 to 100 ppm at the Kanayama mine and no contamination places. *Sargassum thunbergii* was thought to be effective metal sensor for As.

Fig.11 Cu, Zn and As concentration for red seaweed (Rhodophyta), *Caulacanthus ustulatus* and *Ahnfeltiopsis flabelliformis*. They were popular red seaweeds at the sampling place and then effective candidate for a metal sensor. Unfortunately *Ahnfeltiopsis flabelliformis* can not be found in the Shizuki mine however, another places, very common. Cu concentrations of both the red seaweeds were high at the Kanayama mine and low at the no contamination places. Cu concentrations of *Caulacanthus ustulatus* was high, several 100 ppm. Then, both the red seaweeds were thought to be an effective metal sensor for Cu. Zn concentrations of both red seaweeds were several 1000 ppm to several 10000 ppm at the Kanayama mine and several 10 ppm at the Shizuki mine and at the no contamination places. Then, both the red seaweeds were not effective metal sensor for Zn. As concentration of both the red seaweeds were uniform values, several ppm to several 10 ppm. Both the red seaweeds were not effective metal sensor for As. Totally *Sargassum*

*thunbergii* is thought to be an effective seaweed for As, Cu and Zn sensor.

## CONCLUSION

Kanayama mine was thought to be heavily Zn and medium Cu contamination place. Shizuki mine was thought to be heavy Cu and medium Zn and As contamination place. Comparing Cu, Zn and As concentrations for seaweed at the contamination and no contamination places, it was clarified whether metal concentration of the seaweed depended or did not on the contamination condition. As a result, brown seaweed, *Sargassum thunbergii* is thought to be effective for As, Cu and Zn sensor. *Ulvaes*, *Caulacanthus ustulatus* and *Ahnfeltiopsis flabelliformis* are thought to be effective for just Cu sensor.

## REFERENCES

- [1] Lunde G, "Analysis of trace elements in seaweed", J. of Sci. Fd. Agric., Vol. 21, Aug. 1970, pp. 416-418..
- [2] Yamamoto T, and Ishibasi M, "The Content of Trace Elements in Seaweeds", in Proc. 7th Int. Seaweed Symposium, 1971, pp. 511-514.
- [3] Yamamoto T, "Chemical Studies on the Seaweeds (27) The relations between Concentration Factor in Seaweeds and Residence Time of Some Elements in Sea Water", Records of Oceanographic Works in Japan., Vol. 11, No.2, March. 1972, pp. 65-72.
- [4] Hiyama Y and Shimizu M, "On the Concentration Factors of Radioactive Cs, Sr, Cd, Zn and Ce in Marine Organisms", Records of Oceanographic Works in Japan, Vol. 7, No.2, March. 1964, pp. 43-77.
- [5] Hiyama Y and Matsubara JK, "On the Concentration Factors of Radioactive I, Co, Fe and Ru in Marine Organisms", Records of Oceanographic Works in Japan, Vol. 7, No.2, March. 1964, pp. 79-106.
- [6] Ghada F El-Said and Amany El-Sikaily, "Chemical composition of some seaweed from Mediterranean Sea coast, Egypt", Environmental Monitoring and assessment, July 2013, Vol. 185, Issue7, pp 6089-6099
- [7] Alahverdi M and Savabieasfahani M, "Metal Pollution in Seaweed and related Sediment of the Persian Gulf, Iran", Bull Environ. Contam. Toxicol, Vol. 88, 2012, pp. 939-945.
- [8] Griselda MRF, Evgueni S and Ignacio SR, "Heavy metal Pollution monitoring using the brown seaweed *Padina durvillaei* in the coastal zone of the Santa Rosalia mining region, Baja California Peninsula, Mexico", J. Appl. Phycol., Vol. 21, 2009, pp. 19-26.

## **WATER BALANCE ANALYSIS CONSIDERING RUNOFF OF UNGAUGED CATCHMENTS IN IWAKI RIVER BASIN, NORTHERN JAPAN**

Soichiro Kageyama<sup>1</sup>, Shingo Tomiyama<sup>2</sup>, Makoto Ikeda<sup>3</sup> and Hiroyuki Ii<sup>4</sup>  
<sup>1,3</sup>Mitsubishi Materials Techno Corp., Japan, <sup>2</sup>Mitsubishi Materials Corp., Japan,  
<sup>4</sup>Faculty of Systems Engineering, Wakayama University, Japan

### **ABSTRACT**

For integrated and sustainable water resource management, it is essential to understand water balance of river basin. Infiltration calculated by subtracting evapotranspiration and runoff from precipitation is a key factor for groundwater resource development and is an important input data for three-dimensional groundwater flow analysis. For estimation of runoff, it needs a great challenge to establish a method for runoff in ungauged catchments, because gauging stations are usually set up in the limited main rivers. This paper focused on close relation between topography and runoff. Then, the runoff of ungauged catchments in the Iwaki River Basin was estimated by “runoff index” derived from results of geomorphometry and multivariate statistics using digital elevation model data. Comparisons between runoff indices and measured runoff data, showed clear positive correlations. This result proved that runoff index was useful for runoff estimation, and suggested that it was possible to estimate runoff of ungauged catchments from runoff index by linear regression equation.

*Keywords: Water Balance Analysis, DEM, Geomorphometry, Multivariate Statistics, PUB*

### **INTRODUCTION**

For integrated and sustainable water resource management, it is essential to understand water balance of river basin [1]. Water balance is expressed simply by Eq. (1).

$$P = E + R + I \quad (1)$$

Where; P is an amount of precipitation; E is evapotranspiration; R is runoff; and I is infiltration (groundwater recharge). Infiltration calculated by subtracting evapotranspiration and runoff from precipitation is a key factor for groundwater resource development and is an important input data for three-dimensional groundwater flow analysis. Therefore, it is very important that how accuracy amounts of precipitation, evapotranspiration and runoff are estimated. High precision precipitation and evapotranspiration distributions are easily estimated for Japan because of recent progresses for climate data (e.g., “1-km mesh climate data” published by Japan Meteorological Agency [2]). On the other hand, for estimation of runoff, it needs a great challenge to establish a method for runoff in ungauged catchments (Prediction in Ungauged Basin: PUB), because gauging stations are usually set up in the only limited main rivers. As existing researches concerning PUB, while discussions with a focus on hydrology and civil engineering have been made [3], [4], new runoff estimation methods from a topographic perspective have been proposed.

Reference [5] classified catchments based on its terrain feature values as well as quantitative evaluation of terrain feature in each catchment by geomorphometry and multivariate statistics using digital elevation model (hereinafter, DEM) data. Reference [6] performed the flow simulation based on distributed runoff model using kinematic wave equations after conducting catchment classification using the same method. In addition, the authors predicted the runoff of other basins that are a similar terrain feature by applying the constructed flow simulation model and examined its generality and validity. However, there was no study regarding the runoff estimation in catchments with different terrain features. Against the background, Reference [7] focused on close relation between topography and runoff, and suggested that it might be possible to estimate runoff of ungauged catchments by the “runoff index” based on a correlation between terrain features and measured river flow data. This paper is also predicated on same idea. Then the runoff of ungauged catchments in the Iwaki River Basin, northern Japan were estimated by the “runoff index” derived from the result of geomorphometry and multivariate statistics using DEM data.

### **STUDY AREA**

The Iwaki River basin is located in the northernmost part of Honshu, the main island of Japan. The basin contains active volcanic regions with high relief mountains, Mount Iwaki (1,624 m)



in the western part of the basin, Hakkoda Mountains (1,584 m) in the eastern part and Towada volcano in the southeastern part. The Iwaki River is originated in the mountainous area located on the margin part of the basin and flows through the alluvial fans and the Tsugaru Plain to the Sea of Japan. This river has a catchment area of 2,540 km<sup>2</sup>, with a length of 102 km. The study area located in the middle to upper river basin is shown in Fig.1. This area also has regional variations of climate and is suitable for estimating an amount of infiltration on regional scale by a water balance analysis.

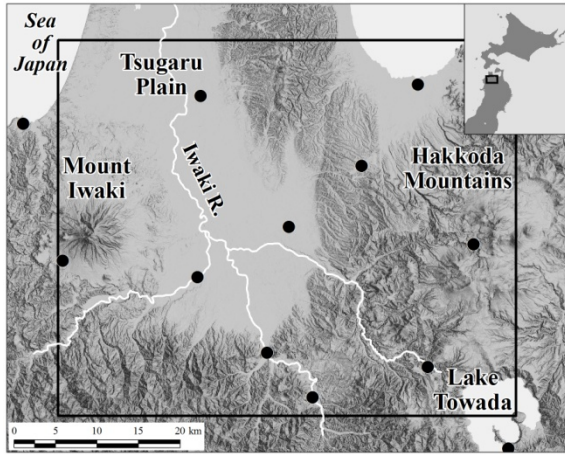


Fig.1 Location map of the study area. The black border in the map denotes the study area and black circles respectively denote the weather observation stations.

## WATER BALANCE ANALYSIS

The water balance analysis performed in this study consists of four items, (1) precipitation estimation using 1-km mesh climate data, (2) evapotranspiration estimation in consideration of land cover using 1-km mesh climate data, (3) runoff estimation by geomorphometry and multivariate statistics using DEM data and (4) infiltration estimation by water balance analysis. As for (3) runoff estimation and (4) infiltration estimation, the duration of estimation is taken as one month of August 2010 due to the river flow data applied to the runoff estimation was measured between 8<sup>th</sup> to 10<sup>th</sup> August 2010 in the study area.

### Estimation of Precipitation

In Japan, the 1-km mesh climate data including average monthly precipitation, temperature and sunshine hours for the past 30 years between 1981 and 2010 is established. The mesh data is estimated by the climate data of about 1,100 weather observation stations of the country, which considers topographical and urban effects on climate.

To estimate monthly precipitation of August 2010, the comparison between the average monthly value for the 30 past years and observed monthly values of August 2010 of 32 weather observation stations located in and near the study area was carried out. In this study, after calculating ratio of average and observed values in each station was derived as a correlation coefficient value for estimation, the correlation coefficient value map of the study area was drawn by interpolating correlation coefficient values of each station by Kriging method. Then, the precipitation distribution of August 2010 was estimated by multiplying the average monthly precipitation map of the mesh data by the correlation coefficient value map. The result of estimation is shown in Fig.2.

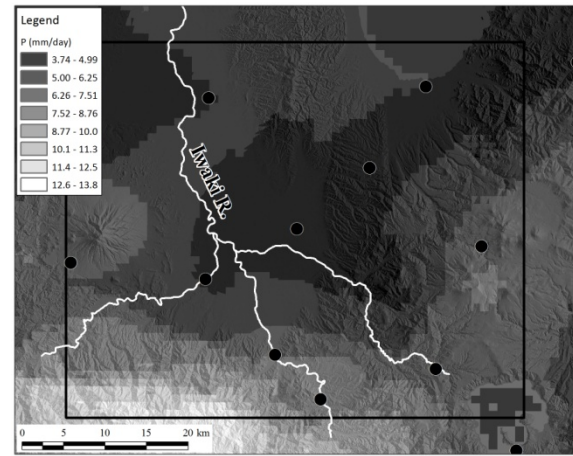


Fig.2 Result of precipitation estimation of August 2008.

### Estimation of Evapotranspiration

The evapotranspiration of the study area was estimated by Makkink equation considering albedo of each land cover class [8] shown in Eq. (2).

$$E = (a + 0.05 - \alpha) \frac{\Delta}{\Delta + \gamma} \frac{R_s}{L} + b \quad (2)$$

$$\frac{\Delta}{\Delta + \gamma} = \frac{1}{1.05 + 1.4 \times \exp(-0.0604T)}$$

Where;  $E$  is daily evapotranspiration;  $a$  and  $b$  are regional constant value ( $a$  is 0.87 and  $b$  is 0.30 in the study area [8]);  $\alpha$  is albedo value of each land cover class;  $\Delta$  is slope of saturation vapor pressure curve;  $\gamma$  is psychrometric constant;  $R_s$  is total solar radiation;  $L$  is latent heat.  $T$  is temperature. Distributions of average monthly total solar radiation, latent heat and temperature for the 30 past years could be calculated by temperature and sunshine hours of 1-km mesh climate data, and the



distributions of August 2010 were estimated by the same method for precipitation estimation. As an albedo value, values of each land use class estimated [9] were adopted. The result of estimation by Makkink equation is shown in Fig.3.

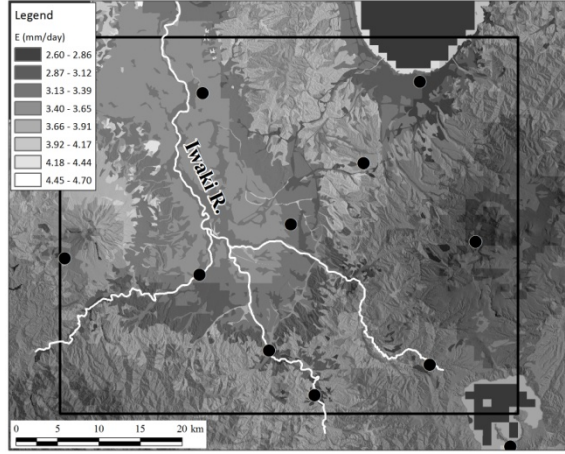


Fig.3 Result of evapotranspiration estimation of August 2008.

### Estimation of Runoff

Focusing on terrain that is closely related to runoff, runoff of ungauged catchments was estimated by comparison examination between terrain features and measured river flow data. The flow chart of runoff estimation is shown in Fig.4.

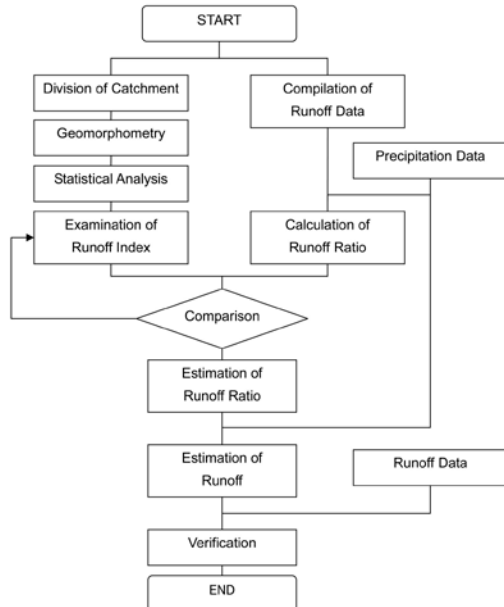


Fig.4 Flow chart of runoff estimation

### Division of sub-catchment

When applying geomorphometry and runoff

estimation, a “sub-catchment” is defined as a basic unit for estimation. The study area was subdivided automatically into 469 sub-catchments and plains by hydrologic analysis using DEM data. The result of division is shown in Fig.5.

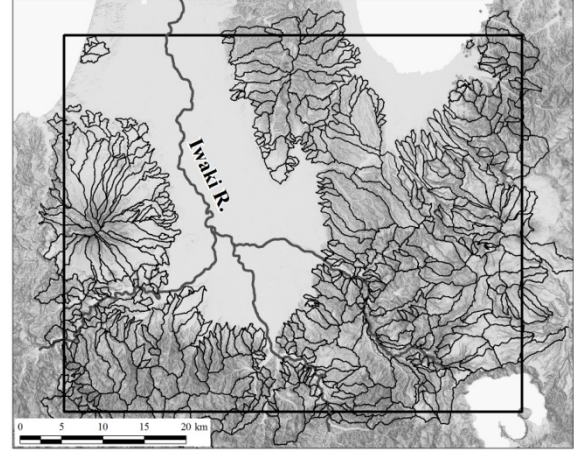


Fig.5 Result of sub-catchment division. The black small borders in the map respectively denote the extracted 469 sub-catchments.

### Geomorphometry

The items of geomorphometry calculated at each sub-catchment are as follows:

“Average erosion height” calculated by Eq. (3) can be used as a factor of surface relief.

$$He = \sum_i^n Es_i - E_i \quad (3)$$

Where;  $He$  is average erosion height of a certain sub-catchment;  $n$  is number of pixels;  $Es_i$  is an elevation of a summit plane of a certain pixel;  $E_i$  is an elevation of a certain pixel. Laplacian of an elevation is defined as a derivation value of gradient and its differences show a grade of surface relief. Laplacian is calculated by Eq. (4).

$$L_{(m,n)} = E_{(m-1,n)} + E_{(m+1,n)} + E_{(m,n-1)} + E_{(m,n+1)} - 4 \times E_{(m,n)} \quad (4)$$

Where  $L_{(m,n)}$  is laplacian of an elevation of a pixel  $(m,n)$ . In addition, a “standard deviation of laplacian” calculated by Eq. (5) is used to evaluate surface texture.

$$Sx_{laplacian} = \sqrt{\frac{\sum_{i=1}^n (L_i - \bar{L})^2}{n}} \quad (5)$$

Where;  $Sx_{laplacian}$  is a standard deviation of laplacian of a certain sub-catchment;  $L_i$  is laplacian of an elevation of a certain pixel;  $L$  is mean laplacian of a certain sub-catchment. "Drainage relief number" is defined as average slope of a certain sub-catchment and is calculated by Eq. (6).

$$Dr = \frac{V}{A^{1.5}} \quad (6)$$

Where;  $Dr$  is average erosion height of a certain sub-catchment;  $V$  is volume of a certain sub-catchment;  $A$  is area of a certain sub-catchment. A "drainage frequency" calculated by Eq. (7) is used to evaluate a drainage network of a certain sub-catchment quantitatively.

$$Fd = \sum_{\omega} \frac{N_{\omega}}{A_{\Omega}} \quad (7)$$

Where;  $Fd$  is a drainage frequency of a certain sub-catchment;  $N_{\omega}$  is number of  $\omega$ th order streams;  $\Omega$  is maximum number of drainage order;  $A$  is area of sub-catchment. "Bifurcation ratio of 1st and 2nd order streams" is calculated by dividing number of pixels of 1<sup>st</sup> order stream by number of pixels of 2<sup>nd</sup> order stream of a certain sub-catchment.

"Drainage form ratio" calculated by Eq. (8), represents length of a main stream against area of sub-catchment.

$$Rl = \frac{(P_{max})^2}{A} \quad (8)$$

Where;  $Rl$  is drainage form ratio of a certain sub-catchment;  $P_{max}$  is maximum distance of drainages of a certain sub-catchment;  $A$  is area of a certain sub-catchment. "Basin form ratio" calculated by Eq. (9) is used to evaluate a shape of a certain sub-catchment.

$$Rf = \frac{(L_{max})^2}{A} \quad (9)$$

Where;  $Rf$  is basin form ratio of a certain sub-catchment;  $L_{max}$  is maximum width of a certain sub-catchment;  $A$  is area of a certain sub-catchment. In general, "kurtosis" and "skewness" are indexes shown as a deviation of distribution data from Gaussian distribution in a field of statistical analysis. In this study, both items were used for measuring a shape and deformation of a certain sub-catchment.

#### Principle component analysis

In order to compile the results of each item and evaluate the runoff of the study area, principle component analysis (hereinafter, PCA) was conducted. The result of PCA is shown in Table 1. In this study, four principal components of the first (hereinafter, PC 1) to the fourth (hereinafter, PC 4) with eigenvalue of more than 1.00 were considered for the examinations. In other words, the terrain feature of the study area is characteristically represented by these four PCs. PC 1 has clearly higher loadings of average erosion height (0.96), standard deviation of laplacian (0.91) and drainage relief number (0.73) compared with those of other items. Since these items are related to relief of terrain, PC 1 is considered to be a factor representing "steepness of terrain". Equally, PC 2, PC 3 and PC 4 are considered to be respectively representing "a shape of sub-catchment and main stream", "deformation of sub-catchment" and "growth of low-order drainages".

Table 1 Result of the PCA

PC	Eigenvalue	Contribution Ratio			
1	2.40	26.7			
2	2.12	23.6			
3	1.40	15.5			
4	1.01	11.2			
5	0.90	10.0			
6	0.62	6.9			
7	0.35	3.9			
8	0.14	1.5			
9	0.07	0.8			

Items	Loading			
	PC 1	PC 2	PC 3	PC 4
Ave. Erosion High	0.96	-0.12	-0.05	-0.06
SD of Laplacian	0.91	-0.22	0.06	-0.09
Drainage Relief No.	0.73	0.44	-0.15	0.13
Drainage Freq.	0.03	0.73	-0.17	0.10
Bif. Ratio (1/2)	-0.06	-0.06	-0.03	0.87
Drainage Form R.	-0.08	0.79	0.44	-0.05
Basin Form R.	0.12	-0.79	0.13	0.29
Kurtosis	0.03	-0.23	0.76	0.37
Skewness	-0.08	0.07	0.77	-0.26

#### Measurement of River Flow

To obtain actual measured runoff data applied to runoff estimation, river flow measurement was carried out between from 8<sup>th</sup> and 10<sup>th</sup> August 2008 in 6 sub-catchments have area of 5.94 to 16.74 km<sup>2</sup>. The river flow measured by a propeller current meter at the mouth of each catchment ranged from 0.08 to 0.50 m<sup>3</sup>/s. In this study, "runoff ratio" was adopted as measured runoff data for considering difference of river flow depending on area of each

sub-catchment. Runoff ratio of a certain sub-catchment is calculated by dividing an amount of river flow by an amount of precipitation during a specific period. The calculated runoff ratio of 6 sub-catchments ranged from 0.13 to 0.54.

#### Runoff Index

To understand relationship between the terrain features and the river flow data of the study area, the comparison between the principle component score (hereinafter, PC score) which shows the topographic features quantitatively and the runoff ratios of 6 measured sub-catchments was conducted. As the result of the comparison, it became obvious that the PC 1 had a strong positive correlation ( $R^2 = 0.75$ ) with the runoff ratio, and PC 4 had a positive correlation ( $R^2 = 0.29$ ) with the runoff ratio. As the PC 1 represents “steepness of terrain”, a sub-catchment with a high PC score shows a steep sloping terrain and a sub-catchment with a low PC score shows a gently sloping landscape. In general, steepness is related to stream velocity; an increase of steepness is connected to an increase of river flow and a decrease of it is connected to a decrease of river flow. Therefore, concerning the PC 1, sub-catchments of higher PC score can be considered as more discharged water in the stream. On the other hand, as the PC 4 represents “growth of low-order drainage”, valleys are developed on a slope of a sub-catchment with a high PC score and valleys are poorly developed on a slope of a sub-catchment with a low PC score. As a slope with many valleys can collect more surface water, sub-catchments of higher PC score can be considered as more discharged water in the stream.

As the result of above discussion, it became obvious that the runoff ratio and the increase-decrease rate of river flow were related to terrain features (“steepness of terrain” and “growth of low-order drainage”) in the study area. Therefore, it suggests that the runoff ratio and river flow of the study area can be estimated by evaluating the PC scores which show two terrain features as above. In this study, the “Runoff Index” [7] was calculated as the indicator of river flow on the basis of PC scores of PC 1 and PC 4, and the runoff index was calculated by Eq. (10).

$$RI = S_{PC1} \times W_{PC1} + S_{PC4} \times W_{PC4} \quad (10)$$

Where;  $RI$  is runoff index;  $S_{PCx}$  is a PC score in PC  $x$ ;  $W_{PCx}$  is weighting of PC  $x$ . Weightings of each PC were calculated by Eq. (11).

$$\begin{aligned} W_{PC1} &= C_{PC1} \div (C_{PC1} + C_{PC4}) \\ W_{PC4} &= C_{PC4} \div (C_{PC1} + C_{PC4}) \end{aligned} \quad (11)$$

Where;  $C_{PCx}$  is contribution ratio in PC  $x$  in Table 1. Then, the runoff index map of the study area is shown in Fig.6. In the map, the sub-catchments with high runoff index are presented by bright colors and ones with the low runoff index are shown as dark colors. Moreover, the comparison between the runoff index and the runoff ratio of 6 measured sub-catchments is shown in Fig.7. The result of comparison shows that the runoff index has a strong positive correlation ( $R^2 = 0.71$ ) with the runoff ratio. This result proves the validity of runoff index, and it suggests that the runoff index can be converted to the runoff ratio by using the regression equation of Fig.7.

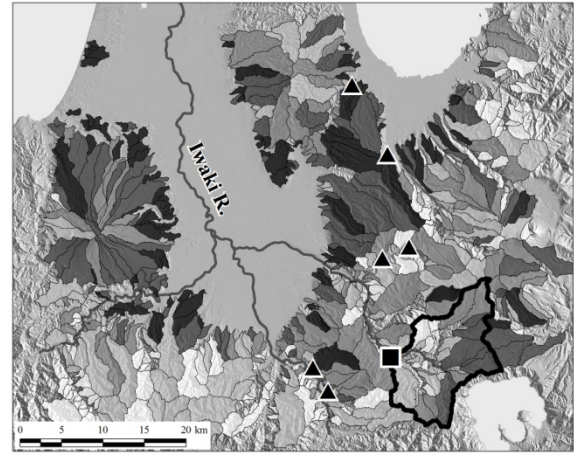


Fig.6 Result of runoff index estimation. The black triangles in the map respectively denote the measuring points of 6 sub-catchments. The black quadrangle denotes Kuzukawa Gauging Station and the black border denotes its catchment.

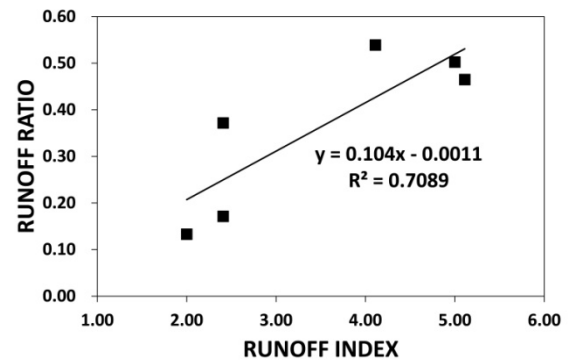


Fig.7 Result of comparison between the runoff index and the runoff ratio of six measured sub-catchments.

#### Prediction of Runoff

The estimated equation of runoff ratio and river flow is shown in Eq. (12).

$$R_{RATIO\_SC} = R_{INDEX\_SC} \times 0.104 - 0.0011 \quad (12)$$

$$R_{SC} = R_{RATIO\_SC} \times P_{SC}$$

Where;  $R_{RATIO\_SC}$  is estimated runoff ratio of a certain sub-catchment;  $R_{INDEX\_SC}$  is runoff index;  $R_{SC}$  is estimated river flow;  $P_{SC}$  is estimated precipitation. By applying the above estimation method, the runoff of sub-catchments only could be estimated. Concerning planes except for sub-catchments, it would be appear that land use contributes runoff of it in comparison to terrain feature. Therefore, the runoff of planes could be estimated by multiplying precipitation by known runoff ratios of each land use (e. g., farm: 0.1, forest: 0.2, paddy field: 0.4, urban area: 0.8, water area: 1.0).

#### Verification of Estimated Runoff

To verify the result of runoff estimation, the comparison between estimated runoff and observed runoff at Kuzukawa Gauging Station located in the southeastern part of the study area (Fig.6) was performed. The amount of estimated runoff for three days from 8<sup>th</sup> August 2008 is 402,113 m<sup>3</sup> and it is 90.2 % based on the observed runoff of 445,836 m<sup>3</sup>. The comparison result suggests that the present method could be generally applied to the runoff estimation due to it could be estimated the runoff with relatively high precision.

#### Estimation of Infiltration

Infiltration could be calculated by subtracting estimated evapotranspiration and runoff from precipitation. The result of infiltration estimation in August 2008 is shown in Fig.8. The amount of estimated infiltration ranged from about 0.1 mm/day to 9.6 mm/day. Verification of estimated infiltration will be carried out by three-dimensional groundwater flow analysis in the study area in future.

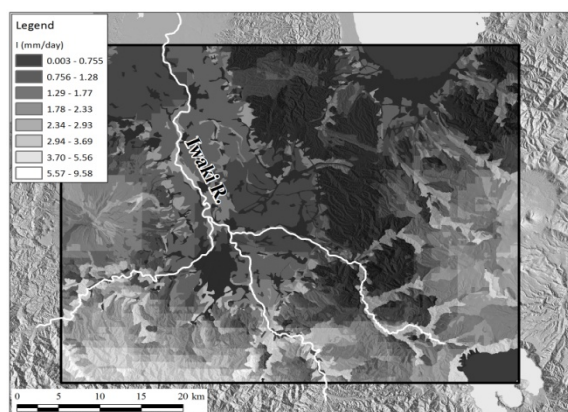


Fig.8 Result of infiltration estimation.

#### CONCLUSION

While the runoff of ungauged catchments in the Iwaki River Basin was estimated by the runoff index derived from geomorphometry and multivariate statistics, the infiltration estimation was carried out by water balance analysis. Comparisons between runoff indices and measured runoff data, showed clear positive correlations. This result suggested that it was possible to estimate runoff of ungauged catchments from runoff index by linear regression equation. Moreover, the result of verification with relatively high precision also indicates that the present method could be generally applied to the runoff estimation.

#### REFERENCES

- [1] Matsuyama H, Oki T, Masuda M, The seasonal change of the water budget in the Congo River Basin, J. of Meteorological Society of Japan, Vol. 72-2, 1994, pp. 281-299.
- [2] Japan Meteorological Agency, 1-km mesh climate data, 2012, Japan Meteorological Business Support Center.
- [3] Tachikawa Y, Sayama T, Takara K, Matsuura H, Yamazaki T, Yamaji A, Michihiro Y, Development of real-time runoff forecasting system using a physically-based distributed hydrologic model and its application to the Yodo River basin, J. of Japan Society for Natural Disaster Science, Vol. 26-2, 2007, pp. 189-201
- [4] Sayama T, Tachikawa Y, Takara K, Data assimilation of a distributed rainfall-runoff prediction system by Kalman filter with bias correction, J. of Japan Society of Civil Engineers, Vol. 64-4, 2008, pp. 226-239.
- [5] Nakayama D, A study of DEM-based drainage basin classification, Geographical Review of Japan Ser. A, Vol. 71-3, 1998, pp. 169-186.
- [6] Sakuma S, Nakayama D, Matsuyama H, Estimation of discharge in ungauged basin using comparative hydrological approach and distributed runoff model, in Proc. of the General Meeting of the Association of Japanese Geographers, Vol. 69, 2006, pp. 239.
- [7] Kageyama S, Ikeda M, Tomiyama S, Water balance analysis considering runoff of ungauged basin in Shimokawa area, Hokkaido, J. Japan Soc. Hydrology and Water Resources, 2010, Vol. 23-4, pp.
- [8] Nagai A, Estimation of evaporation with a measuring instrument of Makkink type, J. Japan Soc. Hydrology and Water Resources, 1993, Vol. 6-3, pp. 238-243.
- [9] Kotoda K, Estimation of river basin evapotranspiration, Environmental Research Venter Papers, University of Tsukuba, 1986, Vol. 8, pp. 1-92.

# REMOVAL OF CESIUM FROM SEA SLUDGE THROUGH DECOMPOSITION OF ORGANIC MATTER WITH AQUEOUS HYDROGEN PEROXIDE

Hirosuke Hirano<sup>1</sup>, Takeshi Toyama<sup>2</sup>, Nobuyuki Nishimiya<sup>3</sup> and Kyoichi Okamoto<sup>4</sup>

<sup>1</sup>Graduate School of Science and Engineering, Nihon University, Japan

<sup>2,3,4</sup>College of Science and Engineering, Nihon University, Japan

**ABSTRACT:** The radioactive cesium scattered from the Fukushima Nuclear Power Plant has caused a pollution problem in Japan. To tackle such accidents, many technologies have been developed to remove radioactive cesium from water. However, the technology to decontaminate the sludge is much less advanced than that for water. Thus, we focus on the decomposition of organic matter by  $H_2O_2$  for decontaminating the sludge. The maximum decontamination of the sea sludge by  $H_2O_2$  was found to be 2.6 times higher than that by water alone, and the greatest decontamination was obtained using 34.5%  $H_2O_2$ . We believe the extent of decontamination increased for this solution because the solution pH was near the pH<sub>pzc</sub>, which would suppress the ability of the sludge to absorb Cs ions. We also examined the effect of time on the decontamination of the sea sludge; however, only a small increase in decontamination (1.7 times the initial value) was observed.

**Keywords:** Cesium, Decontamination, Hydrogen peroxide, Water area

## 1. INTRODUCTION

In 2011, the Fukushima Nuclear Power Plant was destroyed by a tsunami. Radioactive cesium was released across a wide area, contaminating soil and water. As a result, cesium was even found to be present in the sea sludge at the bottom of Tokyo Bay in concentrations that are 1.5–13 times the background level [1].

To recover from this accident, methods to remove radioactive cesium from the sea sludge are needed. There are fewer reports on the decontamination of the sea sludge than on the decontamination from water. In addition, the methods of decontaminating water cannot be simply applied to decontaminate the sea sludge. For example, iron ferrocyanide has been reported to remove  $Cs^+$  from water; however, high concentrations of cyanide accumulated in the sludge when this method was used. Therefore, this method of decontaminating the sludge requires an additional decontamination step for the removal of cyanide [2]. Therefore, in the present study, we have studied easier methods of decontaminating the sea sludge.

### 1.1 Characteristics of Sea Sludge

The sea sludge absorbs cesium and iron ferrocyanide because of the clay minerals contained in the sea sludge [2]. Clay minerals contain hydroxide groups that can coordinate cations such as  $Cs^+$  and  $Fe^{3+}$ . We examined the adsorptivity of the sea sludge for  $Cs^+$  ions. A 10 g of the sea sludge sample was mixed with 20 mL of water containing

1000 ppm of nonradioactive cesium nitrate ( $CsNO_3$ ). This is the same cesium isotope as the radioactive cesium that is the object of the present decontamination study. As shown in Figure 1, the adsorptivity of the sea sludge for  $Cs^+$  in water was found to be 65.1%, and this adsorption occurred instantaneously. Moreover, the properties of the hydroxide groups in the sea sludge are changed at certain pH values. At low pH values, the hydroxide groups are protonated as  $OH_2^+$ . As a result, we assumed the adsorptivity of the sea sludge for cations would decrease. The pH value where this effect occurs is called the isoelectric point (point of zero charge; pH<sub>pzc</sub>). We assumed that the pH of the solution would affect the decontamination.

## 2. PURPOSE OF STUDY

In the present study, we focused on using

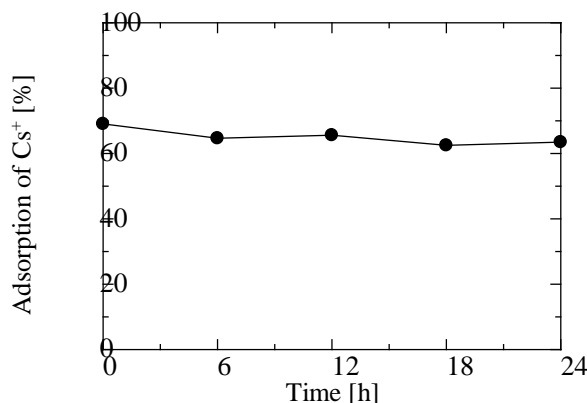


Fig. 1 Adsorption of  $Cs^+$  by sea sludge



hydroxyl radicals as a new way to decontaminate the sludge. This idea was originated from a previous study in which  $\text{Cs}^+$  was removed from the sea sludge, with cleaning sulfide (S) and reducing total nitrogen (T-N) by using hydroxyl radicals in micro-bubbles [3].

The authors proposed that the origin of this decontamination effect was the decomposition of organic matter by hydroxyl radicals or the decomposition of organic matter by aerobic microorganisms that were activated by the micro-bubbles. Therefore, the authors attempted decontamination using anaerobic microorganisms with the same decomposition performance as aerobic microorganisms. However, decontamination of the sea sludge by activation of anaerobic microorganisms could not be confirmed. From this result, the authors concluded that anaerobic conditions were not suitable for removal of cesium and that decontamination was most effective in aerobic conditions. In addition, the authors suggested hydroxyl radicals have shown a decomposition performance that is suitable for decontamination of the sea sludge [4].

In the present study, we studied the decontamination of the sea sludge by hydroxyl radicals. To obtain hydroxyl radicals easily and safely, we suggested using hydrogen peroxide ( $\text{H}_2\text{O}_2$ ).  $\text{H}_2\text{O}_2$  was chosen for two reasons: (i) no equipment, such as micro-bubbles, is required, and (ii) the decontamination ability can easily be compared to the change of  $\text{H}_2\text{O}_2$  concentration. We examined the potential of hydroxyl radicals to decontaminate the sea sludge by varying the concentration of  $\text{H}_2\text{O}_2$  and the stirring time.

### 3. RESULTS AND DISCUSSION

#### 3.1 Purification of Sea Sludge by $\text{H}_2\text{O}_2$

First of all the ability of  $\text{H}_2\text{O}_2$  to purify the sea sludge was examined. A 10 g sea sludge sample collected from the Funabashi port in Chiba prefecture was mixed with 20 mL of aqueous  $\text{H}_2\text{O}_2$

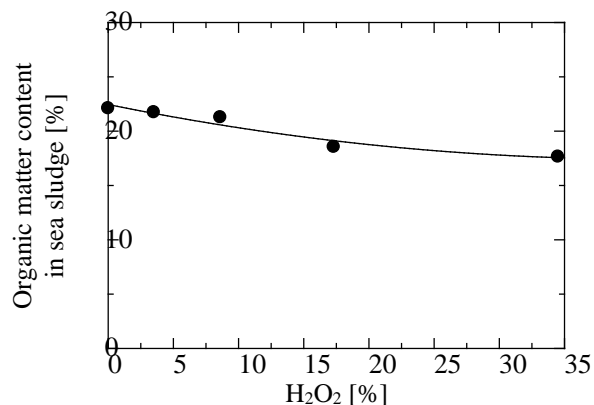


Fig. 2 Change of organic matter content

with a concentration of 0%–34.5%. A powder sample was then made by filtration and drying, and the organic matter content was measured by thermogravimetry (TG) and sulfide content was determined by energy dispersive X-ray spectrometry (EDX). To compare the organic matter content, the difference in the values at 100 °C when water in the sample evaporated and 600 °C when the organic matter is burnt off was used. To compare the sulfide content, the ratio of sulfide in the sea sludge to silicon dioxide ( $\text{SiO}_2$ ) in the sea sludge was used. This ratio was chosen because the content of  $\text{SiO}_2$  in the sea sludge is not greatly affected by  $\text{H}_2\text{O}_2$ .

The change in organic matter content is shown in Figure 2. The organic matter content was found to decrease as the  $\text{H}_2\text{O}_2$  concentration increased. The sulfide concentration, determined as the change in the S/Si ratio, was lower for all  $\text{H}_2\text{O}_2$  concentrations studies compared with the value for 0%, as shown in Figure 3.

These results indicated that purification of the sea sludge by  $\text{H}_2\text{O}_2$  occurs, and was similar to that observed with micro-bubbles. This result indicates that  $\text{H}_2\text{O}_2$  could potentially be used to remove cesium from the sea sludge; thus, the decontamination ability of  $\text{H}_2\text{O}_2$  was determined in the next experiment.

#### 3.2 Decontamination of Sea Sludge by $\text{H}_2\text{O}_2$

The changes in the extent of decontamination using  $\text{H}_2\text{O}_2$  were studied by varying the  $\text{H}_2\text{O}_2$  concentration and the stirring time. Samples were liquids obtained by filtration and the  $\text{Cs}^+$  concentrations were determined. Each 10 g sea sludge sample was mixed with a 20 mL solution of  $\text{H}_2\text{O}_2$  and  $\text{CsNO}_3$ . The concentration of  $\text{H}_2\text{O}_2$  was 0%–34.5%. The concentration of  $\text{CsNO}_3$  was 500–2000 ppm in the experiment where the cesium concentration was varied, and was fixed at 1000 ppm in the experiment where the stirring time was varied. The  $\text{Cs}^+$  concentration and pH in the liquid samples were measured using ion chromatography and a pH meter, respectively.

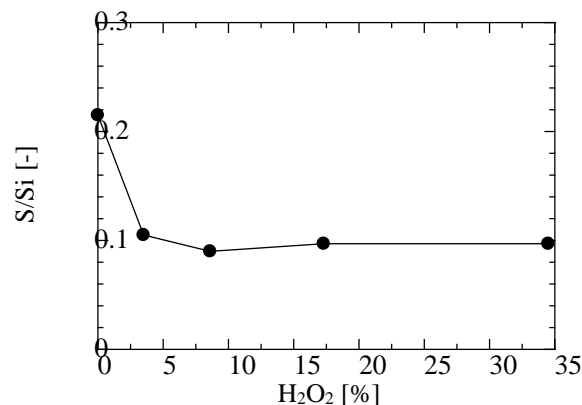


Fig. 3 Change of values in S/Si



### 3.3 Effect of H<sub>2</sub>O<sub>2</sub> Concentration on Sea Sludge Decontamination

The ability of varied concentrations of H<sub>2</sub>O<sub>2</sub> to decontaminate the sludge that contained CsNO<sub>3</sub> was examined. The dissolved Cs<sup>+</sup> concentrations in the liquid phases at different H<sub>2</sub>O<sub>2</sub> concentrations are shown in Figure 4. The concentration of Cs<sup>+</sup> in the liquid phase substantially leveled when the employed H<sub>2</sub>O<sub>2</sub> did not exceed 17.3% H<sub>2</sub>O<sub>2</sub>. The amount of Cs<sup>+</sup> determined in 34.5% H<sub>2</sub>O<sub>2</sub> was much greater than the ones in the other conditions. By dividing the measured values by the value for 0% H<sub>2</sub>O<sub>2</sub>, normalized curves were obtained as shown in Figure 5. A similar trend with H<sub>2</sub>O<sub>2</sub> concentration is observed for all three initial CsNO<sub>3</sub> concentrations, which indicates that the decontamination of the sea sludge by H<sub>2</sub>O<sub>2</sub> was similarly effective under various conditions.

The pH values measured for these solutions are shown in Figure 6. The pH values decreased with increasing H<sub>2</sub>O<sub>2</sub> concentration and were lowest for 34.5% H<sub>2</sub>O<sub>2</sub>. As the extent of decontamination was greatest for 34.5% H<sub>2</sub>O<sub>2</sub>, it is suggested that the pH<sub>pzc</sub> value of the sea sludge is between 3.6 and 4.1 in the present study.

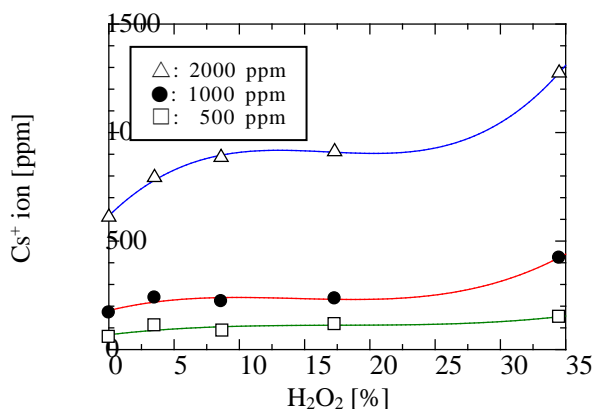


Fig. 4 Removal of Cs<sup>+</sup> from sea sludge by H<sub>2</sub>O<sub>2</sub>

### 3.4 Effect of Stirring Time on Sea Sludge Decontamination

Decontamination results obtained at various H<sub>2</sub>O<sub>2</sub> concentrations (0%–34.5%) and various stirring times (0–24 h) were normalized by dividing the measured values by the value for 0 h stirring as shown in Figure 7. The values obtained for 34.5% H<sub>2</sub>O<sub>2</sub> did not change significantly with stirring time. However, the other concentrations of H<sub>2</sub>O<sub>2</sub> showed peaks in the graph. These peaks were observed at 18 h, 12 h and 6 h for 17.3%, 8.6% and 3.5% H<sub>2</sub>O<sub>2</sub>, respectively. These results indicated that the decontamination of the sludge by H<sub>2</sub>O<sub>2</sub> did not change significantly with time. The peak value was only 1.5 times the 0 hour concentration for 17.3% H<sub>2</sub>O<sub>2</sub> and only 1.7 times the 0 hour concentration for 8.6% H<sub>2</sub>O<sub>2</sub>. From these results, it is not likely that the decontamination effects would be enhanced through prolonged stirring.

### 3.5 Discussion

We have demonstrated the ability of H<sub>2</sub>O<sub>2</sub> to elute Cs<sup>+</sup> from the sea sludge to water. It will be possible to remove Cs<sup>+</sup> from water, using the latest

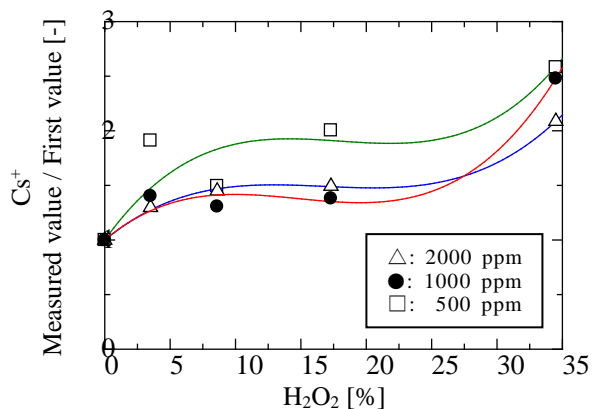


Fig. 5 Normalized removal of Cs<sup>+</sup> from sea sludge by H<sub>2</sub>O<sub>2</sub>

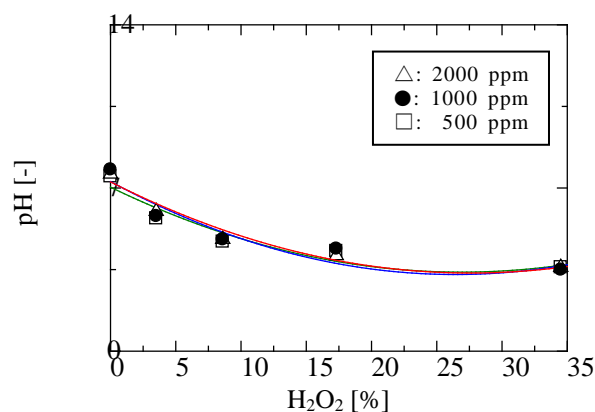


Fig. 6 Change of pH in liquid phase

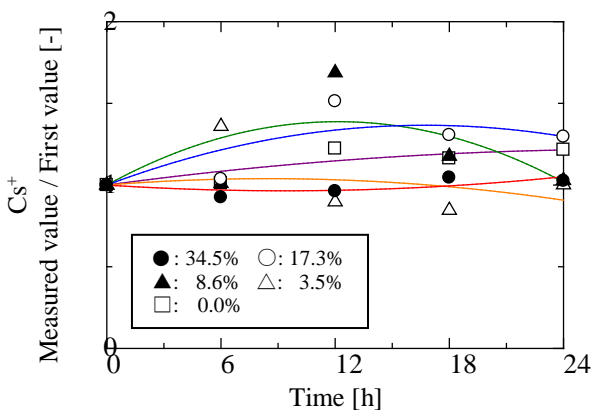


Fig. 7 Change of decontamination with time

decontamination technology, which is currently progressing [6]. From these facts, it will be possible to clean an entire body of water by combining these two technologies for decontamination of the sea sludge and water.

#### 4. CONCLUSION

The removal of  $\text{Cs}^+$  from the sea sludge by  $\text{H}_2\text{O}_2$  was evidenced, and a concentration of 34.5%  $\text{H}_2\text{O}_2$  was found to realize the highest extent of decontamination. In addition, the 34.5%  $\text{H}_2\text{O}_2$  sample had the lowest pH value. Therefore, it is likely that the pH value in 34.5%  $\text{H}_2\text{O}_2$  was less than or equal to the  $\text{pH}_{\text{pzc}}$  value of the sea sludge and that the adsorptivity of the sea sludge for  $\text{Cs}^+$  decreased at that low pH value to enhance the decontamination effect.

Decontamination of the sea sludge by  $\text{H}_2\text{O}_2$  over time was constant for 34.5%  $\text{H}_2\text{O}_2$ , whereas an upward trend of decontamination was observed for 17.3% and 8.6%  $\text{H}_2\text{O}_2$ . However, these values were only 1.5–1.7 times the 0 hour value. The increase in the decontamination ability with time is not large, and decontamination by  $\text{H}_2\text{O}_2$  can be considered substantially instantaneous.

#### 5. REFERENCES

- [1] Yomiuri Shimbun, "Cesium in Tokyo Bay's mud is 13 times higher than 7 months ago", Yomiuri Shimbun, 14th May 2012.
- [2] Aritomi M, Adachi T, Hosobuchi S, Watanabe N, "Decontamination technology of contaminated water with flocculating and settling technology", J. of Power and Energy Systems, Vol. 6, 2012, pp. 412-422.
- [3] Okamoto K, Toyama T, "Ocean decontamination: Elution of radiological cesium from ocean sludge by using micro bubble and activating microorganisms", in The 16th Japan Society of Naval Architects and Ocean Engineers, 2103, pp. 257-258.
- [4] Hirano H, Nishimiya N, Kojima Y, Toyama T, Umegaki T, Okamoto K, "Investigation of radioactive cesium decontamination from sea sludge using microbial activity", in The International Symposium on Inorganic and Environmental Materials 2013, 2013.
- [5] Yonekura N, Oomori T, Koyanagi M, "Coagulation-sedimentation rates of red soil colloids", Bull. of the College of Science, University of the Ryukyus, Vol. 79, 2005, pp. 103-109.
- [6] Sano M, Nakagawa K, Oda H, Obata H, Kitani S, Yamazaki K, "Fundamental study for the development of Cs removal technique from low level radioactive liquid wastes of decontamination processes", The Society of Chemical Engineers, 2014.
- [7] Momonoi K, "The relationship between specific resistance, pH and S-potential on the chemical treatment of sludges", Bull. of Nagaoka University of Technology, 1981, pp. 47-52.
- [8] Yoshida T, "About generation and the removal of the sludge - In bottom sampler examination of the Gulf of Minamata", HEDORO, No. 1, 1974, pp. 11-27.
- [9] Hibino T, Matsumoto H, "Distribution of fluid mud layer in Hiroshima Bay and its seasonal variation", J. of JSCE, B, Vol. 62, 2006, pp. 348-359.

## THE EFFECT OF SUMATRA FAULT EARTHQUAKES ON WEST MALAYSIA

Noushin Naraghi Araghi<sup>1</sup>, Mohd. Nawawi<sup>2</sup>, Syed Mustafizur Rahman<sup>3</sup> and Rosli Saad<sup>4</sup>

<sup>1,2,4</sup> School of Physics, University Science Malaysia

<sup>3</sup> Department of Applied Physics and Electronic Engineering, University of Rajshahi

### ABSTRACT

This paper presents the effect of Sumatra fault earthquakes on west Malaysia by calculating the peak horizontal ground acceleration (PGA). PGA is calculated by a probabilistic seismic hazard assessment (PSHA). A uniform catalogue of earthquakes for the interest region has been provided. We used empirical relations to convert all magnitudes to Moment Magnitude. After eliminating foreshocks and aftershocks in order to achieve reliable results, the completeness of the catalogue and uncertainty of magnitudes have been estimated and seismicity parameters were calculated. Our seismic source model considers the Sumatran strike slip fault that is known historically to generate large earthquakes. The calculations were done using the logic tree method and four attenuation relationships and slip rates for different part of this fault. Seismic hazard assessment carried out for 48 grid points. Eventually, two seismic hazard maps based PGA for 5% and 10% probability of exceedance in 50 year are presented. .

*Keywords: PSHA, Sumatra fault, PGA, seismic parameters*

### INTRODUCTION

Although Malaysia is situated on a stable part of the world, earthquakes in Sumatra effect buildings specially on soft soil area in Malaysia as they have been felt some times specially in high buildings in some part of Malaysia and Singapore[1]. The seismic waves from Sumatra travel long distance to arrive Malaysia bedrock. Normally the high frequency seismic waves damp quickly but low frequency (long period) seismic waves are stronger to energy dissipation and they are able to travel long distances (Fig. 1). Therefore long period waves are considerably amplified as they reach the bedrock of Malaysia, these waves can make resonance in structures with a natural period near the period of the site, and make the large motions [2].

Recently numerous studies are already carried out to determine whether these types of movements could make damage to buildings [3], [4], [5], [6].

### TECTONIC SETTING OF MALAYSIA

Malaysia is situated near two seismically active plates. In the west, Indian Ocean plate moves northeast and subducts under the Sumatra with the estimated velocity of 7 cm/year. This movement produces a great Sumatran fault (Fig. 2).

The Sumatran fault is segmented into 20 parts [7]. From geodetic measurement, each segment has different velocity. The northern segments have higher velocity than the south part (3.7 cm/year and 2cm/year, respectively) [8].

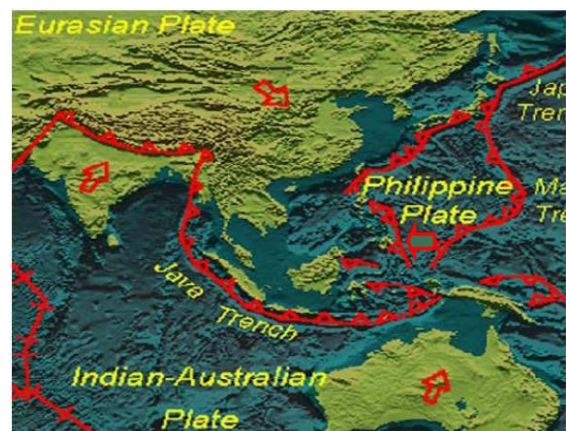


Fig. 2 Major tectonic plates around Malaysia

### EARTHQUAKE SOURCE MODELS

Southeast Asia is a region of variable seismic hazard, ranging from high seismic hazard associated with the subduction process beneath the Indonesian and Philippine archipelagos to moderately low seismic hazard across a large stable region that contains the Malaysian peninsular.

Regarding the historical evidences, west of Malaysia is influenced by earthquakes from two major faults [9], The Sumatran strike slip fault and Sumatran subduction zone.

## SUMATRAN SUBDUCTION ZONE

Subduction of the India-Australian plate beneath the Eurasian plate has produced the Sumatran subduction zone with the slip rate of about 67mm per year. The nearest place of this subduction zone is about 400km to coast of west Malaysia [10]. In this zone, most of the earthquakes are shallow. Historical records show four significant events in the last 300 years (Fig. 3).

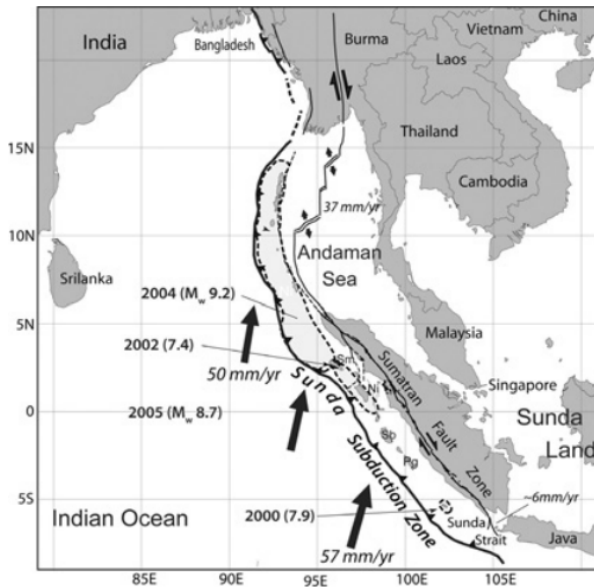


Fig. 3 The Great Sumatran fault zone

## SUMATRAN STRIKE SLIP FAULT

The Sumatran fault runs from beginning to end of the whole length of Sumatra with a length more than 1500km. large historical events with  $M_w$  5.2 and 7.7 are originated from this fault. The closest distance from earthquake source in this fault to the coast of West Malaysia is about 260km. Sumatran fault is divided into 20 major sections including Batee fault.  $M_{max}$  and slip rates calculated for each part of this fault (Fig. 4). We will consider the effect of events caused by this fault on Malaysia [7], [10].

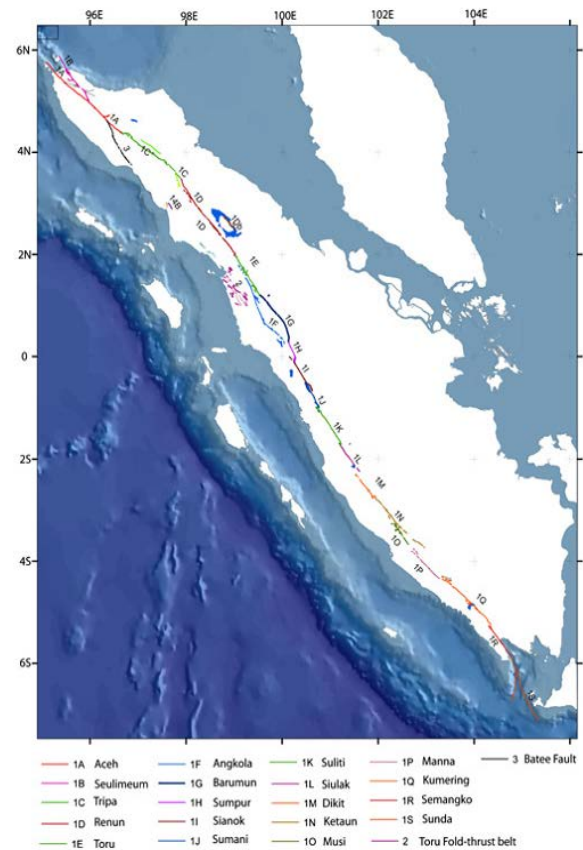


Fig.4 Principal active traces of the Sumatran fault zone

## EARTHQUAKE DATA

Earthquake catalogs are used to estimate future seismic activity from the locations and rates of past earthquakes.

From the locations and frequency-magnitude distributions of past earthquakes we can estimate the locations and rates of future larger shocks that dominate the hazard. For this study we compiled a new catalog of instrumentally recorded earthquakes by combining different catalogues. We used the data from the United States Geological Survey (USGS), the International Seismological Centre (ISC) and the local data in Malaysia (Fig. 5) [11].

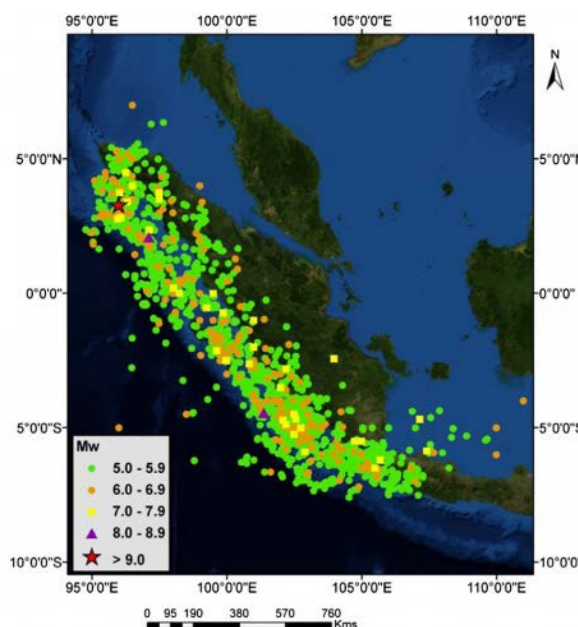


Fig. 5 Seismic events with moment magnitudes larger than 5.0

### EARTHQUAKE RISK ANALYSIS

A homogeneous earthquake catalogue is required for seismicity analysis. As known, moment magnitude ( $M_w$ ) does not saturate for large earthquakes and we will use  $M_w$  for our analysis. To compile a homogeneous earthquake catalog, different magnitudes types like body wave magnitude ( $m_b$ ) and surface wave magnitude ( $M_s$ ), are converted into  $M_w$  using the regression relations derived based on global data [12].

The event list was homogenized and moment magnitude,  $M_w$  was applied in our assessment. Completeness of the catalogue is essential. Obviously, an incomplete catalogue could substantially modify the b-values. The fractions of missing small events would result in a reduction of b-value. Magnitude of completeness ( $M_c$ ) is the smallest amount magnitude and higher than this magnitude, all earthquakes are recorded.  $M_c$  can be evaluated from the observed frequency magnitude distribution.  $M_c$  is someplace that the frequency-magnitude curve begins to digress from a linear trend [13]. The event list would be complete for amount of bigger than  $M_c$ . [14]. In this study  $M_c$  was calculated around 4.5.

Based on the uniform catalogue, seismicity of the region studied, seismicity parameters were calculated utilizing the method proposed by Kijko and Sellevoll [15] (Table 1).

A complete catalog including foreshocks and aftershocks normally will not follow the Poisson distributions, so we will eliminate all foreshocks and aftershocks by windowing method in time and space domains by Gardner and Knopoff [16].

Table 1. Seismic hazard analysis for study area.

Seismic Parameters	$M_c$	$M_{max}$	$\lambda$	a-value	b-value
Value	4.6	7.8	1.17	8.43	$1.1 \pm 0.04$

### ATTENUATION RELATIONS AND ANALYSIS

We used 48 grid points within the study area for seismic hazard assessment (Fig. 6). Quantification of ground motion is important to understand the behavior of any site during an earthquake. Attenuation models are used to predict the probability distribution of ground-shaking intensity, as a function of variables including earthquake magnitude, distance from the site, the faulting mechanism, and near surface site conditions. In the present study, four attenuation relationships were chosen for analysis.

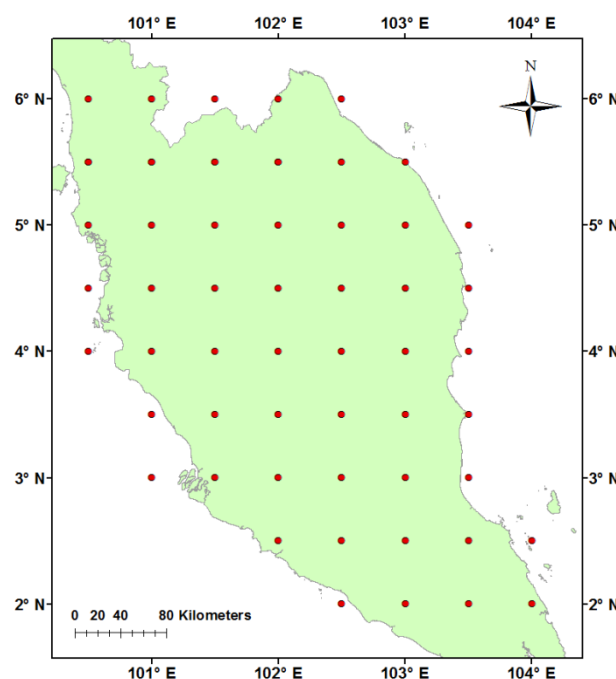


Fig6. Grid points within the study area

Four attenuation relations were used for this study [17], [18], [19], [20]. Peak ground accelerations are generated by EZFRISK with 5% and 10% probability of exceedance in 50 years (Fig 7 and Fig 8).



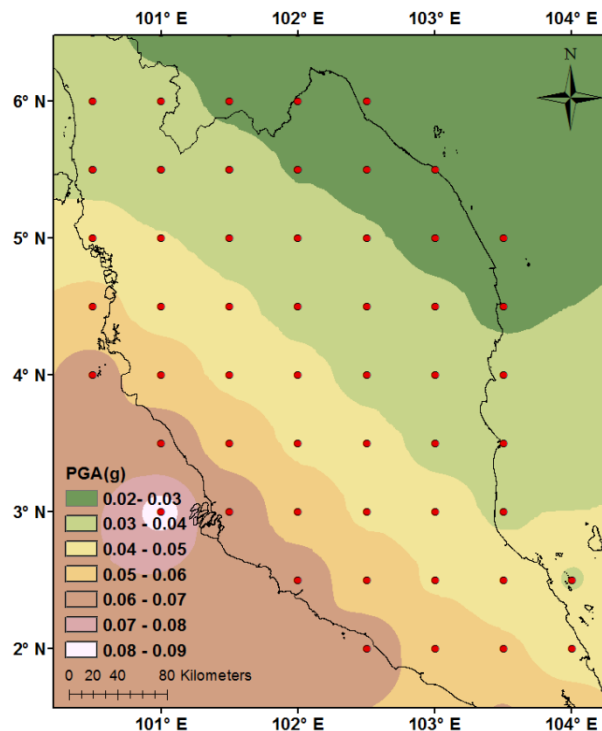


Fig. 7 PGA with 5% probability of exceedance in 50 years (return period: 975 years).

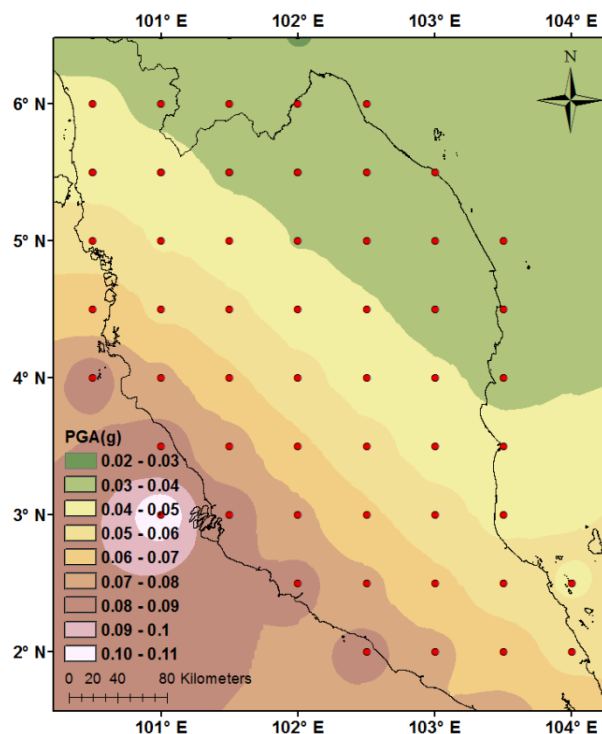


Fig. 8 PGA with 10% probability of exceedance in 50 years (return period: 475 years).

## CONCLUSION

The lack of active faults and earthquakes mean that the Malaysia is located in a tectonically stable

region. Hazard in Sumatra is quite high while in Malaysia it is low. In west Malaysia PGA is 0.02 to 0.09 for 5% probability of exceedance and 0.02 to 0.1 for 10% probability of exceedance. In this assessment, we didn't consider the amplification of soils. This factor can increase the ground motion. The significant results of this study can be summarized as:

- Making complete and updated earthquake catalogue
- Production of a preliminary seismic zoning map based on PGA over bedrock that can be used as a guide for determining the design earthquake.
- Find and use the most suitable attenuation relation for the study area.

## ACKNOWLEDGMENT

The support for the research presented in this paper had been provided by the Universiti Sains Malaysia.

## REFERENCES

- [1] Balendra, T., Tan, T. S., and Lee, S. L. "An analytical model for far-field response spectra with soil amplification effects." *Engineering Structures*, 1990, Vol. 12, No.4, pp 263-268.
- [2] Balendra, T. *Vibration of Buildings to Wind and Earthquake Loading*, Springer-Verlag, London, 1993
- [3] Megawati, K., and Pan, T.-C. "Prediction of the maximum credible ground motion in Singapore due to a great Sumatran subduction earthquake: The worst-case scenario." *Earthquake Engineering and Structural Dynamics*, 2002, Vol. 31, No.8, pp 1501-1523.
- [4] Megawati, K., Pan, T.-C., and Koketsu, K. "Response spectral attenuation relationships for Singapore and the Malay Peninsula due to distant Sumatran-fault earthquakes." *Earthquake Engineering and Structural Dynamics*, 2003, Vol. 32, No.14, pp 2241-2265.
- [5] Megawati, K., Pan, T.-C., and Koketsu, K. "Response spectral attenuation relationships for Sumatran-subduction earthquakes and the seismic hazard implications to Singapore and Kuala Lumpur." *Soil Dynamics and Earthquake Engineering*, 2005, Vol. 25, No.1, pp 11-25.
- [6] Balendra, T., Lam, N. T. K., Wilson, J. L., and Kong, K. H. "Analysis of long-distance earthquake tremors and base shear demand for buildings in Singapore." *Engineering Structures*, 2002, Vol. 24, No.1, pp 99-108.
- [7] Sieh, K. and Natawidjaja, D. Neotectonics of the Sumatran fault, Indonesia. *Journal of Geophysical Research*, 2000, 105, 28,295-28,326.
- [8] Abas, M. R. C. "Earthquake monitoring in Malaysia." *Seismic Risk Seminar*. 2001.



- [9] Balendra, T., and Z. Li. "Seismic hazard of Singapore and Malaysia." *Electron J Struct Eng (special issue, Earthquake engineering in the low and moderate seismic regions of Southeast Asia and Australia)* ,2008, 57-63.
- [10] Mohd Rosaidi, C. A. "Earthquake Monitoring In Malaysia." *Seismic Risk Seminar on 25th September*, 2001.
- [11] Leyu, C. H., Chang, C. F., Arnold, E. P., Kho, S. L., Lim, Y. T., Subramaniam, M., Ong, T. C., Tan, C. K., Yap, K. S., Shu, Y. K., and Goh, H. L, 1985.
- [12] Das, R., Wason, H.R., Sharma, M.L. Global regression relations for conversion of surface wave and body wave magnitudes to moment magnitude. *Nature Hazards* 59,2011, 801–810.
- [13] Nuannin P, Kulhánek O and Persson L. "Spatial and temporal characteristics of aftershocks of the December 26, 2004 and March 28, 2005 earthquakes off NW Sumatra", *Journal of Asian Earth Sciences*, 2012, Vol 46, pp.150-160.
- [14] Nuannin P, Kulhanek O, Persson L. "Variations of b-values preceding large earthquakes in the Andaman-Sumatra subduction zone".*Journal of Asian Earth Sciences*,2012, Vol 61,pp.237-242
- [15] Kijko, A., & Sellevoll, M. A. Estimation of earthquake hazard parameters from incomplete data files. Part II. Incorporation of magnitude heterogeneity. *Bulletin of the Seismological Society of America*, 1992, 82(1), 120-134.
- [16] Knopoff L. and Gardner J. "Homogeneous catalogs of earthquakes", *Proceedings of the National Academy of Sciences*, 1969, Vol. 63, pp.1051-1054.
- [17] D.M. Boore, and G.M. Atkinson, Ground -Motion Prediction Equations for the Average Horizontal Component of PGA, PGV, and 5%-Damped PSA at Spectral Periods between 0.01 s and 10.0s, *Earthquake Spectra*, 24(1), 2008, 99-138.
- [18] Sadigh, K., Chang, C.-Y., Egan, J.A., Makdisi, F., Youngs, R.R. Attenuation relationships for shallow crustal earthquakes based on California strong motion data. *Seismol. Res. Lett*, 1997, 68, 180 – 189.
- [19] Frankel, A., Mueller, C., Barnhard, T., Perkins, D., Leyendecker, E.V., Dickman, N., Hanson, S., Hopper, M. National seismic hazard map: documentation June 1996. Open-File Rep. -U.S. Geol. Surv. 1996, 96-532
- [20] Toro, G.R., Abrahamson, N.A., Schneider, J.F. Model of strong ground motions from earthquakes in Central and Eastern North America: best estimates and uncertainties. *Seismol. Res*, 1997, Lett. 68, 41 – 57.

## **DEVELOPMENT OF SOIL FORMATION CORRESPONDING TO CYCLIC STRESS – DERIVED SHEAR STRAIN BASED ON STRATUM INDEX FACTOR**

Abdull Halim Abdul

Geosciences Department, University Technology PETRONAS, Bandar Seri Iskandar , 31750Tronoh ,  
MALAYSIA

### **ABSTRACT**

This paper discusses the application of Laplace Transform ( LT) method in solving the shear strain equation from stratum index factor , which involve a competitive sequential CPI model and cyclic stress formation . The methodology of these analysis know as modified constant plastic index in consolidated soil –Derived shear strain based on stratum index factor.

*Keywords: Stratum index factor , Shear strain function*

### **INTRODUCTION**

It is well-known that in 1923 Terzaghi [ 1] and his consolidation theory brought the dimension-time into Soil Mechanics. The research about a very soft saturated soil ground consolidation due to self-weight. A lot of evaluation of Terzaghi one dimensional theory has been done to compare the finite element numerical A Constant Plastic Index (CPI ) model was set up that state : a relationship soil consolidation formation exist volume matrix change of shear stress - strains curve . The curve is derived a shear stress function on amplitude strain ( Or , 2001) or mathematical shear strain( Hudson & Harrison ( 1977) due to (  $\frac{1}{2} \alpha$  ) half of stratum index factors

The specific objectives of the research are as follows in Figure 1 as

prediction value to the measured value. In the case of a three dimensional field, the Biot's theory of consolidation which complex the equilibrium of total stress,

continuity of soil mass and strain of soil deformation has been useful (Biot, 1945).

### **OBJECTIVE**

(1) Modification of Constant Plastic Index method on CPI model based on volume matrix change of the consolidation soil .

(2) Derived shear strain function using Laplace Transform ( L T ) and cyclic stress formation as stratum index factor for stress –strain function based on CPI Model

### **MODIFIED CONSTANT PLASTIC INDEX METHOD**

The deformation under cyclic stresses as compression of stratum index factors and it is considered a homogeneous soil subjected to sinusoidal shearing stress of angular velocity stress amplitude and strain amplitude. (Teamrat , A.Ghezzehei , and Dani Or (2001)) [ 3] . The shearing stress applied upon purely elastic soil resulted in proportional and instantaneous strain.

After completing a cyclic load saturation, consolidation and volume matrix change of soil is a steady state case where  $F(e) e_o^x = 1 + e_o$  ( Poulos (1981) Equation 1

The equation ( $S_{sul}$ ) derived will become a mathematical equation as

$$e_o^x = \frac{\Delta e}{S_{sul}} H \quad \text{Equation 2}$$

Where  $H$  is thickness of soil layer  
 $\Delta e$  is a (final void ratio –initial void ratio)  
 $e_0$  is initial void ratio  
 $S_{sul}$  is Ultimate Consolidation Settlement

The equation 2 can be expressed as log10.

$$\log_{e_0} e_0^x = \log_{e_0} \left[ \frac{\Delta e H}{S_{sul}} \right] \quad \text{equation 3}$$

$$\log_{e_0} e_0^x = \log_{e_0} (\Delta e H) - \log_{e_0} S_{sul}$$

$$X = \frac{\ln \left( \frac{\Delta e H}{S_{sul}} \right)}{\ln e_0} \quad \text{equation 4}$$

Where,  $x$  is Constant Plastic Index (CPI)  
 $F(e)$  is Void ratio Function of the potential yields function Elastic soil (Hardin Bankford, 1989) and the equation is follows Hooke Law for a number of clay

$$F(e) = e_0^x \quad \text{equation 5}$$

Where  $F(e)$  is void ratio function

$X$  is constant plastic index (CPI)  
 $e_0$  is initial void ratio

in layer hypothesis in Figure 1 is considered with an initially uniform void ratio  $e_1$  under its own weight, and  $e_2$  is the base of layer which suddenly increased the stress, then remained constant. per surface of this layer is allowed to drain freely, hence its void ratio will immediately reach the new equilibrium state,  $e_2$ . The base of this layer is assumed to be impervious and thus, no drainage can occur across it.

## DERIVED SHEAR STRAIN BASED ON STRATUM INDEX FACTOR

In situation where single drainage is only allowed (Kuantsai 1979)[1] at one of the two boundaries of the stratum, the progress of consolidation will be retarded. In the theory of a linear soil model and the thin layer the actual location of this boundary, whether it is in the surface or the base, does not effected the strain rate of the stratum. This is because identical void ratio changes occur at both boundaries. In the present theory, however, the void ratio changes in both boundaries will be different. Consequently, a difference in the strain rate is expected for different locations of the drainage boundary. This will be

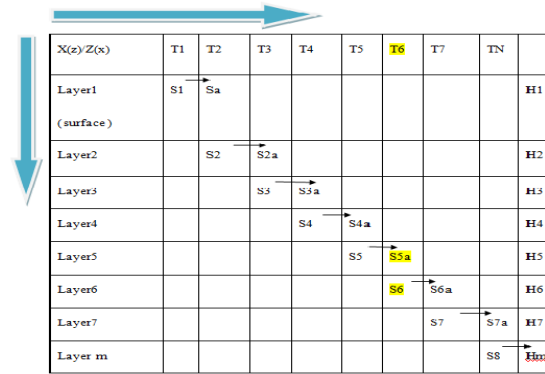


Figure 1 Surface and base of the layer .

In the Langrangian formulation, the compaction within two layers is complicated because of the presence of the fixed boundary. The Constant plastic index (CPI) mechanism of compacted clay between two layers is considered to be integrate Stratum Index Factors ( $\alpha$ ), A characteristic of compacted soil between surface (s) and base (b) of layers is formulated as

$$\alpha = \ln \frac{e_s^{x1}}{e_b^{x2}} \quad \text{equation 6}$$

Furthermore, to obtain the evaluation formula for the expansion characteristic of compaction, it is proposed that the development of CPI ( $x$ ) model and Stratum Index Factor (SIF) model be combined to get the estimate of the CPI ( $x$ ) characteristic of clay.

confirmed in this section by the solutions developed for each case.

The inverse transformation according to the inversion theorem is evaluated in (Lee Kuantsai 1979, pg166) and which it is found that:

$$\beta_n \cos \beta_n + \frac{\alpha}{2} \sin \beta_n = 0 \quad \text{as shear strain function and}$$

$$\beta_n \cos \beta_n - \frac{\alpha}{2} \sin \beta_n = 0 \quad \text{as shear tensile function .}$$

Equation 7

Surface drain The boundary conditions in this case are:

$$q(1, Tv) = \Delta F(e) \quad \text{equation 8}$$

$$\frac{\partial q}{\partial n}(0, Tv) = \alpha q(0, t)$$

equation 9

Using the Laplace transform it is found ( Lee Kuantsai , 1979) that:

$$\bar{q}(n, p) = A_1 \exp(m_1 n) + A_2 \exp(m_2 n) \quad , \quad m_{1,2} = \frac{\alpha}{2} \pm \sqrt{\left(\frac{\alpha^2}{4} + p\right)}$$

equation 10

with,

$$A_1 = \frac{B \Delta F(e)}{p[\exp(m_2) - B \exp(m_1)]}$$

$$A_2 = \frac{a \exp(m_2) - b}{p[\exp(m_2) - \exp(m_1)]} \quad \text{and} \quad B = \frac{m_2 - \alpha}{m_1 - \alpha}$$

The Laplace transform of the local degree of consolidation is given by:

$$\bar{f}(n, p) = \frac{\bar{q}(n, p)}{q(n, \infty)}$$

After some manipulation, this is found to be:

$$\bar{f}(n, p) = \frac{\exp\left[-\frac{\alpha}{2}(n-1)\right] \left\{ \sqrt{\left(\frac{\alpha^2}{4} + p\right)} \cosh\left[n \sqrt{\left(\frac{\alpha^2}{4} + p\right)}\right] + \frac{\alpha}{2} \sinh\left[n \sqrt{\left(\frac{\alpha^2}{4} + p\right)}\right] \right\}}{p \left\{ \sqrt{\left(\frac{\alpha^2}{4} + p\right)} \cosh\left[\sqrt{\left(\frac{\alpha^2}{4} + p\right)}\right] + \frac{\alpha}{2} \sinh\left[\sqrt{\left(\frac{\alpha^2}{4} + p\right)}\right] \right\}}$$

equation 11

The inverse transformation according to the inversion theorem is evaluated in (Lee Kuantsai 1979, pg166) and Figure 2 from which it is found that:

$$f(n, Tv) = 1 -$$

$$2 \sum_n \frac{(-1)^n \left[ \beta_n \cos(\beta_n n) + \frac{\alpha}{2} \sin(\beta_n n) \right]}{\sqrt{\left(\beta_n^2 + \frac{\alpha^2}{4}\right)} \left[ \beta_n + \frac{\alpha^2}{4\beta_n} + \frac{\alpha}{2\beta_n} \right]} \exp \left[ - \left( \beta_n^2 + \frac{\alpha^2}{4} \right) Tv - \frac{\alpha}{2} (n-1) \right]$$

where the  $\beta_n$ s are the zeroes of

$$\beta_n \cos \beta_n + \frac{\alpha}{2} \sin \beta_n = 0 \quad \text{as shear strain and shear rate function}$$

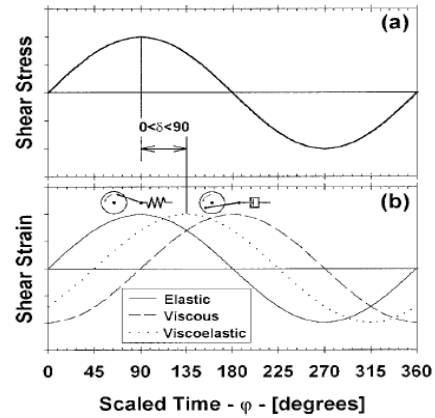


Figure 2 Shear stress and shear strain function

The expression for the void ratio change q can be obtained by:

$$q(n, Tv) = \Delta F(e) \exp[\alpha(n-1)] f(n, Tv)$$

The degree of settlement is found to be:

$$S(Tv) = 1 -$$

$$\frac{2\alpha}{1 - \exp(-\alpha)} \sum_n \frac{\exp \left[ - \left( \beta_n^2 + \frac{\alpha^2}{4} \right) Tv \right]}{\left( \beta_n^2 + \frac{\alpha^2}{4} \right) \left( 1 + \frac{\alpha^2}{4\beta_n^2} + \frac{\alpha}{2\beta_n} \right)}$$

The small time approximation to this can be obtained by considering the behaviour of the Laplace transform, which is:

$$S(p) = \frac{\alpha}{p[1-\exp(-\alpha)]} \frac{1}{\sqrt{\left(\frac{\alpha^2}{4}+p\right)} \coth\left[\sqrt{\left(\frac{\alpha^2}{4}+p\right)}+\frac{\alpha}{2}\right]}$$

As  $p \rightarrow \infty$ ,  $\coth \sqrt{\left(\frac{\alpha^2}{4}+p\right)} \rightarrow 1$

It follows that :

$$s(p) = \frac{\alpha}{1-\exp(-\alpha)} \frac{1}{p\left[\sqrt{\left(\frac{\alpha^2}{4}+p\right)}+\frac{\alpha}{2}\right]} \quad p \rightarrow \infty$$

Since,

In large time an approximate solution can again be obtained by taking the first few terms of the series solution, eq.12 . A comparison of the small and large time approximation (up to the third term in the series) with the exact solution is shown in a typical value of  $\alpha=1$ . The agreement is seen to be very good.

(b) Based drain

The boundary conditions for this case are:

$$q(0, Tv) = \Delta F(e) \exp(-\alpha)$$

$$\frac{\partial q}{\partial n}(1, Tv) = \alpha q(1, Tv)$$

Using the Laplace transform it is found that:

$$L^{-1} \left\{ \frac{1}{p \left[ \sqrt{\left(\frac{\alpha^2}{4}+p\right)}+\frac{\alpha}{2} \right]} \right\} = L^{-1} \left\{ \frac{\sqrt{\left(\frac{\alpha^2}{4}+p\right)}}{p^2} \right\} - \frac{\alpha}{2} Tv$$

It follows from eq.11 that,

$$L^{-1} \left\{ \frac{\sqrt{\left(\frac{\alpha^2}{4}+p\right)}}{p^2} \right\} \simeq 2 \sqrt{\left(\frac{Tv}{\pi}\right)} + \frac{\alpha^2}{2\sqrt{\pi}} \sqrt{(Tv)^3}$$

Which is,

$$S(Tv) = \frac{\alpha}{1-\exp(-\alpha)} \left[ 2 \sqrt{\left(\frac{Tv}{\pi}\right)} - \frac{\alpha}{2} Tv + \frac{\alpha^2}{6\sqrt{\pi}} \sqrt{Tv^3} \right] \quad T \rightarrow 0 \quad \text{equation 12}$$

$$\begin{aligned} \bar{q}(n, p) = & \frac{\Delta F(e) \exp\left(\frac{\alpha}{2}n - \alpha\right)}{p} \left[ \sqrt{\left(\frac{\alpha^2}{4}+p\right)} \cosh \left[ (1-n) \sqrt{\left(\frac{\alpha^2}{4}+p\right)} \right] - \frac{\alpha}{2} \sinh \left[ (1-n) \sqrt{\left(\frac{\alpha^2}{4}+p\right)} \right] \right] \\ & \left[ \sqrt{\left(\frac{\alpha^2}{4}+p\right)} \cosh \sqrt{\left(\frac{\alpha^2}{4}+p\right)} - \frac{\alpha}{2} \sinh \sqrt{\left(\frac{\alpha^2}{4}+p\right)} \right] \end{aligned}$$

and,

$$\bar{f}(n, p) =$$

$$\frac{\exp\left(-\frac{\alpha}{2}n\right)}{p} \frac{\sqrt{\left(\frac{\alpha^2}{4}+p\right)} \cosh \left[ (1-n) \sqrt{\left(\frac{\alpha^2}{4}+p\right)} \right] - \frac{\alpha}{2} \sinh \left[ (1-n) \sqrt{\left(\frac{\alpha^2}{4}+p\right)} \right]}{\sqrt{\left(\frac{\alpha^2}{4}+p\right)} \cosh \sqrt{\left(\frac{\alpha^2}{4}+p\right)} - \frac{\alpha}{2} \sinh \sqrt{\left(\frac{\alpha^2}{4}+p\right)}}$$

The inverse transform of this is also evaluated in Lee Kuantsai page 169 and 59 and this chapter, from which it is found that:

$$f(n, Tv) = 1 -$$

$$2 \sum_n \frac{(-1)^n \left[ \alpha_n \cos \alpha_n (1-n) - \frac{\alpha}{2} \sin \alpha_n (1-n) \right]}{\left( \alpha_n^2 + \frac{\alpha^2}{4} \right) \left( \alpha_n^2 + \frac{\alpha^2}{4\alpha_n} \right)} \exp \left[ - \left( \alpha_n^2 + \frac{\alpha^2}{4} \right) Tv - \frac{\alpha}{2} n \right]$$

and the degree of settlement is:

$$S(Tv) = 1 -$$

$$\frac{2\alpha}{\exp(\alpha)-1} \sum_n \frac{\exp \left[ - \left( \alpha_n^2 + \frac{\alpha^2}{4} \right) Tv \right]}{\left( \alpha_n^2 + \frac{\alpha^2}{4} \right) \left( 1 + \frac{\alpha^2}{4\alpha_n^2} - \frac{\alpha}{2\alpha_n^2} \right)}$$

where the  $\alpha_n$  are the zeroes of

$$\alpha_n \cos \alpha_n - \frac{\alpha}{2} \sin \alpha_n = 0$$

as a shear strain and shear rate function  
equation [13],

Plasticity soil . The small time approximation to the degree of settlement is obtained by Lee Kuantsai (1979) and considering its Laplace transform:

$$\bar{S}(p) = \frac{\alpha}{p[\exp(\alpha)-1]} \frac{1}{\sqrt{\left(\frac{\alpha^2}{4}+p\right)} \coth \sqrt{\left(\frac{\alpha^2}{4}+p\right)} - \frac{\alpha}{2}}$$

equation 14

$$\text{As } p \rightarrow \infty, \quad \coth \sqrt{\left(\frac{\alpha^2}{4}+p\right)} \rightarrow 1$$

it follows that:

$$S(p) = \frac{\alpha}{\exp(\alpha)-1} \frac{1}{p \left[ \sqrt{\left(\frac{\alpha^2}{4}+p\right)} - \frac{\alpha}{2} \right]}$$

The inverse transform of this is, approximately in

Figure 13

$$S(T) = \frac{\alpha}{\exp(\alpha)-1} \left[ 2\sqrt{\left(\frac{Tv}{\pi}\right)} + \frac{\alpha}{2} Tv - \right.$$

$$\left. \frac{\alpha^2}{6} \frac{1}{\sqrt{\pi}} \sqrt{Tv^3} \right] \quad \text{equation 15}$$

It is worth noting that by adding this to the expression for the surface drain case:

$$S_{base} + S_{surface} = \frac{\alpha}{\exp(\alpha)-1} [2(1 +$$

$$\exp(\alpha)) \sqrt{\left(\frac{Tv}{\pi}\right)} - \frac{\alpha}{2} (\exp(\alpha) - 1) Tv +$$

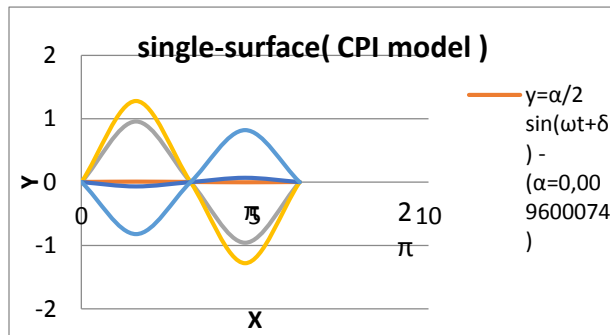
$$\frac{\alpha^2}{6} (1 + \exp(\alpha)) \frac{1}{\sqrt{\pi}} \sqrt{Tv^3} \quad \text{equation 16}$$

## RESULT

The progress of the degree of settlement with the square root of time factors for both surface and base drain cases . The differential of pore water pressure and void ratio change absent and the degree of consolidation will move to lower consolidation . In the surface drain the trend is similar to the double drainage case in that faster consolidation achieved with larger SIF . However the opposite is observed in the base drain case where larger SIF will produce a slower consolidation , and it can be seen that the consolidation with base drain is always slower than the thin layer , while the surface drain will always be faster . It can be seen that the consolidation with stratum coefficient ( Lee Kuantsai 1977 ) [ 1 ] is always slower than the SIF . A



comparison of the small and large time approximation (up to the third term in the series) with the exact



solution is shown in a typical value of  $\alpha=1$ .

Figure 3 Single drainage for surface shear strain

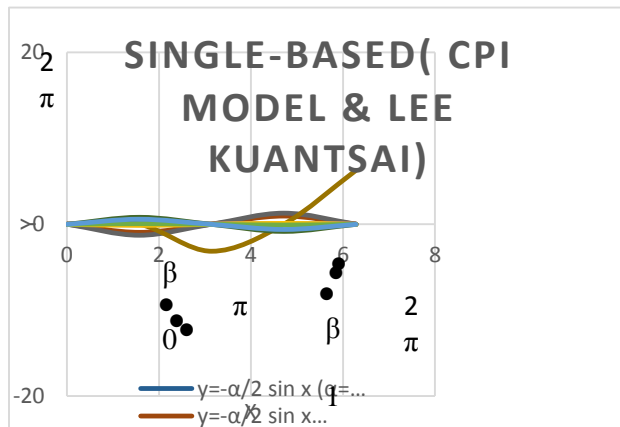


Figure 4 Single drainage for base shear strain function . Single Surface - Case 2— $t=\text{Constant}$ ,  $C_v$  and  $C_F$  = various . Single surface CPI  $S(T_v)$  increased due to Lee Kuantsai method

The inverse transform of this is also evaluated in Lee Kuantsai page 231 and in this chapter, from which it is found that:

$$f(n, T_v) = 1 -$$

$$2 \sum_n \frac{(-1)^n \left[ \alpha_n \cos \alpha_n (1-n) - \frac{\alpha}{2} \sin \alpha_n (1-n) \right]}{\left( \alpha_n^2 + \frac{\alpha^2}{4} \right) \left( \alpha_n^2 + \frac{\alpha^2}{4\alpha_n^2} - \frac{\alpha}{2\alpha_n} \right)} \exp \left[ - \left( \alpha_n^2 + \frac{\alpha^2}{4} \right) T_v - \frac{\alpha}{2} n \right]$$

Degree of settlement is:

$$S(T_v) = 1 - \frac{2\alpha}{\exp(\alpha)-1} \sum_n \frac{\exp \left[ - \left( \alpha_n^2 + \frac{\alpha^2}{4} \right) T_v \right]}{\left( \alpha_n^2 + \frac{\alpha^2}{4} \right) \left( 1 + \frac{\alpha^2}{4\alpha_n^2} - \frac{\alpha}{2\alpha_n} \right)}$$

equation 14

## CONCLUSION

It was found that, the average degree of settlement in critical state for double drainage consolidated faster than for single drainage. Enhanced to increase the degree of settlement of double drainage consolidated was faster than to reduce the degree of settlement.

## REFERENCES

- [1] Kuantsai 1977 "An Analytical And Experimental Study Of Large Strain Soil Consolidation": A Thesis submitted to the University of Oxford for the Degree of Doctor of Philosophy , Trinity Term .
- [ 2 ] Robert Kirk Bowden (1988)  
"Compression Behavior and Shear Strength Characteristics of a Natural Silty Clay Sedimented in the Laboratory", A thesis submitted to the University of Oxford for Degree of Doctor of Philosophy , Trinity Term, 1988.
- [ 3 ] Leonard , G.A ,Altschaeffl, A.G (1964,1976)  
"Compressibility of Clay " Proceeding , ASCE , 90:SM5 :133-156 (1964)
- [4] " Estimating Consolidation Settlement of Shallow Foundation On Over consolidated Clay  
" Special Report No 163 , Transport Research Board , Washington , D.C , pp 13-16 . (1976)
- [4] LisandroPANTELEDIS (2007)"Determining of the Soil Strength Characteristics Through the Plate Bearing Test 'Journal House of Poznan University of Technology , Poznah 2008ISSN 1642-9303 .
- [ 5 ] Ashraf S.Osman , Malcolm D. Bolton (2"A new method to the estimation of untrained settlement of shallow foundation on soft clay ", Journal Engineering Practice and Performance if Soft Deposits .

# UNEXPECTED HIGH CO<sub>2</sub> CONCENTRATION IN CLASSROOMS OF WAKAYAMA UNIVERSITY

Masahiro Yamashita<sup>1</sup> and Hiroyuki Ii<sup>2</sup>

<sup>1</sup>Graduate School of Systems Engineering, Wakayama University, Japan;

<sup>2</sup>Faculty of Systems Engineering, Wakayama University, Japan

## ABSTRACT

CO<sub>2</sub> concentration in most classrooms in Wakayama University was over 1000 ppm, the Japanese school Environmental Standard and sometimes reached over 4000 ppm. Airtightness for each classroom without ventilation was estimated by measuring CO<sub>2</sub> production volume per people number per unit time (CPPT). Airtightness for classroom is variable because of opening door by student during lecture and most of air in classroom was thought to be sometimes exchanged by opening door. Then, effect of opening door and window on CO<sub>2</sub> concentration in classroom was estimated from CO<sub>2</sub> concentration, classroom volume, number of people, and time by comparing CO<sub>2</sub> concentrations under no ventilation condition and ventilation condition opening door or window. As a result, the classroom with volume of 250 to 930 m<sup>3</sup> needs 4.2 to 6.3 m<sup>2</sup> area to open door or window for not increasing CO<sub>2</sub> concentration.

*Keywords: CO<sub>2</sub> concentration, airtightness, ventilation, portable sensor*

## INTRODUCTION

This study is to measure air quality in classroom of Wakayama University by focusing on CO<sub>2</sub> concentration. CO<sub>2</sub> concentration in a classroom is designed based on the Japanese school Environmental Standard. Ministry of Education, Culture, Sport, Science and Technology propose that CO<sub>2</sub> concentration in classrooms is less than 1000 ppm [1]. When it is less than 1000 ppm, there is little impact on the human body. But, there will be various impacts if you are for long time in more than 1000 ppm space. For example, there are drowsiness, languor, vertigo, and headache. Classrooms are likely high population and it isn't customary to do ventilation regularly in University. In addition, buildings in recent years often have high air tightness for improvement of building technology [2]. While this can reduce consumption of air conditioning energy, buildings in recent years are difficult to obtain enough ventilation. CO<sub>2</sub> concentration in classrooms of University may be very high because these reason.

A purpose of this study is to evaluate air condition by measuring CO<sub>2</sub> concentration in lecturing classrooms of Wakayama University.

## METHOD

Survey was performed at 6 buildings in Wakayama University. These are the building of economic, the building of education, the building A of engineering, the building B of engineering, the building of tourism and the building of basic education. The measurement dates are December

2013. Portable sensor GCH-2018 was used for measuring CO<sub>2</sub> concentration as shown in Fig1 Measuring place was at the back side and at 80 cm height of each classroom.

There were two types of measurements. One is short time measurement for obtain roughly CO<sub>2</sub> concentration for many classrooms. Measurement time is about 3 minutes for each classroom and total numbers of classrooms for measurement are 94. The other is one lecture measurement from the beginning of lecture to end of the lecture. Total measurement time is 90 minutes for each lecture with every 15 minutes measurement. The purpose was to clarify change of CO<sub>2</sub> concentration with time, people, volume of classroom, and air condition. The measurement dates are December 2013 and January 2014 as period of winter and April, May and June 2014 as period of spring.



Fig. 1 CO<sub>2</sub> concentration meter (GCH-2018)

## RESULT

### 1. 3 minutes measurement

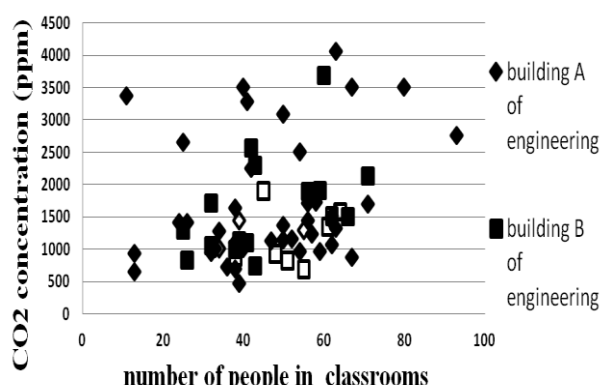


Fig. 2 CO<sub>2</sub> concentration at building A and B of Engineering

Fig. 2 shows CO<sub>2</sub> concentration at building A and B of Engineering for 3 minutes measurement. Solid marks show no ventilation and Open marks show ventilation. Only 20 % numbers of both the buildings were aired by window or air conditioner. CO<sub>2</sub> concentration for many classrooms of both buildings reached over 3000 ppm. However, CO<sub>2</sub> concentrations in ventilated classroom were less than 2000ppm.

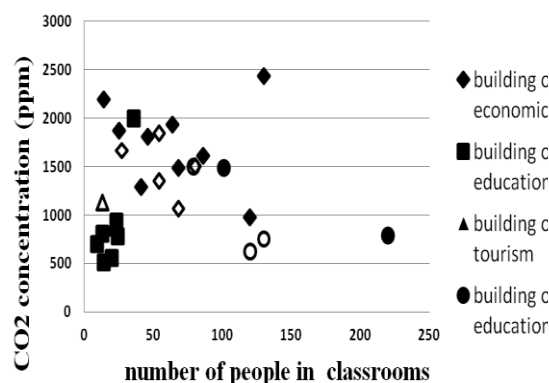


Fig. 3 CO<sub>2</sub> concentration at building of Economic, Education, Tourism and Basic Education

Fig. 3 shows CO<sub>2</sub> concentration at building of Economic, Education, Tourism and Basic Education for 3 minutes measurement. Education buildings were not aired and the half of classrooms for Economic, Tourism and Basic Education buildings were aired. CO<sub>2</sub> concentrations of classrooms for the Economic buildings were often over 2000 ppm. CO<sub>2</sub> concentrations of most of classrooms for Education, Tourism and Basic Education buildings were less than 1500 ppm. CO<sub>2</sub> concentrations of classrooms with ventilation for all buildings were less than 2000

ppm. Therefore, ventilation is useful for reducing CO<sub>2</sub> concentrations of classrooms and keeping less than 2000 ppm.

Table I The CO<sub>2</sub> concentration of classroom for the building

CO <sub>2</sub> concentration (ppm)	building of economic	building of education	building A of engineering	building B of engineering	building of tourism	building of basic education
3001~	0	0	7	1	0	0
2501~3000	0	0	2	1	0	0
2001~2500	2	0	1	2	0	0
1501~2000	6	1	5	7	0	0
1001~1500	4	0	18	5	1	2
~1000	1	8	9	6	2	3

Table I is summary of these results. If comfortable air condition is less than 1000 ppm, building of the Education, building of the Tourism and building of the Basic Education are almost good condition. But, other buildings are often 1000 ppm or more.

Especially in building A of the Engineering, about 35 % is over 1500ppm and about 16 % is over 3000 ppm. As lecture is often done in the same classroom continuously and population density tends to be higher than other buildings, CO<sub>2</sub> concentration was high. It was found that building of the Economic and building B of the Engineering are often bad air condition.

### 2. 90 minutes measurement

From the 3 minutes measurement results, classrooms of the building A and B of Engineering were high CO<sub>2</sub> concentrations and then, 90 minutes measurement was performed in three classrooms of the building A and three classrooms of the building B of Engineering. And one classroom built by woods for the Tourism and two large classrooms for the Basic Education were also studied by 90 minutes measurement. Comparing winter and spring condition, the 90 minutes measurements were performed in December 2013 and January 2014, and April, May and June 2014 for 9 classrooms and 43 total times.

Fig. 4 showed CO<sub>2</sub> concentration change with time of G102 classroom with 970 m<sup>3</sup> volume of the Basic Education under both aired and no aired conditions. Solid rhombus was no ventilation condition with 82 people and open square was ventilation condition with 70 people. Under no ventilation condition, CO<sub>2</sub> concentration increased with time and the increase rate was 6 ppm per minutes. The start CO<sub>2</sub> concentration was high, 1600 ppm and finally, CO<sub>2</sub> concentration reached 2200 ppm. On the other hand, with ventilation by opening a door, the start CO<sub>2</sub> concentration was low, 800 ppm

and it kept low concentration and finally decreased to 700 ppm. The door size was 2.0 m height and 1.0 m width. Then, it was very useful for reducing CO<sub>2</sub> concentration by opening door.

Fig. 5 showed CO<sub>2</sub> concentration change with time of A203 classroom with 530 m<sup>3</sup> volume of building A of Engineering under both aired and no aired conditions. Solid rhombus with 58 people and square with 80 people were no ventilation condition and open triangle with 76 people was ventilation condition opening a door with 2.0 m height and 1.0 m width. However, CO<sub>2</sub> concentration under both ventilated and no ventilated condition increased with time and the increase rate was almost the same. The maximum CO<sub>2</sub> concentration was 4500 ppm.

Fig. 6 showed CO<sub>2</sub> concentration change with time of B203 classroom with 250 m<sup>3</sup> volume of building B of Engineering under both aired and no aired conditions. The people number was about 40 each time. Under no ventilation condition, CO<sub>2</sub> concentration increased with time and the increase rate was 22 ppm per minutes. The start CO<sub>2</sub> concentration was 700 ppm and finally, CO<sub>2</sub> concentration reached 2500 ppm. On the other hand, with ventilation (4/24) by opening a door with 2.0 m height and 1.0 m width, the start CO<sub>2</sub> concentration was 1000 ppm and CO<sub>2</sub> concentration kept 1200 ppm. With ventilation (5/22) by opening a door and window both with 2.0 m height and 1.0 m width, the start CO<sub>2</sub> concentration was 600 ppm and CO<sub>2</sub> concentration kept 600 ppm. With ventilation (6/5) by opening two doors with 2.0 m height and 1.0 m width, the start CO<sub>2</sub> concentration was 700 ppm and CO<sub>2</sub> concentration kept less than 1000 ppm. Therefore, under no ventilation condition, CO<sub>2</sub> concentration reached 2500 ppm and decreased 1500 ppm by ventilation with opening a door. Two doors and both one door and one window were able to keep less than 1000 ppm. Then, CO<sub>2</sub> concentration was thought to depend on people number, classroom size and ventilation method.

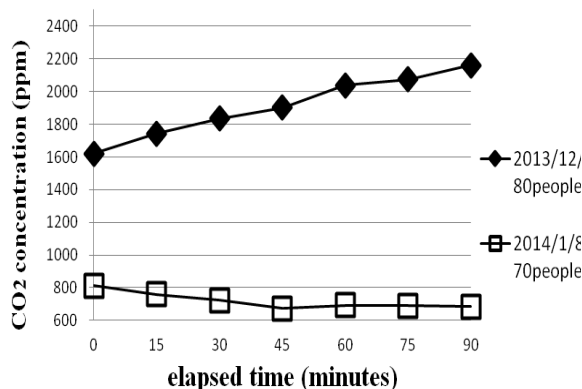


Fig. 4 Measurement result of G102 classroom

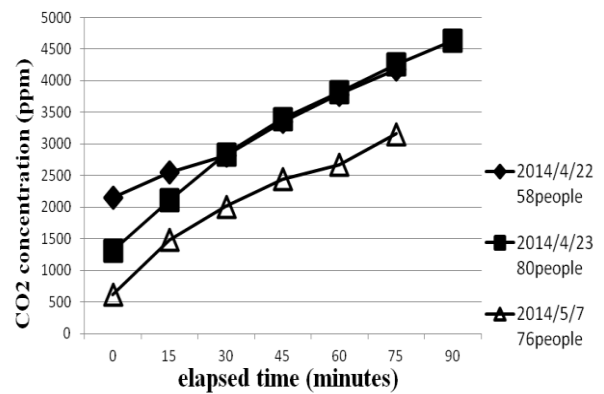


Fig. 5 Measurement result of A203 classroom

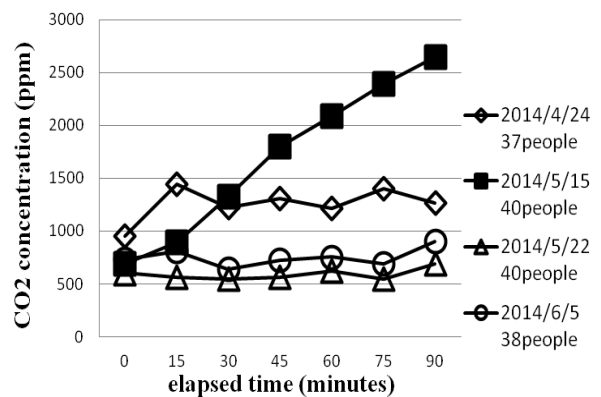


Fig. 6 Measurement result of B203 classroom

Next, under no ventilation condition, CO<sub>2</sub> concentration was estimated by people number, time, and size of classroom. Then, CO<sub>2</sub> concentration increase from the start to the end of lecture was defined by the following equation. CPPT in classroom is CO<sub>2</sub> production volume (10<sup>-6</sup> m<sup>3</sup>/people/minute) per people number per unit time.

*CPPT in classroom*

$$\begin{aligned}
 & \frac{(\text{End CO}_2 \text{ concentration} - \text{Start CO}_2 \text{ concentration})}{\text{Volume of classroom (m}^3\text{)}} \\
 &= \frac{\text{Number of people (people)} * \text{Lecture time (min)} * 10^6}{\dots(1)}
 \end{aligned}$$

The relationship between CO<sub>2</sub> concentration at the start time and CPPT in classroom for 11 no ventilation classrooms in winter and for 7 no ventilation classrooms in spring are shown in Fig. 7 and Fig. 8. CPPT for university student is generally 370\*10<sup>-6</sup> m<sup>3</sup>/people/minute [2]. The value is average per day including exercise for walking. CPPT for rest

time is smaller than CPPT for exercise time and people condition in classroom is rest time. Then, the maximum CPPT in classroom was thought to be in agreement with CPPT for rest time. However, CPPT in classroom calculated in this measurement is variable from  $10 \times 10^{-6}$  to  $250 \times 10^{-6}$  m<sup>3</sup>/minutes/people. The difference between both values was thought to be lack of airtightness for classroom or heterogeneous concentration. Airtightness for classroom is a gap wind even if door and window closed [3]. Even under no ventilation condition, students sometimes opened door during lecture and then exchanged air outside. Measurement point in classroom was just one back side of the classroom. Then, the measured concentration may not be necessary an average value.

Under no ventilation condition, most of CO<sub>2</sub> concentrations in classroom were over 1000 ppm. Next, effect of ventilation on CO<sub>2</sub> concentration of classroom was studied.

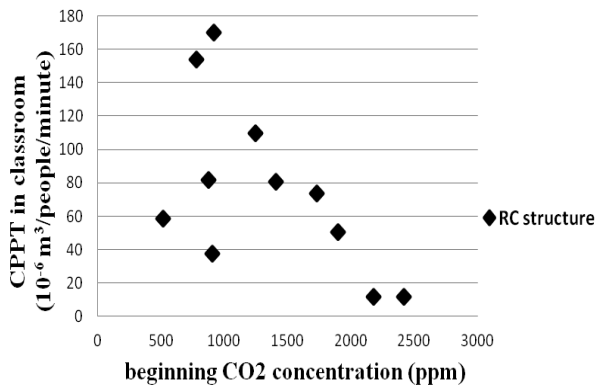


Fig. 7 Beginning CO<sub>2</sub> concentration and CPPT in winter

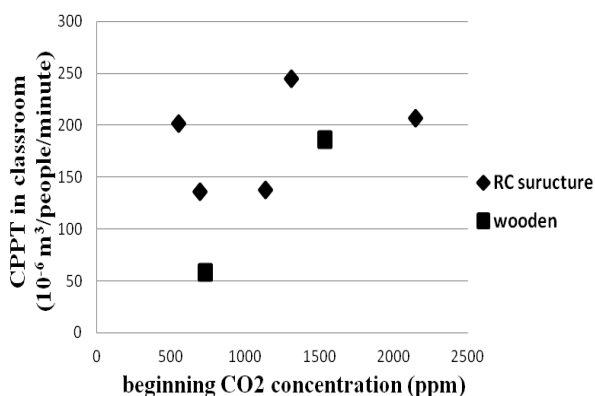


Fig. 8 Beginning CO<sub>2</sub> concentration and CPPT in spring

Fig. 9 and 10 showed relationship between the MAX CO<sub>2</sub> concentration during lecture and population density in winter and in spring. Solid marks were no ventilation and open marks were

ventilation conditions with regression lines for each type of ventilation.

Fig. 9 showed the MAX CO<sub>2</sub> concentration and population density in winter. The ventilation in winter was opening one door with 2.0 m height and 1.0 m width in winter. As population density increased, the MAX CO<sub>2</sub> concentration under both no ventilation and one door ventilation conditions also increased proportionally. Slope, the maximum CO<sub>2</sub> concentration per population density indicated airtightness in classroom and when the value was 0, air exchange is thought to be sufficient and CO<sub>2</sub> concentration does not increase. Slope of regression lines under no ventilation condition and under one door ventilation condition were  $14000 \times 10^{-6}$  m<sup>3</sup>/people and  $7800 \times 10^{-6}$  m<sup>3</sup>/people respectively.

Fig. 10 showed the MAX CO<sub>2</sub> concentration and population density in spring. There were three types of ventilation, one door, two doors, and one door and one window with 2.0 m height and 1.0 m width in spring. Slope of regression line for no ventilation is  $21000 \times 10^{-6}$  m<sup>3</sup>/people. Slope of regression lines for ventilation were  $6000 \times 10^{-6}$  m<sup>3</sup>/people with one door,  $3500 \times 10^{-6}$  m<sup>3</sup>/people with two doors, and  $1500 \times 10^{-6}$  m<sup>3</sup>/people with one door and one window.

Comparing winter and spring, slope of regression line ( $14000 \times 10^{-6}$  m<sup>3</sup>/people) under no ventilation condition in winter was lower than those ( $21000 \times 10^{-6}$  m<sup>3</sup>/people) in spring because some winter results may be controlled by air conditioner. It is difficult to confirm air conditioned or not because room is automatically controlled. Then, spring slope value was thought to be representative value,  $21000 \times 10^{-6}$  m<sup>3</sup>/people under no ventilation condition.

Slope of regression line ( $7800 \times 10^{-6}$  m<sup>3</sup>/people) under one door ventilation condition in winter was higher than those ( $6000 \times 10^{-6}$  m<sup>3</sup>/people) in spring. Under same opening space, comparing two doors and one door and one window open condition, slope of regression line ( $3500 \times 10^{-6}$  m<sup>3</sup>/people) under two doors ventilation condition was higher than those ( $1500 \times 10^{-6}$  m<sup>3</sup>/people) under one door and one window ventilation condition. Opening window was more effective for ventilation.

The slope difference between under no ventilation condition and ventilation condition was ventilation effect. Fig. 11 showed ventilation effect, the difference between  $21000 \times 10^{-6}$  m<sup>3</sup>/people and each ventilated slope value and opening area. When opening area is 0, the effect is 0. Then, regression curve was calculated from origin and ventilation effect results. Two regression curves were calculated because results were variable. When the effect is  $21000 \times 10^{-6}$  m<sup>3</sup>/people, CO<sub>2</sub> concentration does not increase. From the regression curve, opening area is estimated to be 4.9 to 6.3 m<sup>2</sup> when the effect is  $21000 \times 10^{-6}$  m<sup>3</sup>/people. The estimated opening area for keeping no CO<sub>2</sub> concentration increase was 4.9 to 6.3 m<sup>2</sup> based on the maximum CO<sub>2</sub> concentration

results. Next, from CO<sub>2</sub> concentration increase during lecture and population density, opening area for keeping no CO<sub>2</sub> concentration increase is estimated.

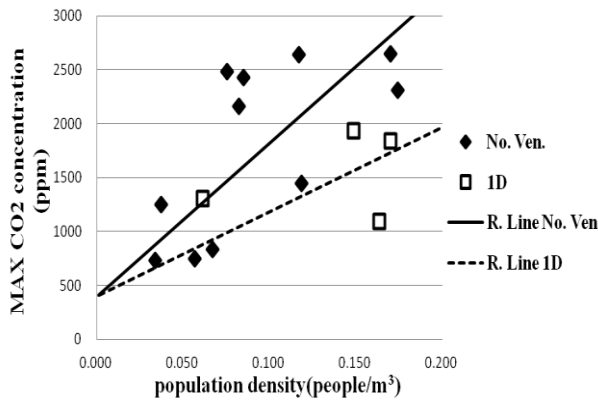


Fig. 9 MAX CO<sub>2</sub> concentration and population density in winter

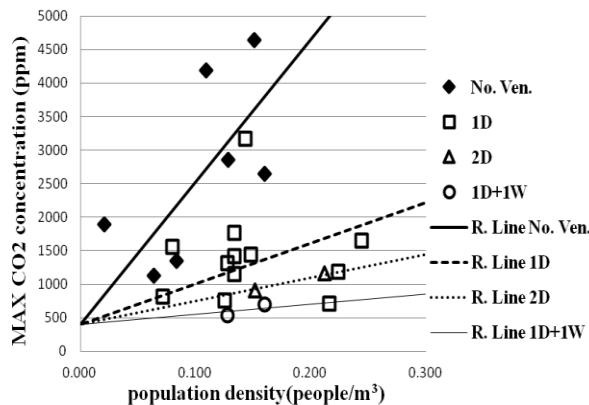


Fig. 10 MAX CO<sub>2</sub> concentration and population density in spring

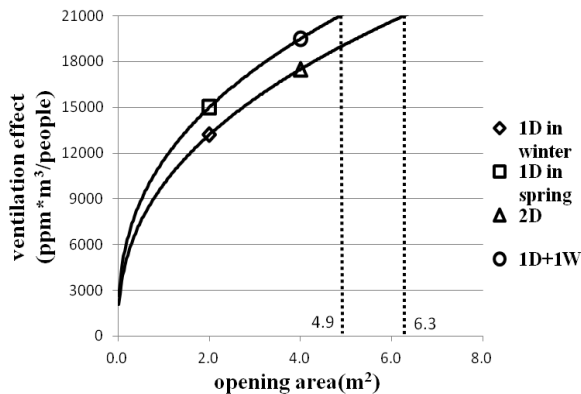


Fig. 11 Effect of ventilation by opening area approached from MAX CO<sub>2</sub> concentration

Next, Fig. 12 and 13 showed relationship between the CO<sub>2</sub> concentration increase during lecture and population density on the basis of the result of 90 minutes measurement in winter and in spring.

Fig. 12 showed the CO<sub>2</sub> concentration increase and population density in winter. As population density increased, the CO<sub>2</sub> concentration increase under both no ventilation and one door ventilation conditions also increased proportionally. Slope of regression lines under no ventilation condition and under one door ventilation condition were  $5000 \times 10^{-6}$  m<sup>3</sup>/people and  $1900 \times 10^{-6}$  m<sup>3</sup>/people respectively.

Fig. 13 showed the CO<sub>2</sub> concentration increase and population density in spring. Slope of regression line for no ventilation is  $15000 \times 10^{-6}$  m<sup>3</sup>/people. Slope of regression lines for ventilation were  $2300 \times 10^{-6}$  m<sup>3</sup>/people with one door,  $920 \times 10^{-6}$  m<sup>3</sup>/people with two doors, and  $90 \times 10^{-6}$  m<sup>3</sup>/people with one door and one window in spring.

Comparing winter and spring, slope of regression line ( $5000 \times 10^{-6}$  m<sup>3</sup>/people) under no ventilation condition in winter was lower than those ( $15000 \times 10^{-6}$  m<sup>3</sup>/people) in spring because some winter results may be controlled by air conditioner. It is difficult to confirm air conditioned or not because room is automatically controlled. Then, spring slope value was thought to be representative value,  $15000 \times 10^{-6}$  m<sup>3</sup>/people under no ventilation condition.

Slope of regression line ( $1900 \times 10^{-6}$  m<sup>3</sup>/people) under one door ventilation condition in winter was higher than those ( $2300 \times 10^{-6}$  m<sup>3</sup>/people) in spring. Under same opening space, comparing two doors and one door and one window open condition, slope of regression line ( $920 \times 10^{-6}$  m<sup>3</sup>/people) under two doors ventilation condition was higher than those ( $90 \times 10^{-6}$  m<sup>3</sup>/people) under one door and one window ventilation condition. Opening window was more effective for ventilation based on the CO<sub>2</sub> concentration increase results.

Fig. 14 showed ventilation effect, the difference between  $15000 \times 10^{-6}$  m<sup>3</sup>/people and each ventilated slope value and opening area. Regression curve was calculated from origin and ventilation effect results. Two regression curves were calculated because results were variable. When the effect is  $15000 \times 10^{-6}$  m<sup>3</sup>/people, CO<sub>2</sub> concentration does not increase. From the regression curve, opening area is estimated to be 4.2 to 6.2 m<sup>2</sup> when the effect is  $15000 \times 10^{-6}$  m<sup>3</sup>/people. The estimated opening area for keeping no CO<sub>2</sub> concentration increase was 4.2 to 6.2 m<sup>2</sup> based on the CO<sub>2</sub> concentration increase results.

The opening areas calculated from the maximum CO<sub>2</sub> concentration and CO<sub>2</sub> concentration increase results respectively were almost the same values, 4.2 to 6.3 m<sup>2</sup>. Opening door or window area to keep no CO<sub>2</sub> concentration increase in the classroom is at least 4.2 to 6.3 m<sup>2</sup>.



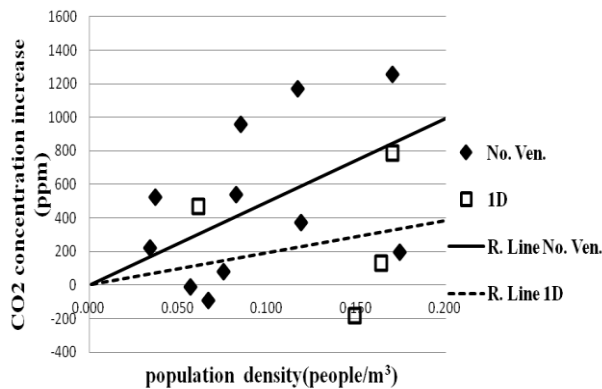


Fig. 12 CO<sub>2</sub> concentration increase and population density in winter

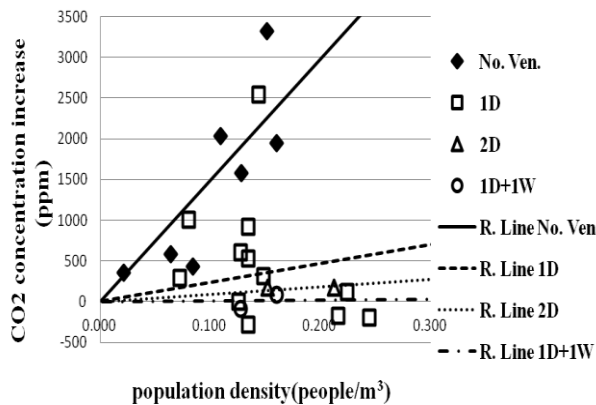


Fig. 13 CO<sub>2</sub> concentration increase and population density in spring

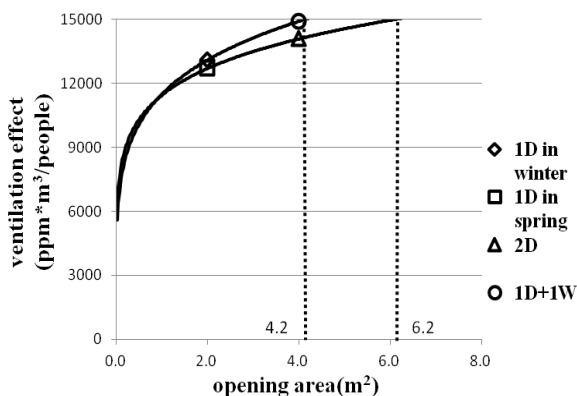


Fig. 14 Effect of ventilation by opening area approached from CO<sub>2</sub> concentration increase

## CONCLUSION

Most classrooms in Wakayama University were not satisfied with comfortable CO<sub>2</sub> concentration. It

is very difficult to maintain less than 1000 ppm without ventilation and CO<sub>2</sub> concentration in some classroom reached over 4000 ppm. From CO<sub>2</sub> concentration for classroom under no ventilation condition, CO<sub>2</sub> production volume per people number per unit time (CPPT) was estimated. The estimated CPPT value in classroom was less than general CPPT value for university student. The difference between both values was thought to depend on lack of airtightness for the classroom such as opening door during lecture. Therefore opening door was thought to be useful for ventilation and then influence of opening door and window on CO<sub>2</sub> concentration in classroom was studied. Comparing CO<sub>2</sub> concentrations under no ventilation condition and ventilation condition opening door or window, ventilation effect was calculated from CO<sub>2</sub> concentration, classroom volume, number of people, and time. The relation between ventilation effect and opening area by door or window was studied. When total area to open door or window in the classroom is at least 4.2 to 6.3 m<sup>2</sup> (one door and one window, two windows), CO<sub>2</sub> concentration in the classroom with volume of 250 to 930 m<sup>3</sup> does not increase.

## REFERENCES

- [1] Noriko Ochiai, Kazunari Yamashita: (2010) Indoor carbon dioxide of Shimane University lecture room and control of air quality
- [2] Homepage of Ministry of Education, Culture, Sport, Science and Technology
- [3] Song SungKi: (2003) Research on the prediction of air conditioning heat load for large space buildings
- [4] Daisuke Kobayashi: (2007) A study on the influence of environment in the classroom brings to children
- [5] Taemi Gohara, Tuyoshi Iwashita: (2002) The indoor air condition measured in elementary school in Kagoshima city

## **ATTENUATION LANDFILL POTENTIAL EVALUATION FOR A MILLENNIUM CITY, IN NIGERIA**

Oluwapeluimi O. Ojuri<sup>1</sup>

<sup>1</sup>Department of Civil and Environmental Engineering, Federal University of Technology, Akure, Nigeria

### **ABSTRACT**

Akure has been selected as a millennium city in Africa by the United Nations Millennium Development Initiative. This research was carried out to study the geotechnical considerations in the design of sanitary landfill, attenuation option for Akure Metropolis, where a dumpsite has been in use for several years. On site investigation and laboratory tests were conducted on depth discrete soil samples up to 3.0 metres depth, to see how suitable the site is, based known engineering regulation for design of an attenuation sanitary landfill. The Cation Exchange Capacity (CEC) values for the site ranged between 9.02 to 10.73 milli-equivalents/100g (Meq./100g) for Na<sup>+</sup>, K<sup>+</sup>, Ca<sup>++</sup>, Mg<sup>++</sup>, and the highest PH value was 7.25. The fines content of the samples ranged from 29.0 to 33.0%. The average unconfined compressive strength of the soil from the unconsolidated undrained triaxial test was 270.0 kN/m<sup>2</sup>, which is adequate for bearing capacity consideration. The coefficient of permeability value ranged between  $2.2 \times 10^{-4}$  and  $4.0 \times 10^{-3}$  cm/sec for all the soil samples tested beneath the dumpsite up to 3.0 metres depth. The attenuation layer of a sanitary landfill should be designed using a low permeability clay-rich soil (hydraulic conductivity  $<10^{-3}$  cm/s), enabling leachate to percolate slowly downwards, simultaneously undergoing attenuation by biodegradation, sorption, filtration and ion exchange. The optimum permeability for attenuation should be in the order of  $10^{-4}$  to  $10^{-6}$  cm/s. The potential for implementing an attenuation landfill at this site is high based on the investigation conducted.

*Keywords: Attenuation landfill, Cation Exchange Capacity, PH, Coefficient of permeability, Specific gravity*

### **INTRODUCTION**

Akure, a growing urban area within latitudes 7° 10'N and 7° 20'N and between longitudes 5° 07'E and 5° 17'E in Ondo State, Southwestern Nigeria was chosen for this research work because it is one of the few towns in Africa and the only one in Nigeria selected as a millennium city by the United Nations Millennium Development Initiative [1]. The contributions of modern sanitary landfills to effective solid waste management in any nation cannot be overemphasized. Control and management of Leachate generated from waste and its associated contaminating effect on groundwater table with related public health issues is one of the major challenges of sanitary landfill design and operation. Two different design strategies are adopted for Leachate treatment and control in sanitary landfills, they are: containment and treatment of Leachate on site and attenuation through degradation, dilution and dispersion of Leachate. Containment requires that all liquid and gaseous emissions produced within the landfill are contained and collected for treatment. The central aim of containment is, therefore, to minimize production of Leachate by restricting access of rainwater to the waste, and to prevent its migration from the landfill of leachate produced. This is accomplished by enclosing the

waste in artificial lining systems consisting of a landfill liner and cap. As a consequence, Leachate drainage systems, containment ponds and leachate treatment facilities are essential additional components of modern containment landfills. Experience has shown that artificial membranes will eventually leak so modern designs usually include composite two, three- and four-layer multi-barrier clay/membrane liner systems. These multi-barrier systems consist of sheets of artificial membrane, most commonly high-density polyethylene, inter layered with natural or bentonite-enriched clay layers [2], [3]. In the European Union for example, landfill regulations make it mandatory to entomb waste using engineered lining systems except at sites with low in-situ hydraulic conductivity (less than  $10^{-9}$  m/s) [4]. Leachate containment with engineered lining systems requires a suitable geological sub-base as a secondary barrier to groundwater when containment structures become permeable. Leakage can result from stress cracking of the membrane, cracking under cold conditions, damage, particularly from stones in the protection layer and from heavy dumping equipment, or failure of the membranes near welded seams [5]. Synthetic liners are also susceptible to failure if installation is not subject to

strict quality controls and favourable weather conditions [6]. Indeed, it is unlikely that any manufactured synthetic membrane is completely free of defects even prior to installation [7]. Lastly, some contaminants are able to diffuse through installed liners including intact geotextiles [8].

A key attraction of an attenuation strategy is avoidance of the excessive costs of containment landfills that are untenable for many developing countries. It also avoids the long-term costs for maintenance and aftercare monitoring, which may be required for containment landfills for decades or even centuries after the site has ceased operating, as long as the waste remains active. Apart from a drainage system and containment ponds to control the leachate head in order to prevent shock loading of the attenuating medium and a monitoring programme, attenuation landfills have little attendant costs. The key constraint of the attenuation strategy, however, is the uncertain but genuine risk of groundwater pollution by leachate if attenuation proves less effective than assumed when selecting the site or if the site is not adequately managed (e.g. with respect to drainage measures).

Little attention has been paid to the siting of landfills. Landfills tend to be located close to urban areas where significant volumes of municipal and industrial wastes are produced. It is safest to position landfills in areas removed from groundwater, drinking-water supply sources and on sites where the underlying geology is able to attenuate to some degree the Leachate that is generated from the stored wastes. Clay and organic-rich materials (overburden or mudstone bedrock) are suitable as they both retard groundwater flow and interact with reactive contaminants in leachate. Unfortunately, it is commonly difficult to choose such ideal locations strictly on the basis of hydro- geological considerations as socio-economic considerations, including the 'not in my back yard' syndrome, tend to dominate the process of selection of landfill sites. [9] notes that landfills and dumps in Africa commonly occur in poorer areas, where residents are often less able to prevent landfill siting in their own backyard, are unlikely to benefit from waste collection services, and invariably depend upon local, often poorly protected sources of water.

## MATERIALS AND METHODS

### Study Area

Akure is a growing urban area within latitudes 7° 10'N and 7° 20'N and between longitudes 5° 07'E and 5° 17'E in Ondo State, Nigeria. The mean annual temperature ranges between 24°C -27°C, while the annual rainfall varies between 1500mm and 3500mm. Initially in Akure, the local government authority was solely responsible for waste collection,

The attenuation strategy allows leachate to migrate outwards from the landfill and takes advantage of the natural subsurface processes of biodegradation, filtration, sorption and ion exchange to attenuate the contaminants in leachate. The attenuation strategy is based on the dilute and disperse principle of leachate management proposed by [10]. Natural geological barriers, may be defined as low permeability clay-rich geological units (hydraulic conductivity  $<10^{-5}$  m/s), which can perform the function of an attenuating layer, enabling leachate to percolate slowly downwards, simultaneously undergoing attenuation by biodegradation, sorption, filtration and ion exchange processes with the clays in the unit [11]. Extremely low permeability geological units (hydraulic conductivity  $<10^{-9}$  m/s) cannot fulfill an attenuation function as they perform in a similar manner to artificial or natural lining systems providing almost complete containment of all emissions. Similarly, geological units with higher permeability (hydraulic conductivity  $>10^{-5}$  m/s) do not provide sufficient confinement to leachate and are thus unsuitable for attenuation. The optimum permeability for attenuation is in the order of  $10^{-6}$  to  $10^{-8}$  m/s [12]

The critical difference between the modern attenuation approach and the former dilute and disperse approach is that attenuation is an active management strategy, requiring the presence of a natural in situ or imported attenuation barrier to attenuate the leachate, whereas dilute and disperse relied on passive subsurface dilution and dispersion processes without the presence of a specific attenuation layer. Although the concepts are similar, it is now recognized that dispersion and dilution alone may not sufficiently attenuate leachate to adequately protect groundwater. More recent studies support the conclusion that clay-rich overburden and mud-rocks have the capacity to attenuate Leachate. The effectiveness of the strategy is further confirmed by the fact that even within geological units of relatively high permeability and supposedly poor attenuation potential, such as sandstone, and sandy overburden, attenuation processes operate very effectively, and most pollutants are moderated within a few hundred metres [7], [13], [14], [15].

transportation, disposal and street sweeping until 1999 when the Ondo State Waste Management Authority (OSWMA) was established as a state government intervention agency. From 1999, curbside and door-to-door collection using government supplied storage facilities or dustbins replaced the communal system. The Government later acquired 7 hectares (17.3 acres) of land along Igbatoro Road in Akure for the purpose of establishing a modern sanitary landfill that will ensure safe and environmental friendly disposal of

solid waste generated in Akure and its environs. The land was cleared for disposal of waste generated in Akure and its surrounding towns in 2001. Fig. 1

shows the map of Akure and its environs, where waste would be generated for disposal in the proposed sanitary landfill.

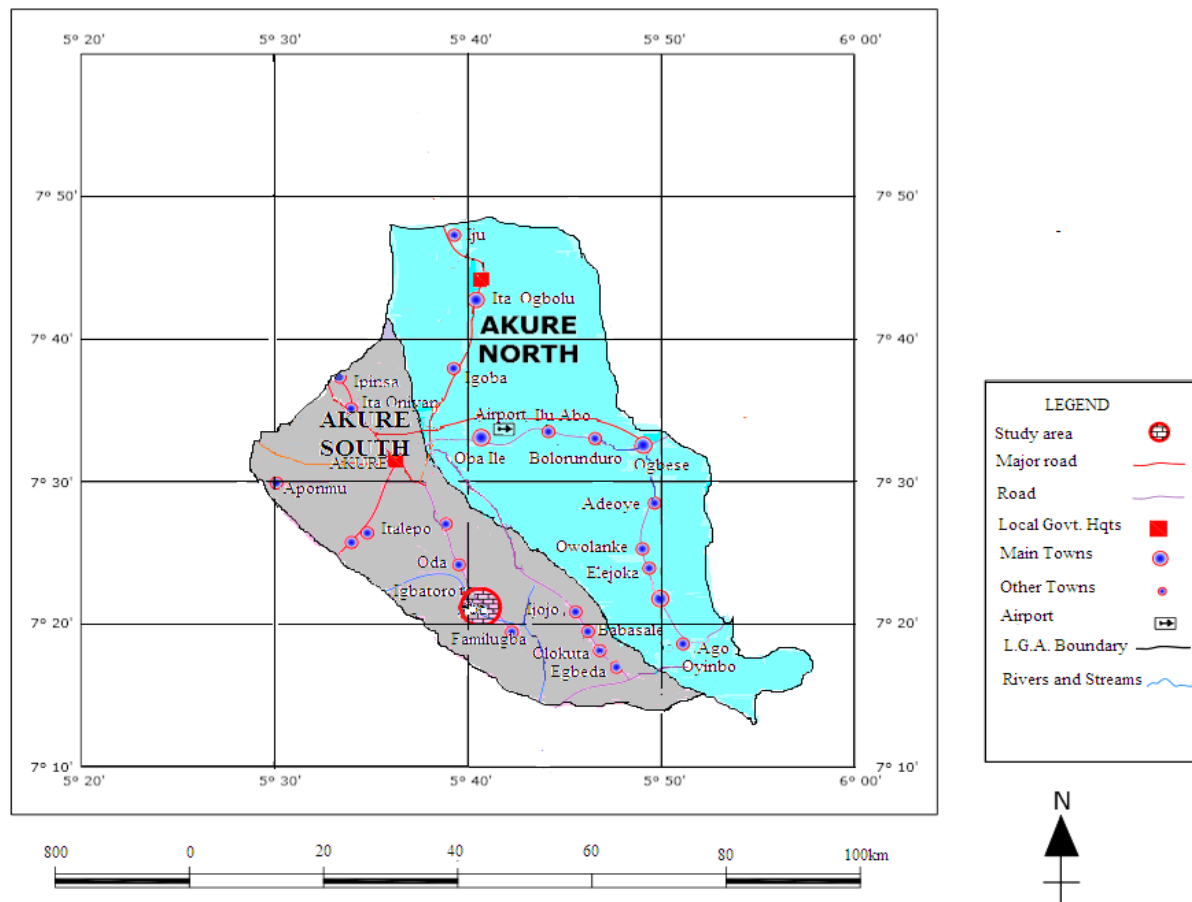


Fig. 1 Map of waste generation areas

### Soil Sampling

The soil samples were taken from test pits covering the specified area of land selected along Igbatoro road in Akure. The samples were collected at different depth from a single test pit; at a depth of 1.5m, 2.0m and 3.0m. Samples from 1.5m, 2.0m and 3.0m depths of various test pits were grouped together and labelled as sample 1, sample 2, and sample 3 respectively. Each of the three soil samples was stored in separate air tight polythene bag to preserve its natural moisture content. They were thereafter taken to the geotechnical laboratory of the Federal University of Technology Akure, where geotechnical tests were carried out on them.

### Methodology

Tests were carried out to determine the suitability of the soil layers from which the samples were taken for functioning as attenuation layers of an

attenuation landfill. The tests are grouped into three classes namely; index property geotechnical tests, geochemical tests, and hydraulic conductivity evaluation test. The tests were carried out in accordance with [16] and [17]. Basic geotechnical characterization tests conducted on the soil samples are; moisture content test, particle size distribution test, Atterberg's limit tests and specific gravity test. Moisture content test was carried out in accordance with section 2.3 of [15] particle size distribution was conducted in accordance with section 2.9 of [16] Atterberg's limit was determined in accordance with sections 2.4 and 2.5 of [16] while, specific gravity was conducted in accordance with section 2.8 of [16]. Geochemical tests that were conducted on the soil samples are pH test and Cation Exchange Capacity (CEC) test; pH test was conducted in accordance with section 3 of [16] while CEC test was conducted in accordance with [17]. The pH values of the soil samples are shown in Table I. PH is the measurement of acidity or alkalinity of a

substance. The exchangeable ions are:  $\text{Na}^+$ ,  $\text{K}^+$ ,  $\text{Ca}^{++}$  and  $\text{Mg}^{++}$ . Permeability test was conducted in

accordance with section 5 of [16].

## RESULTS AND DISCUSSION

### Basic Geotechnical Characterization Tests

The moisture content for soil samples was found to be between 7.2% and 17.1 %. The particle size distribution resulted in percentages passing sieve Number 200 (0.075 mm) [percentage fines] equal to 29.0% for sample 1, 34.8% for sample 2 and 35.8% for sample 3; hydrometer analysis show that, percentage clay (< 0.002 mm) for sample 1 is 11%; sample 2 has 13% percentage clay and sample 3 has 12% percentage clay; the maximum particle size in the samples was 2.5 mm. The specific gravity,  $G_s$  ranged between 2.58 and 2.62. Liquid limit and plastic limit for sample 1 are 45.0 and 25.9 respectively; sample 2 has liquid limit of 28.0 and plastic limit of 19.8; liquid limit for sample 3 was 36.0 and its plastic limit equals 27.9. The plasticity index results show sample 1 to be of medium plasticity, while sample 2 and 3 are of low plasticity. Although the detailed requirements for an attenuation layer vary, the following criteria usually apply: Minimum layer thickness of 3m; minimum clay content of 10%; minimum fines (clay & silt) content >30%; plasticity index >10% and <65%; liquid limit < 90% and maximum particle size of 75mm (USEPA) [12]. The percentage clay content in samples, liquid limit and the maximum particle size in the soil samples are in consonance with USEPA requirements for attenuation layer materials, however plasticity index falls below the requirements for sample 2 and sample 3.

### Geochemical Tests

Geochemical tests conducted on the soil samples are cation exchange capacity (CEC) and pH tests. The CEC is an expression of the number of cation absorption per unit weight of soil. It is defined as the sum total of exchangeable cations absorbed, expressed in milli-equivalents/100g (Meq./100g) of oven dry soil. The results show an increase in CEC value with increase in sample depth. Sample 1 has average CEC of 9.02 Meq./100g, sample 2 has average CEC of 9.49 Meq./100g while sample 3 has average CEC of 10.73 Meq./100g; for all exchangeable ions. The typical CEC for a clayey soil or soil with considerable clay content is between 6.00 Meq./100g to about 15.00 Meq./100g of soil. The results of particle size test shows that, sample 1 contain 29.0% of fines, sample 2 contain 34.8% of fines while sample 3 contain 35.8% of fines. Comparing the typical CEC values for clay soil or soil with considerable clay content with the values of CEC obtained for the three soil samples, it can be shown that sample 1, sample 2 and sample 3 contains a considerable amount of clay content, therefore their CEC values fall within the range of values reported in literature. The ability of natural soil layers to attenuate heavy metal contaminants during the expected life span of the sanitary landfill is enhanced by the cation exchange capacity. Hence, soil samples; 1, 2 and 3 from the site has enough chemical strength to withstand the cations occurring in the Leachate. Table I shows the summary of geochemical tests. Fig. 2 shows the variation of the CEC value with clay contents.

Table I Summary of geochemical of soil samples

Samples serial number	Depth in metres	% clay content	pH values	CEC values (Meq./100g)
1	1.5	11	5.85	9.02
2	2.0	12	6.22	9.49
3	3.0	13	7.25	10.73

From Table I, the pH values of the soil samples increases with depth, the topmost layer has the lowest pH; this may be as a result of previous waste storage on the site in the past. Sample 3 which is collected at the deepest depth has the highest pH value of 7.25, which makes it slightly alkaline, this meet requirement of soil pH of 7.0 or higher for a

sanitary landfill attenuation layer. Since most of the micro-organisms are developed in the acidic environment, an alkaline medium create an unfavorable condition against the growth of the Leachate producing microbes[17].

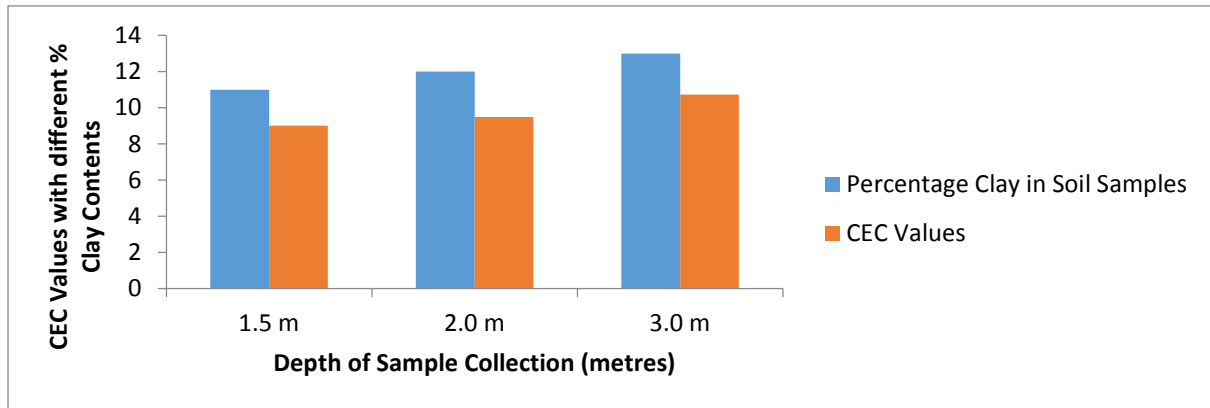


Fig. 2 Variation of CEC values with depth and percentage Clay content.

Figure 3 show the variation of pH with different percentage clay content at various sampling depth. From Fig. 3, pH value of soil samples increases with

depth, the increase may be as a result of higher concentration of acidic constituents from waste leachate on the uppermost layer.

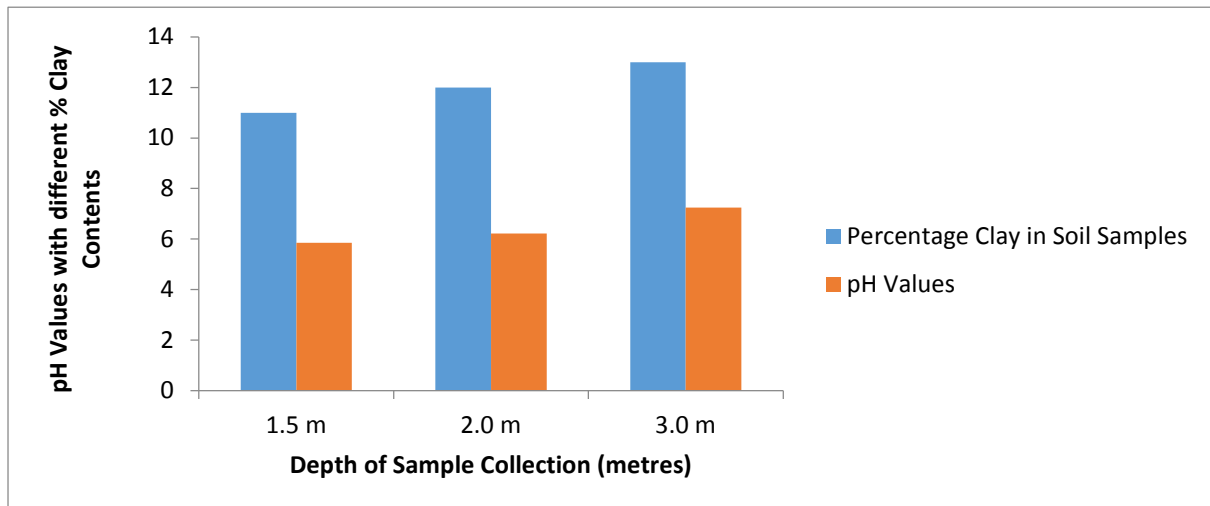


Fig. 3 Variation of pH values with percentage clay content

### Hydraulic Conductivity Evaluation Test

The major geotechnical test conducted on soil samples to assess its attenuation potential was the hydraulic conductivity (coefficient of permeability) test. Once a soil sample satisfies the permeability requirement its chemical characteristics should be determined to assist in the final decision making about site selection. The coefficient of permeability ( $k$ ) for sample 1 was  $3.09 \times 10^{-3} \text{ cm/sec}$ ;  $k$  equals  $2.22 \times 10^{-4} \text{ cm/sec}$  for sample 2 and,  $k$  for sample 3 was  $2.37 \times 10^{-3} \text{ cm/sec}$ . The optimum permeability for attenuation is in the order of  $10^{-6} \text{ cm/sec}$ – $10^{-8} \text{ cm/sec}$

*sec* [18]. Extremely low permeability geological units (hydraulic conductivity  $< 10^{-9} \text{ cm/sec}$ ) cannot fulfill an attenuation function, as they perform in a similar manner to artificial or natural lining systems, providing almost complete containment of all emissions. Similarly, geological units with higher permeability (hydraulic conductivity  $> 10^{-5} \text{ cm/sec}$ ) do not provide sufficient confinement to Leachate and are, thus, unsuitable for attenuation. Table II show the variation of the permeability with the clay content. Figure 4 shows the variation of permeability with percentage clay content in the soil sample



Table II Variation of permeability with clay content

Samples	Permeability	% Clay content	% Fines	Wet Density (kg/m <sup>3</sup> )
1	$3.09 \times 10^{-3}$ cm/sec	11	29.0	2164.5
2	$2.37 \times 10^{-3}$ cm/sec	12	34.8	1966.2
3	$2.22 \times 10^{-4}$ cm/sec	13	35.8	1926.8

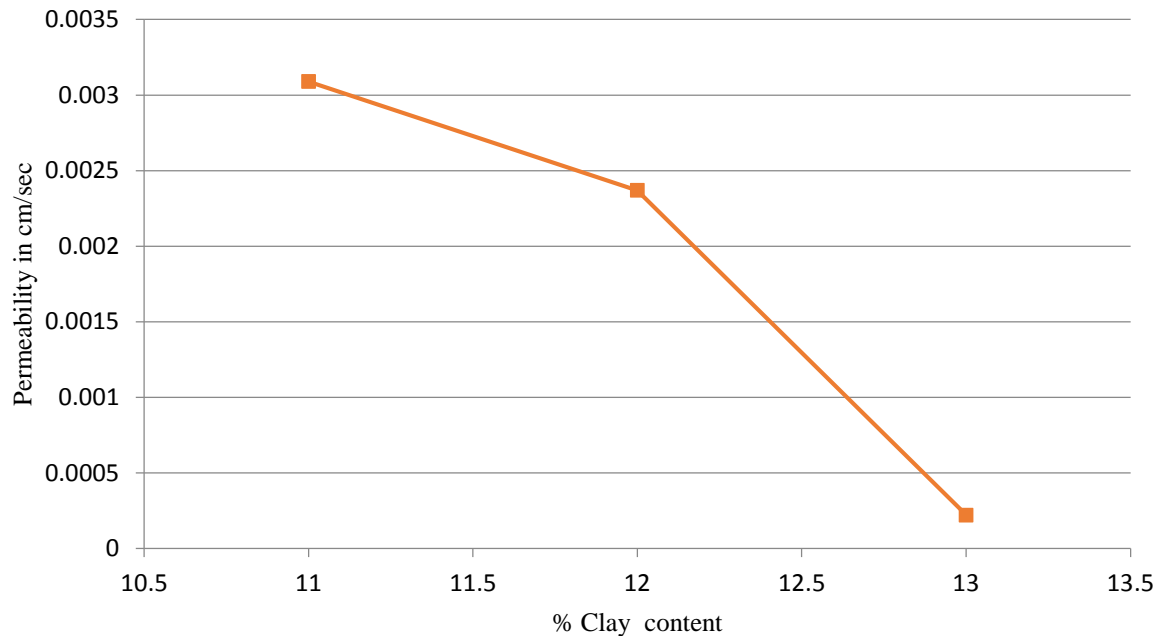


Fig. 4 Graph of permeability against percentage clay content

From the result, the permeability of soil samples reduces with increasing in clay content. This is in agreement with reduction in permeability value with particle size reported by [18]. However, there is a sharp reduction in permeability values of sample 3. This is because, the sample contain the highest percentage of silt in addition to highest clay content. The gradation of a soil and amount of fines it contain, especially its clay content is a major factor that determines the value of its permeability. Permeability test is most important test, in addition to CEC test used to determine the suitability of particular clay materials for construction of sanitary landfill attenuation layer. Even, if the materials to be adopted for the siting of an attenuation landfill do not meet all other criteria; stated in materials characterization, accurate testing is required to demonstrate that the attenuation landfill will have a field hydraulic conductivity of  $1 \times 10^{-6}$  cm/sec or less as reported by [12] in addition to a CEC value ranging between 6 Meq./100g and 15 Meq./100g. From the results, it was discovered that the soil is only adequate in CEC but not adequate in permeability. Hence, in order to use this material for attenuation purpose the materials can be improved with addition of little percentage of bentonite or by

overlaying it with other materials of suitable clay content and permeability.

## CONCLUSION

This study evaluated the attenuation potential of soil on a proposed sanitary attenuation landfill site. From the study, the pH, CEC and permeability of the soil samples collected from the site were carefully assessed. The results obtained are as follows:

- 1) The average pH of the soil at 3m below the ground surface was 7.25 (slightly alkaline). This is suitable for elimination of leachate producing microbes from getting into the water table; as most Leachate producing microbes survive well in acidic medium than in alkaline medium. The soil above this level could be removed in the process of construction.
- 2) The CEC values of the samples collected at various depths were found to range between 9.02 Meq./100g and 10.73 Meq./100g which is in agreement with the range of values reported in literature. This implies that, all the soil samples are of adequate capacity to trap the cation in the leachate from contaminating the underground water.

3) Coefficient of Permeability values of the samples are in the range of  $10^{-4} \text{ cm/sec}$  to  $10^{-3} \text{ cm/sec}$  which is inadequate for materials to be adopted as attenuation landfill site. Soils with higher clay content could be imported and mixed with the in-situ soil to satisfy the permeability requirement. Another option is the improvement of the in-situ soil with bentonite in order to meet the permeability requirement.

## ACKNOWLEDGEMENT

The authors would like to acknowledge the contributions of Ehinmitan, O. O. and Ajibade, A. A. in data collection for this work. The equipment used for this research was made available by the Department of Civil and Environmental Engineering, Federal University of Technology, Akure, Ondo State, Nigeria.

## REFERENCES

- [1] UNIDO (2008). *Millennium Cities Initiative (MCI) Investment Opportunities for Development*, p. 7 Vienna, United Nations Industrial Development Organization (UNIDO)
- [2] Seymour KJ, "Landfill's lining for leachate containment", J. Instit. Water Environ. Man., Vol. 6, 1992, pp. 389-396.
- [3] Cossu R, "The multi-barrier landfill and related engineering problems", In Proc. Sardinia 95, Fifth International Landfill Symposium, (eds. T.H. Christensen, R. Cossu and R. Stegmann), CISA Publisher, Cagliari, Vol. 2, 1995, pp. 3-26.
- [4] Allen A, "Containment landfills: the myth of sustainability", Eng. Geol., Vol. 60, 2001, pp. 3-19.
- [5] Rollin A, Mlynarek J, Lafleur J, and Zanesco A, "An investigation of a seven years old HDPE geomembrane used in a landfill", In: Proc Sardinia 91, Third International Landfill Symposium, (eds. T.H. Christensen, R. Cossu and R. Stegmann), CISA Publisher, Cagliari, 1991, pp. 667-678.
- [6] Aversch U, "Specific problems in the construction of composite landfill liner systems", In Proc. Sardinia 95, Fifth International Landfill Symposium, (eds. T.H. Christensen, R. Cossu and R. Stegmann), CISA Publisher, Cagliari, Vol. 2, 1995, pp. 115-130.
- [7] Christensen TH, Cossu R, and Stegmann R, "Principles of landfill barrier systems", In Landfilling on Waste: Barriers, (eds. T.H. Christensen, R. Cossu and R. Stegmann), 1994, pp. 3-10.
- [8] Potter HAB, and Yong RN, "Waste disposal by landfill in Britain: problems, solutions and the way forward" In Waste Disposal by Landfill, (ed. R.W. Sarsby), Balkema, Rotterdam, 1993, pp. 167-173.
- [9] Onibokun AG, "Synthesis and Recommendations; In Managing the Monster: Urban waste and governance in Africa", (eds A.G. Onibokun), IDRC, Ottawa, 1999, pp. 227-252.
- [10] Gray DA, Mather JD, and Harrison IB, "Review of groundwater pollution from waste disposal sites in England and Wales: with provisional guidelines, for future site selection", Quart. J. Eng. Geol., Vol. 7, 1974, pp. 181-196.
- [11] Allen A, "Attenuation: A Cost Effective Landfill Strategy for Developing Countries", In Engineering Geology for Developing Countries. Proc. 9th Congress of the International Association of Engineering Geology and the Environment, (eds. J.L. van Rooy and C.A. Jermy), South African Institute of Engineering Geology and the Environment, Durban, South Africa, 2002, pp. 156-167.
- [12] USEPA. (US. Environmental Protection Agency), "Municipal solid waste generation, recycling, and disposal in United State", <http://www.epa.gov/osw/nonhaz/municipal/pubs/msw06.pdf>, April 20, 2008.
- [13] Ball JM, and Novella PH, "Coastal Park landfill: leachate plume migration and attenuation", In Proc Sardinia 2003, Ninth International Landfill Symposium, (eds. T.H. Christensen, R. Cossu, and R. Stegmann), CISA Publisher, Cagliari.
- [14] Butler AP, Brook C, Godley A, Lewin K, and Young CP, "Attenuation of landfill leachate in unsaturated sandstone", In Proc. Sardinia 2003, Ninth International Landfill Symposium, (eds. T.H. Christensen, R. Cossu and R. Stegmann), CISA Publisher, Cagliari, 2003.
- [15] Williams GM, (1999) "Natural Attenuation of Contaminants in a Lacustrine Sand Aquifer at Villa Farm, UK", In Proc. Sardinia 99, Seventh International Landfill Symposium, (eds. T.H. Christensen, R. Cossu and R. Stegmann), CISA Publisher, Cagliari, Vol. 4, 1999, pp. 229-236.
- [16] British Standard Institute: BS1377, "Methods of Testing for Soils for Civil Engineering purposes", British Standard Institute, London, 1990.
- [17] ASTM D7503. "Standard Test Method for Measuring Exchange Complex and Cation Exchange Capacity of Inorganic Fine-Grained Soils", *Annual Book of ASTM Standards*, in review, ASTM International, West Conshohocken, PA, 2010.
- [18] Pichtel J, "Waste Management Practice; Municipal, Hazardous, and Industrial" Taylor & Francis Group New York, 2005.
- [19] ASTM (American Society of Testing and Materials), "Annual Book of Standards", West Conshohocken, P A, 1987.

## **SITE REMEDIATION IN NIGERIA: PROVEN AND INNOVATIVE TECHNOLOGIES (RECOVERY OF FREE HYDROCARBON FROM SOIL/GROUNDWATER)**

Oluwapelumi O. Ojuri<sup>1</sup> Samuel A. Ola<sup>1</sup> Olaolu G. Fadugba<sup>1</sup> and Micheal A. Uduebor<sup>1</sup>

<sup>1</sup>Department of Civil and Environmental Engineering, Federal University of Technology, Akure, Nigeria

### **ABSTRACT**

This research is concerned with geo-environmental impact assessment and remediation of contaminated soil/groundwater. The specific study site is Baruwa community (Latitude 06° 35' 12" N, Longitude 03° 16' 21" E), in Alimosho Local government area of Lagos state, Nigeria. The estimated 65,000 people of Baruwa own about 350 hand dug wells for domestic water supply; more than 200 of these wells are at present, under lock and key because of the oil seepage from leaking underground NNPC (Nigerian National Petroleum Corporation) pipeline. The Geoenvironmental Engineering research group in F.U.T.Akure, started Geoenvironmental site assessment, geotechnical, background and natural attenuation studies for the site in 2006. This has enabled delineation of the contaminated zone. Eight (8) hydrocarbon recovery/monitoring wells (W16, W17, W18, W19, W20, W42, W43, and W44) and two bore holes (W401 and W402) were used for the pilot recovery test. Existing contaminated water supply wells were used as hydrocarbon recovery/monitoring wells to minimize cost. Two boreholes were installed for soil vapour extracting and gas surveys in addition to the eight existing wells within the 100m x 100m designated pilot test area. We have already established that water supply wells are covered by pure phase leaking hydrocarbon products from the underground pipes. Tested well waters had been found to be as much as 95 percent petrol and up to 600 mm thickness of free hydrocarbon product on top of the ground water. Volumetric characterization of the pure phase hydrocarbon using Oil/Water Interface meter/ areal measurements and monitoring together with assessment of various technologies (Natural Attenuation, In Situ Chemical Oxidation and Bioremediation) for remediation was implemented for this site.

*Keywords: Petroleum hydrocarbon, Volumetric characterization, Remediation, Pilot test, Innovative Technologies*

### **INTRODUCTION**

The Geoenvironmental Engineering research group in Federal University of Technology, Akure (FUTA), started Geoenvironmental site assessment, geotechnical, background and natural attenuation studies for the site in 2006. The site is now basically characterized with water table contour maps/direction of groundwater flow, liquid hydrocarbon thickness contour map, periodic hydrocarbon isoconcentration maps, periodic geochemical parameter test data and geotechnical/stratigraphic profiles from geophysical and geotechnical data [1]. This has enabled delineation of the contaminated zone and identification of the likely source of hydrocarbon contamination. Numerical modeling has also been used to predict a period of about 48 years for the natural attenuation of hydrocarbon contaminants at this site [2][3]. The prevalence of the casual handling of petroleum hydrocarbon storage, distribution and dispensing facilities (underground tanks, pipelines and gasoline stations) in developing countries like Nigeria

necessitates focus of this study. This is highly relevant in the light of the increasing awareness of the precarious trend of lack of monitoring and remedial feasibility data for the subsoil environment in the thousands of gasoline fuel stations, and petroleum storage/distribution underground infrastructure in Nigeria. In Nigeria, 335,200 deaths occur annually from sanitation, water and hygiene related infections, signifying a 16.7% of total deaths from all sources. This is indicated in the World Health Organization, country-by-country data on the burden of water, sanitation and hygiene related deaths globally [4]. There is now an urgent need to scientifically harness both human and material resources especially in the emerging field of geoenvironmental engineering in order to meet the target 10 (Halve, by 2015, the proportion of people without sustainable access to safe drinking water and basic sanitation) of the pertinent Millennium Development Goal (Goal 7 – Ensure Environmental Sustainability).

FUTA has a mandate to appropriate technology for environmental sustainability through effective management of environmental (air, water and land) resources in order to have a direct impact on the immediate community and the country at large. Effective management of our environmental resources would certainly contribute to the eradication of extreme poverty and hunger, and ultimately ensure environmental sustainability, thereby addressing goals number one (1) and number seven (7) of the United Nations' Millennium Development Goals (MDG) [5].

## METHODOLOGY

### Description of the Study Area

The case study site is Baruwa community in Alimosho Local government area of Lagos state (Latitude 6[degrees] 35' N, Longitude 3[degrees] 16' E). The height above the sea level is about 42meters (141 feet). The neighboring towns near the community to the East are Kadara and Akinogun while Fatode and Oduwale are to the south. It has an abundant rainfall of over 2,000 millimeter per year. "BARUWA" is a Lagos suburb Community in Alimosho Local Government Area of Lagos State; South Western Nigeria (Figure 1a). The community is located between the famous Iyana Ipaja and Ikotun. The petroleum hydrocarbon contaminated site is approximately 940m x 740m in size, within which a pilot scheme area of 100m x 100m is earmarked(Figure1b).

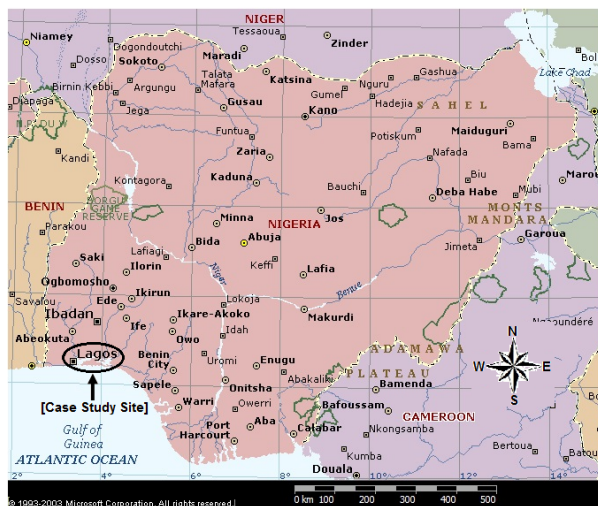


Fig.1a. Map of Nigeria showing Lagos the case study site.

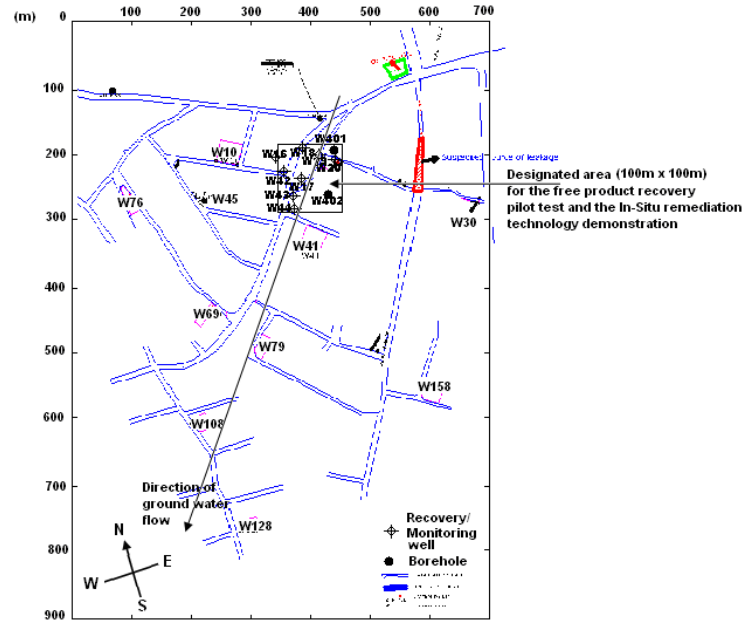


Fig. 1b: Field site (Baruwa, Nigeria) diagram showing location of free product recovery pilot test/In-situ remediation demonstration area.

The estimated 65,000 people of Baruwa own about 350 hand dug wells for domestic water supply and more than 200 of these wells are at present, under lock and key because of the oil seepage from leaking underground NNPC (Nigerian National Petroleum Corporation) pipeline. The Baruwa community is a predominantly residential setting. Majority of the people within this area depend on the groundwater for their survival. Farming was their main occupation until civilization and development brought in diverse infrastructure to the community. This community suffered from the ruptured pipelines of NNPC/PPMC between 1994 and 1996. The leakage went unchecked for several weeks and contaminated the underground water bodies of these areas, polluting wells and boreholes, thus rendering the waters unhealthy for consumption. Nigerian National Petroleum Corporation (NNPC's) Pipeline Product Marketing Company (PPMC's) leaking pipes, running through the community from the Mosimi depot in Shagamu, Ogun State, to the Ejigbo depot in Lagos, had polluted the entire place, destroying farms and making cultivation impossible anymore. The Community's wells had been polluted with no good water available anywhere in the area for the people. Wells and boreholes were covered by leaking products from the pipes. Tested well waters had been found to be as much as 95 percent petrol. Baruwa village is just a few kilometres away from the state capital, Ikeja, but the authorities have failed to stop the pipeline leakage in the community. Because of the oil leaks village

wells have to be kept under lock and key to prevent a potential fire disaster.

### Field Experimental Programme

#### *Design and Implementation of pilot Test:*

There are more than 200 hand dug domestic water supply wells contaminated with floating petroleum product of varying thickness (0.20m to 0.65m) at this site. Groundwater is about 25m below ground surface in the wells. The wells are between 0.75m and 2.00m in diameter. The geotechnical/Geoenvironmental research group in F.U.T.Akure has an inventory of one hundred and sixty seven (167) existing contaminated wells in Baruwa, Nigeria with well identification numbers and exact location description. Remediation started with a pilot scheme area (100m x 100m), with existing 10 wells within the pilot scheme area. Baruwa site is lithologically underlain with inter bedded sands, gravelly sands, silts and clays and reddish lateritic sandy clays. The lithology is essentially an alternating sequence of sands and clay layers from the ground surface to a depth of about 102m (Table 1).

Table 1:- Typical Borehole Log for Study Area

Case> size 0.15-0.200m			G.W.L = 26.55m
Layers	Depths (m)	Thickness (m)	Description of the strata
i.	0.00	3.00	Surface Red Sand
ii.	3.00	7.45	Red and Yellow Clay
iii.	10.45	4.05	Red Clay with Sand
iv.	15.00	1.45	Yellow Coarse Sand
v.	16.45	1.55	Hard with Clay
vi.	18.00	16.45	White Sand with Clay
vii.	34.45	1.55	Black Sand
viii.	36.00	1.20	White Hard Clay
ix.	37.20	2.20	Red Sand
x.	39.00	1.20	Red Sand and Clay
xi.	40.20	1.80	Fine Sand and Yellow Clay
xii.	42.00	3.00	White Sand and Red Clay
xiii.	45.00	3.00	Fine Sand and Yellow Clay
xiv.	48.00	3.00	Casey Clay
xv.	51.00	1.45	Soft Black Clay
xvi.	52.45	4.55	Hard Ash Clay
xvii.	57.00	3.00	Sandy Clay
xviii.	60.00	1.80	White Clay
xix.	61.80	4.20	White Fine Sand
xx.	66.00	2.10	Hard White Clay
xxi.	68.10	2.70	Sandy Clay
xxii.	70.80	0.60	Hard White Clay
xxiii.	71.40	0.60	Soft Black Clay
xxiv.	72.00	3.00	Hard White Clay
xxv.	75.00	1.90	White Coarse Sand
xxvi.	76.90	1.10	Medium Sand
xxvii.	78.00	3.00	Soft Black Clay
xxviii.	81.00	3.18	Medium Sand
xxix.	84.18	2.82	White Coarse Sand
xxx.	87.00	13.90	White Coarse Sand
xxxi.	100.90	1.10	Gravel mixed with Clay
xxxii.	102.00	3.15	White Sand mixed with Clay

**GWL: Groundwater Level**

**Total depth drilled = 102.00m**

**Casing size = 0.150 – 0.200m (6" – 8")**

**Source: Lagos State Water Corporation (2006)**

The method adopted is as follows; use of the PETROTRACTOR (Model 8) BELT OIL SKIMMER (Figure 2a) to remove most of the free petroleum hydrocarbon product from the wells; Use of potassium permanganate ( $\text{KMnO}_4$ ) for in-situ chemical oxidation for the well water together with in-situ bioremediation. The above two methods could be adequate, making it simple and cheap so that it can be replicated in hundreds of such sites in Nigeria. As a contingency, the equipment for air sparge and soil vapour extraction system and dual phase extraction system would be acquired.

There was meeting with the local people to intimate them of the site remediation programme, followed by demarcation of Pilot Test location and site reconnaissance/ identification of monitoring wells and sampling locations for the free product recovery pilot test. Ten (10) hydrocarbon recovery/monitoring wells were earmarked for use in the pilot recovery test (Figure 3). Existing contaminated water supply wells are being used as hydrocarbon recovery/monitoring wells to minimize cost. We have already established that water supply wells are covered by pure phase leaking hydrocarbon products from the underground pipes.

Oil/Water Interface meter (Figure 2) was used to measure the depth to ground water for earmarked wells and to measure thickness of free hydrocarbon on groundwater in water supply wells.

Belt-type oil skimmers use an endless belt of corrosion resistant steel or synthetic medium, were lowered into the well to be skimmed. The belt passes through resilient wiper blades where the oil was removed from both sides of the medium. The Model 8 Oil Skimmer purchased from Abanaki Corporation had a belt 200mm wide and 26 m long.



Fig. 2 Model 122 (CSA) Interface Meter, P8/LM3/60m (Solinst)



## RESULTS/DISCUSSION

### Monitoring

After meeting with the local people and establishing contact with necessary Agencies, Monitoring and Oil skimming started from Mr. Shodende's compound which had a total free hydrocarbon product thickness of 0.52m totaling about 1.33m<sup>3</sup> of Liquid Hydrocarbon. Other wells monitored within and outside the pilot test area had between 0.22 to 0.001m of liquid hydrocarbon

The present status of the examined wells within the pilot scheme area is indicated in Figure 3 and the monitoring test results presented in Table 2 and Figure 4.

It was realized that most compounds had carried out the filling and sealing up of their respective wells. Only three out of the ten wells within the earmarked pilot test scheme were still opened, others wells had been sealed while some others visited had been utilized for effluent discharge and refuse.

It was quite disappointing to realize that many of them cited losing hope in our coming, previous "promise and fail" experiences they had had and the no longer tolerable fume emission from the wells as reasons for embarking on filling and sealing up the wells. Many of them had carried out deep depth borehole drilling in their compounds as substitutes for the filled wells, although they also found the water to be non-drinkable.

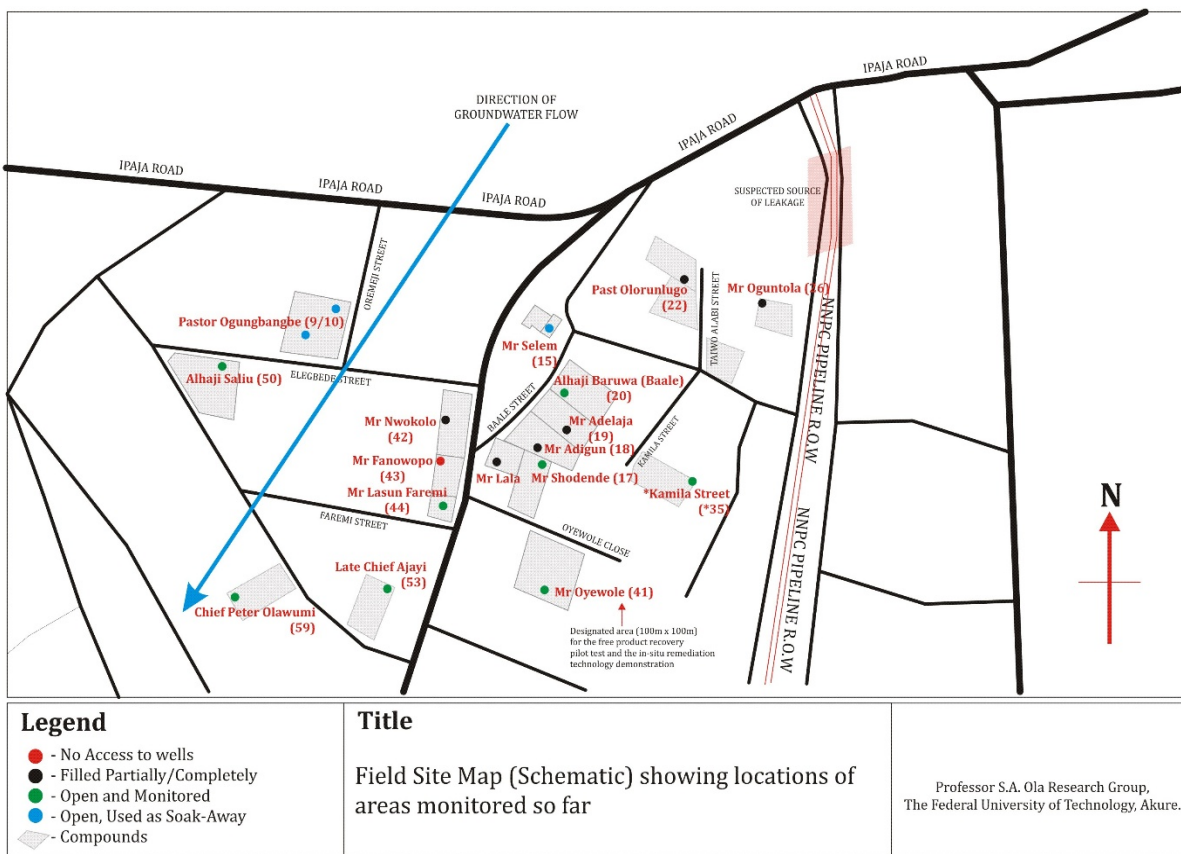


Fig 3 Demarcation of Pilot Test location showing state of the earmarked wells for the pilot recovery test



Table 2: Information from Monitored Wells.

S/N	ID No.	Owners Name	Depth to Liquid Surface from Ground Level (m)	Depth to Water in the Well (m)	Depth to Bottom of Well from Ground Level (m)	Thickness of Liquid Hydrocarbon above water surface in the wells (m)	Thickness of water in the wells (m)	Elevation of Ground level (m)
	20	Alhaji Baruwa	23.721	23.725	24.506	0.004	0.781	49
2	15	Pa Selem	Sealed with Concrete Slab Covering, but on accessing has been converted to soak-away.					50
3	19	Mr. Adelaja	Filled with Sand and Sealed with Concrete.					
4	18	Mr Adigun	Filled with Sand and Sealed with Concrete.					
5	16	Mr Lala	Filled with Earth and other Materials Partially.					
6	42	Mr Nwokolo	Filled with Earth and other Materials Partially.					
7	43	Mr Fanawopo	Building Construction Demolished, No Access to Wells.					
8	44	Mr Lasun Faremi						
9	17	Mr Shodende	23.542	24.033	24.651	<b>0.491</b>	0.618	44
10	41	Pa Oyewole	23.459	23.46	24.179	0.001	0.718	48
11	10	Pastor Ogungbangbe	Converted to soak-away					
12	26	Mr Oguntola	Filled with Earth Partially and currently being used for Refuse Collection					
13	35*	Kamila Street*	24.216	24.437	25.25	0.221	0.813	58
14	22	Pastor Olorunlugo	Filled with Sand and Sealed with Concrete.					
15	50	Alhaji Saliu	24.492	24.493	25.487	0.001	0.993	54
16	59	Chief Peter Olawunmi	23.519	23.52	24.47	0.001	0.95	53
17	53	Late Chief Ajayi	24.022	24.055	25.842	0.033	1.787	57

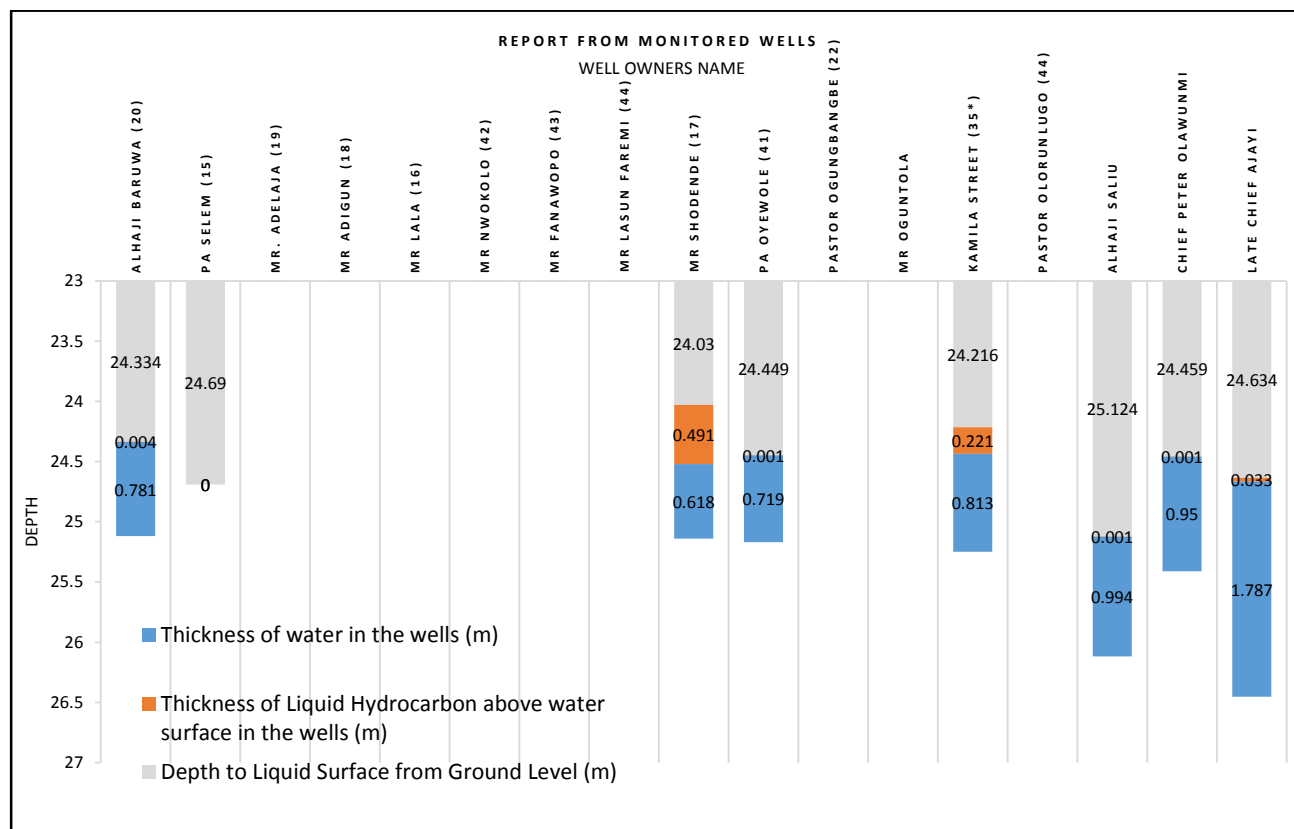


Fig 4 Reports of all wells monitored showing the various thicknesses of free hydrocarbon product and water

## Oil Skimming

The oil skimmer was employed in recovery the free product from the wells where it had been discovered. Skimming essentially started from the well with the highest amount of free product discovered (Well 17) and progressed to others which had just a sheen on the surface of the water within the wells. The placement of the belt/yoke assembly was adjusted to ensure that it was within the hydrocarbon product. Samples were collected at one-hour intervals and analyzed. An improvised bailer was combined with the oil skimmer to increase the rate of recovery of free product. At Well 17, about over 84 Litres of free product hydrocarbon was recovered.

## CONCLUSION

With the use of an improvised bailer and measuring buckets, the bailer was carefully adjusted to fall only within the free product zone so that minimal amount of water/sludge was obtained in the final collection.

It was realized that within a little above an hour, a total of 104.5 litres (Free product – 84 Litres, Sludge – 3.1 Litres, Water – 17.4 Litres) of liquid mixture was bailed out. Bailing was found to be very effective in collection of free product, with very stringent safety measures put in place. Oil Skimming was adopted alongside bailing to bring the free product to almost sheen level. Bailing was found to have recovered more sludge-water mix than the oil skimmer, recovering about 10% more than the use of the oil skimmer. This is still found satisfactory owing to the speed of recovery. Recovered Free Product was still within the 80% range.

Methods employed in recovering free hydrocarbon product on the pilot test scheme site were found to be effective in removing free product from the contaminated wells. Currently, the wells are being pumped and samples collected before and after each pumping to determine the extent of contamination in the water. Other wells would be dug within the area to be able to access the actual amount of contamination within the various strata in the formation of the area.

## ACKNOWLEDGEMENT

The authors would like to acknowledge the TETFUND NATIONAL RESEARCH FUND (NRF) OF THE PROF. S. A. OLA RESEARCH GROUP, FEDERAL UNIVERSITY OF TECHNOLOGY, AKURE, referenced TETF/ES/NRF/013/VOL.I, for the Research Project titled: “Site Remediation in Nigeria: Proven and Innovative Technologies,

Recovery of Free Hydrocarbon from Soil/Groundwater.”

## REFERENCES

- [1] Torres, L. G. B.; Climent, M.; Saquelares, J.; Bandala, E.R.; Urquiza, G.; Iturbe, R., Characterization and treatability of a contaminated soil from an oil exploration zone. “Int. J. Environ. Sci. Tech.”, 4 (3), 2007, 311-322.
- [2] Clement, T.P.; Truex, M.J.; and Lee; P. A case study for demonstrating the application of U.S. EPA’s monitored natural attenuation screening protocol at a hazardous waste site. “Journal of Contaminant Hydrology” 59, No. 1-2, 2002, 133-162.
- [3] Ola S.A. ; Ojuri O.O., “The Use of Sand Tank Experiments to Simulate Field Conditions at the Contaminated Baruwa, Site, Nigeria.” *International Journal of Applied Environmental Sciences (IJEAS)* Vol.4 No.3, 2009, 243-265.
- [4] Ojuri, O.; Ola, S. A. Estimation of contaminant transport parameters for a tropical sand in a sand tank model. *Int. J. Environ. Sci. Tech.*, 7 (2), 2010, 385-394.
- [5] Capel, P. D., K. A. McCarthy, and J. E. Barbash. National, holistic, watershed-scale approach to understand the sources, transport, and fate of agricultural chemicals. *J. Environ. Qual.* 37(3): 2008. 983–993.

## A CASE STUDY ON SLOPE REMEDIATION: A GREEN SOLUTION AND CONSTRUCTION REALITY

Elisabeth Simbolon<sup>1</sup>, Bindumadhava Aery<sup>1</sup>  
<sup>1</sup>Ground Engineering, Aurecon, Brisbane, Australia

### ABSTRACT

This paper presents the case study of the remediation work carried out at Blackmans Gap Road, a part of the Gladstone Regional Council (GRC) road network which was affected by a heavy rainfall event recorded in December 2010 to January 2011 in Queensland. About 750m section of the road section suffered extensive damage and a total of three (3) sites along the road were identified as requiring remediation work.

The remediation solution comprised a “sustainable and flexible” system comprising soil reinforcement and soil nails with flexible facing. This was used successfully in the project, however construction was challenged by variability of ground condition, despite of consistent results of geotechnical investigations. Design parameters considered during design and tender assessments by the contractors, which were based on geotechnical investigations were challenged as variability of ground conditions were encountered during construction requiring modifications of the remediation solution.

The major challenges in geotechnical engineering commonly arise from uncertainties of the ground condition. Often, assumptions and rigorous probabilistic analyses made in the design are not sufficient in particularly when dealing with slope remediation works. An observational approach, monitoring and geotechnical inspections were proven to be the key ingredients of the successful completion in complex ground conditions.

*Keywords: Slope stabilization, Soil nail, Slope stability*

### INTRODUCTION

Blackmans Gap Road is a part of the Gladstone Regional Council (GRC) road network which connects the Boyne Valley with Miriam Vale and Agnes Water, located in Central Queensland, Australia. The road is located on a moderately to steeply sloping hill side at an elevation at least 15m to 20m above the invert level of the gully.

The roadway is likely to have been constructed by cutting into the steep hill face and side-casting the excavated material downslope.

Between December 2010 and January 2011, a 1 in 100 year rainfall event was experienced across Queensland. About 550mm of rainfall was recorded at Gladstone over this period, causing significant damage to the road network at the region, including Blackmans Gap Road.

Approximately 750m of Blackmans Gap Road had sustained damage due to this event and three (3) sites along the road were identified as requiring remediation works, funded by the National Disaster Relief and Recovery Arrangements (NDRRA).

The location of the remediation sites are shown in Figure 1. At the sites, a complete slope failure has not occurred, however slope instability was evident from tension cracks that have formed in the road shoulder. If not remediated, a global failure could occur with the resultant high safety risk to the road users.

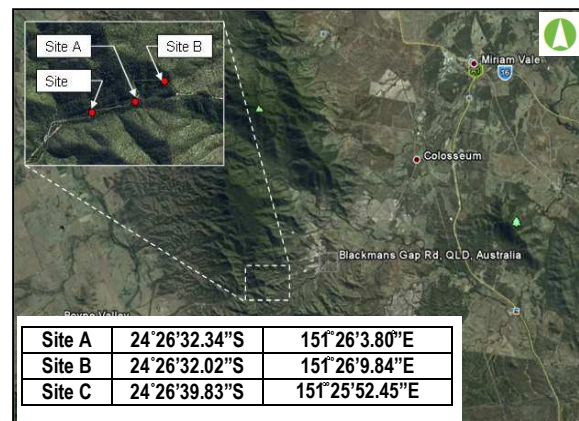


Fig. 1 Plan showing site locations  
 [5] (Google Earth, 2010)

### GEOTECHNICAL CONDITIONS

The typical geotechnical section at Blackmans Gap Road is shown in Figure 2, showing a typical side-cast embankment of fill overlying in-situ rock.

The geological condition underlying the project site is dominated by the intrusive igneous rock of the Castletower Granite formation. The granite rock was evident at the rock cuttings on the uphill slope. The exposed cut face typically reveals a thin (approximately 1 to 2m thick) residual material overlying weathered granite.

Visual observation during geotechnical inspection indicated the granite to be moderately weathered, jointed with dip angle of 20 to 30° into the slope.

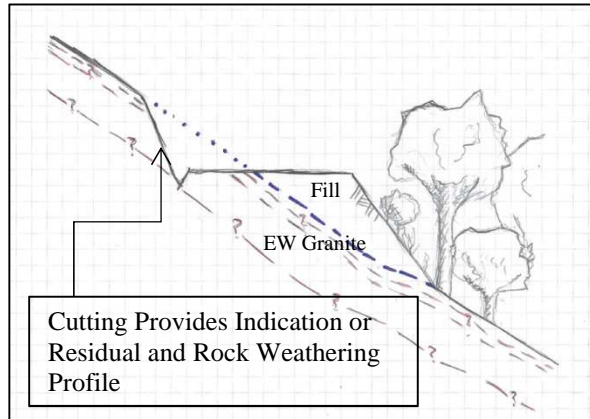


Fig. 2 Typical section at Blackmans Gap Road

The subsurface conditions were investigated by drilling two (2) boreholes at each site and laboratory testing which included particle size distribution and Atterberg's limits of the material.

The geotechnical investigation was scoped to characterise the subsurface conditions, in particular the extent of fill material and strength characteristics of the subsurface material. The borehole rig was positioned as close as possible to the edge of the slope so the approximate extent of the fill section can be determined. The boreholes were drilled through the fill material and terminated in high strength rock material.

Information obtained from boreholes and laboratory testing indicated that the fill material consisted of medium dense silty gravel/gravelly silt with SPT-N values ranging from 10 to 21. The boreholes also intercepted extremely weathered rock material at approximately 1.5m to 2.5m below the existing ground level and consistent across the site.

The rock material was also cored using an NMLC (52mm core barrel) rock coring technique until high strength, less fractured, moderately to slightly weathered rock was encountered at typically 5m depth.

## UNDERSTANDING BACKGROUND OF FAILURES

Understanding the mechanism and causes of slope failure is an important factor to be considered in developing the remediation solution, but also the most challenging task for geotechnical/geological engineers.

Potential causes for slope instability range from deep-seated failures (such as with landslides) to surface erosion (such as when steep slopes cause

water to travel in concentrated flows, eroding a series of gullies) [3] (NCHRP Synthesis 430, 2012).

A site inspection is considered to be the most crucial step in understanding the mechanism of failure as the site conditions often tell a "story". Some signs or indications of failures that should be looked for during inspection include:

- any development of tension cracks
- slumping of materials
- leaning trees or road signage
- scouring or undercutting
- blocked drainage
- weak materials and structure orientation, rock overhanging (for rock cutting)

The geotechnical/geological engineers should consider all the signs on site and assess the likelihood of possible failures and consequences of failures to develop an appropriate remediation solution.

At this site, approximately 2.5cm to 5cm wide longitudinal tension cracks have developed along the edge of the down-slope, which indicated initiation of instability of the down-slope batter. Further saturation of the soil, particularly following a heavy rainfall would lead to a translational slope failure. The roots of trees and vegetation cover on the batter slope has assisted in protection of the slope and prevented further slope movement.

While the heavy rainfall was the trigger of instability, the blocked table drains located at the toe of the up-slope batter were also considered as a contributing factor to saturation of the down-slope fill. As the table drains were blocked, the longitudinal runoff was unable to enter the drainage structures and resulted in sheet flow across the roadway and saturation of the down-slope fill.

Figure 3 shows a sketch of the understanding background of failure.

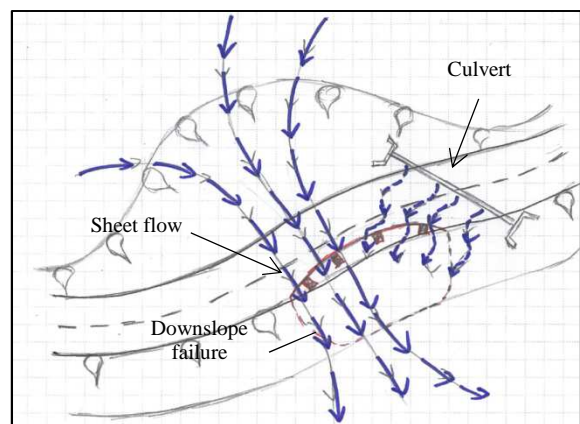


Fig. 3 Failure mode

## AVAILABLE SLOPE STABILISATION METHODS

As the technology is advancing, a large number of slope stabilisation techniques are available, ranging from a) simple solutions of providing sufficient drainage measures, alteration of the slope geometry and rebuilding with suitable fill or rockfill material; to b) the use of slope protection and other bio-engineering techniques to improve the soil strength and, c) the use of soil nailing, gravity wall and other embedded retaining structures to provide a “force system” to resist instability [2] (Oliphent et al., 2000).

The appropriate treatment approach for a site depends on the affected area, budget and feasibility. Although in general perception, the simple solutions would present a cost effective solution, every site is unique and it is critical to understand the site, water, soil and topography as well as the need and extent of the area to be stabilised before selecting an appropriate slope stabilisation techniques. Site conditions and constraints can vary greatly, and a “one-size-fits-all” approach is unlikely to work. Field studies have shown that the combined use of structural and vegetative slope protection system is more cost effective and sustainable than the use of other methods alone. [3] (NCHRP Synthesis 430, 2012).

## DESIGN CONSIDERATIONS AND CRITERIA

Based on discussions with Gladstone Regional Council, the following design guidelines were used to undertake remediation design solution:

- Reinstatement to pre-failure road width and alignment
- Required factor of safety (FOS) of 1.5 for long term conditions and 1.3 during construction
- Sustainability and cost effectiveness of the stabilisation work. A sustainable slope stabilisation treatment is one that poses minimal disturbance to the ecosystem. One way to ensure that a project is low cost and sustainable is to use local or on-site materials.
- Safety to workers and the road users during construction

Safety to workers and the road users during construction was the key driver in the development of the solution. The narrow road width and steep, unstable slope imposed the risks of slope instability and possible collision between the road user and heavy machineries used in construction. Blackmans Gap Road was closed for two (2) months to ensure safety to motorists.

## REMEDIATION WORKS DESIGN

### Soil Nail with Flexible Facing

To meet the design criteria, particularly the stability FOS, a soil nailing solution with flexible facing was adopted in the design. Other options were considered to have higher risks during construction and to have little benefits to achieve the required stability FOS due to the steep down-slope condition and the extent of failure. The main advantages considered for soil nailing solution particularly include:

- Meeting the required FOS for global stability failure
- Installation can be staged by nailing over a stabilised area
- Flexible solution
- Sustainable solution requiring minimal excavation and using local or on-site material as backfill

Soil nailing is essentially an in-situ ground reinforcement technique which involves installing closely-spaced steel bars or nails into the slope to provide reinforcement and strengthening of the existing ground.

The flexible facing comprised mesh and spike plates which is sometimes overlooked in design, for this case also provides an important aspect in the design solution. Rigid shotcrete or concrete finishes were not considered to be acceptable as these types of facings can potentially crack as a result of additional hydrostatic pressure and soil movements mobilised in the long term. A flexible facing using high-tensile strength steel mesh will eliminate the potential of cracking at the face and also provides a “green solution” which blends with the natural environment of the site. The mesh will promote re-vegetation growth or greening of the slope for an aesthetically pleasing, natural looking finish.

High tensile, Tecco Mesh product from Geobrugg was adopted as the flexible facing for the design solution. In standard layout, the high-tensile steel mesh is made of individually twisted 3mm diameter wire of > 1770N/mm<sup>2</sup> tensile strength. The wire has a resilient coating of aluminium-zinc coating for corrosion protection. The mesh has a tensile strength three times greater than traditional twisted mesh. In combination with soil nails, the wire mesh stabilises any superficial instability (0 to 2m depth). The forces are transferred from the mesh into the nail which provides global stability for the slope.

In addition to the soil nail system, the existing table drains were also cleared off debris. Local or on-site materials were used as backfilling materials

to ensure sustainability and cost effectiveness of the solution.

### Development of Design Parameters

Table 1 presents the material parameters used in the design. The most important properties required for the analyses were the unit weight and the shear strength of the material. These parameters were derived from the in-situ and laboratory testing as well as using back analysis of the existing slope profile.

The back analyses were carried out to assess the strength parameters (friction angle,  $\phi'$  and drained cohesion,  $c'$ ) by performing stability assessment on the existing slope geometry. A trial and error method was carried for a range of likely material parameters to achieve a factor of safety of 1.0 against slope failure. It was assumed that the factor of safety against global slope instability was at or close to 1.0 at the time of slope failure.

The back analyses results showed the factor of safety was sensitive to the assumed depth of the critical slip surface and the hydrostatic pressure applied on the slope. To achieve credible strength parameters that would model the failure to be used for design of the remedial works, it was assumed that the translational failure occurred through the fill material and the slope was fully saturated.

The results obtained from back analysis of the material were compared with experience in similar condition and typical material properties and the comparison fell within a reasonable range of expected values.

Table 1 Geotechnical Design Parameters

Material	Existing fill	EW granite	MW-SW granite
Depth (m)	0-2.5	2.5-5	>5
Unit weight, $\gamma$ (kN/m <sup>3</sup> )	19	23	23
Friction angle, $\phi'$ (degree)	32	33	33
Drained cohesion, $c'$ (kPa)	0 to 5	5 to 25	50

### Stability Analysis

Stability assessment was carried out using Slope/W software, which is a limit equilibrium program developed by Geostudio. The software is commonly used in slope stability analysis to generate potential failure surfaces through a slope condition and estimate the factor of safety (FOS) for each generated failure surface. The failure surface with the lowest FOS is selected as the critical case.

Typical slope stability output is presented in Figure 4.

The design of the soil nail system was carried out based on two design conditions. The first design condition considered was the long term condition of the slope to achieve a target stability FOS of 1.5, assuming a low groundwater level. A fully saturated condition was also considered in the design however this was considered to be a short term condition and targeted a FOS of 1.3.

Two (2) rows of soil nails were required to achieve FOS requirements. The design required 28mm diameter steel bar with working load of 133kN per nail and installed at 15degrees to the horizontal and embedded 12m into the EW/HW granite material to satisfy the bond length requirement for the design. Table 2 shows the typical soil nail details used in the project.

Table 2 Soil nail details

Item	Design
Length of soil nails	12m
Diameter of soil nail hole	150mm
Diameter and type of bar	28mm
Working load	133kN
Angle to horizontal	15
Spacing	2m in horizontal – grid pattern
Facing	Tecco G65/3 mm

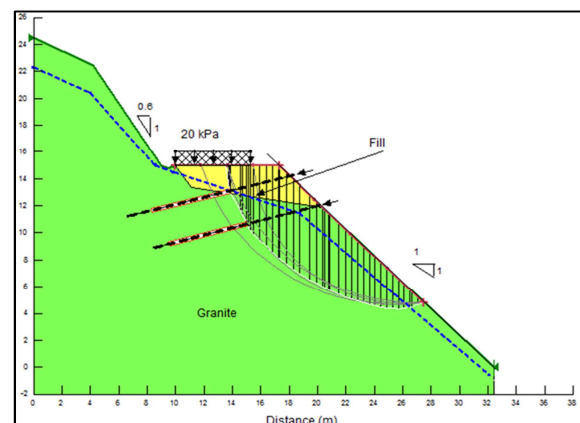


Fig. 4 Typical slope stability output

### Dealing with Geotechnical Uncertainties in Design

The design requirements and assumptions were not only documented in a geotechnical design report but also in the construction drawings and specifications, with the key points being:

- Safety during works



- Subsurface conditions encountered during excavation
- Installation of soil nails
- Foundation conditions

A set of hold points, field testing and construction stages were also presented in the construction drawings and specifications to enable the critical parameters to be reviewed during construction.

Safety during construction was considered the most important aspect in design. A safety in design documentation was created as part of design documentations to ensure that all the hazards associated with construction and design were considered.

Contractors input were also obtained during the design and tender process. The construction stages were developed based on discussions that were carried out with soil nail specialist contractor to ensure that the work can be constructed safely. Potential contractors also carried out a site walkover to assess the site conditions and define the construction methodology and appropriate equipment to be used during construction.

## CONSTRUCTION OF REMEDIATION WORKS

### Issues during Construction

Construction started with preparation of a working platform and excavation to the bottom of fill material to achieve the required subgrade foundation conditions. The soil nails were installed from the top slope by an excavator with a soil nail drill attached to it – shown in Figure 5 and the Tecco mesh was installed following installation of the soil nails.



Fig. 5 Drilling of soil nails

Challenges were faced during construction as a result of variability of the ground condition.

As the initial excavation progressed, it exposed a deeper fill extent in between the two borehole locations which were spaced at 20m. The fact that there was a great variability of ground condition in between boreholes was unexpected, considering the extent of the failures and the consistent subsurface profile obtained from such closely spaced boreholes.

As soon as the issues were encountered, excavation was stopped, as deeper excavation of unstable fill could result in safety issues and increased risk of slope instability. A geotechnical representative inspected the site and carried out Dynamic Cone Penetrometer (DCP) testing to assess the extent of the fill material across the site and in between the boreholes.

The results of the DCP tests were unexpected as it encountered DCP blows of 5 (in average) down to 5m below the existing ground surface. Site inspections also observed a notable amount of organics and some larger boulder sized particles which raised further concerns with regards to suitability of the fill material.

Installation of soil nails also encountered issues with collapsing holes and jammed casing, causing a slow down in production rate.

### Modifications to Remediation Solutions

As the construction fell behind from schedule due to the unforeseen issues encountered during construction, a decision was made to modify the remediation solution to suit the site condition and bring the construction program on schedule. It was essential to complete the project as scheduled as about 20 km of road stretch was closed traffic during construction period. Any delay in completion would cause embarrassment to the council.

The designer reviewed the remediation solution and the site conditions. Following discussion with the contractor, a decision was made to remove the unsuitable soil to maximum depth of 4m. The unsuitable fill was replaced with general fill complying with the Main Roads standards. Safety during construction was managed by performing excavation in slots and inspection by the contractor's geotechnical engineer.

As a result of this modification, the top rows of soil nails were eliminated. Reinforced soil slope with Geogrid as reinforcement were placed in lieu of the top soil nails to increase the localized stability at the face of the downslope. The combined system of better fill, geogrid reinforcement with soil nails also serves benefits to achieve the required global stability FOS.

Eliminating the top rows of soil nails was effective in bringing the construction on schedule and budget.

### Collaborative Approach

A collaborative approach was established between the designers, constructors and the principal to resolve the issues and carry out the work as effectively as possible and in a timely manner.

As the project progressed, an inherent team relationship was developed and it was evident that the constructors, the principals and the inspectors had developed a much better understanding of the technical specifics, demonstrating on many occasions a greater appreciation for the geotechnical issues and risks associated with the project.

Despite the challenges that were encountered, the collaborative approach and commitment of all parties had led to a successful completion of the project and the road was re-opened on the scheduled time. The final remediated road at the completion of construction is shown in Figure 6. The geogrid reinforcement and soil nails have also performed well over the period of heavy rainfall in 2013.



Fig. 6 Final Remediated Road

### CONCLUSIONS

In the presented case study, the soil nailing technique combined with geogrid and flexible facing was concluded to be a feasible slope remediation solution at Blackmans Gap Road. The technique provided a sustainable, cost effective solution.

Challenges were encountered during construction, as a result of variability of the ground condition. Despite of closely spaced boreholes and consistent geotechnical investigation outcomes, unexpected ground conditions were still encountered during

construction.

These challenges were overcome and the project was completed successfully as a result of the high level of commitment by all parties: client, consultant and contractors.

The major challenges in geotechnical engineering commonly arise from uncertainties of the ground condition. It is important for the design to expect variability of the ground condition. The aspects of geotechnical uncertainties must be considered not only in the design analyses but also in tender documentations (such as drawings and specifications).

The geotechnical uncertainties must be managed during construction by carrying out monitoring and geotechnical inspections. A flexible design solution is also considered to be beneficial. As issues are encountered, the designers must be able to review the remediation solution and change the design to suit site condition and construction requirement.

It is also in the opinion of the authors that a major contributing factor to the successful completion of the project is the collaboration of all parties involved.

### ACKNOWLEDGEMENTS

The author would like to acknowledge the Gladstone Regional Council for providing an opportunity to design this project and express her appreciation towards the Aurecon team members in Gladstone and the contractor, the Rix group for their cooperation during the project.

### REFERENCES

- [1] B. Bindumadhava, 'Slope stabilization using grid beam system', in Proc. 2<sup>nd</sup> Int. Conf. on GEOMAT, 2011, pp.5-10
- [2] Oliphant, J., MacCaffey, R. Apted, R., "Soil slope stabilization methods", An Int. Conf. on Geotechnical and Geological Engineering, Melbourne, Australia, November 2000
- [3] Fay, L., Akin, M., Shi, X., "Cost-effective and sustainable road slope stabilization and erosion control", NCHRP Synthesis 430, Transportation Research Board, Washington, DC, 2012
- [4] Farrand, S., Teen, A., "Seismically induced landslide mitigation using flexible slope stabilization systems", in Proc. Con. on NZSEE, 2008
- [5] Google earth website, 2010

## AMMONIA REMOVAL CHARACTERISTICS OF POROUS CONCRETE WITH ZEOLITE FOR ENHANCING SELF-PURIFICATION ABILITY IN RIVER SYSTEM

Fumitake Nishimura<sup>1</sup>, Toshio Yamada<sup>2</sup>, Motohiro Tanaka<sup>2</sup>, Hirofumi Kassai<sup>2</sup> and Michiko Masuda<sup>3</sup>

<sup>1</sup>Department of Environment Engineering, Kyoto University, Japan; <sup>2</sup>Sogo Kaihatsu Co., Inc.; <sup>3</sup>Department of Civil Engineering, Nagoya Institute of Technology, Japan

### ABSTRACT

Ammonia removal characteristics of porous concrete with zeolite are investigated. Ammonia is one of the common pollutants in river water, and it can cause several adverse impacts for human activities such as water supply and agricultural purposes. It has negative impacts on water ecosystem as well. Porous concrete with zeolite can adsorb ammonia by zeolite, and biological nitrification and its promotion can be expected because attached ammonia on the surface of the porous concrete can promote bacterial growth of nitrifying bacteria. It is expected that both chemical effects (ammonia adsorption) and biological effects (nitrification) can remove ammonia effectively from river waters when the porous concrete is applied in the river as an artificial riverbed for example. Experimental discussion is conducted in this study. It was shown that the specific surface area was increased by making porous concrete, and the ammonia removal rate can be increased twice as a result. It was made clear that chemical effect can be produced in the same level as biological effects as well. It is considered that both effects can increase the ammonia removal ability of porous concrete with zeolite effectively.

*Keywords: Porous Concrete, Zeolite, Ammonia, Self-purification of river*

### INTRODUCTION

Concrete constructs are often used in rivers and small channels for river water control and water utilization. Ordinary concrete constructs have been used from the points of durability. On the other hand, environmental functions of rivers attract attention such as self-purification ability of river water, or forming diversified ecosystem surrounding rivers. River Act was revised in 1997 in Japan and environmental functions of rivers have been also focused as well as river water control (flood control) and water utilization (water supply). Therefore, preservation and utilization of the environmental functions of rivers started being paid more attention. There are concrete constructs incorporated in the river, and porous concrete start to be used instead of ordinary concrete because it has wide surface area and a lot of microorganisms can attach on the surface which result in enhancing purification ability of river water quality. Porous property promotes to catch a lot kinds of materials as well as microorganisms, which also helps purifying water quality, therefore purification by porous concrete is expected and porous concrete start to use for the purposes. If the purification is widely applied in the area where sewage system is undeveloped, pollutants loadings in the catchment area can be reduced. Setting porous concrete constructs are easy compared with that of construction of sewerage system. Therefore, several trials have been

conducted, and function analysis of porous concrete from the view point of microbial attachment and purifying ability of water quality[1],[2]. It was reported that the microbial densities in porous concrete were  $10^4 - 10^3$  cells/cm<sup>3</sup> of nitrifying bacteria,  $10^7 - 10^8$  cells/cm<sup>3</sup> of aerobic heterotrophic bacteria, and  $10^7 - 10^8$  cells/gVSS of denitrifying bacteria, respectively[3].

On the other hand, improvements of purifying functions of porous concrete have been tried. One of the cases is using zeolite partly instead of the cement. Zeolite has cation exchange function, and concrete materials can have cation exchange capacity if zeolite is mixed into the concrete. Zeolite can adsorb  $\text{NH}_4^+$ -N especially, which is one of the major pollutants from human activity, therefore it is expected that porous concrete in which zeolite is mixed can have not only biological purification ability but also chemical purification ability, especially  $\text{NH}_4^+$ -N adsorbing ability. The application example for purification of river water quality using porous concrete structure with zeolite have been reported, however most of them is only a report of the application, and detail analyses for purification of water quality have not been conducted from the point of microbial attachment, their activity, and  $\text{NH}_4^+$ -N adsorption.

In this study, water purifying ability of porous concrete were investigated and evaluated through lab-scale experimental setup. Porous concrete can be a good attachment media for bacteria which can

purify river water quality, and the addition of zeolite to concrete enhance adsorption of  $\text{NH}_4^+\text{-N}$ , which can also contribute water purification. It is also expected that adsorption of  $\text{NH}_4^+\text{-N}$  on the surface of the concrete media increase  $\text{NH}_4^+\text{-N}$  concentration which results in the concentrating microorganisms which use  $\text{NH}_4^+\text{-N}$  for their metabolism. Namely the concrete constructs can be a water purifying system if it can have certain amount of microorganisms and other functions such as adsorption of pollutants.

In this study,  $\text{NH}_4^+\text{-N}$  is focused as one of pollutants in river water and its removal efficiency using porous concrete with zeolite was investigated and evaluated. Several kind of porous concrete are targeted and effects of its characteristics such as shape and adding materials on the ability of purification of water body especially river water is investigated.

## MATERIALS AND METHODS

Lab-scale experiments were conducted. Porous concrete pieces with zeolite were prepared and they were incorporated in to a vessel as simulated concrete constructions. Artificial wastewater was introduced into the vessel and the wastewater was purified by microorganisms attached on the surface of the concrete materials and/or concrete material itself by its adsorption function. The outline of the experimental setup is shown in Figure 1. The shape of each concrete piece is cuboid and its size is  $4.9\text{cm} \times 4.9\text{cm} \times 3.2\text{cm}$  in each piece. In the vessel, three different foam types of concrete piece were incorporated. One is the ordinary concrete of which voidage is 0%, and the other two types of concrete pieces were porous concretes of which voidage is 10% and 20%, respectively. 5 concrete pieces of each type were used in a vessel, i.e. 15 concrete pieces were used in an experimental case. 5 experimental cases were set in which mixing ratio of zeolite in the concrete piece was different. The mixing ratio of zeolite in the experimental Cases A was in a range of 0-50%, and effects of mixing ratio

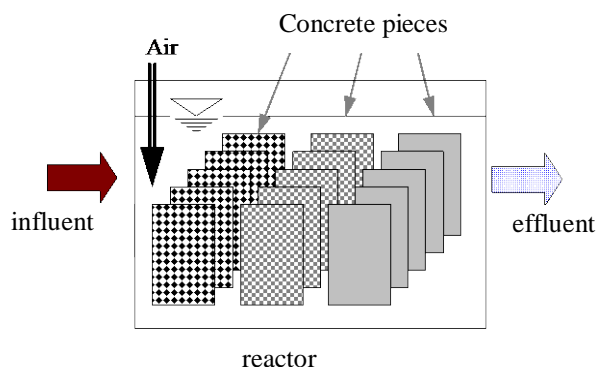


Fig.1 Schematic diagram of experimental apparatus

of zeolite on water purification were investigated.

The experimental condition was summarized in Table 1. These vessels were set in water bath controlled at  $25\text{ }^{\circ}\text{C}$ . Apparent volume ratio of concrete pieces to the total volume was 12.5%, and hydraulic retention time (HRT) was set to be 8hrs. Inorganic artificial wastewater was prepared which is simulated a polluted river water and the  $\text{NH}_4^+\text{-N}$  concentration was set to be  $10\text{ mg/L}$ . The composition is shown in Table 2. Aeration was continued in order to maintain aerobic conditions, and aeration was carefully conducted as not to touch

Table 1 Experimental condition of concrete pieces used in Cases A

Case No.	Mixing ratio of Ca type zeolite (%)	Voidage		
		0%	10%	20%
Case A-1	0%	5	5	5
Case A-2	10%	5	5	5
Case A-3	20%	5	5	5
Case A-4	30%	5	5	5
Case A-5	50%	5	5	5

Table 2 Composition of artificial wastewater

Chemicals	Concentration	
$\text{NH}_4\text{Cl}$	10	$\text{mgN/L}$
$\text{NaHCO}_3$	107	$\text{mgCaCO}_3/\text{L}$
$\text{KH}_2\text{PO}_4$	0.1	$\text{mgP/L}$
$\text{MgSO}_4 \cdot 7\text{H}_2\text{O}$	1	$\text{mgMg/L}$

Table 3 Experimental condition of concrete pieces used in Cases B

Case No.	Zeolite type	Mixing ratio of zeolite (%)	Voidage	
			0%	20%
Case B-1	Fe type	0%	2 pieces	2 pieces
		10%	2 pieces	2 pieces
		20%	2 pieces	2 pieces
		50%	2 pieces	2 pieces
Case B-2	Ca type	0%	2 pieces	2 pieces
		10%	2 pieces	2 pieces
		20%	2 pieces	2 pieces
		50%	2 pieces	2 pieces
Case B-3	Fe and Ca type	0%	2 pieces	2 pieces
		5+5%	2 pieces	2 pieces
		10+10%	2 pieces	2 pieces
		25+25%	2 pieces	2 pieces

Table 4 Composition of the concrete pieces ( $\text{kg/m}^3$ )

	without zeolite	with zeolite (20%)
Cement	322.1kg	234.6kg
zeolite	0.0 kg	46.9 kg
coarse aggregate	1535 kg	1535 kg
water	70.9 kg	75.1 kg

the concrete pieces directly for preventing unwanted agitation on the surface of the biofilm. The artificial wastewater was introduced continuously into the reactor, and growth of biofilm which contains nitrifying bacteria was investigated. The inside of the reactor was maintained under complete mixing condition by the aeration. The continuous reaction was conducted under the room temperature and after accomplishing complete nitrification in which  $\text{NH}_4^+\text{-N}$  was completely oxidized to  $\text{NO}_3^-\text{-N}$ , nitrifying activities were measured by batch experiment. The concrete pieces with nitrifying biofilm were set in a glass vessel with the artificial wastewater, and nitrifying activity was calculated by measuring the nitrate or nitrite increasing rate in the vessel. After the measurement, the attached microorganisms were detached using both ultrasonic homogenizer and pipetting by which concrete piece would not be damaged, and the detached microorganisms were measured as VSS.

Experimental Cases B were set in order to investigate effects of zeolite type on microbial activity. In this study, three types of zeolite were prepared, i.e. Fe type, Ca type, and their mixed type(Fe + Ca type) were investigated.

Three reactors were prepared. They are operated continuously like Case A. In each reactor 8 kind of concrete pieces were incorporated. The types of the concrete pieces about the voidage are 0 and 20%, and in each porosity types, 4 types of the concrete pieces about the mixing ratio of zeolite were prepared, i.e. the value of the ratio was 0, 10, 20, and 50%. Two pieces in each type concrete pieces, totally 16 of concrete piece, were set in a reactor. Porous concretes with Fe type zeolite was set in a reactor and operated as Case B-1. Porous concretes with Ca type zeolite were used in Case B-2, and Porous concretes with both Fe type zeolite and Ca type zeolite were used in Case B-3. The detail of the experimental condition of concrete pieces used in Cases B is summarized in Table 3. Same as the experimental Cases A, concrete pieces were took from the reactors in order to measure nitrifying activity of each concrete piece after complete nitrification was attained at the reactor. The nitrifying activity was measured by batch experiments and investigated ammonia removal characteristics in each concrete piece.

500mL of glass beakers were prepared, and the 400 mL of the artificial wastewater used in each Case was filled. Then a concrete piece was set in carefully in order to submerge it certainly. The liquid in each batch reactor was stirred by magnetic stirrer. Samplings were conducted 5 times, i.e. after 0.25, 1.25, 2.75, 4.75 and 7 hrs after the beginning the batch test. The amount of a liquid sample is determined as 10mL. In order to collect microorganisms attached on the surface of the concrete piece, the piece was submerged in to a

beaker where 300mL of tap water was filled, and then ultrasonic irradiation was conducted twice for 3min. After ultrasonic irradiation, remaining microorganisms was detached from the concrete piece by pipetting.

Mixed liquor with the biofilm is stirred well and sampled for measurement of both SS and number of nitrifying bacteria. Measurement methods of FISH was followed the Amann's procedure[4]. The collected sample was treated with 4% paraformaldehyde immediately and kept under the condition of 4°C for 2hrs. After that the sample was washed for three times with PBS buffer. The sample was preserved under the condition of -20°C after adding the buffer solution which is the mixed liquid of equivalent amount of both PBS and ethanol. Hybridization was conducted under 46°C for 2hrs. Direct counting methods of fluorescing sample was conducted with incident-light fluorescence microscope (OLYMPUS BX-FLA, OLYMPUS BX-50).

The zeolite mixed in the concrete piece is made from coal ash. The coal ash is treated under alkali condition with NaOH, and then Fe or Ca is added in order to change zeolite. CEC of the zeolite is 180-200 meq/100g, and its particle size is in a range of 5-100 $\mu\text{m}$ . whereas micro pore diameter is 5-100Å. The specific surface area is 100-500( $\text{m}^2/\text{g}$ ). The procedure to make porous concrete pieces is as follows; The coarse aggregate is set in a cement mixer, and water is added by bits. After mixing, powder materials(cement and zeolite) are added, and water start to be added in order to make the surface of the coarse aggregate covered by the paste which is the mixture of the powder materials and water. Then the mixed material is set into a steel form unit with using form vibrator. After 1 day waiting, hardening occurs and it is demolded. The composition of the concrete pieces ( $\text{kg}/\text{m}^3$ ) is summarized in Table 4.

For start-up of these experiments, cultivated sludge with culture media shown in Table 2 was added into each reactor in order to attach and grow nitrifying bacteria on the surface of the concrete piece quickly. The sludge itself was originally obtained from domestic wastewater treatment plant (WWTP).

## RESULTS AND DISCUSSION

The results of experimental Case A-5 are shown in Figure 2 for example. Ammonium nitrogen was easily transformed to nitrite nitrogen, oxidation of nitrite nitrogen started and ammonia is quickly oxidized to nitrate nitrogen. And about 40 days after the start up, similar tendency were observed in the other cases. Apparent specific growth rates are calculated from the results of continuous treatment according to the following equation.



Apparent specific growth rate = [net specific growth rate:  $\mu$  (1/day)] - [detachment/death rate:  $d$  (1/day)]

The results of apparent specific growth rates of AOB were 0.330 (1/day) in Case A-1, 0.232(1/day) in Case A-2, 0.297(1/day) in Case A-3, 0.332(1/day) in Case A-4, and 0.363(1/day) in Case A-5, respectively. On the other hand, these of NOB are 0.338(1/day) in Case A-1, 0.117(1/day) in Case A-2, 0.241(1/day) in Case A-3, 0.157(1/day) in Case A-4, 0.186(1/day) in Case A-5, respectively.

Apparent specific growth rates of nitrifying bacteria in the cases where concrete piece without zeolite were used were larger than these in the cases where the pieces with zeolite are used. The apparent specific growth rate also seems to become larger with the increase of zeolite mixing ratio in the cases the pieces with zeolite are used. However, the tendency was not so clear, and there were not big difference about nitrification occurrence among the Cases A. Generally,  $\text{NO}_2^-$ -N accumulation is not observed if ammonia concentration is about 10 mg/L, however,  $\text{NO}_2^-$ -N accumulation happened in all cases in this study. The reason is considered that free ammoniums which can be exist in high ratio under higher pH conditions. The activity of nitrite oxidation enzyme in NOB can be inhibited by FA[5], and the concentration from which the inhibition start is in a range of 1.0 - 10mgFA-N/L[6][7], in this experiment, initial pH value was in a range of 10 - 11.5, which can inhibit the nitrite oxidation enzyme in NOB.  $pK$  at 25°C is 9.25 and the ratio of FA is in a range of 85-99%, therefore partial nitrification was caused by higher pH at the surface of concrete pieces.

Relationship between zeolite containing ratio and biomass attached on the surface of the concrete pieces, or reduction rate of  $\text{NH}_4^+$ -N are shown in Figure 3. There are tendency that biomass on the surface of the concrete pieces increased with the increase of zeolite containing ratio. It is suggested that ion exchange capacity and adsorption capacity of  $\text{NH}_4^+$ -N can promote the phenomena because  $\text{NH}_4^+$ -N is one of the important substrates, and microorganisms themselves were concentrated on the positive charged surface by zeolite because microorganisms are charged negatively charged[8][9]. It was also suggested that pH increase can be suppressed when zeolite was used instead of cement which result in avoiding inhibition of activity of nitrifying bacteria caused by FA relatively.

Amount of microorganisms attaching to the porous concrete was higher than to the ordinary concrete.  $\text{NH}_4^+$ -N reduction rate per unit concrete piece was in a range of 0.39 - 0.81mgN/hr, and the value was on an increasing trend with an increase of voidage or mixing ratio of zeolite. The difference of

the removal rates among them was not so greater than the difference of microbial amount. The thickness of biofilm became larger as attached

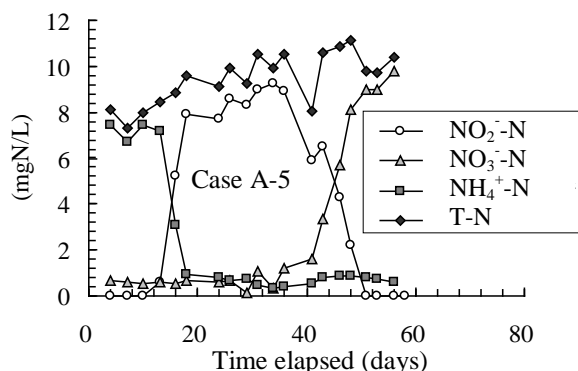


Fig. 2. Time course of nitrogenous compounds (Case A-5)

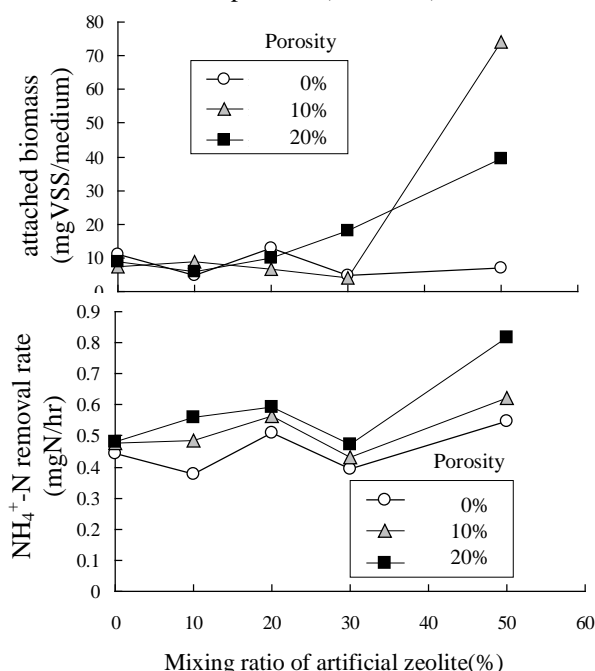


Fig. 3. Relationship between zeolite mixing ratio and attached biomass, or  $\text{NH}_4^+$ -N removal rate

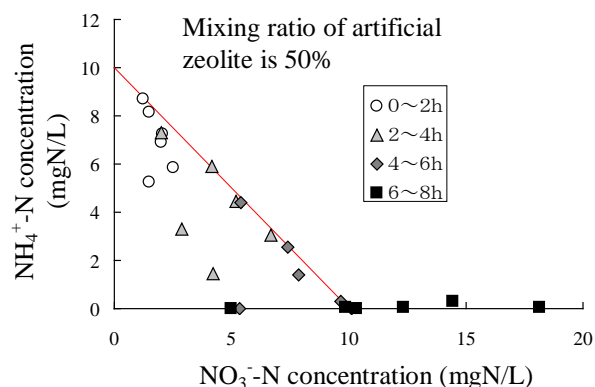


Fig. 4.  $\text{NH}_4^+$ -N removal characteristics



amount of microorganism increased, and microbial activity inside the biofilm can decrease relatively, therefore, the difference of microbial activity was not so large than that of microbial amount.

$\text{NH}_4^+\text{-N}$  removal characteristics by the concrete piece containing zeolite was shown in Figure 4. If the concrete piece cannot adsorb  $\text{NH}_4^+\text{-N}$ , the total concentration of  $\text{NH}_4^+\text{-N}$  and  $\text{NO}_x\text{-N}$  should be 10 mgN/L during the batch experiment and the phenomena is drawn as the solid line. However, the results of the experiment was different and the total concentration of  $\text{NH}_4^+\text{-N}$  and  $\text{NO}_x\text{-N}$  was lower than 10 mgN/L in the initial stage, which shows that adsorption of  $\text{NH}_4^+\text{-N}$  have happened. On the other hand, biological nitrification progressed and the total concentration of nitrogenous compounds was beyond 10mgN/L, which means desorption of  $\text{NH}_4^+\text{-N}$  happens and adsorption ability was regenerated after 6 hrs from the starting the experiment. Finally, total concentration becomes 18 mg/L, and it is calculated that 3.2 mgN of  $\text{NH}_4^+\text{-N}$  was attached on the surface of the concrete pieces. The zeolite used in this study can adsorb  $\text{NH}_4^+\text{-N}$  and its adsorption isotherm is expressed as follows.

$$q = 4.7C^{0.18}$$

where,  $q$ : concentration in solid phase (mgN/gZ)

$C$ : concentration in liquid phase (mgN/L)

The adsorbed amount of  $\text{NH}_4^+\text{-N}$  is calculable from the equation because the concrete piece is in the reactor operated continuously and  $\text{NH}_4^+\text{-N}$  is little existed because nitrification occurs before the batch experiment, therefore adsorbed amount of  $\text{NH}_4^+\text{-N}$  was also little, however, it is shown that attached  $\text{NH}_4^+\text{-N}$  on the surface of the concrete pieces can be nitrified and adsorbing capacity can be regenerated. It is suggested concrete pieces with zeolite can remove  $\text{NH}_4^+\text{-N}$  by both biological process and physicochemical process, which means multifunctional removal system can be accomplished.

Next, the results of Cases B are discussed. About for 40 days from the beginning,  $\text{NO}_2^-\text{-N}$  was accumulated, which were similar as the Cases A. After that, nitrite oxidation started and  $\text{NO}_2^-\text{-N}$  accumulation was resolved by 60 days from the beginning. There were not big difference among Case B-1, Case B-2, and Case B-3 about ammonia and nitrite oxidation, which means the type of zeolite have a small impact on these oxidation.

Relationship between mixing ratio of zeolite in the concrete pieces and ammonium removal rate obtained from the batch experiment were shown in Figure 5. And relationship between mixing ratio of zeolite in the concrete pieces and nitrate generation rate obtained from the batch experiment were shown in Figure 6, as well. Complete nitrification was accomplished and nitrite accumulation was disappeared when batch tests were conducted. Therefore nitrite accumulation was not observed

during the batch experiment.  $\text{NH}_4^+\text{-N}$  removal rate of porous concrete was larger than that of ordinal concrete, and there were clear tendency that  $\text{NH}_4^+\text{-N}$  removal rate becomes larger with the increase of zeolite mixing rate clearly.

Because the removal rate increase according to the increase of specific surface area of the concrete pieces,  $\text{NH}_4^+\text{-N}$  removal rate of porous concrete can be increased due to the increase of surface area where  $\text{NH}_4^+\text{-N}$  can be concentrated with zeolite, which can result in enhancement of adsorption of  $\text{NH}_4^+\text{-N}$  to zeolite. It is understood that the ratio of  $\text{NH}_4^+\text{-N}$  adsorption to total  $\text{NH}_4^+\text{-N}$  removal rate can be the same level of that of biological oxidation. The adsorption of  $\text{NH}_4^+\text{-N}$  occurred quickly and in the first stage, therefore it can be expected that buffering function can acts effectively against the sudden increase of  $\text{NH}_4^+\text{-N}$  concentration in water phase. Clear difference about adsorption function was not observed between zeolite types.

On the other hand, nitrate generation rate was 0.4 -1.6mgN/(L·hr), and the rate of porous concrete was higher than that of normal concrete. There was a tendency that the nitrate generation rate increase d with the increase of zeolite ratio, however the correlation is not so clear than the case of ammonia

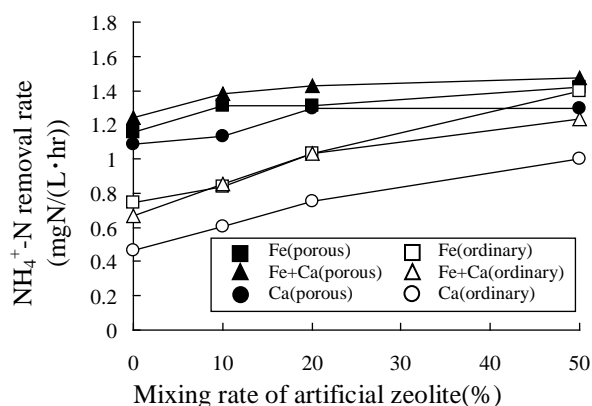


Fig. 5 Relationship between mixing rate of artificial zeolite and  $\text{NH}_4^+\text{-N}$  removal rate

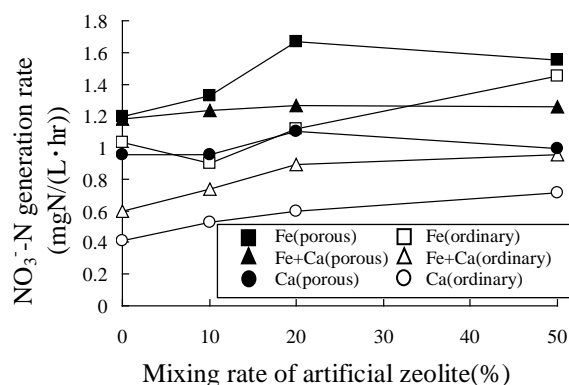


Fig. 6 Relationship between mixing rate of artificial zeolite and  $\text{NO}_3^-\text{-N}$  generation rate

removal rate, and the tendency was observed clearly in the cases of using ordinary concrete compared with the cases of porous concrete. The surface area of porous concrete is wider than the ordinary concrete and it helps forming of much amount of biofilms which can purify the river water quality. Moreover, shape of surface area of porous concrete can increase amount of microorganisms caught at porous, that results in the increase of amount of microorganisms as well. These phenomena result in the increase of self-purifying ability. As results, nitrate generation rate becomes twice compared with the ordinary concrete. There are also tendencies that nitrate generation rate of concrete piece with Fe type zeolite is larger than that with Ca type zeolite. In this study, tap water was used for preparing artificial wastewater, therefore Fe concentration was lower than Ca concentration in the wastewater. Fe is necessary for biological oxidation-reduction reaction because enzymes relating cytochromes uses electron transfer of Fe. It is suggested that nitrification can be promoted by the provision of Fe from zeolite[10]. The nitrifying activity attaching concrete piece with Fe type zeolite was 8.6 mgN/(gMLVSS·hr), which is almost in the same level as previously reported data(4.77 mgN/gTS·hr)[11]. It is shown that using concrete piece with Fe type zeolite can constitute biofilm which accomplish enough nitrification at least.

The density of bacteria attached on the concrete piece is shown in Figure 7. The number of the bacteria on ordinary concrete in Case B-1 and B-2 was counted in a range from  $10^{10}$  to  $10^{11}$  cells by hybridization with probes of Nsm156 and NSR447, respectively, which suggests that the cell number of AOB such as *Nitrosomonas* spp., and NOB such as *Nitrospira* sp. were in the same level. In Case B-3, the number of cells hybridized with probe Nsm156 was around  $10^{10}$ (N), whereas that with probe NSR447 was around  $10^9$ (N). The results mean *Nitrosomonas* spp. exists in priority to *Nitrospira* sp. in the media. However, there were not strong relationships between nitrification activity and density or microbial number of nitrifying bacteria in

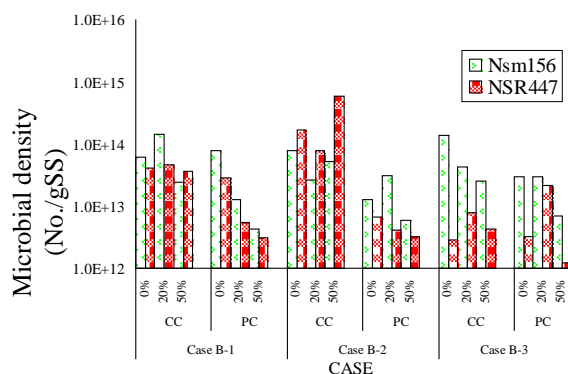


Fig. 7 Density of bacteria attached on the concrete pieces

this study. There was a tendency that the number of cells hybridized with probe Nsm156 decreased with the increase of mixing rate of artificial zeolite(%). It is suggested that biological activity per unit amount of the nitrifying bacteria was not same. By the way, the probe NSR447 is suitable for the detection of *Nitrospira* which is closely related to *Nitrospira moscoviensis* live in freshwater environment. On the other hand, we can't obtain clear image in using NIT3 which is a probe for the detection of *Nitrobacter*. It is also suggested that *Nitrospira* was dominant as NOB compared with *Nitrobacter*. in this research. Investigation of population dynamics of microorganisms on the surface of concrete media could be important research topics for next step.

## CONCLUSIONS

In this study, ammonia removal characteristics of porous concrete with zeolite were investigated by conducting experiments. Some results obtained in this study were summarized as follows.

(1) Concrete pieces containing zeolite can attach microorganisms effectively and the attached amount of microorganisms can increase with the increase of zeolite amount in the concrete pieces. Porous shape can also increase the attaching amount of bacteria. It is suggested that the porous concrete with zeolite can attach microorganisms especially nitrifying bacteria. The concrete piece can adsorb ammonia and the adsorption ability can be regenerated by biologically. The applicability and feasibility to preserve water environment, especially river water quality are suggested.

(2) Nitrification activity of porous concrete with Fe type zeolite was greater than that with Ca type zeolite. Zeolite type would affect the nitrifying ability of concrete pieces.

(3) In this study, clear relationship between nitrifying activity and number of nitrifying bacteria were not observed. Population dynamics on porous concrete will be a challenge for the future.

## ACKNOWLEDGEMENTS

Acknowledgement: We thank students of water environment laboratory in Department of Civil and Environmental Eng., Ehime University, Japan.

## REFERENCES

- [1] Sung-Bum Park, Mang Tia, "An experimental study on the water-purification properties of porous concrete", Cement and Concrete Research, Vol. 34, Issue 2, Feb. 2004, pp. 177 - 184.
- [2] Taghizadeh, M. M., et al. "Feasibility study of water purification using vertical porous concrete

- filter." *Int J of Environ Sci Technol* 4.4, 2007, pp. 505 - 512.
- [3] Tamai, M.: "Adherence of microorganisms onto the porous concrete and water purification; Porous concrete", *Ceramics Japan*, 33(7), pp.542-545, 1998. (in Japanese)
- [4] Amann. R. I.: "In situ identification of microorganisms by whole cell hybridization with rRNA-targeted nucleic acid probes", *Molecular Microbial Ecology Manual* 3.3.6, 1995, pp.1-15.,
- [5] Fernández, B., Vilar, A., Ben, M., Kennes, C, and Veiga,. MC: "Partial nitrification of wastewater from an aminoplastic resin producing factory", *Water Sci. Technol*, Vol.52, No.10-11, 2005, pp.517-524.
- [6] Yang, L., and Alleman, J.E.: "Investigation of batchwise nitrite build-up by an enriched nitrification culture" , *Water Sci. Technol*, Vol.26(5-6), 1992, pp.997-1005.
- [7] A.C. Anthonisen, B.C. Loehr, T.B.S. Prakasam, E.G. Srinath, "Inhibition of nitrification by ammonia and nitrous acid. *J. of Water Pollut. Control Fed.* Vol.48, 1976, pp. 835-852.
- [8] M. Mauret, E. Paul, E. Puech-Costes, M. T. Maurette and P. Baptiste: "Application of experimental research methodology to the study of nitrification in mixed culture", *Water Sci. Technol*, Vol 34(1-2), 1996, pp. 245-252.
- [9] Barbara A. Jucker, Alexander J. B. Zehnder, and Hauke Harms: "Quantification of Polymer Interactions in Bacterial Adhesion, Interaction in Bacterial Adhesion", *Environmental Science and Technology*, Vol. 32, No.19, 1998, pp. 2909-2915.
- [10] Darren A. Lytle: "A systematic comparison of the electrokinetic properties of environmentally important microorganisms in water", *Colloids and Surfaces B*, 24, 2002, pp.91-101.
- [11] Onnis-Hayden, Annalisa; Dair, Daniel; Johnson, Chandler; Schramm, Andreas; Gu, April Z. Kinetics and nitrifying populations in nitrogen removal processes at a full-scale integrated fixed-film activated sludge (IFAS) plant, *Proceedings of the Water Environment Federation, WEFTEC* 2007.

## Authors Index

### **A**

A. K. Alzoubi	225
A. Oya	111
A.S.M. Abdul Awal	388
Abdul Naser Abdul Ghani	427
Abdul Saboor Rahmany	500
Abdull Halim Abdul	566
Ahmad Hilmy Abdul Hamid	427
Ahmet Tuncan	296, 300
Aiassa Martinez Gonzalo	62, 72
Akihiro Fujino	528
Akiko Inoue-Kohama	421
Akinola Johnson Olarewaju	18
Akio Takigawa	472
Akula Pavan	140
Alercia Biga Carolina	72
Alex M. Lechner	416
Alireza Mohammadinia	340
Allan Manalo	124
Alojzy Szymański	196
Aminaton Marto	30
Andreas Nataatmadja	179
Andrzej Głuchowski	196
Anna Szymczak-Graczyk	520
Arif Ali Baig Moghal	315, 411
Arrúa Pedro	62, 72
Arul Arulrajah	340
Athira Ravi	515
Atsushi Fukuda	540
Atul Prabhakaran	208

### **B**

B. Look	145
Barry Wai-Choo Kok	256
Behzad Fatahi	44
Bernat Amat	320
Bertrand Teodosio	167
Bindumadhava Aery	591
Bithin Datta	504
Brian Lamb	224
Burak Evirgen	296, 300
Burt Look	151

### **C**

C H Solanki	262
C. Sreenivasulu	208
Celso Romanel	111
Chaminda Gallage	151, 394
Chane Brits	83
Che Musa Che Omar	477
Chee-Ming Chan	129
Chen-Hui Tsai	36
Chung-Jung Lee	36

### **D**

D. F. Marks	202
D. J. Williams	145
D. Lacey	145
Daisuke Hayasaka	432
Daniel Mellish	145
Darius Macijauskas	173
David Lacey	151

## Authors Index

David Thorpe	359, 455	Hailong Chen	406
Debendra Neupane	162	Hajime Narioka	500
Desai A.K.	310	Hamed Koohpayehzadeh Esfahani	504
Devanmini Halwatura	416	Hanna Szymczak	520
Dimiter Alexiew	484	Harada, H.	13
Dr B. Look	365	Hermie M. Del Pilar	334
Dr. Navin C. Shah	238	Hideaki Yasuhara	162
Dr. Sobha Cyrus	191	Hideyuki Ito	540
Duong Minh Truyen	401	Hirofumi Kassai	597
<b>E</b>		Hiromu Tamba	472
Eberhardt Marcelo	62, 72	Hirosuke Hirano	557
Elisabeth Simbolon	591	Hiroyuki Ii	528, 534, 535, 572
Enos C. Inniss	450	Homayoon Ganji	500
Escolástico Aguiar	320	Hooman Abadi	477
Eva Arifi	382	Hossain, M.Z.	13, 289, 293, 388
<b>F</b>		Hossein Mohammad Hosseini	388
Faizal Pakir, Khairulanam Kasran	30	Huan Wang	406
Francisca Castillo	320	Hudson Jackson	134
Fumitake Nishimura	597	Huu Hung Nguyen	44
Fumitake Nishimura	464	Hyun-Suk Shin	167
<b>G</b>		<b>I</b>	
G. G. N. N. Amarakoon	50	Ian P Craig	455
Graham Thomson	484	Ikeda H	89
Greg You	95	<b>J</b>	
Grzegorz Kmiecik	520	J. N. Kirjan	202
<b>H</b>		J. Rajaraman	103
H. M. A. Rashid	250	J. T. Shahu	353
H.H. Bui	111	Jaehun Ahn	167
Hadi Khabbaz	44	Jay Sanjayan	340

# Authors Index

Jeroen Berends	256	Kunio Minegishi	540
Jia Xie	256	Kyohei Umemura	66
Jim Shiau	83, 124, 202, 244	Kyoichi Okamoto	510, 577
Jing-Cai Jiang	217	<b>L</b>	
Jin-Ung Do	213	L.M. Reddy	353
Jochen Bundschuh	455	L.V. Nuzhdin	267
Jose Carlos Solis Tito	111	Le Hong Thia	401
Jothi M. Ramanujam	346	Lei Han	406
Jothi Ramanujam	394	Limin Zhang	305
Ju-Hyung Lee	213	Lokanantham R. Logitharan	346
Julian Seidel	10	<b>M</b>	
Julius E. Seva	334	M. Boyer	365
Junichi Koseki	185	M. Fujimoto	118
<b>K</b>		M. I. Ibrahimy	289
K. Kawamoto	250	M. I. Ibrahimy	293
K.Chew	365	M. Inanc Onur	296
K.Thiruvenkatasamy	103	M. Inanc Onur	300
Kamarusin Moh Noor	477	M. Z. Hossain	13, 289, 293, 388
Kassim Tarhini	134	M.L. Nuzhdin	267
Katagiri M	89	Maged Almandalawi	95
Kathirgamalingam Somasundaraswaran	346	Mahdi Miri Disfani	340
Kawano M.	89	Makoto Ikeda and Hiroyuki Ii	551
Kazuhiro Oda	66	Manuel Blanco	320
Kazuhito Murakami	421	Marian Drusa	283
Keigo Koizumi	66	Maricar A. Ilagan	334
Keiichi Kato	472	Marta Szejnfeld	520
Kim Dowling	95	Martin Silec	256
Kiyoyama T	89	Masaaki Furuno	432
Koichi Ishimatsu	382	Masaaki Kondo	444, 500
Koichi Yamanaka	540		



## Authors Index

Masahiro Yamashita	572	<b>N</b>	
Masashi Iwata	524	N. Hiraoka	118
Masayoshi Yamanaka	376	Naoki Kinoshita	162
Mashhor Mansor	401	Nathalie Touze-Foltz	320
Md Zahangir Alam	524	Neelima Satyam D.	157
Md. Monjurul Alam	524	Nicholas Hytiris	56
Michael Fraser	56	Nobuyasu Oyama	382
Michal Kuba	283	Nobuyuki Nishimiya	557
Micheal A. Uduebor	585	Nor Zurairahetty Mohd Yunus	30
Michiko Masuda	464	Norimitsu Koike	458
Michiko Masuda	597	Norimitsu Koike	490
Michio Gomyo	421	Noushin Naraghi Araghi	561
Minoru Yamanaka	232	Nursiafitah Kasnon	427
Mitsuhiro Shigeishi	382	<b>O</b>	
Mohamed Redha Menani	494	Ohishi K	89
Mohammad Raihanul Islam	376	Ojiro C.	13
Mohammed Saedi Jami	524	Okuyama, S.	13
Mohannad Sabry	95	Olaolu G. Fadugba	585
Mohd Akmal Azri Jamal	30	Oluwapelumi O. Ojuri.	273, 578, 585
Mohd Zarar Mohd Jenu	129	Osman El Hussien	77
Mohd. Nawawi	561	Ozumi, S.	13
Monesse Andrea Z. Antonio	334	<b>P</b>	
Moshe Livneh	326	P. Moldrup	250
Mosleh Ali Al-Shamrani	411	Pallavi Ravishankar B.	157
Mosleh Ali Al-Shamrani	31 5	Peter Dahlhaus	95
Motohiro Tanaka	597	Peter K. Adegoke	273
Muawia A Dafalla	315	<b>R</b>	
Mustafa Tuncan	296	R. Fukagawa	118
Mustafa Tuncan	300	Rajab M. Abousnina	124
Myint Win Bo	340		

## Authors Index

Ramli Bin Nazir	77	Subha Vishnudas	515
Ravin M. Tailor	238	Subhamoy Bhattacharya	208
Rétyce Ivan Hervé Dodji Togbé Amoussou	382	Sung-Ryul Kim	213
ris Aryanto	370	Suresh R Dash	208
Rosli Saad	561	Susumu Kurahashi	458, 490
Ryota Serizawa	472	Sven Arnold	416
<b>S</b>		Syed Mustafizur Rahman	561
S. M. A. Motakabber	289, 293	<b>T</b>	
S. Narasimha Rao	103	T. Komatsu	250
S. Patel	353	T. Saito.	250
Saki Agatsuma	421	Tadashi Uchiyama	432
Sampei Yamashita	432	Taizo Uchida	432
Samuel A. Ola	585	Takamitsu Kajisa	444, 500
Sandhya Rao Poleneni	450	Takase E	89
Satoru Ishiguro	376	Takashi Minami	432
Satoru Kawasaki	50	Takashi Nakajima	472
Shingo Tomiyama	551	Takefumi Koreeda	50
Shinichi Ito	66	Takeshi Toyama	510, 557
Shiran Jayakody	394	Takuma Kubohara	534
Shoma Nehashi	540	Tamer Y Elkady	315
Shouquan Wang	406	Teruo Arase	432
Shuai Zhang	305	Teruo Arase	438
Shuichi Hasegawa	232	Tetsuo Okano	438
Shukla S.J	310	Thiruvengadam Tamilmani	140
Slobodan B. Mickovski	56	Tomoaki Hachimura	232
Soichiro Kageyama	551	Toshio Yamada	597
Solanki C.H	310	Tsunataka Furuya	217
Stefan Van Baars	173	Tsutomu Namikawa	24
Stephen Buttlng	2		
Stephen Darmawan	340		

## Authors Index

### U

Usama Juniansyah Fauzi 185

### V

Veena. V. 191

Vlastimil Chebeň 283

### W

Waleed M Zahid 411

Weena Lokuge 124

Wen-Yi Hung 36

Wojciech Sas 196

### X

Xuyin Yuan 406

### Y

Yamamoto S 89

Yasuji Shinohara 370

Yi-Chun Tu 36

Yohei Usuki 66

Yoshifuku T 89

Youhei Takanabe 382

### Z

Zakaria Hossain 13, 289, 293, 388

## **Contents of GEOMATE2011-Volume 1(1) and Volume 1(2)**

### ***Geotechnique***

Developments of geosynthetic-reinforced soil technology in Japan: retaining walls and bridge abutments <i>Fumio Tatsuoka</i>	3
Seepage-deformation coupled numerical analysis of unsaturated river embankment using an elasto-plastic model <i>F. Oka, S. Kimoto and R. Kato</i>	15
Progressive failure of shallow anchor in dense sand evaluated by 2D and 3D finite element analysis and model tests <i>T. Sakai and M. Rokouzzaman</i>	23
Design of single pile foundations using the mechanics of unsaturated soils <i>Vanapalli S. and Taylan Z.N.</i>	31
Problematic soil: in search for solution <i>Bujang B.K. Huat</i>	39
Characterization and modeling of various aspects of pre-failure deformation of clayey geomaterials – fundamental theories and analyses <i>J.N. Mukabi</i>	47
The maintenance of ground anchors in Nippon Expressway <i>Yuu Fujiwara and Toshinori Sakai</i>	57
Stress distribution in khon kaen loess under spread footing <i>Pairoj Yodsa-nga and Watcharin Gasaluck</i>	61
The effect of sheet pile length on the capacity of improved pile foundation on sand under vertical and moment loading <i>Tuan Van Nguyen and Pongsakorn Punrattanasin</i>	65
Investigation of a reliable reinforcing method for embankment ground <i>H. M. Shahin, T. Nakai, M. Kikumoto, R. Sakai, Y. Yoshida, I. Saito, N. Nagao and K. Toda</i>	71
Evaluation of stamps and latex shell influence on stabilometer testing results, modeled with simulia abaqus <i>Dmitriy Volik</i>	77
Characterizing the interaction of geomat with fine grained black cotton soils <i>Wekesa S., Mukabi J., Okado J., Kogi S., Ndeda M. and Ogallo J.</i>	81
Soil liquefaction susceptibility zoning due to earthquake using GIS and geotechnical data <i>Bhuyan Md. Habibullah, Rama Mohan Pokhrel, Jiro Kuwano and Shinya Tachibana</i>	87
Evaluation on the results of multistage shear test <i>Hormdee D. and Kaikeerati N.</i>	93
Verification of effects of countermeasures for seepage of river levees by on-site monitoring of the water level of levees <i>Hiroyuki Masuyama, Yukiko Saito, Masanori Ishihara, Tetsuya Sasaki and Hirotoshi Mori</i>	97
Influence of decreasing of soil suction on unconfined compressive strength for bentonite <i>Tomoyoshi Nishimura</i>	103

## **Contents of GEOMATE2011-Volume 1(1) and Volume 1(2)**

The relationship between soil suction and the maximum unsaturated undrained shear strengths of compacted khon kaen soil <i>R. Nuntasarn and W. Wannakul</i>	107
Interpretation of coaxial and non-coaxial strain on directional variation of undrained strength of clay <i>J.Rajaraman and K. Thiruvengkatasamy</i>	113
FEM analysis of innovative shallow foundation system for reactive soils <i>Mostafa A. Ismail and Mohamed A. Shahin</i>	117
Delay times of elastic waves at discontinuities in laminated specimens <i>Yota Togashi, Kazuo Tani, Tetsuji Okada and Hiroaki Sato</i>	123
Geotechnical investigation of valleys using lightweight dynamic cone penetration test for landslide risk assessment <i>Takashi Hanaoka, Takashi Tsuchida, Shoichi Kawabata and Shota Nakagawa</i>	129
Study on individual landslide risk assessment of natural valleys and slopes during heavy rain based on geotechnical investigation and analysis <i>Shouichi Kawabata, Takashi Tsuchida, Takashi Hanaoka and Shouta Nakagawa</i>	135
Analyses of piping under foundation of weirs in different ground density by FEM <i>Okajima Kenji</i>	141
Shear deformation and failure of sandy slope according to pore pressure generation due to rainfall infiltration <i>Katsuo Sasahara and Naoki Sakai</i>	147
Load settlement relationships of circular footing considering dilatancy characteristics of sand <i>Yusuke Tomita, Tatsuaki Nishigata, Takeshi Masui and Shintaro Yao</i>	153
Thermally modifying bentonite for construction industry <i>Abdoullah Namdar</i>	159
Mesh-free analysis of beam on elastic foundation <i>S. M. Binesh</i>	163
Frictional Performance Of Infilled I-Blocks With Geosynthetic Inclusions <i>Faisal Hj Ali, Md. Zahidul Islam Bhuiyan, Firas A. Salman and Siau Lian San</i>	167
Varying ground water level to minimise liquefaction hazards in urban areas <i>Heitor A., Oka F., Kimoto S. and Higo Y.</i>	173
Development of a new type reinforced soil wall <i>Hara T., Tsuji S., Yoshida M., Ito S. and Sawada K.</i>	177
Development of design charts for reinforced embankment using excel spreadsheet slope stability analysis <i>Ito Kazuki, Md. Zakaria Hossain and Toshinori Sakai</i>	183
Numerical simulation of 2D crack growth with frictional contact in brittle materials <i>Kai Zhang, Jing-cai Jiang and Qing Yang</i>	187
Interface behaviour of basalt geosynthetic with sand in direct shear mode <i>M.B. Hossain, M.Z. Hossain and T. Sakai</i>	191
Effect of soil parameter uncertainty on seismic response of buried segmented pipeline <i>Chaminda Gallage, Pathmanathan Rajeev and Jayantha Kodikara</i>	197

## **Contents of GEOMATE2011-Volume 1(1) and Volume 1(2)**

The sorption capacity of cu by sc-soil from batch and column tests <i>Arwut Yimtae, Pongsakorn Punrattanasin and Noppadol Sangiumsak</i>	203
 <b><i>Construction materials</i></b>	
Green construction: the role of palm oil fuel ash in concrete <i>A.S.M. Abdul Awal</i>	211
Behavior of collapsible loessic soil after interparticle cementation <i>Arrua Pedro, Aiassa Gonzalo, Eberhardt Marcelo and Claverie Eliana</i>	221
A study on hardened soil brick using liquid type and powder type hardening agent <i>Jin Sung Ki., Jung Seung Yong. and Kim Tae Ho.</i>	227
The effect of salt content in soil on the sorption capacity of heavy metals <i>Lerd Kerdchaiyaphum and Pongsakorn Punrattanasin</i>	233
Manufacture of Housing Construction Materials with Jute Polymer Composite (Jutin) <i>Mubarak A. Khan, Fahmida Parvin, Jahid M M Islam and Md. Zakaria Hossain</i>	239
Evaluation of strength of granulated construction waste sludge with quick lime and its application to soil structure <i>Makoto Kobayashi, Hiroaki Nakamura and Hideaki Mizuno</i>	245
Analysis of enhanced strength and deformation resistance of some tropical geomaterials through application of in-situ based stabilization techniques <i>Kogi S., Ndeda M., Mukabi J.N. and Wekesa S.</i>	251
Further developments in the swelling model of expansive clays under ASTM 4546 and CBR testing <i>Moshe Livneh</i>	257
The effect of clay, lime and rice husk ash contents on the sorption capacity of Cu, Ni and Zn by Soils <i>Pongsakorn Punrattanasin and Noppadol Sanggiumsak</i>	263
The effect of temperature on the sorption capacity of copper by soils <i>Noppadol Sangiumsak and Pongsakorn Punrattanasin</i>	269
Experimental Investigation for Nitrate Reduction Using Iron Powder in Porous Media <i>Haruka Shimada, Kazuya Inoue, Ikko Ihara, Katsutoshi Suzuki and Tsutomu Tanaka</i>	275
Using spatial moments in conjunction with image processing to estimate macrodispersion in stratified porous formations <i>Katsutoshi Suzuki, Kazuya Inoue, Tsutomu Tanaka and Akira Kobayashi</i>	281
The novel technology of desertification control and ecological restoration with an Hydrolysis Polyurethane(W-OH) <i>Weimin Gao, Zhiren Wu, Zhishen Wu, Kentaro Iwashita, Hirondo Inagaki and Caiqian Yang</i>	287
Migration of radioactive materials through porous media: theory and a solution for an unsteady state problem <i>Khaled I. Hamza</i>	293
Fundamental study on ecosystem support canal using porous concrete <i>Masuma Yoshihiro, Hasegawa Yuki, Md.Rokunuzzaman, Yamada Toshio, Kassai Hirofumi and Sato Shushi</i>	299



## **Contents of GEOMATE2011-Volume 1(1) and Volume 1(2)**

Alternative employment of crushed shell particles in capillary barrier of soil <i>Satoru Nakafusa, Kaoru Kobayashi, Toshihiro Morii, Tomoyoshi Nishimura</i>	305
A novel statistical approach for investigating the significant factors that influence the performance score of the Turkish method <i>Kshama Sundar Roy, Kamrul Islam and Md. Shams Arafat</i>	311
Ultimate strength and fatigue life of concrete structural elements reinforced with carbon fiber sheet <i>Hiddenori Tanaka and Yutaka Toi</i>	317
Development of functional carbon nanotubes -asphalt composites <i>Tatsuo Shirakawa, Akio Tada and Noriyasu Okazaki</i>	323
Hydraulic character of estimation method on roughness coefficient of concrete canal <i>Koichiro Otagaki, Koji Sai, Kenichi Fujisawa, Shinsuke Matsumoto and Shushi Sato</i>	329
Na-bentonite as rock containment barrier against heavy metals and acid leachates <i>Angelica Naka, Takeshi Katsumi, Toru Inui, Giancarlo Flores and Takehiro Ohta</i>	333
The comparison of monotonic behaviors of two different calcareous sands <i>R. Rezvani, H. Shahnazari, H. Salehzadeh and Y. Dehnavi</i>	337
Soaking effect on strength and performance of fine grained soil stabilized with recycled gypsum <i>Aly Ahmed, Keizo Ugai and Taira Jinno</i>	343
Removal of Zinc in soils using natural zeolite <i>Wiparat Nisapai, Arthit Neramittagapong and Sutasinee Neramittagapong</i>	349
Heat control of pavement surface temperature using oyster shell lime <i>Satoru Ishiguro and Masayoshi Yamanaka</i>	353
Buckling behavior of composite triangular plates <i>T.Farsadi, P.Amani and E.Heydarnia</i>	357
Durability of cement treated highway materials <i>Jiraroeth Sukolrat, Apisit Klummeng and Sekchai Anuvechsirikiat</i>	365
Porous geopolymer concrete <i>Tawatchai Tho-in, Vanchai Sata and Prinya Chindaprasirt</i>	371
Design and Fabrication of Composite Technology for Earth Slope Protection <i>Md. Toriqul Islam, Md. Zakaria Hossain and Masaaki Ishida</i>	375
Study of slump testing for hydraulic plastic grout <i>Hiroyasu Ishii, Kenichi Horikoshi and Masaki Kitazume</i>	381
Behavioral comparison of coarse aggregate from various quarry sites of pakistan, effect on hardened concrete, economics and environment <i>Faisal Malik and S. Muhammad Jamil</i>	387
Methods for execution of concrete piles in corrosive and destructive marine environments, based on study of the Persian Gulf marine installations <i>Nasser Arafati, Abdol Hossein Fazli and Seyed Mehdi Mousavi</i>	393
Fundamental study on particle size distribution of coarse materials by image analysis <i>G.H.A.J.J. Kumara, K. Hayano and K. Ogiwara</i>	399

## **Contents of GEOMATE2011-Volume 1(1) and Volume 1(2)**

### ***Environment***

Calibration and simulation of runoff models for developing watershed respond knowledge at tropical area <i>Arien Heryansyah and Zulkifli Yusop</i>	407
Effect of geological succession on macrophyte and microbiota in aquifer ecosystem in urban coastal zone <i>Kazuhito Murakami and Akiko Inoue-Koham</i>	411
Bioclean and liquid biofertilizers a new way to the green area <i>Sittisak Uparivong</i>	417
Massive point cloud acquisition on a soil surface using a stereo camera <i>Masafumi Nakagawa, Anna Nakanishi, Hirotaka Endo and Kenta Ochiai</i>	421
Estimation of earthquake ground motion in Padang, Indonesia <i>Rusnardi Rahmat Putra, J. Kiyono and Y. Ono</i>	425
Groundwater contamination due to irrigation of treated sewage effluent in the werribee delta <i>Hiroyuki Ii, Masanobu Taniguchi, Ataru Satoh, Graeme Allinson, Matt Kitching, George Croatto and Bruce Shelley</i>	431
Process of invading the alien plant species into the river ecosystem <i>Michiko Masuda, Yumie Ito and Fumitake Nishimura</i>	437
Recent meandering pattern of the Irrawaddy, Myanmar <i>Mayumi Matsumoto and Shigeko Haruyama</i>	443
Physical and chemical properties of tsunami deposit in northeast area in Fukushima prefecture after Tohoku-Kanto earthquake <i>Tomonori Fujikawa, Hiromu Okazawa, Takahiko Nakamura, Yasushi Takeuchi and Masaharu Komamura</i>	447
Changes of bottom sediment caused by Construction of the Airport Island in the Ise Bay, Japan. <i>Maki Oyagi, Motohiro Kawase and Akihiko Yagi</i>	453
Proposal of simple measurement method for evaporation rate by using oxygen isotopic ratio in the inawashiro lake <i>Satoshi Miyahara and Hiroyuki Ii</i>	457
Landslide susceptibility mapping using logistic regression model with neighborhood analysis: a case study in mizunami city <i>Wang Liangjie, Sawada Kazuhide and Moriguchi Shuji</i>	463
The evaluation of the river environment and water quality by image analysis in the Yamato River Basin in Japan <i>Masanobu Taniguchi, Hiroyuki Ii and Tatemasa Hirata</i>	469
Distribution of oxygen and hydrogen stable isotopic ratios and estimation of the spring water origin in the Kushiro Moor <i>Natsuki Kawabe and Hiroyuki Ii</i>	473
A debris flow and its risk analysis related to the 2008 Wenchuan earthquake <i>Yange Li, Guangqi Chen, Chuan Tang and Lu Zheng</i>	479
Impact analysis of water price reform of Zhangye, China <i>Atsushi Koike, Zhongmin Xu, Kang Wang and Bunei Itoga</i>	485

## **Contents of GEOMATE2011-Volume 1(1) and Volume 1(2)**

Post earthquake rapid inspection planning for bridges in western Kentucky <i>Norimitsu Koike and Issam E. Harik</i>	491
Organophosphoric acid triesters from landfill sites and sewage plants in Japan <i>Haruki Shimazu</i>	497
Ground water pollution around the Oyachi-Heizu district of Yokkaichi city <i>Yukimasa Takemoto, Masaaki Takahashi, Kayoko Awaya, Mikihiro Ioka and Peng Guo</i>	501
Characteristics of damage to structures induced by the tsunami of the 2011 east Japan mega earthquake <i>Ömer Aydan, Hisataka Tano and Takahiro Iwatate</i>	505
Characteristics of strong motions induced by the 2011 east Japan mega earthquake with an emphasis on Tokyo bay area <i>Takahiro Iwatate, and Ömer Aydan</i>	511
Inquiry of the value of parks in the characteristics and use of park planning through urban revival planning projects in Maebashi city <i>Shinya Tsukada, Tetsuo Morita and Akira Yuzawa</i>	517
A study on evaluation of quality of life in consideration of water/green environment <i>Tetsuo Morita, Yoshihito Kogure, Hiroshi Sugita, Tsuyoshi Baba, Shinya Tsukada and Naoki Miyazato</i>	521
Changes and issues in green space planning in the tokyo metropolitan area: focusing on the "capital region plan" <i>Tetsuo Morita, Yoshihide Nakagawa, Akinori Morimoto, Masateru Maruyama and Yoshimi Hosokawa</i>	527
Application of traffic simulation in road policy assessment accompanied by railway elevation <i>Maekawa Takuya and Hiroshi Inouye</i>	533
Impact estimation of land cover changes of recharge area on spring discharge in marshy environment <i>Masaaki Kondo and Takamitsu Kajisa</i>	541
Numerical Study on Characteristics of Levee Breach Flood Disasters in Alluvial Floodplain <i>Md. Serazul Islam and Tetsuro Tsujimoto</i>	547
Purification system of ocean sludge by activating microorganisms <i>Kyoichi Okamoto, Kenji Hotta, Takeshi Toyama and Hideki Kohno</i>	553
Author index	559

### ***Volume 2***

Characterization and modeling of various aspects of pre-failure deformation of clayey geomaterials – applications in modeling <i>J.N. Mukabi and M.Z. Hossain</i>	563
An emergency medical care information system for fetal monitoring <i>Muhammad Ibn Ibrahimy</i>	573
Effects of gypsum on the swelling and dispersion behaviour of fine grained soils from Sudan <i>Abdul Karim, M. Zein and Ahmed M. Elsharief</i>	577

## **Contents of GEOMATE2011-Volume 1(1) and Volume 1(2)**

Comparison of bearing capacity equations for vertical central loading <i>Muhammad Awais Shafique and Tanvir Iqbal Qayyum</i>	583
Pull-out resistance of selected native plants in Hong Kong <i>Leung F.T.Y., Yan W.M., Tham L.G. and Hau B.C.H.</i>	589
Inland navigation in carrying injured and sick disaster victims in case of a massive earthquake in the Tokyo metropolitan area <i>Kazuya Egami, Keiichi Noto, Wataru Miyazaki, Kazukiyo Yamamoto and Takeo Kondo</i>	593
Model calculation and geotechnical interpretation of the correlation co-efficient between finite and incremental strain path of a formation <i>J.Rajaraman and K. Thiruvengatasamy</i>	597
Geocell reinforced bed subjected to simulated traffic loads <i>P. Sharifi, and S.N. Moghaddas Tafreshi</i>	601
Effects of gradation of various sand deposits of Pakistan on strength of hardened concrete <i>Gauhar Sabih and S. Muhammad Jamil</i>	607
Strengthening of landslide retaining pile wall after geodetic monitoring <i>Frangov G., Zayakova H., and Hamova M.</i>	613
Response of tapered piles under lateral harmonic vibrations <i>Ahmad Dehghanpoor and Mahmoud Ghazavi</i>	627
Investigation of ground movement in soil-nailed walls using 1g models and PIV method <i>H. Mahdavi, and M. Hajjalilue-Bonab</i>	623
Author Index	629

## **Contents of GEOMATE2012 - Volume 2(1)**

### **ID    *Keynote Papers***

1	Use of microbial technology in geotechnical engineering <i>Jian Chu, Volodymyr Ivanov, Jia He and Viktor Stabnikov</i>	1-4
2	A study on slow moving slopes <i>L G Tham and Xu Kai</i>	5-11
3	Bearing capacity and settlement behaviour of shallow foundations in unsaturated sands <i>Sai K. Vanapalli and Fathi M. O. Mohamed</i>	12-21
4	Development of Piled Geo-wall <i>Hara, T., Tsuji, S., Yoshida, M. and Sawada, K.</i>	22-29
5	Measurement of strain distribution along precast driven pile during full scale pile load test <i>Faisal Ali and Lee Sieng Kai</i>	30-39
6	Unique grouting material composed of calcium phosphate compounds <i>S. Kawasaki and M. Akiyama</i>	40-46
7	Stiffness Anisotropy and Resilient Modulus of an Unsaturated Soil under Static and Cyclic loads <i>Charles W.W. Ng, C. Zhou and J. Xu</i>	47-62
8	Nanoparticles for Geotechnical Engineering <i>Mohd Raihan Taha</i>	63-68

### ***Technical Papers***

#### ***Geotechnique***

		69
24	Damage Assessment and Strengthening of R/C Building Constructed on Expansive Soils <i>Osama M. A. Daoud</i>	70-75
29	Gravitational Sphere Packing Method To Find The Porosity Of The Soil Particles With The Identical Size in cylindrical container <i>Mohammad Mahdi Roozbahani , Bujang B. K. Huat, Afshin Asadi</i>	76-78
34	Parametric Study of Piled Raft Foundations to improve the Design Method <i>Tohidi A., MH .Sadagiani</i>	79-84
39	Experimental Study of Suction-Monitored CBR test on Sand-Kaolin Clay Mixture <i>Purwana, Y.M., Nikraz H., and Jitsangiam P.</i>	85-90
41	Foundation Strengthening of Historic Buildings by Micropiles <i>Azza M. Elleboudy</i>	91-96

## **Contents of GEOMATE2012 - Volume 2(1)**

44	Group effects of piles due to lateral soil movement <i>Hongyu Qin1 and Wei Dong Guo</i>	<b>97-102</b>
45	Collapse-Settlement Calculations for Embankments Based on a Collapsible Soil Subgrade <i>Moshe Livneh</i>	<b>103-108</b>
46	The influence of trench soil properties on the accuracy of pressure cell measurements in an earthfill dam <i>D. Elmi, A. A. Mirghasemi</i>	<b>109-112</b>
50	Studying the effects of considering dilation angle over the performance of geotechnical elements using numerical methods <i>Salman Hanifi, Amin Naeimabadi , Mohammad Reza Atrchian</i>	<b>113-117</b>
50a	Comparing the excavating effect of single and twin tunnels on the earth surface settlement by numerical methods <i>Amin Naeimabadi, Salman Hanifi , Mohammad Reza Atrchian</i>	<b>118-124</b>
107	Excess Pore Pressure Characteristics of Sand Mat using Dredged Soil <i>M.S LEE, K. ODA</i>	<b>125-130</b>
110	Effect of clays fraction to california bearing ratio laboratory test value with and without soaked <i>Soewignjo Agus NUGROHO, Syawal Satibi and Ferry Fatnanta</i>	<b>131-136</b>
111	Compressibility Characteristics of Residual Soil Subjected to Microbial Treatment <i>Lee Min Lee, Ng Wei Soon, and Yasuo Tanaka</i>	<b>137-140</b>
115	Strength and aging of cement treated low plastic soils <i>Fabien Szymkiewicz, Antoine Guimond-Barrett, Alain Le Kouby</i>	<b>141-145</b>
119	Performance Of Cantilever Sheet Pile Supporting Excavation Adjacent To Strip Footing <i>Yousry M. Mowafe, Ahmed M. Eltohamy and Ahmed A. Mohamed</i>	<b>146-153</b>
119a	Enhancing Stability of Slopes with Cement Kilin Dust Sand Mixture Layer <i>Al Serif M. Abd Alazez1, Ahmed M. Eltohamy and Ahmed Rusdy Towfek</i>	<b>154-161</b>
122	The effect of confining stress on the analysis of excavations with adjacent existing buildings <i>Sabzi Zahra, Fakher Ali</i>	<b>162-166</b>
125	Bored Pile Socket in Erratic Phyllite of Tuang Formation <i>D.E.L. Ong</i>	<b>167-171</b>
133	Swelling deformation of the bentonite mixed with silica fume or sodium carbonate in calcium hydroxide solution <i>Yuki YOKOYAMA and Kenichiro Nakarai</i>	<b>172-175</b>
136	A Combined Probabilistic Method for Engineering Failure analyses and Applications in Typical Geotechnical Structures <i>Duruo Huang</i>	<b>176-181</b>
137	Parametric Study of Crossing Tunnels at Different Level <i>A. Tohidi, MH.Sadagiani</i>	<b>182-189</b>
143	Use of post-floatation copper tailings in the construction of dump dams <i>Tschuschke W., Wierzbicki J.</i>	<b>190-195</b>



## **Contents of GEOMATE2012 - Volume 2(1)**

150	Effects of Slope Inclination on the Rain-induced Instability of Embankment Slopes <i>Chaminda Gallage, Shiran Jayakody and Taro Uchimura</i>	196-201
225	Extension of an integrated AHP and TOPSIS approach in the earth dam site selection <i>Minatour Yasser, Khazaie Jahangir</i>	202-208
227	Using Geogrid Boxes as a New Approach for Reinforcement of Rock Slopes <i>Ahmad Fahimifar, Arvin Abdolmaleki</i>	209-214
228	Volume Change Characteristics of Clay Mixes with Different Bentonite Percentages <i>J. M. Kate, Sunil Kumar, M. P. Bhorkar</i>	215-218
236	FE Analysis for Settlement of Peat Ground under Embankment Loading <i>Satoshi Nishimoto and Hirochika Hayashi</i>	219-224
237	Seismic behavior of pile group in soil slopes: 1g shake table tests <i>H. Elahi, M. Moradi, A. Ghalandarzadeh and A. Elahi</i>	225-229
239	Electrophoresis of Bacteria and Electro-Biogrouting <i>Hamed A. Keykha, Bujang B. K. Huat, Afshin Asadi, Satoru Kawasaki</i>	230-232
240	Consideration concerning reasonable modified form of Floating-type Improved Ground <i>Hijiri Hashimoto, Satoshi Nishimoto and Hirochika Hayashi</i>	233-236
241	Numerical Study Effect of Nail Angle Change on Stability and Displacement of Excavation Wall in Cohesive and Cemented Non-Cohesive Soils <i>Navid Shahnazi, Jahangir Khazaie, Mohamad Sharifipour and Kiarash Ashtari</i>	237-241
242	An investigation on behavior of geogrid reinforced soil retaining walls applying finite difference method (F.D.M) <i>Jahangir Khazaie and Alireza Sadeghabadi</i>	242-252
243	Effects of humic acid and salt additives on the behaviour of lime-stabilised organic clay. <i>N.Z. Mohd Yunus, D. Wanatowski, and L.R. Stace</i>	253-256
244	Sodium Tripolyphosphate For Stabilizing Of Contaminated Soil <i>Amin Falamaki, Hossein Tavallali and Shahrbanoo Rezanejad Farahmand</i>	257-260
246	Evaluation of Soil Water Characteristic Curves for Sand-Expansive Clay Mixture <i>T. Y. Elkady, M. A. Dafalla, A. M. Al-Mahbashi and Mosleh Al Shamrani</i>	261-265
247	Coastal soils improvement <i>Mohammad reza Atrchian, Morteza Ala, Amin Naeimabadi</i>	266-269
248	A Hybrid Intelligent System of Fuzzy C-Mean Clustering and Neural Networks to Predict the Compaction Characteristics of Fine Grained Soils <i>Iman Ashayeri, Mahnoosh Biglari</i>	270-273
249	Equivalent linear seismic ground response analysis of unsaturated soil deposits <i>Mahnoosh Biglari, Iman Ashayeri</i>	274-278
251	The Correction of Shallow Foundation Settlement Equations by Finite Element Method <i>Mohammad Arab Ameri, Hakime Rabbanifar and Mehdi Arab Ameri</i>	279-284

## **Contents of GEOMATE2012 - Volume 2(1)**

255	Numerical study of earthquake hazards of liquefaction occurring on the site and sustainable transport pipes <i>Hamed Bavanpouri, Jahangir Khazaie, Dr.Hasan Sharafi</i>	<b>285-288</b>
266	Analysis of geogrid reinforced soil retaining walls with limit equilibrium and finite difference method <i>Alireza Sadeghabadi, Jahangir Khazaie and Mostafa Yousefi Rad</i>	<b>289-293</b>
270	Recent Development in Electrokinetic Stabilization of Soft Soil, A review <i>Hossein Moayed, Sina Kazemian, and Bujang B. K. Huat</i>	<b>294-298</b>
275	Application of ion-exchange solution soil stabilizer in increasing CBR values of clayey soils <i>Reza Ziaie Moayed, Seyed Ali Hashemi and Farzad Allahyari</i>	<b>299-302</b>
276	Assessment of Low Strain Wave Attenuation for Piles Cast in Very Dense Granular Soil <i>Ramli Nazir and Osman El Hussien</i>	<b>303-307</b>
279	Dynamic Soil-Structure Interaction Considering Pore-Water Pressure Coupling <i>Qutayba Nazar Al-Saffar, P Akram Y. Al-Sa'aty, Mohamad T. Al-Layla</i>	<b>308-325</b>
281	Analysis and design of tunnel lining in alluvial soil deposits <i>Nuri al-Mohamadi</i>	<b>326-330</b>
285	Effect of silt content on the anisotropic behaviour of silt-sand mixtures <i>Navid Khayat, Abbas Ghalandarzadeh</i>	<b>331-337</b>
288	Optimizing the twin tunnels position for reduction the surface ground movements <i>Mehdi Mokheri, Seyed Ali Farjam</i>	<b>338-344</b>
290	Evaluation of pile lateral capacity in clay applying evolutionary approach <i>Alkroosh I., Nikraz H</i>	<b>345-348</b>
293	Effect of Reservoir Drawdown Rate on Phreatic Line Recession in Homogeneous Earth Dams <i>R. Ziaie Moayed, V. Rashidian</i>	<b>349-352</b>
294	The effect of lime-microsilica stabilization on California Bearing Ratio of silty soils <i>R. Ziaie Moayed, Y. Daghighi, B. Pourhadi and N. Sahebzamani</i>	<b>353-356</b>
295	Effect of elastic modulus varieties in depth on modulus of subgrade reaction on granular soils <i>Reza Ziaie Moayed, Mahdi Ali Bolandi</i>	<b>357-360</b>
296	Flexural Buckling Behavior of Steel Pile with Vertical Load in Liquefied Soil <i>Yoshihiro Kimura and Koichi Onohara</i>	<b>361-365</b>
305	Two-dimensional finite difference pseudo-static deep-seated slope stability analysis of embankments over stone column-improved soft clay <i>Farshad Fayyaz Jahani, Mohammad Sharifipour</i>	<b>366-371</b>
308	Parametric study of Geo-grid soil reinforced retaining walls under dynamic loading by ABAQUS software <i>Artrchian mohammad reza, Daghighi younes, Ghanbari namin hamed</i>	<b>372-380</b>
2010	Sensitivity analysis in soil nail wall for Tehran-Tabriz railway by considering the coefficient of variation for effective parameters in stability analysis <i>Mohammad Moghadaripour, Ardalan Akbari Hamed, Ali Ghozat</i>	<b>381-384</b>

## **Contents of GEOMATE2012 - Volume 2(1)**

2012	Evaluation of Strength Parameters of Improved Collapsible Soils with Current Additives (Case study: Atrak zone, Iran) <i>Mohammad Arab Ameri, Samaneh Kargar and Mehdi Arab Ameri</i>	<b>385-390</b>
2100	Influences of soil material parameters in compaction simulation with soil/water/air coupled F.E. code <i>S. Sakamoto, K. Kawai, V. Phommachanh and A. Iizuka</i>	<b>391-396</b>
2105	Lower bound limit analysis of strip footings resting on cohesive soils <i>S.M. Binesh, A. Gholampour</i>	<b>397-402</b>
2106	Upper bound limit analysis of strip footings resting on cohesive soils <i>S.M. Binesh, S. Raei</i>	<b>403-408</b>
2108	Evaluating and optimizing different methods of treating and cleaning contaminated soil <i>Mohammad Reza Atrechian, Seyed Salman Musavi Khosro Ebrahimkhani</i>	<b>409-412</b>
2112	Experimental study concerning impact characteristics by collision of weight on sand cushion over steel beam <i>Tam Sy Ho, Hiroshi Masuya and Naoto Takashita</i>	<b>413-419</b>
2114	Landslides in Tea Plantation Fields in Shizuoka, Japan <i>Jun Sugawara</i>	<b>420-425</b>
2115	Natural base isolation system for earthquake protection <i>Srijit Bandyopadhyay, Aniruddha Sengupta and G.R. Reddy</i>	<b>426-431</b>
2116	Comparison of Effect of Percent of Compaction, Sand and Cement on The Amount and Time of Swelling of Bentonite <i>Mohammad S. Pakbaz and B. Rafiee</i>	<b>432-435</b>
2118	Prediction of the Axial Bearing Capacity of Piles by SPT-based and Numerical Design Methods <i>Issa Shooshpasha, Ali Hasanzadeh and Abbasali Taghavi</i>	<b>436-439</b>
2120	Application of recently developed mechanistic-empirical methods for the design of heavily loaded pavement structures <i>John N. Mukabi</i>	<b>440-447</b>
2121	Design of support system for excavation in black cotton soils in Guntur, India <i>D. Neelima Satyam, Akhila Manne</i>	<b>448-451</b>
2127	Numerical modeling of pullout capacity of a pile in sand under oblique load <i>Md. Iftekharuzzaman and Dr. Bipul Hawlader</i>	<b>452-457</b>
2130	Slope Failure in Residual Soils of Peru <i>A. Carrillo-Gil</i>	<b>458-461</b>
2131	Back-analysis of Frictional Jacking Forces Based on Shear Box Testing of Excavated Spoils <i>Choo Chung Siung and Dominic Ong E. L.</i>	<b>462-467</b>
2132	Lime Stabilization of Tropical Soft Soils <i>Dygku Salma Awg Ismail, Tan Jui Siang and Siti Noor Linda Taib</i>	<b>468-471</b>
2138	Increase Of Piles Bundle Capacity By Making A Base Joining Them <i>Jan Jaremski</i>	<b>472-478</b>

## **Contents of GEOMATE2012 - Volume 2(1)**

2139	The Effects of soil-Pile Interaction on Seismic Parameters of Superstructure <i>Mahdy KhariI, Khairul Anuar Bin Kassim, Azlan Bin Adnan</i>	<b>479-484</b>
2140	Investigation on Finite Element Modeling of Group of Stone Columns <i>M. Mirshekari , C. Behnia and S. Fakhretaha</i>	<b>485-488</b>
2147	Suction Controlled Triaxial Apparatus for Saturated-Unsaturated Soil Test <i>Luky Handoko, Noriyuki Yasufuku, Kiyoshi Oomine, Hemanta Hazarika</i>	<b>489-493</b>
2154	Monitoring Program and Dilapidation Survey for Grouting of Karst Cavities <i>Hasan A. Kamal and Hassan J. Karam</i>	<b>494-497</b>
2156	Numerical Analysis of Soil Nail Walls under Seismic Condition in 3D Form Excavations <i>Siavash Zamiran, Hamidreza Saba</i>	<b>498-501</b>
2159	Shear strength improvement of fibrous peat due to consolidation pressure <i>Vivi Anggraini, Nurly Gofar and Bujang bin Kim Huat</i>	<b>502-506</b>
2164	Factors affecting the stability analysis of earth dam slopes subjected to reservoir drawdown <i>T. Souliyavong, C. Gallage, P. Egodawatta and B. Maher</i>	<b>507-512</b>
2165	Lateral stress induced due root-water-uptake in unsaturated soils <i>Mu'azu Mohammed Abdullahi and Nazri Bin Ali</i>	<b>513-517</b>
2166	The effect of pre-tensioned rock bolts on seismic behavior of urban tunnels <i>Farshad Fayyaz Jahani, Mohammad Sharifipour</i>	<b>518-523</b>
2170	Effect of silt content on the anisotropic behaviour of silt-sand mixtures <i>Navid Khayat , Abbas Ghalandarzadeh</i>	<b>524-530</b>

### ***Construction Materials***

24b	Production and Properties of High Strength Concrete for Concrete Dam Heightening Project in Sudan <i>Osama M. A. Daoud and, H. S. Sagady</i>	<b>531-537</b>
27	Effect of openings locations of quadratic folded plate roofing systems on their static and dynamic behavior <i>Ahmed Hassan</i>	<b>538-544</b>
48	Improving concrete compression strength using natural additive <i>Abdoullah Namdar, Ideris Bin Zakaria and Nurmunira Binti Muhammad Atan</i>	<b>545-548</b>
53	DEM simulations and laboratory experiments on physical and mechanical properties of sand-gravel mixtures <i>Janaka J. Kumara, Kimitoshi Hayano, Yuuki Shigekuni and Kota Sasaki</i>	<b>549-554</b>
120	Rock slope stability problems in Gold Coast area in Australia <i>Shokouhi Ali, Gratchev Ivan, Charrismanagara Arry</i>	<b>555-558</b>
121	Techno-commercial development of pre-fabricated structures using geopolymer concrete <i>J. Santhosh, R.Sanjeev, P.Sethu Raja, A. Rajendra Prasad, A. Abdul Rahman</i>	<b>559-563</b>

## **Contents of GEOMATE2012 - Volume 2(1)**

124	Mechanical Properties of Recycled Steel Fibre Reinforced Concrete <i>A.S.M. Abdul Awal, Lim Lion Yee, M. Dianah1 and M. Zakaria Hossain</i>	564-569
134	Effects of Gradation of Various Sand Deposits of Pakistan on Strength of Hardened Concrete <i>Gauhar Sabih , S. Muhammad Jamil and Kamran Akhtar</i>	570-574
203	Assessment of recycled concrete aggregates for road base and sub-base <i>S. Jayakody, C. Gallage, A.Kumar</i>	575-579
232	Estimation of consolidation properties of Holocene clays with artificial neural network <i>Kazuhiro ODA , Minsun Lee and Shotaro Kitamura</i>	580-585
250	Measurement of The Crack Displacement Using Digital Photogrammetry for Evaluation of The Soundness of Tunnels <i>A. Kanazawa, S.Nishiyama, T.Yano, T.Kikuchi</i>	586-592
259	Numerical modelling of a small scale shallow foundation reinforced by Soil-Mixing <i>Anna Grzyb, Mahmoud Dhaybi and Frederic Pellet</i>	593-598
262	Physical modelling of a small scale shallow foundation reinforced by Soil-Mixing <i>Mahmoud Dhaybi and Frederic Pellet</i>	599-604
282	Prediction compressive strength of concretes containing silica fume and styrene-butadiene rubber (SBR) with a mathematical model <i>A.Hagholahi, M.Shafieyzadeh</i>	605-610
283	Sliding stability of dry masonry block retaining structure with a resistance plate <i>Akihiro Hashimoto, Noriyuki Yasufuku, Yoshio Suematsu, Kazuo Fujita1 and Toshimitsu Komatsu</i>	611-616
287	Evaluation and Prediction Method on Neutralization of Supplied Long-term Hydraulic Concrete Structure <i>Man-Kwon Choi , Yuki Hasegawa, Shinsuke Matsumoto, Shushi Sato and Tsuguhiro Nonaka</i>	617-621
297	Measurement of tensile properties of geogrids <i>Raid R. Al-Omari and Mohammed K. Fekheraldin</i>	622-631
306	Modeling the Swelling strain and pressure of Weak Rock using Adaptive Network-Based Fuzzy Inference System <i>Ramin Doostmohammadi</i>	632-636
309	Centrifuge Modeling Of Reinforced Embankments On Soft Foundation <i>Ali Sobhanmanesh, Nurly Gofar</i>	637-642
2102	Centrifuge model tests and finite element analyses on the seismic behavior of the quay walls backfilled with cement treated granulate soils <i>Hayano, K., Morikawa, Y., Fukawa, H., Takehana, K. and Tanaka, S.</i>	643-650
2109	Response of Piered Retaining Walls to Lateral Soil Movement Based on Numerical Modeling using Matlab <i>Siamak Pahlevanzadeh</i>	651-654
2122	Evaluation of Thermal Response Tests in Energy Piles <i>Seung-Rae Lee, Seok Yoon, Hyun-Ku Park , Gi-Dae Oh</i>	655-659
2134	Experimental Study on Mechanical Characteristics of Soil-Geosynthetic Interface <i>Md. Bellal Hossain, Md. Zakaria Hossain and Toshinori Sakai</i>	660-665

## **Contents of GEOMATE2012 - Volume 2(1)**

2136	An Interpretation of Mechanical Properties of Bentonite as a Non-linear Elastic Material <i>Y. Takayama, S. Tsurumi, A. Iizuka, K. Kawai</i>	<b>666-671</b>
2149	Effect of carbonation on strength of cement treated sand <i>Kenichiro Nakarai and Tomomi Yoshida</i>	<b>672-675</b>
2167	Application of PML to Analysis of Nonlinear Soil-Structure-Fluid Problem using mixed element <i>Pahaiti Rehemam, Hiroo Shiojiri</i>	<b>676-681</b>

### ***Environment***

28	Recycled Bassanite as a Stabilizing Agent for Cohesion-less Soil <i>Aly Ahmed and Keizo Ugai</i>	<b>682-687</b>
31	The effects of environmental on today construction industry <i>Mahdy KhariI, Khairul Anuar Bin Kassim, Azlan Bin Adnan</i>	<b>688-692</b>
33	A Case History of Quay Wall Failure and Remedial Design <i>C. S. Chen</i>	<b>693-696</b>
37	Environmental economical efficiency in treatment/reutilization of construction sludges considering delay in process flow <i>Shinya Inazumi, Hiroyasu Ohtsu and Takayuki Isoda</i>	<b>697-702</b>
42	Evaluation and validation of elastic-fragile damage modeling for unsaturated porous media in $\theta$ -stock <i>B. Gatmiri , M. Fathalikhani</i>	<b>703-708</b>
43	Estimation of the Landslide Dam Sustainability in the Gigantic Seimareh Landslide Using the Rate of Sedimentation <i>Zieaoddin Shoaiei</i>	<b>709-7012</b>
47	Influence of soil and rock mineralogy and geomorphology on Landslides Occurrence and soil erosion in the Merek Catchment, Iran <i>Mosayeb Heshmati , Nik Muhamad Majid, J. Shamshuddin, Arifin Abdu and Muhamad Ghaituri</i>	<b>713-719</b>
112	The effect of historical land use on landslide initiation <i>Gholamreza Shoaiei</i>	<b>720-723</b>
114	Integrated Environmental Management for Sustained Development <i>J.Rajaraman and K.Thiruvenkatasamy</i>	<b>724-729</b>
114a	Lowland Environmental Geotechnology of Seismosediments of Kandla Port In India <i>J.Rajaraman and K.Thiruvenkatasamy</i>	<b>730-735</b>
123	Single step extraction to find out soluble lead in soil <i>Masahiko Katoh, Satoshi Masaki, Takeshi Sato</i>	<b>736-741</b>
127	Biogas Production from Tannery Sludge <i>A.Rajendra Prasad, A.Dhanalakshmi, S.Usha and A.Abdul Rahman</i>	<b>742-746</b>
131	Water Harvesting and Salinization Prevention by Capillary Barrier of Soil <i>Toshihiro Morii, Mitsuhiro Inoue, Kaoru Kobayashi, Tetsuya Suzuki and Takayuki Kawai</i>	<b>747-752</b>



## **Contents of GEOMATE2012 - Volume 2(1)**

204	Study of the Performance of anaerobic digestion of greasy skim as a renewable energy source <i>Salam J. Bash Al-Maliky</i>	<b>753-756</b>
209	Seismic evaluation of NARGES soil nailed wall under Cyclic loading and Pseudo Static forces <i>Ardalan Akbari Hamed , Mohammad Moghadaripour , Ali Ghazat</i>	<b>757-761</b>
229	Purification System of Ocean Sludge by and Using Coagulants and then Activating Microorganisms <i>Kyoichi Okamoto and Kenji Hotta</i>	<b>762-767</b>
233	Mechanical properties of volcanic products mixed with industrial wastes <i>K. Yamamoto, T. Negami2, M. Hira, N. Aramaki and Y. Hayashi</i>	<b>768-771</b>
235	Measurement of Hydraulic Conductivity for Peat Ground Using CPTU <i>Hirochika Hayashi and Satoshi Nishimoto</i>	<b>772-775</b>
252	Extraction of temporal and spatial properties on habitat of snail by means of statistical approach <i>Masaaki Kondo and Takamitsu Kajisa</i>	<b>776-781</b>
265	The use of Nano Zero Valent Iron to remediation of contaminated soil and groundwater <i>Taghizadeh Maryam , Yousefi Kebria Daryoush and Gholamreza Darvishi</i>	<b>782-785</b>
267	A Multi-parameter Water Quality Analysis by onsite filtered 2mL Sample to Monitor Urban River Eutrophication <i>Akira Kikuchi, Nor Eman Ismail, Narges Janalizadeh, Musa Mutah and Muhamad Faiz</i>	<b>786-790</b>
268	The intelligent performance installations in energy efficiency in green buildings <i>Hooman Abadi, Rouzbeh Abadi, Poona Abadi</i>	<b>791-796</b>
271	Study the Effect of Polyvinyl Chloride (PVC) Addition on the Permeability of Anbar Soils <i>Ahmed H. Abdul Kareem &amp; Omar Mustafa</i>	<b>797-802</b>
274	Monitoring deforestation and rangeland destruction through land use alteration during 1955- 2002, using GIS and RS in Merek sub-basin, west Iran <i>Mohammad Gheitury, Mosayeb Heshmati, Mohammad Ahmadi and Nik Muhamad Majid</i>	<b>803-807</b>
280	The comparison of phytoremediation and electrokinetic methods in remediation of petroleum hydrocarbons contaminated soil <i>Gholami Meade, Yousefi Kebria Daryoush</i>	<b>808-811</b>
286	Using Metacognitive Strategies On Listening Comprehension <i>Mahshid Mirzaaghaee</i>	<b>812-822</b>
298	Evaluation of Run-Off Supply Projects in Hamedan Province(Iran) <i>N. Rostam Afshar, M. Abdoli</i>	<b>823-827</b>
299	Protective measures of the monumental pine in Rikuzentakada with soil-water-air-solved material coupled model <i>Y. Sugiyama, S. Nomura, K. Kawai and A. Iizuka</i>	<b>828-833</b>
304	Effects of Biosurfactants in Electrokinetic Remediation of contaminated soils <i>Bour Moslem and Yousefi kebria Daryoush</i>	<b>834-838</b>
2117	Change in structure of ground-beetle assemblage on river areas after construction of biotopes using the technique, "Nature oriented river works" <i>Michko Masuda, Takaaki Tsukada and Fumitake Nishimura</i>	<b>839-844</b>

## **Contents of GEOMATE2012 - Volume 2(1)**

2123	Dense granular-fluid mixture: the effects of the natural grains characteristics and the interstitial fluid viscosity <i>Anna Maria Pellegrino and Leonardo Schippa</i>	<b>845-850</b>
2131	Back-analysis of Frictional Jacking Forces Based on Shear Box Testing of Excavated Spoils <i>Choo Chung Siung and Dominic Ong E. L.</i>	<b>851-856</b>
2137	An idea of multi-functional reservoirs in mountain regions <i>Jan Jaremski</i>	<b>857-862</b>
2141	Estimation Method of Amount of Tsunami Disaster Wastes during the 2011 off the Pacific Coast of Tohoku Earthquake <i>Minoru Yamanaka, Naoya Toyota, and Shuichi Hasegawa, Atsuko Nonomura</i>	<b>863-866</b>
2143	Assessment of Runoff in the High Humid Foot-hill Areas of Arunachal Himalayas Using Thornthwaite Equation <i>Md. Eahya Al Huda and Surendra Singh</i>	<b>867-871</b>
2161	Natural Radiation level in Groundwater from Katsina, a Semi Arid Region of Northern Nigeria <i>B.G. Muhammad and M.S. Jaafar</i>	<b>872-876</b>
2163	Cost-Performance Studies of Abandoned Shell Husks (ASH) for Soil Reinforcement Applications <i>Md. Toriqul Islam, Md. Zakaria Hossain, Masaaki Ishida, Md. Bellal Hossain and Md, Jamal Uddin</i>	<b>877-880</b>
2171	Cyclones Path and Severities: Effect on Flood Height and Damages of Land and Embankments in Bangladesh <i>Musahaq Ali, Zakaria Hossain and Shigeko Haruyama</i>	<b>881-884</b>
	Author index	<b>885</b>

# Contents of GEOMATE 2013, Nogoya, Japan, Volume 3(1)

Preface	x
Organization	xi
<b><i>ID Keynote Papers</i></b>	<b>1</b>
GROUND DEFORMATION DURING AND AFTER EARTHQUAKES	<b>2</b>
1k –SIMULATION AND PREDICTION BASED ON ELASTO-PLASTIC SOIL MECHANICS- Akira Asaoka	
USE OF RECYCLED AGGREGATES FROM CONSTRUCTION AND DEMOLITION WASTES FOR THE	<b>12</b>
2k CONSTRUCTION OF FLEXIBLE PAVEMENTS Márcio Muniz de Farias, Alejandra María Gómez Jiménez and Ferney Quiñones Sinisterra	
EFFECTIVE STRESS IN UNSATURATED GRANULAR MEDIA IN THE PENDULAR REGIME	<b>24</b>
3k Richard Wan, Sarah Khosravani and Mehdi Pouragha	
RECENT GEOTECHNICAL RESEARCH ADVANCES IN UNIVERSITY PUTRA MALAYSIA	<b>32</b>
4k Bujang B.K.Huat and Afshin Asadi	
	<b>40</b>
<b><i>Technical Papers</i></b>	
	<b>41</b>
<b><i>ID Geotechnique</i></b>	
LANDSLIDES IN BANGLADESH: CAUSES AND RECOMMENDATION	<b>42</b>
3102 Musahaq Ali, Zakaria Hossain and Shigeko Haruyama	
PRECAST SPREAD FOUNDATION IN INDUSTRIALIZED BUILDING SYSTEM	<b>47</b>
3110 Ramli Nazir, Ehsan Momeni, A. Kadir Marsono, Houman Sohaie	
CATEGORISING GEOTECHNICAL PROPERTIES OF SUBSOIL IN SURFERS PARADISE USING	<b>53</b>
3114 GEOGRAPHIC INFORMATION SYSTEM (GIS) Haider Al-Ani, Leila Eslami-Andargoli, Erwin Oh and Gary Chai	
EVALUATION OF CONSTITUTIVE MODEL IN SIMULATING THE BEHAVIOR OF CEMENT-TREATED SOIL	<b>59</b>
3116 Ay Lee Saw, C F Leung and S A Tan	
UPDATING THE PREDICTIVE MODEL FOR THE VERTICAL COLLAPSE PERCENTAGE OF COLLAPSIBLE	<b>65</b>
3122 SOIL SUBGRADES Moshe Livneh and Noam A. Livneh	
INFLUENCE OF FREEZE-THAW ACTION ON AIR-PERMEABILITY OF UNSATURATED SOIL GROUND	<b>71</b>
3123 Tatsuya Ishikawa, Tetsuya Tokoro, Dai Nakamura and Satoshi Yamashita	

## Contents of GEOMATE 2013, Nogoya, Japan, Volume 3(1)

3144	EFFECT OF ROCK SOCKET CHARACTERISTICS ON LOW STRAIN INTEGRITY TEST OF PILES Ramli Bin Nazir and Osman El Hussien	77
3148	CHARACTERISTICS OF SLOPE FAILURES IN MAKINOHARA, JAPAN Jun Sugawara	83
3151	S-PSA WITH USING FEM FOR AN EXISTING ESTUARY DAM T. Hara, M. Iwata, Y. Otake, Y. Honjo, T. Kato, A. Nishida and H. Yukimoto	89
3155	THE ROTATIONAL HARDENING RULE WITHOUT THE LIMIT SURFACE OF HARDENING Hiroyuki Kyokawa, Ryoki Ohashi and Teruo Nakai	95
3157	A STUDY OF THE FORMATION MECHANISM OF BEACHROCK IN OKINAWA, JAPAN: TOWARD MAKING ARTIFICIAL ROCK Takashi Danjo and Satoru Kawasaki	101
3161	A STUDY ON THE SLAKING-INDUCED CREEP DEFORMATION CHARACTERISTICS OF CRUSHED MUDSTONE Sharma Keshab, Kiyota Takashi and Kyokawa Hiroyuki	107
3163	ASTUDY ON GROWTH OF VETIVER GRASS IN TROPICAL REGION FOR SLOPE PROTECTION Mohammad Shariful Islam, B. A. M. Shahriar, Md. Shahidul Islam and Hossain Md. Shahin	113
3164	INTERACTION MECHANISMS OF SOIL-GEOSYNTHETIC REINFORCEMENT Mabrouk Touahmia	119
3165	SIMULATION AND PREDICTION OF LARGE-SETTLEMENT IN ULTRA-SOFT PEAT GROUND BY DEDUCING THE IN-SITU INITIAL CONDITIONS CONSIDERING ARTESIAN PRESSURE Mutsumi Tashiro, Toshihiro Noda and Nguyen Hong Son	124
3175	SEISMIC RESPONSE ANALYSIS OF GEOTECHNICAL STRUCTURES BUILT OF CEMENT-TREATED DREDGED SOIL Takayuki Sakai, Masaki Nakano and Shotaro Yamada	130
3176	DEVELOPMENT OF SPH METHOD WITH AN ELASTO-PLASTIC CONSTITUTIVE MODEL CONSIDERING SOIL SKELETON STRUCTURE AND ITS APPLICATION TO EXCAVATION PROBLEMS Hideto Nonoyama, Masaki Nakano and Toshihiro Noda	136
3178	SOUNDNESS EVALUATION OF THE EMBANKEMENTS FOR EFFECTIVE MAINTENANCE AND LONG-LIFE OF SHIN-TOMEI EXPRESSWAY Masaya Hinokio, Hiroshi Yamato, Kazunari Suzuki, Takayuki Sakai, Masaki Makano and Minoru Kawaïda	142
3184	EVALUATION OF GLASS FIBERS DERIVED-THREE DIMENSIONAL GEOMATERIAL FOR PROBLEMATIC SOIL APPLICATIONS Donovan Mujah, Hemanta Hazarika, Fauziah Ahmad and Muhammad Ekhlaur Rahman	148
3193	STUDY ON MONITORING METHOD OF RETAINING WALL BEHAVIOR USING MEMS SENSOR NETWORK N Minakata, S Nishiyama, T Yano, D.H Lee, J Wu and M Ryu	154
3211	CASE STUDY ON THE USE OF HIGH-RESOLUTION SURFACE WAVE SURVEY FOR EXAMINING THE CAUSE OF SUBSIDENCE OF RECLAIMED ROAD Miura Minami and Shibuya Satoru	160
3217	MODIFICATION OF KAOLIN MINERALOGY AND MORPHOLOGY BY HEAT TREATMENT AND POSSIBILITY OF USE IN GEOTECHNICAL ENGINEERING Nurmunira Muhammad, Ideris Zakaria and Abdoullah Namdar	164
3223	SIMULATING THE EFFECT OF FLOW VOLUME ON SCOURING PROCESS AROUND BREAKWATER UNDER TSUNAMI CONDITION BY SPH METHOD M.R. Islam, K. Hayano and A.M.K.N. Nadeesha	169

## Contents of GEOMATE 2013, Nogoya, Japan, Volume 3(1)

3226	DEVELOPING A NUMERICAL MODEL FOR THE STABILITY DESIGN OF TUNNEL HEADING Jim Shiau and Ryan Kemp	175
3228	INVESTIGATION OF THE OPTIMAL SUPPORT PATTERNS IN BRACED EXCAVATION USING GROUND ANCHORS H. M. Shahin, Teruo Nakai, Okuda Kazuaki and Kato Morihiro	181
3232	SHEAR MODULUS REDUCTION CURVES OF GUAYURIBA SANDS BY CYCLIC TRIAXIAL AND BENDER ELEMENT TESTS J.F. Gaitán-Serrano, M.P. Ortiz-Pulido and J.F. Camacho-Tauta	187
3234	WATER DIVERSION AND DRAINAGE IN SHALLOW LAND WASTE REPOSITORY CONSTRUCTED USING CAPILLARY BARRIER OF SOIL Toshihiro Morii, Kaoru Kobayashi, Kazunobu Matsumoto and Satoru Nakafusa	193
3236	REINFORCING EFFECT OF GEOSYNTHETICS ON BEARING CAPACITY Masuda Saki, H. M. Shahin, Nakai Teruo, Morikawa Yukihiro and Mio Susumu	199
3237	INFLUENCE OF THE STRESS HISTORY ON THE STIFFNESS OF SOIL Asano Kanako, H.M. Shahin, Hiroyuki Kyokawa, Teruo Nakai and Ohashi Ryoki	205
3238	EFFECTIVENESS OF CRASHED TILE IN COUNTERMEASURE AGAINST LIQUEFACTION Morikawa Yukihiro, Maeda Kenichi and Zhang Feng	211
3246	PREDICTION OF NATM TUNNEL EXCAVATION UNDER SHALLOW OVERBURDEN IN PAHANG-SELANGOR RAW WATER TRANSFER TUNNEL PROJECT, MALAYSIA Mohd Ashraf Mohamad Ismail, Goh Chin Ong, Romziah Azit, Zulkifli Nordin, Norzani Mahmood	217
3250	FUNDAMENTAL STUDY ON LATERAL RESISTANCE CHARACTERISTICS OF BALLASTED TRACKS SUBJECTED TO PSEUDO-STATIC INERTIA FORCE Ryuta Ogawa and Kimitoshi Hayano	223
3251	USE OF ACOUSTIC EMISSION TECHNOLOGY TO STUDY THE MECHANICAL BEHAVIOUR OF VARIOUS SANDSTONES: GEOTHERMAL ENERGY Shao, S.S., Ranjith, P.G. and Chen, B.K.	229
3262	UNCONFINED COMPRESSIVE STRENGTH OF CEMENT TREATED SOIL/RAP MIXTURE Jirayut Suebsuk, Aniroot Suksan, Suksun Horpibulsuk and Apichit Kumpala	235
3267	INVESTIGATION OF STRESS REDUCTION EFFECT ON STRUCTURE DUE TO BASEMAT UPLIFT USING ENERGY CONCEPT Takafumi Inoue and Atsushi Mikami	241
3271	SWELLING DEFORMATION OF BENTONITE MIXED WITH INORGANIC MATERIALS IN ALKALINE SOLUTION Yuki Yokoyama and Kenichiro Nakarai	247
3274	USE OF FULLY SOFTENED VERSUS PEAK STRENGTH TO PREDICT THE CAPACITY OF FOOTINGS ON GEOSYNTHETIC REINFORCED SOIL Melia K. Iwamoto, Phillip S.K. Ooi, Jennifer E. Nicks and Michael T. Adams	252
3296	THREE DIMENSIONAL FINITE ELEMENT ANALYSIS OF SOIL NAILS IN GRANITIC SOILS G. Ren and H. Tokhi	258
3298	SIMPLIFIED DYNAMIC AXIAL HEAD PILE STIFFNESS IMPROVEMENT ANALYSIS FOR EXISTING PILED VIADUCT WITH BASE REINFORCEMENT Aglipay Mary Roxanne and Konagai Kazuo	262
3312	PFC3D NUMERICAL EXPERIMENTS OF SELF-BORING IN-SITU SHEAR PRESSURE-METER MODEL TEST Yafei Zhang, Guangli Xu and Jidong Teng	268

## Contents of GEOMATE 2013, Nogoya, Japan, Volume 3(1)

3318	DYNAMIC ANALYSIS OF SLOPE FAILURE USING THE MESH-FREE SPH METHOD N. Hiraoka, A. Oya, Ha H. Bui, P. Rajeev and R. Fukagawa	274
3320	ELECTRICAL RESISTIVITY TOMOGRAPHY TO INSPECT BRIDGE FOUNDATIONS Helsin Wang, Chih-Hsin Hu, and Chung-Yue Wang	280
3323	ULTIMATE BEARING CAPACITY ANALYSIS OF GROUND AGAINST INCLINED LOAD BY TAKING ACCOUNT OF NONLINEAR PROPERTY OF SHEAR STRENGTH Du N L, Ohtsuka S, Hoshina T, Isobe K, and Kaneda K	286
3326	PREDICTION OF SLOPE DEFORMATIONS BY ELASTIC WAVE VELOCITIES IN RELATION TO LANDSLIDE FAILURES Muhammad Irfan and Taro Uchimura	292
3329	BOX-SHAPE RETAINING WALL SYSTEM: EXPERIMENT AND NUMERICAL PREDICTION C.T. Nguyen, Ha H. Bui, and R. Fukagawa	298
3343	PERMEABILITY AND CONSOLIDATION BEHAVIOR OF COMPOSITE GROUND REINFORCED WITH SAND COLUMNS B. A. Mir and Ashish Juneja	304
3347	LABORATORY EVALUATION OF PHYSICO-CHEMICAL VARIATIONS IN BENTONITE UNDER ELECTROKINETIC ENHANCEMENT Nasim Mosavat, Erwin Oh and Gary chai	310
3358	FLOW PATTERN FOR MULTI-SIZE SILOS Yi Yang, Na Li, PengYin and YM Cheng	317
<b>ID</b>	<b><i>Construction Materials</i></b>	<b>322</b>
3132	IMPROVING ENGINEERING PROPERTIES OF FINE-GRAINED SOIL WITH STEEL SLAG FOR USING IN EMBANKMENT EARTHFILL Je-Min Baek, Satoru Shibuya, Jin-Suk Hur and Tara Nidhi Lohani	323
3156	EVALUATION EQUATION OF DIFFUSION COEFFICIENT OF CHLORIDE ION FOR CRACKED CONCRETE Junpei Saito and Satoru Shimobe	327
3160	OPTIMIZATION OF EFFECTIVE DEPTH OF COMPACTION FOR FINE-GRAINED SOILS Girum Y. Yesuf, Inge Hoff and Jan Vaslestad	333
3197	COMPRESSIVE STRENGTH OF CEMENT PASTES EXPOSED TO ELEVATED TEMPERATURE AND DETERIORATION MITIGATION Abdoullah Namdar, Ideris Bin Zakaria and Gurumurthy Hegde	339
3201	PARTICLE SIZE AND OTHER FACTORS AFFECTING THE PULLOUT BEHAVIOR OF GEOCELLS EMBEDDED IN GRAVELLY SOIL BACKFILL Xinye Han, Takashi Kiyota, Michiyuki Harata and Fumio Tatsuoka	345
3202	EFFECT OF LOADING RATE ON STRENGTH CHARACTERISTICS OF GRANULAR BASE COURSE MATERIAL Yuan Zhang, Tatsuya Ishikawa and Tetsuya Tokoro	351
3207	EXPERIMENTAL STUDY OF PLYWOOD COMPARING TO FOAM FILLED HONEYCOMB STRUCTURE Phacharaporn Bunyawanchakul, Chattarin Sunsin, and Thammakorn Sasanawin	357
3249	X-RAY IMAGE ANALYSIS OF POROSITY OF POROUS CONCRETES Jaehun Ahn, Jinwoo Jung and Seungbae Kim	363



## Contents of GEOMATE 2013, Nogoya, Japan, Volume 3(1)

3252	STRESS - STRAIN BEHAVIOUR OF SLAG CEMENT CONCRETE Mustapha Boukendakdji	367
3256	ESTIMATION AND EXPERIMENTAL STUDY ON DIVERSION LENGTH OF CAPILLARY BARRIER USING CRUSHED SHELL PARTICLES Kazunobu Matsumoto, Kaoru Kobayashi , Satoru Nakafusa and Toshihiro Morii	373
3268	EXPERIMENTAL STUDY OF CONCRETE AND MORTAR MIXING WASTE TIRE RUBBER Man-Kwon Choi, Yuki Hasegawa, Shushi Sato, Shinsuke Matsumoto and Hyeon-Tae Kim	379
3287	PILE DRIVING EFFECTS ON NEARBY BUILDING Adhilla Ainun Musir and Abdul Naser Abdul Ghani	384
3317	LABORATORY STUDY ON THE PERFORMANCE OF RECYCLED CONCRETE AGGREGATES BLENDED WITH RECLAIMED ASPHALT PAVEMENT AS A PAVEMENT GRANULAR MATERIAL S. Jayakody, C. Gallage, J. Ramanujam, A.Kumar	389
3322	BEHAVIOR OF PENETRATION AND LEACHING OF CESIUM IN MORTAR HAVING VARIOUS FINE AGGREGATES AND MOISTURE CONTENT Masashi Ito, Kenichiro Nakarai Akihiko Hayashi and Kenji Kawai	394
3324	EFFECTS OF COARSE AGGREGATE CONTENT ON THE EROSION RATE OF CONCRETE DUE TO SULFURIC ACID ATTACK Yuji Hatano, Yutaka Okame and Kenji Kawai	400
3357	STUDY ON PHYSICAL PROPERTIES AND USABILITY OF SOME SELECTED RECYCLED FINE AGGREGATES Mohammad Raihanul Islam, Satoru Ishiguro	406
<b>ID</b>	<b><i>Environment</i></b>	<b>410</b>
3145	COMPUTER MODELING AND ANALYSIS OF THREE PHASE INDUCTION MOTOR UNDER TEMPORARY SHORT CIRCUIT FAULT IN STATOR USING WAVELET TRANSFORM Dicky Nova Wardana, Dimas Anton Asfani, Ardyono Priyadi, and Mauridhi Hery Purnomo	411
3147	ANALYTICAL SOLUTION TO CONTAMINANT EXTRACTION CONSIDERING SMEAR EFFECT H.Y Wang , X.W Tang and B. Bai	416
3152	MECHANISM OF C6H6 OXIDATION IN THE THREE-WAY CATALYTIC CONVERTER EQUIPPED A GASOLINE ENGINE Akio Takigawa, Akihiro Mieda and Yongzhen Peng	422
3177	ROLE OF CURBSIDE CRACK OF ROAD IN URBAN BIODIVERSITY Taizo Uchida, Xue J. Huan, Daisuke Hayasaka, Teruo Arase, William T. Haller and Lyn A. Gettys	427
3185	DYE TRACER EXPERIMENTS FOR IDENTIFYING SOLUTE DISPERSIVITY IN UNSATURATED POROUS MEDIA Kazuya Inoue, Takayuki Fujiwara and Tsutomu Tanaka	433
3188	REUSE OF AGRICULTURAL AND FOOD RESIDUES FOR RETARDING AND ATTENUATING NITRATE IN POROUS MEDIA Kazuya Inoue, Saki Matsuyama and Tsutomu Tanaka	439
3196	MICROSCOPIC RANGE OF IMMOBILIZATION BETWEEN HEAVY METALS AND AMENDMENT IN SOIL THROUGH WATER MIGRATION Shouhei Ogawa, Masahiko Katoh and Takeshi Sato	445
3198	SUB-DARCY-SCALE MODELING OF NON-UNIFORM FLOW THROUGH POROUS MEDIA WITH MIXED WETTABILITES Junichiro Takeuchi, Takuya Takahashi, and Masayuki Fujihara	452

## Contents of GEOMATE 2013, Nogoya, Japan, Volume 3(1)

3218	CAPTURING PEDESTRIAN MOVEMENT SAFETY AND SECURITY ISSUES AT MAJOR TRANSPORTATION INTERCHANGES Zulfadly Azizi Bohari, Syahriah Bachok and Mariana Mohamed Osman	458
3222	ASSESSMENT OF CHROMIUM CONTAMINATION IN SEDIMENTS OF SOUTHERN KAOHSIUNG HARBOR, TAIWAN Cheng-Di Dong, Chih-Feng Chen and Chiu-Wen Chen	464
3224	GPS/GIS IDENTIFICATION OF POTENTIAL BUS STOP LOCATIONS AND PASSENGER'S ACCESS AND EGRESS POINTS Syahriah Bachok, Zakiah Ponrohono, Mariana Mohamed Osman, Zulfadly Azizi Bohari	469
3243	GEOCHEMISTRY OF PALEOGENE RED BEDS IN THE NORTHERN IRAQ FORELAND BASIN: EVIDENCE FOR PROVENANCE Muatasam Hassan, Brian G. Jones, Ali Ismail Al Jubory, Sabah Ahmed Ismail, Abdul Salalm Mehdi Saleh	475
3244	DEVELOPMENT OF BASE MATERIALS FOR SEAWEED BEDS USING VOLCANIC ASHES AND RECYCLING MATERIALS OF INDUSTRIAL WASTES K. Yamamoto, T. Negami, T. Nakajima, H. Yano, Y. Futsuhara and K. Shima	481
3247	CARBON FOOTPRINT AWARENESS – AN INVESTIGATION FROM TRAVEL DIARY SURVEY Nur Sabahiah Abdul Sukorand Nur Khairiyah Basri	487
3248	OPTIMAL MONITORING NETWORK DESIGN FOR EFFICIENT IDENTIFICATION OF UNKNOWN GROUNDWATER POLLUTION SOURCES Om Prakash and Bithin Datta	493
3257	SPATIAL DISTRIBUTION CHARACTERISTICS OF SUBTERRANEAN HOT WATER EVALUATED USING WATER QUALITY CONCENTRATION DATA Takamitsu Kajisa, Si Senfi, Yasunori Mori, Homayoon Ganji, Abdul Saboor Rahmany, Masaaki Kondo and Hajime Narioka	499
3258	IDENTIFICATION OF POLLUTANT SOURCE CHARACTERISTICS UNDER UNCERTAINTY IN CONTAMINATED WATER RESOURCES SYSTEMS USING ADAPTIVE SIMULATED ANEALING AND FUZZY LOGIC Mahsa Amirabdollahian and Bithin Datta	505
3270	POINT-BASED RENDERING FOR MASSIVE POINT CLOUD VISUALIZATION Masafumi Nakagawa	511
3325	REDRAWING AN UNKNOWN MASONRY CAISSON BY GEOPHYSICAL METHODS Ming-Hung Chen, Shun-Min Lee, Yung-Chuan Chou, Yao-Jen Hsu and Chih-Hsin Hu	517
3335	CONTRIBUTION OF GEOLOGICAL MAPPING AND NEW TECHNOLOGIES TO THE IDENTIFICATION OF A MAJOR, PRE-EXISTING AND ACTIVE FAULT OVER THE CAPITAL OF TUNISIA Adnène Kassebi and Fouad Zargouni	523
3338	EFFECT OF GRAIN SIZE ON MINERAL CARBONATION OF COAL COMBUSTION FLY ASH FOR CO <sub>2</sub> SEQUESTRATION N. L Ukwattage and P.G Ranjith	530
3349	STUDY SEISMICITY PARAMETERS OF RUDBAR REGION AND SEISMOLOGICAL ASSESSMENT OF RUDBAR-MANJIL (IRAN) EARTHQUAKE OF JUNE1990 Noushin Naraghi Araghi, Mohd. Nawawi and Syed Mustafizur Rahman	535
3351	UNDERSTANDING TO PREDICT SOIL BEHAVIOR J. Rajaraman, K.Thiruvengkatasamy and S. Narasimha Rao	540
3356	CASE STUDY ON SHALLOW FAILURE OF CONGLOMERATE AND SILTSTONE SLOPES DUE TO A HEAVY RAINFALL Satoshi Kagamiahra, Satoru Shibuya, Byeong - su Kim, Shunzo Kawajiri, Tara Nidhi Lohani and Takashi Okimura	545

# GEOMATE 2015

Fifth International Conference on  
**Geotechnique, Construction Materials & Environment**  
**16-20 November 2015**  
**OSAKA, JAPAN**

**Invitation to participate**

Scopus

EBSCO

CENGAGE  
Learning



GIF  
GLOBAL IMPACT FACTOR

VOLUME 6  
Number 1 & 2  
March-June 2014

ISSN: 2186-2982 (Print)  
ISSN: 2186-2990 (Online)  
Serial 11 & 12

## International Journal of GEOMATE

### Geotechnique, Construction Materials and Environment



Tsu, Japan

<http://www.gi-j.com/>  
[geomate@gi-j.com](mailto:geomate@gi-j.com)

THE GEOMATE INTERNATIONAL SOCIETY